

NASA Technical Memorandum 100910

Bibliography of Lewis Research Center Technical Publications Announced in 1987

(NASA-TM-100910) BIBLIOGRAPHY OF LEWIS
RESEARCH CENTER TECHNICAL PUBLICATIONS
ANNOUNCED IN 1987 (NASA) 362 P CSCL 05B

N88-28832

G3/82 0158869
Unclas

June 1988

NASA

PREFACE

In 1987, Lewis Research Center's 1195 research authors published 493 technical publications that were announced to and reached the worldwide scientific community. This was our highest number of technical publications in 15 years. The 493 papers included 243 symposium/seminar presentations and 77 articles sent directly to journals for publication. The number of seminar presentations was the highest in Lewis history (223 in 1986 and 226 in 1984), while the number of journal articles was the second highest in Lewis history (82 in 1986). For many years, the number of articles submitted directly to journals for publication ranged between 40 and 50. In 1987, Lewis authors published approximately 65 percent of their research contributions in outside publications and the remainder as NASA research reports. Seventy-four percent of Lewis-authored society presentations and journal articles were addressed to members of the following technical societies: AIAA, 99 papers; ASME, 86 papers; SAE, 60 papers; IEEE, 43 papers; American Chemical Society, 34 papers; ASEE (American Society of Engineering Education), 30 papers; American Nuclear Society, 25 papers; AIChE, 24 papers; AIP (American Institute of Physics), 15 papers; and ACS (American Ceramic Society), 13 papers.

In 1987, 239 contractor-authored research reports were produced. In addition, 6 patent applications were filed and 6 patents were issued.

Lewis hosted 14 research conferences in 1987. Five of these resulted in NASA Conference Publications, namely,

- NASA CP-2484, Space Electrochemical Research and Technology (SERT), April 14-16, abstracts/no figures/preprint
- NASA CP-10001, Cryogenic Fluid Management Technology Workshop, April 28-30
- NASA CP-2471, Structural Integrity and Durability of Reusable Space Propulsion Systems, May 12-13
- NASA CP-2493, 1987 Turbine Engine Hot Section Technology (HOST), October 20-21
- NASA CP-10003, Aeropropulsion '87, November 17-19, preprint

Two of these conference publications were published at Lewis and made available to the attendees when they registered at the conference: Space Electrochemical Research and Technology (SERT) and Aeropropulsion '87. Other conferences hosted by Lewis in 1987 included

- Aerospace Education Workshop, February 5-6
- JANNAF Safety and Environmental Protection Meeting, May 5-7
- Electric Propulsion Conference, May 11-13
- 4th North Coast Symposium of the Ohio Chapter of the American Vacuum Society, May 21
- International Symposium on Space Information Systems in the Space Station Era, June 22-24
- The First Structural Mechanics Branch Symposium and Workshop on Composite Mechanics and Related Computer Codes, September 16-17
- Space Station Plasma Interactions and Effects (SSPIE) Working Group Meeting, September 29-30
- High-Speed Commercial Transport Fuels Workshop, October 14-15
- International Workshop on Aircraft Icing Technology, November 4-6

Many Lewis authors have received awards for their contributions; among them are the following:

The 1987 Lewis Distinguished Paper Award was presented to J. L. Smialek and N. S. Jacobson for their paper entitled "Mechanism of Strength Degradation for Hot Corrosion of α -SiC." In addition, a team of researchers led by Robert Hendricks of the Internal Fluid Mechanics Division received ASME's H.H. Jeffcott Award for the paper entitled "Numerical and Analytical Study of Fluid Dynamic Forces in Seals and Bearings" presented at the 11th Biennial ASME Design Engineering Division Conference on Vibration and Noise.

A few Lewis-authored publications are not included in this compilation because of FEDD (For Early Domestic Dissemination) and ITAR (International Traffic in Arms Regulations) considerations which limit their announcement and distribution.

All the publications in this collection were announced in the 1987 issues of STAR (Scientific and Technical Aerospace Reports) and IAA (International Aerospace Abstracts). Some 1987 publications will be announced in the 1988 issues of STAR and IAA and will thus appear in the 1988 Lewis Bibliography.

The arrangement of the material is by NASA subject category, as noted in the Contents. The various indexes will help locate specific publications by subject, author, contractor organization, contract number, and report number.

George Mandel
Chief, Technical Information Services Division

TABLE OF CONTENTS

PREFACE

i

AERONAUTICS

Includes aeronautics (general); aerodynamics; air transportation and safety; aircraft communications and navigation; aircraft design, testing and performance; aircraft instrumentation; aircraft propulsion and power; aircraft stability and control; and research and support facilities (air).

For related information see also *Astronautics*.

01 AERONAUTICS (GENERAL) 1

02 AERODYNAMICS 2

Includes aerodynamics of bodies, combinations, wings, rotors, and control surfaces; and internal flow in ducts and turbomachinery.

For related information see also *34 Fluid Mechanics and Heat Transfer*.

03 AIR TRANSPORTATION AND SAFETY 15

Includes passenger and cargo air transport operations; and aircraft accidents.

For related information see also *16 Space Transportation* and *85 Urban Technology and Transportation*.

04 AIRCRAFT COMMUNICATIONS AND NAVIGATION N.A.

Includes digital and voice communication with aircraft; air navigation systems (satellite and ground based); and air traffic control.

For related information see also *17 Space Communications, Spacecraft Communications, Command and Tracking* and *32 Communications and Radar*.

05 AIRCRAFT DESIGN, TESTING AND PERFORMANCE 17

Includes aircraft simulation technology.

For related information see also *18 Spacecraft Design, Testing and Performance* and *39 Structural Mechanics*. For land transportation vehicles see *85 Urban Technology and Transportation*.

06 AIRCRAFT INSTRUMENTATION N.A.

Includes cockpit and cabin display devices; and flight instruments.

For related information see also *19 Spacecraft Instrumentation* and *35 Instrumentation and Photography*.

07 AIRCRAFT PROPULSION AND POWER 18

Includes prime propulsion systems and systems components, e.g., gas turbine engines and compressors; and onboard auxiliary power plants for aircraft.

For related information see also *20 Spacecraft Propulsion and Power, 28 Propellants and Fuels*, and *44 Energy Production and Conversion*.

08 AIRCRAFT STABILITY AND CONTROL 34

Includes aircraft handling qualities; piloting; flight controls; and autopilots.

For related information see also *05 Aircraft Design, Testing and Performance*.

09 RESEARCH AND SUPPORT FACILITIES (AIR) 34

Includes airports, hangars and runways; aircraft repair and overhaul facilities; wind tunnels; shock tubes; and aircraft engine test stands.

For related information see also *14 Ground Support Systems and Facilities (Space)*.

ASTRONAUTICS

Includes astronautics (general); astrodynamics; ground support systems and facilities (space); launch vehicles and space vehicles; space transportation; space communications, spacecraft communications, command and tracking; spacecraft design, testing and performance; spacecraft instrumentation; and spacecraft propulsion and power.

For related information see also *Aeronautics*.

12 ASTRONAUTICS (GENERAL) 37

For extraterrestrial exploration see *91 Lunar and Planetary Exploration*.

13 ASTRODYNAMICS 37

Includes powered and free-flight trajectories; and orbital and launching dynamics.

14 GROUND SUPPORT SYSTEMS AND FACILITIES (SPACE) 38

Includes launch complexes, research and production facilities; ground support equipment, e.g., mobile transporters; and simulators.

For related information see also *09 Research and Support Facilities (Air)*.

15 LAUNCH VEHICLES AND SPACE VEHICLES 38

Includes boosters; operating problems of launch/space vehicle systems; and reusable vehicles.

For related information see also *20 Spacecraft Propulsion and Power*.

16 SPACE TRANSPORTATION 39

Includes passenger and cargo space transportation, e.g., shuttle operations; and space rescue techniques.

For related information see also *03 Air Transportation and Safety* and *18 Spacecraft Design, Testing and Performance*. For space suits see *54 Man/System Technology and Life Support*.

17 SPACE COMMUNICATIONS, SPACECRAFT COMMUNICATIONS, COMMAND AND TRACKING 41

Includes telemetry; space communications networks; astronavigation and guidance; and radio blackout.

For related information see also *04 Aircraft Communications and Navigation* and *32 Communications and Radar*.

18 SPACECRAFT DESIGN, TESTING AND PERFORMANCE

41

Includes satellites; space platforms; space stations; spacecraft systems and components such as thermal and environmental controls; and attitude controls.

For life support systems see *54 Man/System Technology and Life Support*. For related information see also *05 Aircraft Design, Testing and Performance*, *39 Structural Mechanics*, and *16 Space Transportation*.

19 SPACECRAFT INSTRUMENTATION

N.A.

For related information see also *06 Aircraft Instrumentation* and *35 Instrumentation and Photography*.

20 SPACECRAFT PROPULSION AND POWER

45

Includes main propulsion systems and components, e.g. rocket engines; and spacecraft auxiliary power sources.

For related information see also *07 Aircraft Propulsion and Power*, *28 Propellants and Fuels*, *44 Energy Production and Conversion*, and *15 Launch Vehicles and Space Vehicles*.

CHEMISTRY AND MATERIALS

Includes chemistry and materials (general); composite materials; inorganic and physical chemistry; metallic materials; nonmetallic materials; propellants and fuels; and materials processing.

23 CHEMISTRY AND MATERIALS (GENERAL)

69

24 COMPOSITE MATERIALS

71

Includes physical, chemical, and mechanical properties of laminates and other composite materials.

For ceramic materials see *27 Nonmetallic Materials*.

25 INORGANIC AND PHYSICAL CHEMISTRY

75

Includes chemical analysis, e.g., chromatography; combustion theory; electrochemistry; and photochemistry.

For related information see also *77 Thermodynamics and Statistical Physics*.

26 METALLIC MATERIALS

81

Includes physical, chemical, and mechanical properties of metals, e.g., corrosion; and metallurgy.

27 NONMETALLIC MATERIALS

94

Includes physical, chemical, and mechanical properties of plastics, elastomers, lubricants, polymers, textiles, adhesives, and ceramic materials.

For composite materials see *24 Composite Materials*.

28 PROPELLANTS AND FUELS

106

Includes rocket propellants, igniters and oxidizers; their storage and handling procedures; and aircraft fuels.

For related information see also *07 Aircraft Propulsion and Power*, *20 Spacecraft Propulsion and Power*, and *44 Energy Production and Conversion*.

29 MATERIALS PROCESSING

107

Includes space-based development of products and processes for commercial application.

For biological materials see *55 Space Biology*.

ENGINEERING

Includes engineering (general); communications and radar; electronics and electrical engineering; fluid mechanics and heat transfer; instrumentation and photography; lasers and masers; mechanical engineering; quality assurance and reliability; and structural mechanics.

For related information see also *Physics*.

31 ENGINEERING (GENERAL)

109

Includes vacuum technology; control engineering; display engineering; cryogenics; and fire prevention.

32 COMMUNICATIONS AND RADAR

111

Includes radar; land and global communications; communications theory; and optical communications.

For related information see also *04 Aircraft Communications and Navigation* and *17 Space Communications, Spacecraft Communications, Command and Tracking*. For search and rescue see *03 Air Transportation and Safety*, and *16 Space Transportation*.

33 ELECTRONICS AND ELECTRICAL ENGINEERING

119

Includes test equipment and maintainability; components, e.g., tunnel diodes and transistors; microminiaturization; and integrated circuitry.

For related information see also *60 Computer Operations and Hardware* and *76 Solid-State Physics*.

34 FLUID MECHANICS AND HEAT TRANSFER

130

Includes boundary layers; hydrodynamics; fluidics; mass transfer and ablation cooling.

For related information see also *02 Aerodynamics* and *77 Thermodynamics and Statistical Physics*.

35 INSTRUMENTATION AND PHOTOGRAPHY

152

Includes remote sensors; measuring instruments and gages; detectors; cameras and photographic supplies; and holography.

For aerial photography see *43 Earth Resources and Remote Sensing*. For related information see also *06 Aircraft Instrumentation* and *19 Spacecraft Instrumentation*.

36 LASERS AND MASERS

N.A.

Includes parametric amplifiers.

For related information see also *76 Solid-State Physics*.

37 MECHANICAL ENGINEERING

160

Includes auxiliary systems (nonpower); machine elements and processes; and mechanical equipment.

38 QUALITY ASSURANCE AND RELIABILITY

170

Includes product sampling procedures and techniques; and quality control.

39 STRUCTURAL MECHANICS

173

Includes structural element design and weight analysis; fatigue; and thermal stress.

For applications see *05 Aircraft Design, Testing and Performance* and *18 Spacecraft Design, Testing and Performance*.

GEOSCIENCES

Includes geosciences (general); earth resources and remote sensing; energy production and conversion; environment pollution; geophysics; meteorology and climatology; and oceanography.

For related information see also *Space Sciences*.

42 GEOSCIENCES (GENERAL) N.A.

43 EARTH RESOURCES AND REMOTE SENSING N.A.

Includes remote sensing of earth resources by aircraft and spacecraft; photogrammetry; and aerial photography.

For instrumentation see *35 Instrumentation and Photography*.

44 ENERGY PRODUCTION AND CONVERSION 188

Includes specific energy conversion systems, e.g., fuel cells; global sources of energy; geophysical conversion; and windpower.

For related information see also *07 Aircraft Propulsion and Power*, *20 Spacecraft Propulsion and Power*, and *28 Propellants and Fuels*.

45 ENVIRONMENT POLLUTION N.A.

Includes atmospheric, noise, thermal, and water pollution.

46 GEOPHYSICS 200

Includes aeronomy; upper and lower atmosphere studies; ionospheric and magnetospheric physics; and geomagnetism.

For space radiation see *93 Space Radiation*.

47 METEOROLOGY AND CLIMATOLOGY N.A.

Includes weather forecasting and modification.

48 OCEANOGRAPHY N.A.

Includes biological, dynamic, and physical oceanography; and marine resources.

For related information see also *43 Earth Resources and Remote Sensing*.

LIFE SCIENCES

Includes life sciences (general); aerospace medicine; behavioral sciences; man/system technology and life support; and space biology.

51 LIFE SCIENCES (GENERAL) N.A.

52 AEROSPACE MEDICINE N.A.

Includes physiological factors; biological effects of radiation; and effects of weightlessness on man and animals.

53 BEHAVIORAL SCIENCES N.A.

Includes psychological factors; individual and group behavior; crew training and evaluation; and psychiatric research.

54 MAN/SYSTEM TECHNOLOGY AND LIFE SUPPORT N.A.

Includes human engineering; biotechnology; and space suits and protective clothing.

For related information see also *16 Space Transportation*.

55 SPACE BIOLOGY N.A.

Includes exobiology; planetary biology; and extraterrestrial life.

MATHEMATICAL AND COMPUTER SCIENCES

Includes mathematical and computer sciences (general); computer operations and hardware; computer programming and software; computer systems; cybernetics; numerical analysis; statistics and probability; systems analysis; and theoretical mathematics.

59 MATHEMATICAL AND COMPUTER SCIENCES (GENERAL) N.A.

60 COMPUTER OPERATIONS AND HARDWARE 201

Includes hardware for computer graphics, firmware, and data processing.

For components see *33 Electronics and Electrical Engineering*.

61 COMPUTER PROGRAMMING AND SOFTWARE 201

Includes computer programs, routines, algorithms, and specific applications, e.g., CAD/CAM.

62 COMPUTER SYSTEMS 203

Includes computer networks and special application computer systems.

63 CYBERNETICS N.A.

Includes feedback and control theory, artificial intelligence, robotics and expert systems.

For related information see also *54 Man/System Technology and Life Support*.

64 NUMERICAL ANALYSIS 204

Includes iteration, difference equations, and numerical approximation.

65 STATISTICS AND PROBABILITY N.A.

Includes data sampling and smoothing; Monte Carlo method; and stochastic processes.

66 SYSTEMS ANALYSIS 206

Includes mathematical modeling; network analysis; and operations research.

67 THEORETICAL MATHEMATICS N.A.

Includes topology and number theory.

PHYSICS

Includes physics (general); acoustics; atomic and molecular physics; nuclear and high-energy physics; optics; plasma physics; solid-state physics; and thermodynamics and statistical physics.

For related information see also *Engineering*.

70 PHYSICS (GENERAL) 207

For precision time and time interval (PTTI) see *35 Instrumentation and Photography*; for geophysics, astrophysics or solar physics see *46 Geophysics*, *90 Astrophysics*, or *92 Solar Physics*.

- 71 ACOUSTICS** 208
Includes sound generation, transmission, and attenuation.
For noise pollution see *45 Environment Pollution*.
- 72 ATOMIC AND MOLECULAR PHYSICS** N.A.
Includes atomic structure, electron properties, and molecular spectra.
- 73 NUCLEAR AND HIGH-ENERGY PHYSICS** 213
Includes elementary and nuclear particles; and reactor theory.
For space radiation see *93 Space Radiation*.
- 74 OPTICS** 213
Includes light phenomena and optical devices.
For lasers see *36 Lasers and Masers*.
- 75 PLASMA PHYSICS** 214
Includes magnetohydrodynamics and plasma fusion.
For ionospheric plasmas see *46 Geophysics*. For space plasmas see *90 Astrophysics*.
- 76 SOLID-STATE PHYSICS** 215
Includes superconductivity.
For related information see also *33 Electronics and Electrical Engineering* and *36 Lasers and Masers*.
- 77 THERMODYNAMICS AND STATISTICAL PHYSICS** 219
Includes quantum mechanics; theoretical physics; and Bose and Fermi statistics.
For related information see also *25 Inorganic and Physical Chemistry* and *34 Fluid Mechanics and Heat Transfer*.

SOCIAL SCIENCES

Includes social sciences (general); administration and management; documentation and information science; economics and cost analysis; law, political science, and space policy; and urban technology and transportation.

- 80 SOCIAL SCIENCES (GENERAL)** N.A.
Includes educational matters.
- 81 ADMINISTRATION AND MANAGEMENT** 219
Includes management planning and research.
- 82 DOCUMENTATION AND INFORMATION SCIENCE** N.A.
Includes information management; information storage and retrieval technology; technical writing; graphic arts; and micrography.
For computer documentation see *61 Computer Programming and Software*.
- 83 ECONOMICS AND COST ANALYSIS** N.A.
Includes cost effectiveness studies.

- 84 LAW, POLITICAL SCIENCE AND SPACE POLICY** N.A.
Includes NASA appropriation hearings; aviation law; space law and policy; international law; international cooperation; and patent policy.

- 85 URBAN TECHNOLOGY AND TRANSPORTATION** 220
Includes applications of space technology to urban problems; technology transfer; technology assessment; and surface and mass transportation.
For related information see *03 Air Transportation and Safety*, *16 Space Transportation*, and *44 Energy Production and Conversion*.

SPACE SCIENCES

Includes space sciences (general); astronomy; astrophysics; lunar and planetary exploration; solar physics; and space radiation.

For related information see also *Geosciences*.

- 88 SPACE SCIENCES (GENERAL)** N.A.

- 89 ASTRONOMY** N.A.
Includes radio, gamma-ray, and infrared astronomy; and astrometry.

- 90 ASTROPHYSICS** 223
Includes cosmology; celestial mechanics; space plasmas; and interstellar and interplanetary gases and dust.
For related information see also *75 Plasma Physics*.

- 91 LUNAR AND PLANETARY EXPLORATION** N.A.
Includes planetology; and manned and unmanned flights.

For spacecraft design or space stations see *18 Spacecraft Design, Testing and Performance*.

- 92 SOLAR PHYSICS** N.A.
Includes solar activity, solar flares, solar radiation and sunspots.
For related information see *93 Space Radiation*.

- 93 SPACE RADIATION** N.A.
Includes cosmic radiation; and inner and outer earth's radiation belts.
For biological effects of radiation see *52 Aerospace Medicine*. For theory see *73 Nuclear and High-Energy Physics*.

GENERAL

Includes aeronautical, astronautical, and space science related histories, biographies, and pertinent reports too broad for categorization; histories or broad overviews of NASA programs.

- 99 GENERAL** 223

Note: N.A. means that no abstracts were assigned to this category for this issue.

SUBJECT INDEX	A-1
PERSONAL AUTHOR INDEX	B-1
CORPORATE SOURCE INDEX	C-1
CONTRACT NUMBER INDEX	D-1
REPORT/ACCESSION NUMBER INDEX	E-1

Bibliography of Lewis Research Center Technical Publications Announced in 1987

01

AERONAUTICS (GENERAL)

N87-10003*# Nielsen Engineering and Research, Inc., Mountain View, Calif.

DEVELOPMENT OF A TURBOMACHINERY DESIGN OPTIMIZATION PROCEDURE USING A MULTIPLE-PARAMETER NONLINEAR PERTURBATION METHOD Final Report

S. S. STAHARA Sep. 1984 260 p

(Contract NAS3-20836)

(NASA-CR-3831; NAS 1.26:3831; NEAR-TR-295) Avail: NTIS

HC A12/MF A01 CSCL 01B

An investigation was carried out to complete the preliminary development of a combined perturbation/optimization procedure and associated computational code for designing optimized blade-to-blade profiles of turbomachinery blades. The overall purpose of the procedures developed is to provide demonstration of a rapid nonlinear perturbation method for minimizing the computational requirements associated with parametric design studies of turbomachinery flows. The method combines the multiple parameter nonlinear perturbation method, successfully developed in previous phases of this study, with the NASA TSONIC blade-to-blade turbomachinery flow solver, and the COPES-CONMIN optimization procedure into a user's code for designing optimized blade-to-blade surface profiles of turbomachinery blades. Results of several design applications and a documented version of the code together with a user's manual are provided. Author

N87-15932*# Purdue Univ., West Lafayette, Ind. School of Mechanical Engineering.

JET ENGINE SIMULATION WITH WATER INGESTION THROUGH COMPRESSOR Final Report

T. HAYKIN and S. N. B. MURTHY Jan. 1987 172 p

(Contract NAG3-481; DTFA03-83-A00328)

(NASA-CR-179549; NAS 1.26:179549; FAA/CT-TN87/1;

M/NAFA/TR-1) Avail: NTIS HC A08/MF A01 CSCL 21E

Water ingestion into a jet engine affects most directly the performance of the air compression subsystem of the engine, and also the sensors located in that subsystem providing input to the engine's control system. Such performance changes affect the overall performance of the engine. Considering a generic, high bypass ratio, two-spool gas turbine operating on a stationary test stand with fixed inlet and thrustor nozzle, an attempt was made to establish the transient performance of the engine under a variety of water ingestion and power setting conditions and also when a temperature sensor providing input to the engine control records a lower temperature than the local gas phase temperature. The principal tools utilized in the investigation have been the so called PURDUE code and an engine simulation code. Performance calculations in each selected case have been made under two limiting sets of conditions: (1) total drainage of water, and (2) partial evaporation of water at the entry or exit of the burner with remaining water drained. Although the results are specialized to the generic engine and its control, it is shown in general that: (1)

engine performance is degraded during operation with water ingestion and the amount of degradation is a nonlinear function of inlet water mass fraction; (2) controllability of the engine with respect to operator-initiated power setting changes is affected by water ingestion; and (3) errors in a temperature sensor providing an input to engine control lead to instability in engine operation, eventually causing a limiting condition or parameter to be exceeded. Author

N87-16784*# National Aeronautics and Space Administration. Lewis Research Center, Cleveland, Ohio.

COMPARISON OF THREE EXPLICIT MULTIGRID METHODS FOR THE EULER AND NAVIER-STOKES EQUATIONS

RODRICK V. CHIMA, ELI TURKEL, and STEVE SCHAFER 1987 15 p Presented at the 25th Aerospace Sciences Meeting, Reno, Nev., 12-15 Jan. 1987; sponsored by AIAA

(NASA-TM-88878; ICOMP-86-3; E-3126; NAS 1.15:88878) Avail:

NTIS HC A02/MF A01 CSCL 01B

Three explicit multigrid methods, Ni's method, Jameson's finite-volume method, and a finite-difference method based on Brandt's work, are described and compared for two model problems. All three methods use an explicit multistage Runge-Kutta scheme on the fine grid, and this scheme is also described. Convergence histories for inviscid flow over a bump in a channel for the fine-grid scheme alone show that convergence rate is proportional to Courant number and that implicit residual smoothing can significantly accelerate the scheme. Ni's method was slightly slower than the implicitly-smoothed scheme alone. Brandt's and Jameson's methods are shown to be equivalent in form but differ in their node versus cell-centered implementations. They are about 8.5 times faster than Ni's method in terms of CPU time. Results for an oblique shock/boundary layer interaction problem verify the accuracy of the finite-difference code. All methods slowed considerably on the stretched viscous grid but Brandt's method was still 2.1 times faster than Ni's method. Author

N87-20171*# National Aeronautics and Space Administration. Lewis Research Center, Cleveland, Ohio.

NUMERICAL CALCULATIONS OF TURBULENT REACTING FLOW IN A GAS-TURBINE COMBUSTOR

CHIN-SHUN LIN Apr. 1987 21 p

(Contract NASA ORDER C-99066-G)

(NASA-TM-89842; E-3501; ICOMP-87-2; NAS 1.15:89842) Avail:

NTIS HC A02/MF A01 CSCL 20D

A numerical study for confined, axisymmetrical, turbulent diffusion flames is presented. Local mean gas properties are predicted by solving the appropriate conservation equations in the finite difference form with the corresponding boundary conditions. The k-epsilon two-equation turbulence model is employed to describe the turbulent nature of the flow. A two-step kinetic model is assumed to govern the reaction mechanism. The finite reaction rate is the smaller of an Arrhenius type of reaction rate and a modified version of eddy-breakup model. Reasonable agreement is observed between calculations and measurements, but to obtain better agreement, more work is needed on improvements of the above mathematical models. However, the present numerical study offers an improvement in the analysis and design of the gas turbine combustors. B.G.

01 AERONAUTICS (GENERAL)

N87-25292*# National Aeronautics and Space Administration. Lewis Research Center, Cleveland, Ohio.
ON THE COALESCENCE-DISPERSION MODELING OF TURBULENT MOLECULAR MIXING
PEYMAN GIVI and GEORGE KOSALY (Washington Univ., Seattle.) Jul. 1987 28 p
(NASA-TM-89910; ICOMP-87-3; E-3602; NAS 1.15:89910) Avail: NTIS HC A03/MF A01 CSCL 01B

The general coalescence-dispersion (C/D) closure provides phenomenological modeling of turbulent molecular mixing. The models of Curl and Dopazo and O'Brien appear as two limiting C/D models that bracket the range of results one can obtain by various models. This finding is used to investigate the sensitivity of the results to the choice of the model. Inert scalar mixing is found to be less model-sensitive than mixing accompanied by chemical reaction. Infinitely fast chemistry approximation is used to relate the C/D approach to Toor's earlier results. Pure mixing and infinite rate chemistry calculations are compared to study further a recent result of Hsieh and O'Brien who found that higher concentration moments are not sensitive to chemistry. Author

N87-28501*# National Aeronautics and Space Administration. Lewis Research Center, Cleveland, Ohio.
VORTEX-SCALAR ELEMENT CALCULATIONS OF A DIFFUSION FLAME STABILIZED ON A PLANE MIXING LAYER
AHMED F. GHONIEM (Massachusetts Inst. of Tech., Cambridge.) and PEYMAN GIVI Aug. 1987 26 p Previously announced in IAA as A87-22499
(Contract AF-AFOSR-0356-84; NSF CPE-84-0481)
(NASA-TM-100133; E-3683; NAS 1.15:100133; ICOMP-87-4)
Avail: NTIS HC A03/MF A01 CSCL 01A

The vortex-scalar element method, a scheme which utilizes vortex elements to discretize the region of high vorticity and scalar elements to represent species or temperature fields, is utilized in the numerical simulations of a two-dimensional reacting mixing layer. Computations are performed for a diffusion flame at high Reynolds and Peclet numbers without resorting to turbulence models. In the nonreacting flow, the mean and fluctuation profiles of a conserved scalar show good agreement with experimental measurements. Results for the reacting flow indicate that for temperature independent kinetics, the chemical reaction begins immediately downstream of the splitter plate where mixing starts. Results for the reacting flow with Arrhenius kinetics show an ignition delay, which depends on reactant temperature, before significant chemical reaction occurs. Harmonic forcing changes the structure of the layer, and concomitantly the rates of mixing and reaction, in accordance with experimental results. Strong stretch within the braids in the nonequilibrium kinetics case causes local flame quenching due to the temperature drop associated with the large convective fluxes. Author

02

AERODYNAMICS

Includes aerodynamics of bodies, combinations, wings, rotors, and control surfaces; and internal flow in ducts and turbomachinery.

A87-20886*# Army Propulsion Lab., Cleveland, Ohio.
ROTOR WAKE CHARACTERISTICS OF A TRANSONIC AXIAL-FLOW FAN
M. D. HATHAWAY (U.S. Army, Propulsion Laboratory, Cleveland, OH), J. B. GERTZ, A. H. EPSTEIN (MIT, Cambridge, MA), and A. J. STRAZISAR (NASA, Lewis Research Center, Cleveland, OH) AIAA Journal (ISSN 0001-1452), vol. 24, Nov. 1986, p. 1802-1810. Previously cited in issue 21, p. 3040, Accession no. A85-43974. refs

A87-22414*# Dayton Univ., Ohio.
NAVIER STOKES SOLUTION OF THE FLOWFIELD OVER ICE ACCRETION SHAPES
J. N. SCOTT, W. L. HANKEY, F. J. GIESSLER, and T. P. GIELDA (Dayton, University, OH) AIAA, Aerospace Sciences Meeting, 25th, Reno, NV, Jan. 12-15, 1987. 11 p. refs
(Contract NAG3-665)
(AIAA PAPER 87-0099)

The numerical simulation of flow about ice accretion shapes has been accomplished by solving the Navier-Stokes equations using MacCormack's explicit finite difference scheme. The computations were performed on a CRAY-XMP computer. The influence of turbulence is taken into account by means of an algebraic eddy-viscosity model. In order to optimize the grid spacing and to achieve near orthogonality at the surface of the complex ice shapes, a hyperbolic grid generation scheme is utilized. Particular attention is given to the heat transfer process for which good agreement between the numerical and experimental results is achieved. In addition, liquid water droplet trajectories are coupled within the flowfield along with the resulting collection efficiencies using a parabolized Navier-Stokes formulation. Author

A87-22415*# Akron Univ., Ohio.
NUMERICAL ANALYSIS OF A NACA0012 AIRFOIL WITH LEADING EDGE ICE ACCRETIONS
MARK G. POTAPCZUK (Akron, University, OH) AIAA, Aerospace Sciences Meeting, 25th, Reno, NV, Jan. 12-15, 1987. 10 p. refs
(Contract NAG3-416)
(AIAA PAPER 87-0101)

Analysis of a NACA0012 airfoil with leading edge ice has been performed using a Navier-Stokes code coupled with a grid generation code. The computed results were compared to experimental information obtained for an airfoil with a well defined artificial ice shape. The computations were performed at angles of attack ranging from zero to ten degrees. This range is sufficient to show the development of the separation bubble aft of the ice shape on both the upper and lower surfaces. Velocity profile plots in the separation bubble are examined in order to determine if recirculation patterns are predicted properly and if separation and reattachment points are found within the resolution of the experimental information. Also, the massive separation near the point of stall is examined in order to more accurately evaluate the lift coefficient curve in that region. Lift, drag, and moment coefficients are computed and compared to experiment. Author

A87-22578*# Cornell Univ., Ithaca, N.Y.
A DIAGONAL IMPLICIT MULTIGRID ALGORITHM FOR THE EULER EQUATIONS
DAVID A. CAUGHEY (Cornell University, Ithaca, NY) AIAA, Aerospace Sciences Meeting, 25th, Reno, NV, Jan. 12-15, 1987. 12 p. refs
(Contract NAG3-645; NAG2-373)
(AIAA PAPER 87-0354)

A multigrid implementation of the Alternating Direction Implicit algorithm has been developed to solve the Euler equations of inviscid, compressible flow. The equations are approximated using a finite-volume spatial approximation with added dissipation provided by an adaptive blend of second and fourth differences. For computational efficiency, the equations are diagonalized by a local similarity transformation so that only a decoupled system of scalar pentadiagonal systems need be solved along each line. Results are computed for transonic flows past airfoils and include pressure distributions to verify the accuracy of the basic scheme and convergence histories to demonstrate the efficiency of the method. Author

A87-24010*# Cornell Univ., Ithaca, N.Y.

STALL TRANSIENTS OF AXIAL COMPRESSION SYSTEMS WITH INLET DISTORTION

F. K. MOORE (Cornell University, Ithaca, NY) Journal of Propulsion and Power (ISSN 0748-4658), vol. 2, Nov.-Dec. 1986, p. 552-561. Previously cited in issue 18, p. 2611, Accession no. A85-39740. refs
(Contract NAG3-349)

A87-24901*# Purdue Univ., West Lafayette, Ind.

MEASUREMENT OF A COUNTER ROTATION PROPELLER FLOWFIELD USING A LASER DOPPLER VELOCIMETER

G. L. HARRISON (Embry-Riddle Aeronautical University, Prescott, AZ) and J. P. SULLIVAN (Purdue University, West Lafayette, IN) AIAA, Aerospace Sciences Meeting, 25th, Reno, NV, Jan. 12-15, 1987. 8 p. refs
(Contract NSG-3135)
(AIAA PAPER 87-0008)

This paper is a summary of the results of the experimental investigation of the flow field about a counter-rotating propeller (CRP) system using a Laser Doppler Velocimeter (LDV). The number of configurations available for the CRP system is limitless, thus only a small portion of the number of possible cases were examined. Measurements were made upstream, in between and downstream of the propeller system. The abundance of data readily available from the LDV system clearly identifies the tip vortices and wake regions. The recovery by the downstream propeller of the swirl velocity imparted to the flow by the upstream propeller is very evident. The coefficients of thrust and power were determined using momentum and energy analysis of the data and compared to theory. Author

A87-24929*# Texas A&M Univ., College Station.

EXPERIMENTAL AND THEORETICAL STUDY OF PROPELLER SPINNER/SHANK INTERFERENCE

C. C. CORNELL (Texas A & M University, College Station) AIAA, Aerospace Sciences Meeting, 25th, Reno, NV, Jan. 12-15, 1987. 23 p. refs
(Contract NAG3-272)
(AIAA PAPER 87-0145)

A fundamental investigation into the aerodynamic interference associated with propeller spinner and shank regions has been conducted. The research program involved a theoretical assessment of solutions previously proposed, followed by a systematic experimental study to supplement the existing data base. As a result, a refined computational procedure has been established for prediction of interference effects in terms of either interference drag or propeller thrust and torque coefficients. These quantities have been examined with attention to engineering parameters such as spinner fineness ratio, blade shank form, and number of blades. Also, cascade effects and spinner/shank juncture interference have been semi-empirically modeled using existing theories and placed into a compatible form with an existing propeller performance code. Author

A87-24954*# Boeing Commercial Airplane Co., Seattle, Wash.

AN EXPERIMENTAL INVESTIGATION OF COMPRESSIBLE THREE-DIMENSIONAL BOUNDARY LAYER FLOW IN ANNULAR DIFFUSERS

DEEPAK OM (Boeing Commercial Airplane Co., Seattle, WA) and MORRIS E. CHILDS (Washington, University, Seattle) AIAA, Aerospace Sciences Meeting, 25th, Reno, NV, Jan. 12-15, 1987. 11 p. refs
(Contract NAG3-376)
(AIAA PAPER 87-0366)

An experimental study is described in which detailed wall pressure measurements have been obtained for compressible three-dimensional unseparated boundary layer flow in annular diffusers with and without normal shock waves. Detailed mean flow-field data were also obtained for the diffuser flow without a shock wave. Two diffuser flows with shock waves were investigated. In one case, the normal shock existed over the complete annulus whereas in the second case, the shock existed over a part of the

annulus. The data obtained can be used to validate computational codes for predicting such flow fields. The details of the flow field without the shock wave show flow reversal in the circumferential direction on both inner and outer surfaces. However, there is a lag in the flow reversal between the inner and the outer surfaces. This is an interesting feature of this flow and should be a good test for the computational codes. Author

A87-24992*# Cornell Univ., Ithaca, N.Y.

MULTIGRID SOLUTION OF INVISCID TRANSONIC FLOW THROUGH ROTATING BLADE PASSAGES

WAYNE A. SMITH and DAVID A. CAUGHEY (Cornell University, Ithaca, NY) AIAA, Aerospace Sciences Meeting, 25th, Reno, NV, Jan. 12-15, 1987. 10 p. refs
(Contract NAG3-645)
(AIAA PAPER 87-0608)

A fast Euler solver for three dimensional inviscid transonic flow in rotating domains is described. The time dependent Euler equations are discretized spatially with finite volumes, and are advanced temporally with a multiple stage time stepping scheme. A dramatic increase in the rate of convergence for steady solutions is achieved with a multigrid algorithm that employs the multistage scheme as its smoothing procedure. The effectiveness of the multistage scheme as a multigrid driver is enhanced by the utilization of analytically determined combinations of the governing parameters. Author

A87-24996*# National Aeronautics and Space Administration. Lewis Research Center, Cleveland, Ohio.

SPATIALLY GROWING DISTURBANCES IN A HIGH VELOCITY RATIO TWO-STREAM, COPLANAR JET

JEFFREY H. MILES (NASA, Lewis Research Center, Cleveland, OH) AIAA, Aerospace Sciences Meeting, 25th, Reno, NV, Jan. 12-15, 1987. 11 p. Previously announced in STAR as N87-14283. refs
(AIAA PAPER 87-0056)

The influence of cold and heated secondary flow on the instability of a two-stream, coplanar jet having a 0.7 Mach number heated primary jet for a nominal fan to primary velocity ratio of 0.68 was investigated by means of inviscid linearized stability theory. The instability properties of spatially growing axisymmetric and first order azimuthal disturbances were studied. The instability characteristics of the two-stream jet with a velocity ratio of 0.68 are very different from those of a single stream jet, and a two-stream, coplanar jet having a 0.9 Mach number heated primary jet and a cold secondary jet for a fan to primary velocity ratio of 0.30. For $X/D = 1$ and in comparison to the case where the velocity ratio was 0.3, the presence of the fan stream with a velocity ratio of 0.68 enhanced the instability of the jet and increased the unstable frequency range. However, the axisymmetric mode ($m = 0$) and the first order azimuthal mode ($m = 1$) have similar spatial growth rates where the velocity ratio is 0.68 while for a velocity ratio of 0.3 the growth rate of the first order azimuthal mode ($m = 1$) is greater. Comparing the cold and hot secondary flow results showed that for a velocity ratio of 0.68 the growth rate is greater for cold. Author

A87-25395*# Sverdrup Technology, Inc., Cleveland, Ohio.

A NUMERICAL SIMULATION OF THE INVISCID FLOW THROUGH A COUNTERROTATING PROPELLER

M. L. CELESTINA, R. A. MULAC (Sverdrup Technology, Inc., Middleburg Heights, OH), and J. J. ADAMCZYK (NASA, Lewis Research Center, Cleveland, OH) ASME, Transactions, Journal of Turbomachinery (ISSN 0889-504X), vol. 108, Oct. 1986, p. 187-193. Previously announced in STAR as N86-16195. refs
(ASME PAPER 86-GT-138)

The results of a numerical simulation of the time-averaged inviscid flow field through the blade rows of a multiblade row turboprop configuration are presented. The governing equations are outlined along with a discussion of the solution procedure and coding strategy. Numerical results obtained from a simulation of the flow field through a modern high-speed turboprop will be shown. Author

A87-31106*# National Aeronautics and Space Administration. Lewis Research Center, Cleveland, Ohio.

TWO- AND THREE-DIMENSIONAL VISCOUS COMPUTATIONS OF A HYPERSONIC INLET FLOW

WILLIAM G. KUNIK, THOMAS J. BENSON (NASA, Lewis Research Center, Cleveland, OH), WING-FAI NG, and ARTHUR TAYLOR (Virginia Polytechnic Institute and State University, Blacksburg) AIAA, Aerospace Sciences Meeting, 25th, Reno, NV, Jan. 12-15, 1987. 17 p. Previously announced in STAR as N87-15441. refs (AIAA PAPER 87-0283)

The three-dimensional parabolized Navier-Stokes code has been used to investigate the flow through a Mach 7.4 inlet. A two-dimensional parametric study of grid resolution, turbulence modeling and effect of gamma has been done and compared with experimental results. The results show that mesh resolution of the shock waves, real gas effects and turbulence length scaling are very important to get accurate results for hypersonic inlet flows. In addition a three-dimensional calculation of the Mach 7.4 inlet has been done on a straight sideplate configuration. The results show that the glancing shock/boundary layer interaction phenomena causes significant three-dimensional flow in the inlet.

Author

A87-32191*# National Aeronautics and Space Administration. Lewis Research Center, Cleveland, Ohio.

A GENERALIZED PROCEDURE FOR CONSTRUCTING AN UPWIND-BASED TVD SCHEME

MENG-SING LIOU (NASA, Lewis Research Center, Cleveland, OH) AIAA, Aerospace Sciences Meeting, 25th, Reno, NV, Jan. 12-15, 1987. 16 p. refs (AIAA PAPER 87-0355)

A generalized formulation for constructing second- and higher-order accurate TVD (total variation diminishing) schemes is presented. A given scheme is made TVD by limiting antidiffusive flux differences with some nonlinear functions, so-called limiters. The general idea of the formulation and its mathematical proof of Harten's TVD conditions is shown by applying the Lax-Wendroff method to a scalar nonlinear equation and constant-coefficient system of conservation laws. For the system of equations, several definitions are derived for the argument used in the limiter function and present their performance to numerical experiments. Then the formulation is formally extended to the nonlinear system of equations. It is demonstrated that use of the present procedure allows easy conversion of existing central or upwind, and second- or higher-order differencing schemes so as to preserve monotonicity and to yield physically admissible solutions. The formulation is simple mathematically as well as numerically; neither matrix-vector multiplication nor Riemann solver is required. Roughly twice as much computational effort is needed as compared to conventional scheme. Although the notion of TVD is based on the initial value problem, application to the steady Euler equations of the formulation is also made. Numerical examples including various ranges of problems show both time- and spatial-accuracy in comparison with exact solutions.

Author

A87-32619* Lockheed-Georgia Co., Marietta.

HIGH SPEED WIND TUNNEL TESTS OF THE PTA AIRCRAFT

A. S. ALJABRI and B. H. LITTLE, JR. (Lockheed-Georgia Co., Marietta) SAE, Aerospace Technology Conference and Exposition, Long Beach, CA, Oct. 13-16, 1986. 17 p. refs (Contract NAS3-24339) (SAE PAPER 861744)

Propfans, advanced highly-loaded propellers, are proposed to power transport aircraft that cruise at high subsonic speeds, giving significant fuel savings over the equivalent turbofan-powered aircraft. NASA is currently sponsoring the Propfan Test Assessment Program (PTA) to provide basic data on the structural integrity and acoustic performance of the propfan. The program involves installation design, wind-tunnel tests, and flight tests of the Hamilton Standard SR-7 propfan in a wing-mount tractor installation on the Gulfstream II aircraft. This paper reports on the high-speed wind-tunnel tests and presents the computational aerodynamic methods that were employed in the analyses, design, and

evaluation of the configuration. In spite of the complexity of the configuration, these methods provide aerodynamic predictions which are in excellent agreement with wind-tunnel data. Author

A87-34723*# National Aeronautics and Space Administration. Lewis Research Center, Cleveland, Ohio.

ANALYSIS OF VISCOUS TRANSONIC FLOW OVER AIRFOIL SECTIONS

DENNIS L. HUFF (NASA, Lewis Research Center, Cleveland, OH), JIUNN-CHI WU, and L. N. SANKAR (Georgia Institute of Technology, Atlanta) AIAA, Aerospace Sciences Meeting, 25th, Reno, NV, Jan. 12-15, 1987. 32 p. Previously announced in STAR as N87-17001. refs (AIAA PAPER 87-0420)

A full Navier-Stokes solver has been used to model transonic flow over three airfoil sections. The method uses a two-dimensional, implicit, conservative finite difference scheme for solving the compressible Navier-Stokes equations. Results are presented as prescribed for the Viscous Transonic Airfoil Workshop to be held at the AIAA 25th Aerospace Sciences Meeting. The NACA 0012, RAE 2822 and Jones airfoils have been investigated for both attached and separated transonic flows. Predictions for pressure distributions, loads, skin friction coefficients, boundary layer displacement thickness and velocity profiles are included and compared with experimental data when possible. Overall, the results are in good agreement with experimental data. Author

A87-38496*# Texas Univ., Austin.

ADAPTIVE FINITE ELEMENT METHODS FOR COMPRESSIBLE FLOW PROBLEMS

J. T. ODEN, T. STROUBOULIS, and PH. DEVLOO (Texas, University, Austin) IN: Numerical methods for compressible flows - Finite difference, element and volume techniques; Proceedings of the Winter Annual Meeting, Anaheim, CA, Dec. 7-12, 1986. New York, American Society of Mechanical Engineers, 1986, p. 115-126. refs (Contract NAS8-36647; NAS3-24849; N00014-84-K-0409)

Some recent work on adaptive FEMs for solving transient Euler equations in two-dimensional domains is summarized. The formulation of an FEM model of the Euler equations is shown, and the application of the adaptive strategies to data management schemes is addressed. Sample numerical results from the application of the model and strategies to the flow over a step and to transient cases are given.

C.D.

A87-39528*# United Technologies Research Center, East Hartford, Conn.

INVESTIGATION OF TWO-DIMENSIONAL SHOCK-WAVE/BOUNDARY-LAYER INTERACTIONS

STANLEY A. SKEBE (United Technologies Research Center, East Hartford, CT), ISAAC GREBER (Case Western Reserve University, Cleveland, OH), and WARREN R. HINGST (NASA, Lewis Research Center, Cleveland, OH) AIAA Journal (ISSN 0001-1452), vol. 25, June 1987, p. 777-783. Previously cited in issue 06, p. 701, Accession no. A84-17881. refs (Contract NAG3-61; NAG3-102)

A87-39813*# Sverdrup Technology, Inc., Cleveland, Ohio.

EULER ANALYSIS OF TRANSONIC PROPELLER FLOWS

J. M. BARTON, O. YAMAMOTO (Sverdrup Technology, Inc., Middleburg Heights, OH), and L. J. BOBER (NASA, Lewis Research Center, Cleveland, OH) Journal of Propulsion and Power (ISSN 0748-4658), vol. 3, May-June 1987, p. 277-282. Previously cited in issue 21, p. 3041, Accession no. A85-43977. refs (Contract NAS3-24105)

A87-41157*# General Electric Co., Cincinnati, Ohio.
AERODYNAMIC INSTABILITY PERFORMANCE OF AN ADVANCED HIGH-PRESSURE-RATIO COMPRESSION COMPONENT

W. M. HOSNY and W. G. STEENKEN (General Electric Co., Aircraft Engine Business Group, Cincinnati, OH) AIAA, ASME, SAE, and ASEE, Joint Propulsion Conference, 22nd, Huntsville, AL, June 16-18, 1986. 15 p. refs
 (Contract NAS3-24083; NAS3-24211)
 (AIAA PAPER 86-1619)

The data acquisition and reduction, test procedures, and results of in-stall and in-surge testing of a NASA high-pressure-ratio compression component are discussed, in addition to the compressor-rig configuration and instrumentation used. Data analysis revealed information about rotating stall hysteresis, rotating stall development and cessation times, and rotating-stall-cell flow blockage. It is found that hysteresis exists in the work coefficient as well as in the pressure coefficient. Airflow rakes were designed to study the in-surge transient response of the compressor. The quasi-steady compressor characteristics underlying the transient-surge data were investigated using a parameter-identification technique. R.R.

A87-42057*# National Aeronautics and Space Administration.
 Lewis Research Center, Cleveland, Ohio.

THE UTILIZATION OF PARALLEL PROCESSING IN SOLVING THE INVISCID FORM OF THE AVERAGE-PASSAGE EQUATION SYSTEM FOR MULTISTAGE TURBOMACHINERY

RICHARD A. MULAC, MARK L. CELESTINA (NASA, Lewis Research Center; Sverdrup Technology, Inc., Cleveland, OH), JOHN J. ADAMCZYK (NASA, Lewis Research Center, Cleveland, OH), KENT P. MISEGADES, and JEF M. DAWSON (Cray Research, Inc., Mendota Heights, MN) IN: Computational Fluid Dynamics Conference, 8th, Honolulu, HI, June 9-11, 1987, Technical Papers. New York, American Institute of Aeronautics and Astronautics, 1987, p. 70-80. refs
 (AIAA PAPER 87-1108)

A procedure is outlined which utilizes parallel processing to solve the inviscid form of the average-passage equation system for multistage turbomachinery along with a description of its implementation in a FORTRAN computer code, MSTAGE. A scheme to reduce the central memory requirements of the program is also detailed. Both the multitasking and I/O routines referred to in this paper are specific to the Cray X-MP line of computers and its associated SSD (Solid-state Storage Device). Results are presented for a simulation of a two-stage rocket engine fuel pump turbine. Author

A87-42078*# National Aeronautics and Space Administration.
 Lewis Research Center, Cleveland, Ohio.

COMPOSITE GRID AND FINITE-VOLUME LU IMPLICIT SCHEME FOR TURBINE FLOW ANALYSIS

YUNG K. CHOO (NASA, Lewis Research Center, Cleveland, OH), SEOKKWAN YOON (NASA, Lewis Research Center; Sverdrup Technology, Inc., Cleveland, OH), and KESTUTIS C. CIVINSKAS (NASA, Lewis Research Center; U.S. Army, Propulsion Directorate, Cleveland, OH) IN: Computational Fluid Dynamics Conference, 8th, Honolulu, HI, June 9-11, 1987, Technical Papers. New York, American Institute of Aeronautics and Astronautics, 1987, p. 313-321. Previously announced in STAR as N87-20235. refs
 (AIAA PAPER 87-1129)

A composite grid was generated in an attempt to improve grid quality for a typical turbine blade with large camber in terms of mesh control, smoothness, and orthogonality. This composite grid consists of the C grid (or O grid) in the immediate vicinity of the blade and the H grid in the upstream region and in the middle of the blade passage between the C grids. It provides a good boundary layer resolution around the leading edge region for viscous calculation, has orthogonality at the blade surface and slope continuity at the C-H (or O-H) interface, and has flexibility in controlling the mesh distribution in the upstream region without using excessive grid points. This composite grid eliminates the undesirable qualities of a single grid when generated for a typical

turbine geometry. A finite-volume lower-upper (LU) implicit schemes can be used in solving for the turbine flows on the composite grid. This grid has a special grid node that is connected to more than four neighboring nodes in two dimensions and to more than six nodes in three dimensions. But the finite-volume approach poses no problem at the special point because each interior cell has only four neighboring cells in two dimensions and only six cells in three dimensions. The finite-volume LU implicit scheme was demonstrated to be robust and efficient for both external and internal flows in a broad flow regime. Author

A87-42107*# National Aeronautics and Space Administration.
 Lewis Research Center, Cleveland, Ohio.

NUMERICAL SIMULATION OF TRANSONIC PROPELLER FLOW USING A THREE-DIMENSIONAL SMALL DISTURBANCE CODE EMPLOYING NOVEL HELICAL COORDINATES

AARON SNYDER (NASA, Lewis Research Center, Cleveland, OH) IN: Computational Fluid Dynamics Conference, 8th, Honolulu, HI, June 9-11, 1987, Technical Papers. New York, American Institute of Aeronautics and Astronautics, 1987, p. 647-666. Previously announced in STAR as N87-19350. refs
 (AIAA PAPER 87-1162)

The numerical simulation of three-dimensional transonic flow about propeller blades is discussed. The equations for the unsteady potential flow about propellers is given for an arbitrary coordinate system. From this the small disturbance form of the equation is derived for a new helical coordinate system. The new coordinate system is suited to propeller flow and allows cascade boundary conditions to be applied straightforward. A numerical scheme is employed which solves the steady flow as an asymptotic limit of unsteady flow. Solutions are presented for subsonic and transonic flow about a 5 percent thick bicircular arc blade of an eight bladed cascade. Both high and low advance ratio cases are given which include a lifting case as well as nonlifting cases. The nonlifting cases are compared to solutions from a Euler code. Author

A87-42314*# Mississippi State Univ., Mississippi State.
THREE-DIMENSIONAL UNSTEADY EULER SOLUTIONS FOR PROPFANS AND COUNTER-ROTATING PROPFANS IN TRANSONIC FLOW

D. L. WHITFIELD (Mississippi State University, Mississippi State), T. W. SWAFFORD (Sverdrup Technology, Inc., Arnold Air Force Station, TN), R. A. MULAC (Sverdrup Technology, Inc., Cleveland, OH), D. M. BELK (USAF, Armament Laboratory, Eglin AFB, FL), and J. M. JANUS AIAA, Fluid Dynamics, Plasma Dynamics, and Lasers Conference, 19th, Honolulu, HI, June 8-10, 1987. 15 p. refs

(Contract NAG3-767)

(AIAA PAPER 87-1197)

An Euler code designed for computing the unsteady, three-dimensional, transonic flow about single-rotating and counter-rotating propfans using dynamic blocked-grids is presented. The algorithm is a finite volume, flux-split, upwind, implicit scheme and solves the equations which have been written in a time-dependent curvilinear coordinate system. Relative motion of the blades for counter-rotating configurations is handled by requiring that grid lines be aligned after each discrete rotation of fore and aft rotor grid blocks. The method by which information is passed across block interfaces, as well as how downstream characteristic outflow boundary conditions which enforce simple radial equilibrium are implemented, is discussed. Comparisons of computed flow-field parameters and propfan performance with experimental data indicate good overall agreement between predictions and measurements. Author

A87-44938*# Toledo Univ., Ohio.

AN LDA INVESTIGATION OF THREE-DIMENSIONAL NORMAL SHOCK-BOUNDARY LAYER INTERACTIONS IN A CORNER

R. M. CHRISS, T. G. KEITH, JR. (Toledo, University, OH), W. R. HINGST, A. J. STRAZISAR, and A. R. PORRO (NASA, Lewis Research Center, Cleveland, OH) AIAA, Fluid Dynamics, Plasma Dynamics, and Lasers Conference, 19th, Honolulu, HI, June 8-10, 1987. 12 p. refs

(Contract NAG3-309)

(AIAA PAPER 87-1369)

Nonintrusive, three-dimensional, measurements have been made of a normal shock wave-turbulent boundary layer interaction. The measurements were made in the corner of the test section of a continuous supersonic wind tunnel in which a normal shock wave had been stabilized. LDA, surface pressure measurement and flow visualization techniques were employed for two freestream Mach number test cases: 1.6 and 1.3. The former contained separated flow regions and a system of shock waves. The latter was found to be far less complicated. The reported results are believed to accurately define the flow physics of each case and may be used as benchmark data to verify three-dimensional computer codes. Author

A87-45281*# Lockheed-Georgia Co., Marietta.

WIND TUNNEL TESTS ON A ONE-FOOT DIAMETER SR-7L PROPPAN MODEL

ABDULLAH S. ALJABRI (Lockheed-Georgia Co., Marietta) AIAA, SAE, ASME, and ASEE, Joint Propulsion Conference, 23rd, San Diego, CA, June 29-July 2, 1987. 12 p.

(Contract NAS3-24339)

(AIAA PAPER 87-1892)

Wind tunnel tests have been conducted on a one-foot diameter model of the SR-7L propfan in the Langley 16-Foot and 4 x 7 Meter Wind Tunnels as part of the Propfan Test Assessment (PTA) Program. The model propfan was sized to be used on a 1/9-scale model of the PTA testbed aircraft. The model propeller was tested in isolation and wing-mounted on the aircraft configuration at various Mach numbers and blade pitch angles. Agreement between data obtained from these tests and data from Hamilton Standard validate that the 1/9-scale propeller accurately simulates the aerodynamics of the SR-7L propfan. Predictions from an analytical computer program are presented and show good agreement with the experimental data. Author

A87-45413*# National Aeronautics and Space Administration. Lewis Research Center, Cleveland, Ohio.

TWO-DIMENSIONAL NOZZLE PLUME CHARACTERISTICS

UWE H. VON GLAHN (NASA, Lewis Research Center, Cleveland, OH) AIAA, SAE, ASME, and ASEE, Joint Propulsion Conference, 23rd, San Diego, CA, June 29-July 2, 1987. 20 p. Previously announced in STAR as N87-18540. refs

(AIAA PAPER 87-2111)

Future high performance aircraft will likely feature asymmetric or two-dimensional nozzles with or without ejectors. In order to design two-dimensional nozzle/ejector systems of minimum size and weight, the plume decay and spreading characteristics of basic two-dimensional nozzles must first be established. The present work deals with the experimental analyses of these plume characteristics and includes the effects of nozzle aspect ratio and flow conditions (jet Mach number and temperature) on the plume decay and spreading of two-dimensional nozzles. Correlations including these variables are developed in a manner similar to those previously developed successfully for conic and dual-flow plumes. Author

A87-45414*# National Aeronautics and Space Administration. Lewis Research Center, Cleveland, Ohio.

SECONDARY STREAM AND EXCITATION EFFECTS ON TWO-DIMENSIONAL NOZZLE PLUME CHARACTERISTICS

UWE H. VON GLAHN (NASA, Lewis Research Center, Cleveland, OH) AIAA, SAE, ASME, and ASEE, Joint Propulsion Conference, 23rd, San Diego, CA, June 29-July 2, 1987. 12 p. Previously announced in STAR as N87-18539. refs

(AIAA PAPER 87-2112)

In order to design two-dimensional nozzle/ejector systems for future high performance aircraft, the basic engine exhaust plume velocity and temperature decay as effected by the secondary stream (ejector) and decay augmentation means must be assessed. Included in the assessment of the plume decay characteristics are the effects of nozzle aspect ratio and nozzle/ejector flow conditions. Nozzle/ejector plume decay can be enhanced by suitable excitation of the plume shear layers. Correlations of these factors are developed in a manner similar to those previously developed for conic and dual-flow nozzle plumes. Author

A87-46207*# Pennsylvania State Univ., University Park.

AN EXPERIMENTAL STUDY ON THE EFFECTS OF TIP CLEARANCE ON FLOW FIELD AND LOSSES IN AN AXIAL FLOW COMPRESSOR ROTOR

B. LAKSHMINARAYANA, J. ZHANG, and K. N. S. MURTHY (Pennsylvania State University, University Park) IN: International Symposium on Air Breathing Engines, 8th, Cincinnati, OH, June 14-19, 1987, Proceedings. New York, American Institute of Aeronautics and Astronautics, 1987, p. 273-290. refs

(Contract NSG-3032)

Detailed measurement of the flow field in the tip region of a compressor rotor was carried out using a Laser Doppler Velocimeter (LDV) and a Kiel probe at two different tip clearance heights. At both clearance sizes, the relative stagnation pressure and the axial and tangential components of relative velocities were measured upstream, inside the passage and downstream of the rotor, up to about 20 percent of the blade span from the annulus wall. The velocities, outlet angles, losses, momentum thickness, and force defect thickness are compared for the two clearances. A detailed interpretation of the effect of tip clearance on the flow field is given. There are substantial differences in flow field, on momentum thickness, and performance as the clearance is varied. The losses increase linearly within the passage and their values increase in direct proportion to tip clearance height. No discernable vortex (discrete) is observed downstream of the rotor. Author

A87-46781*# National Aeronautics and Space Administration. Lewis Research Center, Cleveland, Ohio.

LOWER-UPPER IMPLICIT SCHEME FOR HIGH-SPEED INLET ANALYSIS

SEOKKWAN YOON (NASA, Lewis Research Center; Sverdrup Technology, Inc., Cleveland, OH) and ANTHONY JAMESON (Princeton University, NJ) AIAA Journal (ISSN 0001-1452), vol. 25, Aug. 1987, p. 1052, 1053. Abridged.

(Previously cited in issue 20, p. 2915, Accession no. A86-42687)

A87-48719*# National Aeronautics and Space Administration. Lewis Research Center, Cleveland, Ohio.

EULER ANALYSIS OF THE THREE-DIMENSIONAL FLOW FIELD OF A HIGH-SPEED PROPELLER - BOUNDARY CONDITION EFFECTS

M. NALLASAMY (NASA, Lewis Research Center; Sverdrup Technology, Inc., Cleveland, OH), B. J. CLARK, and J. F. GROENEWEG (NASA, Lewis Research Center, Cleveland, OH) ASME, Transactions, Journal of Turbomachinery (ISSN 0889-504X), vol. 109, July 1987, p. 332-339. Previously announced in STAR as N87-16798. refs

(ASME PAPER 87-GT-253)

The results of an investigation of the effects of far field boundary conditions on the solution of the three dimensional Euler equations governing the flow field of a high speed single rotation propeller are presented. The results show that the solutions obtained with

the nonreflecting boundary conditions are in good agreement with experimental data. The specification of nonreflecting boundary conditions is effective in reducing the dependence of the solution on the location of the far field boundary. Details of the flow field within the blade passage and the tip vortex are presented. The dependence of the computed power coefficient on the blade passage and the tip vortex are presented. The dependence of the computed power coefficient on the blade setting angle is examined. Author

A87-48722* # Cambridge Univ. (England).

A METHOD FOR ASSESSING EFFECTS OF CIRCUMFERENTIAL FLOW DISTORTION ON COMPRESSOR STABILITY

T. P. HYNES and E. M. GREITZER (Cambridge University, England) ASME, Transactions, Journal of Turbomachinery (ISSN 0889-504X), vol. 109, July 1987, p. 371-379. Research supported by the Royal Society and SERC. refs
(Contract NSG-3208)

This paper describes the development of a new analysis to predict the onset of flow instability for an axial compressor operating in a circumferentially distorted inlet flow. A relatively simple model is used to examine the influence of various distortions in setting this instability point. It is found that the model reproduces known experimental trends for the loss of stability margin with increasing distortion amplitude and with changes in reduced frequency. In particular, there is a recognizable 'critical sector angle' which characterizes loss of stability margin. To the authors' knowledge, this is the first time the effects described herein have been theoretically demonstrated as the direct result of a fluid dynamic stability. Author

A87-49100* # Sverdrup Technology, Inc., Cleveland, Ohio.

PRELIMINARY AEROTHERMODYNAMIC DESIGN METHOD FOR HYPERSONIC VEHICLES

G. J. HARLOFF and S. L. PETRIE (Sverdrup Technology, Inc., Cleveland, OH) IN: AIAA Applied Aerodynamics Conference, 5th, Monterey, CA, Aug. 17-19, 1987, Technical Papers. New York, American Institute of Aeronautics and Astronautics, 1987, p. 488-496. refs
(Contract NAS3-24105)
(AIAA PAPER 87-2545)

Preliminary design methods are presented for vehicle aerothermodynamics. Predictions are made for Shuttle orbiter, a Mach 6 transport vehicle and a high-speed missile configuration. Rapid and accurate methods are discussed for obtaining aerodynamic coefficients and heat transfer rates for laminar and turbulent flows for vehicles at high angles of attack and hypersonic Mach numbers. Author

A87-49101* # Sverdrup Technology, Inc., Middleburg Heights, Ohio.

HIGH ANGLE OF ATTACK HYPERSONIC AERODYNAMICS

GARY J. HARLOFF (Sverdrup Technology, Inc., Middleburg Heights, OH) IN: AIAA Applied Aerodynamics Conference, 5th, Monterey, CA, Aug. 17-19, 1987, Technical Papers. New York, American Institute of Aeronautics and Astronautics, 1987, p. 497-505. refs
(Contract NAS3-24105)
(AIAA PAPER 87-2548)

A new aerodynamics force model is presented which is based on modified Newtonian theory and empirical correlations. The algebraic model was developed for complete vehicles from take off to orbital speeds and for large angles of attack. Predictions are compared to results for a wind tunnel model at a Mach number of 20, and the full scale Shuttle Orbiter for Mach numbers from 0.25 to 20 for angles of attack from 0 to 50 deg. The maximum shuttle orbiter lift/drag at Mach 10 and 20 is 1.85 at 20-deg angle-of-attack. Aerodynamic force predictions are made for a transatmospheric vehicle, which is a derivative of the Shuttle Orbiter, for Mach numbers from 4 to 27 at angles of attack from 5 to 40 deg. Predicted aerodynamic force data indicate that lift/drag ratios of 5.2 at Mach number 10 and 3.6 at Mach number 26 are obtainable. Changes in force coefficients with changes in: nose

angle, sweep angle, and (volume exp 2/3)/planform area are quantified for Mach numbers of 10 and 26. Lift/drag ratios increase with decreasing nose angle and (volume exp 2/3)/planform area and increasing wing sweep angle. Lift/drag ratios are independent of these variables for angles of attack in excess of 20 deg at Mach 10 and 30 deg at Mach 26. Author

A87-49649* # National Aeronautics and Space Administration, Lewis Research Center, Cleveland, Ohio.

NUMERICAL SIMULATIONS OF UNSTEADY, VISCOUS, TRANSONIC FLOW OVER ISOLATED AND CASCADED AIRFOILS USING A DEFORMING GRID

DENNIS L. HUFF (NASA, Lewis Research Center, Cleveland, OH) AIAA, Fluid Dynamics, Plasma Dynamics, and Lasers Conference, 19th, Honolulu, HI, June 8-10, 1987. 16 p. Previously announced in STAR as N87-24435. refs
(AIAA PAPER 87-1316)

A compressible, unsteady, full Navier-Stokes, finite difference code was developed for modeling transonic flow through two-dimensional, oscillating cascades. The procedure introduces a deforming grid technique to capture the motion of the airfoils. Results using a deforming grid are presented for both isolated and cascaded airfoils. The load histories and unsteady pressure distributions are predicted for the NASA 64A010 isolated airfoil and compared with existing experimental data. Results show that the deforming grid technique can be used to successfully predict the unsteady flow properties around an oscillating airfoil. The deforming grid technique was extended for modeling unsteady flow in a cascade. The use of a deforming grid simplifies the specification of boundary conditions. Unsteady flow solutions similar to the isolated airfoil predictions are found for a NACA 0012 cascade with zero interblade phase angle and zero stagger. Experimental data for these cases are not available for code validation, but computational results are presented to show sample predictions from the code. Applications of the code to typical turbomachinery flow conditions will be presented in future work. Author

A87-50187* # Case Western Reserve Univ., Cleveland, Ohio.

METHOD FOR THE DETERMINATION OF THE THREE DIMENSIONAL AERODYNAMIC FIELD OF A ROTOR-STATOR COMBINATION IN COMPRESSIBLE FLOW

SRIDHAR M. RAMACHANDRA (Case Western Reserve University, Cleveland, OH), LAWRENCE J. BOBER (NASA, Lewis Research Center, Cleveland, OH), and SURESH KHANDELWAL (NASA, Lewis Research Center; Sverdrup Technology, Inc., Cleveland, OH) AIAA, SAE, ASME, and ASEE, Joint Propulsion Conference, 23rd, San Diego, CA, June 29-July 2, 1987. 32 p. Previously announced in STAR as N87-23625. refs
(AIAA PAPER 87-1742)

Using the lifting surface theory and the acceleration potential method for the flow field of an axial turbocompressor stage, a recursive and a direct method are presented that make use of the eigenfunction solutions of the isolated rotor and stator to solve for the rotor-stator interaction problem. The net pressure distribution on the rotor and stator blades is represented by modified Birnbaum series, whose coefficients are determined using a matrix procedure and satisfying the boundary conditions on the surface of the blades. The relation between the matrix operators of the recursive and the direct methods is also shown. Expressions have been given for the blade circulation, the axial and tangential forces on the blade, the rotor power required, and the induced upwash velocity of the stage. Author

02 AERODYNAMICS

A87-52251*# National Aeronautics and Space Administration. Lewis Research Center, Cleveland, Ohio.

WIND TUNNEL PERFORMANCE RESULTS OF AN AEROELASTICALLY SCALED 2/9 MODEL OF THE PTA FLIGHT TEST PROP-FAN

GEORGE L. STEFKO, GARY G. PODBOY (NASA, Lewis Research Center, Cleveland, OH), and GAYLE E. ROSE (NASA, Lewis Research Center; Sverdrup Technology, Inc., Cleveland, OH) AIAA, SAE, ASME, and ASEE, Joint Propulsion Conference, 23rd, San Diego, CA, June 29-July 2, 1987. 49 p. Previously announced in STAR as N87-25294. refs
(AIAA PAPER 87-1893)

High speed wind tunnel aerodynamic performance tests of the SR-7A advanced prop-fan have been completed in support of the Prop-Fan Test Assessment (PTA) flight test program. The test showed that the SR-7A model performed aerodynamically very well. At the cruise design condition, the SR-7A prop fan had a high measured net efficiency of 79.3 percent. R.J.F.

N87-10835*# Sverdrup Technology, Inc., Arnold Air Force Station, Tenn.

LARGE PERTURBATION FLOW FIELD ANALYSIS AND SIMULATION FOR SUPERSONIC INLETS Final Report

M. O. VARNER, W. R. MARTINDALE, W. J. PHARES, K. R. KNEILE, and J. C. ADAMS, JR. Sep. 1984 126 p
(Contract NAS3-23682)
(NASA-CR-174676; NAS 1.26:174676) Avail: NTIS HC A07/MF A01 CSCL 01A

An analysis technique for simulation of supersonic mixed compression inlets with large flow field perturbations is presented. The approach is based upon a quasi-one-dimensional inviscid unsteady formulation which includes engineering models of unstart/restart, bleed, bypass, and geometry effects. Numerical solution of the governing time dependent equations of motion is accomplished through a shock capturing finite difference algorithm, of which five separate approaches are evaluated. Comparison with experimental supersonic wind tunnel data is presented to verify the present approach for a wide range of transient inlet flow conditions. Author

N87-10840*# Hamilton Standard, Windsor Locks, Conn.
EFFECT OF ANGULAR INFLOW ON THE VIBRATORY RESPONSE OF A COUNTER-ROTATING PROPELLER

J. E. TURNBERG and P. C. BROWN 15 Jan. 1985 75 p
(Contract NAS3-24222)
(NASA-CR-174819; NAS 1.26:174819) Avail: NTIS HC A04/MF A01 CSCL 01A

This report presents the results of a propeller vibratory stress survey on the Fairey Gannet aircraft aimed at giving an assessment of the difference in vibratory response between single and counter-rotating propeller operation in angular inflow. The survey showed that counter-rotating operation of the propeller had the effect of increasing the IP response of the rear propeller by approximately 25 percent over comparable single-rotation operation while counter-rotating operation did not significantly influence the IP response of the front propeller. Author

N87-11694*# Atmospheric Science Associates, Bedford, Mass.
CALCULATION OF WATER DROP TRAJECTORIES TO AND ABOUT ARBITRARY THREE-DIMENSIONAL LIFTING AND NONLIFTING BODIES IN POTENTIAL AIRFLOW Final Report

H. G. NORMENT Washington NASA Oct. 1985 168 p
(Contract NAS3-22146)
(NASA-CR-3935; E-2687; NAS 1.26:3935) Avail: NTIS HC A08/MF A01 CSCL 01A

Subsonic, external flow about nonlifting bodies, lifting bodies or combinations of lifting and nonlifting bodies is calculated by a modified version of the Hess lifting code. Trajectory calculations can be performed for any atmospheric conditions and for all water drop sizes, from the smallest cloud droplet to large raindrops. Experimental water drop drag relations are used in the water drop equations of motion and effects of gravity settling are included. Inlet flow can be accommodated, and high Mach number

compressibility effects are corrected for approximately. Seven codes are described: (1) a code used to debug and plot body surface description data; (2) a code that processes the body surface data to yield the potential flow field; (3) a code that computes flow velocities at arrays of points in space; (4) a code that computes water drop trajectories from an array of points in space; (5) a code that computes water drop trajectories and fluxes to arbitrary target points; (6) a code that computes water drop trajectories tangent to the body; and (7) a code that produces stereo pair plots which include both the body and trajectories. Accuracy of the calculations is discussed, and trajectory calculation results are compared with prior calculations and with experimental data.

Author

N87-11701*# Ohio State Univ., Columbus. Dept. of Aero- and Astro-Engineering.

AN EXPERIMENTAL STUDY OF THE AERODYNAMICS OF A NACA 0012 AIRFOIL WITH A SIMULATED GLAZE ICE ACCRETION Interim Technical Report

M. B. BRAGG Nov. 1986 318 p
(Contract NAG3-28; RF PROJ. 712620/762009)
(NASA-CR-179897; NAS 1.26:179897) Avail: NTIS HC A14/MF A01 CSCL 01A

An experimental study was conducted in the Ohio State University subsonic wind tunnel to measure the detailed aerodynamic characteristics of an airfoil with a simulated glaze ice accretion. A NACA 0012 model with interchangeable leading edges and pressure taps every one percent chord was used. Surface pressure and wake data were taken on the airfoil clean, with forced transition and with a simulated glaze ice shape. Lift and drag penalties due to the ice shape were found and the surface pressure clearly showed that large separation bubbles were present. Both total pressure and split-film probes were used to measure velocity profiles, both for the clean model and for the model with a simulated ice accretion. A large region of flow separation was seen in the velocity profiles and was correlated to the pressure measurements. Clean airfoil data were found to compare well to existing airfoil analysis methods. Author

N87-13405*# Scientific Research Associates, Inc., Glastonbury, Conn.

COMPUTATION OF MULTI-DIMENSIONAL VISCOUS SUPERSONIC JET FLOW Final Contractor Report

Y. N. KIM, R. C. BUGGELN, and H. MCDONALD Washington NASA Oct. 1986 128 p
(Contract NAS3-22759)
(NASA-CR-4020; E-3210; NAS 1.26:4020) Avail: NTIS HC A07/MF A01 CSCL 01A

A new method has been developed for two- and three-dimensional computations of viscous supersonic flows with embedded subsonic regions adjacent to solid boundaries. The approach employs a reduced form of the Navier-Stokes equations which allows solution as an initial-boundary value problem in space, using an efficient noniterative forward marching algorithm. Numerical instability associated with forward marching algorithms for flows with embedded subsonic regions is avoided by approximation of the reduced form of the Navier-Stokes equations in the subsonic regions of the boundary layers. Supersonic and subsonic portions of the flow field are simultaneously calculated by a consistently split linearized block implicit computational algorithm. The results of computations for a series of test cases relevant to internal supersonic flow is presented and compared with data. Comparison between data and computation are in general excellent thus indicating that the computational technique has great promise as a tool for calculating supersonic flow with embedded subsonic regions. Finally, a User's Manual is presented for the computer code used to perform the calculations. Author

N87-13406*# Scientific Research Associates, Inc., Glastonbury, Conn.

COMPUTATION OF MULTI-DIMENSIONAL VISCOUS SUPERSONIC FLOW Final Contractor Report

R. C. BUGGELN, Y. N. KIM, and H. MCDONALD Washington

NASA Oct. 1986 194 p

(Contract NAS3-22027)

(NASA-CR-4021; E-3211; NAS 1.26:4021) Avail: NTIS HC

A09/MF A01 CSCL 01A

A method has been developed for two- and three-dimensional computations of viscous supersonic jet flows interacting with an external flow. The approach employs a reduced form of the Navier-Stokes equations which allows solution as an initial-boundary value problem in space, using an efficient noniterative forward marching algorithm. Numerical instability associated with forward marching algorithms for flows with embedded subsonic regions is avoided by approximation of the reduced form of the Navier-Stokes equations in the subsonic regions of the boundary layers. Supersonic and subsonic portions of the flow field are simultaneously calculated by a consistently split linearized block implicit computational algorithm. The results of computations for a series of test cases associated with supersonic jet flow is presented and compared with other calculations for axisymmetric cases. Demonstration calculations indicate that the computational technique has great promise as a tool for calculating a wide range of supersonic flow problems including jet flow. Finally, a User's Manual is presented for the computer code used to perform the calculations. Author

N87-14283*# National Aeronautics and Space Administration. Lewis Research Center, Cleveland, Ohio.

SPATIALLY GROWING DISTURBANCES IN A HIGH VELOCITY RATIO TWO-STREAM, COPLANAR JET

J. H. MILES 1987 12 p Presented at the 25th Aerospace Sciences Meeting, Reno, Nev., 12-15 Jan. 1987; sponsored by AIAA PREVIOUSLY ANNOUNCED IN IAA AS A87-24966

(NASA-TM-88922; E-3255; NAS 1.15:88922; AIAA-87-0056)

Avail: NTIS HC A02/MF A01 CSCL 51A

The influence of cold and heated secondary flow on the instability of a two-stream, coplanar jet having a 0.7 Mach number heated primary jet for a nominal fan to primary velocity ratio of 0.68 was investigated by means of inviscid linearized stability theory. The instability properties of spatially growing axisymmetric and first order azimuthal disturbances were studied. The instability characteristics of the two-stream jet with a velocity ratio of 0.68 are very different from those of a single stream jet, and a two-stream, coplanar jet having a 0.9 Mach number heated primary jet and a cold secondary jet for a fan to primary velocity ratio of 0.30. For $X/D = 1$ and in comparison to the case where the velocity ratio was 0.3, the presence of the fan stream with a velocity ratio of 0.68 enhanced the instability of the jet and increased the unstable frequency range. However, the axisymmetric mode ($m = 0$) and the first order azimuthal mode ($m = 1$) have similar spatial growth rates where the velocity ratio is 0.68 while for a velocity ratio of 0.3 the growth rate of the first order azimuthal mode ($m = 1$) is greater. Comparing the cold and hot secondary flow results showed that for a velocity ratio of 0.68 the growth rate is greater for cold. Author

N87-14284*# National Aeronautics and Space Administration. Lewis Research Center, Cleveland, Ohio.

PROPAGATION OF SOUND WAVES IN TUBES OF NONCIRCULAR CROSS SECTION

W. B. RICHARDS (Oberlin Coll., Ohio) Aug. 1986 33 p

(NASA-TP-2601; E-2690; NAS 1.60:2601) Avail: NTIS HC

A03/MF A01 CSCL 01A

Plane-acoustic-wave propagation in small tubes with a cross section in the shape of a flattened oval is described. Theoretical descriptions of a plane wave propagating in a tube with circular cross section and between a pair of infinite parallel plates, including viscous and thermal damping, are expressed in similar form. For a wide range of useful duct sizes, the propagation constant (whose real and imaginary parts are the amplitude attenuation rate and

the wave number, respectively) is very nearly the same function of frequency for both cases if the radius of the circular tube is the same as the distance between the parallel plates. This suggests that either a circular-cross-section model or a flat-plate model can be used to calculate wave propagation in flat-oval tubing, or any other shape tubing, if its size is expressed in terms of an equivalent radius, given by $g = 2 \times (\text{cross-sectional area})/(\text{length of perimeter})$. Measurements of the frequency response of two sections of flat-oval tubing agree with calculations based on this idea. Flat-plate formulas are derived, the use of transmission-line matrices for calculations of plane waves in compound systems of ducts is described, and examples of computer programs written to carry out the calculations are shown. Author

N87-15173*# National Aeronautics and Space Administration. Lewis Research Center, Cleveland, Ohio.

VISCOUS ANALYSES FOR FLOW THROUGH SUBSONIC AND SUPERSONIC INTAKES

LOUIS A. POVINELLI and CHARLES E. TOWNE 9 Sep. 1986

24 p Presented at the AGARD Propulsion and Energetics Panel Meeting on Engine Response to Distorted Inflow Conditions, Munich, Germany, 8-9 Sep. 1986

(NASA-TM-88831; E-3209; NAS 1.15:88831) Avail: NTIS HC

A02/MF A01 CSCL 01A

A parabolized Navier-Stokes code was used to analyze a number of diffusers typical of a modern inlet design. The effect of curvature of the diffuser centerline and transitioning cross sections was evaluated to determine the primary cause of the flow distortion in the duct. Results are presented for S-shaped intakes with circular and transitioning cross sections. Special emphasis is placed on verification of the analysis to accurately predict distorted flow fields resulting from pressure-driven secondary flows. The effect of vortex generators on reducing the distortion of intakes is presented. Comparisons of the experimental and analytical total pressure contours at the exit of the intake exhibit good agreement. In the case of supersonic inlets, computations of the inlet flow field reveal that large secondary flow regions may be generated just inside of the intake. These strong flows may lead to separated flow regions and cause pronounced distortions upstream of the compressor. Author

N87-15944*# National Aeronautics and Space Administration. Lewis Research Center, Cleveland, Ohio.

A METHOD FOR CALCULATING TURBULENT BOUNDARY LAYERS AND LOSSES IN THE FLOW CHANNELS OF TURBOMACHINES

LAWRENCE F. SCHUMANN 1987 17 p Proposed for presentation at the 32nd International Gas Turbine Conference and Exhibition, Anaheim, Calif., 31 May - 4 Jun. 1987; sponsored by ASME

(NASA-TM-88928; E-3264; NAS 1.15:88928;

USAAVSCOM-TR-86-C-36; AD-A178164) Avail: NTIS HC

A02/MF A01 CSCL 01A

An interactive inviscid core flow-boundary layer method is presented for the calculation of turbomachine channel flows. For this method, a one-dimensional inviscid core flow is assumed. The end-wall and blade surface boundary layers are calculated using an integral entrainment method. The boundary layers are assumed to be collateral and thus are two-dimensional. The boundary layer equations are written in a streamline coordinate system. The streamwise velocity profiles are approximated by power law profiles. Compressibility is accounted for in the streamwise direction but not in the normal direction. Equations are derived for the special cases of conical and two-dimensional rectangular diffusers. For these cases, the assumptions of a one-dimensional core flow and collateral boundary layers are valid. Results using the method are compared with experiment and good quantitative agreement is obtained. Author

02 AERODYNAMICS

N87-16789*# National Aeronautics and Space Administration. Lewis Research Center, Cleveland, Ohio.

MEASUREMENTS OF THE UNSTEADY FLOW FIELD WITHIN THE STATOR ROW OF A TRANSONIC AXIAL-FLOW FAN. 1: MEASUREMENT AND ANALYSIS TECHNIQUE

K. L. SUDER, M. D. HATHAWAY (Army Research and Technology Labs., Cleveland, Ohio), T. H. OKIISHI (Iowa State Univ. of Science and Technology, Ames.), A. J. STRAZISAR, and J. J. ADAMCZYK 1987 17 p Proposed for presentation at the 32nd International Gas Turbine Conference and Exhibition, Anaheim, Calif., 31 May - 4 Jun. 1987; sponsored by ASME (NASA-TM-88945; E-3393; NAS 1.15:88945; USAAVSCOM-TR-86-C-30) Avail: NTIS HC A02/MF A01 CSCL 01A

This two-part paper presents laser anemometer measurements of the unsteady velocity field within the stator row of a transonic axial-flow fan. The objective is to provide additional insight into unsteady blade-row interactions within high speed compressors which affect stage efficiency, energy transfer, and other design considerations. Part 1 describes the measurement and analysis techniques used for resolving the unsteady flow field features. The ensemble-average and variance of the measured velocities are used to identify the rotor wake generated and unresolved unsteadiness, respectively. (Rotor wake generated unsteadiness refers to the unsteadiness generated by the rotor wake velocity deficit and the term unresolved unsteadiness refers to all remaining contributions to unsteadiness such as vortex shedding, turbulence, mass flow fluctuations, etc.). A procedure for calculating auto and cross correlations of the rotor wake generated and unresolved unsteady velocity fluctuations is described. These unsteady-velocity correlations have significance since they also result from a decomposition of the Navier-Stokes equations. This decomposition of the Navier-Stokes equations resulting in the velocity correlations used to describe the unsteady velocity field will also be outlined in this paper. Author

N87-16790*# National Aeronautics and Space Administration. Lewis Research Center, Cleveland, Ohio.

MEASUREMENTS OF THE UNSTEADY FLOW FIELD WITHIN THE STATOR ROW OF A TRANSONIC AXIAL-FLOW FAN. PART 2: RESULTS AND DISCUSSION

M. D. HATHAWAY, K. L. SUDER, T. H. OKIISHI (Iowa State Univ. of Science and Technology, Ames), A. J. STRAZISAR, and J. J. ADAMCZYK 1987 16 p Prepared for presentation at the 32nd International Gas Turbine Conference and Exhibition, Anaheim, Calif., 31 May - 4 Jun. 1987; sponsored by ASME (NASA-TM-88946; E-3394; NAS 1.15:88946; USAAVSCOM-TR-86-C-31) Avail: NTIS HC A02/MF A01 CSCL 01A

Unsteady velocity field measurements made within the stator row of a transonic axial-flow fan are presented. Measurements were obtained at midspan for two different stator blade rows using a laser anemometer. The first stator row consists of double circular-arc airfoils with a solidity of 1.68. The second features controlled-diffusion airfoils with a solidity of 0.85. Both were tested at design-speed peak efficiency conditions. In addition, the controlled-diffusion stator was also tested at near stall conditions. The procedures developed here are used to identify the rotor wake generated and unresolved unsteadiness from the velocity measurements (rotor wake generated unsteadiness refers to the unsteadiness generated by the rotor wake velocity deficit and unresolved unsteadiness refers to all remaining unsteadiness which contributes to the spread in the distribution of velocities such as vortex shedding, turbulence, etc.). Auto and cross correlations of these unsteady velocity fluctuations are presented to show their relative magnitude and spatial distributions. Amplification and attenuation of both rotor wake generated and unresolved unsteadiness are shown to occur within the stator blade passage. Author

N87-16798*# National Aeronautics and Space Administration. Lewis Research Center, Cleveland, Ohio.

EULER ANALYSIS OF THE THREE DIMENSIONAL FLOW FIELD OF A HIGH-SPEED PROPELLER: BOUNDARY CONDITION EFFECTS

M. NALLASAMY (Sverdrup Technology, Inc., Cleveland, Ohio), B. J. CLARK, and J. F. GROENEWEG 1987 18 p Proposed for presentation at the 32nd International Gas Turbine Conference and Exhibition, Anaheim, Calif., 31 May - 4 Jun. 1987; sponsored by ASME (NASA-TM-88955; E-3399; NAS 1.15:88955) Avail: NTIS HC A02/MF A01 CSCL 01A

The results of an investigation of the effects of far field boundary conditions on the solution of the three dimensional Euler equations governing the flow field of a high speed single rotation propeller are presented. The results show that the solutions obtained with the nonreflecting boundary conditions are in good agreement with experimental data. The specification of nonreflecting boundary conditions is effective in reducing the dependence of the solution on the location of the far field boundary. Details of the flow field within the blade passage and the tip vortex are presented. The dependence of the computed power coefficient on the blade passage and the tip vortex are presented. The dependence of the computed power coefficient on the blade setting angle is examined. Author

N87-16799*# National Aeronautics and Space Administration. Lewis Research Center, Cleveland, Ohio.

SPATIALLY GROWING DISTURBANCES IN A TWO-STREAM, COPLANAR JET

JEFFREY H. MILES 1986 30 p Presented at the 24th Aerospace Sciences Meeting, Reno, Nev., 6-8 Jan. 1986; sponsored by AIAA (NASA-TM-88949; E-3398; NAS 1.15:88949; AIAA-86-0041) Avail: NTIS HC A03/MF A01 CSCL 01A

The influence of the outer stream on the instability of a two-stream, coplanar jet with only the primary (central) stream heated for a nominal outer-to-primary velocity ratio of 0.3 was investigated by means of inviscid linearized stability theory. The instability properties of spatially growing axisymmetric and first order azimuthal disturbances were studied. It was found that the instability characteristics of the two stream jet are very different from those of a single stream jet. The presence of the outer stream enhanced the instability of the jet and increased the unstable frequency range for the first order azimuthal mode. Author

N87-16803*# Sverdrup Technology, Inc., Cleveland, Ohio.

A MULTIGRID LU-SSOR SCHEME FOR APPROXIMATE NEWTON ITERATION APPLIED TO THE EULER EQUATIONS Final Report

SEOKKWAN YOON and ANTONY JAMESON (Princeton Univ., N. J.) Sep. 1986 12 p (Contract NAS3-24105) (NASA-CR-179524; E-3104; NAS 1.26:179524) Avail: NTIS HC A02/MF A01 CSCL 01A

A new efficient relaxation scheme in conjunction with a multigrid method is developed for the Euler equations. The LU SSOR scheme is based on a central difference scheme and does not need flux splitting for Newton iteration. Application to transonic flow shows that the new method surpasses the performance of the LU implicit scheme. Author

N87-16804*# Sverdrup Technology, Inc., Cleveland, Ohio.

A HIGH RESOLUTION SHOCK CAPTURING SCHEME FOR HIGH MACH NUMBER INTERNAL FLOW Final Report

SEOKKWAN YOON and ANTONY JAMESON (Princeton Univ., N. J.) Sep. 1986 11 p (Contract NAS3-24105) (NASA-CR-179523; E-3103; NAS 1.26:179523) Avail: NTIS HC A02/MF A01 CSCL 01A

An accurate shock capturing scheme is developed for high speed flow. The flux limited dissipation scheme can be converted to a symmetric TVD scheme in the case of a scalar conservation

law. Application to an oblique shock wave problem shows the improved resolution and accuracy when compared to the results obtained by the adaptive dissipation method, while exhibiting comparable computational efficiency. Author

N87-16805*# National Aeronautics and Space Administration. Lewis Research Center, Cleveland, Ohio.

UNSTEADY FLOWS IN A SINGLE-STAGE TRANSONIC AXIAL-FLOW FAN STATOR ROW Ph.D. Thesis - Iowa State Univ.

MICHAEL D. HATHAWAY Dec. 1986 210 p
(NASA-TM-88929; E-3190; NAS 1.15:88929;
USAAVSCOM-TR-86-C-29) Avail: NTIS HC A10/MF A01 CSCL 01A

Measurements of the unsteady velocity field within the stator row of a transonic axial-flow fan were acquired using a laser anemometer. Measurements were obtained on axisymmetric surfaces located at 10 and 50 percent span from the shroud, with the fan operating at maximum efficiency at design speed. The ensemble-average and variance of the measured velocities are used to identify rotor-wake-generated (deterministic) unsteadiness and turbulence, respectively. Correlations of both deterministic and turbulent velocity fluctuations provide information on the characteristics of unsteady interactions within the stator row. These correlations are derived from the Navier-Stokes equation in a manner similar to deriving the Reynolds stress terms, whereby various averaging operators are used to average the aperiodic, deterministic, and turbulent velocity fluctuations which are known to be present in multistage turbomachines. The correlations of deterministic and turbulent velocity fluctuations throughout the axial fan stator row are presented. In particular, amplification and attenuation of both types of unsteadiness are shown to occur within the stator blade passage. Author

N87-16806*# Sverdrup Technology, Inc., Cleveland, Ohio.
AN LU-SSOR SCHEME FOR THE EULER AND NAVIER-STOKES EQUATIONS Final Report

SEOKKWAN YOON and ANTONY JAMESON (Princeton Univ., N. J.) Dec. 1986 12 p Presented at the 25th Aerospace Sciences Meeting, Reno, Nev., 12-15 Jan. 1987; sponsored by AIAA (Contract NAS3-24105)
(NASA-CR-179556; E-3105; NAS 1.26:179556; AIAA-87-0600)
Avail: NTIS HC A02/MF A01 CSCL 01A

A new multigrid relaxation scheme, lower-upper symmetric successive overrelaxation (LU-SSOR) is developed for the steady-state solution of the Euler and Navier-Stokes equations. The scheme, which is based on central differences, does not require flux splitting for approximate Newton iteration. Application to transonic flow shows that the new method is efficient and robust. The vectorizable LU-SSOR scheme needs only scalar diagonal inversions. Author

N87-17662*# National Aeronautics and Space Administration. Lewis Research Center, Cleveland, Ohio.

GENERATION OF A COMPOSITE GRID FOR TURBINE FLOWS AND CONSIDERATION OF A NUMERICAL SCHEME

Y. CHOO, S. YOON (Sverdrup Technology, Inc., Cleveland, Ohio), and C. RENO (Army Aviation Research and Development Command, Cleveland, Ohio) Nov. 1986 23 p
(NASA-TM-88890; E-3301; NAS 1.15:88890;
USAAVSCOM-TR-86-C-38; AD-A175473) Avail: NTIS HC A02/MF A01 CSCL 01A

A composite grid was generated for flows in turbines. It consisted of the C-grid (or O-grid) in the immediate vicinity of the blade and the H-grid in the middle of the blade passage between the C-grids and in the upstream region. This new composite grid provides better smoothness, resolution, and orthogonality than any single grid for a typical turbine blade with a large camber and rounded leading and trailing edges. The C-H (or O-H) composite grid has an unusual grid point that is connected to more than four neighboring nodes in two dimensions (more than six neighboring nodes in three dimensions). A finite-volume lower-upper (LU) implicit scheme to be used on this grid poses no problem

and requires no special treatment because each interior cell of this composite grid has only four neighboring cells in two dimensions (six cells in three dimensions). The LU implicit scheme was demonstrated to be efficient and robust for external flows in a broad flow regime and can be easily applied to internal flows and extended from two to three dimensions. Author

N87-17665*# National Aeronautics and Space Administration. Lewis Research Center, Cleveland, Ohio.

PRELIMINARY DESIGN OF TURBOPUMPS AND RELATED MACHINERY

GEORGE F. WISLICHENUS Oct. 1986 397 p
(Contract NAS3-13475)
(NASA-RP-1170; E-7389; NAS 1.61:1170) Avail: NTIS HC A17/MF A01 CSCL 01A

Pumps used in large liquid-fuel rocket engines are examined. The term preliminary design denotes the initial, creative phases of design, where the general shape and characteristics of the machine are determined. This compendium is intended to provide the design engineer responsible for these initial phases with a physical understanding and background knowledge of the numerous special fields involved in the design process. Primary attention is directed to the pumping part of the turbopump and hence is concerned with essentially incompressible fluids. However, compressible flow principles are developed. As much as possible, the simplicity and reliability of incompressible flow considerations are retained by treating the mechanics of compressible fluids as a departure from the theory of incompressible fluids. Five areas are discussed: a survey of the field of turbomachinery in dimensionless form; the theoretical principles of the hydrodynamic design of turbomachinery; the hydrodynamic and gas dynamic design of axial flow turbomachinery; the hydrodynamic and gas dynamic design of radial and mixed flow turbomachinery; and some mechanical design considerations of turbomachinery. Theoretical considerations are presented with a relatively elementary mathematical treatment. Author

N87-17669*# National Aeronautics and Space Administration. Lewis Research Center, Cleveland, Ohio.

COMBINED AERODYNAMIC AND STRUCTURAL DYNAMIC PROBLEM EMULATING ROUTINES (CASPER): THEORY AND IMPLEMENTATION

WILLIAM H. JONES Feb. 1985 75 p
(NASA-TP-2418; E-2278; NAS 1.60:2418) Avail: NTIS HC A04/MF A01 CSCL 01A

The Combined Aerodynamic and Structural Dynamic Problem Emulating Routines (CASPER) is a collection of data-base modification computer routines that can be used to simulate Navier-Stokes flow through realistic, time-varying internal flow fields. The Navier-Stokes equation used involves calculations in all three dimensions and retains all viscous terms. The only term neglected in the current implementation is gravitation. The solution approach is of an interactive, time-marching nature. Calculations are based on Lagrangian aerodynamic elements (aeroelements). It is assumed that the relationships between a particular aeroelement and its five nearest neighbor aeroelements are sufficient to make a valid simulation of Navier-Stokes flow on a small scale and that the collection of all small-scale simulations makes a valid simulation of a large-scale flow. In keeping with these assumptions, it must be noted that CASPER produces an imitation or simulation of Navier-Stokes flow rather than a strict numerical solution of the Navier-Stokes equation. CASPER is written to operate under the Parallel, Asynchronous Executive (PAX), which is described in a separate report. Author

02 AERODYNAMICS

N87-18539*# National Aeronautics and Space Administration. Lewis Research Center, Cleveland, Ohio.

SECONDARY STREAM AND EXCITATION EFFECTS ON TWO-DIMENSIONAL NOZZLE PLUME CHARACTERISTICS

UWE H. VONGLAHN 1987 23 p Prepared for presentation at the 23rd Joint Propulsion Conference, San Diego, Calif., 29 Jun. - 2 Jul. 1987; sponsored in part by AIAA, SAE, ASME, and ASEE (NASA-TM-89813; E-3457; NAS 1.15:89813; AIAA-87-2112) Avail: NTIS HC A02/MF A01 CSCL 01A

In order to design two-dimensional nozzle/ejector systems for future high performance aircraft, the basic engine exhaust plume velocity and temperature decay as effected by the secondary stream (ejector) and decay augmentation means must be assessed. Included in the assessment of the plume decay characteristics are the effects of nozzle aspect ratio and nozzle/ejector flow conditions. Nozzle/ejector plume decay can be enhanced by suitable excitation of the plume shear layers. Correlation of these factors are developed in a manner similar to those previously developed for conic and dual-flow nozzle plumes. Author

N87-18540*# National Aeronautics and Space Administration. Lewis Research Center, Cleveland, Ohio.

TWO-DIMENSIONAL NOZZLE PLUME CHARACTERISTICS

UWE H. VONGLAHN 1987 23 p Prepared for presentation at the 23rd Joint Propulsion Conference, San Diego, Calif., 29 Jun. - 2 Jul. 1987; sponsored in part by AIAA, SAE, ASME, and ASEE (NASA-TM-89812; E-3456; NAS 1.15:89812; AIAA-87-2111) Avail: NTIS HC A02/MF A01 CSCL 01A

Future high performance aircraft will likely feature asymmetric or two-dimensional nozzles with or without ejectors. In order to design two-dimensional nozzle/ejector systems of minimum size and weight, the plume decay and spreading characteristics of basic two-dimensional nozzles must first be established. The present work deals with the experimental analyses of these plume characteristics and includes the effects of nozzle aspect ratio and flow conditions (jet Mach number and temperature) on the plume decay and spreading of two-dimensional nozzles. Correlations including these variables are developed in a manner similar to those previously developed successfully for conic and dual-flow plumes. Author

N87-19350*# National Aeronautics and Space Administration. Lewis Research Center, Cleveland, Ohio.

NUMERICAL SIMULATION OF TRANSONIC PROPELLER FLOW USING A 3-DIMENSIONAL SMALL DISTURBANCE CODE EMPLOYING NOVEL HELICAL COORDINATES

AARON SNYDER 1987 23 p Prepared for presentation at the 8th Computational Fluid Dynamics Conference, Honolulu, Hawaii, 9-11 Jun. 1987; sponsored by AIAA (NASA-TM-89826; E-3475; NAS 1.15:89826) Avail: NTIS HC A02/MF A01 CSCL 01A

The numerical simulation of three-dimensional transonic flow about propeller blades is discussed. The equations for the unsteady potential flow about propellers is given for an arbitrary coordinate system. From this the small disturbance form of the equation is derived for a new helical coordinate system. The new coordinate system is suited to propeller flow and allows cascade boundary conditions to be applied straightforward. A numerical scheme is employed which solves the steady flow as an asymptotic limit of unsteady flow. Solutions are presented for subsonic and transonic flow about a 5 percent thick bicircular arc blade of an eight bladed cascade. Both high and low advance ratio cases are given which include a lifting case as well as nonlifting cases. The nonlifting cases are compared to solutions from a Euler code. Author

N87-20235*# National Aeronautics and Space Administration. Lewis Research Center, Cleveland, Ohio.

COMPOSITE GRID AND FINITE-VOLUME LU IMPLICIT SCHEME FOR TURBINE FLOW ANALYSIS

YUNG K. CHOO, SEOKKWAN YOON (Sverdrup Technology, Inc., Cleveland, Ohio.), and KESTUTIS C. CIVINSKAS (Army Aviation Research and Development Command, Cleveland, Ohio.) 1987 12 p Prepared for presentation at the 8th Computational Fluid Dynamics Conference, Honolulu, Hawaii, 8-10 Jun. 1987; sponsored by AIAA (NASA-TM-89828; E-3477; NAS 1.15:89828; USAAVSCOM-TR-87-C-5) Avail: NTIS HC A02/MF A01 CSCL 01A

A composite grid was generated in an attempt to improve grid quality for a typical turbine blade with large camber in terms of mesh control, smoothness, and orthogonality. This composite grid consists of the C grid (or O grid) in the immediate vicinity of the blade and the H grid in the upstream region and in the middle of the blade passage between the C grids. It provides a good boundary layer resolution around the leading edge region for viscous calculation, has orthogonality at the blade surface and slope continuity at the C-H (or O-H) interface, and has flexibility in controlling the mesh distribution in the upstream region without using excessive grid points. This composite grid eliminates the undesirable qualities of a single grid when generated for a typical turbine geometry. A finite-volume lower-upper (LU) implicit scheme can be used in solving for the turbine flows on the composite grid. This grid has a special grid node that is connected to more than four neighboring nodes in two dimensions and to more than six nodes in three dimensions. But the finite-volume approach poses no problem at the special point because each interior cell has only four neighboring cells in two dimensions and only six cells in three dimensions. The finite-volume LU implicit scheme was demonstrated to be robust and efficient for both external and internal flows in a broad flow regime. Author

N87-20238*# National Aeronautics and Space Administration. Lewis Research Center, Cleveland, Ohio.

LEWIS INVERSE DESIGN CODE (LINDES): USERS MANUAL

JOSE M. SANZ Mar. 1987 67 p (NASA-TP-2676; E-3221; NAS 1.60:2676) Avail: NTIS HC A04/MF A01 CSCL 01A

The method of complex characteristics and hodograph transformation for the design of shockless airfoils was introduced by Bauer, Garabedian, and Korn and has been extended by the author to design subcritical and supercritical cascades with high solidities and large inlet angles. This new capability was achieved by introducing a new conformal mapping of the hodograph domain onto an ellipse and expanding the solution in terms of Chebyshev polynomials. A new computer code, the NASA Lewis inverse design code, was developed based on this idea. This new design code is an efficient method for the design of airfoils in cascade. In particular, the design of subcritical cascades of airfoils is a very fast, robust, and versatile process. The inverse design code can be made to interact with a turbulent boundary layer calculation to obtain airfoils with no separated flows at the design condition. This report is intended to serve as a users manual for this design code. Material previously reported by the author is included here for completeness and quick access to the user. The manual contains a description of the method followed by a discussion of the design procedure and examples. The input parameters necessary to run the code are then described and their default values given. Output listings corresponding to six different blade shapes designed with the code are given, as well as the necessary input data to reproduce the computer runs. The examples have been chosen to show that a wide range of applications can be covered with the code, ranging from supercritical propeller sections to wind tunnel turning vanes that can operate with a large inlet flow angle range. Author

N87-20239*# General Electric Co., Cincinnati, Ohio. Aircraft Engine Business Group.

DEVELOPMENT OF A ROTOR WAKE/VORTEX MODEL. VOLUME 2: USER'S MANUAL FOR COMPUTER PROGRAM Final Report

R. K. MAJJIGI and P. R. GLIEBE Jun. 1984 86 p

(Contract NAS3-23681)

(NASA-CR-174850-VOL-2; NAS 1.26:174850-VOL-2) Avail: NTIS HC A05/MF A01 CSCL 01A

The principal objective was to establish a verified rotor wake/vortex model for specific application to fan and compressor rotor-stator interaction and resulting noise generation. A description and flow chart of the Rotor Wake/Vortex Model computer program, a listing of the program, definitions of the input/output parameters, a sample input/output case, and input files for Rotor 55, the JT15D rotor, and Rotor 67, Stage 1 are provided. Author

N87-20243*# Sverdrup Technology, Inc., Cleveland, Ohio.

A NAVIER-STOKES SOLVER USING THE LU-SSOR TVD ALGORITHM Final Contractor Report

SEOKKWAN YOON Mar. 1987 13 p

(Contract NAS3-24105)

(NASA-CR-179608; E-3499; NAS 1.26:179608) Avail: NTIS HC A02/MF A01 CSCL 20D

A new Navier-Stokes solver is developed by combining the efficiency of the LU-SSOR scheme and the accuracy of the flux-limited dissipation scheme. Application to laminar and turbulent flows and hypersonic flows proves the reliability of the new algorithm. Author

N87-22630*# National Aeronautics and Space Administration. Lewis Research Center, Cleveland, Ohio.

APPLICATION OF ADVANCED COMPUTATIONAL CODES IN THE DESIGN OF AN EXPERIMENT FOR A SUPERSONIC THROUGHFLOW FAN ROTOR

JERRY R. WOOD, JAMES F. SCHMIDT, RONALD J. STEINKE, RODRICK V. CHIMA, and WILLIAM G. KUNIK Jun. 1987 30 p Presented at the 32nd International Gas Turbine Conference and Exhibit, Anaheim, Calif., 31 May - 4 Jun. 1987; sponsored by the ASME

(NASA-TM-88915; E-3339; NAS 1.15:88915) Avail: NTIS HC A03/MF A01 CSCL 01A

Increased emphasis on sustained supersonic or hypersonic cruise has revived interest in the supersonic throughflow fan as a possible component in advanced propulsion systems. Use of a fan that can operate with a supersonic inlet axial Mach number is attractive from the standpoint of reducing the inlet losses incurred in diffusing the flow from a supersonic flight Mach number to a subsonic one at the fan face. The design of the experiment using advanced computational codes to calculate the components required is described. The rotor was designed using existing turbomachinery design and analysis codes modified to handle fully supersonic axial flow through the rotor. A two-dimensional axisymmetric throughflow design code plus a blade element code were used to generate fan rotor velocity diagrams and blade shapes. A quasi-three-dimensional, thin shear layer Navier-Stokes code was used to assess the performance of the fan rotor blade shapes. The final design was stacked and checked for three-dimensional effects using a three-dimensional Euler code interactively coupled with a two-dimensional boundary layer code. The nozzle design in the expansion region was analyzed with a three-dimensional parabolized viscous code which corroborated the results from the Euler code. A translating supersonic diffuser was designed using these same codes. Author

N87-23591*# National Aeronautics and Space Administration. Lewis Research Center, Cleveland, Ohio.

ICING OF FLOW CONDITIONERS IN A CLOSED-LOOP WIND TUNNEL M.S. Thesis

JAMES E. NEWTON Jun. 1987 13 p

(NASA-TM-89824; E-3474; NAS 1.15:89824) Avail: NTIS HC A02/MF A01 CSCL 01A

Described are the results of an experiment which determined whether flow conditioning screens and honeycombs would ice up in a closed-loop icing wind tunnel when placed downstream of the heat exchanger and upstream of the spray bars. The experiment was performed in the Icing Research Tunnel (IRT) at NASA Lewis Research Center. The investigation involved two separate tests: one to find the icing characteristics of flow conditioners in the IRT, and the second to find the icing characteristics of flow conditioners in the proposed rehabilitation of the Altitude Wind Tunnel (AWT). Both experiments showed that the heat exchanger removed nearly all of the icing cloud so that icing of the flow conditioners would cause no serious tunnel performance degradation during the course of a day's run. Only extremely cold conditions caused frost formation on the flow conditioners. The significance of this frost formation was minimized because frost buildup on the heat exchanger caused a much more severe pressure drop than did icing of the flow conditioners. Author

N87-23598*# National Aeronautics and Space Administration. Lewis Research Center, Cleveland, Ohio.

COUPLED AERODYNAMIC AND ACOUSTICAL PREDICTIONS FOR TURBOPROPS

BRUCE J. CLARK and JAMES R. SCOTT Mar. 1986 13 p

Presented at the 107th Meeting of the American Acoustical Society, Norfolk, Va., 7-10 May 1984

(NASA-TM-87094; E-2688; NAS 1.15:87094) Avail: NTIS HC A02/MF A01 CSCL 01A

To predict the noise fields for proposed turboprop airplanes, an existing turboprop noise code by Farassat has been modified to accept blade pressure inputs from a three-dimensional aerodynamic code. A Euler-type code can handle the nonlinear transonic flow of these high-speed, highly swept blades. This turboprop code was modified to allow the calculation mesh to extend to about twice the blade radius and to apply circumferential periodicity rather than solid-wall boundary conditions on the blade in the region between the blade tip and the outer shroud. Outputs were added for input to the noise prediction program and for color contour plots of various flow variables. The Farassat input subroutines were modified to read files of blade coordinates and predicted surface pressures. Aerodynamic and acoustic results are shown for the SR-3 model blade. Comparison of the acoustic predicted results with measured data show good agreement. Author

N87-24435*# National Aeronautics and Space Administration. Lewis Research Center, Cleveland, Ohio.

NUMERICAL SIMULATIONS OF UNSTEADY, VISCOUS, TRANSONIC FLOW OVER ISOLATED AND CASCADED AIRFOILS USING A DEFORMING GRID

DENNIS L. HUFF Jun. 1987 16 p Presented at the 19th Fluid Dynamics, Plasma Dynamics and Lasers Conference, Honolulu, Hawaii, 8-10 Jun. 1987; sponsored by AIAA

(NASA-TM-89890; E-3532; NAS 1.15:89890; AIAA-87-1316)

Avail: NTIS HC A02/MF A01 CSCL 01A

A compressible, unsteady, full Navier-Stokes, finite difference code was developed for modeling transonic flow through two-dimensional, oscillating cascades. The procedure introduces a deforming grid technique to capture the motion of the airfoils. Results using a deforming grid are presented for both isolated and cascaded airfoils. The load histories and unsteady pressure distributions are predicted for the NASA 64A010 isolated airfoil and compared with existing experimental data. Results show that the deforming grid technique can be used to successfully predict the unsteady flow properties around an oscillating airfoil. The deforming grid technique was extended for modeling unsteady flow in a cascade. The use of a deforming grid simplifies the

specification of boundary conditions. Unsteady flow solutions similar to the isolated airfoil predictions are found for a NACA 0012 cascade with zero interblade phase angle and zero stagger. Experimental data for these cases are not available for code validation, but computational results are presented to show sample predictions from the code. Applications of the code to typical turbomachinery flow conditions will be presented in future work.

Author

N87-25294*# National Aeronautics and Space Administration. Lewis Research Center, Cleveland, Ohio.

WIND TUNNEL PERFORMANCE RESULTS OF AN AEROELASTICALLY SCALED 2/9 MODEL OF THE PTA FLIGHT TEST PROP-FAN

GEORGE L. STEFKO, GAYLE E. ROSE, and GARY G. PODBOY
Jul. 1987 50 p Presented at the 23rd Joint Propulsion Conference, San Diego, Calif., 29 Jun. - 2 Jul. 1987; cosponsored by AIAA, SAE, ASME, and ASEE Prepared in cooperation with Sverdrup Technology, Inc., Cleveland, Ohio
(NASA-TM-88917; E-3610; NAS 1.15:89917; AIAA-87-1893)
Avail: NTIS HC A03/MF A01 CSCL 01A

High speed wind tunnel aerodynamic performance tests of the SR-7A advanced prop-fan have been completed in support of the Prop-Fan Test Assessment (PTA) flight test program. The test showed that the SR-7A model performed aerodynamically very well. At the cruise design condition, the SR-7A prop fan had a high measured net efficiency of 79.3 percent. R.J.F.

N87-27628*# National Aeronautics and Space Administration. Lewis Research Center, Cleveland, Ohio.

EFFECT OF VARIABLE INLET GUIDE VANES ON THE OPERATING CHARACTERISTICS OF A TILT NACELLE INLET/POWERED FAN MODEL

R. R. WOOLLETT and H. C. PONTONIDES (Grumman Aerospace Corp., Bethpage, N.Y.) Sep. 1987 41 p
(NASA-TM-88983; E-3453; NAS 1.15:88983) Avail: NTIS HC A03/MF A01 CSCL 01A

The effects of a variable inlet guide vane (VIGV) assembly on the operating characteristics of a V/STOL inlet and on the performance of a 20-in. (0.508-m) diameter fan engine were investigated. The data indicate that the VIGVs are effective thrust modulators over a wide range of free-stream velocities, nacelle angles of attack, and fan speeds. The thrust modulation ranges, including choking limits, fan stall limits, and inlet separation boundaries are presented. The presence of the VIGV assembly causes significant losses in inlet angle-of-attack capability and generally increases the blade stress levels at all limit conditions except at high angle of attack and high free-stream velocity. Reducing the fan nozzle exit area limited the positive VIGV actuation range and consequently decreased the range of thrust modulation at all limit conditions except at both high free-stream velocity and high angle of attack conditions. Author

N87-27629*# National Aeronautics and Space Administration. Lewis Research Center, Cleveland, Ohio.

INITIAL TURBULENCE EFFECT ON JET EVOLUTION WITH AND WITHOUT TONAL EXCITATION

G. RAMAN, K. B. M. Q. ZAMAN, and E. J. RICE 1987 17 p
Prepared for presentation at the 11th Aeroacoustics Conference, Sunnyvale, Calif., 19-21 Oct. 1987; sponsored by AIAA
(NASA-TM-100178; E-3702; NAS 1.15:100178; AIAA-87-2725)
Avail: NTIS HC A02/MF A01 CSCL 01A

The effect of initial turbulence level on the development of a jet and on the susceptibility of the jet to discrete tone excitation was experimentally investigated. Turbulence intensity was varied, over the range 0.15 to 5 percent, by using screens and grids placed upstream of an 8.8 cm diameter nozzle. Top-hat mean velocity profiles with approximately identical initial boundary layer states were ensured in all cases; the turbulence spectra were broadband. It was found, contrary to earlier reports, that the natural jet decay remained essentially unchanged for varying initial turbulence. For a fixed amplitude of the tonal excitation, increasing the initial turbulence damped out the growth of the instability wave;

as a result, the excitability, assessed from the mean velocity decay on the axis, was found to diminish. However, the degree of damping in the amplification of the instability wave was only slight compared to the large increase in the initial turbulence. The jet with 5 percent turbulence could be measurably altered by excitation with a velocity perturbation amplitude as little as 0.25 percent of the jet velocity. The amplitude effect data indicate an upper bound of the extent to which a jet could be excited, and thus its plume shortened, by the plane wave, single frequency excitation. An additional data set with no grid or trip, yielding a nominally laminar boundary layer, re-emphasizes the profound effect of initial boundary layer state on jet evolution as well as on its excitability. This jet decayed the fastest naturally, and consequently, it was the least excitable in spite of its turbulence being the least. Author

N87-29412*# City Coll. of the City Univ. of New York. School of Engineering.

AN INVESTIGATION OF THE FLOW CHARACTERISTICS IN THE BLADE ENDWALL CORNER REGION Final Contractor Report
BIRINCHI K. HAZARIKA and RISHI S. RAJ Washington NASA
Jul. 1987 291 p

(Contract NAG3-122)

(NASA-CR-4076; E-3500; NAS 1.26:4076) Avail: NTIS HC A13/MF A01 CSCL 01A

Studies were undertaken to determine the structure of the flow in the blade end wall corner region simulated by attaching two uncambered airfoils on either side of a flat plate with a semicircular leading edge. Detailed measurements of the corner flow were obtained with conventional pressure probes, hot wire anemometry, and flow visualization. The mean velocity profiles and six components of the Reynolds stress tensor were obtained with an inclined single sensor hot wire probe whereas power spectra were obtained with a single sensor oriented normal to the flow. Three streamwise vortices were identified based on the surface streamlines, distortion of total pressure profiles, and variation of mean velocity components in the corner. A horseshoe vortex formed near the leading edge of the airfoil. Within a short distance downstream, a corner vortex was detected between the horseshoe vortex and the surfaces forming the corner. A third vortex was formed at the rear portion of the corner between the corner vortex and the surface of the flat plate. Turbulent shear stress and production of turbulence are negligibly small. A region of negative turbulent shear stress was also observed near the region of low turbulence intensity from the vicinity of the flat plate. Author

N87-29413*# Lockheed-Georgia Co., Marietta.

PROPFAN TEST ASSESSMENT TESTBED AIRCRAFT FLUTTER MODEL TEST REPORT

C. M. J. JENNESS 20 Oct. 1987 102 p
(Contract NAS3-24339)

(NASA-CR-179458; NAS 1.26:179458; LG85ER0187; L86R1350)
Avail: NTIS HC A06/MF A01 CSCL 01A

The PropFan Test Assessment (PTA) program includes flight tests of a propfan power plant mounted on the left wing of a modified Gulfstream II testbed aircraft. A static balance boom is mounted on the right wing tip for lateral balance. Flutter analyses indicate that these installations reduce the wing flutter stabilizing speed and that torsional stiffening and the installation of a flutter stabilizing tip boom are required on the left wing for adequate flutter safety margins. Wind tunnel tests of a 1/9th scale high speed flutter model of the testbed aircraft were conducted. The test program included the design, fabrication, and testing of the flutter model and the correlation of the flutter test data with analysis results. Excellent correlations with the test data were achieved in posttest flutter analysis using actual model properties. It was concluded that the flutter analysis method used was capable of accurate flutter predictions for both the (symmetric) twin propfan configuration and the (unsymmetric) single propfan configuration. The flutter analysis also revealed that the differences between the tested model configurations and the current aircraft design caused the (scaled) model flutter speed to be significantly higher than that of the aircraft, at least for the single propfan configuration without a flutter boom. Verification of the aircraft final design should,

therefore, be based on flutter predictions made with the test validated analysis methods. Author

03

AIR TRANSPORTATION AND SAFETY

N87-29418*# Cleveland State Univ., Ohio. Dept. of Civil Engineering.

ENHANCED MIXING OF AN AXISYMMETRIC JET BY AERODYNAMIC EXCITATION Final Report M.S. Thesis

GANESH RAMAN Mar. 1986 177 p

(Contract NCC3-49)

(NASA-CR-175059; NAS 1.26:175059) Avail: NTIS HC A09/MF A01 CSCL 01A

The main objective of acoustic excitation studies is to gain a high level of control over processes governing free shear flow characteristics. The basic premise is that inherent instability waves in free shear flows are excitable by external perturbations with frequencies close to the natural instability frequency of the flow. An 8.89 cm diameter axisymmetric jet was acoustically excited by four loudspeakers placed upstream of the nozzle exit. Measurements were made at Mach numbers of 0.435 and 0.2. A single hot-wire probe was used to obtain turbulence levels at the nozzle exit and along the centerline, and a microphone at the nozzle exit was used to study the resonance characteristics of the rig. A Pitot probe was stationed at $X/D = 9$ downstream along the nozzle axis to study the Strouhal number dependence and to look at threshold levels for excitation. The test results were obtained after a preliminary evaluation and facility improvement. Excitation at the correct Strouhal number enhanced mixing significantly. The effects were most prominent in the Strouhal number range between 0.4 and 1.0. The effects of acoustic excitation also depend considerably on the sound pressure level at the nozzle exit and were more pronounced at higher sound levels. Other factors which influenced the excitability were valve noise, exit turbulence levels, extraneous noise, and a flanged nozzle. Analysis of the hot-wire signal, in conditions of optimum jet mixing, showed vortex pairing to occur between 2 and 3 diameters downstream. Author

N87-29419*# Ohio State Univ., Columbus. Aeronautical and Astronautical Research Lab.

TRANSONIC INTERFERENCE REDUCTION BY LIMITED VENTILATION WALL PANELS Final Report

JOHN D. LEE Jan. 1986 15 p

(Contract NAG3-109)

(NASA-CR-175039; NAS 1.26:175039) Avail: NTIS HC A02/MF A01 CSCL 01A

In two wind tunnels used for the two-dimensional airfoil tests, each wall above and below the model was modified by replacing small segments of the solid boundaries with perforated plates vented into sealed chambers. Perforated segments having approximately 40 percent open area were found to reduce the transonic wall interference to a negligible level, for a model chord-to-tunnel height ratio of 0.5. This report describes the physical arrangement and presents typical model pressure distributions to illustrate the effectiveness of the technique. Author

N87-29420*# National Aeronautics and Space Administration. Lewis Research Center, Cleveland, Ohio.

CONTROL OF SHEAR FLOWS BY ARTIFICIAL EXCITATION

E. J. RICE and K. B. M. Q. ZAMAN Oct. 1987 12 p Prepared for presentation at the 11th Aeroacoustics Conference, Sunnyvale, Calif., 19-21 Oct. 1987; sponsored by the AIAA

(NASA-TM-100201; E-3794; NAS 1.15:100201; AIAA-87-2722)

Avail: NTIS HC A02/MF A01 CSCL 01A

Investigations involving artificial excitation of various shear flows are reviewed. Potential applications of excitation in flow control, e.g., in enhancing mixing, and in delaying transition and separation are discussed. An account is given of the current activities at NASA Lewis Research Center in this regard. Author

Includes passenger and cargo air transport operations; and aircraft accidents.

A87-17995*# National Aeronautics and Space Administration. Lewis Research Center, Cleveland, Ohio.

IN-FLIGHT PHOTOGRAMMETRIC MEASUREMENT OF WING ICE ACCRETIONS

R. C. MCKNIGHT (NASA, Lewis Research Center, Cleveland, OH), R. L. PALKO, and R. L. HUMES (Carlspring Corp., Arnold Air Force Station, TN) AIAA, Aerospace Sciences Meeting, 24th, Reno, NV, Jan. 6-9, 1986. 14 p. Previously announced in STAR as N86-31562. refs

(AIAA PAPER 86-0483)

A photographic instrumentation system was developed for the Lewis icing research aircraft to measure wind ice accretions during flight. The system generates stereo photographs of the accretions which are then photogrammetrically measured by the Air Force Arnold Engineering and Development Center. The measurements yield a survey of spatial coordinates of an accretion's surface to an accuracy of at least \pm or \pm 0.08 cm. The accretions can then be matched to corresponding icing cloud and aerodynamic measurements. The system is being used to measure rime, mixed, and clear natural ice accretions. Author

A87-22366*# Grumman Aerospace Corp., Bethpage, N.Y.

PARTICLE TRAJECTORY COMPUTER PROGRAM FOR ICING ANALYSIS OF AXISYMMETRIC BODIES - A PROGRESS REPORT

DIMITRIOS G. MALTEZOS (New York, State University, Farmingdale), CHARLES OSONITSCH (Grumman Aerospace Corp., Bethpage, NY), ROBERT J. SHAW (NASA, Lewis Research Center, Cleveland, OH), and ARTHUR KAERCHER (Grumman Data Systems, Bethpage, NY) AIAA, Aerospace Sciences Meeting, 25th, Reno, NV, Jan. 12-15, 1987. 6 p.

(AIAA PAPER 87-0027)

Aircraft exposed to an atmospheric icing environment can accumulate ice, resulting in a sharp increase in drag, a reduction in lift, control surface fouling, and engine damage all of which result in a hazardous flight situation. NASA Lewis Research Center (LeRC) has conducted a program to examine, with the aid of high-speed computer codes, how the trajectories of particles contribute to the ice accumulation on airfoils and engine inlets. For this effort, a computer code was developed to calculate icing particle trajectories and impingement limits for axisymmetric inlets. The original research-oriented NASA code was upgraded and modified to meet the requirements of the design engineer. The improved code is capable of performing trajectory calculations for any atmospheric conditions and droplet sizes. It can handle single droplets or a distribution of various droplet sizes. The four programs that comprise the code are described and the results of a test case using flight conditions for a Fokker F100 icing tunnel test are presented. Author

A87-22464*# Massachusetts Inst. of Tech., Cambridge.

IN-FLIGHT MEASUREMENT OF ICE GROWTH ON AN AIRFOIL USING AN ARRAY OF ULTRASONIC TRANSDUCERS

R. JOHN HANSMAN, JR., MARK S. KIRBY (MIT, Cambridge, MA), ROBERT C. MCKNIGHT (NASA, Lewis Research Center, Cleveland, OH), and ROBERT L. HUMES (Carlspring Corp., Arnold Air Force Station, TN) AIAA, Aerospace Sciences Meeting, 25th, Reno, NV, Jan. 12-15, 1987. 10 p. FAA-supported research. refs

(Contract NGL-22-009-640; NAG3-666)

(AIAA PAPER 87-0178)

Results from three research flights to obtain in-flight ultrasonic pulse-echo measurements of airfoil ice thickness as a function of time using an array of eight ultrasonic transducers mounted flush

03 AIR TRANSPORTATION AND SAFETY

with the leading edge of the airfoil are presented. The accuracy of the thickness measurements is found to be within 0.5 mm of mechanical and stereophotograph measurements of the ice accretion. The ultrasonic measurements demonstrate that the ice growth rate typically varies during the flight, with variations in the ice growth rate for dry ice growth being primarily due to fluctuations in the cloud liquid water content. Discrepancies between experimental results and results predicted by an analytic icing code underline the need for a better understanding of the physics of wet ice growth. R.R.

A87-45635*# Massachusetts Inst. of Tech., Cambridge.
COMPARISON OF WET AND DRY GROWTH IN ARTIFICIAL AND FLIGHT ICING CONDITIONS

R. JOHN HANSMAN, JR. and MARK S. KIRBY (MIT, Cambridge, MA) Journal of Thermophysics and Heat Transfer (ISSN 0887-8722), vol. 1, July 1987, p. 215-221. FAA-supported research. Previously cited in issue 18, p. 2613, Accession no. A86-39948. refs
(Contract NGL-22-009-640; NAG3-6662)

A87-48761* Sverdrup Technology, Inc., Middleburg Heights, Ohio.

EVALUATION OF ICING DRAG COEFFICIENT CORRELATIONS APPLIED TO ICED PROPELLER PERFORMANCE PREDICTION
THOMAS L. MILLER (Sverdrup Technology, Inc., Middleburg Heights, OH), R. J. SHAW (NASA, Lewis Research Center, Cleveland, OH), and K. D. KORKAN (Texas A & M University, College Station) SAE, General Aviation Aircraft Meeting and Exposition, Wichita, KS, Apr. 28-30, 1987. 13 p. refs
(SAE PAPER 871033)

Evaluation of three empirical icing drag coefficient correlations is accomplished through application to a set of propeller icing data. The various correlations represent the best means currently available for relating drag rise to various flight and atmospheric conditions for both fixed-wing and rotating airfoils, and the work presented here illustrates and evaluates one such application of the latter case. The origins of each of the correlations are discussed, and their apparent capabilities and limitations are summarized. These correlations have been made to be an integral part of a computer code, ICEPERF, which has been designed to calculate iced propeller performance. Comparison with experimental propeller icing data shows generally good agreement, with the quality of the predicted results seen to be directly related to the radial icing extent of each case. The code's capability to properly predict thrust coefficient, power coefficient, and propeller efficiency is shown to be strongly dependent on the choice of correlation selected, as well as upon proper specification of radial icing extent. Author

N87-21878*# National Aeronautics and Space Administration. Lewis Research Center, Cleveland, Ohio.

AIRCRAFT ACCIDENT REPORT: NASA 712, CONVAIR 990, N712NA, MARCH AIR FORCE BASE, CALIFORNIA, JULY 17, 1985, EXECUTIVE SUMMARY

BYRON E. BATTHAUER, G. T. MCCARTHY, MICHAEL HANNAH, ROBERT J. HOGAN, FRANK J. MARLOW, WILLIAM D. REYNARD, JANIS H. STOKLOSA, and THOMAS J. YAGER (National Aeronautics and Space Administration. Langley Research Center, Hampton, Va.) Jul. 1986 9 p
(NASA-TM-87356-VOL-1; E-3110; NAS 1.15:87356-VOL-1) Avail: NTIS HC A02/MF A01 CSCL 01C

On July 17, 1985, NASA 712, a Convair 990 aircraft, was destroyed by fire during an aborted takeoff at March Air Force Base in California. Material ejected from a blowout in the tires of the right main landing gear penetrated the right-wing fuel tank. The leaking fuel ignited. Fire engulfed the right wing and fuselage as the aircraft stopped its forward motion. The crew of four and the 15 scientists and technicians aboard escaped without serious injury. Author

N87-21879*# National Aeronautics and Space Administration. Lewis Research Center, Cleveland, Ohio.

AIRCRAFT ACCIDENT REPORT: NASA 712, CONVAIR 990, N712NA, MARCH AIR FORCE BASE, CALIFORNIA, JULY 17, 1985, FACTS AND ANALYSIS

BYRON E. BATTHAUER, G. T. MCCARTHY, MICHAEL HANNAH, ROBERT J. HOGAN, FRANK J. MARLOW, WILLIAM D. REYNARD, JANIS H. STOKLOSA, and THOMAS J. YAGER (National Aeronautics and Space Administration. Langley Research Center, Hampton, Va.) Jul. 1986 59 p
(NASA-TM-87356-VOL-2; E-3110; NAS 1.15:87356-VOL-2) Avail: NTIS HC A04/MF A01 CSCL 01C

On July 17, 1985, at 1810 P.d.t., NASA 712, a Convair 990 aircraft, was destroyed by fire at March Air Force Base, California. The fire started during the rollout after the pilot rejected the takeoff on runway 32. The rejected takeoff was initiated during the takeoff roll because of blown tires on the right landing gear. During the rollout, fragments of either the blown tires or the wheel/brake assemblies penetrated a right-wing fuel tank forward of the right main landing gear. Leaking fuel ignited while the aircraft was rolling, and fire engulfed the right wing and the fuselage after the aircraft was stopped on the runway. The 4-man flightcrew and the 15 scientists and technicians seated in the cabin evacuated the aircraft without serious injury. The fire was not extinguished by crash/rescue efforts and the aircraft was destroyed. Author

N87-29470*# National Aeronautics and Space Administration. Lewis Research Center, Cleveland, Ohio.

NEW METHODS AND MATERIALS FOR MOLDING AND CASTING ICE FORMATIONS

ANDREW L. REEHORST and G. PAUL RICHTER Sep. 1987 16 p
(NASA-TM-100126; E-3673; NAS 1.15:100126) Avail: NTIS HC A02/MF A01 CSCL 01C

This study was designed to find improved materials and techniques for molding and casting natural or simulated ice shapes that could replace the wax and plaster method. By utilizing modern molding and casting materials and techniques, a new methodology was developed that provides excellent reproduction, low-temperature capability, and reasonable turnaround time. The resulting casts are accurate and tough. Author

N87-29471*# National Aeronautics and Space Administration. Lewis Research Center, Cleveland, Ohio.

ANALYSIS OF CONVAIR 990 REJECTED-TAKEOFF ACCIDENT WITH EMPHASIS ON DECISION MAKING, TRAINING AND PROCEDURES

BYRON E. BATTHAUER 1987 23 p Presented at the 40th International Air Safety Seminar, Tokyo, Japan, 26-29 Oct. 1987; sponsored by the Flight Safety Foundation, Inc.
(NASA-TM-100189; E-3771; NAS 1.15:100189) Avail: NTIS HC A02/MF A01 CSCL 01C

This paper analyzes a NASA Convair 990 (CV-990) accident with emphasis on rejected-takeoff (RTO) decision making, training, procedures, and accident statistics. The NASA Aircraft Accident Investigation Board was somewhat perplexed that an aircraft could be destroyed as a result of blown tires during the takeoff roll. To provide a better understanding of tire failure RTO's, The Board obtained accident reports, Federal Aviation Administration (FAA) studies, and other pertinent information related to the elements of this accident. This material enhanced the analysis process and convinced the Accident Board that high-speed RTO's in transport aircraft should be given more emphasis during pilot training. Pilots should be made aware of various RTO situations and statistics with emphasis on failed-tire RTO's. This background information could enhance the split-second decision-making process that is required prior to initiating an RTO. Author

05

AIRCRAFT DESIGN, TESTING AND PERFORMANCE

Includes aircraft simulation technology.

A87-19247* National Aeronautics and Space Administration. Lewis Research Center, Cleveland, Ohio.

FOLDING TILT ROTOR DEMONSTRATOR FEASIBILITY STUDY

J. D. EISENBERG (NASA, Lewis Research Center, Cleveland, OH) and J. V. BOWLES (NASA, Ames Research Center, Moffett Field, CA) IN: American Helicopter Society, Annual Forum, 42nd, Washington, DC, June 2-4, 1986, Proceedings. Volume 2. Alexandria, VA, American Helicopter Society, 1986, p. 563-585. refs

This study considers the modification of existing aircraft to the folding tilt rotor (FTR) design configuration, and then addresses the vehicle design requirements necessary to demonstrate the FTR concept throughout the hover/transition high-speed envelope. Three potential candidates are considered: (1) the Bell/Boeing V-22 Osprey combined with either the existing TF-34 convertible engine or a conceptual convertible engine utilizing the torque-converter-coupled fan configuration; (2) a combination of the same powerplants with a modified Lockheed S-3A Viking; and (3) the NASA/Army/BELL XV-15 airframe mated with a conceptual generic turbofan engine with a fixed-pitch fan coupled to the engine by means of a torque converter. Required aircraft modifications are identified and recommended R&D efforts for engine/rotor/airframe integration are presented. Author

A87-24904*# General Electric Co., Cincinnati, Ohio.

EVALUATION OF CAPILLARY REINFORCED COMPOSITES FOR ANTI-ICING

SAMUEL W. CIARDULLO, STEPHEN C. MITCHELL, and RONALD D. ZERKLE (General Electric Co., Cincinnati, OH) AIAA, Aerospace Sciences Meeting, 25th, Reno, NV, Jan. 12-15, 1987. 11 p.

(Contract NAS3-24386)

(AIAA PAPER 87-0023)

This paper discusses the evaluation of glass capillary reinforced advanced composite structures for anti-icing purposes. The concept involves embedding glass capillary tubes on the surface of a composite structure and ducting heated air through the tubes. A computer program was developed to predict the anti-icing performance of such tubes and a test program was conducted to demonstrate the actual performance of this system. Test data and analytical code results were in excellent agreement. Both indicate the feasibility of using capillary tubes for surface heating in order to combat ice accumulation on advanced composite structures. Author

A87-24905*# National Aeronautics and Space Administration. Lewis Research Center, Cleveland, Ohio.

A HEATER MADE FROM GRAPHITE COMPOSITE MATERIAL FOR POTENTIAL DEICING APPLICATION

CHING-CHEH HUNG (NASA, Lewis Research Center, Cleveland, OH), MICHAEL E. DILLEHAY, and MARK STAHL (Cleveland State University, OH) AIAA, Aerospace Sciences Meeting, 25th, Reno, NV, Jan. 12-15, 1987. 8 p. Previously announced in STAR as N87-12559. refs

(AIAA PAPER 87-0025)

A surface heater was developed using a graphite fiber-epoxy composite as the heating element. This heater can be thin, highly electrically and thermally conductive, and can conform to an irregular surface. Therefore it may be used in an aircraft's thermal deicing system to quickly and uniformly heat the aircraft surface. One-ply of unidirectional graphite fiber-epoxy composite was laminated between two plies of fiber glass-epoxy composite, with nickel foil contacting the end portions of the composite and partly

exposed beyond the composites for electrical contact. The model heater used brominated P-100 fibers from Amoco. The fiber's electrical resistivity, thermal conductivity and density were 50 micro ohms per centimeter, 270 W/m-K and 2.30 gm/cubic cm, respectively. The electricity was found to penetrate through the composite in the transverse direction to make an acceptably low foil-composite contact resistance. When conducting current, the heater temperature increase reached 50 percent of the steady state value within 20 sec. There was no overheating at the ends of the heater provided there was no water corrosion. If the foil-composite bonding failed during storage, liquid water exposure was found to oxidize the foil. Such bonding failure may be avoided if perforated nickel foil is used, so that the composite plies can bond to each other through the perforated holes and therefore lock the foil in place. Author

A87-24918*# Wichita State Univ., Kans.

EXPERIMENTAL, WATER DROPLET IMPINGEMENT DATA ON TWO-DIMENSIONAL AIRFOILS, AXISYMMETRIC INLET AND BOEING 737-300 ENGINE INLET

M. PAPADAKIS (Wichita State University, KS), E. ELANGOAN, G. A. FREUND, JR., and M. D. BREER (Boeing Military Airplane Co., Wichita, KS) AIAA, Aerospace Sciences Meeting, 25th, Reno, NV, Jan. 12-15, 1987. 15 p. refs

(Contract NAG3-566)

(AIAA PAPER 87-0097)

An experimental method has been developed to determine the droplet impingement characteristics on two- and three-dimensional bodies. The experimental results provide the essential droplet impingement data required to validate particle trajectory codes, used in aircraft icing analyses and engine inlet particle separator analyses. A body whose water droplet impingement characteristics are required is covered at strategic locations by thin strips of moisture absorbing (blotter) paper, and then exposed to an air stream containing a dyed-water spray cloud. Water droplet impingement data are extracted from the dyed blotter strips, by measuring the optical reflectance of the dye deposit on the strips, using an automated reflectometer. Impingement efficiency data obtained for a NACA 65(2)015 airfoil section, a supercritical airfoil section, and Boeing 737-300 and axisymmetric inlet models are presented in this paper. Author

N87-12559*# National Aeronautics and Space Administration. Lewis Research Center, Cleveland, Ohio.

A HEATER MADE FROM GRAPHITE COMPOSITE MATERIAL FOR POTENTIAL DEICING APPLICATION

C. C. HUNG, M. E. DILLEHAY (Cleveland State Univ., Ohio), and M. STAHL 1986 22 p Proposed for presentation at the 25th Aerospace Sciences Meeting, Reno, Nev., 12-15 Jan. 1987; sponsored by AIAA

(NASA-TM-88888; E-3298; NAS 1.15:88888) Avail: NTIS HC

A02/MF A01 CSCL 01C

A surface heater was developed using a graphite fiber-epoxy composite as the heating element. This heater can be thin, highly electrically and thermally conductive, and can conform to an irregular surface. Therefore it may be used in an aircraft's thermal deicing system to quickly and uniformly heat the aircraft surface. One-ply of unidirectional graphite fiber-epoxy composite was laminated between two plies of fiber glass-epoxy composite, with nickel foil contacting the end portions of the composite and partly exposed beyond the composites for electrical contact. The model heater used brominated P-100 fibers from Amoco. The fiber's electrical resistivity, thermal conductivity and density were 50 micro ohms per centimeter, 270 W/m-K and 2.30 gm/cubic cm, respectively. The electricity was found to penetrate through the composite in the transverse direction to make an acceptably low foil-composite contact resistance. When conducting current, the heater temperature increase reached 50 percent of the steady state value within 20 sec. There was no overheating at the ends of the heater provided there was no water corrosion. If the foil-composite bonding failed during storage, liquid water exposure was found to oxidize the foil. Such bonding failure may be avoided if perforated nickel foil is used, so that the composite plies can

05 AIRCRAFT DESIGN, TESTING AND PERFORMANCE

bond to each other through the perforated holes and therefore lock the foil in place. Author

N87-16816* National Aeronautics and Space Administration. Lewis Research Center, Cleveland, Ohio.

IDENTIFICATION AND PROPOSED CONTROL OF HELICOPTER TRANSMISSION NOISE AT THE SOURCE

JOHN J. COY (Army Research and Technology Labs., Cleveland, Ohio), ROBERT F. HANDSCHUH, DAVID G. LEWICKI, RONALD G. HUFF, EUGENE A. KREJSA, and ALLAN M. KARCHMER 1987 23 p Proposed for presentation at the NASA/Army Rotorcraft Technology Conference, Moffett Field, Calif., 17-19 Mar. 1987

(NASA-TM-89312; NAS 1.15:89312; USAAVCOM-TR-87-C-2)

Avail: NTIS HC A02/MF A01 CSCL 01C

Helicopter cabin interiors require noise treatment which is expensive and adds weight. The gears inside the main power transmission are major sources of cabin noise. Work conducted by the NASA Lewis Research Center in measuring cabin interior noise and in relating the noise spectrum to the gear vibration of the Army OH-58 helicopter is described. Flight test data indicate that the planetary gear train is a major source of cabin noise and that other low frequency sources are present that could dominate the cabin noise. Companion vibration measurements were made in a transmission test stand, revealing that the single largest contributor to the transmission vibration was the spiral bevel gear mesh. The current understanding of the nature and causes of gear and transmission noise is discussed. It is believed that the kinematical errors of the gear mesh have a strong influence on that noise. The completed NASA/Army sponsored research that applies to transmission noise reduction is summarized. The continuing research program is also reviewed. Author

N87-23615* Hamilton Standard, Windsor Locks, Conn.

DYNAMIC RESPONSE OF TWO COMPOSITE PROP-FAN MODELS ON A NACELLE/WING/FUSELAGE HALF MODEL Final Report

ARTHUR F. SMITH and BENNETT M. BROOKS Oct. 1986 157 p

(Contract NAS3-24088)

(NASA-CR-179589; NAS 1.26:179589; HSER-11058) Avail: NTIS HC A08/MF A01 CSCL 01C

Results are presented for blade response wind tunnel tests of two 62.2 cm diameter Prop-Fan (advanced turboprop) models with swept and unswept graphite/epoxy composite blades. Measurements of dynamic response were made with the rotors mounted on a simulated nacelle/wing/fuselage model, with varying tilt, at flow speeds up to 0.85 Mach number. The presence of the wing, downstream of the rotor, induced 1-P responses that were about twice those previously measured for an isolated nacelle installation. The swept blade had less 1-P response than the unswept (straight) blade. The 2-P response was significant for both blades, and was closely correlated to wing lift. Higher order response was not important for the straight blade, but possibly important for the swept blade near critical speeds, due to the proximity of the blade tips to the wing leading edge. Measurements are compared with theoretically based prediction. Correlations between calculated and measured 1-P response were good for the straight blade, and fair for the swept blade. Improvements to the calculation method were identified and implemented. Author

N87-24457* Sikorsky Aircraft, Stratford, Conn.

A ROTORCRAFT FLIGHT/PROPULSION CONTROL INTEGRATION STUDY Report, Jun. 1984 - Jun. 1986

D. G. C. RUTTLEDGE Nov. 1986 211 p

(Contract NAS3-24343)

(NASA-CR-179574; NAS 1.26:179574; SER-760606) Avail: NTIS HC A10/MF A01 CSCL 01C

An eclectic approach was taken to a study of the integration of digital flight and propulsion controls for helicopters. The basis of the evaluation was the current Gen Hel simulation of the UH-60A Black Hawk helicopter with a model of the GE T700 engine. A list of flight maneuver segments to be used in evaluating the

effectiveness of such an integrated control system was composed, based on past experience and an extensive survey of the U.S. Army Air-to-Air Combat Test data. A number of possible features of an integrated system were examined and screened. Those that survived the screening were combined into a design that replaced the T700 fuel control and part of the control system in the UH-60A Gen Hel simulation. This design included portions of an existing pragmatic adaptive fuel control designed by the Chandler-Evans Company and an linear quadratic regulator (LQR) based N(p) governor designed by the GE company, combined with changes in the basic Sikorsky Aircraft designed control system. The integrated system exhibited improved total performance in many areas of the flight envelope. Author

07

AIRCRAFT PROPULSION AND POWER

Includes prime propulsion systems and systems components, e.g., gas turbine engines and compressors; and onboard auxiliary power plants for aircraft.

A87-13318* National Aeronautics and Space Administration. Lewis Research Center, Cleveland, Ohio.

A REAL-TIME SIMULATION EVALUATION OF AN ADVANCED DETECTION, ISOLATION AND ACCOMMODATION ALGORITHM FOR SENSOR FAILURES IN TURBINE ENGINES

W. C. MERRILL and J. C. DELAAT (NASA, Lewis Research Center, Cleveland, OH) IN: 1986 American Control Conference, 5th, Seattle, WA, June 18-20, 1986, Proceedings. Volume 1. New York, Institute of Electrical and Electronics Engineers, 1986, p. 162-169. Previously announced in STAR as N86-24697. refs

An advanced sensor failure detection, isolation, and accommodation (ADIA) algorithm has been developed for use with an aircraft turbofan engine control system. In a previous paper the authors described the ADIA algorithm and its real-time implementation. Subsequent improvements made to the algorithm and implementation are discussed, and the results of an evaluation presented. The evaluation used a real-time, hybrid computer simulation of an F100 turbofan engine. Author

A87-14123* Flow Research, Inc., Kent, Wash.

PROPELLER DESIGN BY OPTIMIZATION

M. H. RIZK and W.-H. JOU (Flow Research Co., Kent, WA) AIAA Journal (ISSN 0001-1452), vol. 24, Sept. 1986, p. 1554-1556. Previously cited in issue 07, p. 848, Accession no. A86-19678. refs

(Contract NAS3-24533)

A87-17934* Beech Aircraft Corp., Wichita, Kans.

APPLICATION OF PROPFAN PROPULSION TO GENERAL AVIATION

R. W. AWKER (Beech Aircraft Corp., Wichita, KS) AIAA, AHS, and ASEE, Aircraft Systems, Design and Technology Meeting, Dayton, OH, Oct. 20-22, 1986. 16 p. refs

(Contract NAS3-24349)

(AIAA PAPER 86-2698)

Recent studies of advanced propfan propulsion systems have shown significant reductions in fuel consumption of 15-30 percent for transport class aircraft. This paper presents the results of a study which examined applying propfan propulsion to General Aviation class aircraft to determine if similar improvements could be achieved for business aircraft. In addition to the potential performance gains, this paper also addresses the cost aspects of propfan propulsion on General Aviation aircraft emphasizing the significant impact that the cost of capital and tax aspects have on determining the total cost of operation for business aircraft. Author

A87-17993*# National Aeronautics and Space Administration. Lewis Research Center, Cleveland, Ohio.

AN OVERVIEW OF THE SMALL ENGINE COMPONENT TECHNOLOGY (SECT) STUDIES

M. R. VANCO, W. T. WINTUCKY, and R. W. NIEDWIECKI (NASA, Lewis Research Center, Cleveland, OH) AIAA, ASME, SAE, and ASEE, Joint Propulsion Conference, 22nd, Huntsville, AL, June 16-18, 1986. 19 p. Previously announced in STAR as N86-31587. refs
(AIAA PAPER 86-1542)

The objectives of the joint NASA/Army SECT studies were to identify high payoff technologies for year 2000 small gas turbine engine applications and to provide a technology plan for guiding future research and technology efforts applicable to rotorcraft, commuter and general aviation aircraft and cruise missiles. Competitive contracts were awarded to Allison, AVCO Lycoming, Garrett, Teledyne CAE and Williams International. This paper presents an overview of the contractors' study efforts for the commuter, rotorcraft, cruise missile, and auxiliary power (APU) applications with engines in the 250 to 1,000 horsepower size range. Reference aircraft, missions and engines were selected. Advanced engine configurations and cycles with projected year 2000 component technologies were evaluated and compared with a reference engine selected by the contractor. For typical commuter and rotorcraft applications, fuel savings of 22 percent to 42 percent can be attained. For \$1/gallon and \$2/gallon fuel, reductions in direct operating cost range from 6 percent to 16 percent and from 11 percent to 17 percent respectively. For subsonic strategic cruise missile applications, fuel savings of 38 percent to 54 percent can be achieved which allows 35 percent to 60 percent increase in mission range and life cycle cost reductions of 40 percent to 56 percent. High payoff technologies have been identified for all applications. Author

A87-21513*# Williams International, Walled Lake, Mich.
ENGINE STUDIES FOR FUTURE SUBSONIC CRUISE MISSILES
RON PAMPREEN (Williams International, Walled Lake, MI) AIAA, ASME, SAE, and ASEE, Joint Propulsion Conference, 22nd, Huntsville, AL, June 16-18, 1986. 8 p. Army-supported research.
(Contract NAS3-24543)
(AIAA PAPER 86-1547)

A comparative study was conducted to investigate the performance and cost benefits of future engine concepts for subsonic strategic cruise missile propulsion. Technology advancements were projected for component efficiencies, materials and bearing lubrication. Engine configurations studied were an advanced simple cycle (conventional) turbofan and a recuperated turbofan. Results showed the two engines require virtually the same size missile to fly the designated mission. However, there was lower life cycle cost for the advanced simple cycle turbofan engine. Author

A87-21514*# National Aeronautics and Space Administration. Lewis Research Center, Cleveland, Ohio.

VISUALIZATION OF FLOWS IN A MOTORED ROTARY COMBUSTION ENGINE USING HOLOGRAPHIC INTERFEROMETRY

YOLANDA R. HICKS, HAROLD J. SCHOCK (NASA, Lewis Research Center, Cleveland, OH), JAMES E. CRAIG, HOLLY L. UMSTATTER, and DAVID Y. LEE (Spectron Development Laboratories, Inc., Costa Mesa, CA) AIAA, ASME, SAE, and ASEE, Joint Propulsion Conference, 22nd, Huntsville, AL, June 16-18, 1986. 12 p. Previously announced in STAR as N86-31583. refs
(AIAA PAPER 86-1557)

The use of holographic interferometry to view the small- and large-scale flow field structures in the combustion chamber of a motored Wankel engine assembly is described. In order that the flow patterns of interest could be observed, small quantities of helium were injected with the intake air. Variation of the air flow patterns with engine speed, helium flow rate, and rotor position are described. The air flow at two locations within the combustion chamber was examined using this technique. Author

A87-22544*# Clarkson Univ., Potsdam, N.Y.

SOOT LOADING IN A GENERIC GAS TURBINE COMBUSTOR

W. A. ECKERLE (Clarkson University, Potsdam, NY) and T. J. ROSFJORD (United Technologies Research Center, East Hartford, CT) AIAA, Aerospace Sciences Meeting, 25th, Reno, NV, Jan. 12-15, 1987. 11 p. refs
(Contract NAS3-24223)
(AIAA PAPER 87-0297)

Variation in soot loading along the centerline of a generic gas turbine combustor was experimentally investigated. The 12.7-cm dia burner consisted of six sheet-metal louvers. Soot loading along the burner length was quantified by acquiring measurements first at the exit of the full-length combustor and then at upstream stations by sequential removal of liner louvers to shorten the burner length. Alteration of the flow field approaching removed louvers, maintaining a constant liner pressure drop. Burner exhaust flow was sampled at the burner centerline to determine soot mass concentration and smoke number. Characteristic particle size and number density, transmissivity of the exhaust flow, and local radiation from luminous soot particles in the exhaust flow were determined by optical techniques. Four test fuels were burned at three fuel-air ratios to determine fuel chemical property and flow temperature influences. Data were acquired at two combustor pressures. Particulate concentration data indicated a strong oxidation mechanism in the combustor secondary zone, though the oxidation was significantly affected by flow temperature. Soot production was directly related to fuel smoke point. Less soot production and lower secondary-zone oxidation rates were observed at reduced combustor pressure. Author

A87-24944*# Texas A&M Univ., College Station.

COMPUTATIONAL AEROACOUSTICS OF PROPELLER NOISE IN THE NEAR AND FAR FIELD

D. W. FORSYTH and K. D. KORKAN (Texas A & M University, College Station) AIAA, Aerospace Sciences Meeting, 25th, Reno, NV, Jan. 12-15, 1987. 63 p. refs
(Contract NAS3-354)
(AIAA PAPER 87-0254)

Techniques for applying the NASPROP-E computer code (Bober et al., 1983) to characterize the acoustic field of a transonic propfan are described and demonstrated for the case of the SR-3 propfan. It is pointed out that NASPROP E accounts for the nonlinear quadrupole, monopole, and dipole noise sources. The approach used, based on that of White (1984) and Korkan et al. (1985 and 1986), is described in detail, and the results of simulations employing different (reflective and nonreflective) inflow-outflow boundary conditions and azimuthal mesh spacings are presented in graphs and briefly discussed. T.K.

A87-25394*# National Aeronautics and Space Administration. Lewis Research Center, Cleveland, Ohio.

COMPARISON OF CALCULATED AND EXPERIMENTAL CASCADE PERFORMANCE FOR CONTROLLED-DIFFUSION COMPRESSOR STATOR BLADING

N. L. SANGER (NASA, Lewis Research Center, Cleveland, OH) and R. P. SHREEVE (U.S. Naval Postgraduate School, Monterey, CA) ASME, Transactions, Journal of Turbomachinery (ISSN 0889-504X), vol. 108, July 1986, p. 42-50. Previously announced in STAR as N86-16219. refs
(Contract NAVAIR TASK AIR-31OE)
(ASME PAPER 86-GT-35)

The mid-span section of a previously reported controlled-diffusion compressor stator has been experimentally evaluated in cascade. Measurements are taken over a range of incidence angles for blade chord Reynolds numbers from 470,000 to 690,000. Blade chord length is 12.7 cm, aspect ratio is 2.0, and solidity is 1.67. Measurements include conventional cascade performance parameters as well as blade surface pressures. Computations are made for the inviscid flow field, surface boundary layers, and loss for several of the blade inlet angle conditions, are compared against corresponding data. Author

A87-25396*# National Aeronautics and Space Administration. Lewis Research Center, Cleveland, Ohio.

THE EFFECT OF CIRCUMFERENTIAL AERODYNAMIC DETUNING ON COUPLED BENDING-TORSION UNSTALLED SUPERSONIC FLUTTER

D. HOYNIK (NASA, Lewis Research Center, Cleveland, OH) and S. FLEETER (Purdue University, West Lafayette, IN) ASME, Transactions, Journal of Turbomachinery (ISSN 0889-504X), vol. 108, Oct. 1986, p. 253-260. Previously announced in STAR as N86-21513. refs

(ASME PAPER 86-GT-100)

A mathematical model developed to predict the enhanced coupled bending-torsion unstalled supersonic flutter stability due to alternate circumferential spacing aerodynamic detuning of a turbomachine rotor. The translational and torsional unsteady aerodynamic coefficients are developed in terms of influence coefficients, with the coupled bending-torsion stability analysis developed by considering the coupled equations of this aerodynamic detuning on coupled bending-torsion unstalled supersonic flutter as well as the verification of the modeling are then demonstrated by considering an unstable 12 bladed rotor, with Verdon's uniformly spaced Cascade B flow geometry as a baseline. However, with the elastic axis and center of gravity at 60 percent of the chord, this type of aerodynamic detuning has a minimal effect on stability. For both uniform and nonuniform circumferentially space rotors, a single degree of freedom torsion mode analysis was shown to be appropriate for values of the bending-torsion natural frequency ratio lower than 0.6 and higher 1.2. When the elastic axis and center of gravity are not coincident, the effect of detuning on cascade stability was found to be very sensitive to the location of the center of gravity with respect to the elastic axis. In addition, it was determined that when the center of gravity was forward of an elastic axis located at midchord, a single degree of freedom torsion model did not accurately predict cascade stability. Author

A87-27989*# Texas A&M Univ., College Station.

OFF-DESIGN ANALYSIS OF COUNTER-ROTATING PROPELLER CONFIGURATIONS

K. D. KORKAN and J. A. GAZZANIGA (Texas A & M University, College Station) Journal of Propulsion and Power (ISSN 0748-4658), vol. 3, Jan.-Feb. 1987, p. 91-93.

(Contract NAG3-354)

An analysis is conducted to determine whether the counterrotating propeller configuration maintains, and perhaps improves, its excellent performance in the off-design mode for the constant-speed or variable-pitch case. While the twist distribution is maintained, the blade angle is changed to absorb shaft horsepower as a constant rpm setting is maintained under varying freestream velocities. A relatively flat propeller efficiency curve is obtained for advance ratios of 1.5-5.0. O.C.

A87-31277*# National Aeronautics and Space Administration. Lewis Research Center, Cleveland, Ohio.

PREDICTION OF THE STRUCTURE OF FUEL SPRAYS IN CYLINDRICAL COMBUSTION CHAMBERS

JIAN-SHUN SHUEN (NASA, Lewis Research Center; Sverdrup Technology, Inc., Cleveland, OH) Journal of Propulsion and Power (ISSN 0748-4658), vol. 2, Mar.-Apr. 1987, p. 105-113. Previously cited in issue 11, p. 1482, Accession no. A86-26636. refs

(Contract NAS3-24105)

A87-32607* General Electric Co., Fairfield, Conn.

A MODEL PROPULSION SIMULATOR FOR EVALUATING COUNTER ROTATING BLADE CHARACTERISTICS

B. R. DELANEY, C. BALAN, H. WEST (General Electric Co., Fairfield, CT), F. M. HUMENIK (NASA, Lewis Research Center, Cleveland, OH), and G. CRAIG (Boeing Co., Seattle, WA) SAE, Aerospace Technology Conference and Exposition, Long Beach, CA, Oct. 13-16, 1986. 10 p.

(SAE PAPER 861715)

Three Model Propulsion Simulators (MPS) were designed and built to evaluate candidate counterrotation Ultra bypass fan model blade designs of nominally 2-ft (0.61 m) tip diameter for an advanced 'pusher-type' aircraft engine. These propulsion simulators (nominally 1/5 engine size) are capable of operation over a wide range of subsonic conditions and can deliver up to 750 shaft horsepower per rotor at rotor speeds of 10,000 rpm. The rotor thrust and torque, dynamic blade stresses, and system temperature data are transmitted through an integral telemetry system to facilitate data acquisition. Salient features of the design, instrumentation, and operation of these simulators are described in this paper. Author

A87-41156*# National Aeronautics and Space Administration. Lewis Research Center, Cleveland, Ohio.

A PARAMETRIC STUDY OF A GAS-GENERATOR AIRTURBO RAMJET (ATR)

CHRISTOPHER A. SNYDER (NASA, Lewis Research Center, Cleveland, OH) AIAA, ASME, SAE, and ASEE, Joint Propulsion Conference, 22nd, Huntsville, AL, June 16-18, 1986. 18 p. Previously announced in STAR as N86-31586. refs

(AIAA PAPER 86-1681)

Parametric engine performance calculations were carried out for an airturbo ramjet (ATR). A LOX-LH2 rocket powered turbine powered the compressor. The engine was flown over a typical flight path up to Mach 5 to show the effect of engine off design operation. The compressor design efficiency, compressor pressure ratio, rocket turbine efficiency, rocket turbine inlet temperature, and rocket chamber pressure were varied to show their effect on engine net thrust and specific impulse at Mach 5 cruise. Estimates of engine weights as a function of the ratio of compressor air to rocket propellant flow and rocket chamber pressure are also included. In general, the Mach 5 results indicate that increasing the amount of rocket gas produced increased thrust but decreased the specific impulse. The engine performance was fairly sensitive to rocket chamber pressure, especially at higher compressor pressure ratios. At higher compressor pressure ratios, the engine thrust was sensitive to turbine inlet temperature. At all compressor pressure ratios, the engine performance was not sensitive to compressor or turbine efficiency. Author

A87-45239*# United Technologies Research Center, East Hartford, Conn.

SHORT EFFICIENT EJECTOR SYSTEMS

WALTER M. PRESZ, JR. (United Technologies Research Center, East Hartford, CT; Western New England College, Springfield, M, BRUCE L. MORIN (United Technologies, Research Center, East Hartford, CT), and ROGER F. BLINN AIAA, SAE, ASME, and ASEE, Joint Propulsion Conference, 23rd, San Diego, CA, June 29-July 2, 1987. 10 p. refs

(Contract NAG3-610)

(AIAA PAPER 87-1837)

A research program was conducted to improve the performance of low pressure ratio ejector systems. The results show that short, efficient ejectors operating at nearly ideal performance are possible through the use of forced mixer lobes. Forced mixer lobes generate large scale axial vorticity which results in rapid mixing and improved diffuser performance. Ejector testing was conducted using both an ejector wind tunnel. Numerous mixer lobe variations were tested to develop lobe design guidelines. The improved performance of mixer-ejectors is presented over a range of operating conditions. Results of mixer lobe angle, penetration, and alignment are presented. Lobe angles of up to 25 deg, coupled with diffuser wall angles over 20 deg, operate without separation, allowing

efficient, short ejector systems. Both warm and cold flow test results are presented. Temperature similarity expressions previously developed are further formulated and verified. Author

A87-45279*# Purdue Univ., West Lafayette, Ind.

A PANEL METHOD FOR COUNTER ROTATING PROPPANS

M. H. WILLIAMS (Purdue University, West Lafayette, IN) and S. H. CHEN AIAA, SAE, ASME, and ASEE, Joint Propulsion Conference, 23rd, San Diego, CA, June 29-July 2, 1987. 12 p. refs

(Contract NAG3-499)

(AIAA PAPER 87-1890)

A time domain source-doublet surface paneling method is developed for analyzing the unsteady loads on counter rotating propellers in incompressible irrotational flow. A scheme for treating the blade-wake interaction problem is described. Sample results for single rotation propellers are given, with comparisons to alternate theories and experiment. Finally, some preliminary results for quasi-steady and fully unsteady loads on counter rotating systems are presented. Author

A87-45289*# National Aeronautics and Space Administration. Lewis Research Center, Cleveland, Ohio.

CONTINGENCY POWER FOR SMALL TURBOSHAFT ENGINES USING WATER INJECTION INTO TURBINE COOLING AIR

THOMAS J. BIESIADNY, BRETT BERGER (NASA, Lewis Research Center, Cleveland, OH), GARY A. KLANN, and DAVID A. CLARK (NASA, Lewis Research Center; U.S. Army, Propulsion Directorate, Cleveland, OH) AIAA, SAE, ASME, and ASEE, Joint Propulsion Conference, 23rd, San Diego, CA, June 29-July 2, 1987. 9 p. Previously announced in STAR as N87-20280. refs

(AIAA PAPER 87-1906)

Because of one engine inoperative requirements, together with hot-gas reingestion and hot day, high altitude takeoff situations, power augmentation for multiengine rotorcraft has always been of critical interest. However, power augmentation using overtemperature at the turbine inlet will shorten turbine life unless a method of limiting thermal and mechanical stresses is found. A possible solution involves allowing the turbine inlet temperature to rise to augment power while injecting water into the turbine cooling air to limit hot-section metal temperatures. An experimental water injection device was installed in an engine and successfully tested. Although concern for unprotected subcomponents in the engine hot section prevented demonstration of the technique's maximum potential, it was still possible to demonstrate increases in power while maintaining nearly constant turbine rotor blade temperature. Author

A87-45369*# General Electric Co., Evendale, Ohio.

NASA/GE ADVANCED LOW EMISSIONS COMBUSTOR PROGRAM

E. E. EKSTEDT (General Electric Co., Evendale, OH) and J. S. FEAR (NASA, Lewis Research Center, Cleveland, OH) AIAA, SAE, ASME, and ASEE, Joint Propulsion Conference, 23rd, San Diego, CA, June 29-July 2, 1987. 10 p. refs

(AIAA PAPER 87-2035)

The Advanced Low Emissions Combustor Program consisted of the design and testing of advanced combustor concepts utilizing lean, premixed, prevaporized fuel and variable geometry. The objective was to evaluate the potential of these combustor systems to provide very low pollutant emissions levels, superior performance and high durability relative to contemporary combustor designs. Four full annular combustor concepts were designed and fabricated for a 30:1 pressure ratio high bypass turbofan engine. The four full annular combustors with active variable geometry were tested at pressures up to approximately 0.7 MPa with Jet A fuel. The two most promising concepts were also tested in a high pressure sector combustor test rig capable of operation at the maximum engine pressures. The high pressure sector combustor tests were conducted with Jet A and a fuel with reduced hydrogen content. Results of the sector combustor tests are presented in this paper. The potential for very low emissions with premixed fuel was demonstrated. However, autoignition or flashback within the

premixing systems was encountered at high pressures. Further development effort is required to address this problem area. Author

A87-46228*# National Aeronautics and Space Administration. Lewis Research Center, Cleveland, Ohio.

INFLUENCE OF THIRD-DEGREE GEOMETRIC NONLINEARITIES ON THE VIBRATION AND STABILITY OF PRETWISTED, PRECONED, ROTATING BLADES

K. B. SUBRAHMANYAM and K. R. V. KAZA (NASA, Lewis Research Center, Cleveland, OH) IN: International Symposium on Air Breathing Engines, 8th, Cincinnati, OH, June 14-19, 1987, Proceedings. New York, American Institute of Aeronautics and Astronautics, 1987, p. 465-479. Previously announced in STAR as N86-31920. refs

The governing coupled flapwise bending, edgewise bending, and torsional equations are derived including third-degree geometric nonlinear elastic terms by making use of the geometric nonlinear theory of elasticity in which the elongations and shears are negligible compared to unity. These equations are specialized for blades of doubly symmetric cross section with linear variation of Pretwist over the blade length. The nonlinear steady state equations and the linearized perturbation equations are solved by using the Galerkin method, and by utilizing the nonrotating normal modes for the shape functions. Parametric results obtained for various cases of rotating blades from the present theoretical formulation are compared to those produced from the finite element code MSC/NASTRAN, and also to those produced from an in-house experimental test rig. It is shown that the spurious instabilities, observed for thin, rotating blades when second degree geometric nonlinearities are used, can be eliminated by including the third-degree elastic nonlinear terms. Furthermore, inclusion of third degree terms improves the correlation between the theory and experiment. M.G.

A87-46249*# National Aeronautics and Space Administration. Lewis Research Center, Cleveland, Ohio.

AEROELASTIC CONTROL OF STABILITY AND FORCED RESPONSE OF SUPERSONIC ROTORS BY AERODYNAMIC DETUNING

DANIEL HOYNIK (NASA, Lewis Research Center, Cleveland, OH) and SANFORD FLEETER (Purdue University, West Lafayette, IN) IN: International Symposium on Air Breathing Engines, 8th, Cincinnati, OH, June 14-19, 1987, Proceedings. New York, American Institute of Aeronautics and Astronautics, 1987, p. 646-658. refs

Aerodynamic detuning, defined as designed passage-to-pass-age differences in the unsteady aerodynamic flow field of a rotor blade row, is a new approach to passive flutter and forced response control. In this paper, a mathematical model for aerodynamic detuning is developed and utilized to demonstrate the aeroelastic stability enhancement due to aerodynamic detuning of supersonic blade rows. In particular, a model is developed to analyze both the torsion mode and the coupled bending-torsion mode unstalled supersonic flutter and torsion mode aerodynamically forced response characteristics of an aerodynamically detuned rotor operating in a supersonic inlet flow field with a subsonic leading edge locus. As small solidity variations do not have a dominant effect on the steady-state performance of a rotor, the aerodynamic detuning mechanism considered is nonuniform circumferential spacing of adjacent blades. Author

A87-47081*# Garrett Turbine Engine Co., Phoenix, Ariz.

ADVANCED TECHNOLOGY PAYOFFS FOR FUTURE SMALL PROPULSION SYSTEMS

M. A. TURK and P. K. ZEINER (Garrett Turbine Engine Co., Phoenix, AZ) Journal of Propulsion and Power (ISSN 0748-4658), vol. 3, July-Aug. 1987, p. 313-319. Army-supported research. Previously cited in issue 20, p. 2918, Accession no. A86-42704. (Contract NAS3-24544)

07 AIRCRAFT PROPULSION AND POWER

A87-48571*# National Aeronautics and Space Administration. Lewis Research Center, Cleveland, Ohio.

SUPERSONIC THROUGH-FLOW FAN DESIGN

JAMES F. SCHMIDT, ROYCE D. MOORE, JERRY R. WOOD, and RONALD J. STEINKE (NASA, Lewis Research Center, Cleveland, OH) AIAA, SAE, ASME, and ASEE, Joint Propulsion Conference, 23rd, San Diego, CA, June 20-July 2, 1987. 21 p. Previously announced in STAR as N87-22681. refs (AIAA PAPER 87-1746)

The NASA Lewis Research Center has embarked on a program to experimentally prove the concept of a supersonic through-flow fan which is to maintain supersonic velocities throughout the compression system with only weak shock-wave flow losses. The detailed design of a supersonic through-flow fan and estimated off-design performance with the use of advanced computational codes are described. A multistage compressor facility is being modified for the newly designed supersonic through-flow fan and the major aspects of this modification are briefly described.

Author

A87-48766* John Deere Technologies International, Inc., Wood-Ridge, N.J.

ADVANCED LIQUID-COOLED, TURBOCHARGED AND INTERCOOLED STRATIFIED CHARGE ROTARY ENGINES FOR AIRCRAFT

ROBERT E. MOUNT, JOHN BARTEL (John Deere Technologies International, Inc., Wood Ridge, NJ), and WILLIAM F. HADY (NASA, Lewis Research Center, Cleveland, OH) SAE, General Aviation Aircraft Meeting and Exposition, Wichita, KS, Apr. 28-30, 1987. 16 p. refs (SAE PAPER 871039)

Developments concerning stratified-charge rotary (SCR) engines over the past 10 years are reviewed. Aircraft engines being developed using SCR technology are shown and described, and the ability of such technology to meet general aviation engine needs is considered. Production timing and availability of SCR technology for the development of aviation rotary engines are discussed, and continuing efforts toward improving this technology, including NASA efforts, are described. C.D.

A87-50188*# National Aeronautics and Space Administration. Lewis Research Center, Cleveland, Ohio.

PERFORMANCE OF TWO 10-LB/SEC CENTRIFUGAL COMPRESSORS WITH DIFFERENT BLADE AND SHROUD THICKNESSES OPERATING OVER A RANGE OF REYNOLDS NUMBERS

GARY J. SKOCH (NASA, Lewis Research Center; U.S. Army Propulsion Directorate, Cleveland, OH) and ROYCE D. MOORE (NASA, Lewis Research Center, Cleveland, OH) AIAA, SAE, ASME, and ASEE, Joint Propulsion Conference, 23rd, San Diego, CA, June 29-July 2, 1987. 25 p. Previously announced in STAR as N87-23623. refs (AIAA PAPER 87-1745)

Centrifugal compressors often cannot be directly scaled to very small flow sizes because of structural and manufacturing limitations. The inability to directly scale all design parameters leads to a performance loss other than that which can be associated with the lower Reynolds number. A 10-lb/sec centrifugal compressor was scaled down to 2-lb/sec where adjustments to blade and shroud thickness and fillet radii were required. The modified 2-lb/sec compressor was then directly scaled back up to 10 lb/sec so that the effect of the modifications could be determined. The performance of the two 10-lb/sec compressors is compared over a range of speed and mass flow. The effect of variations in Reynolds number, impeller tip clearance, and shroud thickness on compressor performance is also presented. Author

A87-50189*# National Aeronautics and Space Administration. Lewis Research Center, Cleveland, Ohio.

LINER COOLING RESEARCH AT NASA LEWIS RESEARCH CENTER

WALDO A. ACOSTA (NASA, Lewis Research Center; U.S. Army, Propulsion Directorate, Cleveland, OH) AIAA, SAE, ASME, and ASEE, Joint Propulsion Conference, 23rd, San Diego, CA, June 29-July 2, 1987. 18 p. Previously announced in STAR as N87-23624. refs (AIAA PAPER 87-1828)

Described are recently completed and current advanced liner research applicable to advanced small gas turbine engines. Research relating to the evolution of fuel efficient small gas turbine engines capable of meeting future commercial and military aviation needs is currently under way at NASA Lewis Research Center. As part of this research, a reverse-flow combustor geometry was maintained while different advanced liner wall cooling techniques were investigated and compared to a baseline combustor. The performance of the combustors featuring counterflow film-cooled (CFFC) panels, transpiration cooled liner walls (TRANS), and compliant metal/ceramic (CMC) walls was obtained over a range of simulated flight conditions of a 16:1 pressure ratio gas turbine engine and fuel/air ratios up to 0.034. All the combustors featured an identical fuel injection system, identical geometric configuration outline, and similar designed internal aerothermodynamics.

Author

A87-50196*# National Aeronautics and Space Administration. Lewis Research Center, Cleveland, Ohio.

THE SUPERSONIC THROUGH-FLOW TURBOFAN FOR HIGH MACH PROPULSION

LEO C. FRANCISCUS (NASA, Lewis Research Center, Cleveland, OH) AIAA, SAE, ASME, and ASEE, Joint Propulsion Conference, 23rd, San Diego, CA, June 29-July 2, 1987. 14 p. Previously announced in STAR as N87-23626. refs (AIAA PAPER 87-2050)

A study was done to evaluate the potential improvements in aircraft turbine engine performance by incorporating unique supersonic through-flow fans. Engine performance, weight, and mission studies were carried out for conventional turbofan engines using supersonic through-flow fans. A Mach 3 commercial transport mission was considered. The advantages of the supersonic fan engines were evaluated in terms of mission range comparisons between the supersonic fan engines and conventional engines. The installed specific fuel consumption of the supersonic fan engines was 12 percent better than the conventional engines and the installed weight was projected to be 25 percent lighter. For a takeoff gross weight of 550,000 lbs, the aircraft powered by supersonic fan engines had a range capability of 6600 nm compared to 5300 nm (a 25 percent improvement) for conventional engines. Author

A87-50422*# National Aeronautics and Space Administration. Lewis Research Center, Cleveland, Ohio.

FULL-SCALE ENGINE DEMONSTRATION OF AN ADVANCED SENSOR FAILURE DETECTION ISOLATION, AND ACCOMMODATION ALGORITHM - PRELIMINARY RESULTS

WALTER C. MERRILL, JOHN C. DELAAT, STEVEN M. KROSZKEWICZ, and MAHMOOD ABDELWAHAB (NASA, Lewis Research Center, Cleveland, OH) IN: AIAA Guidance, Navigation and Control Conference, Monterey, CA, Aug. 17-19, 1987, Technical Papers. Volume 1. New York, American Institute of Aeronautics and Astronautics, 1987, p. 183-191. Previously announced in STAR as N87-22097. refs (AIAA PAPER 87-2259)

The objective of the advanced detection, isolation, and accommodation (ADIA) program is to improve the overall demonstrated reliability of digital electronic control systems for turbine engines. For this purpose, algorithms were developed which detect, isolate, and accommodate sensor failures using analytical redundancy. Preliminary results of a full scale engine demonstration of the ADIA algorithm are presented. Minimum detectable levels of sensor failures for an F100 turbofan engine control system are

determined and compared to those obtained during a previous evaluation of this algorithm using a real-time hybrid computer simulation of the engine. Author

A87-52245*# Lockheed-Georgia Co., Marietta.

STATIC TESTS OF THE PROPULSION SYSTEM

C. C. WITHERS, H. W. BARTEL (Lockheed-Georgia Co., Marietta), J. E. TURNBERG (United Technologies Corp., Hamilton Standard Div., Windsor Locks, CT), and E. J. GRABER (NASA, Lewis Research Center, Cleveland, OH) AIAA, SAE, ASME, and ASEE, Joint Propulsion Conference, 23rd, San Diego, CA, June 29-July 2, 1987, 12 p.

(Contract NAS3-24339)

(AIAA PAPER 87-1728)

Advanced, highly-loaded, high-speed propellers, called propfans, are promising to revolutionize the transport aircraft industry by offering a 15- to 30-percent fuel savings over the most advanced turbofans without sacrificing passenger comfort or violating community noise standards. NASA Lewis Research Center and industry have been working jointly to develop the needed propfan technology. The NASA-funded Propfan Test Assessment (PTA) Program represents a key element of this joint program. In PTA, Lockheed-Georgia, working in concert with Hamilton Standard, Rohr Industries, Gulfstream Aerospace, and Allison, is developing a propfan propulsion system which will be mounted on the left wing of a modified Gulfstream GII aircraft and flight tested to verify the in-flight characteristics of a 9-foot diameter, single-rotation propfan. The propfan, called SR-7L, was designed and fabricated by Hamilton Standard under a separate NASA contract. Prior to flight testing, the PTA propulsion system was static tested at the Rohr Brown Field facility. In this test, propulsion system operational capability was verified and data was obtained on propfan structural response, system acoustic characteristics, and system performance. This paper reports on the results of the static tests. Author

A87-52246*# General Electric Co., Evendale, Ohio.

A VARIABLE GEOMETRY COMBUSTOR FOR BROADENED PROPERTIES FUELS

W. J. DODDS (General Electric Co., Aircraft Engine Business Group, Evendale, OH) and J. S. FEAR (NASA, Lewis Research Center, Cleveland, OH) AIAA, SAE, ASME, and ASEE, Joint Propulsion Conference, 23rd, San Diego, CA, June 29-July 2, 1987, 9 p. refs

(AIAA PAPER 87-1832)

A program was conducted to design and develop a variable geometry combustor, sized for the cycle and envelope of a large commercial turbofan engine. The combustor uses a variable area swirl cup to control stoichiometry in the primary combustion zone. Potential advantages of this design include improved capability to burn non-standard fuels, short system length, and increased operating temperature range for advanced high performance engine cycles. After considerable development, key program emissions and performance goals were met with the variable geometry combustor. Primary development efforts were to evolve improved variable swirl cup configurations. In particular, air leakage through the variable area swirl cup had a strong effect on low power emissions and performance, while smoke level at high power was affected by features for improved mixing of the fuel and swirler air flow. Additional design and development is still needed to evolve a practical variable geometry combustor. Author

A87-53428* National Aeronautics and Space Administration. Lewis Research Center, Cleveland, Ohio.

COMPOUND CYCLE ENGINE PROGRAM

G. A. BOBULA (NASA, Lewis Research Center; U.S. Army, Army Aviation Research and Technology Activity, Cleveland, OH), W. T. WINTUCKY (NASA, Lewis Research Center, Cleveland, OH), and J. G. CASTOR (Garrett Turbine Engine Co., Phoenix, AZ) IN: Specialists' Meeting on Rotary Wing Propulsion Systems, Williamsburg, VA, Nov. 12-14, 1986, Technical Papers. Alexandria, VA, American Helicopter Society, 1987, 22 p. Previously announced in STAR as N87-11790. refs

The Compound Cycle Engine (CCE) is a highly turbocharged, power compounded power plant which combines the lightweight pressure rise capability of a gas turbine with the high efficiency of a diesel. When optimized for a rotorcraft, the CCE will reduce fuel burn for a typical 2 hr (plus 30 min reserve) mission by 30 to 40 percent when compared to a conventional advanced technology gas turbine. The CCE can provide a 50 percent increase in range-payload product on this mission. A program to establish the technology base for a Compound Cycle Engine is presented. The goal of this program is to research and develop those technologies which are barriers to demonstrating a multicylinder diesel core in the early 1990's. The major activity underway is a three-phased contract with the Garrett Turbine Engine Company to perform: (1) a light helicopter feasibility study, (2) component technology development, and (3) lubricant and material research and development. Other related activities are also presented. Author

N87-10100*# National Aeronautics and Space Administration. Lewis Research Center, Cleveland, Ohio.

RESPONSE OF A SMALL-TURBOSHAFT-ENGINE COMPRESSION SYSTEM TO INLET TEMPERATURE DISTORTION

T. J. BIESADNY, G. A. KLANN (Army Research and Technology Labs., Cleveland, Ohio.), and J. K. LITTLE Sep. 1984 28 p (NASA-TM-83765; E-2198; NAS 1.26:83765; USAVSCOM-TR-84-C-13) Avail: NTIS HC A03/MF A01 CSCL 21E

An experimental investigation was conducted into the response of a small-turboshaft-engine compression system to steady-state and transient inlet temperature distortions. Transient temperature ramps range from less than 100 K/sec to above 610 K/sec and generated instantaneous temperatures to 420 K above ambient. Steady-state temperature distortion levels were limited by the engine hardware temperature list. Simple analysis of the steady-state distortion data indicated that a particle separator at the engine inlet permitted higher levels of temperature distortion before onset of compressor surge than would be expected without the separator. Author

N87-10866*# Lockheed-Georgia Co., Marietta.

PTA TEST BED AIRCRAFT ENGINE INLET MODEL TEST REPORT, REVISED

J. P. HANCOCK May 1985 81 p

(Contract NAS3-24339)

(NASA-CR-174845; NAS 1.26:174845; LG85ER0012-REV) Avail: NTIS HC A05/MF A01 CSCL 21E

The inlet duct test for the Propfan Testbed Assessment (PTA) program was completed in November 1984. The basic test duct was designed using the Lockheed QUADPAN computational code. Test objectives were to experimentally evaluate, modify as required, and eventually verify satisfactory performance as well as duct/engine compatibility. Measured total pressure recovery for the basic duct was 0.993 with no swirl and 0.989 for inflow with a 30 degree simulated swirl angle. This compared to a predicted recovery of 0.979 with no swirl. Measured circumferential distortion with swirl, based on a least-square curve fit of the data, was 0.204 compared to a maximum allowable value of 0.550. Other measured distortion parameters did as well or better relative to their respective maximum allowable values. The basic duct configuration with no refinements is recommended for the PTA inlet as a minimum cost installation. Author

07 AIRCRAFT PROPULSION AND POWER

N87-11191*# Yale Univ., New Haven, Conn. High Temperature Chemical Reaction Engineering Lab.

TURBINE AIRFOIL DEPOSITION MODELS

D. E. ROSNER /in NASA. Lewis Research Center Turbine Engine Hot Section Technology, 1984 22 p Oct. 1984

(Contract NAG3-201)

Avail: NTIS HC A17/MF A01 CSCL 21E

Gas turbine failures associated with sea-salt ingestion and sulfur-containing fuel impurities have directed attention to alkali sulfate deposition and the associated hot corrosion of gas turbine (GT) blades under some GT operating conditions. These salt deposits form thin, molten films which undermine the protective metal oxide coating normally found on GT blades. The prediction of molten salt deposition, flow and oxide dissolution, and their effects on the lifetime of turbine blades are examined. Goals include rationalizing and helping to predict corrosion patterns on operational GT rotor blades and stators, and ultimately providing some of the tools required to design laboratory simulators and future corrosion-resistant high-performance engines. Necessary background developments are reviewed first, and then recent results and tentative conclusions are presented along with a brief account of the present research plans. Author

N87-11196*# Cleveland State Univ., Ohio.

MECHANICAL BEHAVIOR OF THERMAL BARRIER COATINGS FOR GAS TURBINE BLADES

C. C. BERNDT, W. PHUCHAROEN, and G. C. CHANG /in NASA. Lewis Research Center Turbine Engine Hot Section Technology, 1984 12 p Oct. 1984

(Contract NCC3-27)

Avail: NTIS HC A17/MF A01 CSCL 21E

Plasma-sprayed thermal barrier coatings (TBCs) will enable turbine components to operate at higher temperatures and lower cooling gas flow rates; thereby improving their efficiency. Future developments are limited by precise knowledge of the material properties and failure mechanisms of the coating system. Details of this nature are needed for realistic modeling of the coating system which will, in turn, promote advancements in coating technology. Complementary experiments and analytical modeling which were undertaken in order to define and measure the important failure processes for plasma-sprayed coatings are presented. The experimental portion includes two different tests which were developed to measure coating properties. These are termed tensile adhesion and acoustic emission tests. The analytical modeling section details a finite element method which was used to calculate the stress distribution in the coating system. Some preliminary results are presented. Author

N87-11200*# National Aeronautics and Space Administration. Lewis Research Center, Cleveland, Ohio.

AEROTHERMAL MODELING PROGRAM, PHASE 2

E. J. MULARZ /in its Turbine Engine Hot Section Technology, 1984 4 p Oct. 1984

Avail: NTIS HC A17/MF A01 CSCL 21E

The accuracy and utility of current aerothermal models for gas turbine combustors must be improved. Three areas of concern are identified: improved numerical methods for turbulent viscous recirculating flows; flow interaction; and fuel injector-air swirl characterization. Progress in each area is summarized. B.G.

N87-11731*# National Aeronautics and Space Administration. Lewis Research Center, Cleveland, Ohio.

STAEBL: STRUCTURAL TAILORING OF ENGINE BLADES, PHASE 2

M. S. HIRSCHBEIN and K. W. BROWN (Pratt and Whitney Aircraft, East Hartford, Conn.) /in NASA. Langley Research Center Recent Experiences in Multidisciplinary Analysis and Optimization, Part 1 13 p 1984

Avail: NTIS HC A22/MF A01 CSCL 21E

The Structural Tailoring of Engine Blades (STAEBL) program was initiated at NASA Lewis Research Center in 1980 to introduce optimal structural tailoring into the design process for aircraft gas turbine engine blades. The standard procedure for blade design

is highly iterative with the engineer directly providing most of the decisions that control the design process. The goal of the STAEBL program has been to develop an automated approach to generate structurally optimal blade designs. The program has evolved as a three-phase effort with the developmental work being performed contractually by Pratt & Whitney Aircraft. Phase 1 was intended as a proof of concept in which two fan blades were structurally tailored to meet a full set of structural design constraints while minimizing DOC+I (direct operating cost plus interest) for a representative aircraft. This phase was successfully completed and was reported in reference 1 and 2. Phase 2 has recently been completed and is the basis for this discussion. During this phase, three tasks were accomplished: (1) a nonproprietary structural tailoring computer code was developed; (2) a dedicated approximate finite-element analysis was developed; and (3) an approximate large-deflection analysis was developed to assess local foreign object damage. Phase 3 is just beginning and is designed to incorporate aerodynamic analyses directly into the structural tailoring system in order to relax current geometric constraints. Author

N87-11732*# Virginia Polytechnic Inst. and State Univ., Blacksburg. Dept. of Aerospace and Ocean Engineering.

OPTIMIZATION OF CASCADE BLADE MISTUNING UNDER FLUTTER AND FORCED RESPONSE CONSTRAINTS

D. V. MURTHY and R. T. HAFTKA /in NASA. Langley Research Center Recent Experiences in Multidisciplinary Analysis and Optimization, Part 1 15 p 1984

(Contract NAG3-347)

Avail: NTIS HC A22/MF A01 CSCL 21E

In the development of modern turbomachinery, problems of flutter instabilities and excessive forced response of a cascade of blades that were encountered have often turned out to be extremely difficult to eliminate. The study of these instabilities and the forced response is complicated by the presence of mistuning; that is, small differences among the individual blades. The theory of mistuned cascade behavior shows that mistuning can have a beneficial effect on the stability of the rotor. This beneficial effect is produced by the coupling between the more stable and less stable flutter modes introduced by mistuning. The effect of mistuning on the forced response can be either beneficial or adverse. Kaza and Kielb have studied the effects of two types of mistuning on the flutter and forced response: alternate mistuning where alternate blades are identical and random mistuning. The objective is to investigate other patterns of mistuning which maximize the beneficial effects on the flutter and forced response of the cascade. Numerical optimization techniques are employed to obtain optimal mistuning patterns. The optimization program seeks to minimize the amount of mistuning required to satisfy constraints on flutter speed and forced response. Author

N87-11769*# Michigan Univ., Ann Arbor.

ON OPTIMAL DESIGN FOR THE BLADE-ROOT/HUB INTERFACE IN JET ENGINES

N. KIKUCHI and J. E. TAYLOR /in NASA. Langley Research Center Recent Experiences in Multidisciplinary Analysis and Optimization, Part 2 14 p 1984

(Contract NAG3-388)

Avail: NTIS HC A22/MF A01 CSCL 21E

Two major problems identified with the design of the blade-root/hub interface are discussed. The first is the so-called friction contact problem which has two special features: unilateral contact and Coulomb's friction. One of the difficulties in this problem is that the portions of contact and sticking/sliding surfaces are not known a priori. The second is the shape optimization problem which is characterized either by the minimization of the maximum contact pressure or by the minimization of the equivalent stress on the boundary. Design variables are the shapes of the blade-root and the hub. It is noted that friction contact and shape optimization problems are strongly coupled in the present design problem. Author

N87-11788*# Transmission Research, Inc., Cleveland, Ohio.
THE 3600 HP SPLIT-TORQUE HELICOPTER TRANSMISSION
 G. WHITE 18 Dec. 1985 95 p
 (Contract NAS3-23931)
 (NASA-CR-174932; NAS 1.26:174932) Avail: NTIS HC A05/MF
 A01 CSCL 21E

Final design details of a helicopter transmission that is powered by GE twin T 700 engines each rated at 1800 hp are presented. It is demonstrated that in comparison with conventional helicopter transmission arrangements the split torque design offers: weight reduction of 15%; reduction in drive train losses of 9%; and improved reliability resulting from redundant drive paths between the two engines and the main shaft. The transmission fits within the NASA LeRC 3000 hp Test Stand and accepts the existing positions for engine inputs, main shaft, connecting drive shafts, and the cradle attachment points. One necessary change to the test stand involved gear trains of different ratio in the tail drive gearbox. Progressive uprating of engine input power from 3600 to 4500 hp twin engine rating is allowed for in the design. In this way the test transmission will provide a base for several years of analytical, research, and component development effort targeted at improving the performance and reliability of helicopter transmission. Author

N87-11789*# Solar Turbines International, San Diego, Calif.
FABRICATION OF COOLED RADIAL TURBINE ROTOR Final Report
 A. N. HAMMER, G. G. AIGRET, T. P. PSICHOGIOS, and C. RODGERS Jun. 1986 258 p
 (Contract NAS3-22513; DA PROJ. 1L1-612209-AH-76)
 (NASA-CR-179503; NAS 1.26:179503; SR86-R-4938-39) Avail:
 NTIS HC A12/MF A01 CSCL 21E

A design and fabrication program was conducted to evaluate a unique concept for constructing a cooled, high temperature radial turbine rotor. This concept, called split blade fabrication was developed as an alternative to internal ceramic coring. In this technique, the internal cooling cavity is created without flow dividers or any other detail by a solid (and therefore stronger) ceramic plate which can be more firmly anchored within the casting shell mold than can conventional detailed ceramic cores. Casting is conducted in the conventional manner, except that the finished product, instead of having finished internal cooling passages, is now a split blade. The internal details of the blade are created separately together with a carrier sheet. The inserts are superalloy. Both are produced by essentially the same software such that they are a net fit. The carrier assemblies are loaded into the split blade and the edges sealed by welding. The entire wheel is Hot Isostatic Pressed (HIPed), braze bonding the internal details to the inside of the blades. During this program, two wheels were successfully produced by the split blade fabrication technique. Author

N87-11790*# National Aeronautics and Space Administration.
 Lewis Research Center, Cleveland, Ohio.
COMPOUND CYCLE ENGINE PROGRAM
 G. A. BOBULA, W. T. WINTUCKY, and J. G. CASTOR (Garrett Turbine Engine Co., Phoenix, Ariz.) 1986 23 p Presented at the Rotary Wing Propulsion System Specialist Meeting, Williamsburg, Va., 12-14 Nov. 1986; sponsored by the American Helicopter Society
 (Contract DA PROJ. 1L1-62209-AH-76)
 (NASA-TM-88879; E-3286; NAS 1.26:88879;
 USAVSCOM-TR-86-C-37) Avail: NTIS HC A02/MF A01 CSCL 21E

The Compound Cycle Engine (CCE) is a highly turbocharged, power compounded power plant which combines the lightweight pressure rise capability of a gas turbine with the high efficiency of a diesel. When optimized for a rotorcraft, the CCE will reduce fuel burned for a typical 2 hr (plus 30 min reserve) mission by 30 to 40 percent when compared to a conventional advanced technology gas turbine. The CCE can provide a 50 percent increase in range-payload product on this mission. A program to establish the technology base for a Compound Cycle Engine is presented. The

goal of this program is to research and develop those technologies which are barriers to demonstrating a multicylinder diesel core in the early 1990's. The major activity underway is a three-phased contract with the Garrett Turbine Engine Company to perform: (1) a light helicopter feasibility study, (2) component technology development, and (3) lubricant and material research and development. Other related activities are also presented. Author

N87-13441*# Pennsylvania State Univ., State College.
THE MEASUREMENT OF BOUNDARY LAYERS ON A COMPRESSOR BLADE IN CASCADE AT HIGH POSITIVE INCIDENCE ANGLE. 1: EXPERIMENTAL TECHNIQUES AND RESULTS Interim Report
 S. DEUTSCH and W. C. ZIERKE Aug. 1986 65 p
 (Contract NSG-3264)
 (NASA-CR-179491; NAS 1.26:179491) Avail: NTIS HC A04/MF
 A01 CSCL 21E

Measurements of the mean velocity and turbulence intensity were made using a one-component laser Doppler velocimeter in the boundary layer and near wake about a double circular arc, compressor blade in cascade. The measurements were made at a chord Reynolds number of 500,000. Boundary layer measurements on the pressure surface indicate a transition region over the last 40% of the chord. A small separation bubble near the leading edge of the suction surface results in an immediate transition from laminar to turbulent flow. The non-equilibrium turbulent boundary layer separates near the trailing edge of the suction surface. Similarity of the outer region of the turbulent boundary layer ceases to exist in the separated region. Also, similarity does not hold in the near-wake region, a region which includes negative mean velocities because of the separation near the trailing edge on the suction surface. Author

N87-13442*# Pennsylvania State Univ., State College.
THE MEASUREMENT OF BOUNDARY LAYERS ON A COMPRESSOR BLADE IN CASCADE AT HIGH POSITIVE INCIDENCE ANGLE. 2: DATA REPORT Interim Report
 S. DEUTSCH and W. C. ZIERKE Aug. 1986 113 p
 (Contract NSG-3264)
 (NASA-CR-179492; NAS 1.26:179492) Avail: NTIS HC A06/MF
 A01 CSCL 21E

Boundary layer and near-wake velocity measurements have been made in the well documented flow field about a double circular arc compressor blade in cascade, at an incidence angle of 5 deg. and a chord Reynolds number of 500,000. In Part 2 of this report these measurements were analyzed and presented in standard graphical format. The flow geometry, measurement techniques, and physics of the flow field were also discussed. In this, part 2 of the report, raw and analyzed data are presented in tabulated form in an attempt to make this data more accessible to computational comparison. Also included in part 2 is a description of the data analysis employed. A computer tape containing the data is available. Author

N87-13443*# ISTAR, Inc., Santa Monica, Calif.
DETONATION WAVE COMPRESSION IN GAS TURBINES Final Contractor Report
 A. WORTMAN Dec. 1986 77 p
 (Contract NAS3-24854)
 (NASA-CR-179557; NAS 1.26:179557) Avail: NTIS HC A05/MF
 A01 CSCL 81D

A study was made of the concept of augmenting the performance of low pressure ratio gas turbines by detonation wave compression of part of the flow. The concept exploits the constant volume heat release of detonation waves to increase the efficiency of the Brayton cycle. In the models studied, a fraction of the compressor output was channeled into detonation ducts where it was processed by transient transverse detonation waves. Gas dynamic studies determined the maximum cycling frequency of detonation ducts, proved that upstream propagation of pressure pulses represented no problems and determined the variations of detonation duct output with time. Mixing and wave compression were used to recombine the combustor and detonation duct flows

and a concept for a spiral collector to further smooth the pressure and temperature pulses was presented as an optional component. The best performance was obtained with a single firing of the ducts so that the flow could be re-established before the next detonation was initiated. At the optimum conditions of maximum frequency of the detonation ducts, the gas turbine efficiency was found to be 45 percent while that of a corresponding pressure ratio 5 conventional gas turbine was only 26%. Comparable improvements in specific fuel consumption data were found for gas turbines operating as jet engines, turbofans, and shaft output machines. Direct use of the detonation duct output for jet propulsion proved unsatisfactory. Careful analysis of the models of the fluid flow phenomena led to the conclusion that even more elaborate calculations would not diminish the uncertainties in the analysis of the system. Feasibility of the concept to work as an engine now requires validation in an engineering laboratory experiment.

Author

N87-14348*# Sverdrup Technology, Inc., Cleveland, Ohio.
EFFECTS OF DROPLET INTERACTIONS ON DROPLET TRANSPORT AT INTERMEDIATE REYNOLDS NUMBERS Final Contractor Report

J. S. SHUEN Dec. 1986 20 p Presented at the 25th Aerospace Sciences Meeting, Reno, Nev., 12-15 Jan. 1987; sponsored by AIAA

(Contract NAS3-24105)

(NASA-CR-179567; E-3293; NAS 1.26:179567; AIAA-87-0137)

Avail: NTIS HC A02/MF A01 CSCL 21B

Effects of droplet interactions on drag, evaporation, and combustion of a planar droplet array, oriented perpendicular to the approaching flow, are studied numerically. The three-dimensional Navier-Stokes equations, with variable thermophysical properties, are solved using finite-difference techniques. Parameters investigated include the droplet spacing, droplet Reynolds number, approaching stream oxygen concentration, and fuel type. Results are obtained for the Reynolds number range of 5 to 100, droplet spacing from 2 to 24 diameters, oxygen concentrations of 0.1 and 0.2, and methanol and n-butanol fuels. The calculations show that the gasification rates of interacting droplets decrease as the droplet spacings decrease. The reduction in gasification rates is significant only at small spacings and low Reynolds numbers. For the present array orientation, the effects of interactions on the gasification rates diminish rapidly for Reynolds numbers greater than 10 and spacings greater than 6 droplet diameters. The effects of adjacent droplets on drag are shown to be small.

Author

N87-14349*# Garrett Turbine Engine Co., Phoenix, Ariz.
SCALED CENTRIFUGAL COMPRESSOR PROGRAM Final Report

G. CARGILL and C. LINDER 31 Oct. 1986 202 p

(Contract NAS3-23277; DA PROJ. 1L1-62209-AH-76)

(NASA-CR-174912; NAS 1.26:174912; USAVSCOM-TR-85-C-13; GARRETT-21-5464) Avail: NTIS HC A10/MF A01 CSCL 21E

Centrifugal compressors were provided to be used to evaluate the effects of direct scaling, and establishing the methodology for design adjustment when direct scaling is not mechanically feasible. These objectives were accomplished by the following approaches: (1) scaling an existing high-performance centrifugal compressor from 10-lb/sec to 2-lb/sec flow size; (2) making the necessary adjustments to the 2-lb/sec flow size compressor to make it mechanically acceptable; (3) directly scaling the final 2-lb/sec flow size compressor to 10-lb/sec flow size; and (4) fabricating the resulting 10-lb/sec and 2-lb/sec flow size compressors for testing in the NASA-Lewis Compressor Facilities.

Author

N87-16825*# National Aeronautics and Space Administration. Lewis Research Center, Cleveland, Ohio.

OUTDOOR TEST STAND PERFORMANCE OF A CONVERTIBLE ENGINE WITH VARIABLE INLET GUIDE VANES FOR ADVANCED ROTORCRAFT PROPULSION

JACK G. MCARDLE Dec. 1986 25 p Prepared for presentation at the 1987 Rotorcraft Technology Conference, Moffett Field, Calif., 17-19 Mar. 1987; sponsored in part by NASA and Army (NASA-TM-88939; E-3384; NAS 1.15:88939) Avail: NTIS HC A02/MF A01 CSCL 21E

A variable inlet guide van (VIGV) type convertible engine that could be used to power future high-speed rotorcraft was tested on an outdoor stand. The engine ran stably and smoothly in the turbofan, turboshaft, and dual (combined fan and shaft) power modes. In the turbofan mode with the VIGV open fuel consumption was comparable to that of a conventional turbofan engine. In the turboshaft mode with the VIGV closed fuel consumption was higher than that of present turboshaft engines because power was wasted in churning fan-tip airflow. In dynamic performance tests with a specially built digital engine control and using a waterbrake dynamometer for shaft load, the engine responded effectively to large steps in thrust command and shaft torque. Previous mission analyses of a conceptual X-wing rotorcraft capable of 400-knot cruise speed were revised to account for more fan-tip churning power loss than was originally estimated. The new calculations confirm that using convertible engines rather than separate lift and cruise engines would result in a smaller, lighter craft with lower fuel use and direct operating cost.

Author

N87-16826*# National Aeronautics and Space Administration. Lewis Research Center, Cleveland, Ohio.

PARTICLE-LADEN SWIRLING FREE JETS: MEASUREMENTS AND PREDICTIONS

D. L. BULZAN, J.-S. SHUEN (Sverdrup Technology, Inc., Cleveland, Ohio), and G. M. FAETH (Michigan Univ., Dearborn) 1987 29 p Presented at the 25th Aerospace Sciences Meeting, Reno, Nev., 12-15 Jan. 1987; sponsored by AIAA (NASA-TM-88904; E-3307; NAS 1.15:88904; AIAA-87-0303)

Avail: NTIS HC A03/MF A01 CSCL 21E

A theoretical and experimental investigation of single-phase and particle-laden weakly swirling jets was conducted. The jets were injected vertically downward from a 19 mm diameter tube with swirl numbers ranging from 0 to 0.33. The particle-laden jets had a single loading ratio (0.2) with particles having a SMD of 39 microns. Mean and fluctuating properties of both phases were measured using nonintrusive laser based methods while particle mass flux was measured using an isokinetic sampling probe. The continuous phase was analyzed using both a baseline kappa-epsilon turbulence model and an extended version with modifications based on the flux Richardson number to account for effects of streamline curvature. To highlight effects of interphase transport rates and particle/turbulence interactions, effects of the particles were analyzed as follows: (1) locally homogeneous flow (LHF) analysis, where interphase transport rates are assumed to be infinitely fast; (2) deterministic separated flow (DSF) analysis, where finite interphase transport rates are considered but particle/turbulence interactions are ignored; and (3) stochastic separated flow (SSF) analysis, where both effects are considered using random-walk computations.

Author

N87-16827*# National Aeronautics and Space Administration. Lewis Research Center, Cleveland, Ohio.

REPRESENTATION OF THE VAPORIZATION BEHAVIOR OF TURBULENT POLYDISPERSE SPRAYS BY EQUIVALENT MONODISPERSE SPRAYS

S. K. AGGARWAL and J. S. SHUEN (Sverdrup Technology, Inc., Cleveland, Ohio) Dec. 1986 16 p (NASA-TM-88906; E-3300; NAS 1.15:88906) Avail: NTIS HC A02/MF A01 CSCL 21E

The concept of using an equivalent monodisperse spray to represent the vaporization behavior of polydisperse sprays has been examined by numerically solving two turbulent vaporizing sprays. One involves the injection of Freon-11 in a still environment,

whereas the other is a methanol spray in a still but hot environment. The use of three different mean sizes, namely, Sauter mean diameter, volume median diameter, and surface-area mean diameter, has been investigated. Results indicate a good degree of correlation between the polydisperse spray and its equivalent monodisperse sprays represented by the volume median diameter and the Sauter mean diameter, the former giving slightly better results. The surface-area mean diameter does not provide as good a correlation as the other two mean diameters. Author

N87-16830*# Garrett Turbine Engine Co., Phoenix, Ariz.
TRANSITION MIXING STUDY Final Report, Jul. 1984 - Sep. 1986

R. REYNOLDS and C. WHITE Oct. 1986 185 p
(Contract NAS3-24340)
(NASA-CR-175062; NAS 1.26:175062; GARRETT-21-5723)
Avail: NTIS HC A09/MF A01 CSCL 21E

A computer model capable of analyzing the flow field in the transition liner of small gas turbine engines is developed. A FORTRAN code has been assembled from existing codes and physical submodels and used to predict the flow in several test geometries which contain characteristics similar to transition liners, and for which experimental data was available. Comparisons between the predictions and measurements indicate that the code produces qualitative results but that the turbulence models, both K-E and algebraic Reynolds Stress, underestimate the cross-stream diffusion. The code has also been used to perform a numerical experiment to examine the effect of a variety of parameters on the mixing process in transition liners. Comparisons illustrate that geometries with significant curvature show a drift of the jet trajectory toward the convex wall and weaker wake region vortices and decreased penetration for jets located on the convex wall of the liner, when compared to jets located on concave walls. Also shown were the approximate equivalency of angled slots and round holes and a technique by which jet mixing correlations developed for rectangular channels can be used for can geometries. Author

N87-17699*# National Aeronautics and Space Administration.
Lewis Research Center, Cleveland, Ohio.

DESIGN OF 9.271-PRESSURE-RATIO 5-STAGE CORE COMPRESSOR AND OVERALL PERFORMANCE FOR FIRST 3 STAGES

RONALD J. STEINKE May 1986 35 p
(NASA-TP-2597; E-2589; NAS 1.60:2597) Avail: NTIS HC
A03/MF A01 CSCL 21E

Overall aerodynamic design information is given for all five stages of an axial flow core compressor (74A) having a 9.271 pressure ratio and 29.710 kg/sec flow. For the inlet stage group (first three stages), detailed blade element design information and experimental overall performance are given. At rotor 1 inlet tip speed was 430.291 m/sec, and hub to tip radius ratio was 0.488. A low number of blades per row was achieved by the use of low-aspect-ratio blading of moderate solidity. The high reaction stages have about equal energy addition. Radial energy varied to give constant total pressure at the rotor exit. The blade element profile and shock losses and the incidence and deviation angles were based on relevant experimental data. Blade shapes are mostly double circular arc. Analysis by a three-dimensional Euler code verified the experimentally measured high flow at design speed and IGV-stator setting angles. An optimization code gave an optimal IGV-stator reset schedule for higher measured efficiency at all speeds. Author

N87-17700*# National Aeronautics and Space Administration.
Lewis Research Center, Cleveland, Ohio.

SPECTRUM-MODULATING FIBER-OPTIC SENSORS FOR AIRCRAFT CONTROL SYSTEMS

GLENN BEHEIM and KLAUS FRITSCH (John Carroll Univ., Cleveland, Ohio) 1987 9 p Presented at the 1st International Military and Government Fiber-Optic and Communications Exposition, Washington, D.C., 18-19 Mar. 1987; sponsored by the Fiber-Optic Communications Association
(NASA-TM-88968; E-3436; NAS 1.15:88968) Avail: NTIS HC
A02/MF A01 CSCL 01D

A family of fiber-optic sensors for aircraft engine control systems is described. Each of these sensors uses a spectrum-modulation method to obtain an output which is largely independent of the fiber link transmissivity. A position encoder is described which uses a code plate to digitally modulate the sensor output spectrum. Also described are pressure and temperature sensors, each of which uses a Fabry-Perot cavity to modulate the sensor output spectrum as a continuous function of the measurand. A technique is described whereby a collection of these sensors may be effectively combined to perform a number of the measurements which are required by an aircraft-engine control system. Author

N87-17701*# National Aeronautics and Space Administration.
Lewis Research Center, Cleveland, Ohio.

EXPERIMENTAL EVALUATION OF A TRANSLATING NOZZLE SIDEWALL RADIAL TURBINE

RICHARD J. ROELKE and CASIMIR ROGO (Teledyne CAE, Toledo, Ohio) 1987 22 p Proposed for presentation at the 69th Symposium of the AGARD Propulsion and Energetics Panel on Technology for Advanced Aero Engine Components, Paris, France, 4-8 May 1987

(NASA-TM-88963; E-3419; NAS 1.15:88963) Avail: NTIS HC
A02/MF A01 CSCL 21E

Studies have shown that reduced specific fuel consumption of rotorcraft engines can be achieved with a variable capacity engine. A key component in such an engine in a high-work, high-temperature variable geometry gas generator turbine. An optimization study indicated that a radial turbine with a translating nozzle sidewall could produce high efficiency over a wide range of engine flows but substantiating data were not available. An experimental program with Teledyne CAE, Toledo, Ohio was undertaken to evaluate the moving sidewall concept. A variety of translating nozzle sidewall turbine configurations were evaluated. The effects of nozzle leakage and coolant flows were also investigated. Testing was done in warm air (121 C). The results of the contractual program were summarized. Author

N87-20267*# National Aeronautics and Space Administration.
Lewis Research Center, Cleveland, Ohio.

NASA-CHINESE AERONAUTICAL ESTABLISHMENT (CAE) SYMPOSIUM

1986 230 p Symposium held in Cleveland, Ohio, 23-27 Sep. 1985

(NASA-CP-2433; E-3033; NAS 1.55:2433) Avail: NTIS HC
A01/MF A01 CSCL 21E

Several topics relative to combustion research are discussed. A numerical study of combustion processes in afterburners; the modeling of turbulent, reactive flow; gas turbine research; modeling of dilution jet flow fields; and chemical shock tubes as tools for studying high-temperature chemical kinetics are among the topics covered.

N87-20280*# National Aeronautics and Space Administration. Lewis Research Center, Cleveland, Ohio.

CONTINGENCY POWER FOR SMALL TURBOSHAFT ENGINES USING WATER INJECTION INTO TURBINE COOLING AIR

THOMAS J. BIESIADNY, GARY A. KLANN, DAVID A. CLARK (Army Aviation Research and Development Command, Cleveland, Ohio.), and BRETT BERGER 1987 14 p Proposed for presentation at the 23rd Joint Propulsion Conference, San Diego, Calif., 29 Jun. - 2 Jul. 1987; sponsored by the AIAA, ASEE, ASME and SAE

(NASA-TM-89817; E-3462; NAS 1.15:89817; USAAVSCOM-TR-86-C-32; AIAA-87-1906) Avail: NTIS HC A02/MF A01 CSCL 21E

Because of one engine inoperative requirements, together with hot-gas reingestion and hot day, high altitude takeoff situations, power augmentation for multiengine rotorcraft has always been of critical interest. However, power augmentation using overtemperature at the turbine inlet will shorten turbine life unless a method of limiting thermal and mechanical stresses is found. A possible solution involves allowing the turbine inlet temperature to rise to augment power while injecting water into the turbine cooling air to limit hot-section metal temperatures. An experimental water injection device was installed in an engine and successfully tested. Although concern for unprotected subcomponents in the engine hot section prevented demonstration of the technique's maximum potential, it was still possible to demonstrate increases in power while maintaining nearly constant turbine rotor blade temperature.

Author

N87-20282*# National Aeronautics and Space Administration. Lewis Research Center, Cleveland, Ohio.

PERFORMANCE AND EFFICIENCY EVALUATION AND HEAT RELEASE STUDY OF AN OUTBOARD MARINE CORPORATION ROTARY COMBUSTION ENGINE

H. L. NGUYEN, H. E. ADDY, T. H. BOND, C. M. LEE, and K. S. CHUN Apr. 1987 24 p Presented at the International Congress and Exposition, Detroit, Mich., 23-27 Feb. 1987; sponsored by the Society of Automotive Engineers

(NASA-TM-89833; E-3488; NAS 1.15:89833) Avail: NTIS HC A02/MF A01 CSCL 21A

A computer simulation which models engine performance of the Direct Injection Stratified Charge (DISC) rotary engines was used to study the effect of variations in engine design and operating parameters on engine performance and efficiency of an experimental Outboard Marine Corporation (OMC) rotary combustion engine. Engine pressure data were used in a heat release analysis to study the effects of heat transfer, leakage, and crevice flows. Predicted engine data were compared with experimental test data over a range of engine speeds and loads. An examination of methods to improve the performance of the rotary engine using advanced heat engine concepts such as faster combustion, reduced leakage, and turbocharging is also presented.

Author

N87-20996*# Arizona State Univ., Tempe. Dept. of Mechanical and Aerospace Engineering.

ON THE MODELLING OF NON-REACTIVE AND REACTIVE TURBULENT COMBUSTOR FLOWS Final Report

MOHAMMAD NIKJOOY and RONALD M. C. SO Washington NASA Apr. 1987 282 p

(Contract NAG3-167; NAG3-260; N60530-85-C-0191) (NASA-CR-4041; E-3451; NAS 1.26:4041; CR-R86091) Avail: NTIS HC A13/MF A01 CSCL 21E

A study of non-reactive and reactive axisymmetric combustor flows with and without swirl is presented. Closure of the Reynolds equations is achieved by three models: kappa-epsilon, algebraic stress and Reynolds stress closure. Performance of two locally nonequilibrium and one equilibrium algebraic stress models is analyzed assuming four pressure strain models. A comparison is also made of the performance of a high and a low Reynolds number model for combustor flow calculations using Reynolds stress closures. Effects of diffusion and pressure-strain models on these closures are also investigated. Two models for the scalar

transport are presented. One employs the second-moment closure which solves the transport equations for the scalar fluxes, while the other solves the algebraic equations for the scalar fluxes. In addition, two cases of non-premixed and one case of premixed combustion are considered. Fast- and finite-rate chemistry models are applied to non-premixed combustion. Both show promise for application in gas turbine combustors. However, finite rate chemistry models need to be examined to establish a suitable coupling of the heat release effects on turbulence field and rate constants.

Author

N87-21929*# National Aeronautics and Space Administration. Lewis Research Center, Cleveland, Ohio.

SHOCK STRUCTURE MEASURED IN A TRANSONIC FAN USING LASER ANEMOMETRY

JERRY R. WOOD, ANTHONY J. STRAZISAR, and P. SUSAN SIMONYI (Sverdrup Technology, Inc., Middleburg Heights, Ohio.) In AGARD Transonic and Supersonic Phenomena in Turbomachines 14 p Mar. 1987

Avail: NTIS HC A16/MF A01 CSCL 21E

Shock structure measurements acquired in a low aspect ratio transonic fan rotor are presented and analyzed. The rotor aspect ratio is 1.56 and the design tip relative Mach number is 1.38. The rotor flowfield was surveyed at near maximum efficiency and near stall operating conditions. Intra-blade velocity measurements acquired with a laser fringe anemometer on blade-to-blade planes in the supersonic region from 10 to 60% span are presented. The three-dimensional shock surface determined from the velocity measurements is used to determine the shock surface normal Mach number in order to properly calculate the ideal shock jump conditions. The ideal jump conditions are calculated based upon the Mach numbers measured on a surface of revolution and based upon the normal Mach number to indicate the importance of accounting for shock three dimensionality in turbomachinery design. Comparison of the shock locations with those predicted by a 3-D Euler code showed very good agreement and indicated the usefulness of integrating computational and experimental work to enhance the understanding of the flow physics occurring in transonic turbomachinery passages.

Author

N87-21955*# Hamilton Standard, Windsor Locks, Conn. UNSTALLED FLUTTER STABILITY PREDICTIONS AND COMPARISONS TO TEST DATA FOR A COMPOSITE PROP-FAN MODEL Final Report

J. E. TURNBERG 15 Oct. 1986 50 p

(Contract NAS3-24088)

(NASA-CR-179512; NAS 1.26:179512; HSER-11056) Avail: NTIS HC A03/MF A01 CSCL 21E

The aeroelastic stability analyses for three graphite/epoxy composite Prop-Fan designs and post-test stability analysis for one of the designs, the SR-3C-X2 are presented. It was shown that Prop-Fan stability can be effectively analyzed using the F203 modal aeroelastic stability analysis developed at Hamilton Standard and that first mode torsion-bending coupling has a direct effect on blade stability. Positive first mode torsion-bending coupling is a destabilizing factor and the minimization of this parameter will increase Prop-Fan stability. It was also shown that Prop-Fan stability analysis using F203 is sensitive to the blade modal data used as input. Calculated blade modal properties varied significantly with the structural analysis used, and these variations are reflected in the F203 calculations.

Author

N87-21956*# Hamilton Standard, Windsor Locks, Conn. DYNAMIC RESPONSE AND STABILITY OF A COMPOSITE PROP-FAN MODEL Final Report

A. F. SMITH and B. M. BROOKS Oct. 1986 92 p

(Contract NAS3-24088)

(NASA-CR-179528; NAS 1.26:179528; HSER-11057) Avail: NTIS HC A05/MF A01 CSCL 21E

Results are presented for blade response and stability during wind tunnel tests of a 62.2 cm diameter model of a prop-fan, advanced turboprop, with swept graphite/epoxy composite blades. Measurements of dynamic response were made with the rotor

mounted on an isolated nacelle, with varying tilt for nonuniform inflow, at flow speeds from 0.36 to 0.9 Mach number. The blade displayed no instabilities over the operating range tested, up to 0.9 Mach number and 10,000 RPM. Measurements are compared with those for other prop-fan models of both solid metal and graphite composite construction. The swept composite blade had less response than an unswept composite blade. Composite blades had more response than metal blades. Measurements are compared with theoretically based predictions. The 1-P blade response was significantly overpredicted using unimproved methods and somewhat overpredicted using improved methods. Unexpectedly high 2-P strain levels were measured and suggest the presence of nonlinear effects on blade response. Author

N87-22680*# National Aeronautics and Space Administration. Lewis Research Center, Cleveland, Ohio.
ANALYSIS OF AN ADVANCED TECHNOLOGY SUBSONIC TURBOFAN INCORPORATING REVOLUTIONARY MATERIALS
 GERALD KNIP, JR. May 1987 25 p
 (NASA-TM-89868; E-3542; NAS 1.15:89868) Avail: NTIS HC A02/MF A01 CSCL 21E

Successful implementation of revolutionary composite materials in an advanced turbopfan offers the possibility of further improvements in engine performance and thrust-to-weight ratio relative to current metallic materials. The present analysis determines the approximate engine cycle and configuration for an early 21st century subsonic turbopfan incorporating all composite materials. The advanced engine is evaluated relative to a current technology baseline engine in terms of its potential fuel savings for an intercontinental quadjet having a design range of 5500 nmi and a payload of 500 passengers. The resultant near optimum, uncooled, two-spool, advanced engine has an overall pressure ratio of 87, a bypass ratio of 18, a geared fan, and a turbine rotor inlet temperature of 3085 R. Improvements result in a 33-percent fuel saving for the specified mission. Various advanced composite materials are used throughout the engine. For example, advanced polymer composite materials are used for the fan and the low pressure compressor (LPC). Author

N87-22681*# National Aeronautics and Space Administration. Lewis Research Center, Cleveland, Ohio.
SUPERSONIC THROUGH-FLOW FAN DESIGN
 JAMES F. SCHMIDT, ROYCE D. MOORE, JERRY R. WOOD, and RONALD J. STEINKE 1987 21 p Prepared for presentation at the 23rd Joint Propulsion Conference, San Diego, Calif., 29 Jun. - 2 Jul. 1987; sponsored in part by AIAA, SAE, ASME and ASEE
 (NASA-TM-88908; E-3492; NAS 1.15:88908; AIAA-87-1746)
 Avail: NTIS HC A02/MF A01 CSCL 21E

The NASA Lewis Research Center has embarked on a program to experimentally prove the concept of a supersonic through-flow fan which is to maintain supersonic velocities throughout the compression system with only weak shock-wave flow losses. The detailed design of a supersonic through-flow fan and estimated off-design performance with the use of advanced computational codes are described. A multistage compressor facility is being modified for the newly designed supersonic through-flow fan and the major aspects of this modification are briefly described. Author

N87-23622*# Pratt and Whitney Aircraft Group, East Hartford, Conn. Engineering Div.
LIFE PREDICTION AND CONSTITUTIVE MODELS FOR ENGINE HOT SECTION ANISOTROPIC MATERIALS Annual Status Report
 G. A. SWANSON, I. LINASK, D. M. NISSLEY, P. P. NORRIS, T. G. MEYER, and K. P. WALKER Apr. 1987 166 p
 (Contract NAS3-23939)
 (NASA-CR-179594; NAS 1.26:179594; PWA-5968-47; ASR-2; AD-A173875) Avail: NTIS HC A08/MF A01 CSCL 21E

The results are presented of a program designed to develop life prediction and constitutive models for two coated single crystal alloys used in gas turbine airfoils. The two alloys are PWA 1480

and Alloy 185. The two oxidation resistant coatings are PWA 273, an aluminide coating, and PWA 286, an overlay NiCoCrAlY coating. To obtain constitutive and fatigue data, tests were conducted on uncoated and coated specimens loaded in the <100>, <110>, <111> and <123> crystallographic directions. Two constitutive models are being developed and evaluated for the single crystal materials: a micromechanic model based on crystallographic slip systems, and a macroscopic model which employs anisotropic tensors to model inelastic deformation anisotropy. Based on tests conducted on the overlay coating material, constitutive models for coatings also appear feasible and two initial models were selected. A life prediction approach was proposed for coated single crystal materials, including crack initiation either in the coating or in the substrate. The coating initiated failures dominated in the tests at load levels typical of gas turbine operation. Coating life was related to coating stress/strain history which was determined from specimen data using the constitutive models. Author

N87-23623*# National Aeronautics and Space Administration. Lewis Research Center, Cleveland, Ohio.
PERFORMANCE OF TWO 10-LB/SEC CENTRIFUGAL COMPRESSORS WITH DIFFERENT BLADE AND SHROUD THICKNESSES OPERATING OVER A RANGE OF REYNOLDS NUMBERS
 GARY J. SKOCH (Army Aviation Research and Development Command, Cleveland, Ohio.) and ROYCE D. MOORE 1987 25 p Presented at the 23rd Joint Propulsion Conference, San Diego, Calif., 29 Jun. - 2 Jul. 1987; sponsored by AIAA, SAE, ASME and ASEE
 (NASA-TM-100115; E-3660; NAS 1.15:100115; AVSCOM-TR-87-C-21; AIAA-87-1745) Avail: NTIS HC A02/MF A01 CSCL 21E

Centrifugal compressors often cannot be directly scaled to very small flow sizes because of structural and manufacturing limitations. The inability to directly scale all design parameters leads to a performance loss other than that which can be associated with the lower Reynolds number. A 10-lb/sec centrifugal compressor was scaled down to 2-lb/sec where adjustments to blade and shroud thickness and fillet radii were required. The modified 2-lb/sec compressor was then directly scaled back up to 10 lb/sec so that the effect of the modifications could be determined. The performance of the two 10-lb/sec compressors is compared over a range of speed and mass flow. The effect of variations in Reynolds number, impeller tip clearance, and shroud thickness on compressor performance is also presented. Author

N87-23624*# National Aeronautics and Space Administration. Lewis Research Center, Cleveland, Ohio.
LINER COOLING RESEARCH AT NASA LEWIS RESEARCH CENTER
 WALDO A. ACOSTA (Army Aviation Research and Development Command, Cleveland, Ohio.) 1987 18 p Presented at the 23rd Joint Propulsion Conference, San Diego, Calif., 29 Jun. - 2 Jul. 1987; sponsored by AIAA, SAE, ASME and ASEE
 (NASA-TM-100107; E-3647; NAS 1.15:100107; AIAA-87-1828; AVSCOM-TR-87-C-8) Avail: NTIS HC A02/MF A01 CSCL 21E

Described are recently completed and current advanced liner research applicable to advanced small gas turbine engines. Research relating to the evolution of fuel efficient small gas turbine engines capable of meeting future commercial and military aviation needs is currently under way at NASA Lewis Research Center. As part of this research, a reverse-flow combustor geometry was maintained while different advanced liner wall cooling techniques were investigated and compared to a baseline combustor. The performance of the combustors featuring counterflow film-cooled (CFFC) panels, transpiration cooled liner walls (TRANS), and compliant metal/ceramic (CMC) walls was obtained over a range of simulated flight conditions of a 16:1 pressure ratio gas turbine engine and fuel/air ratios up to 0.034. All the combustors featured an identical fuel injection system, identical geometric configuration outline, and similar designed internal aerothermodynamics. Author

07 AIRCRAFT PROPULSION AND POWER

N87-23625*# National Aeronautics and Space Administration. Lewis Research Center, Cleveland, Ohio.

METHOD FOR THE DETERMINATION OF THE THREE-DIMENSIONAL AERODYNAMIC FIELD OF A ROTOR-STATOR COMBINATION TO COMPRESSIBLE FLOW

SRIDHAR M. RAMACHANDRA, LAWRENCE J. BOBER, and SURESH KHANDELWAL (Sverdrup Technology, Inc., Cleveland, Ohio.) Jul. 1987 32 p Presented at the 23rd Joint Propulsion Conference, San Diego, Calif., 29 Jun. - 2 Jul. 1987; cosponsored by AIAA, SAE, ASME and ASEE

(NASA-TM-100118; E-3662; NAS 1.15:100118; AIAA-87-1742)

Avail: NTIS HC A03/MF A01 CSCL 21E

Using the lifting surface theory and the acceleration potential method for the flow field of an axial turbocompressor stage, a recursive and a direct method are presented that make use of the eigenfunction solutions of the isolated rotor and stator to solve for the rotor-stator interaction problem. The net pressure distribution on the rotor and stator blades is represented by modified Birnbaum series, whose coefficients are determined using a matrix procedure and satisfying the boundary conditions on the surface of the blades. The relation between the matrix operators of the recursive and the direct methods is also shown. Expressions have been given for the blade circulation, the axial and tangential forces on the blade, the rotor power required, and the induced upwash velocity of the stage. Author

N87-23626*# National Aeronautics and Space Administration. Lewis Research Center, Cleveland, Ohio.

THE SUPERSONIC THROUGH-FLOW TURBOFAN FOR HIGH MACH PROPULSION

LEO C. FRANCISCUS Jul. 1987 14 p Presented at the 23rd Joint Propulsion Conference, San Diego, Calif., 29 Jun. - 2 Jul. 1987

(NASA-TM-100114; E-3659; NAS 1.15:100114; AIAA-87-2050)

Avail: NTIS HC A02/MF A01 CSCL 21E

A study was done to evaluate the potential improvements in aircraft turbine engine performance by incorporating unique supersonic through-flow fans. Engine performance, weight, and mission studies were carried out for conventional turbofan engines using supersonic through-flow fans. A Mach 3 commercial transport mission was considered. The advantages of the supersonic fan engines were evaluated in terms of mission range comparisons between the supersonic fan engines and conventional engines. The installed specific fuel consumption of the supersonic fan engines was 12 percent better than the conventional engines and the installed weight was projected to be 25 percent lighter. For a takeoff gross weight of 550,000 lbs, the aircraft powered by supersonic fan engines had a range capability of 6600 nm compared to 5300 nm (a 25% improvement) for conventional engines. Author

N87-24419*# National Aeronautics and Space Administration. Lewis Research Center, Cleveland, Ohio.

HOT GAS INGESTION: FROM MODEL RESULTS TO FULL SCALE ENGINE TESTING

ALBERT L. JOHNS, THOMAS J. BIESIADNY, and L. L. PAGEL (McDonnell Aircraft Co., St. Louis, Mo.) /In NASA Ames Research Center Proceedings of the 1985 NASA Ames Research Center's Ground-Effects Workshop p 341-361 Feb. 1987

Avail: NTIS HC A19/MF A01 CSCL 21E

An overview is presented of a joint NASA Lewis McDonnell Aircraft Co. Hot Gas Ingestion (HGI) test program in NASA Lewis' 9 x 15 foot Low Speed Wind Tunnel (LSWT). Advanced short takeoff vertical landing (ASTOVL) aircraft capable of operating from remote sites, damaged runways, aircraft carriers and small air-capable ships are being pursued for deployment around the turn of the century. To achieve this goal, it is important that technologies critical to this unique class of aircraft be developed. One of the ASTOVL concepts, the vectored thrust, has as its critical technology item, the potential of hot gas ingestion (which occurs during vertical flight operation while in ground effect) as a key development issue. Recognizing this need, NASA Lewis Powered Lift Section and McAir have defined a cooperative

program for testing in the Lewis 9 x 15 foot LSWT. This program is described in detail. Author

N87-24469*# National Aeronautics and Space Administration. Lewis Research Center, Cleveland, Ohio.

VISCOUS ANALYSES FOR FLOW THROUGH SUBSONIC AND SUPERSONIC INTAKES

LOUIS A. POVINELLI and CHARLES E. TOWNE /In AGARD Engine Response to Distorted Inflow Conditions 20 p Mar. 1987

Avail: NTIS HC A14/MF A01

A parabolized Navier-Stokes code was used to analyze a number of diffusers typical of a modern inlet design. The effect of curvature of the diffuser centerline and transitioning cross sections was evaluated to determine the primary cause of the flow distortion in the duct. Results are presented for S-shaped intakes with circular and transitioning cross sections. Special emphasis is placed on verification of the analysis to accurately predict distorted flow fields resulting from pressure-driven secondary flows. The effect of vortex generators on reducing the distortion of intakes is presented. Comparisons of the experimental and analytical total pressure contours at the exit of the intake exhibit good agreement. In the case of supersonic inlets, computations of the inlet flow field reveal that large secondary flow regions may be generated just inside of the intake. These strong flows may lead to separated flow regions and cause pronounced distortions upstream of the compressor. Author

N87-24470*# Cambridge Univ. (England).

CALCULATIONS OF INLET DISTORTION INDUCED COMPRESSOR FLOWFIELD INSTABILITY

T. P. HYNES, R. CHUE, E. M. GREITZER, and C. S. TAN (Massachusetts Inst. of Tech., Cambridge.) /In AGARD Engine Response to Distorted Inflow Conditions 16 p Mar. 1987

(Contract NSG-3208)

Avail: NTIS HC A14/MF A01

Calculations are presented predicting the onset of flow instability for a multistage low speed axial compressor operating in circumferentially distorted inlet flow. The most important feature of the model used is that it attempts to properly account for the fluid dynamic interaction between the spoiled and unspoiled sectors of the compressor. The calculations show that there is an approximate stability criterion, the annulus averaged slope of the compressor pressure rise characteristic equal to zero, that is valid whenever the dynamics of the compressor distorted flowfield can be considered independent of the compressor environment. This approximate criterion is used to investigate the relationship between the present model and the parallel compressor model. Further calculations are performed to investigate cases of interest when the dynamics of the flowfield are coupled to the environment. Resonant cases and cases when the distortion is unsteady are studied. In particular, it is shown that rotating distortions which propagate in the rotor direction can have a greater effect on stability margin than stationary or counter-rotational ones. Finally, it is shown that the general predictions of the model are insensitive to the details of the unsteady bladerow dynamics. Author

N87-24477*# National Aeronautics and Space Administration. Lewis Research Center, Cleveland, Ohio.

SUMMARY OF INVESTIGATIONS OF ENGINE RESPONSE TO DISTORTED INLET CONDITIONS

THOMAS J. BIESIADNY, WILLIS M. BRAITHWAITE, RONALD H. SOEDER, and MAHMOOD ABDELWAHAB /In AGARD Engine Response to Distorted Inflow Conditions 21 p Mar. 1987 Previously announced as N86-26336

Avail: NTIS HC A14/MF A01

A survey is presented of experimental and analytical experience of the NASA Lewis Research Center in engine response to inlet temperature and pressure distortions. Results of experimental investigations and analytical modeling are reviewed together with a description of the hardware and the techniques employed. Distortion devices successfully simulated inlet distortion, and knowledge was gained on compression system response to

different types of distortion. A list of NASA research references is included. Author

N87-24481*# National Aeronautics and Space Administration. Lewis Research Center, Cleveland, Ohio.
LOW-COST FM OSCILLATOR FOR CAPACITANCE TYPE OF BLADE TIP CLEARANCE MEASUREMENT SYSTEM
 JOHN P. BARRANGER Jul. 1987 16 p
 (NASA-TP-2746; E-3455; NAS 1.60:2746) Avail: NTIS HC A02/MF A01 CSCL 21E

The frequency-modulated (FM) oscillator described is part of a blade tip clearance measurement system that meets the needs of a wide class of fans, compressors, and turbines. As a result of advancements in the technology of ultra-high-frequency operational amplifiers, the FM oscillator requires only a single low-cost integrated circuit. Its carrier frequency is 42.8 MHz when it is used with an integrated probe and connecting cable assembly consisting of a 0.81 cm diameter engine-mounted capacitance probe and a 61 cm long hermetically sealed coaxial cable. A complete circuit analysis is given, including amplifier negative resistance characteristics. An error analysis of environmentally induced effects is also derived, and an error-correcting technique is proposed. The oscillator can be calibrated in the static mode and has a negative peak frequency deviation of 400 kHz for a rotor blade thickness of 1.2 mm. High-temperature performance tests of the probe and 13 cm of the adjacent cable show good accuracy up to 600 C, the maximum permissible seal temperature. The major source of error is the residual FM oscillator noise, which produces a clearance error of + or - 10 microns at a clearance of 0.5 mm. The oscillator electronics accommodates the high rotor speeds associated with small engines, the signals from which may have frequency components as high as 1 MHz.

Author

N87-25323*# Garrett Turbine Engine Co., Phoenix, Ariz.
COMPOUND CYCLE ENGINE FOR HELICOPTER APPLICATION
 JERE G. CASTOR 25 Apr. 1986 12 p
 (Contract NAS3-24346; DA PROJ. 1L1-61102-AH-45)
 (NASA-CR-175110; NAS 1.26:175110; AD-A180007;
 USAVSCOM-TR-86-C-15) Avail: NTIS HC A02/MF A01 CSCL 21E

The Compound Cycle Engine (CCE) is a highly turbocharged, power compounded, ultra-high power density, light-weight diesel engine. The turbomachinery is similar to a moderate pressure ratio, free power turbine engine and the diesel core is high speed and a low compression ratio. This engine is considered a potential candidate for future military light helicopter applications. This executive summary presents cycle thermodynamic (SFC) and engine weight analyses performed to establish general engine operating parameters and configuration. An extensive performance and weight analysis based on a typical two hour helicopter (+30 minute reserve) mission determined final conceptual engine design. With this mission, CCE performance was compared to that of a T-800 class gas turbine engine. The CCE had a 31% lower-fuel consumption and resulted in a 16% reduction in engine plus fuel and fuel tank weight. Design SFC of the CCE is 0.33 lb-HP-HR and installed wet weight is 0.43 lbs/HP. The major technology development areas required for the CCE are identified and briefly discussed. GRA

N87-25329*# National Aeronautics and Space Administration. Lewis Research Center, Cleveland, Ohio.
FIBER-OPTIC TEMPERATURE SENSOR USING A SPECTRUM-MODULATING SEMICONDUCTOR ETALON
 GLENN BEHEIM, KLAUS FRITSCH, and DONALD J. ANTHAN (Cleveland State Univ., Ohio.) 1987 22 p Presented at the O-E/Fibers '87 Symposium on Fiber Optics and Integrated Optoelectronics, San Diego, Calif., 16-21 Aug. 1987; sponsored by SPIE and International Society for Optical Engineering (NASA-TM-100153; E-3715; NAS 1.15:100153) Avail: NTIS HC A02/MF A01 CSCL 21E

Described is a fiber-optic temperature sensor that uses a spectrum modulating SiC etalon. The spectral output of this type of sensor may be analyzed to obtain a temperature measurement which is largely independent of the transmission properties of the sensor's fiber-optic link. A highly precise laboratory spectrometer is described in detail, and this instrument is used to study the properties of this type of sensor. Also described are a number of different spectrum analyzers that are more suitable for use in a practical thermometer. Author

N87-26908*# Carnegie-Mellon Univ., Pittsburgh, Pa. Dept. of Mechanical Engineering.
BLADED DISK VIBRATION Final Report
 J. H. GRIFFIN Aug. 1987 5 p
 (Contract NAG2-31; NAG3-67)
 (NASA-CR-181203; NAS 1.26:181203) Avail: NTIS HC A02/MF A01 CSCL 21E

The objective was to better understand the vibratory response of bladed disk assemblies that occur in jet engines or turbopumps. Two basic problems were investigated: how friction affects flutter; and how friction, mistuning, and stage aerodynamics affect resonance. Understanding these phenomena allows a better understanding of why some stages have high vibratory stresses, how best to manage those stresses, and what to do about reducing them if they are too large. Author

N87-26910*# National Aeronautics and Space Administration. Lewis Research Center, Cleveland, Ohio.
DESIGN AND PERFORMANCE OF CONTROLLED-DIFFUSION STATOR COMPARED WITH ORIGINAL DOUBLE-CIRCULAR-ARC STATOR
 THOMAS F. GELDER, JAMES F. SCHMIDT, KENNETH L. SUDER, and MICHAEL D. HATHAWAY (Army Aviation Systems Command, Cleveland, Ohio.) 1987 22 p Prepared for presentation at the Aerospace Technology Conference and Exposition, Long Beach, Calif., 5-8 Oct. 1987; sponsored by the Society of Automotive Engineers
 (NASA-TM-100141; AVSCOM-TR-87-C-25; E-3694; NAS 1.15:100141) Avail: NTIS HC A02/MF A01 CSCL 21E

The capabilities of two stators, one with controlled-diffusion (CD) blade sections and one with double-circular-arc (DCA) blade sections, were compared. A CD stator was designed and tested that had the same chord length but half the blades of the DCA stator. The same fan rotor (tip speed, 429 m/sec; pressure ratio, 1.65) was used with each stator row. The design and analysis system is briefly described. The overall stage and rotor performances with each stator are compared, as are selected blade element data. The minimum overall efficiency decrement across the stator was approximately 1 percentage point greater with the CD blade sections than with the DCA blade sections. Author

N87-26914*# General Electric Co., Lynn, Mass. Aircraft Engines.
CERAMIC HIGH PRESSURE GAS PATH SEAL Final Report, Jan. 1982 - Apr. 1987
 G. C. LIOTTA Aug. 1987 138 p
 (Contract NAS3-23174)
 (NASA-CR-180813; NAS 1.26:180813) Avail: NTIS HC A07/MF A01 CSCL 20E

Stage 1 ceramic shrouds (high pressure turbine gas path seal) were developed for the GE T700 turbine helicopter engine under

07 AIRCRAFT PROPULSION AND POWER

the Army/NASA Contract NAS3-23174. This contract successfully proved the viability and benefits of a Stage 1 ceramic shroud for production application. Stage 1 ceramic shrouds were proven by extensive component and engine testing. This Stage 1 ceramic shroud, plasma sprayed ceramic (ZrO₂-BY2O₃) and bond coating (NiCrAlY) onto a cast metal backing, offers significant engine performance improvement. Due to the ceramic coating, the amount of cooling air required is reduced 20% resulting in a 0.5% increase in horsepower and a 0.3% decrease in specific fuel consumption. This is accomplished with a component which is lower in cost than the current production shroud. Stage 1 ceramic shrouds will be introduced into field service in late 1987. Author

N87-28551*# National Aeronautics and Space Administration. Lewis Research Center, Cleveland, Ohio.

TOWARD IMPROVED DURABILITY IN ADVANCED COMBUSTORS AND TURBINES: PROGRESS IN THE PREDICTION OF THERMOMECHANICAL LOADS

DANIEL E. SOKOLOWSKI and C. ROBERT ENSIGN 1986 31 p Presented at the 31st International Gas Turbine Conference and Exhibition, Dusseldorf, West Germany, 8-12 Jun. 1986; sponsored by ASME Previously announced in IAA as A86-48224

(NASA-TM-88932; E-3374; NAS 1.15:88932) Avail: NTIS HC A03/MF A01 CSCL 21E

NASA is sponsoring the Turbine Engine Hot Section Technology (HOST) Project to address the need for improved durability in advanced combustors and turbines. Analytical and experimental activities aimed at more accurate prediction of the aerothermal environment, the thermomechanical loads, the material behavior and structural responses to such loading, and life predictions for high temperature cyclic operation have been underway for several years and are showing promising results. Progress is reported in the development of advanced instrumentation and in the improvement of combustor aerothermal and turbine heat transfer models that will lead to more accurate prediction of thermomechanical loads. Author

N87-28552*# United Technologies Corp., East Hartford, Conn. Pratt and Whitney Engineering Div.

ADVANCED PROPFAN ENGINE TECHNOLOGY (APET) SINGLE- AND COUNTER-ROTATION GEARBOX/PITCH CHANGE MECHANISM Final Report

C. N. REYNOLDS Jul. 1985 288 p (Contract NAS3-23045)

(NASA-CR-168114-VOL-1; NAS 1.26:168114-VOL-1; PWA-5869-88-VOL-1) Avail: NTIS HC A13/MF A01 CSCL 21E

The preliminary design of advanced technology (1992) prop-fan engines for single-rotation prop-fans, the conceptual design of the entire propulsion system, and an aircraft evaluation of the resultant designs are discussed. Four engine configurations were examined. A two-spool engine with all axial compressors and a three-spool engine with axial/centrifugal compressors were selected. Integrated propulsion systems were designed in conjunction with airframe manufacturers. The design efforts resulted in 12,000 shaft horsepower engines installed in over the installations with in-line and offset gearboxes. The prop-fan powered aircraft used 21 percent less fuel and cost 10 percent less to operate than a similar aircraft powered by turbofan engines with comparable technology. Author

N87-28553*# General Electric Co., Cincinnati, Ohio. Aircraft Engine Business Group.

ADVANCED PROPFAN ENGINE TECHNOLOGY (APET) AND SINGLE-ROTATION GEARBOX/PITCH CHANGE MECHANISM

D. F. SARGISSON Jun. 1985 483 p (Contract NAS3-23044)

(NASA-CR-168113; NAS 1.26:168113; R83AEB592) Avail: NTIS HC A21/MF A01 CSCL 21E

The projected performance, in the 1990's time period, of the equivalent technology level high bypass ratio turbofan powered aircraft (at the 150 passenger size) is compared with advanced turboprop propulsion systems. Fuel burn analysis, economic

analysis, and pollution (noise, emissions) estimates were made. Three different cruise Mach numbers were investigated for both the turbofan and the turboprop systems. Aerodynamic design and performance estimates were made for nacelles, inlets, and exhaust systems. Air to oil heat exchangers were investigated for oil cooling advanced gearboxes at the 12,500 SHP level. The results and conclusions are positive in that high speed turboprop aircraft will exhibit superior fuel burn characteristics and lower operating costs when compared with equivalent technology turbofan aircraft.

Author

N87-28554*# General Motors Corp., Indianapolis, Ind. Allison Gas Turbine Div.

ADVANCED PROPFAN ENGINE TECHNOLOGY (APET) DEFINITION STUDY, SINGLE AND COUNTER-ROTATION GEARBOX/PITCH CHANGE MECHANISM DESIGN

R. D. ANDERSON Jul. 1985 289 p

(Contract NAS3-23046)

(NASA-CR-168115; NAS 1.26:168115; EDR-11283) Avail: NTIS HC A13/MF A01 CSCL 21E

Single-rotation propfan-powered regional transport aircraft were studied to identify key technology development issues and programs. The need for improved thrust specific fuel consumption to reduce fuel burned and aircraft direct operating cost is the dominant factor. Typical cycle trends for minimizing fuel consumption are reviewed, and two 10,000 shp class engine configurations for propfan propulsion systems for the 1990's are presented. Recommended engine configurations are both three-spool design with dual spool compressors and free power turbines. The benefits of these new propulsion system concepts were evaluated using an advanced airframe, and results are compared for single-rotation propfan and turbofan advanced technology propulsion systems. The single-rotation gearbox is compared to a similar design with current technology to establish the benefits of the advanced gearbox technology. The conceptual design of the advanced pitch change mechanism identified a high pressure hydraulic system that is superior to the other contenders and completely external to the gearboxes. Author

N87-28555*# United Technologies Corp., Windsor Locks, Conn. Hamilton Standard Div.

ANALYSIS AND TEST EVALUATION OF THE DYNAMIC RESPONSE AND STABILITY OF THREE ADVANCED TURBOPROP MODELS Final Report

P. N. BANSAL, P. J. ARSENEAUX, A. F. SMITH, J. E. TURNBERG, and B. M. BROOKS Aug. 1985 182 p

(Contract NAS3-22393; NAS3-22755)

(NASA-CR-174814; NAS 1.26:174814; HSER-8945) Avail: NTIS HC A09/MF A01 CSCL 21E

Results of dynamic response and stability wind tunnel tests of three 62.2 cm (24.5 in) diameter models of the Prop-Fan, advanced turboprop, are presented. Measurements of dynamic response were made with the rotors mounted on an isolated nacelle, with varying tilt for nonuniform inflow. One model was also tested using a semi-span wing and fuselage configuration for response to realistic aircraft inflow. Stability tests were performed using tunnel turbulence or a nitrogen jet for excitation. Measurements are compared with predictions made using beam analysis methods for the model with straight blades, and finite element analysis methods for the models with swept blades. Correlations between measured and predicted rotating blade natural frequencies for all the models are very good. The IP dynamic response of the straight blade model is reasonably well predicted. The IP response of the swept blades is underpredicted and the wing induced response of the straight blade is overpredicted. Two models did not flutter, as predicted. One swept blade model encountered an instability at a higher RPM than predicted, showing predictions to be conservative. Author

N87-28556*# United Technologies Corp., East Hartford, Conn. Pratt and Whitney Engineering Div.
ADVANCED PROP-FAN ENGINE TECHNOLOGY (APET) SINGLE- AND COUNTER-ROTATION GEARBOX/PITCH CHANGE MECHANISM Final Report
 C. N. REYNOLDS Jul. 1985 170 p
 (Contract NAS3-23045)

(NASA-CR-168114-VOL-2; NAS 1.26:168114-VOL-2; PWA-5869-88-VOL-2) Avail: NTIS HC A08/MF A01 CSCL 21E
 The preliminary design of advanced technology (1992) turboprop engines for single-rotation prop-fans and conceptual designs of pitch change mechanisms for single- and counter-rotation prop-fan application are discussed. The single-rotation gearbox is a split path, in-line configuration. The counter-rotation gearbox is an in-line, differential planetary design. The pitch change mechanisms for both the single- and counter-rotation arrangements are rotary/hydraulic. The advanced technology single-rotation gearbox yields a 2.4 percent improvement in aircraft fuel burn and a one percent improvement in operating cost relative to a current technology gearbox. The 1992 counter-rotation gearbox is 15 percent lighter, 15 percent more reliable, 5 percent lower in cost, and 45 percent lower in maintenance cost than the 1992 single-rotation gearbox. The pitch controls are modular, accessible, and external. Author

N87-28557*# National Aeronautics and Space Administration. Lewis Research Center, Cleveland, Ohio.
MEASUREMENT UNCERTAINTY FOR THE UNIFORM ENGINE TESTING PROGRAM CONDUCTED AT NASA LEWIS RESEARCH CENTER
 MAHMOOD ABDELWAHAB, THOMAS J. BIESIADNY, and DEAN SILVER (Air Force Systems Command, Cleveland, Ohio.) May 1987 54 p
 (NASA-TM-88943; E-3234; NAS 1.15:88943) Avail: NTIS HC A04/MF A01 CSCL 21E

An uncertainty analysis was conducted to determine the bias and precision errors and total uncertainty of measured turbojet engine performance parameters. The engine tests were conducted as part of the Uniform Engine Test Program which was sponsored by the Advisory Group for Aerospace Research and Development (AGARD). With the same engines, support hardware, and instrumentation, performance parameters were measured twice, once during tests conducted in test cell number 3 and again during tests conducted in test cell number 4 of the NASA Lewis Propulsion Systems Laboratory. The analysis covers 15 engine parameters, including engine inlet airflow, engine net thrust, and engine specific fuel consumption measured at high rotor speed of 8875 rpm. Measurements were taken at three flight conditions defined by the following engine inlet pressure, engine inlet total temperature, and engine ram ratio: (1) 82.7 kPa, 288 K, 1.0, (2) 82.7 kPa, 288 K, 1.3, and (3) 20.7 kPa, 288 K, 1.3. In terms of bias, precision, and uncertainty magnitudes, there were no differences between most measurements made in test cells number 3 and 4. The magnitude of the errors increased for both test cells as engine pressure level decreased. Also, the level of the bias error was two to three times larger than that of the precision error. Author

N87-29534*# General Electric Co., Cincinnati, Ohio. Aircraft Engine Business Group.
AERODYNAMIC PERFORMANCE INVESTIGATION OF ADVANCED MECHANICAL SUPPRESSOR AND EJECTOR NOZZLE CONCEPTS FOR JET NOISE REDUCTION Final Report, 1981-1984
 C. D. WAGENKNECHT and E. D. BEDIAKO Feb. 1985 218 p
 (Contract NAS3-23038)
 (NASA-CR-174860; NAS 1.26:174860; R83AEB122-3) Avail: NTIS HC A10/MF A01 CSCL 21E

Advanced Supersonic Transport jet noise may be reduced to Federal Air Regulation limits if recommended refinements to a recently developed ejector shroud exhaust system are successfully carried out. A two-part program consisting of a design study and a subscale model wind tunnel test effort conducted to define an acoustically treated ejector shroud exhaust system for supersonic

transport application is described. Coannular, 20-chute, and ejector shroud exhaust systems were evaluated. Program results were used in a mission analysis study to determine aircraft takeoff gross weight to perform a nominal design mission, under Federal Aviation Regulation (1969), Part 36, Stage 3 noise constraints. Mission trade study results confirmed that the ejector shroud was the best of the three exhaust systems studied with a significant takeoff gross weight advantage over the 20-chute suppressor nozzle which was the second best. Author

N87-29536*# Lockheed-Georgia Co., Marietta.
PROPFAN TEST ASSESSMENT PROPFAN PROPULSION SYSTEM STATIC TEST REPORT Contractor Report, Feb. - Jun. 1986
 D. M. OROURKE Sep. 1987 238 p
 (Contract NAS3-24339)
 (NASA-CR-179613; NAS 1.26:179613; LG86ER0173; L87R1488)
 Avail: NTIS HC A11/MF A01 CSCL 21E

The propfan test assessment (PTA) propulsion system successfully completed over 50 hours of extensive static ground tests, including a 36 hour endurance test. All major systems performed as expected, verifying that the large-scale 2.74 m diameter propfan, engine, gearbox, controls, subsystems, and flight instrumentation will be satisfactory with minor modifications for the upcoming PTA flight tests on the GII aircraft in early 1987. A test envelope was established for static ground operation to maintain propfan blade stresses within limits for propfan rotational speeds up to 105 percent and power levels up to 3880 kW. Transient tests verified stable, predictable response of engine power and propfan speed controls. Installed engine TSFC was better than expected, probably due to the excellent inlet performance coupled with the supercharging effect of the propfan. Near- and far-field noise spectra contained three dominant components, which were dependent on power, tip speed, and direction. The components were propfan blade tones, propfan random noise, and compressor/propfan interaction noise. No significant turbine noise or combustion noise was evident. Author

N87-29537*# National Aeronautics and Space Administration. Lewis Research Center, Cleveland, Ohio.
AIRFLOW CALIBRATION AND EXHAUST PRESSURE/TEMPERATURE SURVEY OF AN F404, S/N 215-109, TURBOFAN ENGINE
 MAUREEN E. BURNS and THOMAS A. KIRCHGEISSNER Sep. 1987 31 p
 (NASA-TM-100159; E-3447; NAS 1.15:100159) Avail: NTIS HC A03/MF A01 CSCL 21E

A General Electric F-404 turbofan engine was calibrated for thrust and airflow at the NASA Lewis Propulsion System Laboratory in support of future flight tests of the X-29 aircraft. Tests were conducted with and without augmentation, over a range of flight conditions, including the two design points of the airplane. Data obtained during the altitude tests will be used to correct two independent gross thrust calculation routines which will be installed and operated on the airplane to determine in-flight gross thrust. Corrected airflow data as a function of corrected fan speed collapsed onto a single curve. Similarly, trends were observed and defined for both augmented and dry thrust. Overall agreement between measured data and F-404 Engine Spec Deck data was within 2 percent for airflow and 6 percent for thrust. The results of an uncertainty analysis for thrust and airflow is presented. In addition to the thrust calibration, the exhaust gas boundary layer pressure and temperatures were surveyed at selected condition and engine power levels to obtain data for another NASA F-404 program. Test data for these surveys are presented. Author

07 AIRCRAFT PROPULSION AND POWER

N87-29538*# General Electric Co., Cincinnati, Ohio.
TURBOFAN AFT DUCT SUPPRESSOR STUDY. CONTRACTOR'S DATA REPORT OF MODE PROBE SIGNAL DATA Final Report
G. H. FISKE, R. E. MOTSINGER, A. A. SYED, M. C. JOSHI, and R. E. KRAFT (Douglas Aircraft Co., Inc., Long Beach, Calif.) Jul. 1983 74 p
(Contract NAS3-22766)
(NASA-CR-175067; NAS 1.26:175067) Avail: NTIS HC A04/MF A01 CSCL 21E

Acoustic modal distributions were measured in a fan test model having an annular exhaust duct for comparison with theoretically predicted acoustic suppression values. This report contains the amplitude and phase data of the acoustic signals sensed by the transducers of the two mode probes employed in the measurement. Each mode probe consisted of an array of 12 transducers sensing the acoustic field at three axial positions and four radial positions.
M.G.

N87-29539*# General Electric Co., Cincinnati, Ohio. Aircraft Engine Business Group.
TURBOFAN AFT DUCT SUPPRESSOR STUDY
A. A. SYED, R. E. MOTSINGER, G. H. FISKE, M. C. JOSHI, and R. E. KRAFT (Douglas Aircraft Co., Inc., Long Beach, Calif.) Jul. 1983 202 p
(Contract NAS3-22766)
(NASA-CR-175067; NAS 1.26:175067; R83AEB566) Avail: NTIS HC A10/MF A01 CSCL 21E

Suppressions due to acoustic treatment in the annular exhaust duct of a model fan were theoretically predicted and compared with measured suppressions. The predictions are based on the modal analysis of sound propagation in a straight annular flow duct with segmented treatment. Modal distributions of the fan noise source (fan-stator interaction only) were measured using in-duct modal probes. The flow profiles were also measured in the vicinity of the modal probes. The acoustic impedance of the single degree of freedom treatment was measured in the presence of grazing flow. The measured values of mode distribution of the fan noise source, the flow velocity profile and the acoustic impedance of the treatment in the duct were used as input to the prediction program. The predicted suppressions, under the assumption of uniform flow in the duct, compared well with the suppressions measured in the duct for all test conditions. The interaction modes generated by the rotor-stator interaction spanned a cut-off ratio range from nearly 1 to 7.
Author

08

AIRCRAFT STABILITY AND CONTROL

Includes aircraft handling qualities; piloting; flight controls; and autopilots.

N87-11797*# Kohlman Systems Research, Inc., Lawrence, Kans.
FLIGHT TEST REPORT OF THE NASA ICING RESEARCH AIRPLANE: PERFORMANCE, STABILITY, AND CONTROL AFTER FLIGHT THROUGH NATURAL ICING CONDITIONS Final Report
J. L. JORDAN, S. J. PLATZ, and W. C. SCHINSTOCK Oct. 1986 159 p
(Contract NAS3-24547)
(NASA-CR-179515; NAS 1.26:179515; KSR-86-01) Avail: NTIS HC A08/MF A01 CSCL 01C

Flight test results are presented documenting the effect of airframe icing on performance and stability and control of a NASA DHC-6 icing research aircraft. Kohlman System Research, Inc., provided the data acquisition system and data analysis under contract to NASA. Performance modeling methods and MMLE techniques were used to determine the effects of natural ice on the aircraft. Results showed that ice had a significant effect on

the drag coefficient of the aircraft and a modest effect on the MMLE derived longitudinal stability coefficients (code version MMLE). Data is also presented on asymmetric power sign slip maneuvers showing rudder floating characteristics with and without ice on the vertical stabilizer.
Author

N87-25331*# National Aeronautics and Space Administration. Lewis Research Center, Cleveland, Ohio.
ADVANCED DETECTION, ISOLATION AND ACCOMMODATION OF SENSOR FAILURES: REAL-TIME EVALUATION
WALTER C. MERRILL, JOHN C. DELAAT, and WILLIAM M. BRUTON Jul. 1987 30 p
(NASA-TP-2740; E-3479; NAS 1.60:2740) Avail: US Patent and Trademark Office CSCL 01C

The objective of the Advanced Detection, Isolation, and Accommodation (ADIA) Program is to improve the overall demonstrated reliability of digital electronic control systems for turbine engines by using analytical redundancy to detect sensor failures. The results of a real time hybrid computer evaluation of the ADIA algorithm are presented. Minimum detectable levels of sensor failures for an F100 engine control system are determined. Also included are details about the microprocessor implementation of the algorithm as well as a description of the algorithm itself.
Author

09

RESEARCH AND SUPPORT FACILITIES (AIR)

Includes airports, hangars and runways; aircraft repair and overhaul facilities; wind tunnels; shock tubes; and aircraft engine test stands.

A87-45203*# National Aeronautics and Space Administration. Lewis Research Center, Cleveland, Ohio.
FULL-SCALE THRUST REVERSER TESTING IN AN ALTITUDE FACILITY
CHARLES M. MEHALIC and ROY A. LOTTIG (NASA, Lewis Research Center, Cleveland, OH) AIAA, SAE, ASME, and ASEE, Joint Propulsion Conference, 23rd, San Diego, CA, June 29-July 2, 1987. 14 p. Previously announced in STAR as N87-18575. refs
(AIAA PAPER 87-1788)

A two-dimensional convergent-divergent exhaust nozzle designed and fabricated by Pratt and Whitney Aircraft was installed on a PW1128 turbofan engine and tested during thrust reverser operation in an altitude facility at NASA Lewis Research Center. A unique collection system was used to capture the thrust reverser exhaust gas and transport it to the primary exhaust collector. Tests were conducted at three flight conditions with varying amounts of thrust reverse at each condition. Some reverser exhaust gas spillage by the collection system was encountered but engine performance was unaffected at all flight conditions tested. Based on the results of this test program, the feasibility of altitude testing of advanced multifunction exhaust nozzle systems has been demonstrated.
Author

A87-50190*# National Aeronautics and Space Administration. Lewis Research Center, Cleveland, Ohio.
REACTIVATION STUDY FOR NASA LEWIS RESEARCH CENTER'S HYPERSONIC TUNNEL FACILITY
JEFFREY E. HAAS (NASA, Lewis Research Center, Cleveland, OH) AIAA, SAE, ASME, and ASEE, Joint Propulsion Conference, 23rd, San Diego, CA, June 29-July 2, 1987. 14 p. Previously announced in STAR as N87-23664. refs
(AIAA PAPER 87-1886)

The Hypersonic Tunnel Facility (HTF) at NASA Lewis Research Center's Plum Brook Station is a blowdown, free-jet, nonvitiated propulsion facility capable of Mach 5, 6, and 7 with true temperature, altitude, and air composition simulation. The facility has been in a

deactivated status for 13 years. Discussed are the capabilities of HTF, and the results of a deactivation study recently conducted to determine the cost, schedule, and technical effort required to restore HTF to its original design operating capabilities are summarized. Author

A87-52494* National Aeronautics and Space Administration. Lewis Research Center, Cleveland, Ohio.

THE NASA STRAIN GAGE LABORATORY

HOWARD F. HOBART and HERBERT A. WILL (NASA, Lewis Research Center, Cleveland, OH) IN: Annual Hostile Environments and High Temperature Measurements Conference, 3rd, Cincinnati, OH, Mar. 25, 26, 1986, Proceedings. Bethel, CT, Society for Experimental Mechanics, Inc., 1986, p. 5-9.

The goal of the NASA-sponsored high-temperature high-strain gage program (which combines in-house, contract, and grant work) is to develop a gage that will measure static strains up to 2000 microstrain to within 10 percent, and at temperatures up to 1250 K (typical for combustors and turbine blades and vanes of gas turbine engines) maintained over 50-h period. The basic equipment of the NASA in-house lab is described (with special attention given to the strain-gage testing system), and some examples of recent test results are discussed. Data are presented on following tests performed on four gages: apparent strain vs temperature at different cooling rates, gage factor at various strain and temperature levels, and drift and creep tests at 133 C. I.S.

N87-16851*# National Aeronautics and Space Administration. Lewis Research Center, Cleveland, Ohio.

A DISTRIBUTED DATA ACQUISITION SYSTEM FOR AERONAUTICS TEST FACILITIES

DENNIS L. FRONEK, ROBERT N. SETTER, PHILIP Z. BLUMENTHAL, and ROBERT R. SMALLEY 1987 8 p Proposed for presentation at the International Instrumentation Symposium, Las Vegas, Nev., 3-8 May 1987; sponsored by the Instrument Society of America (NASA-TM-88961; E-3417; NAS 1.15:88961) Avail: NTIS HC A02/MF A01 CSCL 14B

The NASA Lewis Research Center is in the process of installing a new data acquisition and display system. This new system will provide small and medium sized aeronautics test facilities with a state-of-the-art real-time data acquisition and display system. The new data system will provide for the acquisition of signals from a variety of instrumentation sources. They include analog measurements of temperatures, pressures, and other steady state voltage inputs; frequency inputs to measure speed and flow; discrete I/O for significant events, and modular instrument systems such as multiplexed pressure modules or electronic instrumentation with a IEEE 488 interface. The data system is designed to acquire data, convert it to engineering units, compute test dependent performance calculations, limit check selected channels or calculations, and display the information in alphanumeric or graphical form with a cycle time of one second for the alphanumeric data. This paper describes the system configuration, its salient features, and the expected impact on testing. Author

N87-17717*# National Aeronautics and Space Administration. Lewis Research Center, Cleveland, Ohio.

EXPERIMENTAL EVALUATION OF WALL MACH NUMBER DISTRIBUTIONS OF THE OCTAGONAL TEST SECTION PROPOSED FOR NASA LEWIS RESEARCH CENTER'S ALTITUDE WIND TUNNEL

DOUGLAS E. HARRINGTON, RICHARD R. BURLEY, and ROBERT R. CORBAN Nov. 1986 35 p (NASA-TP-2666; E-3145; NAS 1.60:2666) Avail: NTIS HC A03/MF A01 CSCL 14B

Wall Mach number distributions were determined over a range of test-section free-stream Mach numbers from 0.2 to 0.92. The test section was slotted and had a nominal porosity of 11 percent. Reentry flaps located at the test-section exit were varied from 0 (fully closed) to 9 (fully open) degrees. Flow was bled through the test-section slots by means of a plenum evacuation system (PES) and varied from 0 to 3 percent of tunnel flow. Variations in reentry

flap angle or PES flow rate had little or no effect on the Mach number distributions in the first 70 percent of the test section. However, in the aft region of the test section, flap angle and PES flow rate had a major impact on the Mach number distributions. Optimum PES flow rates were nominally 2 to 2.5 percent with the flaps fully closed and less than 1 percent when the flaps were fully open. The standard deviation of the test-section wall Mach numbers at the optimum PES flow rates was 0.003 or less. Author

N87-18575*# National Aeronautics and Space Administration. Lewis Research Center, Cleveland, Ohio.

FULL-SCALE THRUST REVERSER TESTING IN AN ALTITUDE FACILITY

CHARLES M. MEHALIC and ROY A. LOTTIG 1987 24 p Prepared for presentation at the 23rd Joint Propulsion Conference, San Diego, Calif., 29 Jun. - 2 Jul. 1987; sponsored in part by AIAA, SAE, ASME and ASEE (NASA-TM-88967; AIAA-87-1788; E-3435; NAS 1.15:88967) Avail: NTIS HC A02/MF A01 CSCL 14B

A two-dimensional convergent-divergent exhaust nozzle designed and fabricated by Pratt and Whitney Aircraft was installed on a PW1128 turbofan engine and tested during thrust reverser operation in an altitude facility at NASA Lewis Research Center. A unique collection system was used to capture the thrust reverser exhaust gas and transport it to the primary exhaust collector. Tests were conducted at three flight conditions with varying amounts of thrust reverse at each condition. Some reverser exhaust gas spillage by the collection system was encountered but engine performance was unaffected at all flight conditions tested. Based on the results of this test program, the feasibility of altitude testing of advanced multi-function exhaust nozzle systems has been demonstrated. Author

N87-18576*# National Aeronautics and Space Administration. Lewis Research Center, Cleveland, Ohio.

EXPERIMENTAL EVALUATION OF TWO TURNING VANE DESIGNS FOR FAN DRIVE CORNER OF 0.1-SCALE MODEL OF NASA LEWIS RESEARCH CENTER'S PROPOSED ALTITUDE WIND TUNNEL

DONALD R. BOLDMAN, ROYCE D. MOORE, and RICKEY J. SHYNE Mar. 1987 148 p (NASA-TP-2646; E-3175; NAS 1.60:2646) Avail: NTIS HC A07/MF A01 CSCL 14B

Two turning vane designs were experimentally evaluated for corner 2 of a 0.1 scale model of the NASA Lewis Research Center's proposed Altitude Wind Tunnel (AWT). Corner 2 contained a simulated shaft fairing for a fan drive system to be located downstream of the corner. The corner was tested with a bellmouth inlet followed by a 0.1 scale model of the crossleg diffuser designed to connect corners 1 and 2 of the AWT. Vane A was a controlled-diffusion airfoil shape; vane B was a circular-arc airfoil shape. The A vanes were tested in several arrangements which included the resetting of the vane angle by -5 degrees or the removal of the outer vane. The lowest total pressure loss for vane A configuration was obtained at the negative reset angle. The loss coefficient increased slightly with the Mach number, ranging from 0.165 to 0.175 with a loss coefficient of 0.170 at the inlet design Mach number of 0.24. Removal of the outer vane did not alter the loss. Vane B loss coefficients were essentially the same as those for the reset vane A configurations. The crossleg diffuser loss coefficient was 0.018 at the inlet design Mach number of 0.33. Author

09 RESEARCH AND SUPPORT FACILITIES (AIR)

N87-20295*# National Aeronautics and Space Administration. Lewis Research Center, Cleveland, Ohio.
DETAILED FLOW SURVEYS OF TURNING VANES DESIGNED FOR A 0.1-SCALE MODEL OF NASA LEWIS RESEARCH CENTER'S PROPOSED ALTITUDE WIND TUNNEL
ROYCE D. MOORE, RICKEY J. SHYNE, DONALD R. BOLDMAN, and THOMAS F. GELDER Apr. 1987 151 p
(NASA-TP-2680; E-3294; NAS 1.60:2680) Avail: NTIS HC A08/MF A01 CSCL 14B

Detailed flow surveys downstream of the corner turning vanes and downstream of the fan inlet guide vanes have been obtained in a 0.1-scale model of the NASA Lewis Research Center's proposed Altitude Wind Tunnel. Two turning vane designs were evaluated in both corners 1 and 2 (the corners between the test section and the drive fan). Vane A was a controlled-diffusion airfoil and vane B was a circular-arc airfoil. At given flows the turning vane wakes were surveyed to determine the vane pressure losses. For both corners the vane A turning vane configuration gave lower losses than the vane B configuration in the regions where the flow regime should be representative of two-dimensional flow. For both vane sets the vane loss coefficient increased rapidly near the walls. Author

N87-22694*# National Aeronautics and Space Administration. Lewis Research Center, Cleveland, Ohio.
EXPERIMENTAL EVALUATION OF BLOCKAGE RATIO AND PLENUM EVACUATION SYSTEM FLOW EFFECTS ON PRESSURE DISTRIBUTION FOR BODIES OF REVOLUTION IN 0.1 SCALE MODEL TEST SECTION OF NASA LEWIS RESEARCH CENTER'S PROPOSED ALTITUDE WIND TUNNEL
RICHARD R. BURLEY and DOUGLAS E. HARRINGTON Apr. 1987 26 p
(NASA-TP-2702; E-3267; NAS 1.60:2702) Avail: NTIS HC A03/MF A01 CSCL 14B

An experimental investigation was conducted in the slotted test section of the 0.1-scale model of the proposed Altitude Wind Tunnel to evaluate wall interference effects at tunnel Mach numbers from 0.70 to 0.95 on bodies of revolution with blockage rates of 0.43, 3, 6, and 12 percent. The amount of flow that had to be removed from the plenum chamber (which surrounded the slotted test section) by the plenum evacuation system (PES) to eliminate wall interference effects was determined. The effectiveness of tunnel reentry flaps in removing flow from the plenum chamber was examined. The 0.43-percent blockage model was the only one free of wall interference effects with no PES flow. Surface pressures on the forward part of the other models were greater than interference-free results and were not influenced by PES flow. Interference-free results were achieved on the aft part of the 3- and 6-percent blockage models with the proper amount of PES flow. The required PES flow was substantially reduced by opening the reentry flaps. Author

N87-22774*# National Aeronautics and Space Administration. Lewis Research Center, Cleveland, Ohio.
HEAT FLUX CALIBRATION FACILITY CAPABLE OF SSME CONDITIONS
CURT H. LIEBERT *In its Structural Integrity and Durability of Reusable Space Propulsion Systems* p 47-49 1987
Avail: NTIS HC A10/MF A01 CSCL 14B

There is a need to more thoroughly characterize the hostile space shuttle main engine (SSME) turbopump environment. It has been estimated that component surface heat flux in the hot-gas environment is about 10 MW/square meter, and this is about 50 times that encountered in aircraft engines. Also, material temperature transients can be as high as 1000 K in about 1 second. These transients can cause durability problems such as material cracking. Heat flux sensors placed in the turbopump components can partially characterize this environment by measuring surface heat flux. These heat flux data can be used to verify analytical-stress, boundary-layer, and heat-transfer design models. Preliminary plans were discussed at the first SSME durability conference for designing and fabricating a new facility for the calibration and durability testing of prototype heat flux

sensors for the SSME. This facility, which is necessary for assessment of new heat flux gauge concepts needed in the hostile SSME turbopump environment, is described. Author

N87-23662*# National Aeronautics and Space Administration. Lewis Research Center, Cleveland, Ohio.
EXPERIMENTAL EVALUATION OF HONEYCOMB/SCREEN CONFIGURATIONS AND SHORT CONTRACTION SECTION FOR NASA LEWIS RESEARCH CENTER'S ALTITUDE WIND TUNNEL
RICHARD R. BURLEY and DOUGLAS E. HARRINGTON May 1987 30 p
(NASA-TP-2692; E-3142; NAS 1.60:2692) Avail: NTIS HC A03/MF A01 CSCL 14B

An experimental investigation was conducted in the high speed leg of the 0.1 scale model of the proposed Altitude Wind Tunnel to evaluate flow conditioner configurations in the settling chamber and their effect on the flow through the short contraction section. The lowest longitudinal turbulence intensity measured at the contraction-section entrance, 1.2%, was achieved with a honeycomb-plus three fine-mesh screens. Turbulence intensity in the test section was estimated to be between 0.1 and 0.2% with the honeycomb plus three fine mesh screens in the settling chamber. Adding screens, however, adversely affected the total pressure profile, causing a small defect near the centerline at the contraction section entrance. No significant boundary layer separation was evident in the short contraction section. Author

N87-23664*# National Aeronautics and Space Administration. Lewis Research Center, Cleveland, Ohio.
REACTIVATION STUDY FOR NASA LEWIS RESEARCH CENTER'S HYPERSONIC TUNNEL FACILITY
JEFFREY E. HAAS Jul. 1987 14 p Presented at the 23rd Joint Propulsion Conference, San Diego, Calif., 29 Jun. - 2 Jul. 1987; cosponsored by AIAA, SAE, ASME, and ASEE
(NASA-TM-89918; E-3614; NAS 1.15:89918; AIAA-87-1886)
Avail: NTIS HC A02/MF A01 CSCL 14B

The Hypersonic Tunnel Facility (HTF) at NASA Lewis Research Center's Plum Brook Station is a blowdown, free-jet, nonvibrated propulsion facility capable of Mach 5, 6, and 7 with true temperature, altitude, and air composition simulation. The facility has been in a deactivated status for 13 years. Discussed are the capabilities of HTF, and the results of a deactivation study recently conducted to determine the cost, schedule, and technical effort required to restore HTF to its original design operating capabilities are summarized. Author

N87-25335*# National Aeronautics and Space Administration. Lewis Research Center, Cleveland, Ohio.
ARCJET POWER SUPPLY AND START CIRCUIT Patent Application
ROBERT P. GRUBER, inventor (to NASA) 10 Jun. 1987 10 p
(NASA-CASE-LEW-14374-1; US-PATENT-APPL-SN-060200)
Avail: NTIS HC A02/MF A01 CSCL 14B

A dc power supply for spacecraft arcjet thrusters has an integral automatic starting circuit and an output averaging inductor. The output averaging inductor, in series with the load, provides instantaneous current control, and ignition pulse and an isolated signal proportional to the arc voltage. A pulse width modulated converter, close loop configured, is also incorporated to give fast response output current control. NASA

N87-28571*# National Aeronautics and Space Administration. Lewis Research Center, Cleveland, Ohio.

EXPERIMENTAL EVALUATION OF CORNER TURNING VANES
Summary Report

ROYCE D. MOORE, DONALD R. BOLDMAN, RICKEY J. SHYNE, and THOMAS F. GELDER 1987 27 p Presented at the 1987 Aerospace Technology Conference and Exposition, Long Beach, Calif., 5-8 Oct. 1987; sponsored by the Society of Automotive Engineers

(NASA-TM-100143; E-3695; NAS 1.15:100143) Avail: NTIS HC A03/MF A01 CSCL 14B

Two types of turning vane airfoils (a controlled-diffusion shape and a circular arc shape) have been evaluated in the high-speed and fan-drive corners of a 0.1-scale model of NASA Lewis Research Center's proposed Altitude Wind Tunnel. The high-speed corner was evaluated with and without a simulated engine exhaust removal scoop. The fan-drive corner was evaluated with and without the high-speed corner. Flow surveys of pressure and flow angle were taken for both the corners and the vanes to determine their respective losses. The two-dimensional vane losses were low; however, the overall corner losses were higher because three-dimensional flow was generated by the complex geometry resulting from the turning vanes intersecting the end wall. The three-dimensional effects were especially pronounced in the outer region of the circular corner.

Author

12

ASTRONAUTICS (GENERAL)

A87-18064*# National Aeronautics and Space Administration. Lewis Research Center, Cleveland, Ohio.

SPACECRAFT 2000 - THE CHALLENGE OF THE FUTURE

H. W. BRANDHORST, JR., K. A. FAYMON, and R. W. BERCAW (NASA, Lewis Research Center, Cleveland, OH) IN: IECEC '86; Proceedings of the Twenty-first Intersociety Energy Conversion Engineering Conference, San Diego, CA, August 25-29, 1986. Volume 3. Washington, DC, American Chemical Society, 1986, p. 1397-1400.

The need for spacecraft bus technology advances in order to develop the spacecraft for the 21st century is discussed. Consideration is given to the power and electric propulsion systems for mass-limited satellites such as LEO and GEO. The goal of spacecraft bus technology programs is to design a cost-effective spacecraft which operates well in the satellite environment. The possibility of collaboration between government and industry is examined.

I.F.

A87-46000*# Rockwell International Corp., Canoga Park, Calif.

CONCEPTS FOR SPACE MAINTENANCE OF OTV ENGINES

A. MARTINEZ, B. D. HINES, and C. M. ERICKSON (Rockwell International Corp., Rocketdyne Div., Canoga Park CA) Joint Army-Navy-NASA-Air Force Interagency Propulsion Committee, Propulsion Meeting, New Orleans, LA, Aug. 1986, Paper. 13 p. (Contract NAS3-23773)

In this paper, concepts for space maintainability of Orbital Transfer Vehicles engines are examined. An engine design is developed which is driven by space maintenance requirements and by a Failure Modes and Effects Analysis (FMEA). Modularity within the engine is shown to offer cost benefits and improved space maintenance capabilities. Space-operable disconnects are conceptualized for both engine change-out and for module replacement. Through FME mitigation the modules are conceptualized to contain the most often replaced engine components. A preliminary space maintenance plan is developed around a Controls and Condition Monitoring system using advanced sensors, controls, and conditioning monitoring concepts. Author

N87-17752*# National Aeronautics and Space Administration. Lewis Research Center, Cleveland, Ohio.

LONG RANGE INHABITED SURFACE TRANSPORTATION SYSTEM POWER SOURCE FOR THE EXPLORATION OF MARS (MANNED MARS MISSION)

LISA KOHOUT, MARK BANYAI, and ROBERT AMICK /n NASA. Marshall Space Flight Center Manned Mars Missions. Working Group Papers, Volume 1, Section 1-4 p 397-405 May 1986

Avail: NTIS HC A22/MF A01 CSCL 22A

A hydrogen-oxygen fuel cell system is identified as a viable power source for a long range inhabited surface transportation system for the exploration of Mars. Power system weights and power requirements are determined as a function of vehicle weight. For vehicles weighing from 2700 to 7300 kg in LEO, the total power system weight ranges from 1140 to 1860 kg, with the reactants and energy conversion hardware (fuel cells, reactant storage, and radiator) weighing 430 to 555 kg and 610 to 1110 kg, respectively. Vehicle power requirements range from 45 kW for a 2700 kg vehicle to 110 kW for a 7300 kg vehicle. Power system specific weights and power profiles for housekeeping and the operation of scientific equipment such as coring drills and power tools are also specified.

Author

13

ASTRODYNAMICS

Includes powered and free-flight trajectories; and orbital and launching dynamics.

N87-22700*# Ohio State Univ., Columbus. ElectroScience Lab. **ON ORBITAL ALLOTMENTS FOR GEOSTATIONARY SATELLITES**

DAVID J. A. GONSALVEZ, CHARLES H. REILLY, and CLARK A. MOUNT-CAMPBELL Nov. 1986 151 p

(Contract NAG3-159)

(NASA-CR-181017; NAS 1.26:181017; OS-TR-718688-2) Avail: NTIS HC A08/MF A01 CSCL 03C

The following satellite synthesis problem is addressed: communication satellites are to be allotted positions on the geostationary arc so that interference does not exceed a given acceptable level by enforcing conservative pairwise satellite separation. A desired location is specified for each satellite, and the objective is to minimize the sum of the deviations between the satellites' prescribed and desired locations. Two mixed integer programming models for the satellite synthesis problem are presented. Four solution strategies, branch-and-bound, Benders' decomposition, linear programming with restricted basis entry, and a switching heuristic, are used to find solutions to example synthesis problems. Computational results indicate the switching algorithm yields solutions of good quality in reasonable execution times when compared to the other solution methods. It is demonstrated that the switching algorithm can be applied to synthesis problems with the objective of minimizing the largest deviation between a prescribed location and the corresponding desired location. Furthermore, it is shown that the switching heuristic can use no conservative, location-dependent satellite separations in order to satisfy interference criteria.

Author

N87-25341*# Ohio State Univ., Columbus. ElectroScience Lab. **A SATELLITE SYSTEM SYNTHESIS MODEL FOR ORBITAL ARC ALLOTMENT OPTIMIZATION**

CHARLES H. REILLY Jul. 1987 23 p

(Contract NAG3-159)

(NASA-CR-181150; NAS 1.26:181150; TR-718688-5) Avail: NTIS HC A02/MF A01 CSCL 22A

A mixed integer programming formulation of a satellite system synthesis problem is presented, which is referred to as the arc allotment problem (AAP). Each satellite administration is to be allotted a weighted-length segment of the geostationary orbital

14 GROUND SUPPORT SYSTEMS AND FACILITIES (SPACE)

arc within which its satellites may be positioned at any longitudes. The objective function maximizes the length of the unweighted arc segment allotted to every administration, subject to single-entry co-channel interference restrictions and constraints imposed by the visible arc for each administration. Useful relationships between special cases of AAP and another satellite synthesis problem are established. Solutions to two example problems are presented.

Author

14

GROUND SUPPORT SYSTEMS AND FACILITIES (SPACE)

Includes launch complexes, research and production facilities; ground support equipment, e.g., mobile transporters; and simulators.

A87-29448*# General Dynamics/Convair, San Diego, Calif.
MEASUREMENT OF CENTAUR/ORBITER MULTIPLE REACTION FORCES IN A FULL-SCALE TEST RIG
PHILIP J. MOLE and STAN A. GRIFFIN (General Dynamics Corp., Convair Div., San Diego, CA) IN: Aerospace Testing Seminar, 9th, Los Angeles, CA, Oct. 15-17, 1985, Proceedings. Mount Prospect, IL, Institute of Environmental Sciences, 1986, p. 45-51. (Contract NAS3-22901)

A multiple component load cell for measuring load is described, and its capability and reliability are evaluated by utilizing it to measure the reaction forces between the Centaur and Centaur Support Structure. The system employs 11 six-component balances in a single test rig to react a combination of loads. The vehicle and balance loads, procedures for fabricating each balance, and the assembly of the balances are discussed. The calibration and testing of the balances are examined. It is noted that the multiple component load cell system is a cost-effective method for obtaining an accurate measurement of friction effects and primary loads.

I.F.

N87-13470*# National Aeronautics and Space Administration, Lewis Research Center, Cleveland, Ohio.
HYDROGEN-AIR IGNITION TORCH
G. A. REPAS Nov. 1986 9 p
(NASA-TM-88882; E-3290; NAS 1.15:88882) Avail: NTIS HC A02/MF A01 CSCL 84E

The design and operation of a hydrogen-air ignition torch presently being used to burn off excess hydrogen that accumulates in the scrubber exhaust ducts of two rocket engine test facilities at the NASA Lewis Research Center in Cleveland, Ohio, is described.

Author

15

LAUNCH VEHICLES AND SPACE VEHICLES

Includes boosters; operating problems of launch/space vehicle systems; and reusable vehicles.

A87-33592*# General Dynamics Corp., San Diego, Calif.
SHUTTLE/CENTAUR G-PRIME COMPOSITE ADAPTERS DAMAGE TOLERANCE/REPAIR TEST PROGRAM
TERESA A. SOLLARS (General Dynamics Corp., Space Systems Div., San Diego, CA) IN: Structures, Structural Dynamics and Materials Conference, 28th, Monterey, CA, Apr. 6-8, 1987, Technical Papers. Part 1. New York, American Institute of Aeronautics and Astronautics, 1987, p. 362-375. refs
(Contract NAS3-22901)
(AIAA PAPER 87-0792)

The Space Shuttle/Centaur Composite Adapters Damage Tolerance/Repair Test program had as its goals the determination of probable and potentially critical defects or damages on the adapters' strength and stability, as well as the adequacy of repairs on significantly damaged areas and the generation of NDT data for the upgrading of acceptance criteria. Such rational accept/reject criteria and repair methods reduce both engineering liaison costs and any unnecessary parts-scraping. Successful 'damage tolerant' design ensures that degradations of strength and stability due to undetected defects or damage will not be catastrophic. O.C.

A87-50501*# National Aeronautics and Space Administration, Lewis Research Center, Cleveland, Ohio.

EFFECT OF GIMBAL FRICTION MODELLING TECHNIQUE ON CONTROL STABILITY AND PERFORMANCE FOR CENTAUR UPPER STAGE

RONALD E. GRAHAM (NASA, Lewis Research Center, Cleveland, OH) IN: AIAA Guidance, Navigation and Control Conference, Monterey, CA, Aug. 17-19, 1987, Technical Papers. Volume 2. New York, American Institute of Aeronautics and Astronautics, 1987, p. 914-918. Previously announced in STAR as N87-22755. refs
(AIAA PAPER 87-2455)

The powered-phase autopilot for the Centaur upper stage rocket uses an autopilot forward loop gain scheduler that decreases the proportional gain as propellant mass is depleted. Nonlinear time response simulation studies revealed that Centaur vehicles with low-gain autopilots would have large attitude error limit cycles. These limit cycles were due to the assumed presence of Coulomb friction in the engine gimbals. This situation could be corrected through the use of an harmonic dither, programmed into the on-board digital computer and added to the engine command signal. This would introduce impending motion to the engines, allowing control of the engines even under small commands. Control authority was found to be restored when dither was used. A concern arose that the Centaur could be unacceptably excited at resonances near the dither frequency, if the dither amplitude was to be chosen on the basis of friction level present, a test was conducted to measure this level. Dither characteristics were to be based on the test results. The test results showed that the gimbal friction characteristic was actually hysteretic rather than the assumed Coulomb friction. The simulation results showed that, using this new model of gimbal friction, dither would no longer be necessary.

Author

N87-15996*# National Aeronautics and Space Administration, Lewis Research Center, Cleveland, Ohio.
CENTAUR D1-A SYSTEMS IN A NUTSHELL
ANDREW L. GORDAN Jan. 1987 29 p
(NASA-TM-88880; E-3287; NAS 1.15:88880) Avail: NTIS HC A03/MF A01 CSCL 22D

This report identifies the unique aspects of the Centaur D1-A systems and subsystems. Centaur performance is described in terms of optimality (propellant usage), flexibility, and airborne

computer requirements. Major systems are described narratively with some numerical data given where it may be useful. Author

SPACE TRANSPORTATION

Includes passenger and cargo space transportation, e.g., shuttle operations; and space rescue techniques.

N87-22755*# National Aeronautics and Space Administration. Lewis Research Center, Cleveland, Ohio.

EFFECT OF GIMBAL FRICTION MODELING TECHNIQUE ON CONTROL STABILITY AND PERFORMANCE FOR CENTAUR UPPER-STAGE

RONALD E. GRAHAM 1987 10 p Prepared for presentation at the Guidance, Navigation and Control Conference, Monterey, Calif., 17-19 Aug. 1987; sponsored by AIAA (NASA-TM-89894; E-3582; NAS 1.15:89894) Avail: NTIS HC A02/MF A01 CSCL 22B

The powered-phase autopilot for the Centaur upper stage rocket uses an autopilot forward loop gain scheduler that decreases the proportional gain as propellant mass is depleted. Nonlinear time response simulation studies revealed that Centaur vehicles with low-gain autopilots would have large attitude error limit cycles. These limit cycles were due to the assumed presence of Coulomb friction in the engine gimbals. This situation could be corrected through the use of an harmonic dither, programmed into the on-board digital computer and added to the engine command signal. This would introduce impending motion to the engines, allowing control of the engines even under small commands. Control authority was found to be restored when dither was used. A concern arose that the Centaur could be unacceptably excited at resonances near the dither frequency, if the dither amplitude was to be chosen on the basis of friction level present, a test was conducted to measure this level. Dither characteristics were to be based on the test results. The test results showed that the gimbal friction characteristic was actually hysteretic rather than the assumed Coulomb friction. The simulation results showed that, using this new model of gimbal friction, dither would no longer be necessary. Author

N87-23674*# National Aeronautics and Space Administration. Lewis Research Center, Cleveland, Ohio.

SPECULATIONS ON FUTURE OPPORTUNITIES TO EVOLVE BRAYTON POWERPLANTS ABOARD THE SPACE STATION

ROBERT E. ENGLISH 1987 29 p Presented at the 4th Symposium on Space Nuclear Power Systems, Albuquerque, N. Mex., 12-16 Jan. 1987; sponsored by Sandia National Labs. (NASA-TM-89863; E-3530; NAS 1.15:89863) Avail: NTIS HC A03/MF A01 CSCL 10B

The Space Station provides a unique, low-risk environment in which to evolve new capabilities. In this way, the Space Station will grow in capacity, in its range of capabilities, and its economy of operation as a laboratory and as a center for space operations. Although both Rankine and Brayton cycles, two concepts for solar dynamic power generation, now compete to power the station, this paper confines its attention to the Brayton cycle using a mixture of He and Xe as its working fluid. Such a Brayton powerplant to supply the station's increasing demands for both electric power and heat has the potential to gradually evolve higher and higher performance by exploiting already-evolved materials (ASTAR-811C and molten-Li heat storage), its peak cycle temperature rising ultimately to 1500 K. Adapting the station to exploit long tethers (200 to 300 km long) could yield increases in payloads to LEO, to GEO, and to distant destinations in the solar system. Such tethering of the Space Station would not only require additional power for electric propulsion but also would so increase nuclear safety that nuclear powerplants might provide this power. From an 8000-kWt SP-100 reactor, thermoelectric power generation could produce 300 kWe, or adapted solar-Brayton cycle, 2400 to 2800 kWe. Author

A87-15880*# General Dynamics Corp., San Diego, Calif.

EFFECTS OF TRANSIENT PROPELLANT DYNAMICS ON DEPLOYMENT OF LARGE LIQUID STAGES IN ZERO-GRAVITY WITH APPLICATION TO SHUTTLE/CENTAUR

R. E. MARTIN (General Dynamics Corp., Space Systems Div., San Diego, CA) IAF, International Astronautical Congress, 37th, Innsbruck, Austria, Oct. 4-11, 1986. 11 p. refs (Contract NAS3-22901) (IAF PAPER 86-119)

This paper describes the application of a recently developed CFD program, HYDR-3D, to the analysis of separation of the Centaur G-Prime vehicle from the Shuttle Orbiter. The typical application presented illustrates a particularly difficult design task - deployment of a large, liquid-filled, densely packaged vehicle from a manned vehicle. Since it represents a potential catastrophic hazard, a vast number of conditions and parameters must be analyzed to ensure tolerance of at least two credible failures. Validation of the HYDR-3D program against zero- and low-gravity experimental data is also presented. Using the fluid dynamics program, this approach can be used confidently to analyze and determine design requirements for a variety of OTV/space-station deployment and docking problems. Author

A87-31107*# National Aeronautics and Space Administration. Lewis Research Center, Cleveland, Ohio.

SCIENCE AND TECHNOLOGY ISSUES IN SPACECRAFT FIRE SAFETY

ROBERT FRIEDMAN and KURT R. SACKSTEDER (NASA, Lewis Research Center, Cleveland, OH) AIAA, Aerospace Sciences Meeting, 25th, Reno, NV, Jan. 12-15, 1987. 29 p. Previously announced in STAR as N87-16012. refs (AIAA PAPER 87-0467)

The space station, a permanently-inhabited orbiting laboratory, places new demands on spacecraft fire safety. Long-duration missions may call for more-constrained fire controls, but the accessibility of the space station to a variety of users may call for less-restrictive measures. This paper discusses fire safety issues through a review of the state of the art and a presentation of key findings from a recent NASA Lewis Research Center Workshop. The subjects covered are the fundamental science of low-gravity combustion and the technology advances in fire detection, extinguishment, materials assessment, and atmosphere selection. Key concerns are for the adoption of a fire-safe atmosphere and the substitution for the effective but toxic extinguishant, halon 1301. The fire safety studies and reviews provide several recommendations for further action. One is the expanded research in combustion, sensors, and materials in the low-gravity environment of space. Another is the development of generalized fire-safety standards for spacecraft through cooperative endeavors with aerospace and outside Government and industry sources. Author

A87-33697*# National Aeronautics and Space Administration. Lewis Research Center, Cleveland, Ohio.

THE EFFECT OF NONLINEARITIES ON THE DYNAMIC RESPONSE OF A LARGE SHUTTLE PAYLOAD

TIMOTHY L. SULLIVAN and KELLY S. CARNEY (NASA, Lewis Research Center, Cleveland, OH) IN: Structures, Structural Dynamics and Materials Conference, 28th, Monterey, CA, Apr. 6-8, 1987 and AIAA Dynamics Specialists Conference, Monterey, CA, Apr. 9, 10, 1987, Technical Papers. Part 2A. New York, American Institute of Aeronautics and Astronautics, 1987, p. 440-455. refs (AIAA PAPER 87-0857)

The STS Centaur was designed to be a high energy upper stage for use with the Space Shuttle. Two versions were designed and under development when the program was cancelled. The first version, designated G-prime, was designed for planetary missions. The second version, designated G, was designed to place spacecraft in geosynchronous orbit. As a part of the STS Centaur finite-element model verification effort, test articles of both versions were subjected to a series of static tests. In addition the Centaur G-prime test article was subjected to a series of dynamic tests including a modal survey. Both the static and dynamic tests showed that nonlinearities existed in the Centaur and its support system. The support system included flight-like latches. The nonlinearities were particularly apparent in tests that loaded the forward support structure of the Centaur. These test results were used to aid in the development of two improved finite-element models. The first was a linear model, while the second contained nonlinear elements at the boundaries. Results from both models were compared with the transient response obtained from a step-relaxation or twang test. The linear model was able to accurately match the low frequency response found in the test data. However, only the nonlinear model was able to match higher frequency response that was present in some of the test data. In addition the nonlinear model was able to predict other nonlinear behavior such as the dynamic 'jump' that occurs in systems with nonlinear stiffness. Author

A87-41161*# Rockwell International Corp., Canoga Park, Calif. **CONCEPTS FOR SPACE MAINTENANCE OF OTV ENGINES**

A. MARTINEZ, B. D. HINES, and C. M. ERICKSON (Rockwell International Corp., Rocketdyne Div., Canoga Park, CA) Joint Army-Navy-NASA-Air Force Interagency Propulsion Committee, Propulsion Meeting, New Orleans, LA, Aug. 25-28, 1986, Paper. 13 p.

(Contract NAS3-23773)

Concepts for space maintainability of OTV engines are examined. The advanced efforts are based on work recently completed for NASA Lewis Research Center Space Propulsion Technology Division. An engine design is developed which is driven by space maintenance requirements and by a failure modes and effects analysis. Modularity within the engine is shown to offer cost benefits and improved space maintenance capabilities. Space-operable disconnects are conceptualized for both engine change-out and for module replacement. Through FME mitigation the modules are conceptualized to contain the most often replaced engine components. A preliminary space maintenance plan is developed around a controls and condition monitoring system using advanced sensors, controls, and conditioning monitoring concepts. Author

A87-48573*# National Aeronautics and Space Administration. Lewis Research Center, Cleveland, Ohio.

NUMERICAL MODELING OF ON-ORBIT PROPELLANT MOTION RESULTING FROM AN IMPULSIVE ACCELERATION

JOHN C. AYDELOTT (NASA, Lewis Research Center, Cleveland, OH), RAYMOND C. MJOLNESS, MARTIN D. TORREY (Los Alamos National Laboratory, NM), and JOHN I. HOCHSTEIN (Washington University, St. Louis, MO) AIAA, SAE, ASME, and ASEE, Joint Propulsion Conference, 23rd, San Diego, CA, June 29-July 2, 1987. 23 p. Previously announced in STAR as N87-22757. refs

(AIAA PAPER 87-1766)

In-space docking and separation maneuvers of spacecraft that have large fluid mass fractions may cause undesirable spacecraft motion in response to the impulsive-acceleration-induced fluid motion. An example of this potential low gravity fluid management problem arose during the development of the shuttle/Centaur vehicle. Experimentally verified numerical modeling techniques were developed to establish the propellant dynamics, and subsequent vehicle motion, associated with the separation of the Centaur vehicle from the shuttle orbiter cargo bay. Although the shuttle/Centaur development activity was suspended, the numerical modeling techniques are available to predict on-orbit liquid motion resulting from impulsive accelerations for other missions and spacecraft. Author

N87-16012*# National Aeronautics and Space Administration. Lewis Research Center, Cleveland, Ohio.

SCIENCE AND TECHNOLOGY ISSUES IN SPACECRAFT FIRE SAFETY

ROBERT FRIEDMAN and KURT R. SACKSTEDER Jan. 1987 29 p Presented at the 25th Aerospace Sciences Meeting, Reno, Nev., 12-15 Jan. 1987; sponsored by AIAA (NASA-TM-88933; E-3349; NAS 1.15:88933; AIAA-87-0467) Avail: NTIS HC A03/MF A01 CSCL 22B

The space station, a permanently-inhabited orbiting laboratory, places new demands on spacecraft fire safety. Long-duration missions may call for more-constrained fire controls, but the accessibility of the space station to a variety of users may call for less-restrictive measures. This paper discusses fire safety issues through a review of the state of the art and a presentation of key findings from a recent NASA Lewis Research Center Workshop. The subjects covered are the fundamental science of low-gravity combustion and the technology advances in fire detection, extinguishment, materials assessment, and atmosphere selection. Key concerns are for the adoption of a fire-safe atmosphere and the substitution for the effective but toxic extinguishant, halon 1301. The fire safety studies and reviews provide several recommendations for further action. One is the expanded research in combustion, sensors, and materials in the low-gravity environment of space. Another is the development of generalized fire-safety standards for spacecraft through cooperative endeavors with aerospace and outside Government and industry sources. Author

N87-20342*# National Aeronautics and Space Administration. Lewis Research Center, Cleveland, Ohio.

FIRE SAFETY CONCERNS IN SPACE OPERATIONS

ROBERT FRIEDMAN 1987 13 p Prepared for presentation at the Joint Army-Navy-NASA-Air Force (JANNAF) Safety and Environmental Protection Subcommittee Meeting, Cleveland, Ohio, 4-7 May 1987 (NASA-TM-89848; E-3511; NAS 1.15:89848) Avail: NTIS HC A02/MF A01 CSCL 22A

This paper reviews the state-of-the-art in fire control techniques and identifies important issues for continuing research, technology, and standards. For the future permanent orbiting facility, the space station, fire prevention and control calls for not only more stringent fire safety due to the long-term and complex missions, but also for simplified and flexible safety rules to accommodate the variety of users. Future research must address a better understanding of the microgravity space environment as it influences fire propagation and extinction and the application of the technology of fire

detection, extinguishment, and material assessment. Spacecraft fire safety should also consider the adaptation of methods and concepts derived from aircraft and undersea experience. Author

N87-22757*# National Aeronautics and Space Administration. Lewis Research Center, Cleveland, Ohio.

NUMERICAL MODELING OF ON-ORBIT PROPELLANT MOTION RESULTING FROM AN IMPULSIVE ACCELERATION

JOHN C. AYDELOTT, RAYMOND C. MJOLSNES, MARTIN D. TORREY, and JOHN I. HOCHSTEIN (Washington Univ., St. Louis, Mo.) 1987 24 p Prepared for the 23rd Joint Propulsion Conference, San Diego, Calif., 29 Jun. - 2 Jul. 1987; cosponsored by AIAA, SAE, ASME, and ASEE

(NASA-TM-89873; E-3547; NAS 1.15:89873; AIAA-87-1766)

Avail: NTIS HC A02/MF A01 CSCL 22A

In-space docking and separation maneuvers of spacecraft that have large fluid mass fractions may cause undesirable spacecraft motion in response to the impulsive-acceleration-induced fluid motion. An example of this potential low gravity fluid management problem arose during the development of the shuttle/Centaur vehicle. Experimentally verified numerical modeling techniques were developed to establish the propellant dynamics, and subsequent vehicle motion, associated with the separation of the Centaur vehicle from the shuttle orbiter cargo bay. Although the shuttle/Centaur development activity was suspended, the numerical modeling techniques are available to predict on-orbit liquid motion resulting from impulsive accelerations for other missions and spacecraft. Author

17

SPACE COMM., SPACECRAFT COMM., COMMAND & TRACKING

Includes telemetry; space communications networks; astronavigation and guidance; and radio blackout.

A87-26610* National Aeronautics and Space Administration. Lewis Research Center, Cleveland, Ohio.

OPTICAL TECHNOLOGIES FOR COMMUNICATION SATELLITE APPLICATIONS; PROCEEDINGS OF THE MEETING, LOS ANGELES, CA, JAN. 21, 22, 1986

KUL BHASIN, ED. (NASA, Lewis Research Center, Cleveland, OH) Meeting sponsored by SPIE. Bellingham, WA, Society of Photo-Optical Instrumentation Engineers (SPIE Proceedings. Volume 616), 1986, 307 p. For individual items see A87-26611 to A87-26642.

(SPIE-616)

The present conference considers topics encompassing the fields of satellite communications technology, optical subsystems, transmitters and receivers, subsystems for pointing and tracking, onboard processing- and component-related technologies, fiber-optic distribution networks, and reliability-related considerations. Attention is given to lightwave technology in microwave systems, the status of CO₂ laser technology and homodyne receiver concepts for communication satellite optical links, laser Doppler measurement techniques for spacecraft, fiber-optic gyros for space applications, integrated acoustooptic device modules for communication, signal processing and computing, radiation-hardened optoelectronic components, and radiation effects on fiber-optics. O.C.

18

SPACECRAFT DESIGN, TESTING AND PERFORMANCE

Includes satellites; space platforms; space stations; spacecraft systems and components such as thermal and environmental controls; and attitude controls.

A87-15894*# National Aeronautics and Space Administration. Lewis Research Center, Cleveland, Ohio.

SPACE POWER DEVELOPMENT IMPACT ON TECHNOLOGY REQUIREMENTS

J. F. CASSIDY (NASA, Lewis Research Center, Cleveland, OH), T. J. FITZGERALD, R. I. GILJE, and J. D. GORDON (TRW, Inc., Applied Technology Div., Redondo Beach, CA) IAF, International Astronautical Congress, 37th, Innsbruck, Austria, Oct. 4-11, 1986. 11 p.

(IAF PAPER 86-143)

The paper is concerned with the selection of a specific spacecraft power technology and the identification of technology development to meet system requirements. Requirements which influence the selection of a given technology include the power level required, whether the load is constant or transient in nature, and in the case of transient loads, the time required to recover the power, and overall system safety. Various power technologies, such as solar voltaic power, solar dynamic power, nuclear power systems, and electrochemical energy storage, are briefly described. V.L.

A87-18344* Martin Marietta Aerospace, Denver, Colo.

ON-ORBIT CRYOGENIC STORAGE AND RESUPPLY

R. N. EBERHARDT, J. P. GILLE, and D. A. FESTER (Martin Marietta Co., Denver, CO) IN: International Symposium on Space Technology and Science, 14th, Tokyo, Japan, May 27-June 1, 1984, Proceedings. Tokyo, AGNE Publishing, Inc., 1984, p. 1113-1124.

(Contract NAS3-23355)

Methods of integrating pressure control, liquid acquisition, and liquid transfer concepts for the Cryogenic Fluid Management Facility, a reusable test bed in the Shuttle cargo bay studying the efficient management of cryogens in space, are investigated. Significant design data and criteria for future subcritical cryogenic storage and transfer systems are presented. Technology requirements for liquid storage/supply systems, thermal control systems, and fluid transfer/resupply are addressed, and fluid and thermal analysis pertaining to receiver tank chilldown and no-vent fill of the receiver tank are discussed. C.D.

A87-19907*# National Aeronautics and Space Administration. Lewis Research Center, Cleveland, Ohio.

DEVELOPMENT OF THE VOLT-A SHUTTLE EXPERIMENT

WILLIAM J. BIFANO, JOHN M. BOZEK, and DALE C. FERGUSON (NASA, Lewis Research Center, Cleveland, OH) IN: Photovoltaic Specialists Conference, 18th, Las Vegas, NV, October 21-25, 1985, Conference Record. New York, Institute of Electrical and Electronics Engineers, Inc., 1985, p. 680-687. Previously announced in STAR as N86-14110.

The NASA Lewis Research Center (LeRC) is investigating potential problems associated with the operation of high voltage solar cell arrays in the space plasma environment. At high voltages, interactions between the solar array and the space plasma could result in unacceptable levels of electrical discharge (arcing) and/or parasitic losses (current drains from the array to the plasma). The objective of the Voltage Operating Limit Tests (VOLT-A) Shuttle bay experiment is to characterize space plasma/solar cell panel interactions in low earth orbit. VOLT-A consists of an experiment plate subassembly which contains four solar panels, an electronics subassembly and a Langmuir probe subassembly mounted on an MPES carrier. During a given 8.25 hour data taking period (5-1/2 continuous orbits), the solar panels, which represent state-of-the-art

18 SPACECRAFT DESIGN, TESTING AND PERFORMANCE

solar cell technologies, will be sequentially subjected to bias voltages in steps ranging from minus 626 V to plus 313 V. Appropriate measurements will be made at each voltage to characterize arcing and parasitic losses. Corresponding measurements of the plasma environment (plasma density, electron temperature and neutral density) will also be made. Data will be recorded on an on-board tape recorder for subsequent data reduction and analysis. Author

A87-22401*# National Aeronautics and Space Administration. Lewis Research Center, Cleveland, Ohio.

EFFECT OF AN OXYGEN PLASMA ON THE PHYSICAL AND CHEMICAL PROPERTIES OF SEVERAL FLUIDS FOR THE LIQUID DROPLET RADIATOR

DANIEL A. GULINO and CAROLYN E. COLES (NASA, Lewis Research Center, Cleveland, OH) AIAA, Aerospace Sciences Meeting, 25th, Reno, NV, Jan. 12-15, 1987. 5 p. Previously announced in STAR as N86-31634. (AIAA PAPER 87-0080)

The Liquid Droplet Radiator is one of several radiator systems currently under investigation by NASA Lewis Research Center. It involves the direct exposure of the radiator working fluid to the space environment. An area of concern is the potential harmful effects of the low-Earth-orbit atomic oxygen environment on the radiator working fluid. To address this issue, seven candidate fluids were exposed to an oxygen plasma environment in a laboratory plasma asher. The fluids studied included Dow Corning 705 Diffusion Pump Fluid, polymethylphenylsiloxane and polydimethylsiloxane, both of which are experimental fluids made by Dow Corning, Fomblin Z25, made by Montedison, and three fluids from the Krytox family of fluids, Krytox 143AB, 1502, and 16256, which are made by DuPont. The fluids were characterized by noting changes in visual appearance, physical state, mass, and infrared spectra. Of the fluids tested, the Fomblin and the three Krytox were the least affected by the oxygen plasma. The only effect noted was a change in mass, which was most likely due to an oxygen-catalyzed depolymerization of the fluid molecule. Author

A87-22738*# Massachusetts Inst. of Tech., Cambridge.

RADIATION FROM LARGE SPACE STRUCTURES IN LOW EARTH ORBIT WITH INDUCED AC CURRENTS

D. E. HASTINGS and S. OLBERT (MIT, Cambridge, MA) AIAA, Aerospace Sciences Meeting, 25th, Reno, NV, Jan. 12-15, 1987. 19 p. refs (Contract NAG3-695) (AIAA PAPER 87-0612)

Large conducting space structures in low earth orbit will have a nonnegligible motionally induced potential across their structures. The induced current flow through the body and the ionosphere causes the radiation of Alfvén and lower hybrid waves. This current flow is taken to be ac and the radiated power is studied as a function of the ac frequency. The current may be ac due either to inductive coupling from the power system on the structure or by active modulation. A Space Station-like structure and tether are studied. For the Space Station structure the radiation impedance is particularly high for frequencies in the tens of kilohertz range which suggests that the Space Station may be efficient source of lower hybrid waves. The tether is also shown to be a generator of VLF waves up to source ac frequencies in the megahertz range. The implications for these two structures are discussed. Author

A87-41611*# Hughes Aircraft Co., Los Angeles, Calif.

MODELING OF ENVIRONMENTALLY INDUCED TRANSIENTS WITHIN SATELLITES

N. JOHN STEVENS, GORDON J. BARBAY, MICHAEL R. JONES, and R. VISWANATHAN (Hughes Aircraft Co., Los Angeles, CA) Journal of Spacecraft and Rockets (ISSN 0022-4650), vol. 24, May-June 1987, p. 257-263. refs (Contract NAS3-23869) (AIAA PAPER 85-0387)

A technique is described that allows an estimation of possible spacecraft charging hazards. This technique, called SCREENS

(spacecraft response to environments of space), utilizes the NASA charging analyzer program (NASCAP) to estimate the electrical stress locations and the charge stored in the dielectric coatings due to spacecraft encounter with a geomagnetic substorm environment. This information can then be used to determine the response of the spacecraft electrical system to a surface discharge by means of lumped element models. The coupling into the electronics is assumed to be due to magnetic linkage from the transient currents flowing as a result of the discharge transient. The behavior of a spinning spacecraft encountering a severe substorm is predicted using this technique. It is found that systems are potentially vulnerable to upset if transient signals enter through the ground lines. Author

A87-42585* Massachusetts Inst. of Tech., Cambridge.

THE RADIATION IMPEDANCE OF AN ELECTRODYNAMIC TETHER WITH END CONNECTORS

DANIEL E. HASTINGS and J. WANG (MIT, Cambridge, MA) Geophysical Research Letters (ISSN 0094-8276), vol. 14, May 1987, p. 519-522. refs (Contract NAG3-695)

Electrodynamic tethers are wires deployed across the earth's geomagnetic field through which a current is flowing. The radiation impedance of a tether with end connectors carrying an ac current is computed from classical antenna theory. This simulates the use of a tether on a space structure. It is shown that the current flow pattern at the tether connector is critical to determining the overall radiation impedance. If the tether makes direct electrical contact with the ionosphere then radiation impedances of the order of several thousand Ohms can be expected. If the only electrical contact is through the end connectors then the impedance is only a few Ohms for a dc current rising to several tens of Ohms for an ac current with frequencies in the whistler range. Author

A87-43059*# National Aeronautics and Space Administration. Lewis Research Center, Cleveland, Ohio.

LIQUID DROPLET RADIATOR DEVELOPMENT STATUS

K. ALAN WHITE, III (NASA, Lewis Research Center, Cleveland, OH) AIAA, Thermophysics Conference, 22nd, Honolulu, HI, June 8-10, 1987. 21 p. Previously announced in STAR as N87-20353. refs (AIAA PAPER 87-1537)

Development of the Liquid Droplet Radiator (LDR) is described. Significant published results of previous investigators are presented, and work currently in progress is discussed. Several proposed LDR configurations are described, and the rectangular and triangular configurations currently of most interest are examined. Development of the droplet generator, collector, and auxiliary components are discussed. Radiative performance of a droplet sheet is considered, and experimental results are seen to be in very good agreement with analytical predictions. The collision of droplets in the droplet sheet, the charging of droplets by the space plasma, and the effect of atmospheric drag on the droplet sheet are shown to be of little consequence, or can be minimized by proper design. The LDR is seen to be less susceptible than conventional technology to the effects of micrometeoroids or hostile threats. The identification of working fluids which are stable in the orbital environments of interest is also made. Methods for reducing spacecraft contamination from an LDR to an acceptable level are discussed. Preliminary results of microgravity testing of the droplet generator are presented. Possible future NASA and Air Force missions enhanced or enabled by a LDR are also discussed. System studies indicate that the LDR is potentially less massive than heat pipe radiators. Planned microgravity testing aboard the Shuttle or space station is seen to be a logical next step in LDR development. Author

A87-43073*# National Aeronautics and Space Administration. Lewis Research Center, Cleveland, Ohio.

DEVELOPMENT AND TEST OF THE SHUTTLE/CENTAUR CRYOGENIC TANKAGE THERMAL PROTECTION SYSTEM

R. H. KNOLL (NASA, Lewis Research Center, Cleveland, OH), J. E. ENGLAND, and P. N. MACNEIL (General Dynamics Corp., Space Systems Div., San Diego, CA) AIAA, Thermophysics Conference, 22nd, Honolulu, HI, June 8-10, 1987. 19 p. refs

(Contract NAS3-22901)

(AIAA PAPER 87-1557)

The Thermal Protection System (TPS) for the Shuttle/Centaur had to provide fail-safe thermal protection during prelaunch, launch ascent, and on-orbit operations as well as during potential abort where the Shuttle and Centaur would return to earth. The TPS selected used a helium-purged polyimide foam beneath three radiation shields for the liquid hydrogen (LH2) tank and radiation shields only for the liquid oxygen (LO2) tank (three shields on the tank sidewall and four on the aft bulkhead). An evacuated common intermediate bulkhead separated the two tanks. The LH2 tank had one 1.9-cm thick layer of foam on the forward bulkhead and two layers on the larger area side-wall. Full scale tests of the flight vehicle in a simulated Shuttle cargo bay, that was purged with gaseous nitrogen, gave total prelaunch heating rates of 25.9 kW and 12.9 kW for LH2 and LO2 tanks, respectively. Calorimeter tests on a representative LH2 tank sidewall TPS sample indicated that the measured unit heating rate would rapidly decrease from the prelaunch rate of 300 W/sq m to a desired rate of less than 4 W/sq m once on-orbit.

Author

A87-43081*# General Dynamics Corp., San Diego, Calif.

SELF-REGULATING HEATER APPLICATION TO SHUTTLE-CENTAUR HYDRAZINE FUEL LINE THERMAL CONTROL

DAVID B. UNKRICH (General Dynamics Corp., Space Systems Div., San Diego, CA) AIAA, Thermophysics Conference, 22nd, Honolulu, HI, June 8-10, 1987. 7 p.

(Contract NAS3-22901)

(AIAA PAPER 87-1570)

The Shuttle/Centaur high energy upper stage vehicle thermal environments were more severe than previous Centaur vehicle thermal environments, creating need for a new hydrazine fuel line thermal control technique. Constant power heaters did not satisfy power dissipation requirements, because the power required to maintain fuel line thermal control during cold conditions exceeded the maximum power allowable during hot conditions. Therefore, a Raychem Thermolimit self-regulating heater was selected for this application, and was attached to the hydrazine fuel line with Kapton and aluminum foil tapes. Fuel line/heater thermal modeling and subsequent thermal vacuum chamber testing simulated heater thermal performance during all worst-case Shuttle/Centaur thermal environmental conditions. Fuel line temperatures were maintained between the 4C to 71C limits during all analytical and test cases. Finally, the thermal model predictions were correlated with the test data, thereby ensuring that the model would provide satisfactory predictions for future missions and/or vehicles.

Author

N87-10946*# Hughes Aircraft Co., Los Angeles, Calif. Space and Communications Group.

ENVIRONMENTALLY-INDUCED DISCHARGE TRANSIENT COUPLING TO SPACECRAFT Final Report

R. VISWANATHAN, G. BARBAY, and N. J. STEVENS May 1985 92 p

(Contract NAS3-23869)

(NASA-CR-174922; NAS 1.26:174922) Avail: NTIS HC A05/MF A01 CSCL 22B

The Hughes SCREENS (Space Craft Response to Environments of Space) technique was applied to generic spin and 3-axis stabilized spacecraft models. It involved the NASCAP modeling for surface charging and lumped element modeling for transients coupling into a spacecraft. A differential voltage between antenna and spun shell of approx. 400 V and current of 12 A resulted from discharge at antenna for the spinner and approx. 3 kv and

0.3 A from a discharge at solar panels for the 3-axis stabilized Spacecraft. A typical interface circuit response was analyzed to show that the transients would couple into the Spacecraft System through ground points, which are most vulnerable. A compilation and review was performed on 15 years of available data from electron and ion current collection phenomena. Empirical models were developed to match data and compared with flight data of Pix-1 and Pix-2 mission. It was found that large space power systems would float negative and discharge if operated at or above 300 V. Several recommendations are given to improve the models and to apply them to large space systems.

Author

N87-20353*# National Aeronautics and Space Administration. Lewis Research Center, Cleveland, Ohio.

LIQUID DROPLET RADIATOR DEVELOPMENT STATUS

K. ALAN WHITE, III 1987 28 p Prepared for presentation at the 22nd Thermophysics Conference, Honolulu, Hawaii, 8-10 Jul. 1987; sponsored by AIAA

(NASA-TM-89852; E-3510; NAS 1.15:89852) Avail: NTIS HC

A03/MF A01 CSCL 22B

Development of the Liquid Droplet Radiator (LDR) is described. Significant published results of previous investigators are presented, and work currently in progress is discussed. Several proposed LDR configurations are described, and the rectangular and triangular configurations currently of most interest are examined. Development of the droplet generator, collector, and auxiliary components are discussed. Radiative performance of a droplet sheet is considered, and experimental results are seen to be in very good agreement with analytical predictions. The collision of droplets in the droplet sheet, the charging of droplets by the space plasma, and the effect of atmospheric drag on the droplet sheet are shown to be of little consequence, or can be minimized by proper design. The LDR is seen to be less susceptible than conventional technology to the effects of micrometeoroids or hostile threats. The identification of working fluids which are stable in the orbital environments of interest is also made. Methods for reducing spacecraft contamination from an LDR to an acceptable level are discussed. Preliminary results of microgravity testing of the droplet generator are presented. Possible future NASA and Air Force missions enhanced or enabled by a LDR are also discussed. System studies indicate that the LDR is potentially less massive than heat pipe radiators. Planned microgravity testing aboard the Shuttle or space station is seen to be a logical next step in LDR development.

Author

N87-23685*# National Aeronautics and Space Administration. Lewis Research Center, Cleveland, Ohio.

DESIGN, DEVELOPMENT AND TEST OF SHUTTLE/CENTAUR G-PRIME CRYOGENIC TANKAGE THERMAL PROTECTION SYSTEMS

RICHARD H. KNOLL, PETER N. MACNEIL, and JAMES E. ENGLAND (General Dynamics Corp., San Diego, Calif.) May 1987 42 p Presented at the 22nd Thermophysics Conference, Honolulu, Hawaii, 8-10 Jun. 1987; sponsored by AIAA

(Contract NAS3-22901)

(NASA-TM-89825; E-3473; NAS 1.15:89825; AIAA-87-1557)

Avail: NTIS HC A03/MF A01 CSCL 22B

The thermal protection systems for the shuttle/Centaur would have had to provide fail-safe thermal protection during prelaunch, launch ascent, and on-orbit operations as well as during potential abort. The thermal protection systems selected used a helium-purged polyimide foam beneath three radiation shields for the liquid-hydrogen tank and radiation shields only for the liquid-oxygen tank (three shields on the tank sidewall and four on the aft bulkhead). A double-walled vacuum bulkhead separated the two tanks. The liquid-hydrogen tank had one 0.75-in-thick layer of foam on the forward bulkhead and two layers on the larger area sidewall. Full scale tests of the flight vehicle in a simulated shuttle cargo bay that was purged with gaseous nitrogen gave total prelaunch heating rates of 88,500 Btu/hr and 44,000 Btu/hr for the liquid-hydrogen and -oxygen tanks, respectively. Calorimeter tests on a representative sample of the liquid-hydrogen tank sidewall thermal protection system indicated that the measured

18 SPACECRAFT DESIGN, TESTING AND PERFORMANCE

unit heating rate would rapidly decrease from the prelaunch rate of approx 100 Btu/hr/sq ft to a desired rate of less than 1.3 Btu/hr/sq ft once on orbit.

N87-25419*# Ohio State Univ., Columbus. ElectroScience Lab.
MATHEMATICAL PROGRAMMING FORMULATIONS FOR SATELLITE SYNTHESIS

PUNEET BHASIN and CHARLES H. REILLY Jul. 1987 113 p
(Contract NAG3-159)
(NASA-CR-181151; NAS 1.26:181151; TR-718688-4) Avail: NTIS HC A06/MF A01 CSCL 22B

The problem of satellite synthesis can be described as optimally allotting locations and sometimes frequencies and polarizations, to communication satellites so that interference from unwanted satellite signals does not exceed a specified threshold. In this report, mathematical programming models and optimization methods are used to solve satellite synthesis problems. A nonlinear programming formulation which is solved using Zoutendijk's method and a gradient search method is described. Nine mixed integer programming models are considered. Results of computer runs with these nine models and five geographically compatible scenarios are presented and evaluated. A heuristic solution procedure is also used to solve two of the models studied. Heuristic solutions to three large synthesis problems are presented. The results of our analysis show that the heuristic performs very well, both in terms of solution quality and solution time, on the two models to which it was applied. It is concluded that the heuristic procedure is the best of the methods considered for solving satellite synthesis problems.

Author

N87-26449*# National Aeronautics and Space Administration.
Lewis Research Center, Cleveland, Ohio.

ELECTRODYNAMIC TETHER

MICHAEL PATTERSON *In its* Space Photovoltaic Research and Technology 1986. High Efficiency, Space Environment and Array Technology p 343 Jun. 1987

Avail: NTIS HC A16/MF A01 CSCL 22B

Electrodynamic tethers hold promise for a variety of space applications. Electrodynamic tethers depend upon the interactions between a moving insulated conductor and the Earth's magnetic field. An electric field is generated along the tether as in a conductor moving in the magnetic field of a generator. If the circuit is closed to the ambient space plasma via a plasma gun or other equivalent device, a current is enabled to flow in the tether, and electric power is generated at the expense of orbital mechanical energy. The net effect is a decrease in the altitude of the orbiting tethered system. The situation can be reversed by driving current against the electric field via an external power supply such as a photovoltaic array.

Author

N87-26946*# Alabama Univ., Huntsville. Dept. of Physics.

ELECTRON BEAM EXPERIMENTS AT HIGH ALTITUDES

R. C. OLSEN *In* AGARD, The Aerospace Environment at High Altitudes and its Implications for Spacecraft Charging and Communications 8 p May 1987

(Contract NAG3-620)

Avail: NTIS HC A13/MF A01 CSCL 22B

Experiments with the electron gun on the SCATHA satellite produced evidence of beam-plasma interactions, and heating of the low energy electrons around the satellite. These experiments were conducted near geosynchronous orbit, in the dusk bulge, and plasma sheet, with one short operation in the lobe regions, providing a range of ambient plasma densities. The electron gun was operated at 50 eV, with beam currents of 1, 10, and 100 micro-A. Data from electrostatic analyzers and the DC electric field experiment show that the satellite charged to near the beam energy in sunlight, if the beam current was sufficient. Higher ambient densities required higher beam currents. The electrostatic analyzers showed distribution functions which had peaks, or plateaus, at energies greater than the satellite potential. These measurements indicate heating of the ambient plasma at several Debye lengths from the satellite, with the heated plasma then accelerated into

the satellite. It is likely that the ambient plasma is in fact the photoelectron sheath generated by the satellite.

Author

N87-26950*# National Aeronautics and Space Administration.
Lewis Research Center, Cleveland, Ohio.

SECONDARY ELECTRON GENERATION, EMISSION AND TRANSPORT: EFFECTS ON SPACECRAFT CHARGING AND NASCAP MODELS

IRA KATZ, MYRON MANDELL (Systems Science and Software, La Jolla, Calif.), JAMES C. ROCHE, and CAROLYN PURVIS *In* AGARD, The Aerospace Environment at High Altitudes and its Implications for Spacecraft Charging and Communications 12 p May 1987

Avail: NTIS HC A13/MF A01 CSCL 22B

Secondary electrons control a spacecraft's response to a plasma environment. To accurately simulate spacecraft charging, the NASA Charging Analyzer Program (NASCAP) has mathematical models of the generation, emission and transport of secondary electrons. The importance of each of the processes and the physical basis for each of the NASCAP models are discussed. Calculations are presented which show that the NASCAP formulations are in good agreement with both laboratory and space experiments.

Author

N87-27710*# Communications Satellite Corp., Clarksburg, Md.
ON-BOARD PROCESSING SATELLITE NETWORK ARCHITECTURE AND CONTROL STUDY Final Report

S. JOSEPH CAMPANELLA, B. PONTANO, and H. CHALMERS

Jun. 1987 18 p

(Contract NAS3-24886)

(NASA-CR-180816; NAS 1.26:180816) Avail: NTIS HC A02/MF A01 CSCL 22B

For satellites to remain a vital part of future national and international communications, system concepts that use their inherent advantages to the fullest must be created. Network architectures that take maximum advantage of satellites equipped with onboard processing are explored. Satellite generations must accommodate various services for which satellites constitute the preferred vehicle of delivery. Such services tend to be those that are widely dispersed and present thin to medium loads to the system. Typical systems considered are thin and medium route telephony, maritime, land and aeronautical radio, VSAT data, low bit rate video teleconferencing, and high bit rate broadcast of high definition video. Delivery of services by TDMA and FDMA multiplexing techniques and combinations of the two for individual and mixed service types are studied. The possibilities offered by onboard circuit switched and packet switched architectures are examined and the results strongly support a preference for the latter. A detailed design architecture encompassing the onboard packet switch and its control, the related demand assigned TDMA burst structures, and destination packet protocols for routing traffic are presented. Fundamental onboard hardware requirements comprising speed, memory size, chip count, and power are estimated. The study concludes with identification of key enabling technologies and identifies a plan to develop a POC model.

Author

N87-27711*# Communications Satellite Corp., Clarksburg, Md.
ON-BOARD PROCESSING SATELLITE NETWORK ARCHITECTURE AND CONTROL STUDY Final Report

S. JOSEPH CAMPANELLA, BENJAMIN A. PONTANO, and HARVEY CHALMERS Jun. 1987 207 p

(Contract NAS3-24886)

(NASA-CR-180817; NAS 1.26:180817) Avail: NTIS HC A10/MF A01 CSCL 22B

The market for telecommunications services needs to be segmented into user classes having similar transmission requirements and hence similar network architectures. Use of the following transmission architecture was considered: satellite switched TDMA; TDMA up, TDM down; scanning (hopping) beam TDMA; FDMA up, TDM down; satellite switched MF/TDMA; and switching Hub earth stations with double hop transmission. A candidate network architecture will be selected that: comprises

multiple access subnetworks optimized for each user; interconnects the subnetworks by means of a baseband processor; and optimizes the marriage of interconnection and access techniques. An overall network control architecture will be provided that will serve the needs of the baseband and satellite switched RF interconnected subnetworks. The results of the studies shall be used to identify elements of network architecture and control that require the greatest degree of technology development to realize an operational system. This will be specified in terms of: requirements of the enabling technology; difference from the current available technology; and estimate of the development requirements needed to achieve an operational system. The results obtained for each of these tasks are presented. B.G.

N87-29915*# National Aeronautics and Space Administration. Lewis Research Center, Cleveland, Ohio.

STATUS OF SPACE STATION POWER SYSTEM

COSMO R. BARAONA and DEAN W. SHEIBLEY *In its Space Electrochemical Research and Technology (SERT)* p 1-8 Sep. 1987

Avail: NTIS HC A16/MF A01 CSCL 22B

The major requirements and guidelines that affect the manned space station configuration and the power systems are explained. The evolution of the space station power system from the NASA program development feasibility phase through the current preliminary design phase is described. Several early station concepts are described and linked to the present concept. The recently completed phase B tradeoff study selections of photovoltaic system technologies are described. The present solar dynamic and power management and distribution systems are also summarized for completeness. Author

20

SPACECRAFT PROPULSION AND POWER

Includes main propulsion systems and components, e.g., rocket engines; and spacecraft auxiliary power sources.

A87-14976*# National Aeronautics and Space Administration. Lewis Research Center, Cleveland, Ohio.

VACUUM CHAMBER PRESSURE EFFECTS ON THRUST MEASUREMENTS OF LOW REYNOLDS NUMBER NOZZLES

J. S. SOVEY, P. F. PENKO, S. P. GRISNIK, and M. V. WHALEN (NASA, Lewis Research Center, Cleveland, OH) *Journal of Propulsion and Power* (ISSN 0748-4658), vol. 2, Sept.-Oct. 1986, p. 385-389. Previously announced in STAR as N85-21259. refs

Tests were conducted to investigate the effect of vacuum facility pressure on the performance of small thruster nozzles. Thrust measurements of two converging-diverging nozzles with an area ratio of 140 and an orifice plate flowing unheated nitrogen and hydrogen were taken over a wide range of vacuum facility pressures and nozzle throat Reynolds numbers. In the Reynolds number range of 2200 to 12,000 there was no discernable viscous effect on thrust below an ambient to total pressure ratio of 1000. In nearly all cases, flow separation occurred at a pressure ratio of about 1000. This was the upper limit for obtaining an accurate thrust measurement for a conical nozzle with an area ratio of 140. Author

A87-15900*# National Aeronautics and Space Administration. Lewis Research Center, Cleveland, Ohio.

SPACE POWER - EMERGING OPPORTUNITIES

H. W. BRANDHORST (NASA, Lewis Research Center, Cleveland, OH) IAF, International Astronautical Congress, 37th, Innsbruck, Austria, Oct. 4-11, 1986. 8 p. (IAF PAPER 86-152)

NASA programs directed towards the development of technologies to meet the cost-effective energy needs of future space missions are described. Consideration is given to the space

photovoltaic program, which was developed along two paths: one leading to high-performance ultralight weight solar arrays, the other to high output arrays. The space power materials and energy storage technology are discussed, together with the developmental aspects of an advanced solar dynamic power system and its subsystems. Special attention is given to the Nasa SP-100 Advanced Technology Project and the free-piston Stirling engine technology for nuclear power application. I.S.

A87-16138*# National Aeronautics and Space Administration. Lewis Research Center, Cleveland, Ohio.

ELECTRICAL POWER SYSTEM FOR THE U.S. SPACE STATION

D. L. NORED (NASA, Lewis Research Center, Cleveland, OH) and G. J. HALLINAN (Rockwell International Corp., Rocketdyne Div., Canoga Park, CA) IAF, International Astronautical Congress, 37th, Innsbruck, Austria, Oct. 4-11, 1986. 13 p. Previously announced in STAR as N86-32520. (IAF PAPER 86-37)

The Space Station Electrical Power System presents many interesting challenges. It will be much larger than previous space power systems, and it must be designed for on-orbit maintenance and replacement, along with having a growth capability. The power generation, energy storage, and power management and distribution (PMAD) subsystems comprise the primary elements of the overall system. Each was analyzed by NASA Lewis Research Center and its two contractors Rocketdyne and TRW - in the definition studies of the program to determine the optimum approach to minimize initial costs and life cycle costs. For the PMAD subsystem, a ring bus architecture operating at 440 V, 20 kHz, single phase, was selected. Photovoltaic and solar dynamic power generation subsystems were both studied. Major tradeoffs were made for each subsystem and for the overall system, and a hybrid system (both photovoltaic and solar dynamic) was selected. Author

A87-16929*# National Aeronautics and Space Administration. Lewis Research Center, Cleveland, Ohio.

POWER IS THE KEYSTONE

R. L. THOMAS (NASA, Lewis Research Center, Cleveland, OH) *Aerospace America* (ISSN 0740-722X), vol. 24, Sept. 1986, p. 36-38, 40.

An evaluation is made of the various technologies that have been considered for incorporation into the NASA Space Station's solar power system. A major feature of the system is noted to be the use of both 25 kW capacity of photovoltaic power and two 25-kW turbine-driven generators based on the heating of a working fluid by a mirror concentrator dish. Fuel cells will be used to store excess electrical energy, together with nickel-cadmium batteries. The selection of this manned Space Station power system was arrived at through a comparison of six different configurations. O.C.

A87-17837*# Systems Science and Software, La Jolla, Calif. **COMPUTER SIMULATION OF PLASMA ELECTRON COLLECTION BY PIX-II**

M. J. MANDELL, I. KATZ, G. A. JONGEWARD (Systems, Science and Software, La Jolla, CA), and J. C. ROCHE (NASA, Lewis Research Center, Cleveland, OH) *Journal of Spacecraft and Rockets* (ISSN 0022-4650), vol. 23, Sept.-Oct. 1986, p. 512-518. Previously cited in issue 07, p. 870, Accession no. A85-19715. refs (Contract NAS3-23881)

A87-17992*# National Aeronautics and Space Administration. Lewis Research Center, Cleveland, Ohio.

PERFORMANCE CHARACTERISTICS OF RING-CUSP THRUSTERS WITH XENON PROPELLANT

M. J. PATTERSON (NASA, Lewis Research Center, Cleveland, OH) AIAA, ASME, SAE, and ASEE, Joint Propulsion Conference, 22nd, Huntsville, AL, June 16-18, 1986. 34 p. Previously announced in STAR as N86-31650. refs (AIAA PAPER 86-1392)

The performance characteristics and operating envelope of several 30-cm ring-cusp ion thrusters with xenon propellant were investigated. Results indicate a strong performance dependence on the discharge chamber boundary magnetic fields and resultant distribution of electron currents. Significant improvements in discharge performance over J-series divergent-field thrusters were achieved for large throttling ranges, which translate into reduced cathode emission currents and reduced power dissipation which should be of significant benefit for operation at thruster power levels in excess of 10 kW. Mass spectrometer of the ion beam was documented for both the ring-cusp and J-series thrusters with xenon propellant for determination of overall thruster efficiency, and lifetime. Based on the lower centerline values of doubly charged ions in the ion beam and the lower operating discharge voltage, the screen grid erosion rate of the ring-cusp thruster is expected to be lower than the divergent-field J-series thruster by a factor of 2. Author

A87-17994*# National Aeronautics and Space Administration. Lewis Research Center, Cleveland, Ohio.

THE NONCAVITATING PERFORMANCE AND LIFE OF A SMALL VANE-TYPE POSITIVE DISPLACEMENT PUMP IN LIQUID HYDROGEN

T. E. ULBRICHT and J. A. HEMMINGER (NASA, Lewis Research Center, Cleveland, OH) AIAA, ASME, SAE, and ASEE, Joint Propulsion Conference, 22nd, Huntsville, AL, June 16-18, 1986. 27 p. Previously announced in STAR as N86-31651. refs (AIAA PAPER 86-1438)

The low flow rate and high head rise requirements of hydrogen/oxygen auxiliary propulsion systems make the application of centrifugal pumps difficult. Positive displacement pumps are well-suited for these flow conditions, but little is known about their performance and life characteristics in liquid hydrogen. An experimental and analytical investigation was conducted to determine the performance and life characteristics of a vane-type, positive displacement pump. In the experimental part of this effort, mass flow rate and shaft torque were determined as functions of shaft speed and pump pressure rise. Since liquid hydrogen offers little lubrication in a rubbing situation, pump life is an issue. During the life test, the pump was operated intermittently for 10 hr at the steady-state point of 0.074 lbm/sec (0.03 kg/sec) flow rate, 3000 psid (2.07 MPa) pressure rise, and 9000 rpm (938 rad/sec) shaft speed. Pump performance was monitored during the life test series and the results indicated no loss in performance. Material loss from the vanes was recorded and wear of the other components was documented. In the analytical part of this effort, a comprehensive pump performance analysis computer code, developed in-house, was used to predict pump performance. The results of the experimental investigation are presented and compared with the results of the analysis. Results of the life test are also presented. M.G.

A87-18068*# National Aeronautics and Space Administration. Lewis Research Center, Cleveland, Ohio.

ELECTRICAL POWER SYSTEM DESIGN FOR THE U.S. SPACE STATION

D. L. NORED and D. T. BERNATOWICZ (NASA, Lewis Research Center, Cleveland, OH) IN: IECEC '86; Proceedings of the Twenty-first Intersociety Energy Conversion Engineering Conference, San Diego, CA, August 25-29, 1986. Volume 3. Washington, DC, American Chemical Society, 1986, p. 1416-1422.

The power systems for the Space Station manned core and platforms that have been selected in definition studies are described

in this paper. The selected system for the platforms uses silicon arrays and Ni-H₂ batteries. The power system for the manned core is a hybrid employing arrays and batteries identical to those on the platform along with solar dynamic modules using either Brayton or organic Rankine engines. The power system requirements, candidate technologies, and configurations that were considered, and the basis for selection, are discussed. Author

A87-18093*# National Aeronautics and Space Administration. Lewis Research Center, Cleveland, Ohio.

PARAMETRIC AND CYCLE TESTS OF A 40-AH BIPOLAR NICKEL-HYDROGEN BATTERY

R. L. CATALDO (NASA, Lewis Research Center, Cleveland, OH) IN: IECEC '86; Proceedings of the Twenty-first Intersociety Energy Conversion Engineering Conference, San Diego, CA, August 25-29, 1986. Volume 3. Washington, DC, American Chemical Society, 1986, p. 1547-1553.

The performance of a 12 V, 40 ampere-hour bipolar battery during various charge current, discharge current, temperature, and pressure operating conditions is investigated. The cell voltages, temperatures, ampere-hours, and watt-hours derived from the charge/discharge cycle tests are studied. Consideration is given to battery voltage and discharge capacity as a function of discharge current, the correlation between energy delivered on a discharge and battery temperature, battery voltage response to pulse discharges, and the voltage-temperature relationship. The data reveal that the bipolar Ni-H battery is applicable to high power systems. I.F.

A87-18104* Hughes Research Labs., Malibu, Calif.

CYCLE LIFE OF NICKEL-HYDROGEN CELLS. II - ACCELERATED CYCLE LIFE TEST

H. S. LIM and S. A. VERZWYVELT (Hughes Research Laboratories, Malibu, CA) IN: IECEC '86; Proceedings of the Twenty-first Intersociety Energy Conversion Engineering Conference, San Diego, CA, August 25-29, 1986. Volume 3. Washington, DC, American Chemical Society, 1986, p. 1601-1606. refs (Contract NAS3-22238)

A cycle life test of nickel-hydrogen (Ni/H₂) cells containing electrolytes of various KOH concentrations and a sintered-type nickel electrode were carried out at 23 C using a 45-min accelerated low earth orbit (LEO) cycle regime at 80 percent depth of discharge. Ten cells containing 21 to 36 percent KOH were tested. Since this accelerated test regime accelerated the cycle life roughly twice as fast as a typical LEO regime, the present results indicate that the cells with 26 percent KOH may last over 5 years in an 80 percent depth-of-discharge cycling in an LEO regime. Cells with lower KOH concentrations (21 to 23.5 percent) also showed longer cycle life than those with KOH concentrations of 31 percent or higher, although the life was shorter than those with 26 percent KOH. Author

A87-18107* Life Systems, Inc., Cleveland, Ohio.

ALKALINE WATER ELECTROLYSIS TECHNOLOGY FOR SPACE STATION REGENERATIVE FUEL CELL ENERGY STORAGE

F. H. SCHUBERT (Life Systems, Inc., Cleveland, OH), M. A. HOBERECHT, and M. LE (NASA, Lewis Research Center, Cleveland, OH) IN: IECEC '86; Proceedings of the Twenty-first Intersociety Energy Conversion Engineering Conference, San Diego, CA, August 25-29, 1986. Volume 3. Washington, DC, American Chemical Society, 1986, p. 1617-1627. Research supported by the Life System, Inc. and NASA. refs

The regenerative fuel cell system (RFCS), designed for application to the Space Station energy storage system, is based on state-of-the-art alkaline electrolyte technology and incorporates a dedicated fuel cell system (FCS) and water electrolysis subsystem (WES). In the present study, emphasis is placed on the WES portion of the RFCS. To ensure RFCS availability for the Space Station, the RFCS Space Station Prototype design was undertaken which included a 46-cell 0.93 cu m static feed water electrolysis module and three integrated mechanical components. K.K.

A87-18154*# National Aeronautics and Space Administration. Lewis Research Center, Cleveland, Ohio.

A FEASIBILITY ASSESSMENT OF NUCLEAR REACTOR POWER SYSTEM CONCEPTS FOR THE NASA GROWTH SPACE STATION

H. S. BLOOMFIELD and J. A. HELLER (NASA, Lewis Research Center, Cleveland, OH) IN: IECEC '86; Proceedings of the Twenty-first Intersociety Energy Conversion Engineering Conference, San Diego, CA, August 25-29, 1986. Volume 3. Washington, DC, American Chemical Society, 1986, p. 1924-1932. refs

A preliminary feasibility assessment of the integration of reactor power system concepts with a projected growth Space Station architecture was conducted to address a variety of installation, operational, disposition and safety issues. A previous NASA sponsored study, which showed the advantages of Space Station - attached concepts, served as the basis for this study. A study methodology was defined and implemented to assess compatible combinations of reactor power installation concepts, disposal destinations, and propulsion methods. Three installation concepts that met a set of integration criteria were characterized from a configuration and operational viewpoint, with end-of-life disposal mass identified. Disposal destinations that met current aerospace nuclear safety criteria were identified and characterized from an operational and energy requirements viewpoint, with delta-V energy requirement as a key parameter. Chemical propulsion methods that met current and near-term application criteria were identified and payload mass and delta-V capabilities were characterized. These capabilities were matched against concept disposal mass and destination delta-V requirements to provide a feasibility of each combination. Author

A87-18175* Grumman Aerospace Corp., Bethpage, N.Y.

SOLAR DYNAMIC SPACE POWER SYSTEM HEAT REJECTION

A. W. CARLSON, E. GUSTAFSON (Grumman Aerospace Corp., Bethpage, NY), and K. L. MCLALLIN (NASA, Lewis Research Center, Cleveland, OH) IN: IECEC '86; Proceedings of the Twenty-first Intersociety Energy Conversion Engineering Conference, San Diego, CA, August 25-29, 1986. Volume 3. Washington, DC, American Chemical Society, 1986, p. 2060-2071. refs
(Contract NAS3-24665)

A radiator system concept is described that meets the heat rejection requirements of the NASA Space Station solar dynamic power modules. The heat pipe radiator is a high-reliability, high-performance approach that is capable of erection in space and is maintainable on orbit. Results are present of trade studies that compare the radiator system area and weight estimates for candidate advanced high performance heat pipes. The results indicate the advantages of the dual-slot heat pipe radiator for high temperature applications as well as its weight-reduction potential over the range of temperatures to be encountered in the solar dynamic heat rejection systems. Author

A87-18179*# National Aeronautics and Space Administration. Lewis Research Center, Cleveland, Ohio.

ADVANCED SOLAR THERMAL TECHNOLOGIES FOR THE 21ST CENTURY

L. L. KOHOUT and M. E. PEREZ-DAVIS (NASA, Lewis Research Center, Cleveland, OH) IN: IECEC '86; Proceedings of the Twenty-first Intersociety Energy Conversion Engineering Conference, San Diego, CA, August 25-29, 1986. Volume 3. Washington, DC, American Chemical Society, 1986, p. 2086-2093. refs

The paper considers the present status of solar thermal dynamic space power technologies and projects the various attributes of these systems into the future, to the years 2000 and 2010. By the year 2000, collector weights should decrease from 1.25 kg/sq m (1985 value) to about 1.0 kg/sq m. The specific weight is also expected to decrease from 6.0 kg/kw. By the year 2010, slight improvements in the free piston Stirling energy conversion system are postulated with efficiencies reaching 32 percent. In addition, advanced concentrator concepts should be operational. K.K.

A87-18342* National Aeronautics and Space Administration. Lewis Research Center, Cleveland, Ohio.

THE POTENTIAL IMPACT OF NEW POWER SYSTEM TECHNOLOGY ON THE DESIGN OF A MANNED SPACE STATION

J. S. FORDYCE and H. J. SCHWARTZ (NASA, Lewis Research Center, Cleveland, OH) IN: International Symposium on Space Technology and Science, 14th, Tokyo, Japan, May 27-June 1, 1984, Proceedings. Tokyo, AGNE Publishing, Inc., 1984, p. 1099-1105. Previously announced in STAR as N84-31272. refs

Larger, more complex spacecraft of the future such as a manned Space Station will require electric power systems of 100 kW and more, orders of magnitude greater than the present state of the art. Power systems at this level will have a significant impact on the spacecraft design. Historically, long-lived spacecraft have relied on silicon solar cell arrays, a nickel-cadmium storage battery and operation at 28 V dc. These technologies lead to large array areas and heavy batteries for a Space Station application. This, in turn, presents orbit altitude maintenance, attitude control, energy management and launch weight and volume constraints. Size (area) and weight of such a power system can be reduced if new higher efficiency conversion and lighter weight storage technologies are used. Several promising technology options including concentrator solar photovoltaic arrays, solar thermal dynamic and ultimately nuclear dynamic systems to reduce area are discussed. Also, higher energy storage systems such as nickel-hydrogen and the regenerative fuel cell (RFC) and higher voltage power distribution which add system flexibility, simplicity and reduce weight are examined. Emphasis placed on the attributes and development status of emerging technologies that are sufficiently developed so that they could be available for flight use in the early to mid 1990's. Author

A87-19874*# National Aeronautics and Space Administration. Lewis Research Center, Cleveland, Ohio.

PROTECTION OF SOLAR ARRAY BLANKETS FROM ATTACK BY LOW EARTH ORBITAL ATOMIC OXYGEN

BRUCE A. BANKS, MICHAEL J. MIRTICH, SHARON K. RUTLEDGE, and HENRY K. NAHRA (NASA, Lewis Research Center, Cleveland, OH) IN: Photovoltaic Specialists Conference, 18th, Las Vegas, NV, October 21-25, 1985, Conference Record. New York, Institute of Electrical and Electronics Engineers, Inc., 1985, p. 381-386. refs

The ram impact of low earth orbital atomic oxygen causes oxidation of spacecraft materials including polymers such as polyimides. The rate of oxidation is sufficiently high to potentially compromise the long term durability of Kapton solar array blankets. Ion beam sputter deposited atomic oxygen protective coatings of aluminum oxide, silicon dioxide, and codeposited silicon dioxide with small amounts of polytetrafluoroethylene were evaluated both in RF plasma asher tests and in low earth orbit. Deposition techniques, mechanical properties, and atomic oxygen protection performance are presented. Author

A87-19877*# National Aeronautics and Space Administration. Lewis Research Center, Cleveland, Ohio.

SPACE STATION POWER SYSTEM ISSUES

A. F. FORESTIERI (NASA, Lewis Research Center, Cleveland, OH) IN: Photovoltaic Specialists Conference, 18th, Las Vegas, NV, October 21-25, 1985, Conference Record. New York, Institute of Electrical and Electronics Engineers, Inc., 1985, p. 403-410. refs

A number of attractive options are available for the Space Station Power System. These include a photovoltaic system or solar dynamic system for power generation, batteries or fuel cells for energy storage and ac or dc for power management and distribution. These options are being explored during the present preliminary design and definition phase of the Space Station Program. Final selections are presently targeted for January 1986. Author

A87-21516*# Aerojet TechSystems Co., Sacramento, Calif.

HEAT PIPE COOLED ROCKET ENGINES

D. K. BERKMAN (Aerojet TechSystems Co., Sacramento, CA) and J. TOTH (Thermacore, Inc., Lancaster, PA) AIAA, ASME, SAE, and ASEE, Joint Propulsion Conference, 22nd, Huntsville, AL, June 16-18, 1986. 7 p. refs
(Contract NAS3-23634)
(AIAA PAPER 86-1567)

A concept for a heat-pipe-cooled rocket engine, which involves the use of heat pipes to augment radiation cooling on small, low-flux rocket engines used for attitude control and stationkeeping on satellites, is discussed. Results of the thermal and performance analyses performed on a prototype heat cooled thrust chamber are presented, together with the results of fabrication experiments. A test plan for full-scale hot fire hardware testing is outlined. I.S.

A87-21807* National Aeronautics and Space Administration. Lewis Research Center, Cleveland, Ohio.

NASA GROWTH SPACE STATION MISSIONS AND CANDIDATE NUCLEAR/SOLAR POWER SYSTEMS

JACK A. HELLER and JOSEPH J. NAINIGER (NASA, Lewis Research Center, Cleveland, OH) IN: Space nuclear power systems 1985; Proceedings of the Second Symposium, Albuquerque, NM, Jan. 14-16, 1985. Volume 3. Malabar, FL, Orbit Book Co., Inc., 1987, p. 47-52. NASA sponsored research.

A brief summary is presented of a NASA study contract and in-house investigation on Growth Space Station missions and appropriate nuclear and solar space electric power systems. By the year 2000 some 300 kWe will be needed for missions and housekeeping power for a 12 to 18 person Station crew. Several Space Station configurations employing nuclear reactor power systems are discussed, including shielding requirements and power transmission schemes. Advantages of reactor power include a greatly simplified Station orientation procedure, greatly reduced occultation of views of the earth and deep space, near elimination of energy storage requirements, and significantly reduced station-keeping propellant mass due to very low drag of the reactor power system. The in-house studies of viable alternative Growth Space Station power systems showed that at 300 kWe a rigid silicon solar cell array with NiCd batteries had the highest specific mass at 275 kg/kWe, with solar Stirling the lowest at 40 kg/kWe. However, when 10 year propellant mass requirements are factored in, the 300 kWe nuclear Stirling exhibits the lowest total mass.

Author

A87-23239*# National Aeronautics and Space Administration. Lewis Research Center, Cleveland, Ohio.

STATUS OF ADVANCED PROPULSION FOR SPACE BASED ORBITAL TRANSFER VEHICLE

LARRY P. COOPER and DEAN D. SCHEER (NASA, Lewis Research Center, Cleveland, OH) IAF, International Astronautical Congress, 37th, Innsbruck, Austria, Oct. 4-11, 1986. 31 p. Previously announced in STAR as N87-10959. refs
(IAF PAPER 86-183)

A new Orbital Transfer Vehicle (OTV) propulsion system will be required to meet the needs of space missions beyond the mid-1990's. As envisioned, the advanced OTV will be used in conjunction with earth-to-orbit vehicles, Space Station, and Orbit Maneuvering Vehicle. The OTV will transfer men, large space structures, and conventional payloads between low earth and higher energy orbits. Space probes carried by the OTV will continue the exploration of the solar system. When lunar bases are established, the OTV will be their transportation link to earth. NASA is currently funding the development of technology for advanced propulsion concepts for future Orbital Transfer Vehicles. Progress in key areas during 1986 is presented.

Author

A87-23646* National Aeronautics and Space Administration. Lewis Research Center, Cleveland, Ohio.

AUTOMATING THE U.S. SPACE STATION'S ELECTRICAL POWER SYSTEM

JAMES L. DOLCE and KARL A. FAYMON (NASA, Lewis Research Center, Cleveland, OH) Optical Engineering (ISSN 0091-3286), vol. 25, Nov. 1986, p. 1181-1185. refs

NASA's Lewis Research Center is developing a highly automated system for the generation, storage and distribution of electrical power aboard the projected Space Station. This autonomous power system will employ conventional algorithms, enhanced by expert systems, to schedule power, allocate energy, diagnose causes of failure, propose goals, prepare plans for their implementation, evaluate their consequences, and select optimum plans for their execution. While crew-interactive expert systems will be ready for the initial Space Station, total system autonomy is expected to require additional development time. O.C.

A87-24997*# National Aeronautics and Space Administration. Lewis Research Center, Cleveland, Ohio.

HIGH- AND LOW-THRUST PROPULSION SYSTEMS FOR THE SPACE STATION

ROBERT E. JONES (NASA, Lewis Research Center, Cleveland, OH) AIAA, Aerospace Sciences Meeting, 25th, Reno, NV, Jan. 12-15, 1987. 13 p. Previously announced in STAR as N87-14427. refs
(AIAA PAPER 87-0398)

The purpose of the Advanced Development program was to investigate propulsion options for the space station. Two options were investigated in detail: a high-thrust system consisting of 25 to 50 lbf gaseous oxygen/hydrogen rockets, and a low-thrust system of 0.1 lbf multipropellant resistojets. An effort is also being conducted to determine the life capability of hydrazine-fueled thrusters. During the course of this program, studies clearly identified the benefits of utilizing waste water and other fluids as propellant sources. The results of the H/O thruster test programs are presented and the plan to determine the life of hydrazine thrusters is discussed. The background required to establish a long-life resistojet is presented and the first design model is shown in detail.

Author

A87-24998*# National Aeronautics and Space Administration. Lewis Research Center, Cleveland, Ohio.

AN ANALYTICAL AND EXPERIMENTAL INVESTIGATION OF RESISTOJET PLUMES

LYNNETTE M. ZANA, DAVID J. HOFFMAN (NASA, Lewis Research Center, Cleveland, OH), LORANELL R. BREYLEY, and JOHN S. SERAFINI (Akron, University, OH) AIAA, Aerospace Sciences Meeting, 25th, Reno, NV, Jan. 12-15, 1987. 13 p. Previously announced in STAR as N87-14428. refs
(AIAA PAPER 87-0399)

As a part of the electrothermal propulsion plume research program at the NASA Lewis Research Center, efforts have been initiated to analytically and experimentally investigate the plumes of resistojet thrusters. The method of Simons for the prediction of rocket exhaust plumes is developed for the resistojet. Modifications are made to the source flow equations to account for the increased effects of the relatively large nozzle boundary layer. Additionally, preliminary mass flux measurements of a laboratory resistojet using CO₂ propellant at 298 K have been obtained with a cryogenically cooled quartz crystal microbalance (QCM). There is qualitative agreement between analysis and experiment, at least in terms of the overall number density shape functions in the forward flux region.

Author

A87-31134*# Martin Marietta Corp., Denver, Colo.
**PROPULSION RECOMMENDATIONS FOR SPACE STATION
 FREE FLYING PLATFORMS**

L. R. REDD and L. J. ROSE (Martin Marietta Corp., Denver, CO)
 Joint Army-Navy-NASA-Air Force Interagency Propulsion
 Committee, Propulsion Conference, New Orleans, LA, Aug. 27,
 1986, Paper. 24 p.
 (Contract NAS3-23893)

Propulsion system candidates have been defined for Space
 Station free flying platforms for the purpose of comparison and to
 understand the impact of the various mission requirements on the
 candidate designs. Consideration of the platform mission
 requirements and comparisons of the conceptual propulsion system
 design candidates has led to a fairly clear set of recommendations
 for propulsion for each of the various platforms. Author

A87-31281*# Michigan State Univ., East Lansing.
**MICROWAVE ELECTROTHERMAL THRUSTER PERFORMANCE
 IN HELIUM GAS**

S. WHITEHAIR, J. ASMUSSEN (Michigan State University, East
 Lansing), and S. NAKANISHI (Analex Corp., Cleveland, OH) Journal
 of Propulsion and Power (ISSN 0748-4658), vol. 3, Mar.-Apr. 1987,
 p. 136-144. refs
 (Contract NAG3-305)

The microwave electrothermal thruster presented uses an
 internally tuned, single-mode cylindrical cavity applicator to focus
 and match microwave energy into an electrodeless, high pressure
 flowing gas discharge that is located within a quartz discharge
 chamber. Experimental measurements of microwave coupling
 efficiency, thruster energy efficiency, and specific impulse, are
 obtained for N and He discharges; the efficiency of microwave
 energy transfer to the discharge is found to be of the order of 95
 percent. Higher temperature nozzle materials and more efficient
 discharge chambers will further enhance performance. O.C.

A87-31300*# National Aeronautics and Space Administration.
 Lewis Research Center, Cleveland, Ohio.

**THE SURVIVABILITY OF LARGE SPACE-BORNE REFLECTORS
 UNDER ATOMIC OXYGEN AND MICROMETEOROID IMPACT**

DANIEL A. GULINO (NASA, Lewis Research Center, Cleveland,
 OH) AIAA, Aerospace Sciences Meeting, 25th, Reno, NV, Jan.
 12-15, 1987. 9 p. Previously announced in STAR as N87-14423.
 refs

(AIAA PAPER 87-0341)

Solar dynamic power system mirrors for use on Space Station
 and other spacecraft flown in low earth orbit (LEO) are exposed
 to the harshness of the LEO environment. Both atomic oxygen
 and micrometeoroids/space debris can degrade the performance
 of such mirrors. Protective coatings will be required to protect
 oxidizable reflecting media, such as silver and aluminum, from
 atomic oxygen attack. Several protective coating materials have
 been identified as good candidates for use in this application.
 The durability of these coating/mirror systems after pinhole defects
 have been inflicted during their fabrication and deployment or
 through micrometeoroid/space debris impact once on-orbit is of
 concern. Studies of the effect of an oxygen plasma environment
 on protected mirror surfaces with intentionally induced pinhole
 defects have been conducted at NASA Lewis and are reviewed.
 It has been found that oxidation of the reflective layer and/or the
 substrate in areas adjacent to a pinhole defect, but not directly
 exposed by the pinhole, can occur. Author

A87-36913*# National Aeronautics and Space Administration.
 Lewis Research Center, Cleveland, Ohio.

**SPACE STATION 20-KHZ POWER MANAGEMENT AND
 DISTRIBUTION SYSTEM**

IRVING G. HANSEN and GALE R. SUNDBERG (NASA Lewis
 Research Center, Cleveland, OH) IN: PESC '86; Annual Power
 Electronics Specialists Conference, 17th, Vancouver, Canada, June
 23-27, 1986, Record. New York, Institute of Electrical and
 Electronics Engineers, Inc., 1986, p. 676-683. Previously announced
 in STAR as N86-24747. refs

During the conceptual design phase a 20-kHz power distribution
 system was selected as the reference for the Space Station. The
 system is single-phase 400 VRMS, with a sinusoidal wave form.
 The initial user power level will be 75 kW with growth to 300 kW.
 The high-frequency system selection was based upon
 considerations of efficiency, weight, safety, ease of control,
 interface with computers, and ease of paralleling for growth. Each
 of these aspects will be discussed as well as the associated
 trade-offs involved. An advanced development program has been
 instituted to accelerate the maturation of the high-frequency system.
 Some technical aspects of the advanced development will be
 discussed. Author

A87-37291*# National Aeronautics and Space Administration.
 Lyndon B. Johnson Space Center, Houston, Tex.

MANNED SPACECRAFT ELECTRICAL POWER SYSTEMS

WILLIAM E. SIMON (NASA, Johnson Space Center, Houston, TX)
 and DONALD L. NORED (NASA, Lewis Research Center,
 Cleveland, OH) IEEE, Proceedings (ISSN 0018-9219), vol. 75,
 March 1987, p. 277-307. refs

A brief history of the development of electrical power systems
 from the earliest manned space flights illustrates a natural trend
 toward a growth of electrical power requirements and operational
 lifetimes with each succeeding space program. A review of the
 design philosophy and development experience associated with
 the Space Shuttle Orbiter electrical power system is presented,
 beginning with the state of technology at the conclusion of the
 Apollo Program. A discussion of prototype, verification, and
 qualification hardware is included, and several design improvements
 following the first Orbiter flight are described. The problems
 encountered, the scientific and engineering approaches used to
 meet the technological challenges, and the results obtained are
 stressed. Major technology barriers and their solutions are
 discussed, and a brief Orbiter flight experience summary of early
 Space Shuttle missions is included. A description of projected
 Space Station power requirements and candidate system concepts
 which could satisfy these anticipated needs is presented. Significant
 challenges different from Space Shuttle, innovative concepts and
 ideas, and station growth considerations are discussed. The Phase
 B Advanced Development hardware program is summarized and
 a status of Phase B preliminary tradeoff studies is presented.

Author

A87-38008*# Michigan State Univ., East Lansing.
**A REVIEW OF RESEARCH AND DEVELOPMENT ON THE
 MICROWAVE-PLASMA ELECTROTHERMAL ROCKET**

MARTIN C. HAWLEY, JES ASMUSSEN, JOHN W. FILPUS,
 LYDELL L. FRASCH, STANLEY WHITEHAIR (Michigan State
 University, East Lansing) et al. AIAA, DGLR, and JSASS,
 International Electric Propulsion Conference, 19th, Colorado
 Springs, CO, May 11-13, 1987. 15 p. refs

(Contract NSG-3299)

(AIAA PAPER 87-1011)

The microwave-plasma electrothermal rocket (MWPETR)
 shows promise for spacecraft propulsion and maneuvering, without
 some of the drawbacks of competitive electric propulsion systems.
 In the MWPETR, the electric power is first converted to
 microwave-frequency radiation. In a specially-designed microwave
 cavity system, the electromagnetic energy of the radiation is
 transferred to the electrons in a plasma sustained in the working
 fluid. The resulting high-energy electrons transfer their energy to
 the atoms and molecules of the working fluid by collisions. The
 working fluid, thus heated, expands through a nozzle to generate

20 SPACECRAFT PROPULSION AND POWER

thrust. In the MWPETR, no electrodes are in contact with the working fluid, the energy is transferred into the working fluid by nonthermal mechanisms, and the main requirement for the materials of construction is that the walls of the plasma chamber be insulating and transparent to microwave radiation at operating conditions. In this survey of work on the MWPETR, several experimental configurations are described and compared. Diagnostic methods used in the study are described and compared, including titration, spectroscopy, calorimetry, electric field measurements, gas-dynamic methods, and thrust measurements. Measured and estimated performance efficiencies are reported. Results of computer modeling of the plasma and of the gas flowing from the plasma are summarized. Author

A87-38009*# Michigan State Univ., East Lansing.
A COMPUTER MODEL FOR THE RECOMBINATION ZONE OF A MICROWAVE-PLASMA ELECTROTHERMAL ROCKET
JOHN W. FILPUS and MARTIN C. HAWLEY (Michigan State University, East Lansing) AIAA, DGLR, and JSASS, International Electric Propulsion Conference, 19th, Colorado Springs, CO, May 11-13, 1987. 8 p. refs
(Contract NSG-3299)
(AIAA PAPER 87-1014)

As part of a study of the microwave-plasma electrothermal rocket, a computer model of the flow regime below the plasma has been developed. A second-order model, including axial dispersion of energy and material and boundary conditions at infinite length, was developed to partially reproduce the absence of mass-flow rate dependence that was seen in experimental temperature profiles. To solve the equations of the model, a search technique was developed to find the initial derivatives. On integrating with a trial set of initial derivatives, the values and their derivatives were checked to judge whether the values were likely to attain values outside the practical regime, and hence, the boundary conditions at infinity were likely to be violated. Results are presented and directions for further development are suggested. Author

A87-38017*# GT-Devices, Alexandria, Va.
EXPERIMENTS ON A REPETITIVELY PULSED ELECTROTHERMAL THRUSTER
R. L. BURTON, D. FLEISCHER, S. A. GOLDSTEIN, and D. A. TIDMAN (GT-Devices, Inc., Alexandria, VA) AIAA, DGLR, and JSASS, International Electric Propulsion Conference, 19th, Colorado Springs, CO, May 11-13, 1987. 10 p. Research supported by GT-Devices, Inc. refs
(Contract NAS3-24636)
(AIAA PAPER 87-1043)

This paper presents experimental results from an investigation of a pulsed electrothermal (PET) thruster using water propellant. The PET thruster is operated on a calibrated thrust stand, and produces a thrust to power ratio of $T/P = 0.07 \pm 0.01$ N/kW. The discharge conditions are inferred from a numerical model which predicts pressure and temperature levels of 300-500 atm and 20,000 K, respectively. These values in turn correctly predict the measured values of impulse bit and discharge resistance. The inferred ideal exhaust velocity from these conditions is 17 km/sec, but the injection of water propellant produces a test tank background pressure of 10-20 Torr, which reduces the exhaust velocity to 14 km/sec. This value corresponds to a thrust efficiency of 54 \pm 7 percent when all experimental errors are taken into account. Author

A87-39634*# Rocket Research Corp., Redmond, Wash.
PERFORMANCE CHARACTERIZATION OF A LOW POWER HYDRAZINE ARCJET
S. C. KNOWLES, W. W. SMITH (Rocket Research Co., Redmond, WA), F. M. CURRAN, and T. W. HAAG (NASA, Lewis Research Center, Cleveland, OH) AIAA, DGLR, and JSASS, International Electric Propulsion Conference, 19th, Colorado Springs, CO, May 11-13, 1987. 9 p. refs
(AIAA PAPER 87-1057)

Hydrazine arcjets, which offer substantial performance advantages over alternatives in geosynchronous satellite stationkeeping applications, have undergone startup, materials compatibility, lifetime, and power conditioning unit design issues. Devices in the 1000-3000 W output range have been characterized for several different electrode configurations. Constrictor length and diameter, electrode gap setting, and vortex strength have been parametrically studied in order to ascertain the influence of each on specific impulse and efficiency; specific impulse levels greater than 700 sec have been achieved. O.C.

A87-39635*# Rocket Research Corp., Redmond, Wash.
LOW POWER ARCJET LIFE ISSUES
M. A. SIMON, S. C. KNOWLES (Rocket Research Co., Redmond, WA), F. M. CURRAN, and T. L. HARDY (NASA, Lewis Research Center, Cleveland, OH) AIAA, DGLR, and JSASS, International Electric Propulsion Conference, 19th, Colorado Springs, CO, May 11-13, 1987. 12 p. refs
(AIAA PAPER 87-1059)

The present evaluation of the results of arcjet engine lifetime testing attempts to deepen understanding of the electrode erosion process, with a view to its minimization. Attention is given to the compatibility of materials with N₂H₄, the dependence of electrode erosion on geometry and flow field, and the erosive effects associated with the arcjet power supply. Results are presented for thrusters employing either decomposed N₂H₄ or cold mixed gases, over a power range of 900 to 2000 W. O.C.

A87-39808*# Rockwell International Corp., Canoga Park, Calif.
SMALL CENTRIFUGAL PUMPS FOR LOW-THRUST ROCKETS
R. B. FURST, R. M. BURGESS, N. C. GULBRANDSEN (Rockwell International Corp., Rocketdyne Div., Canoga Park, CA), and D. D. SCHEER (NASA, Lewis Research Center, Cleveland, OH) Journal of Propulsion and Power (ISSN 0748-4658), vol. 3, May-June 1987, p. 241-248. Previously cited in issue 21, p. 3061, Accession no. A85-43978. refs
(Contract NAS3-23164)

A87-40275*# National Aeronautics and Space Administration, Lewis Research Center, Cleveland, Ohio.
THE VOLTAGE THRESHOLD FOR ARCING FOR SOLAR CELLS IN LEO - FLIGHT AND GROUND TEST RESULTS
DALE C. FERGUSON (NASA, Lewis Research Center, Cleveland, OH) AIAA, Aerospace Sciences Meeting, 24th, Reno, NV, Jan. 6-9, 1986. 25 p. Previously announced in STAR as N86-28125. refs
(AIAA PAPER 86-0362)

Ground and flight results of solar cell arcing in low earth orbit (LEO) conditions are compared and interpreted. It is shown that an apparent voltage threshold for arcing may be produced by a storage power law dependence of arc rate on voltage, combined with a limited observation time. The change in this apparent threshold with plasma density is a reflection of the density dependence of the arc rate. A nearly linear dependence of arc rate on density is inferred from the data. A real voltage threshold for arcing for 2 by 2 cm solar cells may exist however, independent of plasma density, near -230 V relative to the plasma. Here, arc rates may change by more than an order of magnitude for a change of only 30 V in array potential. For 5.9 by 5.9 solar cells, the voltage dependence of the arc rate is steeper, and the data are insufficient to indicate the existence of an arcing increased by an atomic oxygen plasma, as is found in LEO, and by arcing from the backs of welded-through substrates. Author

A87-40378*# National Aeronautics and Space Administration. Lewis Research Center, Cleveland, Ohio.

20 KHZ SPACE STATION POWER SYSTEM

IRVING G. HANSEN and FREDRICK J. WOLFF (NASA, Lewis Research Center, Cleveland, OH) IN: EASCON '86; Proceedings of the Nineteenth Annual Electronics and Aerospace Systems Conference, Washington, DC, Sept. 8-10, 1986. New York, Institute of Electrical and Electronics Engineers, Inc., 1986, p. 251-255. Previously announced in STAR as N86-28122. refs

The Space Station represents the next major U.S. commitment in space. The efficient delivery of power to multiple user loads is key to that success. In 1969, NASA Lewis Research Center began a series of studies with component and circuit developments that led to the high frequency bi-directional, four quadrant resonant driven converter. Additional studies and subsequent developments into the early 1980's have shown how the high frequency ac power system could provide overall advantages to many aerospace power systems. Because of its wide versatility, it also has outstanding advantages for the Space Station Program and its wide range of users. High frequency ac power provides higher efficiency, lower cost, and improved safety. The 20 kHz power system has exceptional flexibility, is inherently user friendly, and is compatible with all types of energy sources - photovoltaic, solar dynamic, rotating machines or nuclear Lewis distribution system testbed. The testbed demonstrates flexibility, versatility, and transparency to user technology as well as high efficiency, low mass, and reduced volume. Author

A87-41102*# National Aeronautics and Space Administration. Lewis Research Center, Cleveland, Ohio.

EXPERIMENTAL STUDY OF LOW REYNOLDS NUMBER NOZZLES

STANLEY P. GRISNIK, TAMARA A. SMITH (NASA, Lewis Research Center, Cleveland, OH), and LARRY E. SALTZ (Rocket Research Co., Redmond, WA) AIAA, DGLR, and JSASS, International Electric Propulsion Conference, 19th, Colorado Springs, CO, May 11-13, 1987. 13 p. Previously announced in STAR as N87-20383. refs

(AIAA PAPER 87-0992)

High-performance electrothermal thrusters operate in a low nozzle-throat Reynolds number regime. Under these conditions, the flow boundary layer occupies a large volume inside the nozzle, contributing to large viscous losses. Four nozzles (conical, bell, trumpet, and modified trumpet) and a sharp-edged orifice were evaluated over a Reynolds number range of 500 to 9000 with unheated nitrogen and hydrogen. The nozzles showed significant decreases in specific impulse efficiency with decreasing Reynolds number. At Reynolds numbers less than 1000, all four nozzles were probably filled with a large boundary layer. The discharge coefficient decreased with Reynolds number in the same manner as the specific impulse efficiency. The bell and modified trumpet nozzles had discharge coefficients 4 to 8 percent higher than those of the cone or trumpet nozzles. The Two-Dimensional Kinetics (TDK) nozzle analysis computer program was used to predict nozzle performance. The results were then compared to the experimental results in order to determine the accuracy of the program within this flow regime. Author

A87-41111*# Michigan State Univ., East Lansing.

AN ANALYSIS OF ELECTROMAGNETIC COUPLING AND EIGENFREQUENCIES FOR MICROWAVE ELECTROTHERMAL THRUSTER DISCHARGES

L. L. FRASCH, J. M. GRIFFIN, and J. ASMUSSEN (Michigan State University, East Lansing) AIAA, DGLR, and JSASS, International Electric Propulsion Conference, 19th, Colorado Springs, CO, May 11-13, 1987. 9 p. refs

(Contract NAG3-305)

(AIAA PAPER 87-1012)

This paper discusses the basic approach to developing a comprehensive electromagnetic model for a microwave electrothermal discharge. The discharge and surrounding region are modeled as a section of waveguide loaded with a uniform, cold, lossy plasma. A characteristic equation has been derived

describing all possible system modes. In particular the TM(01) mode is numerically solved. Propagation and attenuation constants for the TM(01) mode are found numerically for a given range of electron-neutral collision frequencies and plasma densities. Results are used to interpret a number of experimental observations in helium. Specifically, they are used to explain high coupling efficiencies and ease of cavity tuning at high pressures. Author

A87-41127*# National Aeronautics and Space Administration. Lewis Research Center, Cleveland, Ohio.

ARCJET COMPONENT CONDITIONS THROUGH A MULTISTART TEST

FRANK M. CURRAN and THOMAS W. HAAG (NASA, Lewis Research Center, Cleveland, OH) AIAA, DGLR, and JSASS, International Electric Propulsion Conference, 19th, Colorado Springs, CO, May 11-13, 1987. 19 p. Previously announced in STAR as N87-20382. refs

(AIAA PAPER 87-1060)

A low power, dc arcjet thruster was tested for starting reliability using hydrogen-nitrogen mixtures simulating the decomposition products of hydrazine. More than 300 starts were accumulated in phases with extended burn-in periods interlaced. A high degree of flow stabilization was built into the arcjet and the power supply incorporated both rapid current regulation and a high voltage, pulsed starting circuit. A nominal current level of 10 A was maintained throughout the test. Photomicrographs of the cathode tip showed a rapid recession to a steady-state operating geometry. A target of 300 starts was selected, as this represents significantly more than anticipated (150 to 240), in missions of 10 yr or less duration. Weighings showed no apparent mass loss. Some anode erosion was observed, particularly at the entrance to the constrictor. This was attributed to the brief period during startup the arc mode attachment point spends in the high pressure region upstream of the nozzle. Based on the results obtained, startup does not appear to be performance or life limiting for the number of starts typical of operational satellite applications. Author

A87-41128*# National Aeronautics and Space Administration. Lewis Research Center, Cleveland, Ohio.

ARCJET STARTING RELIABILITY - A MULTISTART TEST ON HYDROGEN/NITROGEN MIXTURES

THOMAS W. HAAG and FRANK M. CURRAN (NASA, Lewis Research Center, Cleveland, OH) AIAA, DGLR, and JSASS, International Electric Propulsion Conference, 19th, Colorado Springs, CO, May 11-13, 1987. 11 p. refs

(AIAA PAPER 87-1061)

An arcjet starting reliability test was performed to investigate one feasibility issue in the use of arcjets on board a satellite for north-south stationkeeping. A 1 kW arcjet was run on hydrogen/nitrogen gas mixtures simulating decomposed hydrazine. A pulse width modulated power supply with an integral high voltage starting pulser was used for arc ignition and steady-state operation. The test was performed in four phases in order to determine if starting characteristics changed as a result of long term thruster operation. More than 300 successful starts were accumulated over an operating time of 18 hr. Overall results indicate that there is a link between starting characteristics and long term thruster operation; however, the large number of starts had no effect on steady-state performance. Author

A87-41135*# Hughes Research Labs., Malibu, Calif.

PLASMA PROPERTIES IN ELECTRON-BOMBARDMENT ION THRUSTERS

J. N. MATOSSIAN and J. R. BEATTIE (Hughes Research Laboratories, Malibu, CA) AIAA, DGLR, and JSASS, International Electric Propulsion Conference, 19th, Colorado Springs, CO, May 11-13, 1987. 7 p. Research supported by the Hughes Aircraft Co. refs

(Contract NAS3-23775; NAS3-23860)

(AIAA PAPER 87-1076)

The paper describes a technique for computing volume-averaged plasma properties within electron-bombardment ion thrusters, using spatially varying Langmuir-probe measurements.

20 SPACECRAFT PROPULSION AND POWER

Average values of the electron densities are defined by integrating the spatially varying Maxwellian and primary electron densities over the ionization volume, and then dividing by the volume. Plasma properties obtained in the 30-cm-diameter J-series and ring-cusp thrusters are analyzed by the volume-averaging technique. The superior performance exhibited by the ring-cusp thruster is correlated with a higher average Maxwellian electron temperature. The ring-cusp thruster maintains the same fraction of primary electrons as does the J-series thruster, but at a much lower ion production cost. The volume-averaged predictions for both thrusters are compared with those of a detailed thruster performance model. Author

A87-42181*# Toledo Univ., Ohio.

THE EFFECT OF AMBIENT PRESSURE ON THE PERFORMANCE OF A RESISTOJET

D. H. MANZELLA, K. J. DE WITT, T. G. KEITH, JR. (Toledo, University, OH), and P. F. PENKO (NASA, Lewis Research Center, Cleveland, OH) AIAA, DGLR, and JSASS, International Electric Propulsion Conference, 19th, Colorado Springs, CO, May 11-13, 1987. 6 p. refs

(AIAA PAPER 87-0991)

Tests were conducted to investigate the effect of ambient pressure on the measured thrust of a prototype resistojets. The tests were performed using both heated and unheated nitrogen as the propellant at flow rates of 0.0379 and 0.0759 g/s. For the cold flow tests there was no effect on specific impulse over a range of ambient pressures from 1 to 400 microns. The results for the hot flow tests did show as much as a 7 percent variation in specific impulse over the same range of ambient pressures. Author

A87-45256*# National Aeronautics and Space Administration. Lewis Research Center, Cleveland, Ohio.

CONCEPTUAL DESIGN AND INTEGRATION OF A SPACE STATION RESISTOJET PROPULSION ASSEMBLY

R. R. TACINA (NASA, Lewis Research Center, Cleveland, OH) AIAA, SAE, ASME, and ASEE, Joint Propulsion Conference, 23rd, San Diego, CA, June 29-July 2, 1987. 13 p. Previously announced in STAR as N87-20378. refs

(AIAA PAPER 87-1860)

The resistojets propulsion module is designed as a simple, long life, low risk system offering operational flexibility to the space station program. It can dispose of a wide variety of typical space station waste fluids by using them as propellants for orbital maintenance. A high temperature mode offers relatively high specific impulse with long life while a low temperature mode can propulsively dispose of mixtures that contain oxygen or hydrocarbons without reducing thruster life or generating particulates in the plume. A low duty cycle and a plume that is confined to a small aft region minimizes the impacts on the users. Simple interfaces with other space station systems facilitate integration. It is concluded that there are no major obstacles and many advantages to developing, installing, and operating a resistojets propulsion module aboard the Initial Operational Capability (IOC) space station. Author

A87-45390*# National Aeronautics and Space Administration. Lewis Research Center, Cleveland, Ohio.

COMPARISON OF THEORETICAL AND EXPERIMENTAL THRUST PERFORMANCE OF A 1030:1 AREA RATIO ROCKET NOZZLE AT A CHAMBER PRESSURE OF 2413 KN/SQ M (350 PSIA)

TAMARA A. SMITH, ALBERT J. PAVLI, and KENNETH J. KACYNSKI (NASA, Lewis Research Center, Cleveland, OH) AIAA, SAE, ASME, and ASEE, Joint Propulsion Conference, 23rd, San Diego, CA, June 29-July 2, 1987. 22 p. refs

(AIAA PAPER 87-2069)

The Joint Army, Navy, NASA, Air Force (JANNAF) rocket-engine performance-prediction procedure is based on the use of various reference computer programs. One of the reference programs for nozzle analysis is the Two-Dimensional Kinetics (TDK) Program. The purpose of this report is to calibrate the JANNAF procedure

that has been incorporated into the December 1984 version of the TDK program for the high-area-ratio rocket-engine regime. The calibration was accomplished by modeling the performance of a 1030:1 rocket nozzle tested at NASA Lewis. A detailed description of the test conditions and TDK input parameters is given. The results indicate that the computer code predicts delivered vacuum specific impulse to within 0.12 to 1.9 percent of the experimental data. Vacuum thrust coefficient predictions were within + or - 1.3 percent of experimental results. Predictions of wall static pressure were within approximately + or - 5 percent of the measured values. Author

A87-45391*# National Aeronautics and Space Administration. Lewis Research Center, Cleveland, Ohio.

COMPARISON OF TWO PROCEDURES FOR PREDICTING ROCKET ENGINE NOZZLE PERFORMANCE

KENNETH J. DAVIDIAN (NASA, Lewis Research Center, Cleveland, OH) AIAA, SAE, ASME, and ASEE, Joint Propulsion Conference, 23rd, San Diego, CA, June 29-July 2, 1987. 11 p. Previously announced in STAR as N87-20379. refs

(AIAA PAPER 87-2071)

Two nozzle performance prediction procedures which are based on the standardized JANNAF methodology are presented and compared for four rocket engine nozzles. The first procedure required operator intercedence to transfer data between the individual performance programs. The second procedure is more automated in that all necessary programs are collected into a single computer code, thereby eliminating the need for data reformatting. Results from both procedures show similar trends but quantitative differences. Agreement was best in the predictions of specific impulse and local skin friction coefficient. Other compared quantities include characteristic velocity, thrust coefficient, thrust decrement, boundary layer displacement thickness, momentum thickness, and heat loss rate to the wall. Effects of wall temperature profile used as an input to the programs was investigated by running three wall temperature profiles. It was found that this change greatly affected the boundary layer displacement thickness and heat loss to the wall. The other quantities, however, were not drastically affected by the wall temperature profile change. Author

A87-45418*# Pratt and Whitney Aircraft Group, West Palm Beach, Fla.

OXIDIZER HEAT EXCHANGERS FOR ROCKET ENGINE OPERATION IN IDLE MODES

P. G. KANIC and T. D. KMIEC (Pratt and Whitney, West Palm Beach, FL) AIAA, SAE, ASME, and ASEE, Joint Propulsion Conference, 23rd, San Diego, CA, June 29-July 2, 1987. 10 p. refs

(Contract NAS3-24738)

(AIAA PAPER 87-2117)

The heat exchanger concept is discussed together with its role in rocket engine operation in idle modes. Two heat exchanger designs (low and high heat transfer) utilizing different approaches to achieve stable oxygen vaporization are presented as well as their performance test results. It is concluded that compact and lightweight heat exchangers can be used in a stable manner under the 'idle' operating conditions expected with the RL10 rocket engine. K.K.

A87-45725*# National Aeronautics and Space Administration. Lewis Research Center, Cleveland, Ohio.

2000-HOUR CYCLIC ENDURANCE TEST OF A LABORATORY MODEL MULTIPROPELLANT RESISTOJET

W. EARL MORREN and JAMES S. SOVEY (NASA, Lewis Research Center, Cleveland, OH) AIAA, DGLR, and Japan Society for Aeronautical and Space Sciences, International Electric Propulsion Conference, 19th, Colorado Springs, CO, May 11-13, 1987. 22 p. Previously announced in STAR as N87-22237. refs

(AIAA PAPER 87-0993)

The technological readiness of a long-life multipropellant resistojets for space station auxiliary propulsion is demonstrated. A laboratory model resistojets made from grain-stabilized platinum

served as a test bed to evaluate the design characteristics, fabrication methods, and operating strategies for an engineering model multipropellant resistojet developed under contract by the Rocketdyne Division of Rockwell International and Technion Incorporated. The laboratory model thruster was subjected to a 2000-hr, 2400-thermal-cycle endurance test using carbon dioxide propellant. Maximum thruster temperatures were approximately 1400 C. The post-test analyses of the laboratory model thruster included an investigation of component microstructures. Significant observations from the laboratory model thruster are discussed as they relate to the design of the engineering model thruster.

Author

A87-45795*# National Aeronautics and Space Administration. Lewis Research Center, Cleveland, Ohio.

THE NASA ELECTRIC PROPULSION PROGRAM

DAVID C. BYERS (NASA, Lewis Research Center, Cleveland, OH) and ROBERT A. WASEL (NASA, Office of Aeronautics and Space Technology, Washington, DC) AIAA, DGLR, and Japan Society for Aeronautical and Space Sciences, International Electric Propulsion Conference, Colorado Springs, CO, May 11-13, 1987. 21 p. Previously announced in STAR as N87-21037. refs (AIAA PAPER 87-1098)

The NASA OAST Propulsion, Power and Energy Division supports electric propulsion for a broad class of missions. Concepts with potential to significantly benefit or enable space exploration and exploitation are identified and advanced toward applications in the near to far term. Recent program progress in mission/system analyses and in electrothermal, ion, and electromagnetic technologies are summarized.

Author

A87-47003*# National Aeronautics and Space Administration. Lewis Research Center, Cleveland, Ohio.

AN EVALUATION OF METALLIZED PROPELLANTS BASED ON VEHICLE PERFORMANCE

ROBERT L. ZURAWSKI (NASA, Lewis Research Center, Cleveland, OH) and JAMES M. GREEN (NASA, Lewis Research Center; Sverdrup Technology, Inc., Cleveland, OH) AIAA, SAE, ASME, and ASEE, Joint Propulsion Conference, 23rd, San Diego, CA, June 29-July 2, 1987. 27 p. Previously announced in STAR as N87-22806. refs (AIAA PAPER 87-1773)

An analytical study was conducted to determine the improvements in vehicle performance possible by burning metals with conventional liquid bipropellants. These metallized propellants theoretically offer higher specific impulse, increased propellant density and improved vehicle performance compared with conventional liquid bipropellants. Metals considered were beryllium, lithium, aluminum and iron. Liquid bipropellants were H₂/O₂, N₂H₄/N₂O₄, RP-1/O₂ and H₂/F₂. A mission with a delta V = 4267.2 m/sec (14,000 ft/sec) and vehicle with propellant volume fixed at 56.63 cu m (2000 cu ft) and dry mass fixed at 2761.6 kg (6000 lb) was used, roughly representing the transfer of a chemically propelled upper-stage vehicle from a low-Earth orbit to a geosynchronous orbit. The results of thermochemical calculations and mission analysis calculations for bipropellants metallized with beryllium, lithium, aluminum and iron are presented. Technology issues pertinent to metallized propellants are discussed.

Author

A87-48575*# National Aeronautics and Space Administration. Lewis Research Center, Cleveland, Ohio.

LOW POWER DC ARCJET OPERATION WITH HYDROGEN/NITROGEN/AMMONIA MIXTURES

TERRY L. HARDY and FRANCIS M. CURRAN (NASA, Lewis Research Center, Cleveland, OH) AIAA, SAE, ASME, and ASEE, Joint Propulsion Conference, 23rd, San Diego, CA, June 29-July 2, 1987. 25 p. Previously announced in STAR as N87-22804. refs (AIAA PAPER 87-1948)

The effect of gas composition and ambient pressure on arcjet operation was determined. Arcjet operation in different facilities was also compared to determine the validity of tests in small facilities. Volt-ampere characteristics were determined for an arcjet

using hydrogen/nitrogen mixtures (simulating both ammonia and hydrazine), hydrogen/nitrogen/ammonia mixtures, and pure ammonia as propellants at various flow rates. The arcjet had a typical performance of 450 sec specific impulse at 1 kW with hydrogen/nitrogen mixtures. It was determined that the amount of ammonia present in the gas stream had a significant effect on the arcjet volt-ampere characteristics. Also, hydrogen/nitrogen mixtures simulating ammonia gave arc characteristics approximately the same as those of pure ammonia. Finally, no differences in arc volt-ampere characteristics were seen between low and high ambient pressure operation in the same facility. A 3 to 5 V difference was seen when different facilities were compared, but this difference was probably due to differences in the voltage drops across the current connections, and not due to arcjet operational differences in the two facilities.

Author

A87-48677*# Hughes Research Labs., Malibu, Calif.

STATUS OF XENON ION PROPULSION TECHNOLOGY

J. R. BEATTIE, J. N. MATOSSIAN, and R. R. ROBSON (Hughes Research Laboratories, Malibu, CA) AIAA, DGLR, and JSASS, International Electric Propulsion Conference, 19th, Colorado Springs, CO, May 11-13, 1987. 9 p. refs (Contract INTEL-SAT-INTEL-375; NAS3-23860) (AIAA PAPER 87-1003)

This paper describes a working-model xenon ion propulsion subsystem (XIPS) designed for north-south stationkeeping (NSSK) of 2500-kg-class geosynchronous communication satellites. The XIPS consists of a 25-cm-diameter laboratory-model thruster, a breadboard-model power supply, and a flight-prototype pressure regulator (the critical component of the pressure-regulated xenon feed system). With a thrust of 63.5 mN, specific impulse of 2800 sec, and thruster efficiency of 65 percent, the XIPS performance is believed to be the highest ever reported for an ion thruster operated at 1.3-kW input power. The XIPS power supply accepts an input power of about 1.4 kW from a 28- to 35-V bus and converts it into the seven outputs required for startup and operation of the thruster. The simplified power supply contains only about 500 parts and has demonstrated an unprecedented efficiency of 90 percent and a specific mass of about 8 kg/kW. The results of a highly successful wear-mechanism test in which the working-model XIPS was operated for 4350 hours and 3850 ON/OFF cycles are presented. These hours and cycles are equivalent to over ten years of NSSK on large communication satellites.

Author

A87-50191*# National Aeronautics and Space Administration. Lewis Research Center, Cleveland, Ohio.

NUCLEAR POWERED MARS CARGO TRANSPORT MISSION UTILIZING ADVANCED ION PROPULSION

DIANE L. GALECKI (NASA, Lewis Research Center; Sverdrup Technology, Inc., Cleveland, OH) and MICHAEL J. PATTERSON (NASA, Lewis Research Center, Cleveland, OH) AIAA, SAE, ASME, and ASEE, Joint Propulsion Conference, 23rd, San Diego, CA, June 29-July 2, 1987. 29 p. Previously announced in STAR as N87-23692. refs (AIAA PAPER 87-1903)

Nuclear-powered ion propulsion technology was combined with detailed trajectory analysis to determine propulsion system and trajectory options for an unmanned cargo mission to Mars in support of manned Mars missions. A total of 96 mission scenarios were identified by combining two power levels, two propellants, four values of specific impulse per propellant, three starting altitudes, and two starting velocities. Sixty of these scenarios were selected for a detailed trajectory analysis; a complete propulsion system study was then conducted for 20 of these trajectories. Trip times ranged from 344 days for a xenon propulsion system operating at 300 kW total power and starting from lunar orbit with escape velocity, to 770 days for an argon propulsion system operating at 300 kW total power and starting from nuclear start orbit with circular velocity. Trip times for the 3 MW cases studied ranged from 356 kW to 413 days. Payload masses ranged from 5700 to 12,300 kg for the 300 kW power level, and from 72,200 to 81,500 kg for the 3 MW power level.

Author

A87-50192*# National Aeronautics and Space Administration. Lewis Research Center, Cleveland, Ohio.

THE NASA/USAF ARCJET RESEARCH AND TECHNOLOGY PROGRAM

JAMES R. STONE (NASA, Lewis Research Center, Cleveland, OH) and EDWARD S. HUSTON (USAF, Astronautics Laboratory, Edwards AFB, CA) AIAA, SAE, ASME, and ASEE, Joint Propulsion Conference, 23rd, San Diego, CA, June 29-July 2, 1987. 21 p. Previously announced in STAR as N87-24525. refs (AIAA PAPER 87-1946)

Direct current arcjets have the potential to provide specific impulses greater than 500 sec with storable propellants, and greater than 1000 sec with hydrogen. This level of performance can provide significant benefits for such applications as orbit transfer, station keeping, orbit change, and maneuvering. The simplicity of the arcjet system and its elements of commonality with state-of-the-art resistojet systems offer a relatively low risk transition to these enhanced levels of performance for low power (0.5 to 1.5 kW) station keeping applications. Arcjets at power levels of 10 to 30 kW are potentially applicable to orbit transfer missions. Furthermore, with the anticipated development of space nuclear power systems, arcjets at greater than 100 kW may become attractive. This paper describes the ongoing NASA/USAF program and describes major recent accomplishments. Author

A87-50193*# National Aeronautics and Space Administration. Lewis Research Center, Cleveland, Ohio.

LANGMUIR PROBE SURVEYS OF AN ARCJET EXHAUST

LYNNETTE M. ZANA (NASA, Lewis Research Center, Cleveland, OH) AIAA, SAE, ASME, and ASEE, Joint Propulsion Conference, 23rd, San Diego, CA, June 29-July 2, 1987. 30 p. Previously announced in STAR as N87-22807. refs (AIAA PAPER 87-1950)

Electrostatic (Langmuir) probes of both spherical and cylindrical geometry have been used to obtain electron number density and temperature in the exhaust of a laboratory arcjet. The arcjet thruster operated on nitrogen and hydrogen mixtures to simulate fully decomposed hydrazine in a vacuum environment with background pressures less than 0.05 Pa. The exhaust appears to be only slightly ionized (less than 1 percent) with local plasma potentials near facility ground. The current-voltage characteristics of the probes indicate a Maxwellian temperature distribution. Plume data are presented as a function of arcjet operating conditions and also position in the exhaust. Author

A87-50194*# National Aeronautics and Space Administration. Lewis Research Center, Cleveland, Ohio.

LOW POWER ARCJET THRUSTER PULSE IGNITION

CHARLES J. SARMIENTO and ROBERT P. GRUBER (NASA, Lewis Research Center, Cleveland, OH) AIAA, SAE, ASME, and ASEE, Joint Propulsion Conference, 23rd, San Diego, CA, June 29-July 2, 1987. 29 p. Previously announced in STAR as N87-23691. refs (AIAA PAPER 87-1951)

An investigation of the pulse ignition characteristics of a 1 kW class arcjet using an inductive energy storage pulse generator with a pulse width modulated power converter identified several thruster and pulse generator parameters that influence breakdown voltage including pulse generator rate of voltage rise. This work was conducted with an arcjet tested on hydrogen-nitrogen gas mixtures to simulate fully decomposed hydrazine. Over all ranges of thruster and pulser parameters investigated, the mean breakdown voltages varied from 1.4 to 2.7 kV. Ignition tests at elevated thruster temperatures under certain conditions revealed occasional breakdowns to thruster voltages higher than the power converter output voltage. These post breakdown discharges sometimes failed to transition to the lower voltage arc discharge mode and the thruster would not ignite. Under the same conditions, a transition to the arc mode would occur for a subsequent pulse and the thruster would ignite. An automated 11 600 cycle starting and transition to steady state test demonstrated ignition on the first pulse and required application of a second pulse only two times to initiate breakdown. Author

A87-50195*# National Aeronautics and Space Administration. Lewis Research Center, Cleveland, Ohio.

ELECTROMAGNETIC EMISSION EXPERIENCES USING ELECTRIC PROPULSION SYSTEMS - A SURVEY

JAMES S. SOVEY, LYNNETTE M. ZANA (NASA, Lewis Research Center, Cleveland, OH), and STEVEN C. KNOWLES (Rocket Research Co., Redmond, WA) AIAA, SAE, ASME, and ASEE, Joint Propulsion Conference, 23rd, San Diego, CA, June 29-July 2, 1987. 37 p. Previously announced in STAR as N87-22805. refs (AIAA PAPER 87-2028)

As electric propulsion systems become ready to integrate with spacecraft systems, the impact of propulsion system radiated emissions are of significant interest. Radiated emissions from electromagnetic, electrostatic, and electrothermal systems have been characterized and results synopsized from the literature describing 21 space flight programs. Electromagnetic radiated emission results from ground tests and flight experiences are presented with particular attention paid to the performance of spacecraft subsystems and payloads during thruster operations. The impacts to transmission of radio frequency signals through plasma plumes are also reviewed. Author

A87-50197*# National Aeronautics and Space Administration. Lewis Research Center, Cleveland, Ohio.

PRELIMINARY PERFORMANCE CHARACTERIZATIONS OF AN ENGINEERING MODEL MULTIPROPELLANT RESISTOJET FOR SPACE STATION APPLICATION

W. EARL MORREN, THOMAS W. HAAG, JAMES S. SOVEY (NASA, Lewis Research Center, Cleveland, OH), and STUART S. HAY (Purdue University, West Lafayette, IN) AIAA, SAE, ASME, and ASEE, Joint Propulsion Conference, 23rd, San Diego, CA, June 29-July 2, 1987. 24 p. Previously announced in STAR as N87-23821. refs (AIAA PAPER 87-2120)

Presented are the results of a program to describe the operational characteristics of an engineering model multipropellant resistojet for application as an auxiliary propulsion system for the space station. Performance was measured on hydrogen, helium, methane, water (steam), nitrogen, air, argon, and carbon dioxide. Thrust levels ranged from 109 to 355 mN, power levels ranged from 167 to 506 W, and specific impulse values ranged from 93 to 385 sec, depending on the propellant, chamber pressure, and heater current level selected. Detailed thermal maps of the heater and heat exchanger were also obtained for operation with carbon dioxide. Author

A87-50198*# National Aeronautics and Space Administration. Lewis Research Center, Cleveland, Ohio.

IN-SITU ANALYSIS OF HYDRAZINE DECOMPOSITION PRODUCTS

FRANCIS M. CURRAN and MARGARET V. WHALEN (NASA, Lewis Research Center, Cleveland, OH) AIAA, SAE, ASME, and ASEE, Joint Propulsion Conference, 23rd, San Diego, CA, June 29-July 2, 1987. 16 p. Previously announced in STAR as N87-23693. refs (AIAA PAPER 87-2122)

A gas analyzer utilizing a nondispersive infrared (NDIR) detection system was used to monitor the ammonia and water vapor content of the products of a previously unused hydrazine gas generator. This provided an in-situ measurement of the generator's efficiency difficult to obtain by other means. The analyzer was easily installed in both the calibration and hydrazine systems, required no maintenance other than periodic zero adjustments, and performed well for extended periods in the operating range tested. The catalyst bed operated smoothly and repeatedly during the 28 hr of testing. No major transients were observed on startup or during steady state operation. The amount of ammonia in the output stream of the gas generator was found to be a strong function of temperature at catalyst bed temperatures below 450 C. At temperatures above this, the efficiency remained nearly constant. On startup the gas generator efficiency was found to decrease with time until a steady state value was attained.

Elevated catalyst bed temperatures in the periods before steady state operation was found to be responsible for this phenomenon. Author

A87-52247*# Washington Univ., St. Louis, Mo.
TEMPERATURE FIELDS DUE TO JET INDUCED MIXING IN A TYPICAL OTV TANK

J. I. HOCHSTEIN, HYUN-CHUL JI (Washington University, Saint Louis, MO), and J. C. AYDELOTT (NASA, Lewis Research Center, Cleveland, OH) AIAA, SAE, ASME, and ASEE, Joint Propulsion Conference, 23rd, San Diego, CA, June 29-July 2, 1987. 11 p. refs

(Contract NAG3-578)
 (AIAA PAPER 87-2017)

The Eclipse Code is being developed as a general tool for analysis of cryogenic propellant behavior in spacecraft tankage. The focus of the work being reported is on prediction of temperature fields due to introduction of a cold jet along the centerline of a typical Orbit Transfer Vehicle tank. A brief description of the formulations used for modeling heat transfer and turbulent flow is presented. Code performance is verified through comparison to experimental data for mixing in small scale tanks. An unexpected difficulty in computing long duration flows is reviewed. Preliminary results for a partially filled full scale tank are obtained by approximating the free surface by a spherical solid boundary.

Author

A87-52249*# National Aeronautics and Space Administration.
 Lewis Research Center, Cleveland, Ohio.

EXPERIMENTAL EVALUATION OF HEAT TRANSFER ON A 1030:1 AREA RATIO ROCKET NOZZLE

KENNETH J. KACYNSKI, ALBERT J. PAVLI, and TAMARA A. SMITH (NASA, Lewis Research Center, Cleveland, OH) AIAA, SAE, ASME, and ASEE, Joint Propulsion Conference, 23rd, San Diego, CA, June 29-July 2, 1987. 25 p. Previously announced in STAR as N87-25424. refs
 (AIAA PAPER 87-2070)

A 1030:1 carbon steel, heat-sink nozzle was tested. The test conditions included a nominal chamber pressure of 2413 kN/sq m and a mixture ratio range of 2.78 to 5.49. The propellants were gaseous oxygen and gaseous hydrogen. Outer wall temperature measurements were used to calculate the inner wall temperature and the heat flux and heat rate to the nozzle at specified axial locations. The experimental heat fluxes were compared to those predicted by the Two-Dimensional Kinetics (TDK) computer model analysis program. When laminar boundary layer flow was assumed in the analysis, the predicted values were within 15 percent of the experimental values for the area ratios of 20 to 975. However, when turbulent boundary layer conditions were assumed, the predicted values were approximately 120 percent higher than the experimental values. A study was performed to determine if the conditions within the nozzle could sustain a laminar boundary layer. Using the flow properties predicted by TDK, the momentum-thickness Reynolds number was calculated, and the point of transition to turbulent flow was predicted. The predicted transition point was within 0.5 inches of the nozzle throat. Calculations of the acceleration parameter were then made to determine if the flow conditions could produce relaminarization of the boundary layer. It was determined that if the boundary layer flow was inclined to transition to turbulent, the acceleration conditions within the nozzle would tend to suppress turbulence and keep the flow laminar-like.

M.G.

A87-52250*# National Aeronautics and Space Administration.
 Lewis Research Center, Cleveland, Ohio.

ANALYSIS OF QUASI-HYBRID SOLID ROCKET BOOSTER CONCEPTS FOR ADVANCED EARTH-TO-ORBIT VEHICLES

ROBERT L. ZURAWSKI (NASA, Lewis Research Center, Cleveland, OH) and DOUGLAS C. RAPP (Sverdrup Technology, Inc., Cleveland, OH) AIAA, SAE, ASME, and ASEE, Joint Propulsion Conference, 23rd, San Diego, CA, June 29-July 2, 1987. 29 p. Previously announced in STAR as N87-25425. refs
 (AIAA PAPER 87-2082)

A study was conducted to assess the feasibility of quasi-hybrid solid rocket boosters for advanced earth-to-orbit vehicles. Thermochemical calculations were conducted to determine the effect of liquid hydrogen addition, solids composition change plus liquid hydrogen addition, and the addition of an aluminum/liquid hydrogen slurry on the theoretical performance of a PBAN solid propellant rocket. The Space Shuttle solid rocket booster was used as a reference point. All three quasi-hybrid systems theoretically offer higher specific impulse when compared with the Space Shuttle solid rocket boosters. However, based on operational and safety considerations, the quasi-hybrid rocket is not a practical choice for near-term earth-to-orbit booster applications. Safety and technology issues pertinent to quasi-hybrid rocket systems are discussed.

Author

A87-52252*# Akron Univ., Ohio.

EFFECT OF NOZZLE GEOMETRY ON THE RESISTOJET EXHAUST PLUME

LORANELL BREYLEY, JOHN S. SERAFINI (Akron, University, OH), DAVID J. HOFFMAN, and LYNETTE M. ZANA (NASA, Lewis Research Center, Cleveland, OH) AIAA, SAE, ASME, and ASEE, Joint Propulsion Conference, 23rd, San Diego, CA, June 29-July 2, 1987. 10 p. refs
 (Contract NAG3-637)
 (AIAA PAPER 87-2121)

Five nozzle configurations were used to study the effect of geometry on the plume structure of a resistojets exhausting into a vacuum. Mass flux data in the forward and back flux regions were obtained with a cryogenically cooled quartz crystal microbalance. The propellant used was CO₂ at 300 K and a mass flow rate of 0.2 g/s. The data reveal that the percent of mass flow contained within half angles of 10, 30, and 40 deg varied by less than 12 percent from a standard 20 deg half-angle cone nozzle. K.K.

N87-10174*# National Aeronautics and Space Administration.
 Lewis Research Center, Cleveland, Ohio.

COAXIAL TUBE TETHER/TRANSMISSION LINE FOR MANNED NUCLEAR SPACE POWER Patent Application

D. J. BENTS, inventor (to NASA) 18 Aug. 1986 15 p
 (NASA-CASE-LEW-14338-1; US-PATENT-APPL-SN-897239; NAS 1.71:LEW-14338-1) Avail: NTIS HC A02/MF A01 CSCL 10B

A spacecraft comprising a platform, a power system and a power transmission line adapted to transmitting high voltage electrical power in a space environment is disclosed. The transmission power line tethers the suborbiting platform to the power system located in a superorbital position relative to the platform.

NASA

N87-10176*# Rockwell International Corp., Canoga Park, Calif.
 Rocketdyne Div.

COMPOSITE LOAD SPECTRA FOR SELECT SPACE PROPULSION STRUCTURAL COMPONENTS Annual Report

J. F. NEWELL, R. E. KURTH, and H. HO Mar. 1986 365 p
 (Contract NAS3-24382)
 (NASA-CR-179496; NAS 1.26:179496; RI/RD86-123; AR-1)
 Avail: NTIS HC A16/MF A01 CSCL 21H

A multiyear program is performed with the objective to develop generic load models with multiple levels of progressive sophistication to simulate the composite (combined) load spectra that are induced in space propulsion system components, representative of Space Shuttle Main Engines (SSME), such as transfer ducts, turbine blades, and liquid oxygen (LOX) posts. Progress of the first year's effort includes completion of a sufficient

portion of each task -- probabilistic models, code development, validation, and an initial operational code. This code has from its inception an expert system philosophy that could be added to throughout the program and in the future. The initial operational code is only applicable to turbine blade type loadings. The probabilistic model included in the operational code has fitting routines for loads that utilize a modified Discrete Probabilistic Distribution termed RASCAL, a barrier crossing method and a Monte Carlo method. An initial load model was developed by Battelle that is currently used for the slowly varying duty cycle type loading. The intent is to use the model and related codes essentially in the current form for all loads that are based on measured or calculated data that have followed a slowly varying profile. Author

N87-10959*# National Aeronautics and Space Administration. Lewis Research Center, Cleveland, Ohio.

STATUS OF ADVANCED PROPULSION FOR SPACE BASED ORBITAL TRANSFER VEHICLE

L. P. COOPER and D. D. SCHEER 1986 32 p Presented at the 37th Congress of the International Astronautical Federation, Innsbruck, Austria, 4-11 Oct. 1986

(NASA-TM-88848; E-3238; NAS 1.15:88848; IAF-86-183) Avail: NTIS HC A03/MF A01 CSCL 21H

A new Orbital Transfer Vehicle (OTV) propulsion system will be required to meet the needs of space missions beyond the mid-1990's. As envisioned, the advanced OTV will be used in conjunction with Earth-to-orbit vehicles, Space Station, and Orbit Maneuvering Vehicle. The OTV will transfer men, large space structures, and conventional payloads between low Earth and higher energy orbits. Space probes carried by the OTV will continue the exploration of the solar system. When lunar bases are established, the OTV will be their transportation link to Earth. NASA is currently funding the development of technology for advanced propulsion concepts for future Orbital Transfer Vehicles. Progress in key areas during 1986 is presented. Author

N87-10960*# National Aeronautics and Space Administration. Lewis Research Center, Cleveland, Ohio.

OXIDATION-RESISTANT REFLECTIVE SURFACES FOR SOLAR DYNAMIC POWER GENERATION IN NEAR EARTH ORBIT

D. A. GULINO, R. A. EGGER (Cleveland State Univ., Ohio), and W. F. BANHOLZER (General Electric Co., Schenectady, N. Y.) 1986 16 p Presented at the 33rd National Symposium of the National Vacuum Society, Baltimore, Md., 27-31 Oct. 1986

(NASA-TM-88865; E-3268; NAS 1.15:88865) Avail: NTIS HC A02/MF A01 CSCL 10B

Reflective surfaces for space station power generation systems are required to withstand the atomic oxygen-dominated environment of near Earth orbit. Thin films of platinum and rhodium, which are corrosion resistant reflective metals, have been deposited by ion beam sputter deposition onto various substrate materials. Solar reflectances were then measured as a function of time of exposure to a RF-generated air plasma. Similarly, various protective coating materials, including MgF₂, SiO₂, Al₂O₃, and Si₃N₄, were deposited onto silver-coated substrates and then exposed to the plasma. Analysis of the films both before and after exposure by both ESCA and Auger spectroscopy was also performed. The results indicate that Pt and Rh do not suffer any loss in reflectance over the duration of the tests. Also, each of the coating materials survived the plasma environment. The ESCA and Auger analyses are discussed as well. Author

N87-11838*# National Aeronautics and Space Administration. Lewis Research Center, Cleveland, Ohio.

EFFECT OF HARD PARTICLE IMPACTS ON THE ATOMIC OXYGEN SURVIVABILITY OF REFLECTOR SURFACES WITH TRANSPARENT PROTECTIVE OVERCOATS

D. A. GULINO 1986 22 p Proposed for presentation at the 25th Aerospace Sciences Meeting, Reno, Nev. 12-15 Jan. 1987; sponsored by the American Institute of Aeronautics and Astronautics

(NASA-TM-88874; E-3281; NAS 1.15:88874) Avail: NTIS HC A02/MF A01 CSCL 10B

Silver mirror samples with protective coatings were subjected to a stream of 27 microns alumina particles to induce pinhole defects. The protective coating consisted of a layer of aluminum dioxide over silver followed by a layer of silicon dioxide over the alumina. Samples were prepared on both graphite-epoxy composite and fused quartz substrates. After exposure to the hard particle stream, the samples were exposed to an oxygen plasma environment in a laboratory plasma asher. The effects of both the hard particles and the oxygen plasma were documented by both reflectance measurements and scanning electron microscopy. The results indicated that oxidative damage to the silver reflecting layer continues beyond that of the erosively exposed silver. Oxidative undercutting of the silver layer and graphite-epoxy substrate continues in undamaged areas through adjacent, particle damaged defect sites. This may have implications for the use of such mirrors in a space station solar dynamic power system. Author

N87-12606*# National Aeronautics and Space Administration. Lewis Research Center, Cleveland, Ohio.

ADVANCED SOLAR DYNAMIC SPACE POWER SYSTEMS PERSPECTIVES, REQUIREMENTS AND TECHNOLOGY NEEDS

M. O. DUSTIN, J. M. SAVINO, D. E. LACY, R. P. MIGRA (Sverdrup Technology, Inc., Arnold Air Force Station, Tenn.), A. J. JUHASZ, and C. E. COLES 1986 30 p Proposed for presentation at the Solar Energy Conference, Honolulu, Hawaii, 22-23 Mar. 1987; sponsored by ASME, JSME and JSES

(NASA-TM-88884; E-3292; NAS 1.15:88884) Avail: NTIS HC A03/MF A01 CSCL 10B

Projected NASA, Civil, Commercial, and Military missions will require space power systems of increased versatility and power levels. The Advanced Solar Dynamic (ASD) Power systems offer the potential for efficient, lightweight, survivable, relatively compact, long-lived space power systems applicable to a wide range of power levels (3 to 300 kWe), and a wide variety of orbits. The successful development of these systems could satisfy the power needs for a wide variety of these projected missions. Thus, the NASA Lewis Research Center has embarked upon an aggressive ASD research project under the direction of NASA's Office of Aeronautics and Space Technology (DAST). The project is being implemented through a combination of in-house and contracted efforts. Key elements of this project are missions analysis to determine the power systems requirements, systems analysis to identify the most attractive ASD power systems to meet these requirements, and to guide the technology development efforts, and technology development of key components. Author

N87-13486*# Rockwell International Corp., Canoga Park, Calif. Rocketdyne Div.

ENHANCED HEAT TRANSFER COMBUSTOR TECHNOLOGY, SUBTASKS 1 AND 2, TAST C.1 Interim Report

R. D. BAILY 16 Dec. 1986 305 p

(Contract NAS3-23773)

(NASA-CR-179541; NAS 1.26:179541; RI/RD86-199) Avail: NTIS HC A14/MF A01 CSCL 21H

Analytical and experimental studies are being conducted for NASA to evaluate means of increasing the heat extraction capability and service life of a liquid rocket combustor. This effort is being conducted in conjunction with other tasks to develop technologies for an advanced, expander cycle, oxygen/hydrogen engine planned for upper stage propulsion applications. Increased heat extraction, needed to raise available turbine drive energy for higher chamber pressure, is derived from combustion chamber hot gas wall ribs

that increase the heat transfer surface area. Life improvement is obtained through channel designs that enhance cooling and maintain the wall temperature at an acceptable level. Laboratory test programs were conducted to evaluate the heat transfer characteristics of hot gas rib and coolant channel geometries selected through an analytical screening process. Detailed velocity profile maps, previously unavailable for rib and channel geometries, were obtained for the candidate designs using a cold flow laser velocimeter facility. Boundary layer behavior and heat transfer characteristics were determined from the velocity maps. Rib results were substantiated by hot air calorimeter testing. The flow data were analytically scaled to hot fire conditions and the results used to select two rib and three enhanced coolant channel configurations for further evaluation. Author

N87-14422*# National Aeronautics and Space Administration. Lewis Research Center, Cleveland, Ohio.

ELECTRIC PROPULSION OPTIONS FOR THE SP-100 REFERENCE MISSION

T. L. HARDY, V. K. RAWLIN, and M. J. PATTERSON 1987 26 p Presented at the 4th Symposium on Space Nuclear Power Systems, Albuquerque, N. Mex., 12-16 Jan. 1987; sponsored by the Inst. for Space Nuclear Power Studies (NASA-TM-88918; E-3343; NAS 1.15:88918) Avail: NTIS HC A03/MF A01 CSCL 81G

Analyses were performed to characterize and compare electric propulsion systems for use on a space flight demonstration of the SP-100 nuclear power system. The component masses of resistojets, arcjet, and ion thruster systems were calculated using consistent assumptions and the maximum total impulse, velocity increment, and thrusting time were determined, subject to the constraint of the lift capability of a single Space Shuttle launch. From the study it was found that for most systems the propulsion system dry mass was less than 20 percent of the available mass for the propulsion system. The maximum velocity increment was found to be up to 2890 m/sec for resistojets, 3760 m/sec for arcjet, and 23 000 m/sec for ion thruster systems. The maximum thruster time was found to be 19, 47, and 853 days for resistojets, arcjet, and ion thruster systems, respectively. Author

N87-14423*# National Aeronautics and Space Administration. Lewis Research Center, Cleveland, Ohio.

THE SURVIVABILITY OF LARGE SPACE-BORNE REFLECTORS UNDER ATOMIC OXYGEN AND MICROMETEOROID IMPACT

D. A. GULINO 1987 18 p Presented at the 25th Aerospace Sciences Meeting, Reno, Nev., 12-15 Jan. 1987; sponsored by AIAA (NASA-TM-88914; E-3338; NAS 1.15:88914) Avail: NTIS HC A02/MF A01 CSCL 21H

Solar dynamic power system mirrors for use on space station and other spacecraft flown in low Earth orbit (LEO) are exposed to the harshness of the LEO environment. Both atomic oxygen and micrometeoroids/space debris can degrade the performance of such mirrors. Protective coatings will be required to protect oxidizable reflecting media, such as silver and aluminum, from atomic oxygen attack. Several protective coating materials have been identified as good candidates for use in this application. The durability of these coating/mirror systems after pinhole defects have been inflicted during their fabrication and deployment or through micrometeoroid/space debris impact once on-orbit is of concern. Studies of the effect of an oxygen plasma environment on protected mirror surfaces with intentionally induced pinhole defects have been conducted at NASA Lewis and are reviewed. It has been found that oxidation of the reflective layer and/or the substrate in areas adjacent to a pinhole defect, but not directly exposed by the pinhole, can occur. Author

N87-14425*# Page (R. J.) Co., Santa Ana, Calif.

A DESIGN STUDY OF HYDRAZINE AND BIOWASTE RESISTOJETS Final Report

R. J. PAGE, W. A. STONER, and L. BARKER Sep. 1986 149 p (Contract NAS3-23863) (NASA-CR-179510; NAS 1.26:179510) Avail: NTIS HC A07/MF A01 CSCL 21H

A generalized modeling program was adapted in BASIC on a personal computer to compare the performance of four types of biowaste resistojets and two types of hydrazine augmenters. Analyzed biowaste design types were: (1) an electrically conductive ceramic heater-exchanger of zirconia; (2) a truss heater of platinum in cross flow; (3) an immersed bicoiled tubular heater-exchanger; and (4) a nonexposed, refractory metal, radiant heater in a central cavity within a heat exchanger case. Concepts 2 and 3 are designed to have an efficient, stainless steel outer pressure case. The hydrazine design types are: (5) an immersed bicoil heater exchanger and (6) a nonexposed radiant heater now with a refractory metal case. The ceramic biowaste resistojets have the highest specific impulse growth potential at 2000 K of 192.5 (CO₂) and 269 s (H₂O). The bicoil produces the highest augmentor temperature of 1994 K for a 2073 K heater giving 317 s at .73 overall efficiency. Detailed temperature profiles of each of the designs are shown. The scaled layout drawings of each are presented with recommended materials and fabrication methods. Author

N87-14426*# National Aeronautics and Space Administration. Lewis Research Center, Cleveland, Ohio.

LIQUID OXYGEN COOLING OF HIGH PRESSURE LOX/HYDROCARBON ROCKET THRUST CHAMBERS

H. G. PRICE and P. A. MASTERS Aug. 1986 23 p (NASA-TM-88805; E-3149; NAS 1.15:88805) Avail: NTIS HC A02/MF A01 CSCL 21H

An experimental program using liquid oxygen (LOX) and RP-1 as the propellants and supercritical LOX as the coolant was conducted at 4.14, 8.27, and 13.79 MN/sq m (600, 1200, and 2000 psia) chamber pressure. The objectives of this program were to evaluate the cooling characteristics of LOX with the LOX/RP-1 propellants, the buildup of the soot on the hot-gas-side chamber wall, and the effect of an internal LOX leak on the structural integrity of the combustor. Five thrust chambers with throat diameters of 6.6 cm (2.5 in.) were tested successfully. The first three were tested at 4.14 MN/sq m (600 psia) chamber pressure over a mixture ratio range of 2.25 to 2.92. One of these three was tested for over 22 cyclic tests after the first through crack from the coolant channel to the combustion zone was observed with no apparent metal burning or distress. The fourth chamber was tested at 8.27 MN/sq m (1200 psia) chamber pressure over a mixture range of 1.93 to 2.98. The fourth and fifth chambers were tested at 13.79 MN/sq m (2000 psia) chamber pressure over a mixture ratio range of 1.79 to 2.68. Author

N87-14427*# National Aeronautics and Space Administration. Lewis Research Center, Cleveland, Ohio.

HIGH- AND LOW-THRUST PROPULSION SYSTEMS FOR THE SPACE STATION

R. E. JONES 1987 23 p Presented at the 25th Aerospace Sciences Meeting, Reno, Nev., 12-15 Jan. 1987; sponsored by AIAA (NASA-TM-88877; E-3285; NAS 1.15:88877) Avail: NTIS HC A02/MF A01 CSCL 21H

The purpose of the Advanced Development program was to investigate propulsion options for the space station. Two options were investigated in detail: a high-thrust system consisting of 25 to 50 lbf gaseous oxygen/hydrogen rockets, and a low-thrust system of 0.1 lbf multipropellant resistojets. An effort is also being conducted to determine the life capability of hydrazine-fueled thrusters. During the course of this program, studies clearly identified the benefits of utilizing waste water and other fluids as propellant sources. The results of the H₂O thruster test programs are presented and the plan to determine the life of hydrazine thrusters is discussed. The background required to establish a

20 SPACECRAFT PROPULSION AND POWER

long-life resistojet is presented and the first design model is shown in detail. Author

N87-14428*# National Aeronautics and Space Administration. Lewis Research Center, Cleveland, Ohio.
AN ANALYTICAL AND EXPERIMENTAL INVESTIGATION OF RESISTOJET PLUMES

L. M. ZANA, D. J. HOFFMAN, L. R. BREYLEY (Akron Univ., Ohio), and J. S. SERAFINI Jan. 1987 22 p Presented at the 25th Aerospace Sciences Meeting, Reno, Nev., 12-15 Jan. 1987; sponsored by AIAA (NASA-TM-88852; E-3243; NAS 1.15:88852) Avail: NTIS HC A02/MF A01 CSCL 21H

As a part of the electrothermal propulsion plume research program at the NASA Lewis Research Center, efforts have been initiated to analytically and experimentally investigate the plumes of resistojet thrusters. The method of G.A. Simons for the prediction of rocket exhaust plumes is developed for the resistojet. Modifications are made to the source flow equations to account for the increased effects of the relatively large nozzle boundary layer. Additionally, preliminary mass flux measurements of a laboratory resistojet using CO₂ propellant at 298 K have been obtained with a cryogenically cooled quartz crystal microbalance (QCM). There is qualitative agreement between analysis and experiment, at least in terms of the overall number density shape functions in the forward flux region. Author

N87-15267*# National Aeronautics and Space Administration. Lewis Research Center, Cleveland, Ohio.

ELECTRICAL POWER SYSTEM DESIGN FOR THE US SPACE STATION

DONALD L. NORED and DANIEL T. BERNATOWICZ 29 Aug. 1986 19 p Presented at the 21st Intersociety Energy Conversion Engineering Conference, San Diego, Calif., 25-29 Aug. 1986; cosponsored by ACS, SAE, ANS, ASME, IEEE, AIAA and AICHE (NASA-TM-88824; E-3073; NAS 1.15:88824) Avail: NTIS HC A02/MF A01 CSCL 22B

The multipurpose, manned, permanent space station will be our next step toward utilization of space. A multikilowatt electrical power system will be critical to its success. The power systems for the space station manned core and platforms that have been selected in definition studies are described. The system selected for the platforms uses silicon arrays and Ni-H₂ batteries. The power system for the manned core is a hybrid employing arrays and batteries identical to those on the platform along with solar dynamic modules using either Brayton or organic Rankine engines. The power system requirements, candidate technologies, and configurations that were considered, and the basis for selection, are discussed. Author

N87-15269*# Pratt and Whitney Aircraft, West Palm Beach, Fla. Government Products Div.

BREADBOARD RL10-11B LOW THRUST OPERATING MODE Final Test Report, 24-29 Feb. 1984

THOMAS D. KMEIC and DONALD E. GALLER Jan. 1987 83 p (Contract NAS3-24238; NAS3-22902) (NASA-CR-174914; NAS 1.26:174914; FR-18683-2) Avail: NTIS HC A05/MF A01 CSCL 21H

Cryogenic space engines require a cooling process to condition engine hardware to operating temperature before start. This can be accomplished most efficiently by burning propellants that would otherwise be dumped overboard after cooling the engine. The resultant low thrust operating modes are called Tank Head Idle and Pumped Idle. During February 1984, Pratt & Whitney conducted a series of tests demonstrating operation of the RL10 rocket engines at low thrust levels using a previously untried hydrogen/oxygen heat exchanger. The initial testing of the RL10-11B Breadboard Low Thrust Engine is described. The testing demonstrated operation at both tank head idle and pumped idle modes. Author

N87-15270*# Ford Aerospace and Communications Corp., Palo Alto, Calif.

SPACE STATION EXPERIMENT DEFINITION: ADVANCED POWER SYSTEM TEST BED Final Report

H. E. POLLARD and R. E. NEFF 15 Dec. 1986 148 p

(Contract NAS3-24664)

(NASA-CR-179502; NAS 1.26:179502; WDL-TR10939) Avail:

NTIS HC A07/MF A01 CSCL 10B

A conceptual design for an advanced photovoltaic power system test bed was provided and the requirements for advanced photovoltaic power system experiments better defined. Results of this study will be used in the design efforts conducted in phase B and phase C/D of the space station program so that the test bed capabilities will be responsive to user needs. Critical PV and energy storage technologies were identified and inputs were received from the industry (government and commercial, U.S. and international) which identified experimental requirements. These inputs were used to develop a number of different conceptual designs. Pros and cons of each were discussed and a strawman candidate identified. A preliminary evolutionary plan, which included necessary precursor activities, was established and cost estimates presented which would allow for a successful implementation to the space station in the 1994 time frame. Author

N87-15272*# Pratt and Whitney Aircraft, West Palm Beach, Fla. Government Products Div.

LOW HEAT TRANSFER OXIDIZER HEAT EXCHANGER DESIGN AND ANALYSIS Topical Report, Oct. 1985 - Oct. 1986

P. G. KANIC, T. D. KMEIC, and R. J. PECKHAM 30 Jan. 1987 51 p

(Contract NAS3-24238)

(NASA-CR-179488; NAS 1.26:179488; FR-19135-2) Avail: NTIS HC A04/MF A01 CSCL 21H

The RL10-IIB engine, a derivative of the RL10, is capable of multi-mode thrust operation. This engine operates at two low thrust levels: tank head idle (THI), which is approximately 1 to 2 percent of full thrust, and pumped idle (PI), which is 10 percent of full thrust. Operation at THI provides vehicle propellant settling thrust and efficient engine thermal conditioning; PI operation provides vehicle tank pre-pressurization and maneuver thrust for log-g deployment. Stable combustion of the RL10-IIB engine at THI and PI thrust levels can be accomplished by providing gaseous oxygen at the propellant injector. Using gaseous hydrogen from the thrust chamber jacket as an energy source, a heat exchanger can be used to vaporize liquid oxygen without creating flow instability. This report summarizes the design and analysis of a United Aircraft Products (UAP) low-rate heat transfer heat exchanger concept for the RL10-IIB rocket engine. The design represents a second iteration of the RL10-IIB heat exchanger investigation program. The design and analysis of the first heat exchanger effort is presented in more detail in NASA CR-174857. Testing of the previous design is detailed in NASA CR-179487. Author

N87-16024*# National Aeronautics and Space Administration. Lewis Research Center, Cleveland, Ohio.

SOLAR DYNAMIC POWER SYSTEMS FOR SPACE STATION

THOMAS B. IRVINE, MARSHA M. NALL, and ROBERT C. SEIDEL In NASA. Langley Research Center NASA/DOD Control/Structures Interaction Technology, 1986 p 149-166 Nov. 1986

Avail: NTIS HC A23/MF A01 CSCL 14B

The Parabolic Offset Linearly Actuated Reflector (POLAR) solar dynamic module was selected as the baseline design for a solar dynamic power system aboard the space station. The POLAR concept was chosen over other candidate designs after extensive trade studies. The primary advantages of the POLAR concept are the low mass moment of inertia of the module about the transverse boom and the compactness of the stowed module which enables packaging of two complete modules in the Shuttle orbiter payload bay. The fine pointing control system required for the solar dynamic module has been studied and initial results indicate that if disturbances from the station are allowed to back drive the rotary

alpha joint, pointing errors caused by transient loads on the space station can be minimized. This would allow pointing controls to operate in bandwidths near system structural frequencies. The incorporation of the fine pointing control system into the solar dynamic module is fairly straightforward for the three strut concentrator support structure. However, results of structural analyses indicate that this three strut support is not optimum. Incorporation of a vernier pointing system into the proposed six strut support structure is being studied. Author

N87-16065*# Sverdrup Technology, Inc., Cleveland, Ohio.
POTENTIAL PROPELLANT STORAGE AND FEED SYSTEMS FOR SPACE STATION RESISTOJET PROPULSION OPTIONS
Final Report

CLAYTON H. BADER Jan. 1987 63 p

(Contract NAS3-24105)

(NASA-CR-179457; E-3366; NAS 1.26:179457) Avail: NTIS HC A04/MF A01 CSCL 21H

The resistojet system has been defined as part of the baseline propulsion system for the initial Operating Capability Space Station. The resistojet propulsion module will perform a reboost function using a wide variety of fluids as propellants. There are many optional propellants and propellant combinations for use in the resistojet including (but not limited to): hydrazine, hydrogen, oxygen, nitrogen, water, carbon dioxide, and methane. Many different types of propulsion systems have flown or have been conceptualized that may have application for use with resistojets. This paper describes and compares representative examples of these systems that may provide a basis for space station resistojet system design. Author

N87-16874*# Textron Bell Aerospace Co., Buffalo, N. Y.
SPACE STATION AUXILIARY THRUST CHAMBER TECHNOLOGY Final Report

J. M. SENNEFF Aug. 1986 196 p

(Contract NAS3-24656)

(NASA-CR-179552; NAS 1.26:179552; REPT-8911-950001)

Avail: NTIS HC A09/MF A01 CSCL 21H

A program to design, fabricate and test a 50 lb sub f (222 N) thruster was undertaken (Contract NAS 3-24656) to demonstrate the applicability of the reverse flow concept as an item of auxiliary propulsion for the space station. The thruster was to operate at a mixture ratio (O/F) of 4, be capable of operating for 2 million lb sub f-seconds (8.896 million N-seconds) impulse with a chamber pressure of 75 psia (52 N/square cm) and a nozzle area ratio of 40. Superimposed was also the objective of operating with a stainless steel spherical combustion chamber, which limited the wall temperature to 1700 F (1200 K), an objective specific impulse of 400 lb sub f sec/lbm (3923 N-seconds/Kg), and a demonstration of 500,000 lb sub f-seconds (2,224,000 N-seconds) of impulse. The demonstration of these objectives required a number of design iterations which eventually culminated in a very successful 1000 second demonstration, almost immediately followed by a changed program objective imposed to redesign and demonstrate at a mixture ratio (O/F) of 8. This change was made and more than 250,000 lb sub f seconds (1,112,000 N-seconds) of impulse was successfully demonstrated at a mixture ratio of 8. This document contains a description of the effort conducted during the program to design and demonstrate the thrusters involved. Author

N87-16875* National Aeronautics and Space Administration. Lewis Research Center, Cleveland, Ohio.

HEAT EXCHANGER FOR ELECTROTHERMAL DEVICES Patent
 RALPH J. ZAVESKY, inventor (to NASA), JAMES S. SOVEY, inventor (to NASA), MICHAEL J. MIRTICH, inventor (to NASA), CHARALAMPUS MARINOS, inventor (to NASA), and PAUL F. PENKO, inventor (to NASA) 2 Sep. 1986 7 p Filed 31 Jul. 1984 Supersedes N84-32425 (22 - 22, p 3542)
 (NASA-CASE-LEW-14037-1; US-PATENT-4,608,821; US-PATENT-APPL-SN-636463; US-PATENT-CLASS-60-203.1; US-PATENT-CLASS-219-275) Avail: US Patent and Trademark Office CSCL 21H

An improved electrothermal device is disclosed. An electrothermal thruster utilizes a generally cylindrical heat exchanger chamber to convert electricity to heat which raises the propellant temperature. A textured, high emissivity heat element radiatively transfers heat to the inner wall of this chamber that is ion beam morphologically controlled for high absorptivity. This, in turn, raises the temperature of a porous heat exchanger material in an annular chamber surrounding the cylindrical chamber. Propellant gas flows through the annular chamber and is heated by the heat exchanger material.

Official Gazette of the US Patent and Trademark Office

N87-16878*# GT-Devices, Alexandria, Va.
INVESTIGATION OF A REPETITIVE PULSED ELECTROTHERMAL THRUSTER Contract Report, 24 May 1985 - 23 May 1986

R. L. BURTON, D. FLEISCHER, S. A. GOLDSTEIN, D. A. TIDMAN, and N. K. WINSOR 21 Aug. 1986 57 p

(Contract NAS3-24636)

(NASA-CR-179464; NAS 1.26:179464; GTD86-5) Avail: NTIS HC A04/MF A01 CSCL 21H

A pulsed electrothermal (PET) thruster with 1000:1 ratio nozzle is tested in a repetitive mode on water propellant. The thruster is driven by a 60J pulse forming network at repetition rates up to 10 Hz (600W). The pulse forming network has a .31 ohm impedance, well matched to the capillary discharge resistance of .40 ohm, and is directly coupled to the thruster electrodes without a switch. The discharge is initiated by high voltage breakdown, typically at 2500V, through the water vapor in the interelectrode gap. Water is injected as a jet through a .37 mm orifice on the thruster axis. Thruster voltage, current and impulse bit are recorded for several seconds at various power supply currents. Thruster to power ratio is typically T/P = .07 N/kW. Tank background pressure precludes direct measurement of exhaust velocity which is inferred from calculated pressure and temperature in the discharge to be about 14 km/sec. Efficiency, based on this velocity and measured T/P is .54 + or - .07. Thruster ablation is zero at the throat and becomes measurable further upstream, indicating that radiative ablation is occurring late in the pulse. Author

N87-17787*# National Aeronautics and Space Administration. Lewis Research Center, Cleveland, Ohio.

PEGASUS: A MULTI-MEGAWATT NUCLEAR ELECTRIC PROPULSION SYSTEM

EDMUND P. COOMES (Battelle Northwest Labs., Richland, Wash.), JUDITH M. CUTA, BRENT J. WEBB, DAVID Q. KING (Jet Propulsion Lab., California Inst. of Tech., Pasadena), MIKE J. PATTERSON, and FRANK BERKOPEC in NASA. Marshall Space Flight Center Manned Mars Mission. Working Group Papers, V. 2, Sect. 5, App. p 769-786 May 1986

Avail: NTIS HC A24/MF A01 CSCL 21F

A propulsion system (PEGASUS) consisting of an electric thruster driven by a multimegawatt nuclear power system is proposed for a manned Mars mission. Magnetoplasmadynamic and mercury-ion thrusters are considered, based on a mission profile containing a 510-day burn time (for a mission time of approximately 1000 days). Both thrusters are capable of meeting the mission parameters. Electric propulsion systems have significant advantages over chemical systems, because of high specific impulse, lower propellant requirements, and lower system mass. The power for the PEGASUS system is supplied by a boiling

20 SPACECRAFT PROPULSION AND POWER

liquid-metal fast reactor. The power system consists of the reactor, reactor shielding, power conditioning subsystems, and heat rejection subsystems. It is capable of providing a maximum of 8.5 megawatts of electrical power of which 6 megawatts is needed for the thruster system, leaving 1.5 megawatts available for inflight mission applications. Author

N87-17789*# National Aeronautics and Space Administration. Lewis Research Center, Cleveland, Ohio.

POWER SYSTEM TECHNOLOGIES FOR THE MANNED MARS MISSION

DAVE BENTS, MICHAEL J. PATTERSON, F. BERKOPEC, IRA MYERS, and A. PRESLER /in NASA. Marshall Space Flight Center Manned Mars Mission. Working Group Papers, V. 2, Sect. 5, App. p 797-814 May 1986
Avail: NTIS HC A24/MF A01 CSCL 21H

The high impulse of electric propulsion makes it an attractive option for manned interplanetary missions such as a manned mission to Mars. This option is, however, dependent on the availability of high energy sources for propulsive power in addition to that required for the manned interplanetary transit vehicle. Two power system technologies are presented: nuclear and solar. The ion thruster technology for the interplanetary transit vehicle is described for a typical mission. The power management and distribution system components required for such a mission must be further developed beyond today's technology status. High voltage-high current technology advancements must be achieved. These advancements are described. In addition, large amounts of waste heat must be rejected to the space environment by the thermal management system. Advanced concepts such as the liquid droplet radiator are discussed as possible candidates for the manned Mars mission. These thermal management technologies have great potential for significant weight reductions over the more conventional systems. Author

N87-17848*# Rockwell International Corp., Canoga Park, Calif. Rocketdyne Div.

SPACE STATION RESISTOJET SYSTEM REQUIREMENTS AND INTERFACE DEFINITION STUDY Interim Report

BRUCE J. HECKERT Feb. 1987 88 p
(Contract NAS3-24658)
(NASA-CR-179581; NAS 1.26:179581; RI/RD87-109) Avail:
NTIS HC A05/MF A01 CSCL 21H

Preliminary resistojets design requirements were established based on initial technical requirements imposed by the results of NASA and Rocketdyne studies. The requirements are directed toward long life, simplicity, flexibility, and commonality with other space station components. The resistojets assembly is comprised of eight resistojets, fluid components downstream of the waste fluid storage system, a power controller, structure, and shielding. It consists of two identical subassemblies, one of which is redundant. Each subassembly consists of four 500-W resistojets, series redundant latch valves, a power controller, a water vaporizer, two pressure regulators, filters, check valves, disconnects, fluid tubing, and electrical cables. All components are packaged at the end of the stinger aft of the JEM and Columbus modules. Different flow and power control methods were studied. A constant inlet pressure and a two-power setting controller were tentatively selected based on simplicity and reasonably high specific impulse for the range of waste gas compositions that are anticipated. The constant pressure is supplied by pressure regulators. The two set point power control includes individual power supplies to each resistojets heater and water vaporizer. An embedded data processor, a multiplexer-demultiplexer, and a network interface unit that are standard space station components are included in the power controller. The total dry weight of the resistojets assembly is approximately 172 lb. The total cost for design, development, test, evaluation, qualification, and flight hardware is estimated to be \$16 million. Author

N87-20378*# National Aeronautics and Space Administration. Lewis Research Center, Cleveland, Ohio.

CONCEPTUAL DESIGN AND INTEGRATION OF A SPACE STATION RESISTOJET PROPULSION ASSEMBLY

ROBERT R. TACINA 1987 19 p Prepared for presentation at the 23rd Joint Propulsion Conference, San Diego, Calif., 29 Jun. - 21 Jul. 1987; sponsored in part by AIAA, SAE, ASME and ASEE (NASA-TM-89847; E-3483; NAS 1.15:89847) Avail: NTIS HC A02/MF A01 CSCL 21H

The resistojets propulsion module is designed as a simple, long life, low risk system offering operational flexibility to the space station program. It can dispose of a wide variety of typical space station waste fluids by using them as propellants for orbital maintenance. A high temperature mode offers relatively high specific impulse with long life while a low temperature mode can propulsively dispose of mixtures that contain oxygen or hydrocarbons without reducing thruster life or generating particulates in the plume. A low duty cycle and a plume that is confined to a small aft region minimizes the impacts on the users. Simple interfaces with other space station systems facilitate integration. It is concluded that there are no major obstacles and many advantages to developing, installing, and operating a resistojets propulsion module aboard the Initial Operational Capability (IOC) space station. Author

N87-20379*# National Aeronautics and Space Administration. Lewis Research Center, Cleveland, Ohio.

COMPARISON OF TWO PROCEDURES FOR PREDICTING ROCKET ENGINE NOZZLE PERFORMANCE

KENNETH J. DAVIDIAN 1987 16 p Proposed for presentation at the 23rd Joint Propulsion Conference, San Diego, Calif., 29 Jun. - 2 Jul. 1987; sponsored by AIAA, SAE, ASME and ASEE (NASA-TM-89814; E-3458; NAS 1.15:89814) Avail: NTIS HC A02/MF A01 CSCL 21H

Two nozzle performance prediction procedures which are based on the standardized JANNAF methodology are presented and compared for four rocket engine nozzles. The first procedure required operator intercedence to transfer data between the individual performance programs. The second procedure is more automated in that all necessary programs are collected into a single computer code, thereby eliminating the need for data reformatting. Results from both procedures show similar trends but quantitative differences. Agreement was best in the predictions of specific impulse and local skin friction coefficient. Other compared quantities include characteristic velocity, thrust coefficient, thrust decrement, boundary layer displacement thickness, momentum thickness, and heat loss rate to the wall. Effects of wall temperature profile used as an input to the programs was investigated by running three wall temperature profiles. It was found that this change greatly affected the boundary layer displacement thickness and heat loss to the wall. The other quantities, however, were not drastically affected by the wall temperature profile change. Author

N87-20381*# National Aeronautics and Space Administration. Lewis Research Center, Cleveland, Ohio.

EXPERIMENTAL THRUST PERFORMANCE OF A HIGH-AREA-RATIO ROCKET NOZZLE

ALBERT J. PAVLI, KENNETH J. KACYNSKI, and TAMARA A. SMITH Apr. 1987 16 p Presented at the 23rd JANNAF Combustion Meeting, Hampton, Va., 20-24 Oct. 1986 (NASA-TP-2720; E-3236-1; NAS 1.60:2720) Avail: NTIS HC A02/MF A01 CSCL 21H

An experimental investigation was conducted to determine the thrust performance attainable from high-area-ratio rocket nozzles. A modified Rao-contoured nozzle with an expansion area of 1030 was test fired with hydrogen-oxygen propellants at altitude conditions. The nozzle was also tested as a truncated nozzle, at an expansion area ratio of 428. Thrust coefficient and thrust coefficient efficiency values are presented for each configuration at various propellant mixture ratios (oxygen/fuel). Several procedural techniques were developed permitting improved measurement of nozzle performance. The more significant of these

were correcting the thrust for the aneroid effects, determining the effective chamber pressure, and referencing differential pressure transducers to a vacuum reference tank. Author

N87-20382*# National Aeronautics and Space Administration. Lewis Research Center, Cleveland, Ohio.
ARCJET COMPONENT CONDITIONS THROUGH A MULTISTART TEST

FRANK M. CURRAN and THOMAS W. HAAG 1987 20 p
Presented at the 19th International Electric Propulsion Conference, Colorado Springs, Colo., 11-13 May 1987; sponsored by AIAA, DGLR and JSASS

(NASA-TM-89857; E-3525; NAS 1.15:89857; AIAA-87-1060)

Avail: NTIS HC A02/MF A01 CSCL 21H

A low power, dc arcjet thruster was tested for starting reliability using hydrogen-nitrogen mixtures simulating the decomposition products of hydrazine. More than 300 starts were accumulated in phases with extended burn-in periods interlaced. A high degree of flow stabilization was built into the arcjet and the power supply incorporated both rapid current regulation and a high voltage, pulsed starting circuit. A nominal current level of 10 A was maintained throughout the test. Photomicrographs of the cathode tip showed a rapid recession to a steady-state operating geometry. A target of 300 starts was selected, as this represents significantly more than anticipated (150 to 240), in missions of 10 yr or less duration. Weighings showed no apparent mass loss. Some anode erosion was observed, particularly at the entrance to the constrictor. This was attributed to the brief period during startup the arc mode attachment point spends in the high pressure region upstream of the nozzle. Based on the results obtained, startup does not appear to be performance or life limiting for the number of starts typical of operational satellite applications. Author

N87-20383*# National Aeronautics and Space Administration. Lewis Research Center, Cleveland, Ohio.
EXPERIMENTAL STUDY OF LOW REYNOLDS NUMBER NOZZLES

STANLEY P. GRISNIK, TAMARA A. SMITH, and LARRY E. SALTZ (Rocket Research Corp., Redmond, Wash.) 1987 13 p
Presented at the 19th International Electric Propulsion Conference, Colorado Springs, Colo., 11-13 May 1987; sponsored by AIAA, DGLR and JSASS

(NASA-TM-89858; E-3526; NAS 1.15:89858; AIAA-87-0992)

Avail: NTIS HC A02/MF A01 CSCL 21H

High-performance electrothermal thrusters operate in a low nozzle-throat Reynolds number regime. Under these conditions, the flow boundary layer occupies a large volume inside the nozzle, contributing to large viscous losses. Four nozzles (conical, bell, trumpet, and modified trumpet) and a sharp-edged orifice were evaluated over a Reynolds number range of 500 to 9000 with unheated nitrogen and hydrogen. The nozzles showed significant decreases in specific impulse efficiency with decreasing Reynolds number. At Reynolds numbers less than 1000, all four nozzles were probably filled with a large boundary layer. The discharge coefficient decreased with Reynolds number in the same manner as the specific impulse efficiency. The bell and modified trumpet nozzles had discharge coefficients 4 to 8 percent higher than those of the cone or trumpet nozzles. The Two-Dimensional Kinetics (TDK) nozzle analysis computer program was used to predict nozzle performance. The results were then compared to the experimental results in order to determine the accuracy of the program within this flow regime. Author

N87-21037*# National Aeronautics and Space Administration. Lewis Research Center, Cleveland, Ohio.

THE NASA ELECTRIC PROPULSION PROGRAM

DAVID C. BYERS and ROBERT A. WASEL (National Aeronautics and Space Administration, Washington, D.C.) 1987 22 p
Presented at the 19th International Electric Propulsion Conference, Colorado Springs, Colo., 11-13 May 1987; sponsored by AIAA, DGLR and JSASS

(NASA-TM-89856; E-3524; NAS 1.15:89856; AIAA-87-1098)

Avail: NTIS HC A02/MF A01 CSCL 21H

The NASA OAST Propulsion, Power and Energy Division supports electric propulsion for a broad class of missions. Concepts with potential to significantly benefit or enable space exploration and exploitation are identified and advanced toward applications in the near to far term. Recent program progress in mission/system analyses and in electrothermal, ion, and electromagnetism technologies are summarized. Author

N87-21998*# National Aeronautics and Space Administration. Lewis Research Center, Cleveland, Ohio.

ARCJET STARTING RELIABILITY: A MULTISTART TEST ON HYDROGEN/NITROGEN MIXTURES

THOMAS W. HAAG and FRANK M. CURRAN 1987 17 p
Presented at the 19th International Electric Propulsion conference, Colorado Springs, Colo., 11-13 May 1987; sponsored by AIAA, DGLR and JSASS

(NASA-TM-89867; E-3538; NAS 1.15:89867; AIAA-87-1061)

Avail: NTIS HC A02/MF A01 CSCL 21H

An arcjet starting reliability test was performed to investigate one feasibility issue in the use of arcjets onboard a satellite for north-south stationkeeping. A 1 kW arcjet was run on hydrogen/nitrogen gas mixtures simulating decomposed hydrazine. A pulse width modulated power supply with an integral high voltage starting pulser was used for arc ignition and steady-state operation. The test was performed in four phases in order to determine if starting characteristics changed as a result of long term thruster operation. More than 300 successful starts were accumulated over an operating time of 18 hrs. Overall results indicate that there is a link between starting characteristics and long term thruster operation; however, the large number of starts had no effect on steady-state performance. Author

N87-21999*# National Aeronautics and Space Administration. Lewis Research Center, Cleveland, Ohio.

EFFECT OF AN OXYGEN PLASMA ON UNCOATED THIN ALUMINUM REFLECTING FILMS

ROGER L. PARSONS and DANIEL A. GULINO (Cleveland State Univ., Ohio.) May 1987 17 p

(NASA-TM-89882; E-3564; NAS 1.15:89882) Avail: NTIS HC A02/MF A01 CSCL 10B

Thin aluminum films were considered for use as a reflective surface for solar collectors on orbiting solar dynamic power systems. A matter of concern is the durability of such reflective coatings against oxidative attack by highly reactive neutral atomic oxygen, which is the predominate chemical specie in low Earth orbit. Research to date was aimed at evaluating the protective merit of thin dielectric coatings over the aluminum or other reflective metals. However, an uncoated aluminum reflector may self-protect by virtue of the oxide formed from its exposed surface, which constitutes a physical barrier to further oxidation. This possibility was investigated, and an attempt was made to characterize the effects of atomic oxygen on thin Al films using photomicrographs, scanning electron microscopy, spectrophotometry, Auger analysis, and mass measurements. Data collected in a parallel effort is discussed for its comparative value. The results of the investigation of uncoated aluminum supported the self-protection hypothesis, and importantly, it was found that long term specular reflectance for uncoated aluminum exceeded that of Al and Ag reflectors with dielectric coatings. Author

N87-22001*# National Aeronautics and Space Administration. Lewis Research Center, Cleveland, Ohio.

SPACE STATION ELECTRIC POWER SYSTEM REQUIREMENTS AND DESIGN

FRED TERN 1987 15 p Proposed for presentation at the 22nd Intersociety Energy Conversion Engineering Conference, Philadelphia, Pa., 10-14 Aug. 1987; sponsored by AIAA, ANS, ASME, SAE, IEEE, ACS and AIChE (NASA-TM-89889; E-3577; NAS 1.15:89889; AIAA-87-9003) Avail: NTIS HC A02/MF A01 CSCL 22B

An overview of the conceptual definition and design of the space station Electric Power System (EPS) is given. Responsibilities for the design and development of the EPS are defined. The EPS requirements are listed and discussed, including average and peak power requirements, contingency requirements, and fault tolerance. The most significant Phase B trade study results are summarized, and the design selections and rationale are given. Finally, the power management and distribution system architecture is presented. Author

N87-22003*# National Aeronautics and Space Administration. Lewis Research Center, Cleveland, Ohio.

COAXIAL TUBE ARRAY SPACE TRANSMISSION LINE CHARACTERIZATION

COLLEEN A. SWITZER and DAVID J. BENTS 1987 12 p Proposed for presentation at the 22nd Intersociety Energy Conversion Engineering Conference, Philadelphia, Pa., 10-14 Aug. 1987; sponsored by AIAA, ANS, ASME, SAE, IEEE, ACS and AIChE (NASA-TM-89864; E-3531; NAS 1.15:89864) Avail: NTIS HC A02/MF A01 CSCL 09C

The coaxial tube array tether/transmission line used to connect an SP-100 nuclear power system to the space station was characterized over the range of reactor-to-platform separation distances of 1 to 10 km. Characterization was done with respect to array performance, physical dimensions and masses. Using a fixed design procedure, a family of designs was generated for the same power level (300 kWe), power loss (1.5 percent), and meteoroid survival probability (99.5 percent over 10 yr). To differentiate between vacuum insulated and gas insulated lines, two different maximum values of the E field were considered: 20 kV/cm (appropriate to vacuum insulation) and 50 kV/cm (compressed SF6). Core conductor, tube, bumper, standoff, spacer and bumper support dimensions, and masses were also calculated. The results of the characterization show mainly how transmission line size and mass scale with reactor-to-platform separation distance. Author

N87-22004*# National Aeronautics and Space Administration. Lewis Research Center, Cleveland, Ohio.

EMC AND POWER QUALITY STANDARDS FOR 20-KHZ POWER DISTRIBUTION

IRVING G. HANSEN 1987 8 p Proposed for presentation at the 22nd Intersociety Energy Conversion Engineering Conference, Philadelphia, Pa., 10-14 Aug. 1987; sponsored by AIAA, ANS, ASME, SAE, IEEE, ACS and AIChE (NASA-TM-89925; E-3626; NAS 1.15:89925; AIAA-87-9355) Avail: NTIS HC A02/MF A01 CSCL 09C

The Space Station Power Distribution System has been baselined as a sinusoidal single phase, 440 VRMS system. This system has certain unique characteristics directly affecting its application. In particular, existing systematic description and control documents were modified to reflect the high operating frequency. This paper will discuss amendments made on Mil STD 704 (Electrical Power Characteristics), and Mil STD 461-B (Electromagnetic Emission and Susceptibility Requirements for the Control of Electromagnetic Interference). In some cases these amendments reflect changes of several orders of magnitude. Implications and impacts of these changes are discussed. Author

N87-22766*# National Aeronautics and Space Administration. Lewis Research Center, Cleveland, Ohio.

STRUCTURAL INTEGRITY AND DURABILITY OF REUSABLE SPACE PROPULSION SYSTEMS

1987 205 p Conference held in Cleveland, Ohio, 12-13 May 1987 (NASA-CP-2471; E-3512; NAS 1.55:2471) Avail: NTIS HC A10/MF A01 CSCL 21H

A two-day conference on the structural integrity and durability of reusable space propulsion systems was held on May 12 and 13, 1987, at the NASA Lewis research Center. Aerothermodynamic loads; instrumentation; fatigue, fracture, and constitutive modeling; and structural dynamics were discussed.

N87-22783*# National Aeronautics and Space Administration. Lewis Research Center, Cleveland, Ohio.

PROBABILISTIC STRUCTURAL ANALYSIS TO EVALUATE THE STRUCTURAL DURABILITY OF SSME CRITICAL COMPONENTS

CHRISTOS C. CHAMIS *In its* Structural Integrity and Durability of Reusable Space Propulsion Systems p 117-119 1987 Avail: NTIS HC A10/MF A01 CSCL 21H

NASA Lewis Research Center is currently developing probabilistic structural analysis methods for select Space Shuttle Main Engine (SSME) structural components. Briefly, the deterministic, three-dimensional, inelastic analysis methodology developed under the Hot Section Technology (HOST) and R and T Base Programs is being augmented to accommodate the complex probabilistic loading spectra, the thermoviscoplastic material behavior, and the material degradation associated with the environment of space propulsion system structural components representative of the SSME such as turbine blades, transfer ducts, and liquid-oxygen posts. The development of probabilistic structural analysis methodology consists of the following program elements: (1) composite load spectra; (2) probabilistic structural analysis methods; (3) probabilistic finite element theory - new variational principles; and (4) probabilistic structural analysis application. In addition, the program includes deterministic analysis elements: (1) development of structural tailoring computer codes (SSME/STAEBL); (2) development of dynamic creep buckling/ratcheting theory; (3) evaluation of the dynamic characteristics of single-crystal SSME blades; (4) development of SSME blade damper technology; and (5) development of integrated boundary elements for hotfluid structure interaction. Author

N87-22784*# Southwest Research Inst., San Antonio, Tex.

PROBABILISTIC STRUCTURAL ANALYSIS METHODS (PSAM) FOR SELECT SPACE PROPULSION SYSTEM STRUCTURAL COMPONENTS

T. A. CRUSE *In* NASA. Lewis Research Center Structural Integrity and Durability of Reusable Space Propulsion Systems p 121-125 1987

(Contract NAS3-24389) Avail: NTIS HC A10/MF A01 CSCL 21H

The objective is the development of several modular structural analysis packages capable of predicting the probabilistic response distribution for key structural variables such as maximum stress, natural frequencies, transient response, etc. The structural analysis packages are to include stochastic modeling of loads, material properties, geometry (tolerances), and boundary conditions. The solution is to be in terms of the cumulative probability of exceedance distribution (CDF) and confidence bounds. Two methods of probability modeling are to be included as well as three types of structural models - probabilistic finite-element method (PFEM); probabilistic approximate analysis methods (PAAM); and probabilistic boundary element methods (PBEM). The purpose in doing probabilistic structural analysis is to provide the designer with a more realistic ability to assess the importance of uncertainty in the response of a high performance structure. Probabilistic Structural Analysis Method (PSAM) tools will estimate structural safety and reliability, while providing the engineer with information on the confidence that should be given to the predicted behavior. Perhaps most critically, the PSAM results will directly provide

information on the sensitivity of the design response to those variables which are seen to be uncertain. Author

N87-22793*# Rockwell International Corp., Canoga Park, Calif. Rocketdyne Div.

COMPOSITE LOAD SPECTRA FOR SELECT SPACE PROPULSION STRUCTURAL COMPONENTS

J. F. NEWELL / *In* NASA. Lewis Research Center Structural Integrity and Durability of Reusable Space Propulsion Systems p 175-187 1987

(Contract NAS3-24382)

Avail: NTIS HC A10/MF A01 CSCL 21H

The objective of this program is to develop generic load models to simulate the composite load spectra (CLS) that are induced in space propulsion system components representative of the space shuttle main engines (SSME). These models are being developed through describing individual component loads with an appropriate mix of deterministic and state-of-the-art probabilistic models that are related to key generic variables. Combinations of the individual loads are used to synthesize the composite loads spectra. A second approach for developing the composite loads spectra load model simulation, the option portion of the contract will develop coupled models which combine the individual load models. Statistically varying coefficients of the physical models will be used to obtain the composite load spectra. Author

N87-22795*# National Aeronautics and Space Administration. Lewis Research Center, Cleveland, Ohio.

STRUCTURAL TAILORING USING THE SSME/STAEBL CODE

ROBERT RUBINSTEIN / *In* its Structural Integrity and Durability of Reusable Space Propulsion Systems p 201-205 1987

Avail: NTIS HC A10/MF A01 CSCL 21H

Space Shuttle Main Engine/Structural Tailoring of Engine Blades (SSME/STAEBL) was developed by systematically modifying and enhancing the STAEBL code developed by Pratt and Whitney under contract to NASA Lewis Research Center. STAEBL was designed for application to gas turbine blade design. Typical design variables include blade thickness distribution and root chord. Typical constraints include resonance margins, root stress, and root to chord ratios. In this program, the blade is loaded by centrifugal forces only. Additions and modifications of STAEBL included in SSME/STAEBL include (1) thermal stress analysis; (2) gas dynamic (pressure) loads; (3) temperature dependent material and thermal properties; (4) forced vibrations; (5) tip displacement constraints; (6) single crystal material analysis; (7) blade cross section stacking offsets; and (8) direct time integration algorithm for transient dynamic response. Capabilities are also included which permit data transfer from finite element models and stand-alone analysis.

N87-22798*# National Aeronautics and Space Administration. Lewis Research Center, Cleveland, Ohio.

SSME BLADE DAMPER TECHNOLOGY

ROBERT E. KIELB and JERRY H. GRIFFIN (Carnegie-Mellon Univ., Pittsburgh, Pa.) / *In* its Structural Integrity and Durability of Reusable Space Propulsion Systems p 215-217 1987

Avail: NTIS HC A10/MF A01 CSCL 21H

Before 1975 turbine blade damper designs were based on experience and very simple mathematical models. Failure of the dampers to perform as expected showed the need to gain a better understanding of the physical mechanism of friction dampers. Over the last 10 years research on friction dampers for aeronautical propulsion systems has resulted in methods to optimize damper designs. The first-stage turbine blades on the Space Shuttle Main Engine (SSME) high-pressure oxygen pump have experienced cracking problems due to excessive vibration. A solution is to incorporate a well-designed friction dampers to attenuate blade vibration. The subject study, a cooperative effort between NASA Lewis and Carnegie-Mellon University, represents an application of recently developed friction damper technology to the SSME high-pressure oxygen turbopump. The major emphasis was the contractor's design known as the two-piece damper. Damping occurs at the frictional interface between the top half of the damper

and the underside of the platforms of the adjacent blades. The lower half of the damper is an air seal to retard airflow in the volume between blade necks.

N87-22802*# National Aeronautics and Space Administration. Lewis Research Center, Cleveland, Ohio.

IMPACT OF THERMAL ENERGY STORAGE PROPERTIES ON SOLAR DYNAMIC SPACE POWER CONVERSION SYSTEM MASS

ALBERT J. JUHASZ, CAROLYN E. COLES-HAMILTON, and DOVIE E. LACY 1987 10 p Prepared for presentation at the 22nd Intersociety Energy Conversion Engineering Conference, Philadelphia, Pa., 10-14 Aug. 1987; cosponsored by AIAA, ANS, AMSE, SAE, IEEE, ACS, and AIChE

(NASA-TM-89909; E-3601; NAS 1.15:89909; AIAA-87-9442)

Avail: NTIS HC A02/MF A01 CSCL 10C

A 16 parameter solar concentrator/heat receiver mass model is used in conjunction with Stirling and Brayton Power Conversion System (PCS) performance and mass computer codes to determine the effect of thermal energy storage (TES) material property changes on overall PCS mass as a function of steady state electrical power output. Included in the PCS mass model are component masses as a function of thermal power for: concentrator, heat receiver, heat exchangers (source unless integral with heat receiver, heat sink, regenerator), heat engine units with optional parallel redundancy, power conditioning and control (PC and C), PC and C radiator, main radiator, and structure. Critical TES properties are: melting temperature, heat of fusion, density of the liquid phase, and the ratio of solid-to-liquid density. Preliminary results indicate that even though overall system efficiency increases with TES melting temperature up to 1400 K for concentrator surface accuracies of 1 mrad or better, reductions in the overall system mass beyond that achievable with lithium fluoride (LiF) can be accomplished only if the heat of fusion is at least 800 kJ/kg and the liquid density is comparable to that of LiF (1880 kg/cu m. Author

N87-22803*# Pratt and Whitney Aircraft, West Palm Beach, Fla. Government Products Div.

HIGH HEAT TRANSFER OXIDIZER HEAT EXCHANGER DESIGN AND ANALYSIS Final Report, Jan. 1985 - Oct. 1986

THOMAS D. KMIEC, PAUL G. KANIC, and RICHARD J. PECKHAM May 1987 80 p

(Contract NAS3-24738)

(NASA-CR-179596; NAS 1.26:179596; FR-19289-2) Avail: NTIS HC A05/MF A01 CSCL 21H

The RL10-2B engine, a derivative of the RL10, is capable of multimode thrust operation. This engine operates at two low thrust levels: tank head idle (THI), which is approximately 1 to 2% of full thrust, and pumped idle (PI), which is 10% of full thrust. Operation at THI provides vehicle propellant settling thrust and efficient engine thermal conditioning; PI operation provides vehicle tank pre-pressurization and maneuver thrust for low-g deployment. Stable combustion of the RL10-2B engine during the low thrust operating modes can be accomplished by using a heat exchanger to supply gaseous oxygen to the propellant injector. The oxidizer heat exchanger (OHE) vaporizes the liquid oxygen using hydrogen as the energy source. The design, concept verification testing and analysis for such a heat exchanger is discussed. The design presented uses a high efficiency compact core to vaporize the oxygen, and in the self-contained unit, attenuates any pressure and flow oscillations which result from unstable boiling in the core. This approach is referred to as the high heat transfer design. An alternative approach which prevents unstable boiling of the oxygen by limiting the heat transfer is referred to as the low heat transfer design and is reported in Pratt & Whitney report FR-19135-2.

Author

20 SPACECRAFT PROPULSION AND POWER

N87-22804*# National Aeronautics and Space Administration. Lewis Research Center, Cleveland, Ohio.

LOW POWER DC ARCJET OPERATION WITH HYDROGEN/NITROGEN/AMMONIA MIXTURES

TERRY L. HARDY and FRANCIS M. CURRAN Jul. 1987 25 p Prepared for presentation at the 23rd Joint Propulsion Conference, San Diego, Calif., 29 Jun. - 2 Jul. 1987; cosponsored by AIAA, SAE, ASME, and ASEE

(NASA-TM-89876; E-3553; NAS 1.15:89876; AIAA-87-1948)

Avail: NTIS HC A02/MF A01 CSCL 21C

The effect of gas composition and ambient pressure on arcjet operation was determined. Arcjet operation in different facilities was also compared to determine the validity of tests in small facilities. Volt-ampere characteristics were determined for an arcjet using hydrogen/nitrogen mixtures (simulating both ammonia and hydrazine), hydrogen/nitrogen/ammonia mixtures, and pure ammonia as propellants at various flow rates. The arcjet had a typical performance of 450 sec specific impulse at 1 kW with hydrogen/nitrogen mixtures. It was determined that the amount of ammonia present in the gas stream had a significant effect on the arcjet volt-ampere characteristics. Also, hydrogen/nitrogen mixtures simulating ammonia gave arc characteristics approximately the same as those of pure ammonia. Finally, no differences in arc volt-ampere characteristics were seen between low and high ambient pressure operation in the same facility. A 3 to 5 V difference was seen when different facilities were compared, but this difference was probably due to differences in the voltage drops across the current connections, and not due to arcjet operational differences in the two facilities. Author

N87-22805*# National Aeronautics and Space Administration. Lewis Research Center, Cleveland, Ohio.

ELECTROMAGNETIC EMISSION EXPERIENCES USING ELECTRIC PROPULSION SYSTEMS: A SURVEY

JAMES S. SOVEY, LYNNETTE M. ZANA, and STEVEN C. KNOWLES (Rocket Research Corp., Redmond, Wash.) 1987 37 p Presented at the 23rd Joint Propulsion Conference, San Diego, Calif., 29 Jun. - 2 Jul. 1987; sponsored by AIAA, SAE, ASME and ASEE

(NASA-TM-100120; E-3618; NAS 1.15:100120; AIAA-87-2028)

Avail: NTIS HC A03/MF A01 CSCL 21C

As electric propulsion systems become ready to integrate with spacecraft systems, the impact of propulsion system radiated emissions are of significant interest. Radiated emissions from electromagnetic, electrostatic, and electrothermal systems have been characterized and results synopsized from the literature describing 21 space flight programs. Electromagnetic radiated emission results from ground tests and flight experiences are presented with particular attention paid to the performance of spacecraft subsystems and payloads during thruster operations. The impacts to transmission of radio frequency signals through plasma plumes are also reviewed. Author

N87-22806*# National Aeronautics and Space Administration. Lewis Research Center, Cleveland, Ohio.

AN EVALUATION OF METALLIZED PROPELLANTS BASED ON VEHICLE PERFORMANCE

ROBERT L. ZURAWSKI and JAMES M. GREEN (Sverdrup Technology, Inc., Cleveland, Ohio.) 1987 27 p Presented at the 23rd Joint Propulsion Conference, San Diego, Calif., 29 Jun. - 2 Jul. 1987; sponsored by AIAA, SAE, ASME and ASEE

(NASA-TM-100104; E-3639; NAS 1.15:100104; AIAA-87-1773)

Avail: NTIS HC A03/MF A01 CSCL 21H

An analytical study was conducted to determine the improvements in vehicle performance possible by burning metals with conventional liquid bipropellants. These metallized propellants theoretically offer higher specific impulse, increased propellant density and improved vehicle performance compared with conventional liquid bipropellants. Metals considered were beryllium, lithium, aluminum and iron. Liquid bipropellants were H₂/O₂, N₂H₄/N₂O₄, RP-1/O₂ and H₂/F₂. A mission with a delta V = 4267.2 m/sec (14,000 ft/sec) and vehicle with propellant volume fixed at 56.63 cu m (2000 cu ft) and dry mass fixed at 2761.6 kg

(6000 lb) was used, roughly representing the transfer of a chemically propelled upper-stage vehicle from a low-Earth orbit to a geosynchronous orbit. The results of thermochemical calculations and mission analysis calculations for bipropellants metallized with beryllium, lithium, aluminum and iron are presented. Technology issues pertinent to metallized propellants are discussed. Author

N87-22807*# National Aeronautics and Space Administration. Lewis Research Center, Cleveland, Ohio.

LANGMUIR PROBE SURVEYS OF AN ARCJET EXHAUST

LYNNETTE M. ZANA 1987 30 p Presented at the 23rd Joint Propulsion Conference, San Diego, Calif., 29 Jun. - 2 Jul. 1987; sponsored by AIAA, SAE, ASME and ASEE

(NASA-TM-89924; E-3623; NAS 1.15:89924; AIAA-87-1950)

Avail: NTIS HC A03/MF A01 CSCL 21C

Electrostatic (Langmuir) probes of both spherical and cylindrical geometry have been used to obtain electron number density and temperature in the exhaust of a laboratory arcjet. The arcjet thruster operated on nitrogen and hydrogen mixtures to simulate fully decomposed hydrazine in a vacuum environment with background pressures less than 0.05 Pa. The exhaust appears to be only slightly ionized (less than 1 percent) with local plasma potentials near facility ground. The current-voltage characteristics of the probes indicate a Maxwellian temperature distribution. Plume data are presented as a function of arcjet operating conditions and also position in the exhaust. Author

N87-23690*# National Aeronautics and Space Administration. Lewis Research Center, Cleveland, Ohio.

CONTROL CONSIDERATIONS FOR HIGH FREQUENCY, RESONANT, POWER PROCESSING EQUIPMENT USED IN LARGE SYSTEMS

J. W. MILDICE, K. E. SCHREINER, and F. WOLFF 1987 8 p Prepared for presentation at the 22nd Intersociety Energy Conversion Engineering Conference, Philadelphia, Pa., 10-14 Aug. 1987; cosponsored by AIAA, ANS, ASME, SAE, IEEE, ACS, and AICHE

(NASA-TM-89926; E-3629; NAS 1.15:89926; AIAA-87-9353)

Avail: NTIS HC A02/MF A01 CSCL 10B

Addressed is a class of resonant power processing equipment designed to be used in an integrated high frequency (20 KHz domain), utility power system for large, multi-user spacecraft and other aerospace vehicles. It describes a hardware approach, which has been the basis for parametric and physical data used to justify the selection of high frequency ac as the PMAD baseline for the space station. This paper is part of a larger effort undertaken by NASA and General Dynamics to be sure that all potential space station contractors and other aerospace power system designers understand and can comfortably use this technology, which is now widely used in the commercial sector. In this paper, we will examine control requirements, stability, and operational modes; and their hardware impacts from an integrated system point of view. The current space station PMAD system will provide the overall requirements model to develop an understanding of the performance of this type of system with regard to: (1) regulation; (2) power bus stability and voltage control; (3) source impedance; (4) transient response; (5) power factor effects, and (6) limits and overloads. Author

N87-23691*# National Aeronautics and Space Administration. Lewis Research Center, Cleveland, Ohio.

LOW POWER ARCJET THRUSTER PULSE IGNITION

CHARLES J. SARMIENTO and ROBERT P. GRUBER 1987 29 p Presented at the 23rd Joint Propulsion Conference, San Diego, Calif., 29 Jun. - 2 Jul. 1987; sponsored by AIAA, SAE, ASME and ASEE

(NASA-TM-100123; E-3645; NAS 1.15:100123) Avail: NTIS HC A03/MF A01 CSCL 21C

An investigation of the pulse ignition characteristics of a 1 kW class arcjet using an inductive energy storage pulse generator with a pulse width modulated power converter identified several thruster and pulse generator parameters that influence breakdown voltage including pulse generator rate of voltage rise. This work

was conducted with an arcjet tested on hydrogen-nitrogen gas mixtures to simulate fully decomposed hydrazine. Over all ranges of thruster and pulser parameters investigated, the mean breakdown voltages varied from 1.4 to 2.7 kV. Ignition tests at elevated thruster temperatures under certain conditions revealed occasional breakdowns to thruster voltages higher than the power converter output voltage. These post breakdown discharges sometimes failed to transition to the lower voltage arc discharge mode and the thruster would not ignite. Under the same conditions, a transition to the arc mode would occur for a subsequent pulse and the thruster would ignite. An automated 11 600 cycle starting and transition to steady state test demonstrated ignition on the first pulse and required application of a second pulse only two times to initiate breakdown. Author

N87-23692*# National Aeronautics and Space Administration. Lewis Research Center, Cleveland, Ohio.
NUCLEAR POWERED MARS CARGO TRANSPORT MISSION UTILIZING ADVANCED ION PROPULSION
 DIANE L. GALECKI (Sverdrup Technology, Inc., Cleveland, Ohio.) and MICHAEL J. PATTERSON 1987 29 p Presented at the 23rd Joint Propulsion Conference, San Diego, Calif., 29 Jun. - 2 Jul. 1987; sponsored by AIAA, SAE, ASME and ASEE (NASA-TM-100109; E-3641; NAS 1.15:100109; AIAA-87-1903) Avail: NTIS HC A03/MF A01 CSCL 21F

Nuclear-powered ion propulsion technology was combined with detailed trajectory analysis to determine propulsion system and trajectory options for an unmanned cargo mission to Mars in support of manned Mars missions. A total of 96 mission scenarios were identified by combining two power levels, two propellants, four values of specific impulse per propellant, three starting altitudes, and two starting velocities. Sixty of these scenarios were selected for a detailed trajectory analysis; a complete propulsion system study was then conducted for 20 of these trajectories. Trip times ranged from 344 days for a xenon propulsion system operating at 300 kW total power and starting from lunar orbit with escape velocity, to 770 days for an argon propulsion system operating at 300 kW total power and starting from nuclear start orbit with circular velocity. Trip times for the 3 MW cases studied ranged from 356 to 413 days. Payload masses ranged from 5700 to 12,300 kg for the 300 kW power level, and from 72,200 to 81,500 kg for the 3 MW power level. Author

N87-23693*# National Aeronautics and Space Administration. Lewis Research Center, Cleveland, Ohio.
IN-SITU ANALYSIS OF HYDRAZINE DECOMPOSITION PRODUCTS
 FRANCIS M. CURRAN and MARGARET V. WHALEN Jul. 1987 16 p Presented at the 23rd Joint Propulsion Conference, San Diego, Calif., 29 Jun. - 2 Jul. 1987; cosponsored by AIAA, SAE, ASME, and ASEE (NASA-TM-89916; E-3609; NAS 1.15:89916; AIAA-87-2122) Avail: NTIS HC A02/MF A01 CSCL 21I

A gas analyzer utilizing a nondispersive infrared (NDIR) detection system was used to monitor the ammonia and water vapor content of the products of a previously unused hydrazine gas generator. This provided an in-situ measurement of the generator's efficiency difficult to obtain by other means. The analyzer was easily installed in both the calibration and hydrazine systems, required no maintenance other than periodic zero adjustments, and performed well for extended periods in the operating range tested. The catalyst bed operated smoothly and repeatedly during the 28 hr of testing. No major transients were observed on startup or during steady state operation. The amount of ammonia in the output stream of the gas generator was found to be a strong function of temperature at catalyst bed temperatures below 450 C. At temperatures above this, the efficiency remained nearly constant. On startup the gas generator efficiency was found to decrease with time until a steady state value was attained. Elevated catalyst bed temperatures in the periods before steady state operation was found to be responsible for this phenomenon. Author

N87-23695*# Rockwell International Corp., Canoga Park, Calif. Rocketdyne Div.
SPACE STATION WP-04 POWER SYSTEM. VOLUME 1: EXECUTIVE SUMMARY Final Study Report
 G. J. HALLINAN 19 Jan. 1987 92 p (Contract NAS3-24666) (NASA-CR-179587-VOL-1; NAS 1.26:179587-VOL-1; FSR-DR-15-VOL-1) Avail: NTIS HC A05/MF A01 CSCL 14B

Major study activities and results of the phase B study contract for the preliminary design of the space station Electrical Power System (EPS) are summarized. The areas addressed include the general system design, man-tended option, automation and robotics, evolutionary growth, software development environment, advanced development, customer accommodations, operations planning, product assurance, and design and development phase planning. The EPS consists of a combination photovoltaic and solar dynamic power generation subsystem and a power management and distribution (PMAD) subsystem. System trade studies and costing activities are also summarized. M.G.

N87-23696*# Rockwell International Corp., Canoga Park, Calif. Rocketdyne Div.
SPACE STATION WP-04 POWER SYSTEM. VOLUME 2: STUDY RESULTS Final Study Report
 G. J. HALLINAN 19 Jan. 1987 556 p (Contract NAS3-24666) (NASA-CR-179587-VOL-2; NAS 1.26:179587-VOL-2; FSR-DR-15-VOL-2) Avail: NTIS HC A24/MF A01 CSCL 14B

Results of the phase B study contract for the definition of the space station Electric Power System (EPS) are presented in detail along with backup information and supporting data. Systems analysis and trades, preliminary design, advanced development, customer accommodations, operations planning, product assurance, and design and development phase planning are addressed. The station design is a hybrid approach which provides user power of 25 kWe from the photovoltaic subsystem and 50 kWe from the solar dynamic subsystem. The electric power is distributed to users as a utility service; single phase at a frequency of 20 kHz and voltage of 440VAC. The solar array NiH2 batteries of the photovoltaic subsystem are based on commonality to those used on the co-orbiting and solar platforms. M.G.

N87-23809* National Aeronautics and Space Administration. Lewis Research Center, Cleveland, Ohio.
EXPERIMENTAL THRUST PERFORMANCE OF A HIGH AREA-RATIO ROCKET NOZZLE
 A. J. PAVLI, K. J. KACYNSKI, and T. A. SMITH In Johns Hopkins Univ., The 23rd JANNAF Combustion Meeting, Volume 1 p 585-599 Oct. 1986 Previously announced as N87-20381 Avail: CPIA, Laurel, Md. 20707 HC \$70.00 CSCL 21H

An experimental investigation was conducted to determine the thrust performance attainable from high-area-ratio rocket nozzles. A modified Rao-contoured nozzle with an expansion area of 1030 was test fired with hydrogen-oxygen propellants at altitude conditions. The nozzle was also tested as a truncated nozzle, at an expansion area ratio of 428. Thrust coefficient and thrust coefficient efficiency values are presented for each configuration at various propellant mixture ratios (oxygen/fuel). Several procedural techniques were developed permitting improved measurement of nozzle performance. The more significant of these were correcting the thrust for the aneroid effects, determining the effective chamber pressure, and referencing differential pressure transducers to a vacuum reference tank. Author

20 SPACECRAFT PROPULSION AND POWER

N87-24525*# National Aeronautics and Space Administration. Lewis Research Center, Cleveland, Ohio.

THE NASA/USAF ARCJET RESEARCH AND TECHNOLOGY PROGRAM

JAMES R. STONE and EDWARD S. HUSTON (Air Force Astrophysics Lab., Edwards AFB, Calif.) 1987 21 p Presented at the 23rd Joint Propulsion Conference, San Diego, Calif., 29 Jun. - 2 Jul. 1987; sponsored by AIAA, SAE, ASME and ASEE (NASA-TM-100112; E-3656; NAS 1.15:100112; AIAA-87-1946) Avail: NTIS HC A02/MF A01 CSCL 21C

Direct current arcjets have the potential to provide specific impulses greater than 500 sec with storable propellants, and greater than 1000 sec with hydrogen. This level of performance can provide significant benefits for such applications as orbit transfer, station keeping, orbit change, and maneuvering. The simplicity of the arcjet system and its elements of commonality with state-of-the-art resistojet systems offer a relatively low risk transition to these enhanced levels of performance for low power (0.5 to 1.5 kW) station keeping applications. Arcjets at power levels of 10 to 30 kW are potentially applicable to orbit transfer missions. Furthermore, with the anticipated development of space nuclear power systems, arcjets at greater than 100 kW may become attractive. This paper describes the ongoing NASA/USAF program and describes major recent accomplishments. Author

N87-24531*# National Aeronautics and Space Administration. Lewis Research Center, Cleveland, Ohio.

DEVELOPMENT OF AN ADVANCED PHOTOVOLTAIC CONCENTRATOR SYSTEM FOR SPACE APPLICATIONS

MICHAEL F. PISZCZOR, JR. and MARK J. ONEILL (ENTECH Corp., Dallas-Fort Worth Airport, Tex.) 1987 16 p Prepared for presentation at the 22nd Intersociety Energy Conversion Engineering Conference, Philadelphia, Pa., cosponsored by AIAA, ANS, ASME, SAE, IEEE, ACS, and AIChE (NASA-TM-100101; E-3637; NAS 1.15:100101; AIAA-87-9034) Avail: NTIS HC A02/MF A01 CSCL 10B

Recent studies indicate that significant increases in system performance (increased efficiency and reduced system mass) are possible for high power space based systems by incorporating technological developments with photovoltaic power systems. The Advanced Photovoltaic Concentrator Program is an effort to take advantage of recent advancements in refractive optical elements. By using a domed Fresnel lens concentrator and a prismatic cell cover, to eliminate metallization losses, dramatic reductions in the required area and mass over current space photovoltaic systems are possible. The advanced concentrator concept also has significant advantages when compared to solar dynamic Organic Rankine Cycle power systems in Low Earth Orbit applications where energy storage is required. The program is currently involved in the selection of a material for the optical element that will survive the space environment and a demonstration of the system performance of the panel design. Author

N87-24536*# National Aeronautics and Space Administration. Lewis Research Center, Cleveland, Ohio.

RESISTOJET PLUME AND INDUCED ENVIRONMENT ANALYSIS M.S. Thesis - Case Western Reserve Univ.

DAVID J. HOFFMAN May 1987 60 p (NASA-TM-88957; E-3410; NAS 1.15:88957) Avail: NTIS HC A04/MF A01 CSCL 21H

The source flow method developed by G.A. Simons for calculating the far field plume density produced by high thrust rocket nozzles is modified and applied to low thrust resistojet nozzles with Reynolds numbers on the order of 4000 to 7000. Simons' original method and the modified analysis are compared to mass flux measurements taken by Chirivella in a JPL vacuum tank facility. Results of the comparison show the modified analysis presented more accurately predicts the mass flux at large angles from the nozzle centerline than Simons' original method. The modified Simons analysis is then used to calculate the plume structure and two contamination parameters, number column density and back flow, for five nozzle geometries representative of Space Station resistojets. Author

N87-25420*# Georgia Inst. of Tech., Atlanta.

TECHNOLOGY FOR SATELLITE POWER CONVERSION Final Technical Report

M. A. GOUKER, D. P. CAMPBELL, and J. J. GALLAGHER 30 Jun. 1987 110 p (Contract NAG3-282) (NASA-CR-181057; A-3244; NAS 1.26:181057) Avail: NTIS HC A06/MF A01 CSCL 14B

Components were examined that will be needed for high frequency rectenna devices. The majority of the effort was spent on measuring the directivity and efficiency of the half-wave dipole antenna. It is felt that the antenna and diode should be roughly optimized before they are combined into a rectenna structure. An integrated low pass filter had to be added to the antenna structure in order to facilitate the field pattern measurements. A calculation was also made of the power density of the Earth's radiant energy as seen by satellites in Earth orbit. Finally, the feasibility of using a Metal-Oxide-Metal (MOM) diode for rectification of the received power was assessed. B.G.

N87-25422*# National Aeronautics and Space Administration. Lewis Research Center, Cleveland, Ohio.

SPACE STATION PROPULSION SYSTEM TECHNOLOGY

ROBERT E. JONES, PHILLIP R. MENG, STEVEN J. SCHNEIDER, JAMES S. SOVEY, and ROBERT R. TACINA 1987 18 p Proposed for presentation at the 38th International Astronautical Federation Congress, Brighton, England, 10-17 Oct. 1987 (NASA-TM-100108; E-3648; NAS 1.15:100108) Avail: NTIS HC A02/MF A01 CSCL 21H

Two propulsion systems have been selected for the space station: O/H rockets for high thrust applications and the multipropellant resistojets for low thrust needs. These thruster systems integrate very well with the fluid systems on the station. Both thrusters will utilize waste fluids as their source of propellant. The O/H rocket will be fueled by electrolyzed water and the resistojets will use stored waste gases from the environmental control system and the various laboratories. This paper presents the results of experimental efforts with O/H and resistojet thrusters to determine their performance and life capability. Author

N87-25423*# National Aeronautics and Space Administration. Lewis Research Center, Cleveland, Ohio.

COMPARISON OF THEORETICAL AND EXPERIMENTAL THRUST PERFORMANCE OF A 1030:1 AREA RATIO ROCKET NOZZLE AT A CHAMBER PRESSURE OF 2413 KN/M² (350 PSIA)

TAMARA A. SMITH, ALBERT J. PAVLI, and KENNETH J. KACYNSKI 1987 25 p Presented at the 23rd Joint Propulsion Conference, San Diego, Calif., 29 Jun. - 2 Jul. 1987; sponsored by AIAA, SAE, ASME and ASEE (NASA-TP-2725; E-3523; NAS 1.60:2725; AIAA-87-2069) Avail: NTIS HC A02/MF A01 CSCL 21H

The joint Army, Navy, NASA, Air Force (JANNAF) rocket engine performance prediction procedure is based on the use of various reference computer programs. One of the reference programs for nozzle analysis is the Two-Dimensional Kinetics (TDK) Program. The purpose of this report is to calibrate the JANNAF procedure incorporated into the December 1984 version of the TDK program for the high-area-ratio rocket engine regime. The calibration was accomplished by modeling the performance of a 1030:1 rocket nozzle tested at NASA Lewis Research Center. A detailed description of the experimental test conditions and TDK input parameters is given. The results show that the computer code predicts delivered vacuum specific impulse to within 0.12 to 1.9 percent of the experimental data. Vacuum thrust coefficient predictions were within + or - 1.3 percent of experimental results. Predictions of wall static pressure were within approximately + or - 5 percent of the measured values. An experimental value for inviscid thrust was obtained for the nozzle extension between area ratios of 427.5 and 1030 by using an integration of the measured wall static pressures. Subtracting the measured thrust gain produced by the nozzle between area ratios of 427.5 and 1030 from the inviscid thrust gain yielded experimental drag decrements

of 10.85 and 27.00 N (2.44 and 6.07 lb) for mixture ratios of 3.04 and 4.29, respectively. These values correspond to 0.45 and 1.11 percent of the total vacuum thrust. At a mixture ratio of 4.29, the TDK predicted drag decrement was 16.59 N (3.73 lb), or 0.71 percent of the predicted total vacuum thrust. Author

N87-25424*# National Aeronautics and Space Administration. Lewis Research Center, Cleveland, Ohio.
EXPERIMENTAL EVALUATION OF HEAT TRANSFER ON A 1030:1 AREA RATIO ROCKET NOZZLE

KENNETH J. KACYNSKI, ALBERT J. PAVLI, and TAMARA A. SMITH Aug. 1987 28 p Presented at the 23rd Joint Propulsion Conference, San Diego, Calif., 29 Jun. - 2 Jul. 1987; sponsored by AIAA, SAE, ASME and ASEE (NASA-TP-2726; E-3558; NAS 1.60:2726; AIAA-87-2070) Avail: NTIS HC A03/MF A01 CSCL 21H

A 1030:1 carbon steel, heat-sink nozzle was tested. The test conditions included a nominal chamber pressure of 2413 kN/sq m and a mixture ratio range of 2.78 to 5.49. The propellants were gaseous oxygen and gaseous hydrogen. Outer wall temperature measurements were used to calculate the inner wall temperature and the heat flux and heat rate to the nozzle at specified axial locations. The experimental heat fluxes were compared to those predicted by the Two-Dimensional Kinetics (TDK) computer model analysis program. When laminar boundary layer flow was assumed in the analysis, the predicted values were within 15% of the experimental values for the area ratios of 20 to 975. However, when turbulent boundary layer conditions were assumed, the predicted values were approximately 120% higher than the experimental values. A study was performed to determine if the conditions within the nozzle could sustain a laminar boundary layer. Using the flow properties predicted by TDK, the momentum-thickness Reynolds number was calculated, and the point of transition to turbulent flow was predicted. The predicted transition point was within 0.5 inches of the nozzle throat. Calculations of the acceleration parameter were then made to determine if the flow conditions could produce relaminarization of the boundary layer. It was determined that if the boundary layer flow was inclined to transition to turbulent, the acceleration conditions within the nozzle would tend to suppress turbulence and keep the flow laminar-like. M.G.

N87-25425*# National Aeronautics and Space Administration. Lewis Research Center, Cleveland, Ohio.

ANALYSIS OF QUASI-HYBRID SOLID ROCKET BOOSTER CONCEPTS FOR ADVANCED EARTH-TO-ORBIT VEHICLES

ROBERT L. ZURAWSKI and DOUGLAS C. RAPP (Sverdrup Technology, Inc., Cleveland, Ohio.) Aug. 1987 32 p Presented at the 23rd Joint Propulsion Conference, San Diego, Calif. 29 Jun. - 2 Jul. 1987; sponsored by AIAA, SAE, ASME and ASEE (NASA-TP-2751; E-3554; NAS 1.60:2751; AIAA-87-2082) Avail: NTIS HC A03/MF A01 CSCL 21H

A study was conducted to assess the feasibility of quasi-hybrid solid rocket boosters for advanced Earth-to-orbit vehicles. Thermochemical calculations were conducted to determine the effect of liquid hydrogen addition, solids composition change plus liquid hydrogen addition, and the addition of an aluminum/liquid hydrogen slurry on the theoretical performance of a PBAN solid propellant rocket. The space shuttle solid rocket booster was used as a reference point. All three quasi-hybrid systems theoretically offer higher specific impulse when compared with the space shuttle solid rocket boosters. However, based on operational and safety considerations, the quasi-hybrid rocket is not a practical choice for near-term Earth-to-orbit booster applications. Safety and technology issues pertinent to quasi-hybrid rocket systems are discussed. Author

N87-25426*# National Aeronautics and Space Administration. Lewis Research Center, Cleveland, Ohio.

LOW REYNOLDS NUMBER NOZZLE FLOW STUDY M.S. Thesis

MARGARET V. WHALEN Jul. 1987 45 p (NASA-TM-100130; E-3679; NAS 1.15:100130) Avail: NTIS HC A03/MF A01 CSCL 21H

An experimental study of low Reynolds number nozzle flow was performed. A brief comparison was made between some of the experimental performance data and performance predicted by a viscous flow code. The performance of 15, 20, and 25 deg conical nozzles, bell nozzles, and trumpet nozzles was evaluated with unheated nitrogen and hydrogen. The numerical analysis was applied to the conical nozzles only, using an existing viscous flow code that was based on a slender-channel approximation. Although the trumpet and 25 deg conical nozzles had slightly better performance at lower Reynolds numbers, it is unclear which nozzle is superior as all fell within the experimental error band. The numerical results were found to agree with experimental results for nitrogen and for some of the hydrogen data. Some code modification is recommended to improve confidence in the performance prediction. Author

N87-26097*# Rockwell International Corp., Canoga Park, Calif. Rocketdyne Div.

CONCEPTS FOR SPACE MAINTENANCE OF OTV ENGINES Interim Report

A. MARTINEZ, B. D. HINES, and C. M. ERICKSON /in Johns Hopkins Univ., The 1986 JANNAF Propulsion Meeting, Volume 1 p 99-110 Aug. 1986 (Contract NAS3-23773)

Avail: NTIS HC A25/MF A01 CSCL 21H

Concepts for space maintainability of the Orbital Transfer Vehicle (OTV) engines are examined. An engine design is developed which is driven by space maintenance requirements and by a failure modes and effects analysis (FMEA). Modularity within the engine is shown to offer cost benefits and improved space maintenance capabilities. Space-operable disconnects are conceptualized for both engine change-out and for module replacement. A preliminary space maintenance plan is developed around a controls and condition monitoring system using advanced sensors, controls, and condition monitoring concepts. Author

N87-26114*# National Aeronautics and Space Administration. Lewis Research Center, Cleveland, Ohio.

TEST PROGRAM TO PROVIDE CONFIDENCE IN LIQUID OXYGEN COOLING OF HYDROCARBON FUELED ROCKET THRUST CHAMBERS

ELIZABETH S. ARMSTRONG /in Johns Hopkins Univ., The 1986 JANNAF Propulsion Meeting, Volume 1 p 361-367 Aug. 1986 Previously announced as N86-31646

Avail: NTIS HC A25/MF A01 CSCL 21H

In previous tests of liquid oxygen cooling of hydrocarbon fueled rocket engines, small oxygen leaks developed at the throat of the thrust chamber and film cooled the hot gas side of the chamber wall without resulting in catastrophic failure. However, more testing is necessary to demonstrate that a catastrophic failure would not occur if cracks developed further upstream between the injector and the throat, where the boundary layer has not been established. Since under normal conditions cracks are expected to form in the throat region of the thrust chamber, cracks must be initiated artificially in order to control their location. Several methods of crack initiation are discussed here. Author

N87-26129*# Martin Marietta Aerospace, Denver, Colo.
PROPULSION RECOMMENDATIONS FOR SPACE STATION FREE FLYING PLATFORMS

L. R. REDD and L. J. ROSE /in Johns Hopkins Univ., The 1986 JANNAF Propulsion Meeting, Volume 1 p 515-523 Aug. 1986 (Contract NAS3-23893)

Avail: NTIS HC A25/MF A01 CSCL 21H

Propulsion system candidates have been defined for Space Station free flying platforms for the purpose of comparison and to

understand the impact of the various mission requirements on the candidate designs. Recommendations for propulsion for each of the various platforms are given. Author

N87-26133*# National Aeronautics and Space Administration. Lewis Research Center, Cleveland, Ohio.

PROVEN, LONG-LIFE HYDROGEN/OXYGEN THRUST CHAMBERS FOR SPACE STATION PROPULSION

G. PAUL RICHTER and HAROLD G. PRICE /In Johns Hopkins Univ., The 1986 JANNAP Propulsion Meeting, Volume 1 p 547-564 Aug. 1986 Previously announced as N86-32522

Avail: NTIS HC A25/MF A01 CSCL 21H

A 25 lb sub f hydrogen/oxygen thruster has been developed and proven as a viable candidate to meet the needs of the Space Station Program. Likewise, a 50 lb sub f hydrogen/oxygen thrust chamber has been developed and has demonstrated reliable, long-life expectancy at anticipated Space Station operating conditions. Both these thrust chambers were based on design criteria developed in previous thruster programs. Extensive thermal analysis and models were used to design the thrusters to achieve total impulse goals of 2 million lb sub f sec. Test data from each thruster are compared to the analytical predictions for the performance and heat transfer characteristics. Also, the results of thrust chamber life verification tests are presented. Author

N87-26135*# National Aeronautics and Space Administration. Lewis Research Center, Cleveland, Ohio.

WATER-PROPELLANT RESISTOJETS FOR MAN-TENDED PLATFORMS

ALLEN J. LOUVIERE (Space Industries, Inc., Webster, Tex.), ROBERT E. JONES, W. EARL MORREN, and JAMES S. SOVEY 1987 17 p Proposed for presentation at the 38th International Astronautical Federation Congress, Brighton, England, 10-17 Oct. 1987

(NASA-TM-100110; E-3649; NAS 1.15:100110; IAF-87-259)

Avail: NTIS HC A02/MF A01 CSCL 21H

The selection of a propulsion system for a man-tended platform has been influenced by the planned use of resistojets for drag make-up on the manned space station. For that application a resistojet has been designed that is capable of operation with a wide variety of propellants, including water. The reasons for the selection of water as the propellant and the performance of water as a propellant are discussed. The man-tended platform and its mission requirements are described. Author

N87-26141*# National Aeronautics and Space Administration. Lewis Research Center, Cleveland, Ohio.

RECENT DEVELOPMENTS IN INDIUM PHOSPHIDE SPACE SOLAR CELL RESEARCH

DAVID J. BRINKER and IRVING WEINBERG Aug. 1987 13 p Presented at the 22nd Intersociety Energy Conversion Engineering Conference, Philadelphia, Pa., 10-14 Aug. 1987; cosponsored by AIAA, ANS, ASME, SAE, IEEE, ACS, and AICHE

(NASA-TM-100139; E-3690; NAS 1.15:100139; AIAA-87-9053)

Avail: NTIS HC A02/MF A01 CSCL 10B

Recent developments and progress in indium phosphide solar cell research for space application are reviewed. Indium phosphide homojunction cells were fabricated in both the n+p and p+n configurations with total area efficiencies of 17.9 and 15.9% (air mass 0 and 25 C) respectively. Organometallic chemical vapor deposition, liquid phase epitaxy, ion implantation and diffusion techniques were employed in InP cell fabrication. A theoretical model of a radiation tolerant, high efficiency homojunction cell was developed. A realistically attainable AMO efficiency of 20.5% was calculated using this model with emitter and base doping of 6×10^{17} to the 17th power and 5×10^{16} the 16th power/cm respectively. Cells of both configurations were irradiated with 1 MeV electrons and 37 MeV protons. For both proton and electron irradiation, the n+p cells are more radiation resistant at higher fluences than the p+n cells. The first flight module of four InP cells was assembled for the Living Plume Shield III satellite. Author

N87-26144*# National Aeronautics and Space Administration. Lewis Research Center, Cleveland, Ohio.

SPACE STATION ELECTRICAL POWER SYSTEM

THOMAS L. LABUS and THOMAS H. COCHRAN 1987 19 p Proposed for presentation at the 38th International Astronautical Federation Congress, Brighton, England, 10-17 Oct. 1987

(NASA-TM-100140; E-3692; NAS 1.15:100140; IAF-87-234)

Avail: NTIS HC A02/MF A01 CSCL 22B

The purpose of this paper is to describe the design of the Space Station Electrical Power System. This includes the Photovoltaic and Solar Dynamic Power Modules as well as the Power Management and Distribution System (PMAD). In addition, two programmatic options for developing the Electrical Power System will be presented. One approach is defined as the Enhanced Configuration and represents the results of the Phase B studies conducted by the NASA Lewis Research Center over the last two years. Another option, the Phased Program, represents a more measured approach to reaching about the same capability as the Enhanced Configuration. Author

N87-26447*# National Aeronautics and Space Administration. Lewis Research Center, Cleveland, Ohio.

SPACE STATION POWER SYSTEM

COSMO R. BARAONA /In its Space Photovoltaic Research and Technology 1986. High Efficiency, Space Environment and Array Technology p 321-332 Jun. 1987 Previously announced as N86-32521

Avail: NTIS HC A16/MF A01 CSCL 10B

The major requirements and guidelines that affect the space station configuration and power system are explained. The evolution of the space station power system from the NASA program development-feasibility phase through the current preliminary design phase is described. Several early station concepts are described and linked to the present concept. Trade study selections of photovoltaic system technologies are described in detail. A summary of present solar dynamic and power management and distribution systems is also given. Author

N87-26448*# National Aeronautics and Space Administration. Lewis Research Center, Cleveland, Ohio.

SPACECRAFT 2000: THE CHALLENGE OF THE FUTURE

HENRY W. BRANDHORST, JR., KARL A. FAYMON, and ROBERT W. BERCAW /In its Space Photovoltaic Research and Technology 1986. High Efficiency, Space Environment and Array Technology p 333-341 Jun. 1987

Avail: NTIS HC A16/MF A01 CSCL 10B

Considerable opportunity exists to improve the systems, subsystems, components, etc., included in the space station bus, the non-payload portion of the spacecraft. The steps followed to date, the challenges being faced by industry, and the progress toward establishing a new NASA initiative which will identify the technologies required to build spacecraft of the 21st century and which will implement the technology development/validation programs necessary are described. Author

N87-28602*# National Aeronautics and Space Administration. Lewis Research Center, Cleveland, Ohio.

A DETAILED DESCRIPTION OF THE UNCERTAINTY ANALYSIS FOR HIGH AREA RATIO ROCKET NOZZLE TESTS AT THE NASA LEWIS RESEARCH CENTER

KENNETH J. DAVIDIAN, RONALD H. DIECK (Pratt and Whitney Aircraft, West Palm Beach, Fla.), and ISAAC CHUANG 1987 30 p

(NASA-TM-100203; E-3799; NAS 1.15:100203) Avail: NTIS HC A03/MF A01 CSCL 21H

A preliminary uncertainty analysis has been performed for the High Area Ratio Rocket Nozzle test program which took place at the altitude test capsule of the Rocket Engine Test Facility at the NASA Lewis Research Center. Results from the study establish the uncertainty of measured and calculated parameters required for the calculation of rocket engine specific impulse. A generalized description of the uncertainty methodology used is provided. Specific equations and a detailed description of the analysis are

presented. Verification of the uncertainty analysis model was performed by comparison with results from the experimental program's data reduction code. Final results include an uncertainty for specific impulse of 1.30 percent. The largest contributors to this uncertainty were calibration errors from the test capsule pressure and thrust measurement devices. Author

N87-29594*# Boeing Aerospace Co., Kent, Wash. Flight Technology Group.

SPACE STATION PROPULSION-ECLSS INTERACTION STUDY Final Report

SCOTT M. BRENNAN 14 Feb. 1986 92 p

(Contract NAS3-23353)

(NASA-CR-175093; NAS 1.26:175093; D483-10060-1) Avail:

NTIS-NC A05/MF A01 CSCL 21H

The benefits of the utilization of effluents of the Space Station Environmental Control and Life Support (ECLS) system are examined. Various ECLS-propulsion system interaction options are evaluated and compared on the basis of weight, volume, and power requirements. Annual propulsive impulse to maintain station altitude during a complete solar cycle of eleven years and the effect on station resupply are considered. Author

23

CHEMISTRY AND MATERIALS (GENERAL)

A87-22417*# National Aeronautics and Space Administration. Lewis Research Center, Cleveland, Ohio.

EFFECT OF HARD PARTICLE IMPACTS ON THE ATOMIC OXYGEN SURVIVABILITY OF REFLECTOR SURFACES WITH TRANSPARENT PROTECTIVE OVERCOATS

DANIEL A. GULINO (NASA, Lewis Research Center, Cleveland, OH) AIAA, Aerospace Sciences Meeting, 25th, Reno, NV, Jan. 12-15, 1987. 8 p. Previously announced in STAR as N87-11838. refs

(AIAA PAPER 87-0104)

Silver mirror samples with protective coatings were subjected to a stream of 27 microns alumina particles to induce pinhole defects. The protective coating consisted of a layer of aluminum dioxide over silver followed by a layer of silicon dioxide over the alumina. Samples were prepared on both graphite-epoxy composite and fused quartz substrates. After exposure to the hard particle stream, the samples were exposed to an oxygen plasma environment in a laboratory plasma asher. The effects of both the hard particles and the oxygen plasma were documented by both reflectance measurements and scanning electron microscopy. The results indicated that oxidative damage to the silver reflecting layer continues beyond that of the erosively exposed silver. Oxidative undercutting of the silver layer and graphite-epoxy substrate continues in undamaged areas through adjacent, particle damaged defect sites. This may have implications for the use of such mirrors in a space station solar dynamic power system. Author

A87-38472* National Aeronautics and Space Administration. Lewis Research Center, Cleveland, Ohio.

MATERIALS RESEARCH AND APPLICATIONS AT NASA LEWIS RESEARCH CENTER

H. B. PROBST (NASA, Lewis Research Center, Cleveland, OH) Journal of Metals (ISSN 0148-6608), vol. 39, March 1987, p. 62, 63.

The facilities and instruments of the Lewis Research Center specialized for materials research are discussed. The main objectives of the Center are to provide R & D relevant to main propulsion plants and auxiliary power systems for aeronautics, space, and energy conversion applications. The Center is concerned with microstructure-property relations and their effect on processing; intermetallic compounds and high temperature metal

matrix composites; ceramics with improved reliability for use in heat engines; polymer matrix composites for aerospace applications; understanding the high temperature corrosive attack in the hostile environments of aircraft, rockets, and other heat engines; high temperature lubrication and wear; and microgravity materials research. The various types of schemes and techniques, provided by the Center, for analyzing data are described. I.F.

A87-48314*# National Aeronautics and Space Administration. Lewis Research Center, Cleveland, Ohio.

QUANTITATIVE ANALYSIS OF PMR-15 POLYIMIDE RESIN BY HPLC

GARY D. ROBERTS and RICHARD W. LAUVER (NASA, Lewis Research Center, Cleveland, OH) Journal of Applied Polymer Science (ISSN 0021-8995), vol. 33, 1987, p. 2893-2913. refs

The concentration of individual components and of total solids of 50 wt pct PMR-15 resin solutions was determined using reverse-phase HPLC to within + or - 8 percent accuracy. Acid impurities, the major source of impurities in 3,3', 4,4'-benzophenonetetracarboxylic acid (BTDE), were eliminated by recrystallizing the BTDE prior to esterification. Triester formation was not a problem because of the high rate of esterification of the anhydride relative to that of the carboxylic acid. Aging of PMR-15 resin solutions resulted in gradual formation of the mononadimide and bisnadimide of 4,4'-methylenedianiline, with the BTDE concentration remaining constant. Similar chemical reactions occurred at a reduced rate in dried films of PMR-15 resin. R.R.

A87-51176*# National Aeronautics and Space Administration. Lewis Research Center, Cleveland, Ohio.

UP CLOSE - MATERIALS DIVISION OF NASA-LEWIS RESEARCH CENTER

PHILLIP ABEL (NASA, Lewis Research Center, Cleveland, OH) MRS Bulletin (ISSN 0883-7694), vol. 12, Feb. 16-Mar. 16, 1987, p. 85-87.

The eight branches of the Materials Division of NASA-Lewis Research Center are described. The design and capabilities of the Microgravity Materials Science Laboratory are discussed. Consideration is given to the objectives of the ceramic branch, the advanced metallic branch, the metal science branch, and the polymer branch. Also discussed are the research and development efforts of the surface science branch, the environmental durability branch, and the analytic science branch. I.F.

A87-53654* Michigan State Univ., East Lansing.

IPTYCENES - EXTENDED TRIPTYCENES

HAROLD HART, ABDOLLAH BASHIR-HASHEMI, JIHMEI LUO, and MARY ANN MEADOR (Michigan State University, East Lansing) Tetrahedron (ISSN 0040-4020), vol. 42, no. 6, 1986, p. 1641-1654. refs

(Contract NSF CHE-83-19578; NIH-GM-15997; NAG3-670)

Properties of iptycenes and particular structural features of several iptycenes are briefly discussed, as are certain extensions beyond the compounds presented here. Methods for preparing useful synthons are described. Three new, much improved syntheses of triptycene, itself a useful iptycene synthon, are presented. In addition, improved syntheses of pentiptycenes and heptiptycene are described. Author

A87-53656* Michigan State Univ., East Lansing.

TRITRIPTYCENE - A D(3H) C(62) HYDROCARBON WITH THREE U-SHAPED CAVITIES

ABDOLLAH BASHIR-HASHEMI, HAROLD HART, and DONALD L. WARD (Michigan State University, East Lansing) American Chemical Society, Journal (ISSN 0002-7863), vol. 108, 1986, p. 6675-6679. refs

(Contract NSF CHE-83-19578; NAG3-670; NSF CHE-84-03823)

A87-53671* National Aeronautics and Space Administration. Lewis Research Center, Cleveland, Ohio.

A MECHANISTIC STUDY OF POLYIMIDE FORMATION FROM DIESTER-DIACIDS

JAMES C. JOHNSTON, MARY ANN B. MEADOR, and WILLIAM B. ALSTON (NASA, Lewis Research Center, Cleveland, OH) Journal of Polymer Science: Polymer Chemistry Edition (ISSN 0360-6376), vol. 25, 1987, p. 2175-2183. refs

Previous work has noted the presence of anhydride during the imidization step of polyimide polymer processing from diester-diacids and diamines. Comparison of the relative rates of reactions among model compounds demonstrates the intermediacy of anhydride in the imidization reaction. IR and NMR observations of mixtures of monomers confirm the production of anhydride as a necessary intermediate in the imidization reaction. Author

N87-10177*# National Aeronautics and Space Administration. Lewis Research Center, Cleveland, Ohio.

BLACK-AND-WHITE PHOTOGRAPHIC CHEMISTRY: A REFERENCE

E. D. WALKER, comp. Jun. 1986 164 p (NASA-TM-87296; E-3006; NAS 1.15:87296) Avail: NTIS HC A08/MF A01 CSCL 14E

This work is intended as a reference of black-and-white photographic chemistry. Included is a basic history of the photographic processes and a complete description of all chemicals used, formulas for the development and fixation process, and associated formulas such as cleaners, hardeners, and toners. The work contains a complete glossary of photographic terms, a trouble-shooting section listing causes and effects regarding photographic film and papers, and various conversion charts.

Author

N87-11841*# National Aeronautics and Space Administration. Lewis Research Center, Cleveland, Ohio.

SIMULTANEOUS ELECTRICAL RESISTIVITY AND MASS UPTAKE MEASUREMENTS IN BROMINE INTERCALATED FIBERS

D. A. JAWORSKE 1986 10 p Presented at the Fall Meeting of the Materials Research Society, Boston, Mass., 1-5 Dec. 1986 (NASA-TM-88900; E-3324; NAS 1.15:88900) Avail: NTIS HC A02/MF A01 CSCL 11G

Changes in mass and electrical resistivity of several types of pitch-based and vapor-grown graphite fibers were monitored during reaction with bromine. The observed threshold pressure dependent reaction suggested that the fibers were intercalated. In the fully brominated compound, the mass was increased by 44 percent and the resistivity was improved by a factor of 17. In the residue compound, the mass was increased by 22 percent and the resistivity was improved by a factor of 5. Fibers possessing different degrees of graphitization had surprisingly similar changes in both mass and resistivity. Author

N87-14432*# National Aeronautics and Space Administration. Lewis Research Center, Cleveland, Ohio.

SUBSTITUTED 1,1,1-TRIARYL-2,2,2-TRIFLUOROETHANES AND PROCESSES FOR THEIR SYNTHESIS Patent Application

W. B. ALSTON, inventor (to NASA) and R. F. GRATZ, inventor (to NASA) 29 Oct. 1986 24 p (NASA-CASE-LEW-14345-1; NAS 1.71:LEW-14345-1; US-PATENT-APPL-SN-924474) Avail: NTIS HC A02/MF A01 CSCL 990

Synthetic procedures are described for tetraalkyls, tetraacids and dianhydrides substituted 1,1,1-triaryl-2,2,2-trifluoroethanes which comprises: (1) 1,1-bis(dialkylaryl)-1 aryl-2,2,2-trifluoroethane; (2) 1,1-bis(carboxyaryl)-1 aryl-2,2,2-trifluoroethane; or (3) cyclic dianhydride or diamine of 1,1-bis(dialkylaryl)-1 aryl-2,2,2-trifluoroethanes. The synthesis of (1) is accomplished by the condensation reaction of an aryltrifluoromethyl ketone with a dialkylaryl compound. The synthesis of (2) is accomplished by oxidation of (1). The synthesis dianhydride of (3) is accomplished by the conversion of (2) to its corresponding cyclic dianhydride. The synthesis of the diamine is accomplished by the similar reaction

of an aryltrifluoromethyl ketone with aniline or alkyl substituted or disubstituted anilines. Also, other derivatives of the above are formed by nucleophilic displacement reactions. NASA

N87-14433* National Aeronautics and Space Administration. Lewis Research Center, Cleveland, Ohio.

NEW CONDENSATION POLYIMIDES CONTAINING 1,1,1-TRIARYL-2,2,2-TRIFLUOROETHANE STRUCTURES Patent Application

W. B. ALSTON and R. F. GRATZ, inventors (to NASA) 29 Oct. 1986 27 p (NASA-CASE-LEW-14346-1; NAS 1.71:LEW-14346-1; US-PATENT-APPL-SN-934470) Avail: NTIS HC A03/MF A01 CSCL 07A

The invention relates to a condensation polyimide containing a 1,1,1-triaryl-2,2,2-trifluoroethane structure and other related condensation polyimides. The process for their preparation, which comprises polymerization of a cyclic dianhydride with a diamine is also covered. NASA

N87-14434*# Case Western Reserve Univ., Cleveland, Ohio. Dept. of Macromolecular Science.

POLYMER PRECURSORS FOR CERAMIC MATRIX COMPOSITES Annual Contractor Report

M. H. LITT and K. KUMAR Dec. 1986 42 p (Contract NAG3-446) (NASA-CR-179562; NAS 1.26:179562) Avail: NTIS HC A03/MF A01 CSCL 11B

The synthesis and characterization of a polycyclohexasilane is reported. Because of its cyclic structure, it is anticipated that this polymer might serve as a precursor to SiC having a high char yield with little rearrangement to form small, volatile cyclic silanes, and, as such, would be of interest as a precursor to SiC composite matrices and fibers, or as a binder in ceramic processing. Several approaches to the synthesis of a bifunctional cyclic monomer were attempted; the most successful of these was metal coupling of PhMeSiCl₂ and Me₂SiCl₂. The procedure gives six-membered ring compounds with all degrees of phenyl substitution, from none to hexaphenyl. The compounds with from 0-2 groups were isolated and characterized. The fraction with degree of phenyl substitution equal to 2, a mixture of cis and trans 1,2-; 1,3-; and 1,4 isomers, was isolated in 32 percent yield. Pure 1,4 diphenyldecamethylcyclohexasilane was isolated from the mixed diphenyl compounds and characterized. Diphenyldecamethylcyclohexasilanes were dephenylated to dichlorodecamethylcyclohexasilanes by treating with H₂SO₄.NH₄Cl in benzene. The latter were purified and polymerized by reacting with sodium in toluene. The polymers were characterized by HPGPC, elemental analysis, proton NMR, and IR. Thermogravimetric analyses were carried out on the polymers. As the yield of residual SiC was low, polymers were heat treated to increase the residual char yield. As high as 51.52 percent residual char yield was obtained in one case. Author

N87-16879*# Case Western Reserve Univ., Cleveland, Ohio. Dept. of Mechanical and Aerospace Engineering.

OIL FILM THICKNESS MEASUREMENT AND ANALYSIS FOR AN ANGULAR CONTACT BALL BEARING OPERATING IN PARCHED ELASTOHYDRODYNAMIC LUBRICATION M.S. Thesis. Final Report

SCOTT D. HUNTER Sep. 1986 265 p (Contract NCC3-30) (NASA-CR-179506; E-3152; NAS 1.26:179506) Avail: NTIS HC A12/MF A01 CSCL 11H

The capacitance method is used to estimate the oil film thickness in the Hertzian contact zone of an angular contact ball bearing operating in parched elastohydrodynamic lubrication. The parched elastohydrodynamic lubrication regime is characterized by a transient film thickness and basic speed ratio (ball spin rate over combined race speed) and the formation of a friction polymer. The experimental apparatus tests 40 mm 108 H ball bearings in the counter rotating race mode at loads of 200 and 300 lb, a film parameter of 1.6 and nominal inner and outer race speeds of 38

and 26 rps, respectively. Experimental results are presented for the capacitance, thickness, and conductance of the oil film as functions of elapsed time and for the basic speed ratios as a function of elapsed time, load, and amount of lubricant applied to the test bearing. Results indicate that a friction polymer formed from the initial lubricant has an effect on the capacitance and basic speed ratio measurements. Author

N87-22005* National Aeronautics and Space Administration. Lewis Research Center, Cleveland, Ohio.

THE 2,5-DIACYL-1,4-DIMETHYLBENZENES: EXAMPLES OF BISPHOTOENOL EQUIVALENTS

MICHAEL A. MEADOR 1987 15 p Proposed for presentation at the 194th National Meeting of the American Chemical Society, New Orleans, La., 30 Aug. - 4 Sep. 1987 (NASA-TM-89836; E-3493; NAS 1.15:89836) Avail: NTIS HC A02/MF A01 CSCL 07A

The photochemistry of 2,5-dibenzoyl (DBX) and 2,5-diacetyl-1,4-dimethylbenzene (DAX) has been investigated. Both compounds readily undergo photoenolization similar to 0-alkylphenyl ketones. However, unlike 0-alkylphenyl ketones DAX and DBX are each capable of undergoing two tandem photoenolizations. Photoenols derived from 0-alkylphenyl ketones have been successfully trapped with Diels-Alder dienophiles to provide a convenient synthesis of substituted tetralins. Similarly, Diels-Alder trapping of DBX photoenols afforded substituted tetra- and octahydro anthracenes. Further manipulation of these photoproducts provided the corresponding anthracenes in good yield. The photochemistry of DAX and DBX will be discussed, in particular their use in the synthesis of substituted anthracenes.

Author

N87-29599* National Aeronautics and Space Administration. Lewis Research Center, Cleveland, Ohio.

TRIBOLOGY THEORY VERSUS EXPERIMENT

JOHN FERRANTE Oct. 1987 25 p Prepared for presentation at the NSF Workshop on Adhesion Science and Technology, Lake Tahoe, Calif., 15-16 Oct. 1987 (NASA-TM-100198; E-3791; NAS 1.15:100198) Avail: NTIS HC A02/MF A01 CSCL 07A

Tribology, the study of friction and wear of materials, has achieved a new interest because of the need for energy conservation. Fundamental understanding of this field is very complex and requires a knowledge of solid-state physics, material science, chemistry, and mechanical engineering. This paper is meant to be didactic in nature and outlines some of the considerations needed for a tribology research program. The approach is first to present a simple model, a field emission tip in contact with a flat surface, in order to elucidate important considerations, such as contact area, mechanical deformations, and interfacial bonding. Then examples from illustrative experiments are presented. Finally, the current status of physical theories concerning interfacial bonding are presented. Author

24

COMPOSITE MATERIALS

Includes physical, chemical, and mechanical properties of laminates and other composite materials.

A87-12647* National Aeronautics and Space Administration. Lewis Research Center, Cleveland, Ohio.

FIBER-REINFORCED SUPERALLOY COMPOSITES PROVIDE AN ADDED PERFORMANCE EDGE

D. W. PETRASEK (NASA, Lewis Research Center, Cleveland, OH), D. L. MCDANIELS, L. J. WESTFALL, and J. R. STEPHENS Metal Progress (ISSN 0026-0665), Aug. 1986, 5 p.

Fiber reinforcements are being explored as a means to increasing the performance of superalloys past 980 C. Fiber-reinforced superalloys (FRS), particularly tungsten FRS

(TFRS) are candidate materials for rocket-engine turbopump blades for advanced Shuttle engines and in airbreathing and other rocket engines. Refractory metal wires are the reinforcement of choice due to tolerance to fiber/matrix interactions. W alloy fibers have a maximum tensile strength of 2165 MPa at 1095 C and a 100 hr creep rupture strength at stresses up to 1400 MPa. A TFRS has the potential of a service temperature 110 C over the strongest superalloy. Manufacturing processes being evaluated to realize the FRS components are summarized, together with design features which will be introduced in turbine blades to take advantage of the FRS materials and to extend their surface life. M.S.K.

A87-13145* National Aeronautics and Space Administration. Lewis Research Center, Cleveland, Ohio.

SPECIMEN GEOMETRY EFFECTS ON GRAPHITE/PMR-15 COMPOSITES DURING THERMO-OXIDATIVE AGING

K. J. BOWLES (NASA, Lewis Research Center, Cleveland, OH) and A. MEYERS (Ohio, Medical College, Toledo) IN: International SAMPE Symposium and Exhibition, 31st, Los Angeles, CA, April 7-10, 1986, Proceedings. Covina, CA, Society for the Advancement of Material and Process Engineering, 1986, p. 1285-1299. Previously announced in STAR as N86-17477. refs

Studies were conducted to establish the effects of specimen geometry on the thermo-oxidative stability and the mechanical properties retention of unidirectional Celion 12000 graphite fiber reinforced PMR-15 polyimide composites. Weight loss, flexural strength and interlaminar shear strength are measured at isothermal aging times as long as 1639 hr at a temperature of 316 C for three different specimen geometries. It is found that the three different types of specimen surfaces exhibit different values of weight loss/unit area. The mechanical properties retention is also found to be dependent on geometry for these composites. The interlaminar shear strength decreases significantly over the complete range of aging times. The flexural strength retention starts showing geometric dependency after about 1000 hr of aging at 316 C. Weight loss fluxes, associated with the three different types of exposed surfaces, are calculated and used to develop an empirical mathematical model for predicting the weight loss behavior of unidirectional composites of arbitrary geometries. Data are presented comparing experimentally determined weight loss with weight loss values predicted using the empirical model.

Author

A87-15187* National Aeronautics and Space Administration. Lewis Research Center, Cleveland, Ohio.

POLYMER, METAL, AND CERAMIC MATRIX COMPOSITES FOR ADVANCED AIRCRAFT ENGINE APPLICATIONS

D. L. MCDANIELS, T. T. SERAFINI, and J. A. DICARLO (NASA, Lewis Research Center, Cleveland, OH) Journal of Materials for Energy Systems (ISSN 0162-9719), vol. 8, June 1986, p. 80-91. Previously announced in STAR as N86-13407. refs

Advanced aircraft engine research within NASA Lewis is being focused on propulsion systems for subsonic, supersonic, and hypersonic aircraft. Each of these flight regimes requires different types of engines, but all require advanced materials to meet their goals of performance, thrust-to-weight ratio, and fuel efficiency. The high strength/weight and stiffness/weight properties of resin, metal, and ceramic matrix composites will play an increasingly key role in meeting these performance requirements. At NASA Lewis, research is ongoing to apply graphite/polyimide composites to engine components and to develop polymer matrices with higher operating temperature capabilities. Metal matrix composites, using magnesium, aluminum, titanium, and superalloy matrices, are being developed for application to static and rotating engine components, as well as for space applications, over a broad temperature range. Ceramic matrix composites are also being examined to increase the toughness and reliability of ceramics for application to high-temperature engine structures and components. Author

A87-19121* National Aeronautics and Space Administration. Lewis Research Center, Cleveland, Ohio.

ASSESSMENT OF SIMPLIFIED COMPOSITE MICROMECHANICS USING THREE-DIMENSIONAL FINITE-ELEMENT ANALYSIS

J. J. CARUSO and C. C. CHAMIS (NASA, Lewis Research Center, Cleveland, OH) *Journal of Composites Technology and Research* (ISSN 0885-6804), vol. 8, Fall 1986, p. 77-83. refs

Three-dimensional finite-element analyses are used to assess the accuracy of simplified composite micromechanics equations (SME) for hygral, thermal, and mechanical properties of unidirectional composites with orthotropic fibers. The properties predicted by the SME are in reasonably good agreement with those predicted by the three-dimensional finite-element analyses. This correlation demonstrates that the SME can be used with confidence in predicting the hygral, thermal, and mechanical behavior of unidirectional fiber composites. Author

A87-19123* National Aeronautics and Space Administration. Lewis Research Center, Cleveland, Ohio.

FABRICATION AND QUALITY ASSURANCE PROCESSES FOR SUPERHYBRID COMPOSITE FAN BLADES

R. F. LARK and C. C. CHAMIS (NASA, Lewis Research Center, Cleveland, OH) *Journal of Composites Technology and Research* (ISSN 0885-6804), vol. 8, Fall 1986, p. 98-102. Previously announced in STAR as N85-14882. refs

The feasibility of fabricating full-scale fan blades from superhybrid composites (SHC) for use large, commercial gas turbine engines was evaluated. The type of blade construction selected was a metal-spar/SHC-shell configuration, in which the outer shell was adhesively bonded to a short, internal, titanium spar. Various aspects of blade fabrication, inspection, and quality assurance procedures developed in the investigation are described. It is concluded that the SHC concept is feasible for the fabrication of prototype, full-scale, metal-spar/SHC-shell fan blades that have good structural properties and meet dimensional requirements. R.S.F.

A87-20090*# National Aeronautics and Space Administration. Lewis Research Center, Cleveland, Ohio.

SIMPLIFIED COMPOSITE MICROMECHANICS FOR PREDICTING MICROSTRESSES

CHRISTOS C. CHAMIS (NASA, Lewis Research Center, Cleveland, OH) IN: Reinforced Plastics/Composites Institute, Annual Conference, 41st, Atlanta, GA, January 27-31, 1986, Preprint. Lancaster, PA, Technomic Publishing Co., 1986, 11 p. Previously announced in STAR as N86-24759. refs

A unified set of composite micromechanics equations is summarized and described. This unified set is for predicting the ply microstresses when the ply stresses are known. The set consists of equations of simple form for predicting three-dimensional stresses (six each) in the matrix, fiber, and interface. Several numerical examples are included to illustrate use and computational effectiveness of the equations in this unified set. Numerical results from these examples are discussed with respect to their significance on microcrack formation and, therefore, damage initiation in fiber composites. Author

A87-33577*# University of Southern Illinois, Carbondale.

THE SENSITIVITY OF MECHANICAL PROPERTIES OF TFRS COMPOSITES TO VARIATIONS IN REACTION ZONE SIZE AND PROPERTIES

JAMES N. CRADDOCK (Southern Illinois University, Carbondale), DALE A. HOPKINS, DONALD W. PETRASEK, and PAMELA K. BRINDLEY (NASA, Lewis Research Center, Cleveland, OH) IN: Structures, Structural Dynamics and Materials Conference, 28th, Monterey, CA, Apr. 6-8, 1987, Technical Papers. Part 1. New York, American Institute of Aeronautics and Astronautics, 1987, p. 238-244.

(AIAA PAPER 87-0757)

The properties of tungsten fiber reinforced superalloys (TFRS) composites are calculated using a 3-component micromechanical model. The properties and size of the reaction zone are varied and the effect of these variations on the composite properties are

studied. Results are presented in graphical and tabular form. Post-matrix yield behavior is examined in terms of the tangent modulus of the composite and measures of the effective strength of the lamina. Author

A87-38610* National Aeronautics and Space Administration. Lewis Research Center, Cleveland, Ohio.

COMPOSITE SPACE ANTENNA STRUCTURES - PROPERTIES AND ENVIRONMENTAL EFFECTS

C. A. GINTY (NASA, Lewis Research Center, Cleveland, OH) and N. M. ENDRES (Sverdrup Technology, Inc., Middleburg Heights, OH) IN: International SAMPE Technical Conference, 18th, Seattle, WA, Oct. 7-9, 1986, Proceedings. Covina, CA, Society for the Advancement of Material and Process Engineering, 1986, p. 545-560. Previously announced in STAR as N87-16880. refs

The thermal behavior of composite spacecraft antenna reflectors has been investigated with the integrated Composites Analyzer (ICAN) computer code. Parametric studies have been conducted on the face sheets and honeycomb core which constitute the sandwich-type structures. Selected thermal and mechanical properties of the composite faces and sandwich structures are presented graphically as functions of varying fiber volume ratio, temperature, and moisture content. The coefficients of thermal expansion are discussed in detail since these are the critical design parameters. In addition, existing experimental data are presented and compared to the ICAN predictions. Author

A87-38615* National Aeronautics and Space Administration. Langley Research Center, Hampton, Va.

THERMAL EXPANSION BEHAVIOR OF GRAPHITE/GLASS AND GRAPHITE/MAGNESIUM

STEPHEN S. TOMPKINS (NASA, Langley Research Center, Hampton, VA), K. E. ARD (Harris Corp., Aerospace Systems Div., Melbourne, FL), and G. RICHARD SHARP (NASA, Lewis Research Center, Cleveland, OH) IN: International SAMPE Technical Conference, 18th, Seattle, WA, Oct. 7-9, 1986, Proceedings. Covina, CA, Society for the Advancement of Material and Process Engineering, 1986, p. 623-637. refs

The thermal expansion behavior of n (+/- 8)s graphite fiber reinforced magnesium laminate and four graphite reinforced glass-matrix laminates (a unidirectional laminate, a quasi-isotropic laminate, a symmetric low angle-ply laminate, and a random chopped-fiber mat laminate) was determined, and was found, in all cases, to not be significantly affected by thermal cycling. Specimens were cycled up to 100 times between -200 F and 100 F, and the thermal expansion coefficients determined for each material as a function of temperature were found to be low. Some dimensional changes as a function of thermal cycling, and some thermal-strain hysteresis, were observed. R.R.

A87-42684*# Energy Research Corp., Danbury, Conn.

CORROSION OF GRAPHITE COMPOSITES IN PHOSPHORIC ACID FUEL CELLS

L. G. CHRISTNER (Energy Research Corp., Danbury, CT), H. P. DHAR, M. FAROOQUE, and A. K. KUSH National Association of Corrosion Engineers, International Corrosion Forum, Houston, TX, Mar. 17-21, 1986. Paper. 10 p. refs (Contract DEN3-290)

Polymers, polymer-graphite composites and different carbon materials are being considered for many of the fuel cell stack components. Exposure to concentrated phosphoric acid in the fuel cell environment and to high anodic potential results in corrosion. Relative corrosion rates of these materials, failure modes, plausible mechanisms of corrosion and methods for improvement of these materials are investigated. Author

A87-49799* National Aeronautics and Space Administration. Lewis Research Center, Cleveland, Ohio.

MECHANICAL AND ELECTRICAL PROPERTIES OF GRAPHITE FIBER-EPOXY COMPOSITES MADE FROM PRISTINE AND BROMINE INTERCALATED FIBERS

DONALD A. JAWORSKE, RAYMOND D. VANNUCCI (NASA, Lewis Research Center, Cleveland, OH), and REZA ZINOLABEDINI (Cleveland State University, OH) *Journal of Composite Materials* (ISSN 0021-9983), vol. 21, June 1987, p. 580-592. refs

The mechanical and electrical properties of pristine and bromine intercalated graphite fiber-epoxy composites were compared. The two types of composite were similar in terms of tensile modulus, tensile strength, and Poisson's Ratio. However, the interlaminar shear strength of the brominated composite was 18 percent greater than its pristine counterpart. Only slight differences were observed in flexural properties. A five-fold decrease was observed in the electrical resistivity of the brominated composite parallel to the axis of the fibers, resulting in a unidirectional resistivity of about 90 microOmega/cm. Transverse resistivity was unaffected. Both types of composite were subjected to a simulated lightning strike of 10 KJ (at a peak current of 150 kA), and the composite with the intercalated graphite exhibited less damage. Author

A87-50094* National Aeronautics and Space Administration. Lewis Research Center, Cleveland, Ohio.

MECHANICAL PROPERTIES OF SiC FIBER-REINFORCED REACTION-BONDED Si3N4 COMPOSITES

RAMAKRISHNA T. BHATT (NASA, Lewis Research Center, Cleveland, OH) IN: Tailoring multiphase and composite ceramics; *Proceedings of the Twenty-first University Conference on Ceramic Science*, University Park, PA, July 17-19, 1985. New York, Plenum Press, 1986, p. 675-686. Previously announced in STAR as N85-34223. refs

The room temperature mechanical and physical properties of silicon carbide fiber reinforced reaction-bonded silicon nitride composites (SiC/RBSN) have been evaluated. The composites contained 23 and 40 volume fraction of aligned 140 micro m diameter chemically vapor deposited SiC fibers. Preliminary results for composite tensile and bend strengths and fracture strain indicate that the composites displayed excellent properties when compared with unreinforced RBSN of comparable porosity. Fiber volume fraction showed little influence on matrix first cracking strain but did influence the stressed required for matrix first cracking and for ultimate composite fracture strength. It is suggested that by reducing matrix porosity and by increasing the volume fraction of the large diameter SiC fiber, it should be possible to further improve the composite stress at which the matrix first cracks. Author

N87-13491*# National Aeronautics and Space Administration. Lewis Research Center, Cleveland, Ohio.

COMPOSITE INTERLAMINAR FRACTURE TOUGHNESS: THREE-DIMENSIONAL FINITE ELEMENT MODELING FOR MIXED MODE 1, 2 AND 3 FRACTURE

P. L. N. MURTHY (Cleveland State Univ., Ohio) and C. C. CHAMIS 1986 27 p Presented at the 8th Symposium on Composite Materials Testing and Design, Charleston, S. Car., 28-30 Apr. 1986; sponsored by the American Society for Testing and Materials

(NASA-TM-88872; E-3278; NAS 1.15:88872) Avail: NTIS HC A03/MF A01 CSCL 71F

A computational method/procedure is described which can be used to simulate individual and mixed mode interlaminar fracture progression in fiber composite laminates. Different combinations of Modes 1, 2, and 3 fracture are simulated by varying the crack location through the specimen thickness and by selecting appropriate unsymmetric laminate configurations. The contribution of each fracture mode to strain energy release rate is determined by the local crack closure methods while the mixed mode is determined by global variables. The strain energy release rates are plotted versus extending crack length, where slow crack growth, stable crack growth, and rapid crack growth regions are easily identified. Graphical results are presented to illustrate the effectiveness and versatility of the computational simulation for:

(1) evaluating mixed-mode interlaminar fracture, (2) for identifying respective dominant parameters, and (3) for selecting possible simple test methods. Author

N87-16071*# National Aeronautics and Space Administration. Lewis Research Center, Cleveland, Ohio.

PMR POLYIMIDE COMPOSITIONS FOR IMPROVED PERFORMANCE AT 371 DEG C

RAYMOND D. VANNUCCI 1987 13 p Prepared for presentation at the 32nd International SAMPE Symposium and Exhibition, Anaheim, Calif., 6-9 Apr. 1987 (NASA-TM-88942; E-3390; NAS 1.15:88942) Avail: NTIS HC A02/MF A01 CSCL 11D

Studies were conducted to identify matrix resins which have potential for use at 371 C (700 F). Utilizing PMR methodology, neat resin moldings were prepared with various monomer reactants and screened for thermo-oxidative stability at 371 C (700 F) under both ambient and a four-atmosphere air pressure. The results of the resin screening studies indicate that high molecular weight (HMW) formulated resins of first (PMR-15) and second (PMR-II) generation PMR materials exhibit lower levels of weight loss at 371 C (700 F) than PMR-15 and PMR-II resins. The resin systems which exhibited the best overall balance of processability, Tg and thermo-oxidative stability at 371 C were used to prepare unidirectional Celion 6000 and T-40R graphite fiber laminates. Laminates were evaluated for thermo-oxidative stability and 371 C mechanical properties. Results of the laminate evaluation studies indicate that two of the resin compositions have potential for use in 371 C applications. The most promising resin composition provided laminates which exhibited no drop in 371 C mechanical properties and only 11 percent weight loss after 200 hr exposure to 4 atmospheres of air at 371 C. Author

N87-16880*# National Aeronautics and Space Administration. Lewis Research Center, Cleveland, Ohio.

COMPOSITE SPACE ANTENNA STRUCTURES: PROPERTIES AND ENVIRONMENTAL EFFECTS

CAROL A. GINTY and NED M. ENDRES (Sverdrup Technology, Inc., Cleveland, Ohio) 1986 22 p Presented at the 18th International SAMPE Technical Conference, Seattle, Wash., 7-9 Oct. 1986

(NASA-TM-88859; E-3225; NAS 1.15:88859) Avail: NTIS HC A02/MF A01 CSCL 11D

The thermal behavior of composite spacecraft antenna reflectors has been investigated with the integrated Composites Analyzer (ICAN) computer code. Parametric studies have been conducted on the face sheets and honeycomb core which constitute the sandwich-type structures. Selected thermal and mechanical properties of the composite faces and sandwich structures are presented graphically as functions of varying fiber volume ratio, temperature, and moisture content. The coefficients of thermal expansion are discussed in detail since these are the critical design parameters. In addition, existing experimental data are presented and compared to the ICAN predictions. Author

N87-17861*# Gougeon Bros., Inc., Bay City, Mich.

DESIGN OF AN ADVANCED WOOD COMPOSITE ROTOR AND DEVELOPMENT OF WOOD COMPOSITE BLADE TECHNOLOGY Final Report

THOMAS STROEBEL, CURTIS DECHOW, and MICHAEL ZUTECK Dec. 1984 195 p

(Contract DEN3-260; DE-AI01-79ET-20320)

(NASA-CR-174713; DOE/NASA/O260-1; NAS 1.26:174713; GBI-ER-11) Avail: NTIS HC A09/MF A01 CSCL 11D

In support of a program to advance wood composite wind turbine blade technology, a design was completed for a prototype, 90-foot diameter, two-bladed, one-piece rotor, with all wood/epoxy composite structure. The rotor was sized for compatibility with a generator having a maximum power rating of 4000 kilowatts. Innovative features of the rotor include: a teetering hub to minimize the effects of gust loads, untwisted blades to promote rotor power control through stall, joining of blades to the hub structure via an adhesive bonded structural joint, and a blade structural design

which was simplified relative to earlier efforts. The prototype rotor was designed to allow flexibility for configuring the rotor upwind or downwind of the tower, for evaluating various types of teeter dampers and/or elastomeric stops, and with variable delta-three angle settings of the teeter shaft axis. The prototype rotor was also designed with provisions for installing pressure tap and angle of attack instrumentation in one blade. A production version rotor cost analysis was conducted. Included in the program were efforts directed at developing advanced load take-off stud designs for subsequent evaluation testing by NASA, development of aerodynamic tip brake concepts, exploratory testing of a wood/epoxy/graphite concept, and compression testing of wood/epoxy laminate, with scarf-jointed plies. Author

N87-18614*# National Aeronautics and Space Administration. Lewis Research Center, Cleveland, Ohio.

COMPUTATIONAL COMPOSITE MECHANICS FOR AEROSPACE PROPULSION STRUCTURES

CHRISTOS C. CHAMIS 1987 19 p Presented at the 3rd Space Systems Technology Conference, San Diego, Calif., 9-12 Jun. 1986; sponsored by the AIAA Previously announced in IAA as A86-40596

(NASA-TM-88965; E-3023; NAS 1.15:88965) Avail: NTIS HC A02/MF A01 CSCL 11D

Specialty methods are presented for the computational simulation of specific composite behavior. These methods encompass all aspects of composite mechanics, impact, progressive fracture and component specific simulation. Some of these methods are structured to computationally simulate, in parallel, the composite behavior and history from the initial fabrication through several missions and even to fracture. Select methods and typical results obtained from such simulations are described in detail in order to demonstrate the effectiveness of computationally simulating: (1) complex composite structural behavior in general, and (2) specific aerospace propulsion structural components in particular. Author

N87-18615*# National Aeronautics and Space Administration. Lewis Research Center, Cleveland, Ohio.

CERAMIC MATRIX AND RESIN MATRIX COMPOSITES: A COMPARISON

FRANCES I. HURWITZ 1987 14 p Presented at the 32nd National SAMPE Symposium and Exhibition, Anaheim, Calif., 6-9 Apr. 1987

(NASA-TM-89830; E-3481; NAS 1.15:89830) Avail: NTIS HC A02/MF A01 CSCL 11D

The underlying theory of continuous fiber reinforcement of ceramic matrix and resin matrix composites, their fabrication, microstructure, physical and mechanical properties are contrasted. The growing use of organometallic polymers as precursors to ceramic matrices is discussed as a means of providing low temperature processing capability without the fiber degradation encountered with more conventional ceramic processing techniques. Examples of ceramic matrix composites derived from particulate-filled, high char yield polymers and silsesquioxane precursors are provided. Author

N87-20387*# Pratt and Whitney Aircraft, East Hartford, Conn. Engineering Div.

ADVANCED COMPOSITE COMBUSTOR STRUCTURAL CONCEPTS PROGRAM Final Report

M. A. SATTAR and R. P. LOHMANN Dec. 1984 118 p (Contract NAS3-23284)

(NASA-CR-174733; NAS 1.26:174733; PWA-5890-24) Avail: NTIS HC A06/MF A01 CSCL 11D

An analytical study was conducted to assess the feasibility of and benefits derived from the use of high temperature composite materials in aircraft turbine engine combustor liners. The study included a survey and screening of the properties of three candidate composite materials including tungsten reinforced superalloys, carbon-carbon and silicon carbide (SiC) fibers reinforcing a ceramic matrix of lithium aluminosilicate (LAS). The SiC-LAS material was selected as offering the greatest near term potential primarily on

the basis of high temperature capability. A limited experimental investigation was conducted to quantify some of the more critical mechanical properties of the SiC-LAS composite having a multidirection 0/45/-45/90 deg fiber orientation favored for the combustor liner application. Rigorous cyclic thermal tests demonstrated that SiC-LAS was extremely resistant to the thermal fatigue mechanisms that usually limit the life of metallic combustor liners. A thermal design study led to the definition of a composite liner concept that incorporated film cooled SiC-LAS shingles mounted on a Hastelloy X shell. With coolant fluxes consistent with the most advanced metallic liner technology, the calculated hot surface temperatures of the shingles were within the apparent near term capability of the material. Structural analyses indicated that the stresses in the composite panels were low, primarily because of the low coefficient of expansion of the material and it was concluded that the dominant failure mode of the liner would be an as yet unidentified deterioration of the composite from prolonged exposure to high temperature. An economic study, based on a medium thrust size commercial aircraft engine, indicated that the SiC-LAS combustor liner would weigh 22.8N (11.27 lb) less and cost less to manufacture than advanced metallic liner concepts intended for use in the late 1980's. Author

N87-20389*# National Aeronautics and Space Administration. Lewis Research Center, Cleveland, Ohio.

STRAIN ENERGY RELEASE RATES OF COMPOSITE INTERLAMINAR END-NOTCH AND MIXED-MODE FRACTURE: A SUBLAMINATE/PLY LEVEL ANALYSIS AND A COMPUTER CODE

R. R. VALISETTY and C. C. CHAMIS Apr. 1987 88 p Presented at the 8th Symposium on Composite Materials Testing and Design, Charleston, S.C., 29 Apr. - 1 May 1986; sponsored by the American Society for Testing and Materials

(NASA-TM-89827; E-3476; NAS 1.15:89827) Avail: NTIS HC A05/MF A01 CSCL 11D

A computer code is presented for the sublaminate/ply level analysis of composite structures. This code is useful for obtaining stresses in regions affected by delaminations, transverse cracks, and discontinuities related to inherent fabrication anomalies, geometric configurations, and loading conditions. Particular attention is focussed on those layers or groups of layers (sublaminae) which are immediately affected by the inherent flaws. These layers are analyzed as homogeneous bodies in equilibrium and in isolation from the rest of the laminate. The theoretical model used to analyze the individual layers allows the relevant stresses and displacements near discontinuities to be represented in the form of pure exponential-decay-type functions which are selected to eliminate the exponential-precision-related difficulties in sublaminate/ply level analysis. Thus, sublaminate analysis can be conducted without any restriction on the maximum number of layers, delaminations, transverse cracks, or other types of discontinuities. In conjunction with the strain energy release rate (SERR) concept and composite micromechanics, this computational procedure is used to model select cases of end-notch and mixed-mode fracture specimens. The computed stresses are in good agreement with those from a three-dimensional finite element analysis. Also, SERRs compare well with limited available experimental data. Author

N87-21043*# National Aeronautics and Space Administration. Lewis Research Center, Cleveland, Ohio.

STYRENE-TERMINATED POLYSULFONE OLIGOMERS AS MATRIX MATERIAL FOR GRAPHITE REINFORCED COMPOSITES: AN INITIAL STUDY

DANA GARCIA (Goodrich, B. F. Co., Brecksville, Ohio), KENNETH J. BOWLES, and RAYMOND D. VANNUCCI Apr. 1987 30 p

(NASA-TM-89846; E-3472; NAS 1.15:89846) Avail: NTIS HC A03/MF A01 CSCL 11D

Styrene terminated polysulfone oligomers are part of an oligomeric class of compounds with end groups capable of thermal polymerization. These materials can be used as matrices for graphite reinforced composites. The initial evaluation of styrene terminated polysulfone oligomer based composites are summarized

in terms of fabrication methods, and mechanical and environmental properties. In addition, a description and evaluation is provided of the NASA/Industry Fellowship Program for Technology Transfer.

Author

N87-22811*# National Aeronautics and Space Administration. Lewis Research Center, Cleveland, Ohio.

FIBER REINFORCED SUPERALLOYS

DONALD W. PETRASEK, ROBERT A. SIGNORELLI, THOMAS CAULFIELD, and JOHN K. TIEN (Columbia Univ., New York.) Apr. 1987 62 p

(NASA-TM-89865; E-3533; NAS 1.15:89865) Avail: NTIS HC A04/MF A01 CSCL 11D

Improved performance of heat engines is largely dependent upon maximum cycle temperatures. Tungsten fiber reinforced superalloys (TFRS) are the first of a family of high temperature composites that offer the potential for significantly raising hot component operating temperatures and thus leading to improved heat engine performance. This status review of TFRS research emphasizes the promising property data developed to date, the status of TFRS composite airfoil fabrication technology, and the areas requiring more attention to assure their applicability to hot section components of aircraft gas turbine engines.

Author

N87-25432*# National Aeronautics and Space Administration. Lewis Research Center, Cleveland, Ohio.

SILSESQUOXANES AS PRECURSORS TO CERAMIC COMPOSITES

FRANCES I. HURWITZ, LIZBETH H. HYATT, JOY GORECKI, and LISA DAMORE Jan. 1987 16 p Presented at the 11th Annual Conference on Composites, Advanced Ceramics, and Composite Materials, Cocoa Beach, Fla., 18-23 Jan. 1987; cosponsored by NASA, American Ceramic Society and DOD (NASA-TM-89893; E-3581; NAS 1.15:89893) Avail: NTIS HC A02/MF A01 CSCL 11D

Silsesquioxanes having the general structure RSiO_2 sub 1.5, where R = methyl, propyl, or phenyl, melt flow at 70 to 100 C. Above 100 C, free -OH groups condense. At 225 C further crosslinking occurs, and the materials form thermosets. Pyrolysis, with accompanying loss of volatiles, takes place at nominally 525 C. At higher temperatures, the R group serves as an internal carbon source for carbo-thermal reduction to SiC accompanied by the evolution of CO. By blending silsesquioxanes with varying R groups, both the melt rheology and composition of the fired ceramic can be controlled. Fibers can be spun from the melt which are stable in argon in 1400 C. The silsesquioxanes also were used as matrix precursors for Nicalon and alpha-SiC platelet reinforced composites.

Author

N87-28611*# National Aeronautics and Space Administration. Lewis Research Center, Cleveland, Ohio.

DYNAMIC DELAMINATION BUCKLING IN COMPOSITE LAMINATES UNDER IMPACT LOADING: COMPUTATIONAL SIMULATION

JOSEPH E. GRADY, CHRISTOS C. CHAMIS, and ROBERT A. AIELLO 1987 14 p Presented at the 2nd Symposium on Composite Materials: Fatigue and Fracture, Cincinnati, Ohio, 26-30 Apr. 1987; sponsored by the American Society for Testing and Materials

(NASA-TM-100192; E-3779; NAS 1.15:100192) Avail: NTIS HC A02/MF A01 CSCL 11D

A unique dynamic delamination buckling and delamination propagation analysis capability has been developed and incorporated into a finite element computer program. This capability consists of the following: (1) a modification of the direct time integration solution sequence which provides a new analysis algorithm that can be used to predict delamination buckling in a laminate subjected to dynamic loading, and (2) a new method of modeling the composite laminate using plate bending elements and multipoint constraints. This computer program is used to predict both impact induced buckling in composite laminates with initial delaminations and the strain energy release rate due to extension of the delamination. It is shown that delaminations near the outer

surface of a laminate are susceptible to local buckling and buckling-induced delamination propagation when the laminate is subjected to transverse impact loading. The capability now exists to predict the time at which the onset of dynamic delamination buckling occurs, the dynamic buckling mode shape, and the dynamic delamination strain energy release rate.

Author

N87-28612*# Dayton Univ., Ohio.

DESIGN OF TEST SPECIMENS AND PROCEDURES FOR GENERATING MATERIAL PROPERTIES OF DOUGLAS FIR/EPOXY LAMINATED WOOD COMPOSITE MATERIAL: WITH THE GENERATION OF BASELINE DATA AT TWO ENVIRONMENTAL CONDITIONS Final Report, Mar. 1982 - Mar. 1985

PAUL E. JOHNSON Jul. 1985 47 p

(Contract DEN3-286; DE-AI01-79ET-20320)

(NASA-CR-174910; NAS 1.26:174910; DOE/NASA-0286-1;

UDR-TR-85-45) Avail: NTIS HC A03/MF A01 CSCL 11D

In support of the design of wind turbine generator airfoils/blades utilizing Douglas Fir/West System Epoxy laminated composite material, a program was undertaken to define pertinent material properties utilizing small scale test specimens. Task 1 was the development of suitable monotonic tension, compression, short beam shear and full reversed cyclic specimen designs and the companion grips and testing procedures. Task 2 was the generation of the material properties at two environmental conditions utilizing the specimens and procedures developed in Task 1. The monotonic specimens and procedures generated results which compare favorably with other investigators while the cyclic results appear somewhat conservative. Adding moisture and heat or scarf joints degraded the monotonic performance but had a more nebulous effect with cyclic loading.

Author

25

INORGANIC AND PHYSICAL CHEMISTRY

Includes chemical analysis, e.g., chromatography; combustion theory; electrochemistry; and photochemistry.

A87-12598* Pennsylvania State Univ., University Park.

SHOCK-TUBE PYROLYSIS OF ACETYLENE - SENSITIVITY ANALYSIS OF THE REACTION MECHANISM FOR SOOT FORMATION

M. FRENKLACH (Pennsylvania State University, University Park), D. W. CLARY (Louisiana State University; Ethyl Corp., Baton Rouge, LA), W. C. GARDINER, JR. (Louisiana State University, Baton Rouge; Texas, University, Austin), and S. E. STEIN (Louisiana State University, Baton Rouge; NBS, Chemical Kinetics Div., Washington, DC) IN: Shock waves and shock tubes; Proceedings of the Fifteenth International Symposium, Berkeley, CA, July 28-August 2, 1985. Stanford, CA, Stanford University Press, 1986, p. 295-301. Research supported by the Robert A. Welch Foundation. refs

(Contract NAG3-477; NASA ORDER C-80000-E)

The impact of thermodynamic parameters on the sensitivity of model predictions of soot formation by shock-tube pyrolysis of acetylene were assessed analytically. The pyrolysis process was treated as having three components: initiation, the initial pyrolysis stages; cyclization, formation of larger molecules and radicals and small aromatic molecules; and polymerization, further growth of aromatic rings. Rate equations are reviewed for each component. Thermodynamic effects were assessed by varying the C2H-H and C2H3-H bond energies and the Ct-(Ct) group additivity value. Any change in the C2H-H bond energy had a significant impact on the temperature and the maximum amount of the soot yield. The findings underscore the necessity of using accurate thermodynamic data for modeling high-temperature chemical kinetics.

M.S.K.

A87-12599* Louisiana State Univ., Baton Rouge.
EMPIRICAL MODELING OF SOOT FORMATION IN SHOCK-TUBE PYROLYSIS OF AROMATIC HYDROCARBONS
M. FRENKLACH, D. W. CLARY, and R. A. MATULA (Louisiana State University, Baton Rouge) IN: Shock waves and shock tubes; Proceedings of the Fifteenth International Symposium, Berkeley, CA, July 28-August 2, 1985. Stanford, CA, Stanford University Press, 1986, p. 303-309. refs
(Contract DE-FG22-80PC-30247; NAS3-23542; NAG3-477)

A method for empirical modeling of soot formation during shock-tube pyrolysis of aromatic hydrocarbons is developed. The method is demonstrated using data obtained in pyrolysis of argon-diluted mixtures of toluene behind reflected shock waves. The developed model is in good agreement with experiment.

Author

A87-12602* Technion - Israel Inst. of Tech., Haifa.
IGNITION DELAY TIMES OF CYCLOPENTENE OXYGEN ARGON MIXTURES

A. BURCAT (Technion - Israel Institute of Technology, Haifa), C. SNYDER, and T. BRABBS (NASA, Lewis Research Center, Cleveland, OH) IN: Shock waves and shock tubes; Proceedings of the Fifteenth International Symposium, Berkeley, CA, July 28-August 2, 1985. Stanford, CA, Stanford University Press, 1986, p. 335-341. refs

The oxidation of cyclopentene was studied experimentally to expand the database on pyrolysis and the reaction products of five carbon unsaturated ring compounds. Pyrolysis was carried out in a single-pulse shock tube. Data were gathered on the shock speed, wall pressure, and reflected shock temperatures. Four different mixtures of C₅H₈, O₂ and Ar, ranging from 0.25-1 percent cyclopentene and 1.75-7 percent O₂, were examined in 76 different trials. The data showed a shock temperature range of 1323-1816 K and a pressure range of 1.67-7.36 atmospheres. A student-t test analysis of the results led to definition of an ignition delay equation accurate to the 2-sigma level.

M.S.K.

A87-14116*# California Univ., Los Angeles.
THE FLAME STRUCTURE AND VORTICITY GENERATED BY A CHEMICALLY REACTING TRANSVERSE JET

A. R. KARAGOZIAN (California, University, Los Angeles) AIAA Journal (ISSN 0001-1452), vol. 24, Sept. 1986, p. 1502-1507. refs

(Contract NSF MEA-83-05960; NAG3-543)

An analytical model describing the behavior of a turbulent fuel jet injected normally into a cross flow is developed. The model places particular emphasis on the contrarotating vortex pair associated with the jet, and predicts the flame length and shape based on entrainment of the oxidizer by the fuel jet. Effects of buoyancy and density variations in the flame are neglected in order to isolate the effects of large-scale mixing. The results are compared with a simulation of the transverse reacting jet in a liquid (acid-base) system. For a wide range of ratios of the cross flow to jet velocity, the model predicts flame length quite well. In particular, the observed transitional behavior in the flame length between cross-flow velocity to jet velocity of orifice ratios of 0.0 to 0.1, yielding an approximate minimum at the ratio 0.05, is reproduced very clearly by the present model. The transformation in flow structure that accounts for this minimum arises from the differing components of vorticity dominant in the near-field and far-field regions of the jet.

Author

A87-15983*# California Univ., La Jolla.
GRAVITATIONAL EFFECTS ON THE STRUCTURE AND PROPAGATION OF PREMIXED FLAMES

A. HAMINS, M. HEITOR, and P. A. LIBBY (California, University, La Jolla) IAF, International Astronautical Congress, 37th, Innsbruck, Austria, Oct. 4-11, 1986. 18 p. refs
(Contract NAG3-654)

(IAF PAPER 86-279)

The effect of gravity on the propagation velocity and shape of premixed laminar and turbulent flames was studied experimentally, using vertical tubes of two diameter sizes, over the entire

flammability range of methane-air mixtures. In the smaller (5-cm-diam) tube, steady laminar flames with a nearly hemispherical shape were observed, with the upward moving flames propagating faster than the downward moving flames. In the larger (10-cm-diam) tube, the upward propagating flames in both lean and rich mixtures were faster than the downward ones, with the upward propagating flames being roughly hemispherical and the downward propagating flames nearly flat, often with a cellular structure.

I.S.

A87-20223* Pittsburgh Univ., Pa.
REACTIONS OCCURRING DURING THE SULFATION OF SODIUM CHLORIDE DEPOSITED ON ALUMINA SUBSTRATES

C. S. WU (China Steel Corp., Republic of China) and N. BIRKS (Pittsburgh, University, PA) Electrochemical Society, Journal (ISSN 0013-4651), vol. 133, Oct. 1986, p. 2185-2193. refs
(Contract NAG3-44)

The reaction between solid NaCl and air containing 1 pct SO₂ has been studied between 500 and 700 C. The reaction product, Na₂SO₄, forms not only on the surface of the NaCl but also on surrounding areas of the substrate due to the volatility of the NaCl at these temperatures. At the higher temperatures, the vapor pressure of NaCl is so high that the majority of the reaction product is distributed on the substrate. Above 625 C, the reaction product is a liquid solution of NaCl and Na₂SO₄ that exists only so long as NaCl is supplied from the original crystal source. Eventually, the liquid solidifies by constitutional solidification as the NaCl is converted to Na₂SO₄. While it exists, the liquid NaCl-Na₂SO₄ solution is shown to be highly corrosive to Al₂O₃ and, on a scale of Al₂O₃ growing on alloy HOS 875, particularly attacks the grain boundaries of the scale at preferred sites where chromium and iron oxides and sulfides rapidly develop. This is proposed as one mechanism by which NaCl deposition contributes to the initiation of low temperature hot corrosion.

Author

A87-23241* Westinghouse Electric Corp., Pittsburgh, Pa.
MATERIALS CHARACTERIZATION OF PHOSPHORIC ACID FUEL CELL SYSTEM

SRINIVASAN VENKATESH (Westinghouse Electric Corp., Advanced Energy Systems Div., Pittsburgh, PA) National Association of Corrosion Engineers, International Corrosion Forum, Houston, TX, Mar. 17-21, 1986, Paper. 6 p. DOE-supported research. refs

(Contract DEN3-290)

The component materials used in the fabrication of phosphoric acid fuel cells (PAFC) must have mechanical, chemical, and electrochemical stability to withstand the moderately high temperature (200 C) and pressure (500 kPa) and highly oxidizing nature of phosphoric acid. This study discusses the chemical and structural stability, performance and corrosion data on certain catalysts, catalyst supports, and electrode support materials used in PAFC applications.

Author

A87-27165* National Aeronautics and Space Administration.
Lewis Research Center, Cleveland, Ohio.

CORROSION PITTING OF SiC BY MOLTEN SALTS
N. S. JACOBSON and J. L. SMIALEK (NASA, Lewis Research Center, Cleveland, OH) Electrochemical Society, Journal (ISSN 0013-4651), vol. 133, Dec. 1986, p. 2615-2621. refs

The corrosion of SiC by thin films of Na₂CO₃ and Na₂SO₄ at 1000 C is characterized by a severe pitting attack of the SiC substrate. A range of different Si and SiC substrates were examined to isolate the factors critical to pitting. Two types of pitting attack are identified: attack at structural discontinuities and a crater-like attack. The crater-like pits are correlated with bubble formation during oxidation of the SiC. It appears that bubbles create unprotected regions, which are susceptible to enhanced attack and, hence, pit formation.

Author

A87-27400* National Aeronautics and Space Administration. Lewis Research Center, Cleveland, Ohio.

CONCENTRATION OF CARBON DIOXIDE BY A HIGH-TEMPERATURE ELECTROCHEMICAL MEMBRANE CELL
M. P. KANG (NASA, Lewis Research Center, Cleveland, OH; Georgia Institute of Technology, Atlanta) and J. WINNICK (Georgia Institute of Technology, Atlanta) *Journal of Applied Electrochemistry* (ISSN 0021-891X), vol. 15, 1985, p. 431-439. NASA-supported research. refs

The performance of a molten carbonate carbon dioxide concentrator (MCCDC) cell, as a device for removal of CO₂ from manned spacecraft cabins without fuel expenditure, is investigated. The test system consists of an electrochemical cell (with an Li₂CO₃-38 mol pct K₂CO₃ membrane contained in a LiAlO₂ matrix), a furnace, and a flow IR analyzer for monitoring CO₂. Operation of the MCCDC-driven cell was found to be suitable for the task of CO₂ removal: the cell performed at extremely low CO₂ partial pressures (at or above 0.1 mm Hg); cathode CO₂ efficiencies of 97 percent were achieved with 0.25 CO₂ inlet concentration at 19 mA sq cm, at temperatures near 873 K. Anode concentrations of up to 5.8 percent were obtained. Simple cathode and anode performance equations applied to correlate cell performance agreed well with those measured experimentally. A flow diagram for the process is included. I.S.

A87-33987*# Pennsylvania State Univ., University Park.

SYSTEMATIC DEVELOPMENT OF REDUCED REACTION MECHANISMS FOR DYNAMIC MODELING

M. FRENKLACH (Pennsylvania State University, University Park), K. KAILASANATH, and E. S. ORAN (U.S. Navy, Naval Research Laboratory, Washington, DC) IN: Dynamics of reactive systems; International Colloquium on Dynamics of Explosions and Reactive Systems, 10th, Berkeley, CA, Aug. 4-9, 1985, Technical Papers. Part 2. New York, American Institute of Aeronautics and Astronautics, Inc., 1986, p. 365-376. Navy-supported research. refs

(Contract NAG3-477)

A method for systematically developing a reduced chemical reaction mechanism for dynamic modeling of chemically reactive flows is presented. The method is based on the postulate that if a reduced reaction mechanism faithfully describes the time evolution of both thermal and chain reaction processes characteristic of a more complete mechanism, then the reduced mechanism will describe the chemical processes in a chemically reacting flow with approximately the same degree of accuracy. Here this postulate is tested by producing a series of mechanisms of reduced accuracy, which are derived from a full detailed mechanism for methane-oxygen combustion. These mechanisms were then tested in a series of reactive flow calculations in which a large-amplitude sinusoidal perturbation is applied to a system that is initially quiescent and whose temperature is high enough to start ignition processes. Comparison of the results for systems with and without convective flow show that this approach produces reduced mechanisms that are useful for calculations of explosions and detonations. Extensions and applicability to flames are discussed. Author

A87-38787*# National Aeronautics and Space Administration. Lewis Research Center, Cleveland, Ohio.

DIFFUSION FLAME EXTINCTION IN SLOW CONVECTION FLOW UNDER MICROGRAVITY ENVIRONMENT

CHIUN-HSUN CHEN (NASA, Lewis Research Center, Cleveland, OH) IN: Symposium on Microgravity Fluid Mechanics; Proceedings of the Winter Annual Meeting, Anaheim, CA, Dec. 7-12, 1986. New York, American Society of Mechanical Engineers, 1986, p. 13-23. Previously announced in STAR as N86-28378. refs

A theoretical analysis is presented to study the extinction characteristics of a diffusion flame near the leading edge of a thin fuel plate in slow, forced convective flows in a microgravity environment. The mathematical model includes two-dimensional Navier-Stokes momentum, energy and species equations with one-step overall chemical reaction using second-order finite rate Arrhenius kinetics. Radiant heat loss on the fuel plate is applied

in the model as it is the dominant mechanism for flame extinguishment in the small convective flow regime. A parametric study based on the variation of convective flow velocity, which varies the Damkchler number (Da), and the surface radiant heat loss parameter (S) simultaneously, is given. An extinction limit is found in the regime of slow convective flow when the rate of radiant heat loss from fuel surface outweighs the rate of heat generation due to combustion. The transition from existent envelope flame to extinguishment consists of gradual flame contraction in the opposed flow direction together with flame temperature reduction as the convective flow velocity decreases continuously until the extinction limit is reached. A case of flame structure subjected to surface radiant heat loss is also presented and discussed. Author

A87-38958*# National Aeronautics and Space Administration. Lewis Research Center, Cleveland, Ohio.

FAST ALGORITHM FOR CALCULATING CHEMICAL KINETICS IN TURBULENT REACTING FLOW

K. RADHAKRISHNAN (NASA, Lewis Research Center, Cleveland, OH) and D. T. PRATT (Aerofect Propulsion Research Institute, Sacramento, CA) IN: Calculations of turbulent reactive flows; Proceedings of the Winter Annual Meeting, Anaheim, CA, Dec. 7-12, 1986. New York, American Society of Mechanical Engineers, 1986, p. 313-334. refs

(Contract NAG3-294; NAS3-24105)

This paper addresses the need for a fast batch chemistry solver to perform the kinetics part of a split operator formulation of turbulent reacting flows, with special attention focused on the solution of the ordinary differential equations governing a homogeneous gas-phase chemical reaction. For this purpose, a two-part predictor-corrector algorithm which incorporates an exponentially fitted trapezoidal method was developed. The algorithm performs filtering of ill-posed initial conditions, automatic step-size selection, and automatic selection of Jacobi-Newton or Newton-Raphson iteration for convergence to achieve maximum computational efficiency while observing a prescribed error tolerance. The new algorithm, termed CREK1D (combustion reaction kinetics, one-dimensional), compared favorably with the code LSODE when tested on two representative problems drawn from combustion kinetics, and is faster than LSODE. I.S.

A87-40572* California Univ., Berkeley.

FORCED COCURRENT SMOLDERING COMBUSTION

SUDIP S. DOSANJH, PATRICK J. PAGNI, and A. CARLOS FERNANDEZ-PELLO (California, University, Berkeley) *Combustion and Flames* (ISSN 0010-2180), vol. 68, May 1987, p. 131-142. refs

(Contract NAG3-443)

An analytical model of cocurrent smoldering combustion through a very porous solid fuel is developed. Smoldering is initiated at the top of a long radially insulated uniform fuel cylinder, so that the smolder wave propagates downward, opposing an upward-forced flow of oxidizer, with the solid fuel and the gaseous oxidizer entering the reaction zone from the same direction (hence, cocurrent). Radiative heat transfer was incorporated using a diffusion approximation, and smoldering was modeled using a one-step reaction mechanism. The results indicate that, for a given fuel, the final temperature depends only on the initial oxygen mass flux, increasing logarithmically with the mass flux. The smolder velocity is linearly dependent on the initial oxygen mass flux, and, at a fixed value of the flux, increases with initial oxygen mass fraction. The mathematical relationship determining the conditions for steady smolder propagation is presented. I.S.

A87-42677*# Energy Research Corp., Danbury, Conn.
ON THE EFFECT OF THE $Fe(2+)/Fe(3+)$ REDOX COUPLE ON OXIDATION OF CARBON IN HOT H_3PO_4

H. P. DHAR, L. G. CHRISTNER, and A. K. KUSH (Energy Research Corp., Danbury, CT) National Association of Corrosion Engineers, International Corrosion Forum, Houston, TX, Mar. 17-21, 1986, Paper. 15 p. refs
 (Contract DEN3-290)

Oxidation studies of graphite:glassy carbon composites have been carried out at 1 and 4.7 atm. pressures in conc. H_3PO_4 in the presence and absence of iron ions. The concentration of the acid was varied over 85-100 wt pct, and of the iron ions over 30-300 ppm; the temperature varied over 190-210 C. Unlike the effect of Fe, which has been observed to increase the corrosion of carbon in sulphuric acid, the corrosion in phosphoric acid was observed to be slightly decreased or not at all affected. This result arises because of the catalytic reduction of the oxidized surface groups of carbon by $Fe(2+)$ ions. The catalytic reduction is possible because under the experimental conditions the redox potential of the $Fe(2+)/Fe(3+)$ couple is lower than the open-circuit voltage of carbon.

Author

A87-51187* Ohio State Univ., Columbus.
OXYGEN-18 TRACER STUDY OF THE PASSIVE THERMAL OXIDATION OF SILICON

J. D. CAWLEY (Ohio State University, Columbus), J. W. HALLORAN (Ceramic Process Systems, Lexington, MA), and A. R. COOPER (Case Western Reserve University, Cleveland, OH) Oxidation of Metals (ISSN 0030-770X), vol. 28, Aug. 1987, p. 1-16. refs
 (Contract NSG-3291)

This work focuses on the thermal oxidation of silicon near 1273 K using the double-tracer oxidation method. The results confirm that oxidation occurs by the transport of electrically neutral nonnetwork oxygen through the interstitial space of the vitreous silica ($v\text{-SiO}_2$) scale. Simultaneously, self- (or isotopic-) diffusion occurs in the network, resulting in characteristic isotopic fraction distributions near the gas-scale interface. The self-diffusion coefficients calculated from these profiles agree with those reported for tracer diffusion in $v\text{-SiO}_2$, and the diffusion coefficient calculated from the scale growth is consistent with reported O_2 permeation data. An important parameter that describes the double-oxidation behavior is a ratio relating the scale thickness grown during the second oxidation, the network self-diffusion coefficient for oxygen, and the time of the second oxidation.

Author

A87-52248*# National Aeronautics and Space Administration. Lewis Research Center, Cleveland, Ohio.

SIZE AND SHAPE OF SOLID FUEL DIFFUSION FLAMES IN VERY SLOW SPEED FLOWS

CHIUN-HSUN CHEN (NASA, Lewis Research Center, Cleveland, OH), JAMES S. T'EN (Case Western Reserve University, Cleveland, OH), and DAVID W. FOUTCH AIAA, SAE, ASME, and ASEE, Joint Propulsion Conference, 23rd, San Diego, CA, June 29-July 2, 1987. 17 p. refs
 (Contract NGT-36-027-805)
 (AIAA PAPER 87-2030)

The influence of very low speed forced flows on the size and shape of a diffusion flame adjacent to a solid fuel slab is studied experimentally and theoretically. Velocities in the range of 1.5 to 6.3 cm/s and O_2 mole fractions (in the O_2/N_2 atmosphere) in the range of 0.15 to 0.19 were tested. The flames moved farther from the fuel surface as the flow velocity was reduced and closer to the sample as the O_2 concentration was lowered. A corresponding theoretical model was solved using a two-dimensional Navier-Stokes system with a one-step finite-rate chemical reaction and surface radiative loss.

K.K.

N87-11181*# National Aeronautics and Space Administration. Lewis Research Center, Cleveland, Ohio.

COMBUSTION OVERVIEW

D. F. SCHULTZ *In its* Turbine Engine Hot Section Technology, 1984 6 p. Oct. 1984

Avail: NTIS HC A17/MF A01 CSDL 21B

The objective of this effort is to develop improved analytical models of the internal combustor flow field and liner heat transfer as a means to shorten combustor development time and increase turbine engine hot section life. A four-element approach was selected to meet this objective. First, existing models were utilized to determine their deficiencies. Supporting research was then commenced to improve the existing models. While the research effort is in progress, the models are being refined to improve numerics and numerical diffusion. And lastly, the research results and improved numerics will be integrated into existing models.

Author

N87-11204*# National Aeronautics and Space Administration. Lewis Research Center, Cleveland, Ohio.

FLAME RADIATION

J. D. WEAR *In its* Turbine Engine Hot Section Technology, 1984 10 p. Oct. 1984

Avail: NTIS HC A17/MF A01 CSDL 21B

Total radiation and heat flux data was obtained on a combustor liner by advanced instrumentation. If the results obtained by the special instrumentation are considered to be representative of the total radiation and heat flux, then the effect of variation of engine operating parameters and of fuel type can be more easily obtained. The special instrumentation used for these investigations consisted of five total radiometers and two total heat flux gages. The radiometers were arranged axially and circumferentially through sliding air seals in the outer liner. The two heat flux gages were welded in the outer liner between two circumferential radiometers. Static pressures were obtained on both the cold and the hot side of the outer liner in the area of the heat flux gages. Liner metal temperatures were also obtained. The combustor inlet pressure was varied over a nominal range of 0.5 to 2.07 MPa, inlet air temperature from 550 to 670 K, and fuel-air ratio from about 0.015 to 0.040. The two fuels tested were ASTM Jet A and a fuel designated as ERBS V. Results of the tests are discussed. B.G.

N87-11858*# United Technologies Research Center, East Hartford, Conn.

USER'S MANUAL FOR A TEACH COMPUTER PROGRAM FOR THE ANALYSIS OF TURBULENT, SWIRLING REACTING FLOW IN A RESEARCH COMBUSTOR

L. M. CHIAPPETTA Sep. 1983 120 p

(Contract NAS3-22771)

(NASA-CR-179547; NAS 1.26:179547; R83-915540-27) Avail:

NTIS HC A06/MF A01 CSDL 21B

Described is a computer program for the analysis of the subsonic, swirling, reacting turbulent flow in an axisymmetric, bluff-body research combustor. The program features an improved finite-difference procedure designed to reduce the effects of numerical diffusion and a new algorithm for predicting the pressure distribution within the combustor. A research version of the computer program described in the report was supplied to United Technologies Research Center by Professor A. D. Gosman and his students, R. Benodeker and R. I. Issa, of Imperial College, London. The Imperial College staff also supplied much of the program documentation. Presented are a description of the mathematical model for flow within an axisymmetric bluff-body combustor, the development of the finite-difference procedure used to represent the system of equations, an outline of the algorithm for determining the static pressure distribution within the combustor, a description of the computer program including its input format, and the results for representative test cases.

Author

N87-20268*# National Aeronautics and Space Administration. Lewis Research Center, Cleveland, Ohio.

COMBUSTION RESEARCH IN THE INTERNAL FLUID MECHANICS DIVISION

EDWARD J. MULARZ *In its* NASA-Chinese Aeronautical Establishment (CAE) Symposium p 1-6 1986

Avail: NTIS HC A01/MF A01 CSCL 21B

The goal of this research is to bring computational fluid dynamics to a state of practical application for the aircraft engine industry. The approach is to have a strongly integrated computational and experimental program for all the disciplines associated with the gas turbine and other aeropropulsion systems by advancing the understanding of flow physics, heat transfer, and combustion processes. The computational and experimental research is integrated in the following way: the experiments that are performed provide an empirical data set so that physical models can be formulated to describe the processes that are occurring - for example, turbulence or chemical reaction. These experiments also form a data base for those who are doing code development by providing experimental data against which the codes can be verified and assessed. Models are generated as closure to some of the numerical codes, and they also provide physical insight for experiments. At the same time, codes which solve the complete Navier-Stokes equations can be used as a kind of numerical experiment from which far more extensive data can be obtained than ever could be obtained experimentally. This could provide physical insight into the complex processes that are taking place. These codes are also exercised against experimental data to assess the accuracy and applicability of models. Author

N87-22020*# Princeton Univ., N. J. Dept. of Mechanical and Aerospace Engineering.

THE OXIDATION DEGRADATION OF AROMATIC COMPOUNDS Final Report, 1 Sep. 1982 - 30 Aug. 1985

KENNETH BREZINSKY and IRVIN GLASSMAN May 1987 46 p

(Contract NAG3-310)

(NASA-CR-180588; NAS 1.26:180588) Avail: NTIS HC A03/MF A01 CSCL 07D

A series of experiments were conducted which focused on understanding the role that the O atom addition to aromatic rings plays in the oxidation of benzene and toluene. Flow reactor studies of the oxidation of toluene gave an indication of the amount of C atoms available during an oxidation and the degree to which the O atom adds to the ring. Flow reactor studies of the oxidation of toluene and benzene to which NO₂ was added, have shown that NO₂ appears to suppress the formation of O atoms and consequently reduce the amount of phenols and cresols formed by O atom addition. A high temperature pyrolysis study of phenol has confirmed that the major decomposition products are carbon monoxide and cyclopentadiene. A preliminary value for the overall decomposition rate constant was also obtained. Author

N87-23718*# National Aeronautics and Space Administration. Lewis Research Center, Cleveland, Ohio.

ELECTROCHEMICAL PERFORMANCE AND TRANSPORT PROPERTIES OF A NAFION MEMBRANE IN A HYDROGEN-BROMINE CELL ENVIRONMENT

RICHARD S. BALDWIN Jun. 1987 27 p

(NASA-TM-89862; E-3529; NAS 1.15:89862) Avail: NTIS HC A03/MF A01 CSCL 07D

The overall energy conversion efficiency of a hydrogen-bromine energy storage system is highly dependent upon the characteristics and performance of the ion-exchange membrane utilized as a half-cell separator. The electrochemical performance and transport properties of a duPont Nafion membrane in an aqueous HBr-Br₂ environment were investigated. Membrane conductivity data are presented as a function of HBr concentration and temperature for the determination of ohmic voltage losses across the membrane in an operational cell. Diffusion-controlled bromine permeation rates and permeabilities are presented as functions of solution composition and temperature. Relationships between the degree of membrane hydration and the membrane transport characteristics

are discussed. The solution chemistry of an operational hydrogen-bromine cell undergoing charge from 45% HBr to 5% HBr is discussed, and, based upon the experimentally observed bromine permeation behavior, predicted cell coulombic losses due to bromine diffusion through the membrane are presented as a function of the cell state-of-charge. M.G.

N87-23808* National Aeronautics and Space Administration. Langley Research Center, Hampton, Va.

MULTISPECIES CARS MEASUREMENTS IN TURBULENT COMBUSTION

RICHARD R. ANTCLIFF, OLIN JARRETT, JR., R. CLAYTON ROGERS, and THOMAS VANOVERBECK *In* Johns Hopkins Univ., The 23rd JANNAF Combustion Meeting, Volume 1 p 577-583 Oct. 1986 Prepared in cooperation with NASA- Lewis Research Center, Cleveland, Ohio.

Avail: CPIA, Laurel, Md. 20707 HC \$70.00 CSCL 07D

A coherent anti-Stokes Raman scattering (CARS) instrument was upgraded to more accurately measure the number density of oxygen molecules. This instrument is designed to simultaneously measure nitrogen number density, oxygen number density, and the ro-vibrational temperature of nitrogen. The CARS is a nonintrusive diagnostic technique which utilizes a pulsed Nd:YAG laser, broadband dye lasers, a complex optical system, and an intensified photodiode array detector to sample hostile combustion environments. Measurements were made in a flame produced by a coaxial subsonic diffusion hydrogen-air burner. These data were used as a data base for comparison with the results of two separate computational fluid dynamics calculations. Complications which had arisen in previous studies with regard to interpretation of the oxygen data were eliminated. Author

N87-24549*# Sverdrup Technology, Inc., Cleveland, Ohio.

DECOUPLED DIRECT METHOD FOR SENSITIVITY ANALYSIS IN COMBUSTION KINETICS Final Report

KRISHNAN RADHAKRISHNAN Jun. 1987 17 p Presented at the 6th International Symposium on Computer Methods for Partial Differential Equations, Bethlehem, Pa., 23-25 Jun. 1987; sponsored by International Association for Mathematics and Computers (Contract NAS3-24105)

(NASA-CR-179636; E-3635; NAS 1.26:179636) Avail: NTIS HC A02/MF A01 CSCL 21B

An efficient, decoupled direct method for calculating the first order sensitivity coefficients of homogeneous, batch combustion kinetic rate equations is presented. In this method the ordinary differential equations for the sensitivity coefficients are solved separately from , but sequentially with, those describing the combustion chemistry. The ordinary differential equations for the thermochemical variables are solved using an efficient, implicit method (LSODE) that automatically selects the steplength and order for each solution step. The solution procedure for the sensitivity coefficients maintains accuracy and stability by using exactly the same steplengths and numerical approximations. The method computes sensitivity coefficients with respect to any combination of the initial values of the thermochemical variables and the three rate constant parameters for the chemical reactions. The method is illustrated by application to several simple problems and, where possible, comparisons are made with exact solutions and those obtained by other techniques. Author

N87-26188*# National Aeronautics and Space Administration. Lewis Research Center, Cleveland, Ohio.

NEUTRAL ATOMIC OXYGEN BEAM PRODUCED BY ION CHARGE EXCHANGE FOR LOW EARTH ORBITAL (LEO) SIMULATION

BRUCE BANKS, SHARON RUTLEDGE, MARKO BRDAR, CARL OLEN, and CURT STIDHAM (Cleveland State Univ., Ohio.) *In* Jet Propulsion Lab., Proceedings of the NASA Workshop on Atomic Oxygen Effects p 127-134 1 Jun. 1987

Avail: NTIS HC A09/MF A01 CSCL 07D

A low energy neutral atomic oxygen beam system was designed and is currently being assembled at the Lewis Research Center. The system utilizes a 15 cm diameter Kaufman ion source to

produce positive oxygen ions which are charge exchange neutralized to produce low energy (variable from 5 to 150 eV) oxygen atoms at a flux simulating real time low Earth orbital conditions. An electromagnet is used to direct only the singly charged oxygen ions from the ion source into the charge exchange cell. A retarding potential grid is used to slow down the oxygen ions to desired energies prior to their charge exchange. Cryogenically cooled diatomic oxygen gas in the charge exchange cell is then used to transfer charge to the oxygen ions to produce a neutral atomic oxygen beam. Remaining non-charge exchanged oxygen ions are then swept from the beam by electromagnetic or electrostatic deflection depending upon the desired experiment configuration. The resulting neutral oxygen beam of 5 to 10 cm in diameter impinges upon target materials within a sample holder fixture that can also provide for simultaneous heating and UV exposure during the atomic oxygen bombardment. Author

N87-26203* National Aeronautics and Space Administration. Lewis Research Center, Cleveland, Ohio.

AN EVALUATION OF CANDIDATE OXIDATION RESISTANT MATERIALS Abstract Only

SHARON RUTLEDGE, BRUCE BANKS, MICHAEL MIRTICH, FRANK DIFILIPPO, DEBORAH HOTES, RICHARD LABED, TERESE DEVER, and MICHAEL KUSSMAUL (Cleveland State Univ., Ohio.) In Jet Propulsion Lab., Proceedings of the NASA Workshop on Atomic Oxygen Effects p 167 1 Jun. 1987
 Avail: NTIS HC A09/MF A01 CSDL 07D

Ground based testing of materials considered for Kapton solar array blanket protection, graphite epoxy structural member protection, and high temperature radiators was performed in an RF plasma asher. Ashing rates for Kapton were correlated with rates measured on STS-8 to determine the exposure time equivalent to one year in low Earth orbit (LEO) at a constant density space station orbital flux. Protective coatings on Kapton from Tekmat, Andus Corporation, and LeRC were evaluated in the plasma asher and mass loss rates per unit area were measured for each sample. All samples evaluated provided some protection to the underlying surface but ion beam sputter deposited samples of SiO₂ and SiO₂ with 8% polytetrafluoroethylene (PTFE) showed no evidence of degradation after 47 hours of exposure. Mica paint was evaluated as a protective coating for graphite epoxy structural members. Mica appears to be resistant to attack by atomic oxygen but only offers some limited protection as a paint because the paint vehicles evaluated to date were not resistant to atomic oxygen. Four materials were selected for evaluation as candidate radiator materials: stainless steel, copper, niobium-1% zirconium, and titanium-6% aluminum-4% vanadium. These materials were surface textured by various means to improve their emittance. Emittances as high as 0.93 at 2.5 microns for stainless steel and 0.89 at 2.5 microns for Nb-1 Zr were obtained from surface texturing. There were no significant changes in emittance after asher exposure. Author

N87-28628* National Aeronautics and Space Administration. Lewis Research Center, Cleveland, Ohio.

HYDROGEN OXIDATION MECHANISM WITH APPLICATIONS TO (1) THE CHAPERON EFFICIENCY OF CARBON DIOXIDE AND (2) VITIATED AIR TESTING

THEODORE A. BRABBS, ERWIN A. LEZBERG, DAVID A. BITTKER, and THOMAS F. ROBERTSON Sep. 1987 15 p
 (NASA-TM-100186; E-3672; NAS 1.15:100186) Avail: NTIS HC A02/MF A01 CSDL 07D

Ignition delay times for the hydrogen/oxygen/carbon dioxide/argon system were obtained behind reflected shock waves. A detailed kinetic mechanism modeled the experimental hydrogen/oxygen data, Skinner and Ringrose's high-pressure data, and Slack and Grillo's hydrogen/air data. A carbon dioxide chaperon efficiency of 7.0 +/- 0.2 was determined. The reaction pathway H₂O yields H₂O₂ yields OH yields H was required to model the high-pressure data. It is suggested that some of the lowest temperature data points (1.0 and 0.5 atm) for Slack and Grillo's hydrogen/air experiments are in error. It was found that the technique of simplifying a detailed kinetic mechanism for a

limited range of experimental data may render the model useless for other test conditions. Author

N87-28634* Nevada Univ., Las Vegas. Dept. of Physics. **THE TEMPERATURE DEPENDENCE OF INELASTIC LIGHT SCATTERING FROM SMALL PARTICLES FOR USE IN COMBUSTION DIAGNOSTIC INSTRUMENTATION Final Report, 1 Oct. 1982 - 30 Sep. 1986**

STANLEY D. CLOUD 9 Oct. 1987 27 p

(Contract NAG3-368)

(NASA-CR-180399; NAS 1.26:180399) Avail: NTIS HC A03/MF A01 CSDL 21B

A computer calculation of the expected angular distribution of coherent anti-Stokes Raman scattering (CARS) from micrometer size polystyrene spheres based on a Mie-type model, and a pilot experiment to test the feasibility of measuring CARS angular distributions from micrometer size polystyrene spheres by simply suspending them in water are discussed. The computer calculations predict a very interesting structure in the angular distributions that depends strongly on the size and relative refractive index of the spheres. Author

N87-29633* Case Western Reserve Univ., Cleveland, Ohio. Dept. of Physics.

OXYGEN INTERACTION WITH SPACE-POWER MATERIALS Annual Report, 1 May 1986 - 30 Apr. 1987

T. G. ECK and R. W. HOFFMAN Oct. 1987 16 p

(Contract NAG3-696)

(NASA-CR-181396; NAS 1.26:181396) Avail: NTIS HC A02/MF A01 CSDL 07D

Data from the space shuttle flights have established that many materials experience relatively rapid degradation when exposed to the low Earth orbit ambient atmosphere, which is predominately atomic oxygen. While much was learned from samples flown on the shuttle, laboratory simulations of the shuttle environment are necessary for a detailed understanding of the various interactions which contribute to the observed degradations. These laboratory experiments are particularly important for predicting the deterioration to be expected for materials aboard orbiting power systems, which will be exposed for long periods of time and could have components operating at very high temperatures. By using a mass spectrometer to synchronously detect molecules emitted from the surface as a result of amplitude modulated oxygen ion bombardment, quantum yields were obtained as a function of ion energy. A technique was developed to obtain preliminary yield data by slowly scanning the mass setting of the mass spectrometer; measurements were extended down to zero modulation frequency; yield data was obtained for the insulating materials (Nomex, Kevlar, and Teflon) used in the construction of electrodynamic tethers; a heated sample holder was constructed to investigate the effect of sample temperature on quantum yields; and the instrumentation was developed to observe the mass spectrometer signal as a function of time during and following bombardment of the sample by a brief (approximately 1 millisecond) pulse of ions. Author

N87-29635* Drexel Univ., Philadelphia, Pa. Dept. of Mechanical Engineering and Mechanics.

SPARK IGNITION OF MONODISPERSE FUEL SPRAYS Ph.D. Thesis

ALLEN M. DANIS, NICHOLAS P. CERNANSKY, and IZAK NAMER Sep. 1987 150 p

(Contract NAG3-382)

(NASA-CR-181404; NAS 1.26:181404) Avail: NTIS HC A07/MF A01 CSDL 21B

A study of spark ignition energy requirements was conducted with a monodisperse spray system allowing independent control of droplet size, equivalent ratio, and fuel type. Minimum ignition energies were measured for n-heptane and methanol sprays characterized at the spark gap in terms of droplet diameter, equivalence ratio (number density) and extent of prevaporization. In addition to sprays, minimum ignition energies were measured for completely prevaporized mixtures of the same fuels over a range of equivalence ratios to provide data at the lower limit of

droplet size. Results showed that spray ignition was enhanced with decreasing droplet size and increasing equivalence ratio over the ranges of the parameters studied. By comparing spray and prevaporized ignition results, the existence of an optimum droplet size for ignition was indicated for both fuels. Fuel volatility was seen to be a critical factor in spray ignition. The spray ignition results were analyzed using two different empirical ignition models for quiescent mixtures. Both models accurately predicted the experimental ignition energies for the majority of the spray conditions. Spray ignition was observed to be probabilistic in nature, and ignition was quantified in terms of an ignition frequency for a given spark energy. A model was developed to predict ignition frequencies based on the variation in spark energy and equivalence ratio in the spark gap. The resulting ignition frequency simulations were nearly identical to the experimentally observed values.

Author

26

METALLIC MATERIALS

Includes physical, chemical, and mechanical properties of metals, e.g., corrosion; and metallurgy.

A87-11389* Defence Metallurgical Research Lab., Hyderabad (India).

MECHANICAL PROPERTY ANISOTROPY IN SUPERALLOY EL-929 DIRECTIONALLY SOLIDIFIED BY AN EXOTHERMIC TECHNIQUE

D. C. PRADHAN (Defence Research and Development Laboratory, Hyderabad, India), K. K. SHARMA (Defence Metallurgical Research Laboratory, Hyderabad, India), and S. N. TEWARI. *Journal of Materials Science* (ISSN 0022-2461), vol. 21, Aug. 1986, p. 2871-2875. refs

Directional solidification (DS) of the nickel-based superalloy EL-929 was carried out by employing the exothermic technique for preparing several 150 mm long x 55 mm diameter rods. Specimens machined from blanks cut at 0, 45, 75 and 90 deg to the chill surface were tensile and stress-rupture tested at different temperatures. The air-melted DS alloy, when loaded parallel to the growth direction, shows considerable improvement in stress-rupture life and tensile ductility as compared with the vacuum induction melted, forged and heat-treated alloy. However, these property advantages rapidly degrade with the increasing deviation of the load axis from the growth direction.

Author

A87-12029* National Aeronautics and Space Administration. Lewis Research Center, Cleveland, Ohio.

TRANSITION FROM A PLANAR INTERFACE TO CELLULAR AND DENDRITIC STRUCTURES DURING RAPID SOLIDIFICATION PROCESSING

V. LAXMANAN (NASA, Lewis Research Center; Case Western Reserve University, Cleveland, OH). IN: *Rapidly solidified alloys and their mechanical and magnetic properties*; Proceedings of the Symposium, Boston, MA, December 2-4, 1985. Pittsburgh, PA, Materials Research Society, 1986, p. 41-50. NASA-supported research. refs

The development of theoretical models which characterize the planar-cellular and cell-dendrite transitions is described. The transitions are analyzed in terms of the Chalmers number, the solute Peclet number, and the tip stability parameter, which correlate microstructural features and processing conditions. The planar-cellular transition is examined using the constitutional supercooling theory of Chalmers et al., (1953) and it is observed that the Chalmers number is between 0 and 1 during dendritic and cellular growth. Analysis of cell-dendrite transition data reveal that the transition occurs when the solute Peclet number goes through a minimum, the primary arm spacings go through a maximum, and the Chalmers number is equal to 1/2. The relation between the tip stability parameter and the solute Peclet number

is investigated and it is noted that the tip stability parameter is useful for studying dendritic growth in alloys. I.F.

A87-15186* National Aeronautics and Space Administration. Lewis Research Center, Cleveland, Ohio.

MICROSTRUCTURE AND SURFACE CHEMISTRY OF AMORPHOUS ALLOYS IMPORTANT TO THEIR FRICTION AND WEAR BEHAVIOR

K. MIYOSHI and D. H. BUCKLEY (NASA, Lewis Research Center, Cleveland, OH) (Japan Society of Lubrication Engineers, International Tribology Conference, Tokyo, Japan, July 8-10, 1985) *Wear* (ISSN 0043-1648), vol. 110, 1986, p. 295-313. Previously announced in STAR as N84-32508. refs

An investigation was conducted to examine the microstructure and surface chemistry of amorphous alloys, and their effects on tribological behavior. The results indicate that the surface oxide layers present on amorphous alloys are effective in providing low friction and a protective film against wear in air. Clustering and crystallization in amorphous alloys can be enhanced as a result of plastic flow during the sliding process at a low sliding velocity, at room temperature. Clusters or crystallites with sizes to 150 nm and a diffused honeycomb-shaped structure are produced on sizes to 150 nm and a diffused honeycomb-shaped structure are produced on the wear surface. Temperature effects lead to drastic changes in surface chemistry and friction behavior of the alloys at temperatures to 750 C. Contaminants can come from the bulk of the alloys to the surface upon heating and impart to the surface oxides at 350 C and boron nitride above 500 C. The oxides increase friction while the boron nitride reduces friction drastically in vacuum.

Author

A87-17997* National Aeronautics and Space Administration. Lewis Research Center, Cleveland, Ohio.

CORROSION OF METALS AND ALLOYS IN SULFATE MELTS AT 750 C

A. K. MISRA (NASA, Lewis Research Center, Cleveland, OH) *Oxidation of Metals* (ISSN 0030-770X), vol. 25, June 1986, p. 373-396. refs

The corrosion of Ni, Co, Ni-10Cr, Co-21Cr, and IN738 was studied at 750 C in the presence of molten sulfate mixtures (Na₂SO₄-Li₂SO₄ and Na₂SO₄-CoSO₄) and in an atmosphere consisting of O₂ + 0.12 percent SO₂-SO₃. The corrosion was observed to be similar for both Na₂SO₄-Li₂SO₄ and Na₂SO₄-CoSO₄ melts. The corrosion of Ni and Co took place by the formation of a mixed oxide plus sulfide scale, very similar to the corrosion in SO₂ or SO₃ alone. The initial stage for the corrosion of Ni-10Cr involved the formation of a thick NiO + Ni₃S₂ duplex scale, and Cr sulfide was formed during the later stages. A pitting type of morphology was observed for both Co-21Cr and IN738. The pit was Cr sulfide at the beginning, and subsequently the sulfides oxidized to Cr₂O₃. A base-metal oxide layer was present above the pit, and this was observed to be formed very early in the corrosion process. A mechanism is proposed to explain this. In general, the formation of sulfides appears to be the primary mode of degradation in mixed sulfide melts.

Author

A87-19368* Syracuse Univ., N. Y.

GRAIN BOUNDARY OXIDATION AND FATIGUE CRACK GROWTH AT ELEVATED TEMPERATURES

H. W. LIU and Y. OSHIDA (Syracuse University, NY) *Theoretical and Applied Fracture Mechanics* (ISSN 0167-8442), vol. 6, Oct. 1986, p. 85-94. Previously announced in STAR as N87-11873. refs

(Contract NAG3-348)

Fatigue crack growth rate at elevated temperatures can be accelerated by grain boundary oxidation. Grain boundary oxidation kinetics and the statistical distribution of grain boundary oxide penetration depth were studied. At a constant delta K-level and at a constant test temperature, fatigue crack growth rate, da/dN, is a function of cyclic frequency, nu. A fatigue crack growth model of intermittent micro-ruptures of grain boundary oxide is constructed. The model is consistent with the experimental

observations that, in the low frequency region, da/dN is inversely proportional to ν , and fatigue crack growth is intergranular.

Author

A87-23429* National Aeronautics and Space Administration. Lewis Research Center, Cleveland, Ohio.

HIGH TEMPERATURE TENSILE AND CREEP BEHAVIOUR OF LOW PRESSURE PLASMA-SPRAYED Ni-CO-CR-AL-Y COATING ALLOY

M. G. HEB SUR and R. V. MINER (NASA, Lewis Research Center, Cleveland, OH) Materials Science and Engineering (ISSN 0025-5416), vol. 83, 1986, p. 239-245. refs

The high temperature tensile and creep behavior of low pressure plasma-sprayed plates of a typical Ni-Co-Cr-Al-Y alloy has been studied. From room temperature to 800 K, the Ni-Co-Cr-Al-Y alloy studied has nearly a constant low ductility and a high strength. At higher temperatures, it becomes weak and highly ductile. At and above 1123 K, the behavior is highly dependent on strain rate and exhibits classic superplastic characteristics with a high ductility at intermediate strain rates and a strain rate sensitivity of about 0.5. At either higher or lower strain rates, the ductility decreases and the strain rate sensitivities are about 0.2. In the superplastic deformation range, the activation energy for creep is $120 \pm$ or -20 kJ/mol, suggesting a diffusion-aided grain boundary sliding mechanism. Outside the superplastic range, the activation energy for creep is calculated to be $290 \pm$ or -20 kJ/mol.

Author

A87-23843* Michigan Technological Univ., Houghton. FURTHER OBSERVATIONS OF SCC IN ALPHA-BETA BRASS CONSIDERATIONS REGARDING THE APPEARANCE OF CRACK ARREST MARKINGS DURING SCC

M. B. HINTZ, W. K. BLANCHARD, L. A. HELDT (Michigan Technological University, Houghton), and P. K. BRINDLEY (NASA, Lewis Research Center, Cleveland, OH) Metallurgical Transactions A - Physical Metallurgy and Materials Science (ISSN 0360-2133), vol. 17A, June 1986, p. 1081-1086. refs (Contract DE-AC02-81ER-10941)

A series of constant displacement and constant extension rate stress corrosion cracking (SCC) tests was performed on an alpha-beta brass alloy in 1 N Na₂SO₄ solutions. The chosen mechanical and electrochemical conditions resulted in predominantly transgranular, cleavage-like failure at high (about 8 to 50 microns/s) average crack propagation rates. Crack arrest markings were observed on selected transgranular facets, which almost exclusively bordered regions of ductile overload failure. It is proposed that the observed crack velocities and the specific nature of the arrest mark appearance are most consistent with a cracking mechanism involving adsorption or some other interaction with a damaging environmental species.

Author

A87-23848*# National Aeronautics and Space Administration. Lewis Research Center, Cleveland, Ohio.

THE FORMATION OF VOLATILE CORROSION PRODUCTS DURING THE MIXED OXIDATION-CHLORINATION OF COBALT AT 650 C

N. S. JACOBSON (NASA, Lewis Research Center, Cleveland, OH), M. J. MCNALLAN (Illinois, University, Chicago), and Y. Y. LEE Metallurgical Transactions A - Physical Metallurgy and Materials Science (ISSN 0360-2133), vol. 17A, July 1986, p. 1223-1228. DOE-supported research. refs

The reaction of cobalt with 1 pct Cl₂ in 1, 10, and 50 pct O₂/Ar atmospheres has been studied at 650 C with thermogravimetry and mass spectrometry. The principal vapor species appear to be CoCl₂ and CoCl₃. In all cases, CoCl₂(s) forms at the oxide/metal interface and equilibration of the volatile chlorides with Co₃O₄ does not occur in the early stages of the reaction. In the 1 pct Cl₂ 1 pct O₂-Ar case, continuous volatilization occurs. In the 1 pct Cl₂-10 pct O₂-Ar and 1 pct Cl₂-50 pct O₂-Ar cases, volatilization occurs only in the first few minutes of reaction. Afterwards, the reaction is predominantly oxidation.

Author

A87-24040* National Aeronautics and Space Administration. Lewis Research Center, Cleveland, Ohio.

LOW CYCLE FATIGUE BEHAVIOUR OF A PLASMA-SPRAYED COATING MATERIAL

J. GAYDA, T. P. GABB, and R. V. MINER (NASA, Lewis Research Center, Cleveland, OH) International Journal of Fatigue (ISSN 0142-1123), vol. 8, Oct. 1986, p. 217-223. refs

Single crystal nickel-base superalloys employed in turbine blade applications are often used with a plasma spray coating for oxidation and hot corrosion resistance. These coatings may also affect fatigue life of the superalloy substrate. As part of a large program to understand the fatigue behavior of coated single crystals, fully reversed, total strain controlled fatigue tests were run on a free standing NiCoCrAlY coating alloy, PWA 276, at 0.1 Hz. Fatigue tests were conducted at 650 C, where the NiCoCrAlY alloy has modest ductility, and at 1050 C, where it is extremely ductile, showing tensile elongation in excess of 100 percent. At the lower test temperature, deformation induced disordering softened the NiCoCrAlY alloy, while at the higher test temperature cyclic hardening was observed which was linked to gradual coarsening of the two phase microstructure. Fatigue life of the NiCoCrAlY alloy was significantly longer at the higher temperature. Further, the life of the NiCoCrAlY alloy exceeds that of coated, /001/-oriented PWA 1480 single crystals at 1050 C but at 650 C the life of the coated crystal is greater than that of the NiCoCrAlY alloy on a total strain basis.

Author

A87-24110* Michigan Technological Univ., Houghton. THE EFFECTS OF TANTALUM ON THE MICROSTRUCTURE OF TWO POLYCRYSTALLINE NICKEL-BASE SUPERALLOYS - B-1900 + HF AND MAR-M247

R. W. HECKEL, B. J. PLETKA (Michigan Technological University, Houghton), and G. M. JANOWSKI Metallurgical Transactions A - Physical Metallurgy and Materials Science (ISSN 0360-2133), vol. 17A, Nov. 1986, p. 1891-1905. refs (Contract NAG3-216)

The effect of changing the content of Ta on the gamma/gamma-prime carbide microstructure was investigated in two crystalline nickel-base superalloys: conventionally cast B-1900 + Hf, and both conventionally cast and directionally solidified MAR-M247. The changes occurring in the microstructure effects were similar in both alloys. The gamma-prime and carbide volume fractions increased linearly with Ta additions, while the gamma-prime phase compositions did not change. Bulk Ta additions increased the levels of Cr and Co (in addition to that of Ta) of the gamma phase, a result of the approximately constant partitioning ratios for these two elements. The addition of Ta led to a partial replacement of Hf in the MC carbides. In addition, Cr-rich M(23)C(6) carbides formed as a result of MC carbide decomposition during heat treatment.

I.S.

A87-24116* Drexel Univ., Philadelphia, Pa. PROCESSING-STRUCTURE CHARACTERIZATION OF RHEOCAST IN-100 SUPERALLOY

JUNG-JEN ALLEN CHENG, DIRAN APELIAN, and ROGER D. DOHERTY (Drexel University, Philadelphia, PA) Metallurgical Transactions A - Physical Metallurgy and Materials Science (ISSN 0360-2133), vol. 17A, Nov. 1986, p. 2049-2062. refs (Contract NAG3-14)

The rheocasting solidification process was applied in the production of IN-100 nickel base superalloy, and the effects of processing variables, such as stirring speed, isothermal stirring time, and volume fraction solid during isothermal stirring, on the resultant rheocast structure were investigated. Ingots that were furnace cooled at the same rate but without stirring were compared with the rheocast ingots. Rheocasting yielded fine-grained structures, where the extent of microsegregation, the variation in macrostructure, and the solidification-induced porosity and ingot cracking were found to be reduced in comparison to the unstirred ingots. The grain size and nonuniformity were reduced by increasing the stirring speed, isothermal stirring time, or the volume fraction solid during stirring; decreased microsegregation was achieved by an increase in the volume fraction solid. The structures of grain

boundaries lent support to the grain boundary mechanism proposed by Vogel et al. (1977) for rheocasting. I.S.

A87-24119* National Aeronautics and Space Administration. Lewis Research Center, Cleveland, Ohio.
DENDRITIC MICROSTRUCTURE IN ARGON ATOMIZED SUPERALLOY POWDERS

S. N. TEWARI (NASA, Lewis Research Center, Cleveland, OH) and MAHUNDRA KUMAR (Defence Metallurgical Research Laboratory, Hyderabad, India) Metallurgical Transactions A - Physical Metallurgy and Materials Science (ISSN 0360-2133), vol. 17A, Nov. 1986, p. 2099-2102. refs

The dendritic microstructure of atomized nickel base superalloy powders (Ni-20 pct Cr, NIMONIC-80A, ASTROALLOY, and ZHS6-K) was studied. Prealloyed vacuum induction melted ingots were argon-atomized, the powders were cooled to room temperature, and various powder-size fractions were examined by optical metallography. Linear correlations were obtained for the powder size dependence of the secondary dendrite arm spacing, following the expected $d\text{-}\alpha$ (R) to the m power dependence on the particle size for all four superalloy compositions. However, the Ni-20 pct Cr alloy, which had much coarser arm spacing as compared to the other three alloys, had a much larger value of m . I.S.

A87-25048* National Aeronautics and Space Administration. Lewis Research Center, Cleveland, Ohio.

A CRITICAL EXAMINATION OF THE DENDRITE GROWTH MODELS COMPARISON OF THEORY WITH EXPERIMENTAL DATA

S. N. TEWARI and V. LAXMANAN (NASA, Lewis Research Center, Cleveland, OH) Acta Metallurgica (ISSN 0001-6160), vol. 35, Jan. 1987, p. 175-183. NASA-supported research. refs

Three dendrite growth models for directionally solidified succinonitrile-acetone, succinonitrile-salol, aluminum-copper, and lead-palladium alloys are evaluated. The characteristics of the Burden and Hunt (1974) model, the Laxmanan (1985) model, and the Trivedi (1980) model are described. The dendrite tip temperature, tip radius, liquid composition, and primary arm spacing for the alloys are analyzed in terms of growth speed, alloy composition, and temperature gradient. It is observed that the Burden and Hunt model accurately predicts the proper behavior of the parameters, but does not provide good quantitative predictions. A good fit between the experimental data and the Trivedi and Laxmanan models is detected. The advantages of the Trivedi marginal stability analysis and the Laxmanan minimum dendrite tip undercooling approaches are discussed. I.F.

A87-28732* Wisconsin Univ., Madison.
UNDERCOOLING AND CRYSTALLIZATION BEHAVIOUR OF ANTIMONY DROPLETS

J. A. GRAVES and J. H. PEREPEZKO (Wisconsin, University, Madison) Journal of Materials Science (ISSN 0022-2461), vol. 21, Dec. 1986, p. 4215-4220. refs (Contract NAG3-436)

The droplet emulsion technique is presently used to examine the undercooling and crystallization behavior of pure antimony. Control of droplet size and applied cooling rate allowed maximum undercooling to be extended from 0.08 to 0.23 T(m). A droplet coating was produced by means of emulsification which appears to furnish a favorable crystallographic matching for effective nucleation catalysis of a metastable simple cubic structure. Thermal analysis shows the melting temperature of the single cubic phase to be about 625 C. O.C.

A87-28734* Drexel Univ., Philadelphia, Pa.
ANALYSIS OF THE SOLIDIFIED STRUCTURE OF RHEOCAST AND VADER PROCESSED NICKEL-BASE SUPERALLOY
 D. APELIAN and J.-J. A. CHENG (Drexel University, Philadelphia, PA) Journal of Materials Science (ISSN 0022-2461), vol. 21, Dec. 1986, p. 4233-4244. refs (Contract NAG3-14)

Conventional 'ingot' processing of highly alloyed compositions results in a cast product which suffers from extensive macrosegregation, hot tears, and heterogeneities. By controlling the solidification journey, one can produce a fine grained cast product. This is achieved by manipulating the melt in the mushy zone. Rheocasting and vacuum arc double electrode remelting (VADER) are two such technologies where the melt is processed in the mushy zone. IN-100, a nickel based superalloy, was rheocast as well as VADER processed. The resultant cast structures are analyzed, compared and discussed both on micro- and macrostructural levels. The effect of the rheocast processing variables (stirring seed, time and temperature) on the cast microstructure are also discussed. Author

A87-32001* National Aeronautics and Space Administration. Lewis Research Center, Cleveland, Ohio.

REACTION OF IRON WITH HYDROGEN CHLORIDE-OXYGEN MIXTURES AT 550 C

N. S. JACOBSON (NASA, Lewis Research Center, Cleveland, OH) Oxidation of Metals (ISSN 0030-770X), vol. 26, no. 3-4, 1986, p. 157-169. refs

The reaction of iron with 1 percent HCl/0-50 percent O₂/Ar has been studied at 550 C with thermogravimetry to monitor kinetics and scanning electron microscopy to characterize product morphologies. In addition, the volatile species were identified with an atmospheric pressure sampling mass spectrometer. The reaction of 1 percent HCl/Ar produces FeCl₂. The reactions of 1 percent HCl/1, 10, 50 percent O₂/Ar produce Fe₂O₃, Fe₃O₄, FeCl₂, and FeCl₃. In each case condensed phase chlorides form at the oxide/metal interface where the oxygen potential is low. The 10 and 50 percent oxygen mixtures have kinetics in the first 3 hr similar to pure oxidation with some deviations due to iron-chloride formation. The 1 percent oxygen mixture shows enhanced reaction rates over oxidation, very likely due to the formation of a porous scale. Author

A87-32035* Cincinnati Univ., Ohio.
FAULT STRUCTURES IN RAPIDLY QUENCHED NI-MO BINARY ALLOYS

N. JAYARAMAN (Cincinnati, University, OH) and S. N. TEWARI (NASA, Lewis Research Center, Cleveland, OH) Metallurgical Transactions A - Physical Metallurgy and Materials Science (ISSN 0360-2133), vol. 17A, Dec. 1986, p. 2291-2294.

Fault structures in two Ni-Mo alloy ribbons (Ni-28 at. pct Mo and Ni-35 at. pct Mo) cast by a free jet chill block melt spinning process were studied. Thin foils for TEM studies were made by electrochemical thinning using an alcohol/butyl cellosolve/perchloric acid mixture in a twin jet electropolishing device. The samples displayed typical grains containing linear faulted regions on the wheelside of the two alloy ribbons. However, an anomalous diffraction behavior was observed upon continuous tilting of the sample: the network of diffraction spots from a single grain appeared to expand or contract and rotate. This anomalous diffraction behavior was explained by assuming extended spike formation at reciprocal lattice points, resulting in a network of continuous rel rods. The validity of the model was confirmed by observations of a cross section of the reciprocal lattice parallel to the rel rods. I.S.

A87-32040* Georgia Inst. of Tech., Atlanta.

YIELDING AND DEFORMATION BEHAVIOR OF THE SINGLE CRYSTAL SUPERALLOY PWA 1480

WALTER W. MILLIGAN and STEPHEN D. ANTOLOVICH (Georgia Institute of Technology, Atlanta) Metallurgical Transactions A - Physical Metallurgy and Materials Science (ISSN 0360-2133), vol. 18A, Jan. 1987, p. 85-95. Previously announced in STAR as N86-25455. refs
(Contract NAG3-503)

Interrupted tensile tests were conducted to fixed plastic strain levels in 100 ordered single crystals of the nickel based superalloy PWA 1480. Testing was done in the range of 20 to 1093 C, at strain rate of 0.5 and 50 percent/min. The yield strength was constant from 20 to 760 C, above which the strength dropped rapidly and became a strong function of strain rate. The high temperature data were represented very well by an Arrhenius type equation, which resulted in three distinct temperature regimes. The deformation substructures were grouped in the same three regimes, indicating that there was a fundamental relationship between the deformation mechanisms and activation energies. Models of the yielding process were considered, and it was found that no currently available model was fully applicable to this alloy. It was also demonstrated that the initial deformation mechanism (during yielding) was frequently different from that which would be inferred by examining specimens which were tested to failure. Author

A87-32045*# National Aeronautics and Space Administration. Lewis Research Center, Cleveland, Ohio.

ADHERENT AL₂O₃ SCALES FORMED ON UNDOPED NICRAL ALLOYS

JAMES L. SMIALEK (NASA, Lewis Research Center, Cleveland, OH) Metallurgical Transactions A - Physical Metallurgy and Materials Science (ISSN 0360-2133), vol. 18A, Jan. 1987, p. 164-167. refs

Changes in the spalling behavior of Al₂O₃ scales formed on an undoped NiCrAl alloy are described. Two samples of Ni-15Cr-13Al (wt pct), one a control and the other sanded, were subjected to 25 oxidation cycles. It is observed that adherent scales formed on the sanded sample; however, the control sample had speckled, spalled scales. The data reveal that the adherent scales are caused by repeated removal of surface layers after each oxidation cycle. It is determined that interfacial segregation of sulfur influences spallation and sulfur removal increases bonding. The effect of moisture on scale adhesions is investigated. I.F.

A87-32046* Cleveland State Univ., Ohio.

CELLULAR-DENDRITIC TRANSITION IN DIRECTIONALLY SOLIDIFIED BINARY ALLOYS

S. N. TEWARI (Cleveland State University, OH) and V. LAXMANAN (NASA, Lewis Research Center; Case Western Reserve University, Cleveland, OH) Metallurgical Transactions A - Physical Metallurgy and Materials Science (ISSN 0360-2133), vol. 18A, Jan. 1987, p. 167-170. NASA-supported research. refs

The microstructural development of binary alloys during directional solidification is studied. Cellular growth data for the Al-Cu and Pb-Sn binary alloy systems are analyzed in order evaluate the criteria of Kurz and Fisher (1981) and Trivedi (1984) for cellular-dendritic transition. It is observed that the experimental growth values do not correlate with the Kurz and Fisher or Trivedi data. I.F.

A87-34661* Virginia Polytechnic Inst. and State Univ., Blacksburg.

OPENING AND CLOSING OF CRACKS AT HIGH CYCLIC STRAINS

N. S. IYER and N. E. DOWLING (Virginia Polytechnic Institute and State University, Blacksburg) IN: Small fatigue cracks; Proceedings of the Second International Conference/Workshop, Santa Barbara, CA, Jan. 5-10, 1986. Warrendale, PA, Metallurgical Society, Inc., 1986, p. 213-223. refs
(Contract NAG3-438)

The closure behavior of cracks of different length and at different cyclic strain levels (ranging from predominantly elastic to

grossly plastic strains) was studied to observe the effect of residual crack-tip plasticity on crack closure. Cracks were initiated either naturally or artificially (from electric discharge machining pits) in uniaxial test specimens of strengthened alloy steel AISI 4340 with a grain size of 0.016 mm. It was found that, at high strains, cracks closed only when the lowest stress level in the cycle was approached. The stress or the strain opening level depended upon the exact point along the crack length where the observations were made. As the plastic deformation increased, the relative crack opening level was found to decrease and approach the value of stress ratio R. The experimental results were compared with those of three analytical models of crack closure and opening, demonstrating the limitations of the currently available elastic-plastic crack growth analysis. I.S.

A87-34888* Case Western Reserve Univ., Cleveland, Ohio.

ANALYSIS OF NIALTA PRECIPITATES IN BETA-NIAL + 2 AT. PCT TA ALLOY

V. PATHARE, G. M. MICHAL, K. VEDULA (Case Western Reserve University, Cleveland, OH), and M. V. NATHAL (NASA, Lewis Research Center, Cleveland, OH) Scripta Metallurgica (ISSN 0036-9748), vol. 21, March 1987, p. 283-288. NASA-supported research. refs

Results are reported from experiments performed to identify the precipitates, and their orientation in the matrix, in a beta-NiAl alloy containing 2 at. pct. Ta after undergoing creep test at 1300 K. Test specimens formed by extruding hot powders were compressed at 1300 K for about 50 hr at a strain rate averaging 6/1 million per sec. The specimens were then thinned and examined under an electron microscope and by X-ray diffractometry. An intermetallic NiAlTa compound with a hexagonal C14 structure appeared as second phase precipitates in the samples, exhibiting plate-like shapes and a habit plane close to (012). The prism planes of the hexagonal NiAlTa precipitates paralleled the closest packed planes in the cubic beta-NiAl matrix. M.S.K.

A87-36251* National Aeronautics and Space Administration. Lewis Research Center, Cleveland, Ohio.

EFFECT OF COMPOSITION AND GRAIN SIZE ON SLOW PLASTIC FLOW PROPERTIES OF NIAL BETWEEN 1200 AND 1400 K

J. DANIEL WHITTENBERGER (NASA, Lewis Research Center, Cleveland, OH) Journal of Materials Science (ISSN 0022-2461), vol. 22, Feb. 1987, p. 394-402. refs

A series of about 15-micron diameter polycrystalline B2 crystal structure NiAl alloys ranging in composition from 43.9 to 52.7 Al (at. pct) have been compression tested at constant velocities in air between 1200 and 1400 K. All materials were fabricated via powder metallurgy techniques with hot extrusion as the densification process. Seven intermediate compositions were produced by blending various amounts of two master heats of prealloyed powder; in addition, a tenth alloy of identical composition, 48.25 Al, as one of the blended materials, was produced from a third master heat. Comparison of the flow stress-strain rate behavior for the two 48.25 Al alloys revealed that their properties were identical. The creep strength of materials for Al/Ni not above 1.03 was essentially equal, and deformation could be described by a single stress exponent and activation energy. Creep at low temperatures and faster strain rates is independent of grain sizes and appears to be controlled by a subgrain mechanism. However, at higher temperatures and slower strain rates, diffusional creep seems to contribute to the overall deformation rate. Author

A87-38541* Rensselaer Polytechnic Inst., Troy, N.Y.
EFFECTS OF TEMPERATURE AND HOLD TIMES ON LOW CYCLE FATIGUE OF ASTROLOY

S. J. CHOE, N. S. STOLOFF, and D. J. DUQUETTE (Rensselaer Polytechnic Institute, Troy, NY) IN: Strength of metals and alloys; Proceedings of the Seventh International Conference, Montreal, Canada, Aug. 12-16, 1985. Volume 2. Oxford, Pergamon Press, 1986, p. 1291-1298. refs
 (Contract NAG3-22)

Low cycle fatigue (LCF) and creep-fatigue-environment interactions of HIP Astroloy were studied at 650 C and 725 C. The results showed that the model proposed by Kaisand and Mowbray (1979) was successful in predicting the magnitude and trend of the fatigue crack growth rate from LCF data. Raising the temperature from 650 C to 725 C did not change the fracture mode, while employing tensile hold caused a change in fracture mode and was more damaging than raising the temperature by 75 C. All samples displayed multiple fracture origins, which is initiated transgranularly in continuous cycling tests and intergranularly in hold time tests. An examination of the secondary crack showed no apparent creep damage. Oxidation in high purity argon appeared to be the major factor in LCF life degradation due to hold time. Author

A87-39897*# National Aeronautics and Space Administration. Lewis Research Center, Cleveland, Ohio.

HEAT'S ON TO DEVELOP HIGH-TEMPERATURE MATERIALS
 HUGH R. GRAY, HAROLD E. SLINNEY, RAYMOND D. VANNUCCI, STANLEY R. LEVINE, CARL A. STEARNS, and JOSEPH R. STEPHENS (NASA, Lewis Research Center, Cleveland, OH) Aerospace America (ISSN 0740-722X), vol. 25, May 1987, p. 12-14, 16, 18 (9 ff.).

An evaluation is made of the state-of-the-art and foreseeable development prospects in high temperature engineering materials applicable to advanced heat engines and other aerothermodynamically affected structures. Attention is given to monocrystal- and microcrystal-producing metal solidification processes, soft oxide and chemically stable fluoride high temperature solid lubricants, polyimide and other high temperature polymers for propulsion system applications, high strength/toughness ceramics for heat engine structural components, thermal barrier coatings, and metal-matrix composites employing refractory matrices as well as reinforcing fibers. O.C.

A87-40928* National Aeronautics and Space Administration. Lewis Research Center, Cleveland, Ohio.

UNDERSTANDING SINGLE-CRYSTAL SUPERALLOYS
 ROBERT L. DRESHFIELD (NASA, Lewis Research Center, Cleveland, OH) Metal Progress (ISSN 0026-0665), Aug. 1986, 4 p.

The unique properties of single crystals are considered. The anisotropic properties of single crystals, and the relation between crystal orientation and the fatigue life and slip systems of the crystals are examined. The effect of raft formation on the creep-rupture life of the crystals is studied. Proposed research on the properties of and new applications for single crystals is discussed. I.F.

A87-41012* Massachusetts Inst. of Tech., Cambridge.
DENDRITIC GROWTH OF UNDERCOOLED NICKEL-TIN. I, II

Y. WU, T. J. PICCONE, Y. SHIOHARA, and M. C. FLEMINGS (MIT, Cambridge, MA) Metallurgical Transactions A - Physical Metallurgy and Materials Science (ISSN 0360-2133), vol. 18A, May 1987, p. 915-932. refs
 (Contract NSG-7645; NAG3-597)

A comparison is made between high speed cinematography and optical temperature measurements of the solidification of an undercooled Ni-25 wt pct Sn alloy. The first part of this study notes that solidification during the recalescence period at all undercoolings studied occurred in the form of a dendritelike front moving across the sample surface, and that the growth velocities observed agree with calculation results for the dendrite growth model of Lipton et al. (1986); it is concluded that the coarse

structure observed comprises an array of much finer, solute-controlled dendrites. In the second part, attention is given to the solidification of levitated metal samples within a transparent glass medium for the cases of two undercooled Ni-Sn alloys, one of which is eutectic and another hypoeutectic. The data obtained suggest a solidification model involving dendrites of very fine structure growing into the melt at temperatures near the bulk undercooling temperature. O.C.

A87-43396* National Aeronautics and Space Administration. Lewis Research Center, Cleveland, Ohio.

STRESS RUPTURE AND CREEP BEHAVIOR OF A LOW PRESSURE PLASMA-SPRAYED NICOCRALY COATING ALLOY IN AIR AND VACUUM

M. G. HEBUR and R. V. MINER (NASA, Lewis Research Center, Cleveland, OH) Thin Solid Films (ISSN 0040-6090), vol. 147, 1987, p. 143-152. refs

The creep behavior of a NiCoCrAlY coating alloy in air and vacuum at 660 and 850 C is studied. The microstructure of the coating alloy is described. Analysis of the creep curves reveal that the secondary creep rates, the transition from secondary to tertiary creep, and the strain-to-failure are affected by the environment, preexposure, stress, and temperature. It is observed that the rupture lives of the NiCoCrAlY alloy at 660 and 850 C are greater in air than in vacuum. Several mechanisms that may explain the lack of crack growth from surface-connected pores during tests in air are proposed. Author

A87-45336*# National Aeronautics and Space Administration. Lewis Research Center, Cleveland, Ohio.

APPLICATION OF SINGLE CRYSTAL SUPERALLOYS FOR EARTH-TO-ORBIT PROPULSION SYSTEMS

R. L. DRESHFIELD (NASA, Lewis Research Center, Cleveland, OH) and R. A. PARR (NASA, Marshall Space Flight Center, Huntsville, AL) AIAA, SAE, ASME, and ASCE, Joint Propulsion Conference, 23rd, San Diego, CA, June 29-July 2, 1987. 13 p. Previously announced in STAR as N87-22034. refs
 (AIAA PAPER 87-1976)

Single crystal superalloys were first identified as potentially useful engineering materials for aircraft gas turbine engines in the mid-1960s. Although they were not introduced into service as turbine blades in commercial aircraft engines until the early 1980's, they have subsequently accumulated tens of millions of flight hours in revenue producing service. The Space Shuttle main engine (SSME) and potential advanced earth-to-orbit propulsion systems impose severe conditions on turbopump turbine blades which for some potential failure modes are more severe than in aircraft gas turbines. Research activities which are directed at evaluating the potential for single crystal superalloys for application as turbopump turbine blades in the SSME and advanced rocket engines are discussed. The mechanical properties of these alloys are summarized and the effects of hydrogen are noted. The use of high gradient directional solidification and hot isostatic pressing to improve fatigue properties is also addressed. Author

A87-46932* National Aeronautics and Space Administration. Lewis Research Center, Cleveland, Ohio.

THE CHARACTERISTICS OF GAMMA-PRIME DISLOCATION PAIRS IN A NICKEL-BASE SUPERALLOY

T. P. GABB, R. V. MINER (NASA, Lewis Research Center, Cleveland, OH), and G. WELSCH (Case Western Reserve University, Cleveland, OH) Scripta Metallurgica (ISSN 0036-9748), vol. 21, July 1987, p. 987-992. refs

The gamma-prime dislocation pairs of a single crystal nickel-base superalloy, PWA 1480, after tensile and fatigue loading at 650 C are analyzed. The existence and extent of cube cross slip in octahedral slip, and the nature of gamma-prime dislocation pairs in primary cube slip are investigated. It is observed that the PWA 1480 specimens oriented near (001) and (-3 6 10) line directions deform by octahedral slip and specimens oriented near (-1 1 1) and (-2 3 4) lines deform by primary cube slip. It is determined that the overall dislocation distributions are more homogeneous in low cycle fatigue (LCF) loading than in monotonic

tensile loading; however, the gamma-prime dislocation pair characteristics are similar for tensile and LCF test specimens. The data reveal that the gamma-prime dislocation pairs of octahedral slip specimens are near-screw and on the cube cross slip plane and for the cube slip specimens, the dislocation pairs are of various characters and on the primary cube slip plane.

I.F.

A87-47902* National Aeronautics and Space Administration. Lewis Research Center, Cleveland, Ohio.

CHILL BLOCK MELT SPINNING OF NICKEL-MOLYBDENUM ALLOYS

KEVIN J. HEMKER and THOMAS K. GLASGOW (NASA, Lewis Research Center, Cleveland, OH) *Journal of Materials Science* (ISSN 0022-2461), vol. 22, March 1987, p. 798-802. refs

Samples of Ni-Mo alloys ranging in composition from pure nickel to Ni-40 at. pct molybdenum were cast by the chill block melt-spinning rapid solidification technique and examined by optical metallography, X-ray diffraction, and microhardness testing. Casting difficulties were encountered with lean alloys, but richer alloys spread more readily on the casting wheel. Alloy microstructures for 5 to 37.5 at. pct molybdenum ribbons were primarily cellular/dendritic; microstructure feature size decreased with increasing molybdenum content. Extended solubility of molybdenum in gamma-nickel, with fcc lattice parameter increasing with composition to the 1.05 power, was observed up to 37/5 at. pct molybdenum. Substoichiometric Ni-Mo (δ) nucleated on the wheel side of the ribbons of compositions 35, 37.5, and 40 at. pct molybdenum. The amount of partitionless δ -phase thus formed increased with increasing molybdenum content and quench rate. This substoichiometric δ transformed readily to a fine structure gamma- δ mixture.

Author

A87-47932* Defence Metallurgical Research Lab., Hyderabad (India).

EFFECT OF HEAT TREATMENT ON THE FRACTURE BEHAVIOUR OF DIRECTIONALLY SOLIDIFIED (GAMMA/GAMMA-PRIME)-ALPHA ALLOY

A. M. SRIRAMAMURTHY (Defence Metallurgical Research Laboratory, Hyderabad, India) and S. N. TEWARI (NASA, Lewis Research Center, Cleveland, OH) *Journal of Materials Science Letters* (ISSN 0261-8028), vol. 6, April 1987, p. 373-376. Research supported by the Ministry of Defence of India. refs

An investigation is conducted into the influence of various heat treatments on the work of fracture and its relation to microstructure for a directionally solidified Ni-33Mo-5.7Al (wt pct) (gamma/gamma-prime)-alpha alloy. The jagged crack propagation observed is due to delamination of the ligaments and associated plastic deformation. Fracture behavior is examined with respect to alloy microstructures and load-deflection curves. The four heat-treatment conditions considered are: (1) as-directionally solidified, (2) solutionized, (3) directionally solidified and thermally cycled, and (4) solutionized and thermally cycled.

O.C.

A87-48323* National Aeronautics and Space Administration. Lewis Research Center, Cleveland, Ohio.

THE STABILITY OF LAMELLAR GAMMA-GAMMA-PRIME STRUCTURES

M. V. NATHAL and R. A. MACKAY (NASA, Lewis Research Center, Cleveland, OH) *Materials Science and Engineering* (ISSN 0025-5416), vol. 85, 1987, p. 127-138. refs

The stability of stress-annealed gamma/gamma-prime lamellar structures were investigated using three nickel-base single-crystal alloys (the NASAIR 100 and two similar alloys, E and F, containing 5 and 10 wt pct Co, respectively) stress-annealed at 1000 C to form lamellae perpendicular to the applied stress. The rate of the lamellar thickening under various thermal and creep exposures was examined by SEM. For unstressed aging at 1100 C, the lamellar structures of the NASAIR and the E alloys exhibited continuous but slow lamellar coarsening, whereas the lamellae of the alloy F showed pronounced thickening plus spheroidization. Resistance to lamellar thickening was correlated with high magnitudes of lattice mismatch, which promoted a more regular lamellar structure and

a finer spacing of misfit dislocations. Specimens which were tension-annealed prior to compressive creep testing exhibited an earlier onset of tertiary creep in comparison with only heat-treated specimens. This was associated with accelerated lamellar coarsening in the stress-annealed specimens.

I.S.

A87-49558* National Aeronautics and Space Administration. Lewis Research Center, Cleveland, Ohio.

EFFECT OF 15 MPA HYDROGEN ON CREEP-RUPTURE PROPERTIES OF IRON-BASE SUPERALLOYS

S. BHATTACHARYYA (Metallurgical and Engineering Consultants, Ltd., Ranchi, India) and R. H. TITRAN (NASA, Lewis Research Center, Cleveland, OH) IN: High temperature alloys for gas turbines and other applications 1986; Proceedings of the Conference, Liege, Belgium, Oct. 6-9, 1986. Part 2. Dordrecht, Netherlands, D. Reidel Publishing Co., 1986, p. 1317-1332. refs (Contract DEN3-217; DEN3-303)

Six wrought alloys (A-286, Incoloy 800H, N-155, 19-9DL, 12RN72, and CG-27) and four cast alloys (XF-813, CRM-6D, HS-31, and SA-F11), candidate materials for use in Stirling engines, were evaluated with reference to creep-rupture characteristics in 15-MPa H₂ at 705 and 925 C. An analysis of the test results indicates that hydrogen has no effect on the rupture life and the minimum creep rate of the alloys investigated. Rupture ductility in hydrogen is lower than in air, but the mode of fracture is not significantly affected.

V.L.

A87-49570* Ecole Polytechnique Federale de Lausanne (Switzerland).

THERMAL-MECHANICAL FATIGUE CRACK GROWTH IN B-1900+HF

N. MARCHAND (Lausanne, Ecole Polytechnique Federale, Switzerland) and R. M. PELLOUX (MIT, Cambridge, MA) IN: High temperature alloys for gas turbines and other applications 1986; Proceedings of the Conference, Liege, Belgium, Oct. 6-9, 1986. Part 2. Dordrecht, Netherlands, D. Reidel Publishing Co., 1986, p. 1547-1558. refs (Contract NAG3-280)

Thermal-mechanical fatigue crack growth (TMFCG) rates in B-1900+Hf were measured under strain-controlled conditions in the temperature range 400-925 C. A poor correlation between isothermal and TMFCG rates under elastic and fully plastic conditions was observed when test data were analyzed using a strain-based approach. A stress-based approach taking into account the hardening and softening behavior of the material and load shedding provided an adequate description of the isothermal and TMFCG rates. Also, the isothermal crack growth rates at minimum and maximum temperatures provided upper and lower bounds, respectively, on the TMFCG rates.

V.L.

A87-49790* National Aeronautics and Space Administration. Lewis Research Center, Cleveland, Ohio.

DEFECTS IN NICKEL-BASE SUPERALLOYS

ROBERT L. DRESHFIELD (NASA, Lewis Research Center, Cleveland, OH) *Journal of Metals* (ISSN 0148-6608), vol. 39, July 1987, p. 16-21. refs

The presence of substantial amounts of the sigma phase in Ni-base superalloys can drastically reduce the alloy's stress rupture life. No predictive system exists which is entirely successful in anticipating the formation of sigma, mu, and similar phases in new and substantially different alloys. Freckles are defects due to the segregation of elements in quantities that can lead to phase precipitation, and are caused by gravity-driven fluid motion that yields microsegregation in the ingots typically used in the fabrication of structures based on these alloys. Also noted are the effects of porosity and grain boundaries on superalloy mechanical properties.

O.C.

A87-51289* Howmet Turbine Components Corp., White Hall, Mich.

THERMAL STABILITY OF THE NICKEL-BASE SUPERALLOY B-1900 + HF WITH TANTALUM VARIATIONS

B. S. HARMON (Howmet Turbine Components Corp., Whitehall, MI), B. J. PLETKA (Michigan Technological University, Houghton), and G. M. JANOWSKI Metallurgical Transactions A - Physical Metallurgy and Materials Science (ISSN 0360-2133), vol. 18A, Aug. 1987, p. 1341-1351. refs
(Contract NAG3-216)

The microstructure of the solutionized and aged nickel-base superalloy B-1900 + Hf was examined after additional aging at 982 C for 72, 250, and 1000 hours. Alloy compositions that were examined contained the normal 1.34 at. pct (4.3 wt pct) Ta as well as 0.67 at. pct and zero Ta levels. The gamma-prime phase agglomerated, became platelike in morphology, and decreased in volume fraction for all three alloys throughout the aging treatments. Changes which occurred in the gamma and gamma-prime phase compositions were nearly complete after 72 hours of aging while changes in the MC carbide composition continued throughout the aging. Blocky M₆C carbides precipitated along the grain boundaries of all three alloys in the first 72 hours of aging. In addition, an acicular form of this Mo/Cr/Ni-rich carbide developed in the intragranular regions of the Ta-containing alloys. Author

A87-51636* Cincinnati Univ., Ohio.

MICROSTRUCTURES IN RAPIDLY SOLIDIFIED NI-MO ALLOYS
N. JAYARAMAN (Cincinnati, University, OH), S. N. TEWARI, K. J. HEMKER, and T. K. GLASGOW (NASA, Lewis Research Center, Cleveland, OH) IN: Rapidly solidified materials; Proceedings of the International Conference, San Diego, CA, Feb. 3-5, 1986. Metals Park, OH, American Society for Metals, 1986, p. 243-248. Previously announced in STAR as N85-34266. refs

Ni-Mo alloys of compositions ranging from pure Ni to Ni-40 at. percent Mo were rapidly solidified by Chill Block Melt Spinning in vacuum and were examined by optical metallography, X-ray diffraction and transmission electron microscopy. Rapid solidification resulted in an extension of molybdenum solubility in nickel from 28 to 37.5 at. percent. A number of different phases and microstructures were seen at different depths (solidification conditions) from the quenched surface of the melt spun ribbons. Author

A87-51639* Case Western Reserve Univ., Cleveland, Ohio.
ELEVATED TEMPERATURE STRENGTHENING OF A MELT SPUN AUSTENITIC STEEL BY TiB₂

G. M. MICHAL (Case Western Reserve University, Cleveland, OH), T. K. GLASGOW, and T. J. MOORE (NASA, Lewis Research Center, Cleveland, OH) IN: Rapidly solidified materials; Proceedings of the International Conference, San Diego, CA, Feb. 3-5, 1986. Metals Park, OH, American Society for Metals, 1986, p. 265-271. refs

Mechanical properties of an iron-based alloy containing (by wt pct) 33Ni, 2Al, 6Ti, and 2B (resulting in an alloy containing 10 vol pct TiB₂) were evaluated by hardness and tensile testing. The alloy was cast as a ribbon using a dual 'free-jet' variation of Jech et al. (1984) method of chill-block melt-spinning against a copper wheel; to simulate thermal cycles the alloy ribbon would experience during compaction into shapes, various segments of the ribbon were annealed under a vacuum at temperatures ranging from 500 to 1150 C. The results show that maximum strengths at 650 and 760 C were developed in ribbons annealed at 1100 C; in these ribbons an optimal combination of grain coarsening with minimum TiB₂ particle growth was observed. However, the elevated-temperature strength of the TiB₂-strengthened alloy under optimal annealing conditions was poorer than that of conventional iron-based superalloys strengthened by gamma-prime precipitates. I.S.

A87-52282* Michigan Technological Univ., Houghton.

A POINT DEFECT MODEL FOR NICKEL ELECTRODE STRUCTURES

PATRICIA L. LOYSELLE, PHILIP J. KARJALA, and BAHNE C. CORNILSEN (Michigan Technological University, Houghton) IN: Symposium on Electrochemical and Thermal Modeling of Battery, Fuel Cell, and Photoenergy Conversion Systems, San Diego, CA, Oct. 20-22, 1986, Proceedings. Pennington, NJ, Electrochemical Society, Inc., 1986, p. 114-121. refs
(Contract NAG3-519)

The Raman spectra for nickel electrode active mass indicate a single formula-unit crystallographic unit cell of the layered NiOOH-type. Empirical stoichiometric formulas require that extensive point defects, cation dopants and nickel vacancies, be incorporated on nickel sites. Structural differences between the alpha/gamma and beta/beta cycles, and the influence of cobalt addition on the structure will be discussed in terms of the point defect model. Other empirical data supporting the point defect model will be considered. Author

A87-54300* Cleveland State Univ., Ohio.

CELLULAR MICROSTRUCTURE OF CHILL BLOCK MELT SPUN NI-MO ALLOYS

S. N. TEWARI (Cleveland State University, OH) and T. K. GLASGOW (NASA, Lewis Research Center, Cleveland, OH) Metallurgical Transactions A - Physical Metallurgy and Materials Science (ISSN 0360-2133), vol. 18A, Sept. 1987, p. 1663-1678. Research supported by the U.S. National Research Council and NASA. refs

Chill block melt spun ribbons of Ni-Mo binary alloys containing 8.0 to 41.8 wt pct Mo have been prepared under carefully controlled processing conditions. The growth velocity has been determined as a function of distance from the quench surface from the observed ribbon thickness dependence on the melt puddle residence time. Primary arm spacings measured at the midribbon thickness locations show a dependence on growth velocity and alloy composition which is expected from dendritic growth models for binary alloys directionally solidified in a positive temperature gradient. Microsegregation across cells and its variation with distance from the quench surface and alloy composition have been examined and compared with theoretical predictions. Author

A87-54370* National Aeronautics and Space Administration, Lewis Research Center, Cleveland, Ohio.

RESULTS OF AN INTERLABORATORY FATIGUE TEST PROGRAM CONDUCTED ON ALLOY 800H AT ROOM AND ELEVATED TEMPERATURES

J. R. ELLIS (NASA, Lewis Research Center, Cleveland; Akron, University, OH) Journal of Testing and Evaluation (ISSN 0090-3973), vol. 15, Sept. 1987, p. 249-256. Research sponsored by the General Atomic Co. Previously announced in STAR as N85-32340.
(Contract NAG3-379)

The experimental approach adopted for low cycle fatigue tests of alloy 800H involved the use of electrohydraulic test systems, hour glass geometry specimens, diametral extensometers, and axial strain computers. Attempts to identify possible problem areas were complicated by the lack of reliable data for the heat of Alloy 800H under investigation. The method adopted was to generate definitive test data in an Interlaboratory Fatigue Test Program. The laboratories participating in the program were Argonne National Laboratory, Battelle Columbus, Mar-Test, and NASA Lewis. Fatigue tests were conducted on both solid and tubular specimens at temperatures of 20, 593, and 760 C and strain ranges of 2.0, 1.0, and 0.5 percent. The subject test method can, under certain circumstances, produce fatigue data which are serious in error. This approach subsequently was abandoned at General Atomic Company in favor of parallel gage length specimens and axial extensometers. F.M.R.

N87-11182*# National Aeronautics and Space Administration. Lewis Research Center, Cleveland, Ohio.

SURFACE PROTECTION

S. R. LEVINE *In its Turbine Engine Hot Section Technology*, 1984 10 p Oct. 1984

Avail: NTIS HC A17/MF A01 CSCL 11F

The surface protection subproject consists of three major thrusts: airfoil deposition model; metallic coating life prediction; and thermal barrier coating (TBC) life prediction. The time frame for each of these thrusts and the expected outputs are presented. Further details are given for each thrust such as specific element schedules and the status of performance; in-house, via grant, or via contract.

B.G.

N87-11192*# Analox Corp., Dayton, Ohio.

EXPERIMENTAL VERIFICATION OF VAPOR DEPOSITION MODEL IN MACH 0.3 BURNER RIGS

S. A. GOEKOGLU *In NASA. Lewis Research Center Turbine Engine Hot Section Technology*, 1984 13 p Oct. 1984

(Contract NAS3-23293)

Avail: NTIS HC A17/MF A01 CSCL 11F

A comprehensive theoretical framework of deposition from combustion gases was developed covering the spectrum of various mass delivery mechanisms including vapor, thermophoretically enhanced small particle, and inertially impacting large particle deposition. Rational yet simple correlations were provided to facilitate engineering surface arrival rate predictions. Experimental verification of the deposition theory was validated using burner rigs. Toward this end, a Mach 0.3 burner rig apparatus was designed to measure deposition rates from salt-seeded combustion gases on an internally cooled cylindrical collector.

B.G.

N87-11193*# General Electric Co., Fairfield, Conn.

EFFECTS OF SURFACE CHEMISTRY ON HOT CORROSION LIFE

R. E. FRYXELL and B. K. GUPTA (TRW, Inc., Cleveland, Ohio) *In NASA. Lewis Research Center Turbine Engine Hot Section Technology*, 1984 14 p Oct. 1984

(Contract NAS3-23926)

Avail: NTIS HC A17/MF A01 CSCL 11F

Hot corrosion life prediction methodology based on a combination of laboratory test data and field service turbine components, which show evidence of hot corrosion, were examined. Components were evaluated by optical metallography, scanning electron microscopy (SEM), and electron microprobe (EMP) examination.

B.G.

N87-11873*# Syracuse Univ., N. Y. Dept. of Mechanical and Aerospace Engineering.

GRAIN BOUNDARY OXIDATION AND FATIGUE CRACK GROWTH AT ELEVATED TEMPERATURES Final Report

H. W. LIU and Y. OSHIDA Oct. 1986 30 p

(Contract NAG3-348)

(NASA-CR-179529; NAS 1.26:179529) Avail: NTIS HC A03/MF A01 CSCL 11F

Fatigue crack growth rate at elevated temperatures can be accelerated by grain boundary oxidation. Grain boundary oxidation kinetics and the statistical distribution of grain boundary oxide penetration depth were studied. At a constant delta K-level and at a constant test temperature, fatigue crack growth rate, da/dN , is a function of cyclic frequency, ν . A fatigue crack growth model of intermittent micro-ruptures of grain boundary oxide is constructed. The model is consistent with the experimental observations that, in the low frequency region, da/dN is inversely proportional to ν , and fatigue crack growth is intergranular.

Author

N87-11875*# National Aeronautics and Space Administration. Lewis Research Center, Cleveland, Ohio.

PRIMARY ARM SPACING IN CHILL BLOCK MELT SPUN NI-MO ALLOYS

S. N. TEWARI and T. K. GLASGOW 1986 21 p Presented at the Symposium on Enhanced Properties in Structural Metals via Rapid Solidification, Orlando, Fla., 6 Oct. 1986; sponsored by the American Society for Metals

(NASA-TM-88887; E-3297; NAS 1.15:88887) Avail: NTIS HC A02/MF A01 CSCL 11F

Chill block melt spun ribbons of Ni-Mo binary alloys containing 8.0 to 41.8 wt % Mo have been prepared under carefully controlled processing conditions. The growth velocity has been determined as a function of distance from the quench surface from the observed ribbon thickness dependence on the melt puddle residence time. Primary arm spacings measured at the midribbon thickness locations show a dependence on growth velocity and alloy composition which is expected from dendritic growth models for binary alloys directionally solidified in a positive temperature gradient.

Author

N87-13513*# National Aeronautics and Space Administration. Lewis Research Center, Cleveland, Ohio.

THE EFFECT OF ELECTRON BEAM WELDING ON THE CREEP RUPTURE PROPERTIES OF A NB-ZR-C ALLOY Final Report

T. J. MOORE, R. H. TITRAN, and T. L. GROBSTEIN Oct. 1986 15 p Presented at the Metallurgical Society Fall Meeting, Orlando, Fla., 5-9 Oct. 1986; sponsored by AIME

(Contract DE-AI03-86SF-16310)

(NASA-TM-88892; E-3308; DOE/NASA/16310-1; NAS 1.15:88892) Avail: NTIS HC A02/MF A01 CSCL 11F

Creep rupture tests of electron beam welded PWC-11 sheet were conducted at 1350 K. Full penetration, single pass welds were oriented transverse to the testing direction in 1 mm thick sheet. With this orientation, stress was imposed equally on the base metal, weld metal, and heat-affected zone. Tests were conducted in both the postweld annealed and aged conditions. Unwelded specimens with similar heat treatments were tested for comparative purposes. It was found that the weld region is stronger than the base metal for both the annealed and aged conditions and that the PWC-11 material is stronger in the annealed condition than in the aged condition.

Author

N87-13514*# Massachusetts Inst. of Tech., Cambridge. Dept. of Materials Science and Engineering.

THE MATHEMATICAL MODELING OF RAPID SOLIDIFICATION PROCESSING Ph.D. Thesis. Final Report

E. GUTIERREZ-MIRAVETE Nov. 1986 238 p

(Contract NAG3-365)

(NASA-CR-179551; NAS 1.26:179551) Avail: NTIS HC A11/MF A01 CSCL 11F

The detailed formulation of and the results obtained from a continuum mechanics-based mathematical model of the planar flow melt spinning (PFMS) rapid solidification system are presented and discussed. The numerical algorithm proposed is capable of computing the cooling and freezing rates as well as the fluid flow and capillary phenomena which take place inside the molten puddle formed in the PFMS process. The FORTRAN listings of some of the most useful computer programs and a collection of appendices describing the basic equations used for the modeling are included.

B.G.

N87-14482* National Aeronautics and Space Administration. Lewis Research Center, Cleveland, Ohio.

NICKEL BASE COATING ALLOY Patent

C. A. BARRETT, inventor (to NASA) and C. E. LOWELL, inventor (to NASA) 9 Sep. 1986 4 p Filed 23 Mar. 1983 Supersedes N83-24639 (21 - 14, p 2189)

(NASA-CASE-LEW-13834-1; US-PATENT-4,610,736;

US-PATENT-APPL-SN-478131; US-PATENT-CLASS-148-429;

US-PATENT-CLASS-420-460) Avail: US Patent and Trademark Office CSCL 11F

Zirconium is added to a Ni-30 Al (beta) intermetallic alloy in the range of 0.05 w/o to 0.25 w/o. This addition is made during melting or by using metal powders. The addition of zirconium improves the cyclic oxidation resistance of the alloys at temperatures above 1100 C.

Official Gazette of the US Patent and Trademark Office

N87-14483*# National Aeronautics and Space Administration. Lewis Research Center, Cleveland, Ohio.

THE CYCLIC STRESS-STRAIN BEHAVIOR OF PWA 1480 AT 650 DEG C

T. P. GABB and G. E. WELSCH (Case Western Reserve Univ., Cleveland, Ohio) 1986 16 p Presented at the TMS-AIME Annual Meeting, New Orleans, La., 2-6 Mar. 1986 Previously announced as A86-45715

(NASA-TM-87311; E-3038; NAS 1.15:87311) Avail: NTIS HC

A02/MF A01 CSCL 11F

The monotonic plastic flow behavior of several single crystal nickel-base, superalloys has been shown to vary significantly with crystallographic orientation. In the present study, the cyclic plastic flow response of one such alloy, PWA 1480, was examined at 650 deg C in air. Single crystal specimens aligned near several crystallographic directions were tested in fully reversed, total-strain-controlled low cycle fatigue tests at a frequency of 0.1 Hz. The cyclic stress-strain response and general cyclic hardening behavior was analyzed as a function of crystallographic orientation and inelastic strain range. Author

N87-14486*# Massachusetts Inst. of Tech., Cambridge. Dept. of Materials Science and Engineering.

A STUDY OF THE MICROSTRUCTURE OF A RAPIDLY SOLIDIFIED NICKEL-BASE SUPERALLOY MODIFIED WITH BORON M.S. Thesis. Final Contractor Report

J. S. SPECK Nov. 1986 87 p

(Contract NAG3-365)

(NASA-CR-179553; NAS 1.26:179553) Avail: NTIS HC A05/MF A01 CSCL 11F

The microstructures of melt-spun superalloy ribbons with variable boron levels have been studied by transmission electron microscopy. The base alloy was of approximate composition Ni-11% Cr-5%Mo-5%Al-4%Ti with boron levels of 0.06, 0.12, and 0.60 percent (all by weight). Thirty micron thick ribbons display an equiaxed chill zone near the wheel contact side which develops into primary dendrite arms in the ribbon center. Secondary dendrite arms are observed near the ribbon free surface. In the higher boron bearing alloys, boride precipitates are observed along grain boundaries. A concerted effort has been made to elucidate true grain shapes by the use of bright field/dark field microscopy. In the low boron alloy, grain shapes are often convex, and grain faces are flat. Boundary faces frequently have large curvature, and grain shapes form concave polygons in the higher boron level alloys. It is proposed that just after solidification, in all of the alloys studied, grain shapes were initially concave and boundaries were wavy. Boundary straightening is presumed to occur on cooling in the low boron alloy. Boundary migration is precluded in the higher boron alloys by fast precipitation of borides at internal interfaces. Author

N87-14487*# National Aeronautics and Space Administration. Lewis Research Center, Cleveland, Ohio.

THE EFFECT OF LASER GLAZING ON LIFE OF ZRO2 TBCS IN CYCLIC BURNER RIG TESTS

I. ZAPLATYNSKY Aug. 1986 12 p

(NASA-TM-88821; E-3026; NAS 1.15:88821) Avail: NTIS HC

A02/MF A01 CSCL 11F

The performance of laser glazed zirconia (containing 8 wt% Y2O3) TBC's was evaluated in burner rig cyclic oxidation tests at 1000 and 1050 C. It was found that the cycle duration has no effect on life of TBC's and that the increase in thickness of the glazed layer caused a slight reduction in life. Author

N87-14488*# National Aeronautics and Space Administration. Lewis Research Center, Cleveland, Ohio.

THE EFFECT OF CR, CO, AL, MO AND TA ON A SERIES OF CAST NI-BASE SUPERALLOYS ON THE STABILITY OF AN ALUMINIDE COATING DURING CYCLIC OXIDATION IN MACH 0.3 BURNER RIG

I. ZAPLATYNSKY and C. A. BARRETT Oct. 1986 27 p

(NASA-TM-88840; E-3007; NAS 1.15:88840) Avail: NTIS HC

A03/MF A01 CSCL 11F

The influence of varying the content of Co, Cr, Mo, Ta, and Al in a series of cast Ni-based gamma/gamma'superalloys on the behavior of aluminide coatings was studied in burner rig cyclic oxidation tests at 1100 C. The alloys had nominally fixed levels of Ti, W, Cb, Zr, C, and B. The alloy compositions were based on a full 2(sup 5)-fractional statistical design supplemented by 10 star point alloys and a center point alloy. This full central composite design of 43 alloys plus two additional alloys with extreme Al levels allowed a complete second degree estimating equation to be derived from the 5-compositional variables. The weight change/time data for the coated samples fitted well to the parabolic oxidation model and enabled a modified oxidation attack parameter, K'(sub a) to be derived to rank the alloys and log K' (sub a) to be used as the dependent variable in the estimating equation to determine the oxidation resistance of the coating as a function of the underlying alloy content. The most protective aluminide coatings are associated with the highest possible base alloy contents of CR and Al and at a 4 percent Ta level. The Mo and Co effects interact but at fixed levels of 0, 5, or 10% Co. A 4% Mo level is optimum. Author

N87-14489*# National Aeronautics and Space Administration. Lewis Research Center, Cleveland, Ohio.

ESTIMATION OF HIGH TEMPERATURE LOW CYCLE FATIGUE ON THE BASIS OF INELASTIC STRAIN AND STRAINRATE

A. BERKOVITS Sep. 1986 13 p

(NASA-TM-88841; E-3168; NAS 1.15:88841) Avail: NTIS HC

A02/MF A01 CSCL 11F

Fatigue life at elevated temperature can be predicted by introducing parametric values obtained from monotonic constitutive behavior into the Universal-Slopes Equation. For directionally solidified MAR-M200+HF at 975 C, these parameters are the maximum stress achievable under entirely plastic (time-independent) and purely creep (time-dependent) conditions and the corresponding inelastic strains, as well as the elastic modulus. For materials which exhibit plasticity/creep interaction, two more pairs of monotonic parameters must be evaluated for fatigue life prediction. This life-prediction method based on the Universal-Slopes Equation, resulted from a constitutive model characterizing monotonic and cyclic data as inelastic strainrate as a function of inelastic strain. Characterizing monotonic data is this way, permitted distinction between different material responses such as strain-hardening, strain-softening, and dynamic recovery effects. Understanding and defining the region of influence of each of these effects facilitated formulation of the constitutive model in relation to the mechanical and microstructural processes occurring in the material under cyclic loading. Author

N87-15303*# Georgia Inst. of Tech., Atlanta. School of Materials Engineering.

HIGH TEMPERATURE MONOTONIC AND CYCLIC DEFORMATION IN A DIRECTIONALLY SOLIDIFIED NICKEL-BASE SUPERALLOY

ERIC S. HURON May 1986 172 p

(Contract NAG3-503)

(NASA-CR-175101; NAS 1.26:175101; AD-A171480;

USAAVSCOM-TR-86-C-19) Avail: NTIS HC A08/MF A01 CSCL 11F

Directionally solidified (DS) MAR-M246+Hf was tested in tension and fatigue, at temperatures from 20 C to 1093 C. Tests were performed on (001) oriented specimens at strain rates of 50 % and 0.5 % per minute. In tension, the yield strength was constant up to 704 C, above which the strength dropped off rapidly. A strong dependence of strength on strain rate was seen at the higher temperatures. The deformation mode was observed to change from heterogeneous to homogeneous with increasing temperature. Low Cycle Fatigue tests were done using a fully reversed waveform and total strain control. For a given plastic strain range, lives increased with increasing temperature. For a given temperature strain rate had a strong effect on life. At 704 C, decreasing strain rates decreased life, while at the higher temperatures, decreasing strain rates increased life, for a given plastic strain range. These results could be explained through considerations of the deformation modes and stress levels. At the higher temperatures, marked coarsening caused beneficial stress reductions, but oxidation limited the life. The longitudinal grain boundaries were found to influence slip behavior. The degree of secondary slip adjacent to the boundaries was found to be related to the degree of misorientation between the grains. GRA

N87-16113*# National Aeronautics and Space Administration. Lewis Research Center, Cleveland, Ohio.

MORPHOLOGY OF ZIRCONIA PARTICLES EXPOSED TO D.C. ARC PLASMA JET

ISIDOR ZAPLATYNSKY Jan. 1987 17 p

(NASA-TM-88927; E-3325; NAS 1.15:88927) Avail: NTIS HC

A02/MF A01 CSCL 11F

Zirconia particles were sprayed into water with an arc plasma gun in order to determine the effect of various gun operating parameters on their morphology. The collected particles were examined by XRD and SEM techniques. A correlation was established between the content of spherical (molten) particles and the operating parameters by visual inspection and regression analysis. It was determined that the composition of the arc gas and the power input were the predominant parameters that affected the melting of zirconia particles. Author

N87-16902*# National Aeronautics and Space Administration. Lewis Research Center, Cleveland, Ohio.

CONVENTIONALLY CAST AND FORGED COPPER ALLOY FOR HIGH-HEAT-FLUX THRUST CHAMBERS

JOHN M. KAZAROFF and GEORGE A. REPAS Feb. 1987

12 p

(NASA-TP-2694; E-3304; NAS 1.60:2694) Avail: NTIS HC

A02/MF A01 CSCL 11F

The combustion chamber liner of the space shuttle main engine is made of NARloy-Z, a copper-silver-zirconium alloy. This alloy was produced by vacuum melting and vacuum centrifugal casting; a production method that is currently now available. Using conventional melting, casting, and forging methods, NASA has produced an alloy of the same composition called NASA-Z. This report compares the composition, microstructure, tensile properties, low-cycle fatigue life, and hot-firing life of these two materials. The results show that the materials have similar characteristics. Author

N87-17882*# National Aeronautics and Space Administration. Lewis Research Center, Cleveland, Ohio.

ELEVATED TEMPERATURE TENSION, COMPRESSION AND CREEP-RUPTURE BEHAVIOR OF (001)-ORIENTED SINGLE CRYSTAL SUPERALLOY PWA 1480

MOHAN G. HEBBUR and ROBERT V. MINER Feb. 1987 22 p

(NASA-TM-88950; E-3074; NAS 1.15:88950) Avail: NTIS HC

A02/MF A01 CSCL 11F

Tensile and compressive flow behavior at various temperatures and strain rates, and tensile creep rupture behavior at 850 and 1050 C and various stresses were studied for (001)-oriented single crystals of the Ni-base superalloy PWA 1480. At temperatures up to 760 C, the flow stress is insensitive to strain rate and of greater magnitude in tension than in compression. At temperatures of 800 C and above, the flow stress decreases continuously with decreasing strain rate and the tension/compression anisotropy diminishes. The second stage creep rate and rupture time exhibited power law relationships with the applied stress for both 850 and 1050 C, however with different stress dependencies. The stress exponent for the steady state creep rate was about 7 at 1050 C, but much higher at 850 C, about 12. Directional coarsening of the gamma' phase occurred during creep at 1050 C, but not at 850 C. Author

N87-17883*# Garrett Turbine Engine Co., Phoenix, Ariz.

OXIDE-DISPERSION-STRENGTHENED TURBINE BLADES, VOLUME 1

P. P. MILLAN, JR. and J. C. MAYS Oct. 1986 186 p

(Contract NAS3-20073)

(NASA-CR-179537-VOL-1; NAS 1.26:179537-VOL-1;

GARRETT-21-5278-1) Avail: NTIS HC A09/MF A01 CSCL 11F

The objective of Project 4 was to develop a high-temperature, uncooled gas turbine blade using MA6000 alloy. The program objectives were achieved. Production scale up of the MA6000 alloy was achieved with a fair degree of tolerance to nonoptimum processing. The blade manufacturing process was also optimized. The mechanical, environmental, and physical property evaluations of MA6000 were conducted. The ultimate tensile strength, to about 704 C (130 F), is higher than DS MAR-M 247 but with a corresponding lower tensile elongation. Also, above 982 C (180 F) MA6000 tensile strength does not decrease as rapidly as MAR-M 247 because the ODS mechanism still remains active. Based on oxidation resistance and diffusional stability considerations, NiCrAlY coatings are recommended. CoCrAlY coating should be applied on top of a thin NiCrAlY coating. Vibration tests, whirlpit tests, and a high-rotor-rig test were conducted to ensure successful completion of the engine test of the MA6000 TFE731 high pressure turbine blades. The results of these tests were acceptable. In production quantities, the cost of the Project 4 MA6000 blade is estimated to be about twice that of a cast DS MAR-M 247 blade. Author

N87-17884*# National Aeronautics and Space Administration. Lewis Research Center, Cleveland, Ohio.

PRELIMINARY STUDY OF NIOBIUM ALLOY CONTAMINATION BY TRANSPORT THROUGH HELIUM Final Report

COULSON M. SCHEUERMANN, THOMAS J. MOORE, and DONALD R. WHEELER 1987 20 p Presented at the 4th Symposium on Space Nuclear Power Systems, Albuquerque, N. Mex., 12-16 Jan. 1987; sponsored by New Mexico Univ.

(Contract DE-AL03-86SF-16310)

(NASA-TM-88952; DOE/NASA/16310-2; E-3401; NAS

1.15:88952) Avail: NTIS HC A02/MF A01 CSCL 11F

Preliminary tests were conducted to determine if interstitial element transport through a circulating helium working fluid was a potential problem in Brayton and Stirling space power systems. Test specimens exposed to a thermal gradient for up to 3000-hr included Nb-1%Zr, a Sm-Co alloy (referred to as SmCo in this paper), Hiperc 50 steel, and alumina to simulate various engine components of the Brayton and Stirling systems. Results indicate that helium transport of interstitial contaminants can be minimized over a 7-yr life with a monometallic Nb-1%Zr design. Exposure with other materials indicated a potential for interstitial contaminant

transport. Determination of contamination kinetics and the effects on structural integrity will require additional testing. Author

N87-18643*# National Aeronautics and Space Administration. Lewis Research Center, Cleveland, Ohio.

THE ALLOY UNDERCOOLING EXPERIMENT ON THE COLUMBIA STA 61-C SPACE SHUTTLE MISSION

FREDRIC H. HARF, THOMAS J. PICCONE (Massachusetts Inst. of Tech., Cambridge), YANZHONG WU, MERTON C. FLEMINGS, YUH SHIOHARA, LLOYD B. GARDNER (National Aeronautics and Space Administration. Marshall Space Flight Center, Huntsville, Ala.), and EDWARD A. WINSA 1987 38 p Presented at the 25th Aerospace Sciences Meeting, Reno, Nev., 12-15 Jan. 1987; sponsored by AIAA

(NASA-TM-88909; E-3332; NAS 1.15:88909) Avail: NTIS HC A03/MF A01 CSCL 11F

An Alloy Undercooling experiment was performed in an electromagnetic levitator during the Columbia STS 61-C mission in January 1986. One eutectic nickel-tin alloy specimen was partially processed before an equipment failure terminated the experiment. Examination of the specimen showed evidence of undercooling and some unusual microstructural features. Author

N87-20405*# National Aeronautics and Space Administration. Lewis Research Center, Cleveland, Ohio.

CREEP BEHAVIOR OF NIOBIUM ALLOY PWC-11 Final Report

R. H. TITRAN, T. J. MOORE, and T. L. GROBSTEIN 1987 11 p Presented at the 4th Symposium on Space Nuclear Power Systems, Albuquerque, N. Mex., 12-16 Jan. 1987; sponsored by New Mexico Univ.

(Contract DE-AC03-86SF-16310)

(NASA-TM-89834; DOE/NASA/16310-3; E-3306; NAS 1.15:89834) Avail: NTIS HC A02/MF A01 CSCL 11F

The high vacuum creep and creep-rupture behavior of a Nb-1Zr-1C alloy (PWC 11) was investigated at 1350 and 1400 K with an applied stress of 40 MPa. The material was tested in the following four conditions: annealed (1 hr 1755 K/2 hr 1475 K); annealed plus EB welded; annealed plus aged for 1000 hr at 1350 or 1400 K; and annealed, welded, and aged. It was found that the material in the annealed state was the most creep-resistant condition tested, and that aging the alloy for 1000 hr without an applied stress greatly reduced that strength; however, it was still approximately three times as creep resistant as Nb-1Zr. Additionally, the EB weld region was stronger than the base metal in each condition tested, and phase extraction of the dispersed precipitate revealed the presence of a 70%ZrC-30%NbC cubic monocarbide phase. Author

N87-20408*# National Aeronautics and Space Administration. Lewis Research Center, Cleveland, Ohio.

BITHERMAL LOW-CYCLE FATIGUE BEHAVIOR OF A NICOCRALY-COATED SINGLE CRYSTAL SUPERALLOY

J. GAYDA, T. P. GABB, R. V. MINER, and G. R. HALFORD 1987 25 p Presented at the 1987 TMS-AIME Annual Meeting, Denver, Colo., 22-26 Feb. 1987

(NASA-TM-89831; E-3484; NAS 1.15:89831) Avail: NTIS HC A02/MF A01 CSCL 20B

Specimens of a single crystal superalloy, PWA 1480, both bare and coated with a NiCoCrAlY alloy, PWA 276, were tested in low-cycle fatigue at 650 and 1050 C, and in bithermal thermomechanical fatigue tests. In the two bithermal test types, tensile strain was imposed at one of the two temperatures and reversed in compression at the other. In the high-strain regime, lives for both bithermal test types approached that for the 650 C isothermal test on an inelastic strain basis, all being controlled by the low ductility of the superalloy at 650 C. In the low-strain regime, coating cracking reduced life in the 650 C isothermal test. The bithermal test imposing tension at 650 C, termed out-of-phase, also produced rapid surface cracking, but in both coated and bare specimens. Increased crack growth rates also occurred for the out-of-phase test. Increased lives in vacuum suggested that there is a large environmental contribution to damage in the out-of-phase

test due to the 1050 C exposure followed by tensile straining at the low temperature. Author

N87-21077*# National Aeronautics and Space Administration. Lewis Research Center, Cleveland, Ohio.

SUPERALLOY RESOURCES: SUPPLY AND AVAILABILITY

JOSEPH R. STEPHENS Apr. 1987 47 p Submitted for publication

(NASA-TM-89866; E-3305; NAS 1.15:89866) Avail: NTIS HC A03/MF A01 CSCL 11F

Over the past several decades there have been shortages of strategic materials because of our near total import dependence on such metals as chromium, cobalt, and tantalum. In response to the continued vulnerability of U.S. superalloy producers to disruptions in resource supplies, NASA has undertaken a program to address alternatives to the super-alloys containing significant quantities of the strategic materials such as chromium, cobalt, niobium, and tantalum. The research program called Conservation of Strategic Aerospace Materials (COSAM) focuses on substitution, processing, and alternate materials to achieve its goals. In addition to NASA Lewis Research Center, universities and industry play an important role in the COSAM Program. This paper defines what is meant by strategic materials in the aerospace community, presents a strategic materials index, and reviews the resource supply and availability picture from the U.S. point of view. In addition, research results from the COSAM Program are highlighted and future directions for the use of low strategic material alloys or alternate materials are discussed. Author

N87-21078*# National Aeronautics and Space Administration. Lewis Research Center, Cleveland, Ohio.

ANALYSIS OF PLASMA-NITRIDED STEELS

J. SALIK (Arizona Univ., Tucson), J. FERRANTE, F. HONEYC, and R. HOFFMAN, JR. (Case Western Reserve Univ., Cleveland, Ohio) 1986 12 p Presented at the Ion Nitriding Conference, Cleveland, Ohio, 15-17 Sep. 1986; sponsored by the American Society for Metals

(NASA-TM-89815; E-3442; NAS 1.15:89815) Avail: NTIS HC A02/MF A01 CSCL 11F

The analysis of plasma nitrided steels can be divided to two main categories - structural and chemical. Structural analysis can provide information not only on the hardening mechanisms but also on the fundamental processes involved. Chemical analysis can be used to study the kinetics for the nitriding process and its mechanisms. In this paper preliminary results obtained by several techniques of both categories are presented and the applicability of those techniques to the analysis of plasma-nitrided steels is discussed. Author

N87-22034*# National Aeronautics and Space Administration. Lewis Research Center, Cleveland, Ohio.

APPLICATION OF SINGLE CRYSTAL SUPERALLOYS FOR EARTH-TO-ORBIT PROPULSION SYSTEMS

R. L. DRESHFIELD and R. A. PARR (National Aeronautics and Space Administration. Marshall Space Flight Center, Huntsville, Ala.) 1987 15 p Proposed for presentation at the 23rd Joint Propulsion Conference, San Diego, Calif., 29 Jun. - 2 Jul. 1987; sponsored by AIAA, SAE, ASME and ASEE

(NASA-TM-89877; E-3556; NAS 1.15:89877; AIAA-87-1976) Avail: NTIS HC A02/MF A01 CSCL 11F

Single crystal superalloys were first identified as potentially useful engineering materials for aircraft gas turbine engines in the mid-1960's. Although they were not introduced into service as turbine blades in commercial aircraft engines until the early 1980's, they have subsequently accumulated tens of millions of flight hours in revenue producing service. The space shuttle main engine (SSME) and potential advanced earth-to-orbit propulsion systems impose severe conditions on turbopump turbine blades which for some potential failure modes are more severe than in aircraft gas turbines. Research activities which are directed at evaluating the potential for single crystal superalloys for application as turbopump turbine blades in the SSME and advanced rocket engines are discussed. The mechanical properties of these alloys are

26 METALLIC MATERIALS

summarized and the effects of hydrogen are noted. The use of high gradient directional solidification and hot isostatic pressing to improve fatigue properties is also addressed. Author

N87-22777*# National Aeronautics and Space Administration. Lewis Research Center, Cleveland, Ohio.

FATIGUE DAMAGE INTERACTION BEHAVIOR OF PWA 1480

MICHAEL A. MCGAW *In its Structural Integrity and Durability of Reusable Space Propulsion Systems* p 83-87 1987
Avail: NTIS HC A10/MF A01 CSCL 11F

The fatigue damage interaction behavior of PWA 1480 single crystal alloy has been experimentally established for the two-level loading case in which a block of low-cycle fatigue loading is followed by high-cycle fatigue loading to failure. A relative life ratio N_1/N_2 (where N_1 and N_2 are the low- and high-cycle fatigue baseline lives, respectively) of approximately 0.002 was explored to assess the interaction behavior. The experimental results thus far show evidence of a loading order interaction effect to a similar degree of detriment as has been observed in polycrystalline materials. Current generation single crystal alloys in general, and PWA 1480 in particular, contain pores; indeed, it was observed in all cases that specimen failure initiated from pores connected with or immediately below the surface. Detailed fractographic and metallographic studies are currently being made to assess the nature of the porosity in terms of its effect on fatigue life.

Author

N87-23729*# Sverdrup Technology, Inc., Cleveland, Ohio.

THE T55-L-712 TURBINE ENGINE COMPRESSOR HOUSING REFURBISHMENT PROJECT Final Report

GEORGE W. LEISSLER, CLIFF DARLING, and GEORGE GILCHRIST (Corpus Christi Army Depot, Tex.) May 1987 23 p
Prepared in cooperation with Army Aviation Research and Development Command, Cleveland, Ohio
(Contract NAS3-24105; DA PROJ. 1L1-61102-AH-45)
(NASA-CR-179624; E-3571; NAS 1.26:179624;
AVSCOM-TR-87-C-20) Avail: NTIS HC A02/MF A01 CSCL 11F

A study was conducted to access the feasibility of reclaiming T55-L-712 turbine engine compressor housings with an 88 wt % aluminum - 12 wt % silicon alloy applied by the plasma spray processes. Tensile strength testing was conducted on as-sprayed and thermally cycled test specimens which were plasma sprayed from 0.020 to 0.100 in. Satisfactory tensile strength values were observed in the as-sprayed tensile specimens. There was essentially no decrease in tensile strength after thermally cycling the tensile specimens. Author

N87-25456*# Illinois Univ., Urbana-Champaign.

A STUDY OF REDUCED CHROMIUM CONTENT IN A NICKEL-BASE SUPERALLOY VIA ELEMENT SUBSTITUTION AND RAPID SOLIDIFICATION PROCESSING Ph.D. Thesis Final Report

WILLIAM O. POWERS May 1987 288 p
(Contract NAG3-325)
(NASA-CR-179631; NAS 1.26:179631) Avail: NTIS HC A13/MF A01 CSCL 11F

A study of reduced chromium content in a nickel base superalloy via element substitution and rapid solidification processing was performed. The two elements used as partial substitutes for chromium were Si and Zr. The microstructure of conventionally solidified materials was characterized using microscopy techniques. These alloys were rapidly solidified using the chill block melt spinning technique and the rapidly solidified microstructures were characterized using electron microscopy. The spinning technique and the rapidly solidified microstructures was assessed following heat treatments at 1033 and 1272 K. Rapidly solidified material of three alloys was reduced to particulate form and consolidated using hot isostatic pressing (HIP). The consolidated materials were also characterized using microscopy techniques. In order to evaluate the relative strengths of the consolidated alloys, compression tests were performed at room temperature and 1033 K on samples of as-HIPed and HIPed plus solution treated material.

Yield strength, porosity, and oxidation resistance characteristics are given and compared. Author

N87-25459*# National Aeronautics and Space Administration. Lewis Research Center, Cleveland, Ohio.

OBSERVATIONS OF DIRECTIONAL GAMMA PRIME COARSENING DURING ENGINE OPERATION

SUSAN L. DRAPER, DAVID R. HULL, and ROBERT L. DRESHFIELD Feb. 1987 11 p Presented at the TMS Annual Meeting, Denver, Colo., 23-26 Feb. 1987; sponsored by AIME (NASA-TM-100105; E-3642; NAS 1.15:100105) Avail: NTIS HC A02/MF A01 CSCL 11F

Two alloys with negative mismatch parameters, NASAIR 100 and a modified NASAIR 100 called Alloy 3 were run as turbine blades in an experimental ground based Garret TFE731 engine for up to 200 hr. The directional coarsening of gamma prime (rafting) that developed during engine testing was analyzed and compared to previous research from laboratory tests. The blades were found to be rafted normal to the centrifugal stress axis over much of the span, but near the surfaces, the blades were found to be rafted parallel to the centrifugal stress axis for certain cycles. Representative photomicrographs of the blades and the effects of stress and temperature on raft formation are shown. Author

N87-26217*# National Aeronautics and Space Administration. Lewis Research Center, Cleveland, Ohio.

LONG-TIME CREEP BEHAVIOR OF NB-1ZR ALLOY CONTAINING CARBON

R. H. TITRAN Oct. 1986 14 p Presented at the TMS-AIME Fall Meeting, Orlando, Fla., 5-9 Oct. 1986
(Contract DE-AL03-86SF-16310)
(NASA-TM-100142; E-3258; DOE/NASA/16310-4; NAS 1.15:100142) Avail: NTIS HC A02/MF A01 CSCL 11F

Creep tests were conducted on the Nb-1Zr base alloy with and without carbon. Testing was performed at 10 to the -6 MPa in the 1350 to 1400 K range. Creep times, to 1 percent strain, ranged from 60 to 6000 hr. All 1 percent creep data were filled by linear regression to a temperature compensating rate equation. The Nb-1Zr-0.06C alloy, tested in a weakened aged condition, appears to be four times as strong as the Nb-1Zr alloy. Author

N87-27029*# Pratt and Whitney Aircraft, East Hartford, Conn. Engineering Div.

MATERIALS FOR ADVANCED TURBINE ENGINES (MATE). PROJECT 4: EROSION RESISTANT COMPRESSOR AIRFOIL COATING

J. M. RASHID, M. FRELING, and L. A. FRIEDRICH May 1987 88 p
(Contract NAS3-20072)
(NASA-CR-179622; NAS 1.26:179622; PWA-5574-206) Avail: NTIS HC A05/MF A01 CSCL 11F

The ability of coatings to provide at least a 2X improvement in particulate erosion resistance for steel, nickel and titanium compressor airfoils was identified and demonstrated. Coating materials evaluated included plasma sprayed cobalt tungsten carbide, nickel carbide and diffusion applied chromium plus boron. Several processing parameters for plasma spray processing and diffusion coating were evaluated to identify coating systems having the most potential for providing airfoil erosion resistance. Based on laboratory results and analytical evaluations, selected coating systems were applied to gas turbine blades and evaluated for surface finish, burner rig erosion resistance and effect on high cycle fatigue strength. Based on these tests, the following coatings were recommended for engine testing: Gator-Gard plasma spray 88WC-12Co on titanium alloy airfoils, plasma spray 83WC-17Co on steel and nickel alloy airfoils, and Cr+B on nickel alloy airfoils. Author

N87-27030*# National Aeronautics and Space Administration. Lewis Research Center, Cleveland, Ohio.

THE EFFECT OF TRICRESYL-PHOSPHATE (TCP) AS AN ADDITIVE ON WEAR OF IRON (FE)

HIREN M. GHOSE, JOHN FERRANTE, and FRANK C. HONEYC
Aug. 1987 17 p
(NASA-TM-100103; E-2883; NAS 1.15:100103) Avail: NTIS HC A02/MF A01 CSCL 11F

The effect of tricresyl phosphate (TCP) as an antiwear additive in lubricant trimethylol propane triheptanoate (TMPTH) was investigated. The objective was to examine step loading wear by use of surface analysis, wetting, and chemical bonding changes in the lubricant. The investigation consisted of steploading wear studies by a pin or disk tribometer, the effects on wear related to wetting by contact angle and surface tension measurements of various liquid systems, the chemical bonding changes between lubricant and TCP chromatographic analysis, and by determining the reaction between the TCP and metal surfaces through wear scar analysis by Auger emission spectroscopy (AES). The steploading curve for the base fluid alone shows rapid increase of wear rate with load. The steploading curve for the base fluid in presence of 4.25 percent by volume TCP under dry air purge has shown a great reduction of wear rate with all loads studied. It has also been found that the addition of 4.25 percent by volume TCP plus 0.33 percent by volume water to the base lubricant under N₂ purge also greatly reduces the wear rate with all loads studied. AES surface analysis reveals a phosphate type wear resistant film, which greatly increases load-bearing capacity, formed on the iron disk. Preliminary chromatographic studies suggest that this film forms either because of ester oxidation or TCP degradation. Wetting studies show direct correlation between the spreading coefficient and the wear rate.

Author

N87-27771*# Case Western Reserve Univ., Cleveland, Ohio.
DUCTILITY AND FRACTURE IN B2 FEAL ALLOYS Ph.D. Thesis Final Report

MARTIN A. CRIMP Aug. 1987 220 p
(Contract NAG3-563)
(NASA-CR-180810; NAS 1.26:180810) Avail: NTIS HC A10/MF A01 CSCL 11F

The mechanical behavior of B₂FeAl alloys was studied. Stoichiometric Fe-50Al exhibits totally brittle behavior while iron-rich Fe-40Al yields and displays about 3% total strain. This change in behavior results from large decreases in the yield strength with iron-rich deviations from stoichiometry while the fracture stress remains essentially constant. Single crystal studies show that these yield strength decreases are directly related to decreases in the critical resolved shear stress for a group of zone axes //111/ set of (110) planes slip. This behavior is rationalized in terms of the decrease in antiphase boundary energy with decreasing aluminum content. The addition of boron results in improvements in the mechanical behavior of alloys on the iron-rich side of stoichiometry. These improvements are increased brittle fracture stresses of near-stoichiometric alloys, and enhanced ductility of up to 6% in Fe-40Al. These effects were attributed to increased grain boundary adhesion as reflected by changes in fracture mode from intergranular to transgranular failure. The increases in yield strength, which are observed in both polycrystals and single crystals, result from the quenching in of large numbers of thermal vacancies. Hall-Petch plots show that the cooling rate effects are a direct result of changes in the Hall-Petch intercept/lattice resistance flow.

Author

N87-28641*# National Aeronautics and Space Administration. Lewis Research Center, Cleveland, Ohio.

CREEP-RUPTURE BEHAVIOR OF A DEVELOPMENTAL CAST-IRON-BASE ALLOY FOR USE UP TO 800 DEG C Final Report

ROBERT H. TITRAN and COULSON M. SCHEUERMANN Aug. 1987 15 p
(Contract DE-AI01-85CE-50112)
(NASA-TM-100167; DOE/NASA/50112-70; E-3346; NAS 1.26:100167) Avail: NTIS HC A02/MF A01 CSCL 11F

A promising iron-base cast alloy is being developed as part of the DOE/NASA Stirling Engine Systems Project under contract DEN 3-282 with the United Technologies Research Center. This report presents the results of a study at the Lewis Research Center of the alloy's creep-rupture properties. The alloy was tested under a variety of conditions and was found to exhibit the normal 3-stage creep response. The alloy compared favorably with others being used or under consideration for the automotive Stirling engine cylinder/regenerator housing.

Author

N87-28647*# National Aeronautics and Space Administration. Lewis Research Center, Cleveland, Ohio.

HEAT TREATMENT FOR SUPERALLOY Patent

FREDRIC H. HARF, inventor (to NASA) 30 Jun. 1987 6 p
Filed 24 Feb. 1986 Supersedes N86-26414 (24 - 12, p 2706)
(NASA-CASE-LEW-14262-1; US-PATENT-4,676,846;
US-PATENT-APPL-SN-832296; US-PATENT-CLASS-148-162;
US-PATENT-CLASS-148-410) Avail: US Patent and Trademark Office CSCL 11F

A cobalt-free nickel-base superalloy composed of in weight % 15 Cr-5 Mo-3.5 Ti-4 Al-0.07 (max) C-remainder Ni is given a modified heat treatment. With this heat treatment the cobalt-free alloy achieves certain of the mechanical properties of the corresponding cobalt-containing nickel-base superalloy at 1200 F (650 C). Thus, strategic cobalt can be replaced by nickel in the alloy. Official Gazette of the U.S. Patent and Trademark Office

N87-29662*# National Aeronautics and Space Administration. Lewis Research Center, Cleveland, Ohio.

HIGH TEMPERATURE RADIATOR MATERIALS FOR APPLICATIONS IN THE LOW EARTH ORBITAL ENVIRONMENT

SHARON K. RUTLEDGE, BRUCE A. BANKS, MICHAEL J. MIRTICH, RICHARD LEBED, JOYCE BRADY, DEBORAH HOTES, and MICHAEL KUSSMAUL (Cleveland State Univ., Ohio.) 1987 19 p Presented at the 1987 Spring Meeting of the Materials Research Society, Anaheim, Calif., 20-24 Apr. 1987
(NASA-TM-100190; E-3772; NAS 1.15:100190) Avail: NTIS HC A02/MF A01 CSCL 11F

Radiators must be constructed of materials which have high emittance in order to efficiently radiate heat from high temperature space power systems. In addition, if these radiators are to be used for applications in the low Earth orbital environment, they must not be detrimentally affected by exposure to atomic oxygen. Four materials selected as candidate radiator materials (304 stainless steel, copper, titanium-6% aluminum-4% vanadium (Ti-6%Al-4%V), and niobium-1% zirconium (Nb-1%Zr)) were surface modified by acid etching, heat treating, abrading, sputter texturing, electrochemical etching, and combinations of the above in order to improve their emittance. Combination treatment techniques with heat treating as the second treatment provided about a factor of two improvement in emittance for 304 stainless steel, Ti-6%Al-4%V, and Nb-1%Zr. A factor of three improvement in emittance occurred for discharge chamber sputter textured copper. Exposure to atomic oxygen in an RF plasma asher did not significantly change the emittance of those samples that had been heat treated as part of their texturing process. An evaluation of oxygen penetration is needed to understand how oxidation affects the mechanical properties of these materials when heat treated.

Author

NONMETALLIC MATERIALS

Includes physical, chemical, and mechanical properties of plastics, elastomers, lubricants, polymers, textiles, adhesives, and ceramic materials.

A87-12936* National Aeronautics and Space Administration. Lewis Research Center, Cleveland, Ohio.

PARTICLE-SIZE REDUCTION OF Si₃N₄ POWDER WITH Si₃N₄ MILLING HARDWARE

T. P. HERBELL, M. R. FREEDMAN, and J. D. KISER (NASA, Lewis Research Center, Cleveland, OH) Ceramic Engineering and Science Proceedings (ISSN 0196-6219), vol. 7, July-Aug. 1986, p. 817-827. Previously announced in STAR as N86-24839. refs

The grinding of Si₃N₄ powder using reaction bonded Si₃N₄ attrition, vibratory, and ball mills with Si₃N₄ media was examined. The rate of particle size reduction and the change in the chemical composition of the powder were determined in order to compare the grinding efficiency and the increase in impurity content resulting from mill and media wear for each technique. Attrition and vibratory milling exhibited rates of specific surface area increase that were approximately eight times that observed in ball milling. Vibratory milling introduced the greatest impurity pickup. Author

A87-12938* National Aeronautics and Space Administration. Lewis Research Center, Cleveland, Ohio.

CORRELATION OF PROCESSING AND SINTERING VARIABLES WITH THE STRENGTH AND RADIOGRAPHY OF SILICON NITRIDE

W. A. SANDERS (NASA, Lewis Research Center, Cleveland, OH) and G. Y. BAAKLINI (Cleveland State University, OH) Ceramic Engineering and Science Proceedings (ISSN 0196-6219), vol. 7, July-Aug. 1986, p. 839-859. refs

A sintered Si₃N₄-SiO₂-Y₂O₃ composition, NASA 6Y, was developed that reached four-point flexural average strength/standard deviation values of 857/36, 544/33, and 462/59 MPa at room temperature, 1200 and 1370 C, respectively. These strengths represented improvements of 56, 38, and 21 percent over baseline properties at the three test temperatures. At room temperature the standard deviation was reduced by over a factor of three. These accomplishments were realized by the iterative utilization of conventional X-radiography to characterize structural (density) uniformity as affected by systematic changes in powder processing and sintering parameters. Accompanying the improvement in mechanical properties was a change in the type of flaw causing failure from a pore to a large columnar beta-Si₃N₄ grain typically 40-80 micron long, 10-30 micron wide, and with an aspect ratio of 5:1. Author

A87-12939* National Aeronautics and Space Administration. Lewis Research Center, Cleveland, Ohio.

SINTERING, MICROSTRUCTURAL, RADIOGRAPHIC, AND STRENGTH CHARACTERIZATION OF A HIGH-PURITY Si₃N₄-BASED COMPOSITION

J. D. KISER, W. A. SANDERS, and D. M. MIESKOWSKI (NASA, Lewis Research Center, Cleveland, OH) Ceramic Engineering and Science Proceedings (ISSN 0196-6219), vol. 7, July-Aug. 1986, p. 860-883. refs

A commercially available high purity alpha-Si₃N₄ powder (UBE SN-E10) was characterized, milled with additives, and sintered in a high-pressure nitrogen atmosphere at temperatures ranging from 1750 to 2140 C. The composition selected for this study has been previously examined using a different alpha-Si₃N₄ powder. Densification behavior, microstructure characteristics, X-radiographic appearance, room- and high-temperatures flexural strength, and fracture-initiating flaw sites were determined. The high-temperature flexural strengths significantly exceeded those observed in the earlier studies using an identical composition (dif-

ferent alpha-Si₃N₄ powder) and similar processing techniques.

Author

A87-12940* National Aeronautics and Space Administration. Lewis Research Center, Cleveland, Ohio.

IMPROVED CONSOLIDATION OF SILICON CARBIDE

M. R. FREEDMAN (NASA, Lewis Research Center, Cleveland, OH) and M. L. MILLARD (General Electric Co., Evendale, OH) Ceramic Engineering and Science Proceedings (ISSN 0196-6219), vol. 7, July-Aug. 1986, p. 884-892. Previously announced in STAR as N86-24836. refs

Alpha silicon carbide powder was consolidated by both dry and wet methods. Dry pressing in a double acting steel die yielded sintered test bars with an average flexural strength of 235.6 MPa with a critical flaw size of approximately 100 micro m. An aqueous slurry pressing technique produced sintered test bars with an average flexural strength of 440.8 MPa with a critical flaw size of approximately 25 micro m. Image analysis revealed a reduction in both pore area and pore size distribution in the slurry pressed sintered test bars. The improvements in the slurry pressed material properties are discussed in terms of reduced agglomeration and improved particle packing during consolidation. Author

A87-12953* California Univ., Berkeley. Lawrence Berkeley Lab. **DEGRADATION MECHANISMS IN THERMAL-BARRIER COATINGS**

S. L. SHINDE, D. A. OLSON, L. C. DE JONGHE (California, University, Berkeley), and R. A. MILLER (NASA, Lewis Research Center, Cleveland, OH) Ceramic Engineering and Science Proceedings (ISSN 0196-6219), vol. 7, July-Aug. 1986, p. 1032-1038. refs

(Contract DE-AC03-76SF-00098)

The degradation mechanism in a thermal barrier-coating system subjected to prolonged heating in air as well as to thermal cycling was studied. Bond-coat oxidation was found to be the most important reason for degradation. The oxidation produced NiO as well as Al₂O₃ in one set of samples, but the variation in initial coating structure made it difficult to resolve systematic differences between isothermally heated and thermally cycled samples. However, the contribution to degradation from changes in substrate composition seemed less in the cycled sample. Author

A87-12954* National Aeronautics and Space Administration. Lewis Research Center, Cleveland, Ohio.

TRIBOLOGY OF SELECTED CERAMICS AT TEMPERATURES TO 900 C

H. E. SLINNEY, T. P. JACOBSON, D. DEADMORE, and K. MIYOSHI (NASA, Lewis Research Center, Cleveland, OH) Ceramic Engineering and Science Proceedings (ISSN 0196-6219), vol. 7, July-Aug. 1986, p. 1039-1051. Previously announced in STAR as N86-25476. refs

Results of fundamental and focused research on the tribological properties of ceramics are discussed. The basic friction and wear characteristics are given for ceramics of interest for use in gas turbine, adiabatic diesel, and Stirling engine applications. The importance of metal oxides in ceramic/metal sliding combinations is illustrated. The formulation and tribological additives are described. Friction and wear data are given for carbide and oxide-based composite coatings for temperatures to at least 900 C. Author

A87-19504* National Aeronautics and Space Administration. Lewis Research Center, Cleveland, Ohio.

PLASTIC DEFORMATION OF A MAGNESIUM OXIDE 001-PLANE SURFACE PRODUCED BY CAVITATION

S. HATTORI, K. MIYOSHI, D. H. BUCKLEY (NASA, Lewis Research Center, Cleveland, OH), and T. OKADA (Fukui University, Japan) ASLE and ASME, Joint Tribology Conference, Pittsburgh, PA, Oct. 20-22, 1986. 6 p. refs

(ASLE PREPRINT 86-TC-3D-1)

An investigation was conducted to examine plastic deformation of a cleaved single-crystal magnesium oxide 001-plane surface exposed to cavitation. Cavitation damage experiments were carried

out in distilled water at 25 C by using a magnetostrictive oscillator in close proximity (2 mm) to the surface of the cleaved specimen. The dislocation-etch-pit patterns induced by cavitation were examined and compared with that of microhardness indentations. The results revealed that dislocation-etch-pit patterns around hardness indentations contain both screw and edge dislocations, while the etch-pit patterns on the surface exposed to cavitation contain only screw dislocations. During cavitation, deformation occurred in a thin surface layer, accompanied by work-hardening of the ceramic. The row of screw dislocations underwent a stable growth, which was analyzed crystallographically. Author

A87-19625* Case Western Reserve Univ., Cleveland, Ohio.
COLLOIDAL CHARACTERIZATION OF ULTRAFINE SILICON CARBIDE AND SILICON NITRIDE POWDERS
 PAMELA K. WHITMAN and DONALD L. FEKE (Case Western Reserve University, Cleveland, OH) *Advanced Ceramic Materials* (ISSN 0883-5551), vol. 1, Oct. 1986, p. 366-370. refs (Contract NAG3-468)

The effects of various powder treatment strategies on the colloid chemistry of aqueous dispersions of silicon carbide and silicon nitride are examined using a surface titration methodology. Pretreatments are used to differentiate between the true surface chemistry of the powders and artifacts resulting from exposure history. Silicon nitride powders require more extensive pretreatment to reveal consistent surface chemistry than do silicon carbide powders. As measured by titration, the degree of proton adsorption from the suspending fluid by pretreated silicon nitride and silicon carbide powders can both be made similar to that of silica. Author

A87-21470* National Aeronautics and Space Administration. Lewis Research Center, Cleveland, Ohio.
MECHANISM OF STRENGTH DEGRADATION FOR HOT CORROSION OF ALPHA-SiC
 JAMES L. SMIALEK and NATHAN S. JACOBSON (NASA, Lewis Research Center, Cleveland, OH) *American Ceramic Society, Journal* (ISSN 0002-7820), vol. 69, Oct. 1986, p. 741-752. Previously announced in STAR as N85-30135. refs

Sintered alpha SiC was corroded by thin films of Na₂SO₄ and Na₂CO₃ molten salts at 1000 percent. This hot corrosion attack reduced room temperature strengths by as much as 50 percent. Strength degradation was proportional to the degree and uniformity of corrosion pitting attack as controlled by the chemistry of the molten salt. Extensive fractography identified corrosion pits as the most prevalent source of failure. A fracture mechanics treatment of the strength/pit depth relationship produced an average K_{sub} IC equal to 2.6 MPa sub m^{1/2}, which is consistent with published values. E.A.K.

A87-22336* Case Western Reserve Univ., Cleveland, Ohio.
EFFECTS OF SILVER AND GROUP II FLUORIDE SOLID LUBRICANT ADDITIONS TO PLASMA-SPRAYED CHROMIUM CARBIDE COATINGS FOR FOIL GAS BEARINGS TO 650 C
 R. C. WAGNER and HAROLD E. SLINNEY (NASA, Lewis Research Center, Cleveland, OH) *Lubrication Engineering* (ISSN 0024-7154), vol. 42, Oct. 1986, p. 594-600. DOE-supported research. Previously announced in STAR as N85-14928. refs (Contract NCC3-30)

A new self-lubricating coating composition of nickel aluminide-bonded chromium carbide formulated with silver and Group II fluorides was developed in a research program on high temperature solid lubricants. One of the proposed applications for this new coating composition is as a wide temperature spectrum solid lubricant for complaint foil gas bearings. Friction and wear properties were obtained using a foil gas bearing start-stop apparatus at temperatures from 25 to 650 C. The journals were Inconel 748. Some were coated with the plasma sprayed experimental coating, others with unmodified nickel aluminide/chromium carbide as a baseline for comparison. The additional components were provided to assist in achieving low friction over the temperature range of interest. Uncoated, preoxidized Inconel X-750 foil bearings were operated against these

surfaces. The foils were subjected to repeated start/stop cycles under a 14-kPa (2-Psi) bearing unit loading. Sliding contact occurred during lift-off and coastdown at surface velocities less than 6 m/s (3000 rPm). Testing continued until 9000 start/stop cycles were accumulated or until a rise in starting torque indicated the journal/bearing had failed. Comparison in coating performance as well as discussions of their properties and methods of application are given. Author

A87-23702* National Aeronautics and Space Administration. Lewis Research Center, Cleveland, Ohio.
PROPERTIES AND POTENTIAL APPLICATIONS OF BROMINATED P-100 CARBON FIBERS
 D. A. JAWORSKE, J. R. GAIER, C. C. HUNG, and B. A. BANKS (NASA, Lewis Research Center, Cleveland, OH) *SAMPE Quarterly* (ISSN 0036-0821), vol. 18, Oct. 1986, p. 9-14. refs

A review of the properties and potential applications of bromine-intercalated pitch-based carbon fibers is presented. The dynamics of the intercalation reaction are summarized, and characteristics, such as resistivity, density, and stability, are discussed. In addition, the mechanical and electrical properties of bromine-intercalated fiber-epoxy composites will be addressed. With conductivities comparable to stainless steel, these brominated carbon fibers may be used in a number of composite applications, such as electromagnetic interference shielding containers, large conductive space structures, lightning strike-tolerant aircraft surfaces, and aircraft deicing applications. Author

A87-26112* National Aeronautics and Space Administration. Lewis Research Center, Cleveland, Ohio.
A NEW CHROMIUM CARBIDE-BASED TRIBOLOGICAL COATING FOR USE TO 900 C WITH PARTICULAR REFERENCE TO THE STIRLING ENGINE
 HAROLD E. SLINNEY (NASA, Lewis Research Center, Cleveland, OH) *Journal of Vacuum Science and Technology A* (ISSN 0734-2101), vol. 4, Nov.-Dec. 1986, p. 2629-2632. Previously announced in STAR as N86-21682.

A new chromium carbide-based coating (PS 200) is described. This coating is shown to have good friction and wear properties over a wide temperature range. A nickel alloy-bonded chromium carbide coating was used as a baseline material for comparison with experimentally formulated coatings. Coatings were plasma sprayed onto metal disks, then diamond ground to a thickness of 0.025 cm. Friction and wear were determined using a pin on disk tribometer at temperatures from 25 to 900 C in hydrogen, helium, and air. Pin materials included several metallic alloys and silicon carbide. It was found that appropriate additions of metallic silver and of barium fluoride/calcium fluoride eutectic to the baseline carbide composition significantly reduced friction coefficients while preserving, and in some cases, even enhancing wear resistance. The results of this study demonstrate that PS 200 is a promising coating composition to consider for high temperature aerospace and advanced heat engine applications. The excellent results in hydrogen make this coating of particular interest for use in the Stirling engine. Author

A87-27625* National Aeronautics and Space Administration. Lewis Research Center, Cleveland, Ohio.
COUNTERFACE EFFECTS ON THE TRIBOLOGICAL PROPERTIES OF POLYIMIDE COMPOSITES
 ROBERT L. FUSARO (NASA, Lewis Research Center, Cleveland, OH) *Lubrication Engineering* (ISSN 0024-7154), vol. 42, Nov. 1986, p. 668-675; Discussion, p. 675, 676. Previously announced in STAR as N85-26993. refs

Graphite fiber reinforced polyimide composite pins were slid against seven different counterfaces to determine the effect of material type on the tribological properties of polymer composites. In addition, the effect of sliding a new pin on a pre-established transfer film was investigated. The results indicated that almost a five order of magnitude difference in composite wear rate can occur just by varying the counterface material. An attempt to make all surfaces as smooth as possible was made, but due to differences in material composition this was not possible and a range of surface

27 NONMETALLIC MATERIALS

roughnesses were obtained. The results indicate that the smoother the surface, the lower the composite wear rate; but that small protrusions (not discernible with arithmetic surface roughness measurements) can markedly increase wear rates. A pre-established transfer film improved both run in and steady state wear rates. M.G.

A87-27838* National Aeronautics and Space Administration. Lewis Research Center, Cleveland, Ohio.

COMPOSITION OPTIMIZATION OF SELF-LUBRICATING CHROMIUM-CARBIDE-BASED COMPOSITE COATINGS FOR USE TO 760 C

CHRIS DELLACORTE and HAROLD E. SLINEY (NASA, Lewis Research Center, Cleveland, OH) ASLE Transactions (ISSN 0569-8197), vol. 30, Jan. 1987, p. 77-83. Previously announced in STAR as N86-20568.

This paper describes new compositions of self-lubricating coatings that contain chromium carbide. A bonded chromium carbide was used as the base stock because of the known excellent wear resistance and the chemical stability of chromium carbide. Additives were silver and barium fluoride/calcium fluoride eutectic. The coating constituents were treated as a ternary system consisting of: (1) the bonded carbide base material, (2) silver, and (3) the eutectic. A study to determine the optimum amounts of each constituent was performed. The various compositions were prepared by powder blending. The blended powders were then plasma sprayed onto superalloy substrates and diamond ground to the desired coating thickness. Friction and wear studies were performed at temperatures from 25 to 760 C in helium and hydrogen. A variety of counterface materials were evaluated with the objective of discovering a satisfactory metal/coating sliding combination for potential applications such as piston ring/cylinder liner couples for Stirling engines. Author

A87-30621* National Aeronautics and Space Administration. Lewis Research Center, Cleveland, Ohio.

FRACTURE TOUGHNESS OF Si₃N₄ MEASURED WITH SHORT BAR CHEVRON-NOTCHED SPECIMENS

JONATHAN A. SALEM and JOHN L. SHANNON, JR. (NASA, Lewis Research Center, Cleveland, OH) Journal of Materials Science (ISSN 0022-2461), vol. 22, Jan. 1987, p. 321-324. Previously announced in STAR as N86-13495. refs

The short bar chevron-notched specimen is used to measure the plane strain fracture toughness of hot pressed Si₃N₄. Specimen proportions and chevron-notch angle are varied, thereby varying the amount of crack extension to maximum load (upon which K_{sub IC} is based). The measured toughness (4.68 + or 0.19 MNm to the 3/2 power) is independent of these variations, inferring that the material has a flat crack growth resistance curve. Author

A87-34850* National Aeronautics and Space Administration. Lewis Research Center, Cleveland, Ohio.

ETHYNYLATED AROMATICS AS HIGH TEMPERATURE MATRIX RESINS

F. I. HURWITZ (NASA, Lewis Research Center, Cleveland, OH) SAMPE Journal (ISSN 0091-1062), vol. 23, Mar.-Apr. 1987, p. 49-53. refs

Difunctional and trifunctional arylacetylenes were used as monomers to form thermoset matrix resin composites. Composites can be hot-pressed at 180 C to react 80 percent of the acetylene groups. Crosslinking is completed by postcuring at 350 C. The postcured resins are thermally stable to nominally 460 C in air. As a result of their high crosslink density, the matrix exhibits brittle failure when uniaxial composites are tested in tension. Failure of both uniaxial tensile and flexural specimens occurs in shear at the fiber-matrix interface. Tensile fracture stresses for 0-deg composites fabricated with 60 v/o Celion 6K graphite fiber were 827 MPa. The strain to failure was 0.5 percent. Composites fabricated with 8 harness satin Celion cloth (Fiberite 1133) and tested in tension also failed in shear at tensile stresses of 413 MPa. Author

A87-37688* National Aeronautics and Space Administration. Lewis Research Center, Cleveland, Ohio.

A PRELIMINARY STUDY OF ESTER OXIDATION ON AN ALUMINUM SURFACE USING CHEMILUMINESCENCE

WILLIAM R. JONES, JR., MICHAEL A. MEADOR, and WILFREDO MORALES (NASA, Lewis Research Center, Cleveland, OH) ASLE Transactions (ISSN 0569-8197), vol. 30, April 1987, p. 211-219. Previously announced in STAR as N86-24835. refs

The oxidation characteristics of a pure ester (trimethylolpropane triheptanoate) were studied by using a chemiluminescence technique. Tests were run in a thin-film micro-oxidation apparatus with an aluminum alloy catalyst. Conditions included a pure oxygen atmosphere and a temperature range of 176 to 206 C. Results indicated that oxidation of the ester (containing 10 to the minus 3rd power M diphenylanthracene as an intensifier) was accompanied by emission of light. The maximum intensity of light emission (I_{sub max}) was a function of the amount of ester, the concentration of intensifier, and the test temperature. The induction period or the time to reach one-half of maximum intensity (t_{sub 1/2}) was an inverse function of test temperature. Decreases in light emission at the later stages of a test were caused by depletion of the intensifier. Author

A87-38065* National Aeronautics and Space Administration. Lewis Research Center, Cleveland, Ohio.

STRUCTURE AND TENSILE STRENGTH OF LAS(1.4)

J. DANIEL WHITTENBERGER (NASA, Lewis Research Center, Cleveland, OH) and RICHARD H. SMOAK (California Institute of Technology, Jet Propulsion Laboratory, Pasadena) American Ceramic Society, Communications (ISSN 0002-7820), vol. 70, April 1987, p. C-90 to C-92. refs

The tensile strength of LaS(1.4) has been estimated by diametral stress testing at room temperature, 800 and 1300 K. Brittle, tensile-type failures were obtained at all temperatures when the crosshead speed was 0.0021 mm/s; however, a 1300 K test at 0.0085 mm/s produced plastic flow. The microstructure of LaS(1.4) consisted of two phases with beta-La₂S₃ comprising about 15 vol percent of the structure and gamma-La₂S₃ the remainder. Because of the limited amount of material available for testing, no correlation between microstructure and mechanical strength could be drawn. Author

A87-38638* National Aeronautics and Space Administration. Lewis Research Center, Cleveland, Ohio.

STRUCTURE-TO-PROPERTY RELATIONSHIPS IN ADDITION CURED POLYMERS. II - RESIN TG AND COMPOSITE INITIAL MECHANICAL PROPERTIES OF NORBORNENYL CURED POLYIMIDE RESINS

WILLIAM B. ALSTON (NASA, Lewis Research Center; U.S. Army, Propulsion Directorate, Cleveland, OH) IN: International SAMPE Technical Conference, 18th, Seattle, WA, Oct. 7-9, 1986, Proceedings. Covina, CA, Society for the Advancement of Material and Process Engineering, 1986, p. 1006-1014. Previously announced in STAR as N86-29041.

PRM (polymerization of monomeric reactants) methodology was used to prepare thirty different polyimide oligomeric resins. Monomeric composition as well as chain length between sites of crosslinks were varied to examine their effects on glass transition temperature (T_g) of the cured/postcured resins. An almost linear correlation of T_g versus molecular distance between the crosslinks was observed. An attempt was made to correlate T_g with initial mechanical properties (flexural strength and interlaminar shear strength) of unidirectional graphite fiber composites prepared with these resins. However, the scatter in mechanical strength data prevented obtaining as clear a correlation as was observed for the structural modification/crosslink distance versus T_g. Instead, only a range of composite mechanical properties was obtained at the test temperatures studied (room temperature, 288 and 316 C). Perhaps more importantly, what did become apparent during the attempted correlation study was: (1) that PMR methodology could be used to prepare composites from resins that contain a wide variety of monomer modifications, and (2) that these composites almost invariably provided satisfactory initial mechanical

properties as long as the resins selected were melt processable.

Author

A87-40927* Case Western Reserve Univ., Cleveland, Ohio.
**TEM INVESTIGATION OF BETA-SiC GROWN EPITAXIALLY ON
 SI SUBSTRATE BY CVD**

C. M. CHOREY, P. PIROUZ, T. E. MITCHELL (Case Western Reserve University, Cleveland, OH), and J. A. POWELL (NASA, Lewis Research Center, Cleveland, OH) IN: Semiconductor-based heterostructures; Proceedings of the Northeast Regional Meeting, Murray Hill, NJ, May 1, 2, 1986. Warrendale, PA. Metallurgical Society of AIME, May 1987, p. 115-125.
 (Contract NGT-36-027-807)

A transmission electron microscopy study is being conducted on the microstructure of beta-SiC films grown epitaxially on 001-plane silicon by chemical vapor deposition. Observations have been made in plain view and in cross-section. A high density of stacking faults has been found in the bulk of the epilayer which are bounded by partials of the Shockley type with Burgers vectors $1/6$ 211-line. Cross-sectional high resolution electron microscopy of the interface has shown it to be semicoherent with misfit dislocations to accommodate the lattice parameter difference between the substrate and the epilayer. In addition to misfit dislocations, a high density of twins and some stacking faults are present in the SiC near the interface. Mechanisms for the nucleation and growth of these defects are discussed.

Author

A87-41078* National Aeronautics and Space Administration.
 Lewis Research Center, Cleveland, Ohio.

**EFFECTS OF MILLING BROMINATED P-100 GRAPHITE
 FIBERS**

JAMES R. GAIER (NASA, Lewis Research Center, Cleveland, OH), MICHAEL E. DILLEHAY, and PAUL D. HAMBOURGER (Cleveland State University, OH) Journal of Materials Research (ISSN 0003-6951), vol. 2, Mar.-Apr. 1987, p. 195-200. refs
 (Contract NCC3-19)

Preliminary procedures have been developed for the ball milling of pristine and brominated P-100 graphite fibers. Because of the lubricative properties of graphite, large ball loads (50 percent by volume) are required. Use of 2-propanol as a milling medium enhances the efficiency of the process. The fibers, when allowed to settle from the milling medium, tend to be preferentially aligned with rather few fibers standing up. Milled, brominated P-100 fibers have resistivities that are indistinguishable from their pristine counterparts, apparently because of loss of bromine. This suggests that bromine would not be the intercalate of choice in applications where milled fibers of this type are required. It was found that brominated graphite fibers are stable in a wide variety of organic solvents.

Author

A87-42618* National Aeronautics and Space Administration.
 Lewis Research Center, Cleveland, Ohio.

**HOW TO EVALUATE SOLID LUBRICANT FILMS USING A
 PIN-ON-DISK TRIBOMETER**

ROBERT L. FUSARO (NASA, Lewis Research Center, Cleveland, OH) Lubrication Engineering (ISSN 0024-7154), vol. 43, May 1987, p. 330-338; Discussion, p. 338. Previously announced in STAR as N86-19465. refs

Over the years, the author has evaluated and compared hundreds of solid lubricant films using a Pin-on-disk tribometer. The intent of this paper is to describe to the reader experimental techniques and some of the parameters that have been observed to be important for the evaluation and development of new solid lubricant films. Pin-on-disk tribometers will be described and discussed as will experimental methods for evaluating solid lubricant materials. Methods of preparing surfaces for the coating of the thin films and different methods for applying the films will be reviewed. Factors that affect solid lubricant performance will also be discussed. Two different macroscopic mechanisms of solid lubricant film wear exist. These will be characterized schematically, and methods of measuring wear will be examined.

Author

A87-47375* Nebraska Univ., Lincoln.

**TEMPERATURE DEPENDENCE (4K TO 300K) OF THE
 ELECTRICAL RESISTIVITY OF METHANE GROWN CARBON
 FIBERS**

JOHN A. WOOLLAM, HAO CHANG, SURAIYA NAFIS, and DAVID J. SELLMYER (Nebraska, University, Lincoln) Applied Physics Communications (ISSN 0277-9374), vol. 7, no. 1-2, 1987, p. 9-18. Research supported by Sci-Tech, Inc. refs
 (Contract NAG3-95)

Experimental measurements of the electrical resistivity vs temperature of methane vapor grown carbon fibers are presented. The fibers are heat treated from 1100 C (as-grown) to 3000 C. Data are fit to a standard two band model, which yields values for boundary scattering limited electron mobility, in-plane mean free path, energy band overlap, and total carrier density. The data are also fit to an ellipsoidal band model, where data fits yield effective masses, band overlap, Fermi velocity, phonon contributions to scattering, and ionized impurity scattering rates.

Author

A87-47923* Ford Motor Co., Dearborn, Mich.

**FRACTION OF FLASH OXIDIZED, YTTRIA-DOPED SINTERED
 REACTION-BONDED SILICON NITRIDE**

R. K. GOVILA (Ford Motor Co., Dearborn, MI) Journal of Materials Science (ISSN 0022-2461), vol. 22, April 1987, p. 1193-1198. DOE-supported research. refs
 (Contract DEN3-167; NASA ORDER P-192815-D)

The oxidation behavior of a slip cast, yttria-doped, sintered reaction-bonded silicon nitride after 'flash oxidation' was investigated. It was found that both the static oxidation resistance and flexural stress rupture life (creep deformation) were improved at 1000 C in air compared to those of the same material without flash oxidation. Stress rupture data at high temperatures (1000 to 1200 C) are presented to indicate applied stress levels for oxidation-dependent and independent failures.

Author

A87-47958* Southwest Research Inst., San Antonio, Tex.

**FRICTION AND WEAR BEHAVIOUR OF ION BEAM MODIFIED
 CERAMICS**

J. LANKFORD, W. WEI, and R. KOSSOWSKY Journal of Materials Science (ISSN 0022-2461), vol. 22, June 1987, p. 2069-2078. DOE-sponsored research. refs
 (Contract DEN3-352)

In the present study, the sliding friction coefficients and wear rates of carbide, oxide, and nitride materials for potential use as sliding seals (ring/liner) were measured under temperature, environmental, velocity, and loading conditions representative of a diesel engine. In addition, silicon nitride and partially stabilized zirconia discs were modified by ion mixing with TiNi, nickel, cobalt and chromium, and subsequently run against carbide pins, with the objective of producing reduced friction via solid lubrication at elevated temperature. Unmodified ceramic sliding couples were characterized at all temperatures by friction coefficients of 0.24 and above. However, the coefficient at 800 C in an oxidizing environment was reduced to below 0.1, for certain material combinations, by the ion implantation of TiNi or cobalt. This beneficial effect was found to derive from lubricious titanium, nickel, and cobalt oxides.

Author

A87-48324* Michigan State Univ., East Lansing.

**MICROSTRUCTURE-DERIVED MACROSCOPIC RESIDUAL
 RESISTANCE OF BROMINATED GRAPHITE FIBERS**

X. W. QIAN, S. A. SOLIN (Michigan State University, East Lansing), and J. R. GAIER (NASA, Lewis Research Center, Cleveland, OH) Physical Review B, 3rd Series (ISSN 0163-1829), vol. 35, Feb. 15, 1987, p. 2436-2442. Research supported by Exxon. refs
 (Contract NAG3-595; NSF DMR-85-17223)

The microscopic bromine distribution in pitch-based brominated graphite fibers has been measured with a scanning transmission electron microscope by monitoring the Br K alpha1 X-ray intensity. An inhomogeneous distribution of Br along the fiber is found with two distinct cross-sectional distributions, namely, a uniform distribution in Br-rich regions and a Gaussian-like distribution in

Br-poor regions. A model based on these Br distribution measurements is proposed to understand the relation between the Br microstructure and the macroscopic residual resistance of the fiber. This model yields semiquantitative agreement with experimental results. Author

A87-48989* General Motors Corp., Indianapolis, Ind.

SLOW CRACK GROWTH IN SINTERED SILICON NITRIDE

P. K. KHANDELWAL, J. CHANG, and P. W. HEITMAN (General Motors Corp., Allison Gas Turbine Div., Indianapolis, IN) IN: Fracture mechanics of ceramics; Proceedings of the Fourth International Symposium, Blacksburg, VA, June 19-21, 1985. Volume 8. New York, Plenum Press, 1986, p. 351-362. refs (Contract DEN3-17; DEN3-168)

The strength and crack growth characteristics of a sintered silicon nitride were studied at 1000 C. Fractographic analysis of material failing in dynamic fatigue revealed the presence of slow crack growth (SCG) at stressing rates below 6 ksi/min. This material can sustain a 40-ksi flexural stress at 1000 C for 400 h or more but is susceptible to both SCG and creep deformation at higher stress levels. The crack velocity exponent (N) determined both from dynamic and static fatigue experiments lies in a range from 13 to 22. The subcritical crack growth and creep behavior at 1000 C is primarily controlled by the deformation of an intergranular glassy phase. Author

A87-49325* National Aeronautics and Space Administration. Lewis Research Center, Cleveland, Ohio.

ADHESION, FRICTION AND DEFORMATION OF ION-BEAM-DEPOSITED BORON NITRIDE FILMS

K. MIYOSHI, D. H. BUCKLEY, S. A. ALTEROVITZ, J. J. POUCH, and D. C. LIU (NASA, Lewis Research Center, Cleveland, OH) Institution of Mechanical Engineers, International Conference on Tribology, London, England, July 1-3, 1987, Paper. 8 p. Previously announced in STAR as N87-15305. refs

The tribological properties and mechanical strength of boron nitride films were investigated. The BN films were predominantly amorphous and nonstoichiometric and contained small amounts of oxides and carbides. It was found that the yield pressure at full plasticity, the critical load to fracture, and the shear strength of interfacial adhesive bonds (considered as adhesion) depended on the type of metallic substrate on which the BN was deposited. The harder the substrate, the greater the critical load and the adhesion. The yield pressures of the BN film were 12 GPa for the 440C stainless steel substrate, 4.1 GPa for the 304 stainless steel substrate, and 3.3 GPa for the titanium substrate. Author

A87-49370* Goodrich (B. F.) Co., Brecksville, Ohio.

STYRENE-TERMINATED POLYSULFONE OLIGOMERS AS MATRIX MATERIAL FOR GRAPHITE REINFORCED COMPOSITES - AN INITIAL STUDY

DANA GARCIA (B. F. Goodrich Co., Brecksville, OH), KENNETH J. BOWLES, and RAYMOND D. VANNUCCI (NASA, Lewis Research Center, Cleveland, OH) SAMPE Quarterly (ISSN 0036-0821), vol. 18, July 1987, p. 1-9. refs

Results pertaining to graphite reinforced composites containing styrene-terminated oligomers as the matrix material are summarized. The processing parameters are determined and the properties of the resulting composite are evaluated. In terms of solvent impregnation techniques, CH₂Cl₂ is the preferred solvent due to its easy removal during the prepreg drying and consolidation steps. K.K.

A87-51304* Southwest Research Inst., San Antonio, Tex.

CHARACTERIZATION OF ION BEAM MODIFIED CERAMIC WEAR SURFACES USING AUGER ELECTRON SPECTROSCOPY

W. WEI and J. LANKFORD (Southwest Research Institute, San Antonio, TX) Journal of Materials Science (ISSN 0022-2461), vol. 22, July 1987, p. 2387-2396. DOE-supported research. refs (Contract DEN3-352)

An investigation of the surface chemistry and morphology of the wear surfaces of ceramic material surfaces modified by ion

beam mixing has been conducted using Auger electron spectroscopy and secondary electron microscopy. Studies have been conducted on ceramic/ceramic friction and wear couples made up of TiC and NiMo-bonded TiC cermet pins run against Si₃N₄ and partially stabilized zirconia disc surfaces modified by the ion beam mixing of titanium and nickel, as well as unmodified ceramic/ceramic couples in order to determine the types of surface changes leading to the improved friction and wear behavior of the surface modified ceramics in simulated diesel environments. The results of the surface analyses indicate that the formation of a lubricating oxide layer of titanium and nickel, is responsible for the improvement in ceramic friction and wear behavior. The beneficial effect of this oxide layer depends on several factors, including the adherence of the surface modified layer or subsequently formed oxide layer to the disc substrate, the substrate materials, the conditions of ion beam mixing, and the environmental conditions. Author

A87-53352* National Aeronautics and Space Administration. Lewis Research Center, Cleveland, Ohio.

STRUCTURAL CERAMICS IN HEAT ENGINES - THE NASA VIEWPOINT

H. B. PROBST (NASA, Lewis Research Center, Cleveland, OH) IN: Ceramic components for engines. London and New York, Elsevier Applied Science, 1986, p. 45-58. refs

The interest of NASA in the application of ceramics in heat engines is reviewed. This interest started in the early 1950s with attempts to apply oxides, borides, and cermets as gas turbine components. These attempts, as other similar efforts around the world at that time, generally met with failure due to the brittle nature of the materials and a lack of understanding of how to accommodate brittleness by appropriate design approaches. More recent efforts of the 1970s have concentrated on the silicon nitride and silicon carbide family of ceramics. This class of materials demonstrated thermal stability and thermal shock resistance in gas turbine environments. Subsequent programs funded by the DOE and managed by NASA have demonstrated great strides in material fabricability and the application of FEM design concepts. However, the materials remain brittle and lacking in reliability and reproducibility. This reliability/reproducibility problem is viewed as the major current impediment to the application of ceramics in heat engines; approaches to its solution are discussed. Author

A87-53623* National Aeronautics and Space Administration. Lewis Research Center, Cleveland, Ohio.

NEW ZrO₂-Yb₂O₃ PLASMA-SPRAYED COATINGS FOR THERMAL BARRIER APPLICATIONS

STEPHAN STECURA (NASA, Lewis Research Center, Cleveland, OH) Thin Solid Films (ISSN 0040-6090), vol. 150, 1987, p. 15-40. refs

New thermal barrier coatings, whose compositions were chosen on the basis of a limited study of the ZrO₂-Yb₂O₃ system, were evaluated by cyclic testing in a furnace at 1120 C. On Ni-16.2Cr-5.9Al-0.15Y bond coating, ZrO₂-12-12.4Yb₂O₃, ZrO₂-14.7Yb₂O₃ and ZrO₂-17.4Yb₂O₃ coatings have respectively 60, 30, 15 percent longer lives than the near-optimum ZrO₂-6.1Y₂O₃ coating. On Ni-18.3Cr-6.4Al-0.22Yb coating, ZrO₂-12.4Yb₂O₃ has about 40 percent longer life than the ZrO₂-6.1Y₂O₃ coating. The optimum Yb₂O₃ concentration in ZrO₂ at which the maximum life is obtained is believed to be between 12.4 and 14.7 wt pct. The ZrO₂-Yb₂O₃ thermal barrier systems failed through the formation of a crack or cracks in the thermal barrier coating near the bond coating interface. As-received ZrO₂-Yb₂O₃ plasma spray powders had a nonhomogeneous distribution of Yb₂O₃. Monoclinic, cubic, and tetragonal phases in addition to Zr₃Yb₄O₁₂ and an unknown phase were present. C.D.

A87-53652* National Aeronautics and Space Administration. Lewis Research Center, Cleveland, Ohio.

ANNEALING OF ELECTRON DAMAGE IN MID-IR TRANSMITTING FLUORIDE GLASS

NAROTTAM P. BANSAL (NASA, Lewis Research Center, Cleveland, OH; Rensselaer Polytechnic Institute, Troy, NY) and ROBERT H. DOREMUS (Rensselaer Polytechnic Institute, Troy, NY) *Materials Research Bulletin* (ISSN 0025-5408), vol. 21, no. 3, 1986, p. 281-288. refs
(Contract JPL-955870)

Damage in ZrF_4 - BaF_2 - LaF_3 glass induced by high-energy electrons was studied by ESR and optical spectroscopy. An optical absorption band at 314 nm in the irradiated glass annealed rapidly above about 50 C, probably by a second-order reaction at room temperature; the ESR lines annealed very slowly at room temperature. Author

N87-11009* Massachusetts Inst. of Tech., Cambridge. Energy Lab.

PROCESSING OF LASER FORMED SiC POWDER Final Report, 30 Jul. 1982 - 31 Dec. 1985

J. S. HAGGERTY and H. K. BOWEN 31 Dec. 1985 85 p

(Contract NAG3-312)

(NASA-CR-179857; NAS 1.26:179857) Avail: NTIS HC A05/MF A01 CSCL 11G

Superior SiC characteristics can be achieved through the use of ideal constituent powders and careful post-synthesis processing steps. High purity SiC powders of approx. 1000 A uniform diameter, nonagglomerated and spherical were produced. This required major revision of the particle formation and growth model from one based on classical nucleation and growth to one based on collision and coalescence of Si particles followed by their carburization. Dispersions based on pure organic solvents as well as steric stabilization were investigated. Although stable dispersions were formed by both, subsequent part fabrication emphasized the pure solvents since fewer problems with drying and residuals of the high purity particles were anticipated. Test parts were made by the colloidal pressing technique; both liquid filtration and consolidation (rearrangement) stages were modeled. Green densities corresponding to a random close packed structure (approx. 63%) were achieved; this highly perfect structure has a high, uniform coordination number (greater than 11) approaching the quality of an ordered structure without introducing domain boundary effects. After drying, parts were densified at temperatures ranging from 1800 to 2100 C. Optimum densification temperatures will probably be in the 1900 to 2000 C range based on these preliminary results which showed that 2050 C samples had experienced substantial grain growth. Although overfired, the 2050 C samples exhibited excellent mechanical properties. Biaxial tensile strengths up to 714 MPa and Vickers hardness values of 2430 kg/sq mm 2 were both more typical of hot pressed than sintered SiC. Both result from the absence of large defects and the confinement of residual porosity (less than 2.5%) to small diameter, uniformly distributed pores. Author

N87-11194* National Aeronautics and Space Administration. Lewis Research Center, Cleveland, Ohio.

COATING LIFE PREDICTION

J. A. NESBITT and M. A. GEDWILL *In its Turbine Engine Hot Section Technology*, 1984 12 p Oct. 1984

Avail: NTIS HC A17/MF A01 CSCL 11G

Hot-section gas-turbine components typically require some form of coating for oxidation and corrosion protection. Efficient use of coatings requires reliable and accurate predictions of the protective life of the coating. Currently engine inspections and component replacements are often made on a conservative basis. As a result, there is a constant need to improve and develop the life-prediction capability of metallic coatings for use in various service environments. The purpose of this present work is aimed at developing of an improved methodology for predicting metallic coating lives in an oxidizing environment and in a corrosive environment. Author

N87-11195* National Aeronautics and Space Administration. Lewis Research Center, Cleveland, Ohio.

INTRODUCTION TO LIFE MODELING OF THERMAL BARRIER COATINGS

R. A. MILLER *In its Turbine Engine Hot Section Technology*, 1984 6 p Oct. 1984

Avail: NTIS HC A17/MF A01 CSCL 11G

Thermal barrier coatings may be applied to air-cooled turbine section airfoils to insulate such components from hot gases in the engine. The coatings, which typically consist of about 0.01 to 0.04 cm of zirconia-yttria ceramic over about 0.01 cm of NiCrAlY or NiCrAlZr alloy bond coat, allow increased gas temperatures or reduced cooling air flows. This, in turn, leads to marked improvements in engine efficiency and performance. However, certain risks are associated with designing for maximum benefits, and eventually a point is reached where coating loss would immediately jeopardize the underlying component. Therefore, designers must be able to accurately predict the life of a given bill-of-material coating in any particular design. The results of an in-house aeronautics, base research and technology program which is designed to provide the first steps towards developing mission-capable life-prediction models are outlined. Author

N87-11892* Pratt and Whitney Aircraft, East Hartford, Conn. Engineering Div.

THERMAL BARRIER COATING LIFE PREDICTION MODEL DEVELOPMENT Annual Report

J. T. DEMASI 5 Nov. 1986 213 p

(Contract NAS3-23944)

(NASA-CR-179508; NAS 1.26:179508; AR-2) Avail: NTIS HC A10/MF A01 CSCL 11G

A methodology is established to predict thermal barrier coating life in an environment similar to that experienced by gas turbine airfoils. Experiments were conducted to determine failure modes of the thermal barrier coating. Analytical studies were employed to derive a life prediction model. A review of experimental and flight service components as well as laboratory post evaluations indicates that the predominant mode of TBC failure involves thermomechanical spallation of the ceramic coating layer. This ceramic spallation involves the formation of a dominant crack in the ceramic coating parallel to and closely adjacent to the topologically complex metal ceramic interface. This mechanical failure mode clearly is influenced by thermal exposure effects as shown in experiments conducted to study thermal pre-exposure and thermal cycle-rate effects. The preliminary life prediction model developed focuses on the two major damage modes identified in the critical experiments tasks. The first of these involves a mechanical driving force, resulting from cyclic strains and stresses caused by thermally induced and externally imposed mechanical loads. The second is an environmental driving force based on experimental results, and is believed to be related to bond coat oxidation. It is also believed that the growth of this oxide scale influences the intensity of the mechanical driving force. Author

N87-11893* National Aeronautics and Space Administration. Lewis Research Center, Cleveland, Ohio.

THERMAL CONDUCTIVITY OF PRISTINE AND BROMINATED P-100 FIBERS

C. C. HUNG and J. MILLER (Kenyon Coll., Gambier, Ohio) 1986 19 p Presented at the March meeting of the American Physical Society, Las Vegas, Nev., 31 Mar. - 4 Apr. 1986

(NASA-TM-88863; E-3263; NAS 1.15:88863) Avail: NTIS HC A02/MF A01 CSCL 11C

Thermal conductivity of brominated and pristine Union Carbide P-100 graphite fibers in the 30 to 160 C temperature range was determined by measuring thermal conductivities of graphite fiber epoxy composite samples and then excluding the epoxy contribution. A comparative thermal conductivity instrument was used to measure the thermal conductivity of the samples containing fibers. Results showed that the thermal conductivity values were 225 to 370 w/m-K and 215 to 340 w/m-K for pristine and brominated fibers, respectively. Furthermore, the thermal conductivity ratio of brominated to pristine P-100 fibers was 0.89,

27 NONMETALLIC MATERIALS

0.91, and 0.92 at 55 to 80 C; 108 and 130 C, respectively. Such decrease in thermal conductivity results almost entirely from the 10 percent increase in fiber cross sectional area due to bromination. This result suggests that bromination effects on P-100 fiber structure is small, and that some structural changes, presumably the sharp-angled domain wall becomes less sharp, occurring in the 80 to 108 C temperature range. Author

N87-12679*# National Aeronautics and Space Administration. Lewis Research Center, Cleveland, Ohio.

EFFECTS OF GRAPHITIZATION ON THE ENVIRONMENTAL STABILITY OF BROMINATED PITCH-BASED FIBERS

J. R. GAIER and M. E. SLABE (Cleveland State Univ., Ohio) 1986 13 p Presented at the Fall Meeting of the Materials Research Society, Boston, Mass., 1-5 Dec. 1986 (NASA-TM-88899; E-3323; NAS 1.15:88899) Avail: NTIS HC A02/MF A01 CSCL 11C

The residual bromine graphite intercalation compounds of high modulus pitch-based fibers (Amoco P-55, P-75, P-100, and P-120) were formed and their resistances were monitored under a variety of environmental conditions. A threshold graphitization was observed below which the bromination reaction does not occur to an appreciable extent. The graphitization of the P-55 fibers falls below that threshold, precluding an extensive reaction. The P-75, P-100, and P-120 fibers all form bromination compounds which are stable at ambient conditions, under vacuum, and under high humidity (100 percent humidity at 60 C). The thermal stability of the resistivity increased with decreasing graphitization, with the stable temperature for P-120 being 100 C; for P-100, 200 C; and for P-75, 250 C. When cost is a consideration, bromination of pitch-based fibers is an economical way to achieve low resistivities. Author

N87-13539*# General Electric Co., Cincinnati, Ohio. Aircraft Engine Business Group.

THERMAL BARRIER COATING LIFE PREDICTION MODEL Annual Report

R. V. HILLERY, B. H. PILSNER, T. S. COOK, and K. S. KIM Apr. 1986 129 p (Contract NAS3-23943) (NASA-CR-179504; NAS 1.26:179504; R86AEB511; AR-2) Avail: NTIS HC A07/MF A01 CSCL 11B

This is the second annual report of the first 3-year phase of a 2-phase, 5-year program. The objectives of the first phase are to determine the predominant modes of degradation of a plasma sprayed thermal barrier coating system and to develop and verify life prediction models accounting for these degradation modes. The primary TBC system consists of an air plasma sprayed ZrO-Y2O3 top coat, a low pressure plasma sprayed NiCrAlY bond coat, and a Rene' 80 substrate. Task I was to evaluate TBC failure mechanisms. Both bond coat oxidation and bond coat creep have been identified as contributors to TBC failure. Key property determinations have also been made for the bond coat and the top coat, including tensile strength, Poisson's ratio, dynamic modulus, and coefficient of thermal expansion. Task II is to develop TBC life prediction models for the predominant failure modes. These models will be developed based on the results of thermomechanical experiments and finite element analysis. The thermomechanical experiments have been defined and testing initiated. Finite element models have also been developed to handle TBCs and are being utilized to evaluate different TBC failure regimes. Author

N87-13540*# General Electric Co., Cincinnati, Ohio. Aircraft Engine Business Group.

THERMAL BARRIER COATING LIFE PREDICTION MODEL Annual Report

R. V. HILLERY and B. H. PILSNER Apr. 1985 74 p (Contract NAS3-23943) (NASA-CR-175010; NAS 1.26:175010; R85AEB304; AR-1) Avail: NTIS HC A04/MF A01 CSCL 11B

This is the first report of the first phase of a 3-year program. Its objectives are to determine the predominant modes of

degradation of a plasma sprayed thermal barrier coating system, then to develop and verify life prediction models accounting for these degradation modes. The first task (Task I) is to determine the major failure mechanisms. Presently, bond coat oxidation and bond coat creep are being evaluated as potential TBC failure mechanisms. The baseline TBC system consists of an air plasma sprayed ZrO2-Y2O3 top coat, a low pressure plasma sprayed NiCrAlY bond coat, and a Rene'80 substrate. Pre-exposures in air and argon combined with thermal cycle tests in air and argon are being utilized to evaluate bond coat oxidation as a failure mechanism. Unexpectedly, the specimens pre-exposed in argon failed before the specimens pre-exposed in air in subsequent thermal cycles testing in air. Four bond coats with different creep strengths are being utilized to evaluate the effect of bond coat creep on TBC degradation. These bond coats received an aluminide overcoat prior to application of the top coat to reduce the differences in bond coat oxidation behavior. Thermal cycle testing has been initiated. Methods have been selected for measuring tensile strength, Poisson's ratio, dynamic modulus and coefficient of thermal expansion both of the bond coat and top coat layers. Author

N87-14518*# National Aeronautics and Space Administration. Lewis Research Center, Cleveland, Ohio.

HIGH-TEMPERATURE EFFECT OF HYDROGEN ON SINTERED ALPHA-SILICON CARBIDE

G. W. HALLUM and T. P. HERBELL 1986 25 p Presented at the 88th Annual Meeting of the American Ceramic Society, Chicago, Ill., 27 Apr. - 1 May 1986 (NASA-TM-88819; E-3180; NAS 1.15:88819) Avail: NTIS HC A02/MF A01 CSCL 11G

Sintered alpha-silicon carbide was exposed to pure, dry hydrogen at high temperatures for times up to 500 hr. Weight loss and corrosion were seen after 50 hr at temperatures as low as 1000 C. Corrosion of SiC by hydrogen produced grain boundary deterioration at 1100 C and a mixture of grain and grain boundary deterioration at 1300 C. Statistically significant strength reductions were seen in samples exposed to hydrogen for times greater than 50 hr and temperatures above 1100 C. Critical fracture origins were identified by fractography as either general grain boundary corrosion at 1100 C or as corrosion pits at 1300 C. A maximum strength decrease of approximately 33 percent was seen at 1100 and 1300 C after 500 hr exposure to hydrogen. A computer assisted thermodynamic program was also used to predict possible reaction species of SiC and hydrogen. Author

N87-15305*# National Aeronautics and Space Administration. Lewis Research Center, Cleveland, Ohio.

ADHESION, FRICTION, AND DEFORMATION OF ION-BEAM-DEPOSITED BORON NITRIDE FILMS

KAZUHISA MIYOSHI, DONALD H. BUCKLEY, SAMUEL A. ALTEROVITZ, JOHN J. POUCH, and DAVID C. LIU 1987 16 p Prepared for presentation at the International Conference on Tribology, London, England, 1-3 Jul. 1987; Institution of Mechanical Engineers

(NASA-TM-88902; E-3326; NAS 1.15:88902) Avail: NTIS HC A02/MF A01 CSCL 11G

The tribological properties and mechanical strength of boron nitride films were investigated. The BN films were predominantly amorphous and nonstoichiometric and contained small amounts of oxides and carbides. It was found that the yield pressure at full plasticity, the critical load to fracture, and the shear strength of interfacial adhesive bonds (considered as adhesion) depended on the type of metallic substrate on which the BN was deposited. The harder the substrate, the greater the critical load and the adhesion. The yield pressures of the BN film were 12 GPa for the 440C stainless steel substrate, 4.1 GPa for the 304 stainless steel substrate, and 3.3 GPa for the titanium substrate. Author

N87-16140*# National Aeronautics and Space Administration. Lewis Research Center, Cleveland, Ohio.

EFFECTS OF ATMOSPHERE ON THE TRIBOLOGICAL PROPERTIES OF A CHROMIUM CARBIDE BASED COATING FOR USE TO 760 DEG C Final Report

CHRIS DELLACORTE and HAROLD E. SLINEY 1986 20 p
Proposed for presentation at the Annual Meeting of the American Society of Lubrication Engineers, 11-14 May 1987

(Contract DE-AI01-86CE-50162)

(NASA-TM-88894; DOE/NASA/50194-44; E-3311; NAS 1.15:88894) Avail: NTIS HC A02/MF A01 CSCL 11G

The effect of atmosphere on the tribological properties of a plasma-sprayed chromium carbide based self-lubricating coating is reported. The coating contains bonded chromium carbide as the wear resistant base stock to which the lubricants silver and barium fluoride/calcium fluoride eutectic are added. It has been denoted as NASA PS200. Potential applications for the PS200 coating are cylinder wall/piston ring couples for Stirling engines and foil bearing journal lubrication. Friction and wear studies were performed in helium, hydrogen, and moist air at temperatures from 25 to 760 C. In general, the atmosphere had a significant effect on both the friction and the wear of the coating and counterface material. Specimens tested in hydrogen, a reducing environment, exhibited the best tribological properties. Friction and wear increased in helium and air but are still within acceptable limits for intended applications. A variety of X-ray analyses was performed on the test specimens in an effort to explain the results. The following conclusions are made: (1) As the test atmosphere becomes less reducing, the coating experiences a higher concentration level of chromic oxide at the sliding interface which increases both the friction and wear. (2) Beneficial silver transfer from the parent coating to the counter-face material is less effective in air than in helium or hydrogen. (3) There may be a direct relationship between chromic oxide level present at the sliding interface and the friction coefficient. Author

N87-17906*# National Aeronautics and Space Administration. Lewis Research Center, Cleveland, Ohio.

TRIBOLOGICAL PROPERTIES OF POLYMER FILMS AND SOLID BODIES IN A VACUUM ENVIRONMENT

ROBERT L. FUSARO 1987 34 p Prepared for presentation at the Annual Meeting of the American Society of Lubrication Engineers, Anaheim, Calif., 11-14 May 1987

(NASA-TM-88966; E-3429; NAS 1.15:88966) Avail: NTIS HC A03/MF A01 CSCL 11B

The tribological properties of ten different polymer based materials were evaluated in a vacuum environment to determine their suitability for possible lubrication applications in a space environment, such as might be encountered on the proposed space station. A pin-on-disk tribometer was used and the polymer materials were evaluated either as solid body disks or as films applied to 440C HT stainless steel disks. A 440C HT stainless steel hemispherically tipped pin was slid against the polymer materials. For comparison, similar tests were conducted in a controlled air atmosphere of 50 percent relative humidity air. In most instances, the polymer materials lubricated much better under vacuum conditions than in air. Thus, several of the materials show promise as lubricants for vacuum applications. Friction coefficients of 0.05 or less and polymer material wear rates of up to 2 orders of magnitude less than in air were obtained. One material showed considerable promise as a traction drive material. Relatively high friction coefficients (0.36 to 0.52) and reasonably low wear rates were obtained in vacuum. Author

N87-17926*# National Aeronautics and Space Administration. Lewis Research Center, Cleveland, Ohio. Materials and Molecular Research Div.

DEGRADATION MECHANISMS IN THERMAL BARRIER COATINGS

S. L. SHINDE (California Univ., Berkeley. Lawrence Berkeley Lab.), D. A. OLSON, L. C. DEJONGHE, and R. A. MILLER Apr. 1986 19 p Presented at the 10th Annual Conference on Compositors and Advanced Ceramic Materials, Cocoa Beach, Fla., 19 Jan. 1986 Sponsored in part by NASA

(Contract DE-AC03-76SF-00098)

(NASA-TM-89309; NAS 1.15:89309; DE86-015142; LBL-21043;

CONF-860152-7) Avail: NTIS HC A02/MF A01 CSCL 11B

The degradation mechanism in thermal barrier coating systems subjected to prolonged heating in air as well as to thermal cycling was studied. Bond coat oxidation was found to be the most important reason for degradation. The oxidation produced NiO as well as AlO in one set of samples, but the variation in initial coating structure made it difficult to resolve systematic differences between isothermally heated and thermally cycled samples. However, the contribution to degradation from changes in substrate composition seemed less in the cycled sample. DOE

N87-18666*# National Aeronautics and Space Administration. Lewis Research Center, Cleveland, Ohio.

ESTER OXIDATION ON AN ALUMINUM SURFACE USING CHEMILUMINESCENCE

WILLIAM R. JONES, JR., MICHAEL A. MEADOR, and WILFREDO MORALES Jul. 1986 16 p

(NASA-TP-2611; E-2647; NAS 1.60:2611) Avail: NTIS HC A02/MF A01 CSCL 11B

The oxidation characteristics of a pure ester (trimethylpropane triheptanoate) were studied by using a chemiluminescence technique. Tests were run in a thin film microoxidation apparatus with an aluminum alloy catalyst. Conditions included a pure oxygen atmosphere and a temperature range of 176 to 206 C. Results indicated that oxidation of the ester (containing .001 M diphenylanthracene as an intensifier) was accompanied by emission of light. The maximum intensity of light emission was a function of the amount of ester, the concentration of intensifier, and the test temperature. The induction period, or the time to reach one-half of maximum intensity was inversely proportional to test temperature. Decreases in light emission at the later stages of a test were caused by depletion of the intensifier. Author

N87-18668*# National Aeronautics and Space Administration. Lewis Research Center, Cleveland, Ohio.

MECHANICAL STRENGTH AND TRIBOLOGICAL BEHAVIOR OF ION-BEAM DEPOSITED BORON NITRIDE FILMS ON NON-METALLIC SUBSTRATES

KAZUHISA MIYOSHI, DONALD H. BUCKLEY (Case Western Reserve Univ., Cleveland, Ohio), JOHN J. POUCH, SAMUEL A. ALTEROVITZ, and HAROLD E. SLINEY 1987 24 p Presented at the International Conference on Metallurgical Coatings, San Diego, Calif., 23-27 Mar. 1987; sponsored by American Vacuum Society

(NASA-TM-89818; E-3439; NAS 1.15:89818) Avail: NTIS HC A02/MF A01 CSCL 11B

An investigation was conducted to examine the mechanical strength and tribological properties of boron nitride (BN) films ion-beam deposited on silicon (Si), fused silica (SiO₂), gallium arsenide (GaAs), and indium phosphide (InP) substrates in sliding contact with a diamond pin under a load. The results of the investigation indicate that BN films on nonmetallic substrates, like metal films on metallic substrates, deform elastically and plastically in the interfacial region when in contact with a diamond pin. However, unlike metal films and substrates, BN films on nonmetallic substrates can fracture when they are critically loaded. Not only does the yield pressure (hardness) of Si and SiO₂ substrates increase by a factor of 2 in the presence of a BN film, but the critical load needed to fracture increases as well. The presence of films on the brittle substrates can arrest crack formation. The BN film reduces adhesion and friction in the sliding contact. BN

27 NONMETALLIC MATERIALS

adheres to Si and SiO₂ and forms a good quality film, while it adheres poorly to GaAs and InP. The interfacial adhesive strengths were 1 GPa for a BN film on Si and appreciably higher than 1 GPa for a BN film on SiO₂. Author

N87-18670*# National Aeronautics and Space Administration. Lewis Research Center, Cleveland, Ohio.

HARDNESS OF CAF₂ AND BAF₂ SOLID LUBRICANTS AT 25 TO 670 DEG C

DANIEL L. DEADMORE and HAROLD E. SLINEY Mar. 1987 21 p

(NASA-TM-88979; E-3448; NAS 1.15:88979) Avail: NTIS HC A02/MF A01 CSCL 11G

Plastic deformation is a prominent factor in determining the lubricating value of solid lubricants. Little information is available and its direct measurement is difficult so hardness, which is an indirect measure of this property was determined for fluoride solid lubricant compositions. The Vickers hardness of BaF₂ and CaF₂ single crystals was measured up to 670 C in a vacuum. The orientation of the BaF₂ was near the (013) plane and the CaF₂ was about 16 degrees from the degrees from the (1'11) plane. The BaF₂ has a hardness of 83 kg/sq mm at the 25 C and 9 at the 600 C. The CaF₂ is 170 at 25 C and 13 at 670 C. The decrease in hardness in the temperature range of 25 to 100 C is very rapid and amounts to 40% for both materials. Melts of BaF₂ and CaF₂ were made in a platinum crucible in ambient air with compositions of 50 to 100 wt% BaF₂. The Vickers hardness of these polycrystalline binary compositions at 25 C increased with increasing CaF₂ reaching a maximum of 150 kn/sq mm near the eutectic. The polycrystalline CaF₂ was 14% softer than that of the single crystal surface and BaF₂ was 30% harder than the single crystal surface. It is estimated that the brittle to ductile transition temperature for CaF₂ and BaF₂ is less than 100 C for the conditions present in the hardness tester. Author

N87-19518*# National Aeronautics and Space Administration. Lewis Research Center, Cleveland, Ohio.

COMBUSTION OF VELCRO IN LOW GRAVITY

SANDRA L. OLSON and RAYMOND G. SOTOS Mar. 1987 17 p

(NASA-TM-88970; E-3438; NAS 1.15:88970) Avail: NTIS HC A02/MF A01 CSCL 07D

An experimental program was conducted to investigate the low gravity burning characteristics on nylon and Nomex Velcro fastening tapes in an atmosphere of 30-percent oxygen, 70-percent nitrogen at a 70-kPa pressure. The tests were conducted using the NASA Lewis Research Center Zero Gravity Facility. The test results, as documented by high-speed cameras, indicate that both nylon and Nomex burn in low gravity for the full 5.18 sec test time but that Nomex burns less vigorously than nylon. Nylon melts as it burns, whereas Nomex forms a solid char. Nylon also sputters burning droplets as it burns. Thus, from these limited tests, it appears that Nomex Velcro is less hazardous than nylon Velcro for spacecraft applications. The results also show that residual gas velocities, and by analogy spacecraft air circulation, can enhance the low-gravity combustion. Author

N87-20421*# National Aeronautics and Space Administration. Lewis Research Center, Cleveland, Ohio.

INVESTIGATION OF PTFE TRANSFER FILMS BY INFRARED EMISSION SPECTROSCOPY AND PHASE-LOCKED ELLIPSOMETRY

JAMES L. LAUER (Rensselaer Polytechnic Inst., Troy, N.Y.), BRUCE G. BUNTING, and WILLIAM R. JONES, JR. May 1987 16 p Prepared for presentation at the 1987 Annual Meeting of the American Society of Lubrication Engineers, Anaheim, Calif., 11-14 May 1987

(NASA-TM-89844; E-3505; NAS 1.15:89844) Avail: NTIS HC A02/MF A01 CSCL 20L

When a PTFE sheet was rubbed unidirectionally over a smooth surface of stainless steel an essentially monomolecular transfer film was formed. By ellipsometric and emission infrared spectroscopic techniques it was shown that the film was 10 to 15

A thick and birefringent. From the intensity differences of infrared bands obtained with a polarizer passing radiation polarized in mutually perpendicular planes, it was possible to deduce transfer film orientation with the direction of rubbing. After standing in air for several weeks the transfer films apparently increased in thickness by as much as threefold. At the same time both the index of refraction and the absorption index decreased. Examination of the surfaces by optical and electron microscopies showed that the films had become porous and flaky. These observations were consistent with previous tribological measurements. The coefficients of friction decreased with the formation of the transfer film but increased again as the film developed breaks. The applicability of the ellipsometric and polarized infrared emission techniques to the identification of monomolecular tribological transfer films of polymers such as PTFE has been demonstrated. Author

N87-20422*# National Aeronautics and Space Administration. Lewis Research Center, Cleveland, Ohio.

DEFORMATION AND FRACTURE OF SINGLE-CRYSTAL AND SINTERED POLYCRYSTALLINE SILICON CARBIDE PRODUCED BY CAVITATION

KAZUHIISA MIYOSHI, SHUJI HATTORI (Fukui Univ., Japan.), TSUNENORI OKADA, and DONALD H. BUCKLEY (Case Western Reserve Univ., Cleveland, Ohio.) 1987 25 p Proposed for presentation at the 1987 Joint Tribology Conference, San Antonio, Tex., 5-8 Oct. 1987; sponsored by the American Society of Lubrication Engineers and ASME

(NASA-TM-88981; E-3367; NAS 1.15:88981) Avail: NTIS HC A02/MF A01 CSCL 20B

An investigation was conducted to examine the deformation and fracture behavior of single-crystal and sintered polycrystalline SiC surfaces exposed to cavitation. Cavitation erosion experiments were conducted in distilled water at 25 C by using a magnetostrictive oscillator in close proximity (1 mm) to the surface of SiC. The horn frequency was 20 kHz, and the double amplitude of the vibrating disk was 50 microns. The results of the investigation indicate that the SiC (0001) surface could be deformed in a plastic manner during cavitation. Dislocation etch pits were formed when the surface was chemically etched. The number of defects, including dislocations in the SiC (0001) surface, increased with increasing exposure time to cavitation. The presence of intrinsic defects such as voids in the surficial layers of the sintered polycrystalline SiC determined the zones at which fractured grains and fracture pits (pores) were generated. Single-crystal SiC had superior erosion resistance to that of sintered polycrystalline SiC. Author

N87-20425*# National Aeronautics and Space Administration. Lewis Research Center, Cleveland, Ohio.

HOT CORROSION ATTACK AND STRENGTH DEGRADATION OF SiC AND Si(SUB)3N(SUB)4

JAMES L. SMIALEK, DENNIS S. FOX, and NATHAN S. JACOBSON Apr. 1987 12 p Presented at the 3rd Environmental Degradation of Engineering Materials, University Park, Pa., 13-15 Apr. 1987; sponsored by Pennsylvania State Univ.

(NASA-TM-89820; E-3466; NAS 1.15:89820) Avail: NTIS HC A02/MF A01 CSCL 11G

Thin films of Na₂SO₄ and Na₂CO₃ molten salt deposits were used to corrode sintered SiC and Si₃N₄ at 1000 C. The resulting attack produced pitting and grain boundary etching resulting in strength decreases ranging from 15 to 50 percent. Corrosion pits were the predominant sources of fracture. The degree of strength decrease was found to be roughly correlated with the depth of the pit, as predicted from fracture toughness considerations. Gas evolution and bubble formation were key aspects of pit formation. Many of the observations of furnace exposures held true in a more realistic burner rig test. Author

N87-20426*# National Aeronautics and Space Administration. Lewis Research Center, Cleveland, Ohio.

ADDITION POLYMERS FROM 1,4,5,8-TETRAHYDRO-1,4;5,8-DIEPOSYANTHRACENE AND BIS-DIENES: PROCESSABLE RESINS FOR HIGH TEMPERATURE APPLICATION

MARY ANN B. MEADOR 1987 8 p Prepared for presentation at the 194th National Meeting of the American Chemical Society, New Orleans, La., 30 Aug. - 4 Sep. 1987 (NASA-TM-89838; E-3495; NAS 1.15:89838) Avail: NTIS HC A02/MF A01 CSCL 11B

1,4,5,8-Tetrahydro-1,4;5,8-diepoxyanthracene reacts with various anthracene endcapped polyimide oligomers to form Diels-Alder cycloaddition copolymers. The polymers are soluble in common organic solvents, and have molecular weights of approximately 21,000 to 32,000. Interestingly, these resins appear to be more stable in air than in nitrogen. This is shown to be due to a unique dehydration (loss of water ranges from 2 to 5 percent) at temperatures of 390 to 400 C to give thermo-oxidatively stable pentaptycene units along the polymer backbone. Because of their high softening points and good thermo-oxidative stability, the polymers have potential as processible, matrix resins for high temperature composite applications. Author

N87-22048*# National Aeronautics and Space Administration. Lewis Research Center, Cleveland, Ohio.

THERMO-OXIDATIVELY STABLE CONDENSATION POLYIMIDES CONTAINING 1,1,1-TRIARYL-2,2,2-TRIFLUOROETHANE DIANHYDRIDE AND DIAMINE MONOMERS

WILLIAM B. ALSTON and ROY F. GRATZ (Mary Washington Coll., Fredricksburg, Va.) 1987 5 p Proposed for presentation at the Symposium on Recent Advances in Polyimides and Other High Performance Polymers, 13-16 Jul. 1987, Reno, Nev.; sponsored by the American Chemical Society (NASA-TM-89875; E-3551; NAS 1.15:89875; AVSCOM-TR-87-C-7) Avail: NTIS HC A02/MF A01 CSCL 11B

Nine new condensation polyimides containing the trifluorophenylethylidene linkage were synthesized by the amic-acid route. Several other polyimides, including some with the hexafluoroisopropylidene linkage, were also prepared as controls. Amic-acid solutions were characterized by determining their inherent viscosities prior to thermal conversion into polyimide films. Glass transition temperatures (T_{g}), thermogravimetric analysis (TGA), and isothermal weight loss data were obtained for the films. The films were pulverized into molding powders which, in turn, were thermally processed under pressure into neat resin discs. The discs were also characterized by T_{g} and 316 C and 371 C isothermal weight losses. The film study identified two new polyimides with T_{g} greater than 371 C and two new polyimides with low rates of weight loss. The resin discs exhibited the same overall trends in T_{g} and weight loss as the respective films, however the weight loss per unit surface area was always greater, presumably due to voids or to mechanical degradation induced during preparation of the molding powders. Author

N87-22860*# National Aeronautics and Space Administration. Lewis Research Center, Cleveland, Ohio.

FRICTION AND WEAR OF SINTERED ALPHA SIC SLIDING AGAINST IN-718 ALLOY AT 25 TO 800 C IN ATMOSPHERIC AIR AT AMBIENT PRESSURE

DANIEL L. DEADMORE and HAROLD E. SLINEY Jul. 1986 30 p (NASA-TM-87353; E-3107; NAS 1.15:87353) Avail: NTIS HC A03/MF A01 CSCL 11C

The sliding friction and wear of the SiC-nickel based alloy IN-718 couple under line contact test conditions in atmospheric air at a linear velocity of 0.18 m/sec and a load of 6.8 kg (67N) was investigated at temperatures of 25 to 800 C. It was found that the coefficient of friction was 0.6 up to 350 C then decreased to 0.3 at 500 and 800 C. It is suggested that the sharp decrease in the friction in the range of 350 to 550 C is due to the lubrication value of oxidation products. The wear rate reaches a minimum of

1 x 10 to the -10 to 2 x 10 to the -10 cu cm/cm/kg at 400 to 600 C. Author

N87-23736* National Aeronautics and Space Administration. Lewis Research Center, Cleveland, Ohio.

OXIDATION PROTECTION COATINGS FOR POLYMERS Patent JAMES S. SOVEY, inventor (to NASA), BRUCE A. BANKS, inventor (to NASA), and MICHAEL J. MIRTICH, inventor (to NASA) 12 May 1987 7 p Filed 27 Feb. 1986 Supersedes N86-26434 (24-17, p 2709) Division of US-Patent-4,604,181, Patent-Appl-SN-761235, which is a division of US-Patent-4,560,577, US-Patent-Appl-SN-649330

(NASA-CASE-LEW-14072-3; US-PATENT-4,664,980; US-PATENT-APPL-SN-834977; US-PATENT-CLASS-428-421; US-PATENT-CLASS-428-422; US-PATENT-CLASS-428-447; US-PATENT-CLASS-428-473.5; US-PATENT-CLASS-428-702) Avail: US Patent and Trademark Office CSCL 11B

A polymeric substrate is coated with a metal oxide film to provide oxidation protection in low Earth orbital environments. The film contains about four volume percent polymer to provide flexibility. NASA

N87-23750*# National Aeronautics and Space Administration. Lewis Research Center, Cleveland, Ohio.

SOL-GEL SYNTHESIS OF MgO-SiO₂ GLASS COMPOSITIONS HAVING STABLE LIQUID-LIQUID IMMISCIBILITY

NAROTTAM P. BANSAL Apr. 1987 23 p Presented at the 89th Annual Meeting and Exposition of the American Ceramic Society, Pittsburgh, Pa., 26-30 Apr. 1987 (NASA-TM-89905; E-3599; NAS 1.15:89905) Avail: NTIS HC A02/MF A01 CSCL 11B

MgO-SiO₂ glasses containing up to 15 mol % MgO, which could not have been prepared by the conventional glass melting method due to the presence of stable liquid-liquid immiscibility, were synthesized by the sol-gel technique. Clear and transparent gels were obtained from the hydrolysis and polycondensation of silicon tetraethoxide (TEOS) and magnesium nitrate hexahydrate when the water/TEOS mole ratio was four or more. The gelling time decreased with increase in magnesium content, water/TEOS ratio, and reaction temperature. Magnesium nitrate hexahydrate crystallized out of the gels containing 15 and 20 mol % MgO on slow drying. This problem was partially alleviated by drying the gels quickly at higher temperatures. Monolithic gel samples were prepared using glycerol as the drying control additive. The gels were subjected to various thermal treatments and characterized by several methods. No organic groups could be detected in the glasses after heat treatments to approx. 800 C, but trace amounts of hydroxyl groups were still present. No crystalline phase was found from X-ray diffraction in the gel samples to approx. 890 C. At higher temperatures, alpha quartz precipitated out as the crystalline phase in gels containing up to 10 mol % MgO. The overall activation energy for gel formation in 10MgO-90SiO₂ (mol %) system for water/TEOS mole ratio of 7.5 was calculated to be 58.7 kJ/mol. M.G.

N87-24563*# National Aeronautics and Space Administration. Lewis Research Center, Cleveland, Ohio.

STABILITY OF BROMINE, IODINE MONOCHLORIDE, COPPER (II) CHLORIDE, AND NICKEL (II) CHLORIDE INTERCALATED PITCH-BASED GRAPHITE FIBERS

JAMES R. GAIER, MELISSA E. SLABE, and NANETTE SHAFFER (Intercal Co., Port Huron, Mich.) Jul. 1987 18 p Prepared for the 18th Biennial Conference on Carbon, Worcester, Mass., 19-24 Jul. 1987; sponsored by American Carbon Society (NASA-TM-89904; E-3431; NAS 1.15:89904) Avail: NTIS HC A02/MF A01 CSCL 11G

Four different grades of pitch-based graphite fibers (Amoco P-55, P-75, P-100, and P-120) were intercalated with each of four different intercalates: bromine (Br₂), iodine monochloride (ICl), copper (II) chloride (CuCl₂), and nickel (II) chloride (NiCl₂). The P-55 fibers did not react with Br₂ or NiCl₂, and the P-75 did not react with NiCl₂. The stability of the electrical resistance of the intercalated fibers was monitored over long periods of time in

27 NONMETALLIC MATERIALS

ambient, high humidity (100 percent at 60 C), vacuum (10 to the -6 torr), and high temperature (up to 400 C) conditions. Fibers with lower graphitization form graphite intercalation compounds (GIC's) which are more stable than those with higher graphitization (i.e., P-55 (most stable) greater than P-75 greater than P-100 greater than P-120 (least stable). Br₂ formed the most stable GIC's followed in order of decreasing stability by ICl, CuCl₂, and NiCl₂. While Br₂ GIC's had the most stability, ICl had the advantages of forming GIC's with slightly greater reduction in resistance (by about 10%) than Br₂, and the ability to intercalate P-55 fiber. Transition metal chlorides are susceptible to water vapor and high temperature. The stability of fibers in composites differs.

Author

N87-24565*# National Aeronautics and Space Administration. Lewis Research Center, Cleveland, Ohio.

TRIBOLOGICAL PROPERTIES OF COAL SLURRIES

ROBERT L. FUSARO and DALE L. SCHRUBENS 1987 27 p Prepared for presentation at the Joint Tribology Conference, San Antonio, Tex., 5-8 Oct. 1987; cosponsored by American Society of Lubrication Engineers, and ASME (NASA-TM-89930; E-3634; NAS 1.15:89930) Avail: NTIS HC A03/MF A01 CSCL 11G

A pin-on-disk tribometer was used to study the tribological properties of methyl alcohol-coal slurries. Friction coefficients, steel pin wear rates and wear surface morphological studies were conducted on AISI 440C HT and M-50 bearing steels which were slid dry and in solutions of methyl alcohol, methyl alcohol-fine coal particles, and methyl alcohol-fine coal particles-flocking additive. The latter was an oil derived from coal and originally intended to be added to the coal slurry to improve the sedimentation and rheology properties. The results of this study indicated that the addition of the flocking additive to the coal slurry markedly improved the tribological properties, especially wear. In addition, the type of steel was found to be very important in determining the type of wear that took place. Cracks and pits were found on the M-50 steel pin wear surfaces that slid in the coal slurries while 440C HT steel pins showed none.

Author

N87-24566*# National Aeronautics and Space Administration. Lewis Research Center, Cleveland, Ohio.

EFFECT OF ABRASIVE GRIT SIZE ON WEAR OF MANGANESE-ZINC FERRITE UNDER THREE-BODY ABRASION

KAZUHISA MIYOSHI 1987 26 p Proposed for presentation at the 1987 Joint Tribology Conference, San Antonio, Tex., 5-8 Oct. 1987; sponsored by the American Society of Lubrication Engineers and ASME (NASA-TM-89879; E-3559; NAS 1.15:89879) Avail: NTIS HC A03/MF A01 CSCL 11G

Wear experiments were conducted using replication electron microscopy and reflection electron diffraction to study abrasion and deformed layers produced in single-crystal Mn-Zn ferrites under three-body abrasion. The abrasion mechanism of Mn-Zn ferrite changes drastically with the size of abrasive grits. With 15-micron (1000-mesh) SiC grits, abrasion of Mn-Zn ferrite is due principally to brittle fracture; while with 4- and 2-micron (4000- and 6000-mesh) SiC grits, abrasion is due to plastic deformation and fracture. Both microcracking and plastic flow produce polycrystalline states on the wear surfaces of single-crystal Mn-Zn ferrites. Coefficient of wear, total thickness of the deformed layers, and surface roughness of the wear surfaces increase markedly with an increase in abrasive grit size. The total thicknesses of the deformed layers are 3 microns for the ferrite abraded by 15-micron SiC, 0.9 microns for the ferrite abraded by 4-micron SiC, and 0.8 microns for the ferrite abraded by 1-micron SiC.

Author

N87-24573*# Massachusetts Inst. of Tech., Cambridge.

PROCESSING OF LASER FORMED SiC POWDER Final Report

J. S. HAGGERTY and H. K. BOWEN Jun. 1987 80 p (Contract NAG3-312) (NASA-CR-179638; NAS 1.26:179638) Avail: NTIS HC A05/MF A01 CSCL 11B

Processing research was undertaken to demonstrate that superior SiC characteristics could be achieved through the use of ideal constituent powders and careful post-synthesis processing steps. Initial research developed the means to produce approximately 1000 Å uniform diameter, nonagglomerated, spherical, high purity SiC powders. Accomplishing this goal required major revision of the particle formation and growth model from one based on classical nucleation and growth to one based on collision and coalescence of Si particles followed by their carburization. Dispersions based on pure organic solvents as well as steric stabilization were investigated. Test parts were made by the colloidal pressing technique; both liquid filtration and consolidation (rearrangement) stages were modeled. Green densities corresponding to a random close packed structure were achieved. After drying, parts were densified at temperatures ranging from 1800 to 2100 C. This research program accomplished all of its major objectives. Superior microstructures and properties were attained by using powders having ideal characteristics and special post-synthesis processing procedures.

Author

N87-24574*# National Aeronautics and Space Administration. Lewis Research Center, Cleveland, Ohio.

EFFECTS OF SEQUENTIAL TREATMENT WITH FLUORINE AND BROMINE ON GRAPHITE FIBERS

CHING-CHEH HUNG, MARK STAHL, CAROLYN MACIAG, and MELISSA SLABE Jul. 1987 15 p Presented at the 18th Biennial Conference on Carbon, Worcester, Mass., 19-24 Jul. 1987; sponsored by American Carbon Society Prepared in cooperation with Cleveland State Univ., Ohio (NASA-TM-100106; E-3644; NAS 1.15:100106) Avail: NTIS HC A02/MF A01 CSCL 11G

Three pitch based graphite fibers with different degrees of graphitization and one polyacrylonitrile (PAN) based carbon fiber from Amoco Corporation were treated with 1 atm, room temperature fluorine gas for 90 hrs. Fluorination resulted in higher electrical conductivity for all pitch fibers. Further bromination after ambient condition defluorination resulted in further increases in electrical defluorination conductivity for less graphitized, less structurally ordered pitch fibers (P-55) which contain about 3% fluorine by weight before bromination. This product can be stable in 200 C air, or 100% humidity at 60 C. Due to its low cost, this less graphitized fiber may be useful for industrial application, such as airfoil deicer materials. The same bromination process, however, resulted in conductivity decreases for fluorine rich, more graphitized, structurally oriented pitch fibers (P-100 and P-75). Such decreases in electrical conductivity were partially reversed by heating the fibers at 185 C in air. Differential scanning calorimetric (DSC) data indicated that the more graphitized fibers (P-100) contained BrF₃, whereas the less graphitized fibers (P-55) did not.

Author

N87-25476*# Case Western Reserve Univ., Cleveland, Ohio. Inst. of Technology.

STABILITY AND RHEOLOGY OF DISPERSIONS OF SILICON NITRIDE AND SILICON CARBIDE Final Report

DONALD L. FEKE Jun. 1987 74 p (Contract NAG3-468) (NASA-CR-179634; NAS 1.26:179634) Avail: NTIS HC A04/MF A01 CSCL 11G

The relationship between the surface and colloid chemistry of commercial ultra-fine silicon carbide and silicon nitride powders was examined by a variety of standard characterization techniques and by methodologies especially developed for ceramic dispersions. These include electrokinetic measurement, surface titration, and surface spectroscopies. The effects of powder pretreatment and modification strategies, which can be utilized to augment control of processing characteristics, were monitored with these technologies. Both silicon carbide and nitride were found to

exhibit silica-like surface chemistries, but silicon nitride powders possess an additional amine surface functionality. Colloidal characteristics of the various nitride powders in aqueous suspension is believed to be highly dependent on the relative amounts of the two types of surface groups, which in turn is determined by the powder synthesis route. The differences in the apparent colloidal characteristics for silicon nitride powders cannot be attributed to the specific absorption of ammonium ions. Development of a model for the prediction of double-layer characteristics of materials with a hybrid site interface facilitated understanding and prediction of the behavior of both surface charge and surface potential for these materials. The utility of the model in application to silicon nitride powders was demonstrated.

Author

N87-25480* # National Aeronautics and Space Administration. Lewis Research Center, Cleveland, Ohio.

AN EVALUATION OF CANDIDATE OXIDATION RESISTANT MATERIALS FOR SPACE APPLICATIONS IN LEO

SHARON RUTLEDGE, BRUCE BANKS, FRANK DIFILIPPO, JOYCE BRADY, THERESE DEVER, and DEBORAH HOTES (Cleveland State Univ., Ohio.) 1986 16 p Presented at the Workshop on Atomic Oxygen Effects, Pasadena, Calif., 10-11 Nov. 1986; sponsored by JPL (NASA-TM-100122; E-3669; NAS 1.15:100122) Avail: NTIS HC A02/MF A01 CSCL 11C

Ground based testing of materials considered for polyimide (Kapton) solar array blanket protection and graphite-epoxy structural member protection was performed in an RF plasma asher. Protective coatings on Kapton from various commercial sources and from NASA Lewis Research Center were exposed to the air plasma; and mass loss per unit area was measured for each sample. All samples evaluated provided some protection to the underlying surface, but metal-oxide-fluoropolymer coatings provided the best protection by exhibiting very little degradation after 47 hr of asher exposure. Mica paint was evaluated as a protective coating for graphite-epoxy structural members. Mica appeared to be resistant to attack by atomic oxygen, but only offered limited protection as a paint. This is believed to be due to the paint vehicle ashing underneath the mica leaving unattached mica flakes lying on the surface. The protective coatings on Kapton evaluated so far are promising but further research on protection of graphite-epoxy support structures is needed.

Author

N87-26231* # National Aeronautics and Space Administration. Lewis Research Center, Cleveland, Ohio.

THE TRIBOLOGICAL BEHAVIOR OF POLYPHENYL ETHER AND POLYPHENYL THIOETHER AROMATIC LUBRICANTS Ph.D. Thesis - Kyushu Univ., Japan

WILLIAM R. JONES, JR. Jul. 1987 231 p (NASA-TM-100166; E-3424; NAS 1.15:100166) Avail: NTIS HC A11/MF A01 CSCL 11H

The tribological behavior of several polyphenyl ethers and polyphenyl thioethers is reported. Tribological areas covered include: surface tension and wettability measurements, boundary lubrication, ferrography, thermal and oxidative stability and chemiluminescence.

Author

N87-26232* # National Aeronautics and Space Administration. Lewis Research Center, Cleveland, Ohio.

SYNTHESIS, PHYSICAL AND CHEMICAL PROPERTIES, AND POTENTIAL APPLICATIONS OF GRAPHITE FLUORIDE FIBERS

CHING-CHEH HUNG, MARTIN LONG, and MARK STAHL (Cleveland State Univ., Ohio.) Aug. 1987 15 p Prepared for presentation at the Conference on Emerging Technologies in Materials, Minneapolis, Minn., 18-20 Aug. 1987; sponsored by American Inst. of Chemical Engineers. (NASA-TM-100156; E-3699; NAS 1.15:100156) Avail: NTIS HC A02/MF A01 CSCL 11G

Graphite fluoride fibers can be produced by fluorinating pristine or intercalated graphite fibers. The higher the degree of graphitization of the fibers, the higher the temperature needed to

reach the same degree of fluorination. Pitched based fibers were fluorinated to fluorine-to-carbon atom ratios between 0 and 1. The graphite fluoride fibers with a fluorine-to-carbon atom ratio near 1 have extensive visible structural damage. On the other hand, fluorination of fibers pretreated with bromine or fluorine and bromine result in fibers with a fluorine-to-carbon atom ratio nearly equal to 0.5 with no visible structural damage. The electrical resistivity of the fibers is dependent upon the fluorine to carbon atom ratio and ranged from .01 to 10 to the 11th ohm/cm. The thermal conductivity of these fibers ranged from 5 to 73 W/m-k, which is much larger than the thermal conductivity of glass, which is the regular filler in epoxy composites. If graphite fluoride fibers are used as a filler in epoxy or PTFE, the resulting composite may be a high thermal conductivity material with an electrical resistivity in either the insulator or semiconductor range. The electrically insulating product may provide heat transfer with lower temperature gradients than many current electrical insulators. Potential applications are presented.

Author

N87-26233* # Case Western Reserve Univ., Cleveland, Ohio. Dept. of Mechanical and Aerospace Engineering.

COMPOSITION OPTIMIZATION OF CHROMIUM CARBIDE BASED SOLID LUBRICANT COATINGS FOR FOIL GAS BEARINGS AT TEMPERATURES TO 650 C Final Contractor Report

CHRISTOPHER DELLACORTE Jul. 1987 20 p (Contract NCC3-30)

(NASA-CR-179649; E-3681; NAS 1.26:179649) Avail: NTIS HC A02/MF A01 CSCL 11G

A test program to determine the optimum composition of chromium carbide based solid lubricant coatings for compliant gas bearings is described. The friction and wear properties of the coatings are evaluated using a foil gas bearing test apparatus. The various coatings were prepared by powder blending, then plasma sprayed onto Inconel 718 test journals and diamond ground to the desired coating thickness and surface finish. The journals were operated against preoxidized nickel-chromium alloy foils. The test bearings were subjected to repeated start/stop cycles under a 14 kPa (2 psi) bearing unit load. The bearings were tested for 9000 start/stop cycles or until the specimen wear reached a predetermined failure level. In general, the addition of silver and eutectic to the chromium carbide base stock significantly reduced foil wear and increased journal coating wear. The optimum coating composition, PS212 (70 wt% metal bonded Cr3C2, 15 wt% Ag, 15% BaF2/CaF2 eutectic), reduced foil wear by a factor of two and displayed coating wear well within acceptable limits. The load capacity of the bearing using the plasma-sprayed coating prior to and after a run-in period was ascertained and compared to polished Inconel 718 specimens.

Author

N87-27053* # Case Western Reserve Univ., Cleveland, Ohio. **EXPERIMENTAL EVALUATION OF CHROMIUM-CARBIDE-BASED SOLID LUBRICANT COATINGS FOR USE TO 760 C Final Report**

CHRISTOPHER DELLACORTE Aug. 1987 44 p (Contract NCC3-30; DE-AI01-85CE-50162)

(NASA-CR-180808; E-3713; DOE/NASA/0030-2; NAS 1.26:180808) Avail: NTIS HC A03/MF A01 CSCL 11H

A research program is described which further developed and investigated chromium carbide based self-lubricating coatings for use to 760 C. A bonded chromium carbide was used as the base stock because of the known excellent wear resistance and the chemical stability of chromium carbide. Additives were silver and barium fluoride/calcium fluoride eutectic. The three coating components were blended in powder form, applied to stainless steel substrates by plasma spraying and then diamond ground to the desired coating thickness. A variety of coating compositions was tested to determine the coating composition which gave optimum tribological results. Coatings were tested in air, helium, and hydrogen at temperatures from 25 to 760 C. Several counterface materials were evaluated with the objective of discovering a satisfactory metal/coating sliding combination for potential applications, such as piston ring/cylinder liner couples

for Stirling engines. In general, silver and fluoride additions to chromium carbide reduced the friction coefficient and increased the wear resistance relative to the unmodified coating. The lubricant additives acted synergistically in reducing friction and wear.

Author

N87-27810*# National Aeronautics and Space Administration. Lewis Research Center, Cleveland, Ohio.

FIBER REINFORCED CERAMIC MATERIAL Patent Application
15 Apr. 1987 14 p
(NASA-CASE-LEW-14392-2; NAS 1.71:LEW-14392-2;
US-PATENT-APPL-SN-038560) Avail: NTIS HC A02/MF A01
CSCL 11B

A strong and tough SiC/RBSN composite material comprises silicon fibers and a reaction bonded silicon nitride (RBSN) matrix. This composite material may be used at elevated temperatures up to at least 1400 C. NASA

N87-28656* National Aeronautics and Space Administration. Lewis Research Center, Cleveland, Ohio.

METHOD OF PREPARING FIBER REINFORCED CERAMIC MATERIAL Patent

RAMAKRISHNA T. BHATT, inventor (to NASA) 25 Aug. 1987
8 p Filed 16 Jul. 1986 Supersedes N87-14517 (25 - 6, p 753)
(NASA-CASE-LEW-14392-1; US-PATENT-4,689,188;
US-PATENT-APPL-SN-886149; US-PATENT-CLASS-264-60;
US-PATENT-CLASS-264-63; US-PATENT-CLASS-264-332;
US-PATENT-CLASS-428-367) Avail: US Patent and Trademark
Office CSCL 11B

Alternate layers of mats of specially coated SiC fibers and silicon monoxides are hot pressed in two stages to form a fiber reinforced ceramic material. In the first stage a die is heated to about 600 C in a vacuum furnace and maintained at this temperature for about one-half hour to remove fugitive binder. In the second stage the die temperature is raised to about 1000 C and the layers are pressed at between 35 and 138 MPa. The resulting preform is placed in a reactor tube where a nitriding gas is flowed past the preform at 1100 to 1400 C to nitride the same.

Official Gazette of the U.S. Patent and Trademark Office

N87-29679*# National Aeronautics and Space Administration. Lewis Research Center, Cleveland, Ohio.

COMPARISON OF THE TRIBOLOGICAL PROPERTIES OF FLUORINATED COKE AND GRAPHITES

ROBERT L. FUSARO 1987 32 p Proposed for presentation at the 1988 Annual Meeting of the Society of Tribologists and Lubrication Engineers, Cleveland, Ohio, 9-12 May 1988
(NASA-TM-100170; E-3735; NAS 1.15:100170) Avail: NTIS HC A03/MF A01 CSCL 11B

The friction, wear, endurance life, and surface morphology of rubbed (burnished) fluorinated graphite and fluorinated coke materials were studied. Two different coke powders, a graphitic carbon powder, and a graphite powder were fluorinated and then tribologically investigated. In addition, one of the coke powders was reduced in size before fluorinating to evaluate the effect of a finer particle size on the tribological properties. For comparison, graphite and coke powders which were not fluorinated were also tribologically evaluated. Elemental analysis by emission spectroscopy was performed on each sample to determine the impurity content and X-ray diffraction analysis was performed to determine the crystallinity. Coke was found to have very little lubricating ability, but fluorinated coke did possess good lubricating properties. However, the fluorinated graphite and fluorinated graphitic carbon (which gave equivalent results) gave superior results to those obtained with the fluorinated cokes. No tribological benefit was found for using small versus a larger particle size of coke, at least when evaluated as a rubbed film. Author

PROPELLANTS AND FUELS

Includes rocket propellants, igniters, and oxidizers; their storage and handling procedures; and aircraft fuels.

A87-14986*# United Technologies Research Center, East Hartford, Conn.

LONG-TERM DEPOSIT FORMATION IN AVIATION TURBINE FUEL AT ELEVATED TEMPERATURE

A. J. GIOVANETTI and E. J. SZETELA (United Technologies Research Center, East Hartford, CT) Journal of Propulsion and Power (ISSN 0748-4658), vol. 2, Sept.-Oct. 1986, p. 450-456. Previously cited in issue 07, p. 876, Accession no. A86-19929. refs
(Contract NAS3-24091)

A87-45372*# Drexel Univ., Philadelphia, Pa.

DEGRADATION MECHANISMS OF SULFUR AND NITROGEN CONTAINING COMPOUNDS DURING THERMAL STABILITY TESTING OF MODEL FUELS

K. T. REDDY, N. P. CERNANSKY (Drexel University, Philadelphia, PA), and R. S. COHEN (Temple University, Philadelphia, PA) AIAA, SAE, ASME, and ASEE, Joint Propulsion Conference, 23rd, San Diego, CA, June 29-July 2, 1987. 10 p. Research supported by the Drexel University. refs
(Contract NAG3-183)
(AIAA PAPER 87-2039)

The degradation behavior of n-dodecane (singly or in combination with S- and N-containing dopants) was studied using a modified Jet Fuel Thermal Oxidation Tester facility between 200 and 400 C. The products were analyzed by gas chromatography and mass spectrometry. The soluble products consisted mainly of n-alkanes and 1-alkenes, aldehydes, tetrahydrofuran derivatives, dodecanol and dodecanone isomers, C21-C24 alkane isomers, and dodecylhydroperoxide (ROOH) decomposition products. The major products were always the same, with and without dopants, but their distributions varied considerably. The 3,4-dimercaptotoluene and dibutylsulfide dopants added individually to n-dodecane interfered with the hydrocarbon oxidation at the alkylperoxy radical and the alkylhydroperoxide link, respectively, while the 2,5-dimethylpyrrole dopant inhibited ROOH formation. Pyridine, pyrrole, and dibenzothiophene added individually showed few significant effects. I.S.

N87-24577*# Pratt and Whitney Aircraft, East Hartford, Conn.

ANTIMISTING KEROSENE JT3 ENGINE FUEL SYSTEM INTEGRATION STUDY Final Report

A. FIORENTINO Washington NASA Jan. 1987 48 p
(Contract NAS3-24217; NAS3-24353; DTFA03-81-A-00154)
(NASA-CR-4033; NAS 1.26:4033) Avail: NTIS HC A03/MF A01
CSCL 21D

An analytical study and laboratory tests were conducted to assist NASA in determining the safety and mission suitability of the modified fuel system and flight tests for the Full-Scale Transport Controlled Impact Demonstration (CID) program. This twelve-month study reviewed and analyzed both the use of antimisting kerosene (AMK) fuel and the incorporation of a fuel degrader on the operational and performance characteristics of the engines tested. Potential deficiencies and/or failures were identified and approaches to accommodate these deficiencies were recommended to NASA Ames Dryden Flight Research Facility. The result of flow characterization tests on degraded AMK fuel samples indicated levels of degradation satisfactory for the planned missions of the B-720 aircraft. The operability and performance with the AMK in a ground test engine and in the aircraft engines during the test flights were comparable to those with unmodified Jet A. For the final CID test, the JT-3C-7 engines performed satisfactorily while operating on AMK right up to impact. Author

N87-24578* # General Electric Co., Cincinnati, Ohio.
AVIATION FUEL PROPERTY EFFECTS ON ALTITUDE RELIGHT
Final Report, Jan. 1984 - Jun. 1986
 K. VENKATARAMANI May 1987 67 p
 (Contract NAS3-24215)
 (NASA-CR-179582; NAS 1.26:179582; R87AEB111; AD-A183088)
 Avail: NTIS HC A01/MF A01 CSCL 21D

The major objective of this experimental program was to investigate the effects of fuel property variation on altitude relight characteristics. Four fuels with widely varying volatility properties (JP-4, Jet A, a blend of Jet A and 2040 Solvent, and Diesel 2) were tested in a five-swirl-cup-sector combustor at inlet temperatures and flows representative of windmilling conditions of turbofan engines. The effects of fuel physical properties on atomization were eliminated by using four sets of pressure-atomizing nozzles designed to give the same spray Sauter mean diameter (50 + or - 10 micron) for each fuel at the same design fuel flow. A second series of tests was run with a set of air-blast nozzles. With comparable atomization levels, fuel volatility assumes only a secondary role for first-swirl-cup lightoff and complete blowout. Full propagation first-cup blowout were independent of fuel volatility and depended only on the combustor operating conditions. Author

N87-29706* # Drexel Univ., Philadelphia, Pa. Dept. of Mechanical Engineering and Mechanics.
THERMAL STABILITY OF DISTILLATE HYDROCARBON FUELS
Ph.D. Thesis
 KISHENKUMAR TADISINA REDDY and NICHOLAS P. CERNANSKY Oct. 1987 196 p
 (Contract NAG3-183)
 (NASA-CR-181412; NAS 1.26:181412) Avail: NTIS HC A09/MF A01 CSCL 21D

Thermal stability of fuels is expected to become a severe problem in the future due to the anticipated use of broadened specification and alternative fuels. Future fuels will have higher contents of heteroatomic species which are reactive constituents and are known to influence fuel degradation. To study the degradation chemistry of selected model fuels, n-dodecane and n-dodecane plus heteroatoms were aerated by bubbling air through the fuels and stressed on a modified Jet Fuel Thermal Oxidation Tester facility operating at heater tube temperatures between 200 to 400 C. The resulting samples were fractionated to concentrate the soluble products and then analyzed using gas chromatographic and mass spectrometric techniques to quantify and identify the stable reaction intermediate and product specifically. Heteroatom addition showed that the major soluble products were always the same, with and without heteroatoms, but their distributions varied considerably. Author

29

MATERIALS PROCESSING

Includes space-based development of products and processes for commercial applications.

A87-10871* National Aeronautics and Space Administration. Lewis Research Center, Cleveland, Ohio.
CELLULAR AND DENDRITIC GROWTH IN A BINARY MELT - A MARGINAL STABILITY APPROACH
 V. LAXMANAN (NASA, Lewis Research Center; Case Western Reserve University, Cleveland, OH) Journal of Crystal Growth (ISSN 0022-0248), vol. 75, June 1986, p. 573-590. NASA-supported research. refs

A simple model for the constrained growth of an array of cells or dendrites in a binary alloy in the presence of an imposed positive temperature gradient in the liquid is proposed, with the dendritic or cell tip radius calculated using the marginal stability criterion of Langer and Muller-Krumbhaar (1977). This approach, an approach

adopting the ad hoc assumption of minimum undercooling at the cell or dendrite tip, and an approach based on the stability criterion of Trivedi (1980) all predict tip radii to within 30 percent of each other, and yield a simple relationship between the tip radius and the growth conditions. Good agreement is found between predictions and data obtained in a succinonitrile-acetone system, and under the present experimental conditions, the dendritic tip stability parameter value is found to be twice that obtained previously, possibly due to a transition in morphology from a cellular structure with just a few side branches, to a more fully developed dendritic structure. R.R.

A87-22716* # California Univ., La Jolla.
PARTICLE CLOUD KINETICS IN MICROGRAVITY
 A. L. BERLAD, N. D. JOSHI (California, University, La Jolla), H. ROSS, and R. KLIMEK (NASA, Lewis Research Center, Cleveland, OH) AIAA, Aerospace Sciences Meeting, 25th, Reno, NV, Jan. 12-15, 1987. 8 p. NASA-sponsored research. refs
 (AIAA PAPER 87-0577)

Data related to particle-particle agglomeration/deagglomeration and particle-wall attachment are discussed. Particle-cluster cloud interactions and particle-cluster agglomeration/deagglomeration kinetics are studied. An apparatus designed and constructed for examining the agglomeration/deagglomeration effects for lycopodium under the conditions of an acoustically energized mixing process and of alpha-particle-induced deagglomerative processes is described; characteristic features and applications for the apparatus are examined. Requirements for combustion experimentation are discussed. I.F.

A87-23159* # National Bureau of Standards, Gaithersburg, Md.
LOW-GRAVITY EXPERIMENTS IN CRITICAL PHENOMENA
 MICHAEL R. MOLDOVER (NBS, Thermophysics Div., Gaithersburg, MD) IN: Opportunities for academic research in a low-gravity environment. New York, American Institute of Aeronautics and Astronautics, Inc., 1986, p. 57-79. refs
 (Contract NASA ORDER C-86129-D)

Studies of anomalous thermodynamic, transport, and structural phenomena in multibody systems near critical points are reviewed. The nomenclature used to describe critical points is explained; theoretical predictions of the thermodynamic properties of bulk systems are presented; and experimental tests of these predictions systems are discussed, considering equilibration and gravity effects in fluid systems and emphasizing the value of experiments conducted in a reduced-gravity environment. Several such experiments are described, and the available academic-research opportunities are briefly surveyed. T.K.

A87-43141* # Tennessee Univ., Knoxville.
EXPERIMENTS ON THERMOACOUSTIC CONVECTION HEAT TRANSFER IN GRAVITY AND ZERO-GRAVITY ENVIRONMENTS
 MASOOD PARANG (Tennessee, University, Knoxville) and ADEL SALAH-EDDINE AIAA, Thermophysics Conference, 22nd, Honolulu, HI, June 8-10, 1987. 8 p. refs
 (Contract NAG3-239)
 (AIAA PAPER 87-1651)

The results of an experimental study of thermoacoustic convection (TAC) heat transfer in gravity and zero-gravity environments are presented. The experimental apparatus consisted of a cylinder containing air as the compressible fluid. The enclosed air was heated electrically at the top surface which consisted of a thin high-resistance steel foil connected to a power source. Thermocouples were used to measure the transient temperature of the air on the axis of the cylinder and the heated surface in the both zero-gravity and gravity environments. The zero-gravity tests were performed in the Zero-Gravity Drop Tower Facility of NASA-Lewis Research Center. The experimental results were corrected for the error due to radiation absorption by the thermocouples. A conduction-only numerical heat transfer model was developed to compute the transient air temperature in the cylindrical geometry. The results were compared to the experimental data to determine the significance of the

thermoacoustic convection heat transfer mechanism. It is observed that the rate of heat transfer to the air measured during the experiments is consistently higher than that obtained by the conduction-only solution indicating a significant presence of the TAC heat transfer. Further experiments are planned to measure directly (1) the radiative heat transfer contribution to the rise in the air temperature, and (2) the air pressure oscillations within the cylinder that are responsible for the convective heat transfer mode.

Author

A87-45724*# National Aeronautics and Space Administration. Lewis Research Center, Cleveland, Ohio.

THE ALLOY UNDERCOOLING EXPERIMENT ON THE COLUMBIA STS 61-C SPACE SHUTTLE MISSION

FREDRIC H. HARF, EDWARD A. WINSA (NASA, Lewis Research Center, Cleveland, OH), THOMAS J. PICCONE, YANZHONG WU, MERTON C. FLEMINGS, YUH SHIOHARA (MIT, Cambridge, MA), and LLOYD B. GARDNER (NASA, Marshall Space Flight Center, Huntsville, AL) AIAA, Aerospace Sciences Meeting, 25th, Reno, NV, Jan. 12-15, 1987. 37 p. Previously announced in STAR as N87-18643. refs

(AIAA PAPER 87-0506)

An Alloy Undercooling experiment was performed in an electromagnetic levitator during the Columbia STS 61-C mission in January 1986. One eutectic nickel-tin alloy specimen was partially processed before an equipment failure terminated the experiment. Examination of the specimen showed evidence of undercooling and some unusual microstructural features.

Author

N87-15320*# Wyle Labs., Inc., Huntsville, Ala.

EQUIPMENT CONCEPT DESIGN AND DEVELOPMENT PLANS FOR MICROGRAVITY SCIENCE AND APPLICATIONS RESEARCH ON SPACE STATION: COMBUSTION TUNNEL, LASER DIAGNOSTIC SYSTEM, ADVANCED MODULAR FURNACE, INTEGRATED ELECTRONICS LABORATORY

M. L. UHRAN, W. W. YOUNGBLOOD, T. GEORGEKUTTY, M. R. FISKE, and W. O. WEAR Sep. 1986 260 p

(Contract NAS3-24654)

(NASA-CR-179535; NAS 1.26:179535) Avail: NTIS HC A12/MF A01 CSCL 22A

Taking advantage of the microgravity environment of space NASA has initiated the preliminary design of a permanently manned space station that will support technological advances in process science and stimulate the development of new and improved materials having applications across the commercial spectrum. Previous studies have been performed to define from the researcher's perspective, the requirements for laboratory equipment to accommodate microgravity experiments on the space station. Functional requirements for the identified experimental apparatus and support equipment were determined. From these hardware requirements, several items were selected for concept designs and subsequent formulation of development plans. This report documents the concept designs and development plans for two items of experiment apparatus - the Combustion Tunnel and the Advanced Modular Furnace, and two items of support equipment the Laser Diagnostic System and the Integrated Electronics Laboratory. For each concept design, key technology developments were identified that are required to enable or enhance the development of the respective hardware.

Author

N87-16167*# National Aeronautics and Space Administration. Lewis Research Center, Cleveland, Ohio.

SIMULATION OF FLUID FLOWS DURING GROWTH OF ORGANIC CRYSTALS IN MICROGRAVITY

GARY D. ROBERTS, JAMES K. SUTTER, R. BALASUBRAMANIAM, WILLIAM K. FOWLIS (National Aeronautics and Space Administration. Marshall Space Flight Center, Huntsville, Ala.), M. D. RADCLIFFE (Minnesota Mining and Mfg. Co., St. Paul), and M. C. DRAKE 1987 11 p Prepared for presentation at the 32nd International SAMPE Symposium and Exhibition, Anaheim, Calif., 6-9 Apr. 1987

(NASA-TM-88921; E-3354; NAS 1.15:88921) Avail: NTIS HC A02/MF A01 CSCL 22A

Several counter diffusion type crystal growth experiments were conducted in space. Improvements in crystal size and quality are attributed to reduced natural convection in the microgravity environment. One series of experiments called DMOS (Diffusive Mixing of Organic Solutions) was designed and conducted by researchers at the 3M Corporation and flown by NASA on the space shuttle. Since only limited information about the mixing process is available from the space experiments, a series of ground based experiments was conducted to further investigate the fluid dynamics within the DMOS crystal growth cell. Solutions with density differences in the range of 10 to the -7 to 10 to the -4 power g/cc were used to simulate microgravity conditions. The small density differences were obtained by mixing D2O and H2O. Methylene blue dye was used to enhance flow visualization. The extent of mixing was measured photometrically using the 662 nm absorbance peak of the dye. Results indicate that extensive mixing by natural convection can occur even under microgravity conditions. This is qualitatively consistent with results of a simple scaling analysis. Quantitative results are in close agreement with ongoing computational modeling analysis.

Author

N87-16917*# National Aeronautics and Space Administration. Lewis Research Center, Cleveland, Ohio.

RESEARCH OPPORTUNITIES IN MICROGRAVITY SCIENCE AND APPLICATIONS DURING SHUTTLE HIATUS

BRUCE N. ROSENTHAL, THOMAS K. GLASGOW, RICHARD E. BLACK (National Aeronautics and Space Administration. Marshall Space Flight Center, Huntsville, Ala.), and DANIEL D. ELLEMAN (Jet Propulsion Lab., California Inst. of Tech., Pasadena) 1987 10 p Proposed for presentation at the 32nd International SAMPE Symposium and Exhibition, Anaheim, Calif., 6-9 Apr. 1987

(NASA-TM-88964; E-3420; NAS 1.15:88964) Avail: NTIS HC A02/MF A01 CSCL 22A

The opportunity to conduct microgravity and related research still exists, even with the temporary delay in the U.S. Space Shuttle program. Several ground-based facilities are available and use of these facilities is highly recommended for the preparation of near and far term shuttle or space station experiments. Drop tubes, drop towers, aircraft, sounding rockets and a wide variety of other ground-based equipment can be used to simulate microgravity. This paper concentrates on the materials processing capabilities available at NASA Lewis Research Center (NASA Lewis), Marshall Space Flight Center (MSFC), and the California Institute of Technology Jet Propulsion Laboratory (JPL). Also included is information on gaining access to these facilities.

Author

N87-21141*# National Aeronautics and Space Administration. Lewis Research Center, Cleveland, Ohio.

MICROGRAVITY FLUID MANAGEMENT SYMPOSIUM

Apr. 1987 225 p Symposium held in Cleveland, Ohio, 9-10 Sep. 1986

(NASA-CP-2465; E-3386; NAS 1.55:2465) Avail: NTIS HC A10/MF A01 CSCL 22A

The NASA Microgravity Fluid Management Symposium, held at the NASA Lewis Research Center, September 9 to 10, 1986, focused on future research in the microgravity fluid management field. The symposium allowed researchers and managers to review space applications that require fluid management technology, to present the current status of technology development, and to identify the technology developments required for future missions.

The 19 papers covered three major categories: (1) fluid storage, acquisition, and transfer; (2) fluid management applications, i.e., space power and thermal management systems, and environmental control and life support systems; (3) project activities and insights including two descriptions of previous flight experiments and a summary of typical activities required during development of a shuttle flight experiment.

N87-21150*# National Aeronautics and Space Administration. Lewis Research Center, Cleveland, Ohio.

CRYOGENIC FLUID MANAGEMENT FLIGHT EXPERIMENT (CFMFE)

DAVID M. DEFELICE *In its* Microgravity Fluid Management Symposium p 119-124 Apr. 1987

Avail: NTIS HC A10/MF A01 CSCL 22A

Since its foundation, NASA has excelled in the study and development of microgravity fluid management technology. With the advent of space-based vehicles and systems, the use of and the ability to efficiently manage subcritical cryogenics in the space environment has become necessary to our growing space program. The NASA Lewis Research Center is responsible for the planning and execution of a program which will provide advanced in-space cryogenic fluid management technology. A number of future space missions have been identified that will require or could benefit from this technology. These technology needs have been prioritized and the Cryogenic Fluid Management Flight Experiment (CFMFE) is being designed to provide the experimental data necessary for the technological development effort.

Author

N87-21156*# National Aeronautics and Space Administration. Lewis Research Center, Cleveland, Ohio.

SPACE EXPERIMENT DEVELOPMENT PROCESS

JAMES F. DEPAUW *In its* Microgravity Fluid Management Symposium p 189-200 Apr. 1987

Avail: NTIS HC A10/MF A01 CSCL 22A

Described is a process for developing space experiments utilizing the Space Shuttle. The role of the Principal Investigator is described as well as the Principal Investigator's relation with the project development team. Described also is the sequence of events from an early definition phase through the steps of hardware development. The major interactions between the hardware development program and the Shuttle integration and safety activities are also shown. The presentation is directed to people with limited Shuttle experiment experience. The objective is to summarize the development process, discuss the roles of major participants, and list some lessons learned. Two points should be made at the outset. First, no two projects are the same so the process varies from case to case. Second, the emphasis here is on Code EN/Microgravity Science and Applications Division (MSAD).

Author

N87-22865*# Case Western Reserve Univ., Cleveland, Ohio.
THERMOCAPILLARY BUBBLE MIGRATION FOR LARGE MARANGONI NUMBERS Final Report

R. BALASUBRAMANIAM May 1987 15 p

(Contract NAG3-567)

(NASA-CR-179628; E-3515; NAS 1.26:179628) Avail: NTIS HC A02/MF A01 CSCL 22A

The thermocapillary motion of spherical bubbles present in an unbounded liquid with a linear temperature distribution, when the Reynolds number and the Marangoni number are large is analyzed. Previous calculations of the terminal velocity performed for this parametric range did not take into complete consideration the thermal boundary layer present near the surface of the bubble. A scaling analysis is presented for this problem. The thermal boundary layer is analyzed by an integral method. The resulting terminal velocity is lower than the one previously calculated, though it is of the same order of magnitude.

Author

N87-24579*# National Aeronautics and Space Administration. Lewis Research Center, Cleveland, Ohio.

GRAVITATIONAL MACROSEGREGATION IN BINARY PB-SN ALLOY INGOTS

V. LAXMANAN, A. STUDER, L. WANG, J. F. WALLACE (Case Western Reserve Univ., Cleveland, Ohio.), and E. A. WINSA 1986 36 p Presented at the Low Gravity Science Seminar Series, Boulder, Colo, 17 Feb. 1986; sponsored by Colorado Univ.

(NASA-TM-89885; E-3570; NAS 1.15:89885) Avail: NTIS HC

A03/MF A01 CSCL 22A

A space shuttle experiment employing the General Purpose (Rocket) Furnace (GPF) in its isothermal mode of operation is manifested on MSL-3, circa 1989. The central aim of this experiment is to investigate the effect of reduced gravity levels on the segregation behavior in a slowly, and isothermally, cooled sample of a binary Pb-15 wt% Sn alloy. This experiment should be able to simulate, in a small laboratory sample, some aspects of the segregation phenomena occurring in large industrial ingots. Ground-based experiments conducted in the single-cavity simulator of the GPF, in support of the microgravity experiment are described in detail. The results of the MSFC experiments are compared with other related experiments conducted at Case Western Reserve University (CWRS), wherein the isothermal constraints were relaxed. The isothermally processed samples indicate a small and gradual increase in fraction eutectic, and a corresponding increase in tin content, from the bottom to the top of the ingot. The radial variations are minimal near the ingot bottom, but there are large radial variations in the top half. In the CWRU experiments, more severe segregations, including segregation defects known as freckles. Follow up experiments employing the GPF without the isothermal constraints, or other suitably modified space shuttle hardware are suggested.

Author

31

ENGINEERING (GENERAL)

Includes vacuum technology; control engineering; display engineering; cryogenics; and fire prevention.

A87-48313* National Aeronautics and Space Administration. Lewis Research Center, Cleveland, Ohio.

OPPORTUNITIES AND CHALLENGES IN HEAT TRANSFER - FROM THE PERSPECTIVE OF THE GOVERNMENT LABORATORY

ROBERT J. SIMONEAU (NASA, Lewis Research Center, Cleveland, OH) Heat Transfer Engineering (ISSN 0145-7632), vol. 7, no. 3-4, 1986, p. 76-81.

The technological problems in which heat transfer research is required are briefly reviewed, discussing the role of the government laboratory in this research. The Hot Section Technology Program at NASA Lewis is addressed as an example. A building-block approach to turbine aerothermal research is shown, as is an interactive computational/experimental synergism and an interdisciplinary research methodology for life prediction of turbine engine hot-section components. The main issues for government laboratories as organizers and focusers in this area of research are listed, and challenges and opportunities for the future are indicated.

C.D.

31 ENGINEERING (GENERAL)

N87-12708*# National Aeronautics and Space Administration. Lewis Research Center, Cleveland, Ohio.

PLASMA ASSISTED SURFACE COATING/MODIFICATION PROCESSES: AN EMERGING TECHNOLOGY

T. SPALVINS 1986 15 p Presented at the 1st International Ion Nitriding Conference, Cleveland, Ohio, 15-17 Sep. 1985; sponsored by the American Society for Metals (NASA-TM-88885; E-3274; NAS 1.15:88885) Avail: NTIS HC A02/MF A01 CSCL 13H

A broad understanding of the numerous ion or plasma assisted surface coating/modification processes is sought. An awareness of the principles of these processes is needed before discussing in detail the ion nitriding technology. On the basis of surface modifications arising from ion or plasma energizing and interactions, it can be broadly classified as deposition of distinct overlay coatings (sputtering-dc, radio frequency, magnetron, reactive; ion plating-diode, triode) and surface property modification without forming a discrete coating (ion implantation, ion beam mixing, laser beam irradiation, ion nitriding, ion carburizing, plasma oxidation). These techniques offer a great flexibility and are capable in tailoring desirable chemical and structural surface properties independent of the bulk properties. Author

N87-17937*# National Aeronautics and Space Administration. Lewis Research Center, Cleveland, Ohio.

ION PLATED GOLD FILMS: PROPERTIES, TRIBOLOGICAL BEHAVIOR AND PERFORMANCE

TALIVALDIS SPALVINS 1987 15 p Proposed for presentation at the 37th Electronic Components Conference, Boston, Mass., 11-13 May 1987; sponsored by Electronic Industries Association and the Components Hybrids Society IEEE (NASA-TM-88977; E-3425; NAS 1.15:88977) Avail: NTIS HC A02/MF A01 CSCL 20L

The glow discharge energizing favorably modifies and controls the coating/substrate adherence and the nucleation and growth sequence of ion plated gold films. As a result the adherence, coherence, internal stresses, and morphology of the films are significantly improved. Gold ion plated films because of their graded coating/substrate interface and fine uniform densely packed microstructure not only improve the tribological properties but also induce a surface strengthening effect which improves the mechanical properties such as yield, tensile, and fatigue strength. Consequently significant improvements in the tribological performance of ion plated gold films as compared to vapor deposited gold films are shown in terms of decreased friction/wear and prolonged endurance life. Author

N87-19539*# Pratt and Whitney Aircraft, West Palm Beach, Fla. Government Products Div.

CRYOGENIC GEAR TECHNOLOGY FOR AN ORBITAL TRANSFER VEHICLE ENGINE AND TESTER DESIGN Final Report, Apr. - Nov. 1985

M. CALANDRA and G. DUNCAN Jun. 1986 116 p (Contract NAS3-23858)

(NASA-CR-175102; NAS 1.26:175102; PW/GPD-FR-19177) Avail: NTIS HC A06/MF A01 CSCL 22B

Technology available for gears used in advanced Orbital Transfer Vehicle rocket engines and the design of a cryogenic adapted tester used for evaluating advanced gears are presented. The only high-speed, unlubricated gears currently in cryogenic service are used in the RL10 rocket engine turbomachinery. Advanced rocket engine gear systems experience operational load conditions and rotational speed that are beyond current experience levels. The work under this task consisted of a technology assessment and requirements definition followed by design of a self-contained portable cryogenic adapted gear test rig system. Author

N87-21160* National Aeronautics and Space Administration. Lewis Research Center, Cleveland, Ohio.

ION BEAM SPUTTER ETCHING Patent

BRUCE A. BANKS and SHARON K. RUTLEDGE 4 Nov. 1986 10 p Filed 13 Sep. 1985 Supersedes N86-20587 (24 - 11, p 1752)

(NASA-CASE-LEW-13899-1; US-PATENT-4,620,898; US-PATENT-APPL-SN-775968; US-PATENT-CLASS-156-643; US-PATENT-CLASS-156-646; US-PATENT-CLASS-156-659.1; US-PATENT-CLASS-156-661.1; US-PATENT-CLASS-156-904; US-PATENT-CLASS-156-345; US-PATENT-CLASS-204-298) Avail: US Patent and Trademark Office CSCL 13H

An ion beam etching process which forms extremely high aspect ratio surface microstructures using thin sputter masks is utilized in the fabrication of integrated circuits. A carbon rich sputter mask together with unmasked portions of a substrate is bombarded with inert gas ions while simultaneous carbon deposition occurs. The arrival of the carbon deposit is adjusted to enable the sputter mask to have a near zero or even slightly positive increase in thickness with time while the unmasked portions have a high net sputter etch rate.

Official Gazette of the U.S. Patent and Trademark Office

N87-21176*# National Aeronautics and Space Administration. Lewis Research Center, Cleveland, Ohio.

LASER FRINGE ANEMOMETRY FOR AERO ENGINE COMPONENTS

ANTHONY J. STRAZISAR In AGARD Advanced Instrumentation for Aero Engine Components 32 p Nov. 1986 Sponsored by NASA

Avail: NTIS HC A24/MF A01

Advances in flow measurement techniques in turbomachinery continue to be paced by the need to obtain detailed data for use in validating numerical predictions of the flowfield and for use in the development of empirical models for those flow features which cannot be readily modelled numerically. The use of laser anemometry in turbomachinery research has grown over the last 14 years in response to these needs. Based on past applications and current developments, the key issues which are involved when considering the application of laser anemometry to the measurement of turbomachinery flowfields are discussed. Aspects of laser fringe anemometer optical design which are applicable to turbomachinery research are briefly reviewed. Application problems which are common to both laser fringe anemometry (LFA) and laser transit anemometry (LTA) such as seed particle injection, optical access to the flowfield, and measurement of rotor rotational position are covered. The efficiency of various data acquisition schemes is analyzed and issues related to data integrity and error estimation are addressed. Real-time data analysis techniques aimed at capturing flow physics in real time are discussed. Finally, data reduction and analysis techniques are discussed and illustrated using examples taken from several LFA turbomachinery applications. Author

N87-21183*# National Aeronautics and Space Administration. Lewis Research Center, Cleveland, Ohio.

COMBINED FRINGE AND FABRY-PEROT LASER ANEMOMETER FOR 3 COMPONENT VELOCITY MEASUREMENTS IN TURBINE STATOR CASCADE FACILITY

RICHARD G. SEASHOLTZ and LOUIS J. GOLDMAN In AGARD Advanced Instrumentation for Aero Engine Components 15 p Nov. 1986 Previously announced as N86-24967 Sponsored by NASA

Avail: NTIS HC A24/MF A01 CSCL 14B

A laser anemometer is described that was developed for use in a 508 mm diameter annular turbine stator cascade facility. All three velocity components are measured through a single restricted optical port, both within the stator vane row and downstream of the vanes. The measurements are made through a cylindrical window in the casing that matches the tip radius of the cascade. The stator tested has a contoured hub endwall that results in a large radial flow near the hub. The anemometer uses a standard fringe configuration (LFA) with a fluorescent aerosol seed to

measure the axial and circumferential velocity components. The radial component is measured with a confocal Fabry-Perot interferometer. The two configurations are combined in a single optical system and can operate simultaneously. Data are presented to illustrate the capabilities of the system. Author

N87-21204* National Aeronautics and Space Administration. Lewis Research Center, Cleveland, Ohio.

BEAM-MODULATION METHODS IN QUANTITATIVE AND FLOW-VISUALIZATION HOLOGRAPHIC INTERFEROMETRY

ARTHUR J. DECKER /in AGARD Advanced Instrumentation for Aero Engine Components 16 p Nov. 1986 Sponsored by NASA

Avail: NTIS HC A24/MF A01 CSCL 20F

Heterodyne holographic interferometry and time-average holography with a frequency shifted reference beam are discussed. Both methods will be used for the measurement and visualization of internal transonic flows where the target facility is a flutter cascade. The background and experimental requirements for both methods are reviewed. Measurements using heterodyne holographic interferometry are presented. The performance of the laser required for time-average holography of time-varying transonic flows is discussed. Author

N87-23821* National Aeronautics and Space Administration. Lewis Research Center, Cleveland, Ohio.

PRELIMINARY PERFORMANCE CHARACTERIZATIONS OF AN ENGINEERING MODEL MULTIPROPELLANT RESISTOJET FOR SPACE STATION APPLICATION

W. EARL MORREN, STUART S. HAY (Purdue Univ., West Lafayette, Ind.), THOMAS W. HAAG, and JAMES S. SOVEY Jul. 1987 24 p Presented at the 23rd Joint Propulsion Conference, San Diego, Calif., 29 Jun. - 2 Jul. 1987; cosponsored by AIAA, SAE, ASME, and ASEE

(NASA-TM-100113; E-3657; NAS 1.15:100113; AIAA-87-2120)

Avail: NTIS HC A02/MF A01 CSCL 20H

Presented are the results of a program to describe the operational characteristics of an engineering model multipropellant resistojet for application as an auxiliary propulsion system for the space station. Performance was measured on hydrogen, helium, methane, water (steam), nitrogen, air, argon, and carbon dioxide. Thrust levels ranged from 109 to 355 mN, power levels ranged from 167 to 506 W, and specific impulse values ranged from 93 to 385 sec, depending on the propellant, chamber pressure, and heater current level selected. Detailed thermal maps of the heater and heat exchanger were also obtained for operation with carbon dioxide. Author

32

COMMUNICATIONS AND RADAR

Includes radar; land and global communications; communications theory; and optical communications.

A87-18310* Motorola, Inc., Scottsdale, Ariz.

BASEBAND PROCESSOR DEVELOPMENT/TEST PERFORMANCE FOR 30/20 GHZ SS-TDMA COMMUNICATION SYSTEM

L. BROWN, D. SABOURIN, and S. ATTWOOD (Motorola, Inc., Aerospace Electronics Office, Scottsdale, AZ) IN: International Symposium on Space Technology and Science, 14th, Tokyo, Japan, May 27-June 1, 1984, Proceedings. Tokyo, AGNE Publishing, Inc., 1984, p. 867-878.

(Contract NAS3-22502)

The baseband processor (BBP) development for the 30/20 GHz Satellite Communication System is described. The SS-TDMA concept for future satellite communications is reviewed, describing the overall system, the satellite payload, and the frequency plan. A brief general description of the BBP is given, and the

proof-of-concept model of the BBP is summarized. Key technologies and custom LSI developed for the BBP are listed. Finally, key technology developments and test data are reported for the BBP. C.D.

A87-20818* Ohio State Univ., Columbus.

SMI ADAPTIVE ANTENNA ARRAYS FOR WEAK INTERFERING SIGNALS

INDER J. GUPTA (Ohio State University, Columbus) IEEE Transactions on Antennas and Propagation (ISSN 0018-926X), vol. AP-34, Oct. 1986, p. 1237-1242. refs (Contract NAG3-536)

The performance of adaptive antenna arrays in the presence of weak interfering signals (below thermal noise) is studied. It is shown that a conventional adaptive antenna array sample matrix inversion (SMI) algorithm is unable to suppress such interfering signals. To overcome this problem, the SMI algorithm is modified. In the modified algorithm, the covariance matrix is redefined such that the effect of thermal noise on the weights of adaptive arrays is reduced. Thus, the weights are dictated by relatively weak signals. It is shown that the modified algorithm provides the desired interference protection. Author

A87-30775* Toledo Univ., Ohio.

IMAGE DATA COMPRESSION WITH VECTOR QUANTIZATION IN THE TRANSFORM DOMAIN

A. A. ABDELWAHAB and S. C. KWATRA (Toledo, University, OH) IN: ICC '86; Proceedings of the International Conference on Communications, Toronto, Canada, June 22-25, 1986, Conference Record. Volume 2. New York, Institute of Electrical and Electronics Engineers, 1986, p. 1285-1289. refs (Contract NAG3-42)

In this paper, an algorithm is presented for image data compression based upon vector quantization of the two-dimensional discrete cosine transformed coefficients. The ac energies of the transformed blocks are used to classify them into eight different ac classes. The ac coefficients of the transformed blocks of class one are set to zero, while those of classes two through eight are transmitted by seven different code books. The dc coefficients of all eight classes are scalar quantized by an adaptive uniform quantizer. As a result, only 4.5 bits instead of eight bits are required to transmit the dc coefficient with negligible additional degradation. Overall, this algorithm requires approximately 0.75 bits per pixel and gives an average reconstruction error of 7.1. Author

A87-30801* Cincinnati Univ., Ohio.

A HIGH QUALITY IMAGE COMPRESSION SCHEME FOR REAL-TIME APPLICATIONS

P. A. RAMAMOORTHY and T. TRAN (Cincinnati, University, OH) IN: ICC '86; Proceedings of the International Conference on Communications, Toronto, Canada, June 22-25, 1986, Conference Record. Volume 3. New York, Institute of Electrical and Electronics Engineers, 1986, p. 1893-1897.

(Contract NAG3-582)

Many image compression or coding techniques have been developed to reduce the amount of bits of information needed to represent digital images. Among these, Vector Quantization (VQ) seems to have the edge; its theoretical distortion is lower than that of other block coding techniques at comparable bit rates. However, the application of Vector Quantization remains limited due to its high computational complexity. Presently, it is limited to low to medium quality image compression. In this paper it is shown that VQ can be mapped onto VLSI implementation via systolic type architecture, making real time application possible. In addition, it is shown that using multistage or cascade VQ high quality images can be obtained at very low bit rates for real time applications while using smaller codebooks than is necessary in single stage VQ. Examples of processed images are presented. Author

A87-31626* Illinois Univ., Urbana.

RADAR CROSS SECTION OF AN OPEN-ENDED CIRCULAR WAVEGUIDE CALCULATION OF SECOND-ORDER DIFFRACTION TERMS

C. S. LEE and S. W. LEE (Illinois, University, Urbana) Radio Science (ISSN 0048-6604), vol. 22, Jan.-Feb. 1987, p. 2-12. refs (Contract NAG3-475)

The radar cross section of an open-ended, semi-infinite circular waveguide is calculated by the geometrical theory of diffraction and the equivalent-current (EC) method. Both single- and double-diffraction terms are included. It is found that the double-diffraction term is stronger than the single-diffraction term for the horizontal polarization at wide-angle incidence. Its inclusion is necessary in order to check with experimental data and the asymptotic expansion of the exact Wiener-Hopf solution. The EC method is used for the single diffraction. On the other hand the double-diffraction term is obtained by using the EC method for axial incidence and geometrical theory of diffraction for wide-angle incidence. These two solutions are matched with a proper matching function. This technique is computationally more efficient than the matching technique of integration over the equivalent currents.

Author

A87-32829* Northwestern Univ., Evanston, Ill.

A NEW FORMULATION OF ELECTROMAGNETIC WAVE SCATTERING USING AN ON-SURFACE RADIATION BOUNDARY CONDITION APPROACH

GREGORY A. KRIEGSMANN, ALLEN TAFLOVE (Northwestern University, Evanston, IL), and KORADAR R. UMASHANKAR (Illinois, University, Chicago) IEEE Transactions on Antennas and Propagation (ISSN 0018-926X), vol. AP-35, Feb. 1987, p. 153-161. refs

(Contract NAG3-635; NSF MCS-83-00578)

A new formulation of electromagnetic wave scattering by convex, two-dimensional conducting bodies is reported. This formulation, called the on-surface radiation condition (OSRC) approach, is based upon an expansion of the radiation condition applied directly on the surface of a scatterer. It is now shown that application of a suitable radiation condition directly on the surface of a convex conducting scatterer can lead to substantial simplification of the frequency-domain integral equation for the scattered field, which is reduced to just a line integral. For the transverse magnetic case, the integrand is known explicitly. For the transverse electric case, the integrand can be easily constructed by solving an ordinary differential equation around the scatterer surface contour. Examples are provided which show that OSRC yields computed near and far fields which approach the exact results for canonical shapes such as the circular cylinder, square cylinder, and strip. Electrical sizes for the examples are $ka = 5$ and $ka = 10$. The new OSRC formulation of scattering may present a useful alternative to present integral equation and uniform high-frequency approaches for convex cylinders larger than $ka = 1$. Structures with edges or corners can also be analyzed, although more work is needed to incorporate the physics of singular currents at these discontinuities. Convex dielectric structures can also be treated using OSRC.

Author

A87-34527* Communications Satellite Corp., Clarksburg, Md.

20-GHZ PHASED-ARRAY-FED ANTENNAS UTILIZING DISTRIBUTED MMIC MODULES

R. M. SORBELLO, A. I. ZAGHLOUL, S. SIDDIQI, B. D. GELLER (COMSAT Laboratories, Clarksburg, MD), and B. S. LEE (INTELSAT, El Segundo, CA) COMSAT Technical Review, vol. 16, Fall 1986, p. 339-373. refs (Contract NAS3-23250)

The feasibility of phased-array-fed dual-reflector systems with distributed power and phase control, and utilizing monolithic microwave integrated circuit modules, is demonstrated. Secondary radiation patterns for various antenna configurations, calculated using a method in which the phased array for each scanning direction is simulated by a fictitious point source, are computed to determine the achievable EIRP levels, sidelobe isolation, and cross-polarization isolation. The focal-region-fed Cassegrain

reflector was found to be best suited for fixed multiple beam applications, while the phased-array-fed dual-reflector configuration was selected for multiple scanning beams. Key elements of the phased-array design including a radiating square horn and a square orthomode transducer were fabricated and tested. R.R.

A87-42536* Hughes Aircraft Co., El Segundo, Calif.

RCS OF A COATED CIRCULAR WAVEGUIDE TERMINATED BY A PERFECT CONDUCTOR

CHOON S. LEE (Hughes Aircraft Co., El Segundo, CA) and SHUNG-WU LEE (Illinois, University, Urbana) IEEE Transactions on Antennas and Propagation (ISSN 0018-926X), vol. AP-35, April 1987, p. 391-398. refs

(Contract NAG3-475)

The radar cross section (RCS) of a circular waveguide terminated by a perfect electric conductor is calculated by the geometrical theory of diffraction for the rim diffraction and by a physical optics approximation for the interior irradiation. The interior irradiation is generally more than 10 dB higher than the rim diffraction for a/λ equal to or greater than 1 (a is the waveguide radius, λ is the free-space wavelength). At low frequencies (a/λ about 1), the interior irradiation can be significantly reduced over a broad range of incident angle if the interior waveguide wall is coated with a thin layer (1 percent of the radius) of lossy magnetic material. Our theoretical prediction is confirmed by measurements. At higher frequencies (a/λ about 3), a thin layer of coating is effective for the case of near axial incidence, provided that a good transition of the TE(11) mode near the waveguide opening to the HE(11) mode inside the waveguide is made. A thicker layer of coating is required for the RCS reduction over wider incident angle.

Author

A87-43165* National Aeronautics and Space Administration. Lewis Research Center, Cleveland, Ohio.

AN ADVANCED GEOSTATIONARY COMMUNICATIONS PLATFORM

THADDEUS A. HAWKES, WILLIAM CLOPP (RCA, Astro-Space Div., Princeton, NJ), and JACK LEKAN (NASA, Lewis Research Center, Cleveland, OH) IEEE Journal on Selected Areas in Communications (ISSN 0733-8716), vol. SAC-5, May 1987, p. 749-758. refs

A large geostationary communications platform can offer many attractive possibilities for providing lower cost communications. The platform payload concept described in this paper attempts to exploit these possibilities. The use of a combination of spot and wide-area coverage beams accommodates users in both high- and low-density population areas, and provides a good degree of frequency reuse. A standard channel bandwidth, used for most traffic, facilitates interconnectivity among C-, Ku-, and Ka-band users who may all access the platform. Adoption of a 36-MHz channel bandwidth leads to transmission rates that would be easily handled by low-cost terminals providing direct customer premises service. This also lends itself well to a solution using a large number of solid-state power amplifiers operating in all three frequency bands and sharing a common, redundant, conditioned power supply.

Author

A87-44075* Texas Univ., Austin.

RAYS VERSUS MODES - PICTORIAL DISPLAY OF ENERGY FLOW IN AN OPEN-ENDED WAVEGUIDE

HAO LING (Texas, University, Austin), RI-CHEE CHOU, and SHUNG-WU LEE (Illinois, University, Urbana) IEEE Transactions on Antennas and Propagation (ISSN 0018-926X), vol. AP-35, May 1987, p. 605-607. refs

(Contract NAG3-475; NSF ECS-83-11345)

The problem of a plane wave impinging on a semiinfinite parallel-plate waveguide is investigated. It is demonstrated that, for waveguide separation large compared to the wavelength, the fields inside the waveguide obey a single ray optics description. The beam behavior persists for more than 1000 λ into a 50 λ waveguide. For a small 3 λ waveguide, the beam picture begins to blur approximately 5 λ into the guide.

Author

A87-45466* Toledo Univ., Ohio.

AN ADAPTIVE ALGORITHM FOR MOTION COMPENSATED COLOR IMAGE CODING

SUBHASH C. KWATRA (Toledo, University, OH), WAYNE A. WHYTE (NASA, Lewis Research Center, Cleveland, OH), and CHOW-MING LIN (IEEE, IECEJ, ASJ, International Conference on Acoustics, Speech, and Signal Processing, Tokyo, Japan, Apr. 8-11, 1986) IEEE Transactions on Communications (ISSN 0090-6778), vol. COM-35, July 1987, p. 747-754. refs (Contract NAG3-42)

This paper presents an adaptive algorithm for motion compensated color image coding. The algorithm can be used for video teleconferencing or broadcast signals. Activity segmentation is used to reduce the bit rate and a variable stage search is conducted to save computations. The adaptive algorithm is compared with the nonadaptive algorithm and it is shown that with approximately 60 percent savings in computing the motion vector and 33 percent additional compression, the performance of the adaptive algorithm is similar to the nonadaptive algorithm. The adaptive algorithm results also show improvement of up to 1 bit/pel over interframe DPCM coding with nonuniform quantization. The test pictures used for this study were recorded directly from broadcast video in color. Author

A87-45513* National Aeronautics and Space Administration. Lewis Research Center, Cleveland, Ohio.

ACTS EXPERIMENTS PROGRAM

RONALD J. SCHERTLER (NASA, Lewis Research Center, Cleveland, OH) IN: GLOBECOM '86 - Global Telecommunications Conference, Houston, TX, Dec. 1-4, 1986, Conference Record. Volume 1. New York, Institute of Electrical and Electronics Engineers, Inc., 1986, p. 584-592. refs

NASA's Advanced Communications Technology Satellite which will flight test the advanced technologies associated with a Ka-band multibeam antenna, onboard signal processing and switching, and laser communications is described. The ACTS Experiment Program includes flight system technology experiments, ground system technology experiments, network control, propagation experiments, and end-to-end system experiments. Operational communications modes employing the baseband processor and microwave switch matrix are presented as well as the antenna coverage pattern.

K.K.

A87-51403* Northwestern Univ., Evanston, Ill.

THE FINITE-DIFFERENCE TIME-DOMAIN (FD-TD) METHOD FOR ELECTROMAGNETIC SCATTERING AND INTERACTION PROBLEMS

A. TAFLOVE (Northwestern University, Evanston, IL) and K. R. UMASHANKAR (Illinois, University, Chicago) (IEEE, AP-S Symposium and National Radio Science Meeting, Philadelphia, PA, June 12, 1986) Journal of Electromagnetic Waves and Applications (ISSN 0920-5071), vol. 1, no. 3, 1987, p. 243-267. Research supported by the University of California. refs (Contract NAG3-635; NSF ECS-85-15777)

The formulation and recent applications of the finite-difference time-domain (FD-TD) method for the numerical modeling of electromagnetic scattering and interaction problems are considered. It is shown that improvements in FD-TD modeling concepts and software implementation often make it a preferable choice for structures which cannot be easily treated by conventional integral equations and asymptotic approaches. Recent FD-TD modeling validations in research areas including coupling to wires and wire bundles in free space and cavities, scattering from surfaces in relativistic motion, inverse scattering, and radiation condition theory, are reviewed. Finally, the advantages and disadvantages of FD-TD, and guidelines concerning when FD-TD should and should not be used in high-frequency electromagnetic modeling problems, are summarized. R.R.

N87-10225*# Illinois Univ., Urbana-Champaign. Electromagnetics Lab.

THE STUDY OF MICROSTRIP ANTENNA ARRAYS AND RELATED PROBLEMS Semiannual Report, 20 May 1985 - 25 Sep. 1986

Y. T. LO 3 Oct. 1986 61 p

(Contract NAG3-418)

(NASA-CR-179714; NAS 1.26:179714) Avail: NTIS HC A04/MF A01 CSCL 20N

In February, an initial computer program to be used in analyzing the four-element array module was completed. This program performs the analysis of modules composed of four rectangular patches which are corporately fed by a microstrip line network terminated in four identical load impedances. Currently, a rigorous full-wave analysis of various types of microstrip line feed structures and patches is being performed. These tests include the microstrip line feed between layers of different electrical parameters. A method of moments was implemented for the case of a single dielectric layer and microstrip line fed rectangular patches in which the primary source is assumed to be a magnetic current ribbon across the line some distance from the patch. Measured values are compared with those computed by the program. B.G.

N87-11056*# IGI Consulting, Inc., Boston, Mass.

US LONG DISTANCE FIBER OPTIC NETWORKS: TECHNOLOGY, EVOLUTION AND ADVANCED CONCEPTS. VOLUME 1: EXECUTIVE SUMMARY Final Report

Oct. 1986 56 p

(Contract NAS3-24682)

(NASA-CR-179479; NAS 1.26:179479) Avail: NTIS HC A04/MF A01 CSCL 17B

Over the past two decades, fiber optics has emerged as a highly practical and cost-efficient communications technology. Its competitiveness vis-a-vis other transmission media, especially satellite, has become a critical question. This report studies the likely evolution and application of fiber optic networks in the United States to the end of the century. The outlook for the technology of fiber systems is assessed and forecast, scenarios of the evolution of fiber optic network development are constructed, and costs to provide service are determined and examined parametrically as a function of network size and traffic carried. Volume 1 consists of the Executive Summary. Volume 2 focuses on fiber optic technology and long distance fiber optic networks. Volume 3 develops a traffic and financial model of a nationwide long distance transmission network. Among the study's most important conclusions are: revenue requirements per circuit for LATA-to-LATA fiber optic links are less than one cent per call minute; multiplex equipment, which is likely to be required in any competing system, is the largest contributor to circuit costs; the potential capacity of fiber optic cable is very large and as yet undefined; and fiber optic transmission combined with other network optimization schemes can lead to even lower costs than those identified in this study. Author

N87-11057*# IGI Consulting, Inc., Boston, Mass.

US LONG DISTANCE FIBER OPTIC NETWORKS: TECHNOLOGY, EVOLUTION AND ADVANCED CONCEPTS. VOLUME 2: FIBER OPTIC TECHNOLOGY AND LONG DISTANCE NETWORKS Final Report

Oct. 1986 151 p

(Contract NAS3-24682)

(NASA-CR-179480; NAS 1.26:179480) Avail: NTIS HC A08/MF A01 CSCL 17B

The study projects until 2000 the evolution of long distance fiber optic networks in the U.S. Volume 1 is the Executive Summary. Volume 2 focuses on fiber optic components and systems that are directly related to the operation of long-haul networks. Optimistic, pessimistic and most likely scenarios of technology development are presented. The activities of national and regional companies implementing fiber long haul networks are also highlighted, along with an analysis of the market and regulatory forces affecting network evolution. Volume 3 presents advanced fiber optic network concept definitions. Inter-LATA traffic is

quantified and forms the basis for the construction of 11-, 15-, 17-, and 23-node networks. Using the technology projections from Volume 2, a financial model identifies cost drivers and determines circuit mile costs between any two LATAs. A comparison of fiber optics with alternative transmission concludes the report. Author

N87-11915*# IGI Consulting, Inc., Boston, Mass.
US LONG DISTANCE FIBER OPTIC NETWORKS: TECHNOLOGY, EVOLUTION AND ADVANCED CONCEPTS. VOLUME 3: ADVANCED NETWORKS AND ECONOMICS Final Report
 Oct. 1986 598 p
 (Contract NAS3-24682)
 (NASA-CR-179481; NAS 1.26:179481) Avail: NTIS HC A25/MF A01 CSCL 17B

This study projects until 2000 the evolution of long distance fiber optic networks in the U.S. Volume 1 is the executive Summary. Volume 2 focuses on fiber optic components and systems that are directly related to the operation of long-haul networks. Optimistic, pessimistic and most likely scenarios of technology development are presented. The activities of national and regional companies implementing fiber long haul networks are also highlighted, along with an analysis of the market and regulatory forces affecting network evolution. Volume 3 presents advanced fiber optic network concept definitions. Inter-LATA traffic is quantified and forms the basis for the construction of 11-, 15-, 17-, and 23-node networks. Using the technology projections from Volume 2, a financial model identifies cost drivers and determines circuit mile costs between any two LATAs. A comparison of fiber optics with alternative transmission concludes the report. Author

N87-13600*# National Aeronautics and Space Administration. Lewis Research Center, Cleveland, Ohio.
AN ASSESSMENT OF THE STATUS AND TRENDS IN SATELLITE COMMUNICATIONS 1986-2000: AN INFORMATION DOCUMENT PREPARED FOR THE COMMUNICATIONS SUBCOMMITTEE OF THE SPACE APPLICATIONS ADVISORY COMMITTEE
 W. A. POLEY, G. H. STEVENS, S. M. STEVENSON, J. LEKAN, C. H. ARTH, J. E. HOLLANSWORTH, and E. F. MILLER Nov. 1986 102 p
 (NASA-TM-88867; E-3270; NAS 1.15:88867) Avail: NTIS HC A06/MF A01 CSCL 45O

This is a response to a Space Applications Advisory Committee (SAAC) request for information about the status and trends in satellite communications, to be used to support efforts to conceive and recommend long range goals for NASA communications activities. Included in this document are assessments of: (1) the outlook for satellite communications, including current applications, potential future applications, and impact of the changing environment such as optical fiber networks, the Integrated Services Digital Network (ISDN) standard, and the rapidly growing market for Very Small Aperture Terminals (VSAT); (2) the restrictions imposed by our limited spectrum resource; and (3) technology needs indicated by future trends. Potential future systems discussed include: large powerful satellites for providing personal communications; VSAT compatible satellites with onboard switching and having voice capability; large satellites which offer a pervasive T1 network service (primarily for video-phone); and large geostationary communications facilities which support common use by several carriers. Also, discussion is included of NASA particular needs and possible future systems. Based on the mentioned system concepts, specific technology recommendations are provided for the time frames of now - 1993, 1994 - 2000, and 2000 - 2010.

Author

N87-14569*# National Aeronautics and Space Administration. Lewis Research Center, Cleveland, Ohio.

A DESIGN CONCEPT FOR AN MMIC MICROSTRIP PHASED ARRAY

R. Q. LEE, J. SMETANA, and R. ACOSTA 1986 13 p Presented at the 1986 Antenna Applications Symposium, Monticello, Ill., 17-19 Sep. 1986; sponsored by Illinois Univ. and RADCS (NASA-TM-88834; E-3213; NAS 1.15:88834) Avail: NTIS HC A02/MF A01 CSCL 20N

A conceptual design for a microstrip phased array with monolithic microwave integrated circuit (MMIC) amplitude and phase controls is described. The MMIC devices used are 20 GHz variable power amplifiers and variable phase shifters recently developed by NASA contractors for applications in future Ka band advanced satellite communication antenna systems. The proposed design concept is for a general NxN element array of rectangular lattice geometry. Subarray excitation is incorporated in the MMIC phased array design to reduce the complexity of the beam forming network and the number of MMIC components required. The proposed design concept takes into consideration the RF characteristics and actual physical dimensions of the MMIC devices. Also, solutions to spatial constraints and interconnections associated with currently available packaging designs are discussed. Finally, the design of the microstrip radiating elements and their radiation characteristics are examined. Author

N87-16198*# Ohio State Univ., Columbus. ElectroScience Lab.
ENGINEERING CALCULATIONS FOR COMMUNICATIONS SATELLITE SYSTEMS PLANNING Interim Report, 15 Jan. - 11 Jul. 1986

C. H. REILLY, C. A. LEVIS, O. M. BUYUKDURA, and C. A. MOUNT-CAMPBELL Nov. 1986 21 p
 (Contract NAG3-159)
 (NASA-CR-180106; NAS 1.26:180106; TR-718688-1) Avail: NTIS HC A02/MF A01 CSCL 17B

Observed solution times were analyzed for the extended gradient and cyclic coordinate search procedures. The times used in the analysis come from computer runs made during a previously-reported experiment conducted to assess the quality of the solutions to a BSS synthesis problem found by the two search methods. The results of a second experiment with a Fixed Satellite Service (FSS) test problem are also presented. Computational results are summarized for mixed integer programming approaches for solving FSS synthesis problems. A promising heuristic algorithm is described. A synthesis model is discussed for orbital arc allotment optimization. Research plans for the near future are also presented. Author

N87-16953*# Case Western Reserve Univ., Cleveland, Ohio. Dept. of Electrical Engineering and Applied Physics.

INVESTIGATION OF A GAALAS MACH-ZEHNDER ELECTRO-OPTIC MODULATOR M.S. Thesis. Final Contractor Report

DAVID M. MATERNA Jan. 1987 168 p
 (Contract NCC3-54)
 (NASA-CR-179573; NAS 1.26:179573) Avail: NTIS HC A08/MF A01 CSCL 09C

A GaAs modulator operating at 0.78 to 0.88 micron wavelength has the potential to be integrated with a GaAs/GaAlAs laser diode for an integrated fiber-optic transmitter. A travelling-wave Mach-Zehnder modulator using the electro-optic effect of GaAs and operating at a wavelength of 0.82 microns has been investigated for the first time. A four layer Strip-loaded ridge optical waveguide has been analyzed using the effective index method and single mode waveguides have been designed. The electro-optic effect of GaAs has also been analyzed and a modulator using the geometry producing the maximum phase shift has been designed. A coplanar transmission line structure is used in an effort to tap the potentially higher bandwidth of travelling-wave electrodes. The modulator bandwidth has been calculated at 11.95 GHz with a required drive power of 2.335 Watts for full intensity modulation. Finally, some preliminary experiments were performed to characterize a fabrication process for the modulator. Author

N87-16954*# Ford Aerospace and Communications Corp., Palo Alto, Calif. Western Development Lab. Div.

APPLICATION OF ADAPTIVE ANTENNA TECHNIQUES TO FUTURE COMMERCIAL SATELLITE COMMUNICATION Final Report, Apr. 1986 - Jan. 1987

L. ERSOY, E. A. LEE, and E. W. MATTHEWS Jan. 1987 125 p
(Contract NAS3-24892)

(NASA-CR-179566; NAS 1.26:179566; WDL-TR-10941) Avail: NTIS HC A06/MF A01 CSCL 17B

The purpose of this contract was to identify the application of adaptive antenna technique in future operational commercial satellite communication systems and to quantify potential benefits. The contract consisted of two major subtasks. Task 1, Assessment of Future Commercial Satellite System Requirements, was generally referred to as the Adaptive section. Task 2 dealt with Pointing Error Compensation Study for a Multiple Scanning/Fixed Spot Beam Reflector Antenna System and was referred to as the reconfigurable system. Each of these tasks was further sub-divided into smaller subtasks. It should also be noted that the reconfigurable system is usually defined as an open-loop system while the adaptive system is a closed-loop system. The differences between the open- and closed-loop systems were defined. Both the adaptive and reconfigurable systems were explained and the potential applications of such systems were presented in the context of commercial communication satellite systems. Author

N87-16955*# Ford Aerospace and Communications Corp., Palo Alto, Calif. Western Development Lab. Div.

APPLICATION OF ADAPTIVE ANTENNA TECHNIQUES TO FUTURE COMMERCIAL SATELLITE COMMUNICATIONS. EXECUTIVE SUMMARY Final Report, Apr. 1986 - Jan. 1987

L. ERSOY, E. A. LEE, and E. W. MATTHEWS Jan. 1987 17 p
(Contract NAS3-24892)

(NASA-CR-179566-SUMM; NAS 1.26:179566-SUMM; WDL-TR-10941-SUMM) Avail: NTIS HC A02/MF A01 CSCL 17B

The purpose of this contract was to identify the application of adaptive antenna technique in future operational commercial satellite communication systems and to quantify potential benefits. The contract consisted of two major subtasks. Task 1, Assessment of Future Commercial Satellite System Requirements, was generally referred to as the Adaptive section. Task 2 dealt with Pointing Error Compensation Study for a Multiple Scanning/Fixed Spot Beam Reflector Antenna System and was referred to as the reconfigurable system. Each of these tasks was further subdivided into smaller subtasks. It should also be noted that the reconfigurable system is usually defined as an open-loop system while the adaptive system is a closed-loop system. The differences between the open- and closed-loop systems were defined. Both the adaptive and reconfigurable systems were explained and the potential applications of such systems were presented in the context of commercial communication satellite systems. Author

N87-16958*# National Aeronautics and Space Administration. Lewis Research Center, Cleveland, Ohio.

A NEW MODEL FOR BROADBAND WAVEGUIDE TO MICROSTRIP TRANSITION DESIGN

GEORGE E. PONCHAK and ALAN N. DOWNEY Dec. 1986 18 p

(NASA-TM-88905; E-2935; NAS 1.15:88905) Avail: NTIS HC A02/MF A01 CSCL 17B

A new model is presented which permits the prediction of the resonant frequencies created by antipodal finline waveguide to microstrip transitions. The transition is modeled as a tapered transmission line in series with an infinite set of coupled resonant circuits. The resonant circuits are modeled as simple microwave resonant cavities of which the resonant frequencies are easily determined. The model is developed and the resonant frequencies determined for several different transitions. Experimental results are given to confirm the models. Author

N87-17971*# National Aeronautics and Space Administration. Lewis Research Center, Cleveland, Ohio.

BIT-ERROR-RATE TESTING OF HIGH-POWER 30-GHZ TRAVELING WAVE TUBES FOR GROUND-TERMINAL APPLICATIONS

KURT A. SHALKHAUSER and GENE FUJIKAWA Oct. 1986 16 p

(NASA-TP-2635; E-2996; NAS 1.60:2635) Avail: NTIS HC A02/MF A01 CSCL 17B

Tests were conducted at NASA Lewis to measure the bit-error-rate performance of two 30 GHz, 200 W, coupled-cavity traveling wave tubes (TWTs). The transmission effects of each TWT were investigated on a band-limited, 220 Mb/sec SMSK signal. The tests relied on the use of a recently developed digital simulation and evaluation system constructed at Lewis as part of the 30/20 GHz technology development program. The approach taken to test the 30 GHz tubes is described and the resultant test data are discussed. A description of the bit-error-rate measurement system and the adaptations needed to facilitate TWT testing are also presented. Author

N87-18695*# TRW Electronic Systems Group, Redondo Beach, Calif.

ADVANCED SPACE COMMUNICATIONS ARCHITECTURE STUDY. VOLUME 2: TECHNICAL REPORT Contractor Report, Jan. 1986 - Mar. 1987

MICHAEL HORSTEIN and PETER J. HADINGER Mar. 1987 193 p

(Contract NAS3-24743)

(NASA-CR-179592; NAS 1.26:179592) Avail: NTIS HC A09/MF A01 CSCL 17B

The technical feasibility and economic viability of satellite system architectures that are suitable for customer premise service (CPS) communications are investigated. System evaluation is performed at 30/20 GHz (Ka-band); however, the system architectures examined are equally applicable to 14/11 GHz (Ku-band). Emphasis is placed on systems that permit low-cost user terminals. Frequency division multiple access (FDMA) is used on the uplink, with typically 10,000 simultaneous accesses per satellite, each of 64 kbps. Bulk demodulators onboard the satellite, in combination with a baseband multiplexer, convert the many narrowband uplink signals into a small number of wideband data streams for downlink transmission. Single-hop network interconnectivity is accomplished via downlink scanning beams. Each satellite is estimated to weigh 5600 lb and consume 6850W of power; the corresponding payload totals are 1000 lb and 5000 W. Nonrecurring satellite cost is estimated at \$110 million, with the first-unit cost at \$113 million. In large quantities, the user terminal cost estimate is \$25,000. For an assumed traffic profile, the required system revenue has been computed as a function of the internal rate of return (IRR) on invested capital. The equivalent user charge per-minute of 64-kbps channel service has also been determined. Author

N87-18696*# TRW Electronic Systems Group, Redondo Beach, Calif.

ADVANCED SPACE COMMUNICATIONS ARCHITECTURE STUDY. VOLUME 1: EXECUTIVE SUMMARY Contractor Report, Jan. 1986 - Mar. 1987

MICHAEL HORSTEIN and PETER J. HADINGER Mar. 1987 14 p

(Contract NAS3-24743)

(NASA-CR-179591; NAS 1.26:179591) Avail: NTIS HC A02/MF A01 CSCL 17B

The technical feasibility and economic viability of satellite system architectures that are suitable for Customer Premise Service (CPS) communications is investigated. System evaluation is performed at 30/20 GHz (Ka-band); however, the system architectures examined are equally applicable to 14/11 GHz (Ku-band). Emphasis is placed on system that permit low cost user terminals. Frequency Division Multiple Access (FDMA) is used on the uplink, with typically 10,000 simultaneous accesses per satellite, each of 64 kbps. Bulk demodulators onboard the satellite, in combination with a baseband multiplexer, convert the many narrowband uplink signals into a

small number of wideband data streams for downlink transmission. Single hop network interconnectivity is accomplished through use of downlink scanning beams. Each satellite is estimated to weigh 5600 lb and consume 6850W of power; the corresponding payload totals are 1000 lb and 5000W. Nonrecurring satellite cost is estimated at \$110 million, with the first unit cost at \$113 million. In large quantities, the user terminal cost estimate is \$25,000.

Author

N87-18700*# National Aeronautics and Space Administration. Lewis Research Center, Cleveland, Ohio.

PERFORMANCE OF A KA-BAND SATELLITE SYSTEM UNDER VARIABLE TRANSMITTED SIGNAL POWER CONDITIONS

GENE FUJIKAWA and ROBERT J. KERCZEWSKI 1987 12 p
Prepared for presentation at the IEEE MTT-S International Microwave Symposium and Exhibition, Las Vegas, Nev., 9-11 Jun. 1987

(NASA-TM-88984; E-3454; NAS 1.15:88984) Avail: NTIS HC A02/MF A01 CSCL 17B

A laboratory hardware-based satellite communication system simulator has been used to measure the effects of transmitted signal power changes on the performance of a Ka-band system. Such power changes can be used to compensate for signal fade due to rain attenuation. This paper presents and discusses the results of these measurements.

Author

N87-19552*# Communications Satellite Corp., Washington, D.C. Space Communications Div.

INTERSATELLITE LINK (ISL) APPLICATION TO COMMERCIAL COMMUNICATIONS SATELLITES. VOLUME 1: EXECUTIVE SUMMARY Final Report, Mar. - Dec. 1986

S. LEE YOUNG Jan. 1987 44 p

(Contract NAS3-24884)

(NASA-CR-179598-VOL-1; NAS 1.26:179598-VOL-1) Avail: NTIS HC A03/MF A01 CSCL 17B

Based on a comprehensive evaluation of the fundamental Intersatellite Link (ISL) systems characteristics, potential applications of ISLs to domestic, regional, and global commercial satellite communications were identified, and their cost-effectiveness and other systems benefits quantified wherever possible. Implementation scenarios for the cost-effective communications satellite systems employing ISLs were developed for the first launch in 1993 to 1994 and widespread use of ISLs in the early 2000's. Critical technology requirements for both the microwave (60 GHz) and optical (0.85 micron) ISL implementations were identified, and their technology development programs, including schedule and cost estimates, were derived.

Author

N87-19553*# Communications Satellite Corp., Washington, D.C. Space Communications Div.

INTERSATELLITE LINK (ISL) APPLICATION TO COMMERCIAL COMMUNICATIONS SATELLITES. VOLUME 2: TECHNICAL FINAL REPORT Final Report, Mar. - Dec. 1986

S. LEE YOUNG Jan. 1987 304 p

(Contract NAS3-24884)

(NASA-CR-179598-VOL-2; NAS 1.26:179598-VOL-2) Avail: NTIS HC A14/MF A01 CSCL 17B

Intersatellite Link (ISL) applications can improve and expand communication satellite services in a number of ways. As the demand for orbital slots within prime regions of the geostationary arc increases, attention is being focused on ISLs as a method to utilize this resource more efficiently and circumvent saturation. Various GEO-to-GEO applications were determined that provide potential benefits over existing communication systems. A set of criteria was developed to assess the potential applications. Intersatellite link models, network system architectures, and payload configurations were developed. For each of the chosen ISL applications, ISL versus non-ISL satellite systems architectures were derived. Both microwave and optical ISL implementation approaches were evaluated for payload sizing and cost analysis. The technological availability for ISL implementations was assessed. Critical subsystems technology areas were identified,

and an estimate of the schedule and cost to advance the technology to the required state of readiness was made. B.G.

N87-19556*# Raytheon Co., Waltham, Mass. Microwave and Power Tube Div.

RECTENNA TECHNOLOGY PROGRAM: ULTRA LIGHT 2.45 GHZ RECTENNA 20 GHZ RECTENNA

WILLIAM C. BROWN 11 Mar. 1987 98 p

(Contract NAS3-22764)

(NASA-CR-179558; NAS 1.26:179558; PT-6807) Avail: NTIS HC A05/MF A01 CSCL 20N

The program had two general objectives. The first objective was to develop the two plane rectenna format for space application at 2.45 GHz. The resultant foreplane was a thin-film, etched-circuit format fabricated from a laminate composed of 2 mil Kapton F sandwiched between sheets of 1 oz copper. The thin-film foreplane contains half wave dipoles, filter circuits, rectifying Schottky diode, and dc bussing lead. It weighs 160 grams per square meter. Efficiency and dc power output density were measured at 85% and 1 kw/sq m, respectively. Special testing techniques to measure temperature of circuit and diode without perturbing microwave operation using the fluoroptic thermometer were developed. A second objective was to investigate rectenna technology for use at 20 GHz and higher frequencies. Several fabrication formats including the thin-film scaled from 2.45 GHz, ceramic substrate and silk-screening, and monolithic were investigated, with the conclusion that the monolithic approach was the best. A preliminary design of the monolithic rectenna structure and the integrated Schottky diode were made.

Author

N87-20448*# National Aeronautics and Space Administration. Lewis Research Center, Cleveland, Ohio.

UNIQUE BIT-ERROR-RATE MEASUREMENT SYSTEM FOR SATELLITE COMMUNICATION SYSTEMS

MARY JO WINDMILLER Mar. 1987 13 p

(NASA-TP-2699; E-3322; NAS 1.60:2699) Avail: NTIS HC

A02/MF A01 CSCL 17B

Bit-error-rate measurements, necessary to assess the performance of communication systems and components, were required for the ground-based simulation and test bed of a Ka-band, satellite-switched time-division multiple access (SS-TDMA) satellite system at the NASA Lewis Research Center. This report discusses the requirements and design tradeoffs for that system and provides a description of its hardware design.

Author

N87-20450*# National Aeronautics and Space Administration. Lewis Research Center, Cleveland, Ohio.

A STUDY OF THE EFFECT OF GROUP DELAY DISTORTION ON AN SMSK SATELLITE COMMUNICATIONS CHANNEL

ROBERT J. KERCZEWSKI Apr. 1987 39 p

(NASA-TM-89835; E-3491; NAS 1.15:89835) Avail: NTIS HC

A03/MF A01 CSCL 17B

The effects of group delay distortion on an SMSK satellite communications channel have been investigated. Software and hardware simulations have been used to determine the effects of channel group delay variations with frequency on the bit error rate for a 220 Mbps SMSK channel. These simulations indicate that group delay distortions can significantly degrade the bit error rate performance. The severity of the degradation is dependent on the amount, type, and spectral location of the group delay distortion.

Author

N87-21212*# Ford Aerospace and Communications Corp., Palo Alto, Calif. Advanced Systems Dept.

THE USE OF SATELLITES IN NON-GEOSTATIONARY ORBITS FOR UNLOADING GEOSTATIONARY COMMUNICATION SATELLITE TRAFFIC PEAKS. VOLUME 1: EXECUTIVE SUMMARY Final Report, Apr. 1986 - Feb. 1987

K. PRICE, A. TURNER, T. NGUYEN, W. DOONG, and C. WEYANDT May 1987 23 p
(Contract NAS3-24891)
(NASA-CR-179597-VOL-1; NAS 1.26:179597-VOL-1) Avail: NTIS HC A02/MF A01 CSCL 17B

The overall objective of this program was to assess the application, economic benefits, and technology and system implications of satellites in non-geostationary (non-GEO) orbits for off-loading peak traffic from GEO communications satellites. The study was organized into four technical tasks which are described in turn. They are: (1) concepts development; (2) system definition; (3) economic comparisons; and (4) technology requirements definition. Each of these tasks is defined in detail and the results of each are given. Author

N87-21213*# Ford Aerospace and Communications Corp., Palo Alto, Calif. Advanced Systems Dept.

THE USE OF SATELLITES IN NON-GEOSTATIONARY ORBITS FOR UNLOADING GEOSTATIONARY COMMUNICATION SATELLITE TRAFFIC PEAKS. VOLUME 2: TECHNICAL REPORT Final Report, Apr. 1986 - Feb. 1987

K. PRICE, A. TURNER, T. NGUYEN, W. DOONG, and C. WEYANDT May 1987 157 p
(Contract NAS3-24891)
(NASA-CR-179597-VOL-2; NAS 1.26:179597-VOL-2) Avail: NTIS HC A08/MF A01 CSCL 17B

The part of the geostationary (GEO) orbital arc used for United States domestic fixed, communications service is rapidly becoming filled with satellites. One of the factors currently limiting its utilization is that communications satellites must be designed to have sufficient capacity to handle peak traffic loads, and thus are underutilized most of the time. A solution is to use satellites in suitable non-geostationary orbits to unload the traffic peaks. Three different designs for a non-geostationary orbit communications satellite system are presented for the 1995 time frame. The economic performance is analyzed and compared with geostationary satellites for two classes of service, trunking and customer premise service. The result is that the larger payload of the non-geostationary satellite offsets the burdens of increased complexity and worse radiation environment to give improved economic performance. Depending on ground terminal configuration, the improved economic performance of the space segment may be offset by increased ground terminal expenses. Author

N87-22065*# National Aeronautics and Space Administration. Lewis Research Center, Cleveland, Ohio.

RF CHARACTERIZATION OF MONOLITHIC MICROWAVE AND MM-WAVE ICS

R. R. ROMANOVSKY, G. E. PONCHAK, K. A. SHALKHAUSER, and K. B. BHASIN 1986 18 p Presented at the Millimeter Wave/Microwave Measurements and Standards for Miniaturized Systems, Redstone Arsenal, Ala., 6-7 Nov. 1986; sponsored by the Army Missile Command
(NASA-TM-88948; E-3259; NAS 1.15:88948) Avail: NTIS HC A02/MF A01 CSCL 20N

A number of fixturing techniques compatible with automatic network analysis are presented. The fixtures are capable of characterizing GaAs Monolithic Microwave Integrated Circuits (MMICs) at K and Ka band. Several different transitions are used to couple the RF test port to microstrip. Fixtures which provide chip level de-embedding are included. In addition, two advanced characterization techniques are assessed. Author

N87-22089*# National Aeronautics and Space Administration. Lewis Research Center, Cleveland, Ohio.

MICROSTRIP ANTENNA ARRAY WITH PARASITIC ELEMENTS
KAI F. LEE (Akron Univ., Ohio.), ROBERTO J. ACOSTA, and RICHARD Q. LEE 1987 6 p Presented at the 1987 AP-S International Symposium, Blacksburg, Va., 15-17 Jun. 1987; sponsored by IEEE
(NASA-TM-89919; E-3615; NAS 1.15:89919) Avail: NTIS HC A02/MF A01 CSCL 20N

Discussed is the design of a large microstrip antenna array in terms of subarrays consisting of one fed patch and several parasitic patches. The potential advantages of this design are discussed. Theoretical radiation patterns of a subarray in the configuration of a cross are presented. Author

N87-22874*# National Aeronautics and Space Administration. Lewis Research Center, Cleveland, Ohio.

DETECTION OF REFLECTOR SURFACE ERROR FROM NEAR-FIELD DATA: EFFECT OF EDGE DIFFRACTED FIELD
ALAN R. CHERRETTE, SHONG W. LEE (Illinois Univ., Urbana-Champaign.), and ROBERTO J. ACOSTA 1987 6 p Presented at the 1987 AP-S International Symposium, Blacksburg, Va., 15-17 Jun. 1987; sponsored by IEEE
(NASA-TM-89920; E-3616; NAS 1.15:89920) Avail: NTIS HC A02/MF A01 CSCL 20N

The surface accuracy of large reflector antennas must be maintained within certain tolerances if high gain/low sidelobe performance is to be achieved. Thus the measurement of the surface profile is an important part of the quality control procedure when constructing antennas of this type. An efficient method for surface profile measurement has been proposed, i.e., the reflector surface is calculated from the measured near-field phase data using the theory of geometric optics. For a surface profile calculation of this kind, it is necessary to know the margin of error built into the method of calculation. This will enable a specification of the tolerance from which the surface profile can be determined. When calculating the surface profile from near-field phase data, there are two main sources of error. The first is the measurement error in near-field phase data. The second arises from the edge diffracted fields that are superimposed on the reflected fields in the measured near-field data. The error in the calculated surface profile produced by the edge diffracted fields is examined. Author

N87-24605*# Ohio State Univ., Columbus. ElectroScience Lab. **ENGINEERING CALCULATIONS FOR COMMUNICATIONS SATELLITE SYSTEMS PLANNING Interim Report**

CHARLES H. REILLY, ERIC K. WALTON, and PAUL KOHNHORST May 1987 39 p
(Contract NAG3-159)
(NASA-CR-181112; NAS 1.26:181112; REPT-718688-3) Avail: NTIS HC A03/MF A01 CSCL 17B

A procedure is described that was used to calculate minimum required satellite separations based on total link carrier to interference requirements. Also summarized are recent results with a switching algorithm for satellite synthesis problems. Analytic solution value bounds for two of the satellite synthesis models studied are described. Preliminary results from an empirical study of alternate mixed integer programming models for satellite synthesis are presented. Research plans for the near future are discussed. Author

N87-26265*# National Aeronautics and Space Administration. Lewis Research Center, Cleveland, Ohio.

MICROWAVE CHARACTERIZATION AND MODELING OF GAAS/ALGAAS HETEROJUNCTION BIPOLAR TRANSISTORS
RAINEE N. SIMONS and ROBERT R. ROMANOVSKY Jun. 1987 34 p Presented at the EEs of User's Group Meeting, Las Vegas, Nev., 9 Jun. 1987
(NASA-TM-100150; E-3593; NAS 1.15:100150) Avail: NTIS HC A03/MF A01 CSCL 20N

The characterization and modeling of a microwave GaAs/AlGaAs heterojunction Bipolar Transistor (HBT) are

discussed. The de-embedded scattering parameters are used to derive a small signal lumped element equivalent circuit model using EEsof's Touchstone software package. Each element in the equivalent circuit model is shown to have its origin within the device. The model shows good agreement between the measured and modeled scattering parameters over a wide range of bias currents. Further, the MAG (maximum available power gain) and the h_{21} (current gain) calculated from the measured data and those predicted by the model are also in good agreement. Consequently, the model should also be capable of predicting the $f_{sub\ max}$ and the $f_{sub\ T}$ of other HBTs. Author

N87-27085* Illinois Univ., Urbana-Champaign. Electromagnetics Lab.

REDUCTION OF THE RADAR CROSS SECTION OF ARBITRARILY SHAPED CAVITY STRUCTURES

R. CHOU, H. LING, and S. W. LEE Aug. 1987 130 p

(Contract NAG3-475)

(NASA-CR-180307; NAS 1.26:180307; UILU-ENG-87-2560;

UILU-TR-87-6) Avail: NTIS HC A07/MF A01 CSCL 20N

The problem of the reduction of the radar cross section (RCS) of open-ended cavities was studied. The issues investigated were reduction through lossy coating materials on the inner cavity wall and reduction through shaping of the cavity. A method was presented to calculate the RCS of any arbitrarily shaped structure in order to study the shaping problem. The limitations of this method were also addressed. The modal attenuation was studied in a multilayered coated waveguide. It was shown that by employing two layers of coating, it was possible to achieve an increase in both the magnitude of attenuation and the frequency band of effectiveness. The numerical method used in finding the roots of the characteristic equation breaks down when the coating thickness is very lossy and large in terms of wavelength. A new method of computing the RCS of an arbitrary cavity was applied to study the effects of longitudinal bending on RCS reduction. The ray and modal descriptions for the fields in a parallel plate waveguide were compared. To extend the range of validity of the Shooting and Bouncing Ray (SBR) method, the simple ray picture must be modified to account for the beam blurring. B.G.

N87-27848* National Aeronautics and Space Administration. Lewis Research Center, Cleveland, Ohio.

SWEPT FREQUENCY TECHNIQUE FOR DISPERSION MEASUREMENT OF MICROSTRIP LINES

RICHARD Q. LEE In Illinois Univ., Proceedings of the Antenna Applications Symposium held in Urbana, Illinois on 17-19 September 1986, Volume 2 p 597-614 Feb. 1987

(AD-P005420) Avail: NTIS HC A15/MF A01 CSCL 14B

Microstrip lines used in microwave integrated circuits are dispersive. Because a microstrip line is an open structure, the dispersion can not be derived with pure TEM, TE, or TM mode analysis. Dispersion analysis has commonly been done using a spectral domain approach, and dispersion measurement has been made with high Q microstrip ring resonators. Since the dispersion of a microstrip line is fully characterized by the frequency dependent phase velocity of the line, dispersion measurement of microstrip lines requires the measurement of the line wavelength as a function of frequency. In this paper, a swept frequency technique for dispersion measurement is described. GRA

N87-27882* Ohio State Univ., Columbus. ElectroScience Lab. OPTIMIZATION OF ORBITAL ASSIGNMENT AND SPECIFICATION OF SERVICE AREAS IN SATELLITE COMMUNICATIONS

COU-WAY WANG, CURT A. LEVIS, and O. MERIH BUYUKDURA

Feb. 1987 265 p

(Contract NAG3-159)

(NASA-CR-181273; NAS 1.26:181273; REPT-716548-7) Avail:

NTIS HC A12/MF A01 CSCL 17B

The mathematical nature of the orbital and frequency assignment problem for communications satellites is explored, and it is shown that choosing the correct permutations of the orbit locations and frequency assignments is an important step in arriving

at values which satisfy the signal-quality requirements. Two methods are proposed to achieve better spectrum/orbit utilization. The first, called the delta S concept, leads to orbital assignment solutions via either mixed-integer or restricted basis entry linear programming techniques; the method guarantees good single-entry carrier-to-interference ratio results. In the second, a basis for specifying service areas is proposed for the Fixed Satellite Service. It is suggested that service areas should be specified according to the communications-demand density in conjunction with the delta S concept in order to enable the system planner to specify more satellites and provide more communications supply. Author

N87-27883* National Aeronautics and Space Administration. Lewis Research Center, Cleveland, Ohio.

MONOLITHIC MICROWAVE INTEGRATED CIRCUIT (MMIC) TECHNOLOGY FOR SPACE COMMUNICATIONS APPLICATIONS

DENIS J. CONNOLLY, KUL B. BHASIN, and ROBERT R. ROMANOFSKY 1987 18 p Proposed for presentation at the 38th International Astronautical Federation Congress, Brighton, England, 9-17 Oct. 1987

(NASA-TM-100187; E-3763; NAS 1.15:100187; IAF-87-491)

Avail: NTIS HC A02/MF A01 CSCL 09C

Future communications satellites are likely to use gallium arsenide (GaAs) monolithic microwave integrated-circuit (MMIC) technology in most, if not all, communications payload subsystems. Multiple-scanning-beam antenna systems are expected to use GaAs MMICs to increase functional capability, to reduce volume, weight, and cost, and to greatly improve system reliability. RF and IF matrix switch technology based on GaAs MMICs is also being developed for these reasons. MMIC technology, including gigabit-rate GaAs digital integrated circuits, offers substantial advantages in power consumption and weight over silicon technologies for high-throughput, on-board baseband processor systems. For the more distant future pseudomorphic indium gallium arsenide (InGaAs) and other advanced III-V materials offer the possibility of MMIC subsystems well up into the millimeter wavelength region. All of these technology elements are in NASA's MMIC program. Their status is reviewed. Author

N87-28763* National Aeronautics and Space Administration. Lewis Research Center, Cleveland, Ohio.

AP-S WORKSHOP ON CHARACTERIZATION OF MMIC (MONOLITHIC MICROWAVE INTEGRATED CIRCUIT) DEVICES FOR ARRAY ANTENNA

JERRY SMETANA, ed., RAJ MITTRA, ed. (Illinois Univ., Urbana.), NICK LAPRADE, BRYAN EDWARD, and AMIR ZAGHLOUL In Illinois Univ., Proceedings of the Antenna Applications Symposium held in Urbana, Illinois on 17-19 September 1986, Volume 1 p 119-133 Feb. 1987 Workshop held in Philadelphia, Pa., 9-13 Jun. 1986

(AD-P005398) Avail: NTIS HC A16/MF A01 CSCL 09A

The IEEE AP-S ADCOM is attempting to expand its educational, tutorial and information exchange activities as a further benefit to all members. To this end, ADCOM will be forming specialized workshops on topics of interest to its members. The first such workshop on Characterization and Packaging of MMIC Devices for Array Antennas was conceived. The workshop took place on June 13, 1986 as part of the 1986 International Symposium sponsored by IEEE AP-S and URSI in Philadelphia, PA, June 9-13, 1986. The workshop was formed to foster the interchange of ideas among MMIC device users and to provide a forum to collect and focus information among engineers experienced and interested in the topic. After brief presentations by the panelists and comments from attendees on several subtopics, the group was divided into working committees. Each committee evaluated and made recommendations on one of the subtopics. GRA

N87-28769*# National Aeronautics and Space Administration. Lewis Research Center, Cleveland, Ohio.

A DESIGN CONCEPT FOR AN MMIC (MONOLITHIC MICROWAVE INTEGRATED CIRCUIT) MICROSTRIP PHASED ARRAY

RICHARD Q. LEE, JERRY SMETANA, and ROBERTO ACOSTA /n Illinois Univ., Proceedings of the Antenna Applications Symposium held in Urbana, Illinois on 17-19 September 1986, Volume 1 p 239-252 Feb. 1987 (AD-P005404; NASA-TM-88834) Avail: NTIS HC A16/MF A01 CSCL 09A

A conceptual design for a microstrip phased array with monolithic microwave integrated circuit (MMIC) amplitude and phase controls is described. The MMIC devices used are 20 GHz variable power amplifiers and variable phase shifters recently developed by NASA contractors for applications in future Ka proposed design, which concept is for a general NxN element array of rectangular lattice geometry. Subarray excitation is incorporated in the MMIC phased array design to reduce the complexity of the beam forming network and the number of MMIC components required. GRA

N87-28813*# Ohio State Univ., Columbus. ElectroScience Lab. **SMI ADAPTIVE ANTENNA ARRAYS FOR WEAK INTERFERING SIGNALS**

I. J. GUPTA Sep. 1987 57 p

(Contract NAG3-536)

(NASA-CR-181330; NAS 1.26:181330; OSU-TR-716111-5) Avail: NTIS HC A04/MF A01 CSCL 17B

The performance of adaptive antenna arrays is studied when a sample matrix inversion (SMI) algorithm is used to control array weights. It is shown that conventional SMI adaptive antennas, like other adaptive antennas, are unable to suppress weak interfering signals (below thermal noise) encountered in broadcasting satellite communication systems. To overcome this problem, the SMI algorithm is modified. In the modified algorithm, the covariance matrix is modified such that the effect of thermal noise on the weights of the adaptive array is reduced. Thus, the weights are dictated by relatively weak coherent signals. It is shown that the modified algorithm provides the desired interference protection. The use of defocused feeds as auxiliary elements of an SMI adaptive array is also discussed. Author

N87-28814*# Ohio State Univ., Columbus. Dept. of Electrical Engineering.

ADAPTIVE ARRAYS FOR WEAK INTERFERING SIGNALS: AN EXPERIMENTAL SYSTEM M.S. Thesis

JAMES WARD 1987 139 p

(Contract NAG3-536)

(NASA-CR-181181; NAS 1.26:181181) Avail: NTIS HC A07/MF A01 CSCL 20N

An experimental adaptive antenna system was implemented to study the performance of adaptive arrays in the presence of weak interfering signals. It is a sidelobe canceler with two auxiliary elements. Modified feedback loops, which decorrelate the noise components of the two inputs to the loop correlators, control the array weights. Digital processing is used for algorithm implementation and performance evaluation. The results show that the system can suppress interfering signals which are 0 to 10 dB below the thermal noise level in the main channel by 20 to 30 dB. When the desired signal is strong in the auxiliary elements the amount of interference suppression decreases. The amount of degradation depends on the number of interfering signals incident on the communication system. A modified steering vector which overcomes this problem is proposed. Author

N87-28819*# Communications Satellite Corp., Clarksburg, Md. **ONBOARD MULTICHANNEL DEMULTIPLEXER-DEMODULATOR Final Report**

S. JOSEPH CAMPANELLA and SOHEIL SAYEGH 29 Jul. 1987 113 p

(Contract NAS3-24885)

(NASA-CR-180821; NAS 1.26:180821) Avail: NTIS HC A06/MF A01 CSCL 17B

An investigation performed for NASA LeRC by COMSAT Labs, of a digitally implemented on-board demultiplexer/demodulator able to process a mix of uplink carriers of differing bandwidths and center frequencies and programmable in orbit to accommodate variations in traffic flow is reported. The processor accepts high speed samples of the signal carried in a wideband satellite transponder channel, processes these as a composite to determine the signal spectrum, filters the result into individual channels that carry modulated carriers and demodulate these to recover their digital baseband content. The processor is implemented by using forward and inverse pipeline Fast Fourier Transformation techniques. The recovered carriers are then demodulated using a single digitally implemented demodulator that processes all of the modulated carriers. The effort has determined the feasibility of the concept with multiple TDMA carriers, identified critical path technologies, and assessed the potential of developing these technologies to a level capable of supporting a practical, cost effective on-board implementation. The result is a flexible, high speed, digitally implemented Fast Fourier Transform (FFT) bulk demultiplexer/demodulator. Author

33

ELECTRONICS AND ELECTRICAL ENGINEERING

Includes test equipment and maintainability; components, e.g., tunnel diodes and transistors; microminiaturization; and integrated circuitry.

A87-14084*# Systems Science and Software, La Jolla, Calif. **THREE DIMENSIONAL SIMULATION OF THE OPERATION OF A HOLLOW CATHODE ELECTRON EMITTER ON THE SHUTTLE ORBITER**

V. A. DAVIS, I. KATZ, M. J. MANDELL, and D. E. PARKS (Systems Science and Software, La Jolla, CA) NASA, AIAA, and PSN, International Conference on Tethers in Space, Arlington, VA, Sept. 17-19, 1986, Paper. 16 p. refs (Contract NAS3-23881)

Several researchers have suggested using hollow cathodes as plasma contactors for electrodynamic tethers, particularly to prevent the shuttle orbiter from charging to large negative potentials. Previous studies have shown that fluid models with anomalous scattering can describe the electron transport in hollow cathode generated plasmas. An improved theory of the hollow cathode plasmas is developed and computational results using the theory are compared with laboratory experiment. Numerical predictions for a hollow cathode plasma source of the type considered for use on the shuttle are presented as are three-dimensional NASCAP/LEO calculations of the emitted ion trajectories and the resulting potentials in the vicinity of the orbiter. The computer calculations show that the hollow cathode plasma source makes vastly superior contact with the ionospheric plasma compared with either an electron gun or passive ion collection by the orbiter. Author

A87-18115*# National Aeronautics and Space Administration. Lewis Research Center, Cleveland, Ohio.

DESCRIPTION OF A 20 KILOHERTZ POWER DISTRIBUTION SYSTEM

I. G. HANSEN (NASA, Lewis Research Center, Cleveland, OH) IN: IECEC '86; Proceedings of the Twenty-first Intersociety Energy Conversion Engineering Conference, San Diego, CA, August 25-29, 1986. Volume 3. Washington, DC, American Chemical Society, 1986, p. 1693-1695. Previously announced in STAR as N86-31584. refs

A single phase, 440 VRMS, 20 kHz power distribution system with a regulated sinusoidal wave form is discussed. A single phase power system minimizes the wiring, sensing, and control complexities required in a multi-sourced redundantly distributed power system. The single phase addresses only the distribution links multiphase lower frequency inputs and outputs accommodation techniques are described. While the 440 V operating potential was initially selected for aircraft operating below 50,000 ft, this potential also appears suitable for space power systems. This voltage choice recognizes a reasonable upper limit for semiconductor ratings, yet will direct synthesis of 220 V, 3 power. A 20 kHz operating frequency was selected to be above the range of audibility, minimize the weight of reactive components, yet allow the construction of single power stages of 25 to 30 kW. The regulated sinusoidal distribution system has several advantages. With a regulated voltage, most ac/dc conversions involve rather simple transformer rectifier applications. A sinusoidal distribution system, when used in conjunction with zero crossing switching, represents a minimal source of EMI. The present state of 20 kHz power technology includes computer controls of voltage and/or frequency, low inductance cable, current limiting circuit protection, bi-directional power flow, and motor/generator operating using standard induction machines. A status update and description of each of these items and their significance is presented. M.G.

A87-19091* National Aeronautics and Space Administration. Lewis Research Center, Cleveland, Ohio.

ADVANCES IN GALLIUM ARSENIDE MONOLITHIC MICROWAVE INTEGRATED-CIRCUIT TECHNOLOGY FOR SPACE COMMUNICATIONS SYSTEMS

K. B. BHASIN and D. J. CONNOLLY (NASA, Lewis Research Center, Cleveland, OH) IEEE Transactions on Microwave Theory and Techniques (ISSN 0018-9480), vol. MTT-34, Oct. 1986, p. 994-1001. refs

Future communications satellites are likely to use gallium arsenide (GaAs) monolithic microwave integrated-circuit (MMIC) technology in most, if not all, communications payload subsystems. Multiple-scanning-beam antenna systems are expected to use GaAs MMIC's to increase functional capability, to reduce volume, weight, and cost, and to greatly improve system reliability. RF and IF matrix switch technology based on GaAs MMIC's is also being developed for these reasons. MMIC technology, including gigabit-rate GaAs digital integrated circuits, offers substantial advantages in power consumption and weight over silicon technologies for high-throughput, on-board baseband processor systems. In this paper, current developments in GaAs MMIC technology are described, and the status and prospects of the technology are assessed. Author

A87-19104* Illinois Univ., Urbana.

PROPOSAL FOR SUPERSTRUCTURE BASED HIGH EFFICIENCY PHOTOVOLTAICS

M. WAGNER and J. P. LEBURTON (Illinois, University, Urbana) Applied Physics Letters (ISSN 0003-6951), vol. 49, Oct. 6, 1986, p. 886-888. refs (Contract NAG3-507)

A novel class of cascade structures is proposed which features multijunction upper subcells, referred to as superstructure high-efficiency photovoltaics (SHEPs). The additional junctions enhance spectral response and improve radiation tolerance by reducing bulk recombination losses. This is important because ternary III-V alloys, which tend to have short minority-carrier diffusion lengths, are the only viable materials for the high-bandgap

upper subcells required for cascade solar cells. Realistic simulations of AlGaAs SHEPs show that one-sun AMO efficiencies in excess of 26 percent are possible. Author

A87-19996*# National Aeronautics and Space Administration. Lewis Research Center, Cleveland, Ohio.

POTENTIAL FOR USE OF INP SOLAR CELLS IN THE SPACE RADIATION ENVIRONMENT

I. WEINBERG, C. K. SWARTZ, and R. E. HART, JR. (NASA, Lewis Research Center, Cleveland, OH) IN: Photovoltaic Specialists Conference, 18th, Las Vegas, NV, October 21-25, 1985, Conference Record. New York, Institute of Electrical and Electronics Engineers, Inc., 1985, p. 1722-1724. Previously announced in STAR as N86-13645. refs

Indium phosphide solar cells were observed to have significantly higher radiation resistance than either GaAs or Si after exposure to 10 MeV proton irradiation data and previous 1 MeV electron data together with projected efficiencies for InP, it was found that these latter cells produced more output power than either GaAs or Si after specified fluences of 10 MeV protons and 1 MeV electrons. Estimates of expected performance in a proton dominated space orbit yielded much less degradation for InP when compared to the remaining two cell types. It was concluded that, with additional development to increase efficiency, InP solar cells would perform significantly better than either GaAs or Si in the space radiation environment. Author

A87-20666*# National Aeronautics and Space Administration. Lewis Research Center, Cleveland, Ohio.

CARBON AND CARBON-COATED ELECTRODES FOR MULTISTAGE DEPRESSED COLLECTORS FOR ELECTRON-BEAM DEVICES - A TECHNOLOGY REVIEW

ARTHUR N. CURREN (NASA, Lewis Research Center, Cleveland, OH) IEEE Transactions on Electron Devices (ISSN 0018-9383), vol. ED-33, Nov. 1986, pt. 2, p. 1902-1914. refs

Various aspects of carbon and carbon-coated multistaged depressed collector (MDC) electrode technology are reviewed. The physical properties of untreated graphite electrodes, ion-textured graphite electrodes, and textured, carbon-coated copper electrodes, and surface treatment procedures for these electrodes are described. The secondary electron emissions of the three electrode types are analyzed. MDC fabrication methods are discussed. The performances of MDCs fabricated with untreated graphite electrodes, ion-textured graphite electrodes, and textured, carbon-coated copper electrodes are evaluated. MDC and TWT efficiency levels for tubes fabricated with the three materials are measured. I.F.

A87-20667*# National Aeronautics and Space Administration. Lewis Research Center, Cleveland, Ohio.

IMPROVEMENTS IN MDC AND TWT OVERALL EFFICIENCY THROUGH THE APPLICATION OF CARBON ELECTRODE SURFACES

PETER RAMINS and BEN T. EBIHARA (NASA, Lewis Research Center, Cleveland, OH) IEEE Transactions on Electron Devices (ISSN 0018-9383), vol. ED-33, Nov. 1986, pt. 2, p. 1915-1924. refs

The effects of secondary electron emission losses on TWT efficiency are investigated and techniques for minimizing these losses are described. The TWT-multistage depressed collector performance was optimized and measured over a wide range of operating conditions using geometrically identical collectors that utilized copper, pyrolytic graphite, and isotropic graphite electrodes. The data reveal that carbon rather than copper electrodes improve the TWT efficiency, and the ion-textured graphite is most effective in minimizing the secondary electron emission losses. It is noted that degradation of the collector efficiency can be limited to a small percentage with the proper MDC design and the use of low secondary electron yield carbon electrode surfaces. I.F.

A87-23680* National Aeronautics and Space Administration. Lewis Research Center, Cleveland, Ohio.

ANALYSIS OF OPTICALLY CONTROLLED MICROWAVE/MILLIMETER-WAVE DEVICE STRUCTURES

RAINEE N. SIMONS and KUL B. BHASIN (NASA, Lewis Research Center, Cleveland, OH) IEEE Transactions on Microwave Theory and Techniques (ISSN 0018-9480), vol. MTT-34, Dec. 1986, p. 1349-1355. Previously announced in STAR as N86-24907. refs

The light-induced voltage and the change in the source-to-drain channel current under optical illumination higher than the semiconductor bandgap for GaAs MESFET, InP MESFET, Al_{0.3}Ga_{0.7}As/GaAs high electron mobility transistor (HEMT) and GaAs permeable base transistor (PBT) were analytically obtained. The GaAs PBT and GaAs MESFET have much higher sensitivity than InP MESFET. The Al_{0.3}Ga_{0.7}As/GaAs HEMT is observed to have the highest sensitivity. Variation in device parasitics due to optical illumination and its effect on the cutoff frequencies $f_{sub T}$ and $f_{sub max}$ are also investigated. Author

A87-23745* Illinois Univ., Urbana.

MICROWAVE PERFORMANCE OF A QUARTER-MICROMETER GATE LOW-NOISE PSEUDOMORPHIC INGAAS/ALGAAS MODULATION-DOPED FIELD EFFECT TRANSISTOR

T. HENDERSON, M. I. AKSUN, C. K. PENG, HADIS MORKOC (Illinois, University, Urbana), P. C. CHAO (GE Electronics Laboratory, Syracuse, NY) et al. IEEE Electron Device Letters (ISSN 0741-3106), vol. EDL-7, Dec. 1986, p. 649-651. USAF-supported research. refs (Contract NAG3-163)

Excellent dc and millimeter-wave performance is reported in In_{0.15}Ga_{0.85}As/Al_{0.15}Ga_{0.85}As pseudomorphic modulation-doped field effect transistors (MODFET's) with 0.25-micron-length gates. Extrinsic transconductances as high as 495 mS/mm at 300 K and unprecedented power performance in the 60-GHz range were observed. Although not yet optimized, excellent low noise characteristics, 0.9 dB, with an associated gain of 10.4 dB at 18 GHz, and a noise figure of 2.4 dB with an associated gain of 4.4 dB at 62 GHz were obtained. This is the best noise performance ever reported for a MODFET in this frequency range. These results clearly demonstrate the superiority of pseudomorphic MODFET structures in high-frequency applications. Author

A87-23922* Illinois Univ., Urbana.

CHARACTERIZATION OF INGAAS/ALGAAS PSEUDOMORPHIC MODULATION-DOPED FIELD-EFFECT TRANSISTORS

ANDREW A. KETTERSON, WILLIAM T. MASSELINK, JON S. GEDYMIN, JOHN KLEM, CHIN-KUN PENG (Illinois, University, Urbana) et al. IEEE Transactions on Electron Devices (ISSN 0018-9383), vol. ED-33, May 1986, p. 564-571. USAF-supported research. refs (Contract NAG3-613)

High-performance pseudomorphic In_y(Ga)_(1-y)As/Al_{0.15}Ga_{0.85}As $y = 0.05-0.2$ MODFET's grown by MBE have been characterized at dc (300 and 77 K) and RF frequencies. Transconductances as high as 310 and 380 mS/mm and drain currents as high as 290 and 310 mA/mm were obtained at 300 and 77 K, respectively, for 1-micron gate lengths and 3-micron source-drain spacing devices. Lack of persistent trapping effects, I-V collapse, and threshold voltage shifts observed with these devices are attributed to the use of low mole fraction Al_xGa_(1-x)As while still maintaining two-dimensional electron gas concentrations of about 1.3×10^{12} to the 12×10^{12} per sq cm. Detailed microwave S-parameter measurements indicate a current gain cut-off frequency of 24.5 GHz when $y = 0.20$, which is as much as 100 percent better than similar GaAs/AlGaAs MODFET structures, and a maximum frequency of oscillation of 40 GHz. Author

A87-23953* TRW, Inc., Redondo Beach, Calif.

A 30-GHZ MONOLITHIC RECEIVER

LOUIS C. T. LIU (TRW, Inc., Redondo Beach, CA), CAROL S. LIU, JOEL R. KESSLER, SHING-KUO WANG, and CHING-DER CHANG (Hughes Aircraft Co., Microwave Products Div., Torrance, CA) IEEE Transactions on Electron Devices (ISSN 0018-9383), vol. ED-33, Dec. 1986, p. 2079-2083. refs (Contract NAS3-23357)

Several monolithic integrated circuits have been developed to make a 30-GHz receiver. The receiver components include a low-noise amplifier (LNA), an IF amplifier, a mixer, and a phase shifter. The LNA has a 7-dB noise figure with over 17 dB of associated gain. The IF amplifier has a 13-dB gain with a 30-dB control range. The mixer has a conversion loss of 10.5 dB. The phase shifter has a 180-deg phase shift control and a minimum insertion loss of 1.6 dB. Author

A87-30199*# National Aeronautics and Space Administration. Lewis Research Center, Cleveland, Ohio.

TWT EFFICIENCY IMPROVEMENT BY A LOW-COST TECHNIQUE FOR DEPOSITION OF CARBON ON MDC ELECTRODES

BEN T. EBIHARA, PETER RAMINS (NASA, Lewis Research Center, Cleveland, OH), and SHELLY PEET (Case Western Reserve University, Cleveland, OH) IEEE Transactions on Electron Devices (ISSN 0018-9383), vol. ED-34, Feb. 1987, p. 490-493. refs

A simple method of improving the TWT and multistage depressed collector (MDC) efficiency has been demonstrated. The efficiency improvement was produced by the application of a thin layer of carbon to the copper electrodes of the MDC by means of a rapid low-cost technique involving the pyrolysis of hydrocarbon oil in electric arc discharges. Experimental results with a representative TWT and MDC showed an 11 percent improvement in both the TWT and MDC efficiencies as compared to those of the same TWT and MDC with machined copper electrode surfaces. An extended test with a 550-W CW TWT indicated good durability of the carbon-coated electrode surfaces. Author

A87-34525* Honeywell, Inc., Bloomington, Minn.

30 GHZ MONOLITHIC BALANCED MIXERS USING AN ION-IMPLANTED FET-COMPATIBLE 3-INCH GAAS WAFER PROCESS TECHNOLOGY

P. BAUHAHN, A. CONTOLATIS, V. SOKOLOV, and C. CHAO (Honeywell Physical Sciences Center, Bloomington, MN) IEEE, Microwave and Millimeter Wave Monolithic Circuits Symposium, Baltimore, MD, June 4, 5, 1986, Paper. 5 p. (Contract NAS3-23356)

An all ion-implanted Schottky barrier mixer diode which has a cutoff frequency greater than 1000 GHz has been developed. This new device is planar and FET-compatible and employs a projection lithography 3-inch wafer process. A Ka-band monolithic balanced mixer based on this device has been designed, fabricated and tested. A conversion loss of 8 dB has been measured with a LO drive of 10 dBm at 30 GHz. Author

A87-40926* Georgia Inst. of Tech., Atlanta.

MEASUREMENT TECHNIQUES FOR MILLIMETER WAVE SUBSTRATE MOUNTED MMW ANTENNAS

M. A. GOUKER, D. P. CAMPBELL, and J. J. GALLAGHER (Georgia Institute of Technology, Atlanta) Millimeter Wave/Microwave Measurements and Standards for Miniaturized Systems, Huntsville, AL, Nov. 6, 7, 1986, Paper. 6 p. refs (Contract NAG3-282)

An overview of measurement techniques for millimeter wave substrate mounted antennas is presented. Scattering and pickup of the millimeter wave radiation on the low frequency leads is a significant problem in these measurements. Methods to reduce these effects are discussed, and preliminary work on dipole antennas at 230 GHz is presented. Author

A87-41089* Howard Univ., Washington, D. C.
OBSERVATION OF DEEP LEVELS IN CUBIC SILICON CARBIDE

PEIZHEN ZHOU, M. G. SPENCER, G. L. HARRIS, and KONJIT FEKADE (Howard University, Washington, DC) Applied Physics Letters (ISSN 0003-6951), vol. 50, May 11, 1987, p. 1384, 1385. refs
 (Contract NAG3-431)

A deep level transient spectroscopy (DLTS) study on n-type epitaxial cubic silicon carbide grown on Si substrates has been performed. The results of this study indicate the presence of at least two majority-carrier traps. One trap is located 0.34 eV from the conduction-band edge; and the other trap is located 0.68 eV from the conduction-band edge. These two traps have concentrations of approximately 1×10^{15} the 15th/cm. The DLTS spectrum has been investigated as a function of the surface treatment of the SiC. The results of this investigation indicate that one of the levels (SCE2) appears to be formed as a result of high temperature thermal oxidation. Author

A87-41103*# National Aeronautics and Space Administration. Lewis Research Center, Cleveland, Ohio.

RESISTOJET CONTROL AND POWER FOR HIGH FREQUENCY AC BUSES

ROBERT P. GRUBER (NASA, Lewis Research Center, Cleveland, OH) AIAA, DGLR, and JSASS, International Electric Propulsion Conference, 19th, Colorado Springs, CO, May 11-13, 1987. 34 p. Previously announced in STAR as N87-20477. refs
 (AIAA PAPER 87-0994)

Resistojets are operational on many geosynchronous communication satellites which all use dc power buses. Multipropellant resistojets were selected for the Initial Operating Capability (IOC) Space Station which will supply 208 V, 20 kHz power. This paper discusses resistojets heater temperature controllers and passive power regulation methods for ac power systems. A simple passive power regulation method suitable for use with regulated sinusoidal or square wave power was designed and tested using the Space Station multipropellant resistojets. The breadboard delivered 20 kHz power to the resistojets heater. Cold start surge current limiting, a power efficiency of 95 percent, and power regulation of better than 2 percent were demonstrated with a two component, 500 W breadboard power controller having a mass of 0.6 kg. Author

A87-41609*# Systems Science and Software, La Jolla, Calif.
THEORY OF PLASMA CONTACTORS FOR ELECTRODYNAMIC TETHERED SATELLITE SYSTEMS

D. E. PARKS and I. KATZ (Systems, Science and Software, La Jolla, CA) Journal of Spacecraft and Rockets (ISSN 0022-4650), vol. 24, May-June 1987, p. 245-249. Previously announced in STAR as N86-28430. refs
 (Contract NAS3-23881)

Recent data from ground and space experiments indicate that plasma releases from an object dramatically reduce the sheath impedance between the object and the ambient plasma surrounding it. Available data is in qualitative accord with the theory developed to quantify the flow of current in the sheath. Electron transport in the theory is based on a fluid model of a collisionless plasma with an effective collision frequency comparable to frequencies of plasma oscillations. The theory leads to low effective impedances varying inversely with the square root of the injected plasma density. To support such a low impedance mode of operation using an argon plasma source, for example, requires that only one argon ion be injected for each thirty electrons extracted from the ambient plasma. The required plasma flow rates are quite low; to extract one ampere of electron current requires a mass flow rate of about one gram of argon per day. Author

A87-41610*# Massachusetts Inst. of Tech., Cambridge.
THEORY OF PLASMA CONTACTORS USED IN THE IONOSPHERE

D. E. HASTINGS (MIT, Cambridge, MA) Journal of Spacecraft and Rockets (ISSN 0022-4650), vol. 24, May-June 1987, p. 250-256. refs
 (Contract NAS3-24649)

The use of plasma contactors has been proposed as a means of enhancing the current flow through an electrodynamic tether. A simple isothermal spherical model of the plasma cloud around a contactor is outlined for a plasma contactor which is biased positively with respect to the ambient plasma and hence collects electrons. It is shown that for significant current amplification to occur, the plasma cloud must be turbulent. The amount of current amplification is obtained as a function of the ion current through the contactor. For ion currents of several amperes amplification factors of 2-6 can be obtained for potential drops in the range 100-500 V. For smaller ion currents, much larger amplification factors can be obtained. Author

A87-41638* Illinois Univ., Urbana.
NEW SIMPLE FEED NETWORK FOR AN ARRAY MODULE OF FOUR MICROSTRIP ELEMENTS

M. L. OBERHART, Y. T. LO (Illinois, University, Urbana), and R. Q. H. LEE (NASA, Lewis Research Center, Cleveland, OH) Electronics Letters (ISSN 0013-5194), vol. 23, April 23, 1987, p. 436, 437. NASA-supported research.

A simple microstripline feed network for an array module comprising four microstrip elements is described. The advantages and disadvantages of the network are discussed as well as a theoretical explanation for the radiation characteristics of array modules using the network. Author

A87-42681* National Aeronautics and Space Administration. Lewis Research Center, Cleveland, Ohio.

ULTRA SMALL ELECTRON BEAM AMPLIFIERS

J. A. DAYTON, JR. (NASA, Lewis Research Center, Cleveland, OH) and H. G. KOSMAHL (Analex Corp., Cleveland, OH) IN: International Electron Devices Meeting, Los Angeles, CA, Dec. 7-10, 1986, Proceedings. New York, Institute of Electrical and Electronics Engineers, 1986, p. 780-783. refs

Data on field emission and microfabrication technologies relevant to the development of low-power electron-beam amplifiers and oscillators are discussed. The fabrication of a thin-film field-emission (TFE) cathode for a 1-W electron-beam amplifier is examined. Some TFE cathodes have been developed and tested in electron guns. Recent experimental results reveal that a beam can be formed from the field-emission cathode, and the TFE cathode is applicable for devices operating below 3 kV at currents of less than 20 mA. The use of microfabrication techniques to construct slow-wave circuits is studied, and the use of finned structures as the slow-wave circuit for an electron-beam oscillator or amplifier is proposed. I.F.

A87-45511* Watkins-Johnson Co., Palo Alto, Calif.
A 20 GHZ, HIGH EFFICIENCY DUAL MODE TWT FOR THE ACTS PROGRAM

FRANK MUENNEMANN, LOUIS DOMBRO, and JIN LONG (Watkins-Johnson Co., Palo Alto, CA) IN: GLOBECOM '86 - Global Telecommunications Conference, Houston, TX, Dec. 1-4, 1986, Conference Record. Volume 1. New York, Institute of Electrical and Electronics Engineers, Inc., 1986, p. 574-577. Sponsorship: Research supported by TRW, Inc.
 (Contract NAS3-23790)

The development of a 50 W/10 W dual mode K-band downlink TWT is examined, and its performance is evaluated. The designs of the electron gun, RF circuit, and collector for the TWT, which is enclosed in a capsule, are described. It is observed that the high power mode (HPM) power output is at 50 GHz and the low power mode (LPM) output is at 12 GHz; the saturated gain is 52.5 dB for HPM and 3 dB for LPM; the AM-PM is 4.2 dB; the HPM dc power output is 104 W; and the LPM dc output is 42 W;

and the efficiency is 45 percent for the HPM and 28.6 percent for the LPM. I.F.

A87-45899*# Georgia Inst. of Tech., Atlanta.
MEASUREMENT TECHNIQUES FOR MILLIMETER WAVE SUBSTRATE MOUNTED MMW ANTENNAS

M. A. GOUKER, D. P. CAMPBELL, and J. J. GALLAGHER (Georgia Institute of Technology, Atlanta) Conference on Millimeter Wave/Microwave Measurements and Standards for Miniaturized Systems, Huntsville, AL, Nov. 6, 7, 1986, Paper. 7 p. refs (Contract NAG3-282)

An overview of measurement techniques for millimeter wave substrate mounted antennas is presented. Scattering and pickup of the millimeter wave radiation on the low frequency leads is a significant problem in these measurements. Methods to reduce these effects are discussed, and preliminary work on dipole antennas at 230 GHz is presented. Author

A87-47621* IBM Federal Systems Div., Gaithersburg, Md.
MICROSTRIP DISPERSION INCLUDING ANISOTROPIC SUBSTRATES

BRIAN E. KRETCH (IBM Corp., Federal Systems Div., Gaithersburg, MD) and ROBERT E. COLLIN (Case Western Reserve University, Cleveland, OH) IEEE Transactions on Microwave Theory and Techniques (ISSN 0018-9480), vol. MTT-35, Aug. 1987, p. 710-718. refs (Contract NCC3-29)

A perturbation-iteration solution based on potential theory is developed for determining the effective dielectric constant, characteristic impedance, and current-charge distribution on a microstrip transmission line with isotropic and anisotropic substrates. The numerical implementation of the theory is described and is suitable for use on a personal computer. Computed data for several common substrate materials are included. Author

A87-50047* Spire Corp., Bedford, Mass.
INDIUM PHOSPHIDE SHALLOW HOMOJUNCTION SOLAR CELLS MADE BY METALORGANIC CHEMICAL VAPOR DEPOSITION

M. B. SPITZER, C. J. KEAVNEY, S. M. VERNON, and V. E. HAVEN (Spire Corp., Bedford, MA) Applied Physics Letters (ISSN 0003-6951), vol. 51, Aug. 3, 1987, p. 364-366. refs (Contract NAS3-24857)

The fabrication of highly efficient indium phosphide solar cells by metalorganic chemical vapor deposition is reported. Since InP can be annealed at temperatures as low as approximately 100 C and the annealing occurs under solar illumination itself, this accomplishment is relevant to space power systems. A total area air mass zero efficiency of 17.9 percent and an air mass 1.5 efficiency of 20.4 percent are reported. Electrical characterization identifying loss mechanisms is made, and a shallow homojunction design is discussed along with possible improvements. C.D.

N87-10232*# National Aeronautics and Space Administration.
Lewis Research Center, Cleveland, Ohio.

OPTICALLY CONTROLLED GAAS DUAL-GATE MESFET AND PERMEABLE BASE TRANSISTORS

R. N. SIMONS and K. B. BHASIN 1986 7 p Presented at the Conference on Lasers and Electro-Optics (CLEO), San Francisco, Calif., 9-13 Jun. 1986; sponsored by IEEE and Optical Society of America (NASA-TM-88823; E-3183-1; NAS 1.15:88823) Avail: NTIS HC A02/MF A01 CSCL 09A

Optically induced voltage and dc characteristics of the GaAs Dual-gate MESFET and the Permeable Base Transistor (PBT) with optical illumination at wavelength below 0.87 microns were obtained and compared with GaAs MESFET. It was observed that PBT can handle higher current density when illuminated. Author

N87-10237*# Watkins-Johnson Co., Palo Alto, Calif.
DESIGN, CONSTRUCTION AND LONG LIFE ENDURANCE TESTING OF CATHODE ASSEMBLIES FOR USE IN MICROWAVE HIGH-POWER TRANSMITTING TUBES Final Report

R. BATRA and D. MARINO Sep. 1986 99 p (Contract NAS3-23346) (NASA-CR-175116; NAS 1.26:175116) Avail: NTIS HC A05/MF A01 CSCL 09A

The cathode life test program sponsored by NASA Lewis Research Center at Watkins-Johnson Company has been in continuous operation since 1972. Its primary objective has been to evaluate the long life capability of barium dispenser cathodes to produce emission current densities of 2 A sq. cm. or more in an operational environment simulating that of a highpower microwave tube. The life test vehicles were equipped with convergent flow electron guns, drift space tubes with solenoid magnets for electron beam confinement and water-cooled depressed collectors. A variety of cathode types has been tested, including GE Tungstate, Litton Impregnated, Philips Type B and M, Semicon types S and M, and Spectra-Mat Type M. Recent emphasis has been on monitoring the performance of Philips Type M cathodes at 2 A sq. cm. and Spectra-Mat and Semicon Type M cathodes at 4 A sq. cm. These cathodes have been operated at a constant current of 616 mA and a cathode anode voltage on the order of 10 kV. Cathode temperatures were maintained at 1010 C true as measured from black body holes in the backs of the cathodes. This report presents results of the cathode life test program from July 1982 through April 1986. The results include hours of operation and performance data in the form of normalized emission current density versus temperature curves (Miram plots). NASA

N87-11073*# National Aeronautics and Space Administration.
Lewis Research Center, Cleveland, Ohio.

NASA LEWIS EVALUATION OF REGENERATIVE FUEL CELL (RFC) SYSTEMS

N. H. HAGEDORN, O. D. GONZALEZ-SANABRIA, and L. L. KOHOUT /n NASA. Goddard Space Flight Center The 1985 Goddard Space Flight Center Battery Workshop (date) p 13-18 Sep. 1986

Avail: NTIS HC A19/MF A01 CSCL 10C

Evaluation of two regenerative fuel cell (RFC) systems was begun in-house, and under contracts and grants. The passive hydrogen-oxygen RFC offers the possibility of a high-energy density, long-life storage system for geosynchronous Earth orbit missions. The hydrogen-bromine RFC offers the combination of high efficiency and moderate energy density that could ideally suit low Earth orbit missions if successfully developed. Either or both of these systems would be attractive additions to the storage options available to designers of future missions. B.G.

N87-11086*# National Aeronautics and Space Administration.
Lewis Research Center, Cleveland, Ohio.

A FLOODED-STARVED DESIGN FOR NICKEL-CADMIUM CELLS

L. H. THALLER /n NASA. Goddard Space Flight Center The 1985 Goddard Space Flight Center Battery Workshop (date) p 177 - 184 Sep. 1986

Avail: NTIS HC A19/MF A01 CSCL 10C

A somewhat analogous situation among groupings of alkaline fuel cells is described where the stochastic aspects were much more accurately documented and then it was illustrated how this problem was eliminated using straight forward principles of pore size engineering. This is followed by a suggested method of adapting these same design principles to nickel-cadmium cells. It must be kept in mind that when cells are cycled to typically twenty percent depth of discharge that eighty percent of the weight of the cell is simply dead weight. Some of this dead weight might be put to better use by trading it for a scheme that would increase the time during which the cell would be working more closely to its optimum set of operating parameters. Author

N87-11104*# Texas Instruments, Inc., Dallas. Central Research Labs.

THE 20 GHZ GAAS MONOLITHIC POWER AMPLIFIER MODULE DEVELOPMENT Annual Report, 18 May 1983 - 17 May 1984

7 Jun. 1984 66 p

(Contract NAS3-23781)

(NASA-CR-174742; NAS 1.26:174742) Avail: NTIS HC A04/MF A01 CSCL 09A

The development of a 20 GHz GaAs FET monolithic power amplifier module for advanced communication applications is described. Four-way power combing of four 0.6 W amplifier modules is used as the baseline approach. For this purpose, a monolithic four-way traveling-wave power divider/combiner was developed. Over a 20 GHz bandwidth (10 to 30 GHz), an insertion loss of no more than 1.2 dB was measured for a pair of back-to-back connected divider/combiners. Isolation between output ports is better than 20 dB, and VSWRs are better than 21:1. A distributed amplifier with six 300 micron gate width FETs and gate and drain transmission line tapers has been designed, fabricated, and evaluated for use as an 0.6 W module. This amplifier has achieved state-of-the-art results of 0.5 W output power with at least 4 dB gain across the entire 2 to 21 GHz frequency range. An output power of 2 W was achieved at a measurement frequency of 18 GHz when four distributed amplifiers were power-combined using a pair of traveling-wave divider/combiners. Another approach is the direct common-source cascading of three power FET stages. An output power of up to 2W with 12 dB gain and 20% power-added efficiency has been achieved with this approach (at 17 GHz). The linear gain was 14 dB at 1 W output. The first two stages of the three-stage amplifier have achieved an output power of 1.6 W with 9 dB gain and 26% power-added efficiency at 16 GHz.

Author

N87-13637*# National Aeronautics and Space Administration. Lewis Research Center, Cleveland, Ohio.

LOSS-COMPENSATION OF INTENSITY-MODULATING FIBER-OPTIC SENSORS

G. BEHEIM and D. J. ANTHAN (Cleveland State Univ., Ohio) 1986 11 p Presented at Fiber-Optic and Laser Sensors 4, Cambridge, Mass., 21-26 Sep. 1986; sponsored by the Society of Photo-Optical Instrumentation Engineers

(NASA-TM-88825; E-3198; NAS 1.15:88825) Avail: NTIS HC A02/MF A01 CSCL 46C

This report describes a new type of intensity-modulating fiber-optic sensor which has high immunity to the effects of variations in the losses of the fiber-link. A variable-splitting-ratio transducer is used to differentially modulate the intensities of the light which it transmits and reflects. Using a four-fiber optical link, light is impinged onto the transducer from either direction, and, in each case, the transmitted and reflected signals are measured. These four signals are then processed to remove the effects of the fiber and connector losses. Loss-compensated sensors of angular position and displacement are described, and their outputs are shown to be highly stable despite considerable variations in the transmissivities of the fiber-link components.

Author

N87-14597*# National Aeronautics and Space Administration. Lewis Research Center, Cleveland, Ohio.

SWEPT FREQUENCY TECHNIQUE FOR DISPERSION MEASUREMENT OF MICROSTRIP LINES

R. Q. LEE 1986 16 p Presented at the 1986 Antenna Applications Symposium, Monticello, Ill., 17-19 Sep. 1986; sponsored by Illinois Univ. and RADC

(NASA-TM-88836; E-3215; NAS 1.15:88836) Avail: NTIS HC A02/MF A01 CSCL 09C

Microstrip lines used in microwave integrated circuits are dispersive. Because a microstrip line is an open structure, the dispersion can not be derived with pure TEM, TE, or TM mode analysis. Dispersion analysis has commonly been done using a spectral domain approach, and dispersion measurement has been made with high Q microstrip ring resonators. Since the dispersion of a microstrip line is fully characterized by the frequency dependent phase velocity of the line, dispersion measurement of microstrip

lines requires the measurement of the line wavelength as a function of frequency. In this paper, a swept frequency technique for dispersion measurement is described. The measurement was made using an automatic network analyzer with the microstrip line terminated in a short circuit. Experimental data for two microstrip lines on 10 and 30 mil Cuflon substrates were recorded over a frequency range of 2 to 20 GHz. Agreement with theoretical results computed by the spectral domain approach is good. Possible sources of error for the discrepancy are discussed.

Author

N87-16968*# National Aeronautics and Space Administration. Lewis Research Center, Cleveland, Ohio.

ABSOLUTE GAIN MEASUREMENT BY THE IMAGE METHOD UNDER MISMATCHED CONDITION

RICHARD Q. LEE and MAURICE F. BADDOUR 1987 6 p Presented at the International AP-S Symposium, Blacksburg, Va., 15-19 Jun. 1987; sponsored by IEEE

(NASA-TM-88924; E-3359; NAS 1.15:88924) Avail: NTIS HC A02/MF A01 CSCL 09C

Purcell's image method for measuring the absolute gain of an antenna is particularly attractive for small test antennas. The method is simple to use and utilizes only one antenna with a reflecting plane to provide an image for the receiving antenna. However, the method provides accurate results only if the antenna is matched to its waveguide. In this paper, a waveguide junction analysis is developed to determine the gain of an antenna under mismatched condition. Absolute gain measurements for two standard gain horn antennas have been carried out. Experimental results agree closely with published data.

Author

N87-16971*# Colby Coll., Waterville, Maine. Dept. of Physics and Astronomy.

LEO HIGH VOLTAGE SOLAR ARRAY ARCING RESPONSE MODEL Interim Report, Feb. 1987

ROGER N. METZ Feb. 1987 32 p

(Contract NAG3-576)

(NASA-CR-180073; NAS 1.26:180073) Avail: NTIS HC A03/MF A01 CSCL 09A

A series of mathematical models were developed that describe the electrical behavior of a large solar cell array floating electrically in the low Earth orbit (LEO) space plasma and struck by an arc at a point of negative bias. There are now three models in this series: ARCI, which is a fully analytical, linearized model; ARCI, which is an extension of ARCI that includes solar cell inductance as well as load reactance; Nonlinear ARC, which is a numerical model able to treat effects such as non-linearized, i.e., logarithmic solar cell I/V characteristics, conductance switching as a solar cell crosses plasma ground on a voltage excursion and non-ohmic plasma leakage current collection.

Author

N87-16972*# TRW Electronic Systems Group, Redondo Beach, Calif.

THE 20 GHZ POWER GAAS FET DEVELOPMENT Final Report

M. CRANDELL Sep. 1986 52 p

(Contract NAS3-22503)

(NASA-CR-179546; NAS 1.26:179546; S/N-36778) Avail: NTIS HC A04/MF A01 CSCL 09A

The development of power Field Effect Transistors (FET) operating in the 20 GHz frequency band is described. The major efforts include GaAs FET device development (both 1 W and 2 W devices), and the development of an amplifier module using these devices.

Author

N87-17989*# TRW Electronic Systems Group, Redondo Beach, Calif.

THE 20 GHZ SPACECRAFT IMPATT SOLID STATE TRANSMITTER Final Report

T. BEST and Y. C. NGAN Sep. 1986 78 p

(Contract NAS3-22492)

(NASA-CR-179545; NAS 1.26:179545; S/N-36779) Avail: NTIS HC A05/MF A01 CSCL 09A

The engineering development of a solid-state transmitter amplifier operating in the 20-GHz frequency range is described.

This effort involved a multitude of disciplines including IMPATT device development, circulator design, multiple-diode circuit design, and amplifier integration and test. The objective was to develop a transmitter amplifier demonstrating the feasibility of providing an efficient, reliable, lightweight solid-state transmitter to be flown on a 30 to 20 GHz communication demonstration satellite. The work was done under contract from NASA/Lewis Research Center for a period of three years. The result was the development of a GaAs IMPATT diode amplifier capable of an 11-W CW output power and a 2-dB bandwidth of 300 MHz. GaAs IMPATT diodes incorporating diamond heatsink and double-Read doping profile capable of 5.3-W CW oscillator output power and 15.5% efficiency were developed. Up to 19% efficiency was also observed for an output power level of 4.4 W. High performance circulators with a 0.2 dB inserting loss and bandwidth of 5 GHz have also been developed. These represent a significant advance in both device and power combiner circuit technologies in K-band frequencies.

Author

N87-17990*# National Aeronautics and Space Administration. Lewis Research Center, Cleveland, Ohio.

PERFORMANCE OF TEXTURED CARBON ON COPPER ELECTRODE MULTISTAGE DEPRESSED COLLECTORS WITH MEDIUM-POWER TRAVELING WAVE TUBES

PETER RAMINS and ARTHUR N. CURREN Nov. 1986 12 p (NASA-TP-2665; E-3143; NAS 1.60:2665) Avail: NTIS HC A02/MF A01 CSCL 09A

Performance of multistage depressed collectors (MDCs) using textured carbon on copper substrate electrode surfaces was evaluated in conjunction with medium-power traveling wave tubes (TWTs). The MDC and TWT overall efficiencies for these electrodes were measured and compared with those obtained with the same TWT and a copper electrode MDC of identical design. Long-term stability of the carbon-coated copper electrode surfaces was investigated by periodic evaluation of TWT-MDC performance over an extended period of continuous wave (CW) operation. Application of textured carbon coating on copper MDC electrode surfaces produced a 13% improvement in both MDC and TWT overall efficiencies for the TWT-MDC tests. During 1600 hr of CW operation with a medium power TWT, no significant changes in MDC performance were noted. This indicated good stability of the textured carbon electrode surfaces. This stability was confirmed by scanning electron microscope examinations of the electrode surfaces before assembly of the MDC and after completion of the test program.

Author

N87-17991*# National Aeronautics and Space Administration. Lewis Research Center, Cleveland, Ohio.

CALCULATION OF SECONDARY ELECTRON TRAJECTORIES IN MULTISTAGE DEPRESSED COLLECTORS FOR MICROWAVE AMPLIFIERS

DALE A. FORCE Nov. 1986 7 p (NASA-TP-2664; E-3196; NAS 1.60:2664) Avail: NTIS HC A02/MF A01 CSCL 09A

Computational procedures are reported for treating power losses due to secondary electrons in multistage depressed collectors (MDC) for traveling wave tubes (TWT) and other O-type electron tubes. The MDC is modeled with an advanced, multidimensional computer program. Representative beams of secondary electrons are then injected at the points of impact of the primary beams. Separate programs are used to calculate representative beams of high-energy primary electron beams and of low-energy true secondaries. The recomputation of the MDC model including the true secondary beam allows determination of the secondary emission losses, and, if necessary, redesign of the MDC to improve performance. Recomputation of the MDC model including the primary beams is used to check on possible backstreaming from the MDC to the RF interaction structure of the tube. A comparison with experimentally measured values of TWT and MDC efficiencies is made.

Author

N87-17993*# National Aeronautics and Space Administration. Lewis Research Center, Cleveland, Ohio.

MICROWAVE PERFORMANCE OF AN OPTICALLY CONTROLLED ALGAS/GAAS HIGH ELECTRON MOBILITY TRANSISTOR AND GAAS MESFET

RAINEE N. SIMONS and KUL. B. BHASIN 1987 12 p Prepared for presentation at the IEEE MTT-S International Microwave Symposium and Exhibition, Las Vegas, Nev., 9-11 Jun. 1987 (NASA-TM-88980; E-3333; NAS 1.15:88980) Avail: NTIS HC A02/MF A01 CSCL 09A

Direct current and also the microwave characteristics of optically illuminated AlGaAs/GaAs HEMT are experimentally measured for the first time and compared with that of GaAs MESFET. The results showed that the average increase in the gain is 2.89 dB under 1.7 nW/sq cm optical intensity at 0.83 microns. Further, the effect of illumination on S-parameters is more pronounced when the devices are biased close to pinch off. Novel applications of optically illuminated HEMT as a variable gain amplifier, high speed high frequency photo detector, and mixer are demonstrated.

Author

N87-20467*# Ford Aerospace and Communications Corp., Palo Alto, Calif.

SATELLITE ANALOG FDMA/FM TO DIGITAL TDMA CONVERSION Final Report, May - Dec. 1986

T. DRIGGERS, T. NGUYEN, and V. KOLAVENNU Apr. 1987 72 p (Contract NAS3-24890) (NASA-CR-179605; NAS 1.26:179605; WDL-TR11068) Avail: NTIS HC A04/MF A01 CSCL 09C

The results of a study which investigated design issues regarding the use of analog to digital (A/D) conversion on board a satellite are presented. The need for A/D, and of course D/A as well, conversion arose from a satellite design which required analog FDMA/FM up and down links to/from a digitally modulated intersatellite link. There are also some advantages when one must interconnect a large number of various spot beams which are using analog, and therefore cannot take advantage of SS/TDMA switching among the beams, thus resulting in low fill factors. Various tradeoffs were performed regarding the implementation of on-board A/D processing, including mass, power, and costs. The various technologies which were considered included flash ADCs, surface acoustic wave (SAW) devices, and digital signal processing (DSP) chips. Impact analyses were also performed to determine the effect on ground stations to convert to digital if the A/D approach were not implemented.

Author

N87-20468*# National Aeronautics and Space Administration. Lewis Research Center, Cleveland, Ohio.

SYSTEM ARCHITECTURE OF MMIC-BASED LARGE APERTURE ARRAYS FOR SPACE APPLICATION

P. R. HERCZFELD (Drexel Univ., Philadelphia, Pa.), M. KAM, R. R. KUNATH, K. B. BHASIN, and N. LAPRADE (Drexel Univ.,) Jan. 1987 12 p Presented at the O-E/LASE 87 Optoelectronics and Laser Applications in Science and Engineering, Los Angeles, Calif., 11-17 Jan. 1987; sponsored by the Society of Photo-Optical Instrumentation Engineers (NASA-TM-89840; E-3482; NAS 1.15:89840) Avail: NTIS HC A02/MF A01 CSCL 09C

The persistent trend to use millimeter-wave frequencies for satellite communications presents the challenge to design large-aperture phased arrays for space applications. These arrays, which comprise 100 to 10,000 elements, are now possible due to the advent of lightwave technology and the availability of monolithic microwave integrated circuits. In this paper, system aspects of optically controlled array design are studied. In particular, two architectures for a 40 GHz array are outlined, and the main system-related issues are examined: power budget, synchronization in frequency and phase, and stochastic effects.

Author

N87-20469*# National Aeronautics and Space Administration. Lewis Research Center, Cleveland, Ohio.

PROPAGATION CHARACTERISTICS OF SOME NOVEL COPLANAR WAVEGUIDE TRANSMISSION LINES ON GAAS AT MM-WAVE FREQUENCIES

RAINEE N. SIMONS 1986 16 p Presented at the 1986 Conference on Millimeter Wave/Microwave Measurements and Standards for Miniaturized Systems, Redstone Arsenal, Ala., 6-7 Nov. 1986; sponsored by the Army Missile Command (NASA-TM-89839; E-3335; NAS 1.15:89839) Avail: NTIS HC A02/MF A01 CSCL 09C

Three new Coplanar Waveguide (CPW) transmission lines, namely, Suspended CPW (SCPW), Stripline-like Suspended CPW (SSCPW) and Inverted CPW (ICPW), are proposed and also analyzed for their propagation characteristics. The substrate thickness, permittivity and dimensions of housing are assumed to be arbitrary. These structures have the following advantages over conventional CPW. Firstly, the ratio of guide wavelength to free space wavelength is closer to unity which results in larger dimensions and hence lower tolerances. Secondly, the effective dielectric constant is lower and hence the electromagnetic field energies are concentrated more in the air regions which should reduce attenuation. Thirdly, for a prescribed impedance level, the above structures have a wider slot width for identical strip width. Thus, low impedance lines can be achieved with reasonable slot dimensions. Fourthly, in an inverted CPW shunt mounting of active devices, such as Gunn and IMPATT diodes, between the strip and the metal trough is possible. This feature further enhances the attractiveness of the above structures. Lastly, an E-plane probe type transition from a rectangular waveguide to suspended CPW can also be easily realized. The computed results for GaAs at Ka-band illustrate the variation of normalized guide wavelength, effective dielectric constant and the characteristic impedance as a function of the: (1) frequency; (2) distance of separation between the trough side walls; (3) normalized strip and slot widths; and (4) normalized air gap. Author

N87-20474*# National Aeronautics and Space Administration. Lewis Research Center, Cleveland, Ohio.

DESIGN, FABRICATION AND PERFORMANCE OF SMALL, GRAPHITE ELECTRODE, MULTISTAGE DEPRESSED COLLECTORS WITH 200-W, CW, 8- TO 18-GHZ TRAVELING-WAVE TUBES

BEN T. EBIHARA and PETER RAMINS Feb. 1987 22 p (NASA-TP-2693; E-3099; NAS 1.60:2693) Avail: NTIS HC A02/MF A01 CSCL 09A

Small multistage depressed collectors (MDC's) which used pyrolytic graphite, ion-beam-textured pyrolytic graphite, and isotropic graphite electrodes were designed, fabricated, and evaluated in conjunction with 200-W, continuous wave (CW), 8- to 18-GHz traveling-wave tubes (TWT's). The design, construction, and performance of the MDC's are described. The bakeout performance of the collectors, in terms of gas evolution, was indistinguishable from that of typical production tubes with copper collectors. However, preliminary results indicate that some additional radiofrequency (RF) and dc beam processing time (and/or longer or higher temperature bakeouts) may be needed beyond that of typical copper electrode collectors. This is particularly true for pyrolytic graphite electrodes and for TWT's without appendage ion pumps. Extended testing indicated good long-term stability of the textured pyrolytic graphite and isotropic graphite electrode surfaces. The isotropic graphite in particular showed considerable promise as an MDC electrode material because of its high purity, low cost, simple construction, potential for very compact overall size, and relatively low secondary electron emission yield characteristics in the as-machined state. However, considerably more testing experience is required before definitive conclusions on its suitability for electronic countermeasure systems and space TWT's can be made. Author

N87-20475*# National Aeronautics and Space Administration. Lewis Research Center, Cleveland, Ohio.

REFERENCING IN FIBER OPTIC SENSING SYSTEMS

GRIGORY ADAMOVSKY 1987 9 p Proposed for presentation at the Technical Symposium of Optics, Electro-Optics and Sensors, Orlando, Fla., 17-22 May 1987; sponsored by the Society of Photo-Optical Instrumentation Engineers (NASA-TM-89822; E-3468; NAS 1.15:89822) Avail: NTIS HC A02/MF A01 CSCL 20F

Different techniques to account for losses induced by the environment on signals in intensity modulation fiber optic sensing systems are described and analyzed. Author

N87-20477*# National Aeronautics and Space Administration. Lewis Research Center, Cleveland, Ohio.

RESISTOJET CONTROL AND POWER FOR HIGH FREQUENCY AC BUSES

ROBERT P. GRUBER 1987 33 p Presented at the 19th International Electric Propulsion Conference, Colorado Springs, Colo., 11-13 May 1987; sponsored by AIAA, DGLR and JSAS (NASA-TM-89860; E-3527; NAS 1.15:89860; AIAA-87-0994) Avail: NTIS HC A03/MF A01 CSCL 09C

Resistojets are operational on many geosynchronous communication satellites which all use dc power buses. Multipropellant resistojets were selected for the Initial Operating Capability (IOC) Space Station which will supply 208 V, 20 kHz power. This paper discusses resistojet heater temperature controllers and passive power regulation methods for ac power systems. A simple passive power regulation method suitable for use with regulated sinusoidal or square wave power was designed and tested using the Space Station multipropellant resistojet. The breadboard delivered 20 kHz power to the resistojet heater. Cold start surge current limiting, a power efficiency of 95 percent, and power regulation of better than 2 percent were demonstrated with a two component, 500 W breadboard power controller having a mass of 0.6 kg. Author

N87-21234* National Aeronautics and Space Administration. Lewis Research Center, Cleveland, Ohio.

PRECISION TUNABLE RESONANT MICROWAVE CAVITY Patent

SHIGEO NAKANISHI, inventor (to NASA), FRANK S. CALCO, inventor (to NASA), and AUGUST R. SCARPELLI, inventor (to NASA) 10 Feb. 1987 5 p Filed 11 Feb. 1985 Supersedes N85-20248 (23 - 11, p 1628) (NASA-CASE-LEW-13935-1; US-PATENT-4,642,523; US-PATENT-APPL-SN-700255; US-PATENT-CLASS-315-111.81; US-PATENT-CLASS-250-423-R) Avail: US Patent and Trademark Office CSCL 09A

A tunable microwave cavity containing ionizable metallic vapor or gases and an apparatus for precisely positioning a microwave coupling tip in the cavity and for precisely adjusting at least one dimension of the cavity are disclosed. With this combined structure, resonance may be achieved with various types of ionizable gases. A coaxial probe extends into a microwave cavity through a tube. One end of the tube is retained in a spherical joint attached in the cavity wall. This allows the coaxial probe to be pivotally rotated. The coaxial probe is slideable within the tube thus allowing the probe to be extended toward or retracted from the center of the cavity. Official Gazette of the U.S. Patent and Trademark Office

N87-21239*# National Aeronautics and Space Administration. Lewis Research Center, Cleveland, Ohio.

TRAVELING-WAVE-TUBE EFFICIENCY IMPROVEMENT BY A LOW-COST TECHNIQUE FOR DEPOSITION OF CARBON ON MULTISTAGE DEPRESSED COLLECTOR

BEN T. EBIHARA, PETER RAMINS, and SHELLY PEET May 1987 14 p (NASA-TP-2719; E-3416; NAS 1.60:2719) Avail: NTIS HC A02/MF A01 CSCL 09A

A simple method of improving the traveling-wave-tube (TWT) and multistage depressed collector (MDC) efficiency has been demonstrated. The efficiency improvement was produced by the

application of a thin layer of carbon to the copper electrodes of the MDC by means of a rapid, low-cost technique involving the pyrolysis of hydrocarbon oil in electric arc discharges. Experimental results with a representative TWT and MDC showed an 11 percent improvement in both the TWT and MDC efficiencies as compared to those of the same TWT and MDC efficiencies with bare copper electrode surfaces. An extended test with a 500-W, continuous wave (CW) TWT and small-sized MDC indicated good stability of the carbon coated electrode surfaces after a relatively small initial degradation in TWT overall and apparent MDC efficiencies.

Author

N87-22097*# National Aeronautics and Space Administration. Lewis Research Center, Cleveland, Ohio.

FULL-SCALE ENGINE DEMONSTRATION OF AN ADVANCED SENSOR FAILURE DETECTION, ISOLATION AND ACCOMMODATION ALGORITHM: PRELIMINARY RESULTS

WALTER C. MERRILL, JOHN C. DELAAT, STEVEN M. KROSZKEWICZ, and MAHMOOD ABDELWAHAB 1987 14 p Proposed for presentation at the Guidance, Navigation and Control Conference, Monterey, Calif., 17-19 Aug. 1987; sponsored by AIAA

(NASA-TM-89880; E-3561; NAS 1.15:89880; AIAA-87-2259)

Avail: NTIS HC A02/MF A01 CSCL 09C

The objective of the advanced detection, isolation, and accommodation (ADIA) program is to improve the overall demonstrated reliability of digital electronic control systems for turbine engines. For this purpose, algorithms were developed which detect, isolate, and accommodate sensor failures using analytical redundancy. Preliminary results of a full scale engine demonstration of the ADIA algorithm are presented. Minimum detectable levels of sensor failures for an F100 turbofan engine control system are determined and compared to those obtained during a previous evaluation of this algorithm using a real-time hybrid computer simulation of the engine.

Author

N87-22098*# National Aeronautics and Space Administration. Lewis Research Center, Cleveland, Ohio.

RADIATION AND TEMPERATURE EFFECTS IN GALLIUM ARSENIDE, INDIUM PHOSPHIDE AND SILICON SOLAR CELLS

I. WEINBERG, C. K. SWARTZ, R. E. HART, JR., and R. L. STATLER (Naval Research Lab., Washington, D. C.) 1987 14 p Presented at the 19th Photovoltaic Specialists Conference, New Orleans, La., 4-8 May 1987; sponsored by IEEE

(NASA-TM-89870; E-3546; NAS 1.15:89870) Avail: NTIS HC

A02/MF A01 CSCL 09C

The effects of radiation on performance are determined for both $n(+)$ p and $p(+)$ n GaAs and InP cells and for silicon $n(+)$ p cells. It is found that the radiation resistance of InP is greater than that of both GaAs and Si under 1 MeV electron irradiation. For silicon, the observed decreased radiation resistance with decreased resistivity is attributed to the presence of a radiation induced boron-oxygen defect. Comparison of radiation damage in both $p(+)$ n and $n(+)$ p GaAs cells yields a decreased radiation resistance for the $n(+)$ p cell attributable to increased series resistance, decreased shunt resistance, and relatively greater losses in the cell's p-region. For InP, the $n(+)$ p configuration is found to have greater radiation resistance than the $p(+)$ n cell. The increased loss in this latter cell is attributed to losses in the cell's emitter region. Temperature dependency results are interpreted using a theoretical relation for dV_{oc}/dT which predicts that increased V_{oc} should result in decreased numerical values for dP_m/dT . The predicted correlation is observed for GaAs but not for InP a result which is attributed to variations in cell processing.

Author

N87-22102*# National Aeronautics and Space Administration. Lewis Research Center, Cleveland, Ohio.

AUTOMATED MEASUREMENT OF THE BIT-ERROR RATE AS A FUNCTION OF SIGNAL-TO-NOISE RATIO FOR MICROWAVE COMMUNICATIONS SYSTEMS

ROBERT J. KERCZEWSKI, ELAINE S. DAUGHERTY, and IHOR KRAMARCHUK 1987 14 p Presented at the 29th Automatic RF Techniques Group Conference, Las Vegas, Nev., 12-13 Jun. 1987; sponsored by IEEE

(NASA-TM-89898; E-3585; NAS 1.15:89898) Avail: NTIS HC

A02/MF A01 CSCL 17B

The performance of microwave systems and components for digital data transmission can be characterized by a plot of the bit-error rate as a function of the signal to noise ratio (or E_{b}/E_{n}). Methods for the efficient automated measurement of bit-error rates and signal-to-noise ratios, developed at NASA Lewis Research Center, are described. Noise measurement considerations and time requirements for measurement accuracy, as well as computer control and data processing methods, are discussed.

Author

N87-22923*# National Aeronautics and Space Administration. Lewis Research Center, Cleveland, Ohio.

REVISED NASA AXIALLY SYMMETRIC RING MODEL FOR COUPLED-CAVITY TRAVELING-WAVE TUBES

JEFFREY D. WILSON Jan. 1987 17 p

(NASA-TP-2675; E-3220; NAS 1.60:2675) Avail: NTIS HC

A02/MF A01 CSCL 09A

A versatile large-signal, two-dimensional computer program is used by NASA to model coupled-cavity travelling-wave tubes (TWTs). In this model, the electron beam is divided into a series of disks, each of which is further divided into axially symmetric rings which can expand and contract. The trajectories of the electron rings and the radiofrequency (RF) fields are determined from the calculated axial and radial space-charge, RF, and magnetic forces as the rings pass through a sequence of cavities. By varying electrical and geometric properties of individual cavities, the model is capable of simulating severs, velocity tapers, and voltage jumps. The calculated electron ring trajectories can be used in designing magnetic focusing and multidepressed collectors. The details of using the program are presented, and results are compared with experimental data.

Author

N87-23900*# National Aeronautics and Space Administration. Lewis Research Center, Cleveland, Ohio.

OPTICALLY CONTROLLED MICROWAVE DEVICES AND CIRCUITS: EMERGING APPLICATIONS IN SPACE COMMUNICATIONS SYSTEMS

KUL B. BHASIN and RAINEE N. SIMONS Jul. 1987 11 p

Prepared for presentation at the International Microwave Symposium, Rio de Janeiro, Brazil, 27-30 Jul. 1987; cosponsored by Brazilian Microwave Society and the IEEE-MTT

(NASA-TM-89869; E-3543; NAS 1.15:89869) Avail: NTIS HC

A02/MF A01 CSCL 09A

Optical control of microwave devices and circuits by an optical fiber has the potential to simplify signal distribution networks in high frequency communications systems. The optical response of two terminal and three terminal (GaAs MESFET, HEMT, PBT) microwave devices are compared and several schemes for controlling such devices by modulated optical signals examined. Monolithic integration of optical and microwave functions on a single semiconductor substrate is considered to provide low power, low loss, and reliable digital and analog optical links for signal distribution.

Author

N87-23901*# National Aeronautics and Space Administration. Lewis Research Center, Cleveland, Ohio.
ISSUES IN SPACE PHOTOVOLTAIC RESEARCH AND TECHNOLOGY

DENNIS J. FLOOD 30 May 1987 16 p Presented at the 19th Photovoltaic Specialists Conference, New Orleans, La., 4-8 May 1987; sponsored by IEEE
 (NASA-TM-89922; E-3620; NAS 1.15:89922) Avail: NTIS HC A02/MF A01 CSCL 09C

Key issues and opportunities in space photovoltaic research and technology are addressed relative to future NASA mission requirements and drivers. Examples are given of future space missions and/or operational capabilities that are on NASA's planning horizon presenting major technology challenges to the use of photovoltaic power generation in space. A brief description of the capabilities ascribed to the competing technologies of nuclear and solar thermal power systems are given. The performance goals that space photovoltaic power systems must meet to remain competitive are described. Author

N87-23902*# National Aeronautics and Space Administration. Lewis Research Center, Cleveland, Ohio.
SYNCHRONIZATION TRIGGER CONTROL SYSTEM FOR FLOW VISUALIZATION

K. S. CHUN Feb. 1987 18 p Presented at the International Congress and Exposition, Detroit, Mich., 23-27 Feb. 1987; sponsored by SAE
 (NASA-TM-89902; E-3449; SAE-PAPER-870450; NAS 1.15:89902) Avail: NTIS HC A02/MF A01 CSCL 09A

The use of cinematography or holographic interferometry for dynamic flow visualization in an internal combustion engine requires a control device that globally synchronizes camera and light source timing at a predefined shaft encoder angle. The device is capable of 0.35 deg resolution for rotational speeds of up to 73 240 rpm. This was achieved by implementing the shaft encoder signal addressed look-up table (LUT) and appropriate latches. The developed digital signal processing technique achieves 25 nsec of high speed triggering angle detection by using direct parallel bit comparison of the shaft encoder digital code with a simulated angle reference code, instead of using angle value comparison which involves more complicated computation steps. In order to establish synchronization to an AC reference signal whose magnitude is variant with the rotating speed, a dynamic peak followup synchronization technique has been devised. This method scrutinizes the reference signal and provides the right timing within 40 nsec. Two application examples are described. Author

N87-23903*# National Aeronautics and Space Administration. Lewis Research Center, Cleveland, Ohio.

A STUDY OF SCHWARZ CONVERTERS FOR NUCLEAR POWERED SPACECRAFT

THOMAS A. STUART and GENE E. SCHWARZE 1987 11 p Prepared for Presentation at the 22nd Intersociety Energy Conversion Engineering Conference, Philadelphia, Pa., 10-14 Aug. 1987; cosponsored by AIAA, ANS, ASME, SAE, IEEE, ACS, and AICHE
 (NASA-TM-89911; E-3588; NAS 1.15:89911; AIAA-87-9314) Avail: NTIS HC A02/MF A01 CSCL 10B

High power space systems which use low dc voltage, high current sources such as thermoelectric generators, will most likely require high voltage conversion for transmission purposes. This study considers the use of the Schwarz resonant converter for use as the basic building block to accomplish this low-to-high voltage conversion for either a dc or an ac spacecraft bus. The Schwarz converter has the important assets of both inherent fault tolerance and resonant operation; parallel operation in modular form is possible. A regulated dc spacecraft bus requires only a single stage converter while a constant frequency ac bus requires a cascaded Schwarz converter configuration. If the power system requires constant output power from the dc generator, then a second converter is required to route unneeded power to a ballast load. Author

N87-24630*# National Aeronautics and Space Administration. Lewis Research Center, Cleveland, Ohio.

SELF-CONSISTENT INCLUSION OF SPACE-CHARGE IN THE TRAVELING WAVE TUBE

JON C. FREEMAN Jul. 1987 49 p
 (NASA-TM-89928; E-3633; NAS 1.15:89928) Avail: NTIS HC A03/MF A01 CSCL 09C

It is shown how the complete field of the electron beam may be incorporated into the transmission line model theory of the traveling wave tube (TWT). The fact that the longitudinal component of the field due to the bunched beam is not used when formulating the beam-to-circuit coupling equation is not well-known. The fundamental partial differential equation for the traveling wave field is developed and compared with the older (now standard) one. The equation can be solved numerically using the same algorithms, but now the coefficients can be updated continuously as the calculation proceeds down the tube. The coefficients in the older equations are primarily derived from preliminary measurements and some trial and error. The newer coefficients can be found by a recursive method, since each has a well defined physical interpretation and can be calculated once a reasonable first trial solution is postulated. The results of the new expression were compared with those of the older forms, as well as to a field theory model to show the ease in which a reasonable fit to the field prediction is obtained. A complete summary of the existing transmission line modeling of the TWT is given to explain the somewhat vague ideas and techniques in the general area of drifting carrier-traveling circuit wave interactions. The basic assumptions and inconsistencies of the existing theory and areas of confusion in the general literature are examined and hopefully cleared up. Author

N87-25532*# National Aeronautics and Space Administration. Lewis Research Center, Cleveland, Ohio.

ANALYTICAL AND EXPERIMENTAL PERFORMANCE OF A DUAL-MODE TRAVELING WAVE TUBE AND MULTISTAGE DEPRESSED COLLECTOR

PETER RAMINS, DALE A. FORCE, and HENRY G. KOSMAHL Aug. 1987 29 p
 (NASA-TP-2752; E-3470; NAS 1.60:2752) Avail: NTIS HC A03/MF A01 CSCL 09A

A computational procedure for the design of traveling-wave-tube(TWT)/refocuser/multistage depressed collector (MDC) systems was used to design a short, permanent-magnet refocusing system and a highly efficient MDC for a medium-power, dual mode, 4.8- to 9.6-GHz TWT. The computations were carried out with advanced, multidimensional computer programs which model the electron beam and follow the trajectories of representative charges from the radiofrequency (RF) input of the TWT, through the slow-wave structure and refocusing section, to their points of impact in the depressed collector. Secondary emission losses in the MDC were treated semiquantitatively by injecting representative secondary-electron-emission current into the MDA analysis at the point of impact of each primary beam. A comparison of computed and measured TWT and MDC performance showed very good agreement. The electrodes of the MDC were fabricated from a particular form of isotropic graphite that was selected for its low secondary electron yield, ease of machinability, and vacuum properties. Author

N87-26278*# National Aeronautics and Space Administration. Lewis Research Center, Cleveland, Ohio.

COMPUTER CONTROL OF A SCANNING ELECTRON MICROSCOPE FOR DIGITAL IMAGE PROCESSING OF THERMAL-WAVE IMAGES

PERCY GILBERT (Purdue Univ., West Lafayette, Ind.), ROBERT E. JONES, IHOR KRAMARCHUK, WALLACE D. WILLIAMS, and JOHN J. POUCH Aug. 1987 16 p
 (NASA-TM-100157; E-3719; NAS 1.15:100157) Avail: NTIS HC A02/MF A01 CSCL 09C

Using a recently developed technology called thermal-wave microscopy, NASA Lewis Research Center has developed a

computer controlled submicron thermal-wave microscope for the purpose of investigating III-V compound semiconductor devices and materials. This paper describes the system's design and configuration and discusses the hardware and software capabilities. Knowledge of the Concurrent 3200 series computers is needed for a complete understanding of the material presented. However, concepts and procedures are of general interest. Author

N87-27099*# Wittenberg Univ., Springfield, Ohio. Dept. of Physics.

RADIATION EFFECTS ON POWER TRANSISTOR PERFORMANCE Final Report, Apr. - Jun. 1987

ALBERT J. FRASCA Jun. 1987 26 p

(Contract NAG3-793)

(NASA-CR-181188; NAS 1.26:181188) Avail: NTIS HC A03/MF A01 CSCL 09A

The D60T, D62T, and D75T transistors in the nuclear reactor were irradiated with bias voltage and high current I_{subc} vs. V_{subec} curves were obtained to evaluate gain degradation at high power levels. Pre- and post-irradiation high current switching tests were performed to evaluate the response. The gamma ray damage work done at Sandia was correlated with the neutron work done at the O.S.U. reactor with the above specified transistors. Theoretical analyses of damage and electrical performance were conducted in terms of semiconductor physics. The experimental high current pulser was improved in order to measure switching time changes which are less than one microsecond at currents of 100 to 200 amperes for in-situ testing. B.G.

N87-27120*# National Aeronautics and Space Administration. Lewis Research Center, Cleveland, Ohio.

AN EXPERIMENTAL INVESTIGATION OF PARASITIC MICROSTRIP ARRAYS

RICHARD Q. LEE, ROBERTO ACOSTA, J. S. DAHELE, and K. F. LEE (Akron Univ., Ohio.) Sep. 1987 15 p Prepared for presentation at the Symposium on Antenna Application, Monticello, Ill., 23-25 Sep. 1987; sponsored in part by Illinois Univ. and Rome Air Development Center

(NASA-TM-100168; E-3731; NAS 1.15:100168) Avail: NTIS HC A02/MF A01 CSCL 09C

The characteristics of a parasitic microstrip antenna array with a center-fed patch are experimentally investigated. The parasitic array is composed of identical parasitic patches which are symmetrically arranged and electromagnetically coupled to a center-fed patch. The shape and dimensions of the parasitic patches and their positions relative to the center-fed patch are parameters in the study. To show mutual coupling effects between radiating and nonradiating edges of adjacent patches, the impedance and radiation characteristics of a three-element parasitic array excited with (0,1) mode are examined, and compared to that of a single patch. Experimental data indicate that the presence of parasitic patches has significant effects upon the gain, resonant frequency, and impedance bandwidth of the array. Author

N87-27121*# National Aeronautics and Space Administration. Lewis Research Center, Cleveland, Ohio.

DIFFUSION LENGTH MEASUREMENTS IN BULK AND EPITAXIALLY GROWN 3-5 SEMICONDUCTORS USING CHARGE COLLECTION MICROSCOPY

R. P. LEON May 1987 9 p Presented at the 19th Photovoltaic Specialists Conference, New Orleans, La., 4-8 May 1987; sponsored by IEEE

(NASA-TM-100128; E-3677; NAS 1.15:100128) Avail: NTIS HC A02/MF A01 CSCL 20L

Diffusion lengths and surface recombination velocities were measured in GaAs diodes and InP finished solar cells. The basic techniques used was charge collection microscopy also known as electron beam induced current (EBIC). The normalized currents and distances from the pn junction were read directly from the calibrated curves obtained while using the line scan mode in an SEM. These values were then equated to integral and infinite series expressions resulting from the solution of the diffusion equation with both extended generation and point generation

functions. This expands previous work by examining both thin and thick samples. The surface recombination velocity was either treated as an unknown in a system of two equations, or measured directly using low $e(-)$ beam accelerating voltages. These techniques give accurate results by accounting for the effects of surface recombination and the finite size of the generation volume. Author

N87-28825*# Microsemi Corp., Torrance, Calif. Power Technology Components.

SPACE STATION POWER SEMICONDUCTOR PACKAGE

VILNIS BALODIS, ALBERT BERMAN, DARRELL DEVANCE, GERRY LUDLOW, and LEE WAGNER Sep. 1987 115 p

(Contract NAS3-24662)

(NASA-CR-180829; NAS 1.26:180829) Avail: NTIS HC A06/MF A01 CSCL 09A

A package of high-power switching semiconductors for the space station have been designed and fabricated. The package includes a high-voltage (600 volts) high current (50 amps) NPN Fast Switching Power Transistor and a high-voltage (1200 volts), high-current (50 amps) Fast Recovery Diode. The package features an isolated collector for the transistors and an isolated anode for the diode. Beryllia is used as the isolation material resulting in a thermal resistance for both devices of .2 degrees per watt. Additional features include a hermetical seal for long life -- greater than 10 years in a space environment. Also, the package design resulted in a low electrical energy loss with the reduction of eddy currents, stray inductances, circuit inductance, and capacitance. The required package design and device parameters have been achieved. Test results for the transistor and diode utilizing the space station package is given. Author

N87-28832*# National Aeronautics and Space Administration. Lewis Research Center, Cleveland, Ohio.

APPARATUS FOR MOUNTING A FIELD EMISSION CATHODE Patent

BEN T. EBIHARA, inventor (to NASA) and RALPH FORMAN, inventor (to NASA) 18 Aug. 1987 6 p Filed 9 May 1985 Supersedes N85-29149 (23 - 18, p 3094)

(NASA-CASE-LEW-14108-1; US-PATENT-4,687,964;

US-PATENT-APPL-SN-732321; US-PATENT-CLASS-313-237;

US-PATENT-CLASS-313-278) Avail: US Patent and Trademark Office CSCL 09A

A field emission cathode is positioned in a pair of intersecting cross grooves, in the end of a ceramic tube by a metal end cap. A spring in electrical contact with the base of the cathode provides the necessary pressure to maintain continuous circumferential electrical contact between the gate film and a raised edge on the end cap. With this structure the cathode chip is self centering and easily replaceable. Also the gate film of the cathode is not abraded or rubbed during installation, and the holder is readily degassed.

Official Gazette of the U.S. Patent and Trademark Office

N87-29738*# General Dynamics Corp., San Diego, Calif. Space Systems Div.

RESONANT AC POWER SYSTEM PROOF-OF-CONCEPT TEST PROGRAM Contractor Report, Jun. 1981 - Nov. 1985

LORAN J. WAPPES Oct. 1986 243 p

(Contract NAS3-22777)

(NASA-CR-175069-VOL-1; NAS 1.26:175069-VOL-1) Avail: NTIS HC A11/MF A01 CSCL 09C

Proof-of-concept testing was performed on a 20-kHz, resonant power system breadboard from 1981 through 1985. The testing began with the evaluation of a single, 1.0-kW resonant inverter and progressed to the testing of breadboard systems with higher power levels and more capability. The final breadboard configuration tested was a 25.0-kW breadboard with six inverters providing power to three user-interface modules over a 50-meter, 20-kHz bus. The breadboard demonstrated the ability to synchronize multiple resonant inverters to power a common bus. Single-phase and three-phase 20-kHz power distribution was demonstrated. Simple conversion of 20-kHz to dc and

variable-frequency ac was demonstrated as was bidirectional power flow between 20-kHz and dc. Steady state measurements of efficiency, power-factor tolerance, and conducted emissions and conducted susceptibility were made. In addition, transient responses were recorded for such conditions as start up, shut down, load changes. The results showed the 20-kHz resonant system to be a desirable technology for a spacecraft power management and distribution system with multiple users and a utility-type bus. Author

N87-29739*# General Dynamics Corp., San Diego, Calif. Space Systems Div.

RESONANT AC POWER SYSTEM PROOF-OF-CONCEPT TEST PROGRAM, VOLUME 2, APPENDIX 1 Final Report

Oct. 1986 523 p

(Contract NAS3-22777)

(NASA-CR-175069-VOL-2; NAS 1.26:175069-VOL-2) Avail: NTIS HC A22/MF A01 CSCL 09C

This report contains two volumes. The main text (Volume 1) summarizes the tests results and gives a detailed discussion of the response of three early, first generation configurations of ac power system IRAD breadboards to the contracted tests imposed on them. It explains photographs, measurements, and data calculations, as well as any observed anomalies or lessons learned. This volume (No 2, Appendix 1, Test Results and Data), published under separate cover, includes all of the data taken on the 1.0 kW single-phase; 5.0 kW three-phase; and 25.0-kW three-phase system breadboards. The format of this data is raw, i.e., it is a direct copy of the data sheets for the test data notebook. Author

N87-29750*# National Aeronautics and Space Administration. Lewis Research Center, Cleveland, Ohio.

DETECTION OF RADIO-FREQUENCY MODULATED OPTICAL SIGNALS BY TWO AND THREE TERMINAL MICROWAVE DEVICES

K. B. BHASIN, R. N. SIMONS, and S. WOJTCZUK (Cornell Univ., Ithaca, N.Y.) 1987 11 p Presented at the 1987 Technical Symposium on Optics, Electro-Optics and Sensors, Orlando, Fla., 17-22 May 1987; sponsored by the Society of Photo-Optical Instrumentation Engineers

(NASA-TM-100196; E-3698; NAS 1.15:100196) Avail: NTIS HC A02/MF A01 CSCL 09C

An interdigitated photoconductor (two terminal device) on GaAlAs/GaAs heterostructure was fabricated and tested by an electro-optical sampling technique. Further, the photoresponse of GaAlAs/GaAs HEMT (three terminal device) was obtained by illuminating the device with an optical signal modulated up to 8 GHz. Gain-bandwidth product, response time, and noise properties of photoconductor and HEMT devices were obtained. Monolithic integration of these photodetectors with GaAs microwave devices for optically controlled phased array antenna applications is discussed. Author

FLUID MECHANICS AND HEAT TRANSFER

Includes boundary layers; hydrodynamics; fluidics; mass transfer; and ablation cooling.

A87-10920* Arizona State Univ., Tempe.

ON SELF-PRESERVING, VARIABLE-DENSITY, TURBULENT FREE JETS

R. M. C. SO (Arizona State University, Tempe) and T. M. LIU (Rohr Industries, Inc., Chula Vista, CA) Zeitschrift fuer angewandte Mathematik und Physik (ISSN 0044-2275), vol. 37, July 1986, p. 538-558. refs

(Contract NAG3-260; NAG3-167)

Published experimental data on incompressible, compressible, free binary, and confined binary turbulent axisymmetric jet flows are compiled and characterized, and the effect of varying turbulent diffusivity across the mixing region of a free jet is investigated analytically, applying the similarity-solution approach of So and Hwang (1986) to the self-preserving region. It is shown that closed-form solutions, represented by Gaussian error functions and having the turbulent Reynolds number and a profile-shape factor as free parameters, can be obtained if the turbulent diffusivities of momentum, mass, or heat are assumed to be different and to vary in both the streamwise and radial directions. An entrainment function uniquely related to the turbulent Reynolds number is derived, and good agreement between theoretical predictions and experimental measurements is demonstrated in graphs. T.K.

A87-10922* Arizona State Univ., Tempe.

ON SIMILARITY SOLUTIONS FOR TURBULENT AND HEATED ROUND JETS

R. M. C. SO (Arizona State University, Tempe) and B. C. HWANG (David W. Taylor Naval Ship Research and Development Center, Annapolis, MD) Zeitschrift fuer angewandte Mathematik und Physik (ISSN 0044-2275), vol. 37, July 1986, p. 624-631. refs

Commonly used empirical correlations for incompressible, heated round jets are shown to represent similarity solutions of the governing jet equations. These solutions give rise to self-similar eddy viscosities. Not all the similarity solutions are physically valid because some lead to zero eddy viscosities at the jet centerline. One physically valid solution is found to correlate best with round jet measurements and it gives a Gaussian error function description for the normalized mean velocity and temperature. Heat and momentum fluxes thus calculated are also in good agreement with measurements. Therefore, in addition to the classical similarity solution obtained by assuming constant eddy viscosity, another similarity solution to the jet equations is found where the eddy viscosity is self-similar. Author

A87-12060* National Aeronautics and Space Administration. Lewis Research Center, Cleveland, Ohio.

THE GENERATION OF CAPILLARY INSTABILITIES ON A LIQUID JET

S. J. LEIB and M. E. GOLDSTEIN (NASA, Lewis Research Center, Cleveland, OH) Journal of Fluid Mechanics (ISSN 0022-1120), vol. 168, July 1986, p. 479-500. refs

The coupling between imposed disturbances and capillary instabilities on a liquid jet is examined. It is shown that in most physical situations the forcing produces neutral waves, which can then turn into growing waves as the profile relaxes or may be amplified nonlinearly by a mechanism of the type considered by Akyas and Benney (1980). The effectiveness of the coupling is expressed quantitatively by numerically computed values of the 'coupling coefficient'. Author

A87-12251* National Aeronautics and Space Administration. Lewis Research Center, Cleveland, Ohio.

NONLINEAR CRITICAL LAYERS ELIMINATE THE UPPER BRANCH OF SPATIALLY GROWING TOLLMIE-SCHLICHTING WAVES

M. E. GOLDSTEIN and P. A. DURBIN (NASA, Lewis Research Center, Cleveland, OH) Physics of Fluids (ISSN 0031-9171), vol. 29, Aug. 1986, p. 2344, 2345. refs

This letter is concerned with the effect of nonlinear critical layers on spatially growing Tollmien-Schlichting waves in a Blasius boundary layer. It is shown that they effectively eliminate the upper branch of the neutral stability curve predicted by strictly linear theory. Author

A87-13019* Instituto de Estudos Avancados, Sao Jose dos Campos (Brazil).

HEAT TRANSFER IN THE STAGNATION REGION OF THE JUNCTION OF A CIRCULAR CYLINDER PERPENDICULAR TO A FLAT PLATE

J. N. HINCKEL (Instituto de Estudos Avancados, Sao Jose dos Campos, Brazil) and H. T. NAGAMATSU (Rensselaer Polytechnic Institute, Troy, NY) International Journal of Heat and Mass Transfer (ISSN 0017-9310), vol. 29, July 1986, p. 999-1005. refs (Contract NAG3-292; NSF MED-80-06806)

The heat transfer rate in the stagnation region of the junction of a circular cylinder perpendicular to a flat plate was measured for a range of Reynolds numbers varying from 3.0×10^4 to the 4th to 7.0×10^4 to the 5th and a flow Mach number of 0.14. The measurements were performed in a shock-tube facility using a reflected shockwave technique and thin-film platinum heat gages. The heat flux was measured for both the plate and the circular cylinder. A substantial increase in the heat transfer rate in the junction region was observed. The influence of the cylinder over the flat plate extended beyond $3/4$ cylinder diameter for low Reynolds numbers. For high Reynolds numbers the maximum increase in the heat transfer rate was observed to be approximately 100 percent, but for very low Reynolds numbers a maximum increase in the heat flux to the plate by a factor of 5 was observed. The variations in the heat transfer rate to the stagnation point of the cylinder was very small. Author

A87-13506* Garrett Turbine Engine Co., Phoenix, Ariz.
FINITE ANALYTIC NUMERICAL SOLUTION OF TWO-DIMENSIONAL CHANNEL FLOW OVER A BACKWARD-FACING STEP

K.-S. HO (Garrett Turbine Engine Co., Phoenix, AZ) and C.-J. CHEN (Iowa, University, Iowa City) IN: Applied numerical modeling. San Diego, CA, Univelt, Inc., 1986, p. 723-729. refs (Contract NSG-3305)

Laminar channel flow over a backward-facing step is investigated. The finite analytic (FA) method is used to obtain the numerical solution. The FA solutions predict the recirculation zone lengths and the recirculated mass flow rates for Reynolds numbers, Re, of 25, 50, 73, 125, 191 and 229 which correlate well with experimental measurements. The general flow patterns of the recirculation region flows for the Reynolds numbers considered in this study are similar to each other. Author

A87-13843* National Aeronautics and Space Administration. Lewis Research Center, Cleveland, Ohio.

LIQUID FUEL SPRAY PROCESSES IN HIGH-PRESSURE GAS FLOW

R. D. INGEBO (NASA, Lewis Research Center, Cleveland, OH) IN: ICLASS-85; Proceedings of the Third International Conference on Liquid Atomization and Spray Systems, London, England, July 8-10, 1985. Volume 2. London, Institute of Energy, 1986, p. VIA/4/1-VIA/4/18. Previously announced in STAR as N85-21570. refs

Atomization of single liquid jets injected downstream in high pressure and high velocity airflow was investigated to determine the effect of airstream pressure on mean drop size as measured with a scanning radiometer. For aerodynamic - wave breakup of liquid jets, the ratio of orifice diameter D_o to measured mean

drop diameter D_m which is assumed equal to D_{32} or Sauter mean diameter, was correlated with the product of the Weber and Reynolds numbers $WeRe$ and the dimensionless group G/\sqrt{c} , where G is the gravitational acceleration, 1 the mean free molecular path, and square root of C the root mean square velocity, as follows; $D_o/D_{32} = 1.2 (WeRe)$ to the $0.4 (G/\sqrt{c})$ to the 0.15 for values of $WeRe$ 1 million and an airstream pressure range of 0.10 to 2.10 MPa.

G.L.C.

A87-20897*# Wisconsin Univ., Milwaukee.
COMPARISON OF PRESSURE-STRAIN CORRELATION MODELS FOR THE FLOW BEHIND A DISK

R. S. AMANO (Wisconsin, University, Milwaukee) AIAA Journal (ISSN 0001-1452), vol. 24, Nov. 1986, p. 1870-1872. (Contract NAG3-546)

Attention is given to the behavior of Reynolds stresses in the separated wake region behind a disk that is attached in a normal fashion to a long cylinder of small diameter. Computations of the turbulent flow were made in a region beyond a disk by using the second-order closure model of turbulence. It is found that the models of Naot et al. (1970) and Launder et al. (1975) yield similar results and are reliable; the energy distribution may nevertheless be improved for the case of reattaching shear flows by taking the effects of mean strain into account. O.C.

A87-22361*# Dayton Univ., Ohio.
NUMERICAL SIMULATION OF EXCITED JET MIXING LAYERS
J. N. SCOTT and W. L. HANKEY (Dayton, University, OH) AIAA, Aerospace Sciences Meeting, 25th, Reno, NV, Jan. 12-15, 1987. 11 p. refs

(Contract NAG3-526)
(AIAA PAPER 87-0016)

A numerical simulation of unsteady flow in jet mixing layers, both with and without external excitation, has been performed by solving the time-dependent compressible Navier-Stokes equations. Computations were performed on a CRAY X-MP computer using MacCormick's explicit finite difference algorithm. Different excitation methods were investigated and were shown to be very effective in controlling the well organized periodic production, shedding and pairing of large scale vortex structures. It is found that pressure excitation was generally more effective than temperature excitation, and that grid refinement results in substantial improvement in the resolution of unsteady features. The location and orientation, in addition to the frequency, of the excitation source are shown to have a significant influence on the production and interaction of large scale vortex structures in the jet mixing layer. R.R.

A87-22387*# Avco-Everett Research Lab., Mass.
EVALUATION OF NEW TECHNIQUES FOR THE CALCULATION OF INTERNAL RECIRCULATING FLOWS

J. P. VAN DOORMAAL (Advanced Scientific Computing, Ltd., Waterloo, Canada), A. TURAN (AVCO Research Laboratory, Inc., Everett, MA), and G. D. RATHBY (Waterloo, University, Canada) AIAA, Aerospace Sciences Meeting, 25th, Reno, NV, Jan. 12-15, 1987. 11 p. refs

(Contract NAS3-24351)
(AIAA PAPER 87-0059)

The performance of discrete methods for the prediction of fluid flows can be enhanced by improving the convergence rate of solvers and by increasing the accuracy of the discrete representation of the equations of motion. This paper evaluates the gains in solver performance that are available when various acceleration methods are applied. Various discretizations are also examined and two are recommended because of their accuracy and robustness. Insertion of the improved discretization and solver accelerator into a TEACH code, that has been widely applied to combustor flows, illustrates the substantial gains that can be achieved. Author

34 FLUID MECHANICS AND HEAT TRANSFER

A87-22388*# Aerometrics, Inc., Mountain View, Calif.
TWO-PHASE FLOW MEASUREMENTS OF A SPRAY IN A TURBULENT FLOW

R. C. RUDOFF, M. J. HOUSER, and W. D. BACHALO (Aerometrics, Inc., Mountain View, CA) AIAA, Aerospace Sciences Meeting, 25th, Reno, NV, Jan. 12-15, 1987. 11 p. refs
(Contract NAS3-24844)
(AIAA PAPER 87-0062)

The dynamics of spray drop interaction with a turbulent coflowing air stream were investigated using a Phase Doppler Particle Analyzer that determines both drop size and velocity. Detailed measurements obtained included spray drop size, axial and radial velocity, angle of trajectory, drop Reynolds number, and size-velocity correlations. The gas-phase flow field was also ascertained via the behavior of the smallest drops. Also investigated were the drag coefficients of droplets in a turbulent air cross flow for both monodispersions and polydispersions. Most notable aspects of the coflow included the effect of air streams with velocities significantly different from the spray sheet. Local changes in number density were produced as a result of lateral convection and streamwise accelerations and decelerations of various drop size classes. The complexity of the spray field interaction illustrated by this data effectively describes the development of the spray due to the influence of the airflow. The droplet drag measurements showed similar behavior for monodispersed and polydispersed flows and similar trends to previously obtained data. The measurements also pointed out further studies which would assist in creating an improved drag law for polydispersed drops in a turbulent environment. Author

A87-22398*# Rensselaer Polytechnic Inst., Troy, N.Y.
ENDWALL HEAT TRANSFER IN THE JUNCTION REGION OF A CIRCULAR CYLINDER NORMAL TO A FLAT PLATE AT 30 AND 60 DEGREES FROM STAGNATION POINT OF THE CYLINDER

H. T. NAGAMATSU (Rensselaer Polytechnic Institute, Troy, NY) and K. Y. CHOI AIAA, Aerospace Sciences Meeting, 25th, Reno, NV, Jan. 12-15, 1987. 9 p. refs
(Contract NSF MEA-80-06806; NAG3-292)
(AIAA PAPER 87-0077)

The objective of this experimental study was to investigate the influence of horseshoe vortex on the heat transfer on a flat plate near the base of a protruding cylinder. The partial shock reflection technique was used to produce the flow Mach number of 0.14 which simulated the mean inlet flow Mach number for the first stage vanes of the turbine after combustor. Fast response thin-film platinum heat gages were used to measure the heat transfer flux for radial distances of 0.75, 0.875, 1.0, 1.125 cylinder diameter. For a low Reynolds number of 20,000, $r/D = 0.75$, and angular location from the stagnation point = 60 deg, the maximum increase in the heat transfer rate with the cylinder was observed to be approximately 460 percent greater than without the cylinder. On the other hand, the increase in the heat flux for a high Reynolds number of 300,000 was approximately 70 percent greater. For the heat gages located along 30 deg and 60 deg angular locations from the stagnation point, the strong effect of the horseshoe vortex was observed in the junction region. The increase in the heat transfer rate depended on the type of boundary layer and on the boundary layer thickness ahead of the cylinder. Author

A87-22426*# Aerometrics, Inc., Mountain View, Calif.
LASER VELOCIMETRY IN TURBULENT FLOW FIELDS - PARTICLE RESPONSE

W. D. BACHALO, R. RUDOFF, and M. J. HOUSER (Aerometrics, Inc., Mountain View, CA) AIAA, Aerospace Sciences Meeting, 25th, Reno, NV, Jan. 12-15, 1987. 14 p. refs
(Contract NAS3-24844; F49620-86-C-0078)
(AIAA PAPER 87-0118)

Measurements of the particle response in a decelerating flow and a highly turbulent two-phase flow were obtained. Simultaneous measurements of the particle size and velocity served to quantify the particle response to the prevailing flow field. In the case of a flow incident upon a cylinder, the particle lag for a range of size

classes was recorded. Results were also obtained in the flow generated by an atomizer operating on the leeward side of a flat disk bluff body in a coflowing air stream. Measurements of the mean axial, mean radial, and rms velocities and angles of trajectories were obtained for representative particle size classes. The air velocity and turbulence intensity were inferred from the seed particles on the order of one micrometer in diameter. Particles 9 micrometers and larger showed significant differences with respect to the gas phase mean velocity and turbulence intensity even at low velocities. In two-phase flows, reliable measurements of the continuous phase velocity and turbulence parameters requires the simultaneous measurement of particle size as a means for rejecting readings from large particles from the velocity pdf's. Author

A87-22466*# Atmospheric Science Associates, Bedford, Mass.
THREE-DIMENSIONAL TRAJECTORY ANALYSES OF TWO DROP SIZING INSTRUMENTS - PMS OAP AND PMS FSSP

H. G. NORMENT (Atmospheric Science Associates, Bedford, MA), A. QUEALY (Sverdrup Technology, Inc., Middleburg Heights, OH), and R. J. SHAW (NASA, Lewis Research Center, Cleveland, OH) AIAA, Aerospace Sciences Meeting, 25th, Reno, NV, Jan. 12-15, 1987. 12 p. refs
(AIAA PAPER 87-0180)

Flow-induced distortions of water drop fluxes and speeds as seen by the PMS optical array probe (OAP) and the PMS forward scattering spectrometer probe (FSSP) are estimated via three-dimensional flow and trajectory calculation methods. The sensitivities of the instruments to water drop diameter, angle of attack, and free stream air speed are determined. The instruments are first placed in isolation and then mounted under the wing of a Twin Otter airplane. For the wing-mounted OAP at 4-deg angle of attack, partial flow stagnation under the upturned wing causes a significant decrease in both the flux and speed for small water drops. For the wing-mounted FSSP, sensitivity is found to both angle of attack and free stream air speed. K.K.

A87-22509*# Scientific Research Associates, Inc., Glastonbury, Conn.
DUCT FLOWS WITH SWIRL

TOMMY M. TSAI and RALPH LEVY (Scientific Research Associates, Inc., Glastonbury, CT) AIAA, Aerospace Sciences Meeting, 25th, Reno, NV, Jan. 12-15, 1987. 7 p. refs
(Contract NAS3-24224)
(AIAA PAPER 87-0247)

The physics of the flow interaction between swirl and secondary flow was studied in duct bends relevant to the design of advanced aircraft nozzle systems. Both laminar and turbulent subsonic flows were investigated in generic duct bends for different amounts of swirl. The flow calculations are based on an economical three-dimensional spatial marching method employed in an existing computer code (PEPSIG). The computational method and code were extended to allow azimuthal periodicity and solutions in which the polar coordinate singularity occurs in the interior of the flow field. These extensions are needed to address swirling flow and twisted centerlines arising in out-of-plane bends. It was found that appropriate amounts of swirl can reduce total pressure loss relative to nonswirling cases. This conclusion was found to be insensitive to computational mesh. Author

A87-22549*# Oklahoma State Univ., Stillwater.
TWO OPPOSED LATERAL JETS INJECTED INTO SWIRLING CROSSFLOW

D. G. LILLEY (Oklahoma State University, Stillwater), C. B. MCMURRY, and L. H. ONG AIAA, Aerospace Sciences Meeting, 25th, Reno, NV, Jan. 12-15, 1987. 15 p. refs
(Contract NAG3-549)
(AIAA PAPER 87-0307)

Experiments have been conducted to obtain the time-mean and turbulent quantities of opposed lateral jets in a low speed, nonreacting flowfield. A jet-to-crossflow velocity ratio of $R = 4$ was used throughout the experiments, with swirl vane angles of 0 (swirler removed), 45 and 70 degrees used with the crossflow.

Flow visualization techniques used were neutrally-buoyant helium-filled soap bubbles and multispark photography in order to obtain the gross flowfield characteristics. Measurements of time-mean and turbulent quantities were obtained utilizing a six-orientation single hot-wire technique. For the nonswirling case, the jets were found not to penetrate past the test-section centerline, in contrast to the single lateral jet with the same jet-to-crossflow velocity ratio. In the swirling cases, the crossflow remains in a narrow region near the wall of the test section. The opposed jets are swept from their vertical courses into spiral trajectories close to the confining walls. Extensive results are presented in x-x plane plots. Author

A87-22552*# Aerodyne Research, Inc., Billerica, Mass.
MODELING FREE CONVECTIVE GRAVITATIONAL EFFECTS IN
CHEMICAL VAPOR DEPOSITION

C. D. STINESPRING (Aerodyne Research, Inc., Billerica, MA) and K. D. ANNEN (Aerodyne Products Corp., Billerica, MA) AIAA, Aerospace Sciences Meeting, 25th, Reno, NV, Jan. 12-15, 1987. 8 p. refs
 (Contract NAS3-23934)
 (AIAA PAPER 87-0313)

In this paper, a combined fluid-mechanics, mass-transport, and chemistry model describing CVD in an open-tube atmospheric-pressure flow reactor is developed. The model allows gas-phase reactions to proceed to equilibrium and accounts for finite reaction rates at the surface of the deposition substrate. This model is a useful intermediate step toward a model employing fully rate-limited chemistry. The model is used to predict the effects of free convection on flow patterns, temperature and species-concentration profiles, and local deposition rates for silicon deposited by silane pyrolysis. These results are discussed in terms of implications for CVD of silicon and other compounds, microgravity studies, and techniques for testing and validating the model. Author

A87-22645*# Cornell Univ., Ithaca, N.Y.
AN L-U IMPLICIT MULTIGRID ALGORITHM FOR THE
THREE-DIMENSIONAL EULER EQUATIONS

JEFFREY W. YOKOTA and D. A. CAUGHEY (Cornell University, Ithaca, NY) AIAA, Aerospace Sciences Meeting, 25th, Reno, NV, Jan. 12-15, 1987. 12 p. NSERC-supported research. refs
 (Contract NAG3-645)
 (AIAA PAPER 87-0453)

An LU implicit multigrid scheme is developed for the calculation of three-dimensional transonic flow through rotating cascades. This numerical method solves the unsteady Euler equations of gas dynamics in a finite-volume form. The implicit scheme makes it possible to take a much larger time step than is normally permitted in most explicit schemes, while the multigrid method is incorporated to accelerate the convergence rate for steady state calculations. Using this method, computational storage requirements are comparable to those of explicit schemes, while operation counts are considerably less than those found in the more widely-used ADI schemes. Author

A87-22706*# Texas Univ., Austin.
AN ADAPTIVE FINITE ELEMENT STRATEGY FOR COMPLEX
FLOW PROBLEMS

J. T. ODEN, T. STROUBOULIS, PH. DEVLOO (Texas, University, Austin), L. W. SPRADLEY, and J. PRICE (Lockheed Missiles and Space Co., Inc., Huntsville, AL) AIAA, Aerospace Sciences Meeting, 25th, Reno, NV, Jan. 12-15, 1987. 17 p. refs
 (Contract NAS1-17894; NAS3-24849)
 (AIAA PAPER 87-0557)

Adaptive finite element methods for steady and unsteady flow problems in two-dimensional domains are described. Details of a data management scheme are given that provide for the rapid implementation of various CFD algorithms on changing unstructured meshes. The results of several numerical experiments on subsonic and supersonic flow problems are discussed. Author

A87-22859* Houston Univ., Tex.
COHERENT STRUCTURES AND TURBULENCE

A. K. M. FAZLE HUSSAIN (Houston, University, TX) (IUTAM, Symposium on Fluid Mechanics in the Spirit of G. I. Taylor, Cambridge, England, Mar. 24-28, 1986) Journal of Fluid Mechanics (ISSN 0022-1120), vol. 173, Dec. 1986, p. 303-356. NSF-supported research. refs
 (Contract N00014-85-K-0126; NAG3-408)

The present state of understanding of coherent structures is examined with attention focused on their spatial details and dynamical significance. The characteristic measures of coherent structures are discussed and it is emphasized that coherent vorticity is the crucial property. A general scheme for educing structures in any transitional or fully turbulent flow is presented. The role of coherent structures in aerodynamic noise generation is studied and it is argued that the structure breakdown process is the dominant mechanism of noise generation. K.K.

A87-23449* National Aeronautics and Space Administration.
PREDICTION AND RATIONAL CORRELATION OF
THERMOPHORETICALLY REDUCED PARTICLE MASS
TRANSFER TO HOT SURFACES ACROSS LAMINAR OR
TURBULENT FORCED-CONVECTION GAS BOUNDARY
LAYERS

SULEYMAN A. GOKOGLU (NASA, Lewis Research Center, Cleveland, OH) and DANIEL E. ROSNER (Yale University, New Haven, CT) Chemical Engineering Communications (ISSN 0098-6445), vol. 44, 1986, p. 107-119. refs
 (Contract NAG3-590; NCC3-45; AF-AFOSR-84-0034)

A formulation previously developed to predict and correlate the thermophoretically-augmented submicron particle mass transfer rate to cold surfaces is found to account for the thermophoretically reduced particle mass transfer rate to overheated surfaces such that thermophoresis brings about a 10-decade reduction below the convective mass transfer rate expected by pure Brownian diffusion and convection alone. Thermophoretic blowing is shown to produce effects on particle concentration boundary-layer (BL) structure and wall mass transfer rates similar to those produced by real blowing through a porous wall. The applicability of the correlations to developing BL-situations is demonstrated by a numerical example relevant to wet-steam technology. R.R.

A87-23653*# Pennsylvania State Univ., University Park.
TURBULENCE MODELING FOR COMPLEX SHEAR FLOWS

B. LAKSHMINARAYANA (Pennsylvania State University, University Park) AIAA Journal (ISSN 0001-1452), vol. 24, Dec. 1986, p. 1900-1917. Research supported by Sverdrup Technology, Inc. Previously cited in issue 19, p. 2799, Accession no. A85-40752. refs
 (Contract NSG-3266; NSG-3212)

A87-24912*# Analytic and Computational Research, Inc., Los Angeles, Calif.
AN UNCONDITIONALLY-STABLE CENTRAL DIFFERENCING
SCHEME FOR HIGH REYNOLDS NUMBER FLOWS

AKSHAI K. RUNCHAL (Analytic and Computational Research, Inc., Los Angeles, CA), M. S. ANAND, and HUKAM C. MONGIA (General Motors Corp., Allison Gas Turbine Div., Indianapolis, IN) AIAA, Aerospace Sciences Meeting, 25th, Reno, NV, Jan. 12-15, 1987. 13 p. refs
 (Contract NAS3-24350)
 (AIAA PAPER 87-0060)

The central difference scheme (CDS) is a second order accurate scheme which is free of numerical diffusion (in the second order sense) and is simple to implement. However, for grid Peclet numbers larger than 2, the CDS leads to over- and undershoots and is unstable. The present paper describes a method, called CONDIF, which retains the essential nature of the CDS but eliminates the over- and under-shoots. It leads to unconditionally positive coefficients and, in the limit, approaches the CDS for all values of grid Peclet numbers. The CONDIF modifies the CDS by introducing a controlled amount of numerical diffusion based on

the local gradients. In the worst case the scheme yields results similar to those of the hybrid scheme. This paper reports the results obtained from CONDIF for a number of test problems which have been widely used for comparative study of numerical schemes in the published literature. For most of these problems, the CONDIF results are significantly more accurate than the hybrid scheme at high Peclet numbers. In particular, the CONDIF scheme depicts much lower level of numerical diffusion than the hybrid scheme even when the Peclet number is very high and the flow is at large angles to the grid. Author

A87-24913*# Minnesota Univ., Minneapolis.
DEVELOPMENT AND EVALUATION OF IMPROVED NUMERICAL SCHEMES FOR RECIRCULATING FLOWS
 S. V. PATANKAR (Minnesota, University, Minneapolis), K. C. KARKI, and H. C. MONGIA (General Motors Corp., Allison Gas Turbine Div., Indianapolis, IN) AIAA, Aerospace Sciences Meeting, 25th, Reno, NV, Jan. 12-15, 1987. 13 p. refs
 (Contract NAS3-24350)
 (AIAA PAPER 87-0061)

The paper examines the performance of the flux-spline scheme for convection-diffusion. Computations are presented for a number of test cases, both linear and nonlinear. It is shown that in all cases the flux-spline scheme yields results which are superior to those obtained with the lower-order formulations such as hybrid differencing. In order to improve the computational efficiency, the flux-spline scheme has been combined with a direct solution algorithm for the continuity and momentum equations. Such an approach eliminates the need for an equation for pressure or pressure correction and is found to be rapidly convergent. Author

A87-24925*# Washington Univ., Seattle.
MECHANISMS BY WHICH HEAT RELEASE AFFECTS THE FLOW FIELD IN A CHEMICALLY REACTING, TURBULENT MIXING LAYER
 J. J. RILEY (Washington, University, Seattle), R. W. METCALFE (Flow Research Co., Kent, WA), and P. A. MCMURTY AIAA, Aerospace Sciences Meeting, 25th, Reno, NV, Jan. 12-15, 1987. 23 p. refs
 (Contract NAS3-24229)
 (AIAA PAPER 87-0131)

The mechanisms by which heat release affects the fluid dynamics in a turbulent reacting mixing layer are studied by direct numerical simulation. In agreement with previous laboratory experiments, the heat release is observed to lower the rate at which the mixing layer grows and to reduce the rate at which chemical products are formed. The baroclinic torque and thermal expansion in the mixing layer are shown to produce changes in the flame vortex structure that act to produce more diffuse vortices than in the constant density case, resulting in lower rotation rates of fluid elements. Previously unexplained anomalies observed in the mean velocity profiles of reacting jets and mixing layers are shown to result from vorticity generation by baroclinic torques. The density reductions also lower the generation rates of turbulent kinetic energy and the turbulent shear stresses, resulting in less turbulent mixing of fluid elements. Calculations of the energy in the various wave numbers show that the heat release has a stabilizing effect on the growth rates of individual modes. A linear stability analysis of a simplified model problem confirms this, showing that low density fluid in the mixing region will result in a shift of the frequency of the unstable modes to lower wave numbers (longer wavelengths). The growth rates of the unstable modes decrease, contributing to the slower growth of the mixing layer. Author

A87-24926*# National Aeronautics and Space Administration. Lewis Research Center, Cleveland, Ohio.
EFFECTS OF DROPLET INTERACTIONS ON DROPLET TRANSPORT AT INTERMEDIATE REYNOLDS NUMBERS
 JIAN-SHUN SHUEN (NASA, Lewis Research Center; Sverdrup Technology, Inc., Cleveland, OH) AIAA, Aerospace Sciences Meeting, 25th, Reno, NV, Jan. 12-15, 1987. 20 p. refs
 (AIAA PAPER 87-0137)

Effects of droplet interactions on drag, evaporation, and combustion of a planar droplet array, oriented perpendicular to the approaching flow, are studied numerically. The three-dimensional Navier-Stokes equations, with variable thermophysical properties, are solved using finite-difference techniques. Parameters investigated include the droplet spacing, droplet Reynolds number, approaching stream oxygen concentration, and fuel type. Results are obtained for the Reynolds number range of 5 to 100, droplet spacings from 2 to 24 diameters, oxygen concentrations of 0.1 and 0.2, and methanol and n-butanol fuels. The calculations show that the gasification rates of interacting droplets decrease as the droplet spacings decrease. The reduction in gasification rates is significant only at small spacings and low Reynolds numbers. For the present array orientation, the effects of interactions on the gasification rates diminish rapidly for Reynolds numbers greater than 10 and spacings greater than 6 droplet diameters. The effects of adjacent droplets on drag are shown to be small. Author

A87-25281* Oklahoma State Univ., Stillwater.
MULTI-SPARK VISUALIZATION OF TYPICAL COMBUSTOR FLOWFIELDS
 D. G. LILLEY (Oklahoma State University, Stillwater) IN: Fluid control and measurement; Proceedings of the International Symposium, Tokyo, Japan, Sept. 2-5, 1985. Volume 1. Oxford, England and New York, Pergamon Press, 1986, p. 545-551. refs
 (Contract NAG3-549)

The interaction of a deflected jet with a confined tubular nonexpanded cross flow with swirl is investigated experimentally, applying a multiple-spark photographic visualization technique at jet/cross-flow velocity ratios 2, 4, and 6 and inlet-swirl vane angles 0, 45, and 70 deg in the test facility described by Lilley (1985). The visualization technique is described, and the results are presented graphically and briefly characterized. Phenomena observed include jet mixing and spreading, elevation of the vortex core, and reduction of the swirl strength in the lower part of the test section. T.K.

A87-27709*# Wisconsin Univ., Milwaukee.
TURBULENT HEAT TRANSFER IN CORRUGATED-WALL CHANNELS WITH AND WITHOUT FINS
 R. S. AMANO, A. BAGHERLEE (Wisconsin, University, Milwaukee), R. J. SMITH, and T. G. NIESS ASME, Transactions, Journal of Heat Transfer (ISSN 0022-1481), vol. 109, Feb. 1987, p. 62-67. refs
 (Contract NAG3-546)

A numerical study is performed examining flow and heat transfer characteristics in a channel with periodically corrugated walls. The complexity of the flow in this type of channel is demonstrated by such phenomena as flow impingement on the walls, separation at the bend corners, flow reattachment, and flow recirculation. Because of the strong nonisotropic nature of the turbulent flow in the channel, the full Reynolds-stress model was employed for the evaluation of turbulence quantities. Computations are made for several different corrugation periods and for different Reynolds numbers. The results computed by using the present model show excellent agreement with experimental data for mean velocities, the Reynolds stresses, and average Nusselt numbers. The study was further extended to a channel flow where fins are inserted at bends in the channel. It was observed that the insertion of fins in the flow passage has a visible effect on flow patterns and skin friction along the channel wall. Author

A87-27712*# National Aeronautics and Space Administration. Lewis Research Center, Cleveland, Ohio.

TRANSIENT RADIATIVE COOLING OF A DROPLET-FILLED LAYER

R. SIEGEL (NASA, Lewis Research Center, Cleveland, OH) ASME, Transactions, Journal of Heat Transfer (ISSN 0022-1481), vol. 109, Feb. 1987, p. 159-164. refs

A proposed lightweight radiator system for waste heat dissipation in space would eject streams of coolant in the form of small, hot liquid droplets. The droplets would lose radiative energy by direct exposure to the very low-temperature environment of space, and would then be collected for reuse. The cooling behavior of a layer composed of many small droplets was studied by numerical solution of the radiative integral equations. Since there is mutual interference for radiative energy dissipation, an array droplet will cool more slowly than if each drop is exposed individually. Since liquid metal droplets may be used, the study includes results for conditions with high scattering. For optically thin regions, especially with high scattering, the temperature distribution is sufficiently uniform that the cooling can be computed using the approximation of a constant layer emittance. For optically thick layers starting at uniform temperature, the temperature distributions become nonuniform with time. It was found that the cooling process goes through a starting transient; a constant emittance condition is then achieved where the emittance is lower than that for a layer at uniform temperature. Author

A87-27715*# National Aeronautics and Space Administration. Lewis Research Center, Cleveland, Ohio.

EFFECT OF FLOW OSCILLATIONS ON AXIAL ENERGY TRANSPORT IN A POROUS MATERIAL

R. SIEGEL (NASA, Lewis Research Center, Cleveland, OH) ASME, Transactions, Journal of Heat Transfer (ISSN 0022-1481), vol. 109, Feb. 1987, p. 242-244. refs

The effects of flow oscillations on axial energy diffusion in a porous medium, in which the flow is continuously disrupted by the irregularities of the porous structure, are analyzed. The formulation employs an internal heat transfer coefficient that couples the fluid and solid temperatures. The final relationship shows that the axial energy transport per unit cross-sectional area and time is directly proportional to the axial temperature gradient and the square of the maximum fluid displacement. I.S.

A87-27716*# National Aeronautics and Space Administration. Lewis Research Center, Cleveland, Ohio.

INFLUENCE OF OSCILLATION-INDUCED DIFFUSION ON HEAT TRANSFER IN A UNIFORMLY HEATED CHANNEL

R. SIEGEL (NASA, Lewis Research Center, Cleveland, OH) ASME, Transactions, Journal of Heat Transfer (ISSN 0022-1481), vol. 109, Feb. 1987, p. 244-247. refs

An analysis of the effect of flow oscillations on laminar flow heat transfer in a channel with uniform heat addition is presented. It is shown that the effect of flow oscillations will be to reduce the channel heat transfer coefficient. This effect is due to the fact that the heat addition along the channel wall produces an increasing fluid temperature along the channel length. The flow oscillations interacting with this positive temperature gradient will induce a heat flow back toward the channel inlet. This will tend to inhibit the heat transfer process and will raise the wall temperature required to transfer away a given amount of heat at the channel wall. I.S.

A87-27839* National Aeronautics and Space Administration. Lewis Research Center, Cleveland, Ohio.

STARVATION EFFECTS ON THE HYDRODYNAMIC LUBRICATION OF RIGID NONCONFORMAL CONTACTS IN COMBINED ROLLING AND NORMAL MOTION

M. K. GHOSH, D. E. BREWE (NASA, Lewis Research Center, Cleveland, OH), and B. J. HAMROCK (Ohio State University, Columbus) ASLE Transactions (ISSN 0569-8197), vol. 30, Jan. 1987, p. 91-99. Previously announced in STAR as N86-19556. refs

The effect of inlet starvation on the hydrodynamic lubrication of lightly loaded rigid nonconformal contacts in combined rolling and normal motion is determined through a numerical solution of the Reynolds' equation for an isoviscous, incompressible lubricant. Starvation is effected by systematically reducing the fluid inlet level. The pressures are taken to be ambient at the inlet meniscus boundary and Reynolds' boundary condition is applied for film rupture in the exit region. Results are presented for the dynamic performance of the starved contacts in combined rolling and normal motion for both normal approach and separation. During normal approach the dynamic load ratio (i.e. ratio of dynamic to steady state load capacity) increases considerably with increase in the inlet starvation. The effect of starvation on the dynamic peak pressure ratio is relatively small. Further, it has been observed that with increasing starvation, film thickness effects become significant in the dynamic behavior of the nonconformal contacts. For significantly starved contacts the dynamic load ratio increases with increase in film thickness during normal approach and a similar reduction is observed during separation. A similar effect is noted for the dynamic peak pressure ratio. Author

A87-28976* Arizona State Univ., Tempe.

THE NEAR FIELD BEHAVIOR OF TURBULENT GAS JETS IN A LONG CONFINEMENT

RONALD M. C. SO, SAAD A. AHMED, and M. H. YU (Arizona State University, Tempe) Experiments in Fluids (ISSN 0723-4864), vol. 5, no. 1, 1987, p. 2-10. refs
(Contract NAG3-260)

The near-field behavior of a turbulent gas jet (8.73 mm in diameter) in a long confinement was studied using a test rig with a confinement area ratio of about 205 and a length-to-jet diameter ratio of about 1700. Experiments were carried out with CO₂, air, and He/air jets at different jet velocities, using a laser Doppler velocimeter for velocity and turbulence measurements and hot-wire anemometers for a detailed examination of the turbulent shear field of an air jet. The air column inside the tunnel was seen to be first compressed by the jet and then to be slowly pushed out of the tunnel, causing the jet to spread rapidly and to decay quickly. As a result, an equilibrium turbulence field is established in the first two diameters of the jet which bears a similarity to that found in self-preserving turbulent free jets and jets in short confinement. However, in contrast to the cases of the two latter jet types, the near field of jets in a long confinement is independent of jet fluid densities and velocities. I.S.

A87-30281*# Tel-Aviv Univ. (Israel).

COHERENT MOTION IN EXCITED FREE SHEAR FLOWS

ISRAEL J. WYGNANSKI (Tel Aviv University, Israel) and ROBERT A. PETERSEN (Arizona, University, Tucson) AIAA Journal (ISSN 0001-1452), vol. 25, Feb. 1987, p. 201-213. refs
(Contract NSF MEA-82-10876; NAG3-460)
(AIAA PAPER 85-0539)

The application of the inviscid instability approach to externally excited turbulent free shear flows at high Reynolds numbers is explored. Attention is given to the cases of a small-deficit plane turbulent wake, a plane turbulent jet, an axisymmetric jet, the nonlinear evolution of instabilities in free shear flows, the concept of the 'preferred mode', vortex pairing in turbulent mixing layers, and experimental results for the control of free turbulent shear layers. The special features often attributed to pairing or to the preferred mode are found to be difficult to comprehend; the concept of feedback requires further substantiation in the case of incompressible flow. O.C.

A87-30685* Analytic and Computational Research, Inc., Los Angeles, Calif.

CONDIF - A MODIFIED CENTRAL-DIFFERENCE SCHEME WITH UNCONDITIONAL STABILITY AND VERY LOW NUMERICAL DIFFUSION

AKSHAI K. RUNCHAL (Analytic and Computational Research, Inc., Los Angeles, CA) IN: Heat transfer 1986; Proceedings of the Eighth International Conference, San Francisco, CA, Aug. 17-22, 1986. Volume 2. Washington, DC, Hemisphere Publishing Corp., 1986, p. 403-408. Research supported by the General Motors Corp. refs
(Contract NAS3-24350)

This paper describes a method, called CONDIF, which retains the essential nature of the central difference scheme (CDS) but eliminates the over- and under-shoots. It modifies the CDS by introducing a controlled amount of numerical diffusion based on local gradients. The results obtained for a number of test problems show that the CONDIF is significantly more accurate than the hybrid scheme when the Peclet number is very high and the flow is at large angles to the grid. In the worst case, it yields results similar to those of the hybrid scheme. Though the CONDIF is unconditionally stable, under some conditions the rate of convergence deteriorates as the grid Peclet number is increased. Efforts are currently underway to develop a faster converging variation of CONDIF. Author

A87-30720* National Aeronautics and Space Administration. Lewis Research Center, Cleveland, Ohio.

UNSTEADY HEAT TRANSFER AND DIRECT COMPARISON TO STEADY-STATE MEASUREMENTS IN A ROTOR-WAKE EXPERIMENT

J. E. OBRIEN, R. J. SIMONEAU, K. A. MOREHOUSE (NASA, Lewis Research Center, Cleveland, OH), and J. E. LAGRAFF (Syracuse University, NY) IN: Heat transfer 1986; Proceedings of the Eighth International Conference, San Francisco, CA, Aug. 17-22, 1986. Volume 3. Washington, DC, Hemisphere Publishing Corp., 1986, p. 1243-1248. Previously announced in STAR as N86-24934. refs

Circumferentially local and time-resolved heat transfer measurements were obtained for a circular cylinder in crossflow located downstream of a rotating spoked wheel wake generator in a steady flow tunnel. The unsteady heat transfer effects were obtained by developing an extension of a thin film gauge technique employed to date exclusively in short-duration facilities. The time-average thin film results and conventional steady-state heat transfer measurements were compared. Time-averaged wake-induced stagnation heat transfer enhancement levels above the nowake case were about 10 percent for the four cylinder Reynolds numbers. This enhancement level was nearly independent of bar passing frequency and was related directly to the time integral of the heat transfer spikes observed at the bar passing frequency. It is observed that the wake-induced heat transfer spikes have peak magnitudes averaging 30 to 40 percent above the interwake heat transfer level. E.A.K.

A87-30721* National Aeronautics and Space Administration. Lewis Research Center, Cleveland, Ohio.

EFFECT OF A ROTOR WAKE ON THE LOCAL HEAT TRANSFER ON THE FORWARD HALF OF A CIRCULAR CYLINDER

KIM A. MOREHOUSE and ROBERT J. SIMONEAU (NASA, Lewis Research Center, Cleveland, OH) IN: Heat transfer 1986; Proceedings of the Eighth International Conference, San Francisco, CA, Aug. 17-22, 1986. Volume 3. Washington, DC, Hemisphere Publishing Corp., 1986, p. 1249-1255. Previously announced in STAR as N86-21794. refs

Turbine rotor-stator wake dynamics was simulated by a spoked wheel rotating in annular flow, generating rotor wakes. Spanwise averaged circumferentially local heat transfer in the circular cylindrical leading edge region of a turbine airfoil was obtained. Reynolds numbers ranged from 35,000 to 175,000. Strouhal numbers ranged from 0.63 to 2.50. Wakes were generated by 2 sets of circular cylindrical bars, 1.59 and 3.18 mm in diameter. The rotor could be rotated either clockwise or counterclockwise.

Grid turbulence was introduced upstream yielding freestream turbulence of 1.0 to 2.5 percent at the stator. Data represented an extensive body of local heat transfer coefficients, which can be used to model the leading edge region of a turbine airfoil. In the presence of rotor wakes, an asymmetry from the leeward to windward side was noted. Windward side levels were 30 to 40 percent higher than the corresponding leeward side. Author

A87-30728* National Aeronautics and Space Administration. Lewis Research Center, Cleveland, Ohio.

TWO-PHASE FLOWS AND HEAT TRANSFER WITHIN SYSTEMS WITH AMBIENT PRESSURE ABOVE THE THERMODYNAMIC CRITICAL PRESSURE

R. C. HENDRICKS (NASA, Lewis Research Center, Cleveland, OH), M. J. BRAUN (Akron, University, OH), and R. L. MULLEN (Case Western Reserve University, Cleveland, OH) IN: Heat transfer 1986; Proceedings of the Eighth International Conference, San Francisco, CA, Aug. 17-22, 1986. Volume 5. Washington, DC, Hemisphere Publishing Corp., 1986, p. 2331-2336. Previously announced in STAR as N86-19558. refs

In systems where the design inlet and outlet pressure P_{sub} are maintained above the thermodynamic critical pressure $P_{sub,c}$, it is often assumed that heat and mass transfer are governed by single-phase relations and that two-phase flows cannot occur. This simple rule of thumb is adequate in many low-power designs but is inadequate for high-performance turbomachines, boilers, and other systems where two-phase regions can exist even though $P_{sub} > P_{sub,c}$. Heat and mass transfer and rotordynamic-fluid-mechanic restoring forces depend on momentum differences, and those for a two-phase zone can differ significantly from those for a single-phase zone. By using a laminar, variable-property bearing code and a rotating boiler code, pressure and temperature surfaces were determined that illustrate nesting of a two-phase region within a supercritical pressure region. The method of corresponding states is applied to bearings with reasonable rapport. E.A.K.

A87-30732* Texas A&M Univ., College Station.

LOCAL HEAT TRANSFER AUGMENTATION IN CHANNELS WITH TWO OPPOSITE RIBBED SURFACES

J. C. HAN and J. S. PARK (Texas A & M University, College Station) IN: Heat transfer 1986; Proceedings of the Eighth International Conference, San Francisco, CA, Aug. 17-22, 1986. Volume 6. Washington, DC, Hemisphere Publishing Corp., 1986, p. 2885-2890. refs
(Contract NAS3-24227)

The local heat transfer coefficient distribution of a square channel with two opposite ribbed walls was determined. The square channel was connected to a sudden contraction entrance in order to simulate the inlet condition of the turbine blade cooling passages. The test channel was heated by thin stainless steel foils with a thickness of 0.000025 m, and instrumented with 180 thermocouples. The brass ribs of a square cross-section were glued periodically, in line, onto the top and bottom walls of the foil-heated channel in patterns to achieve the desired spacing and angle-of-attack. The local heat transfer coefficients on the smooth side and the ribbed side walls, at the channel entrance and the downstream regions, were measured for eight rib configurations and three Reynolds numbers ($Re = 10,000, 30,000, \text{ and } 60,000$). Author

A87-31176*# Arizona Univ., Tucson.

PERFECT GAS EFFECTS IN COMPRESSIBLE RAPID DISTORTION THEORY

E. J. KERSCHEN and M. R. MYERS (Arizona, University, Tucson) AIAA Journal (ISSN 0001-1452), vol. 25, March 1987, p. 504-507. Research supported by the General Electric Co. refs
(Contract NAG3-357)

The governing equations presented for small amplitude unsteady disturbances imposed on steady, compressible mean flows that are two-dimensional and nearly uniform have their basis in the perfect gas equations of state, and therefore generalize previous results based on tangent gas theory. While these

equations are more complex, this complexity is required for adequate treatment of high frequency disturbances, especially when the base flow Mach number is large; under such circumstances, the simplifying assumptions of tangent gas theory are not applicable. O.C.

A87-31406* Akron Univ., Ohio.

MULTIPLY SCALED CONSTRAINED NONLINEAR EQUATION SOLVERS

JOE PADOVAN and LALA KRISHNA (Akron, University, OH) Numerical Heat Transfer (ISSN 0149-5720), vol. 10, no. 5, 1986, p. 463-482. refs
(Contract NAG3-54)

To improve the numerical stability of nonlinear equation solvers, a partitioned multiply scaled constraint scheme is developed. This scheme enables hierarchical levels of control for nonlinear equation solvers. To complement the procedure, partitioned convergence checks are established along with self-adaptive partitioning schemes. Overall, such procedures greatly enhance the numerical stability of the original solvers. To demonstrate and motivate the development of the scheme, the problem of nonlinear heat conduction is considered. In this context the main emphasis is given to successive substitution-type schemes. To verify the improved numerical characteristics associated with partitioned multiply scaled solvers, results are presented for several benchmark examples. Author

A87-31680* Arizona Univ., Tucson.

ON THE SPATIAL INSTABILITY OF PIECEWISE LINEAR FREE SHEAR LAYERS

T. F. BALSA (Arizona, University, Tucson) Journal of Fluid Mechanics (ISSN 0022-1120), vol. 174, Jan. 1987, p. 553-563. refs
(Contract NAG3-485)

The main goal of this paper is to clarify the spatial instability of a piecewise linear free shear flow. This is done by obtaining numerical solutions to the Orr-Sommerfeld equation of high Reynolds numbers. The velocity profile chosen is very much like a piecewise linear one, with the exception that the corners have been rounded so that the entire profile is infinitely differentiable. It is found that the (viscous) spatial instability of this modified profile is virtually identical to the inviscid spatial instability of the piecewise linear profile and agrees qualitatively with the inviscid results for the tanh profile when the shear layers are convectively unstable. The unphysical features, previously identified for the piecewise linear velocity profile, arise only when the flow is absolutely unstable. It is concluded that there is nothing wrong with the inviscid spatial instability of piecewise linear shear flows. Author

A87-32190*# National Aeronautics and Space Administration. Lewis Research Center, Cleveland, Ohio.

EFFICIENT NUMERICAL SIMULATION OF AN ELECTROTHERMAL DE-ICER PAD

R. J. ROELKE (NASA, Lewis Research Center, Cleveland, OH), T. G. KEITH, JR., K. J. DE WITT, and W. B. WRIGHT (Toledo, University, OH) AIAA, Aerospace Sciences Meeting, 25th, Reno, NV, Jan. 12-15, 1987. 12 p. refs
(AIAA PAPER 87-0024)

In this paper, a new approach to calculate the transient thermal behavior of an iced electrothermal de-icer pad was developed. The method of splines was used to obtain the temperature distribution within the layered pad. Splines were used in order to create a tridiagonal system of equations that could be directly solved by Gauss elimination. The Stefan problem was solved using the enthalpy method along with a recent implicit technique. Only one to three iterations were needed to locate the melt front during any time step. Computational times were shown to be greatly reduced over those of an existing one dimensional procedure without any reduction in accuracy; the current technique was more than 10 times faster. Author

A87-32326* National Aerospace Lab., Kakuda (Japan).

VOLUME-ENERGY PARAMETERS FOR HEAT TRANSFER TO SUPERCRITICAL FLUIDS

A. KUMAKAWA, M. NIINO (National Aerospace Laboratory, Ohgawara, Japan), R. C. HENDRICKS (NASA, Lewis Research Center, Cleveland, OH), P. J. GIARRATANO, and V. D. ARP (NBS, Boulder, CO) IN: International Symposium on Space Technology and Science, 15th, Tokyo, Japan, May 19-23, 1986, Proceedings. Volume 1. Tokyo, AGNE Publishing, Inc., 1986, p. 389-399. refs

Reduced Nusselt numbers of supercritical fluids from different sources were grouped by several volume-energy parameters. A modified bulk expansion parameter was introduced based on a comparative analysis of data scatter. Heat transfer experiments on liquefied methane were conducted under near-critical conditions in order to confirm the usefulness of the parameters. It was experimentally revealed that heat transfer characteristics of near-critical methane are similar to those of hydrogen. It was shown that the modified bulk expansion parameter and the Gibbs-energy parameter grouped the heat transfer data of hydrogen, oxygen and methane including the present data on near-critical methane. It was also indicated that the effects of surface roughness on heat transfer were very important in grouping the data of high Reynolds numbers. Author

A87-34724*# National Aeronautics and Space Administration. Lewis Research Center, Cleveland, Ohio.

AN LU-SSOR SCHEME FOR THE EULER AND NAVIER-STOKES EQUATIONS

SEOKKWAN YOON (NASA, Lewis Research Center; Sverdrup Technology, Inc., Cleveland, OH) and ANTHONY JAMESON (Princeton University, NJ) AIAA, Aerospace Sciences Meeting, 25th, Reno, NV, Jan. 12-15, 1987. 12 p. Previously announced in STAR as N87-16806. refs
(AIAA PAPER 87-0600)

A new multigrid relaxation scheme, lower-upper symmetric successive overrelaxation (LU-SSOR) is developed for the steady-state solution of the Euler and Navier-Stokes equations. The scheme, which is based on central differences, does not require flux splitting for approximate Newton iteration. Application to transonic flow shows that the new method is efficient and robust. The vectorizable LU-SSOR scheme needs only scalar diagonal inversions. Author

A87-34725*# National Aeronautics and Space Administration. Lewis Research Center, Cleveland, Ohio.

COMPARISON OF THREE EXPLICIT MULTIGRID METHODS FOR THE EULER AND NAVIER-STOKES EQUATIONS

RODRICK V. CHIMA, ELI TURKEL, and STEVE SCHAFFER (NASA, Lewis Research Center, Cleveland, OH) AIAA, Aerospace Sciences Meeting, 25th, Reno, NV, Jan. 12-15, 1987. 14 p. Previously announced in STAR as N87-16784. refs
(AIAA PAPER 87-0602)

Three explicit multigrid methods, Ni's method, Jameson's finite-volume method, and a finite-difference method based on Brandt's work, are described and compared for two model problems. All three methods use an explicit multistage Runge-Kutta scheme on the fine grid, and this scheme is also described. Convergence histories for inviscid flow over a bump in a channel for the fine-grid scheme alone show that convergence rate is proportional to Courant number and that implicit residual smoothing can significantly accelerate the scheme. Ni's method was slightly slower than the implicitly-smoothed scheme alone. Brandt's and Jameson's methods are shown to be equivalent in form but differ in their node versus cell-centered implementations. They are about 8.5 times faster than Ni's method in terms of CPU time. Results for an oblique shock/boundary layer interaction problem verify the accuracy of the finite-difference code. All methods slowed considerably on the stretched viscous grid but Brandt's method was still 2.1 times faster than Ni's method. Author

34 FLUID MECHANICS AND HEAT TRANSFER

A87-37208*# Indian Inst. of Tech., Madras.

PERFORMANCE STUDIES ON AN AXIAL FLOW COMPRESSOR STAGE

N. SITARAM (Indian Institute of Technology, Madras, India) Aeronautical Society of India, Journal (ISSN 0001-9267), vol. 38, Nov.-Dec. 1986, p. 267-275. refs
(Contract NSG-3032)

A low-speed, medium loaded axial flow compressor stage is studied experimentally and theoretically. The flow compressor facility, composed of an inlet guide vane row, a rotor blade row, and a stator blade row, and the principles of the streamline curvature method (SCM) and the Douglas-Neumann cascade program are described. The radial distribution of the flow properties, the rotor blade static pressure distribution, and the lift coefficient and relative flow angle derived experimentally and theoretically are compared. It is determined that there is good correlation between the experimental flow properties and the SCM data, the Douglas-Neumann cascade program and experimental rotor blade static pressure data, and the experimental and theoretical lift coefficients only in the midspan region. Modifications to the SCM and the Douglas-Neumann cascade program in order to improve their accuracy are discussed. I.F.

A87-37256* Arizona Univ., Tucson.

THE EVOLUTION OF INSTABILITIES IN THE AXISYMMETRIC JET. I - THE LINEAR GROWTH OF DISTURBANCES NEAR THE NOZZLE. II - THE FLOW RESULTING FROM THE INTERACTION BETWEEN TWO WAVES

J. COHEN (Arizona, University, Tucson) and I. WYGNANSKI (Arizona, University, Tucson; Tel Aviv University, Israel) Journal of Fluid Mechanics (ISSN 0022-1120), vol. 176, March 1987, p. 191-219, 221-235. refs
(Contract NAG3-460; NSF MEA-82-10876)

The modal distribution of coherent structures evolving near the nozzle of a circular jet was studied experimentally and theoretically, with particular attention given to the effects produced on the instability modes by transverse curvature, flow divergence, inhomogeneous inflow conditions, and the detailed shape of the mean velocity profile. Experiments were performed using a specially constructed air-jet facility; hot-wire anemometers were used in conjunction with Disa Model 55P11 sensors for flow measurements. The linear model used as a transfer function is capable of predicting the spectral distribution of the velocity perturbations in a jet. Consideration was also given to studies of leading nonlinear interactions generated by waves externally superimposed on an axisymmetric jet; theoretical predictions were verified experimentally. I.S.

A87-38790*# California Univ., Berkeley.

EQUILIBRIUM FLUID INTERFACES IN THE ABSENCE OF GRAVITY

P. CONCUS (California, University, Berkeley) IN: Symposium on Microgravity Fluid Mechanics; Proceedings of the Winter Annual Meeting, Anaheim, CA, Dec. 7-12, 1986. New York, American Society of Mechanical Engineers, 1986, p. 37, 38.
(Contract NAG3-146; DE-AC03-76SF-00098)

Mathematical properties of capillary surfaces under zero gravity conditions are examined in the framework of the Laplace-Young theory, considering the equilibrium interface between a liquid and a gas or between two immiscible liquids for a cylindrical container of general cross section. The predicted liquid surface behavior is compared with the results obtained in a drop-tower experiment in the Zero-G Facility at the NASA Lewis Research Center. I.S.

A87-38956*# Arizona State Univ., Tempe.

MODELLING OF JET- AND SWIRL-STABILIZED REACTING FLOWS IN AXISYMMETRIC COMBUSTORS

M. NIKJOOY, R. M. C. SO, and R. E. PECK (Arizona State University, Tempe) IN: Calculations of turbulent reactive flows; Proceedings of the Winter Annual Meeting, Anaheim, CA, Dec. 7-12, 1986. New York, American Society of Mechanical Engineers, 1986, p. 233-258. refs
(Contract NAG3-167; NAG3-260; N60530-85-C-0191)

Turbulent nonreactive and reactive flows with and without swirl are analyzed, with particular attention given to the flow fields of a gas-fueled nonpremixed swirl-stabilized combustor and a premixed opposed-jet combustor. Local mean flow properties, including velocity, temperature, and major species concentrations, are calculated by solving numerically the governing partial differential equations with associated submodels for turbulence and combustion. The results of the study indicate that the constant-density k-epsilon turbulence model provides a satisfactory representation of the aerodynamics in most practical combustor flows. The exception is the case of jet-stabilized combustor flow, due to the fact that the k-epsilon model cannot replicate the highly dissipative phenomenon found in such flows. I.S.

A87-39450* National Aeronautics and Space Administration. Lewis Research Center, Cleveland, Ohio.

TIME-MARCHING SOLUTION OF INCOMPRESSIBLE NAVIER-STOKES EQUATIONS FOR INTERNAL FLOW

W. Y. SOH (NASA, Lewis Research Center; Sverdrup Technology, Inc., Cleveland, OH) Journal of Computational Physics (ISSN 0021-9991), vol. 70, May 1987, p. 232-252. refs

Primitive variables with central differencing on a staggered grid are used in the present, factored ADI finite-difference scheme for artificial compressibility method solution of the incompressible Navier-Stokes equations, leading to a close coupling between velocity and pressure that both enhances stability and eliminates the need for artificial damping. Computational efficiency is enhanced through the use of a spatially variable, fixed Courant number-based time-step. The numerical results obtained for a driven cavity at Re of 10,000, with local cell Re as high as 100, exhibits no flow variable spatial oscillations on a 40 x 40 stretched grid solution. O.C.

A87-39805*# National Aeronautics and Space Administration. Lewis Research Center, Cleveland, Ohio.

EFFECTS OF MULTIPLE ROWS AND NONCIRCULAR ORIFICES ON DILUTION JET MIXING

J. D. HOLDEMAN (NASA, Lewis Research Center, Cleveland, OH), R. SRINIVASAN, E. B. COLEMAN, G. D. MEYERS, and C. D. WHITE (Garrett Turbine Engine Co., Phoenix, AZ) Journal of Propulsion and Power (ISSN 0748-4658), vol. 3, May-June 1987, p. 219-226. Previously cited in issue 18, p. 2620, Accession no. A85-39606. refs

A87-39812*# Florida Univ., Gainesville.

NUMERICAL SIMULATION OF THE FLOWFIELD IN A MOTORED TWO-DIMENSIONAL WANKEL ENGINE

T. I.-P. SHIH (Florida, University, Gainesville), H. J. SCHOCK, H. L. NGUYEN, and J. D. STEGEMAN (NASA, Lewis Research Center, Cleveland, OH) Journal of Propulsion and Power (ISSN 0748-4658), vol. 3, May-June 1987, p. 269-276. Previously cited in issue 20, p. 2961, Accession no. A86-42711. refs
(Contract NAG3-363)

A87-40703*# Purdue Univ., West Lafayette, Ind.

TWO COMPONENT LASER VELOCIMETER MEASUREMENTS OF TURBULENCE PARAMETERS DOWNSTREAM OF AN AXISYMMETRIC SUDDEN EXPANSION

RICHARD D. GOULD, WARREN H. STEVENSON, and H. DOYLE THOMPSON (Purdue University, West Lafayette, IN) IN: International Symposium on Applications of Laser Anemometry to Fluid Mechanics, 3rd, Lisbon, Portugal, July 7-9, 1986, Proceedings. Lisbon, Instituto Superior Tecnico, 1986, p. 1.2 (6 p.). refs (Contract NAG3-502)

Simultaneous two-component laser velocimeter measurements were made in an axisymmetric sudden expansion flowfield. A specially designed correction lens was employed to correct optical aberrations introduced by the circular tube. This lens system allowed the accurate simultaneous measurement of axial and radial velocities in the test section. The experimental measurements were compared to predictions generated by a code which employed the k-epsilon turbulence model. Possible sources of differences observed between model predictions and the measurements are discussed. Author

A87-40932* National Aeronautics and Space Administration. Lewis Research Center, Cleveland, Ohio.

TURBULENT SOLUTIONS OF THE NAVIER-STOKES EQUATIONS

R. G. DEISSLER (NASA, Lewis Research Center, Cleveland, OH) IN: Encyclopedia of Fluid Mechanics. Houston, TX, Gulf Publishing Co., 1986, p. 1153-1182. refs

Analytical and numerical approaches to the mechanics of turbulent flow are examined in a general introduction and illustrated with graphs. Topics discussed include the averaged and unaveraged basic equations, numerical solutions and methods, homogeneous fluctuations and turbulence with no mean flow, uniformly sheared fluctuations and turbulence, inhomogeneous fluctuations and turbulence in a developing shear layer, and steady-state homogeneous turbulence with a spatially periodic body force. T.K.

A87-41173*# Houston Univ., Tex.

A MODEL FOR FLUID FLOW DURING SATURATED BOILING ON A HORIZONTAL CYLINDER

K. KHEYRANDISH, C. DALTON, and J. H. LIENHARD (Houston, University, TX) ASME, Transactions, Journal of Heat Transfer (ISSN 0022-1481), vol. 109, May 1987, p. 485-490. refs (Contract NAG3-537; NSF MEA-82-18708)

A model has been developed to represent the vapor removal pattern in the vicinity of a cylinder during nucleate flow boiling across a horizontal cylinder. The model is based on a potential flow representation of the liquid and vapor regions and an estimate of the losses that should occur in the flow. Correlation of the losses shows a weak dependence on the Weber number and a slightly stronger dependence on the saturated liquid-to-vapor density ratio. The vapor jet thickness, which is crucial to the prediction of the burnout heat flux, and the shape of the vapor film are predicted. Both are verified by qualitative experimental observations. Author

A87-41655* National Aeronautics and Space Administration. Lewis Research Center, Cleveland, Ohio.

THE GENERATION OF TOLLMIE-SCHLICHTING WAVES BY LONG WAVELENGTH FREE STREAM DISTURBANCES

M. E. GOLDSTEIN (NASA, Lewis Research Center, Cleveland, OH) IN: Stability of time dependent and spatially varying flows; Proceedings of the Symposium, Hampton, Va, Aug. 19-23, 1985. New York, Springer-Verlag, 1987, p. 58-81. refs

The paper is primarily concerned with explaining how very long wavelength free stream disturbances are able to generate very short wavelength Tollmien-Schlichting waves in laminar boundary layers. Consideration is given to the case where the disturbances are of small amplitude and have harmonic time dependence and where the Mach number is effectively zero. It is shown that the free stream wavelength reduction occurs as a result of nonparallel flow effects which can arise from: (1) the slow viscous growth of

the boundary layer, and (2) small but abrupt changes in surface geometry that produce only very weak static pressure variations. Analyses of these two mechanisms are carried out by linearizing the unsteady motion about an appropriate steady flow and asymptotically expanding the result in inverse powers of an appropriate Reynolds number. The analyses are compared with each other and with available experimental data, and they are used to explain the physics of the two mechanisms. Author

A87-41665* Pennsylvania State Univ., University Park.

THE HUB WALL BOUNDARY LAYER DEVELOPMENT AND LOSSES IN AN AXIAL FLOW COMPRESSOR ROTOR PASSAGE

K. N. S. MURTHY and B. LAKSHMINARAYANA (Pennsylvania State University, University Park) Zeitschrift fuer Flugwissenschaften und Weltraumforschung (ISSN 0342-068X), vol. 11, Jan.-Feb. 1987, p. 1-11. refs (Contract NSG-3212)

The hub wall boundary layer development in a compressor stage including the rotor passage is experimentally investigated. A miniature five-hole probe was employed to measure the hub wall boundary layer inside the inlet guide vane passage, upstream and far downstream of the rotor. The hub wall boundary layer inside the rotor passage was acquired using a rotating miniature five-hole probe. The boundary layer is well behaved upstream and far downstream of the rotor. The migration of the hub wall boundary layer towards the suction surface corner is observed. The limiting streamline angles and static pressure distribution across the stage were also measured. The mean velocity profiles and the integral properties upstream, inside and downstream of the rotor, and the losses are presented and interpreted. Author

A87-42376*# Stanford Univ., Calif.

AN EXPERIMENTAL STUDY OF THE DEVELOPMENT OF LONGITUDINAL VORTEX PAIRS EMBEDDED IN A TURBULENT BOUNDARY LAYER

WAYNE R. PAULEY and JOHN K. EATON (Stanford University, CA) AIAA, Fluid Dynamics, Plasma Dynamics, and Lasers Conference, 19th, Honolulu, HI, June 8-10, 1987. 10 p. refs (Contract DE-FG03-86ER-13608; NAG3-522) (AIAA PAPER 87-1309)

The mean streamwise development of pairs of longitudinal vortices embedded in an otherwise two-dimensional turbulent boundary layer was studied. Planes of closely spaced measurements of the three components of mean velocity were obtained at several streamwise locations, and the vorticity and circulation were calculated. Skin-friction measurements were also made. It was found that the rate of vorticity spreading in a vortex was greatly increased by close proximity of other vortices. The rate of streamwise circulation decrease was significantly greater for corotating vortices than for counter rotating vortices. Boundary-layer thinning and increased skin friction occurred in regions where the secondary flow induced by the pairs was directed toward the wall; the boundary layer was thickened and skin friction reduced where the secondary flow was directed away from the wall. Author

A87-42648*# National Aeronautics and Space Administration. Lewis Research Center, Cleveland, Ohio.

PARTICLE-LADEN SWIRLING FREE JETS - MEASUREMENTS AND PREDICTIONS

D. L. BULZAN (NASA, Lewis Research Center, Cleveland, OH), J.-S. SHUEN (Sverdrup Technology, Inc., Cleveland, OH), and G. M. FAETH (Michigan, University, Ann Arbor) AIAA, Aerospace Sciences Meeting, 25th, Reno, NV, Jan. 12-15, 1987. 29 p. Previously announced in STAR as N87-16826. refs (AIAA PAPER 87-0303)

A theoretical and experimental investigation of single-phase and particle-laden weakly swirling jets was conducted. The jets were injected vertically downward from a 19 mm diameter tube with swirl numbers ranging from 0 to 0.33. The particle-laden jets had a single loading ratio (0.2) with particles having an SMD of 39 micrometers. Mean and fluctuating properties of both phases

34 FLUID MECHANICS AND HEAT TRANSFER

were measured using nonintrusive laser based methods while particle mass flux was measured using an isokinetic sampling probe. The continuous phase was analyzed using both a baseline k-epsilon turbulence model and an extended version with modifications based on the flux Richardson number to account for effects of streamline curvature. To highlight effects of interphase transport rates and particle/turbulence interactions, effects of the particles were analyzed as follows: (1) locally homogeneous flow (LHF) analysis, where interphase transport rates are assumed to be infinitely fast; (2) deterministic separated flow (DSF) analysis, where finite interphase transport rates are considered but particle/turbulence interactions are ignored; and (3) stochastic separated flow (SSF) analysis, where both effects are considered using random-walk computations. Author

A87-43048*# National Aeronautics and Space Administration. Lewis Research Center, Cleveland, Ohio.

LIQUID SHEET RADIATOR

DONALD L. CHUBB and K. ALLAN WHITE, III (NASA, Lewis Research Center, Cleveland, OH) AIAA, Thermophysics Conference, 22nd, Honolulu, HI, June 8-10, 1987. 12 p. Previously announced in STAR as N87-18786. refs (AIAA PAPER 87-1525)

A new external flow radiator concept, the liquid sheet radiator (LSR), is introduced. The LSR sheet flow is described and an expression for the length/width (l/w) ratio is presented. A linear dependence of l/w on velocity is predicted that agrees with experimental results. Specific power for the LSR is calculated and is found to be nearly the same as the specific power of a liquid droplet radiator (LDR). Several sheet thicknesses and widths were experimentally investigated. In no case was the flow found to be unstable. Author

A87-43384*# Pennsylvania State Univ., University Park. **COMPUTATION OF ROTATING TURBULENT FLOW WITH AN ALGEBRAIC REYNOLDS STRESS MODEL**

MATTHEW J. WARFIELD and B. LAKSHMINARAYANA (Pennsylvania State University, University Park) AIAA Journal (ISSN 0001-1452), vol. 25, July 1987, p. 957-964. Previously cited in issue 08, p. 1037, Accession no. A86-22682. refs (Contract NGT-39-009-802; NSG-3266)

A87-43715*# Toledo Univ., Ohio.

NUMERICAL PREDICTION OF COLD TURBULENT FLOW IN COMBUSTOR CONFIGURATIONS WITH DIFFERENT CENTERBODY FLAME HOLDERS

C. N. YUNG, T. G. KEITH, JR., and K. J. DEWITT (Toledo, University, OH) ASME, Winter Annual Meeting, Anaheim, CA, Dec. 7-12, 1986. 9 p. refs (Contract NAG3-355) (ASME PAPER 86-WA/HT-50)

A numerical study of cold turbulent flow in a combustor containing a centerbody flame holder is presented. The axisymmetric Navier-Stokes equations incorporating a k-epsilon turbulence model were solved in a nonorthogonal curvilinear coordinate system. The finite volume method, applied to a staggered grid system, was used to discretize the differential equations. These finite differenced equations were then solved iteratively utilizing the SIMPLE algorithm described by Patankar (1980). Solutions were obtained for two combustor duct geometries with various centerbody flame holders which included a disk, a cone, and a sphere. The extent of mixing due to these bodies was evaluated. A comparison with previously obtained experimental data yielded moderately good agreement. Author

A87-44842*# University of Southern California, Los Angeles.

THE DESIGN AND PERFORMANCE OF A MULTI-STREAM DROPLET GENERATOR FOR THE LIQUID DROPLET RADIATOR

MELISSA ORME, T. FARNHAM, G. PHAM VAN DIEP, E. P. MUNTZ (Southern California, University, Los Angeles, CA), and ALAN WHITE (NASA, Lewis Research Center, Cleveland, OH) AIAA, Thermophysics Conference, 22nd, Honolulu, HI, June 8-10, 1987. 28 p. refs

(Contract NAS3-25068; F04611-84-K-0026)

(AIAA PAPER 87-1538)

Results are presented for the performance capabilities of a multistream droplet generator suitable for use in a spacecraft liquid droplet radiator heat-rejection system. The nozzle-motion mode of stream perturbation initiation was tested with a single droplet stream and found to produce data similar to those generated with the resonant cavity mode of perturbation. Tests then proceeded to a 26-orifice array; the streams of the array responded to the perturbation satisfactorily, forming uniformly separated drops. O.C.

A87-44930*# Flow Research, Inc., Kent, Wash.

ON DIRECT NUMERICAL SIMULATIONS OF TURBULENT REACTING FLOWS

W.-H. JOU (Flow Research Co., Kent, WA) and JAMES J. RILEY (Washington, University, Seattle) AIAA, Fluid Dynamics, Plasma Dynamics, and Lasers Conference, 19th, Honolulu, HI, June 8-10, 1987. 24 p. Research supported by the Johns Hopkins University. refs

(Contract NAS3-23531; NAS3-24229; F49620-85-C-0067;

N00014-84-C-0359; N00014-87-K-0174)

(AIAA PAPER 87-1324)

A description of the emerging field of direct numerical simulations of turbulent, chemically reacting flows is presented. The types of direct numerical simulations, physical issues related to implementing the simulations, as well as the various numerical methods used are described. Examples are presented of recent applications of direct numerical simulations to a variety of problems, displaying both the potential of the method and also some of its limitations. Finally, our view of the potential role of direct numerical simulations in future research on turbulent, chemically reacting flows is presented. Author

A87-44940*# National Aeronautics and Space Administration. Lewis Research Center, Cleveland, Ohio.

SPANWISE STRUCTURES IN TRANSITIONAL FLOW AROUND CIRCULAR CYLINDERS

H. J. KIM (NASA, Lewis Research Center, Cleveland, OH; Minnesota, University, Minneapolis), H. HIGUCHI, and C. FARELL (Minnesota, University, Minneapolis) AIAA, Fluid Dynamics, Plasma Dynamics, and Lasers Conference, 19th, Honolulu, HI, June 8-10, 1987. 5 p. refs

(AIAA PAPER 87-1383)

An experimental investigation of the flow around a smooth circular cylinder at the beginning of the critical transition, where the drag coefficient starts to decrease, was carried out. The measurements disclosed the presence of spanwise structures occurring symmetrically on both sides of the cylinder, associated with large amplitude, low frequency flow components. Mean pressure maps and spanwise cross correlations of pressures and velocities are presented. Author

A87-45325*# National Aeronautics and Space Administration. Lewis Research Center, Cleveland, Ohio.

REPRESENTATION OF THE VAPORIZATION BEHAVIOR OF TURBULENT POLYDISPERSE SPRAYS BY 'EQUIVALENT' MONODISPERSE SPRAYS

S. K. AGGARWAL (NASA, Lewis Research Center, Cleveland, OH) and J. S. SHUEN (NASA, Lewis Research Center; Sverdrup Technology, Inc., Cleveland, OH) AIAA, SAE, ASME, and ASEE, Joint Propulsion Conference, 23rd, San Diego, CA, June 29-July 2, 1987. 8 p. Previously announced in STAR as N87-16827. refs (AIAA PAPER 87-1954)

The concept of using an equivalent monodisperse spray to represent the vaporization behavior of polydisperse sprays has been examined by numerically solving two turbulent vaporizing sprays. One involves the injection of Freon-11 in a still environment, whereas the other is a methanol spray in a still but hot environment. The use of three different mean sizes, namely, Sauter mean diameter, volume median diameter, and surface-area mean diameter, has been investigated. Results indicate a good degree of correlation between the polydisperse spray and its equivalent monodisperse sprays represented by the volume median diameter and the Sauter mean diameter, the former giving slightly better results. The surface-area mean diameter does not provide as good a correlation as the other two mean diameters. Author

A87-45427*# National Aeronautics and Space Administration. Lewis Research Center, Cleveland, Ohio.

AGREEMENT BETWEEN EXPERIMENTAL AND THEORETICAL EFFECTS OF NITROGEN GAS FLOWRATE ON LIQUID JET ATOMIZATION

ROBERT D. INGEBRO (NASA, Lewis Research Center, Cleveland, OH) AIAA, SAE, ASME, and ASEE, Joint Propulsion Conference, 23rd, San Diego, CA, June 29-July 2, 1987. 10 p. Previously announced in STAR as N87-19684. refs (AIAA PAPER 87-2138)

Two-phase flows were investigated by using high velocity nitrogen gas streams to atomize small-diameter liquid jets. Tests were conducted primarily in the acceleration-wave regime for liquid jet atomization, where it was found that the loss of droplets due to vaporization had a marked effect on drop-size measurements. In addition, four identically designed two-fluid atomizers were fabricated and tested for similarity of spray profiles. A scattered-light scanner was used to measure a characteristic drop diameter, which was correlated with nitrogen gas flowrate. The exponent of 1.33 for nitrogen gas flowrate is identical to that predicted by atomization theory for liquid jet breakup in the acceleration-wave regime. This is higher than the value of 1.2 which was previously obtained at a sampling distance of 4.4 cm downstream of the atomizer. The difference is attributed to the fact that drop-size measurements obtained at a 2.2 cm sampling distance are less affected by vaporization and dispersion of small droplets and therefore should give better agreement with atomization theory. Profiles of characteristic drop diameters were also obtained by making at least five line-of-sight measurements across the spray at several horizontal positions above and below the center line of the spray. Author

A87-45637*# National Aeronautics and Space Administration. Lewis Research Center, Cleveland, Ohio.

RADIATIVE COOLING OF A LAYER WITH NONUNIFORM VELOCITY - A SEPARABLE SOLUTION

ROBERT SIEGEL (NASA, Lewis Research Center, Cleveland, OH) Journal of Thermophysics and Heat Transfer (ISSN 0887-8722), vol. 1, July 1987, p. 228-232. refs

Analyzed here is the cooling of a flowing plane layer filled with hot particles or liquid droplets that emit, absorb, and scatter radiation. The velocity distribution is nonuniform across the layer and the specified shape of this distribution affects the layer temperature distribution and emittance. The velocity distribution determined is one that will cause the layer to cool at a uniform temperature. Thus, if the layer initially has a uniform temperature, it will retain the same emittance throughout its length. A separable solution is found that applies in a 'fully developed' region following

an initial cooling length. In this developed region, the solution shows that there is a constant emittance based on the local heat loss and local bulk mean layer temperature. This emittance is a function of the velocity distribution, optical thickness, and scattering albedo. Author

A87-45646*# National Aeronautics and Space Administration. Lewis Research Center, Cleveland, Ohio.

GAS PARTICLE RADIATOR

DONALD L. CHUBB (NASA, Lewis Research Center, Cleveland, OH) Journal of Thermophysics and Heat Transfer (ISSN 0887-8722), vol. 1, July 1987, p. 285-288. refs

The performance of a new space radiator concept, the gas particle radiator (GPR), is studied. The GPR uses a gas containing submicron particles as the radiating medium contained between the radiator's emitting surface and a transparent window. For a modest volume fraction of submicron particles and gas thickness, it is found that the emissivity is determined by the window transmittance. The window must have a high transmittance in the infrared and be structurally strong enough to contain the gas-particle mixture. When the GPR is compared to a proposed titanium wall, potassium heat pipe radiator, with both radiators operating at a power level of 1.01 MW at 775 K, it is found that the GPR mass is 31 percent lower than that of the heat pipe radiator. C.D.

A87-45838* Massachusetts Inst. of Tech., Cambridge.

ROTATIONAL EFFECTS ON IMPINGEMENT COOLING

A. H. EPSTEIN, J. L. KERREBROCK, J. J. KOO, and U. Z. PREISER (MIT, Cambridge, MA) IN: Heat transfer and fluid flow in rotating machinery; Proceedings of the First International Symposium on Transport Phenomena, Honolulu, HI, Apr. 28-May 3, 1985. Washington, DC, Hemisphere Publishing Corp., 1987, p. 86-102. refs

(Contract NAG3-335)

The present consideration of rotation effects on heat transfer in a radially exhausted, impingement-cooled turbine blade model gives attention to experimental results for Reynolds and Rossby numbers and blade/coolant temperature ratio values that are representative of small gas turbine engines. On the basis of a model that encompasses the effects of Coriolis force and buoyancy on heat transfer, buoyancy is identified as the cause of an average Nusselt number that is 20-30 percent lower than expected from previous nonrotating data. A heuristic model is proposed which predicts that the impingement jets nearest the blade roots should deflect inward, due to a centripetal force generated by their tangential velocity counter to the blade motion. Potentially serious thermal stresses must be anticipated from rotation effects in the course of blade design. O.C.

A87-45851* Akron Univ., Ohio.

FINITE DIFFERENCE SOLUTION FOR A GENERALIZED REYNOLDS EQUATION WITH HOMOGENEOUS TWO-PHASE FLOW

M. J. BRAUN, R. L. WHEELER, III (Akron, University, OH), R. C. HENDRICKS (NASA, Lewis Research Center, Cleveland, OH), and R. L. MULLEN (Case Western Reserve University, Cleveland, OH) IN: Heat transfer and fluid flow in rotating machinery; Proceedings of the First International Symposium on Transport Phenomena, Honolulu, HI, Apr. 28-May 3, 1985. Washington, DC, Hemisphere Publishing Corp., 1987, p. 424-439. refs

An attempt is made to relate elements of two-phase flow and kinetic theory to the modified generalized Reynolds equation and to the energy equation, in order to arrive at a unified model simulating the pressure and flows in journal bearings, hydrostatic journal bearings, or squeeze film dampers when a two-phase situation occurs due to sudden fluid depressurization and heat generation. The numerical examples presented furnish a test of the algorithm for constant properties, and give insight into the effect of the shaft fluid heat transfer coefficient on the temperature profiles. The different level of pressures achievable for a given angular velocity depends on whether the bearing is thermal or

nonisothermal; upwind differencing is noted to be essential for the derivation of a realistic profile. O.C.

A87-45852* Case Western Reserve Univ., Cleveland, Ohio.
COMPARISON OF GENERALIZED REYNOLDS AND NAVIER STOKES EQUATIONS FOR FLOW OF A POWER LAW FLUID

R. L. MULLEN (Case Western Reserve University, Cleveland, OH), A. PREKWA (CHAM of North America, Inc., Huntsville, AL), M. J. BRAUN (Akron, University, OH), and R. C. HENDRICKS (NASA, Lewis Research Center, Cleveland, OH) IN: Heat transfer and fluid flow in rotating machinery; Proceedings of the First International Symposium on Transport Phenomena, Honolulu, HI, Apr. 28-May 3, 1985. Washington, DC, Hemisphere Publishing Corp., 1987, p. 440-460. refs

This paper compares a finite element solution of a modified Reynolds equation with a finite difference solution of the Navier-Stokes equation for a power law fluid. Both the finite element and finite difference formulation are reviewed. Solutions to spiral flow in parallel and conical geometries are compared. Comparison with experimental results are also given. The effects of the assumptions used in the Reynolds equation are discussed.

Author

A87-46199*# Aerometrics, Inc., Mountain View, Calif.
TWO-PHASE MEASUREMENTS OF A SPRAY IN THE WAKE OF A BLUFF BODY

R. C. RUDOFF, M. J. HOUSER, and W. D. BACHALO (Aerometrics, Inc., Mountain View, CA) IN: International Symposium on Air Breathing Engines, 8th, Cincinnati, OH, June 14-19, 1987, Proceedings. New York, American Institute of Aeronautics and Astronautics, 1987, p. 200-208. refs
 (Contract NAS3-24844; F49620-86-C-0078)

The dynamics of spray drop interaction with the turbulent, recirculating wake of a flat disk bluff body were investigated using a phase Doppler particle analyzer to determine drop size and velocity and the gas-phase velocity. Detailed measurements obtained included spray drop size, axial and radial velocity, angle of trajectory, and size-velocity correlations. The gas-phase velocity was determined from seeding of the two-phase flow. Results showed dramatic differences in drop behavior for various size classes when interacting with the turbulent flow field. Small drops were quickly entrained and recirculated, while initially, the larger drops continued in the general direction of the spray cone. Further downstream, significant numbers of large drops recirculated, generating a bifurcated size-velocity correlation. These lateral convections and streamwise accelerations and decelerations strongly influenced the number density along with size and velocity distributions. The complex interaction of the spray with the turbulent air-flow points out the need for spatially-resolved measurements that determine drop behavior for individual size classes, rather than characterizing a spray only via simple integral quantities such as the Sauter mean diameter.

Author

A87-47158* Brown Univ., Providence, R. I.
NONLINEAR BINARY-MODE INTERACTIONS IN A DEVELOPING MIXING LAYER

D. E. NIKITPOULOS and J. T. C. LIU (Brown University, Providence, RI) Journal of Fluid Mechanics (ISSN 0022-1120), vol. 179, June 1987, p. 345-370. DARPA-supported research. refs

(Contract NAG1-379; NAG3-673; NSF MSM-83-20307; NSF INT-85-14196; NATO-343/85)

This paper presents the formulation and results of two-wave interactions in a spatially developing shear layer, directed at understanding and interpreting the physical mechanisms that underlie the results of quantitative observation. The study confirms the existence of Kelly's (1967) mechanism that augments the growth of a subharmonic disturbance by extracting energy from its fundamental or vice versa. This mechanism is shown to be strongest in the region where the fundamental begins to return energy to the mean flow and the two wave modes are of comparable energy levels. It is found that the initial conditions and, especially, the initial phase angle between the two

disturbances play a very significant role in the modal development and that of the shear layer itself. A doubling of the shear-layer thickness is shown to take place; the two successive plateaux in its growth are attributed to the peaking in the energy production rates of the fundamental and subharmonic fluctuations. Author

A87-48047* National Aeronautics and Space Administration.
 Lewis Research Center, Cleveland, Ohio.
SHEAR FLOW INSTABILITY GENERATED BY NON-HOMOGENEOUS EXTERNAL FORCING

P. A. DURBIN (NASA, Lewis Research Center, Cleveland, OH) Journal of Sound and Vibration (ISSN 0022-460X), vol. 116, July 8, 1987, p. 188-190. refs

An experiment has been designed and conducted in order to ascertain whether instability waves can be generated by nonhomogeneous forcing, using a biconvex vane located outside the mixing layer whose oscillation was induced by an electromagnetic shaker through a linkage. The vane was oscillated at 20 Hz, and the resulting spectra were computed by a spectrum analyzer. The data are judged to provide an example of instability waves generated solely through nonhomogeneous forcing. O.C.

A87-48450* National Aeronautics and Space Administration.
 Lewis Research Center, Cleveland, Ohio.
SEPARATION OF VARIABLES SOLUTION FOR NON-LINEAR RADIATIVE COOLING

ROBERT SIEGEL (NASA, Lewis Research Center, Cleveland, OH) International Journal of Heat and Mass Transfer (ISSN 0017-9310), vol. 30, May 1987, p. 959-965. refs

A separation of variables solution has been obtained for transient radiative cooling of an absorbing-scattering plane layer. The solution applies after an initial transient period required for adjustment of the temperature and scattering source function distributions. The layer emittance, equal to the instantaneous heat loss divided by the fourth power of the instantaneous mean temperature, becomes constant. This emittance is a function of only the optical thickness of the layer and the scattering albedo; its behavior as a function of these quantities is considerably different than for a layer at constant temperature. Author

A87-48572*# National Aeronautics and Space Administration.
 Lewis Research Center, Cleveland, Ohio.

THERMODYNAMIC ANALYSIS AND SUBSCALE MODELING OF SPACE-BASED ORBIT TRANSFER VEHICLE CRYOGENIC PROPELLANT RESUPPLY

DAVID M. DEFELICE and JOHN C. AYDELOTT (NASA, Lewis Research Center, Cleveland, OH) AIAA, SAE, ASME, and ASCE, Joint Propulsion Conference, 23rd, San Diego, CA, June 29-July 2, 1987. 21 p. Previously announced in STAR as N87-22949. refs
 (AIAA PAPER 87-1764)

The resupply of the cryogenic propellants is an enabling technology for spacebased orbit transfer vehicles. As part of the NASA Lewis ongoing efforts in microgravity fluid management, thermodynamic analysis and subscale modeling techniques were developed to support an on-orbit test bed for cryogenic fluid management technologies. Analytical results have shown that subscale experimental modeling of liquid resupply can be used to validate analytical models when the appropriate target temperature is selected to relate the model to its prototype system. Further analyses were used to develop a thermodynamic model of the tank chilldown process which is required prior to the no-vent fill operation. These efforts were incorporated into two FORTRAN programs which were used to present preliminary analytical results. Author

A87-48726*# Clemson Univ., S.C.

HEAT TRANSFER AND FLUID MECHANICS MEASUREMENTS IN TRANSITIONAL BOUNDARY LAYERS ON CONVEX-CURVED SURFACES

T. WANG (Clemson, University, SC) and T. W. SIMON (Minnesota, University, Minneapolis) ASME, Transactions, Journal of Turbomachinery (ISSN 0889-504X), vol. 109, July 1987, p. 443-452. Research supported by the University of Minnesota and AMOCO Foundation. refs

(Contract NAG3-286)

(ASME PAPER 85-MT-60)

The test section of the present experiment to ascertain the effects of convex curvature and freestream turbulence on boundary layer momentum and heat transfer during natural transition provided a two-dimensional boundary layer flow on a uniformly heated curved surface, with bending to various curvature radii, R . Attention is given to results for the cases of $R = \text{infinity}$, 180 cm, and 90 cm, each with two freestream turbulence intensity levels. While the mild convex curvature of $R = 180$ cm delays transition, further bending to $R = 90$ cm leads to no significant further delay of transition. Cases with both curvature and higher freestream disturbance effects exhibit the latter's pronounced dominance. These data are pertinent to the development of transition prediction models for gas turbine blade design. O.C.

A87-48751* National Aeronautics and Space Administration. Lewis Research Center, Cleveland, Ohio.

NUMERICAL SIMULATION OF THE FLOW FIELD AND FUEL SPRAYS IN AN IC ENGINE

H. L. NGUYEN, H. J. SCHOCK (NASA, Lewis Research Center, Cleveland, OH), J. I. RAMOS (Carnegie-Mellon University, Pittsburgh, PA), M. H. CARPENTER (NASA, Langley Research Center, Hampton, VA), and J. D. STEGEMAN (Toledo, University, OH) SAE, International Congress and Exposition, Detroit, MI, Feb. 23-27, 1987. 28 p. Research supported by the U.S. Spain Committee for Scientific and Technological Cooperation. refs

(Contract NAG3-21; NAG3-689; NAG3-533)

(SAE PAPER 870599)

A two-dimensional model for axisymmetric piston-cylinder configurations is developed to study the flow field in two-stroke direct-injection Diesel engines under motored conditions. The model accounts for turbulence by a two-equation model for the turbulence kinetic energy and its rate of dissipation. A discrete droplet model is used to simulate the fuel spray, and the effects of the gas phase turbulence on the droplets is considered. It is shown that a fluctuating velocity can be added to the mean droplet velocity every time step if the step is small enough. Good agreement with experimental data is found for a range of ambient pressures in Diesel engine-type microenvironments. The effects of the intake swirl angle in the spray penetration, vaporization, and mixing in a uniflow-scavenged two-stroke Diesel engine are analyzed. It is found that the swirl increases the gas phase turbulence levels and the rates of vaporization. C.D.

A87-49551* National Aeronautics and Space Administration. Lewis Research Center, Cleveland, Ohio.

EXPERIMENTAL VERIFICATION OF CORROSIVE VAPOR DEPOSITION RATE THEORY IN HIGH VELOCITY BURNER RIGS

SULEYMAN A. GOKOGLU (NASA, Lewis Research Center; Case Western Reserve University, Cleveland, OH) and GILBERT J. SANTORO (NASA, Lewis Research Center; Cleveland, OH) IN: High temperature alloys for gas turbines and other applications 1986; Proceedings of the Conference, Liege, Belgium, Oct. 6-9, 1986. Part 2. Dordrecht, Netherlands, D. Reidel Publishing Co., 1986, p. 1117-1126. Previously announced in STAR as N86-22890. refs

The ability to predict deposition rates is required to facilitate modelling of high temperature corrosion by fused salt condensates in turbine engines. A corrosive salt vapor deposition theory based on multicomponent chemically frozen boundary layers (CFBL) has been successfully verified by high velocity burner rig experiments. The experiments involved internally air-impingement cooled, both

rotating full and stationary segmented cylindrical collectors located in the crossflow of sodium-seeded combustion gases. Excellent agreement is found between the CFBL theory and the experimental measurements for both the absolute amounts of Na_2SO_4 deposition rates and the behavior of deposition rate with respect to collector temperature, mass flowrate (velocity) and Na concentration. Author

A87-52049* Michigan State Univ., East Lansing.

A CRITICAL ANALYSIS OF TRANSVERSE VORTICITY MEASUREMENTS IN A LARGE PLANE SHEAR LAYER

J. F. FOSS, S. K. ALI, and R. C. HAW (Michigan State University, East Lansing) IN: Advances in turbulence; Proceedings of the First European Turbulence Conference, Ecully, France, July 1-4, 1986. Berlin and New York, Springer-Verlag, 1987, p. 446-455. Research supported by the Alexander von Humboldt-Stiftung. refs

(Contract NAG3-671)

An evaluation is made of the roles played in four-wire hot wire probe arrays by the influence of (1) the transverse velocity component on pitch angle measurement; (2) the instantaneous spatial gradient of the pitch angle on transverse vorticity computation; (3) the uncertainties in the magnitude of instantaneous pitch angle spatial gradient in the transverse vorticity computation; and (4) the spatial dimension of the microcirculation domain and the evaluation of transverse vorticity. Attention is given to the probe configuration and its computation algorithm. O.C.

A87-52320* Stanford Univ., Calif.

SIMULTANEOUS MEASUREMENTS OF TWO-DIMENSIONAL VELOCITY AND PRESSURE FIELDS IN COMPRESSIBLE FLOWS THROUGH IMAGE-INTENSIFIED DETECTION OF LASER-INDUCED FLUORESCENCE

BERNHARD HILLER, LAWRENCE M. COHEN, and RONALD K. HANSON (Stanford University, CA) IN: Flow visualization IV; Proceedings of the Fourth International Symposium, Paris, France, Aug. 26-29, 1986. Washington, DC, Hemisphere Publishing Corp., 1987, p. 173-178. refs

(Contract F49620-83-K-0004; NAG3-285)

A87-53589*# Houston Univ., Tex.

TRANSITION BOILING HEAT TRANSFER AND THE FILM TRANSITION REGIME

J. M. RAMILISON and J. H. LIENHARD (Houston, University, TX) ASME, Transactions, Journal of Heat Transfer (ISSN 0022-1481), vol. 109, Aug. 1987, p. 746-752. refs

(Contract NSF MEA-82-18708; NAG3-537)

The Berenson (1960) flat-plate transition-boiling experiment has been recreated with a reduced thermal resistance in the heater, and an improved access to those portions of the transition boiling regime that have a steep negative slope. Tests have been made in Freon-113, acetone, benzene, and n-pentane boiling on horizontal flat copper heaters that have been mirror-polished, 'roughened', or teflon-coated. The resulting data reproduce and clarify certain features observed by Berenson: the modest surface finish dependence of boiling burnout, and the influence of surface chemistry on both the minimum heat flux and the mode of transition boiling, for example. A rational scheme of correlation yields a prediction of the heat flux in what Witte and Lienhard (1982) previously identified as the 'film-transition boiling' region. It is also shown how to calculate the heat flux at the boundary between the pure-film, and the film-transition, boiling regimes, as a function of the advancing contact angle. Author

A87-54365* National Aeronautics and Space Administration. Lewis Research Center, Cleveland, Ohio.

GENERATION OF TOLLMIE-SCHLICHTING WAVES ON INTERACTIVE MARGINALLY SEPARATED FLOWS

M. E. GOLDSTEIN, S. J. LEIB (NASA, Lewis Research Center, Cleveland, OH), and S. J. COWLEY (Imperial College of Science and Technology, London, England) *Journal of Fluid Mechanics* (ISSN 0022-1120), vol. 181, Aug. 1987, p. 485-517. refs

This paper is concerned with the interaction of very-long-wavelength free-stream disturbances with the small but abrupt changes in the mean flow that occur near the minimum-skin-friction point in an interactive marginally separated boundary layer. The source frequency is chosen so that the eigensolutions with that frequency have an 'interactive' structure in the region of marginal separation. The eigensolution wavelength scale must then differ from the lengthscale of the marginal separation, and a composite expansion technique has to be used to obtain the solution. The initial instability wave amplitude turns out to be exponentially small, but eventually dominates the original disturbance owing to its exponential growth. It then begins to decay but ultimately turns into a standard spatially growing Tollmien-Schlichting wave much further downstream. Author

A87-54366* National Aeronautics and Space Administration. Lewis Research Center, Cleveland, Ohio.

A NOTE ON THE GENERATION OF TOLLMIE-SCHLICHTING WAVES BY SUDDEN SURFACE-CURVATURE CHANGE

M. E. GOLDSTEIN and LENNART S. HULTGREN (NASA, Lewis Research Center, Cleveland, OH) *Journal of Fluid Mechanics* (ISSN 0022-1120), vol. 181, Aug. 1987, p. 519-525. refs

This note is primarily concerned with the generation of spatially growing Tollmien-Schlichting waves by the interaction of very long-wavelength free-stream disturbances with a discontinuity in the curvature of a bounding surface (whose slope may or may not be continuous). The theory is combined with a numerical solution of the local Orr-Sommerfeld equation, and the result is used to predict the Tollmien-Schlichting amplitude in a relevant experiment carried out by Leehey and Shapiro (1980). The calculated results are in satisfactory agreement with their observations. Author

N87-11124*# National Aeronautics and Space Administration. Lewis Research Center, Cleveland, Ohio.

THERMOHYDRODYNAMIC ANALYSIS FOR LAMINAR LUBRICATING FILMS

H. G. ELROD and D. E. BREWE 1986 14 p Presented at the Leeds-Lyon Symposium on Tribology, Leeds, England, 8-12 Sep. 1986

(NASA-TM-88845; E-3235; NAS 1.15:88845; USAAVSCOM-TR-86-C-33) Avail: NTIS HC A02/MF A01 CSCL 20M

A Galerkin-type analysis to include thermal effects in laminar lubricating films was performed. The lubricant properties were assumed constant except for a temperature-dependent Newtonian viscosity. The cross-film temperature profile is established by collocation at the film boundaries and two interior Lobatto points. The interior temperatures are determined by requiring that the zeroth and first moment of the energy equation be satisfied across the film. The fluidity is forced to conform to a third-degree polynomial appropriate to the Lobatto-point temperatures. Preliminary indications are that the use of just two such sampling points enables satisfactory prediction of bearing performance even in the presence of substantial viscosity variation. Author

N87-11184*# National Aeronautics and Space Administration. Lewis Research Center, Cleveland, Ohio.

HOST TURBINE HEAT TRANSFER OVERVIEW

J. E. ROHDE *In its Turbine Engine Hot Section Technology*, 1984 6 p Oct. 1984

Avail: NTIS HC A17/MF A01 CSCL 20D

Improved methods of predicting airfoil local metal temperatures require advances in the understanding of the physics and methods of analytically predicting the following four aerothermal loads: hot

gas flow over airfoils, heat transfer rates on the gas-side of airfoils, cooling air flow inside airfoils, and heat transfer rates on the coolant-side of airfoils. A systematic building block research approach is being pursued to investigate these four areas of concern from both the experimental and analytical sides. Experimental approaches being pursued start with fundamental experiments using simple shapes and flat plates in wind tunnels, progress to more realistic cold and hot cascade tests using airfoils, continue to progress in large low-speed rigs and turbines and warm turbines, and finally, combine all the interactive effects in tests using real engines or real engine type turbine rigs. Analytical approaches being pursued also build from relatively simple steady two dimensional inviscid flow and boundary layer heat transfer codes to more advanced steady two and three dimensional viscous flow and heat transfer codes. These advanced codes provide more physics to model better the interactive effects and the true real-engine environment. Author

N87-11201*# United Technologies Research Center, East Hartford, Conn.

MASS AND MOMENTUM TURBULENT TRANSPORT EXPERIMENTS

B. V. JOHNSON and R. ROBACK *In NASA. Lewis Research Center Turbine Engine Hot Section Technology*, 1984 10 p Oct. 1984

(Contract NAS3-22771)

Avail: NTIS HC A17/MF A01 CSCL 20D

An experimental study of mixing downstream of axial and swirling coaxial jets is being conducted to obtain data for the evaluation and improvement of turbulent transport models currently employed in a variety of computational procedures used throughout the propulsion community. Effort was directed toward the acquisition of length scale and dissipation rate data that will provide more accurate inlet boundary conditions for the computational procedures and a data base to evaluate the turbulent transport models in the near jet region where recirculation does not occur. Mass and momentum turbulent transport data with a blunt inner-jet inlet configuration will also be acquired. B.G.

N87-11219*# General Motors Corp., Detroit, Mich. Gas Turbine Div.

TURBINE AIRFOIL GAS SIDE HEAT TRANSFER

E. R. TURNER *In NASA. Lewis Research Center Turbine Engine Hot Section Technology*, 1984 14 p Oct. 1984

(Contract NAS3-23695)

Avail: NTIS HC A17/MF A01 CSCL 20D

Work is currently underway to develop and characterize an analytical approach, based on boundary layer theory, for predicting the effects of leading edge (showerhead) film cooling on downstream gas side heat transfer rates. Parallel to this work, experiments are being conducted to build a relevant data base for present and future methods verification. Author

N87-11220*# Scientific Research Associates, Inc., Glastonbury, Conn.

CALCULATION OF TWO- AND THREE-DIMENSIONAL TRANSONIC CASCADE FLOW FIELD USING THE NAVIER-STOKES EQUATIONS

B. C. WEINBERG, R. J. YANG, S. J. SHAMROTH, and H. MCDONALD *In NASA. Lewis Research Center Turbine Engine Hot Section Technology*, 1984 8 p Oct. 1984

(Contract NAS3-23695)

Avail: NTIS HC A17/MF A01 CSCL 20D

A Navier-Stokes analysis employing the time-dependent Linearized Block Implicit scheme (LBI) was applied to two-dimensional and three-dimensional transonic turbulent cascade flows. In general, the geometrical configuration of the turbine blade impacts both the grid construction procedure and the implementation of the numerical algorithm. Since modern turbine blades of interest are characterized by very blunt leading edges, rounded trailing edges and high stacking angles, a robust grid construction procedure is required that can accommodate the severe body shape while resolving regions of large flow gradients. A

constructive O-type grid generation technique, suitable for cascades with rounded trailing edges, was developed and used to construct the C3X turbine cascade coordinate grid. Two-dimensional calculations were performed employing the Navier-Stokes procedure for the C3X turbine cascade, and the predicted pressure coefficients and heat transfer rates were compared with the experimental data. Three-dimensional Navier-Stokes calculations were also performed. B.G.

**N87-11223*# Tennessee Univ. Space Inst., Tullahoma.
GAS FLOW ENVIRONMENTAL AND HEAT TRANSFER
NONROTATING 3D PROGRAM**

R. A. CRAWFORD /in NASA. Lewis Research Center Turbine Engine Hot Section Technology, 1984 5 p Oct. 1984
(Contract NAS3-23278)

Avail: NTIS HC A17/MF A01 CSCL 20D

The experimental contract objective is to provide a complete set of benchmark quality data for the flow within a large rectangular turning duct. The data are to be used to evaluate and verify three-dimensional internal viscous flow models and computational codes. The analytical contract objective is to select such a computational code and define the capabilities of this code to predict the experimental results. Details of the proper code operation will be defined and improvements to the code modeling capabilities will be formulated. Author

**N87-11224*# United Technologies Research Center, East
Hartford, Conn.
ASSESSMENT OF A 3-D BOUNDARY LAYER CODE TO
PREDICT HEAT TRANSFER AND FLOW LOSSES IN A
TURBINE**

O. L. ANDERSON /in NASA. Lewis Research Center Turbine Engine Hot Section Technology, 1984 6 p Oct. 1984
(Contract NAS3-23716)

Avail: NTIS HC A17/MF A01 CSCL 20D

Zonal concepts are utilized to delineate regions of application of three-dimensional boundary layer (DBL) theory. The zonal approach requires three distinct analyses. A modified version of the 3-DBL code named TABLET is used to analyze the boundary layer flow. This modified code solves the finite difference form of the compressible 3-DBL equations in a nonorthogonal surface coordinate system which includes coriolis forces produced by coordinate rotation. These equations are solved using an efficient, implicit, fully coupled finite difference procedure. The nonorthogonal surface coordinate system is calculated using a general analysis based on the transfinite mapping of Gordon which is valid for any arbitrary surface. Experimental data is used to determine the boundary layer edge conditions. The boundary layer edge conditions are determined by integrating the boundary layer edge equations, which are the Euler equations at the edge of the boundary layer, using the known experimental wall pressure distribution. Starting solutions along the inflow boundaries are estimated by solving the appropriate limiting form of the 3-DBL equations. B.G.

**N87-11961*# Wisconsin Univ., Milwaukee. Dept. of Mechanical
Engineering.**

**THIRD-MOMENT CLOSURE OF TURBULENCE FOR
PREDICTIONS OF SEPARATING AND REATTACHING SHEAR
FLOWS: A STUDY OF REYNOLDS-STRESS CLOSURE MODEL
Final Report**

R. S. AMANO and P. GOEL Sep. 1986 91 p
(Contract NAG3-546)

(NASA-CR-177055; NAS 1.26:177055; TF/86/9) Avail: NTIS HC A05/MF A01 CSCL 20D

A numerical study of computations in backward-facing steps with flow separation and reattachment, using the Reynolds stress closure is presented. The highlight of this study is the improvement of the Reynold-stress model (RSM) by modifying the diffusive transport of the Reynolds stresses through the formulation, solution and subsequent incorporation of the transport equations of the third moments, $\bar{u}(i)\bar{u}(j)\bar{u}(k)$, into the turbulence model. The diffusive transport of the Reynolds stresses, represented by the

gradients of the third moments, attains greater significance in recirculating flows. The third moments evaluated by the development and solution of the complete transport equations are superior to those obtained by existing algebraic correlations. A low-Reynolds number model for the transport equations of the third moments is developed and considerable improvement in the near-wall profiles of the third moments is observed. The values of the empirical constants utilized in the development of the model are recommended. The Reynolds-stress closure is consolidated by incorporating the equations of k and ϵ , containing the modified diffusion coefficients, and the transport equations of the third moments into the Reynolds stress equations. Computational results obtained by the original k - ϵ model, the original RSM and the consolidated and modified RSM are compared with experimental data. Overall improvement in the predictions is seen by consolidation of the RMS and a marked improvement in the profiles of $\bar{u}(i)\bar{u}(j)\bar{u}(k)$ is obtained around the reattachment region. M.G.

**N87-11962*# National Aeronautics and Space Administration.
Lewis Research Center, Cleveland, Ohio.**

**EFFECT OF VIBRATION AMPLITUDE ON VAPOR CAVITATION
IN JOURNAL BEARINGS**

D. E. BREWE and B. O. JACOBSON (Lulea Univ, Sweden)
1986 17 p Presented at the Nordic Symposium on Tribology, Lulea, Sweden, 15-18 Jun. 1986; sponsored by the Royal Swedish Academy of Engineering Sciences

(NASA-TM-88826; E-3200; NAS 1.15:88826;
USAAVSCOM-TR-86-C-26) Avail: NTIS HC A02/MF A01 CSCL 20D

Computational movies were used to analyze the formation and collapse of vapor cavitation bubbles in a submerged journal bearing. The effect of vibration amplitude on vapor cavitation was studied for a journal undergoing circular whirl. The boundary conditions were implemented using Elrod's algorithm, which conserves mass flow through the cavitation bubble as well as through the oil-film region of the bearing. The vibration amplitudes for the different cases studied resulted in maximum eccentricity ratios ranging from 0.4 to 0.9. The minimum eccentricity ratio reached in each case was 0.1. For the least vibration amplitude studied in which the eccentricity ratio varied between 0.1 and 0.4, no vapor cavitation occurred. The largest vibration amplitude (i.e., eccentricity ratios of 0.1 to 0.9) resulted in vapor cavitation present 76 percent of one complete orbit. Author

**N87-13661*# General Motors Corp., Indianapolis, Ind. Allison
Gas Turbine Div.**

**TURBINE VANE EXTERNAL HEAT TRANSFER. VOLUME 2.
NUMERICAL SOLUTIONS OF THE NAVIER-STOKES
EQUATIONS FOR TWO- AND THREE-DIMENSIONAL TURBINE
CASCADES WITH HEAT TRANSFER Final Report**

R. J. YANG, B. C. WEINBERG, S. J. SHAMROTH, and H. MCDONALD Jul. 1985 160 p

(Contract NAS3-23695)

(NASA-CR-174828; NAS 1.26:174828; ALLISON-EDR-11984)

Avail: NTIS HC A08/MF A01 CSCL 20D

The application of the time-dependent ensemble-averaged Navier-Stokes equations to transonic turbine cascade flow fields was examined. In particular, efforts focused on an assessment of the procedure in conjunction with a suitable turbulence model to calculate steady turbine flow fields using an O-type coordinate system. Three cascade configurations were considered. Comparisons were made between the predicted and measured surface pressures and heat transfer distributions wherever available. In general, the pressure predictions were in good agreement with the data. Heat transfer calculations also showed good agreement when an empirical transition model was used. However, further work in the development of laminar-turbulent transitional models is indicated. The calculations showed most of the known features associated with turbine cascade flow fields. These results indicate the ability of the Navier-Stokes analysis to predict, in reasonable amounts of computation time, the surface pressure distribution, heat transfer rates, and viscous flow

34 FLUID MECHANICS AND HEAT TRANSFER

development for turbine cascades operating at realistic conditions. Author

N87-15441*# National Aeronautics and Space Administration. Lewis Research Center, Cleveland, Ohio.

TWO- AND THREE-DIMENSIONAL VISCOUS COMPUTATIONS OF A HYPERSONIC INLET FLOW

WILLIAM G. KUNIK, THOMAS J. BENSON, WING-FAI NG (Virginia Polytechnic Inst. and State Univ., Blacksburg), and ARTHUR TAYLOR Jan. 1987 17 p Prepared for the 25th Aerospace Sciences Meeting, Reno, Nev., 12-15 Jan. 1987; sponsored by AIAA

(NASA-TM-88923; E-3356; NAS 1.15:88923; AIAA-87-0283)

Avail: NTIS HC A02/MF A01 CSCL 20D

The three-dimensional parabolized Navier-Stokes code has been used to investigate the flow through a Mach 7.4 inlet. A two-dimensional parametric study of grid resolution, turbulence modeling and effect of gamma has been done and compared with experimental results. The results show that mesh resolution of the shock waves, real gas effects and turbulence length scaling are very important to get accurate results for hypersonic inlet flows. In addition a three-dimensional calculation of the Mach 7.4 inlet has been done on a straight sideplate configuration. The results show that the glancing shock/boundary layer interaction phenomena causes significant three-dimensional flow in the inlet.

Author

N87-15442*# National Aeronautics and Space Administration. Lewis Research Center, Cleveland, Ohio.

EVALUATION OF SEALS FOR HIGH-PERFORMANCE CRYOGENIC TURBOMACHINES

R. C. HENDRICKS, L. T. TAM (CHAM of North America, Inc., Huntsville, Ala.), M. J. BRAUN (Akron Univ., Ohio), and B. L. VLCEK (Rensselaer Polytechnic Inst., Troy, N.Y.) 1987 15 p Prepared for presentation at the 17th International Congress of Refrigeration, Vienna, Austria, 24-29 Aug. 1987

(NASA-TM-88919; E-3348; NAS 1.15:88919) Avail: NTIS HC

A02/MF A01 CSCL 11A

An approach to computing flow and dynamic characteristics for seals or bearings is discussed. The local average velocity was strongly influenced by inlet and exit effects and fluid injection, which in turn drove zones of secondary flow. For the restricted three-dimensional model considered, the integral averaged results were in reasonable agreement with selected data. Unidirectional pressure measurements alone were insufficient to define such flow variations. However, for seal and bearing leakage correlations the principles of corresponding states were found to be useful. Also discussed are three phenomena encountered during testing of three eccentric nonrotating seal configurations for the Space Shuttle Main Engine (SSME) Program. Fluid injection, choking within a seal, and pressure profile crossover are related to postulated zones of secondary flow or separation and to direct stiffness.

Author

N87-17001*# National Aeronautics and Space Administration. Lewis Research Center, Cleveland, Ohio.

ANALYSIS OF VISCOUS TRANSONIC FLOW OVER AIRFOIL SECTIONS

DENNIS L. HUFF, JIUNN-CHI WU (Georgia Inst. of Tech., Atlanta), and L. N. SANKAR Jan. 1987 32 p Presented at the 25th Aerospace Sciences Meeting, Reno, Nev., 12-15 Jan. 1987; sponsored by AIAA

(NASA-TM-88912; E-3340; NAS 1.15:88912; AIAA-87-0420)

Avail: NTIS HC A03/MF A01 CSCL 20D

A full Navier-Stokes solver has been used to model transonic flow over three airfoil sections. The method uses a two-dimensional, implicit, conservative finite difference scheme for solving the compressible Navier-Stokes equations. Results are presented as prescribed for the Viscous Transonic Airfoil Workshop to be held at the AIAA 25th Aerospace Sciences Meeting. The NACA 0012, RAE 2822 and Jones airfoils have been investigated for both attached and separated transonic flows. Predictions for pressure distributions, loads, skin friction coefficients, boundary layer

displacement thickness and velocity profiles are included and compared with experimental data when possible. Overall, the results are in good agreement with experimental data. Author

N87-17002*# National Aeronautics and Space Administration. Lewis Research Center, Cleveland, Ohio.

A GENERAL METHOD FOR UNSTEADY STAGNATION REGION HEAT TRANSFER AND RESULTS FOR MODEL TURBINE FLOWS

TUNCER CEBECI (California State Univ., Long Beach), ANDREAS KRAINER (Naval Postgraduate School, Monterey, Calif.), ROBERT J. SIMONEAU, and MAX F. PLATZER 1987 8 p Proposed for presentation at the 2nd Thermal Engineering Conference, Honolulu, Hawaii, 22-27 Mar. 1987; sponsored by the ASME and JSME

(NASA-TM-88903; E-3329; NAS 1.15:88903) Avail: NTIS HC

A02/MF A01 CSCL 20D

Recent experiments suggest that the heat-transfer characteristics of stator blades are influenced by the frequency of passing of upstream rotor blades. The calculation of these effects requires that the movement of the stagnation point with variations in freestream velocity is properly represented together with the possible effects of turbulence characteristics on the thin leading-edge boundary layer. A procedure to permit the achievement of these purposes is described for laminar flows in this paper together with results of its application to two model problems which demonstrate its abilities and quantify the influence of wake characteristics on fluid-dynamic and heat-transfer properties of the flow and their effects on surface heat transfer. Author

N87-17003*# Texas A&M Univ., College Station. Turbomachinery Labs.

MEASUREMENT OF HEAT TRANSFER AND PRESSURE DROP IN RECTANGULAR CHANNELS WITH TURBULENCE PROMOTERS Final Report

J. C. HAN, J. S. PARK, and M. Y. IBRAHIM Washington NASA Sep. 1986 203 p

(Contract NAS3-24227; DA PROJ. 1L1-62209-AH-76)

(NASA-CR-4015; E-3164; NAS 1.26:4015; AVSCOM-TR-86-C-25)

Avail: NTIS HC A10/MF A01 CSCL 20D

Periodic rib turbulators were used in advanced turbine cooling designs to enhance the internal heat transfer. The objective of the present project was to investigate the combined effects of the rib angle of attack and the channel aspect ratio on the local heat transfer and pressure drop in rectangular channels with two opposite ribbed walls for Reynolds number varied from 10,000 to 60,000. The channel aspect ratio (W/H) was varied from 1 to 2 to 4. The rib angle of attack (α) was varied from 90 to 60 to 45 to 30 degree. The highly detailed heat transfer coefficient distribution on both the smooth side and the ribbed side walls from the channel sharp entrance to the downstream region were measured. The results showed that, in the square channel, the heat transfer for the slant ribs ($\alpha = 30$ -45 deg) was about 30% higher than that of the transverse ribs ($\alpha = 90$ deg) for a constant pumping power. However, in the rectangular channels (W/H = 2 and 4, ribs on W side), the heat transfer at $\alpha = 30$ -45 deg was only about 5% higher than 90 deg. The average heat transfer and friction correlations were developed to account for rib spacing, rib angle, and channel aspect ratio over the range of roughness Reynolds number. GRA

N87-18034*# National Aeronautics and Space Administration. Lewis Research Center, Cleveland, Ohio.

JET MODEL FOR SLOT FILM COOLING WITH EFFECT OF FREE-STREAM AND COOLANT TURBULENCE

FREDERICK F. SIMON Oct. 1986 21 p

(NASA-TP-2655; E-2961; NAS 1.60:2655) Avail: NTIS HC

A02/MF A01 CSCL 20D

An analysis was performed utilizing the model of a wall jet for obtaining equations that will predict slot film-cooling efficiency under conditions of variable turbulence intensity, flow, and temperature. The analysis, in addition to assessing the effects of the above

variables, makes a distinction between an initial region and a fully developed region. Such a distinction is important in determining the role that the turbulence intensity of the coolant plays in effecting film-cooling effectiveness in the area of the slot exit. The results of the analysis were used in the correlation of the results of a well-designed film-cooling experiment. The result of the analysis and experiment was equations that predicted film-cooling efficiency within + or - 4% average deviation for lateral free-stream turbulence intensities up to 24% and blowing rates up to 1.9. These equations should be useful in determining the optimum quantity of cooling air required for protecting the wall of a combustor. Author

N87-18035*# National Aeronautics and Space Administration. Lewis Research Center, Cleveland, Ohio.

VELOCITY PROFILES IN LAMINAR DIFFUSION FLAMES

VALERIE J. LYONS and JANICE M. MARGLE (Pennsylvania State Univ., Abington) May 1986 13 p Presented at the Combustion Inst. Meeting, Cleveland, Ohio, 5-6 May 1986 (NASA-TP-2596; E-2879; NAS 1.60:2596) Avail: NTIS HC A02/MF A01 CSCL 20D

Velocity profiles in vertical laminar diffusion flames were measured by using laser Doppler velocimetry (LDV). Four fuels were used: n-heptane, iso-octane, cyclohexane, and ethyl alcohol. The velocity profiles were similar for all the fuels, although there were some differences in the peak velocities. The data compared favorably with the theoretical velocity predictions. The differences could be attributed to errors in experimental positioning and in the prediction of temperature profiles. Error in the predicted temperature profiles are probably due to the difficulty in predicting the radiative heat losses from the flame. Author

N87-18784*# National Aeronautics and Space Administration. Lewis Research Center, Cleveland, Ohio.

THERMOMECHANICAL BEHAVIOR OF PLASMA-SPRAYED ZRO2-Y2O3 COATINGS INFLUENCED BY PLASTICITY, CREEP AND OXIDATION

J. PADOVAN (Akron Univ., Ohio), B. T. F. CHUNG, GLEN E. MCDONALD, and ROBERT C. HENDRICKS 1987 15 p Presented at the 11th Annual Conference on Composites, Advanced Ceramics and Composite Materials, Cocoa Beach, Fla., 18-23 Jan. 1987; sponsored by NASA, DOD and the American Ceramic Society (NASA-TM-88940; E-3385; NAS 1.15:88940) Avail: NTIS HC A02/MF A01 CSCL 20D

Thermocycling of ceramic-coated turbomachine components produces high thermomechanical stresses that are mitigated by plasticity and creep but aggravated by oxidation, with residual stresses exacerbated by all three. These residual stresses, coupled with the thermocyclic loading, lead to high compressive stresses that cause the coating to spall. A ceramic-coated gas path seal is modeled with consideration given to creep, plasticity, and oxidation. The resulting stresses and possible failure modes are discussed. Author

N87-18786*# National Aeronautics and Space Administration. Lewis Research Center, Cleveland, Ohio.

LIQUID SHEET RADIATOR

DONALD L. CHUBB and K. ALAN WHITE, III 1987 13 p Prepared for presentation at the 22nd Thermophysics Conference, Honolulu, Hawaii, 8-10 Jul. 1987; sponsored by AIAA (NASA-TM-89841; E-3497; NAS 1.15:89841) Avail: NTIS HC A02/MF A01 CSCL 20D

A new external flow radiator concept; the liquid sheet radiator (LSR), is introduced. The LSR sheet flow is described and an expression for the length/width (l/w), ratio is presented. A linear dependence of l/w on velocity is predicted that agrees with experimental results. Specific power for the LSR is calculated and is found to be nearly the same as the specific power of a liquid droplet radiator; (LDR). Several sheet thicknesses and widths were experimentally investigated. In no case was the flow found to be unstable. Author

N87-19647*# Georgia Inst. of Tech., Atlanta. School of Mechanical Engineering.

FEASIBILITY ANALYSIS OF RECIPROCATING MAGNETIC HEAT PUMPS Semiannual Status Report, 2 Jul. 1985 - 2 Jan. 1986

A. V. LARSON, J. G. HARTLEY, S. V. SHELTON, and M. M. SMITH Jan. 1986 11 p (Contract NAG3-600) (NASA-CR-180262; NAS 1.26:180262) Avail: NTIS HC A02/MF A01 CSCL 20D

The conceptual design selected for detailed system analysis and optimization is the reciprocating gadolinium core in a regenerative fluid column within the bore of a superconducting magnet. The thermodynamic properties of gadolinium are given. A computerized literature search for relevant papers was conducted and is being analyzed. Contact was made with suppliers of superconducting magnets and accessories, magnetic materials, and various types of hardware. A description of the model for the thermal analysis of the core and regenerator fluids is included. B.G.

N87-20270*# National Aeronautics and Space Administration. Lewis Research Center, Cleveland, Ohio.

MODELING TURBULENT, REACTING FLOW

RUSSELL W. CLAUS In its NASA-Chinese Aeronautical Establishment (CAE) Symposium p 31-46 1986 Avail: NTIS HC A01/MF A01 CSCL 20D

Several of the approximations or models involved in the development of a numerical combustor flow code are examined. In the first section, the importance of numerical accuracy is illustrated, and the impact that improved-accuracy schemes have on slowing convergence is demonstrated. Solution algorithms that can speed convergence are discussed and some performance features of these algorithms are illustrated. A sample calculation displaying the importance of boundary conditions on a three-dimensional numerical prediction is presented. The inaccuracy of a current turbulence model in highly turbulent (nonequilibrium) regions is described. Finally, the surprisingly good performance of a six-flux model in describing radiation heat transfer is displayed. In all the areas examined, continued research is still needed, but valuable engineering tools are available today. Author

N87-20272*# National Aeronautics and Space Administration. Lewis Research Center, Cleveland, Ohio.

TWO-PHASE FLOW

ROBERT R. TACINA In its NASA-Chinese Aeronautical Establishment (CAE) Symposium p 63-87 1986 Avail: NTIS HC A01/MF A01 CSCL 20D

An experimental program to characterize the spray from candidate nozzles for icing-cloud simulation is discussed. One candidate nozzle, which is currently used for icing research, has been characterized for flow and drop size. The median-volume diameter (MVD) from this air-assist nozzle is compared with correlations in the literature. The new experimental spray facility is discussed, and the drop-size instruments are discussed in detail. Since there is no absolute standard for drop-size measurements and there are other limitations, such as drop-size range and velocity range, several instruments are used and results are compared. A two-phase model was developed at Pennsylvania State University. The model uses the k-epsilon model of turbulence in the continuous phase. Three methods for treating the discrete phase are used: (1) a locally homogeneous flow (LHF) model, (2) a deterministic separated flow (DSF) model, and (3) a stochastic separated flow (SSF) model. In the LHF model both phases have the same velocity and temperature at each point. The DSF model provides interphase transport but ignores the effects of turbulent fluctuations. In the SSF model the drops interact with turbulent eddies whose properties are determined by the k-epsilon turbulence model. The two-phase flow model has been extended to include the effects of evaporation and combustion. Author

N87-20276*# National Aeronautics and Space Administration. Lewis Research Center, Cleveland, Ohio.

EXPERIMENTS AND MODELING OF DILUTION JET FLOW FIELDS

JAMES D. HOLDEMAN *In its* NASA-Chinese Aeronautical Establishment (CAE) Symposium p 149-174 1986
 Avail: NTIS HC A01/MF A01 CSCL 20D

Experimental and analytical results of the mixing of single, double, and opposed rows of jets with an isothermal or variable-temperature main stream in a straight duct are presented. This study was performed to investigate flow and geometric variations typical of the complex, three-dimensional flow field in the dilution zone of gas-turbine-engine combustion chambers. The principal results, shown experimentally and analytically, were the following: (1) variations in orifice size and spacing can have a significant effect on the temperature profiles; (2) similar distributions can be obtained, independent of orifice diameter, if momentum-flux ratio and orifice spacing are coupled; (3) a first-order approximation of the mixing of jets with a variable-temperature main stream can be obtained by superimposing the main-stream and jets-in-an-isothermal-crossflow profiles; (4) the penetration of jets issuing mixing is slower and is asymmetric with respect to the jet centerlines, which shift laterally with increasing downstream distance; (5) double rows of jets give temperature distributions similar to those from a single row of equally spaced, equal-area circular holes; (6) for opposed rows of jets, with the orifice centerlines in line, the optimum ratio of orifice spacing to duct height is one-half the optimum value for single-side injection at the same momentum-flux ratio and (7) for opposed rows of jets, with the orifice centerlines staggered, the optimum ratio of orifice spacing to duct height is twice the optimum value for single-side injection at the same momentum-flux ratio. Author

N87-20504*# National Aeronautics and Space Administration. Lewis Research Center, Cleveland, Ohio.

A FINITE DIFFERENCE SCHEME FOR THREE-DIMENSIONAL STEADY LAMINAR INCOMPRESSIBLE FLOW

DANNY P. HWANG and HUNG T. HUYNH 1987 16 p Proposed for presentation at the 5th International Conference on Numerical Methods in Laminar and Turbulent Flow, Montreal, Quebec, 6-10 Jul. 1987; sponsored by Concordia Univ., P and W Canada, International Journal for Numerical Methods in Fluids (NASA-TM-89851; E-3513; NAS 1.15:89851) Avail: NTIS HC A02/MF A01 CSCL 20D

A finite difference scheme for three-dimensional steady laminar incompressible flows is presented. The Navier-Stokes equations are expressed conservatively in terms of velocity and pressure increments (delta form). First order upwind differences are used for first order partial derivatives of velocity increments resulting in a diagonally dominant matrix system. Central differences are applied to all other terms for second order accuracy. The SIMPLE pressure correction algorithm is used to satisfy the continuity equation. Numerical results are presented for cubic cavity flow problems for Reynolds numbers up to 2000 and are in good agreement with other numerical results. Author

N87-21257*# United Technologies Research Center, East Hartford, Conn. Experimental Gas Dynamics Group.

FLOWFIELD MEASUREMENTS IN A SEPARATED AND REATTACHED FLAT PLATE TURBULENT BOUNDARY LAYER Final Report

WILLIAM P. PATRICK Washington NASA Mar. 1987 245 p (Contract NAS3-22770) (NASA-CR-4052; E-3254; NAS 1.26:4052) Avail: NTIS HC A11/MF A01 CSCL 20D

The separation and reattachment of a large-scale, two-dimensional turbulent boundary layer at low subsonic speed on a flat plate has been studied experimentally. The separation bubble was 55 cm long and had a maximum bubble thickness, measured to the height of the mean dividing streamline, of 17 cm, which was twice the thickness of the inlet boundary layer. A combination of laser velocimetry, hot-wire anemometry, pneumatic probing techniques, and flow visualization were used as diagnostics.

Principal findings were that an outer inviscid rotational flow was defined which essentially convected over the blockage associated with the inner, viscously dominated bubble recirculation region. A strong backflow region in which the flow moved upstream 100 percent of the time was measured near the test surface over the central 35 percent of the bubble. A laminar backflow boundary layer having pseudo-turbulent characteristics including a log-linear velocity profile was generated under the highly turbulent backflow. Velocity profile shapes in the reversed flow region matched a previously developed universal backflow profile at the upstream edge of the separation region but not in the steady backflow region downstream. A smoke flow visualization movie and hot-film measurements revealed low frequency nonperiodic flapping at reattachment. However, forward flow fraction data at reattachment and mean velocity profiles in the redeveloping boundary layer downstream of reattachment correlated with backward-facing step data when the axial dimension was scaled by the distance from the maximum bubble thickness to reattachment. Author

N87-22122*# National Aeronautics and Space Administration. Lewis Research Center, Cleveland, Ohio.

EFFECT OF SHAFT FREQUENCY ON CAVITATION IN A JOURNAL BEARING FOR NONCENTERED CIRCULAR WHIRL

DAVID E. BREWE and M. M. KHONSARI (Ohio State Univ., Columbus.) 1987 23 p Presented at the 1987 Annual Meeting of the American Society of Lubrication Engineers, Anaheim, Calif., 11-14 May 1987

(NASA-TM-88925; E-3361; NAS 1.15:88925; USAAVSCOM-TR-86-C-41) Avail: NTIS HC A02/MF A01 CSCL 20D

The effect of shaft frequency on the performance of a submerged journal undergoing noncentered circular whirl is examined. The main emphasis of the paper is on the behavior of the vapor cavitation bubble and its effect on the bearing performance as a function of frequency. A cavitation algorithm due to Elrod was implemented in a computer program which solves a time-dependent Reynolds equation. This algorithm automatically handles the boundary conditions by using a switch function and a control volume approach which conserves mass throughout the entire flow. The shaft frequencies in this investigation ranged from 0 rad/s (squeeze-film damper) to -104 rad/s (a case in which oil-whip condition was produced momentarily). For the particular vibration amplitude chosen in this investigation it was observed that vapor cavitation had an effect on the load components for the full range of shaft frequencies investigated. Author

N87-22171*# National Aeronautics and Space Administration. Lewis Research Center, Cleveland, Ohio.

STATUS OF COMMERCIAL FUEL CELL POWERPLANT SYSTEM DEVELOPMENT Final Report

MARVIN WARSHAY 1987 8 p Proposed for presentation at the 22nd Intersociety Energy Conversion Engineering Conference, Philadelphia, Pa., 10-14 Aug. 1987; sponsored by AIAA, ANS, ASME, SAE, IEEE, ACS and AlChE

(Contract DE-AI21-80ET-17088) (NASA-TM-89896; DOE/NASA/17088-5; E-3586; NAS 1.15:89896; AIAA-87-9081) Avail: NTIS HC A02/MF A01 CSCL 20D

The primary focus is on the development of commercial Phosphoric Acid Fuel Cell (PAFC) powerplant systems because the PAFC, which has undergone extensive development, is currently the closest fuel cell system to commercialization. Shorter discussions are included on the high temperature fuel cell systems which are not as mature in their development, such as the Molten Carbonate Fuel Cell (MCFC) and the Solid Oxide Fuel Cell (SOFC). The alkaline and the Solid Polymer Electrolyte (SPE) fuel cell systems, are also included, but their discussions are limited to their prospects for commercial development. Currently, although the alkaline fuel cell continues to be used for important space applications there are no commercial development programs of significant size in the USA and only small efforts outside. The market place for fuel cells and the status of fuel cell programs in the USA receive extensive treatment. The fuel cell efforts outside

the USA, especially the large Japanese programs, are also discussed. Author

N87-22174*# National Aeronautics and Space Administration. Lewis Research Center, Cleveland, Ohio.

SELECTION OF HIGH TEMPERATURE THERMAL ENERGY STORAGE MATERIALS FOR ADVANCED SOLAR DYNAMIC SPACE POWER SYSTEMS

DOVIE E. LACY, CAROLYN COLES-HAMILTON, and ALBERT JUHASZ 1987 13 p Proposed for presentation at the 22nd Intersociety Energy Conversion Engineering Conference, Philadelphia, Pa., 10-14 Aug. 1987; sponsored by AIAA, ANS, ASME, SAE, IEEE, ACS and AIChE (NASA-TM-89886; E-3569; NAS 1.15:89886) Avail: NTIS HC A02/MF A01 CSCL 10B

Under the direction of NASA's Office of Aeronautics and Technology (OAST), the NASA Lewis Research Center has initiated an in-house thermal energy storage program to identify combinations of phase change thermal energy storage media for use with a Brayton and Stirling Advanced Solar Dynamic (ASD) space power system operating between 1070 and 1400 K. A study has been initiated to determine suitable combinations of thermal energy storage (TES) phase change materials (PCM) that result in the smallest and lightest weight ASD power system possible. To date the heats of fusion of several fluoride salt mixtures with melting points greater than 1025 K have been verified experimentally. The study has indicated that these salt systems produce large ASD systems because of their inherent low thermal conductivity and low density. It is desirable to have PCMs with high densities and high thermal conductivities. Therefore, alternate phase change materials based on metallic alloy systems are also being considered as possible TES candidates for future ASD space power systems. Author

N87-22767*# National Aeronautics and Space Administration. Lewis Research Center, Cleveland, Ohio.

UNSTEADY STATOR/ROTOR INTERACTION

PHILIP C. E. JORGENSEN and RODRICK V. CHIMA *In its* Structural Integrity and Durability of Reusable Space Propulsion Systems p 5-11 1987
Avail: NTIS HC A10/MF A01 CSCL 20D

The major thrust of the computational analysis of turbomachinery to date has been the steady-state solution of isolated blades using mass-averaged inlet and exit conditions. Unsteady flows differ from the steady solution due to interaction of pressure waves and wakes between blade rows. To predict the actual complex flow conditions one must look at the time accurate solution of the entire turbomachine. Three quasi-three-dimensional Euler and thin layer Navier-Stokes equations are solved for unsteady turbomachinery flows. Author

N87-22768*# National Aeronautics and Space Administration. Lewis Research Center, Cleveland, Ohio.

SIMULATION OF MULTISTAGE TURBINE FLOWS

JOHN J. ADAMCZYK and RICHARD A. MULAC (Sverdrup Technology, Inc., Middleburg Heights, Ohio.) *In its* Structural Integrity and Durability of Reusable Space Propulsion Systems p 13-20 1987
Avail: NTIS HC A10/MF A01 CSCL 20D

A flow model has been developed for analyzing multistage turbomachinery flows. This model, referred to as the average passage flow model, describes the time-averaged flow field with a typical passage of a blade row embedded within a multistage configuration. Computer resource requirements, supporting empirical modeling, formulation code development, and multitasking and storage are discussed. Illustrations from simulations of the space shuttle main engine (SSME) fuel turbine performed to date are given. Author

N87-22769*# National Aeronautics and Space Administration. Lewis Research Center, Cleveland, Ohio.

PROGRESS IN THE PREDICTION OF UNSTEADY HEAT TRANSFER ON TURBINE BLADES

T. CEBECI, R. J. SIMONEAU, A. KRAINER, and M. F. PLATZER (Naval Postgraduate School, Monterey, Calif.) *In its* Structural Integrity and Durability of Reusable Space Propulsion Systems p 21-27 1987

Avail: NTIS HC A10/MF A01 CSCL 20D

Progress toward developing a general method for predicting unsteady heat transfer on turbine blades subject to blade-passing frequencies and Reynolds numbers relevant to the Space Shuttle Main Engine (SSME) is discussed. The method employs an inviscid/viscous interactive procedure which has been tested extensively for steady subsonic and transonic external airfoil problems. One such example is shown. The agreement with experimental data and with Navier-Stokes calculations yields confidence in the method. The technique is extended to account for wake generated unsteadiness. The flow reversals around the stagnation point caused by the nonuniform onset velocity are accounted for by using the Characteristic Box scheme developed by Cebeci and Stewartson. The coupling between the inviscid and viscous methods is achieved by using a special procedure, which, with a novel inverse finite-difference boundary-layer method, allows the calculations to be performed for a wide range of flow conditions, including separation. Preliminary results are presented for the stagnation region of turbine blades for both laminar and turbulent flows. A laminar model problem corresponding to a flow on a circular cylinder which experiences the periodic passing of wakes from turbine blades is presented to demonstrate the ability of the method to calculate flow reversals around the stagnation region. Author

N87-22948*# Massachusetts Inst. of Tech., Cambridge. Dept. of Aeronautics and Astronautics.

A LINEARIZED EULER ANALYSIS OF UNSTEADY FLOWS IN TURBOMACHINERY Final Report

KENNETH C. HALL and EDWARD F. CRAWLEY Jun. 1987 183 p

(Contract NSG-3079)

(NASA-CR-180987; NAS 1.26:180987) Avail: NTIS HC A09/MF A01 CSCL 20D

A method for calculating unsteady flows in cascades is presented. The model, which is based on the linearized unsteady Euler equations, accounts for blade loading shock motion, wake motion, and blade geometry. The mean flow through the cascade is determined by solving the full nonlinear Euler equations. Assuming the unsteadiness in the flow is small, then the Euler equations are linearized about the mean flow to obtain a set of linear variable coefficient equations which describe the small amplitude, harmonic motion of the flow. These equations are discretized on a computational grid via a finite volume operator and solved directly subject to an appropriate set of linearized boundary conditions. The steady flow, which is calculated prior to the unsteady flow, is found via a Newton iteration procedure. An important feature of the analysis is the use of shock fitting to model steady and unsteady shocks. Use of the Euler equations with the unsteady Rankine-Hugoniot shock jump conditions correctly models the generation of steady and unsteady entropy and vorticity at shocks. In particular, the low frequency shock displacement is correctly predicted. Results of this method are presented for a variety of test cases. Predicted unsteady transonic flows in channels are compared to full nonlinear Euler solutions obtained using time-accurate, time-marching methods. The agreement between the two methods is excellent for small to moderate levels of flow unsteadiness. The method is also used to predict unsteady flows in cascades due to blade motion (flutter problem) and incoming disturbances (gust response problem). M.G.

N87-22949*# National Aeronautics and Space Administration. Lewis Research Center, Cleveland, Ohio.

THERMODYNAMIC ANALYSIS AND SUBSCALE MODELING OF SPACE-BASED ORBIT TRANSFER VEHICLE CRYOGENIC PROPELLANT RESUPPLY

DAVID M. DEFELICE and JOHN C. AYDELOTT Jul. 1987 21 p Prepared for presentation at the 23rd Joint Propulsion Conference, San Diego, Calif., 29 Jun. - 2 Jul. 1987; cosponsored by AIAA, SAE, ASME, and ASEE

(NASA-TM-89921; E-3617; NAS 1.15:89921; AIAA-87-1764)

Avail: NTIS HC A02/MF A01 CSCL 20D

The resupply of the cryogenic propellants is an enabling technology for spacebased orbit transfer vehicles. As part of the NASA Lewis ongoing efforts in microgravity fluid management, thermodynamic analysis and subscale modeling techniques were developed to support an on-orbit test bed for cryogenic fluid management technologies. Analytical results have shown that subscale experimental modeling of liquid resupply can be used to validate analytical models when the appropriate target temperature is selected to relate the model to its prototype system. Further analyses were used to develop a thermodynamic model of the tank chilldown process which is required prior to the no-vent fill operation. These efforts were incorporated into two FORTRAN programs which were used to present preliminary analytical results.

Author

N87-23921*# National Aeronautics and Space Administration. Lewis Research Center, Cleveland, Ohio.

THREE-STEP LABYRINTH SEAL FOR HIGH-PERFORMANCE TURBOMACHINES

ROBERT C. HENDRICKS Jun. 1987 75 p

(NASA-TP-1848; E-3186; NAS 1.60:1848) Avail: NTIS HC

A04/MF A01 CSCL 20D

A three-step labyrinth seal with 12, 11, and 10 labyrinth teeth per step, respectively, was tested under static (nonrotating) conditions. The configuration represented the seal for a high-performance turbopump (e.g., the space shuttle main engine fuel pump). The test data included critical mass flux and pressure profiles over a wide range of fluid conditions at concentric, partially eccentric, and fully eccentric seal positions. The seal mass fluxes (leakage rates) were lower over the entire range of fluid conditions tested than those for data collected for similar straight and three-step cylindrical seals, and this conformed somewhat to expectations. However, the pressure profiles for the eccentric positions indicated little, if any, direct stiffness for this configuration in contrast to significant direct stiffness reported for the straight and three-step cylindrical seals over the range of test conditions. Seal dynamics depend on geometric configuration, inlet and exit parameters, fluid phase, and rotation. The method of corresponding states was applied to the mass flux data, which were found to have a pressure dependency for helium.

Author

N87-23925*# Virginia Polytechnic Inst. and State Univ., Blacksburg. Turbomachinery Research Group.

THERMODYNAMIC EVALUATION OF TRANSONIC COMPRESSOR ROTORS USING THE FINITE VOLUME APPROACH Final Report, 20 Dec. 1984 - 19 Dec. 1986

JOHN MOORE, STEPHEN NICHOLSON, and JOAN G. MOORE 19 Dec. 1986 83 p

(Contract NAG3-593)

(NASA-CR-180587; NAS 1.26:180587; JM/87-4) Avail: NTIS HC

A05/MF A01 CSCL 20D

The development of a computational capability to handle viscous flow with an explicit time-marching method based on the finite volume approach is summarized. Emphasis is placed on the extensions to the computational procedure which allow the handling of shock induced separation and large regions of strong backflow. Appendices contain abstracts of papers and whole reports generated during the contract period.

N87-23933*# National Aeronautics and Space Administration. Lewis Research Center, Cleveland, Ohio.

DIRECT NUMERICAL SIMULATIONS OF A TEMPORALLY EVOLVING MIXING LAYER SUBJECT TO FORCING

RUSSELL W. CLAUS 1986 22 p Presented at the 10th Symposium on Turbulence, Rolla, Mo., 22-24 Sep. 1986; sponsored by ONR and Missouri Univ.

(NASA-TM-88896; E-3313; NAS 1.15:88896) Avail: NTIS HC

A02/MF A01 CSCL 20D

The vortical evolution of mixing layers subject to various types of forcing is numerically simulated using pseudospectral methods. The effect of harmonic forcing and random noise in the initial conditions is examined with some results compared to experimental data. Spanwise forcing is found to enhance streamwise vorticity in a nonlinear process leading to a slow, secondary growth of the shear layer. The effect of forcing on a chemical reaction is favorably compared with experimental data at low Reynolds numbers. Combining harmonic and subharmonic forcing is shown to both augment and later destroy streamwise vorticity.

Author

N87-23934*# National Aeronautics and Space Administration. Lewis Research Center, Cleveland, Ohio.

COMPUTATION OF FULL-COVERAGE FILM-COOLED AIRFOIL TEMPERATURES BY TWO METHODS AND COMPARISON WITH HIGH HEAT FLUX DATA

H. J. GLADDEN, F. C. YEH, and P. J. AUSTIN, JR. Jun. 1987 18 p Presented at the 32nd International Gas Turbine Conference and Exhibition, Anaheim, Calif., 31 May - 4 Jun. 1987; sponsored by ASME

(NASA-TM-88931; E-3372; NAS 1.15:88931) Avail: NTIS HC

A02/MF A01 CSCL 20D

Two methods were used to calculate the heat flux to full-coverage film cooled airfoils and, subsequently, the airfoil wall temperatures. The calculated wall temperatures were compared to measured temperatures obtained in the Hot Section Facility operating at real engine conditions. Gas temperatures and pressures up to 1900 K and 18 atm with a Reynolds number up to 1.9 million were investigated. Heat flux was calculated by the convective heat transfer coefficient adiabatic wall method and by the superposition method which incorporates the film injection effects in the heat transfer coefficient. The results of the comparison indicate the first method can predict the experimental data reasonably well. However, superposition overpredicted the heat flux to the airfoil without a significant modification of the turbulent Prandtl number. The results suggest that additional research is required to model the physics of full-coverage film cooling where there is significant temperature/density differences between the gas and the coolant.

Author

N87-23936*# National Aeronautics and Space Administration. Lewis Research Center, Cleveland, Ohio.

STRAIGHT CYLINDRICAL SEAL FOR HIGH-PERFORMANCE TURBOMACHINES

ROBERT C. HENDRICKS Jun. 1987 76 p

(NASA-TP-1850; E-3184; NAS 1.60:1850) Avail: NTIS HC

A05/MF A01 CSCL 20D

A straight cylindrical seal configuration representing the seal for a high-performance turbopump (e.g., the space shuttle main engine fuel pump) was tested under static (nonrotating) conditions. The test data included critical mass flux and pressure profiles over a wide range of inlet temperatures and pressures for fluid nitrogen and fluid hydrogen with the seal in concentric and fully eccentric positions. The critical mass fluxes (or leakage rates) for the concentric and fully eccentric configurations were nearly the same when based on stagnation conditions upstream of the seal. The fully eccentric configuration pressure profiles of the gas and liquid were different. Further, the pressure differences between the maximum and the minimum clearance positions were highly dependent on the geometric conditions, the temperature, and the absolute pressure at both the inlet and the exit. The pressure differences were greatest in the inlet region. The results, although complex, tend to follow the corresponding-states principles for critical flows. Gaseous injection near the seal exit plane significantly

altered the pressure profiles and could be used to control turbomachine instabilities. Author

N87-24639*# National Aeronautics and Space Administration. Lewis Research Center, Cleveland, Ohio.

THREE-STEP CYLINDRICAL SEAL FOR HIGH-PERFORMANCE TURBOMACHINES

ROBERT C. HENDRICKS Jun. 1987 79 p
(NASA-TP-1849; E-3185; NAS 1.60:1849) Avail: NTIS HC A05/MF A01 CSCL 20D

A three-step cylindrical seal configuration representing the seal for a high performance turbopump (e.g., the space shuttle main engine fuel pump) was tested under static (nonrotating) conditions. The test data included critical mass flux and pressure profiles over a wide range of inlet temperatures and pressures for fluid nitrogen and fluid hydrogen with the seal in concentric and fully eccentric positions. The critical mass flux (leakage rate) was 70% that of an equivalent straight cylindrical seal with a correspondingly higher pressure drop based on the same flow areas of 0.3569 sq cm but 85% that of the straight seal based on the third-step flow area of 0.3044 sq cm. The mass flow rates for the three step cylindrical seal in the fully eccentric and concentric positions were essentially the same, and the trends in flow coefficient followed those of a simple axisymmetric inlet configuration. However, for inlet stagnation temperatures less than the thermodynamic critical temperature the pressure profiles exhibited a flat region throughout the third step of the seal, with the pressure magnitude dependent on the inlet stagnation temperature. Such profiles represent an extreme positive direct stiffness. These conditions engendered a crossover in the pressure profile upstream of the postulated choke that resulted in a local negative stiffness. Flat and crossover profiles resulting from choking within the seal are practically unknown to the seal designer. However, they are of critical importance to turbomachine stability and must be integrated into any dynamic analysis of a seal of this configuration. In addition, choking is highly dependent on geometry, inlet-to-backpressure ratio, and inlet temperature and can occur within the seal even though the backpressure is above the critical pressure. M.G.

N87-24641*# Beech Aircraft Corp., Boulder, Colo.
SPACE STATION EXPERIMENT DEFINITION: LONG-TERM CRYOGENIC FLUID STORAGE Final Report

R. L. JETLEY and R. D. SCARLOTTI Washington NASA Jun. 1987 257 p
(Contract NAS3-24661)
(NASA-CR-4072; E-3463; NAS 1.26:4072; BAC-ER-18056-8)
Avail: NTIS HC A12/MF A01 CSCL 20D

The conceptual design of a space station Technology Development Mission (TDM) experiment to demonstrate and evaluate cryogenic fluid storage and transfer technologies is presented. The experiment will be deployed on the initial operational capability (IOC) space station for a four-year duration. It is modular in design, consisting of three phases to test the following technologies: passive thermal technologies (phase 1), fluid transfer (phase 2), and active refrigeration (phase 3). Use of existing hardware was a primary consideration throughout the design effort. A conceptual design of the experiment was completed, including configuration sketches, system schematics, equipment specifications, and space station resources and interface requirements. These requirements were entered into the NASA Space Station Mission Data Base. A program plan was developed defining a twelve-year development and flight plan. Program cost estimates are given. Author

N87-24646*# National Aeronautics and Space Administration. Lewis Research Center, Cleveland, Ohio.

STABILITY OF A RIGID ROTOR SUPPORTED ON FLEXIBLE OIL JOURNAL BEARINGS

BANKIM C. MAJUMDAR, DAVID E. BREWE, and MICHAEL M. KHONSARI (Ohio State Univ., Columbus.) 1987 29 p Proposed for presentation at the 1987 Joint Tribology Conference, San Antonio, Tex., 5-8 Oct. 1987; sponsored by the American Society of Lubrication Engineers and ASME
(NASA-TM-89899; E-3408; NAS 1.15:89899;
AVSCOM-TR-87-C-12) Avail: NTIS HC A01/MF A01 CSCL 20D

This investigation deals with the stability characteristics of oil journal bearings, including the effect of elastic distortions in the bearing liner. Graphical results are presented for (1) steady-state load, (2) stiffness and damping coefficients, and (3) the stability. These results are given for various slenderness ratios, eccentricity ratios, and elasticity parameters. The lubricant is first assumed to be isoviscous. The analysis is then extended to the case of a pressure-dependent viscosity. It has been found that stability decreases with increase of the elasticity parameter of the bearing liner for heavily loaded bearings. Author

N87-26002*# National Aeronautics and Space Administration. Lewis Research Center, Cleveland, Ohio.

INTERNAL COMPUTATIONAL FLUID MECHANICS ON SUPERCOMPUTERS FOR AEROSPACE PROPULSION SYSTEMS

BERNHARD H. ANDERSEN and THOMAS J. BENSON /n NASA. Ames Research Center, Supercomputing in Aerospace p 35-48 Mar. 1987
Avail: NTIS HC A13/MF A01 CSCL 12A

The accurate calculation of three-dimensional internal flowfields for application towards aerospace propulsion systems requires computational resources available only on supercomputers. A survey is presented of three-dimensional calculations of hypersonic, transonic, and subsonic internal flowfields conducted at the Lewis Research Center. A steady state Parabolized Navier-Stokes (PNS) solution of flow in a Mach 5.0, mixed compression inlet, a Navier-Stokes solution of flow in the vicinity of a terminal shock, and a PNS solution of flow in a diffusing S-bend with vortex generators are presented and discussed. All of these calculations were performed on either the NAS Cray-2 or the Lewis Research Center Cray XMP. Author

N87-26302*# National Aeronautics and Space Administration. Lewis Research Center, Cleveland, Ohio.

TURBULENCE MODELING AND SURFACE HEAT TRANSFER IN A STAGNATION FLOW REGION

CHI R. WANG and FREDERICK C. YEH 1987 22 p Prepared for presentation at the Winter Annual Meeting of the American Society of Mechanical Engineers, Boston, Mass., 13-18 Dec. 1987
(NASA-TM-100132; E-3682; NAS 1.15:100132) Avail: NTIS HC A02/MF A01 CSCL 20D

Analysis for the turbulent flow field and the effect of freestream turbulence on the surface heat transfer rate of a stagnation flow is presented. The emphasis is on modeling and its augmentation of surface heat transfer rate. The flow field considered is the region near the forward stagnation point of a circular cylinder in a uniform turbulent mean flow. Author

N87-27161*# National Aeronautics and Space Administration. Lewis Research Center, Cleveland, Ohio.

APPLICATION OF TURBULENCE MODELING TO PREDICT SURFACE HEAT TRANSFER IN STAGNATION FLOW REGION OF CIRCULAR CYLINDER

CHI R. WANG and FREDERICK C. YEH Sep. 1987 25 p
(NASA-TP-2758; E-3418; NAS 1.60:2758) Avail: NTIS HC A02/MF A01 CSCL 20D

A theoretical analysis and numerical calculations for the turbulent flow field and for the effect of free-stream turbulence on the surface heat transfer rate of a stagnation flow are presented.

The emphasis is on the modeling of turbulence and its augmentation of surface heat transfer rate. The flow field considered is the region near the forward stagnation point of a circular cylinder in a uniform turbulent mean flow. The free stream is steady and incompressible with a Reynolds number of the order of 10 to the 5th power and turbulence intensity of less than 5 percent. For this analysis, the flow field is divided into three regions: (1) a uniform free-stream region where the turbulence is homogeneous and isotropic; (2) an external viscous flow region where the turbulence is distorted by the variation of the mean flow velocity; and, (3) an anisotropic turbulent boundary layer region over the cylinder surface. The turbulence modeling techniques used are the kappa-epsilon two-equation model in the external flow region and the time-averaged turbulence transport equation in the boundary layer region. The turbulence double correlations, the mean velocity, and the mean temperature within the boundary layer are solved numerically from the transport equations. The surface heat transfer rate is calculated as functions of the free-stream turbulence longitudinal microlength scale, the turbulence intensity, and the Reynolds number. Author

N87-27949* Georgia Inst. of Tech., Atlanta. School of Aerospace Engineering.
STUDIES OF UNSTEADY VISCOUS FLOWS USING A TWO-EQUATION MODEL OF TURBULENCE Semiannual Status Report, 1 Jan. - 30 Jun. 1987
 L. N. SANKAR and JIUNN-CHI WU 1987 11 p
 (Contract NAG3-768)
 (NASA-CR-181293; NAS 1.26:181293) Avail: NTIS HC A02/MF A01 CSCL 20D

A two equation model of turbulence, based on the turbulent kinetic energy and energy dissipation, suitable for prediction of unsteady viscous flows, was developed. Also, the performance of the two equation model was compared with simpler algebraic models such as the Baldwin-Lomax two layer eddy viscosity model, and a model by Johnson and King which accounts for upstream history of the turbulent kinetic energy. A brief discussion of this study is given. Author

N87-27973* Purdue Univ., West Lafayette, Ind. School of Mechanical Engineering.
TURBULENCE CHARACTERISTICS OF AN AXISYMMETRIC REACTING FLOW Final Report
 RICHARD D. GOULD, WARREN H. STEVENSON, and H. DOYLE THOMPSON 15 Sep. 1987 219 p
 (Contract NAG3-502)
 (NASA-CR-180697; NAS 1.26:180697) Avail: NTIS HC A10/MF A01 CSCL 20D

Simultaneous two-component laser velocimeter measurements were made in the turbulent flow field following an axisymmetric sudden expansion with and without combustion. The fuel (propane) and air were fully premixed to give a constant fuel-air ratio of 0.032 at the inlet for the combustor flow measurements. Reynolds number based on step height was 55,700. The primary objective was to obtain detailed measurements which would be of use to modelers. Quantities measured included mean axial and radial velocities, Reynolds stresses, and turbulent triple products. In addition, simultaneous time resolved temperature measurements were made in the reacting flow using high speed thermocouples. This permitted the computation of velocity-temperature correlations. Experimental results were compared to predictions from a widely used numerical code based on the kappa-epsilon turbulence model and the combustion model of Magnussen and Hjertager. Relatively good agreement was found for the cold flow case as in previous studies, but predicted values of temperature in the reacting flow case deviated substantially from the measurements. Sizable errors in the predictions for the velocity field also were found. Possible sources for the observed differences and suggestions for future model development are suggested. Author

N87-27977* National Aeronautics and Space Administration. Lewis Research Center, Cleveland, Ohio.

CONTROLLED EXCITATION OF A COLD TURBULENT SWIRLING FREE JET

R. TAGHAVI, E. J. RICE, and S. FAROKHI (Kansas Univ., Lawrence.) 1987 13 p Prepared for presentation at the Winter Annual Meeting of the American Society of Mechanical Engineers, Boston, Mass., 13-18 Dec. 1987
 (NASA-TM-100173; E-3741; NAS 1.15:100173) Avail: NTIS HC A02/MF A01 CSCL 20D

Experimental results from acoustic excitation of a cold free turbulent jet with and without swirl are presented. A flow with a swirl number of 0.35 (i.e., moderate swirl) is excited internally by plane acoustic waves at a constant sound pressure level and at various frequencies. It is observed that the cold swirling jet is excitable by plane waves, and that the instability waves grow about 50 percent less in peak rms amplitude, and saturate further upstream compared to corresponding waves in a jet without swirl having the same axial mass flux. The preferred Strouhal number based on the mass-averaged axial velocity and nozzle exit diameter for both swirling and nonswirling flows is 0.4. So far no change in the mean velocity components of the swirling jet is observed as a result of excitation. Author

N87-28860* Indiana Univ., Indianapolis. Dept. of Aeronautical and Astronautical Engineering.
THREE DIMENSIONAL BOUNDARY LAYERS IN INTERNAL FLOWS Final Report
 R. J. BODONYI 28 Sep. 1987 26 p
 (Contract NAG3-528)
 (NASA-CR-181336; NAS 1.26:181336) Avail: NTIS HC A03/MF A01 CSCL 20D

A numerical study of the effects of viscous-inviscid interactions in three-dimensional duct flows is presented. In particular interacting flows for which the oncoming flow is not fully-developed were considered. In this case there is a thin boundary layer still present upstream of the surface distortion, as opposed to the fully-developed pipe flow situation wherein the flow is viscous across the cross section. Author

35

INSTRUMENTATION AND PHOTOGRAPHY

Includes remote sensors; measuring instruments and gages; detectors; cameras and photographic supplies; and holography.

A87-11048* Nebraska Univ., Lincoln.
EFFECTS OF NON-SPHERICAL DROPS ON A PHASE DOPPLER SPRAY ANALYZER

D. R. ALEXANDER, K. J. WILES, S. A. SCHAUB, and M. P. SEEMAN (Nebraska, University, Lincoln) IN: Particle sizing and spray analysis; Proceedings of the Meeting, San Diego, CA, August 21, 1985. Bellingham, WA, Society of Photo-Optical Instrumentation Engineers, 1985, p. 67-72. Research supported by the University of Nebraska. refs
 (Contract NAG3-634; DAAA15-85-K-0001)

A phase/Doppler spray analyzer (P/D SA) and a laser imaging system was used to study the response of a P/D SA to nonspherical particles. Methanol particles with an aspect ratio ranging from 0.7 to 1.4 were used in this investigation. Results indicated that the P/D SA was quite sensitive to particle shape. A Berglund-Liu generator was used to produce particles of 98 microns (volumetric diameter). The P/D SA instrument measured particle sizes ranging from 142 microns for a particle of aspect ratio 0.7, to 84 microns for an aspect ratio of 1.4. Particle diameters based on averaged x and y diameters for the laser imaging system ranged from 95 microns to 92 microns over the same range of aspect ratios. Author

A87-11049* California Univ., Irvine.

PERFORMANCE COMPARISON OF TWO INTERFEROMETRIC DROPLET SIZING TECHNIQUES

T. A. JACKSON and G. S. SAMUELSEN (California, University, Irvine) IN: Particle sizing and spray analysis; Proceedings of the Meeting, San Diego, CA, August 21, 1985. Bellingham, WA, Society of Photo-Optical Instrumentation Engineers, 1985, p. 73-79. refs (Contract NAS3-24350; F08635-83-C-0052; N00014-83-C-9151)

In this paper, two interferometric techniques (Visibility/Intensity Validation and Phase Doppler) are critically examined in characterizing the spray of an air-assist nozzle with Sauter mean diameter of less than 35 microns. The two techniques are compared to each other and are evaluated against a Malvern diffraction unit. With the use of a rotating grating for Visibility/Intensity Validation, the interference techniques compare well to each other and to the diffraction method. The Phase Doppler technique is more easily applied to the spray, due largely to its broadened size and velocity ranges. The consistency of the interferometric results raises questions with regard to the use of the Malvern's most frequently applied distribution model. Author

A87-13878* National Bureau of Standards, Gaithersburg, Md. VISCOMETER FOR LOW FREQUENCY, LOW SHEAR RATE MEASUREMENTS

R. F. BERG and M. R. MOLDOVER (NBS, Thermophysics Div., Gaithersburg, MD) Review of Scientific Instruments (ISSN 0034-6748), vol. 57, Aug. 1986, p. 1667-1672. refs (Contract NASA ORDER C-86129-D)

A computer-controlled torsion-oscillator viscometer with low 0.5 Hz frequency and very low 0.05/s shear rate is designed to precisely study shear-sensitive fluids such as microemulsions, gels, polymer solutions and melts, colloidal solutions undergoing coagulation, and liquid mixtures near critical points. The viscosities are obtained from measurements of the logarithmic decrement of an underdriven oscillator. The viscometer is found to have a resolution of 0.2 percent when used with liquid samples and a resolution of 0.4 percent when used with a dense gaseous sample. The design is compatible with submillikelvin temperature control. R.R.

A87-17320*# National Aeronautics and Space Administration. Lewis Research Center, Cleveland, Ohio.

LARGE APERTURE INTERFEROMETER WITH PHASE-CONJUGATE SELF-REFERENCE BEAM

W. L. HOWES (NASA, Lewis Research Center, Cleveland, OH) Applied Optics (ISSN 0003-6935), vol. 25, Sept. 15, 1986, p. 3167-3170. refs

A large aperture self-referencing interferometer consisting of a Twyman-Green interferometer using a self-pumped phase conjugator in series with test section optics is described and experimentally demonstrated. This interferometer provides twice the fringe shift of a Mach-Zehnder (M-Z) interferometer for a given optical phase change induced within the test section. It also provides greater irradiance in the reference beam than does a similar series setup utilizing a M-Z interferometer incorporating a local reference beam. Whereas the ordinary interferometer records instantaneous conditions, the new one records average conditions if a BaTiO₃ crystal is used as the phase conjugator. C.D.

A87-19186*# National Aeronautics and Space Administration. Lewis Research Center, Cleveland, Ohio.

FIBER-OPTIC INTERFEROMETER USING FREQUENCY-MODULATED LASER DIODES

G. BEHEIM (NASA, Lewis Research Center, Cleveland, OH) Applied Optics (ISSN 0003-6935), vol. 25, Oct. 1, 1986, p. 3469-3472. refs

This paper describes an electrically passive fiber-optic interferometer which uses dual frequency-modulated laser diodes. Experimental results show that this type of interferometer can attain a displacement range of 100 micron with subnanometer resolution. This technique can serve as the basis for a number of high-precision fiber-optic sensors. Author

A87-23899* Massachusetts Inst. of Tech., Cambridge.

A COMPUTERIZED TEST SYSTEM FOR THERMAL-MECHANICAL FATIGUE CRACK GROWTH

N. MARCHAND and R. M. PELLOUX (MIT, Cambridge, MA) Journal of Testing and Evaluation (ISSN 0090-3973), vol. 14, Nov. 1986, p. 303-311. refs (Contract NAG3-280)

A computerized testing system to measure fatigue crack growth under thermal-mechanical fatigue conditions is described. Built around a servohydraulic machine, the system is capable of a push-pull test under stress-controlled or strain-controlled conditions in the temperature range of 25 to 1050 C. Temperature and mechanical strain are independently controlled by the closed-loop system to simulate the complex inservice strain-temperature relationship. A d-c electrical potential method is used to measure crack growth rates. The correction procedure of the potential signal to take into account powerline and RF-induced noises and thermal changes is described. It is shown that the potential drop technique can be used for physical mechanism studies and for modelling crack tip processes. Author

A87-25948*# National Aeronautics and Space Administration. Lewis Research Center, Cleveland, Ohio.

FIBER-OPTIC THERMOMETER USING TEMPERATURE DEPENDENT ABSORPTION, BROADBAND DETECTION, AND TIME DOMAIN REFERENCING

GRIGORY ADAMOVSKY and NANCY D. PILTCH (NASA, Lewis Research Center, Cleveland, OH) Applied Optics (ISSN 0003-6935), vol. 25, Dec. 1, 1986, p. 4439-4443. refs (Contract NAG3-366)

A fiber-optic thermometer based on temperature dependent absorption in Nd(3+) doped glass is demonstrated over the 298-573 K range. A broadband detection technique allows the use of the complete spectrum of a pulse modulated light emitting diode. A fiber-optic recirculating loop is employed to construct a reference channel in the time domain by generating a train of pulses from one initial pulse. A theoretical model is developed, and experimental data are shown to compare well with the theory. Possible sources of error and instability are identified, and ways to enhance the performance of the system are proposed. Author

A87-26109* California Univ., Los Angeles.

THIN-FILM TEMPERATURE SENSORS FOR GAS TURBINE ENGINES PROBLEMS AND PROSPECTS

R. C. BUDHANI, S. PRAKASH, and R. F. BUNSHAH (California, University, Los Angeles) Journal of Vacuum Science and Technology A (ISSN 0734-2101), vol. 4, Nov.-Dec. 1986, p. 2609-2617. refs (Contract NAG3-451)

The erosion and corrosion of thermocouples used to measure the temperature in turbine engines are studied. Structural and metallurgical interactions and instabilities at thermocouple interfaces are analyzed. Consideration is given to the adhesion, dielectric quality, surface topography, and hardness of the thermal oxides; it is observed that the structural and thermoelectric stability of thin-film thermocouple elements depends on adhesion, surface topography, and dielectric strength. The electrical conductivity and impurity content of the oxide scale are evaluated. Methods for improving the adhesion of thermocouples on the alumina surfaces are described. Compositional inhomogeneities in the sensors and contamination of the thermocouple elements are examined. The fabrication of the thermocouples is discussed. It is noted that Al₂O₃ and Si₃N₄ are useful for developing stable thermocouple elements on the surface of the blades and vanes. I.F.

A87-32152* National Aeronautics and Space Administration. Lewis Research Center, Cleveland, Ohio.

LOSS-COMPENSATION TECHNIQUE FOR FIBER-OPTIC SENSORS AND ITS APPLICATION TO DISPLACEMENT MEASUREMENTS

GLENN BEHEIM (NASA, Lewis Research Center, Cleveland, OH) Applied Optics (ISSN 0003-6935), vol. 26, Feb. 1, 1987, p. 452-455. refs

This report describes a new type of intensity-modulating fiber-optic sensor which has high immunity to the effects of variations in the losses of the fiber-link. A variable-splitting-ratio transducer is used to differentially modulate the intensities of the light which it transmits and reflects. Using a four-fiber optical link, light is impinged onto the transducer from either direction, and in each case, the transmitted and reflected signals are measured. These four signals are then processed to remove the effects of the fiber and connector losses. Loss-compensated sensors of angular position and displacement are described, and their outputs are shown to be highly stable despite considerable variations in the transmissivities of the fiber-link components. Author

A87-34566* National Aeronautics and Space Administration. Lewis Research Center, Cleveland, Ohio.

FIBER-OPTIC PHOTOELASTIC PRESSURE SENSOR WITH FIBER-LOSS COMPENSATION

G. BEHEIM (NASA, Lewis Research Center, Cleveland, OH) and D. J. ANTHAN (Cleveland State University, OH) Optics Letters (ISSN 0146-9592), vol. 12, March 1987, p. 220-222. refs

A new fiber-optic pressure sensor is described that has high immunity to the effects of fiber-loss variations. This device uses the photoelastic effect to modulate the proportion of the light from each of two input fibers that is coupled into each of two output fibers. This four-fiber link permits two detectors to be used to measure the sensor's responses to the light from each of two independently controlled sources. These four detector outputs are processed to yield a loss-compensated signal that is a stable and sensitive pressure indicator. Author

A87-37698* National Aeronautics and Space Administration. Lewis Research Center, Cleveland, Ohio.

AN ANEMOMETER FOR HIGHLY TURBULENT OR RECIRCULATING FLOWS

P. A. DURBIN, D. J. MCKINZIE (NASA, Lewis Research Center, Cleveland, OH), and E. J. DURBIN (Princeton University, NJ) Experiments in Fluids (ISSN 0723-4864), vol. 5, no. 3, 1987, p. 184-188. refs

An anemometer which determines flow velocity by ionizing air and sensing the convective displacement of the ions is described. It is suited to measurement in low speed, highly unsteady gas flows. Comparisons to hot wire spectra suggest the corona anemometer has adequate frequency response to make it a useful tool for fluid dynamics measurement. Author

A87-40725*# National Aeronautics and Space Administration. Lewis Research Center, Cleveland, Ohio.

A PARAMETRIC STUDY OF THE BEAM REFRACTION PROBLEMS ACROSS LASER ANEMOMETER WINDOWS

ALBERT K. OWEN (NASA, Lewis Research Center, Cleveland, OH) IN: International Symposium on Applications of Laser Anemometry to Fluid Mechanics, 3rd, Lisbon, Portugal, July 7-9, 1986, Proceedings. Lisbon, Instituto Superior Tecnico, 1986, p. 10.7 (6 p.). Previously announced in STAR as N86-31857. refs

The experimenter is often required to view flows through a window with a different index of refraction than either the medium being observed or the medium that the laser anemometer is immersed in. The refraction that occurs at the window surfaces may lead to undesirable changes in probe volume position or beam crossing angle and can lead to partial or complete beam uncrossing. This report describes the results of a parametric study of this problem using a ray tracing technique to predict these changes. The windows studied were a flat plate and a simple cylinder. For the flat-plate study: (1) surface thickness, (2) beam crossing angle, (3) bisecting line - surface normal angle, and (4)

incoming beam plane surface orientation were varied. For the cylindrical window additional parameters were also varied: (1) probe volume immersion, (2) probe volume off-radial position, and (3) probe volume position out of the r-theta plane of the lens. A number of empirical correlations were deduced to aid the reader in determining the movement, uncrossing, and change in crossing angle for a particular situations. Author

A87-40750*# Case Western Reserve Univ., Cleveland, Ohio. LASER ANEMOMETRY MEASUREMENTS OF NATURAL CIRCULATION FLOW IN A SCALE MODEL PWR REACTOR SYSTEM

J. R. KADAMBI (Case Western Reserve University, Cleveland, OH), S. J. SCHNEIDER (NASA, Lewis Research Center, Cleveland, OH), and W. A. STEWART (Westinghouse Electric Corp., Pittsburgh, PA) IN: International Symposium on Applications of Laser Anemometry to Fluid Mechanics, 3rd, Lisbon, Portugal, July 7-9, 1986, Proceedings. Lisbon, Instituto Superior Tecnico, 1986, p. 21.3 (6 p.). Research supported by the Electric Power Research Institute.

The natural circulation of a single phase fluid in a scale model of a pressurized water reactor system during a postulated grade core accident is analyzed. The fluids utilized were water and SF6. The design of the reactor model and the similitude requirements are described. Four LDA tests were conducted: water with 28 kW of heat in the simulated core, with and without the participation of simulated steam generators; water with 28 kW of heat in the simulated core, with the participation of simulated steam generators and with cold upflow of 12 lbm/min from the lower plenum; and SF6 with 0.9 kW of heat in the simulated core and without the participation of the simulated steam generators. For the water tests, the velocity of the water in the center of the core increases with vertical height and continues to increase in the upper plenum. For SF6, it is observed that the velocities are an order of magnitude higher than those of water; however, the velocity patterns are similar. I.F.

A87-42374*# Rockwell International Corp., Canoga Park, Calif. FEASIBILITY OF MAPPING VELOCITY FLOWFIELDS IN AN SSME POWERHEAD USING LASER ANEMOMETRY TECHNIQUES

D. G. PELACCIO, L. K. SHARMA, and T. V. FERGUSON (Rockwell International Corp., Rocketdyne Div., Canoga Park, CA) AIAA, Fluid Dynamics, Plasma Dynamics, and Lasers Conference, 19th, Honolulu, HI, June 8-10, 1987. 12 p. (Contract NAS3-24356) (AIAA PAPER 87-1306)

Nonintrusive anemometry measurement techniques are investigated for a NASA study of steady and unsteady aerothermal flow phenomena present in three engine component flow environments in the Space Shuttle Main Engine powerhead, the: (1) high-pressure fuel turbopump preburner; (2) turbine; and (3) turnaround duct. Issues considered include identification of feasible means of optical access to the high-pressure high-temperature measurement flow regions, and measurement system compatibility with the test environment. Descriptions of the two-component LDV and Laser Two Focus measurement systems are given whose capabilities include measurements of the time-averaged values of velocity magnitude and flow direction, turbulence intensity, and velocity component correlations. R.R.

A87-42546* John Carroll Univ., Cleveland, Ohio.

LINEAR CAPACITIVE DISPLACEMENT SENSOR WITH FREQUENCY READOUT

KLAUS FRITSCH (John Carroll University, Cleveland, OH) Review of Scientific Instruments (ISSN 0034-6748), vol. 58, May 1987, p. 861-863. (Contract NAG3-571)

A simple, inherently linear technique for measuring changes in the separation of the mirrors of an optical cavity is reported. The capacitor, made up of the reflective metallic coatings, is part of a feedback loop which adjusts the frequency of an oscillator to be proportional to the mirror separation. A linearity of 0.2 percent full

scale was achieved for separations up to 0.5 mm with a resolution of 10 nm. Author

A87-45128* # National Aeronautics and Space Administration. Lewis Research Center, Cleveland, Ohio.

RAMP-INTEGRATION TECHNIQUE FOR CAPACITANCE-TYPE BLADE-TIP CLEARANCE MEASUREMENT

GARIMELLA R. SARMA and JOHN P. BARRANGER (NASA, Lewis Research Center, Cleveland, OH) IN: International Instrumentation Symposium, 32nd, Seattle, WA, May 5-8, 1986, Proceedings. Research Triangle Park, NC, Instrument Society of America, 1986, p. 591-600.

The analysis of a proposed new technique for capacitance type blade tip clearance measurement is presented. The capacitance between the blade tip and a mounted capacitance electrode within a guard ring forms one of the feedback elements of a high speed operational amplifier. The differential equation governing the operational amplifier circuit is formulated and solved for two types of inputs to the amplifier - a constant voltage and a ramp. The resultant solution shows an output that contains a term that is proportional to the derivative of the product of the input voltage and the time constant of the feedback network. The blade tip clearance capacitance is obtained by subtracting the output of a balancing reference channel followed by integration. The proposed sampled data algorithm corrects for environmental effects and varying rotor speeds on-line, making the system suitable for turbine instrumentation. System requirements, block diagrams, and a typical application are included. Author

A87-45842* National Aeronautics and Space Administration. Lewis Research Center, Cleveland, Ohio.

FLOW VISUALIZATION STUDY OF THE EFFECT OF INJECTION HOLE GEOMETRY ON AN INCLINED JET IN CROSSFLOW

FREDERICK F. SIMON and MICHAEL L. CIANCONE (NASA, Lewis Research Center, Cleveland, OH) IN: Heat transfer and fluid flow in rotating machinery; Proceedings of the First International Symposium on Transport Phenomena, Honolulu, HI, Apr. 28-May 3, 1985. Washington, DC, Hemisphere Publishing Corp., 1987, p. 170-192. Previously announced in STAR as N85-20269. refs

A flow visualization was studied by using neutrally buoyant, helium-filled soap bubbles, to determine the effect of injection hole geometry on the trajectory of an air jet in a crossflow and to investigate the mechanisms involved in jet deflection. Experimental variables were the blowing rate, and the injection hole geometry cusp facing upstream (CUS), cusp facing downstream (CDS), round, swirl passage, and oblong. It is indicated that jet deflection is governed by both the pressure drag forces and the entrainment of free-stream fluid into the jet flow. For injection hole geometries with similar cross-sectional areas and similar mass flow rates, the jet configuration with the larger aspect ratio experienced a greater deflection. Entrainment arises from lateral shearing forces on the sides of the jet, which set up a dual vortex motion within the jet and thereby cause some of the main-stream fluid momentum to be swept into the jet flow. This additional momentum forces the jet nearer the surface. Of the jet configurations, the oblong, CDS, and CUS configurations exhibited the largest deflections. The results correlate well with film cooling effectiveness data, which suggests a need to determine the jet exit configuration of optimum aspect ratio to provide maximum film cooling effectiveness. E.A.K.

N87-10377* # , United Technologies Corp., East Hartford, Conn. **DEMONSTRATION OF LASER SPECKLE SYSTEM ON BURNER LINER CYCLIC RIG Final Report**

K. A. STETSON Jun. 1986 28 p
(Contract NAS3-24615)

(NASA-CR-179509; NAS 1.26:179509; R86-927298-10) Avail: NTIS HC A03/MF A01 CSCL 14B

A demonstration test was conducted to apply speckle photogrammetry to the measurement of strains on a sample of combustor liner material in a cyclic fatigue rig. A system for recording specklegrams was assembled and shipped to the NASA Lewis Research Center, where it was set up and operated during

rig tests. Data in the form of recorded specklegrams were sent back to United Technologies Research Center for processing to extract strains. Difficulties were found in the form of warping and bowing of the sample during the tests which degraded the data. Steps were taken by NASA personnel to correct this problem and further tests were run. Final data processing indicated erratic patterns of strain on the burner liner sample. Author

N87-11144* # United Technologies Corp., East Hartford, Conn. **HOT SECTION VIEWING SYSTEM**

W. W. MOREY Sep. 1984 141 p
(Contract NAS3-23156)

(NASA-CR-174773; NAS 1.26:174773; R84-925830-33) Avail: NTIS HC A07/MF A01 CSCL 14B

This report covers the development and testing of a prototype combustor viewing system. The system allows one to see and record images from the inside of an operating gas turbine combustor. The program proceeded through planned phases of conceptual design, preliminary testing to resolve problem areas, prototype design and fabrication, and rig testing. Successful tests were completed with the viewing system in the laboratory, in a high pressure combustor rig, and on a Pratt and Whitney PW20307 jet engine. Both film and video recordings were made during the tests. Digital image analysis techniques were used to enhance images and bring out special effects. The use of pulsed laser illumination was also demonstrated as a means for observing liner surfaces in the presence of luminous flame. Author

N87-11187* # National Aeronautics and Space Administration. Lewis Research Center, Cleveland, Ohio.

LASER ANEMOMETERS OF HOT-SECTION APPLICATIONS

R. G. SEASHOLTZ, L. G. OBERLE, and D. H. WEIKLE In its Turbine Engine Hot Section Technology, 1984 11 p Oct. 1984
Avail: NTIS HC A17/MF A01 CSCL 14B

Laser anemometers are being developed for use in the turbine facilities at Lewis that are involved in the Turbine Engine Hot Section Technology Program. The status of the program is given along with some results accomplished since 1983. B.G.

N87-11189* # National Aeronautics and Space Administration. Lewis Research Center, Cleveland, Ohio.

EVALUATION RESULTS OF THE 700 DEG C CHINESE STRAIN GAGES

H. F. HOBART In its Turbine Engine Hot Section Technology, 1984 8 p Oct. 1984

Avail: NTIS HC A17/MF A01 CSCL 14B

There is a continuing interest and need for resistance strain gages capable of making static strain measurements on components located in the hot section of gas turbine engines. A paper by Tsen-tai Wu describes the development and evaluation of high temperature gauges fabricated from specially developed Fe-Cr-Al-V-Ti-Y alloy wire. Several of these gages and a quantity of P12-2 ceramic adhesive were purchased for evaluation. Nine members of the aircraft turbine engine community were invited to participate in an evaluation of these gages. Each participant was sent one strain gage, a small amount of ceramic adhesive, instructions for mounting the gage on a test beam, and a set of suggestions for the experiment. Data on gage factor variation with temperature, apparent strain, and drift are discussed. Author

N87-12829* # General Electric Co., Schenectady, N.Y. Corporate Research and Development Dept.

ADVANCED OPTICAL SMOKE METERS FOR JET ENGINE EXHAUST MEASUREMENT Final Report

R. W. PITZ Sep. 1986 43 p
(Contract NAS3-24084)

(NASA-CR-179459; NAS 1.26:179459) Avail: NTIS HC A03/MF A01 CSCL 14B

Smoke meters with increased sensitivity, improved accuracy, and rapid response are needed to measure the smoke levels emitted by modern jet engines. The standard soiled tape meter in current use is based on filtering, which yields long term averages and is insensitive to low smoke levels. Two new optical smoke

35 INSTRUMENTATION AND PHOTOGRAPHY

meter techniques that promise to overcome these difficulties have been experimentally evaluated: modulated transmission (MODTRAN) and photothermal deflection spectroscopy (PDS). Both techniques are based on light absorption by smoke, which is closely related to smoke density. They are variations on direct transmission measurements which produce a modulated signal that can be easily measured with phase sensitive detection. The MODTRAN and PDS techniques were tested on low levels of smoke and diluted samples of NO₂ in nitrogen, simulating light adsorption due to smoke. The results are evaluated against a set of ideal smoke meter criteria that include a desired smoke measurement range of 0.1 to 12 mg cu.m. (smoke numbers of 1 to 50) and a frequency response of 1 per second. The MODTRAN instrument is found to be inaccurate for smoke levels below 3 mg/cu.m. and is able to make a only about once every 20 seconds because of its large sample cell. The PDS instrument meets nearly all the characteristics of an ideal smoke meter: it has excellent sensitivity over a range of smoke levels from 0.1 to 20 mg/cu.m. (smoke numbers of 1 to 60) and good frequency response (1 per second). Author

N87-13731*# National Aeronautics and Space Administration. Lewis Research Center, Cleveland, Ohio.

EVALUATION OF DIFFUSE-ILLUMINATION HOLOGRAPHIC CINEMATOGRAPHY IN A FLUTTER CASCADE

A. J. DECKER Jul. 1986 33 p
(NASA-TP-2593; E-2937; NAS 1.60:2593) Avail: NTIS HC A03/MF A01 CSCL 14E

Since 1979, the Lewis Research Center has examined holographic cinematography for three-dimensional flow visualization. The Nd:YAG lasers used were Q-switched, double-pulsed, and frequency-doubled, operating at 20 pulses per second. The primary subjects for flow visualization were the shock waves produced in two flutter cascades. Flow visualization was by diffuse-illumination, double-exposure, and holographic interferometry. The performances of the lasers, holography, and diffuse-illumination interferometry are evaluated in single-window wind tunnels. The fringe-contrast factor is used to evaluate the results. The effects of turbulence on shock-wave visualization in a transonic flow are discussed. The depth of field for visualization of a turbulent structure is demonstrated to be a measure of the relative density and scale of that structure. Other items discussed are the holographic emulsion, tests of coherence and polarization, effects of windows and diffusers, hologram bleaching, laser configurations, influence and handling of specular reflections, modes of fringe localization, noise sources, and coherence requirements as a function of the pulse energy. Holography and diffuse illumination interferometry are also reviewed. Author

N87-15452*# National Aeronautics and Space Administration. Lewis Research Center, Cleveland, Ohio.

GAS PARTICLE RADIATOR Patent Application

DONALD L. CHUBB, inventor (to NASA) 9 Oct. 1986 8 p
(NASA-CASE-LEW-14297-1; NAS 1.71:LEW-14297-1; US-PATENT-APPL-SN-917125) Avail: NTIS HC A02/MF A01 CSCL 82B

A gas particle radiator adapted to operate in a microgravity space environment having a transparent boundary which transmits energy in the infrared spectrum, and a gas particle mixture that yields high absorption and emittances are described. NASA

N87-18057*# National Aeronautics and Space Administration. Lewis Research Center, Cleveland, Ohio.

FOUR SPOT LASER ANEMOMETER AND OPTICAL ACCESS TECHNIQUES FOR TURBINE APPLICATIONS

MARK P. WERNET 1987 16 p Proposed for presentation at the 12th International Congress on Instrumentation in Aerospace Simulation Facilities, Williamsburg, Va., 22-25 Jun. 1987; sponsored by IEEE Aerospace and Electric Systems Society and NASA Langley Research Center
(NASA-TM-88972; E-3440; NAS 1.15:88972) Avail: NTIS HC A02/MF A01 CSCL 14B

A time-of-flight anemometer (TOFA) system, utilizing a spatial lead-lag filter for bipolar pulse generation was constructed and tested. This system, called a Four Spot Laser Anemometer, was specifically designed for use in high speed, turbulent flows in the presence of walls or surfaces. The TOFA system uses elliptical spots to increase the flow acceptance angle to be comparable with that of a fringe type anemometer. The tightly focused spots used in the Four Spot yield excellent flare light rejection capabilities. Good results were obtained to 75 microns normal to a surface, with a f/2.5 collecting lens. This system is being evaluated for use in a warm turbine facility. Results from both a particle lag velocity experiment and boundary layer profiles will be discussed. In addition, an analysis of the use of curved windows in a turbine casing will be presented. Curved windows, matching the inner radius of the turbine casing, preserve the flow conditions, but introduce astigmatic aberrations. A correction optic was designed that virtually eliminates these astigmatic aberrations throughout the intrablade survey region for normal incidence. Author

N87-18801*# National Aeronautics and Space Administration. Lewis Research Center, Cleveland, Ohio.

ACCELERATION DISPLAY SYSTEM FOR AIRCRAFT ZERO-GRAVITY RESEARCH

MARC G. MILLIS Mar. 1987 22 p
(NASA-TM-87358; E-3117; NAS 1.15:87358) Avail: NTIS HC A02/MF A01 CSCL 01D

The features, design, calibration, and testing of Lewis Research Center's acceleration display system for aircraft zero-gravity research are described. Specific circuit schematics and system specifications are included as well as representative data traces from flown trajectories. Other observations learned from developing and using this system are mentioned where appropriate. The system, now a permanent part of the Lewis Learjet zero-gravity program, provides legible, concise, and necessary guidance information enabling pilots to routinely fly accurate zero-gravity trajectories. Regular use of this system resulted in improvements of the Learjet zero-gravity flight techniques, including a technique to minimize later accelerations. Lewis Gates Learjet trajectory data show that accelerations can be reliably sustained within 0.01 g for 5 consecutive seconds, within 0.02 g for 7 consecutive seconds, and within 0.04 g for up to 20 second. Lewis followed the past practices of acceleration measurement, yet focussed on the acceleration displays. Refinements based on flight experience included evolving the ranges, resolutions, and frequency responses to fit the pilot and the Learjet responses. Author

N87-19684*# National Aeronautics and Space Administration. Lewis Research Center, Cleveland, Ohio.

AGREEMENT BETWEEN EXPERIMENTAL AND THEORETICAL EFFECTS OF NITROGEN GAS FLOWRATE ON LIQUID JET ATOMIZATION

ROBERT D. INGEBO 1987 11 p Prepared for presentation at the 23rd Joint Propulsion Conference, San Diego, Calif., 29 Jun. - 2 Jul. 1987; sponsored by AIAA, ASME, and SAE
(NASA-TM-89821; E-3467; NAS 1.15:89821; AIAA-87-2138) Avail: NTIS HC A02/MF A01 CSCL 20D

Two-phase flows were investigated by using high velocity nitrogen gas streams to atomize small-diameter liquid jets. Tests were conducted primarily in the acceleration-wave regime for liquid jet atomization, where it was found that the loss of droplets due to vaporization had a marked effect on drop size measurements. In addition, four identically designed two-fluid atomizers were

fabricated and tested for similarity of spray profiles. A scattered-light scanner was used to measure a characteristic drop diameter, which was correlated with nitrogen gas flowrate. The exponent of 1.33 for nitrogen gas flowrate is identical to that predicted by atomization theory for liquid jet breakup in the acceleration-wave regime. This is higher than the value of 1.2 which was previously obtained at a sampling distance of 4.4 cm downstream of the atomizer. The difference is attributed to the fact that drop-size measurements obtained at a 2.2 cm sampling distance are less effected by vaporization and dispersion of small droplets and therefore should give better agreement with atomization theory. Profiles of characteristic drop diameters were also obtained by making at least five line-of-sight measurements across the spray at several horizontal positions above and below the center line of the spray.

Author

N87-19686*# Pratt and Whitney Aircraft, West Palm Beach, Fla. Government Products Div.

FURTHER DEVELOPMENT OF THE DYNAMIC GAS TEMPERATURE MEASUREMENT SYSTEM. VOLUME 1: TECHNICAL EFFORTS Final Report

D. L. ELMORE, W. W. ROBINSON, and W. B. WATKINS Aug. 1986 157 p

(Contract NAS3-24228)

(NASA-CR-179513-VOL-1; NAS 1.26:179513-VOL-1; P/W/GPD-FR-19381-VOL-1) Avail: NTIS HC A08/MF A01 CSCL 14B

A compensated dynamic gas temperature thermocouple measurement method was experimentally verified. Dynamic gas temperature signals from a flow passing through a chopped-wheel signal generator and an atmospheric pressure laboratory burner were measured by the dynamic temperature sensor and other fast-response sensors. Compensated data from dynamic temperature sensor thermoelements were compared with fast-response sensors. Results from the two experiments are presented as time-dependent waveforms and spectral plots. Comparisons between compensated dynamic temperature sensor spectra and a commercially available optical fiber thermometer compensated spectra were made for the atmospheric burner experiment. Increases in precision of the measurement method require optimization of several factors, and directions for further work are identified.

Author

N87-20279*# National Aeronautics and Space Administration. Lewis Research Center, Cleveland, Ohio.

THE CHEMICAL SHOCK TUBE AS A TOOL FOR STUDYING HIGH-TEMPERATURE CHEMICAL KINETICS

THEODORE A. BRABBS *In its* NASA-Chinese Aeronautical Establishment (CAE) Symposium p 207-224 1986

Avail: NTIS HC A01/MF A01 CSCL 14B

Although the combustion of hydrocarbons is our primary source of energy today, the chemical reactions, or pathway, by which even the simplest hydro-carbon reacts with atmospheric oxygen to form CO₂ and water may not always be known. Furthermore, even when the reaction pathway is known, the reaction rates are always under discussion. The shock tube has been an important and unique tool for building a data base of reaction rates important in the combustion of hydrocarbon fuels. The ability of a shock wave to bring the gas sample to reaction conditions rapidly and homogeneously makes shock-tube studies of reaction kinetics extremely attractive. In addition to the control and uniformity of reaction conditions achieved with shock-wave methods, shock compression can produce gas temperatures far in excess of those in conventional reactors. Argon can be heated to well over 10 000 K, and temperatures around 5000 K are easily obtained with conventional shock-tube techniques. Experiments have proven the validity of shock-wave theory; thus, reaction temperatures and pressures can be calculated from a measurement of the incident shock velocity. A description is given of the chemical shock tube and auxiliary equipment and of two examples of kinetic experiments conducted in a shock tube.

Author

N87-20515*# National Aeronautics and Space Administration. Lewis Research Center, Cleveland, Ohio.

PRETEST UNCERTAINTY ANALYSIS FOR CHEMICAL ROCKET ENGINE TESTS

KENNETH J. DAVIDIAN 1987 16 p Presented at the 33rd International Instrumentation Symposium, Las Vegas, Nev., 3-8 May 1987; sponsored by the Instrument Society of America (NASA-TM-89819; E-3465; NAS 1.15:89819) Avail: NTIS HC A02/MF A01 CSCL 14B

A parametric pretest uncertainty analysis has been performed for a chemical rocket engine test at a unique 1000:1 area ratio altitude test facility. Results from the parametric study provide the error limits required in order to maintain a maximum uncertainty of 1 percent on specific impulse. Equations used in the uncertainty analysis are presented.

Author

N87-20516*# National Aeronautics and Space Administration. Lewis Research Center, Cleveland, Ohio.

A COMPUTER CONTROLLED SIGNAL PREPROCESSOR FOR LASER FRINGE ANEMOMETER APPLICATIONS

LAWRENCE G. OBERLE Mar. 1987 28 p Presented at the Conference on the Use of Computers in Laser Velocimetry, Saint-Louis, France

(NASA-TM-88982; E-3452; NAS 1.15:88982) Avail: NTIS HC A03/MF A01 CSCL 14B

The operation of most commercially available laser fringe anemometer (LFA) counter-processors assumes that adjustments are made to the signal processing independent of the computer used for reducing the data acquired. Not only does the researcher desire a record of these parameters attached to the data acquired, but changes in flow conditions generally require that these settings be changed to improve data quality. Because of this limitation, on-line modification of the data acquisition parameters can be difficult and time consuming. A computer-controlled signal preprocessor has been developed which makes possible this optimization of the photomultiplier signal as a normal part of the data acquisition process. It allows computer control of the filter selection, signal gain, and photo-multiplier voltage. The raw signal from the photomultiplier tube is input to the preprocessor which, under the control of a digital computer, filters the signal and amplifies it to an acceptable level. The counter-processor used at Lewis Research Center generates the particle interarrival times, as well as the time-of-flight of the particle through the probe volume. The signal preprocessor allows computer control of the acquisition of these data. Through the preprocessor, the computer also can control the hand shaking signals for the interface between itself and the counter-processor. Finally, the signal preprocessor splits the pedestal from the signal before filtering, and monitors the photo-multiplier dc current, sends a signal proportional to this current to the computer through an analog to digital converter, and provides an alarm if the current exceeds a predefined maximum. Complete drawings and explanations are provided in the text as well as a sample interface program for use with the data acquisition software.

Author

N87-22179*# United Technologies Research Center, East Hartford, Conn.

HIGH TEMPERATURE STATIC STRAIN GAGE ALLOY DEVELOPMENT PROGRAM Final Report

C. O. HULSE, R. S. BAILEY, and F. D. LEMKEY Mar. 1985 90 p

(Contract NAS3-23169)

(NASA-CR-174833; NAS 1.26:174833; R85-915952-13) Avail: NTIS HC A05/MF A01 CSCL 14B

The literature, applicable theory and finally an experimental program were used to identify new candidate alloy systems for use as the electrical resistance elements in static strain gages up to 1250K. The program goals were 50 hours of use in the environment of a test stand gas turbine engine with measurement accuracies equal to or better than 10 percent of full scale for strains up to + or - 2000 microstrain. As part of this effort, a computerized electrical resistance measurement system was constructed for use at temperatures between 300K and 1250K

35 INSTRUMENTATION AND PHOTOGRAPHY

and heating and cooling rates of 250K/min and 10K/min. The two best alloys were an iron-chromium-aluminum alloy and a palladium base alloy. Although significant progress was made, it was concluded that a considerable additional effort would be needed to fully optimize and evaluate these candidate systems.

Author

N87-22181*# National Aeronautics and Space Administration. Lewis Research Center, Cleveland, Ohio.

USE OF A LIQUID-CRYSTAL, HEATER-ELEMENT COMPOSITE FOR QUANTITATIVE, HIGH-RESOLUTION HEAT TRANSFER COEFFICIENTS ON A TURBINE AIRFOIL, INCLUDING TURBULENCE AND SURFACE ROUGHNESS EFFECTS

STEVEN A. HIPPENSTEELE, LOUIS M. RUSSELL, and FELIX J. TORRES May 1987 16 p Presented at the Winter Annual Meeting of the American Society of Mechanical Engineers, Anaheim, Calif., 7-12 Dec. 1986

(NASA-TM-87355; E-3021; NAS 1.15:87355) Avail: NTIS HC A02/MF A01 CSCL 14B

Local heat transfer coefficients were measured along the midchord of a three-times-size turbine vane airfoil in a static cascade operated at room temperature over a range of Reynolds numbers. The test surface consisted of a composite of commercially available materials: a Mylar sheet with a layer of cholestric liquid crystals, which change color with temperature, and a heater made of a polyester sheet coated with vapor-deposited gold, which produces uniform heat flux. After the initial selection and calibration of the composite sheet, accurate, quantitative, and continuous heat transfer coefficients were mapped over the airfoil surface. Tests were conducted at two free-stream turbulence intensities: 0.6 percent, which is typical of wind tunnels; and 10 percent, which is typical of real engine conditions. In addition to a smooth airfoil, the effects of local leading-edge sand roughness were also examined for a value greater than the critical roughness. The local heat transfer coefficients are presented for both free-stream turbulence intensities for inlet Reynolds numbers from 1.20 to 5.55 x 10 to the 5th power. Comparisons are also made with analytical values of heat transfer coefficients obtained from the STAN5 boundary layer code.

Author

N87-22772*# National Aeronautics and Space Administration. Lewis Research Center, Cleveland, Ohio.

PROGRESS ON THIN-FILM SENSORS FOR SPACE PROPULSION TECHNOLOGY

WALTER S. KIM *In its* Structural Integrity and Durability of Reusable Space Propulsion Systems p 39-42 1987

Avail: NTIS HC A10/MF A01 CSCL 14B

The objective is to develop thin-film thermocouples for Space Shuttle Main Engine (SSME) components. Thin-film thermocouples have been developed for aircraft gas turbine engines and are in use for temperature measurement on turbine blades to 1800 F. The technology established for aircraft gas turbine engines will be adapted to the materials and environment encountered in the SSME. Specific goals are to expand the existing in-house thin-film sensor technology and to test the survivability and durability of thin-film sensors in the SSME environment.

Author

N87-22959*# National Aeronautics and Space Administration. Lewis Research Center, Cleveland, Ohio.

LASER ANEMOMETRY TECHNIQUES FOR TURBINE APPLICATIONS

MARK P. WERNET and LAWRENCE G. OBERLE Jun. 1987 17 p Presented at the 32nd International Gas Turbine Conference and Exhibition, Anaheim, Calif., 31 May - 4 Jun. 1987; sponsored by ASME

(NASA-TM-88953; E-3369; NAS 1.15:88953) Avail: NTIS HC A02/MF A01 CSCL 14B

Laser anemometry offers a nonintrusive means for obtaining flow field information. Current research at NASA Lewis Research Center is focused on instrumenting a warm turbine facility with a laser anemometer system. In an effort to determine the laser anemometer system best qualified for the warm turbine environment, the performance of a conventional laser fringe

anemometer and a two spot time of flight system were compared with a new, modified time of flight system, called a Four Spot laser anemometer. The comparison measurements were made in highly turbulent flows near walls. The Four Spot anemometer uses elliptical spots to increase the flow acceptance angle to be comparable to that of a Laser Fringe Anemometer. Also, the Four Spot uses an optical code that vastly simplifies the pulse detection processor. The results of the comparison measurements will exemplify which laser anemometer system is best suited to the hostile environment typically encountered in warm rotating turbomachinery.

Author

N87-22960*# Sverdrup Technology, Inc., Cleveland, Ohio.

OPTICAL STRAIN MEASUREMENT SYSTEM DEVELOPMENT, PHASE 1 Final Report

CHRISTIAN T. LANT and WALID QAQISH May 1987 39 p (Contract NAS3-24105)

(NASA-CR-179619; E-3550; NAS 1.26:179619) Avail: NTIS HC A03/MF A01 CSCL 14B

A laser speckle, differential strain measurement system was built and tested for future applications in hostile environments. One dimensional electronic correlation of speckle pattern movement allows a quasi-real time measure of strain. The system was used successfully to measure uniaxial strain reaching into plastic deformation of a test specimen, at temperatures ranging to 450 C. A resolution of 16 microstrain is given by the photodiode array sensor pitch and the specimen to sensor separation. The strain measurement limit of the gauge is determined by air density perturbations causing decorrelation of the reference and shifted speckle patterns, and may be improved by limiting convective flow in the immediate vicinity of the test specimen.

Author

N87-25552*# United Technologies Research Center, East Hartford, Conn.

ADVANCED HIGH TEMPERATURE STATIC STRAIN SENSOR DEVELOPMENT Final Report

C. O. HULSE, K. A. STETSON, H. P. GRANT, S. M. JAMEIKIS, W. W. MOREY, P. RAYMONDO, T. W. GRUDKOWSKI, and R. S. BAILEY Aug. 1986 205 p

(Contract NAS3-22126)

(NASA-CR-179520; NAS 1.26:179520; R86-995875-28) Avail: NTIS HC A10/MF A01 CSCL 14B

An examination was made into various techniques to be used to measure static strain in gas turbine liners at temperatures up to 1150 K (1600 F). The methods evaluated included thin film and wire resistive devices, optical fibers, surface acoustic waves, the laser speckle technique with a heterodyne readout, optical surface image and reflective approaches and capacitive devices. A preliminary experimental program to develop a thin film capacitive device was dropped because calculations showed that it would be too sensitive to thermal gradients. In a final evaluation program, the laser speckle technique appeared to work well up to 1150 K when it was used through a relatively stagnant air path. The surface guided acoustic wave approach appeared to be interesting but to require too much development effort for the funds available. Efforts to develop a FeCrAl resistive strain gage system were only partially successful and this part of the effort was finally reduced to a characterization study of the properties of the 25 micron diameter FeCrAl (Kanthal A-1) wire. It was concluded that this particular alloy was not suitable for use as the resistive element in a strain gage above about 1000 K.

Author

N87-25562*# National Aeronautics and Space Administration. Lewis Research Center, Cleveland, Ohio.

AMPLITUDE SPECTRUM MODULATION TECHNIQUE FOR ANALOG DATA PROCESSING IN FIBER OPTIC SENSING SYSTEM WITH TEMPORAL SEPARATION OF CHANNELS

GRIGORY ADAMOVSKY 1987 10 p Presented at the O-E/Fibers '87 Symposium on Fiber Optics and Integrated Optoelectronics, San Diego, Calif., 16-21 Aug. 1987; sponsored by SPIE and International Society for Optical Engineering (NASA-TM-100152; E-3714; NAS 1.15:100152) Avail: NTIS HC A02/MF A01 CSCL 14B

A novel technique to analyze analog data in fiber optic sensing systems with temporal separation of channels is proposed. A theoretical explanation of the process is presented and an experimental setup that was used to obtain data is described.

Author

N87-26326*# Sverdrup Technology, Inc., Arnold Air Force Station, Tenn.

OPTICAL STRAIN MEASUREMENT SYSTEM DEVELOPMENT Final Report

CHRISTIAN T. LANT and WALID QAQISH Jul. 1987 15 p Prepared for presentation at the O-E/Fibers Symposium on Fiber Optics and Integrated Optoelectronics, San Diego, Calif., 16-21 Aug. 1987; sponsored in part by SPIE and The International Society for Optical Engineering (Contract NAS3-24105)

(NASA-CR-179646; E-3678; NAS 1.26:179646) Avail: NTIS HC A02/MF A01 CSCL 14B

A laser speckle, differential strain measurement system has been built and tested for future applications in hostile environments. One-dimensional electronic correlation of speckle pattern movement allows a quasi-real time measure of strain. The system has been used successfully to measure uniaxial strain reaching into plastic deformation of a test specimen, at temperatures ranging to 450 C. A resolution of 16 microstrain is given by the photodiode array sensor pitch and the specimen to sensor separation. The strain measurement error is estimated to be ± 18 microstrain ± 3 percent of the strain reading. The upper temperature limit of the gauge is determined by air density perturbations causing decorrelation of the reference and shifted speckle patterns, and may be improved by limiting convective flow in the immediate vicinity of the test specimen.

Author

N87-26327*# Cleveland State Univ., Ohio. Dept. of Civil Engineering.

OPTICAL STRAIN MEASURING TECHNIQUES FOR HIGH TEMPERATURE TENSILE TESTING

JOHN Z. GYEKENYESI and JOHN H. HEMANN Jun. 1987 55 p

(Contract NAG3-749)

(NASA-CR-179637; NAS 1.26:179637) Avail: NTIS HC A04/MF A01 CSCL 14B

A number of optical techniques used for the analysis of in-plane displacements or strains are reviewed. The application would be for the high temperature, approximately 1430 C (2600 F), tensile testing of ceramic composites in an oxidizing atmosphere. General descriptions of the various techniques and specifics such as gauge lengths and sensitivities are noted. Also, possible problems with the use of each method in the given application are discussed.

Author

N87-28869*# United Technologies Research Center, East Hartford, Conn.

HIGH TEMPERATURE STATIC STRAIN GAGE DEVELOPMENT CONTRACT, TASKS 1 AND 2 Interim Report

C. O. HULSE, R. S. BAILEY, H. P. GRANT, and J. S. PRZYBYSZEWSKI Jul. 1987 82 p

(Contract NAS3-23722)

(NASA-CR-180811; NAS 1.26:180811; R87-916527-1) Avail: NTIS HC A05/MF A01 CSCL 14B

Results are presented for the first two tasks to develop resistive strain gage systems for use up to 1250 K on blades and vanes in

gas turbine engines under tests. The objective of these two tasks was to further improve and evaluate two static strain gage alloys identified as candidates in a previous program. Improved compositions were not found for either alloy. Further efforts on the Fe-11.9Al-10.6Cr weight percent alloy were discontinued because of time dependent drift problems at 1250 K in air. When produced as a 6.5 micrometer thick sputtered film, the Pd-13Cr weight percent alloys is not sufficiently stable for this use in air at 1250 K and a protective overcoat system will need to be developed.

B.G.

N87-28880*# National Aeronautics and Space Administration. Lewis Research Center, Cleveland, Ohio.

BONDING LEXAN AND SAPPHIRE TO FORM HIGH-PRESSURE, FLAME-RESISTANT WINDOW

WILLIAM R. RICHARDSON and ERNIE D. WALKER 1987 8 p Proposed for presentation at the 129th Technical Conference and Equipment Exhibit, Los Angeles, Calif., 31 Oct. - 4 Nov. 1987; sponsored by the Society of Motion Picture and Television Engineers

(NASA-TM-100188; E-3769; NAS 1.15:100188) Avail: NTIS HC A02/MF A01 CSCL 13H

Flammable materials have been studied in normal gravity and microgravity for many years. Photography plays a major role in the study of the combustion process giving a permanent visual record that can be analyzed. When these studies are extended to manned spacecraft, safety becomes a primary concern. The need for a high-pressure, flame-resistant, shatter-resistant window permitting photographic recording of combustion experiments in manned spacecraft prompted the development of a method for bonding Lexan and sapphire. Materials that resist shattering (e.g., Lexan) are not compatible with combustion experiments; the material loses strength at combustion temperatures. Sapphire is compatible with combustion temperatures in oxygen-enriched atmospheres but is subject to shattering. Combining the two materials results in a shatter-resistant, flame-resistant window. Combustion in microgravity produces a low-visibility flame; however, flame propagation and flame characteristics are readily visible as long as there is no deterioration of the image. Since an air gap between the Lexan and the sapphire would reduce transmission, a method was developed for bonding these unlike materials to minimize light loss.

Author

N87-28883*# Pratt and Whitney Aircraft Group, East Hartford, Conn. Commercial Engineering Dept.

THIN FILM STRAIN GAGE DEVELOPMENT PROGRAM Final Program

H. P. GRANT, J. S. PRZYBYSZEWSKI, W. L. ANDERSON, and R. G. CLAING Dec. 1983 194 p

(Contract NAS3-21262)

(NASA-CR-174707; NAS 1.26:174707; PWA-5628-69) Avail: NTIS HC A09/MF A01 CSCL 14B

Sputtered thin-film dynamic strain gages of 2 millimeter (0.08 in) gage length and 10 micrometer (0.0004 in) thickness were fabricated on turbojet engine blades and tested in a simulated compressor environment. Four designs were developed, two for service to 600 K (600 F) and two for service to 900 K (1200 F). The program included a detailed study of guidelines for formulating strain-gage alloys to achieve superior dynamic and static gage performance. The tests included gage factor, fatigue, temperature cycling, spin to 100,000 G, and erosion. Since the installations are 30 times thinner than conventional wire strain gage installations, and any alteration of the aerodynamic, thermal, or structural performance of the blade is correspondingly reduced, dynamic strain measurement accuracy higher than that attained with conventional gages is expected. The low profile and good adherence of the thin film elements is expected to result in improved durability over conventional gage elements in engine tests.

Author

MECHANICAL ENGINEERING

Includes auxiliary systems (nonpower); machine elements and processes; and mechanical equipment.

A87-14656*# National Aeronautics and Space Administration. Lewis Research Center, Cleveland, Ohio.

FACTORS THAT AFFECT THE FATIGUE STRENGTH OF POWER TRANSMISSION SHAFTING AND THEIR IMPACT ON DESIGN

S. H. LEOWENTHAL (NASA, Lewis Research Center, Cleveland, OH) ASME, Transactions, Journal of Mechanisms, Transmission, and Automation in Design, vol. 108, March 1986, p. 106-114; Discussion, p. 115-118; Author's Closure, p. 118. Previously announced in STAR as N84-26029. refs

A long standing objective in the design of power transmission shafting is to eliminate excess shaft material without compromising operational reliability. A shaft design method is presented which accounts for variable amplitude loading histories and their influence on limited life designs. The effects of combined bending and torsional loading are considered along with a number of application factors known to influence the fatigue strength of shafting materials. Among the factors examined are surface condition, size, stress concentration, residual stress and corrosion fatigue. Author

A87-17269* National Aeronautics and Space Administration. Lewis Research Center, Cleveland, Ohio.

A SIMPLE METHOD FOR MONITORING SURFACE TEMPERATURES IN PLASMA TREATMENTS

R. R. MANORY (NASA, Lewis Research Center, Cleveland, OH) Journal of Vacuum Science and Technology A (ISSN 0734-2101), vol. 4, Sept.-Oct. 1986, p. 2392-2394.

A method consisting of applying temperature markers on the specimen is described for measuring the highest temperature reached by very thin films in situ during deposition. In the first test setup, lowering the input power to 500 W only effected the 177-C marker, while increasing the input power to 1.25 kW effected the 274-C marker. In tests conducted in a dc plasma with markers placed on the uncooled cathode in Ar plasma, the maximum temperatures indicated by the thermocouple matched a change in color of the markers, and no effect of earlier sublimation or decomposition was noted. R.R.

A87-18033* National Aeronautics and Space Administration. Lewis Research Center, Cleveland, Ohio.

OVERVIEW OF THE 1986 FREE-PISTON STIRLING SP-100 ACTIVITIES AT THE NASA LEWIS RESEARCH CENTER

J. G. SLABY (NASA, Lewis Research Center, Cleveland, OH) IN: IECEC '86; Proceedings of the Twenty-first Intersociety Energy Conversion Engineering Conference, San Diego, CA, August 25-29, 1986. Volume 1. Washington, DC, American Chemical Society, 1986, p. 420-429. Previously announced in STAR as N86-26261. refs

An overview of the NASA Lewis Research Center SP-100 free-piston Stirling engine activities is presented. These activities include a free-piston Stirling space-power technology feasibility demonstration project as part of the SP-100 program being conducted in support of the Department of Defense (DOD), Department of Energy (DOE), and NASA. The space-power Stirling advanced technology effort, under SP-100, addresses the status of the 25 kWe Space Power Demonstrator Engine (SPDE) including test results. Future space-power projections are presented along with a description of a study that will investigate the feasibility of scaling a single-cylinder free-piston Stirling space-power module to the 150 kW power range. Design parameters and conceptual design features will be presented for a 25 kWe, single-cylinder free-piston Stirling space-power converter. A description of a hydrodynamic gas bearing concept is presented whereby the displacer of a 1 kWe free-piston Stirling engine is modified to demonstrate the bearing concept. And finally the goals of a

conceptual design for a 25 kWe Solar Advanced Stirling Conversion System capable of delivering electric power to an electric utility grid are discussed. Author

A87-18036* National Aeronautics and Space Administration. Lewis Research Center, Cleveland, Ohio.

TESTING OF A VARIABLE-STROKE STIRLING ENGINE

L. G. THIEME (NASA, Lewis Research Center, Cleveland, OH) and D. J. ALLEN (Sverdrup Technology, Inc., Cleveland, OH) IN: IECEC '86; Proceedings of the Twenty-first Intersociety Energy Conversion Engineering Conference, San Diego, CA, August 25-29, 1986. Volume 1. Washington, DC, American Chemical Society, 1986, p. 457-462.

Testing of a variable-stroke Stirling engine at NASA Lewis has been completed. In support of the DOE Stirling Engine Highway Vehicle Systems Program, the engine was tested for about 70 hours total with both He and H₂ working fluids over a range of pressures and strokes. A direct comparison was made of part-load efficiencies obtained with variable-stroke (VS) and variable-pressure operation. Two failures with the variable-angle swash-plate drive system limited testing to low power levels. These failures are not thought to be caused by problems inherent with the VS concept but do emphasize the need for careful design in the area of the crossheads. Author

A87-18037* Mechanical Technology, Inc., Latham, N. Y.

EVALUATION OF STIRLING ENGINE APPENDIX GAP LOSSES

S. C. HUANG and R. BERGGREN (Mechanical Technology, Inc., Latham, NY) IN: IECEC '86; Proceedings of the Twenty-first Intersociety Energy Conversion Engineering Conference, San Diego, CA, August 25-29, 1986. Volume 1. Washington, DC, American Chemical Society, 1986, p. 562-568. DOE-sponsored research. refs

(Contract DEN3-32)

The efficiency of a Stirling engine can be strongly influenced by the heat transfer losses associated with its appendix gap region. The cyclic energy flows in this region are related to the temperature gradient along the piston and cylinder partition walls, the reciprocating motion of the piston, the pressure variation in the Stirling cycle and the leakage flow across the cold-end seal. This paper outlines a numerical model to simulate these cyclic energy flows and the subsequent effort to correlate it with engine test data. The sensitivity of the appendix gap loss to selected parameters and comparisons with test results are presented. Author

A87-19502* Akron Univ., Ohio.

THERMAL SHAFT EFFECTS ON LOAD-CARRYING CAPACITY OF A FULLY COUPLED, VARIABLE-PROPERTIES CRYOGENIC JOURNAL BEARING

M. J. BRAUN, R. L. WHEELER, III (Akron, University, OH), and R. C. HENDRICKS (NASA, Lewis Research Center, Cleveland, OH) ASLE and ASME, Joint Tribology Conference, Pittsburgh, PA, Oct. 20-22, 1986. 11 p. refs

(Contract NAG3-304)

(ASLE PREPRINT 86-TC-6B-1)

The purpose of this work was to perform a rather complete analysis for a cryogenic (oxygen) journal bearing. The Reynolds equation required coupling and simultaneous solution with the fluid energy equation. To correctly account for the changes in the fluid viscosity, the fluid energy equation was coupled with the shaft and bearing heat conduction energy equations. The effects of pressure and temperature on the density, viscosity, and load-carrying capacity were further discussed as analysis parameters, with respect to relative eccentricity and the angular velocity. The isothermal fluid case and the adiabatic fluid case represented the limiting boundaries. The discussion was further extrapolated to study the Sommerfeld number dependency on the fluid Nusselt number and its consequence on possible total loss of load-carrying capacity and/or seizure (catastrophic failure).

Author

A87-19529*# Texas A&M Univ., College Station.
COMPARISON OF HIRS' EQUATION WITH MOODY'S
EQUATION FOR DETERMINING ROTORDYNAMIC
COEFFICIENTS OF ANNULAR PRESSURE SEALS

C. C. NELSON and D. T. NGUYEN (Texas A & M University, College Station) ASME and ASLE, Joint Tribology Conference, Pittsburgh, PA, Oct. 20-22, 1986. 5 p. refs (Contract NAS3-181)

(ASME PAPER 86-TRIB-19)

The rotordynamic coefficients of an incompressible-flow annular pressure seal were determined using a bulk-flow model in conjunction with two different friction factor relationships. The first, Hirs' equation, assumes the friction factor is a function of Reynolds number only. The second, Moody's equation, approximates Moody's diagram and assumes the friction factor is a function of both Reynolds number and relative roughness. For each value of relative roughness, Hirs' constants were determined so that both equations gave the same magnitude and slope of the friction factor. For smooth seals, both relationships give the same results. For rough seals, Moody's equation predicts 44 percent greater direct stiffness, 35 percent greater cross-coupled stiffness, 19 percent smaller cross-coupled damping, 59 percent smaller cross-coupled inertia, and nominally the same direct damping and direct inertia.

Author

A87-19536*# Akron Univ., Ohio.

A FULLY COUPLED VARIABLE PROPERTIES
THERMOHYDRAULIC MODEL FOR A CRYOGENIC
HYDROSTATIC JOURNAL BEARING

M. J. BRAUN, R. L. WHEELER, III (Akron, University, OH), and R. C. HENDRICKS (NASA, Lewis Research Center, Cleveland, OH) ASME and ASLE, Joint Tribology Conference, Pittsburgh, PA, Oct. 20-22, 1986. 10 p. refs

(ASME PAPER 86-TRIB-55)

The goal set forth here is to continue the work started by Braun et al. (1984-1985) and present an integrated analysis of the behavior of the two row, 20 staggered pockets, hydrostatic cryogenic bearing used by the turbopumps of the Space Shuttle main engine. The variable properties Reynolds equation is fully coupled with the two-dimensional fluid film energy equation. The three-dimensional equations of the shaft and bushing model the boundary conditions of the fluid film energy equation. The effects of shaft eccentricity, angular velocity, and inertia pressure drops at pocket edge are incorporated in the model. Their effects on the bearing fluid properties, load carrying capacity, mass flow, pressure, velocity, and temperature form the ultimate object of this paper.

Author

A87-22501*# National Aeronautics and Space Administration.
 Lewis Research Center, Cleveland, Ohio.

THE EFFECTS OF ENGINE SPEED AND INJECTION
CHARACTERISTICS ON THE FLOW FIELD AND FUEL/AIR
MIXING IN MOTORED TWO-STROKE DIESEL ENGINES

H. L. NGUYEN (NASA, Lewis Research Center, Cleveland, OH), M. H. CARPENTER (NASA, Langley Research Center, Hampton, VA), and J. I. RAMOS (Carnegie-Mellon University, Pittsburgh, PA) AIAA, Aerospace Sciences Meeting, 25th, Reno, NV, Jan. 12-15, 1987. 39 p. Research supported by the U.S.-Spain Joint Committee for Scientific and Technological Cooperation. refs (Contract NAG3-21; NAG3-689)

(AIAA PAPER 87-0227)

A numerical analysis is presented on the effects of the engine speed, injection angle, droplet distribution function, and spray cone angle on the flow field, spray penetration and vaporization, and turbulence in a turbocharged motored two-stroke diesel engine. The results indicate that the spray penetration and vaporization, velocity, and turbulence kinetic energy increase with the intake swirl angle. Good spray penetration, vaporization, and mixing can be achieved by injecting droplets of diameters between 50 and 100 microns along a 120-deg cone at about 315 deg before top-dead-center for an intake swirl angle of 30 deg. The spray penetration and vaporization were found to be insensitive to the turbulence levels within the cylinder. The results have also indicated

that squish is necessary in order to increase the fuel vaporization rate and mixing. I.S.

A87-28624* Florida Univ., Gainesville.

A TWO-DIMENSIONAL NUMERICAL STUDY OF THE FLOW
INSIDE THE COMBUSTION CHAMBER OF A MOTORED
ROTARY ENGINE

T. I-P. SHIH, S. L. YANG (Florida, University, Gainesville), and H. J. SCHOCK (NASA, Lewis Research Center, Cleveland, OH) SAE, International Congress and Exposition, Detroit, MI, Feb. 24-28, 1986. 16 p. Previously announced in STAR as N86-19289. refs (SAE PAPER 860615)

A numerical study was performed to investigate the unsteady, multidimensional flow inside the combustion chambers of an idealized, two-dimensional, rotary engine under motored conditions. The numerical study was based on the time-dependent, two-dimensional, density-weighted, ensemble-averaged conservation equations of mass, species, momentum, and total energy valid for two-component ideal gas mixtures. The ensemble-averaged conservation equations were closed by a K-epsilon model of turbulence. This K-epsilon model of turbulence was modified to account for some of the effects of compressibility, streamline curvature, low-Reynolds number, and preferential stress dissipation. Numerical solutions to the conservation equations were obtained by the highly efficient implicit-factored method of Beam and Warming. The grid system needed to obtain solutions were generated by an algebraic grid generation technique based on transfinite interpolation. Results of the numerical study are presented in graphical form illustrating the flow patterns during intake, compression, gaseous fuel injection, expansion, and exhaust.

Author

A87-29275* Carnegie-Mellon Univ., Pittsburgh, Pa.

COMPARISONS BETWEEN THERMODYNAMIC AND ONE-DI-
MENSIONAL COMBUSTION MODELS OF SPARK-IGNITION
ENGINES

J. I. RAMOS (Carnegie-Mellon University, Pittsburgh, PA) Applied Mathematical Modelling (ISSN 0307-904X), vol. 10, Dec. 1986, p. 409-422. Sponsorship: U.S.-Spain Joint Committee for Scientific and Technological Cooperation. refs (Contract USSJCSTC-020; NAG3-21)

Results from a one-dimensional combustion model employing a constant eddy diffusivity and a one-step chemical reaction are compared with those of one-zone and two-zone thermodynamic models to study the flame propagation in a spark-ignition engine. One-dimensional model predictions are found to be very sensitive to the eddy diffusivity and reaction rate data. The average mixing temperature found using the one-zone thermodynamic model is higher than those of the two-zone and one-dimensional models during the compression stroke, and that of the one-dimensional model is higher than those predicted by both thermodynamic models during the expansion stroke. The one-dimensional model is shown to predict an accelerating flame even when the front approaches the cold cylinder wall.

R.R.

A87-35332* National Aeronautics and Space Administration.
 Lewis Research Center, Cleveland, Ohio.

A REVIEW OF RECENT ADVANCES IN SOLID FILM
LUBRICATION

T. SPALVINS (NASA, Lewis Research Center, Cleveland, OH) Journal of Vacuum Science and Technology A (ISSN 0734-2101), vol. 5, Mar.-Apr. 1987, p. 212-219. refs

Thin, adherent sputtered MoS₂ and ion plated metallic (Au, Ag, Pb) lubricating films are primarily used in precision contacting triboelement surfaces where wear debris formation is critical and high reliability requirements have to be satisfied. Detailed structural and compositional characterization of solid film lubricants is of prime importance. It is this information from the nano-micro-macro level which is needed to interpret and improve the frictional behavior and assure long endurance lives. The purpose of this paper is to summarize in a concise review the solid lubricant film structure and morphology and their effects on the tribological properties of the lubricant systems. The tribological performance of thin

lubricating films has significantly advanced through progressive understanding of the film parameters such as adhesion, cohesion, interface formation, nucleation and microstructural growth, critical film thickness and substrate finish, and temperature. Sputtered MoS₂ and ion plated Au, Ag, and Pb films are separately discussed and evaluated in terms of the above film parameters to establish the most desirable film structures and thicknesses in order to achieve effective lubrication. Author

A87-37686* National Aeronautics and Space Administration. Lewis Research Center, Cleveland, Ohio.

EFFECT OF INTERFERENCE FITS ON ROLLER BEARING FATIGUE LIFE

HAROLD H. COE and ERWIN V. ZARETSKY (NASA, Lewis Research Center, Cleveland, OH) ASLE Transactions (ISSN 0569-8197), vol. 30, April 1987, p. 131-140; Discussion, p. 140. Previously announced in STAR as N86-19616. refs

An analysis was performed to determine the effects of inner-ring speed and press fits on roller bearing fatigue life. The effects of the resultant hoop and radial stresses on the principal stresses were considered. The maximum shear stresses below the Hertzian contact were determined for different conditions of inner-ring speed and load, and were applied to a conventional roller bearing life analysis. The effect of mean stress was determined using Goodman diagram approach. Hoop stresses caused by press fits and centrifugal force can reduce bearing life by as much as 90 percent. Use of a Goodman diagram predicts life reduction of 20 to 30 percent. The depth of the maximum shear stress remains virtually unchanged. Author

A87-37687* Carnegie-Mellon Univ., Pittsburgh, Pa. CENTRIFUGAL INERTIA EFFECTS IN TWO-PHASE FACE SEAL FILMS

P. BASU, W. F. HUGHES, and R. M. BEELER (Carnegie-Mellon University, Pittsburgh, PA) ASLE Transactions (ISSN 0569-8197), vol. 30, April 1987, p. 177-186. refs (Contract NAG3-166)

A simplified, semianalytical model has been developed to analyze the effect of centrifugal inertia in two-phase face seals. The model is based on the assumption of isothermal flow through the seal, but at an elevated temperature, and takes into account heat transfer and boiling. Using this model, seal performance curves are obtained with water as the working fluid. It is shown that the centrifugal inertia of the fluid reduces the load-carrying capacity dramatically at high speeds and that operational instability exists under certain conditions. While an all-liquid seal may be starved at speeds higher than a 'critical' value, leakage always occurs under boiling conditions. Author

A87-38464*# Arizona State Univ., Tempe. OPTIMAL PLACEMENT OF CRITICAL SPEEDS IN ROTOR-BEARING SYSTEMS

M. RAJAN, S. D. RAJAN, H. D. NELSON (Arizona State University, Tempe), and W. J. CHEN ASME, Transactions, Journal of Vibration, Acoustics, Stress, and Reliability in Design (ISSN 0739-3717), vol. 109, April 1987, p. 152-157. refs (Contract NAG3-580)

The design of a rotor-bearing system is an iterative process in which the parameters that influence the design are modified until the desired design objectives are achieved. Primary among the design objectives is the minimization of the response amplitude within the operating range of the rotor system. An automated design procedure for the optimal placement of the critical speeds of a rotor is presented. The desired design objective is cast as a nonlinear programming problem that minimizes an objective function subject to constraints. The optimization program interacts with an analysis program to search for the feasible optimal design. Author

A87-45398*# General Electric Co., Cincinnati, Ohio. DYNAMIC DATA ACQUISITION, REDUCTION, AND ANALYSIS FOR THE IDENTIFICATION OF HIGH-SPEED COMPRESSOR COMPONENT POST-STABILITY CHARACTERISTICS

S. D. DVORAK, W. M. HOSNY, W. G. STEENKEN (General Electric Co., Aircraft Engine Business Group, Cincinnati, OH), and J. H. TAYLOR (General Electric Co., Schenectady, NY) AIAA, SAE, ASME, and ASEE, Joint Propulsion Conference, 23rd, San Diego, CA, June 29-July 2, 1987. 14 p. refs (Contract NAS3-2483; NAS3-24211) (AIAA PAPER 87-2089)

A compressor test was conducted in which transient data were obtained for the purpose of identifying the high-speed post-stability characteristics. The transient, surge-cycle nature of high-speed post-stability operation precludes the possibility of obtaining the characteristics in a steady-state manner, as is possible during low-speed poststability operation, which is characterized by quasi-steady rotating-stall behavior. Specialized compressor instrumentation was developed and was used to obtain the necessary surge-cycle performance data, which were then digitized, filtered, and analyzed. The high-speed post-stability characteristics were obtained through the use of a maximum likelihood-parameter estimation technique. The estimated characteristics were found to be insensitive to the presence of measurement noise and unmodelled system dynamics, but the compressor time-response constants, which were also estimated, were more sensitive to these same disturbances. Author

A87-45846* National Aeronautics and Space Administration. Lewis Research Center, Cleveland, Ohio.

ANALYSIS OF EXPERIMENTAL SHAFT SEAL DATA FOR HIGH-PERFORMANCE TURBOMACHINES - AS FOR SPACE SHUTTLE MAIN ENGINES

R. C. HENDRICKS (NASA, Lewis Research Center, Cleveland, OH), R. L. MULLEN (Case Western Reserve University, Cleveland, OH), M. J. BRAUN (Akron, University, OH), R. E. BURCHAM, and W. A. DIAMOND (Rockwell International Corp., Rocketdyne Div., Canoga Park, CA) IN: Heat transfer and fluid flow in rotating machinery; Proceedings of the First International Symposium on Transport Phenomena, Honolulu, HI, Apr. 28-May 3, 1985. Washington, DC, Hemisphere Publishing Corp., 1987, p. 288-303. Previously announced in STAR as N85-21569. refs

High-pressure, high-temperature seal flow (leakage) data for nonrotating and rotating Raleigh-step and convergent-tapered-bore seals were characterized in terms of a normalized flow coefficient. The data for normalized Rayleigh-step and nonrotating tapered-bore seals were in reasonable agreement with theory, but data for the rotating tapered-bore seals were not. The tapered-bore-seal operational clearances estimated from the flow data were significantly larger than calculated. Although clearances are influenced by wear from conical to cylindrical geometry and errors in clearance corrections, the problem was isolated to the shaft temperature - rotational speed clearance correction. The geometric changes support the use of some conical convergence in any seal. Under these conditions rotation reduced the normalized flow coefficient by nearly 10 percent. Author

A87-48500* Dartmouth Coll., Hanover, N.H. THE ROLE OF NEAR-SURFACE PLASTIC DEFORMATION IN THE WEAR OF LAMELLAR SOLIDS

F. E. KENNEDY, L. A. HARTMAN, K. E. HAUCK, and V. A. SURPRENANT (Dartmouth College, Hanover, NH) IN: Wear of materials 1985; Proceedings of the International Conference, Vancouver, Canada, Apr. 14-18, 1985. New York, American Society of Mechanical Engineers, 1985, p. 273-279. refs (Contract NSG-3253)

It is shown in this paper that the role of surface and near-surface plastic deformation is especially significant in both sliding and abrasive wear of lamellar composites. Lamellar structures were produced artificially from alternate layers of pure copper and pure tin or lead foils. The resulting composites were tested in three different wear tests: single-pass abrasion by a sharp, hard abrader; multiple-pass rubbing by a hard, rounded abrader; and pin-on-disk

sliding. In each case the counterface was a hard alloy steel. Tests were run with the composite lamellae in two orientations: perpendicular and parallel to the sliding direction. It was found that the composites had much less wear resistance and greater abrasability when oriented perpendicular to the rub direction. The mechanisms for wear particle removal and the role of plastic deformation in the process were studied by plasticity analysis and by microscopic (SEM and optical) observation. Author

A87-48780* Mechanical Technology, Inc., Latham, N. Y.

MOD II ENGINE PERFORMANCE

ALBERT E. RICHEY and SHYAN-CHERNG HUANG (Mechanical Technology, Inc., Latham, NY) SAE, International Congress and Exposition, Detroit, MI, Feb. 23-27, 1987. 8 p. DOE-supported research.

(Contract DEN3-32)

(SAE PAPER 870101)

The testing of a prototype of an automotive Stirling engine, the Mod II, is discussed. The Mod II is a one-piece cast block with a V-4 single-crankshaft configuration and an annular regenerator/cooler design. The initial testing of Mod II concentrated on the basic engine, with auxiliaries driven by power sources external to the engine. The performance of the engine was tested at 720 C set temperature and 820 C tube temperature. At 720 C, it is observed that the power deficiency is speed dependent and linear, with a weak pressure dependency, and at 820 C, the power deficiency is speed and pressure dependent. The effects of buoyancy and nozzle spray pattern on the heater temperature spread are investigated. The characterization of the oil pump and the operating cycle and temperature spread tests are proposed for further evaluation of the engine. I.F.

A87-48781* Mechanical Technology, Inc., Latham, N. Y.

AUTOMOTIVE STIRLING ENGINE SYSTEM COMPONENT REVIEW

CHIP HINDES and ROBERT STOTTS (Mechanical Technology, Inc., Latham, NY) SAE, International Congress and Exposition, Detroit, MI, Feb. 23-27, 1987. 7 p.

(Contract DEN3-32)

(SAE PAPER 870102)

The design and testing of the power and combustion control system for the basic Stirling engine, Mod II, are examined. The power control system is concerned with transparent operation, and the Mod II uses engine working gas pressure variation to control the power output of the engine. The main components of the power control system, the power control valve, the pump-down system, and the hydrogen stable system, are described. The combustion control system consists of a combustion air supply system and an air/fuel ratio control system, and the system is to maintain constant heater head temperature, and to maximize combustion efficiency and to minimize exhaust emissions. I.F.

A87-48783* Florida Univ., Gainesville.

FUEL-AIR MIXING AND COMBUSTION IN A TWO-DIMENSIONAL WANKEL ENGINE

T. I.-P. SHIH (Florida, University, Gainesville), H. J. SCHOCK (NASA, Lewis Research Center, Cleveland, OH), and J. I. RAMOS (Carnegie-Mellon University, Pittsburgh, PA) SAE, International Congress and Exposition, Detroit, MI, Feb. 23-27, 1987. 31 p. Research supported by the U.S.-Spain Joint Committee for Scientific and Technological Cooperation. refs

(Contract NAG3-363; NAG3-689)

(SAE PAPER 870408)

A two-equation turbulence model, an algebraic grid generalization method, and an approximate factorization time-linearized numerical technique are used to study the effects of mixture stratification at the intake port and gaseous fuel injection on the flow field and fuel-air mixing in a two-dimensional rotary engine model. The fuel distribution in the combustion chamber is found to be a function of the air-fuel mixture fluctuations at the intake port. It is shown that the fuel is advected by the flow field induced by the rotor and is concentrated near the leading apex during the intake stroke, while during compression, the fuel

concentration is highest near the trailing apex and is lowest near the rotor. It is also found that the fuel concentration near the trailing apex and rotor is small except at high injection velocities.

R.R.

A87-48787* National Aeronautics and Space Administration. Lewis Research Center, Cleveland, Ohio.

ESTIMATION OF INSTANTANEOUS HEAT TRANSFER COEFFICIENTS FOR A DIRECT-INJECTION STRATIFIED-CHARGE ROTARY ENGINE

C. M. LEE, H. E. ADDY, T. H. BOND, K. S. CHUN (NASA, Lewis Research Center, Cleveland, OH), and C. Y. LU (Cleveland State University, OH) SAE, International Congress and Exposition, Detroit, MI, Feb. 23-27, 1987. 11 p. refs

(SAE PAPER 870444)

The main objective of this report was to derive equations to estimate heat transfer coefficients in both the combustion chamber and coolant passage of a rotary engine. This was accomplished by making detailed temperature and pressure measurements in a direct-injection stratified-charge rotary engine under a range of conditions. For each specific measurement point, the local physical properties of the fluids were calculated. Then an empirical correlation of the coefficients was derived by using a multiple regression program. This correlation expresses the Nusselt number as a function of the Prandtl number and Reynolds number.

Author

A87-48790* Garrett Turbine Engine Co., Phoenix, Ariz.

A TECHNOLOGY DEVELOPMENT SUMMARY FOR THE AGT101 ADVANCED GAS TURBINE PROGRAM

GARY L. BOYD, JAMES R. KIDWELL, and DANIEL M. KREINER (Garrett Turbine Engine Co., Phoenix, AZ) SAE, International Congress and Exposition, Detroit, MI, Feb. 23-27, 1987. 23 p. DOE-supported research.

(Contract DEN3-167)

(SAE PAPER 870466)

A summary is presented of significant technology developments that have been made in the AGT101 advanced gas turbine program. The AGT101 design features are reviewed, and the power section testing and results are addressed in detail. The results of component testing and evaluation are described for the compressor, turbine, regenerator, and foil bearing. Ceramic component development is discussed, including that of the static seal, turbine shroud seal, regenerator shield planar seal, regenerator shield piston ring, stator rig, ceramic combustor, and turbine rotor. Important areas to be addressed by the Advanced Turbine Technology Applications Project now in the planning stage at DOE and NASA are briefly reviewed. C.D.

A87-48791* Department of Energy, Washington, D. C.

THE ADVANCED TURBINE TECHNOLOGY APPLICATIONS PROGRAM (ATTAP)

SAUNDERS B. KRAMER (DOE, Washington, DC), PAUL T. KERWIN (NASA, Lewis Research Center, Cleveland, OH), and JOHN C. SCHETTINO (ORI, Inc., Rockville, MD) SAE, International Congress and Exposition, Detroit, MI, Feb. 23-27, 1987. 8 p.

(SAE PAPER 870467)

The need for advances in ceramic techniques in order to manufacture reliable cost-effective ceramic components for automotive gas turbine engines, in particular in the hot section of the engine, is examined. The objectives of the ATTAP is to establish the reliability of ceramic component designs and materials in automotive gas turbines; to expand the experimental data base in the operation environment; and to complete the development of analytical tools needed to support industry in the successful application of ceramics to long-life turbine engines. The role of industry and the government in the development of the gas turbine engine is discussed. I.F.

37 MECHANICAL ENGINEERING

A87-50777* National Aeronautics and Space Administration. Lewis Research Center, Cleveland, Ohio.

REFRIGERATED DYNAMIC SEAL TO 6.9 MPA (1000 PSI)

ROBERT C. HENDRICKS (NASA, Lewis Research Center, Cleveland, OH), R. L. MULLEN (Case Western Reserve University, Cleveland, OH), and M. J. BRAUN (Akron, University, OH) IN: Advances in cryogenic engineering. Volume 31; Proceedings of the Cryogenic Engineering Conference, Cambridge, MA, Aug. 12-16, 1985. New York, Plenum Press, 1986, p. 1007-1016. Previously announced in STAR as N85-34356. refs

The self sealing, high shear flow passage approach which was extended to large pressure differences was studied. In a refrigerated seal the fluid to be sealed flows through a refrigerated housing or constriction. The fluid can be frozen to the housing during the transient phase. Under steady state conditions the refrigerated seal proves to be a dynamic low leakage seal. The concept is extended to pressure differences of 6.9 MPa. Author

A87-53420* Illinois Univ., Chicago.

NEW GENERATION METHODS FOR SPUR, HELICAL, AND SPIRAL-BEVEL GEARS

F. L. LITVIN, W.-J. TSUNG (Illinois, University, Chicago), J. J. COY, R. F. HANDSCHUH (NASA, Lewis Research Center; U.S. Army, Army Aviation Research and Technology Activity, Cleveland, OH), and C.-B. P. TSAY (National Chiao Tung University, Hsinchu, Republic of China) IN: Specialists' Meeting on Rotary Wing Propulsion Systems, Williamsburg, VA, Nov. 12-14, 1986, Technical Papers. Alexandria, VA, American Helicopter Society, 1987, 25 p. Previously announced in STAR as N87-15466. refs

New methods for generating spur, helical, and spiral-bevel gears are proposed. These methods provide the gears with conjugate gear tooth surfaces, localized bearing contact, and reduced sensitivity to gear misalignment. Computer programs have been developed for simulating gear meshing and bearing contact.

Author

A87-53422* Akron Univ., Ohio.

GEAR MESH COMPLIANCE MODELING

M. SAVAGE, R. J. CALDWELL, G. D. WISOR (Akron, University, OH), and D. G. LEWICKI (NASA, Lewis Research Center; U.S. Army, Army Aviation Research and Technology Activity, Cleveland, OH) IN: Specialists' Meeting on Rotary Wing Propulsion Systems, Williamsburg, VA, Nov. 12-14, 1986, Technical Papers. Alexandria, VA, American Helicopter Society, 1987, 16 p. Previously announced in STAR as N87-18092. refs

(Contract NAG3-55)
A computer model has been constructed to simulate the compliance and load sharing in a spur gear mesh. The model adds the effect of rim deflections to previously developed state-of-the-art gear tooth deflection models. The effects of deflections on mesh compliance and load sharing are examined. The model can treat gear meshes composed of two external gears or an external gear driving an internal gear. The model includes deflection contributions from the bending and shear in the teeth, the Hertzian contact deformations, and primary and secondary rotations of the gear rims. The model shows that rimmed gears increase mesh compliance and, in some cases, improve load sharing. Author

N87-10391*# National Aeronautics and Space Administration. Lewis Research Center, Cleveland, Ohio.

TESTING OF UH-60A HELICOPTER TRANSMISSION IN NASA LEWIS 2240-KW (3000-HP) FACILITY

A. M. MITCHELL, F. B. OSWALD, and H. H. COE Aug. 1986 30 p
(NASA-TP-2626; E-2941; NAS 1.60:2626) Avail: NTIS HC A03/MF A01 CSCL 131

The U.S. Army's UH-60A Black Hawk 2240-kW (3000-hp) class, twin-engine helicopter transmission was tested at the NASA Lewis Research Center. The vibration and efficiency test results will be used to enhance the data base for similar-class helicopters. Most of the data were obtained for a matrix of test conditions of 50 to 100 percent of rated rotor speed and 20 to 100 percent of rated

input power. The transmission's mechanical efficiency at 100 percent of rated power was 97.3 and 97.5 percent with its inlet oil maintained at 355 and 372 K (180 and 210 F), respectively. The highest vibration reading was 72 g's rms at the upper housing side wall. Other vibration levels measured near the gear meshes are reported. Author

N87-11158*# Mechanical Technology, Inc., Latham, N. Y.

FATIGUE LIFE OF LASER CUT METALS Final Report

M. R. MARTIN Sep. 1986 54 p
(Contract NAS3-23942; DA PROJ. 1L1-61102-AH-45)
(NASA-CR-179501; NAS 1.26:179501; USAAVSCOM-TR-86-C-34; MTI-86TR40) Avail: NTIS HC A04/MF A01 CSCL 131

Fatigue tests were conducted to determine the actual reduction in fatigue life due to weight removal for balancing by: hand grinding, low power (20 watt) Nd:glass laser, and high power (400 watt) Nd:YAG laser. Author

N87-11993*# National Aeronautics and Space Administration. Lewis Research Center, Cleveland, Ohio.

SELECTION OF ROLLING-ELEMENT BEARING STEELS FOR LONG-LIFE APPLICATION

E. V. ZARETSKY 1986 76 p Presented at International Symposium on the Effect of Steel Manufacturing Processes on the Quality of Bearing Steels, Phoenix, Ariz., 4-6 Nov. 1986; sponsored by American Society for Testing and Materials (NASA-TM-88881; E-3288; NAS 1.15:88881) Avail: NTIS HC A05/MF A01 CSCL 131

Nearly four decades of research in bearing steel metallurgy and processing have resulted in improvements in bearing life by a factor of 100 over that obtained in the early 1940's. For critical applications such as aircraft, these improvements have resulted in longer lived, more reliable commercial aircraft engines. Material factors such as hardness, retained austenite, grain size and carbide size, number, and area can influence rolling-element fatigue life. Bearing steel processing such as double vacuum melting can have a greater effect on bearing life than material chemistry. The selection and specification of a bearing steel is dependent on the integration of all these considerations into the bearing design and application. The paper reviews rolling-element fatigue data and analysis which can enable the engineer or metallurgist to select a rolling-element bearing steel for critical applications where long life is required.

Author

N87-11995*# General Motors Corp., Indianapolis, Ind. Gas Turbine Div.

ADVANCED GAS TURBINE (AGT) TECHNOLOGY PROJECT Final Annual Report, 1985

1 Sep. 1986 160 p
(Contract DEN3-168)
(NASA-CR-179484; DOE/NASA/0168-10; NAS 1.26:179484; EDR-12344) Avail: NTIS HC A08/MF A01 CSCL 21A

Engine testing, ceramic component fabrication and evaluation, component performance rig testing, and analytical studies comprised AGT 100 activities during the 1985 year. Ten experimental assemblies (builds) were evaluated using two engines. Accrued operating time was 120 hr of burning and 170 hr total, bringing cumulative total operating time to 395 hr, all devoid of major failures. Tests identified the generator seals as the primary working fluid leakage sources. Power transfer clutch operation was demonstrated. An alpha SiC gasifier rotor engine test resulted in blade tip failures. Recurring case vibration and shaft whip have limited gasifier shaft speeds to 84%. Ceramic components successfully engine tested now include the SiC scroll assembly, Si3N3 turbine rotor, combustor assembly, regenerator disk bulkhead, turbine vanes, piston rings, and couplings. A compressor shroud design change to reduce heat recirculation back to the inlet was executed. Ceramic components activity continues to focus on the development of state-of-the-art material strength characteristics in full-scale engine hardware. Fiber reinforced glass-ceramic composite turbine (inner) backplates were fabricated by Corning Glass Works. The BMAS/III material performed well in

engine testing. Backplates of MAS material have not been engine tested. Author

N87-13755*# National Aeronautics and Space Administration. Lewis Research Center, Cleveland, Ohio.

EFFECT OF DESIGN VARIABLES, TEMPERATURE GRADIENTS AND SPEED OF LIFE AND RELIABILITY OF A ROTATING DISK

E. V. ZARETSKY, T. E. SMITH (Sverdrup Technology, Inc., Cleveland, Ohio), and R. AUGUST 1986 26 p Proposed for presentation at the 2nd Thermal Engineering Conference, Honolulu, Hawaii, 22-27 Mar. 1987; sponsored by ASME and JSME (NASA-TM-88883; E-3291; NAS 1.15:88883) Avail: NTIS HC A03/MF A01 CSCL 940

A generalized methodology to predict the fatigue life and reliability of a rotating disk such as used for aircraft engine turbines and compressors is advanced. The approach incorporates the computed life of elemental stress volumes to predict system life and reliability. Disk speed and thermal gradients as well as design variables such as disk diameter and thickness and bolt hole size, number and location are considered. Author

N87-15466*# National Aeronautics and Space Administration. Lewis Research Center, Cleveland, Ohio.

NEW GENERATION METHODS FOR SPUR, HELICAL, AND SPIRAL-BEVEL GEARS

F. L. LITVIN (Illinois Univ., Chicago), W.-J. TSUNG, J. J. COY (Army Aviation Research and Technology Activity, Cleveland, Ohio), R. F. HANDSCHUH, and C.-B. P. TSAY (National Chiao Tung Univ., Hsinchu Taiwan) Nov. 1986 26 p Presented at the Rotary Wing Propulsion System Specialist Meeting, Williamsburg, Va., 12-14 Nov. 1986; sponsored by American Helicopter Society (NASA-TM-88862; E-3216; NAS 1.15:88862; USAAVSCOM-TR-86-C-27; AD-A178145) Avail: NTIS HC A03/MF A01 CSCL 131

New methods for generating spur, helical, and spiral-bevel gears are proposed. These methods provide the gears with conjugate gear tooth surfaces, localized bearing contact, and reduced sensitivity to gear misalignment. Computer programs have been developed for simulating gear meshing and bearing contact. Author

N87-15467*# National Aeronautics and Space Administration. Lewis Research Center, Cleveland, Ohio.

LUBRICANT EFFECTS ON BEARING LIFE

ERWIN V. ZARETSKY Dec. 1986 22 p Presented at the OEM Design Conference, New York, N.Y., 9-11 Dec. 1986 (NASA-TM-88875; E-3253; NAS 1.15:88875) Avail: NTIS HC A02/MF A01 CSCL 11H

Lubricant considerations for rolling-element bearings have within the last two decades taken on added importance in the design and operation of mechanical systems. The phenomenon which limits the useful life of bearings is rolling-element or surface pitting fatigue. The elastohydrodynamic (EHD) film thickness which separates the ball or roller surface from those of the raceways of the bearing directly affects bearing life. Chemical additives added to the lubricant can also significantly affect bearings life and reliability. The interaction of these physical and chemical effects is important to the design engineer and user of these systems. Design methods and lubricant selection for rolling-element bearings are presented and discussed. Author

N87-16336*# National Aeronautics and Space Administration. Lewis Research Center, Cleveland, Ohio.

EVALUATION OF A HIGH-TORQUE BACKLASH-FREE ROLLER ACTUATOR

BRUCE M. STEINETZ, DOUGLAS A. ROHN, and WILLIAM ANDERSON (NASTEC, Inc., Cleveland, Ohio) In its The 20th Aerospace Mechanics Symposium p 205-230 May 1986 Avail: NTIS HC A14/MF A01 CSCL 131

The results are presented of a test program that evaluated the stiffness, accuracy, torque ripple, frictional losses, and torque holding capability of a 16:1 ratio, 430 N-m (320 ft-lb) planetary

roller drive for a potential space vehicle actuator application. The drive's planet roller supporting structure and bearings were found to be the largest contributors to overall drive compliance, accounting for more than half of the total. In comparison, the traction roller contacts themselves contributed only 9 percent of the drive's compliance based on an experimentally verified stiffness model. The drive exhibited no backlash although 8 arc sec of hysteresis deflection were recorded due to microcreep within the contact under torque load. Because of these load-dependent displacements, some form of feedback control would be required for arc second positioning applications. Torque ripple tests showed the drive to be extremely smooth, actually providing some damping of input torsional oscillations. The drive also demonstrated the ability to hold static torque with drifts of 7 arc sec or less over a 24 hr period at 35 percent of full load. Author

N87-16342*# Akron Univ., Ohio.

A MECHANISM FOR PRECISE LINEAR AND ANGULAR ADJUSTMENT UTILIZING FLEXURES

J. R. ELLIS In NASA. Lewis Research Center The 20th Aerospace Mechanics Symposium p 291-302 May 1986 (Contract NAG3-379; N7405-ENG-26)

Avail: NTIS HC A14/MF A01 CSCL 131

The design and development of a mechanism for precise linear and angular adjustment is described. This work was in support of the development of a mechanical extensometer for biaxial strain measurement. A compact mechanism was required which would allow angular adjustments about perpendicular axes with better than 0.001 degree resolution. The approach adopted was first to develop a means of precise linear adjustment. To this end, a mechanism based on the toggle principle was built with inexpensive and easily manufactured parts. A detailed evaluation showed that the resolution of the mechanism was better than 1 micron and that adjustments made by using the device were repeatable. In the second stage of this work, the linear adjustment mechanisms were used in conjunction with a simple arrangement of flexural pivots and attachment blocks to provide the required angular adjustments. Attempts to use the mechanism in conjunction with the biaxial extensometer under development proved unsuccessful. Any form of in situ adjustment was found to cause erratic changes in instrument output. These changes were due to problems with the suspension system. However, the subject mechanism performed well in its own right and appeared to have potential for use in other applications. Author

N87-17033*# National Aeronautics and Space Administration. Lewis Research Center, Cleveland, Ohio.

COMMON PROBLEMS AND PITFALLS IN GEAR DESIGN

DENNIS P. TOWNSEND Dec. 1986 18 p Presented at the Original Equipment Manufacturing Design Conference, New York, N.Y., 9-11 Dec. 1986

(NASA-TM-88858; E-3223; NAS 1.15:88858) Avail: NTIS HC A02/MF A01 CSCL 131

There are several pitfalls and problems associated with the successful design of a new gear transmission. A new design will require the knowledge and experience of several technical areas of engineering. Most of the pitfalls and problems associated with a new design are related to an inadequate evaluation of several areas, such as, the lubrication and cooling requirements, complete static and dynamic load analysis, evaluation of materials and heat treatment and the latest manufacturing technology. Some of the common problems of the gear design process are discussed with recommendations made for avoiding these conditions. Author

37 MECHANICAL ENGINEERING

N87-18092*# National Aeronautics and Space Administration. Lewis Research Center, Cleveland, Ohio.

GEAR MESH COMPLIANCE MODELING

M. SAVAGE (Akron Univ., Ohio), R. J. CALDWELL, G. D. WISOR, and D. G. LEWICKI (Army Aviation Research and Development Command, Cleveland, Ohio) 1986 17 p Presented at the Rotary Wing Propulsion System Specialist Meeting, Williamsburg, Va., 12-14 Nov. 1986; sponsored by the American Helicopter Society

(Contract NAG3-55)

(NASA-TM-88843; E-3230; NAS 1.15:88843;

USAAVSCOM-TR-86-C-28) Avail: NTIS HC A02/MF A01 CSCL 131

A computer model has been constructed to simulate the compliance and load sharing in a spur gear mesh. The model adds the effect of rim deflections to previously developed state-of-the-art gear tooth deflection models. The effects of deflections on mesh compliance and load sharing are examined. The model can treat gear meshes composed to two external gears or an external gear driving an internal gear. The model includes deflection contributions from the bending and shear in the teeth, the Hertzian contact deformations, and primary and secondary rotations of the gear rims. The model shows that rimmed gears increase mesh compliance and, in some cases, improve load sharing.

Author

N87-18095*# National Aeronautics and Space Administration. Lewis Research Center, Cleveland, Ohio.

PREDICTED EFFECT OF DYNAMIC LOAD ON PITTING FATIGUE LIFE FOR LOW-CONTACT-RATIO SPUR GEARS

DAVID G. LEWICKI Jun. 1986 19 p

(NASA-TP-2610; E-2989; NAS 1.60:2610; AD-A170906;

AVSCOM-TR-86-C-21) Avail: NTIS HC A02/MF A01 CSCL 131

How dynamic load affects the surface pitting fatigue life of external spur gears was predicted by using the NASA computer program TELSGE. Parametric studies were performed over a range of various gear parameters modeling low-contact-ratio involute spur gears. In general, gear life predictions based on dynamic loads differed significantly from those based on static loads, with the predictions being strongly influenced by the maximum dynamic load during contact. Gear mesh operating speed strongly affected predicted dynamic load and life. Meshes operating at a resonant speed or one-half the resonant speed had significantly shorter lives. Dynamic life factors for gear surface pitting fatigue were developed on the basis of the parametric studies. In general, meshes with higher contact ratios had higher dynamic life factors than meshes with lower contact ratios. A design chart was developed for hand calculations of dynamic life factors.

Author

N87-18096*# Texas A&M Univ., College Station. Turbomachinery Labs.

A COMPARISON OF EXPERIMENTAL AND THEORETICAL RESULTS FOR LABYRINTH GAS SEALS Ph.D. Thesis

JOSEPH KIRK SCHARRE Feb. 1987 233 p

(Contract NAG3-181)

(NASA-CR-180194; NAS 1.26:180194; TRC-SEAL-3-87) Avail:

NTIS HC A11/MF A01 CSCL 11A

The basic equations are derived for a two control volume model for compressible flow in a labyrinth seal. The flow is assumed to be completely turbulent and isoenergetic. The wall friction factors are determined using the Blasius formula. Jet flow theory is used for the calculation of the recirculation velocity in the cavity. Linearized zeroth and first order perturbation equations are developed for small motion about a centered position by an expansion in the eccentricity ratio. The zeroth order pressure distribution is found by satisfying the leakage equation. The circumferential velocity distribution is determined by satisfying the momentum equations. The first order equations are solved by a separation of variable solution. Integration of the resultant pressure distribution along and around the seal defines the reaction force developed by the seal and the corresponding dynamic coefficients. The results of this analysis are compared to experimental test results.

Author

N87-18820*# National Aeronautics and Space Administration. Lewis Research Center, Cleveland, Ohio.

EFFECTS OF SURFACE REMOVAL ON ROLLING-ELEMENT FATIGUE

ERWIN V. ZARETSKY 1987 20 p Prepared for presentation at the International Conference on Tribology, Lubrication and Wear; 50 Years On, London, England, 1-3 Jul. 1987; sponsored by Inst. of Mechanical Engineers.

(NASA-TM-88871; E-3231; NAS 1.15:88871) Avail: NTIS HC A02/MF A01 CSCL 131

The Lundberg-Palmgren equation was modified to show the effect on rolling-element fatigue life of removing by grinding a portion of the stressed volume of the raceways of a rolling-element bearing. Results of this analysis show that depending on the amount of material removed, and depending on the initial running time of the bearing when material removal occurs, the 10-percent life of the reground bearings ranges from 74 to 100 percent of the 10-percent life of a brand new bearing. Three bearing types were selected for testing. A total of 250 bearings were reground. Of this matter, 30 bearings from each type were endurance tested to 1600 hr. No bearing failure occurred related to material removal. Two bearing failures occurred due to defective rolling elements and were typical of those which may occur in new bearings.

Author

N87-19723*# Hamilton Standard, Windsor Locks, Conn.

EXPANSION OF EPICYCLIC GEAR DYNAMIC ANALYSIS PROGRAM Final Report

LINDA SMITH BOYD and JAMES A. PIKE 1987 94 p

(Contract NAS3-24614)

(NASA-CR-179563; NAS 1.26:179563; HSER-10853) Avail: NTIS HC A05/MF A01 CSCL 131

The multiple mesh/single stage dynamics program is a gear tooth analysis program which determines detailed geometry, dynamic loads, stresses, and surface damage factors. The program can analyze a variety of both epicyclic and single mesh systems with spur or helical gear teeth including internal, external, and buttress tooth forms. The modifications refine the options for the flexible carrier and flexible ring gear rim and adds three options: a floating Sun gear option; a natural frequency option; and a finite element compliance formulation for helical gear teeth. The option for a floating Sun incorporates two additional degrees of freedom at the Sun center. The natural frequency option evaluates the frequencies of planetary, star, or differential systems as well as the effect of additional springs at the Sun center and those due to a flexible carrier and/or ring gear rim. The helical tooth pair finite element calculated compliance is obtained from an automated element breakup of the helical teeth and then is used with the basic gear dynamic solution and stress postprocessing routines. The flexible carrier or ring gear rim option for planetary and star spur gear systems allows the output torque per carrier and ring gear rim segment to vary based on the dynamic response of the entire system, while the total output torque remains constant.

Author

N87-20552*# Akron Univ., Ohio. Dept. of Mechanical Engineering.

FLEXIBILITY EFFECTS ON TOOTH CONTACT LOCATION IN SPIRAL BEVEL GEAR TRANSMISSIONS

P. C. ALTIDIS and M. SAVAGE Washington NASA Mar. 1987 201 p

(Contract NAG3-55; DA PROJ. 1L1-61102-AH-45)

(NASA-CR-4055; E-3360; NAS 1.26:4055) Avail: NTIS HC A10/MF A01 CSCL 131

An analytical method to predict the shift of the contact ellipse between the meshing teeth in a spiral bevel gear set is presented in this report. The contact ellipse shift of interest is the motion of the nominal tooth contact location on each tooth from the ideal pitch point to the point of contact between the two teeth considering the elastic motions of the gears and their supporting shafts. This is the shift of the pitch point from the ideal, unloaded position on each tooth to the nominal contact location on the tooth when the gears are fully loaded. It is assumed that the major contributors

of this motion are the elastic deflections of the gear shafts, the slopes of the shafts under load and the radial deflections of the four gear shaft bearings. The motions of the two pitch point locations on the pinion and the gear tooth surfaces are calculated in a FORTRAN program which also calculates the size and orientation of the Hertzian contact ellipse on the tooth faces. Based on the curvatures of the two spiral bevel gear teeth and the size of the contact ellipse, the program also predicts the basic dynamic capacity of the tooth pair. A complete numerical example is given to illustrate the use of the program. Author

N87-20555* National Aeronautics and Space Administration. Lewis Research Center, Cleveland, Ohio.

VIBRATION CHARACTERISTICS OF OH-58A HELICOPTER MAIN ROTOR TRANSMISSION

DAVID G. LEWICKI and JOHN J. COY Apr. 1987 18 p (NASA-TP-2705; E-3368; NAS 1.60:2705; AVSCOM-TR-86-C-42; AD-A180364) Avail: NTIS HC A01/MF A01 CSCL 01C

Experimental vibration tests covering a range of torque and speed conditions were performed on the OH-58A helicopter main rotor transmission at the NASA Lewis Research Center. Signals from accelerometers located on the transmission housing were analyzed by using Fourier spectra, power spectral density functions, and averaging techniques. Most peaks of the Fourier spectra occurred at the spiral bevel and planetary gear mesh harmonics. The highest level of vibration occurred at the spiral bevel meshing frequency. Transmission speed and vibration measurement location had a significant effect on measured vibration; transmission torque and measurement direction had a small effect. Author

N87-20556* National Aeronautics and Space Administration. Lewis Research Center, Cleveland, Ohio.

EXPERIMENTAL AND ANALYTICAL EVALUATION OF DYNAMIC LOAD AND VIBRATION OF A 2240-KW (300-HP) ROTORCRAFT TRANSMISSION

FRED K. CHOY, DENNIS P. TOWNSEND, and FRED B. OSWALD Mar. 1987 18 p Presented at the Design Engineering Conference and Show, Chicago, Ill., 2-5 Mar. 1987; sponsored by ASME (NASA-TM-88975; E-3380; NAS 1.15:88975) Avail: NTIS HC A02/MF A01 CSCL 13I

A dynamic analysis of a 2240-kW (3000-hp) helicopter planetary system is presented. Results from both analytical and experimental studies show good correlation in gear-tooth loads. A parametric study indicates that the mesh damping ratio has a significant effect on maximum gear tooth load, stress, and vibration. Correlation with experimental results indicates that the Sun-planet mesh damping ratio can significantly differ from the planet ring mesh damping ratio. A numerical fast Fourier transform (FFT) procedure was applied to examine the mesh load components in the frequency domain and the magnitudes of multiple tooth pass frequencies excited by nonsynchronous meshing of the planets. Effects of tooth-spacing errors and tooth-profile modifications with tip relief are examined. A general discussion of results and correlation with the experimental study are also presented. Author

N87-22199* National Aeronautics and Space Administration. Lewis Research Center, Cleveland, Ohio.

ROTORDYNAMIC INSTABILITY PROBLEMS IN HIGH-PERFORMANCE TURBOMACHINERY, 1986

Jan. 1987 548 p Workshop held in College Station, Tex., 2-4 Jun. 1986; sponsored in cooperation with Texas A&M Univ., Army Research Office, and Air Force Aeropropulsion Lab. (NASA-CP-2443; E-3136; NAS 1.55:2443) Avail: NTIS HC A23/MF A01 CSCL 13I

The first rotordynamics workshop proceedings (NASA CP-2133, 1980) emphasized a feeling of uncertainty in predicting the stability of characteristics of high-performance turbomachinery. In the second workshop proceedings (NASA CP-2250, 1982) these uncertainties were reduced through programs established to systematically resolve problems, with emphasis on experimental validation of the forces that influence rotordynamics. In third proceedings (NASA CP-2338, 1984) many programs for predicting

or measuring forces and force coefficients in high-performance turbomachinery produced results. Data became available for designing new machines with enhanced stability characteristics or for upgrading existing machines. The present workshop proceedings illustrates a continued trend toward a more unified view of rotordynamic instability problems and several encouraging new analytical developments.

N87-22212* Texas A&M Univ., College Station.

EXPERIMENTAL ROTORDYNAMIC COEFFICIENT RESULTS FOR TEETH-ON-ROTOR AND TEETH-ON-STATOR LABYRINTH GAS SEALS

DARA W. CHILDS and JOSEPH K. SCHARRER In NASA. Lewis Research Center Rotordynamic Instability Problems in High-Performance Turbomachinery, 1986 p 259-275 Jan. 1987 (Contract NAS3-181; F49620-82-K-0033) Avail: NTIS HC A23/MF A01 CSCL 13I

An experimental test facility is used to measure the rotordynamic coefficients of teeth-on-rotor and teeth-on-stator labyrinth gas seals. Direct damping coefficients are presented for these seals for the first time. The results are presented for the two seal configurations at identical operating conditions, and show that, in a rotordynamic sense, the teeth-on-stator seal is more stable than the teeth-on-rotor seal, for inlet tangential velocity in the direction of rotation. Author

N87-22235* National Aeronautics and Space Administration. Lewis Research Center, Cleveland, Ohio.

GEAR TOOTH STRESS MEASUREMENTS ON THE UH-60A HELICOPTER TRANSMISSION

FRED B. OSWALD Mar. 1987 17 p (NASA-TP-2698; E-3357; NAS 1.60:2698) Avail: NTIS HC A02/MF A01 CSCL 13I

The U.S. Army UH-60A (Black Hawk) 2200-kW (3000-hp) class twin-engine helicopter transmission was tested at the NASA Lewis Research Center. Results from these experimental (strain-gage) stress tests will enhance the data base for gear stress levels in transmissions of a similar power level. Strain-gage measurements were performed on the transmission's spiral-bevel combining pinions, the planetary Sun gear, and ring gear. Tests were performed at rated speed and at torque levels 25 to 100 percent that of rated. One measurement series was also taken at a 90 percent speed level. The largest stress found was 760 MPa (110 ksi) on the combining pinion fillet. This is 230 percent greater than the AGMA index stress. Corresponding mean and alternating stresses were 300 and 430 MPa (48 and 62 ksi). These values are within the range of successful test experience reported for other transmissions. On the fillet of the ring gear, the largest stress found was 410 MPa (59 ksi). The ring-gear peak stress was found to be 11 percent less than an analytical (computer simulation) value and it is 24 percent greater than the AGMA index stress. A peak compressive stress of 650 MPa (94 ksi) was found at the center of the Sun gear tooth root. Author

N87-22237* National Aeronautics and Space Administration. Lewis Research Center, Cleveland, Ohio.

A 2000-HOUR CYCLIC ENDURANCE TEST OF A LABORATORY MODEL MULTIPROPELLANT RESISTOJET

W. EARL MORREN and JAMES S. SOVEY 1987 24 p Presented at the 19th International Electric Propulsion Conference, Colorado Springs, Colo., 11-13 May 1987; sponsored by AIAA, DGLR and JSASS (NASA-TM-89854; E-3521; NAS 1.15:89854; AIAA-87-0993) Avail: NTIS HC A02/MF A01 CSCL 13I

The technological readiness of a long-life multipropellant resistojets for space station auxiliary propulsion is demonstrated. A laboratory model resistojets made from grain-stabilized platinum served as a test bed to evaluate the design characteristics, fabrication methods, and operating strategies for an engineering model multipropellant resistojets developed under contract by the Rocketdyne Division of Rockwell International and Technion Incorporated. The laboratory model thruster was subjected to a 2000-hr, 2400-thermal-cycle endurance test using carbon dioxide

propellant. Maximum thruster temperatures were approximately 1400 C. The post-test analyses of the laboratory model thruster included an investigation of component microstructures. Significant observations from the laboratory model thruster are discussed as they relate to the design of the engineering model thruster.

Author

N87-22245*# General Electric Co., Cincinnati, Ohio. Aircraft Engine Business Group.

DEVELOPMENT OF GAS-TO-GAS LIFT PAD DYNAMIC SEALS, VOLUMES 1 AND 2 Final Report

A. N. POPE and D. W. PUGH May 1987 189 p

(Contract NAS3-20043)

(NASA-CR-179486; NAS 1.26:179486; R87-AEB432) Avail: NTIS HC A09/MF A01 CSCL 11A

Dynamic tests were performed on self acting (hydrodynamic) carbon face rotary shaft seals to assess their potential, relative to presently used labyrinth seals, for improving performance of aircraft gas turbine engines by reducing air leakage flow rate at compressor end seal locations. Three self acting bearing configurations, designed to supply load support at the interface of the stationary carbon seal and rotating seal race, were tested. Two configurations, the shrouded taper and shrouded flat step, were incorporated on the face of the stationary carbon seal element. The third configuration, inward pumping spiral grooves, was incorporated on the hard faced surface of the rotating seal race. Test results demonstrated seal leakage air flow rates from 75 to 95% lower than can be achieved with best state-of-the-art labyrinth designs and led to identification of the need for a more geometrically stable seal design configuration which is presently being manufactured for subsequent test evaluation.

Author

N87-22246*# Mechanical Technology, Inc., Latham, N. Y. **EHD ANALYSIS OF AND EXPERIMENTS ON PUMPING LENINGRADER SEALS Final Report**

M. W. EUSEPI and J. A. WALOWIT Jun. 1986 93 p

(Contract DEN3-343; DE-AI01-85CE-50112)

(NASA-CR-179570; DOE/NASA/0343-1; NAS 1.26:179570;

MTI-86TR33) Avail: NTIS HC A05/MF A01 CSCL 11A

Analysis and design charts have been generated to provide design data for Pumping Leningrader Reciprocating Rod Seals. The analytical treatment divides the seal into three regions: an inlet zone, induced with the use of an expansion ring, a contact zone, and an exit zone. Complete solutions have been obtained by matching elasticity equations with hydrodynamic theory. Experiments, although of a limited nature, did demonstrate the ability of the seal design analysis to provide viable seals.

Author

N87-22978*# National Aeronautics and Space Administration. Lewis Research Center, Cleveland, Ohio.

HELICOPTER TRANSMISSION TESTING AT NASA LEWIS RESEARCH CENTER

DAVID G. LEWICKI and JOHN J. COY Jun. 1987 18 p Presented at the Testing of Aerospace Transmissions Conference, Derby, England, 10 Jun. 1987; sponsored by the Institute of Mechanical Engineers

(NASA-TM-89912; E-3603; NAS 1.15:89912;

AVSCOM-TR-87-C-10) Avail: NTIS HC A02/MF A01 CSCL 13I

The helicopter has evolved into a highly valuable air mobile vehicle for both military and civilian needs. The helicopter transmission requires advanced studies to develop a technology base for future rotorcraft advances. A joint helicopter transmission research program between the NASA Lewis Research Center and the U.S. Army Aviation Systems Command has existed since 1970. Program goals are to reduce weight and noise and to increase life and reliability. The current experimental activities at Lewis consist of full-scale helicopter transmission testing, a base effort in gearing technology, and a future effort in noise reduction technology. The experimental facilities at Lewis for helicopter transmission testing are described. A description of each of the rigs is presented along with some significant results and near-term plans.

Author

N87-23969*# Cincinnati Univ., Ohio.

COMPUTER AIDED DESIGN AND ANALYSIS OF GEAR TOOTH GEOMETRY Final Report

S. H. CHANG and R. L. HUSTON May 1987 84 p

(Contract NSG-3188)

(NASA-CR-179611; NAS 1.26:179611; AVSCOM-TR-87-C-13)

Avail: NTIS HC A05/MF A01 CSCL 13I

A simulation method for gear hobbing and shaping of straight and spiral bevel gears is presented. The method is based upon an enveloping theory for gear tooth profile generation. The procedure is applicable in the computer aided design of standard and nonstandard tooth forms. An inverse procedure for finding a conjugate gear tooth profile is presented for arbitrary cutter geometry. The kinematic relations for the tooth surfaces of straight and spiral bevel gears are proposed. The tooth surface equations for these gears are formulated in a manner suitable for their automated numerical development and solution.

Author

N87-23977*# Northwestern Univ., Evanston, Ill.

A SIMPLIFIED COMPUTER SOLUTION FOR THE FLEXIBILITY MATRIX OF CONTACTING TEETH FOR SPIRAL BEVEL GEARS Final Report

C. Y. HSU and H. S. CHENG Jun. 1987 73 p

(Contract NAG3-3143)

(NASA-CR-179620; NAS 1.26:179620; AVSCOM-TR-87-C-16)

Avail: NTIS HC A04/MF A01 CSCL 13I

A computer code, FLEXM, was developed to calculate the flexibility matrices of contacting teeth for spiral bevel gears using a simplified analysis based on the elementary beam theory for the deformation of gear and shaft. The simplified theory requires a computer time at least one order of magnitude less than that needed for the complete finite element method analysis reported earlier by H. Chao, and it is much easier to apply for different gear and shaft geometries. Results were obtained for a set of spiral bevel gears. The teeth deflections due to torsion, bending moment, shearing strain and axial force were found to be in the order 10(-5), 10(-6), 10(-7), and 10(-8) respectively. Thus, the torsional deformation was the most predominant factor. In the analysis of dynamic load, response frequencies were found to be larger when the mass or moment of inertia was smaller or the stiffness was larger. The change in damping coefficient had little influence on the resonance frequency, but has a marked influence on the dynamic load at the resonant frequencies.

M.G.

N87-23978*# National Aeronautics and Space Administration. Lewis Research Center, Cleveland, Ohio.

THE IMPACT DAMPED HARMONIC OSCILLATOR IN FREE DECAY

G. V. BROWN and C. M. NORTH 1987 23 p Prepared for presentation at the Vibrations Conference, Boston, Mass., 27-30 Sep. 1987; sponsored by the ASME

(NASA-TM-89897; E-3587; NAS 1.15:89897) Avail: NTIS HC

A02/MF A01 CSCL 13I

The impact-damped oscillator in free decay is studied by using time history solutions. A large range of oscillator amplitude is covered. The amount of damping is correlated with the behavior of the impacting mass. There are three behavior regimes: (1) a low amplitude range with less than one impact per cycle and very low damping, (2) a useful middle amplitude range with a finite number of impacts per cycle, and (3) a high amplitude range with an infinite number of impacts per cycle and progressively decreasing damping. For light damping the impact damping in the middle range is: (1) proportional to impactor mass, (2) additive to proportional damping, (3) a unique function of vibration amplitude, (4) proportional to 1-epsilon, where epsilon is the coefficient of restitution, and (5) very roughly inversely proportional to amplitude. The system exhibits jump phenomena and period doublings. An impactor with 2 percent of the oscillator's mass can produce a loss factor near 0.1.

Author

N87-23984*# National Aeronautics and Space Administration. Lewis Research Center, Cleveland, Ohio.

EXPERIMENTS ON DYNAMIC STIFFNESS AND DAMPING OF TAPERED BORE SEALS

DAVID P. FLEMING 1987 13 p Prepared for presentation at the Vibrations Conference, Boston, Mass., 27-30 Sep. 1987; sponsored by ASME

(NASA-TM-89895; E-3552; NAS 1.15:89895) Avail: NTIS HC A02/MF A01 CSCL 11A

Stiffness and damping were measured in tapered bore ring seals with air as the sealed fluid. Excitation was provided by a known unbalance in the shaft which rotated in the test seals. Results were obtained for various seal supply pressures, clearances, unbalance amounts, and shaft speeds. Stiffness and damping varied little with unbalance level, indicating linearity of the seal. Greater variation was observed with speed and particularly supply pressure. A one-dimensional analysis predicted stiffness fairly well, but considerably overestimated damping. Author

N87-25578*# Sikorsky Aircraft, Stratford, Conn.

AUTOMATED INSPECTION AND PRECISION GRINDING OF SPIRAL BEVEL GEARS Final Report

HAROLD FRINT Washington NASA Jul. 1987 83 p (Contract NAS3-25465; DA PROJ. 1L1-62209-AH-76)

(NASA-CR-4083; E-3604; SER-510220; NAS 1.26:4083; AVSCOM-TR-87-C-11; AD-A183726) Avail: NTIS HC A05/MF A01 CSCL 13I

The results are presented of a four phase MM&T program to define, develop, and evaluate an improved inspection system for spiral bevel gears. The improved method utilizes a multi-axis coordinate measuring machine which maps the working flank of the tooth and compares it to nominal reference values stored in the machine's computer. A unique feature of the system is that corrective grinding machine settings can be automatically calculated and printed out when necessary to correct an errant tooth profile. This new method eliminates most of the subjective decision making involved in the present method, which compares contact patterns obtained when the gear set is run under light load in a rolling test machine. It produces a higher quality gear with significant inspection time and cost savings. Author

N87-25579*# Bolt, Beranek, and Newman, Inc., Cambridge, Mass.

ANALYSIS OF THE VIBRATORY EXCITATION ARISING FROM SPIRAL BEVEL GEARS Final Report

WILLIAM D. MARK Washington NASA Jul. 1987 122 p (Contract NAS3-23703)

(NASA-CR-4081; E-3580; REPT-6451; NAS 1.26:4081) Avail: NTIS HC A06/MF A01 CSCL 13I

Tools required to understand and predict in terms of its underlying causes the vibratory excitation arising from meshing spiral bevel gears are developed. A generalized three component transmission error of meshing spiral bevel gears is defined. Equations are derived that yield the three components of the generalized transmission error in terms of deviations of tooth running surfaces from equispaced perfect spherical involute surfaces and tooth/gearbody elastic deformations arising from the three components of the generalized force transmitted by the meshing gears. A method for incorporating these equations into the equations of motion of a gear system is described. Equations are derived for the three components of the generalized force transmitted by the gears which are valid whenever inertial effects of the meshing gears and their supports are negligible. Bearing offsets from the positions occupied by the shaft centerlines of perfect spherical involute bevel gears and bearing/bearing support flexibilities enter into the computation of these forces. Author

N87-25585*# National Aeronautics and Space Administration. Lewis Research Center, Cleveland, Ohio.

CARBIDE-FLUORIDE-SILVER SELF-LUBRICATING COMPOSITE Patent Application

HAROLD E. SLINNEY, inventor (to NASA) 28 May 1987 13 p (NASA-CASE-LEW-14196-2; US-PATENT-APPL-SN-054983)

Avail: NTIS HC A02/MF A01 CSCL 11H

A self-lubricating, friction and wear reducing composite material is described for use over a wide temperature spectrum from cryogenic temperature to about 900 C in a chemically reactive environment comprising silver, barium fluoride/calcium fluoride eutectic, and metal bonded chromium carbide. NASA

N87-26356*# Illinois Univ., Chicago. Dept. of Mechanical Engineering.

GENERATION OF SPIRAL BEVEL GEARS WITH CONJUGATE TOOTH SURFACES AND TOOTH CONTACT ANALYSIS Final Report

FAYDOR L. LITVIN, WEI-JIUNG TSUNG, and HONG-TAO LEE Washington NASA Aug. 1987 127 p

(Contract NAG3-48)

(NASA-CR-4088; E-3670; NAS 1.26:4088; AVSCOM-TR-87-C-22)

Avail: NTIS HC A07/MF A01 CSCL 13I

A new method for generation of spiral bevel gears is proposed. The main features of this method are as follows: (1) the gear tooth surfaces are conjugated and can transform rotation with zero transmission errors; (2) the tooth bearing contact is localized; (3) the center of the instantaneous contact ellipse moves in a plane that has a fixed orientation; (4) the contact normal performs in the process of meshing a parallel motion; (5) the motion of the contact ellipse provides improved conditions of lubrication; and (6) the gears can be manufactured by use of Gleason's equipment. Author

N87-26358*# Northwestern Univ., Evanston, Ill. Center for Engineering Tribology.

A COMPUTER SOLUTION FOR THE DYNAMIC LOAD, LUBRICANT FILM THICKNESS AND SURFACE TEMPERATURES IN SPIRAL BEVEL GEARS Final Contractor Report

H. C. CHAO and H. S. CHENG Washington NASA Jul. 1987 206 p

(Contract NSG-3143)

(NASA-CR-4077; E-3540; NAS 1.26:4077; AVSCOM-TR-87-C-17)

Avail: NTIS HC A10/MF A01 CSCL 11H

A complete analysis of spiral bevel gear sets is presented. The gear profile is described by the movements of the cutting tools. The contact patterns of the rigid body gears are investigated. The tooth dynamic force is studied by combining the effects of variable teeth meshing stiffness, speed, damping, and bearing stiffness. The lubrication performance is also accomplished by including the effects of the lubricant viscosity, ambient temperature, and gear speed. A set of numerical results is also presented. Author

N87-27197*# Ohio State Univ., Columbus. Dept. of Mechanical Engineering.

THE DESIGN AND ANALYSIS OF SINGLE FLANK TRANSMISSION ERROR TESTER FOR LOADED GEARS Final Report

DUANE E. BASSETT and DONALD R. HOUSER Jun. 1987 138 p

(Contract NAG3-541)

(NASA-CR-179621; NAS 1.26:179621; AVSCOM-TR-87-C-15;

REPT-764038/716109) Avail: NTIS HC A07/MF A01 CSCL 13I

To strengthen the understanding of gear transmission error and to verify mathematical models which predict them, a test stand that will measure the transmission error of gear pairs under design loads has been investigated. While most transmission error testers have been used to test gear pairs under unloaded conditions, the goal of this report was to design and perform dynamic analysis of a unique tester with the capability of measuring

the transmission error of gears under load. This test stand will have the capability to continuously load a gear pair at torques up to 16,000 in-lb at shaft speeds from 0 to 5 rpm. Error measurement will be accomplished with high resolution optical encoders and the accompanying signal processing unit from an existing unloaded transmission error tester. Input power to the test gear box will be supplied by a dc torque motor while the load will be applied with a similar torque motor. A dual input, dual output control system will regulate the speed and torque of the system. This control system's accuracy and dynamic response were analyzed and it was determined that proportional plus derivative speed control is needed in order to provide the precisely constant torque necessary for error-free measurement. Author

N87-28918*# National Aeronautics and Space Administration. Lewis Research Center, Cleveland, Ohio.

PROFILE MODIFICATION TO MINIMIZE SPUR GEAR DYNAMIC LOADING

HSIANG HSI LIN (Memphis State Univ., Tenn.), DENNIS P. TOWNSEND, and FRED B. OSWALD 1987 22 p. Proposed for presentation at the Design Engineering Technical Conference, Orlando, Fla., 24-28 Sep. 1988; sponsored by ASME (NASA-TM-89901; E-3597; NAS 1.15:89901) Avail: NTIS HC A02/MF A01 CSCL 13I

An analytical computer simulation program for dynamic modeling of low-contact-ratio spur gear systems is presented. The procedure computes the static transmission error of the gears operating under load and uses a fast Fourier transform to generate the frequency spectrum of the static transmission error at various tooth profile modifications. The dynamic loading response of an unmodified (perfect involute) gear pair was compared with that of gears with various profile modifications. Correlations were found between various profile modifications and the resulting dynamic loads. An effective error, obtained from frequency domain analysis of the static transmission error of the gears, gave a very good indication of the optimum profile modification to reduce gear dynamic loading. Design curves generated by dynamic simulation at various profile modifications are given for gear systems operated at various loads. Optimum profile modifications can be determined from these design curves for improved gear design. Author

N87-29840*# Michigan Technological Univ., Houghton. Dept. of Mechanical Engineering and Engineering Mechanics.

AN INVESTIGATION OF THE DYNAMIC RESPONSE OF SPUR GEAR TEETH WITH MOVING LOADS Final Report

C. E. PASSERELLO and L. W. SHUEY Aug. 1987 238 p (Contract NAG3-344) (NASA-CR-179643; NAS 1.26:179643; AVSCOM-TR-87-C-23) Avail: NTIS HC A11/MF A01 CSCL 13I

Two concepts relating to gear dynamics were studied. The first phase of the analysis involved the study of the effect of the speed of a moving load on the dynamic deflections of a gear tooth. A single spur gear tooth modelled using finite elements was subjected to moving loads with variable velocities. The tooth tip deflection time histories were plotted, from which it was seen that the tooth tip deflection consisted of a quasistatic response with an oscillatory response superimposed on it whose amplitude was dependent on the type of load engagement. Including the rim in the analysis added flexibility to the model but did not change the general behavior of the system. The second part of the analysis involved an investigation to determine the effect on the dynamic response of the inertia of the gear tooth. A simplified analysis using meshing cantilever beams was used. In one case, the beams were assumed massless. In the other, the mass (inertia) of the beams was included. From this analysis it was found that the inertia of the tooth did not affect the dynamic response of meshing cantilever beams. Author

N87-29846*# Chicago Univ., Ill.

HELICAL GEARS WITH CIRCULAR ARC TEETH: GENERATION, GEOMETRY, PRECISION AND ADJUSTMENT TO ERRORS, COMPUTER AIDED SIMULATION OF CONDITIONS OF MESHING AND BEARING CONTACT Final Report

FAYDOR L. LITVIN and CHUNG-BIAU TSAY Washington NASA Oct. 1987 95 p (Contract NAG3-655) (NASA-CR-4089; E-3541; NAS 1.26:4089) Avail: NTIS HC A05/MF A01 CSCL 13I

The authors have proposed a method for the generation of circular arc helical gears which is based on the application of standard equipment, worked out all aspects of the geometry of the gears, proposed methods for the computer aided simulation of conditions of meshing and bearing contact, investigated the influence of manufacturing and assembly errors, and proposed methods for the adjustment of gears to these errors. The results of computer aided solutions are illustrated with computer graphics. Author

38

QUALITY ASSURANCE AND RELIABILITY

Includes product sampling procedures and techniques; and quality control.

A87-14300* Cleveland State Univ., Ohio.

PROBABILITY OF DETECTION OF INTERNAL VOIDS IN STRUCTURAL CERAMICS USING MICROFOCUS RADIOGRAPHY

G. Y. BAAKLINI (Cleveland State University, OH) and D. J. ROTH (NASA, Lewis Research Center, Cleveland, OH) Journal of Materials Research (ISSN 0884-2914), vol. 1, May-June 1986, p. 457-467. Previously announced in STAR as N86-13749. refs

The reliability of microfocus X-radiography for detecting subsurface voids in structural ceramic test specimens was statistically evaluated. The microfocus system was operated in the projection mode using low X-ray photon energies (20 keV) and a 10 micro m focal spot. The statistics were developed for implanted subsurface voids in green and sintered silicon carbide and silicon nitride test specimens. These statistics were compared with previously-obtained statistics for implanted surface voids in similar specimens. Problems associated with void implantation are discussed. Statistical results are given as probability-of-detection curves at a 95 percent confidence level for voids ranging in size from 20 to 528 micro m in diameter. Author

A87-32200* Illinois Univ., Urbana.

NONDESTRUCTIVE EVALUATION OF ADHESIVE BOND STRENGTH USING THE STRESS WAVE FACTOR TECHNIQUE

HENRIQUE L. M. DOS REIS (Illinois, University, Urbana) and HAROLD E. KRAUTZ (NASA, Lewis Research Center, Cleveland, OH) Journal of Acoustic Emission (ISSN 0730-0050), vol. 5, Oct.-Dec. 1986, p. 144-147. refs

Acousto-ultrasonic nondestructive evaluation has been conducted to evaluate the adhesive bond strength between rubber and steel plates using the stress wave factor (SWF) measurement technique. Specimens with different bond strength were manufactured and tested using the SWF technique. Two approaches were used to define the SWF. One approach defines the SWF as the signal energy and the other approach defines the SWF as the square root of the zero moment of the frequency spectrum of the received signal. The strength of the rubber-steel adhesive joint was then evaluated using the destructive peel strength test method. It was observed that in both approaches higher values of the SWF measurements correspond to higher values of the peel strength test data. Therefore, these results show that the stress wave factor technique has the potential of

being used in quality assurance of the adhesive bond strength between rubber and steel substrates. Author

A87-48702*# National Aeronautics and Space Administration. Lewis Research Center, Cleveland, Ohio.

NDE RELIABILITY AND PROCESS CONTROL FOR STRUCTURAL CERAMICS

G. Y. BAAKLINI (NASA, Lewis Research Center, Cleveland, OH) ASME, Transactions, Journal of Engineering for Gas Turbines and Power (ISSN 0022-0825), vol. 109, July 1987, p. 263-266. Previously announced in STAR as N87-12910. refs (ASME PAPER 87-GT-8)

The reliability of microfocus X-radiography and scanning laser acoustic microscopy for detecting microvoids in silicon nitride and silicon carbide was statistically evaluated. Materials- and process-related parameters that influenced the statistical findings in research samples are discussed. The use of conventional X-radiography in controlling and optimizing the processing and sintering of an $\text{Si}_3\text{N}_4\text{-SiO}_2\text{-Y}_2\text{O}_3$ composition designated NASA 6Y is described. Radiographic evaluation and guidance helped develop uniform high-density Si_3N_4 modulus-of-rupture bars with improved four-point flexural strength (857, 544, and 462 MPa at room temperature, 1200 C, and 1370 C, respectively) and reduced strength scatter. Author

A87-51974*# National Aeronautics and Space Administration. Lewis Research Center, Cleveland, Ohio.

QUANTITATIVE VOID CHARACTERIZATION IN STRUCTURAL CERAMICS BY USE OF SCANNING LASER ACOUSTIC MICROSCOPY

D. J. ROTH, E. R. GENERAZIO (NASA, Lewis Research Center, Cleveland, OH), and G. Y. BAAKLINI (Cleveland State University, OH) Materials Evaluation (ISSN 0025-5327), vol. 45, Aug. 1987, p. 958-966. Previously announced in STAR as N86-31913. refs

The ability of scanning laser acoustic microscopy (SLAM) to characterize artificially seeded voids in sintered silicon nitride structural ceramic specimens was investigated. Using trigonometric relationships and Airy's diffraction theory, predictions of internal void depth and size were obtained from acoustic diffraction patterns produced by the voids. Agreement was observed between actual and predicted void depths. However, predicted void diameters were generally much greater than actual diameters. Precise diameter predictions are difficult to obtain due to measurement uncertainty and the limitations of 100 MHz SLAM applied to typical ceramic specimens. Author

N87-10399*# National Aeronautics and Space Administration. Lewis Research Center, Cleveland, Ohio.

ULTRASONIC DETERMINATION OF RECRYSTALLIZATION

E. R. GENERAZIO 1986 15 p Presented at the Review of Progress in Quantitative NDE, La Jolla, Calif. 3-8 Aug. 1986; sponsored by Ames Lab. and Iowa State Univ. (NASA-TM-88855; E-3248; NAS 1.15:88855) Avail: NTIS HC A02/MF A01 CSCL 14D

Ultrasonic attenuation was measured for cold worked Nickel 200 samples annealed at increasing temperatures. Localized dislocation density variations, crystalline order and volume percent of recrystallized phase were determined over the anneal temperature range using transmission electron microscopy, X-ray diffraction, and metallurgy. The exponent of the frequency dependence of the attenuation was found to be a key variable relating ultrasonic attenuation to the thermal kinetics of the recrystallization process. Identification of this key variable allows for the ultrasonic determination of onset, degree, and completion of recrystallization. B.G.

N87-11213*# Pratt and Whitney Aircraft, East Hartford, Conn. **CREEP FATIGUE LIFE PREDICTION FOR ENGINE HOT SECTION MATERIALS (ISOTROPIC): TWO YEAR UPDATE** V. MORENO In NASA. Lewis Research Center Turbine Engine Hot Section Technology, 1984 6 p Oct. 1984 (Contract NAS3-23288)

Avail: NTIS HC A17/MF A01 CSCL 14D

Requirements for increased durability of gas turbine hot section components have placed a greater degree of importance on accurate structural analysis and life prediction. Various life prediction approaches for high temperature applications were investigated. Basic models were selected and developed for simple-cycle, isothermal loading conditions. Models will be developed which address thermomechanical cycling, multiaxial conditions, cumulative loading, environmental effects, and cyclic mean stress. Verification tests of models will be conducted on an alternate material and coating system. B.G.

N87-12910*# National Aeronautics and Space Administration. Lewis Research Center, Cleveland, Ohio.

NDE RELIABILITY AND PROCESS CONTROL FOR STRUCTURAL CERAMICS

G. Y. BAAKLINI 1986 17 p Proposed for presentation at the 32nd International Gas Turbine Conference and Exhibition, Anaheim, Calif., 31 May - 4 Jun. 1987; sponsored by ASME (NASA-TM-88870; E-3276; NAS 1.15:88870) Avail: NTIS HC A02/MF A01 CSCL 14D

The reliability of microfocus x-radiography and scanning laser acoustic microscopy for detecting microvoids in silicon nitride and silicon carbide was statistically evaluated. Materials- and process-related parameters that influenced the statistical findings in research samples are discussed. The use of conventional x-radiography in controlling and optimizing the processing and sintering of an $\text{Si}_3\text{N}_4\text{-SiO}_2\text{-Y}_2\text{O}_3$ composition designated NASA 6Y is described. Radiographic evaluation and guidance helped develop uniform high-density Si_3N_4 modulus-of-rupture bars with improved four-point flexural strength (857, 544, and 462 MPa at room temperature, 1200 C, and 1370 C, respectively) and reduced strength scatter. Author

N87-13779*# Massachusetts Inst. of Tech., Cambridge. Dept. of Mechanical Engineering.

MODES OF VIBRATION ON SQUARE FIBERGLASS EPOXY COMPOSITE THICK PLATE Final Report

J. H. WILLIAMS, JR., E. R. C. MARQUES, and S. S. LEE Washington NASA Sep. 1986 29 p (Contract NAG3-328)

(NASA-CR-4018; E-3195; NAS 1.26:4018) Avail: NTIS HC A03/MF A01 CSCL 20K

The frequencies and nodal patterns of a square thick plate of unidirectional fiberglass epoxy composite are measured experimentally. The constituent material is transversely isotropic. The plate is transversely excited at the center of the upper face, its resonant frequencies in the frequency range of 3 kHz to 21.73 kHz are detected and the measured nodal patterns are sketched. Author

N87-13781*# Massachusetts Inst. of Tech., Cambridge. Dept. of Mechanical Engineering.

ULTRASONIC DETERMINATION OF THE ELASTIC CONSTANTS OF THE STIFFNESS MATRIX FOR UNIDIRECTIONAL FIBERGLASS EPOXY COMPOSITES Final Report

E. R. C. MARQUES and J. H. WILLIAMS, JR. Washington NASA Dec. 1986 27 p (Contract NAG3-328)

(NASA-CR-4034; E-3271; NAS 1.26:4034) Avail: NTIS HC A03/MF A01 CSCL 94B

The elastic constants of a fiberglass epoxy unidirectional composite are determined by measuring the phase velocities of longitudinal and shear stress waves via the through transmission ultrasonic technique. The waves introduced into the composite specimens were generated by piezoceramic transducers. Geometric lengths and the times required to travel those lengths were used

to calculate the phase velocities. The model of the transversely isotropic medium was adopted to relate the velocities and elastic constants. Author

N87-13782*# Massachusetts Inst. of Tech., Cambridge. Dept. of Mechanical Engineering.

PARAMETERIZED MATERIALS AND DYNAMIC RESPONSE CHARACTERIZATIONS IN UNIDIRECTIONAL COMPOSITES Final Report

J. H. WILLIAMS, JR. and E. R. C. MARQUES Washington
NASA Dec. 1986 37 p
(Contract NAG3-328)
(NASA-CR-4032; E-3272; NAS 1.26:4032) Avail: NTIS HC
A03/MF A01 CSCL 94B

The values of phase velocities of ultrasonic waves in transversely isotropic media are presented in terms of the fiber volume fraction of a unidirectional fiberglass epoxy composite with constant matrix properties and the ratio between extensional moduli in the longitudinal and transverse directions of the composite when the properties of the fibers are changed, at a constant fiber volume fraction. The model of a homogeneous transversely isotropic medium is adopted to describe the relations between elastic properties and velocities. The displacements due to an oscillatory point source in an infinite medium are used as one measure of comparison of the behavior of the unidirectional composite according to the variations of the parameters, as described above. Values of phase velocities, elastic moduli, Poisson's ratios and displacements due to a point source can be read from the parameterized plots for a known fiber volume fraction or a known ratio between extensional moduli of the composite. Alternatively fiber volume fraction and the ratio between extensional moduli can be inferred from the plots when the values of the phase velocities are known; for example from experimental measurements. Therefore, such parameterized curves may be useful in nondestructive mechanical property and material degradation characterizations. Author

N87-18109*# National Aeronautics and Space Administration. Lewis Research Center, Cleveland, Ohio.

NONDESTRUCTIVE EVALUATION OF STRUCTURAL CERAMICS

STANLEY J. KLIMA, GEORGE Y. BAAKLINI (Cleveland State Univ., Ohio), and PHILLIP B. ABEL 1987 23 p Presented at the 24th Automotive Technology Development Contractors Coordination Meeting, Dearborn, Mich., 27-30 Oct. 1986; sponsored by DOE
(NASA-TM-88978; E-3446; NAS 1.15:88978) Avail: NTIS HC
A02/MF A01 CSCL 14D

A review is presented on research and development of techniques for nondestructive evaluation and characterization of advanced ceramics for heat engine applications. Highlighted in this review are Lewis Research Center efforts in microfocus radiography, scanning laser acoustic microscopy (SLAM), scanning acoustic microscopy (SAM), scanning electron acoustic microscopy (SEAM), and photoacoustic microscopy (PAM). The techniques were evaluated by applying them to research samples of green and sintered silicon nitride and silicon carbide in the form of modulus-of-rupture bars containing seeded voids. Probabilities of detection of voids were determined for diameters as small as 20 microns for microfocus radiography, SLAM, and SAM. Strengths and limitations of the techniques for ceramic applications are identified. Application of ultrasonics for characterizing ceramic microstructures is also discussed. Author

N87-20562*# National Aeronautics and Space Administration. Lewis Research Center, Cleveland, Ohio.

THE ACOUSTO-ULTRASONIC APPROACH

ALEX VARY 1987 30 p Prepared for presentation at the Conference on Acousto-Ultrasonics: Theory and Application, Blacksburg, Va., 12-15 Jul. 1987; sponsored in part by NASA and American Society for Nondestructive Testing
(NASA-TM-89843; E-3504; NAS 1.15:89843) Avail: NTIS HC
A03/MF A01 CSCL 14D

The nature and underlying rationale of the acousto-ultrasonic approach is reviewed, needed advanced signal analysis and evaluation methods suggested, and application potentials discussed. Acousto-ultrasonics is an NDE technique combining aspects of acoustic emission methodology with ultrasonic simulation of stress waves. This approach uses analysis of simulated stress waves for detecting and mapping variations of mechanical properties. Unlike most NDE, acousto-ultrasonics is less concerned with flaw detection than with the assessment of the collective effects of various flaws and material anomalies. Acousto-ultrasonics has been applied chiefly to laminated and filament-wound fiber reinforced composites. It has been used to assess the significant strength and toughness reducing effects that can be wrought by combinations of essentially minor flaws and diffuse flaw populations. Acousto-ultrasonics assesses integrated defect states and the resultant variations in properties such as tensile, shear, and flexural strengths and fracture resistance. Matrix cure state, porosity, fiber orientation, fiber volume fraction, fiber-matrix bonding, and interlaminar bond quality are underlying factors. Author

N87-23987*# National Aeronautics and Space Administration. Lewis Research Center, Cleveland, Ohio.

APPLICATION OF SCANNING ACOUSTIC MICROSCOPY TO ADVANCED STRUCTURAL CERAMICS

ALEX VARY and STANLEY J. KLIMA Jul. 1987 14 p Prepared for presentation at the Symposium on Characterization of Advanced Materials, Monterey, Calif., 27-28 Jul. 1987; sponsored by International Metallographic Society
(NASA-TM-89929; E-3632; NAS 1.15:89929) Avail: NTIS HC
A02/MF A01 CSCL 14D

A review is presented of research investigations of several acoustic microscopy techniques for application to structural ceramics for advanced heat engines. Results obtained with scanning acoustic microscopy (SAM), scanning laser acoustic microscopy (SLAM), scanning electron acoustic microscopy (SEAM), and photoacoustic microscopy (PAM) are compared. The techniques were evaluated on research samples of green and sintered monolithic silicon nitrides and silicon carbides in the form of modulus-of-rupture bars containing deliberately introduced flaws. Strengths and limitations of the techniques are described with emphasis on statistics of detectability of flaws that constitute potential fracture origins. Author

N87-24707*# Massachusetts Inst. of Tech., Cambridge. Dept. of Mechanical Engineering.

ONE-DIMENSIONAL WAVE PROPAGATION IN RODS OF VARIABLE CROSS SECTION: A WKBJ SOLUTION Final Report

SIMEON C. U. OCHI and JAMES H. WILLIAMS, JR. Washington NASA Jul. 1987 92 p
(Contract NAG3-328)
(NASA-CR-4086; E-3651; NAS 1.26:4086) Avail: NTIS HC
A05/MF A01 CSCL 14D

As an important step in the characterization of a particular dynamic surface displacement transducer (IQI Model 501), a one-dimensional wave propagation in isotropic nonpiezoelectric and piezoelectric rods of variable cross section are presented. With the use of the Wentzel-Kramers-Brillouin-Jeffreys (WKBJ) approximate solution technique, an approximate formula, which relates the ratio of the amplitudes of a propagating wave observed at any two locations along the rod to the ratio of the cross sectional radii at these respective locations, is derived. The domains of

frequency for which the approximate solution is valid are discussed for piezoelectric and nonpiezoelectric materials. Author

N87-25589*# National Aeronautics and Space Administration. Lewis Research Center, Cleveland, Ohio.

RAY PROPAGATION PATH ANALYSIS OF ACOUSTO-ULTRASONIC SIGNALS IN COMPOSITES

HAROLD E. KAUTZ 1987 20 p Presented at Acousto-Ultrasonics: Theory and Application, Blacksburg, Va., 12-15 Jul. 1987; sponsored by NASA (NASA-TM-100148; E-3706; NAS 1.15:100148) Avail: NTIS HC A02/MF A01 CSCL 14D

The most important result was the demonstration that acousto-ultrasonic (AU) energy introduced into a laminated graphite/resin propagates by two modes through the structure. The first mode, along the graphite fibers, is the faster. The second mode, through the resin matrix, besides being slower is also more strongly attenuated at the higher frequencies. This demonstration was accomplished by analyzing the time and frequency domain of the composite AU signal and comparing them to the same for a neat resin specimen of the same chemistry and geometry as the composite matrix. Analysis of the fine structure of AU spectra was accomplished by various geometrical strategies. It was shown that the multitude of narrow peaks associated with AU spectra are the effect of the many pulse arrivals in the signal. The shape and distribution of the peaks is mainly determined by the condition of nonnormal reflections of ray paths. A cepstrum analysis was employed which can be useful in detecting characteristic times. Analysis of propagation modes can be accomplished while ignoring the fine structure. Author

N87-26361*# Massachusetts Inst. of Tech., Cambridge. **ACOUSTO-ULTRASONIC INPUT-OUTPUT CHARACTERIZATION OF UNIDIRECTIONAL FIBER COMPOSITE PLATE BY SH WAVES** Final Report

JAMES H. WILLIAMS, JR. and PETER LIAO Washington NASA Aug. 1987 50 p (Contract NAG3-328) (NASA-CR-4087; E-3650; NAS 1.26:4087) Avail: NTIS HC A03/MF A01 CSCL 14D

A unidirectional fiberglass epoxy composite plate specimen is modeled as a homogeneous transversely isotropic continuum plate medium. Acousto-ultrasonic non-contact input-output characterization by tracing SH waves in the continuum is studied theoretically with a transmitting and receiving transducer located on the same face of the plate. It is found that the directional dependence of the phase velocity of the SH waves travelling in the transversely isotropic medium has a significant effect on the delay time as opposed to the phase velocity of the SH wave travelling in an isotropic medium. Author

N87-26362*# National Aeronautics and Space Administration. Lewis Research Center, Cleveland, Ohio.

ULTRASONIC NDE OF STRUCTURAL CERAMICS FOR POWER AND PROPULSION SYSTEMS

ALEX VARY, EDWARD R. GENERAZIO, DON J. ROTH, and GEORGE Y. BAKLINI (Cleveland State Univ., Ohio.) 1987 12 p Presented at the 4th European Conference on Non-Destructive Testing, London, England, 13-18 Sep. 1987; sponsored by the British Inst. of Non-Destructive Testing (NASA-TM-100147; E-3705; NAS 1.15:100147) Avail: NTIS HC A02/MF A01 CSCL 14D

A review of research investigations of several ultrasonic evaluation techniques applicable to structural ceramics for advanced heat engines is presented. This review highlights recent work conducted under the sponsorship of and at the Lewis Research Center. Results obtained with scanning acoustic microscopy, scanning laser acoustic microscopy, photo acoustic microscopy, and scanning electron acoustic microscopy are compared. In addition to these flaw imaging techniques, microstructure characterization by analytical ultrasonics is described. The techniques were evaluated by application to research samples of monolithic silicon nitride and silicon carbide

in the form of discs and bars containing naturally occurring and deliberately-introduced flaws and microstructural anomalies. Strengths and limitations of the techniques are discussed. Author

39

STRUCTURAL MECHANICS

Includes structural element design and weight analysis; fatigue; and thermal stress.

A87-10893* Georgia Inst. of Tech., Atlanta.

NOTES AND COMMENTS ON COMPUTATIONAL ELASTOPLASTICITY - SOME NEW MODELS AND THEIR NUMERICAL IMPLEMENTATION

S. N. ATLURI (Georgia Institute of Technology, Atlanta) IN: Finite elements in computational mechanics - FEICOM '85; Proceedings of the International Conference, Bombay, India, December 2-6, 1985. Volume 1. Oxford, Pergamon Press, 1985, p. 271-289. refs (Contract NAG3-346; N00014-78-C-0636)

The following topics are discussed in this paper: (1) the basic interactive nature of classical elasto-plasticity and a redefinition of elastic and plastic processes that facilitates numerical calculations, (2) generalized mid-point or end-point algorithms to determine the stress increment in an elastic-plastic solid from a given strain increment, (3) an endochronic (internal time) rate theory of time-independent plasticity which encompasses various multiple-yield-surface theories and nonlinear kinematic hardening theories as its specializations, and (4) comments on finite element and boundary element methods for solving boundary value problems in elasto-plasticity. Author

A87-11106*# Ohio State Univ., Columbus.

THREE-DIMENSIONAL VIBRATIONS OF TWISTED CANTILEVERED PARALLELEPIPEDS

A. LEISSA (Ohio State University, Columbus) and K. I. JACOB ASME, Transactions, Journal of Applied Mechanics (ISSN 0021-8936), vol. 53, Sept. 1986, p. 614-618. refs (Contract NAG3-424)

A large number of references dealing with the vibrations of twisted, cantilevered beams and plates exist in the literature. These works show considerable disagreement concerning the effect of twist angle upon frequencies. The present work is the first three-dimensional study of the problem. Displacement components are assumed in the form of algebraic polynomials which satisfy the fixed face conditions exactly, and which are mathematically complete. The Ritz method is then applied. Accurate frequencies are calculated for twisted thick plates and are compared with ones obtained recently by others using beam, shell, and finite element theory. Author

A87-13496* Toledo Univ., Ohio.

THERMAL ANALYSIS OF AN ORTHOTROPIC ENGINEERING BODY

K.-C. FU and D.-R. JENG (Toledo, University, OH) IN: Applied numerical modeling. San Diego, CA, Univelt, Inc., 1986, p. 559-564. (Contract NAG3-373)

This work is an effort in determining the temperature distribution of an orthotropic engineering body. First the governing partial differential equation is derived, then, a finite element procedure using variational approach is developed for the solution of the governing equation. Finally, a computer program provides a set of satisfactory results. Author

A87-13882* State Univ. of New York, Buffalo.
FREE VIBRATION ANALYSIS BY BEM USING PARTICULAR INTEGRALS

S. AHMAD and P. K. BANERJEE (New York, State University, Buffalo) Journal of Engineering Mechanics (ISSN 0733-9399), vol. 112, July 1986, p. 682-695. refs
 (Contract NAS3-23697)

A new method for the free-vibration analysis using the boundary element technique is presented. The method utilizes a fictitious vector function to approximate the inertia forces and then uses the well-known concept of complementary functions and particular integrals to solve the resulting governing differential equations. The necessary particular integrals are defined for the two and three-dimensional analyses, and the present formulation is applied to a number of two-dimensional problems to show its accuracy and efficiency in the solution of realistic engineering problems.

Author

A87-14316* Akron Univ., Ohio.
ANALYSIS OF THERMOMECHANICAL OXIDATION FIELDS IN THERMAL BARRIER COATINGS

J. PADOVAN, P. PADOVAN, and Y. XIARU (Akron, University, OH) Journal of Thermal Stresses (ISSN 0149-5739), vol. 9, no. 3, 1986, p. 251-277. refs
 (Contract NAG3-256)

This paper considers the problem of the thermomechanical oxidation response of thermal barrier coatings. Overall, this involves the formulation of the requisite field equations and their associated boundary conditions, including the effects of oxide scale developing either on external surfaces or at interlaminar regions. To establish the potential effects of growing scale layers, the solution to the thermomechanical oxidation response of a cylindrically configured thermal barrier coating is developed. This includes handling the overall thermomechanical oxidation history.

Author

A87-15798* Massachusetts Inst. of Tech., Cambridge.
KI-SOLUTIONS FOR SINGLE EDGE NOTCH SPECIMENS UNDER FIXED END DISPLACEMENTS

N. MARCHAND, D. M. PARKS, and R. M. PELLOUX (MIT, Cambridge, MA) International Journal of Fracture (ISSN 0376-9429), vol. 31, May 1986, p. 53-65. refs
 (Contract NAG3-280; N00014-80-C-0706)

The KI solution for a finite length single-edge notch specimen loaded under fixed-end displacements is derived using a crack compliance analysis. Numerical and experimental checks of the KI solution are provided. Good agreement between the experimental and numerical solutions is observed. The applicability of conventional fracture mechanics to correlate crack growth data generated under displacement control is discussed.

Author

A87-17799* National Aeronautics and Space Administration.
 Lewis Research Center, Cleveland, Ohio.
ELASTIC ANALYSIS OF A MODE II FATIGUE CRACK TEST SPECIMEN

B. GROSS, R. J. BUZZARD, and W. F. BROWN, JR. (NASA, Lewis Research Center, Cleveland, OH) International Journal of Fracture (ISSN 0376-9429), vol. 31, June 1986, p. 151-157.

Elastic displacements and stress intensity measurements for a mode II specimen have been obtained over a range of a/W values between 0.500 and 0.900 using the MARC general purpose finite element program. Stress intensity factors were experimentally determined using load point displacement values. Good general agreement between numerical and experimental results for crack mouth, crack surface, and load point displacements, and for stress intensity factors, demonstrates the accuracy of the present method.

R.R.

A87-17988*# National Aeronautics and Space Administration.
 Lewis Research Center, Cleveland, Ohio.

SCARE - A POSTPROCESSOR PROGRAM TO MSC/NASTRAN FOR RELIABILITY ANALYSIS OF STRUCTURAL CERAMIC COMPONENTS

J. P. GYEKENYESI (NASA, Lewis Research Center, Cleveland, OH) ASME, Transactions, Journal of Engineering for Gas Turbines and Power (ISSN 0022-0825), vol. 108, July 1986, p. 540-546. Previously announced in STAR as N86-14688. refs
 (ASME PAPER 86-GT-34)

A computer program was developed for calculating the statistical fast fracture reliability and failure probability of ceramic components. The program includes the two-parameter Weibull material fracture strength distribution model, using the principle of independent action for polyaxial stress states and Batdorf's shear-sensitive as well as shear-insensitive crack theories, all for volume distributed flaws in macroscopically isotropic solids. Both penny-shaped cracks and Griffith cracks are included in the Batdorf shear-sensitive crack response calculations, using Griffith's maximum tensile stress or critical coplanar strain energy release rate criteria to predict mixed mode fracture. Weibull material parameters can also be calculated from modulus of rupture bar tests, using the least squares method with known specimen geometry and fracture data. The reliability prediction analysis uses MSC/NASTRAN stress, temperature and volume output, obtained from the use of three-dimensional, quadratic, isoparametric, or axisymmetric finite elements. The statistical fast fracture theories employed, along with selected input and output formats and options, are summarized. An example problem to demonstrate various features of the program is included.

Author

A87-20892*# Georgia Inst. of Tech., Atlanta.
BOUNDING SOLUTIONS OF GEOMETRICALLY NONLINEAR VISCOELASTIC PROBLEMS

JOHN M. STUBSTAD and GEORGE J. SIMITSES (Georgia Institute of Technology, Atlanta) (Structures, Structural Dynamics, and Materials Conference, 27th, San Antonio, TX, May 19-21, 1986, Technical Papers. Part 1, p. 343-352) AIAA Journal (ISSN 0001-1452), vol. 24, Nov. 1986, p. 1843-1850. Previously cited in issue 18, p. 2655, Accession no. A86-38838. refs
 (Contract NAG3-534)

A87-22128* Case Western Reserve Univ., Cleveland, Ohio.
RE-EXAMINATION OF CUMULATIVE FATIGUE DAMAGE ANALYSIS - AN ENGINEERING PERSPECTIVE

S. S. MANSON (Case Western Reserve University, Cleveland, OH) and G. R. HALFORD (NASA, Lewis Research Center, Cleveland, OH) (IUTAM, Israel Academy of Science and Humanities, U.S. Army, et al., Symposium on Mechanics of Damage and Fatigue, Haifa and Tel Aviv, Israel, July 1-4, 1985) Engineering Fracture Mechanics (ISSN 0013-7944), vol. 25, no. 5-6, 1986, p. 539-571. Previously announced in STAR as N86-27680. refs

A method which has evolved in the laboratories for the past 20 yr is re-examined with the intent of improving its accuracy and simplicity of application to engineering problems. Several modifications are introduced both to the analytical formulation of the Damage Curve Approach, and to the procedure for modifying this approach to achieve a Double Linear Damage Rule formulation which immensely simplifies the calculation. Improvements are also introduced in the treatment of mean stress for determining fatigue life of the individual events that enter into a complex loading history. While the procedure is completely consistent with the results of numerous two level tests that have been conducted on many materials, it is still necessary to verify applicability to complex loading histories. Caution is expressed that certain phenomenon can also influence the applicability - for example, unusual deformation and fracture modes inherent in complex loading especially if stresses are multiaxial. Residual stresses at crack tips, and metallurgical factors are also important in creating departures from the cumulative damage theories; examples of departures are provided.

Author

A87-22775* State Univ. of New York, Buffalo.
CONFORMING VERSUS NON-CONFORMING BOUNDARY ELEMENTS IN THREE-DIMENSIONAL ELASTOSTATICS
 G. D. MANOLIS and P. K. BANERJEE (New York, State University, Buffalo) International Journal for Numerical Methods in Engineering (ISSN 0029-5981), vol. 23, Oct. 1986, p. 1885-1904. Research supported by Pratt and Whitney. refs
 (Contract NAS3-23967)

A critical comparison of two basic formulations in three-dimensional elastostatics, using conforming and nonconforming boundary elements, is presented. The basic structure of the boundary element method is developed. The peculiarities that both types of boundary elements present in relation to the numerical implementation are discussed. Through selected examples, key issues such as the computational advantages and disadvantages of both formulations, mesh discretization and accuracy questions, and optimal location of the collocation nodes in the case of nonconforming elements are addressed. It is shown that conforming elements are able to produce more accurate results than nonconforming ones, with substantial economy in the final size of the system equations.

I.S.

A87-25407* National Aeronautics and Space Administration. Lewis Research Center, Cleveland, Ohio.
DESIGN CONCEPTS/PARAMETERS ASSESSMENT AND SENSITIVITY ANALYSES OF SELECT COMPOSITE STRUCTURAL COMPONENTS

C. C. CHAMIS (NASA, Lewis Research Center, Cleveland, OH) International Journal of Materials and Product Technology (ISSN 0268-1900), vol. 1, Oct. 1986, p. 211-229. refs

Formal approaches are summarized to evaluate design concepts and perform sensitivity analyses on design parameters of composite structural components for vehicles. The formal approaches include structural analyses coupled with composite micromechanics to assess the structural response of beams made from various intraply hybrids, finite element analysis in conjunction with composite mechanics to assess the structural response of panels made from strip hybrids, and sensitivity analysis through optimization to assess the effects of various design parameters on the optimum design of a panel made from angleply composite laminates. Results obtained from these approaches are presented in graphical and tabular form to illustrate parametric studies and acceptable ranges of various design parameters. Author

A87-25775* Case Western Reserve Univ., Cleveland, Ohio.
COMPLIANCE MATRICES FOR CRACKED BODIES
 R. BALLARINI (Case Western Reserve University, Cleveland, OH) International Journal of Fracture (ISSN 0376-9429), vol. 31, Aug. 1986, p. R63-R66. refs
 (Contract NCC3-46)

An algorithm is developed to construct the compliance matrix for a cracked solid in the integral-equation formulation of two-dimensional linear-elastic fracture mechanics. The integral equation is reduced to a system of algebraic equations for unknown values of the dislocation-density function at discrete points on the interval from -1 to 1, using the numerical procedure described by Gerasoulis (1982). Sample numerical results are presented, and it is suggested that the algorithm is especially useful in cases where iterative solutions are required; e.g., models of fiber-reinforced concrete, rocks, or ceramics where microcracking, fiber bridging, and other nonlinear effects are treated as nonlinear springs along the crack surfaces (Ballarini et al., 1984). T.K.

A87-25924* Akron Univ., Ohio.
ON THE NUMERICAL PERFORMANCE OF THREE-DIMENSIONAL THICK SHELL ELEMENTS USING A HYBRID-MIXED FORMULATION
 W. GRAF, T. Y. CHANG, and A. F. SALEEB (Akron, University, OH) Finite Elements in Analysis and Design (ISSN 0168-874X), vol. 2, Dec. 1986, p. 357-375. refs
 (Contract NAG3-307)

Three-dimensional thick shell elements with 8, 16, and 18 nodes are formulated by using the hybrid/mixed method. In bending applications, these elements are free from locking effect and give improved stress predictions. Finite element equations are derived from the Hellinger-Reissner variational principle in which both the displacement and stress fields are approximated by independent interpolation functions. For the assumption of stress parameters, three guidelines are followed: (1) suppression of kinematic deformation modes, (2) invariant element property, and (3) the constraint index exhibited by the element, when applied to constrained-media problems, must be greater than or equal to one. Numerical results are presented to show the element's behavior characteristics regarding sensitivity to locking, distortion effect (patch tests), mesh convergence and the accuracy of stress evaluation. Author

A87-27945*# Georgia Inst. of Tech., Atlanta.
THERMODYNAMICALLY CONSISTENT CONSTITUTIVE EQUATIONS FOR NONISOTHERMAL LARGE-STRAIN, ELASTOPLASTIC, CREEP BEHAVIOR
 RICHARD RIFF, ROBERT L. CARLSON, and GEORGE J. SIMITSES (Georgia Institute of Technology, Atlanta) AIAA Journal (ISSN 0001-1452), vol. 25, Jan. 1987, p. 114-122. Previously cited in issue 17, p. 2527, Accession no. A85-38425. refs
 (Contract NAG3-534)

A87-27986*# National Aeronautics and Space Administration. Lewis Research Center, Cleveland, Ohio.
FATIGUE CRITERION TO SYSTEM DESIGN, LIFE, AND RELIABILITY
 ERWIN Y. ZARETSKY (NASA, Lewis Research Center, Cleveland, OH) Journal of Propulsion and Power (ISSN 0748-4658), vol. 3, Jan.-Feb. 1987, p. 76-83. Previously cited in issue 19, p. 2818, Accession no. A85-40814. refs

A87-28543* Rockwell International Corp., Downey, Calif.
MODELING OF MULTI-ROTOR TORSIONAL VIBRATIONS IN ROTATING MACHINERY USING SUBSTRUCTURING
 FOLA R. SOARES (Rockwell International Corp., Space Transportation Systems Div., Downey, CA) IN: International Modal Analysis Conference, 4th, Los Angeles, CA, Feb. 3-6, 1986, Proceedings. Volume 1. Schenectady, NY, Union College, 1986, p. 360-370. refs
 (Contract NAG3-391)

The application of FEM modeling techniques to the analysis of torsional vibrations in complex rotating systems is described and demonstrated, summarizing results reported by Soares (1985). A substructuring approach is used for determination of torsional natural frequencies and resonant-mode shapes, steady-state frequency-sweep analysis, identification of dynamically unstable speed ranges, and characterization of transient linear and nonlinear systems. Results for several sample problems are presented in diagrams, graphs, and tables. STORV, a computer code based on this approach, is in use as a preliminary design tool for drive-train torsional analysis in the High Altitude Wind Tunnel at NASA Lewis. T.K.

A87-28982* Case Western Reserve Univ., Cleveland, Ohio.

AN ANALYSIS FOR CRACK LAYER STABILITY

K. SEHANOBI, J. BOTSIS, A. MOET, and A. CHUDNOVSKY (Case Western Reserve University, Cleveland, OH) *International Journal of Fracture* (ISSN 0376-9429), vol. 32, Sept. 1986, p. 21-33. Research supported by the Gas Research Institute. refs (Contract NAG3-585)

The problem of uncontrolled crack propagation and crack arrest is considered with respect to crack layer (CL) translational stability. CL propagation is determined by the difference between the energy release rate and the amount of energy required for material transformation, and necessary and sufficient conditions for CL instability are derived. CL propagation in polystyrene is studied for two cases. For the case of remotely applied fixed load fatigue, the sufficient condition of instability is shown to be met before the necessary condition, and the necessary condition controls the stability. For the fixed displacement case, neither of the instability conditions are met, and CL propagation remains stable, resulting in crack arrest. R.R.

A87-33579*# Northwestern Univ., Evanston, Ill.

A PROBABILISTIC HU-WASHIZU VARIATIONAL PRINCIPLE

W. K. LIU, T. BELYTSCHKO (Northwestern University, Evanston, IL), and G. H. BESTERFIELD IN: Structures, Structural Dynamics and Materials Conference, 28th, Monterey, CA, Apr. 6-8, 1987, Technical Papers. Part 1. New York, American Institute of Aeronautics and Astronautics, 1987, p. 252-259. refs (Contract NAG3-535) (AIAA PAPER 87-0764)

A Probabilistic Hu-Washizu Variational Principle (PHWVP) for the Probabilistic Finite Element Method (PFEM) is presented. This formulation is developed for both linear and nonlinear elasticity. The PHWVP allows incorporation of the probabilistic distributions for the constitutive law, compatibility condition, equilibrium, domain and boundary conditions into the PFEM. Thus, a complete probabilistic analysis can be performed where all aspects of the problem are treated as random variables and/or fields. The Hu-Washizu variational formulation is available in many conventional finite element codes thereby enabling the straightforward inclusion of the probabilistic features into present codes. Author

A87-33581*# Sverdrup Technology, Inc., Cleveland, Ohio.

PROBABILISTIC STRUCTURAL ANALYSIS TO QUANTIFY UNCERTAINTIES ASSOCIATED WITH TURBOPUMP BLADES

VINOD K. NAGPAL, ROBERT RUBINSTEIN (Sverdrup Technology, Inc., Cleveland, OH), and CHRISTOS C. CHAMIS (NASA, Lewis Research Center, Cleveland, OH) IN: Structures, Structural Dynamics and Materials Conference, 28th, Monterey, CA, Apr. 6-8, 1987, Technical Papers. Part 1. New York, American Institute of Aeronautics and Astronautics, 1987, p. 268-274. refs (AIAA PAPER 87-0766)

A probabilistic study of turbopump blades has been in progress at NASA Lewis Research Center for over the last two years. The objectives of this study are to evaluate the effects of uncertainties in geometry and material properties on the structural response of the turbopump blades to evaluate the tolerance limits on the design. A methodology based on probabilistic approach has been developed to quantify the effects of the random uncertainties. The results of this study indicate that only the variations in geometry have significant effects. Author

A87-33604*# Georgia Inst. of Tech., Atlanta.

SOLUTION METHODS FOR ONE-DIMENSIONAL VISCOELASTIC PROBLEMS

JOHN M. STUBSTAD and GEORGE J. SIMITSES (Georgia Institute of Technology, Atlanta) IN: Structures, Structural Dynamics and Materials Conference, 28th, Monterey, CA, Apr. 6-8, 1987, Technical Papers. Part 1. New York, American Institute of Aeronautics and Astronautics, 1987, p. 458-465. refs (Contract NAG3-534) (AIAA PAPER 87-0804)

A recently developed differential methodology for solution of one-dimensional nonlinear viscoelastic problems is presented. Using the example of an eccentrically loaded cantilever beam-column, the results from the differential formulation are compared to results generated using a previously published integral solution technique. It is shown that the results obtained from these distinct methodologies exhibit a surprisingly high degree of correlation with one another. A discussion of the various factors affecting the numerical accuracy and rate of convergence of these two procedures is also included. Finally, the influences of some 'higher order' effects, such as straining along the centroidal axis are discussed. Author

A87-33605*# Georgia Inst. of Tech., Atlanta.

NON-ISOTHERMAL ELASTOVISCOPLASTIC SNAP-THROUGH AND CREEP BUCKLING OF SHALLOW ARCHES

G. J. SIMITSES and R. RIFF (Georgia Institute of Technology, Atlanta) IN: Structures, Structural Dynamics and Materials Conference, 28th, Monterey, CA, Apr. 6-8, 1987, Technical Papers. Part 1. New York, American Institute of Aeronautics and Astronautics, 1987, p. 466-472. refs (Contract NAG3-534) (AIAA PAPER 87-0806)

The problem of buckling of shallow arches under transient thermomechanical loads is investigated. The analysis is based on nonlinear geometric and constitutive relations, and is expressed in a rate form. The material constitutive equations are capable of reproducing all non-isothermal, elasto-viscoplastic characteristics. The solution scheme is capable of predicting response which includes pre and postbuckling with creep and plastic effects. The solution procedure is demonstrated through several examples which include both creep and snap-through behavior. Author

A87-33624*# Massachusetts Inst. of Tech., Cambridge.

A VERSATILE AND LOW ORDER HYBRID STRESS ELEMENT FOR GENERAL SHELL GEOMETRY

DAVID S. KANG and THEODORE H. H. PIAN (MIT, Cambridge, MA) IN: Structures, Structural Dynamics and Materials Conference, 28th, Monterey, CA, Apr. 6-8, 1987, Technical Papers. Part 1. New York, American Institute of Aeronautics and Astronautics, 1987, p. 633-641. refs (Contract NAG3-33) (AIAA PAPER 87-0840)

A hybrid stress general shell element is developed based on the Hellinger-Reissner principle modified for relaxed element compatibility conditions. The element is based on a consistent first order thin shell theory with Love Kirchhoff hypotheses. It is of quadrilateral shape with only four corner nodes and five degrees of freedom per node. The geometry of the element is approximated through a bi-cubic polynomial surface patch. Numerical examples consist of torsion-loaded slit cylinder and pinched cylinder with open ends and rigid diaphragmed ends. Also, the representation of the rigid body motion is studied by series of parametric eigenvalue analysis of the stiffness matrix. Author

A87-33645*# National Aeronautics and Space Administration. Lewis Research Center, Cleveland, Ohio.

ADVANCES IN 3-D INELASTIC ANALYSIS METHODS FOR HOT SECTION COMPONENTS

CHRISTOS C. CHAMIS (NASA, Lewis Research Center, Cleveland, OH) IN: Structures, Structural Dynamics and Materials Conference, 28th, Monterey, CA, Apr. 6-8, 1987, Technical Papers. Part 1. New York, American Institute of Aeronautics and Astronautics, 1987, p. 802-811.

(AIAA PAPER 87-0719)

3-D Inelastic Analysis Methods are described. These methods consist of a series of new computer codes embodying a progression of mathematical models (mechanics of materials, specialty finite element, boundary element) for streamlined analysis of: (1) combustor liners, (2) turbine blades, and (3) turbine vanes. These models address the effects of high temperatures and thermal/mechanical loadings on the local (stress/strain) and global (dynamics, buckling) structural behavior of the three selected components. Three computer codes, referred to as MOMM (Mechanics of Materials Model), MHOST (MARC-Hot Section Technology), and BEST (Boundary Element Stress Technology), have been developed and are briefly described in this paper.

Author

A87-33648*# Pratt and Whitney Aircraft Group, East Hartford, Conn.

STRUCTURAL TAILORING OF ADVANCED TURBOPROPS

K. W. BROWN, P. R. HARVEY (Pratt and Whitney, East Hartford, CT), and C. C. CHAMIS (NASA, Lewis Research Center, Cleveland, OH) IN: Structures, Structural Dynamics and Materials Conference, 28th, Monterey, CA, Apr. 6-8, 1987, Technical Papers. Part 1. New York, American Institute of Aeronautics and Astronautics, 1987, p. 827-837. refs

(AIAA PAPER 87-0753)

A computer program has been developed for the performance of numerical optimizations of highly swept propfan blades by minimizing an objective function that is defined either as direct operating cost or the aeroelastic difference between a blade and its scaled model. Three component analysis categories are employed: an optimization algorithm, approximate analysis procedures for objective function and constraint evaluation, and refined analysis procedures for optimum design validation. The analyses conducted by the program encompass aerodynamic efficiency evaluation, finite element stress and vibration analysis, acoustics, flutter, and forced response life prediction. O.C.

A87-33719*# Georgia Inst. of Tech., Atlanta.

A TECHNIQUE FOR THE PREDICTION OF AIRFOIL FLUTTER CHARACTERISTICS IN SEPARATED FLOW

JIUNN-CHI WU, L. N. SANKAR (Georgia Institute of Technology, Atlanta), and K. R. V. KAZA (NASA, Lewis Research Center, Cleveland, OH) IN: Structures, Structural Dynamics and Materials Conference, 28th, Monterey, CA, Apr. 6-8, 1987 and AIAA Dynamics Specialists Conference, Monterey, CA, Apr. 9, 10, 1987, Technical Papers. Part 2B. New York, American Institute of Aeronautics and Astronautics, 1987, p. 664-673. refs

(Contract NAG3-730)

(AIAA PAPER 87-0910)

A solution procedure is described for determining the two-dimensional, one- or two-degree-of-freedom flutter characteristics of arbitrary airfoils at large angles of attack. The same procedure is used to predict stall flutter. This procedure requires a simultaneous integration in time of the solid and fluid equations of motion. The fluid equations of motion are the unsteady compressible Navier-Stokes equations, solved in a body-fitted moving coordinate system using an approximate factorization scheme. The solid equations of motion are integrated in time using an Euler implicit scheme. Flutter is said to occur if small disturbances imposed on the airfoil attitude lead to divergent oscillatory motions at subsequent times. Results for a number of special cases are presented to demonstrate the suitability of this scheme to predict flutter at large mean angles of attack. Some stall flutter applications are also presented. Author

A87-33756*# National Aeronautics and Space Administration. Lewis Research Center, Cleveland, Ohio.

APPROXIMATIONS TO EIGENVALUES OF MODIFIED GENERAL MATRICES

DURBHA V. MURTHY (NASA, Lewis Research Center, Cleveland; Toledo, University, OH) and RAPHAEL T. HAFTKA (Virginia Polytechnic Institute and State University, Blacksburg) IN: Structures, Structural Dynamics and Materials Conference, 28th, Monterey, CA, Apr. 6-8, 1987 and AIAA Dynamics Specialists Conference, Monterey, CA, Apr. 9, 10, 1987, Technical Papers. Part 2B. New York, American Institute of Aeronautics and Astronautics, 1987, p. 1032-1045. refs

(Contract NAG3-347; NAG1-224)

(AIAA PAPER 87-0947)

The reanalysis of non-self-adjoint dynamic models is computationally very expensive in design optimization applications. This paper describes several approximations that can be applied to eigenvalues of non-hermitian matrices to reduce that computational cost. Approximations based on eigenvector derivatives, generalized Rayleigh quotient and the trace theorem are presented and their accuracy and computational cost are estimated. The accuracy and cost estimates are verified by applying the approximations to random matrices and matrices arising in flutter analysis of compressor blades. Recommendations are made for selection of the best approximation when the derivatives are available and when they are not. In particular, it is concluded that the quadratic approximation for eigenvalues should never be used as higher order approximations are always more accurate as well as more efficient. Author

A87-35334* Virginia Polytechnic Inst. and State Univ., Blacksburg.

J-INTEGRAL ESTIMATES FOR CRACKS IN INFINITE BODIES

N. E. DOWLING (Virginia Polytechnic Institute and State University, Blacksburg) Engineering Fracture Mechanics (ISSN 0013-7944), vol. 26, no. 3, 1987, p. 333-348. Previously announced in STAR as N86-28467. refs

(Contract NAG3-438)

An analysis and discussion is presented of existing estimates of the J-integral for cracks in infinite bodies. Equations are presented which provide convenient estimates for Ramberg-Osgood type elasto-plastic materials containing cracks and subjected to multiaxial loading. The relationship between J and the strain normal to the crack is noted to be only weakly dependent on state of stress. But the relationship between J and the stress normal to the crack is strongly dependent on state of stress. A plastic zone correction term often employed is found to be arbitrary, and its magnitude is seldom significant. Author

A87-35656*# Indian Inst. of Science, Bangalore.

A HIGHER ORDER THEORY OF LAMINATED COMPOSITE CYLINDRICAL SHELLS

A. V. KRISHNA MURTHY (Indian Institute of Science, Bangalore, India) and T. S. R. REDDY (NASA, Lewis Research Center, Cleveland, OH) Aeronautical Society of India, Journal (ISSN 0001-9267), vol. 38, Aug. 1986, p. 161-171. Research supported by the Aeronautical Research and Development Board. refs

A new higher order theory has been proposed for the analysis of composite cylindrical shells. The formulation allows for arbitrary variation of inplane displacements. Governing equations are presented in the form of a hierarchy of sets of partial differential equations. Each set describes the shell behavior to a certain degree of approximation. The natural frequencies of simply-supported isotropic and laminated shells and stresses in a ring loaded composite shell have been determined to various orders of approximation and compared with three dimensional solutions. These numerical studies indicate the improvements achievable in estimating the natural frequencies and the interlaminar shear stresses in laminated composite cylinders. Author

A87-36926* Illinois Univ., Chicago.

ELASTIC INTERACTION OF A CRACK WITH A MICROCRACK ARRAY. I - FORMULATION OF THE PROBLEM AND GENERAL FORM OF THE SOLUTION. II - ELASTIC SOLUTION FOR TWO CRACK CONFIGURATIONS (PIECEWISE CONSTANT AND LINEAR APPROXIMATIONS)

A. CHUDNOVSKY (Illinois, University, Chicago), A. DOLGOPOLSKY (Delaware, University, Newark), and M. KACHANOV (Tufts University, Medford, MA) International Journal of Solids and Structures (ISSN 0020-7683), vol. 23, no. 1, 1987, p. 1-21. refs (Contract NAG3-23; AF-AFOSR-84-0321; DAAG29-84-K-0184)

The elastic interactions of a two-dimensional configuration consisting of a crack with an array of microcracks located near the tip are studied. The general form of the solution is based on the potential representations and approximations of tractions on the microcracks by polynomials. In the second part, the technique is applied to two simple two-dimensional configurations involving one and two microcracks. The problems of stress shielding and stress amplification (the reduction or increase of the effective stress intensity factor due to the presence of microcracks) are discussed, and the refinements introduced by higher order polynomial approximations are illustrated. R.R.

A87-39896*# National Aeronautics and Space Administration. Lewis Research Center, Cleveland, Ohio.

NONLINEAR VIBRATION AND STABILITY OF ROTATING, PRETWISTED, PRECONED BLADES INCLUDING CORIOLIS EFFECTS

K. B. SUBRAHMANYAM, K. R. V. KAZA, G. V. BROWN, and C. LAWRENCE (NASA, Lewis Research Center, Cleveland, OH) Journal of Aircraft (ISSN 0021-8669), vol. 24, May 1987, p. 342-352. Previously announced in STAR as N86-17789. refs

The coupled bending-bending-torsional equations of dynamic motion of rotating, linearly pretwisted blades are derived including large precone, second degree geometric nonlinearities and Coriolis effects. The equations are solved by the Galerkin method and a linear perturbation technique. Accuracy of the present method is verified by comparisons of predicted frequencies and steady state deflections with those from MSC/NASTRAN and from experiments. Parametric results are generated to establish where inclusion of only the second degree geometric nonlinearities is adequate. The nonlinear terms causing torsional divergence in thin blades are identified. The effects of Coriolis terms and several other structurally nonlinear terms are studied, and their relative importance is examined. Author

A87-40056*# Case Western Reserve Univ., Cleveland, Ohio. **CRACK LAYER THEORY**

A. CHUDNOVSKY (Case Western Reserve University, Cleveland, OH) IN: U.S. National Congress of Applied Mechanics, 10th, Austin, TX, June 16-20, 1986, Proceedings. New York, American Society of Mechanical Engineers, 1987, p. 97-106. Research supported by the Dow Chemical Co. and CASC. Previously announced in STAR as N84-22980. refs (Contract NAG3-585)

A damage parameter is introduced in addition to conventional parameters of continuum mechanics and consider a crack surrounded by an array of microdefects within the continuum mechanics framework. A system consisting of the main crack and surrounding damage is called crack layer (CL). Crack layer propagation is an irreversible process. The general framework of the thermodynamics of irreversible processes are employed to identify the driving forces (causes) and to derive the constitutive equation of CL propagation, that is, the relationship between the rates of the crack growth and damage dissemination from one side and the conjugated thermodynamic forces from another. The proposed law of CL propagation is in good agreement with the experimental data on fatigue CL propagation in various materials. The theory also elaborates material toughness characterization. M.A.C.

A87-40496*# National Aeronautics and Space Administration. Lewis Research Center, Cleveland, Ohio.

ANALYTICAL AND EXPERIMENTAL INVESTIGATION OF MISTUNING IN PROPFAN FLUTTER

KRISHNA RAO V. KAZA, ORAL MEHMED (NASA, Lewis Research Center, Cleveland, OH), MARC WILLIAMS (Purdue University, West Lafayette, IN), and LARRY A. MOSS (Sverdrup Technology, Inc., Cleveland, OH) IN: Structures, Structural Dynamics and Materials Conference, 28th, Monterey, CA, Apr. 6-8, 1987 and AIAA Dynamics Specialists Conference, Monterey, CA, Apr. 9, 10, 1987, Technical Papers. Part 2A. New York, American Institute of Aeronautics and Astronautics, 1987, p. 98-110. Previously announced in STAR as N87-18116. refs (AIAA PAPER 87-0739)

An analytical and experimental investigation of the effects of mistuning on propfan subsonic flutter was performed. The analytical model is based on the normal modes of a rotating composite blade and a three-dimensional subsonic unsteady lifting surface aerodynamic theory. Theoretical and experimental results are compared for selected cases at different blade pitch angles, rotational speeds, and free-stream Mach numbers. The comparison shows a reasonably good agreement between theory and experiment. Both theory and experiment showed that combined mode shape, frequency, and aerodynamic mistuning can have a beneficial or adverse effect on blade damping depending on Mach number. Additional parametric results showed that alternative blade frequency mistuning does not have enough potential for it to be used as a passive flutter control in propfans similar to the one studied. It can be inferred from the results that a laminated composite propfan blade can be tailored to optimize its flutter speed by selecting the proper ply angles. Author

A87-40497*# National Aeronautics and Space Administration. Lewis Research Center, Cleveland, Ohio.

ANALYTICAL FLUTTER INVESTIGATION OF A COMPOSITE PROPFAN MODEL

K. R. V. KAZA, O. MEHMED (NASA, Lewis Research Center, Cleveland, OH), G. V. NARAYANAN (Sverdrup Technology, Inc., Cleveland, OH), and D. V. MURTHY (Toledo, University, OH) IN: Structures, Structural Dynamics and Materials Conference, 28th, Monterey, CA, Apr. 6-8, 1987 and AIAA Dynamics Specialists Conference, Monterey, CA, Apr. 9, 10, 1987, Technical Papers. Part 2A. New York, American Institute of Aeronautics and Astronautics, 1987, p. 84-97. Previously announced in STAR as N87-18115. refs (AIAA PAPER 87-0738)

A theoretical model and an associated computer program for predicting subsonic bending-torsion flutter in propfans are presented. The model is based on two-dimensional unsteady cascade strip theory and three-dimensional steady and unsteady lifting surface aerodynamic theory in conjunction with a finite element structural model for the blade. The analytical results compare well with published experimental data. Additional parametric studies are also presented illustrating the effects on flutter speed of steady aeroelastic deformations, blade setting angle, rotational speed, number of blades, structural damping, and number of modes. Author

A87-45994* Akron Univ., Ohio.

AN EFFICIENT QUADRILATERAL ELEMENT FOR PLATE BENDING ANALYSIS

A. F. SALEEB and T. Y. CHANG (Akron, University, OH) International Journal for Numerical Methods in Engineering (ISSN 0029-5981), vol. 24, June 1987, p. 1123-1155. refs (Contract NAG3-307)

A simple, shear flexible, quadrilateral plate element is developed based on the Hellinger/Reissner mixed variational principle with independently assumed displacement and stress fields. The crucial point of the selection of appropriate stress parameters is emphasized in the formulation. For this purpose, a set of guidelines is formulated based on the following considerations: (1) suppression of all kinematic deformation modes, (2) the element has a favorable value for the constraint index in the thin plate limit, and (3) element

properties are frame-invariant. For computer implementation the components of the element stiffness matrix are evaluated analytically using the symbolic manipulation package MACSYMA. The effectiveness and practical usefulness of the proposed element are demonstrated by the numerical results of a variety of problems involving thin and moderately thick plates under different loading and support conditions. Author

A87-49275* National Aeronautics and Space Administration. Lewis Research Center, Cleveland, Ohio.

SIMPLIFIED COMPOSITE MICROMECHANICS FOR PREDICTING MICROSTRESSES

CHRISTOS C. CHAMIS (NASA, Lewis Research Center, Cleveland, OH) (Society of Plastics Industry, Conference, 41st, Atlanta, GA, Jan. 1986) *Journal of Reinforced Plastics and Composites* (ISSN 0731-6844), vol. 6, July 1987, p. 268-284. refs

A unified set of composite micromechanics equations is summarized and described. This unified set is for predicting the ply microstresses when the ply stresses are known. The set consists of equations of simple form for predicting three-dimensional stresses (six each) in the matrix, fiber, and interface. Several numerical examples are included to illustrate use and computational effectiveness of the equations in this unified set. Numerical results from these examples are discussed with respect to their significance on microcrack formation and, therefore, damage initiation in fiber composites. Author

A87-51167* Cooper Union for the Advancement of Science and Art, New York.

STOCHASTIC AND FRACTAL ANALYSIS OF FRACTURE TRAJECTORIES

MICHAEL H. BESSENDORF (Cooper Union for the Advancement of Science and Art, New York) *International Journal of Engineering Science* (ISSN 0020-7225), vol. 25, no. 6, 1987, p. 667-672. refs

(Contract NAG3-223)

Analyses of fracture trajectories are used to investigate structures that fall between 'micro' and 'macro' scales. It was shown that fracture trajectories belong to the class of nonstationary processes. It was also found that correlation distance, which may be related to a characteristic size of a fracture process, increases with crack length. An assemblage of crack trajectory processes may be considered as a diffusive process. Chudnovsky (1981-1985) introduced a 'crack diffusion coefficient' d which reflects the ability of the material to deviate the crack trajectory from the most energetically efficient path and thus links the material toughness to its structure. For the set of fracture trajectories in AISI 304 steel, d was found to be equal to 1.04 microns. The fractal dimension D for the same set of trajectories was found to be 1.133. Author

A87-53796* Akron Univ., Ohio.

A QUADRILATERAL SHELL ELEMENT USING A MIXED FORMULATION

A. F. SALEEB, T. Y. CHANG, and W. GRAF (Akron, University, OH) *Computers and Structures* (ISSN 0045-7949), vol. 26, no. 5, 1987, p. 787-803. refs

(Contract NAG3-307)

A simple quadrilateral shell element consisting of five nodes, four corner nodes and a central node, is developed for linear elastic analysis of thin as well as moderately thick shells. Based on a modified Hellinger-Reissner principle, finite element equations are derived from the assumed displacement and strain fields. By carefully choosing appropriate strain terms, all kinematic deformation modes are suppressed. Although the present element is similar to a displacement-based degenerated shell, no locking is experienced when it is applied to thin shell problems. Five examples are given to illustrate the analysis capability of the shell element. Numerical results indicate that the element shows fast mesh convergence and gives excellent stress predictions. Author

N87-11180* National Aeronautics and Space Administration. Lewis Research Center, Cleveland, Ohio.

TURBINE ENGINE HOT SECTION TECHNOLOGY, 1984

Oct. 1984 400 p Conference held in Cleveland, Ohio, 23-24 Oct. 1984

(NASA-CP-2339; E-2267; NAS 1.55:2339) Avail: NTIS HC A17/MF A01 CSCL 20K

Presentations were made concerning the hot section environment and behavior of combustion liners, turbine blades, and waves. The presentations were divided into six sessions: instrumentation, combustion, turbine heat transfer, structural analysis, fatigue and fracture, and surface properties. The principal objective of each session was to disseminate research results to date, along with future plans. Topics discussed included modeling of thermal and fluid flow phenomena, structural analysis, fatigue and fracture, surface protective coatings, constitutive behavior, stress-strain response, and life prediction methods.

N87-11183* National Aeronautics and Space Administration. Lewis Research Center, Cleveland, Ohio.

FATIGUE AND FRACTURE: OVERVIEW

G. R. HALFORD *In its Turbine Engine Hot Section Technology*, 1984 4 p Oct. 1984

Avail: NTIS HC A17/MF A01 CSCL 20K

A brief overview of the status of the fatigue and fracture programs is given. The programs involve the development of appropriate analytic material behavior models for cyclic stress-strain-temperature-time/cyclic crack initiation, and cyclic crack propagation. The underlying thrust of these programs is the development and verification of workable engineering methods for the calculation, in advance of service, of the local cyclic stress-strain response at the critical life governing location in hot section compounds, and the resultant crack initiation and crack growth lifetimes. B.G.

N87-11209* National Aeronautics and Space Administration. Lewis Research Center, Cleveland, Ohio.

HIGH TEMPERATURE STRESS-STRAIN ANALYSIS

R. L. THOMPSON *In its Turbine Engine Hot Section Technology*, 1984 14 p Oct. 1984

Avail: NTIS HC A17/MF A01 CSCL 20K

The objectives are threefold: to assist in developing predictive tools needed to improve design analyses and procedures for the efficient and accurate prediction of burner liner structural performance and response; to calibrate, validate, and evaluate these predictive tools by comparing the predicted results with the experimental data; and to evaluate existing as well as advanced temperature and strain measurement instrumentation, through both contact and noncontact efforts, in a simulated turbine engine combustor environment. As the predictive tool, tests, test methods, instrumentation, and data acquisition and reduction methods are developed and evaluated, a proven, integrated analysis/experiment method will be developed that will permit the accurate prediction of the cyclic life of a burner liner. Author

N87-11210* Akron Univ., Ohio.

HIGH-TEMPERATURE CONSTITUTIVE MODELING

D. N. ROBINSON and J. R. ELLIS *In NASA. Lewis Research Center Turbine Engine Hot Section Technology*, 1984 11 p Oct. 1984

(Contract NAG3-379)

Avail: NTIS HC A17/MF A01 CSCL 20K

Thermomechanical service conditions for high-temperature levels, thermal transients, and mechanical loads severe enough to cause measurable inelastic deformation are studied. Structural analysis in support of the design of high-temperature components depends strongly on accurate mathematical representations of the nonlinear, hereditary, inelastic behavior of structural alloys at high temperature, particularly in the relatively small strain range. Progress is discussed in the following areas: multiaxial experimentation to provide a basis for high-temperature multiaxial constitutive relationships; nonisothermal testing and theoretical development toward a complete thermomechanically path

39 STRUCTURAL MECHANICS

dependent formulation of viscoplasticity; and development of viscoplastic constitutive model accounting for initial anisotropy.
B.G.

N87-12017*# National Aeronautics and Space Administration. Lewis Research Center, Cleveland, Ohio.
CONCENTRATED MASS EFFECTS ON THE FLUTTER OF A COMPOSITE ADVANCED TURBOPROP MODEL
J. K. RAMSEY and K. R. V. KAZA Oct. 1986 22 p
(NASA-TM-88854; E-3247; NAS 1.15:88854) Avail: NTIS HC A02/MF A01 CSCL 20K

The effects on bending-torsion flutter due to the addition of a concentrated mass to an advanced turboprop model blade with rigid hub are studied. Specifically the effects of the magnitude and location of added mass on the natural frequencies, mode shapes, critical interblade phase angle, and flutter Mach number are analytically investigated. The flutter of a propfan model is shown to be sensitive to the change in mass distribution. Static unbalance effects, like those for fixed wings, were shown to occur as the concentrated mass was moved from the leading edge to the trailing edge with the exception of one mass location. Mass balancing is also inferred to be a feasible method for increasing the flutter speed.
Author

N87-12021*# Virginia Polytechnic Inst. and State Univ., Blacksburg. Dept. of Aerospace and Ocean Engineering.
SENSITIVITY ANALYSIS AND APPROXIMATION METHODS FOR GENERAL EIGENVALUE PROBLEMS Final Report
D. V. MURTHY and R. T. HAFTKA Oct. 1986 124 p
(Contract NAG3-347)
(NASA-CR-179538; NAS 1.26:179538) Avail: NTIS HC A06/MF A01 CSCL 20K

Optimization of dynamic systems involving complex non-hermitian matrices is often computationally expensive. Major contributors to the computational expense are the sensitivity analysis and reanalysis of a modified design. The present work seeks to alleviate this computational burden by identifying efficient sensitivity analysis and approximate reanalysis methods. For the algebraic eigenvalue problem involving non-hermitian matrices, algorithms for sensitivity analysis and approximate reanalysis are classified, compared and evaluated for efficiency and accuracy. Proper eigenvector normalization is discussed. An improved method for calculating derivatives of eigenvectors is proposed based on a more rational normalization condition and taking advantage of matrix sparsity. Important numerical aspects of this method are also discussed. To alleviate the problem of reanalysis, various approximation methods for eigenvalues are proposed and evaluated. Linear and quadratic approximations are based directly on the Taylor series. Several approximation methods are developed based on the generalized Rayleigh quotient for the eigenvalue problem. Approximation methods based on trace theorem give high accuracy without needing any derivatives. Operation counts for the computation of the approximations are given. General recommendations are made for the selection of appropriate approximation technique as a function of the matrix size, number of design variables, number of eigenvalues of interest and the number of design points at which approximation is sought.
Author

N87-12915*# Case Western Reserve Univ., Cleveland, Ohio. Dept. of Civil Engineering.
ANALYSIS OF MIXED-MODE CRACK PROPAGATION USING THE BOUNDARY INTEGRAL METHOD Final Report
A. MENDELSON and L. J. GHOSH Sep. 1986 194 p
(Contract NAG3-396)
(NASA-CR-179518; NAS 1.26:179518) Avail: NTIS HC A09/MF A01 CSCL 20K

Crack propagation in a rotating inner raceway of a high speed roller bearing is analyzed using the boundary integral equation method. The method consists of an edge crack in a plate under tension, upon which varying Hertzian stress fields are superimposed. A computer program for the boundary integral equation method was written using quadratic elements to determine

the stress and displacement fields for discrete roller positions. Mode I and Mode II stress intensity factors and crack extension forces $G_{sub 00}$ (energy release rate due to tensile opening mode) and $G_{sub r0}$ (energy release rate due to shear displacement mode) were computed. These calculations permit determination of that crack growth angle for which the change in the crack extension forces is maximum. The crack driving force was found to be the alternating mixed-mode loading that occurs with each passage of the most heavily loaded roller. The crack is predicted to propagate in a step-like fashion alternating between radial and inclined segments, and this pattern was observed experimentally. The maximum changes $\Delta G_{sub 00}$ and $\Delta G_{sub r0}$ of the crack extension forces are found to be good measures of the crack propagation rate and direction.
Author

N87-12923*# Pratt and Whitney Aircraft, East Hartford, Conn.
ON 3-D INELASTIC ANALYSIS METHODS FOR HOT SECTION COMPONENTS (BASE PROGRAM) Annual Status Report
R. B. WILSON, M. J. BAK, S. NAKAZAWA, and P. K. BANERJEE
Feb. 1986 206 p
(Contract NAS3-23697)
(NASA-CR-175060; NAS 1.26:175060; ASR-2; PWA-5940-36)
Avail: NTIS HC A10/MF A01 CSCL 29K

A 3-D Inelastic Analysis Method program is described. This program consists of a series of new computer codes embodying a progression of mathematical models (mechanics of materials, special finite element, boundary element) for streamlined analysis of: (1) combustor liners, (2) turbine blades, and (3) turbine vanes. These models address the effects of high temperatures and thermal/mechanical loadings on the local (stress/strain) and global (dynamics, buckling) structural behavior of the three selected components. Three computer codes, referred to as MOMM (Mechanics of Materials Model), MHOST (Marc-Hot Section Technology), and BEST (Boundary Element Stress Technology), have been developed and are briefly described in this report.
Author

N87-12924*# National Aeronautics and Space Administration. Lewis Research Center, Cleveland, Ohio.
A CONSTITUTIVE LAW FOR FINITE ELEMENT CONTACT PROBLEMS WITH UNCLASSICAL FRICTION
M. E. PLESHA and B. M. STEINETZ Nov. 1986 19 p
(NASA-TM-88838; E-3181; NAS 1.15:88838; ICOMP-86-1) Avail: NTIS HC A02/MF A01 CSCL 20K

Techniques for modeling complex, unclassical contact-friction problems arising in solid and structural mechanics are discussed. A constitutive modeling concept is employed whereby analytic relations between increments of contact surface stress (i.e., traction) and contact surface deformation (i.e., relative displacement) are developed. Because of the incremental form of these relations, they are valid for arbitrary load-deformation histories. The motivation for the development of such a constitutive law is that more realistic friction idealizations can be implemented in finite element analysis software in a consistent, straightforward manner. Of particular interest is modeling of two-body (i.e., unlubricated) metal-metal, ceramic-ceramic, and metal-ceramic contact. Interfaces involving ceramics are of engineering importance and are being considered for advanced turbine engines in which higher temperature materials offer potential for higher engine fuel efficiency.
Author

N87-13790*# Akron Univ., Ohio.
A VISCOPLASTIC CONSTITUTIVE THEORY FOR METAL MATRIX COMPOSITES AT HIGH TEMPERATURE Final Contractor Report
D. N. ROBINSON, S. F. DUFFY (Cleveland State Univ., Ohio), and J. R. ELLIS Nov. 1986 21 p
(Contract NAG3-379)
(NASA-CR-179530; E-3279; NAS 1.26:179530) Avail: NTIS HC A02/MF A01 CSCL 20K

A viscoplastic constitutive theory is presented for representing the high-temperature deformation behavior of metal matrix composites. The point of view taken is a continuum one where

the composite is considered a material in its own right, with its own properties that can be determined for the composite as a whole. It is assumed that a single preferential (fiber) direction is identifiable at each material point (continuum element) admitting the idealization of local transverse isotropy. A key ingredient in this work is the specification of an experimental program for the complete determination of the material functions and parameters for characterizing a particular metal matrix composite. The parameters relating to the strength of anisotropy can be determined through tension/torsion tests on longitudinally and circumferentially reinforced thin-walled tubes. Fundamental aspects of the theory are explored through a geometric interpretation of some basic features analogous to those of the classical theory of plasticity.

Author

N87-13794*# National Aeronautics and Space Administration. Lewis Research Center, Cleveland, Ohio.

PROBABILISTIC STRUCTURAL ANALYSIS METHODS FOR SPACE PROPULSION SYSTEM COMPONENTS

C. C. CHAMIS 1986 25 p Presented at the 3rd Space Systems Technology Conference, San Diego, Calif., 9-12 Jun. 1986; sponsored by the American Institute of Aeronautics and Astronautics

(NASA-TM-88861; E-3015; NAS 1.15:88861) Avail: NTIS HC A02/MF A01 CSCL 46E

The development of a three-dimensional inelastic analysis methodology for the Space Shuttle main engine (SSME) structural components is described. The methodology is composed of: (1) composite load spectra, (2) probabilistic structural analysis methods, (3) the probabilistic finite element theory, and (4) probabilistic structural analysis. The methodology has led to significant technical progress in several important aspects of probabilistic structural analysis. The program and accomplishments to date are summarized.

Author

N87-14730*# National Aeronautics and Space Administration. Lewis Research Center, Cleveland, Ohio.

A LOW-COST OPTICAL DATA ACQUISITION SYSTEM FOR VIBRATION MEASUREMENT

S. J. POSTA and G. V. BROWN Dec. 1986 21 p (NASA-TM-88907; E-3330; NAS 1.15:88907) Avail: NTIS HC A02/MF A01 CSCL 20K

A low cost optical data acquisition system was designed to measure deflection of vibrating rotor blade tips. The basic principle of the new design is to record raw data, which is a set of blade arrival times, in memory and to perform all processing by software following a run. This approach yields a simple and inexpensive system with the least possible hardware. Functional elements of the system were breadboarded and operated satisfactorily during rotor simulations on the bench, and during a data collection run with a two-bladed rotor in the Lewis Research Center Spin Rig. Software was written to demonstrate the sorting and processing of data stored in the system control computer, after retrieval from the data acquisition system. The demonstration produced an accurate graphical display of deflection versus time.

Author

N87-15491*# Pratt and Whitney Aircraft, East Hartford, Conn. Engineering Div.

CREEP FATIGUE LIFE PREDICTION FOR ENGINE HOT SECTION MATERIALS (ISOTROPIC) Interim Report

R. S. NELSON, J. F. SCHOENDORF, and L. S. LIN Dec. 1986 162 p

(Contract NAS3-23288) (NASA-CR-179550; NAS 1.26:179550) Avail: NTIS HC A08/MF A01 CSCL 20K

The specific activities summarized include: verification experiments (base program); thermomechanical cycling model; multiaxial stress state model; cumulative loading model; screening of potential environmental and protective coating models; and environmental attack model.

B.G.

N87-16321*# National Aeronautics and Space Administration. Lewis Research Center, Cleveland, Ohio.

THE 20TH AEROSPACE MECHANICS SYMPOSIUM

May 1986 316 p Symposium held in Cleveland, Ohio, 7-9 May 1986; sponsored by NASA, the California Inst. of Tech. and LMSC

(NASA-CP-2423-REV; E-2904; NAS 1.55:2423-REV) Avail: NTIS HC A14/MF A01 CSCL 20K

Numerous topics related to aerospace mechanisms were discussed. Deployable structures, electromagnetic devices, tribology, hydraulic actuators, positioning mechanisms, electric motors, communication satellite instruments, redundancy, lubricants, bearings, space stations, rotating joints, and teleoperators are among the topics covered.

N87-17087*# National Aeronautics and Space Administration. Lewis Research Center, Cleveland, Ohio.

SURFACE FLAW RELIABILITY ANALYSIS OF CERAMIC COMPONENTS WITH THE SCARE FINITE ELEMENT POSTPROCESSOR PROGRAM

JOHN P. GYEKENYESI and NOEL N. NEMETH (WLT Corp., Cleveland, Ohio) 1987 17 p Proposed for presentation at the 32nd International Gas Turbine Conference and Exhibit, Anaheim, Calif., 31 May - 4 Jun. 1987; sponsored by ASME

(NASA-TM-88901; E-3229; NAS 1.15:88901) Avail: NTIS HC A02/MF A01 CSCL 20K

The SCARE (Structural Ceramics Analysis and Reliability Evaluation) computer program on statistical fast fracture reliability analysis with quadratic elements for volume distributed imperfections is enhanced to include the use of linear finite elements and the capability of designing against concurrent surface flaw induced ceramic component failure. The SCARE code is presently coupled as a postprocessor to the MSC/NASTRAN general purpose, finite element analysis program. The improved version now includes the Weibull and Batdorf statistical failure theories for both surface and volume flaw based reliability analysis. The program uses the two-parameter Weibull fracture strength cumulative failure probability distribution model with the principle of independent action for poly-axial stress states, and Batdorf's shear-sensitive as well as shear-insensitive statistical theories. The shear-sensitive surface crack configurations include the Griffith crack and Griffith notch geometries, using the total critical coplanar strain energy release rate criterion to predict mixed-mode fracture. Weibull material parameters based on both surface and volume flaw induced fracture can also be calculated from modulus of rupture bar tests, using the least squares method with known specimen geometry and grouped fracture data. The statistical fast fracture theories for surface flaw induced failure, along with selected input and output formats and options, are summarized. An example problem to demonstrate various features of the program is included.

Author

N87-18112*# National Aeronautics and Space Administration. Lewis Research Center, Cleveland, Ohio.

THE EFFECT OF NONLINEARITIES ON THE DYNAMIC RESPONSE OF A LARGE SHUTTLE PAYLOAD

TIMOTHY L. SULLIVAN and KELLY S. CARNEY 1987 31 p Proposed for presentation at the 28th Structures, Structural Dynamics and Materials Conference, Monterey, Calif., 6-8 Apr. 1987; sponsored by AIAA

(NASA-TM-88941; E-3387; NAS 1.15:88941) Avail: NTIS HC A03/MF A01 CSCL 20K

The STS Centaur was designed to be a high energy upper stage for use with the Space Shuttle. Two versions were designed under development when the program was cancelled. The first version, designated G-prime, was for planetary missions. The second version, designated G, was to place spacecraft in geosynchronous orbit. As a part of the STS Centaur finite-element model verification effort, test articles of both versions were subjected to a series of static tests. In addition the Centaur G-prime test article was subjected to a series of dynamic tests including a modal survey. Both the static and dynamic tests showed that nonlinearities existed in the Centaur and its support system. The

39 STRUCTURAL MECHANICS

support system included flight-like latches. The nonlinearities were particularly apparent in tests that loaded the forward support structure of the Centaur. These test results were used to aid in the development of two improved finite-element models. The first was a linear model, while the second contained nonlinear elements at the boundaries. Results from both models were compared with the transient response obtained from a step-relaxation or twang test. The linear model was able to accurately match the low frequency response found in the test data. However, only the nonlinear model was able to match higher frequency response that was present in some of the test data. In addition the nonlinear model was able to predict other nonlinear behavior such as the dynamic jump that occurs in systems with nonlinear stiffness.

Author

N87-18115*# National Aeronautics and Space Administration. Lewis Research Center, Cleveland, Ohio.

ANALYTICAL FLUTTER INVESTIGATION OF A COMPOSITE PROPFAN MODEL

K. R. V. KAZA, O. MEHMED, G. V. NARAYANAN (Sverdrup Technology, Inc., Cleveland, Ohio), and D. V. MURTHY (Toledo Univ., Ohio) 1987 24 p. Proposed for presentation at the 28th Structures, Structural Dynamics and Materials Conference, Monterey, Calif., 6-8 Apr. 1987; sponsored by AIAA, ASME, AHS and ASEE

(NASA-TM-88944; E-3392; NAS 1.15:88944; AIAA-87-0738)

Avail: NTIS HC A02/MF A01 CSCL 20K

A theoretical model and an associated computer program for predicting subsonic bending-torsion flutter in propfans are presented. The model is based on two-dimensional unsteady cascade strip theory and three-dimensional steady and unsteady lifting surface aerodynamic theory in conjunction with a finite element structural model for the blade. The analytical results compare well with published experimental data. Additional parametric studies are also presented illustrating the effects on flutter speed of steady aeroelastic deformations, blade setting angle, rotational speed, number of blades, structural damping, and number of modes.

Author

N87-18116*# National Aeronautics and Space Administration. Lewis Research Center, Cleveland, Ohio.

ANALYTICAL AND EXPERIMENTAL INVESTIGATION OF MISTUNING IN PROPFAN FLUTTER

KRISHNA RAO V. KAZA, ORAL MEHMED, MARC WILLIAMS (Purdue Univ., West Lafayette, Ind.), and LARRY A. MOSS (Sverdrup Technology, Inc., Cleveland, Ohio) 1987 21 p. Proposed for presentation at the 28th Structures, Structural Dynamics and Materials Conference, Monterey, Calif., 6-8 Apr. 1987; sponsored by AIAA, ASME, AHS and ASEE

(NASA-TM-88959; E-3412; NAS 1.15:88959; AIAA-87-0739)

Avail: NTIS HC A02/MF A01 CSCL 20K

An analytical and experimental investigation of the effects of mistuning on propfan subsonic flutter was performed. The analytical model is based on the normal modes of a rotating composite blade and a three-dimensional subsonic unsteady lifting surface aerodynamic theory. Theoretical and experimental results are compared for selected cases at different blade pitch angles, rotational speeds, and free-stream Mach numbers. The comparison shows a reasonably good agreement between theory and experiment. Both theory and experiment showed that combined mode shape, frequency, and aerodynamic mistuning can have a beneficial or adverse effect on blade damping depending on Mach number. Additional parametric results showed that alternative blade frequency mistuning does not have enough potential for it to be used as a passive flutter control in propfans similar to the one studied. It can be inferred from the results that a laminated composite propfan blade can be tailored to optimize its flutter speed by selecting the proper ply angles.

Author

N87-18117*# Pratt and Whitney Aircraft, East Hartford, Conn. Engineering Div.

CREEP FATIGUE LIFE PREDICTION FOR ENGINE HOT SECTION MATERIALS (ISOTROPIC) Annual Report

VITO MORENO, DAVID NISSLEY, and LI-SEN JIM LIN Mar. 1985 141 p

(Contract NAS3-23288)

(NASA-CR-174844; NAS 1.26:174844; PWA-5894-34; AR-2)

Avail: NTIS HC A07/MF A01 CSCL 20K

The first two years of a two-phase program aimed at improving the high temperature crack initiation life prediction technology for gas turbine hot section components are discussed. In Phase 1 (baseline) effort, low cycle fatigue (LCF) models, using a data base generated for a cast nickel base gas turbine hot section alloy (B1900+Hf), were evaluated for their ability to predict the crack initiation life for relevant creep-fatigue loading conditions and to define data required for determination of model constants. The variables included strain range and rate, mean strain, strain hold times and temperature. None of the models predicted all of the life trends within reasonable data requirements. A Cycle Damage Accumulation (CDA) was therefore developed which follows an exhaustion of material ductility approach. Material ductility is estimated based on observed similarities of deformation structure between fatigue, tensile and creep tests. The cycle damage function is based on total strain range, maximum stress and stress amplitude and includes both time independent and time dependent components. The CDA model accurately predicts all of the trends in creep-fatigue life with loading conditions. In addition, all of the CDA model constants are determinable from rapid cycle, fully reversed fatigue tests and monotonic tensile and/or creep data.

Author

N87-18121*# Akron Univ., Ohio. Dept. of Mechanical Engineering.

STRUCTURAL PROPERTIES OF IMPACT ICES ACCRETED ON AIRCRAFT STRUCTURES Final Report

R. J. SCAVUZZO and M. L. CHU Jan. 1987 59 p

(Contract NAG3-479)

(NASA-CR-179580; NAS 1.26:179580) Avail: NTIS HC A04/MF

A01 CSCL 01C

The structural properties of ice accretions formed on aircraft surfaces are studied. The overall objectives are to measure basic structural properties of impact ices and to develop finite element analytical procedures for use in the design of all deicing systems. The Icing Research Tunnel (IRT) was used to produce simulated natural ice accretion over a wide range of icing conditions. Two different test apparatus were used to measure each of the three basic mechanical properties: tensile, shear, and peeling. Data was obtained on both adhesive shear strength of impact ices and peeling forces for various icing conditions. The influences of various icing parameters such as tunnel air temperature and velocity, icing cloud drop size, material substrate, surface temperature at ice/material interface, and ice thickness were studied. A finite element analysis of the shear test apparatus was developed in order to gain more insight in the evaluation of the test data. A comparison with other investigators was made. The result shows that the adhesive shear strength of impact ice typically varies between 40 and 50 psi, with peak strength reaching 120 psi and is not dependent on the kind of substrate used, the thickness of accreted ice, and tunnel temperature below 4 C.

Author

N87-18852*# Cincinnati Univ., Ohio. Dept. of Aerospace Engineering and Engineering Mechanics.

A CONSTITUTIVE MODEL FOR THE INELASTIC MULTIAXIAL CYCLIC RESPONSE OF A NICKEL BASE SUPERALLOY RENE 80 Ph.D. Thesis. Final Report

V. G. RAMASWAMY Washington NASA Jul. 1986 245 p

Previously announced as N86-25472

(Contract NAS3-23927)

(NASA-CR-3998; E-3069; NAS 1.26:3998) Avail: NTIS HC

A11/MF A01 CSCL 20K

The objective was to develop unified constitutive equations which can model a variety of nonlinear material phenomena

observed in Rene 80 at elevated temperatures. A constitutive model was developed based on back stress and drag stress. The tensorial back stress was used to model directional effects; whereas, the scalar drag stress was used to model isotropic effects and cyclic hardening or softening. A flow equation and evolution equations for the state variables were developed in multiaxial form. Procedures were developed to generate the material parameters. The model predicted very well the monotonic tensile, cyclic, creep, and stress relaxation behavior of Rene 80 at 982 C. The model was then extended to 871, 760, and 538 C. It was shown that strain rate dependent behavior at high temperatures and strain rate independent behavior at the lower temperatures could be predicted very well. A large number of monotonic tensile, creep, stress relation, and cyclic experiments were predicted. The multiaxial capabilities of the model were verified extensively for combined tension/torsion experiments. The prediction of the model agreed very well for proportional, nonproportional, and pure shear cyclic loading conditions at 982 and 871 C. Author

N87-18881*# National Aeronautics and Space Administration. Lewis Research Center, Cleveland, Ohio.

THE EFFECTS OF CRACK SURFACE FRICTION AND ROUGHNESS ON CRACK TIP STRESS FIELDS

ROBERTO BALLARINI (Case Western Reserve Univ., Cleveland, Ohio) and MICHAEL E. PLESHA (Wisconsin Univ., Madison) Feb. 1987 19 p

(Contract NCC3-46; NASA ORDER C-99066-G; DAAL03-86-K-0134)

(NASA-TM-88976; ICOMP-87-1; E-3445; NAS 1.15:88976) Avail: NTIS HC A02/MF A01 CSCL 20K

A model is presented which can be used to incorporate the effects of friction and tortuosity along crack surfaces through a constitutive law applied to the interface between opposing crack surfaces. The problem of a crack with a saw-tooth surface in an infinite medium subjected to a far-field shear stress is solved and the ratios of Mode-I stress intensity to Mode-II stress intensity are calculated for various coefficients of friction and material properties. The results show that tortuosity and friction lead to an increase in fracture loads and alter the direction of crack propagation. Author

N87-18882*# National Aeronautics and Space Administration. Lewis Research Center, Cleveland, Ohio.

FATIGUE FAILURE OF REGENERATOR SCREENS IN A HIGH FREQUENCY STIRLING ENGINE

DAVID R. HULL, DONALD L. ALGER, THOMAS J. MOORE, and COULSON M. SCHEUERMANN Mar. 1987 22 p

(NASA-TM-88974; E-3443; NAS 1.15:88974) Avail: NTIS HC A02/MF A01 CSCL 10B

Failure of Stirling Space Power Demonstrator Engine (SPDE) regenerator screens was investigated. After several hours of operation the SPDE was shut down for inspection and on removing the regenerator screens, debris of unknown origin was discovered along with considerable cracking of the screens in localized areas. Metallurgical analysis of the debris determined it to be cracked-off-deformed pieces of the 41 micron thickness Type 304 stainless steel wire screen. Scanning electron microscopy of the cracked screens revealed failures occurring at wire crossovers and fatigue striations on the fracture surface of the wires. Thus, the screen failure can be characterized as a fatigue failure of the wires. The crossovers were determined to contain a 30 percent reduction in wire thickness and a highly worked microstructure occurring from the manufacturing process of the wire screens. Later it was found that reduction in wire thickness occurred because the screen fabricator had subjected it to a light cold-roll process after weaving. Installation of this screen left a clearance in the regenerator allowing the screens to move. The combined effects of the reduction in wire thickness, stress concentration (caused by screen movement), and highly worked microstructure at the wire crossovers led to the fatigue failure of the screens. Author

N87-18883*# National Aeronautics and Space Administration. Lewis Research Center, Cleveland, Ohio.

A COMPARATIVE STUDY OF SOME DYNAMIC STALL MODELS

T. S. R. REDDY (Toledo Univ., Ohio) and K. R. V. KAZA Mar. 1987 79 p

(NASA-TM-88917; E-3342; NAS 1.15:88917) Avail: NTIS HC A05/MF A01 CSCL 20K

Three semi-empirical aerodynamic stall models are compared with respect to their lift and moment hysteresis loop prediction, limit cycle behavior, easy implementation, and feasibility in developing the parameters required for stall flutter prediction of advanced turbines. For the comparison of aeroelastic response prediction including stall, a typical section model and a plate structural model are considered. The response analysis includes both plunging and pitching motions of the blades. In model A, a correction to the angle of attack is applied when the angle of attack exceeds the static stall angle. In model B, a synthesis procedure is used for angles of attack above static stall angles and the time history effects are accounted through the Wagner function. In both models the life and moment coefficients for angle of attack below stall are obtained from tabular data for a given Mach number and angle of attack. In model C, referred to as the ONERA model, the life and moment coefficients are given in the form of two differential equations, one for angles below stall, and the other for angles above stall. The parameters of those equations are nonlinear functions of the angle of attack. Author

N87-19756*# Georgia Inst. of Tech., Atlanta. School of Aerospace Engineering.

ANALYSIS OF SHELL-TYPE STRUCTURES SUBJECTED TO TIME-DEPENDENT MECHANICAL AND THERMAL LOADING Semiannual Status Report

G. J. SIMITSES, R. L. CARLSON, and R. RIFF Apr. 1987 22 p

(Contract NAG3-534)

(NASA-CR-180349; NAS 1.26:180349) Avail: NTIS HC A02/MF A01 CSCL 20K

A general mathematical model and solution methodologies are being developed for analyzing structural response of thin, metallic shell-type structures under large transient, cyclic, or static thermomechanical loads. Among the system responses, which were associated with these load conditions, were thermal buckling, creep buckling, and ratcheting. Thus, geometric as well as material-type nonlinearities (of high order) can be anticipated and must be considered in the development of the mathematical model. Furthermore, this must also be accommodated in the solution process. Author

N87-20565*# National Aeronautics and Space Administration. Lewis Research Center, Cleveland, Ohio.

CALCULATION OF THERMOMECHANICAL FATIGUE LIFE BASED ON ISOTHERMAL BEHAVIOR

GARY R. HALFORD and JAMES F. SALTSMAN 1987 22 p

Prepared for presentation at the 5th National Congress on Pressure Vessel and Piping Technology, San Diego, Calif., 28 Jun. - 2 Jul. 1987; sponsored by ASME

(NASA-TM-88864; E-2940; NAS 1.15:88864) Avail: NTIS HC A02/MF A01 CSCL 20K

The isothermal and thermomechanical fatigue (TMF) crack initiation response of a hypothetical material was analyzed. Expected thermomechanical behavior was evaluated numerically based on simple, isothermal, cyclic stress-strain - time characteristics and on strainrange versus cyclic life relations that have been assigned to the material. The attempt was made to establish basic minimum requirements for the development of a physically accurate TMF life-prediction model. A worthy method must be able to deal with the simplest of conditions: that is, those for which thermal cycling, per se, introduces no damage mechanisms other than those found in isothermal behavior. Under these assumed conditions, the TMF life should be obtained uniquely from known isothermal behavior. The ramifications of making more complex assumptions will be dealt with in future studies. Although analyses are only in their early stages, considerable insight has

been gained in understanding the characteristics of several existing high-temperature life-prediction methods. The present work indicates that the most viable damage parameter is based on the inelastic strainrange. Author

N87-20566*# National Aeronautics and Space Administration. Lewis Research Center, Cleveland, Ohio.

SHOT PEENING FOR Ti-6Al-4V ALLOY COMPRESSOR BLADES

GERALD A. CAREK Apr. 1987 9 p
(NASA-TP-2711; E-3430; NAS 1.60:2711) Avail: NTIS HC A01/MF A01 CSCL 20K

A text program was conducted to determine the effects of certain shot-peening parameters on the fatigue life of the Ti-6Al-4V alloys as well as the effect of a demarcation line on a test specimen. This demarcation line, caused by an abrupt change from untreated surface to shot-peened surface, was thought to have caused the failure of several blades in a multistage compressor at the NASA Lewis Research Center. The demarcation line had no detrimental effect upon bending fatigue specimens tested at room temperature. Procedures for shot peening Ti-6Al-4V compressor blades are recommended for future applications. Author

N87-21375*# National Aeronautics and Space Administration. Lewis Research Center, Cleveland, Ohio.

A NASTRAN PRIMER FOR THE ANALYSIS OF ROTATING FLEXIBLE BLADES

CHARLES LAWRENCE, ROBERT A. AIELLO, MICHAEL A. ERNST, and OLIVER G. MCGEE (Ohio State Univ., Columbus) May 1987 23 p
(NASA-TM-89861; E-3528; NAS 1.15:89861) Avail: NTIS HC A02/MF A01 CSCL 20K

This primer provides documentation for using MSC NASTRAN in analyzing rotating flexible blades. The analysis of these blades includes geometrically nonlinear (large displacement) analysis under centrifugal loading, and frequency and mode shape (normal modes) determination. The geometrically nonlinear analysis using NASTRAN Solution sequence 64 is discussed along with the determination of frequencies and mode shapes using Solution Sequence 63. A sample problem with the complete NASTRAN input data is included. Items unique to rotating blade analyses, such as setting angle and centrifugal softening effects are emphasized. Author

N87-22267*# General Electric Co., Cincinnati, Ohio. Aircraft Engine Business Group.

ELEVATED TEMPERATURE CRACK GROWTH Annual Report

S. N. MALIK, R. H. VANSTONE, K. S. KIM, and J. H. LAFFEN Jan. 1987 43 p
(Contract NAS3-23940)
(NASA-CR-179601; NAS 1.26:179601) Avail: NTIS HC A03/MF A01 CSCL 20K

The objective of the Elevated Temperature Crack Growth Program is to evaluate proposed nonlinear fracture mechanics methods for application to hot section components of aircraft gas turbine engines. Progress during the past year included linear-elastic fracture mechanics data reduction on nonlinear crack growth rate data on Alloy 718. The bulk of the analytical work centered on thermal gradient problems and proposed fracture mechanics parameters. Good correlation of thermal gradient experimental displacement data and finite element prediction was obtained. Author

N87-22273*# National Aeronautics and Space Administration. Lewis Research Center, Cleveland, Ohio.

STRUCTURAL AND AEROELASTIC ANALYSIS OF THE SR-7L PROPPAN

MURRAY HIRSCHBEIN, ROBERT KIELB, ROBERT AIELLO, MARSHA NALL, and CHARLES LAWRENCE Mar. 1985 31 p
(NASA-TM-86877; E-2338; NAS 1.15:86877) Avail: NTIS HC A03/MF A01 CSCL 20K

A structural and aeroelastic analysis of a large scale advanced turboprop rotor blade is presented. This 8-blade rotor is designed

to operate at Mach 0.8 at an altitude of 35,000 ft. The blades are highly swept and twisted and of spar/shell construction. Due to the complexity of the blade geometry and its high performance, it is subjected to much higher loads and tends to be much less stable than conventional blades. Four specific analyses were conducted: (1) steady deflection; (2) natural frequencies and mode shapes; (3) steady stresses; and (4) aeroelastic stability. State-of-the-art methods were used to analyze the blades including a large deflection, finite element structural analysis, and an aeroelastic analysis including interblade aerodynamic coupling (cascade effects). The study found the blade to be structurally sound and aeroelastically stable. However, it clearly indicated that advanced turboprop blades are much less robust than conventional blades and must be analyzed and fabricated much more carefully in order to assure that they are structurally sound and aeroelastically stable. Author

N87-22779*# National Aeronautics and Space Administration. Lewis Research Center, Cleveland, Ohio.

NONLINEAR HEAT TRANSFER AND STRUCTURAL ANALYSES OF SSME TURBINE BLADES

A. ABDUL-AZIZ (Sverdrup Technology, Inc., Middleburg Heights, Ohio.) and A. KAUFMAN *In its* Structural Integrity and Durability of Reusable Space Propulsion Systems p 95-104 1987
Avail: NTIS HC A10/MF A01 CSCL 20K

Three-dimensional nonlinear finite-element heat transfer and structural analyses were performed for the first stage high-pressure fuel turbopump blade of the space shuttle main engine (SSME). Directionally solidified (DS) MAR-M 246 material properties were considered for the analyses. Analytical conditions were based on a typical test stand engine cycle. Blade temperature and stress-strain histories were calculated using MARC finite-element computer code. The study was undertaken to assess the structural response of an SSME turbine blade and to gain greater understanding of blade damage mechanisms, convective cooling effects, and the thermal-mechanical effects. Author

N87-22785*# MARC Analysis Research Corp., Palo Alto, Calif.

THE NESSUS FINITE ELEMENT CODE

J. B. DIAS, J. C. NAGIEGAAL, and S. NAKAZAWA *In* NASA. Lewis Research Center Structural Integrity and Durability of Reusable Space Propulsion Systems p 127-131 1987
(Contract NAS3-24389)
Avail: NTIS HC A10/MF A01 CSCL 20K

The objective of this development is to provide a new analysis tool which integrates the structural modeling versatility of a modern finite element code with the latest advances in the area of probabilistic modeling and structural reliability. Version 2.0 of the NESSUS finite element code was released last February, and is currently being exercised on a set of problems which are representative of typical Space Shuttle Main Engine (SSME) applications. NESSUS 2.0 allows linear elastostatic and eigenvalue analysis of structures with uncertain geometry, material properties and boundary conditions, which are subjected to a random mechanical and thermal loading environment. The NESSUS finite element code is a key component in a broader software system consisting of five major modules. NESSUS/EXPERT is an expert system under development at Southwest Research Institute, with the objective of centralizing all component-specific knowledge useful for conducting probabilistic analysis of typical Space Shuttle Main Engine (SSME) components. NESSUS/FEM contains the finite element code used for the structural analysis and parameter sensitivity evaluation of these components. The task of parametrizing a finite element mesh in terms of the random variables present is facilitated with the use of the probabilistic data preprocessor in NESSUS/PRE. An external database file is used for managing the bulk of the data generated by NESSUS/FEM. Author

N87-22790*# Northwestern Univ., Evanston, Ill.

PROBABILISTIC FINITE ELEMENTS

TED BELYTSCHKO and KAM LIU WING /in NASA. Lewis Research Center Structural Integrity and Durability of Reusable Space Propulsion Systems p 153-159 1987

(Contract NAG3-535)

Avail: NTIS HC A10/MF A01 CSCL 20K

In the Probabilistic Finite Element Method (PFEM), finite element methods have been efficiently combined with second-order perturbation techniques to provide an effective method for informing the designer of the range of response which is likely in a given problem. The designer must provide as input the statistical character of the input variables, such as yield strength, load magnitude, and Young's modulus, by specifying their mean values and their variances. The output then consists of the mean response and the variance in the response. Thus the designer is given a much broader picture of the predicted performance than with simply a single response curve. These methods are applicable to a wide class of problems, provided that the scale of randomness is not too large and the probabilistic density functions possess decaying tails. By incorporating the computational techniques we have developed in the past 3 years for efficiency, the probabilistic finite element methods are capable of handling large systems with many sources of uncertainties. Sample results for an elastic-plastic ten-bar structure and an elastic-plastic plane continuum with a circular hole subject to cyclic loadings with the yield stress on the random field are given.

Author

N87-22796*# Georgia Inst. of Tech., Atlanta.

NONISOTHERMAL ELASTO-VISCO-PLASTIC RESPONSE OF SHELL-TYPE STRUCTURES

G. J. SIMITSES, R. L. CARLSON, and R. RIFF /in NASA. Lewis Research Center Structural Integrity and Durability of Reusable Space Propulsion Systems p 207-214 1987

(Contract NAG3-534)

Avail: NTIS HC A10/MF A01 CSCL 20K

A mathematical model and solution methodologies for analyzing structural response of thin, metallic shell-type structures under large transient, cyclic or static thermomechanical loads is discussed. Among the system responses, which are associated with these load conditions, are thermal buckling and creep buckling. Thus, geometric as well as material-type nonlinearities (of high order) can be anticipated and have been considered in the development of the mathematical model. Furthermore, this was accommodated in the solution procedures. A complete true ab-initio rate theory of kinematics and kinetics for continuum and curved thin structures, without any restriction on the magnitude of the strains or the deformation, was formulated. The time dependence and large strain behavior are incorporated through the introduction of the time rates of the metric and curvature in two coordinate systems, a fixed (spatial) one and a convected (material) coordinate system. The relations between the time derivative and the covariant derivatives (gradients) have been developed for curved space and motion, so that the velocity components supply the connection between the equations of motion and the time rate of change of the metric and curvature tensors.

Author

N87-22996*# Pratt and Whitney Aircraft, East Hartford, Conn.
ON 3-D INELASTIC ANALYSIS METHODS FOR HOT SECTION COMPONENTS. VOLUME 1: SPECIAL FINITE ELEMENT MODELS Annual Status Report, 14 Feb. 1985 - 14 Feb. 1986

S. NAKAZAWA Mar. 1987 102 p

(Contract NAS3-23697)

(NASA-CR-179494; NAS 1.26:179494; PWA-5940-46-VOL-1;

ASR-3) Avail: NTIS HC A06/MF A01 CSCL 20K

This Annual Status Report presents the results of work performed during the third year of the 3-D Inelastic Analysis Methods for Hot Section Components program (NASA Contract NAS3-23697). The objective of the program is to produce a series of new computer codes that permit more accurate and efficient three-dimensional analysis of selected hot section components, i.e., combustor liners, turbine blades, and turbine vanes. The computer codes embody a progression of mathematical models

and are streamlined to take advantage of geometrical features, loading conditions, and forms of material response that distinguish each group of selected components. This report is presented in two volumes. Volume 1 describes effort performed under Task 4B, Special Finite Element Special Function Models, while Volume 2 concentrates on Task 4C, Advanced Special Functions Models.

Author

N87-23010*# National Aeronautics and Space Administration. Lewis Research Center, Cleveland, Ohio.

FINITE ELEMENT IMPLEMENTATION OF ROBINSON'S UNIFIED VISCOPLASTIC MODEL AND ITS APPLICATION TO SOME UNIAXIAL AND MULTIAXIAL PROBLEMS

V. K. ARYA and A. KAUFMAN Jun. 1987 20 p

(NASA-TM-89891; E-3583; NAS 1.15:89891) Avail: NTIS HC

A02/MF A01 CSCL 20K

A description of the finite element implementation of Robinson's unified viscoplastic model into the General Purpose Finite Element Program (MARC) is presented. To demonstrate its application, the implementation is applied to some uniaxial and multiaxial problems. A comparison of the results for the multiaxial problem of a thick internally pressurized cylinder, obtained using the finite element implementation and an analytical solution, is also presented. The excellent agreement obtained confirms the correct finite element implementation of Robinson's model.

Author

N87-24006*# National Aeronautics and Space Administration. Lewis Research Center, Cleveland, Ohio.

IDENTIFICATION OF STRUCTURAL INTERFACE CHARACTERISTICS USING COMPONENT MODE SYNTHESIS

A. A. HUCKELBRIDGE (Case Western Reserve Univ., Cleveland, Ohio.) and C. LAWRENCE 1987 14 p Prepared for presentation at the Vibrations Conference, Boston, Mass., 27-30 Sep. 1987; sponsored by ASME

(NASA-TM-88960; E-3415; NAS 1.15:88960) Avail: NTIS HC

A02/MF A01 CSCL 20K

The inability to adequately model connections has limited the ability to predict overall system dynamic response. Connections between structural components are often mechanically complex and difficult to accurately model analytically. Improved analytical models for connections are needed to improve system dynamic predictions. This study explores combining Component Mode synthesis methods for coupling structural components with Parameter Identification procedures for improving the analytical modeling of the connections. Improvements in the connection properties are computed in terms of physical parameters so the physical characteristics of the connections can be better understood, in addition to providing improved input for the system model. Two sample problems, one utilizing simulated data, the other using experimental data from a rotor dynamic test rig are presented.

Author

N87-24007*# National Aeronautics and Space Administration. Lewis Research Center, Cleveland, Ohio.

ENVIRONMENTAL DEGRADATION OF 316 STAINLESS STEEL IN HIGH TEMPERATURE LOW CYCLE FATIGUE

SREERAMESH KALLURI, S. STANFORD MANSON, and GARY R. HALFORD Apr. 1987 17 p Presented at the 3rd International Conference on Environmental Degradation of Engineering Materials, University Park, Pa., 13-15 Apr. 1987; sponsored by the Pennsylvania State Univ.

(Contract NAG3-337; NAG3-553)

(NASA-TM-89931; E-3636; NAS 1.15:89931) Avail: NTIS HC

A02/MF A01 CSCL 20K

Procedures based on modification of the conventional Strainrange Partitioning method are proposed to characterize the time-dependent degradation of engineering alloys in high-temperature, low-cycle fatigue. Creep-fatigue experiments were conducted in air using different waveforms of loading on 316 stainless steel at 816 C (1500 F) to determine the effect of exposure time on cyclic life. Reductions in the partitioned cyclic lives were observed with an increase in the time of exposure (or with the corresponding decrease in the steady-state creep rate)

for all the waveforms involving creep strain. Excellent correlations of the experimental data were obtained by modifying the Conventional Strainrange Partitioning life relationships involving creep strain using a power-law term of either: (1) time of exposure, or (2) steady-state creep rate of the creep-fatigue test. Environmental degradation due to oxidation, material degradation due to the precipitation of carbides along the grain boundaries and detrimental deformation modes associated with the prolonged periods of creep were observed to be the main mechanisms responsible for life reductions at long exposure times. Author

N87-24722*# National Aeronautics and Space Administration. Lewis Research Center, Cleveland, Ohio.

HUB FLEXIBILITY EFFECTS ON PROPPAN VIBRATION

MICHAEL A. ERNST and CHARLES LAWRENCE Jul. 1987 16 p

(NASA-TM-89900; E-3596; NAS 1.15:89900) Avail: NTIS HC A02/MF A01 CSCL 20K

The significance of hub flexibility in the nonlinear static and dynamic analyses of advanced turboprop blades is assessed. The chosen blade is the 0.175 scale model of the GE-A7-B4 unducted fan blade. A procedure for coupling the effective hub stiffness matrix to an MSC/NASTRAN finite element model is defined and verified. A series of nonlinear static and dynamic analyses are conducted on the blade for both rigid and flexible hub configurations. Results indicate that hub flexibility is significant in the nonlinear static and dynamic analyses of the GE-A7-B4. In order to insure accuracy in analyses of other blades, hub flexibility should always be considered. Author

N87-25607*# Tulane Univ., New Orleans, La. Dept. of Mechanical Engineering.

MACROCRACK INTERACTION WITH TRANSVERSE ARRAY OF MICROCRACKS Final Contractor Report

A. A. RUBINSTEIN and H. C. CHOI (Illinois Univ., Urbana-Champaign.) Jul. 1987 25 p

(Contract NAG3-751) (NASA-CR-180806; NAS 1.26:180806) Avail: NTIS HC A02/MF A01 CSCL 20K

General formulation of a problem involving a macrocrack propagating through an area with microcracks is considered. The analysis is based on the simultaneous solution of a system of singular integral equations. Various methods described in the literature are discussed in detail and compared. The specific problem considered was a macrocrack approaching an infinite transverse array of microcracks. Results illustrate the effects of different loading types and can be used for interpretation of the microcrack toughening mechanisms. Numerical comparisons are made with data recently appearing in literature which demonstrates the importance of numerical accuracy. Reported results differ by a factor in certain cases as compared with data given in other literature. Author

N87-26384*# Sverdrup Technology, Inc., Cleveland, Ohio.

SSME SINGLE CRYSTAL TURBINE BLADE DYNAMICS Final Report

LARRY A. MOSS and TODD E. SMITH Jul. 1987 27 p

(Contract NAS3-24105) (NASA-CR-179644; E-3671; NAS 1.26:179644) Avail: NTIS HC A03/MF A01 CSCL 20K

A study was performed to determine the dynamic characteristics of the Space Shuttle main engine high pressure fuel turbopump (HPFTP) blades made of single crystal (SC) material. The first and second stage drive turbine blades of HPFTP were examined. The nonrotating natural frequencies were determined experimentally and analytically. The experimental results of the SC second stage blade were used to verify the analytical procedures. The analytical study examined the SC first stage blade natural frequencies with respect to crystal orientation at typical operating conditions. The SC blade dynamic response was predicted to be less than the directionally solidified blade. Crystal axis orientation optimization indicated the third mode interference will exist in any SC orientation. Author

N87-26385*# National Aeronautics and Space Administration. Lewis Research Center, Cleveland, Ohio.

FINITE ELEMENT ANALYSIS OF FLEXIBLE, ROTATING BLADES

OLIVER G. MCGEE Jul. 1987 40 p

(NASA-TM-89906; E-3674; NAS 1.15:89906) Avail: NTIS HC A03/MF A01 CSCL 20K

A reference guide that can be used when using the finite element method to approximate the static and dynamic behavior of flexible, rotating blades is given. Important parameters such as twist, sweep, camber, co-planar shell elements, centrifugal loads, and inertia properties are studied. Comparisons are made between NASTRAN elements through published benchmark tests. The main purpose is to summarize blade modeling strategies and to document capabilities and limitations (for flexible, rotating blades) of various NASTRAN elements. Author

N87-26399*# National Aeronautics and Space Administration. Lewis Research Center, Cleveland, Ohio.

A HIGH TEMPERATURE FATIGUE AND STRUCTURES TESTING FACILITY

PAUL A. BARTOLOTTA and MICHAEL A. MCGAW Aug. 1987 24 p

(NASA-TM-100151; E-3712; NAS 1.15:100151) Avail: NTIS HC A02/MF A01 CSCL 20K

As man strives for higher levels of sophistication in air and space transportation, awareness of the need for accurate life and material behavior predictions for advanced propulsion system components is heightened. Such sophistication will require complex operating conditions and advanced materials to meet goals in performance, thrust-to-weight ratio, and fuel efficiency. To accomplish these goals will require that components be designed using a high percentage of the material's ultimate capabilities. This serves only to complicate matters dealing with life and material behavior predictions. An essential component of material behavior model development is the underlying experimentation which must occur to identify phenomena. To support experimentation, the NASA Lewis Research Center's High Temperature Fatigue and Structures Laboratory has been expanded significantly. Several new materials testing systems have been added, as well as an extensive computer system. The intent of this paper is to present an overview of the laboratory, and to discuss specific aspects of the test systems. A limited discussion of computer capabilities will also be presented. Author

N87-27267*# Pratt and Whitney Aircraft, East Hartford, Conn. Engineering Div.

3-D INELASTIC ANALYSIS METHODS FOR HOT SECTION COMPONENTS. VOLUME 2: ADVANCED SPECIAL FUNCTIONS MODELS Annual Status Report No. 3

R. B. WILSON and P. K. BANERJEE Aug. 1987 87 p

(Contract NAS3-23697) (NASA-CR-179517; NAS 1.26:179517; PWA-5940-46-VOL-2) Avail: NTIS HC A05/MF A01 CSCL 20K

This Annual Status Report presents the results of work performed during the third year of the 3-D Inelastic Analysis Methods for Hot Sections Components program (NASA Contract NAS3-23697). The objective of the program is to produce a series of computer codes that permit more accurate and efficient three-dimensional analyses of selected hot section components, i.e., combustor liners, turbine blades, and turbine vanes. The computer codes embody a progression of mathematical models and are streamlined to take advantage of geometrical features, loading conditions, and forms of material response that distinguish each group of selected components. Author

N87-27268*# National Aeronautics and Space Administration. Lewis Research Center, Cleveland, Ohio.

SINDA-NASTRAN INTERFACING PROGRAM THEORETICAL DESCRIPTION AND USER'S MANUAL

STEVEN R. WINEGAR Aug. 1987 31 p
(NASA-TM-100158; E-3720; NAS 1.15:100158) Avail: NTIS HC A03/MF A01 CSCL 20K

The task of converting SINDA finite difference thermal model temperature results into NASTRAN finite element model thermal loads can be very labor intensive if there is not one node-to-one element, or systematic node-to-element, correlation between models. This paper describes the SINDA-NASTRAN Interfacing Program (SNIP), a FORTRAN computer code that generates NASTRAN structural model thermal load cards given by SINDA (or similar thermal model) temperature results and thermal model geometric data. SNIP generates NASTRAN thermal load cards for NASTRAN plate, shell, bar, and beam elements. The paper describes the interfacing procedures used by SNIP, and discusses set-up and operation of the program. Sample cases are included to demonstrate use of the program and show its performance under a variety of conditions. SNIP can provide structural model thermal loads that accurately reflect thermal model results while reducing the time required to interface thermal and structural models when compared to other methods. Author

N87-27269*# National Aeronautics and Space Administration. Lewis Research Center, Cleveland, Ohio.

FRACTURE MECHANICS CONCEPTS IN RELIABILITY ANALYSIS OF MONOLITHIC CERAMICS

JANE M. MANDERSCHIED and JOHN P. GYEKENYESI Aug. 1987 16 p Presented at the Testing High Performance Ceramics, Boston, Mass., 25-27 Aug. 1987; sponsored in part by American Ceramic Society, and the American Society for Nondestructive Testing.

(NASA-TM-100174; E-3743; NAS 1.15:100174) Avail: NTIS HC A02/MF A01 CSCL 20K

Basic design concepts for high-performance, monolithic ceramic structural components are addressed. The design of brittle ceramics differs from that of ductile metals because of the inability of ceramic materials to redistribute high local stresses caused by inherent flaws. Random flaw size and orientation requires that a probabilistic analysis be performed in order to determine component reliability. The current trend in probabilistic analysis is to combine linear elastic fracture mechanics concepts with the two parameter Weibull distribution function to predict component reliability under multiaxial stress states. Nondestructive evaluation supports this analytical effort by supplying data during verification testing. It can also help to determine statistical parameters which describe the material strength variation, in particular the material threshold strength (the third Weibull parameter), which in the past was often taken as zero for simplicity. Author

N87-28058*# National Aeronautics and Space Administration. Lewis Research Center, Cleveland, Ohio.

A COMPUTATIONAL PROCEDURE FOR AUTOMATED FLUTTER ANALYSIS

DURBHA V. MURTHY (Toledo Univ., Ohio.) and KRISHNA RAO V. KAZA Aug. 1987 17 p
(NASA-TM-100171; E-3736; NAS 1.15:100171) Avail: NTIS HC A02/MF A01 CSCL 20K

A direct solution procedure for computing the flutter Mach number and the flutter frequency is applied to the aeroelastic analysis of propfans using a finite element structural model and an unsteady aerodynamic model based on a three-dimensional subsonic compressible lifting surface theory. An approximation to the Jacobian matrix that improves the efficiency of the iterative process is presented. The Jacobian matrix is indirectly approximated from approximate derivatives of the flutter matrix. Examples are used to illustrate the convergence properties. The direct solution procedure facilitates the automated flutter analysis in addition to contributing to the efficient use of computer time as well as the analyst's time. Author

N87-28944*# National Aeronautics and Space Administration. Lewis Research Center, Cleveland, Ohio.

EXPOSURE TIME CONSIDERATIONS IN HIGH TEMPERATURE LOW CYCLE FATIGUE

S. KALLURI, S. S. MANSON (Case Western Reserve Univ., Cleveland, Ohio.), and G. R. HALFORD Jun. 1987 12 p Presented at the 5th International Conference on Mechanical Behaviour of Materials, Beijing, China, 3-6 Jun. 1987; sponsored in part by the Chinese Society of Metals, and the Chinese Society of Mechanics

(Contract NAG3-337; NAG3-553)

(NASA-TM-88934; E-3375; NAS 1.15:88934) Avail: NTIS HC A02/MF A01 CSCL 20K

The Conventional Strainrange Partitioning (CSRP) method for High-Temperature, Low-Cycle Fatigue (HTLCF) life prediction has its origins in the modeling of first-order, creep-fatigue waveform effects while treating as second-order effects, the influence of metallurgical or environmental time dependencies. Procedures are proposed to include the latter explicitly in the inelastic strainrange-life relations. For brevity, only the CP life relation will be presented in detail. The exposure-time effect within the CP inelastic strainrange (tensile creep reversed by compressive plasticity) was determined by tensile stresshold-time experiments for 316 SS at 816 C. Reductions in CP cyclic life of a factor of about two were observed with an increase in exposure time or a corresponding decrease in creep rate by a factor of about 100. The CP life relation has been modified to be expressed in terms of either Steady State Creep Rate (SSCR) or Exposure Time (ET). The applicability and accuracy of the time-dependent CP life relations is demonstrated by conducting verification experiments involving complex hysteresis loops. Metallographic examination revealed time-dependent degradation attributable to oxide formation and precipitation of carbides along grain boundaries. Author

N87-29896*# Georgia Inst. of Tech., Atlanta. School of Aerospace Engineering.

THERMO-ELASTO-VISCOPLASTIC ANALYSIS OF PROBLEMS IN EXTENSION AND SHEAR

R. RIFF and G. J. SIMITSES 1987 20 p

(Contract NAG3-534)

(NASA-CR-181410; NAS 1.26:181410) Avail: NTIS HC A02/MF A01 CSCL 20K

The problems of extension and shear behavior of structural elements made of carbon steel and subjected to large thermomechanical loads are investigated. The analysis is based on nonlinear geometric and constitutive relations, and is expressed in a rate form. The material constitutive equations are capable of reproducing all nonisothermal, elasto-viscoplastic characteristics. The results of the test problems show that: (1) the formulation can accommodate very large strains and rotations; (2) the model incorporates the simplification associated with rate-insensitive elastic response without losing the ability to model a rate-temperature dependent yield strength and plasticity; and (3) the formulation does not display oscillatory behavior in the stresses for the simple shear problem. Author

N87-29897*# Georgia Inst. of Tech., Atlanta.

THE DYNAMIC ASPECTS OF THERMO-ELASTO-VISCOPLASTIC SNAP-THROUGH AND CREEP BUCKLING PHENOMENA

R. RIFF and G. J. SIMITSES 1987 4 p

(Contract NAG3-534)

(NASA-CR-181411; NAS 1.26:181411) Avail: NTIS HC A02/MF A01 CSCL 20K

Use of a mathematical model and solution methodology, to examine dynamic buckling and dynamic postbuckling behavior of shallow arches and spherical caps made of a realistic material and undergoing non-isothermal, elasto-viscoplastic deformation was examined. Thus, geometric as well as material type nonlinearities of higher order are included in this analysis. The dynamic stability problem is studied under impulsive loading and suddenly applied loading with loads of constant magnitude and infinite duration. A finite element model was derived directly from the incrementally formulated nonlinear shell equations, by using a

44 ENERGY PRODUCTION AND CONVERSION

tensor-oriented procedure. As an example of the results, the time history of the midspan displacement of a damped shallow circular arch is presented. B.G.

44

ENERGY PRODUCTION AND CONVERSION

Includes specific energy conversion systems, e.g., fuel cells; global sources of energy; geophysical conversion; and windpower.

A87-12338* Energy Research Corp., Danbury, Conn.
PERFORMANCE STUDY OF A FUEL CELL PT-ON-C ANODE IN PRESENCE OF CO AND CO₂, AND CALCULATION OF ADSORPTION PARAMETERS FOR CO POISONING
H. P. DHAR, L. G. CHRISTNER, A. K. KUSH, and H. C. MARU (Energy Research Corp., Danbury, CT) Electrochemical Society, Journal (ISSN 0013-4651), vol. 133, Aug. 1986, p. 1574-1582. DOE-supported research. refs
(Contract DEN3-290)

A87-18071*# National Aeronautics and Space Administration. Lewis Research Center, Cleveland, Ohio.
INDIUM PHOSPHIDE SOLAR CELLS - STATUS AND PROSPECTS FOR USE IN SPACE
I. WEINBERG and D. J. BRINKER (NASA, Lewis Research Center, Cleveland, OH) IN: IECEC '86; Proceedings of the Twenty-first Intersociety Energy Conversion Engineering Conference, San Diego, CA, August 25-29, 1986. Volume 3. Washington, DC, American Chemical Society, 1986, p. 1431-1435. Previously announced in STAR as N86-26520. refs

The current status of indium phosphide cell research is reviewed and state of the art efficiencies compared to those of GaAs and Si. It is shown that the radiation resistance of InP cells is superior to that of either GaAs or Si under 1 MeV electron and 10 MeV proton irradiation. Using lightweight blanket technology, a SEP array structure and projected cell efficiencies, array specific powers are obtained for all three cell types. Array performance is calculated as a function of time in orbit. The results indicate that arrays using InP cells can outperform those using GaAs or Si in orbits where radiation is a significant cell degradation factor. It is concluded that InP solar cells are excellent prospects for future use in the space radiation environment. Author

A87-18073* Varian Associates, Palo Alto, Calif.
HIGH-EFFICIENCY GAAS SOLAR CONCENTRATOR CELLS FOR SPACE AND TERRESTRIAL APPLICATIONS
H. C. HAMAKER, J. G. WERTHEN, C. W. FORD, G. F. VIRSHUP, and N. R. KAMINAR (Varian Research Center, Palo Alto, CA) IN: IECEC '86; Proceedings of the Twenty-first Intersociety Energy Conversion Engineering Conference, San Diego, CA, August 25-29, 1986. Volume 3. Washington, DC, American Chemical Society, 1986, p. 1441-1445. Research supported by Sandia National Laboratories. refs
(Contract NAS3-23876)

High-efficiency Al(x)Ga(1-x)As/GaAs heteroface solar concentrator cells have been developed for both space and terrestrial applications. The cells, which were grown using metalorganic chemical vapor deposition, have been fabricated in both the p-n and n-p configurations. Magnesium and zinc are used as p-type dopants, and Se is used as the n-type dopant. The space cells, which are designed for use in a Cassegrainian concentrator operating at 100 suns, AMO, have a circular illuminated area 4 mm in diameter on a 5 mm x 5 mm cell. These cells have exhibited flash-tested efficiencies as high as 23.6 percent at 28 C and 21.6 percent at 80 C. The terrestrial cells have a circular illuminated area 0.2 inches in diameter and are intended for use in a module which operates at 940 suns, AM1.5. These cells have shown a peak efficiency of 26 percent at 753 suns and over 25 percent at greater than 1000 suns. Author

A87-18074* Spectrolab, Inc., Sylmar, Calif.
FURTHER ADVANCES IN SILICON SOLAR CELL TECHNOLOGY FOR SPACE APPLICATION

D. R. LILLINGTON and J. R. KUKULKA (Spectrolab, Inc., Sylmar, CA) IN: IECEC '86; Proceedings of the Twenty-first Intersociety Energy Conversion Engineering Conference, San Diego, CA, August 25-29, 1986. Volume 3. Washington, DC, American Chemical Society, 1986, p. 1446-1451. refs
(Contract NAS3-24672)

Recent improvements relating to the design of high efficiency cells are presented. A conceptual design using passivation techniques is discussed, which potentially increases the open circuit voltage to approximately 650 mV. This concept is supported by experimental data using only silicon passivation beneath contacts. The use of thin thermal oxides of silicon for passivation between contacts is also discussed. A number of novel structures have also been fabricated to investigate reduction in the thermal alpha of planar and sculptured cells. It is shown that this may be as low as 0.63 on glassed gridded back cells, and that the IR rejection beyond 1.1 microns may approach 100 percent if the backside is AR coated. Finally, experimental data is given to support the existence of free electron absorption in heavily doped emitters on sculptured cells. Author

A87-18103*# National Aeronautics and Space Administration. Lewis Research Center, Cleveland, Ohio.
NICKEL-HYDROGEN SEPARATOR DEVELOPMENT
O. D. GONZALEZ-SANABRIA (NASA, Lewis Research Center, Cleveland, OH) IN: IECEC '86; Proceedings of the Twenty-first Intersociety Energy Conversion Engineering Conference, San Diego, CA, August 25-29, 1986. Volume 3. Washington, DC, American Chemical Society, 1986, p. 1598-1600.

The separator technology is a critical element in the nickel-hydrogen (Ni-H₂) systems. Previous research and development work carried out at NASA Lewis Research Center has determined that separators made from zirconium oxide (ZrO₂) and potassium titanate (PKT) fibers will function satisfactorily in Ni-H₂ cells without exhibiting the problems associated with the asbestos separators. A program has been established to transfer the separator technology into a commercial production line. A detailed plan of this program will be presented and the preliminary results will be discussed. Author

A87-18105*# National Aeronautics and Space Administration. Lewis Research Center, Cleveland, Ohio.
EFFECT OF IMPREGNATION METHOD ON CYCLE LIFE OF THE NICKEL ELECTRODE

J. J. SMITHRICK (NASA, Lewis Research Center, Cleveland, OH) IN: IECEC '86; Proceedings of the Twenty-first Intersociety Energy Conversion Engineering Conference, San Diego, CA, August 25-29, 1986. Volume 3. Washington, DC, American Chemical Society, 1986, p. 1607-1611. Previously announced in STAR as N86-31980. refs

The nickel electrode has been identified as the life limiting component for individual pressure vessel (IPV) nickel-hydrogen cells when cycled under a low earth orbit (LEO) cycle regime at deep depths of discharge. As a part of an overall program to develop a long life nickel electrode for nickel-hydrogen cells, the effect of two different methods of electrochemical impregnation on the cycle life of the nickel electrode was investigated. One method was the Pickett (aqueous/ethanolic) process. The other was the modified Bell (aqueous) process. The plaques for both impregnation methods were made by sintering dry carbonyl nickel powder in a reducing atmosphere. The plaques contain a nickel screen substrate. Electrodes made from both processes were cycled in Air Force design IPV nickel-hydrogen cells. The only factor different for this test was the method of plaque impregnation; all other factors were the same. The cells were cycled to failure under a 90 min LEO cycle regime at a deep depth of discharge (80 percent DOD). Failure for this test was defined to occur when the cell voltage degraded to 1.0 V prior to the completion of the 35 min discharge. Author

44 ENERGY PRODUCTION AND CONVERSION

A87-21823* National Aeronautics and Space Administration. Lewis Research Center, Cleveland, Ohio.

RELIABILITY AND MASS ANALYSIS OF DYNAMIC POWER CONVERSION SYSTEMS WITH PARALLEL OR STANDBY REDUNDANCY

ALBERT J. JUHASZ and HARVEY S. BLOOMFIELD (NASA, Lewis Research Center, Cleveland, OH) IN: Space nuclear power systems 1985; Proceedings of the Second Symposium, Albuquerque, NM, Jan. 14-16, 1985. Volume 4. Malabar, FL, Orbit Book Co., Inc., 1987, p. 205-212. NASA-sponsored research.

A combinatorial reliability approach was used to identify potential dynamic power conversion systems for space mission applications. A reliability and mass analysis was also performed, specifically for a 100-kWe nuclear Brayton power conversion system with parallel redundancy. Although this study was done for a reactor outlet temperature of 1100 K, preliminary system mass estimates are also included for reactor outlet temperatures ranging up to 1500 K. Author

A87-25475*# National Aeronautics and Space Administration. Lewis Research Center, Cleveland, Ohio.

OVERVIEW OF THE NEW ASME PERFORMANCE TEST CODE FOR WIND TURBINES

DAVID A. SPERA (NASA, Lewis Research Center, Cleveland, OH) ASME and IEEE, Joint Power Generation Conference, Portland, OR, Oct. 19-23, 1986. 9 p. (ASME PAPER 86-JPGC-PTC-4)

The principal technical features of the ASME Performance Test Code for wind turbines are presented and such issues as what sizes and types of wind turbines should be included, what the principal measure of performance should be, and how wind speed should be measured are discussed. It is concluded that the present test code is applicable to wind turbine systems of all sizes. The principal measure of performance as defined by this code is net energy output and the primary performance parameter is the 'test energy ratio' which is based on a comparison between the measured and predicted energy output for the test period. K.K.

A87-33777* National Aeronautics and Space Administration. Lewis Research Center, Cleveland, Ohio.

STATUS OF COMMERCIAL PHOSPHORIC ACID FUEL CELL POWER PLANT SYSTEM DEVELOPMENT

M. WARSHAY (NASA, Lewis Research Center, Cleveland, OH) IN: Progress in batteries and solar cells. Volume 6. Cleveland, OH, JEC Press, Inc., 1987, p. 1-6. refs

A technology development and commercial feasibility evaluation is presented for phosphoric acid fuel cells (PAFCs) applicable to electric utility operations. The correction of identified design deficiencies in the control card and water treatment subsystems is projected to be able to substantially increase average powerplant availability from the 63 percent achieved in recent field tests of a PAFC system. Current development work is proceeding under NASA research contracts at the output levels of a multimewatt facility for electric utility use, a multikilowatt on-site integrated energy generation facility, and advanced electrocatalysts applicable to PAFCs. O.C.

A87-33787* National Aeronautics and Space Administration. Lewis Research Center, Cleveland, Ohio.

ADVANCED TECHNOLOGY FOR EXTENDED ENDURANCE ALKALINE FUEL CELLS

D. W. SHEIBLEY (NASA, Lewis Research Center, Cleveland, OH) and R. A. MARTIN (International Fuel Cells Corp., South Windsor, CT) IN: Progress in batteries and solar cells. Volume 6. Cleveland, OH, JEC Press, Inc., 1987, p. 155-158.

Advanced components have been developed for alkaline fuel cells with a view to the satisfaction of NASA Space Station design requirements for extended endurance. The components include a platinum-on-carbon catalyst anode, a potassium titanate-bonded electrolyte matrix, a lightweight graphite electrolyte reservoir plate, a gold-plated nickel-perforated foil electrode substrate, a polyphenylene sulfide cell edge frame material, and a nonmagnesium cooler concept. When incorporated into the alkaline

fuel cell unit, these components are expected to yield regenerative operation in a low earth orbit Space Station with a design life greater than 5 years. O.C.

A87-33788* National Aeronautics and Space Administration. Lewis Research Center, Cleveland, Ohio.

COMPUTER-BASED PHOSPHORIC ACID FUEL CELL ANALYTICAL TOOLS DESCRIPTIONS AND USAGES

C. LU and A. F. PRESLER (NASA, Lewis Research Center, Cleveland, OH) IN: Progress in batteries and solar cells. Volume 6. Cleveland, OH, JEC Press, Inc., 1987, p. 165-167.

Simulation models have been developed for the prediction of phosphoric acid fuel cell (PAFC) powerplant system performance under both transient and steady operation conditions, as well as for the design of component configurations and for optimal systems synthesis. These models, which are presently computer-implemented, are an engineering and a system model; the former being solved by the finite difference method to determine the balances and properties of different sections, and the latter using thermodynamic balances to set up algebraic equations that yield physical and chemical properties of the stream for one operating condition. O.C.

A87-33789* National Aeronautics and Space Administration. Lewis Research Center, Cleveland, Ohio.

CATALYST AND ELECTRODE RESEARCH FOR PHOSPHORIC ACID FUEL CELLS

A. C. ANTOINE and R. B. KING (NASA, Lewis Research Center, Cleveland, OH) IN: Progress in batteries and solar cells. Volume 6. Cleveland, OH, JEC Press, Inc., 1987, p. 168-171.

An account is given of the development status of phosphoric acid fuel cells' high performance catalyst and electrode materials. Binary alloys have been identified which outperform the baseline platinum catalyst; it has also become apparent that pressurized operation is required to reach the desired efficiencies, calling in turn for the use of graphitized carbon blacks in the role of catalyst supports. Efforts to improve cell performance and reduce catalyst costs have led to the investigation of a class of organometallic cathode catalysts represented by the tetraazaannulenes, and a mixed catalyst which is a mixture of carbons catalyzed with an organometallic and a noble metal. O.C.

A87-47088*# National Aeronautics and Space Administration. Lewis Research Center, Cleveland, Ohio.

COMBINATION SOLAR PHOTOVOLTAIC HEAT ENGINE ENERGY CONVERTER

DONALD L. CHUBB (NASA, Lewis Research Center, Cleveland, OH) Journal of Propulsion and Power (ISSN 0748-4658), vol. 3, July-Aug. 1987, p. 365-374. Previously announced in STAR as N87-23028. refs

A combination solar photovoltaic heat engine converter is proposed. Such a system is suitable for either terrestrial or space power applications. The combination system has a higher efficiency than either the photovoltaic array or the heat engine alone can attain. Advantages in concentrator and radiator area and receiver mass of the photovoltaic heat engine system over a heat-engine-only system are estimated. A mass and area comparison between the proposed space station organic Rankine power system and a combination PV-heat engine system is made. The critical problem for the proposed converter is the necessity for high temperature photovoltaic array operation. Estimates of the required photovoltaic temperature are presented. Author

A87-19840*# National Aeronautics and Space Administration. Lewis Research Center, Cleveland, Ohio.

A 25.5 PERCENT AMO GALLIUM ARSENIDE GRATING SOLAR CELL

V. G. WEIZER and M. P. GODLEWSKI (NASA, Lewis Research Center, Cleveland, OH) IN: Photovoltaic Specialists Conference, 18th, Las Vegas, NV, October 21-25, 1985, Conference Record. New York, Institute of Electrical and Electronics Engineers, Inc., 1985, p. 100-104. Previously announced in STAR as N86-11671. refs

Recent calculations have shown that significant open circuit voltage gains are possible with a dot grating junction geometry. The feasibility of applying the dot geometry to the GaAs cell was investigated. This geometry is shown to result in voltage approach 1.120 V and efficiencies well over 25 percent (AMO) if good collection efficiency can be maintained. The latter is shown to be possible if one chooses the proper base resistivity and cell thickness. The above advances in efficiency are shown to be possible in the P-base cell with only minor improvements in existing technology. Author

A87-19842*# National Aeronautics and Space Administration. Lewis Research Center, Cleveland, Ohio.

USE OF A CORRUGATED SURFACE TO ENHANCE RADIATION TOLERANCE IN A GAAS SOLAR CELL

ROSA P. LEON and MICHAEL F. PISZCZOR, JR. (NASA, Lewis Research Center, Cleveland, OH) IN: Photovoltaic Specialists Conference, 18th, Las Vegas, NV, October 21-25, 1985, Conference Record. New York, Institute of Electrical and Electronics Engineers, Inc., 1985, p. 111-115. refs

The use of a corrugated surface on a GaAs solar cell and its effects on radiation resistance were studied. A compute code was developed to determine the performance of the cell for various geometric parameters. The large optical absorption coefficient of GaAs allows grooves to be only 4-5 micrometers deep. Using accepted material parameters for GaAs solar cells the theoretical performances were compared for various corrugated cells before and after minority carrier diffusion length degradation. The total power output was maximized for both n(+)/p and p(+)/n cells. Optimum values of 1.0-1.5 and 5.0 micrometers for groove and ridge widths respectively were determined. Author

A87-19859* National Aeronautics and Space Administration. Lewis Research Center, Cleveland, Ohio.

A PHOTOVOLTAIC POWER SYSTEM AND A LOW-POWER SATELLITE EARTH STATION FOR INDONESIA

RICHARD DELOMBARD (NASA, Lewis Research Center, Cleveland, OH) and KENT EVERSON (Dawn Engineering, Plano, TX) IN: Photovoltaic Specialists Conference, 18th, Las Vegas, NV, October 21-25, 1985, Conference Record. New York, Institute of Electrical and Electronics Engineers, Inc., 1985, p. 269-274.

A photovoltaic power system and a low-power, two-way satellite earth station have been installed at Wawotobi, Sulawesi, Indonesia to provide university classroom communications for audio teleconferencing and video graphics. This project is a part of the Agency for International Development's Rural Satellite Program. The purpose of this program is to demonstrate the use of satellite communications for development assistance applications. The purpose of the photovoltaic power system is to demonstrate the suitability of a hybrid photovoltaic/engine-generator power system for a remote satellite earth station. This paper describes the design, installation and initial operation of the photovoltaic power system and the earth station. Author

A87-19871*# National Aeronautics and Space Administration. Lewis Research Center, Cleveland, Ohio.

PERFORMANCE OF GAAS AND SILICON CONCENTRATOR CELLS UNDER 1 MEV ELECTRON IRRADIATION

H. B. CURTIS and C. K. SWARTZ (NASA, Lewis Research Center, Cleveland, OH) IN: Photovoltaic Specialists Conference, 18th, Las Vegas, NV, October 21-25, 1985, Conference Record. New York, Institute of Electrical and Electronics Engineers, Inc., 1985, p. 356-361.

Gallium arsenide concentrator cells from three sources and silicon concentrator cells from one source were exposed to 1 MeV electrons at fluences up to 1×10^{15} to the 15th electrons per square cm. Performance data were taken after several fluences, at two temperatures (25 and 80 C), and at concentration levels from 1 to about 150X AMO. Data at one sun and 25 C were taken with an X-25 xenon lamp solar simulator. Data at concentrations were taken using a pulsed solar simulator with the assumption of a linear relationship between short-circuit current and irradiance. The cells are 5 mm x 5 mm with a 4 mm diameter illuminated area. Author

A87-19882* Delaware Univ., Newark.

AN OPTIMIZED TOP CONTACT DESIGN FOR SOLAR CELL CONCENTRATORS

GREGORY C. DESALVO and ALLEN M. BARNETT (Delaware University, Newark) IN: Photovoltaic Specialists Conference, 18th, Las Vegas, NV, October 21-25, 1985, Conference Record. New York, Institute of Electrical and Electronics Engineers, Inc., 1985, p. 435-440. refs (Contract NAG3-422)

A new grid optimization scheme is developed for point focus solar cell concentrators which employs a separated grid and busbar concept. Ideally, grid lines act as the primary current collectors and receive all of the current from the semiconductor region. Busbars are the secondary collectors which pick up current from the grids and carry it out of the active region of the solar cell. This separation of functions leads to a multithickness metallization design, where the busbars are made larger in cross section than the grids. This enables the busbars to carry more current per unit area of shading, which is advantageous under high solar concentration where large current densities are generated. Optimized grid patterns using this multilayer concept can provide a 1.6 to 20 percent increase in output power efficiency over optimized single thickness grids. Author

A87-19915* Cleveland State Univ., Ohio.

A PROPOSED GAAS-BASED SUPERLATTICE SOLAR CELL STRUCTURE WITH HIGH EFFICIENCY AND HIGH RADIATION TOLERANCE

CHANDRA GORADIA, RALPH CLARK (Cleveland State University, OH), and DAVID BRINKER (NASA, Lewis Research Center, Cleveland, OH) IN: Photovoltaic Specialists Conference, 18th, Las Vegas, NV, October 21-25, 1985, Conference Record. New York, Institute of Electrical and Electronics Engineers, Inc., 1985, p. 776-781. NASA-supported research. refs

A solar cell structure is proposed which uses a GaAs nipi doping superlattice. An important feature of this structure is that photogenerated minority carriers are very quickly collected in a time shorter than bulk lifetime in the fairly heavily doped n and p layers and these carriers are then transported parallel to the superlattice layers to selective ohmic contacts. Assuming that these already-separated carriers have very long recombination lifetimes, due to their being across an indirect bandgap in real space, it is argued that the proposed structure may exhibit superior radiation tolerance along with reasonably high beginning-of-life efficiency. Author

A87-52288* Energy Research Corp., Danbury, Conn.
MODELING FOR CO POISONING OF A FUEL CELL ANODE
 H. P. DHAR, A. K. KUSH, D. N. PATEL, and L. G. CHRISTNER
 (Energy Research Corp., Danbury, CT) IN: Symposium on
 Electrochemical and Thermal Modeling of Battery, Fuel Cell, and
 Photoenergy Conversion Systems, San Diego, CA, Oct. 20-22,
 1986, Proceedings. Pennington, NJ, Electrochemical Society, Inc.,
 1986, p. 284-297. Research supported by Westinghouse Electric
 Corp. and DOE. refs
 (Contract DEN3-290)

Poisoning losses in a half-cell in the 110-190 C temperature range have been measured in 100 wt pct H₃PO₄ for various mixtures of H₂, CO, and CO₂ gases in order to investigate the polarization loss due to poisoning by CO of a porous fuel cell Pt anode. At a fixed current density, the poisoning loss was found to vary linearly with ln of the CO/H₂ concentration ratio, although deviations from linearity were noted at lower temperatures and higher current densities for high CO/H₂ concentration ratios. The surface coverages of CO were also found to vary linearly with ln of the CO/H₂ concentration ratio. A general adsorption relationship is derived. Standard free energies for CO adsorption were found to vary from -14.5 to -12.1 kcal/mol in the 130-190 C temperature range. The standard entropy for CO adsorption was found to be -39 cal/mol per deg K. R.R.

N87-10531*# Paragon Pacific, Inc., Torrance, Calif.
WEST-3 WIND TURBINE SIMULATOR DEVELOPMENT. VOLUME 2: VERIFICATION Final Report
 S. SRIDHAR Jul. 1985 31 p
 (Contract DEN3-247; DE-AI01-76ET-20320)
 (NASA-CR-174982; DOE/NASA-0247/2; NAS 1.26:174982;
 PPI-FID-300102-VOL-2) Avail: NTIS HC A03/MF A01 CSCL 10A

The details of a study to validate WEST-3, a new time wind turbine simulator developed by Paragib Pacific Inc., are presented in this report. For the validation, the MOD-0 wind turbine was simulated on WEST-3. The simulation results were compared with those obtained from previous MOD-0 simulations, and with test data measured during MOD-0 operations. The study was successful in achieving the major objective of proving that WEST-3 yields results which can be used to support a wind turbine development process. The blade bending moments, peak and cyclic, from the WEST-3 simulation correlated reasonably well with the available MOD-0 data. The simulation was also able to predict the resonance phenomena observed during MOD-0 operations. Also presented in the report is a description and solution of a serious numerical instability problem encountered during the study. The problem was caused by the coupling of the rotor and the power train models. The results of the study indicate that some parts of the existing WEST-3 simulation model may have to be refined for future work; specifically, the aerodynamics and procedure used to couple the rotor model with the tower and the power train models. Author

N87-11344*# Engelhard Corp., Edison, N.J. Research and Development Dept.
DEVELOP AND TEST FUEL CELL POWERED ON SITE INTEGRATED TOTAL ENERGY SYSTEMS. PHASE 3: FULL-SCALE POWER PLANT DEVELOPMENT Quarterly Report, Nov. 1985 - Jan. 1986
 A. KAUFMAN, B. OLSON, S. PUDICK, C. L. WANG, J. WERTH, and J. A. WHELAN 17 Mar. 1986 20 p
 (Contract DEN3-241)
 (NASA-CR-175118; DOE/NASA-0241-21; NAS 1.26:175118;
 QR-19) Avail: NTIS HC A02/MF A01 CSCL 10A

The third in a series of 4kW stacks, consisting of 24 cells of the 13 inch x 23 inch cell size, has been on test for about 1600 hours. This stack is similar to the first two stacks, which ran 7000 and 8400 hours, respectively. The present stack incorporates technology improvements relating to the electrolyte-matrix, the current-collector assembly, and a reduction in the number of cooling plates. Performance is currently averaging about 0.64 per cell at 161 mA sq cm. Author

N87-11345*# National Aeronautics and Space Administration. Lewis Research Center, Cleveland, Ohio.
COMPONENT TESTING OF A GROUND BASED GAS TURBINE STEAM COOLED RICH-BURN PRIMARY ZONE COMBUSTOR FOR EMISSIONS CONTROL OF NITROGENOUS FUELS Final Report
 D. F. SCHULTZ 1986 21 p Presented at the Inter-Agency Advanced Power Group, Washington, D.C., 15-16 Oct. 1986
 (NASA-TM-88873; DOE/NASA-13111/16; E-3280; NAS 1.15:88873) Avail: NTIS HC A02/MF A01 CSCL 10A

This effort summarizes the work performed on a steam cooled, rich-burn primary zone, variable geometry combustor designed for combustion of nitrogenous fuels such as heavy oils or synthetic crude oils. The steam cooling was employed to determine its feasibility and assess its usefulness as part of a ground based gas turbine bottoming cycle. Variable combustor geometry was employed to demonstrate its ability to control primary and secondary zone equivalence ratios and overall pressure drop. Both concepts proved to be highly successful in achieving their desired objectives. The steam cooling reduced peak liner temperatures to less than 800 K. This low temperature offers the potential of both long life and reduced use of strategic materials for liner fabrication. These degrees of variable geometry were successfully employed to control air flow distribution within the combustor. A variable blade angle axial flow air swirler was used to control primary zone air flow, while the secondary and tertiary zone air flows were controlled by rotating bands which regulated air flow to the secondary zone quench holes and the dilutions holes respectively. Author

N87-11346*# Engelhard Corp., Edison, N.J. Research and Development Dept.
DEVELOP AND TEST FUEL CELL POWERED ON-SITE INTEGRATED TOTAL ENERGY SYSTEMS. PHASE 3: FULL-SCALE POWER PLANT DEVELOPMENT Quarterly Report, Aug. - Oct. 1985
 A. KAUFMAN, B. OLSON, S. PUDICK, C. L. WANG, J. WERTH, and J. A. WHELAN 3 Feb. 1986 22 p
 (Contract DEN3-241)
 (NASA-CR-175117; DOE/NASA-0241/20; NAS 1.26:175117;
 QR-18) Avail: NTIS HC A02/MF A01 CSCL 10A

The testing of two 25-cell stacks of the 13 inch x 23 inch cell size (about 4kW) was carried out for 7000 and 8400 hours, respectively. A 25kW stack containing 175 cells of the same size and based on the same technology was constructed and is on test. A third 4kW stack, which will contain 24 cells, will comprise several new technology features; these will be assessed for performance and durability in long-term testing. Author

N87-11347*# Engelhard Corp., Edison, N.J. Research and Development Dept.
DEVELOP AND TEST FUEL CELL POWERED ON SITE INTEGRATED TOTAL ENERGY SYSTEMS. PHASE 3: FULL-SCALE POWER PLANT DEVELOPMENT Quarterly Report, May - Jul. 1985
 A. KAUFMAN, B. OLSON, S. PUDICK, C. L. WANG, J. WERTH, and J. A. WHELAN 9 Oct. 1986 23 p
 (Contract DEN3-241)
 (NASA-CR-175075; DOE/NASA-0241/19; NAS 1.26:175075;
 QR-17) Avail: NTIS HC A02/MF A01 CSCL 10A

A 25-cell stack of the 13 inch x 23 inch cell size (about 4kW) remains on test after 8300 hours, using simulated reformat fuel. A similar stack was previously shut down after 7000 hours on load. These tests have been carried out for the purpose of assessing the durability of fuel cell stack components developed through the end of 1983. A 25kW stack containing 175 cells of the same size and utilizing a technology base representative of the 25-cell stacks has been constructed and is undergoing initial testing. A third 4kW stack is being prepared, and this stack will incorporate several new technology features. Author

44 ENERGY PRODUCTION AND CONVERSION

N87-11348*# Paragon Pacific, Inc., El Segundo, Calif.
WEST-3 WIND TURBINE SIMULATOR DEVELOPMENT.
VOLUME 1: SUMMARY Final Report
S. SRIDHAR Jul. 1985 24 p
(Contract DEN3-247; DE-AI01-76ET-20320)
(NASA-CR-174981; DOE/NASA-0247/1-VOL-1; NAS 1.26:174981;
PPI-FID-300101-VOL-1) Avail: NTIS HC A02/MF A01 CSCL
10A

This report is a summary description of WEST-3, a new real-time wind turbine simulator developed by Paragon Pacific Inc. WEST-3 is an all digital, fully programmable, high performance parallel processing computer. Contained in the report are descriptions of the WEST-3 hardware and software. WEST-3 consists of a network of Computational Units (CUs) working in parallel. Each CU is a custom designed high speed digital processor operating independently of other CUs. The CU, which is the main building block of the system, is described in some detail. A major contributor to the high performance of the system is the use of a unique method for transferring data among the CUs. The software aspects of WEST-3 covered in the report include the preparation of the simulation model (reformulation, scaling and normalization), and the use of the system software (Translator, Linker, Assembler and Loader). Also given is a description of the wind turbine simulation model used in WEST-3, and some sample results from a study conducted to validate the system. Finally, efforts currently underway to enhance the user friendliness of the system are outlined; these include the 32-bit floating point capability, and major improvements in system software. Author

N87-12046*# Paragon Pacific, Inc., Torrance, Calif.
WEST-3 WIND TURBINE SIMULATOR DEVELOPMENT
J. A. HOFFMAN and S. SRIDHAR Jul. 1985 236 p
(Contract DEN3-247; DE-AI01-76ET-20320)
(NASA-CR-174983; DOE/NASA-0247-3; NAS 1.26:174983;
PPI-FID-300086-VOL-3) Avail: NTIS HC A11/MF A01 CSCL
10A

The software developed for WEST-3, a new, all digital, and fully programmable wind turbine simulator is given. The process of wind turbine simulation on WEST-3 is described in detail. The major steps are, the processing of the mathematical models, the preparation of the constant data, and the use of system software generated executable code for running on WEST-3. The mechanics of reformulation, normalization, and scaling of the mathematical models is discussed in detail, in particular, the significance of reformulation which leads to accurate simulations. Descriptions for the preprocessor computer programs which are used to prepare the constant data needed in the simulation are given. These programs, in addition to scaling and normalizing all the constants, relieve the user from having to generate a large number of constants used in the simulation. Also given are brief descriptions of the components of the WEST-3 system software: Translator, Assembler, Linker, and Loader. Also included are: details of the aeroelastic rotor analysis, which is the center of a wind turbine simulation model, analysis of the gimbal subsystem; and listings of the variables, constants, and equations used in the simulation. Author

N87-12047*# Mechanical Technology, Inc., Latham, N. Y.
CERAMIC AUTOMOTIVE STIRLING ENGINE PROGRAM
Aug. 1986 187 p
(Contract DEN3-311; DE-AI01-85CE-50112)
(NASA-CR-175042; DOE/NASA-0311/1; NAS 1.26:175042;
MTI-85SESD24) Avail: NTIS HC A09/MF A01 CSCL 10B

The Ceramic Automotive Stirling Engine Program evaluated the application of advanced ceramic materials to an automotive Stirling engine. The objective of the program was to evaluate the technical feasibility of utilizing advanced ceramics to increase peak engine operating temperature, and to evaluate the performance benefits of such an increase. Manufacturing cost estimates were also developed for various ceramic engine components and compared with conventional metallic engine component costs. Author

N87-13856*# National Aeronautics and Space Administration.
Lewis Research Center, Cleveland, Ohio.
TUNISIA RENEWABLE ENERGY PROJECT SYSTEMS
DESCRIPTION REPORT
L. R. SCUDDER, J. E. MARTZ, and A. F. RATAJCZAK Oct.
1986 44 p Prepared for the Agency for International
Development
(NASA-TM-88789; E-3124; NAS 1.15:88789) Avail: NTIS HC
A03/MF A01 CSCL 10A

In 1979, the Agency for International Development (AID) initiated a renewable energy project with the Government of Tunisia to develop an institutional capability to plan and institute renewable energy technologies in a rural area. The specific objective of the district energy applications subproject was to demonstrate solar and wind energy systems in a rural village setting. The NASA Lewis Research Center was asked by the AID Near East Bureau to manage and implement this subproject. This report describes the project and gives detailed descriptions of the various systems. Author

N87-14771*# Sverdrup Technology, Inc., Cleveland, Ohio.
CONCEPTUAL DEFINITION OF A TECHNOLOGY
DEVELOPMENT MISSION FOR ADVANCED SOLAR DYNAMIC
POWER SYSTEMS Final Report
R. P. MIGRA Jul. 1986 128 p
(Contract NAS3-24105)
(NASA-CR-179482; E-3132; NAS 1.26:179482) Avail: NTIS HC
A07/MF A01 CSCL 10B

An initial conceptual definition of a technology development mission for advanced solar dynamic power systems is provided, utilizing a space station to provide a dedicated test facility. The advanced power systems considered included Brayton, Stirling, and liquid metal Rankine systems operating in the temperature range of 1040 to 1400 K. The critical technologies for advanced systems were identified by reviewing the current state of the art of solar dynamic power systems. The experimental requirements were determined by planning a system test of a 20 kWe solar dynamic power system on the space station test facility. These requirements were documented via the Mission Requirements Working Group (MRWG) and Technology Development Advocacy Group (TDAG) forms. Various concepts or considerations of advanced concepts are discussed. A preliminary evolutionary plan for this technology development mission was prepared. Author

N87-16445*# National Aeronautics and Space Administration.
Lewis Research Center, Cleveland, Ohio.
INITIAL PERFORMANCE OF ADVANCED DESIGNS FOR IPV
NICKEL-HYDROGEN CELLS
JOHN J. SMITHRICK Sep. 1986 13 p Presented at the 15th
International Power Sources Symposium, Brighton, England, 7-11
Sep. 1986 Supersedes NASA-TM-87029
(NASA-TM-87282; E-2992; NAS 1.15:87282) Avail: NTIS HC
A02/MF A01 CSCL 10C

Advanced designs for individual pressure vessel nickel-hydrogen cells have been conceived which should improve the cycle life at deep depths-of-discharge and improve thermal management. Features of the designs which are new and not incorporated in either of the contemporary cells (Air Force/Hughes, Comsat) are: (1) use of alternate methods of oxygen recombination, (2) use of serrated edge separators to facilitate movement of gas within the cell while still maintaining required physical contact with the wall wick, and (3) use of an expandable stack to accommodate some of the nickel electrode expansion. The designs also consider electrolyte volume requirements over the life of the cells, and are fully compatible with the Air Force/Hughes design. Author

N87-17400*# Electrotek Concepts, Inc., Knoxville, Tenn.
UTILITY INTERCONNECTION ISSUES FOR WIND POWER GENERATION Status Report

J. I. HERRERA, J. S. LAWLER, T. W. REDDOCH, and R. L. SULLIVAN Jun. 1986 45 p
 (Contract NAS3-24105; DE-AI01-76ET-20320)
 (NASA-CR-175056; DOE/NASA/4105-3; NAS 1.26:175056)
 Avail: NTIS HC A03/MF A01 CSCL 10B

This document organizes the total range of utility related issues, reviews wind turbine control and dynamic characteristics, identifies the interaction of wind turbines to electric utility systems, and identifies areas for future research. The material is organized at three levels: the wind turbine, its controls and characteristics; connection strategies as dispersed or WPSS; and the composite issue of planning and operating the electric power system with wind generated electricity. Author

N87-17401*# Cleveland State Univ., Ohio.
DESIGN AND DYNAMIC SIMULATION OF A FIXED PITCH 56 KW WIND TURBINE DRIVE TRAIN WITH A CONTINUOUSLY VARIABLE TRANSMISSION Final Report

C. GALLO, R. KASUBA, A. PINTZ, and J. SPRING Mar. 1986 45 p
 (Contract NCC3-6; DE-AI01-76ET-20320)
 (NASA-CR-179543; DOE/NASA/0006-3; NAS 1.26:179543)
 Avail: NTIS HC A03/MF A01 CSCL 10B

The dynamic analysis of a horizontal axis fixed pitch wind turbine generator (WTG) rated at 56 kW is discussed. A mechanical Continuously Variable Transmission (CVT) was incorporated in the drive train to provide variable speed operation capability. One goal of the dynamic analysis was to determine if variable speed operation, by means of a mechanical CVT, is capable of capturing the transient power in the WTG/wind environment. Another goal was to determine the extent of power regulation possible with CVT operation. Author

N87-18229*# Georgia Tech Research Inst., Atlanta.
TECHNOLOGY FOR SATELLITE POWER CONVERSION Semiannual Technical Report

M. A. GOUKER, D. P. CAMPBELL, and J. J. GALLAGHER 27 Feb. 1987 21 p
 (Contract NAG3-282; PROJ. 3244)
 (NASA-CR-180162; NAS 1.26:180162) Avail: NTIS HC A02/MF A01 CSCL 10A

The work in this reporting period was concentrated on electronically calibrating the bolometer detectors. The calibration is necessary for two reasons: first, the power delivered to the rectifying circuit must be known in order to choose a diode with the appropriate barrier height, and second, the power captured by the antenna must be measured if the efficiency of the rectenna is to be divided into antenna efficiency and rectification efficiency. The millimeter wave region operation of the bolometers was simulated with a VHF (10 to 90 MHz) test signal. These detectors are accurate to within roughly 10%. The typical responsivity of the bolometers is 10 volts/watt and the NEP at 20 Hz is 5 times 10 to the minus 9th power W(Hz)^{-1/2}. Author

N87-18230*# National Aeronautics and Space Administration. Lewis Research Center, Cleveland, Ohio.

USER EVALUATION OF PHOTOVOLTAIC-POWERED VACCINE REFRIGERATOR/FREEZER SYSTEMS Final Report

ANTHONY F. RATAJCZAK Mar. 1987 75 p
 (Contract DE-AI01-79ET-20485; PASA-NASA/DSB-5710-2-79)
 (NASA-TM-88830; E-3206; DOE/NASA/20485-80; NAS 1.15:88830) Avail: NTIS HC A04/MF A01 CSCL 10B

The NASA Lewis Research Center has concluded a project to develop and field test photovoltaic-powered refrigerator/freezers for vaccine storage in remote areas of developing countries. As a conclusion to this project, questionnaires were sent to the in-country administrators for each test site probing user acceptance of the systems and attitudes regarding procurement of additional systems. Responses indicate that the systems had a positive effect on the local communities, that they made a positive impression on the

local health authorities, and that system cost and scarcity of funds are the major barriers to procurements of additional systems.

Author

N87-18922*# AeroVironment, Inc., Monrovia, Calif.
DEVELOPMENT AND TESTING OF VORTEX GENERATORS FOR SMALL HORIZONTAL AXIS WIND TURBINES Final Report

G. W. GYATT Jul. 1986 45 p
 (Contract DEN3-367; DE-AI01-76ET-20320)
 (NASA-CR-179514; DOE/NASA/0367-1; NAS 1.26:179514; AV-FR-86/822) Avail: NTIS HC A03/MF A01 CSCL 10A

Vortex generators (VGs) for a small (32 ft diameter) horizontal axis wind turbine, the Carter Model 25, have been developed and tested. Arrays of VGs in a counterrotating arrangement were tested on the inbound half-span, outboard half-span, and on the entire blade. VG pairs had their centerlines spaced at a distance of 15% of blade chord, with a spanwise width of 10% of blade chord. Each VG had a length/height ratio of 4, with a height of between 0.5% and 1.0% of the blade chord. Tests were made with roughness strips to determine whether VGs alleviated the sensitivity of some turbines to an accumulation of bugs and dirt on the leading edge. Field test data showed that VGs increased power output up to 20% at wind speeds above 10 m/s with only a small (less than 4%) performance penalty at lower speeds. The VGs on the outboard span of the blade were more effective than those on inner sections. For the case of full span coverage, the energy yearly output increased almost 6% at a site with a mean wind speed of 16 mph. The VGs did reduce the performance loss caused by leading edge roughness. An increase in blade pitch angle has an effect on the power curve similar to the addition of VGs. VGs alleviate the sensitivity of wind turbine rotors to leading edge roughness caused by bugs and drift. Author

N87-19804*# ECO Energy Conversion, Somerville, Mass.
ORGANOMETALLIC CATALYSTS FOR PRIMARY PHOSPHORIC ACID FUEL CELLS Final Report, Nov. 1981 - Nov. 1985

FRASER WALSH Mar. 1987 92 p
 (Contract DEN3-206; DE-AI21-80ET-17088)
 (NASA-CR-179490; DOE/NASA/0206-16; NAS 1.26:179490)
 Avail: NTIS HC A05/MF A01 CSCL 10A

A continuing effort by the U.S. Department of Energy to improve the competitiveness of the phosphoric acid fuel cell by improving cell performance and/or reducing cell cost is discussed. Cathode improvement, both in performance and cost, available through the use of a class of organometallic cathode catalysts, the tetraazaannulenes (TAAs), was investigated. A new mixed catalyst was identified which provides improved cathode performance without the need for the use of a noble metal. This mixed catalyst was tested under load for 1000 hr. in full cell at 160 to 200 C in phosphoric acid H₃PO₄, and was shown to provide stable performance. The mixed catalyst contains an organometallic to catalyze electroreduction of oxygen to hydrogen peroxide and a metal to catalyze further electroreduction of the hydrogen peroxide to water. Cathodes containing an exemplar mixed catalyst (e.g., Co bisphenyl TAA/Mn) operate at approximately 650 mV vs DHE in 160 C, 85% H₃PO₄ with oxygen as reactant. In developing this mixed catalyst, a broad spectrum of TAAs were prepared, tested in half-cell and in a rotating ring-disk electrode system. TAAs found to facilitate the production of hydrogen peroxide in electroreduction were shown to be preferred TAAs for use in the mixed catalyst. Manganese (Mn) was identified as a preferred metal because it is capable of catalyzing hydrogen peroxide electroreduction, is lower in cost and is of less strategic importance than platinum, the cathode catalyst normally used in the fuel cell. Author

N87-22307*# National Aeronautics and Space Administration. Lewis Research Center, Cleveland, Ohio.

STRESS-LIFE INTERRELATIONSHIPS ASSOCIATED WITH ALKALINE FUEL CELLS

LAWRENCE H. THALLER, RONALD E. MARTIN, and JAMES K. STEDMAN (International Fuel Cells Corp., South Windsor, Conn.) 1987 8 p Proposed for presentation at the 22nd Intersociety Energy Conversion Engineering Conference, Philadelphia, Pa., 10-14 Aug. 1987; sponsored by AIAA, ANS, ASME, SAE, IEEE, ACS and AIChE

(NASA-TM-89881; E-3562; NAS 1.15:89881; AIAA-87-9198)

Avail: NTIS HC A02/MF A01 CSCL 10B

A review is presented concerning the interrelationships between applied stress and the expected service life of alkaline fuel cells. Only the physical, chemical, and electrochemical phenomena that take place within the fuel cell stack portion of an overall fuel cell system will be discussed. A brief review will be given covering the significant improvements in performance and life over the past two decades as well as summarizing the more recent advances in understanding which can be used to predict the performance and life characteristics of fuel cell systems that have yet to be built. Author

N87-22308*# National Aeronautics and Space Administration. Lewis Research Center, Cleveland, Ohio.

EFFECT OF STORAGE AND LEO CYCLING ON MANUFACTURING TECHNOLOGY IPV NICKEL-HYDROGEN CELLS

JOHN J. SMITHRICK 1987 9 p Proposed for presentation at the 22nd Intersociety Energy Conversion Engineering Conference, Philadelphia, Pa., 10-14 Aug. 1987; sponsored by AIAA, ANS, ASME, SAE, IEEE, ACS and AIChE

(NASA-TM-89883; E-3566; NAS 1.15:89883; AIAA-87-9318)

Avail: NTIS HC A02/MF A01 CSCL 10C

Yardney Manufacturing Technology (MANTECH) 50 A-hr space weight individual pressure vessel nickel-hydrogen cells were evaluated. This consisted of investigating: the effect of storage and charge/discharge cycling on cell performance. For the storage test the cells were precharged with hydrogen, by the manufacturer, to a pressure of 14.5 psia. After undergoing activation and acceptance tests, the cells were discharged at C/10 rate (5A) to 0.1 V or less. The terminals were then shorted. The cells were shipped to NASA Lewis Research Center where they were stored at room temperature in the shorted condition for 1 year. After storage, the acceptance tests were repeated at NASA Lewis. A comparison of test results indicate no significant degradation in electrical performance due to 1 year storage. For the cycle life test the regime was a 90 minute low earth orbit at deep depths of discharge (80 and 60 percent). At the 80 percent DOD the three cells failed on the average at cycle 741. Failure for this test was defined to occur when the cell voltage degraded to 1 V prior to completion of the 35 min discharge. The DOD was reduced to 60 percent. The cycle life test was continued. Author

N87-22310*# National Aeronautics and Space Administration. Lewis Research Center, Cleveland, Ohio.

REGENERATIVE FUEL CELL STUDY FOR SATELLITES IN GEO ORBIT

LESLIE VANDINE, OLGA GONZALEZ-SANABRIA, and ALEXANDER LEVY (International Fuel Cells Corp., South Windsor, Conn.) 1987 8 p Proposed for presentation at the 22nd Intersociety Energy Conversion Engineering Conference, Philadelphia, Pa., 10-14 Aug. 1987; sponsored by AIAA, ANS, ASME, SAE, IEEE, ACS and AIChE

(NASA-TM-89914; E-3607; NAS 1.15:89914; AIAA-87-9200)

Avail: NTIS HC A02/MF A01 CSCL 10B

The results of a 12 month study to identify high performance regenerative hydrogen-oxygen fuel cell concepts for geosynchronous satellite application are summarized. Emphasis was placed on concepts with the potential for high energy density and passive means for water and heat management to maximize system reliability. Both polymer membrane and alkaline electrolyte fuel cells were considered, with emphasis on the alkaline cell

because of its high performance, advanced state of development, and proven ability to operate in a launch and space environment. Three alkaline system concepts were studied. Results indicate that using near term technology energy densities between 46 and 52 watt-hour/lb can be achieved at efficiencies of 55 percent. Using advanced light weight cell construction which was achieved in experimental cells, composite tankage material for the reactant gases and the reversible stack concept, system energy densities of 115 watt-hours/lb can be projected. Author

N87-22311*# National Aeronautics and Space Administration. Lewis Research Center, Cleveland, Ohio.

A PREDICTION MODEL OF THE DEPTH-OF-DISCHARGE EFFECT ON THE CYCLE LIFE OF A STORAGE CELL

LAWRENCE H. THALLER and HONG S. LIM (Hughes Research Labs., Malibu, Calif.) 1987 9 p Proposed for presentation at the 22nd Intersociety Energy Conversion Engineering Conference, Philadelphia, Pa., 10-14 Aug. 1987; sponsored by AIAA, ANS, ASME, SAE, IEEE, ACS and AIChE

(NASA-TM-89915; E-3608; NAS 1.15:89915; AIAA-87-9080)

Avail: NTIS HC A02/MF A01 CSCL 10C

Cycle life requirements are very high for batteries used in aerospace applications in low Earth orbit. The data base required to establish confidence in a particular cell design is thus both extensive and expensive. Reliable accelerated cycle life testing and performance decay modeling represent attractive alternatives to real-time tests of cycle life. In light of certain long-term cycle life test results, this paper examines a very simple performance decay model developed earlier. Application of that model to available data demonstrates a rigid relationship between a battery's expected cycle life and the depth of discharge of cycling. Further, modeling analysis of the data suggests that a significantly improved cycle life can be obtained with advanced components, materials, and designs; and that cycle life can be reliably predicted from the results of accelerated testing. Author

N87-23020*# National Aeronautics and Space Administration. Lewis Research Center, Cleveland, Ohio.

HIGH TEMPERATURE SOLID OXIDE REGENERATIVE FUEL CELL FOR SOLAR PHOTOVOLTAIC ENERGY STORAGE

DAVID J. BENTS 1987 19 p Prepared for presentation at the 22nd Intersociety Energy Conversion Engineering Conference, Philadelphia, Pa., 10-14 Aug. 1987; sponsored in part by AIAA, ANS, ASME, SAE, IEEE, ACS, and AIChE

(NASA-TM-89872; E-3549; NAS 1.15:89872; AIAA-87-9203)

Avail: NTIS HC A02/MF A01 CSCL 10C

A hydrogen-oxygen regenerative fuel cell (RFC) energy storage system based on high temperature solid oxide fuel cell (SOFC) technology is described. The reactants are stored as gases in lightweight insulated pressure vessels. The product water is stored as a liquid in saturated equilibrium with the fuel gas. The system functions as a secondary battery and is applicable to darkside energy storage for solar photovoltaics. Author

N87-23027*# National Aeronautics and Space Administration. Lewis Research Center, Cleveland, Ohio.

SP-100 ADVANCED TECHNOLOGY PROGRAM

RONALD J. SOVIE 1987 12 p Proposed for presentation at the 22nd Intersociety Energy Conversion Engineering Conference, Philadelphia, Pa., 10-14 Aug. 1987; sponsored by AIAA, ANS, ASME, SAE, IEEE, ACS and AIChE

(NASA-TM-89888; E-3576; NAS 1.15:89888; AIAA-87-9232)

Avail: NTIS HC A02/MF A01 CSCL 10B

The goal of the triagency SP-100 Program is to develop long-lived, compact, lightweight, survivable nuclear reactor space power systems for application to the power range 50 kWe to 1 MWe. The successful development of these systems should enable or significantly enhance many of the future NASA civil and commercial missions. The NASA SP-100 Advanced Technology Program strongly augments the parallel SP-100 Ground Engineering System Development program and enhances the chances for success of the overall SP-100 program. The purpose of this paper is to discuss the key technical elements of the Advanced

Technology Program and the progress made in the initial year and a half of the project. Author

N87-23028*# National Aeronautics and Space Administration. Lewis Research Center, Cleveland, Ohio.

PERFORMANCE CHARACTERISTICS OF A COMBINATION SOLAR PHOTOVOLTAIC HEAT ENGINE ENERGY CONVERTER

DONALD L. CHUBB 1987 14 p Prepared for presentation at the 22nd Intersociety Energy Conversion Engineering Conference, Philadelphia, Pa., 10-14 Aug. 1987; cosponsored by AIAA, ANS, ASME, SAE, IEEE, ACS, AIChE (NASA-TM-89908; E-3591; NAS 1.15:89908; AIAA-87-9035) Avail: NTIS HC A02/MF A01 CSCL 10A

A combination solar photovoltaic heat engine converter is proposed. Such a system is suitable for either terrestrial or space power applications. The combination system has a higher efficiency than either the photovoltaic array or the heat engine alone can attain. Advantages in concentrator and radiator area and receiver mass of the photovoltaic heat engine system over a heat-engine-only system are estimated. A mass and area comparison between the proposed space station organic Rankine power system and a combination PV-heat engine system is made. The critical problem for the proposed converter is the necessity for high temperature photovoltaic array operation. Estimates of the required photovoltaic temperature are presented. Author

N87-23029*# National Aeronautics and Space Administration. Lewis Research Center, Cleveland, Ohio.

COMPONENT VARIATIONS AND THEIR EFFECTS ON BIPOLAR NICKEL-HYDROGEN CELL PERFORMANCE

MICHELLE A. MANZO, RANDALL F. GAHN, OLGA D. GONZALEZ-SANABRIA, ROBERT L. CATALDO, and RUSSEL P. GEMEINER 1987 6 p Prepared for presentation at the 22nd Intersociety Energy Conversion Engineering Conference, Philadelphia, Pa., 10-14 Aug. 1987; cosponsored by AIAA, ANS, ASME, SAE, IEEE, ACS, and AIChE (NASA-TM-89907; E-3600; NAS 1.15:89907; AIAA-87-9260) Avail: NTIS HC A02/MF A01 CSCL 10C

A 50 cell bipolar nickel-hydrogen battery was assembled to demonstrate the feasibility of constructing a high voltage stack of cells. Various component combinations were tested in this battery. The battery had approximately 1 ampere-hour of capacity and was constructed from components with an active area of 2' X 2'. The components were parametrically varied to give a comparison of nickel electrodes, hydrogen electrodes, separators, fill procedures and electrolyte reservoir plate thicknesses. Groups of five cells were constructed using the same components; ten combinations were tested in all. The battery was thoroughly characterized at various charge and discharge rates as well as with various pulse patterns and rates. Over a period of 1400 40% DOD LEO cycles some of the groups began to exhibit performance differences. In general, only separator variations had a significant effect on cell performance. It also appears that shunt currents may have been operating within the stack, resulting in electrolyte transfer from one cell to another, thus contributing to cell performance variations. Author

N87-23030*# Solavolt International, Phoenix, Ariz.
DESIGN, DEVELOPMENT AND DEPLOYMENT OF PUBLIC SERVICE PHOTOVOLTAIC POWER/LOAD SYSTEMS FOR THE GABONESE REPUBLIC Final Report

WILLIAM J. KASZETA Apr. 1987 235 p (Contract DEN3-347) (NASA-CR-179603; NAS 1.26:179603) Avail: NTIS HC A11/MF A01 CSCL 10B

Five different types of public service photovoltaic power/load systems installed in the Gabonese Republic are discussed. The village settings, the systems, performance results and some problems encountered are described. Most of the systems performed well, but some of the systems had problems due to failure of components or installation errors. The project was reasonably successful in collecting and reporting data for system

performance evaluation that will be useful for guiding officials and system designers involved in village power applications in developing countries. R.J.F.

N87-24026*# National Aeronautics and Space Administration. Lewis Research Center, Cleveland, Ohio.

FLUORIDE SALTS AND CONTAINER MATERIALS FOR THERMAL ENERGY STORAGE APPLICATIONS IN THE TEMPERATURE RANGE 973 TO 1400 K

AJAY K. MISRA (Case Western Reserve Univ., Cleveland, Ohio.) and J. DANIEL WHITTENBERGER 1987 23 p Proposed for presentation at the 22nd Intersociety Energy Conversion Engineering Conference, Philadelphia, Pa., 10-14 Aug. 1987; sponsored by AIAA, ANS, ASME, SAE, IEEE, ACS and AIChE (NASA-TM-89913; E-3563; NAS 1.15:89913; AIAA-87-9226) Avail: NTIS HC A02/MF A01 CSCL 10C

Multicomponent fluoride salt mixtures were characterized for use as latent heat of fusion heat storage materials in advanced solar dynamic space power systems with operating temperatures in the range of 973 to 1400 K. The melting points and eutectic composition for many systems with published phase diagrams were verified, and several new eutectic compositions were identified. Additionally, the heats of fusion of several binary and ternary eutectics and congruently melting intermediate compounds were measured by differential scanning calorimetry. The extent of corrosion of various metals by fluoride melts was estimated from thermodynamic considerations, and equilibrium conditions inside a containment vessel were calculated as functions of the initial moisture content of the salt and free volume above the molten salt. Preliminary experimental data on the corrosion of commercial, high-temperature alloys in LiF-19.5CaF₂ and NaF-27CaF₂-36MgF₂ melts are presented and compared to the thermodynamic predictions. Author

N87-24029*# National Aeronautics and Space Administration. Lewis Research Center, Cleveland, Ohio.

TEST RESULTS OF A 60 VOLT BIPOLAR NICKEL-HYDROGEN BATTERY

RUSSELL L. CATALDO, OLGA GONZALEZ-SANABRIA, RANDALL F. GAHN, MICHELLE A. MANZO, and RUSSEL P. GEMEINER 1987 7 p Prepared for presentation at the 22nd Intersociety Energy Conversion Engineering Conference, Philadelphia, Pa., 10-14 Aug. 1987; cosponsored by AIAA, ANS, ASME, SAE, IEEE, ACS, and AIChE (NASA-TM-89927; E-3631; NAS 1.15:89927; AIAA-87-9262) Avail: NTIS HC A02/MF A01 CSCL 10C

In July, 1986, a high-voltage nickel-hydrogen battery was assembled at the NASA Lewis Research Center. This battery incorporated bipolar construction techniques to build a 50-cell stack with approximately 1.0 A-hr capacity (C) and an open-circuit voltage of 65 V. The battery was characterized at both low and high current rates prior to pulsed and nonpulsed discharges. Pulse discharges at 5 and 10 C were performed before placing the battery on over 1400, 40% depth-of-discharge, low-earth-orbit cycles. The successful demonstration of a high-voltage bipolar battery in one containment vessel has advanced the technology to where nickel-hydrogen high-voltage systems can be constructed of several modules instead of hundreds of individual cells. Author

N87-24838*# National Aeronautics and Space Administration. Lewis Research Center, Cleveland, Ohio.

EFFECT OF COMPONENT COMPRESSION ON THE INITIAL PERFORMANCE OF AN IPV NICKEL-HYDROGEN CELL

RANDALL F. GAHN 1987 17 p Prepared for presentation at the 22nd Intersociety Energy Conversion Engineering Conference, Philadelphia, Pa., 10-14 Aug. 1987; cosponsored by AIAA, ANS, ASME, SAE, IEEE, ACS, and AIChE (NASA-TM-100102; E-3590; NAS 1.15:100102; AIAA-87-9257) Avail: NTIS HC A02/MF A01 CSCL 10C

An experimental method was developed for evaluating the effect of component compression on the charge and discharge voltage characteristics of a 3 1/2 in. diameter boiler plate cell. A standard

44 ENERGY PRODUCTION AND CONVERSION

boiler plate pressure vessel was modified by the addition of a mechanical feedthrough on the bottom of the vessel which permitted different compressions to be applied to the components without disturbing the integrity of the stack. Compression loadings from 0.94 to 27.4 psi were applied by suspending weights from the feedthrough rod. Cell voltages were measured for 0.96-C, 55-min charge and for 1.37-C, 35-min and 2-C, 24-min discharges. An initial change in voltage performance on both charge and discharge as the loading increased was attributed to seating of the components. Subsequent variation of the compression from 2.97 to 27.4 psi caused only minor changes in either the charge or the discharge voltages. Several one month open-circuit voltage stands and 1100 cycles under LEO conditions at the maximum loading have produced no change in performance. Author

N87-25621*# Ohio State Univ., Columbus.
WIND TUNNEL EVALUATION OF A TRUNCATED NACA 64-621 AIRFOIL FOR WIND TURBINE APPLICATIONS Final Report
S. P. LAW and G. M. GREGOREK Jul. 1987 37 p
(Contract NAG3-330)
(NASA-CR-180803; DOE/NASA/0330-2; NAS 1.26:180803)
Avail: NTIS HC A03/MF A01 CSCL 10A

An experimental program to measure the aerodynamic performance of a NACA 64-621 airfoil with a truncated trailing edge for wind turbine applications has been conducted in the Ohio State University Aeronautical and Astronautical Research Laboratory 6 in. by 21 in. pressurized wind tunnel. The blunted or trailing edge truncated (TET) airfoil has an advantage over similar trailing edge airfoils because it is able to streamline a larger spar structure, while also providing aerodynamic properties that are quite good. Surface pressures were measured and integrated to determine the lift, pressure drag, and moment coefficients over angles of attack ranging from -14 to +90 deg at Mach 0.2 and Reynolds numbers of 1,000,000 and 600,000. Results are compared to the NACA 0025, 0030, and 0035 thick airfoils with sharp trailing edges. Comparison shows that the 30 percent thick NACA 64-621-TET airfoil has higher maximum lift, higher lift curve slope, lower drag at higher lift coefficients, and higher chordwise force coefficient than similar thick airfoils with sharp trailing edges. Author

N87-25630*# National Aeronautics and Space Administration. Lewis Research Center, Cleveland, Ohio.
COMBINATION PHOTOVOLTAIC-HEAT ENGINE ENERGY CONVERTER Patent Application
DONALD L. CHUBB, inventor (to NASA) 9 Jul. 1987 10 p
(NASA-CASE-LEW-14252-1; US-PATENT-APPL-SN-071678)
Avail: NTIS HC A02/MF A01 CSCL 10B

A combination photovoltaic array heat engine solar energy converter that converts the entire solar spectrum into electrical energy is disclosed. Photons from the solar spectrum of predetermined wavelengths are directed to the photovoltaic array and converted to electrical energy. Also, a combination of electrical energy and thermal energy storage is provided to insure electrical power throughout the spacecraft orbit. NASA

N87-26413*# National Aeronautics and Space Administration. Lewis Research Center, Cleveland, Ohio.
SPACE PHOTOVOLTAIC RESEARCH AND TECHNOLOGY 1986. HIGH EFFICIENCY, SPACE ENVIRONMENT, AND ARRAY TECHNOLOGY
Jun. 1987 375 p Conference held in Cleveland, Ohio, 7-9 Oct. 1986
(NASA-CP-2475; E-3450; NAS 1.55:2475) Avail: NTIS HC A16/MF A01 CSCL 10B

The conference provided a forum to assess the progress made, the problems remaining, and the strategy for the future of photovoltaic research. Cell research and technology, space environmental effects, array technology and applications were discussed.

N87-26417*# Varian Associates, Palo Alto, Calif.
HIGH-EFFICIENCY GAAS CONCENTRATOR SPACE CELLS
J. G. WERTHEN, G. F. VIRSHUP, H. F. MACMILLAN, C. W. FORD, and H. C. HAMAKER In NASA. Lewis Research Center, Space Photovoltaic Research and Technology 1986. High Efficiency, Space Environment and Array Technology p 25-31 Jun. 1987 (Contract NAS3-23876)

Avail: NTIS HC A16/MF A01 CSCL 10B

High efficiency Al sub x Ga sub 1-x As/GaAs heteroface solar concentrator cells have been developed for space applications. The cells, which were grown using metalorganic chemical vapor deposition (MOCVD), have been fabricated in both the p-n and n-p configurations. Magnesium and zinc are used as the p-type dopants, and Se is used as the n-type dopant. The space cells, which are designed for use in a Cassegrainian concentrator operating at 100 suns, AMO, have a circular illuminated area 4 mm in diameter on a 5 mm by 5 mm cell. These cells have exhibited flash-tested efficiencies as high as 23.6 percent at 28 C and 21.6 percent at 80 C. Author

N87-26422*# National Aeronautics and Space Administration. Lewis Research Center, Cleveland, Ohio.

DESIGN CONSIDERATIONS FOR A GAAS NIPI DOPING SUPERLATTICE SOLAR CELL

RALPH CLARK, CHANDRA GORADIA (Cleveland State Univ., Ohio.), and DAVID BRINKER In its Space Photovoltaic Research and Technology 1986. High Efficiency, Space Environment and Array Technology p 73-80 Jun. 1987

Avail: NTIS HC A16/MF A01 CSCL 10B

A new GaAs nipi doping superlattice solar cell structure is presented, which holds promise for high efficiency coupled with very high radiation tolerance. The structure has all contacts on the unilluminated side. Design constraints are presented which this structure must satisfy in order to exhibit high efficiency and high radiation tolerance. The results of self-consistent quantum mechanical calculations are presented which show that a viable design of this cell would include relatively thick n and p layers which are fairly heavily doped. Author

N87-26427*# National Aeronautics and Space Administration. Lewis Research Center, Cleveland, Ohio.

DEVELOPMENT OF A FRESNEL LENS CONCENTRATOR FOR SPACE APPLICATION

MARK J. ONEILL (ENTECH Corp., Dallas-Fort Worth Airport, Tex.) and MICHAEL F. PISZCZOR In its Space Photovoltaic Research and Technology 1986. High Efficiency, Space Environment and Array Technology p 119-132 Jun. 1987 (Contract NAS3-24871)

Avail: NTIS HC A16/MF A01 CSCL 10B

The selected conceptual design of the dome lens photovoltaic concentrator for space applications uses a 3.7 cm square aperture dome lens to focus onto a 0.4 cm active diameter gallium arsenide cell. The selected configuration will provide 91.5 percent lens optical efficiency and 21.4 percent cell efficiency at 100 suns irradiance and 100 C cell temperature, for an overall cell efficiency of 19.6 percent. The selected configuration will tolerate 1 degree tracking errors with negligible loss of performance. The selected panel weight is 2.5 kg/sq.m. Author

N87-26430*# National Aeronautics and Space Administration. Lewis Research Center, Cleveland, Ohio.

THE EFFECT OF INTERNAL STRESSES ON SOLAR CELL EFFICIENCY

VICTOR G. WEIZER In its Space Photovoltaic Research and Technology 1986. High Efficiency, Space Environment and Array Technology p 151-161 Jun. 1987

Avail: NTIS HC A16/MF A01 CSCL 10B

Diffusion induced stresses in silicon are shown to result in large localized changes in the minority carrier mobility which in turn have a significant effect on cell output. Evidence is given that both compressive and tensile stresses can be generated in either the emitter or the base region. Tensile stresses appear to be much more effective in altering cell performance. While most

stress related effects appear to degrade cell efficiency, this is not always the case. Evidence is presented showing that arsenic induced stresses can result in emitter characteristics comparable to those found in the MINP cell without requiring a high degree of surface passivation. Author

N87-26434*# National Aeronautics and Space Administration. Lewis Research Center, Cleveland, Ohio.

THE USE OF MULTIPLE EBIC CURVES AND LOW VOLTAGE ELECTRON MICROSCOPY IN THE MEASUREMENT OF SMALL DIFFUSION LENGTHS

R. P. LEON *In its* Space Photovoltaic Research and Technology 1986. High Efficiency, Space Environment and Array Technology p 185-193 Jun. 1987

Avail: NTIS HC A16/MF A01 CSCL 10B

Accurate evaluations of diffusion lengths for heavily to moderately doped III-V semiconductors and/or radiation damaged solar cells have been made possible by using experimental and numerical techniques. The techniques employed were electron beam induced current and low voltage electron microscopy. Author

N87-26435*# National Aeronautics and Space Administration. Lewis Research Center, Cleveland, Ohio.

RESULTS OF 1 MEV PROTON IRRADIATION OF FRONT AND BACK SURFACES OF SILICON SOLAR CELLS

B. E. ANSPAUGH, R. KACHARE (Jet Propulsion Lab., California Inst. of Tech., Pasadena.), and V. G. WEIZER *In its* Space Photovoltaic Research and Technology 1986. High Efficiency, Space Environment and Array Technology p 195-206 Jun. 1987

Avail: NTIS HC A16/MF A01 CSCL 10B

Several silicon solar cells with and without back surface fields (BSF), having thicknesses of 200 microns and 63 microns were irradiated with 1 MeV protons having fluences between 1 times 10 to the 10th power and 1 times 10 to the 12th power p/square cm. The irradiation was performed using both normal and isotropic incidence on the front as well as back surfaces of the solar cells. The results of the back surface irradiations are analyzed using a model in which irradiation induced defects across the high-low (BSF) junction are considered. It is concluded that degradation of the high-low junction is responsible for the severe performance loss in thinner cells when irradiated from the rear. Author

N87-26438*# National Aeronautics and Space Administration. Lewis Research Center, Cleveland, Ohio.

PERFORMANCE OF ALGAS, GaaS AND INGaaS CELLS AFTER 1 MEV ELECTRON IRRADIATION

HENRY B. CURTIS and RUSSELL E. HART, JR. *In its* Space Photovoltaic Research and Technology 1986. High Efficiency, Space Environment and Array Technology p 223-234 Jun. 1987

Avail: NTIS HC A16/MF A01 CSCL 10B

Electron irradiations were made on three different types of III-V cells. AlGaAs, GaAs, and InGaAs cells with bandgaps of approximately 1.72, 1.43, and 1.1 eV, respectively, were tested. All of the cells were concentrator cells and performance data from one sun to beyond 100x AMO were taken. The total 1 MeV electron fluence was 3 times 10 to the 15th power e/square cm with data taken at several intermediate fluences. Cell performance is presented as a function of electron fluence for various concentration ratios and two different temperatures (25 and 80 C). Since these three cell types are potential candidates for the individual cells in a cascade structure, it is possible to calculate the loss in performance of cascade cells under 1 MeV irradiation. Data are presented which show the calculated performance of both series-connected and separately connected cascade cells. Author

N87-26440*# Spire Corp., Bedford, Mass.

STATUS OF INDIUM PHOSPHIDE SOLAR CELL DEVELOPMENT AT SPIRE

M. B. SPITZER, C. J. KEAVNEY, and S. M. VERNON *In* NASA. Lewis Research Center, Space Photovoltaic Research and Technology 1986. High Efficiency, Space Environment and Array Technology p 247-259 Jun. 1987 (Contract NAS3-24857)

Avail: NTIS HC A16/MF A01 CSCL 10B

On-going development of indium phosphide solar cells for space applications is presented. The development is being carried out with a view towards both high conversion efficiency and simplicity of manufacture. The cell designs comprise the ion-implanted cell, the indium tin oxide top contact cell, and the epitaxial cell grown by metal organic chemical vapor deposition. Modelling data on the limit to the efficiency are presented and comparison is made to measured performance data. Author

N87-26441*# National Aeronautics and Space Administration. Lewis Research Center, Cleveland, Ohio.

COMPARATIVE PERFORMANCE OF DIFFUSED JUNCTION INDIUM PHOSPHIDE SOLAR CELLS

I. WEINBERG, C. K. SWARTZ, R. E. HART, JR., S. K. GHANDHI, J. M. BORREGO, and K. K. PARAT (Rensselaer Polytechnic Inst., Troy, N.Y.) *In its* Space Photovoltaic Research and Technology 1986. High Efficiency, Space Environment and Array Technology p 261-271 Jun. 1987

Avail: NTIS HC A16/MF A01 CSCL 10B

A comparison is made between indium phosphide solar cells whose p-n junctions were processed by open tube capped diffusion, and closed tube uncapped diffusion, of sulfur into Czochralski grown p-type substrates. Air mass zero, total area, efficiencies ranged from 10 to 14.2 percent; the latter value attributed to cells processed by capped diffusion. The radiation resistance of these latter cells was slightly better, under 1 MeV electron irradiation. However, rather than being process dependent, the difference in radiation resistance could be attributed to the effects of increased base dopant concentration. In agreement with previous results, both cells exhibited radiation resistance superior to that of gallium arsenide. The lowest temperature dependency of maximum power was exhibited by the cells prepared by open tube capped diffusion. Contrary to previous results, no correlation was found between open circuit voltage and the temperature dependency of Pmax. It was concluded that additional process optimization was necessary before concluding that one process was better than another. Author

N87-26443*# National Aeronautics and Space Administration. Lewis Research Center, Cleveland, Ohio.

NEAR-OPTIMUM DESIGN OF THE INP HOMOJUNCTION SOLAR CELL

CHANDRA GORADIA, JAMES V. GEIER (Cleveland State Univ., Ohio.), and IRVING WEINBERG *In its* Space Photovoltaic Research and Technology 1986. High Efficiency, Space Environment and Array Technology p 285-293 Jun. 1987

Avail: NTIS HC A16/MF A01 CSCL 10B

Using a fairly comprehensive model, researchers have done a parametric variation study of the InP n+p homojunction solar cell for AMO, 25 C operation. The results of this study are presented. These results indicate that an efficiency of about 25 percent should be realistically possible in a shallow homojunction InP solar cell with near-optimum design. Author

44 ENERGY PRODUCTION AND CONVERSION

N87-26444*# Rensselaer Polytechnic Inst., Troy, N.Y.
SOLAR CELLS IN BULK INP USING AN OPEN TUBE DIFFUSION PROCESS

K. K. PARAT, S. BOTHRA, J. M. BORREGO, and S. K. GHANDHI / *In* NASA. Lewis Research Center, Space Photovoltaic Research and Technology 1986. High Efficiency, Space Environment and Array Technology p 295-300 Jun. 1987 (Contract NAG3-604)

Avail: NTIS HC A16/MF A01 CSCL 10B

A simple open tube diffusion technique for the fabrication of n+p junction solar cells is described. Large area (greater than 0.25 square cm) solar cells have been made by this process with a photovoltaic conversion efficiency of 15.2 percent under simulated AMO illumination. An ideality factor is 1.04 and a saturation current density of 9.6 times 10 to the minus 16th power A/square cm have been observed for these cells. These are the lowest (best) values reported to date for diffused structures in bulk INP.

Author

N87-26452*# National Aeronautics and Space Administration.
Lewis Research Center, Cleveland, Ohio.

HIGH POWER/LARGE AREA PV SYSTEMS

JOSEPH WISE (Air Force Wright Aeronautical Labs., Wright-Patterson AFB, Ohio.) and COSMO BARAONA / *In* its Space Photovoltaic Research and Technology 1986. High Efficiency, Space Environment and Array Technology p 355-359 Jun. 1987

Avail: NTIS HC A16/MF A01 CSCL 10B

The major photovoltaic power system technology drivers for a wide variety of mission types were ranked. Each technology driver was ranked on a scale of high, medium, or low in terms of importance to each particular mission type. The rankings were then compiled to determine the overall importance of each driver over the entire range of space missions. In each case cost was ranked the highest.

Author

N87-26455*# National Aeronautics and Space Administration.
Lewis Research Center, Cleveland, Ohio.

SURFACE PRESSURE MEASUREMENTS ON THE BLADE OF AN OPERATING MOD-2 WIND TURBINE WITH AND WITHOUT VORTEX GENERATORS

TED W. NYLAND Aug. 1987 37 p

(Contract DE-AI01-76ET-20320)

(NASA-TM-89903; E-3595; DOE/NASA/20320-72; NAS 1.15:89903) Avail: NTIS HC A03/MF A01 CSCL 10A

Pressure measurements covering a range of wind velocities were made at one span location on the surface of an operating Mod-2, 2500 kW, wind turbine blade. The data, which were taken with and without vortex generators installed on the leading edge, show the existence of higher pressure coefficients than would be expected from two-dimensional wind tunnel data. These high pressure ratios may be the result of three-dimensional flow over the blade, which delays flow separation. Data are presented showing the repetitiveness of abrupt changes in the pressure distribution that occur as the blade rotates. Calculated values of suction and flap coefficients are also presented.

Author

N87-27324*# International Fuel Cells Corp., South Windsor, Conn.

REGENERATIVE FUEL CELL STUDY FOR SATELLITES IN GEO ORBIT Final Contractor Report

ALEXANDER LEVY, LESLIE L. VANDINE, and JAMES K. STEDMAN Jul. 1987 82 p

(Contract NAS3-22234)

(NASA-CR-179609; NAS 1.26:179609; FCR-8347) Avail: NTIS HC A05/MF A01 CSCL 10B

Summarized are the results of a 12-month study to identify high performance regenerative hydrogen-oxygen fuel cell concepts for geosynchronous satellite application. Emphasis was placed on concepts with the potential for high energy density (W-hr/lb) and passive means for water and heat management to maximize system reliability. Both polymer membrane and alkaline electrolyte fuel cells were considered, with emphasis on the alkaline cell because

of its high performance, advanced state of development, and proven ability to operate in a launch and space environment. Three alkaline system concepts were studied. The first, the integrated design, utilized a configuration in which the fuel cell and electrolysis cells are alternately stacked inside a pressure vessel. Product water is transferred by diffusion during electrolysis and waste heat is conducted through the pressure wall, thus using completely passive means for transfer and control. The second alkaline system, the dedicated design, uses a separate fuel cell and electrolysis stack so that each unit can be optimized in size and weight based on its orbital operating period. The third design was a dual function stack configuration, in which each cell can operate in both fuel cell and electrolysis mode, thus eliminating the need for two separate stacks and associated equipment. Results indicate that using near term technology energy densities between 46 and 52 W-hr/lb can be achieved at efficiencies of 55 percent. System densities of 115 W-hr/lb are contemplated.

Author

N87-27327*# Wichita State Univ., Kans.
PERFORMANCE AND AERODYNAMIC BRAKING OF A HORIZONTAL-AXIS WIND TURBINE FROM SMALL-SCALE WIND TUNNEL TESTS Final Report

H. V. CAO and W. H. WENTZ, JR. Jul. 1987 43 p

(Contract NSG-3277)

(NASA-CR-180812; DOE/NASA/3277-4; NAS 1.26:180812)

Avail: NTIS HC A03/MF A01 CSCL 10A

Wind tunnel tests of three 20' diameter, zero twist, zero pitch wind turbine rotor models were conducted in a 7' x 10' wind tunnel to determine the performance of such rotors with NACA 23024 and NACA 64 sub 3-621 airfoil sections. Aerodynamic braking characteristics of a 38% span, 30% chord, vented aileron configuration were measured on the NACA 23024 rotor. Surface flow patterns were observed using fluorescent mini-tufts attached to the suction side of the rotor blades. Experimental results with and without ailerons are compared to predictions using airfoil section data and a momentum performance code. Results of the performance studies show that the 64 sub 3-621 rotor produces higher peak power than the 23024 rotor for a given rotor speed. Analytical studies, however, indicate that the 23024 should produce higher power. Transition strip experiments show that the 23024 rotor is much more sensitive to roughness than the 64 sub 3-621 rotor. These trends agree with analytical predictions. Results of the aileron test show that this aileron, when deflected, produces a braking torque at all tip speed ratios. In free wheeling coastdowns the rotor blade stopped, then rotated backward at a tip speed ratio of -0.6.

Author

N87-28960# National Aeronautics and Space Administration.
Lewis Research Center, Cleveland, Ohio.

THE SPACE STATION POWER SYSTEM

COSMO R. BARAONA / *In* ESA Proceedings of the Fifth European Symposium on Photovoltaic Generators in Space p 3-11 Nov. 1986

Avail: NTIS HC A21/MF A01

The major requirements and guidelines that affect the NASA Space Station configuration and the power system are explained. The evolution of the Space Station power system from the NASA program development-feasibility phase through the preliminary design phase is described. Early station concepts, both fanciful and feasible, are described and linked to the present concept. The Phase B trade study selections of photovoltaic system technologies are detailed. Solar dynamic and power management and distribution systems are summarized.

ESA

N87-28961# National Aeronautics and Space Administration. Lewis Research Center, Cleveland, Ohio.

ALTERNATIVE POWER GENERATION CONCEPTS FOR SPACE

HENRY W. BRANDHORST, JR., ALBERT J. JUHASZ, and BARBARA I. JONES /In ESA Proceedings of the Fifth European Symposium on Photovoltaic Generators in Space p 13-19 Nov. 1986

Avail: NTIS HC A21/MF A01

Trade and optimization studies that highlight the potential of solar and nuclear dynamic systems relative to photovoltaic power systems are summarized. The solar dynamic case is the LEO Stirling system, while the nuclear system is the SP-100 system goal. Nuclear systems have the potential for the lightest weight, least area, sunlight independent, radiation-durable system. Solar dynamic systems pose a stiff challenge to photovoltaic systems in the midaltitudes because of their insensitivity to the Van Allen radiation belts. While the initial operational capability space station power system is only slightly superior to the SOA PV system, with development focused on the key technologies, advanced solar dynamic systems are fully competitive in LEO midaltitudes with the advanced photovoltaic systems. Advances in energy storage systems (100 Whrs/kg required) are essential. ESA

N87-29018# National Aeronautics and Space Administration. Lewis Research Center, Cleveland, Ohio.

RADIATION DAMAGE IN PROTON IRRADIATED INDIUM PHOSPHIDE SOLAR CELLS

I. WEINBERG, C. K. SWARTZ, R. E. HART, JR., and MASAFUMI YAMAGUCHI (Nippon Telegraph and Telephone Public Corp., Tokai, Japan) /In ESA Proceedings of the Fifth European Symposium on Photovoltaic Generators in Space p 415-420 Nov. 1986

Avail: NTIS HC A21/MF A01

Indium phosphide solar cells exposed to 10 MeV proton irradiations were found to have significantly greater radiation resistance than either GaAs or Si. Performance predictions were obtained for two proton dominated orbits and one in which both protons and electrons were significant cell degradation factors. Array specific power was calculated using lightweight blanket technology, a SEP array structure, and projected cell efficiencies. Results indicate that arrays using fully developed InP cells should out-perform those using GaAs or Si in orbits where radiation is a significant cell degradation factor. ESA

N87-29914*# National Aeronautics and Space Administration. Lewis Research Center, Cleveland, Ohio.

SPACE ELECTROCHEMICAL RESEARCH AND TECHNOLOGY (SERT)

Sep. 1987 364 p Conference held in Cleveland, Ohio, 14-16 Apr. 1987

(NASA-CP-2484; E-3506; NAS 1.55:2484) Avail: NTIS HC A16/MF A01 CSCL 10C

The conference provided a forum to assess critical needs and technologies for the NASA electrochemical energy conversion and storage program. It was aimed at providing guidance to NASA on the appropriate direction and emphasis of that program. A series of related overviews were presented in the areas of NASA advanced mission models (space stations, low and geosynchronous Earth orbit missions, planetary missions, and space transportation). Papers were presented and workshops conducted in a variety of technical areas, including advanced rechargeables, advanced concepts, critical physical electrochemical issues, and modeling.

N87-29920*# Hughes Research Labs., Malibu, Calif.

KOH CONCENTRATION EFFECT ON CYCLE LIFE OF NICKEL-HYDROGEN CELLS

HONG S. LIM and S. A. VERZWYVELT /In NASA-Lewis Research Center, Space Electrochemical Research and Technology (SERT) p 29-39 Sep. 1987 Submitted for publication (Contract NAS3-22238)

Avail: NTIS HC A16/MF A01 CSCL 10C

A cycle life test of Ni/H₂ cells containing electrolytes of various KOH concentrations and a sintered type nickel electrode was carried out at 23 C using a 45 min accelerated low Earth orbit (LEO) cycle regime at 80 percent depth of discharge. One of three cells containing 26 percent KOH has achieved over 28,000 cycles, and the other two 19,000 cycles, without a sign of failure. Two other cells containing 31 percent KOH electrolyte, which is the concentration presently used in aerospace cells, failed after 2,979 and 3,620 cycles. This result indicates that the cycle life of the present type of Ni/H₂ cells may be extended by a factor of 5 to 10 simply by lowering the KOH concentration. Long cycle life of a Ni/H₂ battery at high depth-of-discharge operation is desired, particularly for an LEO spacecraft application. Typically, battery life of about 30,000 cycles is required for a five year mission in an LEO. Such a cycle life with presently available cells can be assured only at a very low depth-of-discharge operation. Results of testing already show that the cycle life of an Ni/H₂ cell is tremendously improved by simply using an electrolyte of low KOH concentration. Author

N87-29940*# Giner, Inc., Waltham, Mass.

OXYGEN ELECTRODES FOR RECHARGEABLE ALKALINE FUEL CELLS

LARRY SWETTE and JOSE GINER /In NASA-Lewis Research Center, Space Electrochemical Research and Technology (SERT) p 237-244 Sep. 1987

(Contract NAS3-24635)

Avail: NTIS HC A16/MF A01 CSCL 10C

Electrocatalysts and supports for the positive electrode of moderate temperature single unit rechargeable alkaline fuel cells were investigated and developed. The electrocatalysts are defined as the material with a higher activity for the oxygen electrode reaction than the support. Advanced development will require that the materials be prepared in high surface area forms, and may also entail integration of various candidate materials. Eight candidate support materials and seven electrocatalysts were investigated. Of the 8 support, 3 materials meet the preliminary requirements in terms of electrical conductivity and stability. Emphasis is now on preparing in high surface area form and testing under more severe corrosion stress conditions. Of the 7 electrocatalysts prepared and evaluated, at least 5 materials remain as potential candidates. The major emphasis remains on preparation, physical characterization and electrochemical performance testing. Author

N87-29945*# Case Western Reserve Univ., Cleveland, Ohio. Dept. of Chemical Engineering.

THEORETICAL PERFORMANCE OF HYDROGEN-BROMINE RECHARGEABLE SPE FUEL CELL

ROBERT F. SAVINELL and S. D. FRITTS /In NASA-Lewis Research Center, Space Electrochemical Research and Technology (SERT) p 321-340 Sep. 1987

(Contract NAG3-500; NSF CPE-83-51849)

Avail: NTIS HC A16/MF A01 CSCL 10C

A mathematical model was formulated to describe the performance of a hydrogen-bromine fuel cell. Porous electrode theory was applied to the carbon felt flow-by electrode and was coupled to theory describing the solid polymer electrolyte (SPE) system. Parametric studies using the numerical solution to this model were performed to determine the effect of kinetic, mass transfer, and design parameters on the performance of the fuel cell. The results indicate that the cell performance is most sensitive to the transport properties of the SPE membrane. The model was also shown to be a useful tool for scale-up studies. Author

N87-29956* # National Aeronautics and Space Administration. Lewis Research Center, Cleveland, Ohio.

PERFORMANCE AND POWER REGULATION CHARACTERISTICS OF TWO AILERON-CONTROLLED ROTORS AND A PITCHABLE TIP-CONTROLLED ROTOR ON THE MOD-0 TURBINE Final Report

ROBERT D. CORRIGAN, CLINTON B. F. ENSWORTH, III, and DEAN R. MILLER Oct. 1987 21 p
(Contract DE-A101-76ET-20320)

(NASA-TM-100136; DOE/NASA/20320-73; E-3686; NAS 1.15:100136) Avail: NTIS HC A02/MF A01 CSCL 10B

Tests were conducted on the DOE/NASA mod-0 horizontal axis wind turbine to compare and evaluate the performance and the power regulation characteristics of two aileron-controlled rotors and a pitchable tip-controlled rotor. The two aileron-controlled rotor configurations used 20 and 38 percent chord ailerons, while the tip-controlled rotor had a pitchable blade tip. The ability of the control surfaces to regulate power was determined by measuring the change in power caused by an incremental change in the deflection angle of the control surface. The data shows that the change in power per degree of deflection angle for the tip-controlled rotor was four times the corresponding value for the 2-percent chord ailerons. The root mean square power deviation about a power setpoint was highest for the 20 percent chord aileron, and lowest for the 38 percent chord aileron. Author

N87-29957* # Illinois Univ., Urbana-Champaign.

COMPUTER MODELLING OF ALUMINUM-GALLIUM ARSENIDE/GALLIUM ARSENIDE MULTILAYER PHOTOVOLTAICS M.S. Thesis

MICHAEL BRODERICK WAGNER 1987 39 p

(Contract NAG3-507)

(NASA-CR-181418; NAS 1.26:181418) Avail: NTIS HC A03/MF A01 CSCL 10A

The modeled cascade cells offer an alternative to conventional series cascade designs that require a monolithic intercell ohmic contact. Selective electrodes provide a simple means of fabricating three-terminal devices, which can be configured in complementary pairs to circumvent the attendant losses and fabrication complexities of intercell ohmic contacts. Moreover, selective electrodes allow incorporation of additional layers in the upper subcell which can improve spectral response and increase radiation tolerance. Realistic simulations of such cells operating under one-sun AMO conditions show that the seven-layer structure is optimum from the standpoint of beginning-of-life efficiency and radiation tolerance. Projected efficiencies exceed 26 percent. Under higher concentration factors, it should be possible to achieve efficiencies beyond 30 percent. However, to simulate operation at high concentration will require a model for resistive losses. Overall, these devices appear to be a promising contender for future space applications. Author

N87-29958* # Illinois Univ., Urbana-Champaign. Dept. of Electrical and Computer Engineering.

MODELLING OF MULTIJUNCTION CASCADE PHOTOVOLTAICS FOR SPACE APPLICATIONS M.S. Thesis, 1988

JAMES LOUIS EDUCATO 1987 42 p

(Contract NAG3-507)

(NASA-CR-181417; NAS 1.26:181417) Avail: NTIS HC A03/MF A01 CSCL 10A

An alternative class of photovoltaics was presented, which is designed to overcome two problem areas with conventional cascade designs: poor upper subcell performance and lossy intercell ohmic contact (IOC). It was shown that upper subcell quality can be improved by incorporating additional junctions into the upper subcell and that the problems with monolithic IOCs may be circumvented by using complementary pairs of three-terminal cells or a 1 x 2 voltage-matched configuration. Realistic simulations show that AlGaAs-GaAs and AlGaAs-InGaAs multijunction, multiband-gap solar cells (MJSC) may achieve beginning-of-life (BOL) one-sun, AMO efficiencies of 26 and 28 percent, respectively. Complementary cells made in the AlGaAs-InGaAs system can achieve BOL one-sun AMO efficiencies

in excess of 27 percent. Seven-layer MJSCs are most advantageous for space applications due to their superior tolerance to radiation degradation. Author

GEOPHYSICS

Includes aeronomy; upper and lower atmosphere studies; ionospheric and magnetospheric physics; and geomagnetism.

A87-24672* Iowa Univ., Iowa City.

MEASUREMENTS OF PLASMA PARAMETERS IN THE VICINITY OF THE SPACE SHUTTLE

G. MURPHY, J. PICKETT, N. DANGELO, and W. S. KURTH (Iowa, University, Iowa City) Planetary and Space Science (ISSN 0032-0633), vol. 34, Oct. 1986, p. 993-1004. refs
(Contract NAG3-449; NAS8-32807)

A Langmuir probe flown as part of the Plasma Diagnostics Package aboard the third Space Shuttle flight was used to determine electron densities, temperatures, and plasma potential in the vicinity of the Shuttle Orbiter. Measurements taken both in the cargo bay and 10 m above the cargo bay on the Remote Manipulator System arm are consistent with small satellite and laboratory results, in that reduced densities and elevated temperatures are observed in the Shuttle wake. The primary difference in the Shuttle measurements is one of magnitude; i.e., orders-of-magnitude density decreases and factor-of-five temperature enhancements. Analysis of data taken in (Delta N)/N turbulence can be as high as a few percent, and the most intense turbulence seems to occur near regions with a steep gradient in plasma pressure. Author

A87-31322* California Univ., La Jolla.

THE DYNAMIC BEHAVIOR OF PLASMAS OBSERVED NEAR GEOSYNCHRONOUS ORBIT

C. E. MCILWAIN and E. C. WHIPPLE (California, University, La Jolla) IEEE Transactions on Plasma Science (ISSN 0093-3813), vol. PS-14, Dec. 1986, p. 874-890. refs
(Contract NGL-05-005-007; NSG-3150; NSG-7623; NSF INT-82-19963; NSF ATM-83-08366; NAS5-21055; NAS8-33982; F04701-77-C-0062)

The behavior of plasmas observed by the ATS-6, ATS-5, and SCATHA spacecraft in the vicinity of synchronous orbit in the earth's magnetosphere is investigated. Two predominant features noted are the sudden appearance of injections, and the presence of marked magnetic field-aligned structure. Injections are geosynchronous manifestations of the global acceleration process producing the aurora. Field-aligned fluxes can be as much as two orders of magnitude larger than perpendicular fluxes, and ions and electrons often display different field-aligned structure which changes with energy, suggesting field-aligned acceleration processes. Other observed phenomena include particle and field wave activity, and various kinds of plasma heating. Spacecraft charging events illustrate the effects of the hot magnetospheric plasma on material objects. R.R.

A87-51713* Maxwell Labs., Inc., San Diego, Calif.

RAM ION SCATTERING CAUSED BY SPACE SHUTTLE V x B INDUCED DIFFERENTIAL CHARGING

I. KATZ and V. A. DAVIS (Maxwell Laboratories, Inc., S-Cubed Div., La Jolla, CA) Journal of Geophysical Research (ISSN 0148-0227), vol. 92, Aug. 1, 1987, p. 8787-8791. refs
(Contract NAS3-23881)

Observations of secondary, high-inclination ions streams have been reported in the literature. The authors of these previous papers attributed the source of the secondary ions to a disturbed region in the plasma about 10 m from the Space Shuttle Orbiter. A new theory has been developed which shows how $v \times B$ induced differential charging on the plasma diagnostics package (PDP) can

scatter the ram ion flux. Some of these ions are reflected back to the PDP and may be the source of the observed ion distributions. The effect is unique to large spacecraft; it occurs only when the magnitude of the induced $v \times B$ potentials are much larger than the electron thermal energy and of the order of the ion ram energy. That the ion streams observed at large angles must have been reflected from the PDP surface is demonstrated with three-dimensional sheath and particle trajectory calculations using the low earth orbit version of the NASA Charging Analyzer Program (NASCAP/LEO).
Author

60

COMPUTER OPERATIONS AND HARDWARE

Includes hardware for computer graphics, firmware, and data processing.

A87-11895* Cornell Univ., Ithaca, N.Y.

TOWARDS EFFECTIVE INTERACTIVE THREE-DIMENSIONAL COLOUR POSTPROCESSING

B. C. BAILEY, J. F. HAJJAR, and J. F. ABEL (Cornell University, Ithaca, NY) Engineering Computations (ISSN 0264-4401), vol. 3, June 1986, p. 90-98. refs
(Contract NAG3-395)

Recommendations for the development of effective three-dimensional, graphical color postprocessing are made. First, the evaluation of large, complex numerical models demands that a postprocessor be highly interactive. A menu of available functions should be provided and these operations should be performed quickly so that a sense of continuity and spontaneity exists during the post-processing session. Second, an agenda for three-dimensional color postprocessing is proposed. A postprocessor must be versatile with respect to application and basic algorithms must be designed so that they are flexible. A complete selection of tools is necessary to allow arbitrary specification of views, extraction of qualitative information, and access to detailed quantitative and problem information. Finally, full use of advanced display hardware is necessary if interactivity is to be maximized and effective postprocessing of today's numerical simulations is to be achieved.
Author

A87-45512* Motorola, Inc., Phoenix, Ariz.

ACTS BASEBAND PROCESSING

RICHARD L. MOAT (Motorola, Inc., Government Electronics Group, Chandler, AZ) IN: GLOBECOM '86 - Global Telecommunications Conference, Houston, TX, Dec. 1-4, 1986, Conference Record. Volume 1. New York, Institute of Electrical and Electronics Engineers, Inc., 1986, p. 578-583. refs
(Contract NAS3-23790)

The baseband processor designed for NASA's ACTS experimental system operating in Ka band is described. The ACTS baseband processor facilitates the interconnection necessary to support scanning spot beam low bit rate communications. The dynamic reconfiguration of message routing and the individual application of forward correction coding to overcome localized rain fading are among the processors many advantages. Preliminary hardware testing results are reviewed.
K.K.

61

COMPUTER PROGRAMMING AND SOFTWARE

Includes computer programs, routines, and algorithms, and specific applications, e.g., CAD/CAM.

A87-18499* Akron Univ., Ohio.

ON THE SYMBOLIC MANIPULATION AND CODE GENERATION FOR ELASTO-PLASTIC MATERIAL MATRICES

T. Y. CHANG, A. F. SALEEB (Akron, University, OH), P. S. WANG, and H. Q. TAN (Kent State University, OH) Engineering with Computers (ISSN 0177-0667), vol. 1, no. 4, 1986, p. 205-215. refs
(Contract NAG3-307; NAG3-298)

A computerized procedure for symbolic manipulations and FORTRAN code generation of elastoplastic material matrix for finite element applications is presented. Special emphasis is placed on expression simplifications during intermediate derivations, optimal code generation, and interface with the main program. A systematic procedure is outlined to avoid redundant algebraic manipulations. Symbolic expressions of the derived material stiffness matrix are automatically converted to RATFOR code which is then translated into FORTRAN statements through a preprocessor. To minimize the interface problem with the main program, a template file is prepared so that the translated FORTRAN statements can be merged into the file to form a subroutine (or a submodule). Three constitutive models; namely, von Mises plasticity, the Drucker-Prager model, and a concrete plasticity model, are used as illustrative examples.
Author

A87-33614*# University of Western Michigan, Kalamazoo.

OPTIMIZATION AND ANALYSIS OF GAS TURBINE ENGINE BLADES

D. J. VANDENBRINK (Western Michigan University, Kalamazoo, MI) and D. A. HOPKINS (NASA, Lewis Research Center, Cleveland, OH) IN: Structures, Structural Dynamics and Materials Conference, 28th, Monterey, CA, Apr. 6-8, 1987, Technical Papers. Part 1. New York, American Institute of Aeronautics and Astronautics, 1987, p. 535-537. refs
(AIAA PAPER 87-0827)

A gas turbine engine blade design is optimized using STAEBL. To validate the STAEBL analysis, the optimized blade design is analyzed using MARC, MHOST and BEST3D. The results show good agreement between STAEBL, MARC, and MHOST. The conclusion is that STAEBL can be used to optimize an engine blade design.
Author

A87-35718* Arizona State Univ., Tempe.

A HYBRID NONLINEAR PROGRAMMING METHOD FOR DESIGN OPTIMIZATION

S. D. RAJAN (Arizona State University, Tempe) Journal of Structural Mechanics (ISSN 0360-1218), vol. 14, no. 4, 1986, p. 455-474. refs
(Contract NAG3-580)

Solutions to engineering design problems formulated as nonlinear programming (NLP) problems usually require the use of more than one optimization technique. Moreover, the interaction between the user (analysis/synthesis) program and the NLP system can lead to interface, scaling, or convergence problems. An NLP solution system is presented that seeks to solve these problems by providing a programming system to ease the user-system interface. A simple set of rules is used to select an optimization technique or to switch from one technique to another in an attempt to detect, diagnose, and solve some potential problems. Numerical examples involving finite element based optimal design of space trusses and rotor bearing systems are used to illustrate the applicability of the proposed methodology.
Author

A87-45900* Cornell Univ., Ithaca, N.Y.

INTERACTIVE GRAPHICS AND ANALYSIS ACCURACY

J. F. ABEL, M. J. PANTHAKI, and P. A. WAWRZYNEK (Cornell University, Ithaca, NY) IN: Reliability of Methods for Engineering Analysis; Proceedings of the International Conference, Swansea, Wales, June 9-11, 1986. Swansea, Wales, Pineridge Press, 1986, p. 305-318. Research sponsored by the Grumman Corp. refs (Contract NAG3-395; NSF ATM-83-51914)

An important objective of graphical finite element postprocessing is the facility to indicate to the engineer the accuracy of analysis results. The inclusion of mesh quality sensors permits a subjective evaluation of the adequacy of a single analysis being interpreted. For graphical approaches, both strain energy density gradients and discontinuities of unsmoothed responses and their gradients have proved to be effective sensors. Graphical tools which can display discontinuity information effectively are described; these are essentially different from the ordinary methods used for the viewing of smoothed results. Author

A87-52534*# National Aeronautics and Space Administration. Lewis Research Center, Cleveland, Ohio.

MATHEMATICAL MODEL PARTITIONING AND PACKING FOR PARALLEL COMPUTER CALCULATION

DALE J. ARPASI and EDWARD J. MILNER (NASA, Lewis Research Center, Cleveland, OH) IN: 1986 International Conference on Parallel Processing, University Park, PA, Aug. 19-22, 1986, Proceedings. Washington, DC, IEEE Computer Society Press, 1986, p. 67-74. refs

This paper deals with the development of multiprocessor simulations from a serial set of ordinary differential equations describing a physical system. The identification of computational parallelism within the model equations is discussed. A technique is presented for identifying this parallelism and for partitioning the equations for parallel solution on a multiprocessor. Next, an algorithm which packs the equations into a minimum number of processors is described. The results of applying the packing algorithm to a turboshaft engine model are presented. Author

A87-52541*# National Aeronautics and Space Administration. Lewis Research Center, Cleveland, Ohio.

INCREASING PROCESSOR UTILIZATION DURING PARALLEL COMPUTATION RUNDOWN

WILLIAM H. JONES (NASA, Lewis Research Center, Cleveland, OH) IN: 1986 International Conference on Parallel Processing, University Park, PA, Aug. 19-22, 1986, Proceedings. Washington, DC, IEEE Computer Society Press, 1986, p. 139-144. Previously announced in STAR as N86-26914.

Some parallel processing environments provide for asynchronous execution and completion of general purpose parallel computations from a single computational phase. When all the computations from such a phase are complete, a new parallel computational phase is begun. Depending upon the granularity of the parallel computations to be performed, there may be a shortage of available work as a particular computational phase draws to a close (computational rundown). This can result in the waste of computing resources and the delay of the overall problem. In many practical instances, strict sequential ordering of phases of parallel computation is not totally required. In such cases, the beginning of one phase can be correctly computed before the end of a previous phase is completed. This allows additional work to be generated somewhat earlier to keep computing resources busy during each computational rundown. The conditions under which this can occur are identified and the frequency of occurrence of such overlapping in an actual parallel Navier-Stokes code is reported. A language construct is suggested and possible control strategies for the management of such computational phase overlapping are discussed. Author

N87-14872*# Ohio State Univ., Columbus. ElectroScience Lab. **ALTERNATIVE MATHEMATICAL PROGRAMMING FORMULATIONS FOR FSS SYNTHESIS**

C. H. REILLY, C. A. MOUNT-CAMPBELL, D. J. A. GONSALVEZ, and C. A. LEVIS Oct. 1986 35 p

(Contract NAG3-159)
(NASA-CR-180030; NAS 1.26:180030; TR-716548-6) Avail: NTIS HC A03/MF A01 CSCL 09B

A variety of mathematical programming models and two solution strategies are suggested for the problem of allocating orbital positions to (synthesizing) satellites in the Fixed Satellite Service. Mixed integer programming and almost linear programming formulations are presented in detail for each of two objectives: (1) positioning satellites as closely as possible to specified desired locations, and (2) minimizing the total length of the geostationary arc allocated to the satellites whose positions are to be determined. Computational results for mixed integer and almost linear programming models, with the objective of positioning satellites as closely as possible to their desired locations, are reported for three six-administration test problems and a thirteen-administration test problem. Author

N87-17441*# National Aeronautics and Space Administration. Lewis Research Center, Cleveland, Ohio.

A COMPARISON OF FIVE BENCHMARKS

JANICE E. HUSS and JAMES A. PENNLINE Feb. 1987 15 p
(NASA-TM-88956; E-3411; NAS 1.15:88956) Avail: NTIS HC A02/MF A01 CSCL 09B

Five benchmark programs were obtained and run on the NASA Lewis CRAY X-MP/24. A comparison was made between the programs codes and between the methods for calculating performance figures. Several multitasking jobs were run to gain experience in how parallel performance is measured. Author

N87-18997*# Cornell Univ., Ithaca, N.Y.

COLOR POSTPROCESSING FOR 3-DIMENSIONAL FINITE ELEMENT MESH QUALITY EVALUATION AND EVOLVING GRAPHICAL WORKSTATION

MALCOLM J. PANTHAKI Mar. 1987 188 p Original document contains color illustrations

(Contract NAG3-395)
(NASA-CR-180215; NAS 1.26:180215; PCG-REPT-87-1) Avail: NTIS HC A09/MF A01 CSCL 09B

Three general tasks on general-purpose, interactive color graphics postprocessing for three-dimensional computational mechanics were accomplished. First, the existing program (POSTPRO3D) is ported to a high-resolution device. In the course of this transfer, numerous enhancements are implemented in the program. The performance of the hardware was evaluated from the point of view of engineering postprocessing, and the characteristics of future hardware were discussed. Second, interactive graphical tools implemented to facilitate qualitative mesh evaluation from a single analysis. The literature was surveyed and a bibliography compiled. Qualitative mesh sensors were examined, and the use of two-dimensional plots of unaveraged responses on the surface of three-dimensional continua was emphasized in an interactive color raster graphics environment. Finally, a postprocessing environment was designed for state-of-the-art workstation technology. Modularity, personalization of the environment, integration of the engineering design processes, and the development and use of high-level graphics tools are some of the features of the intended environment. Author

N87-18998*# Cornell Univ., Ithaca, N.Y.

UNIFICATION OF COLOR POSTPROCESSING TECHNIQUES FOR 3-DIMENSIONAL COMPUTATIONAL MECHANICS

BRUCE CHARLES BAILEY Aug. 1985 143 p

(Contract NAG3-395)
(NASA-CR-180214; NAS 1.26:180214; PCG-REPT-85-1) Avail: NTIS HC A07/MF A01 CSCL 09B

To facilitate the understanding of complex three-dimensional numerical models, advanced interactive color postprocessing techniques are introduced. These techniques are sufficiently flexible

so that postprocessing difficulties arising from model size, geometric complexity, response variation, and analysis type can be adequately overcome. Finite element, finite difference, and boundary element models may be evaluated with the prototype postprocessor. Elements may be removed from parent models to be studied as independent subobjects. Discontinuous responses may be contoured including responses which become singular, and nonlinear color scales may be input by the user for the enhancement of the contouring operation. Hit testing can be performed to extract precise geometric, response, mesh, or material information from the database. In addition, stress intensity factors may be contoured along the crack front of a fracture model. Stepwise analyses can be studied, and the user can recontour responses repeatedly, as if he were paging through the response sets. As a system, these tools allow effective interpretation of complex analysis results. Author

N87-19002* National Aeronautics and Space Administration. Lewis Research Center, Cleveland, Ohio.

AUTOMATING THE PARALLEL PROCESSING OF FLUID AND STRUCTURAL DYNAMICS CALCULATIONS

DALE J. ARPASI and GARY L. COLE 1987 11 p Prepared for presentation at the Summer Computer Simulation Conference, Montreal, Quebec, 27-30 Jul., 1987; sponsored by the Society for Computer Simulation (NASA-TM-89837; E-3494; NAS 1.15:89837) Avail: NTIS HC A02/MF A01 CSCL 09B

The NASA Lewis Research Center is actively involved in the development of expert system technology to assist users in applying parallel processing to computational fluid and structural dynamic analysis. The goal of this effort is to eliminate the necessity for the physical scientist to become a computer scientist in order to effectively use the computer as a research tool. Programming and operating software utilities have previously been developed to solve systems of ordinary nonlinear differential equations on parallel scalar processors. Current efforts are aimed at extending these capabilities to systems of partial differential equations, that describe the complex behavior of fluids and structures within aerospace propulsion systems. This paper presents some important considerations in the redesign, in particular, the need for algorithms and software utilities that can automatically identify data flow patterns in the application program and partition and allocate calculations to the parallel processors. A library-oriented multiprocessing concept for integrating the hardware and software functions is described. Author

N87-20766* National Aeronautics and Space Administration. Lewis Research Center, Cleveland, Ohio.

TIME-PARTITIONING SIMULATION MODELS FOR CALCULATION ON PARALLEL COMPUTERS

EDWARD J. MILNER, RICHARD A. BLECH, and RODRICK V. CHIMA 1987 15 p Proposed for presentation at the 1987 Summer Computer Simulation Conference, Montreal, Quebec, 27-30 Jul. 1987; sponsored by the Society for Computer Simulation (NASA-TM-89850; E-3517; NAS 1.15:89850) Avail: NTIS HC A02/MF A01 CSCL 09B

A technique allowing time-staggered solution of partial differential equations is presented in this report. Using this technique, called time-partitioning, simulation execution speedup is proportional to the number of processors used because all processors operate simultaneously, with each updating of the solution grid at a different time point. The technique is limited by neither the number of processors available nor by the dimension of the solution grid. Time-partitioning was used to obtain the flow pattern through a cascade of airfoils, modeled by the Euler partial differential equations. An execution speedup factor of 1.77 was achieved using a two processor Cray X-MP/24 computer. Author

N87-22422* Cornell Univ., Ithaca, N.Y. Program of Computer Graphics.

INTERACTIVE COLOR DISPLAY OF 3-D ENGINEERING ANALYSIS RESULTS Final Technical Report, 1 Mar. 1983 - 28 Feb. 1987

JOHN F. ABEL, ANTHONY R. INGRAFFEA, and DONALD P. GREENBERG 28 May 1987 6 p (Contract NAG3-395) (NASA-CR-180589; NAS 1.26:180589) Avail: NTIS HC A02/MF A01 CSCL 09B

A general approach to three-dimensional postprocessing of engineering analyses is presented. The approach is versatile and may handle the results from a wide range of engineering analysis methods which involve the discretization of continua. To facilitate the understanding of complex three-dimensional numerical models, advanced interactive color postprocessing techniques are introduced. Finite element, finite difference, and boundary element models are evaluated with the prototype postprocessor. The existing color graphics program (POSTPRO3D) was ported to a high-resolution device. Interactive graphic tools were implemented to facilitate qualitative mesh evaluation from a single analysis. A postprocessing environment was design for workstation technology. B.G.

62

COMPUTER SYSTEMS

Includes computer networks and special application computer systems.

A87-53631* Duke Univ., Durham, N. C.

EXTRAPOLATION METHODS FOR VECTOR SEQUENCES

DAVID A. SMITH (Duke University, Durham, NC), WILLIAM F. FORD (NASA, Lewis Research Center, Cleveland, OH), and AVRAM SIDI (Technion - Israel Institute of Technology, Haifa) SIAM Review (ISSN 0036-1445), vol. 29, June 1987, p. 199-233. refs (Contract NSG-3160)

This paper derives, describes, and compares five extrapolation methods for accelerating convergence of vector sequences or transforming divergent vector sequences to convergent ones. These methods are the scalar epsilon algorithm (SEA), vector epsilon algorithm (VEA), topological epsilon algorithm (TEA), minimal polynomial extrapolation (MPE), and reduced rank extrapolation (RRE). MPE and RRE are first derived and proven to give the exact solution for the right 'essential degree' k . Then, Brezinski's (1975) generalization of the Shanks-Schmidt transform is presented; the generalized form leads from systems of equations to TEA. The necessary connections are then made with SEA and VEA. The algorithms are extended to the nonlinear case by cycling, the error analysis for MPE and VEA is sketched, and the theoretical support for quadratic convergence is discussed. Strategies for practical implementation of the methods are considered. C.D.

N87-20767* National Aeronautics and Space Administration. Lewis Research Center, Cleveland, Ohio.

THE HYPERCLUSTER: A PARALLEL PROCESSING TEST-BED ARCHITECTURE FOR COMPUTATIONAL MECHANICS APPLICATIONS

RICHARD A. BLECH 1987 11 p Proposed for presentation at the Summer Computer Simulation Conference, Montreal, Canada, 27-30 Jul. 1987; sponsored by the Society for Computer Simulation (NASA-TM-89823; E-3469; NAS 1.15:89823) Avail: NTIS HC A02/MF A01 CSCL 09B

The development of numerical methods and software tools for parallel processors can be aided through the use of a hardware test-bed. The test-bed architecture must be flexible enough to support investigations into architecture-algorithm interactions. One way to implement a test-bed is to use a commercial parallel

processor. Unfortunately, most commercial parallel processors are fixed in their interconnection and/or processor architecture. In this paper, we describe a modified n cube architecture, called the hypercluster, which is a superset of many other processor and interconnection architectures. The hypercluster is intended to support research into parallel processing of computational fluid and structural mechanics problems which may require a number of different architectural configurations. An example of how a typical partial differential equation solution algorithm maps on to the hypercluster is given. Author

N87-23202*# National Aeronautics and Space Administration. Lewis Research Center, Cleveland, Ohio.

APPLICATIONS AND REQUIREMENTS FOR REAL-TIME SIMULATORS IN GROUND-TEST FACILITIES

DALE J. ARPASI and RICHARD A. BLECH Dec. 1986 26 p (NASA-TP-2672; E-3189; NAS 1.60:2672) Avail: NTIS HC A03/MF A01 CSCL 09B

This report relates simulator functions and capabilities to the operation of ground test facilities, in general. The potential benefits of having a simulator are described to aid in the selection of desired applications for a specific facility. Configuration options for integrating a simulator into the facility control system are discussed, and a logical approach to configuration selection based on desired applications is presented. The functional and data path requirements to support selected applications and configurations are defined. Finally, practical considerations for implementation (i.e., available hardware and costs) are discussed. Author

64

NUMERICAL ANALYSIS

Includes iteration, difference equations, and numerical approximation.

A87-21968* National Aeronautics and Space Administration. Lewis Research Center, Cleveland, Ohio.

SOLUTION OF ELLIPTIC PDES BY FAST POISSON SOLVERS USING A LOCAL RELAXATION FACTOR

SIN-CHUNG CHANG (NASA, Lewis Research Center, Cleveland, OH) Journal of Computational Physics (ISSN 0021-9991), vol. 67, Nov. 1986, p. 91-123. refs

A large class of two- and three-dimensional, nonseparable elliptic partial differential equations (PDEs) is presently solved by means of novel one-step (D'Yakanov-Gunn) and two-step (accelerated one-step) iterative procedures, using a local, discrete Fourier analysis. In addition to being easily implemented and applicable to a variety of boundary conditions, these procedures are found to be computationally efficient on the basis of the results of numerical comparison with other established methods, which lack the present one's: (1) insensitivity to grid cell size and aspect ratio, and (2) ease of convergence rate estimation by means of the coefficient of the PDE being solved. The two-step procedure is numerically demonstrated to outperform the one-step procedure in the case of PDEs with variable coefficients. O.C.

A87-35575* National Aeronautics and Space Administration. Lewis Research Center, Cleveland, Ohio.

EXTRAPOLATION METHODS FOR DIVERGENT OSCILLATORY INFINITE INTEGRALS THAT ARE DEFINED IN THE SENSE OF SUMMABILITY

AVRAM SIDI (NASA, Lewis Research Center, Cleveland, OH; Technion Israel Institute of Technology, Haifa) Journal of Computational and Applied Mathematics (ISSN 0377-0427), vol. 17, Feb. 1987, p. 105-114. Research supported by the Technion - Israel Institute of Technology. refs

In a recent work by the author an extrapolation method, the W-transformation, was developed, by which a large class of oscillatory infinite integrals can be computed very efficiently. The

results of this work are extended to a class of divergent oscillatory infinite integrals in the present paper. It is shown in particular that these divergent integrals exist in the sense of Abel summability and that the W-transformation can be applied to them without any modifications. Convergence results are stated and numerical examples given. Author

A87-41239*# Texas Univ., Austin.

RECENT ADVANCES IN ERROR ESTIMATION AND ADAPTIVE IMPROVEMENT OF FINITE ELEMENT CALCULATIONS

J. T. ODEN, T. STROUBOULIS, PH. DEVLOO, and M. HOWE (Texas, University, Austin) IN: Computational mechanics - Advances and trends; Proceedings of the Session - Future Directions of Computational Mechanics of the ASME Winter Annual Meeting, Anaheim, CA, Dec. 7-12, 1986. New York, American Society of Mechanical Engineers, 1986, p. 369-410. refs (Contract N00014-84-K-0409; NAS3-24849; NAS8-36647)

Recent advances in adaptive finite elements are summarized. General concepts behind a posteriori error estimation, h-method data management, and algorithms for fluid-mechanics applications are then examined, and some results of numerical experiments with new adaptive codes are given. Numerical examples include supersonic flow over a 20-deg ramp, supersonic flow in expansion corners, the reflecting-shock problem, and the rotating-cone problem. Finally, future directions of research in the field are outlined. V.L.

A87-42069*# National Aeronautics and Space Administration. Lewis Research Center, Cleveland, Ohio.

ON THE VALIDITY OF THE MODIFIED EQUATION APPROACH TO THE STABILITY ANALYSIS OF FINITE-DIFFERENCE METHODS

SIN-CHUNG CHANG (NASA, Lewis Research Center, Cleveland, OH) IN: Computational Fluid Dynamics Conference, 8th, Honolulu, HI, June 9-11, 1987, Technical Papers. New York, American Institute of Aeronautics and Astronautics, 1987, p. 210-229. refs (AIAA PAPER 87-1120)

The validity of the modified equation stability analysis introduced by Warming and Hyett was investigated. It is shown that the procedure used in the derivation of the modified equation is flawed and generally leads to invalid results. Moreover, the interpretation of the modified equation as the exact partial differential equation solved by a finite-difference method generally cannot be justified even if spatial periodicity is assumed. For a two-level scheme, due to a series of mathematical quirks, the connection between the modified equation approach and the von Neuman method established by Warming and Hyett turns out to be correct despite its questionable original derivation. However, this connection is only partially valid for a scheme involving more than two time levels. In the von Neumann analysis, the complex error multiplication factor associated with a wave number generally has (L-1) roots for an L-level scheme. It is shown that the modified equation provides information about only one of these roots. Author

A87-49821* Los Alamos National Lab., N. Mex.

SOME PLANE CURVATURE APPROXIMATIONS

R. C. MJOLNESS and BLAIR SWARTZ (Los Alamos National Laboratory, NM) Mathematics of Computation (ISSN 0025-5718), vol. 49, July 1987, p. 215-230. refs (Contract NASA ORDER C-67846-D; W-7405-ENG-36)

An analytical technique is developed to estimate (with second-order accuracy) the curvature of a sufficiently smooth plane curve defined in finite form. The derivation of the approximations from local information is explained in detail; the continuity and invariance of the estimates under translation and rotation are demonstrated; and examples, error estimates, and a broken-line extension are presented. The suitability of the present technique for computer implementation is indicated. T.K.

A87-52865* National Aeronautics and Space Administration. Lewis Research Center, Cleveland, Ohio.

MULTIGRID-SINC METHODS

STEVE SCHAFFER (NASA, Lewis Research Center, Cleveland, OH) and FRANK STENGER (Utah, University, Salt Lake City) (USAF and Gesellschaft fuer Mathematik und Datenverarbeitung, Copper Mountain Conference on Multigrid Methods, 2nd, Copper Mountain, CO, Mar. 31-Apr. 3, 1985) Applied Mathematics and Computation (ISSN 0096-3003), vol. 19, July 1986, p. 311-319. refs

A Galerkin method using Whittaker cardinal or 'sinc' functions as basis functions is described for the solution of boundary-value problems. When the solution is analytic in the interior of the domain, the error of approximation using $2N + 1$ points is $O(e^{-\gamma \sqrt{N}})$ even if derivatives of the solution are singular at the boundaries. A multigrid method with overall complexity $O(N \log N)$ is used to solve the discrete equations. This paper contains a description of the multigrid-sinc algorithm along with some preliminary numerical results for two-point boundary-value problems. Author

A87-53675* Analytic and Computational Research, Inc., Los Angeles, Calif.

CONDIF - A MODIFIED CENTRAL-DIFFERENCE SCHEME FOR CONVECTIVE FLOWS

AKSHAI K. RUNCHAL (Analytic and Computational Research, Inc., Los Angeles, CA) International Journal for Numerical Methods in Engineering (ISSN 0029-5981), vol. 24, Aug. 1987, p. 1593-1608. Research supported by the General Motors Corp. refs (Contract NAS3-24350)

The paper presents a method, called CONDIF, which modifies the CDS (central-difference scheme) by introducing a controlled amount of numerical diffusion based on the local gradients. The numerical diffusion can be adjusted to be negligibly low for most problems. CONDIF results are significantly more accurate than those obtained from the hybrid scheme when the Peclet number is very high and the flow is at large angles to the grid. Author

N87-11543*# National Aeronautics and Space Administration. Lewis Research Center, Cleveland, Ohio.

AN EFFICIENT METHOD FOR SOLVING THE STEADY EULER EQUATIONS

M. S. LIOU 1986 18 p Presented at the 4th Joint Fluid Mechanics, Plasma Dynamics and Lasers Conference, Atlanta, Ga., 12-14 May 1986; sponsored by AIAA and ASME Previously announced in IAA as A86-38442 (Contract AF-AFOSR-0327-84)

(NASA-TM-87329; E-3051; NAS 1.15:87329; AIAA-86-1079) Avail: NTIS HC A02/MF A01 CSCL 12A

An efficient numerical procedure for solving a set of nonlinear partial differential equations is given, specifically for the steady Euler equations. Solutions of the equations were obtained by Newton's linearization procedure, commonly used to solve the roots of nonlinear algebraic equations. In application of the same procedure for solving a set of differential equations we give a theorem showing that a quadratic convergence rate can be achieved. While the domain of quadratic convergence depends on the problems studied and is unknown a priori, we show that first and second-order derivatives of flux vectors determine whether the condition for quadratic convergence is satisfied. The first derivatives enter as an implicit operator for yielding new iterates and the second derivatives indicate smoothness of the flows considered. Consequently flows involving shocks are expected to require larger number of iterations. First-order upwind discretization in conjunction with the Steger-Warming flux-vector splitting is employed on the implicit operator and a diagonal dominant matrix results. However the explicit operator is represented by first- and second-order upwind differencings, using both Steger-Warming's and van Leer's splittings. We discuss treatment of boundary conditions and solution procedures for solving the resulting block matrix system. With a set of test problems for one- and two-dimensional flows, we show detailed study as to the efficiency, accuracy, and convergence of the present method. Author

N87-14918*# National Aeronautics and Space Administration. Lewis Research Center, Cleveland, Ohio.

SOLUTION OF ELLIPTIC PARTIAL DIFFERENTIAL EQUATIONS BY FAST POISSON SOLVERS USING A LOCAL RELAXATION FACTOR. 2: TWO-STEP METHOD

S. C. CHANG May 1986 17 p (NASA-TP-2530; E-2528-1; NAS 1.60:2530) Avail: NTIS HC A02/MF A01 CSCL 12A

A two-step semidirect procedure is developed to accelerate the one-step procedure described in NASA TP-2529. For a set of constant coefficient model problems, the acceleration factor increases from 1 to 2 as the one-step procedure convergence rate decreases from $+\infty$ to 0. It is also shown numerically that the two-step procedure can substantially accelerate the convergence of the numerical solution of many partial differential equations (PDE's) with variable coefficients. Author

N87-24132*# National Aeronautics and Space Administration. Lewis Research Center, Cleveland, Ohio.

A GENERALIZED PROCEDURE FOR CONSTRUCTING AN UPWIND BASED TVD SCHEME

MENG-SING LIOU Jan. 1987 27 p Presented at the 25th Aerospace Sciences Meeting, Reno, Nev., 12-15 Jan. 1987; sponsored by AIAA

(NASA-TM-88926; E-3364; NAS 1.15:88926; AIAA-87-0355)

Avail: NTIS HC A03/MF A01 CSCL 12A

A generalized formulation for constructing second- and higher-order accurate TVD (total variation diminishing) schemes is presented. A given scheme is made TVD by limiting antidiffusive flux differences with some linear functions, so-called limiters. The general idea of the formulation and its mathematical proof of Harten's TVD conditions is shown by applying the Lax-Wendroff method to scalar nonlinear equations and a constant-coefficient system of conservation laws. For the system of equations, several definitions are derived for the argument used in the limiter function and present their performance in numerical experiments. The formulation is extended to the nonlinear system. It is demonstrated that the present procedure can easily convert existing central or upwind, and second- or higher-order differencing schemes to preserve monotonicity and yield physically admissible solutions. The formulation is simple mathematically as well as numerically; both matrix-vector multiplication and Riemann solver are avoided. Although the notion of TVD is based on the initial value problem, application to the steady Euler equations of the formulation is also made. Author

N87-24930*# National Aeronautics and Space Administration. Lewis Research Center, Cleveland, Ohio.

AN EXPONENTIAL FINITE DIFFERENCE TECHNIQUE FOR SOLVING PARTIAL DIFFERENTIAL EQUATIONS M.S. Thesis - Toledo Univ., Ohio

ROBERT F. HANDSCHUH (Army Aviation Research and Development Command, Cleveland, Ohio.) Jun. 1987 135 p (NASA-TM-89874; E-3544; NAS 1.15:89874; AVSCOM-TR-87-C-19) Avail: NTIS HC A07/MF A01 CSCL 12A

An exponential finite difference algorithm, as first presented by Bhattacharya for one-dimensional steady-state, heat conduction in Cartesian coordinates, has been extended. The finite difference algorithm developed was used to solve the diffusion equation in one-dimensional cylindrical coordinates and applied to two- and three-dimensional problems in Cartesian coordinates. The method was also used to solve nonlinear partial differential equations in one (Burger's equation) and two (Boundary Layer equations) dimensional Cartesian coordinates. Predicted results were compared to exact solutions where available, or to results obtained by other numerical methods. It was found that the exponential finite difference method produced results that were more accurate than those obtained by other numerical methods, especially during the initial transient portion of the solution. Other applications made using the exponential finite difference technique included unsteady one-dimensional heat transfer with temperature varying thermal

64 NUMERICAL ANALYSIS

conductivity and the development of the temperature field in a laminar Couette flow. Author

N87-29212*# Northwestern Univ., Evanston, Ill. Dept. of Mechanical Engineering.

VARIATIONAL APPROACH TO PROBABILISTIC FINITE ELEMENTS Final Report, 1 May 1984 - 31 Aug. 1987

T. BELYTSCHKO, W. K. LIU, A. MANI, and G. BESTERFIELD
28 Sep. 1987 178 p

(Contract NAG3-535)

(NASA-CR-181343; NAS 1.26:181343) Avail: NTIS HC A09/MF A01 CSCL 12A

Probabilistic finite element method (PFEM), synthesizing the power of finite element methods with second-moment techniques, are formulated for various classes of problems in structural and solid mechanics. Time-invariant random materials, geometric properties, and loads are incorporated in terms of their fundamental statistics viz. second-moments. Analogous to the discretization of the displacement field in finite element methods, the random fields are also discretized. Preserving the conceptual simplicity, the response moments are calculated with minimal computations. By incorporating certain computational techniques, these methods are shown to be capable of handling large systems with many sources of uncertainties. By construction, these methods are applicable when the scale of randomness is not very large and when the probabilistic density functions have decaying tails. The accuracy and efficiency of these methods, along with their limitations, are demonstrated by various applications. Results obtained are compared with those of Monte Carlo simulation and it is shown that good accuracy can be obtained for both linear and nonlinear problems. The methods are amenable to implementation in deterministic FEM based computer codes. Author

66

SYSTEMS ANALYSIS

Includes mathematical modeling; network analysis; and operations research.

N87-17472*# Ford Aerospace and Communications Corp., Palo Alto, Calif.

COMMUNICATIONS SATELLITE SYSTEMS OPERATIONS WITH THE SPACE STATION. VOLUME 1: EXECUTIVE SUMMARY Final Report, Jul. 1985 - Sep. 1986

K. PRICE, J. DIXON, and C. WEYANDT Feb. 1987 17 p

(Contract NAS3-24253)

(NASA-CR-179526; NAS 1.26:179526) Avail: NTIS HC A02/MF A01 CSCL 12B

The benefits of new space-based activities are quantified and the impacts on the satellite design and the space station are assessed. B.G.

N87-17473*# Ford Aerospace and Communications Corp., Palo Alto, Calif.

COMMUNICATIONS SATELLITE SYSTEMS OPERATIONS WITH THE SPACE STATION, VOLUME 2 Final Report, Jul. 1985 - Sep. 1986

K. PRICE, J. DIXON, and C. WEYANDT Feb. 1987 190 p

(Contract NAS3-24253)

(NASA-CR-179527; NAS 1.26:179527) Avail: NTIS HC A09/MF A01 CSCL 12B

A financial model was developed which described quantitatively the economics of the space segment of communication satellite systems. The model describes the economics of the space system throughout the lifetime of the satellite. The expected state-of-the-art status of communications satellite systems and operations beginning service in 1995 were assessed and described. New or enhanced space-based activities and associated satellite system designs that have the potential to achieve future communications

satellite operations in geostationary orbit with improved economic performance were postulated and defined. Three scenarios using combinations of space-based activities were analyzed: a spin stabilized satellite, a three axis satellite, and assembly at the Space Station and GEO servicing. Functional and technical requirements placed on the Space Station by the scenarios were detailed. Requirements on the satellite were also listed. B.G.

N87-27475*# The Futures Group, Glastonbury, Conn.

NASA LEWIS RESEARCH CENTER FUTURING WORKSHOP Final Report

MARK BOROUSH, JOHN STOVER, and CHARLES THOMAS Jan. 1987 156 p Workshop held in Cleveland, Ohio, 21-22 Oct. 1986

(Contract NASA ORDER C-21030)

(NASA-CR-179577; NAS 1.26:179577) Avail: NTIS HC A08/MF A01 CSCL 12B

On October 21 and 22, 1986, the Futures Group ran a two-day Futuring Workshop on the premises of NASA Lewis Research Center. The workshop had four main goals: to acquaint participants with the general history of technology forecasting; to familiarize participants with the range of forecasting methodologies; to acquaint participants with the range of applicability, strengths, and limitations of each method; and to offer participants some hands-on experience by working through both judgmental and quantitative case studies. Among the topics addressed during this workshop were: information sources; judgmental techniques; quantitative techniques; merger of judgment with quantitative measurement; data collection methods; and dealing with uncertainty. Author

N87-30132*# National Aeronautics and Space Administration. Lewis Research Center, Cleveland, Ohio.

OPTIMIZING THE ANTENNA SYSTEM OF A MICROWAVE SPACE POWER STATION: IMPLICATIONS FOR THE SELECTION OF OPERATING POWER, FREQUENCY AND ANTENNA SIZE

ROBERT M. MANNING Sep. 1987 9 p

(NASA-TM-100184; E-3761; NAS 1.15:100184) Avail: NTIS HC A02/MF A01 CSCL 12B

A design for a space power station that is to transmit power to the surface of a planet via high powered microwaves should commence with the optimum design of the transmitting and receiving antenna combination to be employed. Once one has assured that the desired amount of power has been transferred (which, after all, is the purpose of any power transmission system), one can, from the constraints imposed by such a design, tailor other parameters of the system such as antenna sizes and weights, power density in the planet's atmosphere (e.g., to avoid electrical breakdown), and frequency of operation. It is the purpose of this brief analysis to provide the working equations of such an optimized antenna system, and to give examples of their use. Related problems that should be analyzed in the future will then be discussed and a flow chart of the indicated order of priority presented. The analysis given here differs from previous work on this subject in that the development given will allow analytical expressions to be obtained for the relevant parameters. This is made possible by employing an approximation procedure to be given during the exposition. Author

PHYSICS (GENERAL)

A87-37542* Trinity Coll., Dublin (Ireland).

NONCOMMUTATIVE-GEOMETRY MODEL FOR CLOSED BOSONIC STRINGS

SIDDHARTHA SEN (Trinity College, Dublin, Ireland) and R. HOLMAN (NASA/Fermilab Astrophysics Center, Batavia, IL) Physical Review Letters (ISSN 0031-9007), vol. 58, March 30, 1987, p. 1304-1307. NASA-DOE-supported research. refs

It is shown how Witten's (1986) noncommutative geometry may be extended to describe the closed bosonic string. For closed strings, an explicit representation is provided of the integral operator needed to construct an action and of an associative product on string fields. The proper choice of the action of the integral operator and the associative product in order to give rise to a reasonable theory is explained, and the consequences of such a choice are discussed. It is shown that the ghost numbers of the operator and associative product can be chosen arbitrarily for both open and closed strings, and that this construct can be used as an action for interacting closed bosonic strings. C.D.

N87-14956*# National Aeronautics and Space Administration. Lewis Research Center, Cleveland, Ohio.

FINITE ELEMENT MODELING OF ELECTROMAGNETIC PROPAGATION IN COMPOSITE STRUCTURES

K. J. BAUMEISTER 1987 7 p Proposed for presentation at the AP-S International Symposium, Blacksburg, Va., 15-19 Jun. 1987; sponsored by IEEE (NASA-TM-88916; E-3341; NAS 1.15:88916) Avail: NTIS HC A02/MF A01 CSCL 460

A finite element Galerkin formulation has been developed to study electromagnetic propagation in complex two-dimensional absorbing ducts. The reflection and transmission at entrance and exit boundaries are determined by coupling the finite element solutions at the entrance and exit to the eigenfunctions of an infinite uniform perfect conducting duct. Example solutions are presented for electromagnetic propagation with absorbing duct walls and propagating through dielectric-metallic matrix materials.

Author

N87-18391*# National Aeronautics and Space Administration. Lewis Research Center, Cleveland, Ohio.

FINITE ELEMENT ANALYSIS OF ELECTROMAGNETIC PROPAGATION IN AN ABSORBING WAVE GUIDE

KENNETH J. BAUMEISTER Dec. 1986 54 p Presented at the Winter Annual Meeting of the American Society of Mechanical Engineers, Anaheim, Calif., 7-12 Dec. 1986 (NASA-TM-88866; E-3133; NAS 1.15:88866) Avail: NTIS HC A04/MF A01 CSCL 20C

Wave guides play a significant role in microwave space communication systems. The attenuation per unit length of the guide depends on its construction and design frequency range. A finite element Galerkin formulation has been developed to study TM electromagnetic propagation in complex two-dimensional absorbing wave guides. The analysis models the electromagnetic absorptive characteristics of a general wave guide which could be used to determine wall losses or simulate resistive terminations fitted into the ends of a guide. It is believed that the general conclusions drawn by using this simpler two-dimensional geometry will be fundamentally the same for other geometries. Author

N87-25821*# National Aeronautics and Space Administration. Lewis Research Center, Cleveland, Ohio.

A FINITE ELEMENT MODEL FOR WAVE PROPAGATION IN AN INHOMOGENEOUS MATERIAL INCLUDING EXPERIMENTAL VALIDATION

KENNETH J. BAUMEISTER and MILO D. DAHL 1987 15 p Prepared for presentation at the 11th Aeroacoustics Conference, Sunnyvale, Calif., 19-21 Oct. 1987; sponsored by AIAA (NASA-TM-100149; E-3471; NAS 1.15:100149) Avail: NTIS HC A02/MF A01 CSCL 20C

A finite element model was developed to solve for the acoustic pressure field in a nonhomogeneous region. The derivations from the governing equations assumed that the material properties could vary with position resulting in a nonhomogeneous variable property two-dimensional wave equation. This eliminated the necessity of finding the boundary conditions between the different materials. For a two media region consisting of part air (in the duct) and part bulk absorber (in the wall), a model was used to describe the bulk absorber properties in two directions. An experiment to verify the numerical theory was conducted in a rectangular duct with no flow and absorbing material mounted on one wall. Changes in the sound field, consisting of planar waves was measured on the wall opposite the absorbing material. As a function of distance along the duct, fairly good agreement was found in the standing wave pattern upstream of the absorber and in the decay of pressure level opposite the absorber. Author

N87-25823*# National Aeronautics and Space Administration. Lewis Research Center, Cleveland, Ohio.

ENHANCED THERMAL EMITTANCE OF SPACE RADIATORS BY ION-DISCHARGE CHAMBER TEXTURING

MICHAEL J. MIRTICH and MICHAEL T. KUSSMAUL (Cleveland State Univ., Ohio.) 1987 14 p Presented at the International Conference on Metallurgical Coatings, San Diego, Calif. 23-27 Mar. 1987; sponsored by the American Vacuum Society (NASA-TM-100137; E-3687; NAS 1.15:100137) Avail: NTIS HC A02/MF A01 CSCL 20C

The discharge chamber of a 30-cm argon ion source was successfully used to texture potential space radiator materials for the purpose of obtaining values of thermal emittance greater than 0.85 at 700 and 900 K. Some samples were also treated in acid prior to texturing. To evaluate the durability of the textured materials to atomic oxygen, samples were exposed to an RF air plasma environment. The spectral emittance between 2.0 and 15.0 microns was measured before and after the textured materials were exposed to the plasma asher. The results indicate that copper with extremely high values of emittance after texturing (0.978 and 0.983) at 700 and 900 K, respectively, did not change its values of emittance after ashing, whereas the emittance of stainless steel fell below 0.85 after ashing. These data, along with scanning electron photomicrographs, and the results of texturing and ashing titanium and Nb(1)Zr are presented. Author

ACOUSTICS

Includes sound generation, transmission, and attenuation.

A87-10772* National Aeronautics and Space Administration. Lewis Research Center, Cleveland, Ohio.

ULTRASONIC VERIFICATION OF MICROSTRUCTURAL CHANGES DUE TO HEAT TREATMENT

E. R. GENERAZIO (NASA, Lewis Research Center, Cleveland, OH) IN: Review of progress in quantitative nondestructive evaluation. Volume 5B - Proceedings of the Twelfth Annual Review, Williamsburg, VA, June 23-28, 1985. New York, Plenum Press, 1986, p. 1315-1326. Previously announced in STAR as N86-22977. refs

Ultrasonic attenuation was measured for polycrystalline samples of nickel and copper with various grain-size distributions produced by heat treatment. Attenuation as a function of frequency was determined for a sample having a known mean grain diameter. Once this function was determined, it could be scaled to determine the mean grain size of other samples of the same material with different mean grain diameters. These results were obtained by using broadband pulse-echo ultrasound in the 25 to 100 MHz frequency range. The results suggest an ultrasonic, nondestructive approach for verifying heat treatment of metals. R.J.F.

A87-11768* Florida State Univ., Tallahassee.

ON BROADBAND SHOCK ASSOCIATED NOISE OF SUPERSONIC JETS

C. K. W. TAM (Florida State University, Tallahassee) IN: Recent advances in aeroacoustics. New York, Springer-Verlag, 1986, p. 25-51. refs

(Contract NAG3-182)

The characteristics and generation mechanisms of noise associated with the interactions of turbulence with the quasi-periodic broadband shock cells of supersonic jet engines are reviewed. The noise possesses broadband spectra and directionality that are completely different from noise caused by turbulence. Experimental data have shown that broadband noise is most prominent in the forward arc, with peak frequencies being a function of the observation angle and the pressure mismatch in the engine. The noise originates in the engine as turbulence-shock interactions occur during downstream movement. Features of the phased point-source array model and the large turbulence structures-shock cells interaction model are defined and model predictions are compared with experimental data on noise sources. Only a scaling of the noise component is found to be currently possible. More complete characterization depends on consideration of the jet temperature and analysis of turbulence-shock interactions, broadband shock and screech tones and shock noise in several flow configurations. M.S.K.

A87-13587* Arizona Univ., Tucson.

INFLUENCE OF AIRFOIL MEAN LOADING ON CONVECTED GUST INTERACTION NOISE

E. J. KERSCHEN and M. R. MYERS (Arizona, University, Tucson) IN: Aero- and hydro-acoustics; Proceedings of the Symposium, Ecully, France, July 3-6, 1985. Berlin and New York, Springer-Verlag, 1986, p. 13-20. refs

(Contract NAG3-357)

A theoretical model is developed for the noise generated when a convected vortical or entropic gust encounters an airfoil at nonzero angle of attack. The analysis is based on Rapid Distortion Theory. High frequency gusts, whose wavelengths are short compared to the airfoil chord, are considered. The noise generation is shown to be concentrated near the airfoil leading edge. The level of the generated noise is increased by airfoil mean loading, with the appropriate scaling parameter being the local leading edge incidence angle. The trailing edge simply scatters the leading edge sound field, and here the mean loading effects scale on the

airfoil total lift. Calculations are presented which illustrate that, at high frequencies, moderate levels of airfoil steady loading can dramatically increase the noise produced by airfoil convected gust interactions. Author

A87-17991*# National Aeronautics and Space Administration. Lewis Research Center, Cleveland, Ohio.

MODELING THE EFFECTS OF WIND TUNNEL WALL ABSORPTION ON THE ACOUSTIC RADIATION CHARACTERISTICS OF PROPELLERS

K. J. BAUMEISTER (NASA, Lewis Research Center, Cleveland, OH) and W. EVERSMAN (Missouri-Rolla, University, Rolla) AIAA, Aeroacoustics Conference, 10th, Seattle, WA, July 9-11, 1986. 19 p. Previously announced in STAR as N86-29630. refs (AIAA PAPER 86-1876)

Finite element theory is used to calculate the acoustic field of a propeller in a soft walled circular wind tunnel and to compare the radiation patterns to the same propeller in free space. Parametric solutions are present for a 'Gutin' propeller for a variety of flow Mach numbers, admittance values at the wall, microphone position locations, and propeller to duct radius ratios. Wind tunnel boundary layer is not included in this analysis. For wall admittance nearly equal to the characteristic value of free space, the free field and ducted propeller models agree in pressure level and directionality. In addition, the need for experimentally mapping the acoustic field is discussed. Author

A87-24978*# National Aeronautics and Space Administration. Lewis Research Center, Cleveland, Ohio.

HIGH-SPEED PROPELLER NOISE PREDICTIONS - EFFECTS OF BOUNDARY CONDITIONS USED IN BLADE LOADING CALCULATIONS

M. NALLASAMY (NASA, Lewis Research Center; Sverdrup Technology, Inc., Cleveland, OH), B. J. CLARK, and J. F. GROENEWEG (NASA, Lewis Research Center, Cleveland, OH) AIAA, Aerospace Sciences Meeting, 25th, Reno, NV, Jan. 12-15, 1987. 25 p. Previously announced in STAR as N87-14957. refs (AIAA PAPER 87-0525)

The acoustics of an advanced single rotation SR-3 propeller at cruise conditions are studied employing a time-domain approach. The study evaluates the acoustic significance of the differences in blade pressures computed using nonreflecting rather than hard wall boundary conditions in the three-dimensional Euler code solution. The directivities of the harmonics of the blade passing frequency tone and the effects of chordwise loading on tone directivity are examined. The results show that the maximum difference in the computed sound pressure levels due to the use of blade pressure distributions obtained with the nonreflecting rather than the hard wall boundary conditions is about 1.5 dB. The blade passing frequency tone directivity obtained in the present study shows good agreement with jetstar flight data. Author

A87-31109*# National Aeronautics and Space Administration. Lewis Research Center, Cleveland, Ohio.

MEASURED NOISE OF A SCALE MODEL HIGH SPEED PROPELLER AT SIMULATED TAKEOFF/APPROACH CONDITIONS

RICHARD P. WOODWARD (NASA, Lewis Research Center, Cleveland, OH) AIAA, Aerospace Sciences Meeting, 25th, Reno, NV, Jan. 12-13, 1987. 21 p. Previously announced in STAR as N87-16588. refs (AIAA PAPER 87-0526)

A model high-speed advanced propeller, SR-7A, was tested in the NASA Lewis 9 x 15 foot anechoic wind tunnel at simulated takeoff/approach conditions of 0.2 Mach number. These tests were in support of the full-scale Propfan Text Assessment (PTA) flight program. Acoustic measurements were taken with fixed microphone arrays and with an axially translating microphone probe. Limited aerodynamic measurements were also taken to establish the propeller operating conditions. Tests were conducted with the propeller alone and with three down-stream wing configurations. The propeller was run over a range of blade setting angles from 32.0 deg. to 43.6 deg., tip speeds from 183 to 290 m/sec (600 to

950 ft/sec), and angles of attack from -10 deg. to +15 deg. The propeller alone BPF tone noise was found to increase 10 dB in the flyover plane at 15 deg. propeller axis angle of attack. The installation of the straight wing at minimum spacing of 0.54 wing chord increased the tone noise 5 dB under the wing of 10 deg. propeller axis angle of attack, while a similarly spaced inboard upswept wing only increased the tone noise 2 dB. Author

A87-31110*# National Aeronautics and Space Administration. Lewis Research Center, Cleveland, Ohio.

STRUCTUREBORNE NOISE CONTROL IN ADVANCED TURBOPROP AIRCRAFT

IRVIN J. LOEFFLER (NASA, Lewis Research Center, Cleveland, OH) AIAA, Aerospace Sciences Meeting, 25th, Reno, NV, Jan. 12-15, 1987. 21 p. Previously announced in STAR as N87-16587. refs

(AIAA PAPER 87-0530)

Structureborne noise is discussed as a contributor to propeller aircraft interior noise levels that are nonresponsive to the application of a generous amount of cabin sidewall acoustic treatment. High structureborne noise levels may jeopardize passenger acceptance of the fuel-efficient high-speed propeller transport aircraft designed for cruise at Mach 0.65 to 0.85. These single-rotation tractor and counter-rotation tractor and pusher propulsion systems will consume 15 to 30 percent less fuel than advanced turbofan systems. Structureborne noise detection methodologies and the importance of development of a structureborne noise sensor are discussed. A structureborne noise generation mechanism is described in which the periodic components or propeller swirl produce periodic torques and forces on downstream wings and airfoils that are propagated to the cabin interior as noise. Three concepts for controlling structureborne noise are presented: (1) a stator row swirl remover, (2) selection of a proper combination of blade numbers in the rotor/stator system of a single-rotation propeller, and the rotor/rotor system of a counter-rotation propeller, and (3) a tuned mechanical absorber.

Author

A87-31144*# National Aeronautics and Space Administration. Lewis Research Center, Cleveland, Ohio.

AIRCRAFT TURBOFAN NOISE

J. F. GROENEWEG and E. J. RICE (NASA, Lewis Research Center, Cleveland, OH) ASME, Transactions, Journal of Turbomachinery (ISSN 0889-504X), vol. 109, Jan. 1987, p. 130-141. Previously announced in STAR as N83-18405. refs

Turbofan noise generation and suppression in aircraft engines are reviewed. The chain of physical processes which connect unsteady flow interactions with fan blades to far field noise is addressed. Mechanism identification and description, duct propagation, radiation, and acoustic suppression are discussed. The experimental techniques of fan inflow static tests are discussed. Rotor blade surface pressure and wake velocity measurements aid in the determination of the types and strengths of the generation mechanisms. Approaches to predicting or measuring acoustic mode content, optimizing treatment impedance to maximize attenuation, translating impedance into porous wall structure, and interpreting far field directivity patterns are illustrated by comparisons of analytical and experimental results. The interdependence of source and acoustic treatment design to minimize far field noise is emphasized. Areas requiring further research are discussed, and the relevance of aircraft turbofan results to quieting other turbomachinery installation is addressed.

S.L.

A87-37628* Lockheed-Georgia Co., Marietta.

ACOUSTIC POWER MEASUREMENT FOR SINGLE AND ANNULAR STREAM DUCT-NOZZLE SYSTEMS UTILIZING A MODAL DECOMPOSITION SCHEME

M. SALIKUDDIN and R. RAMAKRISHNAN (Lockheed-Georgia Co., Marietta) Journal of Sound and Vibration (ISSN 0022-460X), vol. 113, March 22, 1987, p. 441-472. refs
(Contract NAS3-20797)

A refined acoustic impulse technique was used to evaluate the adequacy of single point in-duct pressure measurements for determining the acoustic power for incident, reflected, and transmitted fields for single and annular stream duct-nozzle systems at various flow conditions. The spatial distributions of incident and reflected pressure fields were measured at several radial and azimuthal locations inside the duct. A modal decomposition scheme was used to derive the acoustic power of each duct mode from the complex pressure measurements. The total sums of these individual modal acoustic powers were compared with the area-weighted acoustic power distributions that were evaluated from measured pressure data. It was found that a single-point measurement near the duct wall is adequate for estimating the transmitted power for both single and annular stream duct-nozzle systems. Author

A87-37629* Lockheed-Georgia Co., Marietta.

SOUND RADIATION FROM SINGLE AND ANNULAR STREAM NOZZLES, WITH MODAL DECOMPOSITION OF IN-DUCT ACOUSTIC POWER

M. SALIKUDDIN (Lockheed-Georgia Co., Marietta) Journal of Sound and Vibration (ISSN 0022-460X), vol. 113, March 22, 1987, p. 473-501. refs
(Contract NAS3-20797)

An experimental program was carried out to study the acoustic characteristics of single and annular stream duct-nozzle systems at various flow conditions by using a refined acoustic impulse technique. In this technique, signal synthesis and signal averaging processes are incorporated to generate a desired impulsive signal from acoustic driver(s) and to eliminate background noise (flow noise) from in-duct and far field signals, respectively. The contribution of higher order modes to incident reflected and transmitted acoustic powers is accounted for by using a modal decomposition process. The annular stream terminations were tested statically at various annular stream flow velocities with no inner stream flow. The results derived from the experiments include in-duct acoustic powers, termination reflection coefficients, transmission coefficients, far field power, and acoustic dissipation.

Author

A87-45282*# Hamilton Standard, Windsor Locks, Conn.

RESULTS OF ACOUSTIC TESTS OF A PROP-FAN MODEL

F.B. METZGER and P. C. BROWN (United Technologies Corp., Hamilton Standard Div., Windsor Locks, CT) AIAA, SAE, ASME, and ASEE, Joint Propulsion Conference, 23rd, San Diego, CA, June 29-July 2, 1987. 8 p.

(Contract NAS3-24222)

(AIAA PAPER 87-1894)

Results of acoustic tests in a low speed open jet anechoic wind tunnel are presented for a counter rotation Prop-Fan model. The model tested had 5 front and 5 rear rotor blades with swept planform. Noise spectra are presented showing the influence of operating and configuration variables such as: (1) power absorption, (2) tip speed, (3) rotor-rotor spacing, (4) power split between the front and rear blade rows, (5) variation of the RPM ratio between front and rear blade rows, (6) tractor versus pusher (pylon effects), and (7) angle of attack. In addition to model scale results, calculated levels derived from test are presented showing the influence of the above variables on Effective Perceived Noise Level of a 13.1 ft diameter Prop-Fan at a flyover distance of 1500 ft. It was found that the strongest effects are caused by tip speed and power absorption. A significant finding was that there is an optimum operating tip speed for minimum noise for a given power absorption. Effects of other parametric variations are generally small but measurable. In order to minimize noise to meet airplane certification

limits, operation at moderate tip speeds and power absorption is shown to be desirable. Accuracy of predicted Effective Perceived Noise Level is shown to be good with the best accuracy in the 590 to 670 ft/sec tip speed range. Author

A87-48760* Sverdrup Technology, Inc., Arnold Air Force Station, Tenn.

THE ACOUSTIC EXPERIMENTAL INVESTIGATION OF COUNTERROTATING PROPELLER CONFIGURATIONS

JOHN A. GAZZANIGA (Sverdrup Technology, Inc., Arnold Air Force Station, TN) SAE, General Aviation Aircraft Meeting and Exposition, Wichita, KS, Apr. 28-30, 1987. 21 p. refs

(Contract NAG3-354)

(SAE PAPER 871031)

An experimental study of scale counterrotating propellers operating in an anechoic facility has been conducted. Various configurations of counterrotation for equal numbers of blades per disk have been tested along with single-rotation propellers, underscoring the fundamental acoustic differences between single and counterrotation propeller operation. In addition it is shown that, as the loading on the counterrotating system is increased, the overall sound-pressure level is also increased in both the disk plane and axial direction. Author

N87-10752*# General Electric Co., Cincinnati, Ohio.

FREE JET FEASIBILITY STUDY OF A THERMAL ACOUSTIC SHIELD CONCEPT FOR AST/VCE APPLICATION: DUAL STREAM NOZZLES Final Report

B. A. JANARDAN, J. F. BRAUSCH, and R. K. MAJJIGI Washington NASA Mar. 1985 203 p

(Contract NAS3-22137)

(NASA-CR-3867; E-2392; NAS 1.26:3867) Avail: NTIS HC

A10/MF A01 CSCL 20A

The influence of selected geometric and aerodynamic flow variables of an unsuppressed coannular plug nozzle and a coannular plug nozzle with a 20-chute outer stream suppressor were experimentally determined. A total of 136 static and simulated flight acoustic test points were conducted with 9 scale model nozzles. Also, aerodynamic measurements of four selected plumes were made with a laser velocimeter. The presence of the 180 deg shield produced different mixing characteristics on the shield side compared to the unshield side because of the reduced mixing with ambient air on the shielded side. This resulted in a stretching of the jet, yielding a higher peak mean velocity up to a length of 10 equivalent diameters from the nozzle exit. The 180 deg shield in community orientation around the suppressed coannular plug nozzle yielded acoustic benefit at all observer angles for a simulated takeoff. While the effect of shield-to-outer stream velocity ratio was small at angles up to 120 deg, beyond this angle significant acoustic benefit was realized with a shield-to-outer stream velocity ratio of 0.64. Author

N87-10753*# General Electric Co., Cincinnati, Ohio. Aircraft Engine Business Group.

FREE-JET ACOUSTIC INVESTIGATION OF HIGH-RADIUS-RATIO COANNULAR PLUG NOZZLES Final Report

P. R. KNOTT, B. A. JANARDAN, R. K. MAJJIGI, P. K. BHUTIANI, and P. G. VOGT Washington NASA Oct. 1984 218 p

(Contract NAS3-20619)

(NASA-CR-3818; E-2177; NAS 1.26:3818; R83AEB574) Avail:

NTIS HC A10/MF A01 CSCL 20A

The experimental and analytical results of a scale model simulated flight acoustic exploratory investigation of high radius ratio coannular plug nozzles with inverted velocity and temperature profiles are summarized. Six coannular plug nozzle configurations and a baseline convergent conical nozzle were tested for simulated flight acoustic evaluation. The nozzles were tested over a range of test conditions that are typical of a Variable Cycle Engine for application to advanced high speed aircraft. It was found that in simulate flight, the high radius ratio coannular plug nozzles maintain their jet noise and shock noise reduction features previously observed in static testing. The presence of nozzle bypass struts

will not significantly affect the acoustic noise reduction features of a General Electric type nozzle design. A unique coannular plug nozzle flight acoustic spectral prediction method was identified and found to predict the measured results quite well. Special laser velocimeter and acoustic measurements were performed which have given new insights into the jet and shock noise reduction mechanisms of coannular plug nozzles with regard to identifying further beneficial research efforts. Author

N87-13252*# National Aeronautics and Space Administration. Lewis Research Center, Cleveland, Ohio.

CRUISE NOISE OF COUNTERROTATION PROPELLER AT ANGLE OF ATTACK IN WIND TUNNEL

J. H. DITTMAR Oct. 1986 35 p

(NASA-TM-88869; E-3275; NAS 1.15:88869) Avail: NTIS HC

A03/MF A01 CSCL 20A

The noise of a counterrotation propeller at angle of attack was measured in the NASA Lewis 8- by 6-Foot Supersonic Wind Tunnel at cruise conditions. Noise increases of as much as 4 dB were measured at positive angles of attack on the tunnel side wall, which represented an airplane fuselage. These noise increases could be minimized or eliminated by operating the counterrotation propeller with the front propeller turning up-inboard. This would require oppositely rotating propellers on opposite sides of the airplane. Noise analyses at different bandwidths enabled the separate front- and rear-propeller tones, as well as the total noise, at each harmonic to be determined. A simplified noise model was explored to show how the observed circumferential noise patterns of the separate propeller tones might have occurred. The total noise pattern, which represented the sum of the front- and rear-propeller tones at a particular harmonic, showed trends that would be hard to interpret without the separate-tone results. Therefore it is important that counterrotation angle-of-attack noise data be taken in such a manner that the front- and rear-propeller tones can be separated. Author

N87-14957*# National Aeronautics and Space Administration. Lewis Research Center, Cleveland, Ohio.

HIGH-SPEED PROPELLER NOISE PREDICTIONS: EFFECTS OF BOUNDARY CONDITIONS USED IN BLADE LOADING CALCULATIONS

M. NALLASAMY (Sverdrup Technology, Inc., Cleveland, Ohio.), B. J. CLARK, and J. F. GROENEWEG 1987 26 p Presented at the 25th Aerospace Sciences Meeting, Reno, Nev., 12-15 Jan. 1987; sponsored by AIAA

(NASA-TM-88913; E-3337; NAS 1.15:88913; AIAA-87-0525)

Avail: NTIS HC A03/MF A01 CSCL 20A

The acoustics of an advanced single rotation SR-3 propeller at cruise conditions are studied employing a time-domain approach. The study evaluates the acoustic significance of the differences in blade pressures computed using nonreflecting rather than hard wall boundary conditions in the three-dimensional Euler code solution. The directivities of the harmonics of the blade passing frequency tone and the effects of chordwise loading on tone directivity are examined. The results show that the maximum difference in the computed sound pressure levels due to the use of blade pressure distributions obtained with the nonreflecting rather than the hard wall boundary conditions is about 1.5 dB. The blade passing frequency tone directivity obtained in the present study shows good agreement with jetstar flight data. Author

N87-16586*# National Aeronautics and Space Administration. Lewis Research Center, Cleveland, Ohio.

NOISE GENERATED BY FLOW THROUGH LARGE BUTTERFLY VALVES

RONALD G. HUFF Jan. 1987 17 p

(NASA-TM-88911; E-3336; NAS 1.15:88911) Avail: NTIS HC

A01/MF A01 CSCL 20A

A large butterfly valve (1.37 m diam) was acoustically tested to measure the noise generated and propagating in both the upstream and downstream directions. The experimental investigation used wall mounted pressure transducers to measure the fluctuating component of the pipe static pressure upstream

and downstream of the valve. Microphones upstream of the pipe inlet and located in a plenum were used to measure the noise radiated from the valve in the upstream direction. Comparison of the wall pressure downstream of the valve to a prediction were made. Reasonable agreement was obtained with the valve operating at a choked condition. The noise upstream of the valve is 30 dB less than that measured downstream. Author

N87-16587*# National Aeronautics and Space Administration. Lewis Research Center, Cleveland, Ohio.

STRUCTUREBORNE NOISE CONTROL IN ADVANCED TURBOPROP AIRCRAFT

IRVIN J. LOEFFLER Jan. 1987 24 p Presented at the 25th Aerospace Sciences Meeting, Reno, Nev., 12-15 Jan. 1987; sponsored by AIAA

(NASA-TM-88947; E-3362; NAS 1.15:88947; AIAA-87-0530)

Avail: NTIS HC A02/MF A01 CSCL 20A

Structureborne noise is discussed as a contributor to propeller aircraft interior noise levels that are nonresponsive to the application of a generous amount of cabin sidewall acoustic treatment. High structureborne noise levels may jeopardize passenger acceptance of the fuel-efficient high-speed propeller transport aircraft designed for cruise at Mach 0.65 to 0.85. These single-rotation tractor and counter-rotation tractor and pusher propulsion systems will consume 15 to 30 percent less fuel than advanced turbofan systems. Structureborne noise detection methodologies and the importance of development of a structureborne noise sensor are discussed. A structureborne noise generation mechanism is described in which the periodic components or propeller swirl produce periodic torques and forces on downstream wings and airfoils that are propagated to the cabin interior as noise. Three concepts for controlling structureborne noise are presented: (1) a stator row swirl remover, (2) selection of a proper combination of blade numbers in the rotor/stator system of a single-rotation propeller, and the rotor/rotor system of a counter-rotation propeller, and (3) a tuned mechanical absorber. Author

N87-16588*# National Aeronautics and Space Administration. Lewis Research Center, Cleveland, Ohio.

MEASURED NOISE OF A SCALE MODEL HIGH SPEED PROPELLER AT SIMULATED TAKEOFF/APPROACH CONDITIONS

RICHARD P. WOODWARD Jan. 1987 29 p Presented at the 25th Aerospace Sciences Meeting, Reno, Nev., 12-15 Jan. 1987; sponsored by AIAA

(NASA-TM-88920; E-3352; NAS 1.15:88920; AIAA-87-0526)

Avail: NTIS HC A03/MF A01 CSCL 20A

A model high-speed advanced propeller, SR-7A, was tested in the NASA Lewis 9x15 foot anechoic wind tunnel at simulated takeoff/approach conditions of 0.2 Mach number. These tests were in support of the full-scale Propfan Text Assessment (PTA) flight program. Acoustic measurements were taken with fixed microphone arrays and with an axially translating microphone probe. Limited aerodynamic measurements were also taken to establish the propeller operating conditions. Tests were conducted with the propeller alone and with three down-stream wing configurations. The propeller was run over a range of blade setting angles from 32.0 deg. to 43.6 deg., tip speeds from 183 to 290 m/sec (600 to 950 ft/sec), and angles of attack from -10 deg. to +15 deg. The propeller alone BPF tone noise was found to increase 10 dB in the flyover plane at 15 deg. propeller axis angle of attack. The installation of the straight wing at minimum spacing of 0.54 wing chord increased the tone noise 5 dB under the wing of 10 deg. propeller axis angle of attack, while a similarly spaced inboard upswept wing only increased the tone noise 2 dB. Author

N87-17480*# National Aeronautics and Space Administration. Lewis Research Center, Cleveland, Ohio.

COMBUSTION NOISE FROM GAS TURBINE AIRCRAFT ENGINES MEASUREMENT OF FAR-FIELD LEVELS

EUGENE A. KREJSA 1987 8 p Proposed for presentation at the 1987 National Conference on Noise Control Engineering, University Park, Pa., 8-10 Jun. 1987

(NASA-TM-88971; E-3407; NAS 1.15:88971) Avail: NTIS HC A02/MF A01 CSCL 20A

Combustion noise can be a significant contributor to total aircraft noise. Measurement of combustion noise is made difficult by the fact that both jet noise and combustion noise exhibit broadband spectra and peak in the same frequency range. Since in-flight reduction of jet noise is greater than that of combustion noise, the latter can be a major contributor to the in-flight noise of an aircraft but will be less evident, and more difficult to measure, under static conditions. Several methods for measuring the far-field combustion noise of aircraft engines are discussed in this paper. These methods make it possible to measure combustion noise levels even in situations where other noise sources, such as jet noise, dominate. Measured far-field combustion noise levels for several turbofan engines are presented. These levels were obtained using a method referred to as three-signal coherence, requiring that fluctuating pressures be measured at two locations within the engine core in addition to the far-field noise measurement. Cross-spectra are used to separate the far-field combustion noise from far-field noise due to other sources. Spectra and directivities are presented. Comparisons with existing combustion noise predictions are made. Author

N87-17481*# General Electric Co., Cincinnati, Ohio. Aircraft Engine Business Group.

SIMULATED FLIGHT ACOUSTIC INVESTIGATION OF TREATED EJECTOR EFFECTIVENESS ON ADVANCED MECHANICAL SUPPRESSORS FOR HIGH VELOCITY JET NOISE REDUCTION Final Contractor Report

J. F. BRAUSCH, R. E. MOTSINGER, and D. J. HOERST Washington NASA Nov. 1986 413 p

(Contract NAS3-23275)

(NASA-CR-4019; E-3134; NAS 1.26:4019; R85AEB518) Avail: NTIS HC A18/MF A01 CSCL 20A

Ten scale-model nozzles were tested in an anechoic free-jet facility to evaluate the acoustic characteristics of a mechanically suppressed inverted-velocity-profile coannular nozzle with an acoustically treated ejector system. The nozzle system used was developed from aerodynamic flow lines evolved in a previous contract, defined to incorporate the restraints imposed by the aerodynamic performance requirements of an Advanced Supersonic Technology/Variable Cycle Engine system through all its mission phases. Acoustic data of 188 test points were obtained, 87 under static and 101 under simulated flight conditions. The tests investigated variables of hardwall ejector application to a coannular nozzle with 20-chute outer annular suppressor, ejector axial positioning, treatment application to ejector and plug surfaces, and treatment design. Laser velocimeter, shadowgraph photograph, aerodynamic static pressure, and temperature measurement were acquired on select models to yield diagnostic information regarding the flow field and aerodynamic performance characteristics of the nozzles. Author

N87-19057*# National Aeronautics and Space Administration. Lewis Research Center, Cleveland, Ohio.

NOISE REDUCTION FOR MODEL COUNTERROTATION PROPELLER AT CRUISE BY REDUCING AFT-PROPELLER DIAMETER

JAMES H. DITTMAR and DAVID B. STANG (Sverdrup Technology, Inc., Cleveland, Ohio) 1987 31 p Prepared for presentation at the 113th Meeting of the Acoustical Society of America, Indianapolis, Ind., 11-15 May 1987

(NASA-TM-88936; E-3378; NAS 1.15:88936) Avail: NTIS HC A03/MF A01 CSCL 20A

The forward propeller of a model counterrotation propeller was tested with its original aft propeller and with a reduced diameter

aft propeller. Noise reductions with the reduced diameter aft propeller were measured at simulated cruise conditions. Reductions were as large as 7.5 dB for the aft-propeller passing tone and 15 dB in the harmonics at specific angles. The interaction tones, mostly the first, were reduced probably because the reduced-diameter aft-propeller blades no longer interacted with the forward propeller tip vortex. The total noise (sum of primary and interaction noise) at each harmonic was significantly reduced. The chief noise reduction at each harmonic came from reduced aft-propeller-alone noise, with the interaction tones contributing little to the totals at cruise. Total cruise noise reductions were as much as 3 dB at given angles for the blade passing tone and 10 dB for some of the harmonics. These reductions would measurably improve the fuselage interior noise levels and represent a definite cruise noise benefit from using a reduced diameter aft propeller.

Author

N87-25826*# National Aeronautics and Space Administration. Lewis Research Center, Cleveland, Ohio.

EFFECTS OF FIBER MOTION ON THE ACOUSTIC BEHAVIOR OF AN ANISOTROPIC, FLEXIBLE FIBROUS MATERIAL

MILO D. DAHL, EDWARD J. RICE, and DONALD E. GROESBECK May 1987 33 p Presented at the 113th Meeting of the Acoustical Society of America, Indianapolis, Ind., 11-16 May 1987

(NASA-TM-89884; E-3568; NAS 1.15:89884) Avail: NTIS HC A03/MF A01 CSCL 20A

The acoustic behavior of a flexible fibrous material was studied experimentally. The material consisted of cylindrically shaped fibers arranged in a batting with the fibers primarily aligned parallel to the face of the batting. This type of material was considered anisotropic, with the acoustic propagation constant depending on whether the direction of sound propagation was parallel or normal to the fiber arrangement. Normal incidence sound absorption measurements were taken for both fiber orientations over the frequency range 140 to 1500 Hz and with bulk densities ranging from 4.6 to 67 kg/cu m. When the sound propagated in a direction normal to the fiber alignment, the measured sound absorption showed the occurrence of a strong resonance, which increased absorption above that attributed to viscous and thermal effects. When the sound propagated in a direction parallel to the fiber alignment, indications of strong resonances in the data were not present. The resonance in the data for fibers normal to the direction of sound propagation is attributed to fiber motion. An analytical model was developed for the acoustic behavior of the material displaying the same fiber motion characteristics shown in the measurements.

Author

N87-26615*# National Aeronautics and Space Administration. Lewis Research Center, Cleveland, Ohio.

AEROACOUSTICS OF SUBSONIC TURBULENT SHEAR FLOWS

MARVIN E. GOLDSTEIN 1987 12 p Proposed for presentation at the 11th Aeroacoustics Conference, Sunnyvale, Calif., 19-21 Oct. 1987; sponsored by AIAA

(NASA-TM-100165; E-3730; NAS 1.15:100165) Avail: NTIS HC A02/MF A01 CSCL 20A

Sound generation in turbulent shear flows is examined. The emphasis is on simultaneous calculation of the turbulent flow along with the resulting sound generation rather than the alternative acoustic analogy approach. The first part of the paper is concerned with solid surface interaction. The second part concentrates on the sound generated by turbulence interacting with itself.

Author

N87-28396*# National Aeronautics and Space Administration. Lewis Research Center, Cleveland, Ohio.

THE EFFECT OF FRONT-TO-REAR PROPELLER SPACING ON THE INTERACTION NOISE OF A MODEL COUNTERROTATION PROPELLER AT CRUISE CONDITIONS

JAMES H. DITTMAR Aug. 1987 18 p
(NASA-TM-100121; E-3667; NAS 1.15:100121) Avail: NTIS HC A02/MF A01 CSCL 20A

The effect of front-to-rear propeller spacing on the interaction noise of a counterrotation propeller model was measured at cruise conditions. The data taken at an axial Mach number of 0.80 behaved as expected: interaction noise was reduced with increased spacing. The data taken at $M=0.76$ and $M=0.72$ did not behave as expected. At some of the test conditions the noise was unchanged; others even showed noise increases with increased spacing. A possible explanation, involving the amount of downstream blade area impacted by the tip vortex, is presented.

Author

N87-28398*# National Aeronautics and Space Administration. Lewis Research Center, Cleveland, Ohio.

CRUISE NOISE OF THE 2/9TH SCALE MODEL OF THE LARGE-SCALE ADVANCED PROPFAN (LAP) PROPELLER, SR-7A

JAMES H. DITTMAR and DAVID B. STANG (Sverdrup Technology, Inc., Cleveland, Ohio.) Sep. 1987 52 p Prepared for presentation at the 11th AIAA Aeroacoustics Conference, Sunnyvale, Calif., 19-21 Oct. 1987

(NASA-TM-100175; E-3746; NAS 1.15:100175) Avail: NTIS HC A04/MF A01 CSCL 20A

Noise data on the Large-scale Advanced Propfan (LAP) propeller model SR-7A were taken in the NASA Lewis Research Center 8 x 6 foot Wind Tunnel. The maximum blade passing tone noise first rises with increasing helical tip Mach number to a peak level, then remains the same or decreases from its peak level when going to higher helical tip Mach numbers. This trend was observed for operation at both constant advance ratio and approximately equal thrust. This noise reduction or, leveling out at high helical tip Mach numbers, points to the use of higher propeller tip speeds as a possible method to limit airplane cabin noise while maintaining high flight speed and efficiency. Projections of the tunnel model data are made to the full scale LAP propeller mounted on the test bed aircraft and compared with predictions. The prediction method is found to be somewhat conservative in that it slightly overpredicts the projected model data at the peak.

Author

N87-29315*# General Electric Co., Cincinnati, Ohio. Aircraft Engine Business Group.

FREE-JET INVESTIGATION OF MECHANICALLY SUPPRESSED, HIGH RADIUS RATIO COANNULAR PLUG MODEL NOZZLES Final Report

B. A. JANARDAN, R. K. MAJUMGI, J. F. BRAUSCH, and P. R. KNOTT May 1985 250 p
(Contract NAS3-21608)

(NASA-CR-3596; E-2472; NAS 1.26:3596; R81AEG484) Avail: NTIS HC A11/MF A01 CSCL 20A

The experimental and analytical acoustic results of a scale-model investigation of unsuppressed and mechanically suppressed high-radius ratio coannular plug nozzles with inverted velocity and temperature profiles are summarized. Nine coannular nozzle configurations along with a reference conical nozzle were evaluated in the Anechoic Free-Jet Facility for a total of 212 acoustic test points. Most of the tests were conducted at variable cycle engine conditions applicable to advanced high speed aircraft. The tested nozzles included coannular plug nozzles with both convergent and convergent-divergent (C-D) terminations in order to evaluate C-D effectiveness in the reduction of shock-cell noise and 20 and 40 shallow-chute mechanical suppressors in the outer stream in order to evaluate their effectiveness in the reduction of jet noise. In addition to the acoustic tests, mean and turbulent velocity measurements were made on selected plumes of the 20 shallow-chute configuration using a laser velocimeter. At a mixed

jet velocity of 700 m/sec, the 20 shallow-chute suppressor configuration yielded peak aft quadrant suppression of 11.5 and 9 PNdB and forward quadrant suppression of 7 and 6 PNdB relative to a baseline conical nozzles during static and simulated flight, respectively. The C-D terminations were observed to reduce shock-cell noise. An engineering spectral prediction method was formulated for mechanically suppressed coannular plug nozzles.

Author

73

NUCLEAR AND HIGH-ENERGY PHYSICS

Includes elementary and nuclear particles; and reactor theory.

N87-25838* National Aeronautics and Space Administration. Lewis Research Center, Cleveland, Ohio.

NUCLEAR REACTOR POWER FOR A SPACE-BASED RADAR. SP-100 PROJECT

HARVEY BLOOMFIELD, JACK HELLER, LEONARD JAFFE, RICHARD BEATTY, PRADEEP BHANDARI, EDWIN CHOW, WILLIAM DEININGER, RICHARD EWELL, TOSHIO FUJITA, MERLIN GROSSMAN et al. 31 Aug. 1986 176 p Prepared in cooperation with JPL, Pasadena, Calif. and Los Alamos National Lab., N. Mex.

(Contract NAS7-918; DE-AI03-86SF-16013)

(NASA-TM-89295; JPL-PUB-86-47; NAS 1.15:89295) Avail: NTIS HC A09/MF A01 CSCL 18I

A space-based radar mission and spacecraft, using a 300 kW nuclear reactor power system, has been examined, with emphasis on aspects affecting the power system. The radar antenna is a horizontal planar array, 32 X 64 m. The orbit is at 61 deg, 1088 km. The mass of the antenna with support structure is 42,000 kg; of the nuclear reactor power system, 8,300 kg; of the whole spacecraft about 51,000 kg, necessitating multiple launches and orbital assembly. The assembly orbit is at 57 deg, 400 km, high enough to provide the orbital lifetime needed for orbital assembly. The selected scenario uses six Shuttle launches to bring the spacecraft and a Centaur G upper-stage vehicle to assembly orbit. After assembly, the Centaur places the spacecraft in operational orbit, where it is deployed on radio command, the power system started, and the spacecraft becomes operational. Electric propulsion is an alternative and allows deployment in assembly orbit, but introduces a question of nuclear safety.

Author

N87-27495* Oregon State Univ., Corvallis. Dept. of Nuclear Engineering.

AN ASSESSMENT AND VALIDATION STUDY OF NUCLEAR REACTORS FOR LOW POWER SPACE APPLICATIONS Final Report 1986, 1 Nov. - 30 Apr. 1987

A. C. KLEIN, S. R. GEDEON, and D. C. MOREY 26 Jun. 1987 53 p

(Contract NAG3-752)

(NASA-CR-180672; NAS 1.26:180672; OSU-NE-8702) Avail: NTIS HC A04/MF A01 CSCL 18N

The feasibility and safety of six conceptual small, low power nuclear reactor designs was evaluated. Feasibility evaluations included the determination of sufficient reactivity margins for seven years of full power operation and safe shutdown as well as handling during pre-launch assembly phases. Safety evaluations were concerned with the potential for maintaining subcritical conditions in the event of launch or transportation accidents. These included water immersion accident scenarios both with and without water flooding the core. Results show that most of the concepts can potentially meet the feasibility and safety requirements; however, due to the preliminary nature of the designs considered, more detailed designs will be necessary to enable these concepts to fully meet the safety requirements.

Author

74

OPTICS

Includes light phenomena; and optical devices.

A87-18171* Harris Government Aerospace Systems Div., Melbourne, Fla.

SOLAR CONCENTRATOR MATERIALS DEVELOPMENT

D. E. MOREL, S. R. AYERS (Harris Corp., Government Aerospace Systems Div., Melbourne, FL), D. A. GULINO (NASA, Lewis Research Center, Cleveland, OH), R. C. TENNYSON (Toronto, University, Canada), and R. A. EGGER (Cleveland State University, OH) IN: IECEC '86; Proceedings of the Twenty-first Intersociety Energy Conversion Engineering Conference, San Diego, CA, August 25-29, 1986. Volume 3. Washington, DC, American Chemical Society, 1986, p. 2032-2038. refs

(Contract NAS3-24670)

Materials with potential applications in reflective and refractive solar dynamic concentrators are tested for resistance to atomic oxygen degradation. It is found that inorganic coatings such as MgF₂, SiO₂(x), and ITO provide excellent protection for reflective surfaces while organic materials are much more susceptible to erosion and mass loss. Of the organic polymers tested, the silicones have the highest intrinsic resistance to atomic oxygen degradation.

K.K.

A87-18173* Harris Corp., Melbourne, Fla.

OPTIMIZATION OF SPHERICAL FACETS FOR PARABOLIC SOLAR CONCENTRATORS

J. E. WHITE, R. J. ERIKSON, J. D. STURGIS (Harris Corp., Melbourne, FL), and T. B. ELFE (Georgia Institute of Technology, Atlanta) IN: IECEC '86; Proceedings of the Twenty-first Intersociety Energy Conversion Engineering Conference, San Diego, CA, August 25-29, 1986. Volume 3. Washington, DC, American Chemical Society, 1986, p. 2045-2049. refs

(Contract NAS3-24666; NAS3-24670)

Solar concentrator designs which employ deployable hexagonal panels are being developed for space power systems. An offset optical configuration has been developed which offers significant system level advantages over previously proposed collector designs for space applications. Optical analyses have been performed which show offset reflector intercept factors to be only slightly lower than those for symmetric reflectors with the same slope error. Fluxes on the receiver walls are asymmetric but manageable by varying the tilt angle of the receiver. Greater producibility is achieved by subdividing the hexagonal panels into triangular mirror facets of spherical contour. Optical analysis has been performed upon these to yield near-optimum sizes and radii.

Author

N87-30180* Ohio State Univ., Columbus. ElectroScience Lab. DESIGN, IMPLEMENTATION AND INVESTIGATION OF AN IMAGE GUIDE-BASED OPTICAL FLIP-FLOP ARRAY

P. C. GRIFFITH Jul. 1987 99 p

(Contract NSG-3302)

(NASA-CR-181382; NAS 1.26:181382; ESL-TR-712257-5) Avail: NTIS HC A05/MF A01 CSCL 20F

Presented is the design for an image guide-based optical flip-flop array created using a Hughes liquid crystal light valve and a flexible image guide in a feedback loop. This design is used to investigate the application of image guides as a communication mechanism in numerical optical computers. It is shown that image guides can be used successfully in this manner but mismatch match between the input and output fiber arrays is extremely limiting.

Author

PLASMA PHYSICS

Includes magnetohydrodynamics and plasma fusion.

A87-18735* Tuskegee Inst., Ala.

RAIL GUN PERFORMANCE AND PLASMA CHARACTERISTICS DUE TO WALL ABLATION

P. K. RAY (Tuskegee Institute, AL) (DARPA, Symposium on Electromagnetic Launch Technology, 3rd, University of Texas, Austin, Apr. 20-24, 1986) IEEE Transactions on Magnetics (ISSN 0018-9464), vol. MAG-22, Nov. 1986, p. 1699-1705. refs (Contract NAG3-76)

The experiment of Bauer, et al. (1982) is analyzed by considering wall ablation and viscous drag in the plasma. Plasma characteristics are evaluated through a simple fluid-mechanical analysis considering only wall ablation. By equating the energy dissipated in the plasma with the radiation heat loss, the average properties of the plasma are determined as a function of time. Author

A87-22712*# Systems Science and Software, La Jolla, Calif.

HOLLOW CATHODES AS ELECTRON EMITTING PLASMA CONTACTORS THEORY AND COMPUTER MODELING

V. A. DAVIS, I. KATZ, M. J. MANDELL, and D. E. PARKS (Systems Science and Software, La Jolla, CA) AIAA, Aerospace Sciences Meeting, 25th, Reno, NV, Jan. 12-15, 1987. 7 p. refs (Contract NAS3-23881) (AIAA PAPER 87-0569)

Several researchers have suggested using hollow cathodes as plasma contactors for electrodynamic tethers, particularly to prevent the Shuttle Orbiter from charging to large negative potentials. Previous studies have shown that fluid models with anomalous scattering can describe the electron transport in hollow cathode generated plasmas. An improved theory of the hollow cathode plasmas is developed and computational results using the theory are compared with laboratory experiments. Numerical predictions for a hollow cathode plasma source of the type considered for use on the Shuttle are presented, as are three-dimensional NASCAP/LEO calculations of the emitted ion trajectories and the resulting potentials in the vicinity of the Orbiter. The computer calculations show that the hollow cathode plasma source makes vastly superior contact with the ionospheric plasma compared with either an electron gun or passive ion collection by the Orbiter. Author

A87-22714*# Massachusetts Inst. of Tech., Cambridge.

ENHANCED CURRENT FLOW THROUGH A PLASMA CLOUD BY INDUCTION OF PLASMA TURBULENCE

D. E. HASTINGS and A. GIOULEKAS (MIT, Cambridge, MA) AIAA, Aerospace Sciences Meeting, 25th, Reno, NV, Jan. 12-15, 1987. 15 p. refs (Contract NAG3-681) (AIAA PAPER 87-0573)

Electrodynamic tethers have been proposed as a means of generating power in low earth orbit. One of the limitations on the power generated is the relatively low electron current that can be collected. It is proposed that the electron current can be significantly enhanced by means of current induced plasma turbulence in a plasma cloud around the collecting anode. This is examined for the specific case of lower hybrid turbulence. An important conclusion is that the use of plasma clouds in the ionosphere will entail a high impedance (no instability) and a low impedance (lower hybrid instability) mode of operation depending on the current density. Author

A87-31211*# National Aeronautics and Space Administration. Lewis Research Center, Cleveland, Ohio.

PLASMA CONTACTORS FOR ELECTRODYNAMIC TETHERS

MICHAEL J. PATTERSON (NASA, Lewis Research Center, Cleveland, OH) and PAUL J. WILBUR (Colorado State University, Fort Collins) Aerospace America (ISSN 0740-722X), vol. 25, Feb. 1987, p. 32-34.

Plasma contactors could be used to ground satellites to space plasma to acquire a flow of electrons to propel or power the satellites. A tether would cut across geomagnetic field lines, producing a potential difference between the ends of the tether. Closing the connection between the ends would form a circuit in which an electrical load could be inserted. Design constraints of the circuit are low impedance and a fully reversible high current. The contactor would generate a neutral plasma to connect to the ionospheric plasma. The surface area of the connection would have to be kept large enough for the current density to be equal to the random electron current density in the unperturbed space plasmas. The other contactor would feed electrons and draw ions from the space plasma. Experimental results from spaceborne and ground-based space plasma simulator tests of hollow cathodes that have shown that multiampere currents can be collected are described. M.S.K.

A87-32192*# National Aeronautics and Space Administration. Lewis Research Center, Cleveland, Ohio.

HOLLOW CATHODE-BASED PLASMA CONTACTOR EXPERIMENTS FOR ELECTRODYNAMIC TETHER

MICHAEL J. PATTERSON (NASA, Lewis Research Center, Cleveland, OH) AIAA, Aerospace Sciences Meeting, 25th, Reno, NV, Jan. 12-15, 1987. 46 p. refs (AIAA PAPER 87-0572)

The role plasma contactors play in effective electrodynamic tether operation is discussed. Hollow cathodes and hollow cathode-based plasma sources have been identified as leading candidates for the electrodynamic tether plasma contactor. Present experimental efforts to evaluate the suitability of these devices as plasma contactors are reviewed. This research includes the definition of preliminary plasma contactor designs, and the characterization of their operation as electron collectors from a simulated space plasma. The discovery of an 'ignited mode' regime of high contactor efficiency and low impedance is discussed, as well as is the application of recent models of the plasma coupling process to contactor operation. Results indicate that ampere-level electron currents can be exchanged between hollow cathode-based plasma contactors and a dilute plasma in this regime. A discussion of design considerations for plasma contactors is given which includes expressions defining the total mass flow rate and power requirements of plasma contactors operating in both the cathodic and anodic regimes, and correlation of this to the tether current. Finally, future ground and spaceflight experiments are proposed to resolve critical issues of plasma contactor operation. Author

A87-48241* Massachusetts Inst. of Tech., Cambridge.

ENHANCED CURRENT FLOW THROUGH A PLASMA CLOUD BY INDUCTION OF PLASMA TURBULENCE

D. E. HASTINGS (MIT, Cambridge, MA) Journal of Geophysical Research (ISSN 0148-0227), vol. 92, July 1, 1987, p. 7716-7722. refs (Contract NAG3-681)

Electrodynamic tethers have been proposed as a means of generating power in low earth orbit. One of the limitations on the power generated is the relatively low electron current that can be collected. It is proposed that the electron current can be significantly enhanced by means of current-induced plasma turbulence in a plasma cloud around the collecting anode. This is examined for the specific case of ion acoustic turbulence. An important conclusion is that the use of plasma clouds in the ionosphere will entail a high-impedance (no instability) and a low-impedance (ion acoustic instability) mode of operation. The low-impedance mode of operation will have two submodes, one steady state and one pulsed. Author

N87-14998*# National Aeronautics and Space Administration. Lewis Research Center, Cleveland, Ohio.

ASYMPTOTIC ANALYSIS OF CORONA DISCHARGE FROM THIN ELECTRODES

P. A. DURBIN Sep. 1986 7 p
(NASA-TP-2645; E-3151; NAS 1.60:2645) Avail: NTIS HC A02/MF A01 CSCL 201

The steady discharge of a high-voltage corona is analyzed as a singular perturbation problem. The small parameter is the ratio of the length of the ionization region to the total gap length. By this method, current versus voltage characteristics can be calculated analytically. Author

N87-16614*# Iowa Univ., Iowa City. Dept. of Physics and Astronomy.

MEASUREMENTS OF PLASMA DENSITY AND TURBULENCE NEAR THE SHUTTLE ORBITER

A. TRIBBLE, N. DANIELO, G. MURPHY, and J. PICKETT Jan. 1987 12 p
(Contract NAS8-32807; NAG3-449)
(NASA-CR-180102; NAS 1.26:180102) Avail: NTIS HC A02/MF A01 CSCL 201

In August 1985 the University of Iowa's Plasma Diagnostics Package was used in the Spacelab 2 mission to study the plasma environment near the shuttle orbiter. Measurements of the plasma density and the percentage density fluctuations yielded information about the structure of the orbiter's wake. These data appear to be in general agreement with previous shuttle results and with laboratory observations of plasma flow-body interactions. Author

N87-18428*# National Aeronautics and Space Administration. Lewis Research Center, Cleveland, Ohio.

PLASMA CONTACTORS FOR ELECTRODYNAMIC TETHER

MICHAEL J. PATTERSON and PAUL J. WILBUR Sep. 1986 31 p Presented at the International Conference on Tethers in Space, Arlington, Va., 17-19 Sep. 1986; sponsored in part by NASA, AIAA and PSN Prepared in cooperation with Colorado State Univ., Fort Collins
(NASA-TM-88850; E-3242; NAS 1.15:88850) Avail: NTIS HC A03/MF A01 CSCL 201

The role plasma contactors play in effective electrodynamic tether operation is discussed. Hollow cathodes and hollow cathode-based plasma sources have been identified as leading candidates for the electrodynamic tether plasma contactor. Present experimental efforts to evaluate the suitability of these devices as plasma contactors, conducted concurrently at NASA Lewis Research Center and Colorado State University, are reviewed. These research programs include the definition of preliminary plasma contactor designs, and the characterization of their operation both as electron emitters and electron collectors to and from a simulated space plasma. Results indicate that ampere-level electron currents, sufficient for electrodynamic tether operation, can be exchanged between hollow cathode-based plasma contactors and a dilute plasma. Author

N87-22508*# Alabama Univ., Huntsville. College of Science.
INVESTIGATION OF BEAM-PLASMA INTERACTIONS Final Report

RICHARD C. OLSEN May 1987 29 p
(Contract NAG3-620)
(NASA-CR-180579; NAS 1.26:180579) Avail: NTIS HC A03/MF A01 CSCL 201

Data from the SCATHA satellite was analyzed to solve the problems of establishing electrical contact between a satellite and the ambient plasma. The original focus of the work was the electron gun experiments conducted near the geosynchronous orbit, which resulted in observations which bore a startling similarity to observations of the SEPAC experiments on SPACELAB 1. The study has evolved to include the ion gun experiments on SCATHA, a modest laboratory effort in hollow cathode performance, and preparation for flight experiments pertinent to tether technology. These areas are addressed separately. Author

N87-28423*# National Aeronautics and Space Administration. Lewis Research Center, Cleveland, Ohio.

GROUND-BASED PLASMA CONTRACTOR CHARACTERIZATION

MICHAEL J. PATTERSON (Washington Univ., Seattle.) and RANDALL S. AADLAND 1987 17 p Prepared for presentation at the 2nd International Conference on Tethers in Space, Venice, Italy, 6-8 Oct. 1987; sponsored in part by ESA, AIAA and AAS (NASA-TM-100194; E-3784; NAS 1.15:100194) Avail: NTIS HC A02/MF A01 CSCL 201

Presented are recent NASA Lewis Research Center (LeRC) plasma contractor experimental results, as well as a description of the plasma contractor test facility. The operation of a 24 cm diameter plasma source with hollow cathode was investigated in the lighted-mode regime of electron current collection from 0.1 to 7.0 A. These results are compared to those obtained with a 12 cm plasma source. Full two-dimensional plasma potential profiles were constructed from emissive probe traces of the contractor plume. The experimentally measured dimensions of the plume sheaths were then compared to those theoretically predicted using a model of a spherical double sheath. Results are consistent for currents up to approximately 1.0 A. For currents above 1.0 A, substantial deviations from theory occur. These deviations are due to sheath asphericity, and possibly volume ionization in the double-sheath region. Author

76

SOLID-STATE PHYSICS

Includes superconductivity.

A87-11242* Case Western Reserve Univ., Cleveland, Ohio.

BEHAVIOR OF INVERSION LAYERS IN 3C SILICON CARBIDE

R. E. AVILA, J. J. KOPANSKI, and C. D. FUNG (Case Western Reserve University, Cleveland, OH) Applied Physics Letters (ISSN 0003-6951), vol. 49, Aug. 11, 1986, p. 334-336. refs
(Contract NAG3-490; NAG3-389)

A study on the field-induced surface-charge region in 3C silicon carbide (SiC) using 1 MHz capacitance-voltage (C-V) measurements at room temperature is here reported. A double column mercury probe was used on oxidized SiC substrates to form metal-oxide-semiconductor (MOS) structures. These structures were characterized in terms of the substrate doping profile, effective fixed oxide charge, and interface trap density. A distinctive feature of the MOS C-V curves from accumulation to inversion is that after going into deep depletion the capacitance rises to its equilibrium inversion level during the voltage sweep. Capacitance transient measurements indicate that the minority-carrier generation occurs at the SiO₂/SiC interface. Author

A87-12292* Case Western Reserve Univ., Cleveland, Ohio.

STOICHIOMETRIC DISTURBANCES IN COMPOUND SEMICONDUCTORS DUE TO ION IMPLANTATION

R. E. AVILA and C. D. FUNG (Case Western Reserve University, Cleveland, OH) Journal of Applied Physics (ISSN 0021-8979), vol. 60, Sept. 1, 1986, p. 1602-1606. refs
(Contract NAG3-490; NAG3-389)

A method is developed to calculate the depth distribution of the local stoichiometric disturbance (SD) resulting from ion implantation in binary-compound substrates. The calculation includes first-order recoils considering projected range straggle of projectiles and recoils and lateral straggle of recoils. The method uses tabulated final-range statistics to infer the projectile range distributions at intermediate energies. This approach greatly simplifies the calculation with little compromise on accuracy as compared to existing procedures. As an illustration, the SD profile is calculated for implantation of boron, silicon, and aluminum in silicon carbide. The results for the latter case suggest that the SD may be responsible for otherwise unexplained distortions in

the annealed aluminum profile. A comparison with calculations by other investigators using the Boltzmann transport equation shows good agreement. Author

A87-14222* National Aeronautics and Space Administration. Lewis Research Center, Cleveland, Ohio.

CELL PERFORMANCE AND DEFECT BEHAVIOR IN PROTON-IRRADIATED LITHIUM-COUNTERDOPED N(+)-P SILICON SOLAR CELLS

I. WEINBERG, J. W. STUPICA, C. K. SWARTZ (NASA, Lewis Research Center, Cleveland, OH), and C. GORADIA (Cleveland State University, OH). Journal of Applied Physics (ISSN 0021-8979), vol. 60, Sept. 15, 1986, p. 2179-2181. refs

Lithium-counterdoped n(+)-p silicon solar cells were irradiated by 10-MeV protons, and their performance was determined as a function of fluence. It was found that the cell with the highest lithium concentration exhibited the higher radiation resistance. Deep-level transient spectroscopy studies of deep-level defects were used to identify two lithium-related defects. Defect energy levels obtained after the present 10-MeV irradiations were found to be markedly different than those observed after previous 1-MeV electron irradiations. However, the present DLTS data are consistent with previous suggestion by Weinberg et al. (1984) of a lithium-oxygen interaction which tends to inhibit formation of an interstitial boron-oxygen defect. Author

A87-15071* Case Western Reserve Univ., Cleveland, Ohio.

COMPENSATION IN EPITAXIAL CUBIC SiC FILMS

B. SEGALL (Case Western Reserve University, Cleveland, OH), S. A. ALTEROVITZ, E. J. HAUGLAND, and L. G. MATUS (NASA, Lewis Research Center, Cleveland, OH). Applied Physics Letters (ISSN 0003-6951), vol. 49, Sept. 8, 1986, p. 584-586. refs (Contract NCC3-25)

Hall measurements on four n-type cubic SiC films epitaxially grown by chemical vapor deposition on (100) Si substrates are presented, and the temperature-dependent carrier concentrations are analyzed. Samples are found to be highly compensated (greater than 90 percent) contrary to the assumption made in previously published work, and the donor ionization energies, E(D), are shown to be less than one-half the values quoted previously. New E(D) and donor concentration values, however, provide evidence for identifying the donors as nitrogen in cubic SiC. R.R.

A87-20519* Nebraska Univ., Lincoln.

VARIABLE ANGLE OF INCIDENCE SPECTROSCOPIC ELLIPSOMETRY APPLICATION TO GaAs-Al(x)Ga(1-x)As MULTIPLE HETEROSTRUCTURES

PAUL G. SNYDER, MARTIN C. ROST, GEORGE H. BU-ABBUD, JOHN A. WOOLLAM (Nebraska, University, Lincoln), and SAMUEL A. ALTEROVITZ (NASA, Lewis Research Center, Cleveland, OH). Journal of Applied Physics (ISSN 0021-8979), vol. 60, Nov. 1, 1986, p. 3293-3302. refs (Contract NAG3-154)

The sensitivity of spectroscopic ellipsometry data to multilayer model parameters is shown to be a strong function of the angle of incidence. A quantitative study of sensitivity versus angle of incidence is performed for a GaAs-Al(x)Ga(1-x)As-GaAs substrate structure, showing that maximum sensitivity to layer thicknesses and AlGaAs composition occurs near the wavelength-dependent principal angle. These results are verified by experimental measurements on two molecular-beam epitaxy grown samples. Author

A87-21237* National Aeronautics and Space Administration. Lewis Research Center, Cleveland, Ohio.

FORMATION OF A PN JUNCTION ON AN ANISOTROPICALLY ETCHED GaAs SURFACE USING METALORGANIC CHEMICAL VAPOR DEPOSITION

R. P. LEON, S. G. BAILEY, G. A. MAZARIS, and W. D. WILLIAMS (NASA, Lewis Research Center, Cleveland, OH). Applied Physics Letters (ISSN 0003-6951), vol. 49, Oct. 13, 1986, p. 945-947. refs

A continuous p-type GaAs epilayer has been deposited on an n-type sawtooth GaAs surface using MOCVD. A wet chemical etching process was used to expose the intersecting (111)Ga and (-1 -1 1)Ga planes with 6-micron periodicity. Charge-collection microscopy was used to verify the presence of the pn junction thus formed and to measure its depth. The ultimate goal of this work is to fabricate a V-groove GaAs cell with improved absorptivity, high short-circuit current, and tolerance to particle radiation. Author

A87-23967* National Aeronautics and Space Administration. Lewis Research Center, Cleveland, Ohio.

ELLIPSOMETRIC AND OPTICAL STUDY OF AMORPHOUS HYDROGENATED CARBON FILMS

S. A. ALTEROVITZ, J. D. WARNER, D. C. LIU, and J. J. POUCH (NASA, Lewis Research Center, Cleveland, OH). Electrochemical Society, Journal (ISSN 0013-4651), vol. 133, Nov. 1986, p. 2339-2342. refs

A low-frequency plasma deposition system was used to prepare amorphous hydrogenated carbon (a-C:H) films. The growth energy was varied by changing the power and/or pressure of the plasma. Ellipsometry and optical absorption were used to obtain the optical energy gap, the density of states, and the refractive index. Ion sputtering was used in conjunction with ellipsometry and Auger electron spectroscopy to get absolute sputtering rates. The plasma deposited a-C:H is amorphous with an optical energy gap of approximately 2.0-2.4 eV. These a-C:H films have higher density and/or hardness, higher refractive index, and lower optical energy gaps with increasing energy of the particles in the plasma, while the density of states remains unchanged. These results are in agreement with, and give a fine-tuned positive confirmation to, an existing conjecture on the nature of the a-C:H films (Kaplan et al., 1985). Author

A87-27198* Nebraska Univ., Lincoln.

THERMAL AND STRUCTURAL STABILITY OF COSPUTTERED AMORPHOUS Ta(x)Cu(1-x) ALLOY THIN FILMS ON GaAs

J. E. OH, J. A. WOOLLAM, K. D. AYLESWORTH, D. J. SELLMYER (Nebraska, University, Lincoln), and J. J. POUCH (NASA, Lewis Research Center, Cleveland, OH). Journal of Applied Physics (ISSN 0021-8979), vol. 60, Dec. 15, 1986, p. 4281-4286. refs (Contract NAG3-154; NSF INT-84-19546)

The characteristics of thin films of Ta-Cu, prepared over a wide range of compositions by cosputter deposition onto GaAs and fused quartz substrates, are studied by X-ray diffraction and van der Pauw resistivity measurement. Results show films to be amorphous over the range of 55-95 at. pct, and show Ta(93)Cu(7) barriers to be effective in preventing Au in-diffusion, with a 3000-A layer remaining unpenetrated after an annealing at 700 C for 20 min. Diffusion of Ga and/or As into amorphous 93 at. pct Ta is found to be more rapid than that of Au, and interfacial reactions were shown to form compounds including Ta₃Au, CuAu, TaAs₂, and Ga₃Cu₇ above 700 C. R.R.

A87-28295* Nebraska Univ., Lincoln.

ANTICORRELATION OF SHUBNIKOV-DEHAAS AMPLITUDES AND NEGATIVE MAGNETORESISTANCE MAGNITUDES IN INTERCALATED PITCH BASED GRAPHITE FIBERS

JOHN A. WOOLLAM, V. NATARAJAN (Nebraska, University, Lincoln), and BRUCE BRANDT (MIT, Cambridge, MA) Applied Physics Communications (ISSN 0277-9374), vol. 6, no. 2-3, 1986, p. 121-129. NSF-supported research. refs
(Contract NAG3-95)

In pitch based carbon fibers at low temperatures, simultaneous presence of a negative magnetoresistance and the Shubnikov-deHaas effect are found. The strengths of these effects correlate inversely. These results can be understood in terms of the amount of order vs disorder in the fiber, as described by Guigon and Oberlin from structural studies. Author

A87-30023* Rensselaer Polytechnic Inst., Troy, N.Y.

SHALLOW N(+) DIFFUSION INTO INP BY AN OPEN-TUBE DIFFUSION TECHNIQUE

SORAB K. GHANDHI and KRISHNA K. PARAT (Rensselaer Polytechnic Institute, Troy, NY) Applied Physics Letters (ISSN 0003-6951), vol. 50, Jan. 26, 1987, p. 209-211. refs
(Contract NAG3-604)

Very shallow n(+) layers have been obtained in InP by using gallium sulfide as a source for sulfur diffusion, and chemically vapor-deposited SiO₂ as a cap. Diffusions were carried out from 585 to 725 C in an open-tube system with a nitrogen ambient. The doping profile of sulfur in InP is estimated to be of the complementary error function type with a surface concentration of 5.6×10^{18} to the 18th/cc and a diffusion constant of 1.1×10^{-14} to the -14th sq cm/s at 670 C. Diodes made on n(+)-p junctions obtained by this diffusion technique show ideality factors close to unity and saturation current densities as low as 3.4×10^{-10} to the -15th A/sq cm, signifying the presence of a defect-free junction. These diffusions, with junction depths in the 400-700 Å range, are ideal for solar cell applications. Author

A87-30025* Case Western Reserve Univ., Cleveland, Ohio.

ANTIPHASE BOUNDARIES IN EPITAXIALLY GROWN BETA-SiC

P. PIROUZ, C. M. CHOREY (Case Western Reserve University, Cleveland, OH), and J. A. POWELL (NASA, Lewis Research Center, Cleveland, OH) Applied Physics Letters (ISSN 0003-6951), vol. 50, Jan. 26, 1987, p. 221-223. refs
(Contract NGT-36-027-807)

When the surface of beta-SiC, grown epitaxially on (001) silicon by chemical vapor deposition, is chemically etched, boundaries appear which may be observed by optical or scanning electron microscopy. Examination by plan-view and cross-sectional transmission electron microscopy shows boundaries in the film which exhibit line or fringe contrast. Convergent beam electron diffraction has been used to show that these boundaries separate domains that are in an antiphase relationship to each other. A model is presented which discusses the formation of these domains from independent nucleation on a stepped substrate surface. Author

A87-39687* University of Southern California, Los Angeles.

NONLINEAR ABSORPTION IN ALGaAs/GaAs MULTIPLE QUANTUM WELL STRUCTURES GROWN BY METALORGANIC CHEMICAL VAPOR DEPOSITION

H. C. LEE, A. HARIZ, P. D. DAPKUS, A. KOST, M. KAWASE (Southern California, University, Los Angeles, CA) et al. Applied Physics Letters (ISSN 0003-6951), vol. 50, April 27, 1987, p. 1182-1184. Research supported by University of Southern California, U.S. Army, and NSF. refs
(Contract AF-AFOSR-84-305; AF-AFOSR-85-0297; NAG3-529)

This paper reports the study of growth conditions for achieving the sharp exciton resonances and low-intensity saturation of these resonances in AlGaAs-GaAs multiple quantum well structures grown by metalorganic chemical vapor deposition. Low growth temperature is necessary to observe this sharp resonance feature at room temperature. The optimal growth conditions are a tradeoff

between the high temperatures required for high quality AlGaAs and low temperatures required for high-purity GaAs. A strong optical saturation of the excitonic absorption has been observed. A saturation density as low as 250 W/sq cm is reported. Author

A87-42846* Case Western Reserve Univ., Cleveland, Ohio.

COMMENT ON 'TEMPERATURE DEPENDENCE OF ELECTRICAL PROPERTIES OF NON-DOPED AND NITROGEN-DOPED BETA-SiC SINGLE CRYSTALS GROWN BY CHEMICAL VAPOR DEPOSITION'

B. SEGALL (Case Western Reserve University, Cleveland, OH), S. A. ALTEROVITZ, E. J. HAUGLAND, and L. G. MATUS (NASA, Lewis Research Center, Cleveland, OH) Applied Physics Letters (ISSN 0003-6951), vol. 50, May 25, 1987, p. 1533, 1534; Reply, p. 1534. refs

A87-44562* Nebraska Univ., Lincoln.

INTERACTIONS OF AMORPHOUS TA(X)CU(1-X) (X = 0.93 AND 0.80) ALLOY FILMS WITH AU OVERLAYERS AND GaAs SUBSTRATES

JAE E. OH, JOHN A. WOOLLAM (Nebraska, University, Lincoln), and JOHN J. POUCH (NASA, Lewis Research Center, Cleveland, OH) Applied Physics Letters (ISSN 0003-6951), vol. 50, June 15, 1987, p. 1722-1724. refs
(Contract NAG3-154)

Amorphous Ta(93)Cu(7) and Ta(80)Cu(20) alloy films are prepared by cosputtering of pure Ta and pure Cu targets with a rotating sample holder table. To investigate the possible application of these materials as diffusion barriers for the Au-GaAs system, vacuum annealings are made in the temperature range from 200 to 800 C. Resistivity change, X-ray diffraction, and Auger electron spectroscopy measurements are performed to find the chemical and metallurgical stabilities of these materials in this system. The reaction temperature for Ta(x)Cu(1-x) in contact with GaAs lies between 500 and 700 C. For Au in contact with Ta(x)Cu(1-x) the reaction occurs at about 600 C. Amorphous Ta(93)Cu(7) shows different interdiffusion characteristics with surrounding elements than does Ta(80)Cu(20). Author

A87-44875* National Aeronautics and Space Administration. Lewis Research Center, Cleveland, Ohio.

GROWTH AND CHARACTERIZATION OF CUBIC SiC SINGLE-CRYSTAL FILMS ON Si

J. ANTHONY POWELL, G. MATUS, and MARIA A. KUCZMARSKI (NASA, Lewis Research Center, Cleveland, OH) Electrochemical Society, Journal (ISSN 0013-4651), vol. 134, June 1987, p. 1558-1565. refs

Morphological and electrical characterization results are presented for cubic SiC films grown by chemical vapor deposition on single-crystal Si substrates. The films, up to 40 microns thick, were characterized by optical microscopy, (SEM), (TEM), electron channeling, surface profilometry, and Hall measurements. A variety of morphological features observed on the SiC films are described. Electrical measurements showed a decrease in the electron mobility with increasing electron carrier concentration, similar to that observed in Si. Room-temperature electron mobilities up to 520 sq cm/V-s (at an electron carrier concentration of 5×10^{18} to the 16th/cu cm) were measured. Finally, a number of parameters believed to be important in the growth process were investigated, and some discussion is given of their possible effects on the film characteristics. Author

A87-48733* National Aeronautics and Space Administration. Lewis Research Center, Cleveland, Ohio.

DENDRITIC SOLIDIFICATION IN A BINARY ALLOY MELT - COMPARISON OF THEORY AND EXPERIMENT

V. LAXMANAN (NASA, Lewis Research Center, Cleveland, OH) Journal of Crystal Growth (ISSN 0022-0248), vol. 83, no. 3, June 1987, p. 391-402. NASA-supported research. refs

A simple model for 'constrained' growth of an 'array' of cells or dendrites in a binary alloy melt, in the presence of a positive temperature gradient in the liquid ahead of the tips, is presented. The cell or dendrite tip radius is calculated by adopting both the

'ad hoc' assumption of minimum undercooling at the tips as well as the more recently proposed hypothesis of dendritic growth under conditions of 'marginal stability'. Theoretical predictions of the model have been compared with experimental data in binary succinonitrile-acetone alloys. It has been shown that, according to the present model, the 'marginally stable' state may be virtually indistinguishable from the 'minimum undercooled' state, under the usual conditions of dendritic growth. Author

N87-17515*# M/A-COM, Inc., Burlington, Mass.
THE 60 GHZ IMPATT DIODE DEVELOPMENT Final Report, Mar. 1982 - Jul. 1986

ROVINDRA DAT, MURTHY AYYAGARI, DAVID HOAG, DAVID SLOAT, YOGI ANAND, and STAN WHITELEY Jul. 1986 174 p (Contract NAS3-23339)
 (NASA-CR-179536; NAS 1.26:179536) Avail: NTIS HC A08/MF A01 CSCL 20L

The objective is to develop 60 GHz IMPATT diodes suitable for communications applications. The performance goals of the 60 GHz IMPATT is 1W CW output power with a conversion efficiency of 15 percent and 10-year lifetime. The final design of the 60 GHz IMPATT structure evolved from computer simulations performed at the University of Michigan. The initial doping profile, involving a hybrid double-drift (HDD) design, was derived from a drift-diffusion model that used the static velocity-field characteristics for GaAs. Unfortunately, the model did not consider the effects of velocity undershoot and delay of the avalanche process due to energy relaxation. Consequently, the initial devices were oscillating at a much lower frequency than anticipated. With a revised simulation program that included the two effects given above, a second HDD profile was generated and was used as a basis for fabrication efforts. In the area of device fabrication, significant progress was made in epitaxial growth and characterization, wafer processing, and die assembly. The organo-metallic chemical vapor deposition (OMCVD) was used. Starting with a baseline X-Band IMPATT technology, appropriate processing steps were modified to satisfy the device requirements at V-Band. In terms of efficiency and reliability, the device requirements dictate a reduction in its series resistance and thermal resistance values. Qualitatively, researchers were able to reduce the diodes' series resistance by reducing the thickness of the N+ GaAs substrate used in its fabrication. Author

N87-20821*# National Aeronautics and Space Administration. Lewis Research Center, Cleveland, Ohio.

RAPID THERMAL ANNEALING OF AMORPHOUS HYDROGENATED CARBON (A-C:H) FILMS

SAMUEL A. ALTEROVITZ, JOHN J. POUCH, and JOSEPH D. WARNER Apr. 1987 8 p Presented at the Spring Meeting of the Materials Research Society, Anaheim, Calif., 21-25 Apr. 1987 (NASA-TM-89859; E-3519; NAS 1.15:89859) Avail: NTIS HC A02/MF A01 CSCL 20L

Amorphous hydrogenated carbon (a-C:H) films were deposited on silicon and quartz substrates by a 30 kHz plasma discharge technique using methane. Rapid thermal processing of the films was accomplished in nitrogen gas using tungsten halogen light. The rapid thermal processing was done at several fixed temperatures (up to 600 C), as a function of time (up to 1800 sec). The films were characterized by optical absorption and by ellipsometry in the near UV and the visible. The bandgap, estimated from extrapolation of the linear part of a Tauc plot, decreases both with the annealing temperature and the annealing time, with the temperature dependence being the dominating factor. The density of states parameter increases up to 25 percent and the refractive index changes up to 20 percent with temperature increase. Possible explanations of the mechanisms involved in these processes are discussed. Author

N87-23304*# National Aeronautics and Space Administration. Lewis Research Center, Cleveland, Ohio.

ALGAS GROWTH BY OMCVD USING AN EXCIMER LASER

JOSEPH D. WARNER, DAVID M. WILT, JOHN J. POUCH, and PAUL R. ARON Dec. 1986 11 p Presented at the Fall Meeting of the Materials Research Society, Boston, Mass., 1-5 Dec. 1986

(NASA-TM-88937; E-3379; NAS 1.15:88937) Avail: NTIS HC A02/MF A01 CSCL 20B

AlGaAs has been grown on GaAs by laser assisted OMCVD using an excimer laser, wavelength 193 nm, and a Cambridge OMCVD reactor. Films were grown at temperatures of 450 and 500 C with the laser beam parallel to the surface and impinging onto the surface at 15 deg from parallel. The samples were heated by RF coils while the laser beam was perpendicular to the gas flow. Typical gas flow parameters are 12 slm of H₂, 15 sccm of Ga(CH₃)₃, 13 sccm of Al(CH₃)₃, and a pressure of 250 mbar. The initial energy density of the beam at the surface was 40 mJ/sq cm, the pulse rate was 20 pps, and the growth time was 7 min. The films were analyzed by Auger electron spectroscopy for the aluminum concentration and by TEM for the surface morphology. Author

N87-25017*# National Aeronautics and Space Administration. Lewis Research Center, Cleveland, Ohio.

BORON NITRIDE: COMPOSITION, OPTICAL PROPERTIES AND MECHANICAL BEHAVIOR

JOHN J. POUCH, SAMUEL A. ALTEROVITZ, KAZUHISA MIYOSHI, and JOSEPH D. WARNER Apr. 1987 9 p Presented at the Spring Meeting of the Materials Research Society, Anaheim, Calif., 21-25 Apr. 1987

(NASA-TM-89849; E-3514; NAS 1.15:89849) Avail: NTIS HC A02/MF A01 CSCL 20L

A low energy ion beam deposition technique was used to grow boron nitride films on quartz, germanium, silicon, gallium arsenide, and indium phosphate. The film structure was amorphous with evidence of a hexagonal phase. The peak boron concentration was 82 at %. The carbon and oxygen impurities were in the 5 to 8 at % range. Boron-nitrogen and boron-boron bonds were revealed by X-ray photoelectron spectroscopy. The index of refraction varied from 1.65 to 1.67 for films deposited on III-V compound semiconductors. The coefficient of friction for boron nitride in sliding contact with diamond was less than 0.1. The substrate was silicon. Author

N87-27541*# National Aeronautics and Space Administration. Lewis Research Center, Cleveland, Ohio.

A V-GROOVED ALGAS/GAAS PASSIVATED PN JUNCTION

SHEILA G. BAILEY, ROSA P. LEON, and ANNE ARRISON May 1987 12 p Presented at the 19th Photovoltaic Specialists Conference, New Orleans, La., 4-8 May 1987; sponsored by AIEEE

(NASA-TM-100138; E-3688; NAS 1.15:100138) Avail: NTIS HC A02/MF A01 CSCL 20L

A passivated, V-grooved GaAs solar cell offers important advantages in terms of improved optical coupling, higher short circuit current, and increased tolerance to particle radiation when compared to the planar cell configuration. An AlGaAs epilayer has been deposited on a p-type GaAs epilayer grown on an n-type V-grooved GaAs surface using MOCVD. A wet chemical etching process was used to produce a V-pattern with a 7.0 micron periodicity. Reflectivity measurements substantiate the expected decrease in solar reflectance. Scanning electron microscopy techniques were used to confirm the presence of the AlGaAs layer and verify the existence of a pn junction. Author

N87-28741*# GTE Labs., Inc., Waltham, Mass.

A COMPARATIVE STUDY OF THE INFLUENCE OF BUOYANCY DRIVEN FLUID FLOW ON GAAS CRYSTAL GROWTH

J. A. KAFALIS and A. H. BELLOWES *In* ESA, Proceedings of the Sixth European Symposium on Material Sciences under Microgravity Conditions p 525-527 Feb. 1987

(Contract NAS3-24664)

Avail: NTIS HC A99/MF A01; print copy avail. EPD, ESTEC, Noordwijk, The Netherlands Dfl 100 CSCL 20B

An experiment on the effect of gravity-driven fluid flow on GaAs crystal growth under a variety of Earth-based conditions and in microgravity aboard the space shuttle is described. Earth-based growth is performed under stabilizing and destabilizing temperature gradients, with and without applied magnetic fields. The space growth experiment is flown in a self-contained payload container through NASA's Get Away Special program. The scope of the experiment and the experimental apparatus are outlined. Results of the Earth-based portions of the experiment are presented.

ESA

77

THERMODYNAMICS AND STATISTICAL PHYSICS

Includes quantum mechanics; theoretical physics; and Bose and Fermi statistics.

A87-14665* National Aeronautics and Space Administration. Lewis Research Center, Cleveland, Ohio.

A UNIVERSAL EQUATION OF STATE FOR SOLIDS

P. VINET, J. FERRANTE (NASA, Lewis Research Center, Cleveland, OH), J. R. SMITH (GM Research Laboratories, Warren, MI), and J. H. ROSE (Iowa State University of Science and Technology, Ames) *Journal of Physics C - Solid State Physics* (ISSN 0022-3719), vol. 19, 1986, p. L467-L473. Research supported by the Ministere des Relations Exterieures. refs

(Contract W-7405-ENG-82)

The total energy versus interatomic spacing of ionic, metallic, covalent, and rare-gas solids is examined, and a universal form for pressure as a function of volume for all classes of solids in compression is derived. The relation is shown to hold for pressure-volume data for hydrogen and deuterium, xenon, cesium, molybdenum, sodium chloride, and magnesium oxide. R.R.

A87-51962* National Aeronautics and Space Administration. Lewis Research Center, Cleveland, Ohio.

COMPRESSIBILITY OF SOLIDS

P. VINET, J. FERRANTE (NASA, Lewis Research Center, Cleveland, OH), J. H. ROSE (DOE, Ames Laboratory, IA), and J. R. SMITH (GM Research Laboratories, Warren, MI) *Journal of Geophysical Research* (ISSN 0148-0227), vol. 92, Aug. 10, 1987, p. 9319-9325. Research supported by the Ministere des Relations Exterieures. refs

(Contract W-7405-ENG-82)

A universal form is proposed for the equation of state (EOS) of solids. Good agreement is found for a variety of test data. The form of the EOS is used to suggest a method of data analysis, which is applied to materials of geophysical interest. The isothermal bulk modulus is discussed as a function of the volume and of the pressure. The isothermal compression curves for materials of geophysical interest are examined. C.D.

N87-20274*# National Aeronautics and Space Administration. Lewis Research Center, Cleveland, Ohio.

THERMODYNAMICS AND COMBUSTION MODELING

FRANK J. ZELENK. *In its* NASA-Chinese Aeronautical Establishment (CAE) Symposium p 113-133 1986

Avail: NTIS HC A01/MF A01 CSCL 20M

Modeling fluid phase phenomena blends the conservation equations of continuum mechanics with the property equations of

thermodynamics. The thermodynamic contribution becomes especially important when the phenomena involve chemical reactions as they do in combustion systems. The successful study of combustion processes requires (1) the availability of accurate thermodynamic properties for both the reactants and the products of reaction and (2) the computational capabilities to use the properties. A discussion is given of some aspects of the problem of estimating accurate thermodynamic properties both for reactants and products of reaction. Also, some examples of the use of thermodynamic properties for modeling chemically reacting systems are presented. These examples include one-dimensional flow systems and the internal combustion engine. Author

N87-20277*# National Aeronautics and Space Administration. Lewis Research Center, Cleveland, Ohio.

THEORETICAL KINETIC COMPUTATIONS IN COMPLEX REACTING SYSTEMS

DAVID A. BITTKER *In its* NASA-Chinese Aeronautical Establishment (CAE) Symposium p.175-189 1986

Avail: NTIS HC A01/MF A01 CSCL 20M

Nasa Lewis' studies of complex reacting systems at high temperature are discussed. The changes which occur are the result of many different chemical reactions occurring at the same time. Both an experimental and a theoretical approach are needed to fully understand what happens in these systems. The latter approach is discussed. The differential equations which describe the chemical and thermodynamic changes are given. Their solution by numerical techniques using a detailed chemical mechanism is described. Several different comparisons of computed results with experimental measurements are also given. These include the computation of (1) species concentration profiles in batch and flow reactions, (2) rocket performance in nozzle expansions, and (3) pressure versus time profiles in hydrocarbon ignition processes. The examples illustrate the use of detailed kinetic computations to elucidate a chemical mechanism and to compute practical quantities such as rocket performance, ignition delay times, and ignition lengths in flow processes. Author

81

ADMINISTRATION AND MANAGEMENT

Includes management planning and research.

N87-12384*# National Aeronautics and Space Administration. Lewis Research Center, Cleveland, Ohio.

STRATEGIC PLAN, 1985

1985 33 p

(NASA-TM-89263; NAS 1.15:89263) Avail: NTIS HC A03/MF A01 CSCL 05A

The Lewis Strategic Plan was updated for 1985 and beyond. Major programs for the space station, the advanced turboprop, the Advanced Communications Technology Satellite (ACTS), and the Altitude Wind Tunnel were begun or greatly expanded during 1984. In parallel, The Lewis aeropropulsion research and technology program was extensively evaluated and reviewed; a reduced and reoriented program emerged. The thrusts and implementation plans for these programs are described as they pertain to the individual directorates. Other key accomplishments and plans are summarized. B.G.

URBAN TECHNOLOGY AND TRANSPORTATION

Includes applications of space technology to urban problems; technology transfer; technology assessment; and surface and mass transportation.

A87-18034*# National Aeronautics and Space Administration. Lewis Research Center, Cleveland, Ohio.

DOE/NASA AUTOMOTIVE STIRLING ENGINE PROJECT - OVERVIEW 86

D. G. BEREMAND and R. K. SHALTENS (NASA, Lewis Research Center, Cleveland, OH) IN: IECEC '86; Proceedings of the Twenty-first Intersociety Energy Conversion Engineering Conference, San Diego, CA, August 25-29, 1986. Volume 1. Washington, DC, American Chemical Society, 1986, p. 430-438. Previously announced in STAR as N86-29731. refs

The DOE/NASA Automotive Stirling Engine Project is reviewed and its technical progress and status are presented. Key technologies in materials, seals, and piston rings are progressing well. Seven first-generation engines, and modifications thereto, have accumulated over 15,000 hr of test time, including 1100 hr of in-vehicle testing. Results indicate good progress toward the program goals. The first second-generation engine is now undergoing initial testing. It is expected that the program goal of a 30-percent improvement in fuel economy will be achieved in tests of a second-generation engine in a Celebrity vehicle.

Author

N87-10777*# Argonne National Lab., Ill.

ANL/RBC: A COMPUTER CODE FOR THE ANALYSIS OF RANKINE BOTTOMING CYCLES, INCLUDING SYSTEM COST EVALUATION AND OFF-DESIGN PERFORMANCE Final Report

G. A. MCLENNAN May 1986 68 p
(Contract NASA ORDER C-80002-E; DE-AI01-86CE-50162)
(NASA-CR-179462; NAS 1.26:179462; DOE/NASA/80002-1;
ANL/CT-86-3) Avail: NTIS HC A04/MF A01 CSCL 10B

This report describes, and is a User's Manual for, a computer code (ANL/RBC) which calculates cycle performance for Rankine bottoming cycles extracting heat from a specified source gas stream. The code calculates cycle power and efficiency and the sizes for the heat exchangers, using tabular input of the properties of the cycle working fluid. An option is provided to calculate the costs of system components from user defined input cost functions. These cost functions may be defined in equation form or by numerical tabular data. A variety of functional forms have been included for these functions and they may be combined to create very general cost functions. An optional calculation mode can be used to determine the off-design performance of a system when operated away from the design-point, using the heat exchanger areas calculated for the design-point.

Author

N87-13359*# National Aeronautics and Space Administration. Lewis Research Center, Cleveland, Ohio.

PROGRESS OF STIRLING CYCLE ANALYSIS AND LOSS MECHANISM CHARACTERIZATION Final Report

R. C. TEW, JR. 1986 19 p Presented at the 24th Automotive Technology Development Meeting, Dearborn, Mich., 27-30 Oct. 1986; sponsored by Society of Automotive Engineers
(NASA-TM-88891; DOE/NASA-50112/67; E-3302; NAS 1.15:88891) Avail: NTIS HC A01/MF A01 CSCL 10B

An assessment of Stirling engine thermodynamic modeling and design codes shows a general deficiency; this deficiency is due to poor understanding of the fluid flow and heat transfer phenomena that occur in the oscillating flow and pressure level environment within the engines. Stirling engine thermodynamic loss mechanisms are listed. Several experimental and computational research efforts now underway to characterize various loss mechanisms are reviewed. The need for additional experimental rigs and rig upgrades is discussed. Recent developments and current efforts

in Stirling engine thermodynamic modeling are also reviewed.

Author

N87-15030*# Garrett Turbine Engine Co., Phoenix, Ariz.

BRAYTON CYCLE SOLARIZED ADVANCED GAS TURBINE Final Report, Feb. 1980 - Mar. 1986

Dec. 1986 135 p

(Contract DEN3-181)

(NASA-CR-179559; DOE/NASA-0181; NAS 1.26:179559;
GARRETT-31-6190) Avail: NTIS HC A07/MF A01 CSCL 10B

Described is the development of a Brayton Engine/Generator Set for solar thermal to electrical power conversion, authorized under DOE/NASA Contract DEN3-181. The objective was to design, fabricate, assemble, and test a small, hybrid, 20-kW Brayton-engine-powered generator set. The latter, called a power conversion assembly (PCA), is designed to operate with solar energy obtained from a parabolic dish concentrator, 11 meters in diameter, or with fossil energy supplied by burning fuels in a combustor, or by a combination of both (hybrid model). The CPA consists of the Brayton cycle engine, a solar collector, a belt-driven 20-kW generator, and the necessary control systems for automatic operation in solar-only, fuel-only, and hybrid modes to supply electrical power to a utility grid. The original configuration of the generator set used the GTEC Model GTP36-51 gas turbine engine for the PCA prime mover. However, subsequent development of the GTEC Model AGT101 led to its selection as the powersource for the PCA. Performance characteristics of the latter, thermally coupled to a solar collector for operation in the solar mode, are presented. The PCA was successfully demonstrated in the fuel-only mode at the GTEC Phoenix, Arizona, facilities prior to its shipment to Sandia National Laboratory in Albuquerque, New Mexico, for installation and testing on a test bed concentrator (parabolic dish). Considerations relative to Brayton-engine development using the all-ceramic AGT101 when it becomes available, which would satisfy the DOE heat engine efficiency goal of 35 to 41 percent, are also discussed in the report.

Author

N87-15031*# National Aeronautics and Space Administration. Lewis Research Center, Cleveland, Ohio.

ADVANCED STIRLING CONVERSION SYSTEMS FOR TERRESTRIAL APPLICATIONS Final Report

R. K. SHALTENS 1987 26 p To be presented at the Solar Energy Conference, Honolulu, Hawaii, 22-27 Mar. 1987; cosponsored by ASME, JSME and JSES

(Contract DE-AT04-85AL-33408)

(NASA-TM-88897; E-3314; DOE/NASA-33408/1; NAS 1.15:88897) Avail: NTIS HC A03/MF A01 CSCL 10B

Under the Department of Energy's (DOE) Solar Thermal Technology Program, Sandia National Laboratories (SNLA) is developing heat engines for terrestrial Solar Distributed Heat Receivers. SNLA has identified the Stirling to be one of the most promising candidates for the terrestrial applications. The free-piston Stirling engine (FPSE) has the potential to meet the DOE goals for both performance and cost. The National Aeronautics and Space Administration (NASA) Lewis Research Center (LeRC) is conducting free-piston Stirling activities which are directed toward a dynamic power source for space applications. Space power system requirements include high efficiency, very long life, high reliability and low vibration. The FPSE has the potential for future high power space conversion systems, either solar or nuclear. Generic free-piston technology is currently being developed by LeRC for DOE/ORNL for use with a residential heat pump under an Interagency Agreement. Since 1983, the SP-100 Program (DOD/NASA/DOE) is developing dynamic power sources for space. Although both applications (heat pump and space power) appear to be quite different, their requirements complement each other. A cooperative Interagency Agreement (IAA) was signed in 1985 with NASA Lewis to provide technical management for an Advanced Stirling Conversion System (ASCS) for SNLA. Conceptual design(s) using a free-piston Stirling (FPSE), and a heat pipe will be discussed. The ASCS will be designed using technology which can reasonably be expected to be available in the 1980's.

Author

N87-16663*# National Aeronautics and Space Administration. Lewis Research Center, Cleveland, Ohio.

OVERVIEW OF THE 1986 FREE-PISTON STIRLING ACTIVITIES AT NASA LEWIS RESEARCH CENTER

DONALD L. ALGER Oct. 1986 17 p Presented at the 24th Automotive Technology Development Contractors Coordination Meeting, Dearborn, Mich., 27-30 Oct. 1986; sponsored by DOE (NASA-TM-88895; E-3312; NAS 1.15:88895) Avail: NTIS HC A02/MF A01 CSCL 13F

An overview of the NASA Lewis Research Center's free-piston Stirling engine research is presented, including efforts to improve and advance its design for use in specific space power applications. These efforts are a part of the SP-100 program being conducted to support the Department of Defense (DOD), Department of Energy (DOE) and NASA. Such efforts include: (1) the testing and improvement of 25 kWe Stirling Space Power Demonstrator Engine (SPDE); (2) the preliminary design of 25 kWe single-cylinder Experimental Stirling Space Engine (ESSE); and, (3) a study to determine the feasibility of scaling a single-cylinder free-piston Stirling engine/linear alternator to 150 kWe. Other NASA Lewis free-piston Stirling engine activities will be described, directed toward the advancement of general free-piston Stirling engine technology and its application in specific terrestrial applications. One such effort, supported by DOE/Oak Ridge National Laboratory (DRNL), is the development of a free-piston Stirling engine which produces hydraulic power. Finally, a terrestrial solar application involving a conceptual design of a 25 kWe Solar Advanced Stirling Conversion System (ASCS) capable of delivering power to an electric utility grid will be discussed. The latter work is supported by DOE/Sandia National Laboratory (SNLA). Author

N87-16664*# National Aeronautics and Space Administration. Lewis Research Center, Cleveland, Ohio.

EFFECT OF WATER ON HYDROGEN PERMEABILITY Final Report

DAVID HULLIGAN and WILLIAM A. TOMAZIC Jan. 1987 25 p (Contract DE-AI01-85CE-50112) (NASA-TM-88898; E-3321; DOE/NASA-50112-68; NAS 1.15:88898) Avail: NTIS HC A02/MF A01 CSCL 07D

Doping of hydrogen with CO and CO₂ was developed to reduce hydrogen permeation in Stirling engines by forming a low permeability oxide coating on the inner surface of the heater head tubes. Although doping worked well, under certain circumstances the protective oxide could be chemically reduced by the hydrogen in the engine. Some oxygen is required in the hydrogen to prevent reduction. Eventually, all the oxygen in the hydrogen gas - whatever its source - shows up as water. This is the result of hydrogen reducing the CO, CO₂, or the protective inner surface oxides. This water can condense in the engine system under the right conditions. If the concentration of water vapor is reduced to a low enough level, the hydrogen can chemically reduce the oxide coating, resulting in an increase in permeability. This work was done to define the minimum water content required to avoid this reduction in the oxide coating. The results of this testing show that a minimum of approximately 750 ppm water is required to prevent an increase in permeability of CG-27, a high temperature metal alloy selected for Stirling engine heater tubes. Author

N87-18470*# SKF Industries, Inc., King of Prussia, Pa.

SOLID LUBRICATION DESIGN METHODOLOGY, PHASE 2 Final Report

R. A. PALLINI, L. D. WEDEVEN, M. A. RAGEN, and B. B. AGGARWAL Feb. 1986 122 p Prepared in cooperation with Department of Energy, Washington, D.C.

(Contract DEN3-323) (NASA-CR-175114; DOE/NASA/0323-2; NAS 1.26:175114; AT86D002) Avail: NTIS HC A06/MF A01 CSCL 11G

The high temperature performance of solid lubricated rolling elements was conducted with a specially designed traction (friction) test apparatus. Graphite lubricants containing three additives (silver, phosphate glass, and zinc orthophosphate) were evaluated from room temperature to 540 C. Two hard coats were also evaluated. The evaluation of these lubricants, using a burnishing method of

application, shows a reasonable transfer of lubricant and wear protection for short duration testing except in the 200 C temperature range. The graphite lubricants containing silver and zinc orthophosphate additives were more effective than the phosphate glass material over the test conditions examined. Traction coefficients ranged from a low of 0.07 to a high of 0.6. By curve fitting the traction data, empirical equations for slope and maximum traction coefficient as a function of contact pressure (P), rolling speed (U), and temperature (T) can be developed for each lubricant. A solid lubricant traction model was incorporated into an advanced bearing analysis code (SHABERTH). For comparison purposes, preliminary heat generation calculations were made for both oil and solid lubricated bearing operation. A preliminary analysis indicated a significantly higher heat generation for a solid lubricated ball bearing in a deep groove configuration. An analysis of a cylindrical roller bearing configuration showed a potential for a low friction solid lubricated bearing. Author

N87-20137*# Mechanical Technology, Inc., Latham, N. Y.

AUTOMOTIVE STIRLING ENGINE DEVELOPMENT PROGRAM Semiannual Technical Progress Report, 1 Jan. - 30 Jun. 1985

W. ERNST, A. RICHEY, R. FARRELL, G. RIECKE, G. SMITH, R. HOWARTH, M. CRONIN, M. SIMETKOSKY, and J. MEACHER Feb. 1986 115 p

(Contract DEN3-32)

(NASA-CR-174972; DOE/NASA/0032-26; NAS 1.26:174972;

MTI-85ASE476SA8) Avail: NTIS HC A06/MF A01 CSCL 13F

The major accomplishments were the completion of the Basic Stirling Engine (BSE) and the Stirling Engine System (SES) designs on schedule, the approval and acceptance of those designs by NASA, and the initiation of manufacture of BSE components. The performance predictions indicate the Mod II engine design will meet or exceed the original program goals of 30% improvement in fuel economy over a conventional Internal Combustion (IC) powered vehicle, while providing acceptable emissions. This was accomplished while simultaneously reducing Mod II engine weight to a level comparable with IC engine power density, and packaging the Mod II in a 1985 Celebrity with no external sheet metal changes. The projected mileage of the Mod II Celebrity for the combined urban and highway CVS cycle is 40.9 mpg which is a 32% improvement over the IC Celebrity. If additional potential improvements are verified and incorporated in the Mod II, the mileage could increase to 42.7 mpg. B.G.

N87-21756*# National Aeronautics and Space Administration. Lewis Research Center, Cleveland, Ohio.

A 1987 OVERVIEW OF FREE-PISTON STIRLING TECHNOLOGY FOR SPACE POWER APPLICATION

JACK G. SLABY and DONALD L. ALGER 1987 13 p Proposed for presentation at the 22nd Intersociety Energy Conversion Engineering Conference, Philadelphia, Pa., 10-14 Aug. 1987; sponsored by AIAA, ANS, ASME, SAE, IEEE, ACS and AIChE (NASA-TM-89832; E-3485; NAS 1.15:89832) Avail: NTIS HC A02/MF A01 CSCL 10B

An overview is presented of the NASA Lewis Research Center free-piston Stirling engine activities directed toward space-power application. NASA Lewis serves as the project office to manage the newly initiated NASA SP-100 Advanced Technology Program. One of the major elements of this five-year program is the development of advanced power conversion concepts of which the Stirling cycle is a viable growth candidate. Under this program the status of the 25 kWe opposed-piston Space Power Demonstrator Engine (SPDE) is presented. Included in the SPDE discussion are comparisons between predicted and experimental engine performance, enhanced performance resulting from regenerator modification, increased operating stroke brought about by isolating the gas bearing flow between the displacer and power piston, identifying excessive energy losses and recommending corrective action, and a better understanding of linear alternator design and operation. Technology work is also conducted on heat exchanger concepts, both design and fabrication. Design parameters and conceptual design features are also presented

for a 25 kWe, single-cylinder free-piston Stirling space-power converter. Author

N87-22561*# National Aeronautics and Space Administration. Lewis Research Center, Cleveland, Ohio.

CALIBRATION AND COMPARISON OF THE NASA LEWIS FREE-PISTON STIRLING ENGINE MODEL PREDICTIONS WITH RE-1000 TEST DATA

STEVEN M. GENG 1987 22 p Proposed for presentation at the 22nd Intersociety Energy Conversion Engineering Conference, Philadelphia, Pa., 10-14 Aug. 1987; sponsored by AIAA, ANS, ASME, SAE, IEEE, ACS and AIChE (NASA-TM-89853; E-3520; NAS 1.15:89853) Avail: NTIS HC A02/MF A01 CSCL 13F

A free-piston Stirling engine performance code is being upgraded and validated at the NASA Lewis Research Center under an interagency agreement between the Department of Energy's Oak Ridge National Laboratory and NASA Lewis. Many modifications were made to the free-piston code in an attempt to decrease the calibration effort. A procedure was developed that made the code calibration process more systematic. Engine-specific calibration parameters are often used to bring predictions and experimental data into better agreement. The code was calibrated to a matrix of six experimental data points. Predictions of the calibrated free-piston code are compared with RE-1000 free-piston Stirling engine sensitivity test data taken at NASA Lewis. Reasonable agreement was obtained between the code predictions and the experimental data over a wide range of engine operating conditions. Author

N87-22562*# National Aeronautics and Space Administration. Lewis Research Center, Cleveland, Ohio.

AUTOMOTIVE STIRLING ENGINE DEVELOPMENT PROGRAM: A SUCCESS Final Report

W. K. TABATA 1987 10 p Proposed for presentation at the Intersociety Energy Conversion Engineering Conference, Philadelphia, Pa., 10-14 Aug. 1987; sponsored by AIAA (Contract DE-AI01-85CE-50112) (NASA-TM-89892; DOE/NASA/50112-69; E-3579; NAS 1.15:89892) Avail: NTIS HC A02/MF A01 CSCL 13F

The original 5-yr Automotive Stirling Engine Development Program has been extended to 10 years due to reduced annual funding levels. With an estimated completion date of April 1988, the technical achievements and the perspectives of meeting the original program objectives are reviewed. Various other applications of this developed Stirling engine technology are also discussed. Author

N87-27564*# National Aeronautics and Space Administration. Lewis Research Center, Cleveland, Ohio.

COMPARISON OF STIRLING ENGINES FOR USE WITH A 25-KW DISK-ELECTRIC CONVERSION SYSTEM

RICHARD K. SHALTENS Aug. 1987 18 p (NASA-TM-100111; E-3655; NAS 1.15:100111; AIAA-87-9069; DOE/NASA-33408-2) Avail: NTIS HC A02/MF A01 CSCL 13F

Heat engines were evaluated for terrestrial solar heat receivers. The Stirling Engine was identified as one of the most promising engines for terrestrial applications. The potential to meet the Department of Energy (DOE) goals for performance and cost can be met by the free-piston Stirling engine. NASA Lewis is providing technical management for an Advanced Stirling Conversion System (ASCS) through a cooperative interagency agreement with DOE. Parallel contracts were awarded for conceptual designs of an ASCS. Each design will feature a free-piston Stirling engine, a liquid-metal heat pipe receiver, and a means to provide about 25 kW of electric power to a utility grid while meeting long-term performance and goals. The Mechanical Technology, Ins. (MTI) design incorporates a linear alternator to directly convert the solar energy to electricity while the Stirling Technology Company (STC) generates electrical power indirectly by using a hydraulic output to a ground-based hydraulic pump/motor coupled to a rotating alternator. Both designs use technology which can reasonably be expected to be available in the 1980's. The ASCS designs using

a free-piston Stirling engine, a heat transport system, a receiver, and the methods of providing electricity to the utility grid will be discussed. Author

N87-28470*# Cummins Engine Co., Inc., Columbus, Ind. **TECHNICAL AND ECONOMIC STUDY OF STIRLING AND RANKINE CYCLE BOTTOMING SYSTEMS FOR HEAVY TRUCK DIESEL ENGINES Final Report**

I. KUBO Sep. 1987 171 p (Contract DEN3-361; DE-AI01-86CE-50162) (NASA-CR-180833; DOE/NASA-0361-1; NAS 1.26:180833; CTR-0723-87001) Avail: NTIS HC A08/MF A01 CSCL 13F

Bottoming cycle concepts for heavy duty transport engine applications were studied. In particular, the following tasks were performed: (1) conceptual design and cost data development for Stirling systems; (2) life-cycle cost evaluation of three bottoming systems - organic Rankine, steam Rankine, and Stirling cycles; and (3) assessment of future directions in waste heat utilization research. Variables considered for the second task were initial capital investments, fuel savings, depreciation tax benefits, salvage values, and service/maintenance costs. The study shows that none of the three bottoming systems studied are even marginally attractive. Manufacturing costs have to be reduced by at least 65%. As a new approach, an integrated Rankine/Diesel system was proposed. It utilizes one of the diesel cylinders as an expander and capitalizes on the in-cylinder heat energy. The concept eliminates the need for the power transmission device and a sophisticated control system, and reduces the size of the exhaust evaporator. Results of an economic evaluation indicate that the system has the potential to become an attractive package for end users. Author

N87-30223*# Mechanical Technology, Inc., Latham, N. Y. Engine Systems Div.

AUTOMOTIVE STIRLING ENGINE DEVELOPMENT PROGRAM Semiannual Technical Progress Report, 1 Jul. - 31 Dec. 1984

N. NIGHTINGALE, A. RICHEY, R. FARRELL, G. RIECKE, W. ERNST, R. HOWARTH, M. CRONIN, M. SIMETKOSKY, G. SMITH, and J. MEACHER Nov. 1985 87 p (Contract DEN3-32; DE-AI01-85CE-50112) (NASA-CR-174873; DOE/NASA/0032-25; DOE/NASA/0032-80/7; NAS 1.26:174873; MTI-85ASE445SA7) Avail: NTIS HC A05/MF A01 CSCL 13F

Development test activities on Mod I engines directed toward evaluating technologies for potential inclusion in the Mod II engine are summarized. Activities covered include: test of a 12-tube combustion gas recirculation combustor; manufacture and flow-distribution test of a two-manifold annular heater head; piston rod/piston base joint; single-solid piston rings; and a digital air/fuel concept. Also summarized are results of a formal assessment of candidate technologies for the Mod II engine, and preliminary design work for the Mod II. The overall program philosophy weight is outlined, and data and test results are presented. Author

N87-30225*# Garrett Turbine Engine Co., Phoenix, Ariz. **ADVANCED GAS TURBINE (AGT) TECHNOLOGY DEVELOPMENT PROJECT Annual Interim Report, 1 Jul. 1985 - 30 Jun. 1986**

Feb. 1987 132 p (Contract DEN3-167) (NASA-CR-180818; DOE/NASA/0167-11; NAS 1.26:180818; GARRETT-31-3725(11)) Avail: NTIS HC A07/MF A01 CSCL 13F

This report is the eleventh in the series of Technical Summary reports for the Advanced Gas Turbine (AGT) Technology Development Project, authorized under NASA Contract DEN3-167, and sponsored by the Department of Energy (DOE). This report was prepared by Garrett Turbine Engine Company, A Division of the Garrett Corporation, and includes information provided by Ford Motor Company, the Standard Oil Company, and AiResearch Casting Company. This report covers plans and progress for the period July 1, 1985 through June 30, 1986. Technical progress during the reported period was highlighted by the 85-hour

endurance run of an all-ceramic engine operating in the 2000 to 2250 F temperature regime. Component development continued in the areas of the combustion/fuel injection system, regenerator and seals system, and ceramic turbine rotor attachment design. Component rig testing saw further refinements. Ceramic materials showed continued improvements in required properties for gas turbine applications; however, continued development is needed before performance and reliability goals can be set. Author

90

ASTROPHYSICS

Includes cosmology; celestial mechanics; space plasmas; and interstellar and interplanetary gases and dust.

A87-26927*# Rome Univ. (Italy).

QUASARS AS INDICATORS OF GALACTIC AGES

A. CAVALIERE (Roma II, Università, Rome, Italy), A. SZALAY (NASA/Fermilab Astrophysics Group, Batavia, IL; Eotvos Lorand Tudományegyetem, Budapest, Hungary), and F. VAGNETTI (Roma II, Università; Roma I, Università, Rome, Italy) (CNR, Osservatorio Astronomico di Roma, I Università di Roma, et al., International Colloquium on the Age of Stellar Systems, Rome, Italy, Apr. 15-18, 1986) Società Astronomica Italiana, Memorie (ISSN 0037-8720), vol. 57, no. 3, 1986, p. 595-603. refs

Theoretical models of QSO evolution and their use in estimating the ages of galaxies containing QSOs are discussed, with a focus on the problems involved in extrapolating from statistical data on relatively nearby objects (z less than 2) to characterize distant objects. Graphs and histograms are provided, and it is concluded that the sharp decrease in the number of QSOs between $z = 2$ and $z = 3$, if not the result of obscuration or some other selection effect, makes it probable that the galaxy-formation processes which led to the formation of the QSOs occurred at z greater than 5. In that case, the QSOs would be one of the only observational probes of these processes. Mechanisms which could account for the time delay between galaxy formation and QSO turn-on are considered.

T.K.

A87-40651* California Univ., Berkeley.

THE LARGE-SCALE PECULIAR VELOCITY FIELD IN FLAT MODELS OF THE UNIVERSE

NICOLA VITTORIO (California, University, Berkeley) and MICHAEL S. TURNER (NASA/Fermilab Astrophysics Center, Batavia; Chicago, University, IL) Astrophysical Journal, Part 1 (ISSN 0004-637X), vol. 316, May 15, 1987, p. 475-482. NASA-supported research. refs

(Contract DE-AT03-84ER-40161)

The inflationary universe scenario predicts a flat universe and both adiabatic and isocurvature primordial density perturbations with the Zel'dovich spectrum. The two simplest realizations, models dominated by hot or cold dark matter, seem to be in conflict with observations. Flat models with two components of mass density, where one of the components of mass density is smoothly distributed, are examined, and the large-scale peculiar velocity field for these models is computed. For the smooth component the authors consider relativistic particles, a relic cosmological term, and light strings. At present the observational situation is unsettled, but, in principle, the large-scale peculiar velocity field is a very powerful discriminator between these different models. Author

99

GENERAL

N87-17656*# National Aeronautics and Space Administration. Lewis Research Center, Cleveland, Ohio.

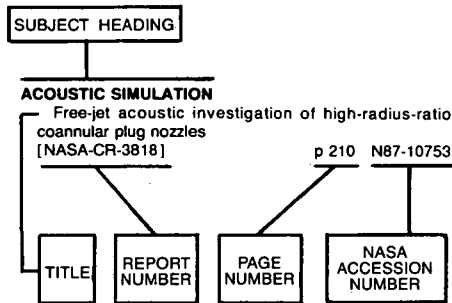
RESEARCH AND TECHNOLOGY Annual Report, 1986

1986 103 p

(NASA-TM-88868; NAS 1.15:88868) Avail: NTIS HC A06/MF A01 CSCL 05A

The research and technology accomplishments of the NASA Lewis Research Center are summarized for the fiscal year 1986, the 45th anniversary year of the Center. Five major sections are presented covering: aeronautics, aerospace technology, space communications, space station systems, and computational technology support. A table of contents by subjects was developed to assist the reader in finding articles of special interest. Author

Typical Subject Index Listing



The subject heading is a key to the subject content of the document. Titles, report numbers, and accession numbers of pertinent documents are provided under each subject heading. When the title is insufficiently descriptive of the document content, a title extension has been added, separated from the title by three hyphens. The report number helps to indicate the type of document cited (e.g., NASA report, NASA translation, NASA contractor report). The NASA accession number is the number by which the document abstracts are arranged in this journal and by which the document is sold or requested. The title, with title extensions if present, are arranged under each subject heading in ascending accession number order. The subject headings have been selected from the latest revision of the *NASA Thesaurus*.

A

ABEL FUNCTION

Extrapolation methods for divergent oscillatory infinite integrals that are defined in the sense of summability
[NASA-TM-89879] p 204 N87-35575

ABLATION

Rail gun performance and plasma characteristics due to wall ablation p 214 A87-18735

ABORTED MISSIONS

Aircraft accident report: NASA 712, Convair 990, N712NA, March Air Force Base, California, July 17, 1985, facts and analysis
[NASA-TM-87356-VOL-2] p 16 N87-21879

Analysis of Convair 990 rejected-takeoff accident with emphasis on decision making, training and procedures
[NASA-TM-100189] p 16 N87-29471

ABRASION

Effect of abrasive grit size on wear of manganese-zinc ferrite under three-body abrasion
[NASA-TM-89879] p 104 N87-24566

ABSORPTION SPECTRA

Fiber-optic thermometer using temperature dependent absorption, broadband detection, and time domain referencing p 153 A87-25948

ABSORPTIVITY

Heat exchanger for electrothermal devices
[NASA-CASE-LEW-14037-1] p 59 N87-16875

AC GENERATORS

Resistojet control and power for high frequency ac buses
[AIAA PAPER 87-0994] p 122 A87-41103

Resistojet control and power for high frequency ac buses
[NASA-TM-89860] p 126 N87-20477

ACCELERATED LIFE TESTS

Cycle life of nickel-hydrogen cells. II - Accelerated cycle life test p 46 A87-18104

Effect of storage and LEO cycling on manufacturing technology IPV nickel-hydrogen cells
[NASA-TM-89883] p 194 N87-22308
KOH concentration effect on cycle life of nickel-hydrogen cells p 199 N87-29920

ACCELERATION (PHYSICS)

Numerical modeling of on-orbit propellant motion resulting from an impulsive acceleration
[AIAA PAPER 87-1766] p 40 A87-48573

Acceleration display system for aircraft zero-gravity research
[NASA-TM-87358] p 156 N87-18801

Numerical modeling of on-orbit propellant motion resulting from an impulsive acceleration
[NASA-TM-89873] p 41 N87-22757

ACCELERATORS

Improvements in MDC and TWT overall efficiency through the application of carbon electrode surfaces --- Multistage Depressed Collectors p 120 A87-20667

Performance of textured carbon on copper electrode multistage depressed collectors with medium-power traveling wave tubes
[NASA-TP-2665] p 125 N87-17990

Calculation of secondary electron trajectories in multistage depressed collectors for microwave amplifiers
[NASA-TP-2664] p 125 N87-17991

Design, fabrication and performance of small, graphite electrode, multistage depressed collectors with 200-W, CW, 8- to 18-GHz traveling-wave tubes
[NASA-TP-2693] p 126 N87-20474

Analytical and experimental performance of a dual-mode traveling wave tube and multistage depressed collector
[NASA-TP-2752] p 128 N87-25532

ACETYLENE

Shock-tube pyrolysis of acetylene - Sensitivity analysis of the reaction mechanism for soot formation p 75 A87-12598

ACIDS

A mechanistic study of polyimide formation from diester-diols p 70 A87-53671

ACOUSTIC DUCTS

Sound radiation from single and annular stream nozzles, with modal decomposition of in-duct acoustic power p 209 A87-37629

ACOUSTIC EMISSION

Nondestructive evaluation of adhesive bond strength using the stress wave factor technique p 170 A87-32200

ACOUSTIC EXCITATION

Initial turbulence effect on jet evolution with and without tonal excitation
[NASA-TM-100178] p 14 N87-27629

Controlled excitation of a cold turbulent swirling free jet
[NASA-TM-100173] p 152 N87-27977

Enhanced mixing of an axisymmetric jet by aerodynamic excitation
[NASA-CR-175059] p 15 N87-29418

Control of shear flows by artificial excitation
[NASA-TM-100201] p 15 N87-29420

ACOUSTIC MEASUREMENT

Acoustic power measurement for single and annular stream duct-nozzle systems utilizing a modal decomposition scheme p 209 A87-37628

Combustion noise from gas turbine aircraft engines measurement of far-field levels
[NASA-TM-88971] p 211 N87-17480

Coupled aerodynamic and acoustical predictions for turbofans
[NASA-TM-87094] p 13 N87-23598

Ray propagation path analysis of acousto-ultrasonic signals in composites
[NASA-TM-100148] p 173 N87-25589

Effects of fiber motion on the acoustic behavior of an anisotropic, flexible fibrous material
[NASA-TM-89884] p 212 N87-25826

ACOUSTIC MICROSCOPES

Quantitative void characterization in structural ceramics by use of scanning laser acoustic microscopy p 171 A87-51974

Application of scanning acoustic microscopy to advanced structural ceramics
[NASA-TM-89929] p 172 N87-23987

ACOUSTIC PROPERTIES

DOE/NASA automotive Stirling engine project - Overview 86 p 220 A87-18034

Experiments on thermoacoustic convection heat transfer in gravity and zero-gravity environments
[AIAA PAPER 87-1651] p 107 A87-43141

ACOUSTIC SIMULATION

Free-jet acoustic investigation of high-radius-ratio conannular plug nozzles
[NASA-CR-3818] p 210 N87-10753

ACOUSTICS

Modeling the effects of wind tunnel wall absorption on the acoustic radiation characteristics of propellers
[AIAA PAPER 86-1876] p 208 A87-17991

The acousto-ultrasonic approach
[NASA-TM-89843] p 172 N87-20562

Acousto-ultrasonic input-output characterization of unidirectional fiber composite plate by SH waves
[NASA-CR-4087] p 173 N87-26361

Proplan test assessment proplan propulsion system static test report
[NASA-CR-179613] p 33 N87-29536

ACTIVATION

Reactivation study for NASA Lewis Research Center's Hypersonic Tunnel Facility
[AIAA PAPER 87-1886] p 34 A87-50190

Reactivation study for NASA Lewis Research Center's hypersonic tunnel facility
[NASA-TM-89918] p 36 N87-23664

ACTUATORS

The 20th Aerospace Mechanics Symposium
[NASA-CP-2423-REV] p 181 N87-16321

Evaluation of a high-torque backlash-free roller actuator p 165 N87-16336

ADAPTIVE CONTROL

SMI adaptive antenna arrays for weak interfering signals --- Sample Matrix Inversion p 111 A87-20818

Recent advances in error estimation and adaptive improvement of finite element calculations p 204 A87-41239

Application of adaptive antenna techniques to future commercial satellite communication
[NASA-CR-179566] p 115 N87-16954

Application of adaptive antenna techniques to future commercial satellite communications. Executive summary
[NASA-CR-179566-SUMM] p 115 N87-16955

SMI adaptive antenna arrays for weak interfering signals
[NASA-CR-181330] p 119 N87-28813

Adaptive arrays for weak interfering signals: An experimental system
[NASA-CR-181181] p 119 N87-28814

ADDITION RESINS

Addition polymers from 1,4,5,8-tetrahydro-1,4,5,8-diepoxyanthracene and Bis-dienes: Processable resins for high temperature application
[NASA-TM-89838] p 103 N87-20426

ADDITIVES

Cell performance and defect behavior in proton-irradiated lithium-counterdoped n(+)-p silicon solar cells p 216 A87-14222

An evaluation of metallized propellants based on vehicle performance
[AIAA PAPER 87-1773] p 53 A87-47003

An evaluation of metallized propellants based on vehicle performance
[NASA-TM-100104] p 64 N87-22806

Design considerations for a GaAs nipi doping superlattice solar cell p 196 N87-26422

The effect of Tricresyl-Phosphate (TCP) as an additive on wear of iron (Fe)
[NASA-TM-100103] p 93 N87-27030

ADHESION

Adherent Al₂O₃ scales formed on undoped NiCrAl alloys p 84 A87-32045

ADHESIVE BONDING

Nondestructive evaluation of adhesive bond strength using the stress wave factor technique

Adhesion, friction and deformation of ion-beam-deposited boron nitride films

Adhesion, friction, and deformation of ion-beam-deposited boron nitride films [NASA-TM-88902]

ADIABATIC CONDITIONS

Fast algorithm for calculating chemical kinetics in turbulent reacting flow

Solid lubrication design methodology, phase 2 [NASA-CR-175114]

ADSORPTION

Modeling for CO poisoning of a fuel cell anode

AEROACOUSTICS

On broadband shock associated noise of supersonic jets

Computational aeroacoustics of propeller noise in the near and far field [AIAA PAPER 87-0254]

High-speed propeller noise predictions - Effects of boundary conditions used in blade loading calculations [AIAA PAPER 87-0525]

Results of acoustic tests of a Prop-Fan model [AIAA PAPER 87-1894]

The acoustic experimental investigation of counterrotating propeller configurations [SAE PAPER 87-1031]

High-speed propeller noise predictions: Effects of boundary conditions used in blade loading calculations [NASA-TM-88913]

A finite element model for wave propagation in an inhomogeneous material including experimental validation [NASA-TM-100149]

Aeroacoustics of subsonic turbulent shear flows [NASA-TM-100165]

AEROBRAKING

Performance and aerodynamic braking of a horizontal-axis wind turbine from small-scale wind tunnel tests

[NASA-CR-180812]

AERODYNAMIC BRAKES

Performance and aerodynamic braking of a horizontal-axis wind turbine from small-scale wind tunnel tests

[NASA-CR-180812]

AERODYNAMIC CHARACTERISTICS

Unsteady heat transfer and direct comparison to steady-state measurements in a rotor-wake experiment

Lower-upper implicit scheme for high-speed inlet analysis

Method for the determination of the three dimensional aerodynamic field of a rotor-stator combination in compressible flow

[AIAA PAPER 87-1742]

An experimental study of the aerodynamics of a NACA 0012 airfoil with a simulated glaze ice accretion [NASA-CR-179897]

Turbine vane external heat transfer. Volume 2. Numerical solutions of the Navier-Stokes equations for two- and three-dimensional turbine cascades with heat transfer [NASA-CR-174828]

Method for the determination of the three-dimensional aerodynamic field of a rotor-stator combination to compressible flow [NASA-TM-100118]

[NASA-TM-100118]

[NASA-TM-100118]

[NASA-TM-100118]

[NASA-TM-100118]

[NASA-TM-100118]

[NASA-TM-100118]

[NASA-TM-100118]

[NASA-TM-100118]

[NASA-TM-100118]

[NASA-TM-100118]

[NASA-TM-100118]

[NASA-TM-100118]

[NASA-TM-100118]

[NASA-TM-100118]

[NASA-TM-100118]

[NASA-TM-100118]

[NASA-TM-100118]

[NASA-TM-100118]

[NASA-TM-100118]

[NASA-TM-100118]

[NASA-TM-100118]

[NASA-TM-100118]

AERODYNAMIC FORCES

High angle of attack hypersonic aerodynamics [AIAA PAPER 87-2548]

AERODYNAMIC HEAT TRANSFER

Navier Stokes solution of the flowfield over ice accretion shapes

[AIAA PAPER 87-0099]

AERODYNAMIC INTERFERENCE

Experimental and theoretical study of propeller spinner/shank interference

[AIAA PAPER 87-0145]

Transonic interference reduction by limited ventilation wall panels [NASA-CR-175039]

AERODYNAMIC LOADS

Influence of airfoil mean loading on convected gust interaction noise

Surface pressure measurements on the blade of an operating Mod-2 wind turbine with and without vortex generators [NASA-TM-89903]

AERODYNAMIC NOISE

Coherent structures and turbulence

Cruise noise of the 2/9th scale model of the Large-scale Advanced Propfan (LAP) propeller, SR-7A [NASA-TM-100175]

AERODYNAMIC STABILITY

Aerodynamic instability performance of an advanced high-pressure-ratio compression component

[AIAA PAPER 86-1619]

Aeroelastic control of stability and forced response of supersonic rotors by aerodynamic detuning

[AIAA PAPER 86-1619]

AERODYNAMIC STALLING

Stall transients of axial compression systems with inlet distortion

A comparative study of some dynamic stall models [NASA-TM-88917]

AERODYNAMICS

Euler analysis of the three-dimensional flow field of a high-speed propeller - Boundary condition effects [ASME PAPER 87-GT-253]

Euler analysis of the three dimensional flow field of a high-speed propeller: Boundary condition effects [NASA-TM-88955]

Coupled aerodynamic and acoustical predictions for turboprops [NASA-TM-87094]

Bladed disk vibration [NASA-CR-181203]

AEROELASTICITY

Analytical flutter investigation of a composite propfan model [AIAA PAPER 87-0738]

Aeroelastic control of stability and forced response of supersonic rotors by aerodynamic detuning

[AIAA PAPER 87-0738]

Analytical flutter investigation of a composite propfan model [NASA-TM-88944]

Unstalled flutter stability predictions and comparisons to test data for a composite prop-fan model [NASA-CR-179512]

Structural and aeroelastic analysis of the SR-7L propfan [NASA-TM-86877]

[NASA-TM-86877]

[NASA-TM-86877]

[NASA-TM-86877]

[NASA-TM-86877]

[NASA-TM-86877]

[NASA-TM-86877]

[NASA-TM-86877]

[NASA-TM-86877]

[NASA-TM-86877]

[NASA-TM-86877]

[NASA-TM-86877]

[NASA-TM-86877]

[NASA-TM-86877]

[NASA-TM-86877]

[NASA-TM-86877]

[NASA-TM-86877]

[NASA-TM-86877]

[NASA-TM-86877]

[NASA-TM-86877]

[NASA-TM-86877]

[NASA-TM-86877]

[NASA-TM-86877]

Tribological properties of polymer films and solid bodies in a vacuum environment

[NASA-TM-88966]

Liquid droplet radiator development status [NASA-TM-88952]

Microgravity Fluid Management Symposium [NASA-CP-2465]

SP-100 Advanced Technology Program [NASA-TM-89888]

Test results of a 60 volt bipolar nickel-hydrogen battery [NASA-TM-89927]

AEROSPACE INDUSTRY

Superalloy resources: Supply and availability [NASA-TM-89866]

AEROTHERMODYNAMICS

Comparison of wet and dry growth in artificial and flight icing conditions

Preliminary aerothermodynamic design method for hypersonic vehicles [AIAA PAPER 87-2545]

Host turbine heat transfer overview

Aerothermal modeling program, phase 2

Structural Integrity and Durability of Reusable Space Propulsion Systems [NASA-CP-2471]

[NASA-CP-2471]

AGING (METALLURGY)

Thermal stability of the nickel-base superalloy B-1900 + Hf with tantalum variations

The effect of electron beam welding on the creep rupture properties of a Nb-Zr-C alloy [NASA-TM-88892]

[NASA-TM-88892]

AILERONS

Performance and power regulation characteristics of two aileron-controlled rotors and a pitchable tip-controlled rotor on the Mod-O turbine

[NASA-TM-100136]

AIR

Hydrogen-air ignition torch [NASA-TM-88882]

Hydrogen oxidation mechanism with applications to (1) the chaperon efficiency of carbon dioxide and (2) vitiated air testing [NASA-TM-100186]

[NASA-TM-100186]

AIR BREATHING BOOSTERS

A parametric study of a gas-generator air turbo ramjet (ATR) [AIAA PAPER 86-1681]

[AIAA PAPER 86-1681]

AIR COOLING

Fabrication of cooled radial turbine rotor [NASA-CR-179503]

[NASA-CR-179503]

AIR FLOW

Liquid fuel spray processes in high-pressure gas flow

Two-phase flow measurements of a spray in a turbulent flow [AIAA PAPER 87-0062]

Calculation of water drop trajectories to and about arbitrary three-dimensional lifting and nonlifting bodies in potential airflow [NASA-CR-3935]

Development of gas-to-gas lift pad dynamic seals, volumes 1 and 2 [NASA-CR-179486]

Airflow calibration and exhaust pressure/temperature survey of an F404, S/N 215-109, turbofan engine [NASA-TM-100159]

[NASA-TM-100159]

AIR JETS

Flow visualization study of the effect of injection hole geometry on an inclined jet in crossflow

[NASA-TM-87356-VOL-1]

[NASA-TM-87356-VOL-1]

[NASA-TM-87356-VOL-1]

[NASA-TM-87356-VOL-1]

[NASA-TM-87356-VOL-1]

[NASA-TM-87356-VOL-1]

[NASA-TM-87356-VOL-1]

[NASA-TM-87356-VOL-1]

[NASA-TM-87356-VOL-1]

[NASA-TM-87356-VOL-1]

[NASA-TM-87356-VOL-1]

[NASA-TM-87356-VOL-1]

[NASA-TM-87356-VOL-1]

[NASA-TM-87356-VOL-1]

[NASA-TM-87356-VOL-1]

[NASA-TM-87356-VOL-1]

AIRCRAFT CONFIGURATIONS

- Application of propfan propulsion to general aviation [AIAA PAPER 86-2698] p 18 A87-17934
- Advanced Propfan Engine Technology (APET) single- and counter-rotation gearbox/pitch change mechanism [NASA-CR-168114-VOL-1] p 32 N87-28552

AIRCRAFT CONSTRUCTION MATERIALS

- Fiber-reinforced superalloy composites provide an added performance edge p 71 A87-12647

AIRCRAFT DESIGN

- Propeller design by optimization p 18 A87-14123
- Application of propfan propulsion to general aviation [AIAA PAPER 86-2698] p 18 A87-17934
- Folding tilt rotor demonstrator feasibility study p 17 A87-19247
- Response of a small-turboshaft-engine compression system to inlet temperature distortion [NASA-TM-83765] p 23 N87-10100
- An investigation of the flow characteristics in the blade endwall corner region [NASA-CR-4076] p 14 N87-29412
- Propfan test assessment testbed aircraft flutter model test report [NASA-CR-179458] p 14 N87-29413

AIRCRAFT ENGINES

- Polymer, metal, and ceramic matrix composites for advanced aircraft engine applications p 71 A87-15187
- An overview of the small engine component technology (SECT) studies --- commuter, rotorcraft, cruise missile and auxiliary power applications in year 2000 [AIAA PAPER 86-1542] p 19 A87-17993
- Evaluation of capillary reinforced composites for anti-icing [AIAA PAPER 87-0023] p 17 A87-24904
- Aircraft turbofan noise p 209 A87-31144
- Aerodynamic instability performance of an advanced high-pressure-ratio compression component [AIAA PAPER 86-1619] p 5 A87-41157
- Advanced liquid-cooled, turbocharged and intercooled stratified charge rotary engines for aircraft [SAE PAPER 87-1039] p 22 A87-48766
- Static tests of the propulsion system --- Propfan Test Assessment program [AIAA PAPER 87-1728] p 23 A87-52245
- Structural ceramics in heat engines - The NASA viewpoint p 98 A87-53352
- Turbine Engine Hot Section Technology, 1984 [NASA-CP-2339] p 179 N87-11180
- STAEBL: Structural tailoring of engine blades, phase 2 p 24 N87-11731
- Analysis of mixed-mode crack propagation using the boundary integral method [NASA-CR-179518] p 180 N87-12915
- Advanced composite combustor structural concepts program [NASA-CR-174733] p 74 N87-20387
- Analysis of an advanced technology subsonic turbofan incorporating revolutionary materials [NASA-TM-89868] p 29 N87-22680
- Fiber reinforced superalloys [NASA-TM-89865] p 75 N87-22811

AIRCRAFT EQUIPMENT

- A heater made from graphite composite material for potential deicing application [AIAA PAPER 87-0025] p 17 A87-24905
- A heater made from graphite composite material for potential deicing application [NASA-TM-88888] p 17 N87-12559

AIRCRAFT FUELS

- Long-term deposit formation in aviation turbine fuel at elevated temperature p 106 A87-14986
- Degradation mechanisms of sulfur and nitrogen containing compounds during thermal stability testing of model fuels [AIAA PAPER 87-2039] p 106 A87-45372
- A variable geometry combustor for broadened properties fuels [AIAA PAPER 87-1832] p 23 A87-52246
- Aircraft accident report: NASA 712, Convair 990, N712NA, March Air Force Base, California, July 17, 1985, executive summary [NASA-TM-87356-VOL-1] p 16 N87-21878
- Aviation fuel property effects on altitude relight [NASA-CR-179582] p 107 N87-24578

AIRCRAFT HAZARDS

- Comparison of wet and dry growth in artificial and flight icing conditions p 16 A87-45635

AIRCRAFT INSTRUMENTS

- Three-dimensional trajectory analyses of two drop sizing instruments - PMS OAP and PMS FSPP --- Optical Array Probe and Forward Scattering Spectrometer Probe [AIAA PAPER 87-0180] p 132 A87-22466

AIRCRAFT MODELS

- Wind tunnel tests on a one-foot diameter SR-7L propfan model [AIAA PAPER 87-1892] p 6 A87-45281

AIRCRAFT NOISE

- Influence of airfoil mean loading on convected gust interaction noise p 208 A87-13587
- Structureborne noise control in advanced turboprop aircraft [AIAA PAPER 87-0530] p 209 A87-31110
- Aircraft turbofan noise p 209 A87-31144
- The acoustic experimental investigation of counterrotating propeller configurations [SAE PAPER 87-1031] p 210 A87-48760
- Cruise noise of counterrotation propeller at angle of attack in wind tunnel [NASA-TM-88869] p 210 N87-13252
- Structureborne noise control in advanced turboprop aircraft [NASA-TM-88947] p 211 N87-16587
- Identification and proposed control of helicopter transmission noise at the source [NASA-TM-89312] p 18 N87-16816
- Combustion noise from gas turbine aircraft engines measurement of far-field levels [NASA-TM-88971] p 211 N87-17480
- Cruise noise of the 2/9th scale model of the Large-scale Advanced Propfan (LAP) propeller, SR-7A [NASA-TM-100175] p 212 N87-28398
- Aerodynamic performance investigation of advanced mechanical suppressor and ejector nozzle concepts for jet noise reduction [NASA-CR-174860] p 33 N87-29534
- Propfan test assessment propfan propulsion system static test report [NASA-CR-179613] p 33 N87-29536

AIRCRAFT PERFORMANCE

- Flight test report of the NASA icing research airplane: Performance, stability, and control after flight through natural icing conditions [NASA-CR-179515] p 34 N87-11797

AIRCRAFT SAFETY

- Flight test report of the NASA icing research airplane: Performance, stability, and control after flight through natural icing conditions [NASA-CR-179515] p 34 N87-11797
- Antimisting kerosene JT3 engine fuel system integration study [NASA-CR-4033] p 106 N87-24577
- New methods and materials for molding and casting ice formations [NASA-TM-100126] p 16 N87-29470

AIRCRAFT STRUCTURES

- Particle trajectory computer program for icing analysis of axisymmetric bodies - A progress report [AIAA PAPER 87-0027] p 15 A87-22366
- 3-D inelastic analysis methods for hot section components. Volume 2: Advanced special functions models [NASA-CR-179517] p 186 N87-27267

AIRCRAFT TIRES

- Analysis of Convair 990 rejected-takeoff accident with emphasis on decision making, training and procedures [NASA-TM-100189] p 16 N87-29471

AIRFOIL OSCILLATIONS

- A technique for the prediction of airfoil flutter characteristics in separated flow [AIAA PAPER 87-0910] p 177 A87-33719

AIRFOIL PROFILES

- Evaluation of icing drag coefficient correlations applied to iced propeller performance prediction [SAE PAPER 87-1033] p 16 A87-48761
- Development of a turbomachinery design optimization procedure using a multiple-parameter nonlinear perturbation method [NASA-CR-3831] p 1 N87-10003

AIRFOILS

- Influence of airfoil mean loading on convected gust interaction noise p 208 A87-13587
- Numerical analysis of a NACA0012 airfoil with leading edge ice accretions [AIAA PAPER 87-0101] p 2 A87-22415
- In-flight measurement of ice growth on an airfoil using an array of ultrasonic transducers [AIAA PAPER 87-0178] p 15 A87-22464
- Experimental, water droplet impingement data on two-dimensional airfoils, axisymmetric inlet and Boeing 737-300 engine inlet [AIAA PAPER 87-0097] p 17 A87-24918
- Effect of a rotor wake on the local heat transfer on the forward half of a circular cylinder p 136 A87-30721
- Analysis of viscous transonic flow over airfoil sections [AIAA PAPER 87-0420] p 4 A87-34723

- Numerical simulations of unsteady, viscous, transonic flow over isolated and cascaded airfoils using a deforming grid [AIAA PAPER 87-1316] p 7 A87-49649

- Turbine Engine Hot Section Technology, 1984 [NASA-CP-2339] p 179 N87-11180
- Surface protection p 88 N87-11182
- Host turbine heat transfer overview p 144 N87-11184

- An experimental study of the aerodynamics of a NACA 0012 airfoil with a simulated glaze ice accretion [NASA-CR-179897] p 8 N87-11701

- Analysis of viscous transonic flow over airfoil sections [NASA-TM-88912] p 146 N87-17001

- Development and testing of vortex generators for small horizontal axis wind turbines [NASA-CR-179514] p 193 N87-18922

- Lewis inverse design code (LINDES): Users manual [NASA-TP-2676] p 12 N87-20238

- Use of a liquid-crystal, heater-element composite for quantitative, high-resolution heat transfer coefficients on a turbine airfoil, including turbulence and surface roughness effects [NASA-TM-87355] p 158 N87-22181

- Fiber reinforced superalloys [NASA-TM-89865] p 75 N87-22811

- Life prediction and constitutive models for engine hot section anisotropic materials [NASA-CR-179594] p 29 N87-23622

- Computation of full-coverage film-cooled airfoil temperatures by two methods and comparison with high heat flux data [NASA-TM-88931] p 150 N87-23934

- Numerical simulations of unsteady, viscous, transonic flow over isolated and cascaded airfoils using a deforming grid [NASA-TM-89890] p 13 N87-24435

- Wind tunnel evaluation of a truncated NACA 64-621 airfoil for wind turbine applications [NASA-CR-180803] p 196 N87-25621

- Experimental evaluation of corner turning vanes [NASA-TM-100143] p 37 N87-28571

- Transonic interference reduction by limited ventilation wall panels [NASA-CR-175039] p 15 N87-29419

ALGORITHMS

- A real-time simulation evaluation of an advanced detection, isolation and accommodation algorithm for sensor failures in turbine engines p 18 A87-13318

- Fast algorithm for calculating chemical kinetics in turbulent reacting flow p 77 A87-38958

- An adaptive algorithm for motion compensated color image coding p 113 A87-45466

- Full-scale engine demonstration of an advanced sensor failure detection isolation, and accommodation algorithm - Preliminary results [AIAA PAPER 87-2259] p 22 A87-50422

- A Navier-Stokes solver using the LU-SSOR TVD algorithm [NASA-CR-179608] p 13 N87-20243

- Full-scale engine demonstration of an advanced sensor failure detection, isolation and accommodation algorithm: Preliminary results [NASA-TM-89880] p 127 N87-22097

- Engineering calculations for communications satellite systems planning [NASA-CR-181112] p 117 N87-24605

ALIGNMENT

- A mechanism for precise linear and angular adjustment utilizing flexures p 165 N87-16342

ALKALINE BATTERIES

- Alkaline water electrolysis technology for Space Station regenerative fuel cell energy storage p 46 A87-18107
- Advanced technology for extended endurance alkaline fuel cells p 190 A87-33787
- Oxygen electrodes for rechargeable alkaline fuel cells p 199 N87-29940

ALLOYS

- Corrosion of metals and alloys in sulfate melts at 750 C p 81 A87-17997
- Results of an interlaboratory fatigue test program conducted on alloy 800H at room and elevated temperatures p 87 A87-54370
- High temperature static strain gage alloy development program [NASA-CR-174833] p 157 N87-22179
- Friction and wear of sintered Alpha SiC sliding against IN-718 alloy at 25 to 800 C in atmospheric air at ambient pressure [NASA-TM-87353] p 103 N87-22860
- High temperature static strain gage development contract, tasks 1 and 2 [NASA-CR-180811] p 159 N87-28869

ALTERNATING CURRENT

Radiation from large space structures in low earth orbit with induced ac currents
[AIAA PAPER 87-0612] p 42 A87-22738
20 kHz Space Station power system

Resonant AC power system proof-of-concept test program
[NASA-CR-175069-VOL-1] p 129 N87-29738
Resonant AC power system proof-of-concept test program, volume 2, appendix 1
[NASA-CR-175069-VOL-2] p 130 N87-29739

ALTERNATING DIRECTION IMPLICIT METHODS

A diagonal implicit multigrid algorithm for the Euler equations
[AIAA PAPER 87-0354] p 2 A87-22578
Time-marching solution of incompressible Navier-Stokes equations for internal flow p 138 A87-39450

ALTITUDE SIMULATION

Full-scale thrust reverser testing in an altitude facility
[AIAA PAPER 87-1788] p 34 A87-45203
Full-scale thrust reverser testing in an altitude facility
[NASA-TM-88967] p 35 N87-18575
Detailed flow surveys of turning vanes designed for a 0.1-scale model of NASA Lewis Research Center's proposed altitude wind tunnel
[NASA-TP-2680] p 36 N87-20295

ALUMINUM

Investigation of a GaAlAs Mach-Zehnder electro-optic modulator
[NASA-CR-179573] p 114 N87-16953
Shot peening for Ti-6Al-4V alloy compressor blades
[NASA-TP-2711] p 184 N87-20566
AlGaAs growth by OMCD using an excimer laser
[NASA-TM-88937] p 218 N87-23304

ALUMINUM ALLOYS

Analysis of NiAlTa precipitates in beta-NiAl + 2 at. pct Ta alloy p 84 A87-34888
Effect of composition and grain size on slow plastic flow properties of NiAl between 1200 and 1400 K p 84 A87-36251

A preliminary study of ester oxidation on an aluminum surface using chemiluminescence p 96 A87-37688
Effect of heat treatment on the fracture behaviour of directionally solidified (gamma/gamma-prime)-alpha alloy p 86 A87-47932

Ester oxidation on an aluminum surface using chemiluminescence
[NASA-TP-2611] p 101 N87-18666

ALUMINUM COATINGS

The effect of Cr, Co, Al, Mo and Ta on a series of cast Ni-base superalloys on the stability of an aluminide coating during cyclic oxidation in Mach 0.3 burner rig
[NASA-TM-88840] p 89 N87-14488
Effect of an oxygen plasma on uncoated thin aluminum reflecting films
[NASA-TM-89882] p 61 N87-21999

ALUMINUM GALLIUM ARSENIDES

Variable angle of incidence spectroscopic ellipsometry Application to GaAs-Al(x)Ga(1-x)As multiple heterostructures p 216 A87-20519
Microwave performance of a quarter-micrometer gate low-noise pseudomorphic InGaAs/AlGaAs modulation-doped field effect transistor p 121 A87-23745

Characterization of InGaAs/AlGaAs pseudomorphic modulation-doped field-effect transistors p 121 A87-23922

Nonlinear absorption in AlGaAs/GaAs multiple quantum well structures grown by metalorganic chemical vapor deposition p 217 A87-39687

Microwave performance of an optically controlled AlGaAs/GaAs high electron mobility transistor and GaAs MESFET
[NASA-TM-88980] p 125 N87-17993

Microwave characterization and modeling of GaAs/AlGaAs heterojunction bipolar transistors
[NASA-TM-100150] p 117 N87-26265
High-efficiency GaAs concentrator space cells p 196 N87-26417

Performance of AlGaAs, GaAs and InGaAs cells after 1 MeV electron irradiation p 197 N87-26438
A V-grooved AlGaAs/GaAs passivated PN junction
[NASA-TM-100138] p 218 N87-27541

ALUMINUM OXIDES

Reactions occurring during the sulfation of sodium chloride deposited on alumina substrates p 76 A87-20223
Adherent Al₂O₃ scales formed on undoped NiCrAl alloys p 84 A87-32045

AMBIENT TEMPERATURE

Results of an interlaboratory fatigue test program conducted on alloy 800H at room and elevated temperatures p 87 A87-54370

Friction and wear of sintered Alpha SiC sliding against IN-718 alloy at 25 to 800 C in atmospheric air at ambient pressure
[NASA-TM-87353] p 103 N87-22860

AMMONIA

Low power dc arcjet operation with hydrogen/nitrogen/ammonia mixtures
[AIAA PAPER 87-1948] p 53 A87-48575
Low power DC arcjet operation with hydrogen/nitrogen/ammonia mixtures
[NASA-TM-89876] p 64 N87-22804

AMORPHOUS MATERIALS

High-temperature effect of hydrogen on sintered alpha-silicon carbide
[NASA-TM-88819] p 100 N87-14518
Rapid thermal annealing of Amorphous Hydrogenated Carbon (a-C:H) films
[NASA-TM-89859] p 218 N87-20821

AMORPHOUS SEMICONDUCTORS

Interactions of amorphous Ta(x)Cu(1-x) (x = 0.93 and 0.80) alloy films with Au overlayers and GaAs substrates p 217 A87-44562

AMORPHOUS SILICON

Friction and wear of sintered Alpha SiC sliding against IN-718 alloy at 25 to 800 C in atmospheric air at ambient pressure
[NASA-TM-87353] p 103 N87-22860

AMPLITUDE MODULATION

Amplitude spectrum modulation technique for analog data processing in fiber optic sensing system with temporal separation of channels
[NASA-TM-100152] p 159 N87-25562

AMPLITUDES

A design concept for an MMIC microstrip phased array
[NASA-TM-88834] p 114 N87-14569

ANALOG DATA

Amplitude spectrum modulation technique for analog data processing in fiber optic sensing system with temporal separation of channels
[NASA-TM-100152] p 159 N87-25562

ANALOG TO DIGITAL CONVERTERS

Satellite analog FDMA/FM to digital TDMA conversion
[NASA-CR-179605] p 125 N87-20467

ANEMOMETERS

An anemometer for highly turbulent or recirculating flows p 154 A87-37698

ANGLE OF ATTACK

High angle of attack hypersonic aerodynamics
[AIAA PAPER 87-2548] p 7 A87-49101
Cruise noise of counterrotation propeller at angle of attack in wind tunnel
[NASA-TM-88869] p 210 N87-13252

ANGLES (GEOMETRY)

A mechanism for precise linear and angular adjustment utilizing flexures p 165 N87-16342

ANGULAR DISTRIBUTION

The temperature dependence of inelastic light scattering from small particles for use in combustion diagnostic instrumentation
[NASA-CR-180399] p 80 N87-28634

ANISOTROPIC MEDIA

Mechanical property anisotropy in superalloy EI-929 directionally solidified by an exothermic technique p 81 A87-11389
Microstrip dispersion including anisotropic substrates p 123 A87-47621

ANISOTROPY

Effects of fiber motion on the acoustic behavior of an anisotropic, flexible fibrous material
[NASA-TM-89884] p 212 N87-25826

ANNEALING

Interactions of amorphous Ta(x)Cu(1-x) (x = 0.93 and 0.80) alloy films with Au overlayers and GaAs substrates p 217 A87-44562

The stability of lamellar gamma-gamma-prime structures --- nickel-base superalloy p 86 A87-48323
Annealing of electron damage in mid-IR transmitting fluoride glass p 99 A87-53652
Rapid thermal annealing of Amorphous Hydrogenated Carbon (a-C:H) films
[NASA-TM-89859] p 218 N87-20821

ANNULAR DUCTS

Acoustic power measurement for single and annular stream duct-nozzle systems utilizing a modal decomposition scheme p 209 A87-37628
Turbofan aft duct suppressor study. Contractor's data report of mode probe signal data
[NASA-CR-175067] p 34 N87-29538

Turbofan aft duct suppressor study
[NASA-CR-175067] p 34 N87-29539

ANNULAR NOZZLES

An experimental investigation of compressible three-dimensional boundary layer flow in annular diffusers
[AIAA PAPER 87-0366] p 3 A87-24954

The evolution of instabilities in the axisymmetric jet. I - The linear growth of disturbances near the nozzle. II - The flow resulting from the interaction between two waves p 138 A87-37256
Sound radiation from single and annular stream nozzles, with modal decomposition of in-duct acoustic power p 209 A87-37629

Free jet feasibility study of a thermal acoustic shield concept for AST/VCE application: Dual stream nozzles
[NASA-CR-3867] p 210 N87-10752
Free-jet acoustic investigation of high-radius-ratio coannular plug nozzles
[NASA-CR-3818] p 210 N87-10753

Free-jet investigation of mechanically suppressed, high radius ratio coannular plug model nozzles
[NASA-CR-3596] p 212 N87-29315

ANTENNA ARRAYS

SMI adaptive antenna arrays for weak interfering signals --- Sample Matrix Inversion p 111 A87-20818
New simple feed network for an array module of four microstrip elements p 122 A87-41638
The study of microstrip antenna arrays and related problems

[NASA-CR-179714] p 113 N87-10225
An experimental investigation of parasitic microstrip arrays
[NASA-TM-100168] p 129 N87-27120
APS-Workshop on Characterization of MMIC (Monolithic Microwave Integrated Circuit) Devices for Array Antenna [AD-P005398] p 118 N87-28763
SMI adaptive antenna arrays for weak interfering signals

[NASA-CR-181330] p 119 N87-28813
Adaptive arrays for weak interfering signals: An experimental system
[NASA-CR-181181] p 119 N87-28814

ANTENNA COMPONENTS

Composite space antenna structures - Properties and environmental effects p 72 A87-38610
Composite space antenna structures: Properties and environmental effects p 73 N87-16880
[NASA-TM-88859]

ANTENNA DESIGN

The study of microstrip antenna arrays and related problems
[NASA-CR-179714] p 113 N87-10225
Application of adaptive antenna techniques to future commercial satellite communication
[NASA-CR-179566] p 115 N87-16954
Rectenna Technology Program: Ultra light 2.45 GHz rectenna 20 GHz rectenna
[NASA-CR-179558] p 116 N87-19556

Technology for satellite power conversion
[NASA-CR-181057] p 66 N87-25420
An experimental investigation of parasitic microstrip arrays
[NASA-TM-100168] p 129 N87-27120

Optimizing the antenna system of a microwave space power station: Implications for the selection of operating power, frequency and antenna size
[NASA-TM-100184] p 206 N87-30132

ANTENNA FEEDS

20-GHz phased-array-fed antennas utilizing distributed MMIC modules p 112 A87-34527
New simple feed network for an array module of four microstrip elements p 122 A87-41638

ANTENNA RADIATION PATTERNS

Measurement techniques for millimeter wave substrate mounted MMW antennas p 121 A87-40926
Absolute gain measurement by the image method under mismatched condition
[NASA-TM-88924] p 124 N87-16968

Microstrip antenna array with parasitic elements
[NASA-TM-89919] p 117 N87-22089
Detection of reflector surface error from near-field data: Effect of edge diffracted field
[NASA-TM-89920] p 117 N87-22874

ANTENNAS

System architecture of MMIC-based large aperture arrays for space application
[NASA-TM-89840] p 125 N87-20468

ANTI-FRICTION BEARINGS

Selection of rolling-element bearing steels for long-life application
[NASA-TM-88881] p 164 N87-11993

ANTI-CORROSION ADDITIVES

Evaluation of capillary reinforced composites for anti-icing
[AIAA PAPER 87-0023] p 17 A87-24904

ANTIMISTING FUELS

Antimisting kerosene JT3 engine fuel system integration study
[NASA-CR-4033] p 106 N87-24577

ANTIMONY

Undercooling and crystallization behaviour of antimony droplets p 83 A87-28732

ANTIREFLECTION COATINGS

Effect of hard particle impacts on the atomic oxygen survivability of reflector surfaces with transparent protective overcoats
[AIAA PAPER 87-0104] p 69 A87-22417

APPLICATIONS PROGRAMS (COMPUTERS)

Thermodynamic analysis and subscale modeling of space-based orbit transfer vehicle cryogenic propellant resupply
[AIAA PAPER 87-1764] p 142 A87-48572

The study of microstrip antenna arrays and related problems
[NASA-CR-179714] p 113 N87-10225

Predicted effect of dynamic load on pitting fatigue life for low-contact-ratio spur gears
[NASA-TP-2610] p 166 N87-18095

Strain energy release rates of composite interlaminar end-notch and mixed-mode fracture: A sublaminate/ply level analysis and a computer code
[NASA-TM-89827] p 74 N87-20389

Use of a liquid-crystal, heater-element composite for quantitative, high-resolution heat transfer coefficients on a turbine airfoil, including turbulence and surface roughness effects
[NASA-TM-87355] p 158 N87-22181

Calibration and comparison of the NASA Lewis free-piston Stirling engine model predictions with RE-1000 test data
[NASA-TM-89853] p 222 N87-22561

Application of advanced computational codes in the design of an experiment for a supersonic throughflow fan rotor
[NASA-TM-88915] p 13 N87-22630

Thermodynamic analysis and subscale modeling of space-based orbit transfer vehicle cryogenic propellant resupply
[NASA-TM-89921] p 150 N87-22949

Finite element implementation of Robinson's unified viscoplastic model and its application to some uniaxial and multiaxial problems
[NASA-TM-89891] p 185 N87-23010

3-D inelastic analysis methods for hot section components. Volume 2: Advanced special functions models
[NASA-CR-179517] p 186 N87-27267

APPROXIMATION

Some plane curvature approximations
p 204 A87-49821

Sensitivity analysis and approximation methods for general eigenvalue problems
[NASA-CR-179538] p 180 N87-12021

A multigrid LU-SSOR scheme for approximate Newton iteration applied to the Euler equations
[NASA-CR-179524] p 10 N87-16803

Experiments and modeling of dilution jet flow fields
p 148 N87-20276

ARC JET ENGINES

Performance characterization of a low power hydrazine arcjet
[AIAA PAPER 87-1057] p 50 A87-39634

Low power arcjet life issues
[AIAA PAPER 87-1059] p 50 A87-39635

Arcjet component conditions through a multistart test
[AIAA PAPER 87-1060] p 51 A87-41127

Arcjet starting reliability - A multistart test on hydrogen/nitrogen mixtures
[AIAA PAPER 87-1061] p 51 A87-41128

The NASA Electric Propulsion Program
[AIAA PAPER 87-1098] p 53 A87-45795

Low power dc arcjet operation with hydrogen/nitrogen/ammonia mixtures
[AIAA PAPER 87-1948] p 53 A87-48575

The NASA/USAF arcjet research and technology program
[AIAA PAPER 87-1946] p 54 A87-50192

Langmuir probe surveys of an arcjet exhaust
[AIAA PAPER 87-1950] p 54 A87-50193

Low power arcjet thruster pulse ignition
[AIAA PAPER 87-1951] p 54 A87-50194

Electric propulsion options for the SP-100 reference mission
[NASA-TM-88918] p 57 N87-14422

Arcjet component conditions through a multistart test
[NASA-TM-89857] p 61 N87-20382

The NASA Electric Propulsion Program
[NASA-TM-89856] p 61 N87-21037

Arcjet starting reliability: A multistart test on hydrogen/nitrogen mixtures
[NASA-TM-89867] p 61 N87-21998

Low power DC arcjet operation with hydrogen/nitrogen/ammonia mixtures
[NASA-TM-89876] p 64 N87-22804

Langmuir probe surveys of an arcjet exhaust
[NASA-TM-89924] p 64 N87-22807

Low power arcjet thruster pulse ignition
[NASA-TM-100123] p 64 N87-23691

The NASA/USAF arcjet research and technology program

[NASA-TM-100112] p 66 N87-24525

Arcjet power supply and start circuit
[NASA-CASE-LEW-14374-1] p 36 N87-25335

ARC MELTING

Analysis of the solidified structure of rheocast and VADER processed nickel-base superalloy
p 83 A87-28734

ARC SPRAYING

Morphology of zirconia particles exposed to D.C. arc plasma jet
[NASA-TM-88927] p 90 N87-16113

ARCHES

Non-isothermal elastoviscoplastic snap-through and creep buckling of shallow arches
[AIAA PAPER 87-0806] p 176 A87-33605

The dynamic aspects of thermo-elasto-viscoplastic snap-through and creep buckling phenomena
[NASA-CR-181411] p 187 N87-29897

ARCHITECTURE

System architecture of MMIC-based large aperture arrays for space application
[NASA-TM-89840] p 125 N87-20468

ARCHITECTURE (COMPUTERS)

Satellite analog FDMA/FM to digital TDMA conversion
[NASA-CR-179605] p 125 N87-20467

The hypercluster: A parallel processing test-bed architecture for computational mechanics applications
[NASA-TM-89823] p 203 N87-20767

On-board processing satellite network architecture and control study
[NASA-CR-180816] p 44 N87-27710

On-board processing satellite network architecture and control study
[NASA-CR-180817] p 44 N87-27711

AREA

Experimental thrust performance of a high-area-ratio rocket nozzle
[NASA-TP-2720] p 60 N87-20381

Experimental thrust performance of a high area-ratio rocket nozzle
p 65 N87-23809

ARGON PLASMA

A simple method for monitoring surface temperatures in plasma treatments
p 160 A87-17269

AROMATIC COMPOUNDS

Ethynylated aromatics as high temperature matrix resins
p 96 A87-34850

ARRAYS

Performance characteristics of a combination solar photovoltaic heat engine energy converter
[NASA-TM-89908] p 195 N87-23028

Macrocrack interaction with transverse array of microcracks
[NASA-CR-180806] p 186 N87-25607

Design, implementation and investigation of an image guide-based optical flip-flop array
[NASA-CR-181382] p 213 N87-30180

ARSENIC

The effect of internal stresses on solar cell efficiency
p 196 N87-26430

ARTIFICIAL SATELLITES

Regenerative fuel cell study for satellites in GEO orbit
[NASA-CR-179609] p 198 N87-27324

ASTROLOY (TRADEMARK)

Effects of temperature and hold times on low cycle fatigue of Astroloy
p 85 A87-38541

ASTRONOMICAL MODELS

The large-scale peculiar velocity field in flat models of the universe
p 223 A87-40651

ASYMPTOTIC METHODS

Asymptotic analysis of corona discharge from thin electrodes
[NASA-TP-2645] p 215 N87-14998

ASYMPTOTIC PROPERTIES

Low-gravity experiments in critical phenomena
p 107 A87-23159

Radar cross section of an open-ended circular waveguide
Calculation of second-order diffraction terms
p 112 A87-31626

ATMOSPHERES

Effects of atmosphere on the tribological properties of a chromium carbide based coating for use to 760 deg C
[NASA-TM-88894] p 101 N87-16140

ATMOSPHERIC PRESSURE

Friction and wear of sintered Alpha SiC sliding against IN-718 alloy at 25 to 800 C in atmospheric air at ambient pressure
[NASA-TM-87353] p 103 N87-22860

ATOMIC BEAMS

Neutral atomic oxygen beam produced by ion charge exchange for Low Earth Orbital (LEO) simulation
p 79 N87-26188

ATOMIZING

Liquid fuel spray processes in high-pressure gas flow
p 131 A87-13643

Agreement between experimental and theoretical effects of nitrogen gas flowrate on liquid jet atomization
[AIAA PAPER 87-2138] p 141 A87-45427

Agreement between experimental and theoretical effects of nitrogen gas flowrate on liquid jet atomization
[NASA-TM-89821] p 156 N87-19684

ATTACHMENT

Flowfield measurements in a separated and reattached flat plate turbulent boundary layer
[NASA-CR-4052] p 148 N87-21257

AUGER SPECTROSCOPY

Characterization of ion beam modified ceramic wear surfaces using Auger electron spectroscopy
p 98 A87-51304

AUGMENTATION

Enhanced thermal emittance of space radiators by ion-discharge chamber texturing
[NASA-TM-100137] p 207 N87-25823

AUSTENITIC STAINLESS STEELS

Elevated temperature strengthening of a melt spun austenitic steel by TiB2
p 87 A87-51639

AUTOMATIC CONTROL

Automating the parallel processing of fluid and structural dynamics calculations
[NASA-TM-89837] p 203 N87-19002

Automated inspection and precision grinding of spiral bevel gears
[NASA-CR-4083] p 169 N87-25578

A computational procedure for automated flutter analysis
[NASA-TM-100171] p 187 N87-28058

AUTOMATIC FLIGHT CONTROL

A rotorcraft flight/propulsion control integration study
[NASA-CR-179574] p 18 N87-24457

AUTOMATIC PILOTS

Effect of gimbal friction modelling technique on control stability and performance for Centaur upper stage
[AIAA PAPER 87-2455] p 38 A87-50501

Effect of Gimbal friction modeling technique on control stability and performance for Centaur upper-stage
[NASA-TM-89894] p 39 N87-22755

AUTOMATIC TEST EQUIPMENT

Automated measurement of the bit-error rate as a function of signal-to-noise ratio for microwave communications systems
[NASA-TM-89898] p 127 N87-22102

AUTOMATION

Automating the U.S. Space Station's electrical power system
p 48 A87-23646

AUTOMOBILE ENGINES

Testing of a variable-stroke Stirling engine
p 160 A87-18036

Mod II engine performance
[SAE PAPER 870101] p 163 A87-48780

Automotive Stirling engine system component review
[SAE PAPER 870102] p 163 A87-48781

The Advanced Turbine Technology Applications Program (ATTAP)
[SAE PAPER 870467] p 163 A87-48791

Effect of 15 MPa hydrogen on creep-rupture properties of iron-base superalloys
p 86 A87-49558

Advanced Gas Turbine (AGT) Technology Project
[NASA-CR-179484] p 164 N87-11995

Ceramic automotive Stirling engine program
[NASA-CR-175042] p 192 N87-12047

Automotive Stirling engine development program: A success
[NASA-TM-89892] p 222 N87-22562

Creep-rupture behavior of a developmental cast-iron-base alloy for use up to 800 deg C
[NASA-TM-100167] p 93 N87-28641

AUTOMOBILES

Automotive Stirling engine development program
[NASA-CR-174972] p 221 N87-20137

AUXILIARY PROPULSION

Arcjet component conditions through a multistart test
[AIAA PAPER 87-1060] p 51 A87-41127

Advanced technology payoffs for future small propulsion systems
p 21 A87-47081

The NASA/USAF arcjet research and technology program
[AIAA PAPER 87-1946] p 54 A87-50192

Preliminary performance characterizations of an engineering model multipropellant resistojet for space station application
[AIAA PAPER 87-2120] p 54 A87-50197

Arcjet component conditions through a multistart test
[NASA-TM-89857] p 61 N87-20382

Preliminary performance characterizations of an engineering model multipropellant resistojet for space station application
[NASA-TM-100113] p 111 N87-23821

The NASA/USAF arcjet research and technology program
[NASA-TM-100112] p 66 N87-24525

AVALANCHE DIODES

- The 60 GHz IMPATT diode development
[NASA-CR-179536] p 218 N87-17515
The 20 GHz spacecraft IMPATT solid state transmitter
[NASA-CR-179545] p 124 N87-17989

AXIAL FLOW

- Rotor wake characteristics of a transonic axial-flow fan p 2 A87-20886
Stall transients of axial compression systems with inlet distortion p 3 A87-24010
Measurements of the unsteady flow field within the stator row of a transonic axial-flow fan. 1: Measurement and analysis technique
[NASA-TM-88945] p 10 N87-16789

AXIAL FLOW TURBINES

- Measurements of the unsteady flow field within the stator row of a transonic axial-flow fan. Part 2: Results and discussion
[NASA-TM-88946] p 10 N87-16790
Unsteady flows in a single-stage transonic axial-flow fan stator row
[NASA-TM-88929] p 11 N87-16805

AXIAL LOADS

- J-integral estimates for cracks in infinite bodies
p 177 A87-35334

AXIAL STRAIN

- Results of an interlaboratory fatigue test program conducted on alloy 800H at room and elevated temperatures p 87 A87-54370
A simplified computer solution for the flexibility matrix of contacting teeth for spiral bevel gears
[NASA-CR-179620] p 168 N87-23977

AXISYMMETRIC BODIES

- Particle trajectory computer program for icing analysis of axisymmetric bodies - A progress report
[AIAA PAPER 87-0027] p 15 A87-22366
Revised NASA axially symmetric ring model for coupled-cavity traveling-wave tubes
[NASA-TP-2675] p 127 N87-22923

AXISYMMETRIC FLOW

- The evolution of instabilities in the axisymmetric jet. I - The linear growth of disturbances near the nozzle. II - The flow resulting from the interaction between two waves p 138 A87-37256
Modelling of jet- and swirl-stabilized reacting flows in axisymmetric combustors p 138 A87-38956
Initial turbulence effect on jet evolution with and without tonal excitation p 14 N87-27629
Enhanced mixing of an axisymmetric jet by aerodynamic excitation
[NASA-CR-175059] p 15 N87-29418

B**BACKWARD FACING STEPS**

- Finite analytic numerical solution of two-dimensional channel flow over a backward-facing step p 131 A87-13506
Third-moment closure of turbulence for predictions of separating and reattaching shear flows: A study of Reynolds-stress closure model
[NASA-CR-177055] p 145 N87-11961

BALL BEARINGS

- Lubricant effects on bearing life
[NASA-TM-88875] p 165 N87-15467
Oil film thickness measurement and analysis for an angular contact ball bearing operating in parched elastohydrodynamic lubrication
[NASA-CR-179506] p 70 N87-16879

BARIUM FLUORIDES

- Hardness of CaF₂ and BaF₂ solid lubricants at 25 to 670 deg C
[NASA-TM-88979] p 102 N87-18670

BARIUM TITANATES

- Large aperture interferometer with phase-conjugate self-reference beam p 153 A87-17320

BEAM CURRENTS

- Electron beam experiments at high altitudes p 44 N87-26946

BEAMS (RADIATION)

- Rays versus modes - Pictorial display of energy flow in an open-ended waveguide p 112 A87-44075
Beam-modulation methods in quantitative and flow-visualization holographic interferometry p 111 N87-21204

BEARING ALLOYS

- Selection of rolling-element bearing steels for long-life application
[NASA-TM-88881] p 164 N87-11993

BEARINGS

- A fully coupled variable properties thermohydraulic model for a cryogenic hydrostatic journal bearing
[ASME PAPER 86-TRIB-55] p 161 A87-19536

- A hybrid nonlinear programming method for design optimization p 201 A87-35718

- Flexibility effects on tooth contact location in spiral bevel gear transmissions
[NASA-CR-4055] p 166 N87-20552

BENDING

- The effect of circumferential aerodynamic detuning on coupled bending-torsion unstalled supersonic flutter
[ASME PAPER 86-GT-100] p 20 A87-25396

BENDING MOMENTS

- An efficient quadrilateral element for plate bending analysis p 178 A87-45994
A simplified computer solution for the flexibility matrix of contacting teeth for spiral bevel gears
[NASA-CR-179620] p 168 N87-23977

BENDING VIBRATION

- Nonlinear vibration and stability of rotating, pretwisted, precone blades including Coriolis effects p 178 A87-39896

BENZENE

- Triptycene - A D(3h) C(62) hydrocarbon with three U-shaped cavities p 69 A87-53656
The 2,5-diacyl-1,4-dimethylbenzenes: Examples of bisphotoenol equivalents
[NASA-TM-89836] p 71 N87-22005
The oxidation degradation of aromatic compounds
[NASA-CR-180588] p 79 N87-22020

BINARY ALLOYS

- Cellular and dendritic growth in a binary melt - A marginal stability approach p 107 A87-10871
Fault structures in rapidly quenched Ni-Mo binary alloys p 83 A87-32035
Cellular-dendritic transition in directionally solidified binary alloys p 84 A87-32046
The alloy undercooling experiment on the Columbia STS 61-C Space Shuttle mission
[AIAA PAPER 87-0506] p 108 A87-45724
Dendritic solidification in a binary alloy melt - Comparison of theory and experiment p 217 A87-48733
Primary arm spacing in chill block melt spun Ni-Mo alloys
[NASA-TM-88887] p 88 N87-11875
The alloy undercooling experiment on the Columbia STA 61-C space shuttle mission
[NASA-TM-88909] p 91 N87-18643

BINARY SYSTEMS (MATERIALS)

- Centrifugal inertia effects in two-phase face seal films p 162 A87-37687

BIOMASS

- A design study of hydrazine and biowaste resists
[NASA-CR-179510] p 57 N87-14425

BIPOLAR TRANSISTORS

- Microwave characterization and modeling of GaAs/AlGaAs heterojunction bipolar transistors
[NASA-TM-100150] p 117 N87-26265

BIPOLARITY

- Develop and test fuel cell powered on-site integrated total energy systems. Phase 3: Full-scale power plant development
[NASA-CR-175117] p 191 N87-11346
Component variations and their effects on bipolar nickel-hydrogen cell performance
[NASA-TM-89907] p 195 N87-23029

BIT ERROR RATE

- Bit-error-rate testing of high-power 30-GHz traveling wave tubes for ground-terminal applications
[NASA-TP-2635] p 115 N87-17971
Unique bit-error-rate measurement system for satellite communication systems p 116 N87-20448
Automated measurement of the bit-error rate as a function of signal-to-noise ratio for microwave communications systems
[NASA-TM-89898] p 127 N87-22102

BLACK AND WHITE PHOTOGRAPHY

- Black-and-white photographic chemistry: A reference
[NASA-TM-87296] p 70 N87-10177

BLADE TIPS

- Ramp-integration technique for capacitance-type blade-tip clearance measurement p 155 A87-45128
An experimental study on the effects of tip clearance on flow field and losses in an axial flow compressor rotor p 6 A87-46207
Low-cost FM oscillator for capacitance type of blade tip clearance measurement system
[NASA-TP-2746] p 31 N87-24481
Performance and power regulation characteristics of two aileron-controlled rotors and a pitchable tip-controlled rotor on the Mod-O turbine
[NASA-TM-100136] p 200 N87-29956

BLADES

- Performance of two 10-lb/sec centrifugal compressors with different blade and shroud thicknesses operating over a range of Reynolds numbers
[AIAA PAPER 87-1745] p 22 A87-50188

- A NASTRAN primer for the analysis of rotating flexible blades

- [NASA-TM-89861] p 184 N87-21375
Performance of two 10-lb/sec centrifugal compressors with different blade and shroud thicknesses operating over a range of Reynolds numbers
[NASA-TM-100115] p 29 N87-23623

BLASIUS FLOW

- Nonlinear critical layers eliminate the upper branch of spatially growing Tollmien-Schlichting waves p 131 A87-12251

BLOWOUTS

- Aircraft accident report: NASA 712, Convair 990, N712NA, March Air Force Base, California, July 17, 1985, executive summary p 16 N87-21878
Aircraft accident report: NASA 712, Convair 990, N712NA, March Air Force Base, California, July 17, 1985, facts and analysis
[NASA-TM-87356-VOL-2] p 16 N87-21879
Analysis of Convair 990 rejected-takeoff accident with emphasis on decision making, training and procedures
[NASA-TM-100189] p 16 N87-29471

BLUFF BODIES

- Two-phase measurements of a spray in the wake of a bluff body p 142 A87-46199

BODY CENTERED CUBIC LATTICES

- Analysis of NiAlTa precipitates in beta-NiAl + 2 at. pct Ta alloy p 84 A87-34888

BOEING 737 AIRCRAFT

- Experimental, water droplet impingement data on two-dimensional airfoils, axisymmetric inlet and Boeing 737-300 engine inlet
[AIAA PAPER 87-0097] p 17 A87-24918

BOLOMETERS

- Technology for satellite power conversion
[NASA-CR-180162] p 193 N87-18229

BOLTZMANN TRANSPORT EQUATION

- Stoichiometric disturbances in compound semiconductors due to ion implantation p 215 A87-12292

BORON

- A study of the microstructure of a rapidly solidified nickel-base superalloy modified with boron
[NASA-CR-179553] p 89 N87-14486

BORON ALLOYS

- Elevated temperature strengthening of a melt spun austenitic steel by TiB₂ p 87 A87-51639

BORON NITRIDES

- Adhesion, friction and deformation of ion-beam-deposited boron nitride films p 98 A87-49325
Adhesion, friction, and deformation of ion-beam-deposited boron nitride films
[NASA-TM-88902] p 100 N87-15305
Mechanical strength and tribological behavior of ion-beam deposited boron nitride films on non-metallic substrates p 101 N87-18668
Boron nitride: Composition, optical properties and mechanical behavior
[NASA-TM-89849] p 218 N87-25017

BOSONS

- Noncommutative-geometry model for closed bosonic strings p 207 A87-37542

BOUNDARY ELEMENT METHOD

- Conforming versus non-conforming boundary elements in three-dimensional elastostatics p 175 A87-22775

BOUNDARY INTEGRAL METHOD

- Free vibration analysis by BEM using particular integrals p 174 A87-13882

BOUNDARY LAYER EQUATIONS

- DOE/NASA automotive Stirling engine project - Overview 86 p 220 A87-18034

BOUNDARY LAYER FLOW

- Endwall heat transfer in the junction region of a circular cylinder normal to a flat plate at 30 and 60 degrees from stagnation point of the cylinder
[AIAA PAPER 87-0077] p 132 A87-22398
The hub wall boundary layer development and losses in an axial flow compressor rotor passage p 139 A87-41665

- Radiative cooling of a layer with nonuniform velocity - A separable solution p 141 A87-45637
Heat transfer and fluid mechanics measurements in transitional boundary layers on convex-curved surfaces
[ASME PAPER 85-MT-60] p 143 A87-48726

- Third-moment closure of turbulence for predictions of separating and reattaching shear flows: A study of Reynolds-stress closure model
[NASA-CR-177055] p 145 N87-11961
Flowfield measurements in a separated and reattached flat plate turbulent boundary layer
[NASA-CR-4052] p 148 N87-21257

BOUNDARY LAYER SEPARATION

Generation of Tollmien-Schlichting waves on interactive marginally separated flows p 144 A87-54365

BOUNDARY LAYER STABILITY

The generation of Tollmien-Schlichting waves by long wavelength free stream disturbances p 139 A87-41655

BOUNDARY LAYER TRANSITION

Heat transfer and fluid mechanics measurements in transitional boundary layers on convex-curved surfaces [ASME PAPER 85-MT-60] p 143 A87-48726

BOUNDARY LAYERS

Nonlinear critical layers eliminate the upper branch of spatially growing Tollmien-Schlichting waves p 131 A87-12251

Comparison of calculated and experimental cascade performance for controlled-diffusion compressor stator blading [ASME PAPER 86-GT-35] p 19 A87-25394

The measurement of boundary layers on a compressor blade in cascade at high positive incidence angle. 1: Experimental techniques and results [NASA-CR-179491] p 25 N87-13441

The measurement of boundary layers on a compressor blade in cascade at high positive incidence angle. 2: Data report [NASA-CR-179492] p 25 N87-13442

A general method for unsteady stagnation region heat transfer and results for model turbine flows [NASA-TM-88903] p 146 N87-17002

Direct numerical simulations of a temporally evolving mixing layer subject to forcing [NASA-TM-88896] p 150 N87-23933

BOUNDARY VALUE PROBLEMS

A new formulation of electromagnetic wave scattering using an on-surface radiation boundary condition approach p 112 A87-32829

Numerical simulations of unsteady, viscous, transonic flow over isolated and cascaded airfoils using a deforming grid [AIAA PAPER 87-1316] p 7 A87-49649

Multigrid-sinc methods p 205 A87-52865

Mass and momentum turbulent transport experiments p 144 N87-11201

Analysis of mixed-mode crack propagation using the boundary integral method [NASA-CR-179518] p 180 N87-12915

Strain energy release rates of composite interlaminar end-notch and mixed-mode fracture: A sublaminate/ply level analysis and a computer code [NASA-TM-89827] p 74 N87-20389

Numerical simulations of unsteady, viscous, transonic flow over isolated and cascaded airfoils using a deforming grid [NASA-TM-89890] p 13 N87-24435

Diffusion length measurements in bulk and epitaxially grown 3-5 semiconductors using charge collection microscopy [NASA-TM-100128] p 129 N87-27121

Three dimensional boundary layers in internal flows [NASA-CR-181336] p 152 N87-28860

BRASSES

Further observations of SCC in alpha-beta brass Considerations regarding the appearance of crack arrest markings during SCC p 82 A87-23843

BRAYTON CYCLE

Brayton cycle solarized advanced gas turbine [NASA-CR-179559] p 220 N87-15030

Speculations on future opportunities to evolve Brayton powerplants aboard the space station [NASA-TM-89863] p 39 N87-23674

BREADBOARD MODELS

Breadboard RL10-11B low thrust operating mode [NASA-CR-174914] p 58 N87-15269

BROADBAND

On broadband shock associated noise of supersonic jets p 208 A87-11768

A new model for broadband waveguide to microstrip transition design [NASA-TM-88905] p 115 N87-16958

BROMINATION

Effects of milling brominated P-100 graphite fibers p 97 A87-41078

Microstructure-derived macroscopic residual resistance of brominated graphite fibers p 97 A87-48324

Thermal conductivity of pristine and brominated P-100 fibers [NASA-TM-88863] p 99 N87-11893

Effects of graphitization on the environmental stability of brominated pitch-based fibers [NASA-TM-88899] p 100 N87-12679

Effects of sequential treatment with fluorine and bromine on graphite fibers [NASA-TM-100106] p 104 N87-24574

BROMINE

Properties and potential applications of brominated P-100 carbon fibers p 95 A87-23702

Mechanical and electrical properties of graphite fiber-epoxy composites made from pristine and bromine intercalated fibers p 73 A87-49799

Simultaneous electrical resistivity and mass uptake measurements in bromine intercalated fibers [NASA-TM-88900] p 70 N87-11841

Electrochemical performance and transport properties of a Nafion membrane in a hydrogen-bromine cell environment [NASA-TM-89862] p 79 N87-23718

Stability of bromine, iodine monochloride, copper (II) chloride, and nickel (II) chloride intercalated pitch-based graphite fibers [NASA-TM-89904] p 103 N87-24563

BUBBLES

Thermocapillary bubble migration for large Marangoni Numbers [NASA-CR-179628] p 109 N87-22865

BUCKLING

Non-isothermal elastoviscoplastic snap-through and creep buckling of shallow arches [AIAA PAPER 87-0806] p 176 A87-33605

Dynamic delamination buckling in composite laminates under impact loading: Computational simulation [NASA-TM-100192] p 75 N87-28611

The dynamic aspects of thermo-elasto-viscoplastic snap-through and creep buckling phenomena [NASA-CR-181411] p 187 N87-29897

BUOYANCY

A comparative study of the influence of buoyancy driven fluid flow on GaAs crystal growth p 219 N87-28741

BURNERS

Experimental verification of corrosive vapor deposition rate theory in high velocity burner rigs p 143 A87-49551

Experimental verification of vapor deposition model in Mach 0.3 burner rigs p 88 N87-11192

High temperature stress-strain analysis p 179 N87-11209

BUTTERFLY VALVES

Noise generated by flow through large butterfly valves [NASA-TM-88911] p 210 N87-16586

BYPASS RATIO

A model propulsion simulator for evaluating counter rotating blade characteristics [SAE PAPER 861715] p 20 A87-32607

C**C-135 AIRCRAFT**

Acceleration display system for aircraft zero-gravity research [NASA-TM-87358] p 156 N87-18801

CALCIUM FLUORIDES

Hardness of CaF₂ and BaF₂ solid lubricants at 25 to 670 deg C [NASA-TM-88979] p 102 N87-18670

CALCULUS OF VARIATIONS

A generalized procedure for constructing an upwind based TVD scheme [NASA-TM-88926] p 205 N87-24132

CALIBRATING

An anemometer for highly turbulent or recirculating flows Technology for satellite power conversion [NASA-CR-180162] p 193 N87-18229

Calibration and comparison of the NASA Lewis free-piston Stirling engine model predictions with RE-1000 test data [NASA-TM-89853] p 222 N87-22561

Heat flux calibration facility capable of SSME conditions p 36 N87-22774

Airflow calibration and exhaust pressure/temperature survey of an F404, S/N 215-109, turbofan engine [NASA-TM-100159] p 33 N87-29537

CANTILEVER BEAMS

Solution methods for one-dimensional viscoelastic problems [AIAA PAPER 87-0804] p 176 A87-33604

An investigation of the dynamic response of spur gear teeth with moving loads [NASA-CR-179643] p 170 N87-29840

CANTILEVER PLATES

Three-dimensional vibrations of twisted cantilevered parallelepipeds p 173 A87-11106

CAPACITANCE

Ramp-integration technique for capacitance-type blade-tip clearance measurement p 155 A87-45128

Oil film thickness measurement and analysis for an angular contact ball bearing operating in parched elastohydrodynamic lubrication [NASA-CR-179506] p 70 N87-16879

CAPACITANCE-VOLTAGE CHARACTERISTICS

Behavior of inversion layers in 3C silicon carbide p 215 A87-11242

CAPILLARY FLOW

Thermocapillary bubble migration for large Marangoni Numbers [NASA-CR-179628] p 109 N87-22865

CAPILLARY WAVES

The generation of capillary instabilities on a liquid jet p 130 A87-12060

CARBIDES

Carbide-fluoride-silver self-lubricating composite [NASA-CASE-LEW-14196-2] p 169 N87-25585

CARBON

Carbon and carbon-coated electrodes for multistage depressed collectors for electron-beam devices - A technology review p 120 A87-20666

Ellipsometric and optical study of amorphous hydrogenated carbon films p 216 A87-23967

TWT efficiency improvement by a low-cost technique for deposition of carbon on MDC electrodes p 121 A87-30199

Rapid thermal annealing of Amorphous Hydrogenated Carbon (a-C:H) films [NASA-TM-89859] p 218 N87-20821

Traveling-wave-tube efficiency improvement by a low-cost technique for deposition of carbon on multistage depressed collector [NASA-TP-2719] p 126 N87-21239

Long-time creep behavior of Nb-1Zr alloy containing carbon [NASA-TM-100142] p 92 N87-26217

Comparison of the tribological properties of fluorinated cokes and graphites [NASA-TM-100170] p 106 N87-29679

CARBON DIOXIDE

Performance study of a fuel cell Pt-on-C anode in presence of CO and CO₂, and calculation of adsorption parameters for CO poisoning p 188 A87-12338

Concentration of carbon dioxide by a high-temperature electrochemical membrane cell p 77 A87-27400

Hydrogen oxidation mechanism with applications to (1) the chaperon efficiency of carbon dioxide and (2) vitiated air testing [NASA-TM-100186] p 80 N87-28628

CARBON FIBERS

Properties and potential applications of brominated P-100 carbon fibers p 95 A87-23702

Anticorrelation of Shubnikov-deHaas amplitudes and negative magnetoresistance magnitudes in intercalated pitch based graphite fibers p 217 A87-28295

Thermal expansion behavior of graphite/glass and graphite/magnesium p 72 A87-38615

Effects of milling brominated P-100 graphite fibers p 97 A87-41078

Temperature dependence (4K to 300K) of the electrical resistivity of methane grown carbon fibers p 97 A87-47375

Microstructure-derived macroscopic residual resistance of brominated graphite fibers p 97 A87-48324

Effects of graphitization on the environmental stability of brominated pitch-based fibers [NASA-TM-88899] p 100 N87-12679

Stability of bromine, iodine monochloride, copper (II) chloride, and nickel (II) chloride intercalated pitch-based graphite fibers [NASA-TM-89904] p 103 N87-24563

CARBON MONOXIDE POISONING

Performance study of a fuel cell Pt-on-C anode in presence of CO and CO₂, and calculation of adsorption parameters for CO poisoning p 188 A87-12338

Modeling for CO poisoning of a fuel cell anode p 191 A87-52288

CARBON-CARBON COMPOSITES

Advanced composite combustor structural concepts program [NASA-CR-174733] p 74 N87-20387

CARBURIZING

Processing of laser formed SiC powder [NASA-CR-179638] p 104 N87-24573

CARGO SPACECRAFT

Nuclear powered Mars cargo transport mission utilizing advanced ion propulsion [AIAA PAPER 87-1903] p 53 A87-50191

Nuclear powered Mars cargo transport mission utilizing advanced ion propulsion [NASA-TM-100109] p 65 N87-23692

CARRIER DENSITY (SOLID STATE)

Compensation in epitaxial cubic SiC films p 216 A87-15071

CASCADE FLOW

An L-U implicit multigrid algorithm for the three-dimensional Euler equations [AIAA PAPER 87-0453] p 133 A87-22645

- Comparison of calculated and experimental cascade performance for controlled-diffusion compressor stator blading [ASME PAPER 86-GT-35] p 19 A87-25394
- Numerical simulations of unsteady, viscous, transonic flow over isolated and cascaded airfoils using a deforming grid [AIAA PAPER 87-1316] p 7 A87-49649
- The measurement of boundary layers on a compressor blade in cascade at high positive incidence angle. 1: Experimental techniques and results [NASA-CR-179491] p 25 N87-13441
- The measurement of boundary layers on a compressor blade in cascade at high positive incidence angle. 2: Data report [NASA-CR-179492] p 25 N87-13442
- Combined fringe and Fabry-Perot laser anemometer for 3 component velocity measurements in turbine stator cascade facility p 110 N87-21183
- Unsteady stator/rotor interaction p 149 N87-22767
- A linearized Euler analysis of unsteady flows in turbomachinery [NASA-CR-180987] p 149 N87-22948
- Numerical simulations of unsteady, viscous, transonic flow over isolated and cascaded airfoils using a deforming grid [NASA-TM-89890] p 13 N87-24435
- CAST ALLOYS**
- Cellular-dendritic transition in directionally solidified binary alloys p 84 A87-32046
- High temperature monotonic and cyclic deformation in a directionally solidified nickel-base superalloy [NASA-CR-175101] p 90 N87-15303
- CASTING**
- Fabrication of cooled radial turbine rotor [NASA-CR-179503] p 25 N87-11789
- New methods and materials for molding and casting ice formations [NASA-TM-100126] p 16 N87-29470
- CATALYSTS**
- Organometallic catalysts for primary phosphoric acid fuel cells [NASA-CR-179490] p 193 N87-19804
- CATALYTIC ACTIVITY**
- Catalytic and electrode research for phosphoric acid fuel cells p 190 A87-33789
- CATHODES**
- Design, construction and long life endurance testing of cathode assemblies for use in microwave high-power transmitting tubes [NASA-CR-175116] p 123 N87-10237
- Apparatus for mounting a field emission cathode [NASA-CASE-LEW-14108-1] p 129 N87-28832
- CAVITATION CORROSION**
- Plastic deformation of a magnesium oxide 001-plane surface produced by cavitation [ASLE PREPRINT 86-TC-3D-1] p 94 A87-19504
- Deformation and fracture of single-crystal and sintered polycrystalline silicon carbide produced by cavitation [NASA-TM-88981] p 102 N87-20422
- CAVITATION FLOW**
- Two-phase flows and heat transfer within systems with ambient pressure above the thermodynamic critical pressure p 136 A87-30728
- Effect of vibration amplitude on vapor cavitation in journal bearings [NASA-TM-88826] p 145 N87-11962
- Effect of shaft frequency on cavitation in a journal bearing for noncentered circular whirl [NASA-TM-88925] p 148 N87-22122
- CAVITIES**
- Revised NASA axially symmetric ring model for coupled-cavity traveling-wave tubes [NASA-TP-2675] p 127 N87-22923
- Reduction of the radar cross section of arbitrarily shaped cavity structures [NASA-CR-180307] p 118 N87-27085
- CAVITY RESONATORS**
- Linear capacitive displacement sensor with frequency readout p 154 A87-42546
- CELL ANODES**
- Performance study of a fuel cell Pt-on-C anode in presence of CO and CO₂, and calculation of adsorption parameters for CO poisoning p 188 A87-12338
- Modeling for CO poisoning of a fuel cell anode p 191 A87-52288
- CELL CATHODES**
- Organometallic catalysts for primary phosphoric acid fuel cells [NASA-CR-179490] p 193 N87-19804
- CENTAUR LAUNCH VEHICLE**
- Effects of transient propellant dynamics on deployment of large liquid stages in zero-gravity with application to Shuttle/Centaur [IAF PAPER 86-119] p 39 A87-15880
- Measurement of Centaur/Orbiter multiple reaction forces in a full-scale test rig p 38 A87-29448
- Shuttle/Centaur G-prime composite adapters damage tolerance/repair test program [AIAA PAPER 87-0792] p 38 A87-33592
- The effect of nonlinearities on the dynamic response of a large Shuttle payload [AIAA PAPER 87-0857] p 40 A87-33697
- Development and test of the Shuttle/Centaur cryogenic tankage thermal protection system [AIAA PAPER 87-1557] p 43 A87-43073
- Self-regulating heater application to Shuttle/Centaur hydrazine fuel line thermal control [AIAA PAPER 87-1570] p 43 A87-43081
- Effect of gimbal friction modelling technique on control stability and performance for Centaur upper stage [AIAA PAPER 87-2455] p 38 A87-50501
- Centaur D1-A systems in a nutshell [NASA-TM-88880] p 38 N87-15996
- Effect of Gimbal friction modeling technique on control stability and performance for Centaur upper-stage [NASA-TM-88894] p 39 N87-22755
- Design, development and test of shuttle/Centaur G-prime cryogenic tankage thermal protection systems [NASA-TM-88825] p 43 N87-23685
- CENTERBODIES**
- Numerical prediction of cold turbulent flow in combustor configurations with different centerbody flame holders [ASME PAPER 86-WA/HT-50] p 140 A87-43715
- CENTRIFUGAL COMPRESSORS**
- Performance of two 10-lb/sec centrifugal compressors with different blade and shroud thicknesses operating over a range of Reynolds numbers [AIAA PAPER 87-1745] p 22 A87-50188
- Scaled centrifugal compressor program [NASA-CR-174912] p 26 N87-14349
- Performance of two 10-lb/sec centrifugal compressors with different blade and shroud thicknesses operating over a range of Reynolds numbers [NASA-TM-100115] p 29 N87-23623
- CENTRIFUGAL PUMPS**
- Small centrifugal pumps for low-thrust rockets p 50 A87-39808
- CENTRIFUGES**
- Centrifugal inertia effects in two-phase face seal films p 162 A87-37687
- CEPSTRAL ANALYSIS**
- Ray propagation path analysis of acousto-ultrasonic signals in composites [NASA-TM-100148] p 173 N87-25589
- CERAMIC BONDING**
- Fracture of flash oxidized, yttria-doped sintered reaction-bonded silicon nitride p 97 A87-47923
- CERAMIC COATINGS**
- Degradation mechanisms in thermal-barrier coatings p 94 A87-12953
- New ZrO₂-Yb₂O₃ plasma-sprayed coatings for thermal barrier applications p 98 A87-53623
- Thermal barrier coating life prediction model development [NASA-CR-179508] p 99 N87-11892
- Advanced Gas Turbine (AGT) Technology Project [NASA-CR-179484] p 164 N87-11995
- CERAMIC FIBERS**
- Silsesquioxanes as precursors to ceramic composites [NASA-TM-88993] p 75 N87-25432
- CERAMIC MATRIX COMPOSITES**
- Polymer, metal, and ceramic matrix composites for advanced aircraft engine applications p 71 A87-15187
- Thermal expansion behavior of graphite/glass and graphite/magnesium p 72 A87-38615
- Advanced Gas Turbine (AGT) Technology Project [NASA-CR-179484] p 164 N87-11995
- Polymer precursors for ceramic matrix composites [NASA-CR-179562] p 70 N87-14434
- Ceramic matrix and resin matrix composites: A comparison [NASA-TM-89830] p 74 N87-18615
- Advanced composite combustor structural concepts program [NASA-CR-174733] p 74 N87-20387
- Silsesquioxanes as precursors to ceramic composites [NASA-TM-89893] p 75 N87-25432
- Fiber reinforced ceramic material [NASA-CASE-LEW-14392-2] p 106 N87-27810
- Method of preparing fiber reinforced ceramic material [NASA-CASE-LEW-14392-1] p 106 N87-28656
- CERAMICS**
- Tribology of selected ceramics at temperatures to 900 C p 94 A87-12954
- Probability of detection of internal voids in structural ceramics using microfocus radiography p 170 A87-14300
- SCARE - A postprocessor program to MSC/NASTRAN for reliability analysis of structural ceramic components [ASME PAPER 86-GT-34] p 174 A87-17988
- Plastic deformation of a magnesium oxide 001-plane surface produced by cavitation [ASLE PREPRINT 86-TC-3D-1] p 94 A87-19504
- Friction and wear behaviour of ion beam modified ceramics p 97 A87-47958
- NDE reliability and process control for structural ceramics [ASME PAPER 87-GT-8] p 171 A87-48702
- A technology development summary for the AGT101 advanced gas turbine program [SAE PAPER 870466] p 163 A87-48790
- The Advanced Turbine Technology Applications Program (ATTAP) [SAE PAPER 870467] p 163 A87-48791
- Quantitative void characterization in structural ceramics by use of scanning laser acoustic microscopy p 171 A87-51974
- Structural ceramics in heat engines - The NASA viewpoint p 98 A87-53352
- Ceramic automotive Stirling engine program [NASA-CR-175042] p 192 N87-12047
- NDE reliability and process control for structural ceramics [NASA-TM-88870] p 171 N87-12910
- A constitutive law for finite element contact problems with unclassical friction [NASA-TM-88838] p 180 N87-12924
- Surface flaw reliability analysis of ceramic components with the SCARE finite element postprocessor program [NASA-TM-88901] p 181 N87-17087
- Nondestructive evaluation of structural ceramics [NASA-TM-88978] p 172 N87-18109
- Thermomechanical behavior of plasma-sprayed ZrO₂-Y₂O₃ coatings influenced by plasticity, creep and oxidation [NASA-TM-88940] p 147 N87-18784
- Analysis of an advanced technology subsonic turbofan incorporating revolutionary materials [NASA-TM-89868] p 29 N87-22680
- Application of scanning acoustic microscopy to advanced structural ceramics [NASA-TM-88929] p 172 N87-23987
- Stability and rheology of dispersions of silicon nitride and silicon carbide [NASA-CR-179634] p 104 N87-25476
- Ultrasonic NDE of structural ceramics for power and propulsion systems [NASA-TM-100147] p 173 N87-26362
- Ceramic high pressure gas path seal [NASA-CR-180813] p 31 N87-26914
- Fracture mechanics concepts in reliability analysis of monolithic ceramics [NASA-TM-100174] p 187 N87-27269
- Fiber reinforced ceramic material [NASA-CASE-LEW-14392-2] p 106 N87-27810
- Advanced Gas Turbine (AGT) Technology Development Project [NASA-CR-180818] p 222 N87-30225
- CHANNEL FLOW**
- Finite analytic numerical solution of two-dimensional channel flow over a backward-facing step p 131 A87-13506
- Turbulent heat transfer in corrugated-wall channels with and without fins p 134 A87-27709
- Influence of oscillation-induced diffusion on heat transfer in a uniformly heated channel p 135 A87-27716
- Local heat transfer augmentation in channels with two opposite ribbed surfaces p 136 A87-30732
- A method for calculating turbulent boundary layers and losses in the flow channels of turbomachines [NASA-TM-88928] p 9 N87-15944
- Measurement of heat transfer and pressure drop in rectangular channels with turbulence promoters [NASA-CR-4015] p 146 N87-17003
- CHARACTERIZATION**
- Acousto-ultrasonic input-output characterization of unidirectional fiber composite plate by SH waves [NASA-CR-4087] p 173 N87-26361
- CHARGE EFFICIENCY**
- Effect of storage and LEO cycling on manufacturing technology IPV nickel-hydrogen cells [NASA-TM-89883] p 194 N87-22308
- CHARGE EXCHANGE**
- Neutral atomic oxygen beam produced by ion charge exchange for Low Earth Orbital (LEO) simulation p 79 N87-26188
- CHEMICAL ANALYSIS**
- Analysis of plasma-nitrided steels [NASA-TM-89815] p 91 N87-21078
- CHEMICAL ATTACK**
- Corrosion pitting of SiC by molten salts p 76 A87-27165

- The effect of Cr, Co, Al, Mo and Ta on a series of cast Ni-base superalloys on the stability of an aluminide coating during cyclic oxidation in Mach 0.3 burner rig [NASA-TM-88840] p 89 N87-14488
- CHEMICAL BONDS**
Triptycene - A D(3h) C(62) hydrocarbon with three U-shaped cavities p 69 A87-53656
- CHEMICAL COMPOSITION**
Particle-size reduction of Si₃N₄ powder with Si₃N₄ milling hardware p 94 A87-12936
Composition optimization of self-lubricating chromium-carbide-based composite coatings for use to 760 C p 96 A87-27838
The effect of Cr, Co, Al, Mo and Ta on a series of cast Ni-base superalloys on the stability of an aluminide coating during cyclic oxidation in Mach 0.3 burner rig [NASA-TM-88840] p 89 N87-14488
Boron nitride: Composition, optical properties and mechanical behavior [NASA-TM-89849] p 218 N87-25017
The tribological behavior of polyphenyl ether and polyphenyl thioether aromatic lubricants [NASA-TM-100166] p 105 N87-26231
Composition optimization of chromium carbide based solid lubricant coatings for foil gas bearings at temperatures to 650 C [NASA-CR-179649] p 105 N87-26233
- CHEMICAL EFFECTS**
Effect of an oxygen plasma on uncoated thin aluminum reflecting films [NASA-TM-89882] p 61 N87-21999
Oxygen interaction with space-power materials [NASA-CR-181396] p 80 N87-29633
- CHEMICAL PROPERTIES**
Effect of an oxygen plasma on the physical and chemical properties of several fluids for the Liquid Droplet Radiator [AIAA PAPER 87-0080] p 42 A87-22401
Plasma assisted surface coating/modification processes: An emerging technology [NASA-TM-88885] p 110 N87-12708
Aviation fuel property effects on altitude relight [NASA-CR-179582] p 107 N87-24578
- CHEMICAL REACTIONS**
Black-and-white photographic chemistry: A reference [NASA-TM-87296] p 70 N87-10177
Theoretical kinetic computations in complex reacting systems p 219 N87-20277
The chemical shock tube as a tool for studying high-temperature chemical kinetics p 157 N87-20279
Stress-life interrelationships associated with alkaline fuel cells [NASA-TM-89881] p 194 N87-22307
- CHEMILUMINESCENCE**
A preliminary study of ester oxidation on an aluminum surface using chemiluminescence p 96 A87-37688
Ester oxidation on an aluminum surface using chemiluminescence [NASA-TP-2611] p 101 N87-18666
The tribological behavior of polyphenyl ether and polyphenyl thioether aromatic lubricants [NASA-TM-100166] p 105 N87-26231
- CHLORIDES**
The formation of volatile corrosion products during the mixed oxidation-chlorination of cobalt at 650 C p 82 A87-23848
Stability of bromine, iodine monochloride, copper (II) chloride, and nickel (II) chloride intercalated pitch-based graphite fibers [NASA-TM-89904] p 103 N87-24563
- CHROMIUM**
A study of reduced chromium content in a nickel-base superalloy via element substitution and rapid solidification processing [NASA-CR-179631] p 92 N87-25456
- CHROMIUM CARBIDES**
Effects of silver and group II fluoride solid lubricant additions to plasma-sprayed chromium carbide coatings for foil gas bearings to 650 C p 95 A87-22336
A new chromium carbide-based tribological coating for use to 900 C with particular reference to the Stirling engine p 95 A87-26112
Composition optimization of self-lubricating chromium-carbide-based composite coatings for use to 760 C p 96 A87-27838
Composition optimization of chromium carbide based solid lubricant coatings for foil gas bearings at temperatures to 650 C [NASA-CR-179649] p 105 N87-26233
Experimental evaluation of chromium-carbide-based solid lubricant coatings for use to 760 C [NASA-CR-180808] p 105 N87-27053
- CHRONOLOGY**
Quasars as indicators of galactic ages p 223 A87-26927
- CINEMATOGRAPHY**
Evaluation of diffuse-illumination holographic cinematography in a flutter cascade [NASA-TP-2593] p 156 N87-13731
- CIRCUITS**
Arcjet power supply and start circuit [NASA-CASE-LEW-14374-1] p 36 N87-25335
- CIRCULAR CYLINDERS**
Heat transfer in the stagnation region of the junction of a circular cylinder perpendicular to a flat plate p 131 A87-13019
Endwall heat transfer in the junction region of a circular cylinder normal to a flat plate at 30 and 60 degrees from stagnation point of the cylinder [AIAA PAPER 87-0077] p 132 A87-22398
Effect of a rotor wake on the local heat transfer on the forward half of a circular cylinder p 136 A87-30721
A new formulation of electromagnetic wave scattering using an on-surface radiation boundary condition approach p 112 A87-32829
Spanwise structures in transitional flow around circular cylinders [AIAA PAPER 87-1383] p 140 A87-44940
Progress in the prediction of unsteady heat transfer on turbine blades p 149 N87-22769
Application of turbulence modeling to predict surface heat transfer in stagnation flow region of circular cylinder [NASA-TP-2758] p 151 N87-27161
- CIRCULAR WAVEGUIDES**
Radar cross section of an open-ended circular waveguide Calculation of second-order diffraction terms p 112 A87-31626
RCS of a coated circular waveguide terminated by a perfect conductor p 112 A87-42536
- CLEAN FUELS**
NASA/GE advanced low emissions combustor program [AIAA PAPER 87-2035] p 21 A87-45369
- CLEARANCES**
Ramp-integration technique for capacitance-type blade-tip clearance measurement p 155 A87-45128
- CLOSED ECOLOGICAL SYSTEMS**
Space station propulsion-ECLSS interaction study [NASA-CR-175093] p 69 N87-29594
- CLOUD GLACIATION**
Comparison of wet and dry growth in artificial and flight icing conditions p 16 A87-45635
- CLOUDS**
Particle cloud kinetics in microgravity [AIAA PAPER 87-0577] p 107 A87-22716
- COAL**
Tribological properties of coal slurries [NASA-TM-89930] p 104 N87-24565
- COALESCING**
On the coalescence-dispersion modeling of turbulent molecular mixing [NASA-TM-89910] p 2 N87-25292
- COATINGS**
How to evaluate solid lubricant films using a Pin-on-disk tribometer p 97 A87-42618
Materials for Advanced Turbine Engines (MATE). Project 4: Erosion resistant compressor airfoil coating [NASA-CR-179622] p 92 N87-27029
- COAXIAL CABLES**
Coaxial tube tether/transmission line for manned nuclear space power [NASA-CASE-LEW-14338-1] p 55 N87-10174
Coaxial tube array space transmission line characterization [NASA-TM-89864] p 62 N87-22003
- COBALT**
Corrosion of metals and alloys in sulfate melts at 750 C p 81 A87-17997
- COBALT ALLOYS**
Low cycle fatigue behaviour of a plasma-sprayed coating material p 82 A87-24040
- COBALT OXIDES**
The formation of volatile corrosion products during the mixed oxidation-chlorination of cobalt at 650 C p 82 A87-23848
- CODES**
Overview of the new ASME Performance Test Code for wind turbines [ASME PAPER 86-JPGC-PTC-4] p 190 A87-25475
- CODING**
A high quality image compression scheme for real-time applications p 111 A87-30801
Composite load spectra for select space propulsion structural components [NASA-CR-179496] p 55 N87-10176
ANL/RBC: A computer code for the analysis of Rankine bottoming cycles, including system cost evaluation and off-design performance [NASA-CR-179462] p 220 N87-10777
- Gas flow environmental and heat transfer nonrotating 3D program p 145 N87-11223
On 3-D inelastic analysis methods for hot section components (base program) [NASA-CR-175060] p 180 N87-12923
Lewis inverse design code (LINDES): Users manual [NASA-TP-2676] p 12 N87-20238
On 3-D inelastic analysis methods for hot section components. Volume 1: Special finite element models [NASA-CR-179494] p 185 N87-22996
Low Reynolds number nozzle flow study [NASA-TM-100130] p 67 N87-25426
- COEFFICIENT OF FRICTION**
Friction and wear behaviour of ion beam modified ceramics p 97 A87-47958
The effects of crack surface friction and roughness on crack tip stress fields [NASA-TM-88976] p 183 N87-18881
Experimental rotordynamic coefficient results for teeth-on-rotor and teeth-on-stator labyrinth gas seals p 167 N87-22212
Friction and wear of sintered Alpha SiC sliding against IN-718 alloy at 25 to 800 C in atmospheric air at ambient pressure [NASA-TM-87353] p 103 N87-22860
- COHERENCE**
Coherent structures and turbulence p 133 A87-22859
- COKE**
Comparison of the tribological properties of fluorinated cokes and graphites [NASA-TM-100170] p 106 N87-29679
- COLD WORKING**
Ultrasonic determination of recrystallization [NASA-TM-88855] p 171 N87-10399
- COLLOIDS**
Colloidal characterization of ultrafine silicon carbide and silicon nitride powders p 95 A87-19625
- COLOR**
Towards effective interactive three-dimensional colour postprocessing p 201 A87-11895
Unification of color postprocessing techniques for 3-dimensional computational mechanics [NASA-CR-180214] p 202 N87-18998
Interactive color display of 3-D engineering analysis results [NASA-CR-180589] p 203 N87-22422
- COLOR TELEVISION**
An adaptive algorithm for motion compensated color image coding p 113 A87-45466
- COMBUSTIBLE FLOW**
Visualization of flows in a motored rotary combustion engine using holographic interferometry [AIAA PAPER 86-1557] p 19 A87-21514
The effects of engine speed and injection characteristics on the flow field and fuel/air mixing in motored two-stroke diesel engines [AIAA PAPER 87-0227] p 161 A87-22501
Mechanisms by which heat release affects the flow field in a chemically reacting, turbulent mixing layer [AIAA PAPER 87-0131] p 134 A87-24925
Systematic development of reduced reaction mechanisms for dynamic modeling p 77 A87-33987
Modelling of jet- and swirl-stabilized reacting flows in axisymmetric combustors p 138 A87-38956
Fast algorithm for calculating chemical kinetics in turbulent reacting flow p 77 A87-38958
On direct numerical simulations of turbulent reacting flows [AIAA PAPER 87-1324] p 140 A87-44930
On the modelling of non-reactive and reactive turbulent combustor flows [NASA-CR-4041] p 28 N87-20996
- COMBUSTION**
Science and technology issues in spacecraft fire safety [AIAA PAPER 87-0467] p 39 A87-31107
Effects of droplet interactions on droplet transport at intermediate Reynolds numbers [NASA-CR-179567] p 26 N87-14348
Science and technology issues in spacecraft fire safety [NASA-TM-88933] p 40 N87-16012
Combustion noise from gas turbine aircraft engines measurement of far-field levels [NASA-TM-88971] p 211 N87-17480
NASA-Chinese Aeronautical Establishment (CAE) Symposium [NASA-CP-2433] p 27 N87-20267
The temperature dependence of inelastic light scattering from small particles for use in combustion diagnostic instrumentation [NASA-CR-180399] p 80 N87-28634

COMBUSTION CHAMBERS

- Visualization of flows in a motored rotary combustion engine using holographic interferometry
[AIAA PAPER 86-1557] p 19 A87-21514
- Soot loading in a generic gas turbine combustor
[AIAA PAPER 87-0297] p 19 A87-22544
- Multi-spark visualization of typical combustor flowfields
p 134 A87-25281

A two-dimensional numerical study of the flow inside the combustion chamber of a motored rotary engine
[SAE PAPER 860615] p 161 A87-28624

Prediction of the structure of fuel sprays in cylindrical combustion chambers
p 20 A87-31277

Advances in 3-D Inelastic Analysis Methods for hot section components
[AIAA PAPER 87-0719] p 177 A87-33645

Modelling of jet- and swirl-stabilized reacting flows in axisymmetric combustors
p 138 A87-38956

Effects of multiple rows and noncircular orifices on dilution jet mixing
p 138 A87-39805

Numerical prediction of cold turbulent flow in combustor configurations with different centerbody flame holders
[ASME PAPER 86-WA/HT-50] p 140 A87-3715

NASA/GE advanced low emissions combustor program
[AIAA PAPER 87-2035] p 21 A87-45369

Liner cooling research at NASA Lewis Research Center -- for gas turbine combustion chambers
[AIAA PAPER 87-1828] p 22 A87-50189

A variable geometry combustor for broadened properties fuels
[AIAA PAPER 87-1832] p 23 A87-52246

Demonstration of laser speckle system on burner liner cyclic rig
[NASA-CR-179509] p 155 A87-10377

Hot section viewing system
[NASA-CR-174773] p 155 A87-11144

Combustion overview
p 78 A87-11181

Flame radiation
p 78 A87-11204

Component testing of a ground based gas turbine steam cooled rich-burn primary zone combustor for emissions control of nitrogenous fuels
[NASA-TM-88873] p 191 A87-11345

User's manual for a TEACH computer program for the analysis of turbulent, swirling reacting flow in a research combustor
[NASA-CR-179547] p 78 A87-11858

Enhanced heat transfer combustor technology, subtasks 1 and 2, task C.1
[NASA-CR-179541] p 56 A87-13486

Liquid oxygen cooling of high pressure LOX/hydrocarbon rocket thrust chambers
[NASA-TM-88805] p 57 A87-14426

Transition mixing study
[NASA-CR-175062] p 27 A87-16830

Space station auxiliary thrust chamber technology
[NASA-CR-179552] p 59 A87-16874

Conventionally cast and forged copper alloy for high-heat-flux thrust chambers
[NASA-TP-2694] p 90 A87-16902

Numerical calculations of turbulent reacting flow in a gas-turbine combustor
[NASA-TM-89842] p 1 A87-20171

Modeling turbulent, reacting flow
p 147 A87-20270

Advanced composite combustor structural concepts program
[NASA-CR-174733] p 74 A87-20387

Liner cooling research at NASA Lewis Research Center
[NASA-TM-100107] p 29 A87-23624

Toward improved durability in advanced combustors and turbines: Progress in the prediction of thermomechanical loads
[NASA-TM-88932] p 32 A87-28551

Bonding Lexan and sapphire to form high-pressure, flame-resistant window
[NASA-TM-100188] p 159 A87-28880

COMBUSTION CHEMISTRY

Decoupled direct method for sensitivity analysis in combustion kinetics
[NASA-CR-179636] p 79 A87-24549

COMBUSTION EFFICIENCY

Numerical calculations of turbulent reacting flow in a gas-turbine combustor
[NASA-TM-89842] p 1 A87-20171

Performance and efficiency evaluation and heat release study of an outboard Marine Corporation Rotary Combustion Engine
[NASA-TM-89833] p 28 A87-20282

Synchronization trigger control system for flow visualization
[NASA-TM-89902] p 128 A87-23902

COMBUSTION PHYSICS

Particle cloud kinetics in microgravity
[AIAA PAPER 87-0577] p 107 A87-22716

Effects of droplet interactions on droplet transport at intermediate Reynolds numbers
[AIAA PAPER 87-0137] p 134 A87-24926

Forced cocurrent smoldering combustion
p 77 A87-40572

Combustion research in the Internal Fluid Mechanics Division
p 79 A87-20268

Thermodynamics and combustion modeling
p 219 A87-20274

The oxidation degradation of aromatic compounds
[NASA-CR-180588] p 79 A87-22020

The temperature dependence of inelastic light scattering from small particles for use in combustion diagnostic instrumentation
[NASA-CR-180399] p 80 A87-28634

COMBUSTION PRODUCTS

Hydrogen-air ignition torch
[NASA-TM-88882] p 38 A87-13470

Combustion of velcro in low gravity
[NASA-TM-88970] p 102 A87-19518

Thermodynamics and combustion modeling
p 219 A87-20274

COMBUSTION STABILITY

Liquid oxygen cooling of high pressure LOX/hydrocarbon rocket thrust chambers
[NASA-TM-88805] p 57 A87-14426

COMMERCIAL ENERGY

Status of commercial fuel cell powerplant system development
[NASA-TM-89896] p 148 A87-22171

COMMUNICATION

Research and technology
[NASA-TM-88868] p 223 A87-17656

COMMUNICATION NETWORKS

US long distance fiber optic networks: Technology, evolution and advanced concepts. Volume 2: Fiber optic technology and long distance networks
[NASA-CR-179480] p 113 A87-11057

US long distance fiber optic networks: Technology, evolution and advanced concepts. Volume 3: Advanced networks and economics
[NASA-CR-179481] p 114 A87-11915

An assessment of the status and trends in satellite communications 1986-2000: An information document prepared for the Communications Subcommittee of the Space Applications Advisory Committee
[NASA-CR-88867] p 114 A87-13600

Application of adaptive antenna techniques to future commercial satellite communication
[NASA-CR-179566] p 115 A87-16954

Application of adaptive antenna techniques to future commercial satellite communications. Executive summary
[NASA-CR-179566-SUMM] p 115 A87-16955

Unique bit-error-rate measurement system for satellite communication systems
[NASA-TP-2699] p 116 A87-20448

COMMUNICATION SATELLITES

Advances in gallium arsenide monolithic microwave integrated-circuit technology for space communications systems
p 120 A87-19091

A 20 GHz, high efficiency dual mode TWT for the ACTS program -- Advanced Communications Technology Satellite
p 122 A87-45511

ACTS baseband processing -- Advanced Communications Technology Satellite
p 201 A87-45512

ACTS experiments program -- Advanced Communications Technology Satellite
p 113 A87-45513

Strategic plan, 1985
[NASA-TM-89263] p 219 A87-12384

Engineering calculations for communications satellite systems planning
[NASA-CR-180106] p 114 A87-16198

Communications satellite systems operations with the space station. Volume 1: Executive summary
[NASA-CR-179526] p 206 A87-17472

Communications satellite systems operations with the space station, volume 2
[NASA-CR-179527] p 206 A87-17473

The use of satellites in non-geostationary orbits for unloading geostationary communication satellite traffic peaks. Volume 1: Executive summary
[NASA-CR-179597-VOL-1] p 117 A87-21212

The use of satellites in non-geostationary orbits for unloading geostationary communication satellite traffic peaks. Volume 2: Technical report
[NASA-CR-179597-VOL-2] p 117 A87-21213

On orbital allotments for geostationary satellites
[NASA-CR-181017] p 37 A87-22700

Engineering calculations for communications satellite systems planning
[NASA-CR-181112] p 117 A87-24605

A satellite system synthesis model for orbital arc allotment optimization
[NASA-CR-181150] p 37 A87-25341

Mathematical programming formulations for satellite synthesis
[NASA-CR-181151] p 44 A87-25419

On-board processing satellite network architecture and control study
[NASA-CR-180816] p 44 A87-27710

Optimization of orbital assignment and specification of service areas in satellite communications
[NASA-CR-181273] p 118 A87-27882

Monolithic Microwave Integrated Circuit (MMIC) technology for space communications applications
[NASA-TM-100187] p 118 A87-27883

COMPARISON

Comparison of calculated and experimental cascade performance for controlled-diffusion compressor stator blading
[ASME PAPER 86-GT-35] p 19 A87-25394

Comparison of three explicit multigrid methods for the Euler and Navier-Stokes equations
[AIAA PAPER 87-0602] p 137 A87-34725

Comparison of three explicit multigrid methods for the Euler and Navier-Stokes equations
[NASA-TM-88878] p 1 A87-16784

Advanced Propan Engine Technology (APET) and single-rotation gearbox/pitch change mechanism
[NASA-CR-168113] p 32 A87-28553

Comparison of the tribological properties of fluorinated cokes and graphites
[NASA-TM-100170] p 106 A87-29679

COMPATIBILITY

Space station resistojet system requirements and interface definition study
[NASA-CR-179581] p 60 A87-17848

COMPONENT RELIABILITY

Probabilistic structural analysis to quantify uncertainties associated with turbopump blades
[AIAA PAPER 87-0766] p 176 A87-33581

Optical strain measurement system development, phase 1
[NASA-CR-179619] p 158 A87-22960

Fracture mechanics concepts in reliability analysis of monolithic ceramics
[NASA-TM-100174] p 187 A87-27269

COMPOSITE FUNCTIONS

Composite grid and finite-volume LU implicit scheme for turbine flow analysis
[AIAA PAPER 87-1129] p 5 A87-42078

Composite load spectra for select space propulsion structural components
[NASA-CR-179496] p 55 A87-10176

Generation of a composite grid for turbine flows and consideration of a numerical scheme
[NASA-TM-88890] p 11 A87-17662

Composite grid and finite-volume LU implicit scheme for turbine flow analysis
[NASA-TM-89828] p 12 A87-20235

COMPOSITE MATERIALS

Polymer, metal, and ceramic matrix composites for advanced aircraft engine applications
p 71 A87-15187

Simplified composite micromechanics for predicting microstresses
p 72 A87-20090

On the effect of the Fe(2+)/Fe(3+) redox couple on oxidation of carbon in hot H3PO4
p 78 A87-42677

Composite interlaminar fracture toughness: Three-dimensional finite element modeling for mixed mode I, 2 and 3 fracture
[NASA-TM-88872] p 73 A87-13491

Parameterized materials and dynamic response characterizations in unidirectional composites
[NASA-CR-4032] p 172 A87-13782

PMR polyimide compositions for improved performance at 371 deg C
[NASA-TM-88942] p 73 A87-16071

Carbide-fluoride-silver self-lubricating composite
[NASA-CASE-LEW-14196-2] p 169 A87-25585

Fiber reinforced ceramic material
[NASA-CASE-LEW-14392-2] p 106 A87-27810

Dynamic delamination buckling in composite laminates under impact loading: Computational simulation
[NASA-TM-100192] p 75 A87-28611

COMPOSITE STRUCTURES

Evaluation of capillary reinforced composites for anti-icing
[AIAA PAPER 87-0023] p 17 A87-24904

Design concepts/parameters assessment and sensitivity analyses of select composite structural components
p 175 A87-25407

Shuttle/Centaur G-prime composite adapters damage tolerance/repair test program
[AIAA PAPER 87-0792] p 38 A87-33592

A higher order theory of laminated composite cylindrical shells
p 177 A87-35656

Composite space antenna structures - Properties and environmental effects p 72 A87-38610

Finite element modeling of electromagnetic propagation in composite structures [NASA-TM-88916] p 207 N87-14956

Composite space antenna structures: Properties and environmental effects [NASA-TM-88859] p 73 N87-16880

Nondestructive evaluation of structural ceramics [NASA-TM-88978] p 172 N87-18109

Computational composite mechanics for aerospace propulsion structures [NASA-TM-88965] p 74 N87-18614

Strain energy release rates of composite interlaminar end-notch and mixed-mode fracture: A sublaminar/ply level analysis and a computer code [NASA-TM-89827] p 74 N87-20389

COMPRESSIBILITY

Compressibility of solids p 219 A87-51962

COMPRESSIBLE FLOW

An experimental investigation of compressible three-dimensional boundary layer flow in annular diffusers [AIAA PAPER 87-0366] p 3 A87-24954

Perfect gas effects in compressible rapid distortion theory p 136 A87-31176

Adaptive finite element methods for compressible flow problems p 4 A87-38496

Method for the determination of the three dimensional aerodynamic field of a rotor-stator combination in compressible flow [AIAA PAPER 87-1742] p 7 A87-50187

Simultaneous measurements of two-dimensional velocity and pressure fields in compressible flows through image-intensified detection of laser-induced fluorescence p 143 A87-52320

Elevated temperature tension, compression and creep-rupture behavior of (001)-oriented single crystal superalloy PWA 1480 [NASA-TM-88950] p 90 N87-17882

A comparison of experimental and theoretical results for labyrinth gas seals [NASA-CR-180194] p 166 N87-18096

Method for the determination of the three-dimensional aerodynamic field of a rotor-stator combination to compressible flow [NASA-TM-100118] p 30 N87-23625

COMPRESSING

The effect of internal stresses on solar cell efficiency p 196 N87-26430

COMPRESSION LOADS

Effect of component compression on the initial performance of an IPV nickel-hydrogen cell [NASA-TM-100102] p 195 N87-24838

COMPRESSION WAVES

Detonation wave compression in gas turbines [NASA-CR-179557] p 25 N87-13443

COMPRESSOR BLADES

Rotor wake characteristics of a transonic axial-flow fan p 2 A87-20886

Comparison of calculated and experimental cascade performance for controlled-diffusion compressor stator blading [ASME PAPER 86-GT-35] p 19 A87-25394

Approximations to eigenvalues of modified general matrices [AIAA PAPER 87-0947] p 177 A87-33756

The measurement of boundary layers on a compressor blade in cascade at high positive incidence angle. 1: Experimental techniques and results [NASA-CR-179491] p 25 N87-13441

The measurement of boundary layers on a compressor blade in cascade at high positive incidence angle. 2: Data report [NASA-CR-179492] p 25 N87-13442

Shot peening for Ti-6Al-4V alloy compressor blades [NASA-TP-2711] p 184 N87-20566

Materials for Advanced Turbine Engines (MATE). Project 4: Erosion resistant compressor airfoil coating [NASA-CR-179622] p 92 N87-27029

Thin film strain gage development program [NASA-CR-174707] p 159 N87-28883

COMPRESSOR EFFICIENCY

Performance studies on an axial flow compressor stage p 138 A87-37208

Calculations of inlet distortion induced compressor flowfield instability p 30 N87-24470

COMPRESSOR ROTORS

The hub wall boundary layer development and losses in an axial flow compressor rotor passage p 139 A87-41665

An experimental study on the effects of tip clearance on flow field and losses in an axial flow compressor rotor p 6 A87-46207

Thermodynamic evaluation of transonic compressor rotors using the finite volume approach [NASA-CR-180587] p 150 N87-23925

COMPRESSORS

Comparison of calculated and experimental cascade performance for controlled-diffusion compressor stator blading [ASME PAPER 86-GT-35] p 19 A87-25394

Aerodynamic instability performance of an advanced high-pressure-ratio compression component [AIAA PAPER 86-1619] p 5 A87-41157

Dynamic data acquisition, reduction, and analysis for the identification of high-speed compressor component post-stability characteristics [AIAA PAPER 87-2089] p 162 A87-45398

Response of a small-turboshaft-engine compression system to inlet temperature distortion [NASA-TM-83765] p 23 N87-10100

Jet engine simulation with water ingestion through compressor [NASA-CR-179549] p 1 N87-15932

Design of 9.271-pressure-ratio 5-stage core compressor and overall performance for first 3 stages [NASA-TP-2597] p 27 N87-17699

The T55-L-712 turbine engine compressor housing refurbishment project [NASA-CR-179624] p 92 N87-23729

COMPUTATION

Comparison of calculated and experimental cascade performance for controlled-diffusion compressor stator blading [ASME PAPER 86-GT-35] p 19 A87-25394

Increasing processor utilization during parallel computation rundown p 202 A87-52541

Sensitivity analysis and approximation methods for general eigenvalue problems [NASA-CR-179538] p 180 N87-12021

Theoretical kinetic computations in complex reacting systems p 219 N87-20277

Computation of full-coverage film-cooled airfoil temperatures by two methods and comparison with high heat flux data [NASA-TM-88931] p 150 N87-23934

A computational procedure for automated flutter analysis [NASA-TM-100171] p 187 N87-28058

COMPUTATIONAL FLUID DYNAMICS

On similarity solutions for turbulent and heated round jets p 130 A87-10922

Finite analytic numerical solution of two-dimensional channel flow over a backward-facing step p 131 A87-13506

Effects of transient propellant dynamics on deployment of large liquid stages in zero-gravity with application to Shuttle/Centaur [IAF PAPER 86-119] p 39 A87-15880

Numerical simulation of excited jet mixing layers [AIAA PAPER 87-0016] p 131 A87-22361

Evaluation of new techniques for the calculation of internal recirculating flows [AIAA PAPER 87-0059] p 131 A87-22387

Navier Stokes solution of the flowfield over ice accretion shapes [AIAA PAPER 87-0099] p 2 A87-22414

Numerical analysis of a NACA0012 airfoil with leading edge ice accretions [AIAA PAPER 87-0101] p 2 A87-22415

Duct flows with swirl [AIAA PAPER 87-0247] p 132 A87-22509

A diagonal implicit multigrid algorithm for the Euler equations [AIAA PAPER 87-0354] p 2 A87-22578

An adaptive finite element strategy for complex flow problems [AIAA PAPER 87-0557] p 133 A87-22706

Turbulence modeling for complex shear flows p 133 A87-23653

An unconditionally-stable central differencing scheme for high Reynolds number flows [AIAA PAPER 87-0060] p 133 A87-24912

Development and evaluation of improved numerical schemes for recirculating flows [AIAA PAPER 87-0061] p 134 A87-24913

Mechanisms by which heat release affects the flow field in a chemically reacting, turbulent mixing layer [AIAA PAPER 87-0131] p 134 A87-24925

CONDIF - A modified central-difference scheme with unconditional stability and very low numerical diffusion p 136 A87-30685

On the spatial instability of piecewise linear free shear layers p 137 A87-31680

A generalized procedure for constructing an upwind-based TVD scheme [AIAA PAPER 87-0355] p 4 A87-32191

Analysis of viscous transonic flow over airfoil sections [AIAA PAPER 87-0420] p 4 A87-34723

An LU-SSOR scheme for the Euler and Navier-Stokes equations [AIAA PAPER 87-0600] p 137 A87-34724

Comparison of three explicit multigrid methods for the Euler and Navier-Stokes equations [AIAA PAPER 87-0602] p 137 A87-34725

Adaptive finite element methods for compressible flow problems p 4 A87-38496

Euler analysis of transonic propeller flows p 4 A87-39813

Turbulent solutions of the Navier-Stokes equations p 139 A87-40932

A model for fluid flow during saturated boiling on a horizontal cylinder p 139 A87-41173

Recent advances in error estimation and adaptive improvement of finite element calculations p 204 A87-41239

The generation of Tollmien-Schlichting waves by long wavelength free stream disturbances p 139 A87-41655

The utilization of parallel processing in solving the inviscid form of the average-passage equation system for multistage turbomachinery [AIAA PAPER 87-1108] p 5 A87-42057

Computation of rotating turbulent flow with an algebraic Reynolds stress model p 140 A87-43384

Numerical prediction of cold turbulent flow in combustor configurations with different centerbody flame holders [ASME PAPER 86-WA/HT-50] p 140 A87-43715

Radiative cooling of a layer with nonuniform velocity - A separable solution p 141 A87-45637

Lower-upper implicit scheme for high-speed inlet analysis p 6 A87-46781

Separation of variables solution for non-linear radiative cooling p 142 A87-48450

Numerical modeling of on-orbit propellant motion resulting from an impulsive acceleration [AIAA PAPER 87-1766] p 40 A87-48573

Euler analysis of the three-dimensional flow field of a high-speed propeller - Boundary condition effects [ASME PAPER 87-GT-253] p 6 A87-48719

A method for assessing effects of circumferential flow distortion on compressor stability p 7 A87-48722

Numerical simulations of unsteady, viscous, transonic flow over isolated and cascaded airfoils using a deforming grid [AIAA PAPER 87-1316] p 7 A87-49649

Some plane curvature approximations p 204 A87-49821

CONDIF - A modified central-difference scheme for convective flows p 205 A87-53675

Generation of Tollmien-Schlichting waves on interactive marginally separated flows p 144 A87-54365

Mass and momentum turbulent transport experiments p 144 N87-11201

Calculation of two- and three-dimensional transonic cascade flow field using the Navier-Stokes equations p 144 N87-11220

Gas flow environmental and heat transfer nonrotating 3D program p 145 N87-11223

Third-moment closure of turbulence for predictions of separating and reattaching shear flows: A study of Reynolds-stress closure model [NASA-CR-177055] p 145 N87-11961

Computation of multi-dimensional viscous supersonic jet flow [NASA-CR-4020] p 8 N87-13405

Computation of multi-dimensional viscous supersonic flow [NASA-CR-4021] p 9 N87-13406

Comparison of three explicit multigrid methods for the Euler and Navier-Stokes equations [NASA-TM-88878] p 1 N87-16784

Euler analysis of the three dimensional flow field of a high-speed propeller: Boundary condition effects [NASA-TM-88955] p 10 N87-16798

A high resolution shock capturing scheme for high Mach number internal flow [NASA-CR-179523] p 10 N87-16804

An LU-SSOR scheme for the Euler and Navier-Stokes equations [NASA-CR-179556] p 11 N87-16806

Analysis of viscous transonic flow over airfoil sections [NASA-TM-88912] p 146 N87-17001

Combined aerodynamic and structural dynamic problem emulating routines (CASPER): Theory and implementation [NASA-TP-2418] p 11 N87-17669

Automating the parallel processing of fluid and structural dynamics calculations [NASA-TM-88837] p 203 N87-19002

Combustion research in the Internal Fluid Mechanics Division p 79 N87-20268

Modeling turbulent, reacting flow p 147 N87-20270

Application of advanced computational codes in the design of an experiment for a supersonic throughflow fan rotor

[NASA-TM-88915] p 13 N87-22630

Numerical modeling of on-orbit propellant motion resulting from an impulsive acceleration

[NASA-TM-89873] p 41 N87-22757

Unsteady stator/rotor interaction p 149 N87-22767

Simulation of multistage turbine flows

p 149 N87-22768

Progress in the prediction of unsteady heat transfer on turbine blades

p 149 N87-22769

A linearized Euler analysis of unsteady flows in turbomachinery

[NASA-CR-180987] p 149 N87-22948

Multispecies CARS measurements in turbulent combustion

p 79 N87-23808

Thermodynamic evaluation of transonic compressor rotors using the finite volume approach

[NASA-CR-180587] p 150 N87-23925

Numerical simulations of unsteady, viscous, transonic flow over isolated and cascaded airfoils using a deforming grid

[NASA-TM-89890] p 13 N87-24435

Viscous analyses for flow through subsonic and supersonic intakes

p 30 N87-24469

Calculations of inlet distortion induced compressor flowfield instability

p 30 N87-24470

Internal computational fluid mechanics on supercomputers for aerospace propulsion systems

p 151 N87-26002

COMPUTATIONAL GRIDS

A diagonal implicit multigrid algorithm for the Euler equations

[AIAA PAPER 87-0354] p 2 A87-22578

An L-U implicit multigrid algorithm for the three-dimensional Euler equations

[AIAA PAPER 87-0453] p 133 A87-22645

An adaptive finite element strategy for complex flow problems

[AIAA PAPER 87-0557] p 133 A87-22706

Multigrid solution of inviscid transonic flow through rotating blade passages

[AIAA PAPER 87-0608] p 3 A87-24992

A two-dimensional numerical study of the flow inside the combustion chamber of a motored rotary engine

[SAE PAPER 860615] p 161 A87-28624

Two- and three-dimensional viscous computations of a hypersonic inlet flow

[AIAA PAPER 87-0283] p 4 A87-31106

Comparison of three explicit multigrid methods for the Euler and Navier-Stokes equations

[AIAA PAPER 87-0602] p 137 A87-34725

Composite grid and finite-volume LU implicit scheme for turbine flow analysis

[AIAA PAPER 87-1129] p 5 A87-42078

Multigrid-sinc methods p 205 A87-52865

Calculation of two- and three-dimensional transonic cascade flow field using the Navier-Stokes equations

p 144 N87-11220

Two- and three-dimensional viscous computations of a hypersonic inlet flow

[NASA-TM-88923] p 146 N87-15441

Comparison of three explicit multigrid methods for the Euler and Navier-Stokes equations

[NASA-TM-88878] p 1 N87-186784

A multigrid LU-SSOR scheme for approximate Newton iteration applied to the Euler equations

[NASA-CR-179524] p 10 N87-16803

Generation of a composite grid for turbine flows and consideration of a numerical scheme

[NASA-TM-88890] p 11 N87-17662

Composite grid and finite-volume LU implicit scheme for turbine flow analysis

[NASA-TM-89828] p 12 N87-20235

Time-partitioning simulation models for calculation on parallel computers

[NASA-TM-89850] p 203 N87-20766

COMPUTER AIDED DESIGN

Towards effective interactive three-dimensional colour postprocessing

p 201 A87-11895

Structural tailoring of advanced turboprops

[AIAA PAPER 87-0753] p 177 A87-33648

A hybrid nonlinear programming method for design optimization

p 201 A87-35718

Supersonic through-flow fan design

[AIAA PAPER 87-1746] p 22 A87-48571

Mathematical model partitioning and packing for parallel computer calculation

p 202 A87-52534

STAEBL: Structural tailoring of engine blades, phase 2

p 24 N87-11731

On optimal design for the blade-root/hub interface in jet engines

p 24 N87-11769

The 60 GHz IMPATT diode development

[NASA-CR-179536] p 218 N87-17515

Color postprocessing for 3-dimensional finite element mesh quality evaluation and evolving graphical workstation

[NASA-CR-180215] p 202 N87-18997

Unification of color postprocessing techniques for 3-dimensional computational mechanics

[NASA-CR-180214] p 202 N87-18998

Interactive color display of 3-D engineering analysis results

[NASA-CR-180589] p 203 N87-22422

Supersonic through-flow fan design

[NASA-TM-88908] p 29 N87-22681

Probabilistic Structural Analysis Methods (PSAM) for select space propulsion system structural components

p 62 N87-22784

The NESSUS finite element code p 184 N87-22785

Probabilistic finite elements p 185 N87-22790

Structural tailoring using the SSME/STAEBL code

p 63 N87-22795

Computer aided design and analysis of gear tooth geometry

[NASA-CR-179611] p 168 N87-23969

COMPUTER GRAPHICS

Towards effective interactive three-dimensional colour postprocessing

p 201 A87-11895

Interactive graphics and analysis accuracy

p 202 A87-45900

On optimal design for the blade-root/hub interface in jet engines

p 24 N87-11769

Color postprocessing for 3-dimensional finite element mesh quality evaluation and evolving graphical workstation

[NASA-CR-180215] p 202 N87-18997

Unification of color postprocessing techniques for 3-dimensional computational mechanics

[NASA-CR-180214] p 202 N87-18998

Interactive color display of 3-D engineering analysis results

[NASA-CR-180589] p 203 N87-22422

COMPUTER PROGRAMMING

A computer controlled signal preprocessor for laser fringe anemometer applications

[NASA-TM-88982] p 157 N87-20516

A satellite system synthesis model for orbital arc allotment optimization

[NASA-CR-181150] p 37 N87-25341

COMPUTER PROGRAMS

Particle trajectory computer program for icing analysis of axisymmetric bodies - A progress report

[AIAA PAPER 87-0027] p 15 A87-22366

Advances in 3-D Inelastic Analysis Methods for hot section components

[AIAA PAPER 87-0719] p 177 A87-33645

Analytical flutter investigation of a composite propfan model

[AIAA PAPER 87-0738] p 178 A87-40497

Comparison of two procedures for predicting rocket engine nozzle performance

[AIAA PAPER 87-2071] p 52 A87-45391

Numerical modeling of on-orbit propellant motion resulting from an impulsive acceleration

[AIAA PAPER 87-1766] p 40 A87-48573

Composite load spectra for select space propulsion structural components

[NASA-CR-179496] p 55 N87-10176

Calculation of water drop trajectories to and about arbitrary three-dimensional lifting and nonlifting bodies in potential airflow

[NASA-CR-3935] p 8 N87-11694

On 3-D inelastic analysis methods for hot section components (base program)

[NASA-CR-175060] p 180 N87-12923

Engineering calculations for communications satellite systems planning

[NASA-CR-180106] p 114 N87-16198

Surface flaw reliability analysis of ceramic components with the SCARE finite element postprocessor program

[NASA-TM-88901] p 181 N87-17087

Analytical flutter investigation of a composite propfan model

[NASA-TM-88944] p 182 N87-18115

Comparison of two procedures for predicting rocket engine nozzle performance

[NASA-TM-89814] p 60 N87-20379

Numerical modeling of on-orbit propellant motion resulting from an impulsive acceleration

[NASA-TM-89873] p 41 N87-22757

On 3-D inelastic analysis methods for hot section components. Volume 1: Special finite element models

[NASA-CR-179494] p 185 N87-22996

Engineering calculations for communications satellite systems planning

[NASA-CR-181112] p 117 N87-24605

Low Reynolds number nozzle flow study

[NASA-TM-100130] p 67 N87-25426

Computer control of a scanning electron microscope for digital image processing of thermal-wave images

[NASA-TM-100157] p 128 N87-26278

COMPUTER SYSTEMS PERFORMANCE

A comparison of five benchmarks

[NASA-TM-88956] p 202 N87-17441

COMPUTER TECHNIQUES

A computerized test system for thermal-mechanical fatigue crack growth

p 153 A87-23899

Automated inspection and precision grinding of spiral bevel gears

[NASA-CR-4083] p 169 N87-25578

COMPUTERIZED SIMULATION

A real-time simulation evaluation of an advanced detection, isolation and accommodation algorithm for sensor failures in turbine engines

p 18 A87-13318

Computer simulation of plasma electron collection by PIX-II — solar array-space plasma interaction

p 45 A87-17837

SCARE - A postprocessor program to MSC/NASTRAN for reliability analysis of structural ceramic components

[ASME PAPER 86-GT-34] p 174 A87-17988

Computational aeroacoustics of propeller noise in the near and far field

[AIAA PAPER 87-0254] p 19 A87-24944

Computer-based phosphoric acid fuel cell analytical tools Descriptions and usages

p 190 A87-33788

A computer model for the recombination zone of a microwave-plasma electrothermal rocket

[AIAA PAPER 87-1014] p 50 A87-38009

On direct numerical simulations of turbulent reacting flows

[AIAA PAPER 87-1324] p 140 A87-44930

Comparison of theoretical and experimental thrust performance of a 1030:1 area ratio rocket nozzle at a chamber pressure of 2413 kN/sq m (350 psia)

[AIAA PAPER 87-2069] p 52 A87-45390

Temperature fields due to jet induced mixing in a typical OTV tank

[AIAA PAPER 87-2017] p 55 A87-52247

Gear mesh compliance modeling

p 164 A87-53422

WEST-3 wind turbine simulator development. Volume 2: Verification

[NASA-CR-174982] p 191 N87-10531

Combined aerodynamic and structural dynamic problem emulating routines (CASPER): Theory and implementation

[NASA-TP-2418] p 11 N87-17669

Gear mesh compliance modeling

[NASA-TM-88843] p 166 N87-18092

Performance and efficiency evaluation and heat release study of an outboard Marine Corporation Rotary Combustion Engine

[NASA-TM-89833] p 28 N87-20282

Time-partitioning simulation models for calculation on parallel computers

[NASA-TM-89850] p 203 N87-20766

Effect of shaft frequency on cavitation in a journal bearing for noncentered circular whirl

[NASA-TM-88925] p 148 N87-22122

Simulation of multistage turbine flows

p 149 N87-22768

Composite load spectra for select space propulsion structural components

p 63 N87-22793

Computer aided design and analysis of gear tooth geometry

[NASA-CR-179611] p 168 N87-23969

A simplified computer solution for the flexibility matrix of contacting teeth for spiral bevel gears

[NASA-CR-179620] p 168 N87-23977

Dynamic delamination buckling in composite laminates under impact loading: Computational simulation

[NASA-TM-100192] p 75 N87-28611

Helical gears with circular arc teeth: Generation, geometry, precision and adjustment to errors, computer aided simulation of conditions of meshing and bearing contact

[NASA-CR-4089] p 170 N87-29846

Computer modelling of aluminum-gallium arsenide/gallium arsenide multilayer photovoltaics

[NASA-CR-181418] p 200 N87-29957

CONCENTRATION (COMPOSITION)

Concentration of carbon dioxide by a high-temperature electrochemical membrane cell

p 77 A87-27400

CONCENTRATORS

High-efficiency GaAs solar concentrator cells for space and terrestrial applications

p 188 A87-18073

Optimization of spherical facets for parabolic solar concentrators

p 213 A87-18173

Performance of GaAs and silicon concentrator cells under 1 MeV electron irradiation

p 189 A87-19871

An optimized top contact design for solar cell concentrators

p 189 A87-19882

Development of an advanced photovoltaic concentrator system for space applications

[NASA-TM-100101] p 66 N87-24531

High-efficiency GaAs concentrator space cells
p 196 N87-26417

Development of a Fresnel lens concentrator for space application
p 196 N87-26427

Performance of AlGaAs, GaAs and InGaAs cells after 1 MeV electron irradiation
p 197 N87-26438

CONDUCTIVE HEAT TRANSFER

Evaluation of Stirling engine appendix gap losses
p 160 A87-18037

Multiply scaled constrained nonlinear equation solvers -- for nonlinear heat conduction problems
p 137 A87-31406

CONDUCTIVITY

Oil film thickness measurement and analysis for an angular contact ball bearing operating in parched elastohydrodynamic lubrication
[NASA-CR-179506] p 70 N87-16879

CONFERENCES

Optical technologies for communication satellite applications; Proceedings of the Meeting, Los Angeles, CA, Jan. 21, 22, 1986
[SPIE-616] p 41 A87-26610

Turbine Engine Hot Section Technology, 1984
[NASA-CP-2339] p 179 N87-11180

The 20th Aerospace Mechanics Symposium
[NASA-CP-2423-REV] p 181 N87-16321

Microgravity Fluid Management Symposium
[NASA-CP-2465] p 108 N87-21141

Structural Integrity and Durability of Reusable Space Propulsion Systems
[NASA-CP-2471] p 62 N87-22766

Space Photovoltaic Research and Technology 1986. High Efficiency, Space Environment, and Array Technology
[NASA-CP-2475] p 196 N87-26413

NASA Lewis Research Center Futuring Workshop
[NASA-CR-179577] p 206 N87-27475

CONICAL NOZZLES

Free-jet investigation of mechanically suppressed, high radius ratio conical plug model nozzles
[NASA-CR-3596] p 212 N87-29315

CONSERVATION LAWS

A generalized procedure for constructing an upwind-based TVD scheme
[AIAA PAPER 87-0355] p 4 A87-32191

A generalized procedure for constructing an upwind based TVD scheme
[NASA-TM-88926] p 205 N87-24132

CONSTITUTIVE EQUATIONS

A viscoplastic constitutive theory for metal matrix composites at high temperature
[NASA-CR-179530] p 180 N87-13790

A constitutive model for the inelastic multiaxial cyclic response of a nickel base superalloy Rene 80
[NASA-CR-3998] p 182 N87-18852

CONSTRUCTION MATERIALS

Ultrasonic NDE of structural ceramics for power and propulsion systems
[NASA-TM-100147] p 173 N87-26362

CONTACT LOADS

Flexibility effects on tooth contact location in spiral bevel gear transmissions
[NASA-CR-4055] p 166 N87-20552

A simplified computer solution for the flexibility matrix of contacting teeth for spiral bevel gears
[NASA-CR-179620] p 168 N87-23977

Analysis of the vibratory excitation arising from spiral bevel gears
[NASA-CR-4081] p 169 N87-25579

CONTACTORS

Plasma contactors for electrodynamic tethers
p 214 A87-31211

Hollow cathode-based plasma contactor experiments for electrodynamic tether
[AIAA PAPER 87-0572] p 214 A87-32192

Theory of plasma contactors for electrodynamic tethered satellite systems
p 122 A87-41609

Theory of plasma contactors used in the ionosphere
p 122 A87-41610

Plasma contactors for electrodynamic tether
[NASA-TM-88850] p 215 N87-18428

CONTAMINATION

Response of a small-turboshaft-engine compression system to inlet temperature distortion
[NASA-TM-83765] p 23 N87-10100

An analytical and experimental investigation of resistojet plumes
[NASA-TM-88852] p 58 N87-14428

Preliminary study of niobium alloy contamination by transport through helium
[NASA-TM-88952] p 90 N87-17884

CONTINGENCY

Contingency power for small turboshaft engines using water injection into turbine cooling air
[AIAA PAPER 87-1906] p 21 A87-45289

Contingency power for small turboshaft engines using water injection into turbine cooling air
[NASA-TM-89817] p 28 N87-20280

CONTINUUM MECHANICS

The mathematical modeling of rapid solidification processing
[NASA-CR-179551] p 88 N87-13514

CONTRACTORS

Ground-based plasma contractor characterization
[NASA-TM-100194] p 215 N87-28423

CONTRAROTATING PROPELLERS

A panel method for counter rotating propfans
[AIAA PAPER 87-1890] p 21 A87-45279

The acoustic experimental investigation of counterrotating propeller configurations
[SAE PAPER 871031] p 210 A87-48760

Cruise noise of counterrotation propeller at angle of attack in wind tunnel
[NASA-TM-88869] p 210 N87-13252

CONTROL

A computer controlled signal preprocessor for laser fringe anemometer applications
[NASA-TM-88982] p 157 N87-20516

Computer control of a scanning electron microscope for digital image processing of thermal-wave images
[NASA-TM-100157] p 128 N87-26278

CONTROL EQUIPMENT

Full-scale engine demonstration of an advanced sensor failure detection isolation, and accommodation algorithm - Preliminary results
[AIAA PAPER 87-2259] p 22 A87-50422

Microwave performance of an optically controlled AlGaAs/GaAs high electron mobility transistor and GaAs MESFET
[NASA-TM-88980] p 125 N87-17993

Full-scale engine demonstration of an advanced sensor failure detection, isolation and accommodation algorithm: Preliminary results
[NASA-TM-89880] p 127 N87-22097

Optically controlled microwave devices and circuits: Emerging applications in space communications systems
[NASA-TM-89869] p 127 N87-23900

CONTROL STABILITY

Effect of gimbal friction modelling technique on control stability and performance for Centaur upper stage
[AIAA PAPER 87-2455] p 38 A87-50501

Flight test report of the NASA icing research airplane: Performance, stability, and control after flight through natural icing conditions
[NASA-CR-179515] p 34 N87-11797

Effect of Gimbal friction modeling technique on control stability and performance for Centaur upper-stage
[NASA-TM-89894] p 39 N87-22755

CONTROL SURFACES

Performance and power regulation characteristics of two aileron-controlled rotors and a pitchable tip-controlled rotor on the Mod-O turbine
[NASA-TM-100136] p 200 N87-29956

CONTROL SYSTEMS DESIGN

Component testing of a ground based gas turbine steam cooled rich-burn primary zone combustor for emissions control of nitrogenous fuels
[NASA-TM-88873] p 191 N87-11345

Synchronization trigger control system for flow visualization
[NASA-TM-89902] p 128 N87-23902

Control of shear flows by artificial excitation
[NASA-TM-100201] p 15 N87-29420

CONTROLLERS

Electrodynamic tether
p 44 N87-26449

CONVECTIVE FLOW

Development and evaluation of improved numerical schemes for recirculating flows
[AIAA PAPER 87-0061] p 134 A87-24913

Diffusion flame extinction in slow convection flow under microgravity environment
p 77 A87-38787

CONDIF - A modified central-difference scheme for convective flows
p 205 A87-53675

CONVECTIVE HEAT TRANSFER

Influence of oscillation-induced diffusion on heat transfer in a uniformly heated channel
p 135 A87-27716

Experiments on thermoacoustic convection heat transfer in gravity and zero-gravity environments
[AIAA PAPER 87-1651] p 107 A87-43141

CONVERGENCE

Extrapolation methods for vector sequences
p 203 A87-53631

CONVERGENT-DIVERGENT NOZZLES

On broadband shock associated noise of supersonic jets
p 208 A87-11768

Vacuum chamber pressure effects on thrust measurements of low Reynolds number nozzles
p 45 A87-14976

CONVERTERS

A study of Schwarz converters for nuclear powered spacecraft
[NASA-TM-89911] p 128 N87-23903

Resonant AC power system proof-of-concept test program
[NASA-CR-175069-VOL-1] p 129 N87-29738

COOLANTS

Effect of an oxygen plasma on the physical and chemical properties of several fluids for the Liquid Droplet Radiator
[AIAA PAPER 87-0080] p 42 A87-22401

COOLING

Undercooling and crystallization behaviour of antimony droplets
p 83 A87-28732

Local heat transfer augmentation in channels with two opposite ribbed surfaces
p 136 A87-30732

Rotational effects on impingement cooling
p 141 A87-45838

Liner cooling research at NASA Lewis Research Center --- for gas turbine combustion chambers
[AIAA PAPER 87-1828] p 22 A87-50189

Component testing of a ground based gas turbine steam cooled rich-burn primary zone combustor for emissions control of nitrogenous fuels
[NASA-TM-88873] p 191 N87-11345

The mathematical modeling of rapid solidification processing
[NASA-CR-179551] p 88 N87-13514

Liquid oxygen cooling of high pressure LOX/hydrocarbon rocket thrust chambers
[NASA-TM-88805] p 57 N87-14426

Liner cooling research at NASA Lewis Research Center
[NASA-TM-100107] p 29 N87-23624

COOLING FINNS

Enhanced heat transfer combustor technology, subtasks 1 and 2, task C.1
[NASA-CR-179541] p 56 N87-13486

COOLING SYSTEMS

Heat pipe cooled rocket engines
[AIAA PAPER 86-1567] p 48 A87-21516

Advanced liquid-cooled, turbocharged and intercooled stratified charge rotary engines for aircraft
[SAE PAPER 871039] p 22 A87-48766

COPLANARITY

Spatially growing disturbances in a high velocity ratio two-stream, coplanar jet
[AIAA PAPER 87-0056] p 3 A87-24996

Spatially growing disturbances in a high velocity ratio two-stream, coplanar jet
[NASA-TM-88922] p 9 N87-14283

Propagation characteristics of some novel coplanar waveguide transmission lines on GaAs at MM-wave frequencies
[NASA-TM-89839] p 126 N87-20469

COPPER

Ultrasonic verification of microstructural changes due to heat treatment
p 208 A87-10772

Traveling-wave-tube efficiency improvement by a low-cost technique for deposition of carbon on multistage depressed collector
[NASA-TP-2719] p 126 N87-21239

Stability of bromine, iodine monochloride, copper (II) chloride, and nickel (II) chloride intercalated pitch-based graphite fibers
[NASA-TM-89904] p 103 N87-24563

COPPER ALLOYS

Conventionally cast and forged copper alloy for high-heat-flux thrust chambers
[NASA-TP-2694] p 90 N87-16902

CORIOLIS EFFECT

Nonlinear vibration and stability of rotating, pretwisted, precone blades including Coriolis effects
p 178 A87-39896

CORNER FLOW

Turbulent heat transfer in corrugated-wall channels with and without fins
p 134 A87-27709

Experimental evaluation of two turning vane designs for fan drive corner of 0.1-scale model of NASA Lewis Research Center's proposed altitude wind tunnel
[NASA-TP-2646] p 35 N87-18576

Experimental evaluation of corner turning vanes
[NASA-TM-100143] p 37 N87-28571

CORONAS

An anemometer for highly turbulent or recirculating flows
p 154 A87-37698

CORRELATION

Volume-energy parameters for heat transfer to supercritical fluids
p 137 A87-32326

CORRELATION COEFFICIENTS

Evaluation of icing drag coefficient correlations applied to iced propeller performance prediction
[SAE PAPER 871033] p 16 A87-48761

CORROSION PREVENTION

Protection of solar array blankets from attack by low earth orbital atomic oxygen p 47 A87-19874
 Oxidation protection coatings for polymers [NASA-CASE-LEW-14072-3] p 103 N87-23736

CORROSION RESISTANCE

Mechanism of strength degradation for hot corrosion of alpha-SiC p 95 A87-21470
 Corrosion pitting of SiC by molten salts p 76 A87-27165
 Reaction of iron with hydrogen chloride-oxygen mixtures at 550 C p 83 A87-32001
 High temperature static strain gage development contract, tasks 1 and 2 [NASA-CR-180811] p 159 N87-28869

CORROSION TESTS

The formation of volatile corrosion products during the mixed oxidation-chlorination of cobalt at 650 C p 82 A87-23848

CORRUGATING

Use of a corrugated surface to enhance radiation tolerance in a GaAs solar cell p 189 A87-19842

COSMOLOGY

The large-scale peculiar velocity field in flat models of the universe p 223 A87-40651

COST EFFECTIVENESS

20 kHz Space Station power system p 51 A87-40378

Advanced Stirling conversion systems for terrestrial applications [NASA-TM-88897] p 220 N87-15031

Intersatellite Link (ISL) application to commercial communications satellites. Volume 1: Executive summary [NASA-CR-179598-VOL-1] p 116 N87-19552

COST ESTIMATES

Space station experiment definition: Advanced power system test bed [NASA-CR-179502] p 58 N87-15270

COST REDUCTION

An overview of the small engine component technology (SECT) studies — commutator, rotorcraft, cruise missile and auxiliary power applications in year 2000 [AIAA PAPER 86-1542] p 19 A87-17993

COSTS

High power/large area PV systems p 198 N87-26452

COUNTER ROTATION

Measurement of a counter rotation propeller flowfield using a Laser Doppler Velocimeter [AIAA PAPER 87-0008] p 3 A87-24901

Off-design analysis of counter-rotating propeller configurations p 20 A87-27989

A model propulsion simulator for evaluating counter rotating blade characteristics [SAE PAPER 861715] p 20 A87-32607

A panel method for counter rotating propellers [AIAA PAPER 87-1890] p 21 A87-45279

Effect of angular inflow on the vibratory response of a counter-rotating propeller [NASA-CR-174819] p 8 N87-10840

Noise reduction for model counterrotation propeller at cruise by reducing aft-propeller diameter [NASA-TM-88936] p 211 N87-19057

The effect of front-to-rear propeller spacing on the interaction noise of a model counterrotation propeller at cruise conditions [NASA-TM-100121] p 212 N87-28396

COUNTER-ROTATING WHEELS

Advanced Propfan Engine Technology (APET) definition study, single and counter-rotation gearbox/pitch change mechanism design [NASA-CR-168115] p 32 N87-28554

COUPLED MODES

The effect of circumferential aerodynamic detuning on coupled bending-torsion unstalled supersonic flutter [ASME PAPER 86-GT-100] p 20 A87-25396

An analysis of electromagnetic coupling and eigenfrequencies for microwave electrothermal thruster discharges [AIAA PAPER 87-1012] p 51 A87-41111

Revised NASA axially symmetric ring model for coupled-cavity traveling-wave tubes [NASA-TP-2675] p 127 N87-22923

COUPLING CIRCUITS

Environmentally-induced discharge transient coupling to spacecraft [NASA-CR-174922] p 43 N87-10946

CRACK ARREST

Further observations of SCC in alpha-beta brass. Considerations regarding the appearance of crack arrest markings during SCC p 82 A87-23843

An analysis for crack layer stability p 176 A87-28982

CRACK CLOSURE

Opening and closing of cracks at high cyclic strains p 84 A87-34661

CRACK GEOMETRY

An analysis for crack layer stability p 176 A87-28982

Opening and closing of cracks at high cyclic strains p 84 A87-34661

Crack layer theory p 178 A87-40056

CRACK INITIATION

Crack layer theory p 178 A87-40056

Creep fatigue life prediction for engine hot section materials (ISOTROPIC) [NASA-CR-179550] p 181 N87-15491

Test program to provide confidence in liquid oxygen cooling of hydrocarbon fueled rocket thrust chambers p 67 N87-26114

CRACK PROPAGATION

KI-solutions for single edge notch specimens under fixed end displacements p 174 A87-15798

Elastic analysis of a mode II fatigue crack test specimen p 174 A87-17799

Grain boundary oxidation and fatigue crack growth at elevated temperatures p 81 A87-19368

Simplified composite micromechanics for predicting microstresses p 72 A87-20090

A computerized test system for thermal-mechanical fatigue crack growth p 153 A87-23899

An analysis for crack layer stability p 176 A87-28982

Fracture toughness of Si3N4 measured with short bar chevron-notched specimens p 96 A87-30621

Opening and closing of cracks at high cyclic strains p 84 A87-34661

Crack layer theory p 178 A87-40056

Corrosion of graphite composites in phosphoric acid fuel cells p 72 A87-42684

Effect of heat treatment on the fracture behaviour of directionally solidified (gamma/gamma-prime)-alpha alloy p 86 A87-47932

Slow crack growth in sintered silicon nitride p 98 A87-48989

Thermal-mechanical fatigue crack growth in B-1900 + Hf p 86 A87-49570

Stochastic and fractal analysis of fracture trajectories p 179 A87-51167

Grain boundary oxidation and fatigue crack growth at elevated temperatures [NASA-CR-179529] p 88 N87-11873

Analysis of mixed-mode crack propagation using the boundary integral method [NASA-CR-179518] p 180 N87-12915

High temperature monotonic and cyclic deformation in a directionally solidified nickel-base superalloy [NASA-CR-175101] p 90 N87-15303

Elevated temperature crack growth [NASA-CR-179601] p 184 N87-22267

Macrocrack interaction with transverse array of microcracks [NASA-CR-180806] p 186 N87-25607

CRACK TIPS

Re-examination of cumulative fatigue damage analysis - An engineering perspective p 174 A87-22128

Compliance matrices for cracked bodies p 175 A87-25775

Elastic interaction of a crack with a microcrack array. I - Formulation of the problem and general form of the solution. II - Elastic solution for two crack configurations (piecewise constant and linear approximations) p 178 A87-36926

The effects of crack surface friction and roughness on crack tip stress fields [NASA-TM-88976] p 183 N87-18881

CRACKING (FRACTURING)

SCARE - A postprocessor program to MSC/NASTRAN for reliability analysis of structural ceramic components [ASME PAPER 86-GT-34] p 174 A87-17988

Crack layer theory p 178 A87-40056

Fracture of flash oxidized, yttria-doped sintered reaction-bonded silicon nitride p 97 A87-47923

CRACKS

J-integral estimates for cracks in infinite bodies p 177 A87-35334

Surface flaw reliability analysis of ceramic components with the SCARE finite element postprocessor program [NASA-TM-88901] p 181 N87-17087

Test program to provide confidence in liquid oxygen cooling of hydrocarbon fueled rocket thrust chambers p 67 N87-26114

CRAY COMPUTERS

Internal computational fluid mechanics on supercomputers for aerospace propulsion systems p 151 N87-26002

CREEP ANALYSIS

Thermodynamically consistent constitutive equations for nonisothermal large-strain, elastoplastic, creep behavior p 175 A87-27945

CREEP PROPERTIES

High temperature tensile and creep behaviour of low pressure plasma-sprayed Ni-Co-Cr-Al-Y coating alloy p 82 A87-23429

Effects of temperature and hold times on low cycle fatigue of Astroloy p 85 A87-38541

Thermomechanical behavior of plasma-sprayed ZrO2-Y2O3 coatings influenced by plasticity, creep and oxidation [NASA-TM-88940] p 147 N87-18784

Analysis of shell-type structures subjected to time-dependent mechanical and thermal loading [NASA-CR-180349] p 183 N87-19756

Creep behavior of niobium alloy PWC-11 [NASA-TM-89834] p 91 N87-20405

Finite element implementation of Robinson's unified viscoplastic model and its application to some uniaxial and multiaxial problems [NASA-TM-89891] p 185 N87-23010

The dynamic aspects of thermo-elasto-viscoplastic snap-through and creep buckling phenomena [NASA-CR-181411] p 187 N87-29897

CREEP RUPTURE STRENGTH

Stress rupture and creep behavior of a low pressure plasma-sprayed NiCoCrAlY coating alloy in air and vacuum p 85 A87-43396

Effect of 15 MPa hydrogen on creep-rupture properties of iron-base superalloys p 86 A87-49558

The effect of electron beam welding on the creep rupture properties of a Nb-Zr-C alloy [NASA-TM-88892] p 88 N87-13513

Elevated temperature tension, compression and creep-rupture behavior of (001)-oriented single crystal superalloy PWA 1480 [NASA-TM-88950] p 90 N87-17882

Creep behavior of niobium alloy PWC-11 [NASA-TM-89834] p 91 N87-20405

Observations of directional gamma prime coarsening during engine operation [NASA-TM-100105] p 92 N87-25459

Creep-rupture behavior of a developmental cast-iron-base alloy for use up to 800 deg C [NASA-TM-100167] p 93 N87-28641

Heat treatment for superalloy [NASA-CASE-LEW-14262-1] p 93 N87-28647

CREEP STRENGTH

Creep fatigue life prediction for engine hot section materials (isotropic) [NASA-CR-174844] p 182 N87-18117

Exposure time considerations in high temperature low cycle fatigue [NASA-TM-88934] p 187 N87-28944

CREEP TESTS

Long-time creep behavior of Nb-1Zr alloy containing carbon [NASA-TM-100142] p 92 N87-26217

CRITICAL POINT

Low-gravity experiments in critical phenomena p 107 A87-23159

CRITICAL VELOCITY

Optimal placement of critical speeds in rotor-bearing systems p 162 A87-38464

CROSS FLOW

The flame structure and vorticity generated by a chemically reacting transverse jet p 76 A87-14116

Two opposed lateral jets injected into swirling crossflow [AIAA PAPER 87-0307] p 132 A87-22549

A model for fluid flow during saturated boiling on a horizontal cylinder p 139 A87-41173

Flow visualization study of the effect of injection hole geometry on an inclined jet in crossflow p 155 A87-45842

Experiments and modeling of dilution jet flow fields p 148 N87-20276

CRUISE MISSILES

Engine studies for future subsonic cruise missiles [AIAA PAPER 86-1547] p 19 A87-21513

Advanced technology payoffs for future small propulsion systems p 21 A87-47081

CRUISING FLIGHT

Cruise noise of counterrotation propeller at angle of attack in wind tunnel [NASA-TM-88869] p 210 N87-13252

Noise reduction for model counterrotation propeller at cruise by reducing aft-propeller diameter [NASA-TM-88936] p 211 N87-19057

The effect of front-to-rear propeller spacing on the interaction noise of a model counterrotation propeller at cruise conditions [NASA-TM-100121] p 212 N87-28396

CRYOGENIC EQUIPMENT

The noncavitating performance and life of a small vane-type positive displacement pump in liquid hydrogen [AIAA PAPER 86-1438] p 46 A87-17994

Thermal shaft effects on load-carrying capacity of a fully coupled, variable-properties cryogenic journal bearing [ASLE PREPRINT 86-TC-6B-1] p 160 A87-19502

A fully coupled variable properties thermohydraulic model for a cryogenic hydrostatic journal bearing [ASME PAPER 86-TRIB-55] p 161 A87-19536

Development and test of the Shuttle/Centaur cryogenic tankage thermal protection system [AIAA PAPER 87-1557] p 43 A87-43073

Evaluation of seals for high-performance cryogenic turbomachines [NASA-TM-88919] p 146 A87-15442

CRYOGENIC FLUID STORAGE

On-orbit cryogenic storage and resupply p 41 A87-18344

Thermodynamic analysis and subscale modeling of space-based orbit transfer vehicle cryogenic propellant resupply [AIAA PAPER 87-1764] p 142 A87-48572

Cryogenic Fluid Management Flight Experiment (CFMFE) p 109 A87-21150

Thermodynamic analysis and subscale modeling of space-based orbit transfer vehicle cryogenic propellant resupply [NASA-TM-89921] p 150 A87-22949

Space station experiment definition: Long-term cryogenic fluid storage [NASA-CR-4072] p 151 A87-24641

CRYOGENIC ROCKET PROPELLANTS

On-orbit cryogenic storage and resupply p 41 A87-18344

Thermodynamic analysis and subscale modeling of space-based orbit transfer vehicle cryogenic propellant resupply [AIAA PAPER 87-1764] p 142 A87-48572

Breadboard RL10-11B low thrust operating mode [NASA-CR-174914] p 58 A87-15269

Thermodynamic analysis and subscale modeling of space-based orbit transfer vehicle cryogenic propellant resupply [NASA-TM-89921] p 150 A87-22949

Design, development and test of shuttle/Centaur G-prime cryogenic tankage thermal protection systems [NASA-TM-89825] p 43 A87-23685

CRYOGENIC STORAGE

Design, development and test of shuttle/Centaur G-prime cryogenic tankage thermal protection systems [NASA-TM-89825] p 43 A87-23685

CRYSTAL DEFECTS

Cell performance and defect behavior in proton-irradiated lithium-counterdoped n^+p silicon solar cells p 216 A87-14222

Fault structures in rapidly quenched Ni-Mo binary alloys p 83 A87-32035

Defects in nickel-base superalloys p 86 A87-49790

Gravitational macrosegregation in binary Pb-Sn alloy ingots [NASA-TM-89885] p 109 A87-24579

CRYSTAL DISLOCATIONS

The characteristics of gamma-prime dislocation pairs in a nickel-base superalloy p 85 A87-46932

Ductility and fracture in B2 FeAl alloys [NASA-CR-180810] p 93 A87-27771

CRYSTAL GROWTH

A critical examination of the dendrite growth models Comparison of theory with experimental data p 83 A87-25048

Dendritic growth of undercooled nickel-tin. I, II p 85 A87-41012

Growth and characterization of cubic SiC single-crystal films on Si p 217 A87-44875

Dendritic solidification in a binary alloy melt - Comparison of theory and experiment p 217 A87-48733

Simulation of fluid flows during growth of organic crystals in microgravity [NASA-TM-88921] p 108 A87-16167

High-efficiency GaAs concentrator space cells p 196 A87-26417

A comparative study of the influence of buoyancy driven fluid flow on GaAs crystal growth p 219 A87-28741

CRYSTAL LATTICES

Transition from a planar interface to cellular and dendritic structures during rapid solidification processing p 81 A87-12029

CRYSTAL OPTICS

Large aperture interferometer with phase-conjugate self-reference beam p 153 A87-17320

CRYSTAL STRUCTURE

Growth and characterization of cubic SiC single-crystal films on Si p 217 A87-44875

A point defect model for nickel electrode structures p 87 A87-52282

CRYSTALLIZATION

Thermal and structural stability of cosputtered amorphous Ta(x)Cu(1-x) alloy thin films on GaAs p 216 A87-27198

Undercooling and crystallization behaviour of antimony droplets p 83 A87-28732

CUBIC LATTICES

Compensation in epitaxial cubic SiC films p 216 A87-15071

Growth and characterization of cubic SiC single-crystal films on Si p 217 A87-44875

CURRENT AMPLIFIERS

Theory of plasma contactors used in the ionosphere p 122 A87-41610

CURRENT CONVERTERS (AC TO DC)

Description of a 20 kilohertz power distribution system p 120 A87-18115

CURRENT DENSITY

Modeling for CO poisoning of a fuel cell anode p 191 A87-52288

Performance of textured carbon on copper electrode multistage depressed collectors with medium-power traveling wave tubes [NASA-TP-2665] p 125 A87-17990

CURRENT DISTRIBUTION

Description of a 20 kilohertz power distribution system p 120 A87-18115

CURVATURE

Heat transfer and fluid mechanics measurements in transitional boundary layers on convex-curved surfaces [ASME PAPER 85-MT-60] p 143 A87-48726

Some plane curvature approximations p 204 A87-49821

A note on the generation of Tollmien-Schlichting waves by sudden surface-curvature change p 144 A87-54366

CURVES (GEOMETRY)

Computer aided design and analysis of gear tooth geometry [NASA-CR-179611] p 168 A87-23969

A satellite system synthesis model for orbital arc allotment optimization [NASA-CR-181150] p 37 A87-25341

CV-990 AIRCRAFT

Aircraft accident report: NASA 712, Convair 990, N712NA, March Air Force Base, California, July 17, 1985, facts and analysis [NASA-TM-87356-VOL-2] p 16 A87-21879

CYCLES

The effect of laser glazing on life of ZrO₂ TBCs in cyclic burner rig tests [NASA-TM-88821] p 89 A87-14487

CYCLIC LOADS

An analysis for crack layer stability p 176 A87-28982

Opening and closing of cracks at high cyclic strains p 84 A87-34661

Results of an interlaboratory fatigue test program conducted on alloy 800H at room and elevated temperatures p 87 A87-54370

Estimation of high temperature low cycle fatigue on the basis of inelastic strain and strainrate [NASA-TM-88841] p 89 A87-14489

Biternal low-cycle fatigue behavior of a NiCoCrAlY-coated single crystal superalloy [NASA-TM-89831] p 91 A87-20408

Environmental degradation of 316 stainless steel in high temperature low cycle fatigue [NASA-TM-89931] p 185 A87-24007

Exposure time considerations in high temperature low cycle fatigue [NASA-TM-88934] p 187 A87-28944

CYCLOHEXANE

Velocity profiles in laminar diffusion flames [NASA-TP-2596] p 147 A87-18035

CYLINDRICAL BODIES

A new formulation of electromagnetic wave scattering using an on-surface radiation boundary condition approach p 112 A87-32829

A model for fluid flow during saturated boiling on a horizontal cylinder p 139 A87-41173

Straight cylindrical seal for high-performance turbomachines [NASA-TP-1850] p 150 A87-23936

CYLINDRICAL SHELLS

A higher order theory of laminated composite cylindrical shells p 177 A87-35656

DAMAGE

Shuttle/Centaur G-prime composite adapters damage tolerance/repair test program [AIAA PAPER 87-0792] p 38 A87-33592

DAMAGE ASSESSMENT

Re-examination of cumulative fatigue damage analysis - An engineering perspective p 174 A87-22128

Crack layer theory p 178 A87-40056

Expansion of epicyclic gear dynamic analysis program [NASA-CR-179563] p 166 A87-19723

DAMPING

The impact damped harmonic oscillator in free decay [NASA-TM-89897] p 168 A87-23978

DATA ACQUISITION

Dynamic data acquisition, reduction, and analysis for the identification of high-speed compressor component post-stability characteristics [AIAA PAPER 87-2089] p 162 A87-45398

A low-cost optical data acquisition system for vibration measurement [NASA-TM-88907] p 181 A87-14730

A distributed data acquisition system for aeronautics test facilities [NASA-TM-88961] p 35 A87-16851

DATA COMPRESSION

Image data compression with vector quantization in the transform domain p 111 A87-30775

A high quality image compression scheme for real-time applications p 111 A87-30801

DATA FLOW ANALYSIS

Sound radiation from single and annular stream nozzles, with modal decomposition of in-duct acoustic power p 209 A87-37629

DATA PROCESSING

Dynamic data acquisition, reduction, and analysis for the identification of high-speed compressor component post-stability characteristics [AIAA PAPER 87-2089] p 162 A87-45398

Amplitude spectrum modulation technique for analog data processing in fiber optic sensing system with temporal separation of channels [NASA-TM-100152] p 159 A87-25562

DATA REDUCTION

An adaptive algorithm for motion compensated color image coding p 113 A87-45466

DECAY RATES

The impact damped harmonic oscillator in free decay [NASA-TM-89897] p 168 A87-23978

DECISION MAKING

NASA Lewis Research Center Futuring Workshop [NASA-CR-179577] p 206 A87-27475

DECOMPOSITION

In-situ analysis of hydrazine decomposition products [AIAA PAPER 87-2122] p 54 A87-50198

In-situ analysis of hydrazine decomposition products [NASA-TM-89916] p 65 A87-23693

DECOUPLING

Decoupled direct method for sensitivity analysis in combustion kinetics [NASA-CR-179636] p 79 A87-24549

DEFLECTION

Flexibility effects on tooth contact location in spiral bevel gear transmissions [NASA-CR-40055] p 166 A87-20552

A simplified computer solution for the flexibility matrix of contacting teeth for spiral bevel gears [NASA-CR-179620] p 168 A87-23977

An investigation of the dynamic response of spur gear teeth with moving loads [NASA-CR-179643] p 170 A87-29840

DEFORMATION

Bounding solutions of geometrically nonlinear viscoelastic problems p 174 A87-20892

Re-examination of cumulative fatigue damage analysis - An engineering perspective p 174 A87-22128

Yielding and deformation behavior of the single crystal superalloy PWA 1480 p 84 A87-32040

Adhesion, friction and deformation of ion-beam-deposited boron nitride films p 98 A87-49325

High temperature monotonic and cyclic deformation in a directionally solidified nickel-base superalloy [NASA-CR-175101] p 90 A87-15303

Adhesion, friction, and deformation of ion-beam-deposited boron nitride films [NASA-TM-88902] p 100 A87-15305

Deformation and fracture of single-crystal and sintered polycrystalline silicon carbide produced by cavitation [NASA-TM-88981] p 102 A87-20422

DEGRADATION

Degradation mechanisms in thermal barrier coatings [NASA-TM-89309] p 101 A87-17926

Effect of storage and LEO cycling on manufacturing technology IPV nickel-hydrogen cells [NASA-TM-89883] p 194 A87-22308

Environmental degradation of 316 stainless steel in high temperature low cycle fatigue [NASA-TM-89931] p 185 A87-24007

The effect of internal stresses on solar cell efficiency p 196 A87-26430

- Results of 1 MeV proton irradiation of front and back surfaces of silicon solar cells p 197 N87-26435
- Oxygen interaction with space-power materials [NASA-CR-181396] p 80 N87-29633
- Thermal stability of distillate hydrocarbon fuels [NASA-CR-181412] p 107 N87-29706
- DEICERS**
- Efficient numerical simulation of an electrothermal de-icer pad [AIAA PAPER 87-0024] p 137 A87-32190
- DEICING**
- A heater made from graphite composite material for potential deicing application [AIAA PAPER 87-0025] p 17 A87-24905
- A heater made from graphite composite material for potential deicing application [NASA-TM-88888] p 17 N87-12559
- Structural properties of impact ices accreted on aircraft structures [NASA-CR-179580] p 182 N87-18121
- DELAMINATING**
- Dynamic delamination buckling in composite laminates under impact loading: Computational simulation [NASA-TM-100192] p 75 N87-28611
- DELPHI METHOD (FORECASTING)**
- NASA Lewis Research Center Futuring Workshop [NASA-CR-179577] p 206 N87-27475
- DEMULATION**
- Onboard multichannel demultiplexer/demodulator [NASA-CR-180821] p 119 N87-28819
- DEMULPLEXING**
- Onboard multichannel demultiplexer/demodulator [NASA-CR-180821] p 119 N87-28819
- DENDRITIC CRYSTALS**
- Cellular and dendritic growth in a binary melt - A marginal stability approach p 107 A87-10871
- Dendritic microstructure in argon atomized superalloy powders p 83 A87-24119
- A critical examination of the dendrite growth models Comparison of theory with experimental data p 83 A87-25048
- Cellular-dendritic transition in directionally solidified binary alloys p 84 A87-32046
- Dendritic growth of undercooled nickel-tin. I, II p 85 A87-41012
- Dendritic solidification in a binary alloy melt - Comparison of theory and experiment p 217 A87-48733
- DENSITY (NUMBER/VOLUME)**
- Multiplicity CARS measurements in turbulent combustion p 79 N87-23808
- DENSITY MEASUREMENT**
- Improved consolidation of silicon carbide p 94 A87-12940
- DEPOLYMERIZATION**
- Effect of an oxygen plasma on the physical and chemical properties of several fluids for the Liquid Droplet Radiator [AIAA PAPER 87-0080] p 42 A87-22401
- DEPOSITION**
- Adhesion, friction and deformation of ion-beam-deposited boron nitride films p 98 A87-49325
- Adhesion, friction, and deformation of ion-beam-deposited boron nitride films [NASA-TM-88902] p 100 N87-15305
- Mechanical strength and tribological behavior of ion-beam deposited boron nitride films on non-metallic substrates [NASA-TM-89818] p 101 N87-18668
- Traveling-wave-tube efficiency improvement by a low-cost technique for deposition of carbon on multistage depressed collector [NASA-TP-2719] p 126 N87-21239
- DEPOSITS**
- Long-term deposit formation in aviation turbine fuel at elevated temperature p 106 A87-14986
- Turbine airfoil deposition models p 24 N87-11191
- Experimental verification of vapor deposition model in Mach 0.3 burner rigs p 88 N87-11192
- DESCENT TRAJECTORIES**
- Calculation of water drop trajectories to and about arbitrary three-dimensional lifting and nonlifting bodies in potential airflow [NASA-CR-3935] p 8 N87-11694
- DESIGN ANALYSIS**
- Propeller design by optimization p 18 A87-14123
- Factors that affect the fatigue strength of power transmission shafting and their impact on design p 160 A87-14656
- An optimized top contact design for solar cell concentrators p 189 A87-19882
- Optimization and analysis of gas turbine engine blades [AIAA PAPER 87-0827] p 201 A87-33614
- Approximations to eigenvalues of modified general matrices [AIAA PAPER 87-0947] p 177 A87-33756

- The design and performance of a multi-stream droplet generator for the liquid droplet radiator [AIAA PAPER 87-1538] p 140 A87-44842
- Development of a turbomachinery design optimization procedure using a multiple-parameter nonlinear perturbation method [NASA-CR-3831] p 1 N87-10003
- High temperature stress-strain analysis p 179 N87-11209
- Effect of design variables, temperature gradients and speed of life and reliability of a rotating disk [NASA-TM-88883] p 165 N87-13755
- A design study of hydrazine and biowaste resistojets [NASA-CR-179510] p 57 N87-14425
- A design concept for an MMIC microstrip phased array [NASA-TM-88834] p 114 N87-14569
- Brayton cycle solarized advanced gas turbine [NASA-CR-179559] p 220 N87-15030
- Low heat transfer oxidizer heat exchanger design and analysis [NASA-CR-179488] p 58 N87-15272
- Common problems and pitfalls in gear design [NASA-TM-88858] p 165 N87-17033
- Design and dynamic simulation of a fixed pitch 56 kW wind turbine drive train with a continuously variable transmission [NASA-CR-179543] p 193 N87-17401
- Design of 9.271-pressure-ratio 5-stage core compressor and overall performance for first 3 stages [AIAA-TP-2597] p 27 N87-17699
- Lewis inverse design code (LINDES): Users manual [NASA-TP-2676] p 12 N87-20238
- Design, fabrication and performance of small, graphite electrode, multistage depressed collectors with 200-W, CW, 8- to 18-GHz traveling-wave tubes [NASA-TP-2693] p 126 N87-20474
- EHD analysis of and experiments on pumping Leningrad seals [NASA-CR-179570] p 168 N87-22246
- Application of advanced computational codes in the design of an experiment for a supersonic throughflow fan rotor [NASA-TM-88915] p 13 N87-22630
- Design, development and test of shuttle/Centaur G-prime cryogenic tankage thermal protection systems [NASA-TM-89825] p 43 N87-23685
- Space station WP-04 power system. Volume 1: Executive summary [NASA-CR-179587-VOL-1] p 65 N87-23695
- Space station WP-04 power system. Volume 2: Study results [NASA-CR-179587-VOL-2] p 65 N87-23696
- A computer solution for the dynamic load, lubricant film thickness and surface temperatures in spiral bevel gears [NASA-CR-4077] p 169 N87-26358
- Design and performance of controlled-diffusion stator compared with original double-circular-arc stator [NASA-TM-100141] p 31 N87-26910
- The design and analysis of single flank transmission error tester for loaded gears [NASA-CR-179621] p 169 N87-27197
- Comparison of Stirling engines for use with a 25-kW disk-electric conversion system [NASA-TM-100111] p 222 N87-27564
- Helical gears with circular arc teeth: Generation, geometry, precision and adjustment to errors, computer aided simulation of conditions of meshing and bearing contact [NASA-CR-4089] p 170 N87-29846
- DETECTION**
- A real-time simulation evaluation of an advanced detection, isolation and accommodation algorithm for sensor failures in turbine engines p 18 A87-13318
- Detection of radio-frequency modulated optical signals by two and three terminal microwave devices [NASA-TM-100196] p 130 N87-29750
- DETONATION WAVES**
- Detonation wave compression in gas turbines [NASA-CR-179557] p 25 N87-13443
- DIELECTRICS**
- RCS of a coated circular waveguide terminated by a perfect conductor p 112 A87-42536
- The study of microstrip antenna arrays and related problems [NASA-CR-179714] p 113 N87-10225
- DIES**
- Improved consolidation of silicon carbide p 94 A87-12940
- DIESEL ENGINES**
- The effects of engine speed and injection characteristics on the flow field and fuel/air mixing in motored two-stroke diesel engines [AIAA PAPER 87-0227] p 161 A87-22501

- Numerical simulation of the flow field and fuel sprays in an IC engine [SAE PAPER 870599] p 143 A87-48751
- Compound cycle engine program p 23 A87-53428
- Compound cycle engine program [NASA-TM-88879] p 25 N87-11790
- Solid lubrication design methodology, phase 2 [NASA-CR-175114] p 221 N87-18470
- Compound cycle engine for helicopter application [NASA-CR-175110] p 31 N87-25323
- Technical and economic study of Stirling and Rankine cycle bottoming systems for heavy truck diesel engines [NASA-CR-180833] p 222 N87-28470
- DIFFERENCE EQUATIONS**
- A generalized procedure for constructing an upwind based TVD scheme [NASA-TM-88926] p 205 N87-24132
- DIFFERENTIAL EQUATIONS**
- Studies of unsteady viscous flows using a two-equation model of turbulence [NASA-CR-181293] p 152 N87-27949
- DIFFERENTIAL GEOMETRY**
- Noncommutative-geometry model for closed bosonic strings p 207 A87-37542
- DIFFRACTION**
- Detection of reflector surface error from near-field data: Effect of edge diffracted field [NASA-TM-89920] p 117 N87-22874
- DIFFUSERS**
- An experimental investigation of compressible three-dimensional boundary layer flow in annular diffusers [AIAA PAPER 87-0366] p 3 A87-24954
- Short efficient ejector systems [AIAA PAPER 87-1837] p 20 A87-45239
- DIFFUSION**
- Comparison of calculated and experimental cascade performance for controlled-diffusion compressor stator blading [ASME PAPER 86-GT-35] p 19 A87-25394
- A method for calculating turbulent boundary layers and losses in the flow channels of turbomachines [NASA-TM-88928] p 9 N87-15944
- Solar cells in bulk InP using an open tube diffusion process p 198 N87-26444
- Design and performance of controlled-diffusion stator compared with original double-circular-arc stator [NASA-TM-100141] p 31 N87-26910
- Diffusion length measurements in bulk and epitaxially grown 3-5 semiconductors using charge collection microscopy [NASA-TM-100128] p 129 N87-27121
- DIFFUSION COEFFICIENT**
- Oxygen-18 tracer study of the passive thermal oxidation of silicon p 78 A87-51187
- DIFFUSION FLAMES**
- Diffusion flame extinction in slow convection flow under microgravity environment p 77 A87-38787
- Size and shape of solid fuel diffusion flames in very slow speed flows [AIAA PAPER 87-2030] p 78 A87-52248
- Velocity profiles in laminar diffusion flames [NASA-TP-2596] p 147 N87-18035
- Vortex-scalar element calculations of a diffusion flame stabilized on a plane mixing layer [NASA-TM-100133] p 2 N87-28501
- DIFFUSION THEORY**
- Development and evaluation of improved numerical schemes for recirculating flows [AIAA PAPER 87-0061] p 134 A87-24913
- Influence of oscillation-induced diffusion on heat transfer in a uniformly heated channel p 135 A87-27716
- CONDIF - A modified central-difference scheme with unconditional stability and very low numerical diffusion p 136 A87-30685
- DIFFUSION WELDING**
- Materials for Advanced Turbine Engines (MATE). Project 4: Erosion resistant compressor airfoil coating [NASA-CR-179622] p 92 N87-27029
- DIGITAL ELECTRONICS**
- Full-scale engine demonstration of an advanced sensor failure detection isolation, and accommodation algorithm - Preliminary results [AIAA PAPER 87-2259] p 22 A87-50422
- Full-scale engine demonstration of an advanced sensor failure detection, isolation and accommodation algorithm: Preliminary results [NASA-TM-89880] p 127 N87-22097
- DIGITAL SIMULATION**
- WEST-3 wind turbine simulator development [NASA-CR-174983] p 192 N87-12046
- Automating the parallel processing of fluid and structural dynamics calculations [NASA-TM-89837] p 203 N87-19002

DIGITAL SYSTEMS

- Automating the parallel processing of fluid and structural dynamics calculations
[NASA-TM-89837] p 203 N87-19002

DIGITAL TECHNIQUES

- Computer control of a scanning electron microscope for digital image processing of thermal-wave images
[NASA-TM-100157] p 128 N87-26278

DIPOLE ANTENNAS

- Measurement techniques for millimeter wave substrate mounted MMW antennas p 121 A87-40926
Technology for satellite power conversion
[NASA-CR-181057] p 66 N87-25420

DIRECT CURRENT

- Arcjet power supply and start circuit
[NASA-CASE-LEW-14374-1] p 36 N87-25335

DIRECTIONAL SOLIDIFICATION (CRYSTALS)

- Mechanical property anisotropy in superalloy El-929 directionally solidified by an exothermic technique p 81 A87-11389

- Cellular-dendritic transition in directionally solidified binary alloys p 84 A87-32046

- Effect of heat treatment on the fracture behaviour of directionally solidified (gamma/gamma-prime)-alpha alloy p 86 A87-47932

- Dendritic solidification in a binary alloy melt - Comparison of theory and experiment p 217 A87-48733

- SSME single crystal turbine blade dynamics
[NASA-CR-179644] p 186 N87-26384

DISCRETE FUNCTIONS

- Evaluation of new techniques for the calculation of internal recirculating flows
[AIAA PAPER 87-0059] p 131 A87-22387

DISKS (SHAPES)

- Bladed disk vibration
[NASA-CR-181203] p 31 N87-26908

DISPERSION

- On the coalescence-dispersion modeling of turbulent molecular mixing
[NASA-TM-89910] p 2 N87-25292

DISPERSIONS

- Representation of the vaporization behavior of turbulent polydisperse sprays by 'equivalent' monodisperse sprays
[AIAA PAPER 87-1954] p 141 A87-45325

- Swept frequency technique for dispersion measurement of microstrip lines
[NASA-TM-88836] p 124 N87-14597

- Representation of the vaporization behavior of turbulent polydisperse sprays by equivalent monodisperse sprays
[NASA-TM-88906] p 26 N87-16827

DISPLACEMENT

- KI-solutions for single edge notch specimens under fixed end displacements p 174 A87-15798
A parametric study of the beam refraction problems across laser anemometer windows p 154 A87-40725

DISPLACEMENT MEASUREMENT

- Fiber-optic interferometer using frequency-modulated laser diodes p 153 A87-19186
Linear capacitive displacement sensor with frequency readout p 154 A87-42546

DISPLAY DEVICES

- Acceleration display system for aircraft zero-gravity research
[NASA-TM-87358] p 156 N87-18801

DISTRIBUTED PROCESSING

- A distributed data acquisition system for aeronautics test facilities
[NASA-TM-88961] p 35 N87-16851

DONOR MATERIALS

- Compensation in epitaxial cubic SiC films p 216 A87-15071

DOPED CRYSTALS

- Shallow n(+) diffusion into InP by an open-tube diffusion technique p 217 A87-30023
Comment on 'Temperature dependence of electrical properties of non-doped and nitrogen-doped beta-SiC single crystals grown by chemical vapor deposition' p 217 A87-42846

- Thermal stability of distillate hydrocarbon fuels
[NASA-CR-181412] p 107 N87-29706

DOPPLER EFFECT

- Effects of non-spherical drops on a phase Doppler spray analyzer p 152 A87-11048

DOWNLINKING

- A 20 GHz, high efficiency dual mode TWT for the ACTS program --- Advanced Communications Technology Satellite p 122 A87-45511

- Engineering calculations for communications satellite systems planning
[NASA-CR-181112] p 117 N87-24605

DROP SIZE

- Effects of non-spherical drops on a phase Doppler spray analyzer p 152 A87-11048

- Performance comparison of two interferometric droplet sizing techniques p 153 A87-11049

- Liquid fuel spray processes in high-pressure gas flow p 131 A87-13843

- Two-phase flow measurements of a spray in a turbulent flow

- [AIAA PAPER 87-0062] p 132 A87-22388

- Three-dimensional trajectory analyses of two drop sizing instruments - PMS OAP and PMS FSSP --- Optical Array Probe and Forward Scattering Spectrometer Probe
[AIAA PAPER 87-0180] p 132 A87-22466

- Agreement between experimental and theoretical effects of nitrogen gas flowrate on liquid jet atomization
[AIAA PAPER 87-2138] p 141 A87-45427

- Two-phase measurements of a spray in the wake of a bluff body p 142 A87-46199

- Effects of droplet interactions on droplet transport at intermediate Reynolds numbers
[NASA-CR-179567] p 26 N87-14348

- Agreement between experimental and theoretical effects of nitrogen gas flowrate on liquid jet atomization
[NASA-TM-89821] p 156 N87-19684

DROPS (LIQUIDS)

- Experimental, water droplet impingement data on two-dimensional airfoils, axisymmetric inlet and Boeing 737-300 engine inlet
[AIAA PAPER 87-0097] p 17 A87-24918

- Effects of droplet interactions on droplet transport at intermediate Reynolds numbers p 134 A87-24926

- [AIAA PAPER 87-0137] p 134 A87-24926

- Transient radiative cooling of a droplet-filled layer p 135 A87-27712

- Liquid droplet radiator development status --- waste heat rejection devices for future space vehicles
[AIAA PAPER 87-1537] p 42 A87-43059

- The design and performance of a multi-stream droplet generator for the liquid droplet radiator
[AIAA PAPER 87-1538] p 140 A87-44842

- Calculation of water drop trajectories to and about arbitrary three-dimensional lifting and nonlifting bodies in potential airflow p 8 N87-11694

- [NASA-CR-3935] p 8 N87-11694

- Effects of droplet interactions on droplet transport at intermediate Reynolds numbers p 26 N87-14348

- Liquid droplet radiator development status
[NASA-TM-89852] p 43 N87-20353

DUCTED FLOW

- DOE/NASA automotive Stirling engine project - Overview 86 p 220 A87-18034

- Duct flows with swirl p 132 A87-22509

- Acoustic power measurement for single and annular stream duct-nozzle systems utilizing a modal decomposition scheme p 209 A87-37628

- Experiments and modeling of dilution jet flow fields p 148 N87-20276

DUCTILITY

- Ductility and fracture in B2 FeAl alloys
[NASA-CR-180810] p 93 N87-27771

DUCTS

- Gas flow environmental and heat transfer nonrotating 3D program p 145 N87-11223

DURABILITY

- 2000-hour cyclic endurance test of a laboratory model multipropellant resistorjet p 52 A87-45725

- [AIAA PAPER 87-0993] p 52 A87-45725

- A 2000-hour cyclic endurance test of a laboratory model multipropellant resistorjet p 167 N87-22237

- [NASA-TM-89854] p 167 N87-22237

- Structural Integrity and Durability of Reusable Space Propulsion Systems
[NASA-CP-2471] p 62 N87-22766

DYNAMIC CHARACTERISTICS

- Flexibility effects on tooth contact location in spiral bevel gear transmissions p 166 N87-20552

DYNAMIC LOADS

- Approximations to eigenvalues of modified general matrices
[AIAA PAPER 87-0947] p 177 A87-33756

- Predicted effect of dynamic load on pitting fatigue life for low-contact-ratio spur gears p 166 N87-18095

- [NASA-TP-2610] p 166 N87-18095

- Expansion of epicyclic gear dynamic analysis program
[NASA-CR-179563] p 166 N87-19723

- Experimental and analytical evaluation of dynamic load and vibration of a 2240-kW (300-hp) rotorcraft transmission
[NASA-TM-88975] p 167 N87-20556

- Effect of shaft frequency on cavitation in a journal bearing for noncentered circular whirl p 148 N87-22122

- [NASA-TM-88925] p 148 N87-22122

- A computer solution for the dynamic load, lubricant film thickness and surface temperatures in spiral bevel gears
[NASA-CR-4077] p 169 N87-26358

- Dynamic delamination buckling in composite laminates under impact loading: Computational simulation
[NASA-TM-100192] p 75 N87-28611

- Profile modification to minimize spur gear dynamic loading
[NASA-TM-89901] p 170 N87-28918

- An investigation of the dynamic response of spur gear teeth with moving loads
[NASA-CR-179643] p 170 N87-29840

DYNAMIC MODELS

- Systematic development of reduced reaction mechanisms for dynamic modeling p 77 A87-33987

- Dynamic data acquisition, reduction, and analysis for the identification of high-speed compressor component post-stability characteristics
[AIAA PAPER 87-0899] p 162 A87-45398

DYNAMIC RESPONSE

- The effect of nonlinearities on the dynamic response of a large Shuttle payload p 40 A87-33697

- Approximations to eigenvalues of modified general matrices
[AIAA PAPER 87-0947] p 177 A87-33756

- Parameterized materials and dynamic response characterizations in unidirectional composites
[NASA-CR-4032] p 172 N87-13782

- The effect of nonlinearities on the dynamic response of a large shuttle payload
[NASA-TM-88941] p 181 N87-18112

- A comparative study of some dynamic stall models
[NASA-TM-88917] p 183 N87-18883

- Dynamic response and stability of a composite prop-fan model
[NASA-CR-179528] p 28 N87-21956

- Dynamic response of two composite prop-fan models on a nacelle/wing/fuselage half model
[NASA-CR-179589] p 18 N87-23615

- Analysis and test evaluation of the dynamic response and stability of three advanced turboprop models
[NASA-CR-174814] p 32 N87-28555

- An investigation of the dynamic response of spur gear teeth with moving loads
[NASA-CR-179643] p 170 N87-29840

- The dynamic aspects of thermo-elasto-viscoplastic snap-through and creep buckling phenomena
[NASA-CR-181411] p 187 N87-29897

DYNAMIC STABILITY

- Dynamic response and stability of a composite prop-fan model
[NASA-CR-179528] p 28 N87-21956

- Three-step cylindrical seal for high-performance turbomachines
[NASA-TP-1849] p 151 N87-24639

DYNAMIC STRUCTURAL ANALYSIS

- Solar dynamic power systems for space station p 58 N87-16024

- Combined aerodynamic and structural dynamic problem emulating routines (CASPER): Theory and implementation
[NASA-TP-2418] p 11 N87-17669

- The effect of nonlinearities on the dynamic response of a large shuttle payload
[NASA-TM-88941] p 181 N87-18112

- Automating the parallel processing of fluid and structural dynamics calculations
[NASA-TM-89837] p 203 N87-19002

- Structural and aeroelastic analysis of the SR-7L propfan
[NASA-TM-86877] p 184 N87-22273

- Structural Integrity and Durability of Reusable Space Propulsion Systems
[NASA-CP-2471] p 62 N87-22766

- Probabilistic finite elements p 185 N87-22790

- Nonisothermal elasto-visco-plastic response of shell-type structures p 185 N87-22796

- Identification of structural interface characteristics using component mode synthesis
[NASA-TM-88960] p 185 N87-24006

- Variational approach to probabilistic finite elements
[NASA-CR-181343] p 206 N87-29212

E**EARTH ORBITAL ENVIRONMENTS**

- Space power - Emerging opportunities
[IAF PAPER 86-152] p 45 A87-15900

- Solar concentrator materials development p 213 A87-18171

- Protection of solar array blankets from attack by low earth orbital atomic oxygen p 47 A87-19874

- Radiation from large space structures in low earth orbit with induced ac currents
[AIAA PAPER 87-0612] p 42 A87-22738

- Status of advanced propulsion for space based orbital transfer vehicle
[IAF PAPER 86-183] p 48 A87-23239
- Measurements of plasma parameters in the vicinity of the Space Shuttle p 200 A87-24672
- Status of advanced propulsion for space based orbital transfer vehicle
[NASA-TM-88848] p 56 N87-10959
- Oxidation-resistant reflective surfaces for solar dynamic power generation in near Earth orbit
[NASA-TM-88865] p 56 N87-10960
- An evaluation of candidate oxidation resistant materials for space applications in LEO
[NASA-TM-100122] p 105 N87-25480
- Neutral atomic oxygen beam produced by ion charge exchange for Low Earth Orbital (LEO) simulation
p 79 N87-26188
- An evaluation of candidate oxidation resistant materials p 80 N87-26203
- High temperature radiator materials for applications in the low Earth orbital environment
[NASA-TM-100190] p 93 N87-29662
- EARTH ORBITS**
- Development of the VOLT-A Shuttle experiment --- Volt Operating Limit Tests p 41 A87-19907
- The voltage threshold for arcing for solar cells in Leo - Flight and ground test results
[AIAA PAPER 86-0362] p 50 A87-40275
- Centaur D1-A systems in a nutshell
[NASA-TM-88880] p 38 N87-15996
- ECONOMIC ANALYSIS**
- The use of satellites in non-geostationary orbits for unloading geostationary communication satellite traffic peaks. Volume 1: Executive summary
[NASA-CR-179597-VOL-1] p 117 N87-21212
- The use of satellites in non-geostationary orbits for unloading geostationary communication satellite traffic peaks. Volume 2: Technical report
[NASA-CR-179597-VOL-2] p 117 N87-21213
- Technical and economic study of Stirling and Rankine cycle bottoming systems for heavy truck diesel engines
[NASA-CR-180833] p 222 N87-28470
- ECONOMICS**
- Communications satellite systems operations with the space station. Volume 1: Executive summary
[NASA-CR-179526] p 206 N87-17472
- Communications satellite systems operations with the space station, volume 2
[NASA-CR-179527] p 206 N87-17473
- EDDY VISCOSITY**
- On similarity solutions for turbulent and heated round jets p 130 A87-10922
- EDGES**
- Detection of reflector surface error from near-field data: Effect of edge diffracted field
[NASA-TM-89920] p 117 N87-22874
- EFFICIENCY**
- 20 kHz Space Station power system p 51 A87-40378
- EIGENVALUES**
- Approximations to eigenvalues of modified general matrices
[AIAA PAPER 87-0947] p 177 A87-33756
- Sensitivity analysis and approximation methods for general eigenvalue problems
[NASA-CR-179538] p 180 N87-12021
- EJECTORS**
- Short efficient ejector systems
[AIAA PAPER 87-1837] p 20 A87-45239
- Two-dimensional nozzle plume characteristics
[AIAA PAPER 87-2111] p 6 A87-45413
- Two-dimensional nozzle plume characteristics
[NASA-TM-89812] p 12 N87-18540
- ELASTIC ANISOTROPY**
- Life prediction and constitutive models for engine hot section anisotropic materials
[NASA-CR-179594] p 29 N87-23622
- ELASTIC BENDING**
- Influence of third-degree geometric nonlinearities on the vibration and stability of pretwisted, preloaded, rotating blades p 21 A87-46228
- ELASTIC DEFORMATION**
- Thermodynamically consistent constitutive equations for nonisothermal large-strain, elastoplastic, creep behavior p 175 A87-27945
- A simplified computer solution for the flexibility matrix of contacting teeth for spiral bevel gears
[NASA-CR-179620] p 168 N87-23977
- ELASTIC PROPERTIES**
- Elastic analysis of a mode II fatigue crack test specimen p 174 A87-17799
- A quadrilateral shell element using a mixed formulation p 179 A87-53796
- Fracture mechanics concepts in reliability analysis of monolithic ceramics
[NASA-TM-100174] p 187 N87-27269
- ELASTOHYDRODYNAMICS**
- Starvation effects on the hydrodynamic lubrication of rigid nonconformal contacts in combined rolling and normal motion p 135 A87-27839
- Oil film thickness measurement and analysis for an angular contact ball bearing operating in parched elastohydrodynamic lubrication
[NASA-CR-179506] p 70 N87-16879
- ELASTOPLASTICITY**
- Notes and comments on computational elastoplasticity - Some new models and their numerical implementation p 173 A87-10893
- On the symbolic manipulation and code generation for elasto-plastic material matrices p 201 A87-18499
- Thermodynamically consistent constitutive equations for nonisothermal large-strain, elastoplastic, creep behavior p 175 A87-27945
- Non-isothermal elastoviscoplastic snap-through and creep buckling of shallow arches
[AIAA PAPER 87-0806] p 176 A87-33605
- Opening and closing of cracks at high cyclic strains p 84 A87-34661
- J-integral estimates for cracks in infinite bodies p 177 A87-35334
- Nonisothermal elasto-visco-plastic response of shell-type structures p 185 N87-22796
- The dynamic aspects of thermo-elasto-viscoplastic snap-through and creep buckling phenomena
[NASA-CR-181411] p 187 N87-29897
- ELASTOSTATICS**
- Conforming versus non-conforming boundary elements in three-dimensional elastostatics p 175 A87-22775
- ELECTRIC ARCS**
- The voltage threshold for arcing for solar cells in Leo - Flight and ground test results
[AIAA PAPER 86-0362] p 50 A87-40275
- ELECTRIC BATTERIES**
- High temperature solid oxide regenerative fuel cell for solar photovoltaic energy storage
[NASA-TM-89872] p 194 N87-23020
- Space Electrochemical Research and Technology (SERT)
[NASA-CP-2484] p 199 N87-29914
- ELECTRIC CHARGE**
- Investigation of beam-plasma interactions
[NASA-CR-180579] p 215 N87-22508
- Effect of component compression on the initial performance of an IPV nickel-hydrogen cell
[NASA-TM-100102] p 195 N87-24838
- ELECTRIC CORONA**
- Asymptotic analysis of corona discharge from thin electrodes
[NASA-TP-2645] p 215 N87-14998
- ELECTRIC CURRENT**
- A heater made from graphite composite material for potential deicing application
[AIAA PAPER 87-0025] p 17 A87-24905
- A heater made from graphite composite material for potential deicing application
[NASA-TM-88888] p 17 N87-12559
- ELECTRIC DISCHARGES**
- Environmentally-induced discharge transient coupling to spacecraft
[NASA-CR-174922] p 43 N87-10946
- Asymptotic analysis of corona discharge from thin electrodes
[NASA-TP-2645] p 215 N87-14998
- A prediction model of the depth-of-discharge effect on the cycle life of a storage cell
[NASA-TM-89915] p 194 N87-22311
- Effect of component compression on the initial performance of an IPV nickel-hydrogen cell
[NASA-TM-100102] p 195 N87-24838
- ELECTRIC GENERATORS**
- Enhanced current flow through a plasma cloud by induction of plasma turbulence p 214 A87-48241
- ELECTRIC POTENTIAL**
- Effect of component compression on the initial performance of an IPV nickel-hydrogen cell
[NASA-TM-100102] p 195 N87-24838
- ELECTRIC POWER PLANTS**
- Status of commercial phosphoric acid fuel cell power plant system development p 190 A87-33777
- ELECTRIC POWER SUPPLIES**
- Electrical power system design for the U.S. Space Station p 46 A87-18068
- Space Station 20-kHz power management and distribution system p 49 A87-36913
- Space station electric power system requirements and design
[NASA-TM-89889] p 62 N87-22001
- ELECTRIC POWER TRANSMISSION**
- Factors that affect the fatigue strength of power transmission shafting and their impact on design p 160 A87-14656
- Utility interconnection issues for wind power generation
[NASA-CR-175056] p 193 N87-17400
- ELECTRIC PROPULSION**
- Microwave electrothermal thruster performance in helium gas p 49 A87-31281
- Experiments on a repetitively pulsed electrothermal thruster
[AIAA PAPER 87-1043] p 50 A87-38017
- Arcjet component conditions through a multistart test
[AIAA PAPER 87-1060] p 51 A87-41127
- Low power dc arcjet operation with hydrogen/nitrogen/ammonia mixtures
[AIAA PAPER 87-1948] p 53 A87-48575
- Electromagnetic emission experiences using electric propulsion systems - A survey
[AIAA PAPER 87-2028] p 54 A87-50195
- Electric propulsion options for the SP-100 reference mission
[NASA-TM-88918] p 57 N87-14422
- Investigation of a repetitively pulsed electrothermal thruster
[NASA-CR-179464] p 59 N87-16878
- Arcjet component conditions through a multistart test
[NASA-TM-89857] p 61 N87-20382
- Low power DC arcjet operation with hydrogen/nitrogen/ammonia mixtures
[NASA-TM-89876] p 64 N87-22804
- Electromagnetic emission experiences using electric propulsion systems: A survey
[NASA-TM-100120] p 64 N87-22805
- ELECTRIC RELAYS**
- Hollow cathodes as electron emitting plasma contactors Theory and computer modeling
[AIAA PAPER 87-0569] p 214 A87-22712
- ELECTRICAL GROUNDING**
- Environmentally-induced discharge transient coupling to spacecraft
[NASA-CR-174922] p 43 N87-10946
- ELECTRICAL PROPERTIES**
- Properties and potential applications of brominated P-100 carbon fibers p 95 A87-23702
- Comment on 'Temperature dependence of electrical properties of non-doped and nitrogen-doped beta-SiC single crystals grown by chemical vapor deposition' p 217 A87-42846
- Mechanical and electrical properties of graphite fiber-epoxy composites made from pristine and bromine intercalated fibers p 73 A87-49799
- LEO high voltage solar array arcing response model
[NASA-CR-180073] p 124 N87-16971
- ELECTRICAL RESISTANCE**
- Temperature dependence (4K to 300K) of the electrical resistivity of methane grown carbon fibers p 97 A87-47375
- High temperature static strain gage alloy development program
[NASA-CR-174833] p 157 N87-22179
- ELECTRICAL RESISTIVITY**
- Microstructure-derived macroscopic residual resistance of brominated graphite fibers p 97 A87-48324
- Evaluation results of the 700 deg C Chinese strain gages p 155 N87-11189
- Simultaneous electrical resistivity and mass uptake measurements in bromine intercalated fibers
[NASA-TM-88900] p 70 N87-11841
- Effects of sequential treatment with fluorine and bromine on graphite fibers
[NASA-TM-100106] p 104 N87-24574
- Synthesis, physical and chemical properties, and potential applications of graphite fluoride fibers
[NASA-TM-100156] p 105 N87-26232
- ELECTRICITY**
- Heat exchanger for electrothermal devices
[NASA-CASE-LEW-14037-1] p 59 N87-16875
- Comparison of Stirling engines for use with a 25-kW disk-electric conversion system
[NASA-TM-100111] p 222 N87-27564
- ELECTRO-OPTICS**
- Investigation of a GaAlAs Mach-Zehnder electro-optic modulator
[NASA-CR-179573] p 114 N87-16953
- ELECTROCATALYSTS**
- Catalyst and electrode research for phosphoric acid fuel cells p 190 A87-33789
- Space Electrochemical Research and Technology (SERT)
[NASA-CP-2484] p 199 N87-29914
- Oxygen electrodes for rechargeable alkaline fuel cells p 199 N87-29940
- ELECTROCHEMICAL CELLS**
- Concentration of carbon dioxide by a high-temperature electrochemical membrane cell p 77 A87-27400
- Initial performance of advanced designs for IPV nickel-hydrogen cells
[NASA-TM-87282] p 192 N87-16445

- Component variations and their effects on bipolar nickel-hydrogen cell performance
[NASA-TM-89907] p 195 N87-23029
- ELECTROCHEMICAL CORROSION**
Corrosion of graphite composites in phosphoric acid fuel cells
p 72 A87-42684
- ELECTROCHEMISTRY**
Organometallic catalysts for primary phosphoric acid fuel cells
[NASA-CR-179490] p 193 N87-19804
Stress-life interrelationships associated with alkaline fuel cells
[NASA-TM-89881] p 194 N87-22307
Electrochemical performance and transport properties of a Nafion membrane in a hydrogen-bromine cell environment
[NASA-TM-89862] p 79 N87-23718
Space Electrochemical Research and Technology (SERT)
[NASA-CP-2484] p 199 N87-29914
- ELECTRODE MATERIALS**
Effect of impregnation method on cycle life of the nickel electrode
p 188 A87-18105
Low power arcjet life issues
[AIAA PAPER 87-1059] p 50 A87-39635
On the effect of the $Fe(2+)/Fe(3+)$ redox couple on oxidation of carbon in hot H_3PO_4 p 78 A87-42677
Oxygen electrodes for rechargeable alkaline fuel cells
p 199 N87-29940
- ELECTRODEPOSITION**
TWT efficiency improvement by a low-cost technique for deposition of carbon on MDC electrodes
p 121 A87-30199
- ELECTRODES**
Effect of impregnation method on cycle life of the nickel electrode
p 188 A87-18105
TWT efficiency improvement by a low-cost technique for deposition of carbon on MDC electrodes
p 121 A87-30199
Asymptotic analysis of corona discharge from thin electrodes
[NASA-TP-2645] p 215 N87-14998
Performance of textured carbon on copper electrode multistage depressed collectors with medium-power traveling wave tubes
[NASA-TP-2665] p 125 N87-17990
Design, fabrication and performance of small, graphite electrode, multistage depressed collectors with 200-W, CW, 8- to 18-GHz traveling-wave tubes
[NASA-TP-2693] p 126 N87-20474
Traveling-wave-tube efficiency improvement by a low-cost technique for deposition of carbon on multistage depressed collector
[NASA-TP-2719] p 126 N87-21239
- ELECTRODYNAMICS**
Theory of plasma contactors for electrodynamic tethered satellite systems
p 122 A87-41609
The radiation impedance of an electrodynamic tether with end connectors
p 42 A87-42585
Plasma contactors for electrodynamic tether
[NASA-TM-88850] p 215 N87-18428
Electrodynamic tether
p 44 N87-26449
Ground-based plasma contractor characterization
[NASA-TM-100194] p 215 N87-28423
Oxygen interaction with space-power materials
[NASA-CR-181396] p 80 N87-29633
- ELECTROHYDRAULIC FORMING**
Results of an interlaboratory fatigue test program conducted on alloy 800H at room and elevated temperatures
p 87 A87-54370
- ELECTROLYSIS**
Alkaline water electrolysis technology for Space Station regenerative fuel cell energy storage
p 46 A87-18107
- ELECTROMAGNETIC ABSORPTION**
Finite element analysis of electromagnetic propagation in an absorbing wave guide
[NASA-TM-88866] p 207 N87-18391
- ELECTROMAGNETIC INTERACTIONS**
An analysis of electromagnetic coupling and eigenfrequencies for microwave electrothermal thruster discharges
[AIAA PAPER 87-1012] p 51 A87-41111
- ELECTROMAGNETIC INTERFERENCE**
EMC and power quality standards for 20-kHz power distribution
[NASA-TM-89925] p 62 N87-22004
Optimization of orbital assignment and specification of service areas in satellite communications
[NASA-CR-181273] p 118 N87-27882
SMI adaptive antenna arrays for weak interfering signals
[NASA-CR-181330] p 119 N87-28813
Adaptive arrays for weak interfering signals: An experimental system
[NASA-CR-181181] p 119 N87-28814
- ELECTROMAGNETIC MEASUREMENT**
Measurement techniques for millimeter wave substrate mounted MMW antennas
p 121 A87-40926
- ELECTROMAGNETIC PROPULSION**
The NASA Electric Propulsion Program
[AIAA PAPER 87-1098] p 53 A87-45795
The NASA Electric Propulsion Program
[NASA-TM-89856] p 61 N87-21037
Arcjet starting reliability: A multistart test on hydrogen/nitrogen mixtures
[NASA-TM-89867] p 61 N87-21998
- ELECTROMAGNETIC RADIATION**
Electromagnetic emission experiences using electric propulsion systems - A survey
[AIAA PAPER 87-2028] p 54 A87-50195
The finite-difference time-domain (FD-TD) method for electromagnetic scattering and interaction problems
p 113 A87-51403
Finite element analysis of electromagnetic propagation in an absorbing wave guide
[NASA-TM-88866] p 207 N87-18391
Electromagnetic emission experiences using electric propulsion systems: A survey
[NASA-TM-100120] p 64 N87-22805
- ELECTROMAGNETIC SCATTERING**
A new formulation of electromagnetic wave scattering using an on-surface radiation boundary condition approach
p 112 A87-32829
- ELECTROMAGNETIC WAVE TRANSMISSION**
Finite element modeling of electromagnetic propagation in composite structures
[NASA-TM-88916] p 207 N87-14956
- ELECTRON BEAM WELDING**
The effect of electron beam welding on the creep rupture properties of a Nb-Zr-C alloy
[NASA-TM-88892] p 88 N87-13513
- ELECTRON BEAMS**
Carbon and carbon-coated electrodes for multistage depressed collectors for electron-beam devices - A technology review
p 120 A87-20666
Ultra small electron beam amplifiers
p 122 A87-42681
Self-consistent inclusion of space-charge in the traveling wave tube
[NASA-TM-89928] p 128 N87-24630
Analytical and experimental performance of a dual-mode traveling wave tube and multistage depressed collector
[NASA-TP-2752] p 128 N87-25532
The use of multiple EBIC curves and low voltage electron microscopy in the measurement of small diffusion lengths
p 197 N87-26434
- ELECTRON BOMBARDMENT**
Plasma properties in electron-bombardment ion thrusters
[AIAA PAPER 87-1076] p 51 A87-41135
- ELECTRON DENSITY (CONCENTRATION)**
Rail gun performance and plasma characteristics due to wall ablation
p 214 A87-18735
Plasma properties in electron-bombardment ion thrusters
[AIAA PAPER 87-1076] p 51 A87-41135
- ELECTRON DIFFRACTION**
Antiphase boundaries in epitaxially grown beta-SiC
p 217 A87-30025
- ELECTRON DIFFUSION**
The use of multiple EBIC curves and low voltage electron microscopy in the measurement of small diffusion lengths
p 197 N87-26434
- ELECTRON EMISSION**
Three dimensional simulation of the operation of a hollow cathode electron emitter on the Shuttle orbiter
p 119 A87-14084
Improvements in MDC and TWT overall efficiency through the application of carbon electrode surfaces --- Multistage Depressed Collectors
p 120 A87-20667
Hollow cathodes as electron emitting plasma contactors
Theory and computer modeling
[AIAA PAPER 87-0569] p 214 A87-22712
Design, construction and long life endurance testing of cathode assemblies for use in microwave high-power transmitting tubes
[NASA-CR-175116] p 123 N87-10237
Performance of textured carbon on copper electrode multistage depressed collectors with medium-power traveling wave tubes
[NASA-TP-2665] p 125 N87-17990
Calculation of secondary electron trajectories in multistage depressed collectors for microwave amplifiers
[NASA-TP-2664] p 125 N87-17991
Secondary electron generation, emission and transport: Effects on spacecraft charging and NASCAP models
p 44 N87-26950
- ELECTRON GUNS**
Investigation of beam-plasma interactions
[NASA-CR-180579] p 215 N87-22508
- Electron beam experiments at high altitudes
p 44 N87-26946
- ELECTRON IRRADIATION**
Performance of GaAs and silicon concentrator cells under 1 MeV electron irradiation
p 189 A87-19871
Radiation and temperature effects in gallium arsenide, indium phosphide and silicon solar cells
[NASA-TM-89870] p 127 N87-22098
Performance of AlGaAs, GaAs and InGaAs cells after 1 MeV electron irradiation
p 197 N87-26438
- ELECTRON MICROSCOPY**
TEM investigation of beta-SiC grown epitaxially on Si substrate by CVD
p 97 A87-40927
Microstructures in rapidly solidified Ni-Mo alloys
p 87 A87-51636
Computer control of a scanning electron microscope for digital image processing of thermal-wave images
[NASA-TM-100157] p 128 N87-26278
The use of multiple EBIC curves and low voltage electron microscopy in the measurement of small diffusion lengths
p 197 N87-26434
Diffusion length measurements in bulk and epitaxially grown 3-5 semiconductors using charge collection microscopy
[NASA-TM-100128] p 129 N87-27121
- ELECTRON PARAMAGNETIC RESONANCE**
Annealing of electron damage in mid-IR transmitting fluoride glass
p 99 A87-53652
- ELECTRON PLASMA**
Computer simulation of plasma electron collection by PIX-II --- solar array-space plasma interaction
p 45 A87-17837
- ELECTRON RADIATION**
Annealing of electron damage in mid-IR transmitting fluoride glass
p 99 A87-53652
- ELECTRON TUBES**
Carbon and carbon-coated electrodes for multistage depressed collectors for electron-beam devices - A technology review
p 120 A87-20666
- ELECTRONS**
Secondary electron generation, emission and transport: Effects on spacecraft charging and NASCAP models
p 44 N87-26950
- ELECTROSTATIC CHARGE**
Investigation of beam-plasma interactions
[NASA-CR-180579] p 215 N87-22508
- ELECTROSTATIC ENGINES**
Precision tunable resonant microwave cavity
[NASA-CASE-LEW-13935-1] p 126 N87-21234
- ELECTROSTATIC PROBES**
Measurements of plasma parameters in the vicinity of the Space Shuttle
p 200 A87-24672
Langmuir probe surveys of an arcjet exhaust
[AIAA PAPER 87-1950] p 54 A87-50193
Langmuir probe surveys of an arcjet exhaust
[NASA-TM-89924] p 64 N87-22807
- ELECTROSTATICS**
Electron beam experiments at high altitudes
p 44 N87-26946
- ELECTROTHERMAL ENGINES**
A review of research and development on the microwave-plasma electrothermal rocket
[AIAA PAPER 87-1011] p 49 A87-38008
A computer model for the recombination zone of a microwave-plasma electrothermal rocket
[AIAA PAPER 87-1014] p 50 A87-38009
Experiments on a repetitively pulsed electrothermal thruster
[AIAA PAPER 87-1043] p 50 A87-38017
Experimental study of low Reynolds number nozzles
[AIAA PAPER 87-0992] p 51 A87-41102
An analysis of electromagnetic coupling and eigenfrequencies for microwave electrothermal thruster discharges
[AIAA PAPER 87-1012] p 51 A87-41111
The NASA/USAF arcjet research and technology program
[AIAA PAPER 87-1946] p 54 A87-50192
Heat exchanger for electrothermal devices
[NASA-CASE-LEW-14037-1] p 59 N87-16875
Investigation of a repetitively pulsed electrothermal thruster
[NASA-CR-179464] p 59 N87-16878
Experimental study of low Reynolds number nozzles
[NASA-TM-89858] p 61 N87-20383
The NASA/USAF arcjet research and technology program
[NASA-TM-100112] p 66 N87-24525
- ELLIPSOMETERS**
Variable angle of incidence spectroscopic ellipsometry
Application to GaAs-Al(x)Ga(1-x)As multiple heterostructures
p 216 A87-20519
Ellipsometric and optical study of amorphous hydrogenated carbon films
p 216 A87-23967

- Investigation of PTFE transfer films by infrared emission spectroscopy and phase-locked ellipsometry
[NASA-TM-89844] p 102 N87-20421
- ELLIPTIC DIFFERENTIAL EQUATIONS**
- Solution of elliptic PDEs by fast Poisson solvers using a local relaxation factor p 204 N87-21968
- Solution of elliptic partial differential equations by fast Poisson solvers using a local relaxation factor. 2: Two-step method
[NASA-TP-2530] p 205 N87-14918
- ELLIPTIC FUNCTIONS**
- Solution of elliptic partial differential equations by fast Poisson solvers using a local relaxation factor. 2: Two-step method
[NASA-TP-2530] p 205 N87-14918
- ELLIPTICAL CYLINDERS**
- Propagation of sound waves in tubes of noncircular cross section
[NASA-TM-2601] p 9 N87-14284
- EMISSION**
- Component testing of a ground based gas turbine steam cooled rich-burn primary zone combustor for emissions control of nitrogenous fuels
[NASA-TM-88873] p 191 N87-11345
- EMISSIVITY**
- Gas particle radiator p 141 A87-45646
- EMITTANCE**
- High temperature radiator materials for applications in the low Earth orbital environment
[NASA-TM-100190] p 93 N87-29662
- ENERGY CONSERVATION**
- Polymer, metal, and ceramic matrix composites for advanced aircraft engine applications p 71 A87-15187
- Automotive Stirling engine development program
[NASA-CR-174972] p 221 N87-20137
- ENERGY CONVERSION**
- Tunisia Renewable Energy Project systems description report
[NASA-TM-88789] p 192 N87-13856
- Status of commercial fuel cell powerplant system development
[NASA-TM-89896] p 148 N87-22171
- ENERGY CONVERSION EFFICIENCY**
- Overview of the 1986 free-piston Stirling SP-100 activities at the NASA Lewis Research Center p 160 A87-18033
- Further advances in silicon solar cell technology for space application p 188 A87-18074
- A 25.5 percent AMO gallium arsenide grating solar cell p 189 A87-19840
- Performance of GaAs and silicon concentrator cells under 1 MeV electron irradiation p 189 A87-19871
- A proposed GaAs-based superlattice solar cell structure with high efficiency and high radiation tolerance p 189 A87-19915
- TWT efficiency improvement by a low-cost technique for deposition of carbon on MDC electrodes p 121 A87-30199
- Develop and test fuel cell powered on site integrated total energy systems. Phase 3: Full-scale power plant development
[NASA-CR-175118] p 191 N87-11344
- Develop and test fuel cell powered on site integrated total energy systems: Phase 3: Full-scale power plant development
[NASA-CR-175075] p 191 N87-11347
- Brayton cycle solarized advanced gas turbine
[NASA-CR-179559] p 220 N87-15030
- Impact of thermal energy storage properties on solar dynamic space power conversion system mass
[NASA-TM-89909] p 63 N87-22802
- Space Photovoltaic Research and Technology 1986. High Efficiency, Space Environment, and Array Technology p 196 N87-26413
- High-efficiency GaAs concentrator space cells p 196 N87-26417
- The effect of internal stresses on solar cell efficiency p 196 N87-26430
- Status of indium phosphide solar cell development at Spire p 197 N87-26440
- Near-optimum design of the InP homojunction solar cell p 197 N87-26443
- Resonant AC power system proof-of-concept test program, volume 2, appendix 1
[NASA-CR-175069-VOL-2] p 130 N87-29739
- Modelling of multijunction cascade photovoltaics for space applications
[NASA-CR-181417] p 200 N87-29958
- ENERGY DISSIPATION**
- Evaluation of Stirling engine appendix gap losses p 160 A87-18037

- ENERGY GAPS (SOLID STATE)**
- Analysis of optically controlled microwave/millimeter-wave device structures p 121 A87-23680
- Ellipsometric and optical study of amorphous hydrogenated carbon films p 216 A87-23967
- ENERGY STORAGE**
- Alkaline water electrolysis technology for Space Station regenerative fuel cell energy storage p 46 A87-18107
- The potential impact of new power system technology on the design of a manned Space Station p 47 A87-18342
- NASA Lewis evaluation of Regenerative Fuel Cell (RFC) systems p 123 N87-11073
- Regenerative fuel cell study for satellites in GEO orbit
[NASA-TM-89914] p 194 N87-22310
- Effect of component compression on the initial performance of an IPV nickel-hydrogen cell
[NASA-TM-100102] p 195 N87-24838
- Theoretical performance of hydrogen-bromine rechargeable SPE fuel cell p 199 N87-29945
- ENERGY TECHNOLOGY**
- Space power - Emerging opportunities
[IAF PAPER 86-152] p 45 A87-15900
- Nickel-hydrogen separator development p 188 A87-18103
- Advanced solar thermal technologies for the 21st century p 47 A87-18179
- Materials characterization of phosphoric acid fuel cell system p 76 A87-23241
- Overview of the new ASME Performance Test Code for wind turbines p 190 A87-25475
- Status of commercial phosphoric acid fuel cell power plant system development p 190 A87-33777
- Advanced technology for extended endurance alkaline fuel cells p 190 A87-33787
- ENERGY TRANSFER**
- Comparison of pressure-strain correlation models for the flow behind a disk p 131 A87-20897
- Effect of flow oscillations on axial energy transport in a porous material p 135 A87-27715
- Gas particle radiator
[NASA-CASE-LEW-14297-1] p 156 N87-15452
- Technology for satellite power conversion
[NASA-CR-181057] p 66 N87-25420
- ENGINE CONTROL**
- Spectrum-modulating fiber-optic sensors for aircraft control systems
[NASA-TM-88968] p 27 N87-17700
- A rotorcraft flight/propulsion control integration study
[NASA-CR-179574] p 18 N87-24457
- Advanced detection, isolation and accommodation of sensor failures: Real-time evaluation
[NASA-TP-2740] p 34 N87-25331
- ENGINE COOLANTS**
- Contingency power for small turboshaft engines using water injection into turbine cooling air
[AIAA PAPER 87-1906] p 21 A87-45289
- Contingency power for small turboshaft engines using water injection into turbine cooling air
[NASA-TM-89817] p 28 N87-20280
- ENGINE DESIGN**
- An overview of the small engine component technology (SECT) studies --- commuter, rotorcraft, cruise missile and auxiliary power applications in year 2000
[AIAA PAPER 86-1542] p 19 A87-17993
- Fabrication and quality assurance processes for superhybrid composite fan blades p 72 A87-19123
- The effects of engine speed and injection characteristics on the flow field and fuel/air mixing in motored two-stroke diesel engines
[AIAA PAPER 87-0227] p 161 A87-22501
- Optimization and analysis of gas turbine engine blades
[AIAA PAPER 87-0827] p 201 A87-33614
- Euler analysis of transonic propeller flows p 4 A87-39813
- A parametric study of a gas-generator air turbo ramjet (ATR)
[AIAA PAPER 86-1681] p 20 A87-41156
- NASA/GE advanced low emissions combustor program
[AIAA PAPER 87-2035] p 21 A87-45369
- Dynamic data acquisition, reduction, and analysis for the identification of high-speed compressor component post-stability characteristics
[AIAA PAPER 87-2089] p 162 A87-45398
- Advanced liquid-cooled, turbocharged and intercooled stratified charge rotary engines for aircraft
[SAE PAPER 871039] p 22 A87-48766
- Mod II engine performance
[SAE PAPER 870101] p 163 A87-48780
- Automotive Stirling engine system component review
[SAE PAPER 870102] p 163 A87-48781
- On optimal design for the blade-root/hub interface in jet engines p 24 N87-11769

- Ceramic automotive Stirling engine program
[NASA-CR-175042] p 192 N87-12047
- Low heat transfer oxidizer heat exchanger design and analysis
[NASA-CR-179488] p 58 N87-15272
- Space station auxiliary thrust chamber technology
[NASA-CR-179552] p 59 N87-16874
- Experimental evaluation of a translating nozzle sidewall radial turbine
[NASA-TM-88963] p 27 N87-17701
- Cryogenic gear technology for an orbital transfer vehicle engine and tester design
[NASA-CR-175102] p 110 N87-19539
- Automotive Stirling engine development program
[NASA-CR-174972] p 221 N87-20137
- Numerical calculations of turbulent reacting flow in a gas-turbine combustor
[NASA-TM-89842] p 1 N87-20171
- Structural tailoring using the SSME/STAEBL code p 63 N87-22795
- High heat transfer oxidizer heat exchanger design and analysis --- RL10-2B engine p 63 N87-22803
- Compound cycle engine for helicopter application
[NASA-CR-175110] p 31 N87-25323
- Concepts for space maintenance of OTV engines p 67 N87-26097
- Technical and economic study of Stirling and Rankine cycle bottoming systems for heavy truck diesel engines
[NASA-CR-180833] p 222 N87-28470
- Automotive Stirling Engine Development Program
[NASA-CR-174873] p 222 N87-30223
- ENGINE FAILURE**
- Jet engine simulation with water ingestion through compressor
[NASA-CR-179549] p 1 N87-15932
- Advanced detection, isolation and accommodation of sensor failures: Real-time evaluation
[NASA-TP-2740] p 34 N87-25331
- ENGINE INLETS**
- Experimental, water droplet impingement data on two-dimensional airfoils, axisymmetric inlet and Boeing 737-300 engine inlet
[AIAA PAPER 87-0097] p 17 A87-24918
- An experimental investigation of compressible three-dimensional boundary layer flow in annular diffusers
[AIAA PAPER 87-0366] p 3 A87-24954
- Lower-upper implicit scheme for high-speed inlet analysis p 6 A87-46781
- Viscous analyses for flow through subsonic and supersonic intakes p 30 N87-24469
- ENGINE NOISE**
- Computational aeroacoustics of propeller noise in the near and far field
[AIAA PAPER 87-0254] p 19 A87-24944
- Aeroacoustics of subsonic turbulent shear flows
[NASA-TM-100165] p 212 N87-26615
- Turbofan aft duct suppressor study. Contractor's data report of mode probe signal data
[NASA-CR-175067] p 34 N87-29538
- Turbofan aft duct suppressor study
[NASA-CR-175067] p 34 N87-29539
- ENGINE PARTS**
- An overview of the small engine component technology (SECT) studies --- commuter, rotorcraft, cruise missile and auxiliary power applications in year 2000
[AIAA PAPER 86-1542] p 19 A87-17993
- Evaluation of capillary reinforced composites for anti-icing
[AIAA PAPER 87-0023] p 17 A87-24904
- Stress rupture and creep behavior of a low pressure plasma-sprayed NiCoCrAlY coating alloy in air and vacuum p 85 A87-43396
- Application of single crystal superalloys for earth-to-orbit propulsion systems
[AIAA PAPER 87-1976] p 85 A87-45336
- Automotive Stirling engine system component review
[SAE PAPER 870102] p 163 A87-48780
- A technology development summary for the AGT101 advanced gas turbine program
[SAE PAPER 870466] p 163 A87-48790
- Structural ceramics in heat engines - The NASA viewpoint p 98 A87-53352
- High-temperature constitutive modeling p 179 N87-11210
- Probabilistic structural analysis methods for space propulsion system components
[NASA-TM-88861] p 181 N87-13794
- Nondestructive evaluation of structural ceramics
[NASA-TM-88978] p 172 N87-18109
- Computational composite mechanics for aerospace propulsion structures
[NASA-TM-88965] p 74 N87-18614

Thermomechanical behavior of plasma-sprayed ZrO₂-Y₂O₃ coatings influenced by plasticity, creep and oxidation
[NASA-TM-88940] p 147 N87-18784

Advanced composite combustor structural concepts program
[NASA-CR-174733] p 74 N87-20387

Application of single crystal superalloys for Earth-to-orbit propulsion systems
[NASA-TM-89877] p 91 N87-22034

Composite load spectra for select space propulsion structural components
p 63 N87-22793

High heat transfer oxidizer heat exchanger design and analysis — RL10-2B engine
[NASA-CR-179596] p 63 N87-22803

Advanced Gas Turbine (AGT) Technology Development Project
[NASA-CR-180818] p 222 N87-30225

ENGINE STARTERS

Arcjet starting reliability: A multistart test on hydrogen/nitrogen mixtures
[NASA-TM-89867] p 61 N87-21998

ENGINE TESTS

Testing of a variable-stroke Stirling engine
p 160 A87-18036

A parametric study of a gas-generator air turbo ramjet (ATR)
[AIAA PAPER 86-1681] p 20 A87-41156

Aerodynamic instability performance of an advanced high-pressure-ratio compression component
[AIAA PAPER 86-1619] p 5 A87-41157

The effect of ambient pressure on the performance of a resistojet
[AIAA PAPER 87-0991] p 52 A87-42181

Full-scale thrust reverser testing in an altitude facility
[AIAA PAPER 87-1788] p 34 A87-45203

Results of acoustic tests of a Prop-Fan model
[AIAA PAPER 87-1894] p 209 A87-45282

Contingency power for small turboshaft engines using water injection into turbine cooling air
[AIAA PAPER 87-1906] p 21 A87-45289

Opportunities and challenges in heat transfer - From the perspective of the government laboratory
p 109 A87-48313

Mod II engine performance
[SAE PAPER 870101] p 163 A87-48780

A technology development summary for the AGT101 advanced gas turbine program
[SAE PAPER 870466] p 163 A87-48790

Static tests of the propulsion system — Propan Test Assessment program
[AIAA PAPER 87-1728] p 23 A87-52245

Response of a small-turboshaft-engine compression system to inlet temperature distortion
[NASA-TM-83765] p 23 N87-10100

PTA test bed aircraft engine inlet model test report, revised
[NASA-CR-174845] p 23 N87-10866

Breadboard RL10-11B low thrust operating mode
[NASA-CR-174914] p 58 N87-15269

Full-scale thrust reverser testing in an altitude facility
[NASA-TM-88967] p 35 N87-18575

Contingency power for small turboshaft engines using water injection into turbine cooling air
[NASA-TM-89817] p 28 N87-20280

Pretest uncertainty analysis for chemical rocket engine tests
[NASA-TM-89819] p 157 N87-20515

Arcjet starting reliability: A multistart test on hydrogen/nitrogen mixtures
[NASA-TM-89867] p 61 N87-21998

Synchronization trigger control system for flow visualization
[NASA-TM-89902] p 128 N87-23902

Hot gas ingestion: From model results to full scale engine testing
p 30 N87-24419

Comparison of theoretical and experimental thrust performance of a 1030:1 area ratio rocket nozzle at a chamber pressure of 2413 kN/m² (350 psia)
[NASA-TP-2725] p 66 N87-25423

Observations of directional gamma prime coarsening during engine operation
[NASA-TM-100105] p 92 N87-25459

Proven, long-life hydrogen/oxygen thrust chambers for space station propulsion
p 68 N87-26133

Measurement uncertainty for the Uniform Engine Testing Program conducted at NASA Lewis Research Center
[NASA-TM-88943] p 33 N87-28557

Advanced Gas Turbine (AGT) Technology Development Project
[NASA-CR-180818] p 222 N87-30225

ENGINEERING MANAGEMENT

Preliminary performance characterizations of an engineering model multipropellant resistojet for space station application
[AIAA PAPER 87-2120] p 54 A87-50197

Preliminary performance characterizations of an engineering model multipropellant resistojet for space station application
[NASA-TM-100113] p 111 N87-23821

ENGINES

Tribology of selected ceramics at temperatures to 900 C
p 94 A87-12954

ENTHALPY

Efficient numerical simulation of an electrothermal de-icer pad
[AIAA PAPER 87-0024] p 137 A87-32190

ENVIRONMENT POLLUTION

Resistojet plume and induced environment analysis
[NASA-TM-88957] p 66 N87-24536

ENVIRONMENTAL CHEMISTRY

Environmental degradation of 316 stainless steel in high temperature low cycle fatigue
[NASA-TM-89931] p 185 N87-24007

ENVIRONMENTAL CONTROL

Concentration of carbon dioxide by a high-temperature electrochemical membrane cell
p 77 A87-27400

ENVIRONMENTAL MONITORING

Effects of graphitization on the environmental stability of brominated pitch-based fibers
[NASA-TM-88899] p 100 N87-12679

ENVIRONMENTAL TESTS

Effect of an oxygen plasma on the physical and chemical properties of several fluids for the Liquid Droplet Radiator
[AIAA PAPER 87-0080] p 42 A87-22401

An evaluation of candidate oxidation resistant materials
p 80 N87-26203

EPITAXY

TEM investigation of beta-SiC grown epitaxially on Si substrate by CVD
p 97 A87-40927

Observation of deep levels in cubic silicon carbide
p 122 A87-41089

AlGaAs growth by OMCVD using an excimer laser
[NASA-TM-88937] p 218 N87-23304

EPOXY MATRIX COMPOSITES

Modes of vibration on square fiberglass epoxy composite thick plate
[NASA-CR-4018] p 171 N87-13779

Ultrasonic determination of the elastic constants of the stiffness matrix for unidirectional fiberglass epoxy composites
[NASA-CR-4034] p 171 N87-13781

EQUATIONS OF STATE

A universal equation of state for solids
p 219 A87-14665

Compressibility of solids
p 219 A87-51962

EQUIPMENT SPECIFICATIONS

Advanced solar thermal technologies for the 21st century
p 47 A87-18179

NASA Lewis evaluation of Regenerative Fuel Cell (RFC) systems
p 123 N87-11073

Acceleration display system for aircraft zero-gravity research
[NASA-TM-87358] p 156 N87-18801

Optical strain measurement system development, phase 1
[NASA-CR-179619] p 158 N87-22960

EROSION

Low power arcjet life issues
[AIAA PAPER 87-1059] p 50 A87-39635

ERROR ANALYSIS

Recent advances in error estimation and adaptive improvement of finite element calculations
p 204 A87-41239

A critical analysis of transverse vorticity measurements in a large plane shear layer
p 143 A87-52049

Surface flaw reliability analysis of ceramic components with the SCARE finite element postprocessor program
[NASA-TM-88901] p 181 N87-17087

Pretest uncertainty analysis for chemical rocket engine tests
[NASA-TM-89819] p 157 N87-20515

Low-cost FM oscillator for capacitance type of blade tip clearance measurement system
[NASA-TP-2746] p 31 N87-24481

The design and analysis of single flank transmission error tester for loaded gears
[NASA-CR-179621] p 169 N87-27197

Measurement uncertainty for the Uniform Engine Testing Program conducted at NASA Lewis Research Center
[NASA-TM-88943] p 33 N87-28557

Profile modification to minimize spur gear dynamic loading
[NASA-TM-89901] p 170 N87-28918

ERROR FUNCTIONS

On self-preserving, variable-density, turbulent free jets
p 130 A87-10920

ERRORS

Helical gears with circular arc teeth: Generation, geometry, precision and adjustment to errors, computer aided simulation of conditions of meshing and bearing contact
[NASA-CR-4089] p 170 N87-29846

ESTERS

A preliminary study of ester oxidation on an aluminum surface using chemiluminescence
p 96 A87-37688

A mechanistic study of polyimide formation from diester-diacids
p 70 A87-53671

Ester oxidation on an aluminum surface using chemiluminescence
[NASA-TP-2611] p 101 N87-18666

ESTIMATES

Potential for use of InP solar cells in the space radiation environment
p 120 A87-19996

ESTIMATING

Estimation of high temperature low cycle fatigue on the basis of inelastic strain and strainrate
[NASA-TM-88841] p 89 N87-14489

ETALONS

Fiber-optic temperature sensor using a spectrum-modulating semiconductor etalon
[NASA-TM-100153] p 31 N87-25329

ETCHING

Formation of a pn junction on an anisotropically etched GaAs surface using metalorganic chemical vapor deposition
p 216 A87-21237

Ion beam sputter etching
[NASA-CASE-LEW-13899-1] p 110 N87-21160

ETHYL ALCOHOL

Velocity profiles in laminar diffusion flames
[NASA-TP-2596] p 147 N87-18035

EULER EQUATIONS OF MOTION

A diagonal implicit multigrid algorithm for the Euler equations
[AIAA PAPER 87-0354] p 2 A87-22578

An L-U implicit multigrid algorithm for the three-dimensional Euler equations
[AIAA PAPER 87-0453] p 133 A87-22645

An LU-SSOR scheme for the Euler and Navier-Stokes equations
[AIAA PAPER 87-0600] p 137 A87-34724

Comparison of three explicit multigrid methods for the Euler and Navier-Stokes equations
[AIAA PAPER 87-0602] p 137 A87-34725

Adaptive finite element methods for compressible flow problems
p 4 A87-38496

Three-dimensional unsteady Euler solutions for propfans and counter-rotating propfans in transonic flow
[AIAA PAPER 87-1197] p 5 A87-42314

Euler analysis of the three-dimensional flow field of a high-speed propeller - Boundary condition effects
[ASME PAPER 87-GT-253] p 6 A87-48719

An efficient method for solving the steady Euler equations
[NASA-TM-87329] p 205 N87-11543

Comparison of three explicit multigrid methods for the Euler and Navier-Stokes equations
[NASA-TM-88878] p 1 N87-16784

Euler analysis of the three dimensional flow field of a high-speed propeller: Boundary condition effects
[NASA-TM-88955] p 10 N87-16798

A multigrid LU-SSOR scheme for approximate Newton iteration applied to the Euler equations
[NASA-CR-179524] p 10 N87-16803

An LU-SSOR scheme for the Euler and Navier-Stokes equations
[NASA-CR-179556] p 11 N87-16806

A linearized Euler analysis of unsteady flows in turbomachinery
[NASA-CR-180987] p 149 N87-22948

EVACUATING (VACUUM)

Experimental evaluation of blockage ratio and plenum evacuation system flow effects on pressure distribution for bodies of revolution in 0.1 scale model test section of NASA Lewis Research Center's proposed altitude wind tunnel
[NASA-TP-2702] p 36 N87-22694

EVALUATION

A real-time simulation evaluation of an advanced detection, isolation and accommodation algorithm for sensor failures in turbine engines
p 18 A87-13318

Evaluation of seals for high-performance cryogenic turbomachines
[NASA-TM-88919] p 146 N87-15442

Performance of a Ka-band satellite system under variable transmitted signal power conditions
[NASA-TM-88984] p 116 N87-18700

Experimental and analytical evaluation of dynamic load and vibration of a 2240-kW (300-hp) rotorcraft transmission
[NASA-TM-88975] p 167 N87-20556

The acousto-ultrasonic approach
[NASA-TM-88943] p 172 N87-20562

- Experimental evaluation of blockage ratio and plenum evacuation system flow effects on pressure distribution for bodies of revolution in 0.1 scale model test section of NASA Lewis Research Center's proposed altitude wind tunnel
[NASA-TP-2702] p 36 N87-22694
- An evaluation of candidate oxidation resistant materials for space applications in LEO
[NASA-TM-100122] p 105 N87-25480
- Ultrasonic NDE of structural ceramics for power and propulsion systems
[NASA-TM-100147] p 173 N87-26362
- Performance and power regulation characteristics of two aireron-controlled rotors and a pitchable tip-controlled rotor on the Mod-O turbine
[NASA-TM-100136] p 200 N87-29956
- EXCIMER LASERS**
AlGaAs growth by OMCVD using an excimer laser
[NASA-TM-88937] p 218 N87-23304
- EXCITATION**
Secondary stream and excitation effects on two-dimensional nozzle plume characteristics
[AIAA PAPER 87-2112] p 6 A87-45414
- Secondary stream and excitation effects on two-dimensional nozzle plume characteristics
[NASA-TM-89813] p 12 N87-18539
- Analysis of the vibratory excitation arising from spiral bevel gears
[NASA-CR-4081] p 169 N87-25579
- EXHAUST EMISSION**
NASA/GE advanced low emissions combustor program
[AIAA PAPER 87-2035] p 21 A87-45369
- Langmuir probe surveys of an arcjet exhaust
[AIAA PAPER 87-1950] p 54 A87-50193
- Langmuir probe surveys of an arcjet exhaust
[NASA-TM-89924] p 64 N87-22807
- EXHAUST GASES**
An analytical and experimental investigation of resistojet plumes
[AIAA PAPER 87-0399] p 48 A87-24998
- Effect of nozzle geometry on the resistojet exhaust plume
[AIAA PAPER 87-2121] p 55 A87-52252
- Laser anemometers of hot-section applications
p 155 N87-11187
- An analytical and experimental investigation of resistojet plumes
[NASA-TM-88852] p 58 N87-14428
- Theoretical kinetic computations in complex reacting systems
p 219 N87-20277
- Hot gas ingestion: From model results to full scale engine testing
p 30 N87-24419
- Airflow calibration and exhaust pressure/temperature survey of an F404, S/N 215-109, turbofan engine
[NASA-TM-100159] p 33 N87-29537
- EXHAUST NOZZLES**
Experimental evaluation of heat transfer on a 1030:1 area ratio rocket nozzle
[AIAA PAPER 87-2070] p 55 A87-52249
- Experimental evaluation of heat transfer on a 1030:1 area ratio rocket nozzle
[NASA-TP-2726] p 67 N87-25424
- EXHAUST SYSTEMS**
Short efficient ejector systems
[AIAA PAPER 87-1837] p 20 A87-45239
- EXOTHERMIC REACTIONS**
Mechanical property anisotropy in superalloy EI-929 directionally solidified by an exothermic technique
p 81 A87-11389
- Mechanisms by which heat release affects the flow field in a chemically reacting, turbulent mixing layer
[AIAA PAPER 87-0131] p 134 A87-24925
- EXPERIMENT DESIGN**
Feasibility of mapping velocity flowfields in an SSME powerhead using laser anemometry techniques
[AIAA PAPER 87-1306] p 154 A87-42374
- Cryogenic Fluid Management Flight Experiment (CFMFE)
p 109 N87-21150
- Space experiment development process
p 109 N87-21156
- A finite element model for wave propagation in an inhomogeneous material including experimental validation
[NASA-TM-100149] p 207 N87-25821
- EXPERIMENTATION**
Comparison of calculated and experimental cascade performance for controlled-diffusion compressor stator blading
[ASME PAPER 86-GT-35] p 19 A87-25394
- EXPERT SYSTEMS**
Composite load spectra for select space propulsion structural components
p 63 N87-22793

EXPONENTIAL FUNCTIONS

- An exponential finite difference technique for solving partial differential equations
[NASA-TM-89874] p 205 N87-24930

EXPOSURE

- Effects of atmosphere on the tribological properties of a chromium carbide based coating for use to 760 deg C
[NASA-TM-88894] p 101 N87-16140
- Exposure time considerations in high temperature low cycle fatigue
[NASA-TM-88934] p 187 N87-28944

EXTENSIONS

- Thermo-elasto-viscoplastic analysis of problems in extension and shear
[NASA-CR-181410] p 187 N87-29896

EXTENSOMETERS

- Results of an interlaboratory fatigue test program conducted on alloy 800H at room and elevated temperatures
p 87 A87-54370
- A mechanism for precise linear and angular adjustment utilizing flexures
p 165 N87-16342

EXTINGUISHING

- Diffusion flame extinction in slow convection flow under microgravity environment
p 77 A87-38787

EXTRAPOLATION

- Extrapolation methods for divergent oscillatory infinite integrals that are defined in the sense of summability
p 204 A87-35575
- Extrapolation methods for vector sequences
p 203 A87-53631

EXTREMELY HIGH FREQUENCIES

- Baseband processor development/test performance for 30/20 GHz SS-TDMA communication system
p 111 A87-18310
- A 20 GHz, high efficiency dual mode TWT for the ACTS program --- Advanced Communications Technology Satellite
p 122 A87-45511
- Performance of a Ka-band satellite system under variable transmitted signal power conditions
[NASA-TM-88984] p 116 N87-18700

F**FABRICATION**

- Nickel-hydrogen separator development
p 188 A87-18103
- Fabrication and quality assurance processes for superhybrid composite fan blades
p 72 A87-19123
- Brayton cycle solarized advanced gas turbine
[NASA-CR-179559] p 220 N87-15030
- Design, fabrication and performance of small, graphite electrode, multistage depressed collectors with 200-W, CW, 8- to 18-GHz traveling-wave tubes
[NASA-TP-2693] p 126 N87-20474
- FABRY-PEROT INTERFEROMETERS**
Combined fringe and Fabry-Perot laser anemometer for 3 component velocity measurements in turbine stator cascade facility
p 110 N87-21183
- FACE CENTERED CUBIC LATTICES**
Understanding single-crystal superalloys
p 85 A87-40928
- The characteristics of gamma-prime dislocation pairs in a nickel-base superalloy
p 85 A87-46932

FAILURE ANALYSIS

- SCARE - A postprocessor program to MSC/NASTRAN for reliability analysis of structural ceramic components
[ASME PAPER 86-GT-34] p 174 A87-17988
- Re-examination of cumulative fatigue damage analysis - An engineering perspective
p 174 A87-22128
- Yielding and deformation behavior of the single crystal superalloy PWA 1480
p 84 A87-32040
- Full-scale engine demonstration of an advanced sensor failure detection isolation, and accommodation algorithm - Preliminary results
[AIAA PAPER 87-2259] p 22 A87-50422
- Thermal barrier coating life prediction model
[NASA-CR-179504] p 100 N87-13539
- Full-scale engine demonstration of an advanced sensor failure detection, isolation and accommodation algorithm: Preliminary results
[NASA-TM-89880] p 127 N87-22097
- Effect of storage and LEO cycling on manufacturing technology IPV nickel-hydrogen cells
[NASA-TM-89883] p 194 N87-22308
- FAILURE MODES**
A real-time simulation evaluation of an advanced detection, isolation and accommodation algorithm for sensor failures in turbine engines
p 18 A87-13318
- Re-examination of cumulative fatigue damage analysis - An engineering perspective
p 174 A87-22128
- Structure and tensile strength of LaS(1,4)
p 96 A87-38065

- Thermomechanical behavior of plasma-sprayed ZrO₂-Y₂O₃ coatings influenced by plasticity, creep and oxidation
[NASA-TM-88940] p 147 N87-18784
- Fatigue failure of regenerator screens in a high frequency Stirling engine
[NASA-TM-88974] p 183 N87-18882
- Strain energy release rates of composite interlaminar end-notch and mixed-mode fracture: A sublaminar/ply level analysis and a computer code
[NASA-TM-89827] p 74 N87-20389
- Stress-life interrelationships associated with alkaline fuel cells
[NASA-TM-89881] p 194 N87-22307
- FAN BLADES**
Fabrication and quality assurance processes for superhybrid composite fan blades
p 72 A87-19123
- Rotor wake characteristics of a transonic axial-flow fan
p 2 A87-20886
- Aircraft turbofan noise
p 209 A87-31144
- A model propulsion simulator for evaluating counter rotating blade characteristics
[SAE PAPER 861715] p 20 A87-32607
- Application of advanced computational codes in the design of an experiment for a supersonic throughflow fan rotor
[NASA-TM-88915] p 13 N87-22630
- Hub flexibility effects on propfan vibration
[NASA-TM-89900] p 186 N87-24722
- FAR FIELDS**
Computational aeroacoustics of propeller noise in the near and far field
[AIAA PAPER 87-0254] p 19 A87-24944
- Aircraft turbofan noise
p 209 A87-31144
- FASTENERS**
Combustion of velcro in low gravity
[NASA-TM-88970] p 102 N87-19518
- FATIGUE (MATERIALS)**
Factors that affect the fatigue strength of power transmission shafting and their impact on design
p 160 A87-14656
- Fatigue criterion to system design, life, and reliability
p 175 A87-27986
- Crack layer theory
p 178 A87-40056
- Fatigue and fracture: Overview
p 179 N87-11183
- Creep fatigue life prediction for engine hot section materials (ISOTROPIC)
p 181 N87-15491
- Predicted effect of dynamic load on pitting fatigue life for low-contact-ratio spur gears
[NASA-TP-2610] p 166 N87-18095
- Fatigue failure of regenerator screens in a high frequency Stirling engine
[NASA-TM-88974] p 183 N87-18882
- Structural Integrity and Durability of Reusable Space Propulsion Systems
[NASA-CP-2471] p 62 N87-22766
- Environmental degradation of 316 stainless steel in high temperature low cycle fatigue
[NASA-TM-89931] p 185 N87-24007
- FATIGUE LIFE**
Re-examination of cumulative fatigue damage analysis - An engineering perspective
p 174 A87-22128
- Effect of interference fits on roller bearing fatigue life
p 162 A87-37686
- Fatigue life of laser cut metals
[NASA-CR-179501] p 164 N87-11158
- Estimation of high temperature low cycle fatigue on the basis of inelastic strain and strain rate
[NASA-TM-88841] p 89 N87-14489
- High temperature monotonic and cyclic deformation in a directionally solidified nickel-base superalloy
[NASA-CR-175101] p 90 N87-15303
- Lubricant effects on bearing life
[NASA-TM-88875] p 165 N87-15467
- Effects of surface removal on rolling-element fatigue
[NASA-TM-88871] p 166 N87-18820
- Advanced composite combustor structural concepts program
[NASA-CR-174733] p 74 N87-20387
- Bithermal low-cycle fatigue behavior of a NiCoCrAlY-coated single crystal superalloy
[NASA-TM-89831] p 91 N87-20408
- Calculation of thermomechanical fatigue life based on isothermal behavior
[NASA-TM-88864] p 183 N87-20565
- Fatigue damage interaction behavior of PWA 1480
p 92 N87-22777
- Probabilistic structural analysis to evaluate the structural durability of SSME critical components
p 62 N87-22783
- Exposure time considerations in high temperature low cycle fatigue
[NASA-TM-88934] p 187 N87-28944

FATIGUE TESTING MACHINES

A computerized test system for thermal-mechanical fatigue crack growth p 153 A87-23899

FATIGUE TESTS

Elastic analysis of a mode II fatigue crack test specimen p 174 A87-17799

Low cycle fatigue behaviour of a plasma-sprayed coating material p 82 A87-24040

Slow crack growth in sintered silicon nitride p 98 A87-48989

Thermal-mechanical fatigue crack growth in B-1900+Hf p 86 A87-49570

Results of an interlaboratory fatigue test program conducted on alloy 800H at room and elevated temperatures p 87 A87-54370

The cyclic stress-strain behavior of PWA 1480 at 650 deg C p 89 A87-14483

Advanced composite combustor structural concepts program p 74 A87-20387

Fatigue damage interaction behavior of PWA 1480 p 92 A87-22777

A high temperature fatigue and structures testing facility p 186 A87-26399

Design of test specimens and procedures for generating material properties of Douglas fir/epoxy laminated wood composite material: With the generation of baseline data at two environmental conditions p 75 A87-28612

[NASA-TM-100151] p 186 A87-26399

Design of test specimens and procedures for generating material properties of Douglas fir/epoxy laminated wood composite material: With the generation of baseline data at two environmental conditions p 75 A87-28612

[NASA-TM-100151] p 186 A87-26399

Design of test specimens and procedures for generating material properties of Douglas fir/epoxy laminated wood composite material: With the generation of baseline data at two environmental conditions p 75 A87-28612

[NASA-TM-100151] p 186 A87-26399

Design of test specimens and procedures for generating material properties of Douglas fir/epoxy laminated wood composite material: With the generation of baseline data at two environmental conditions p 75 A87-28612

[NASA-TM-100151] p 186 A87-26399

Design of test specimens and procedures for generating material properties of Douglas fir/epoxy laminated wood composite material: With the generation of baseline data at two environmental conditions p 75 A87-28612

[NASA-TM-100151] p 186 A87-26399

Design of test specimens and procedures for generating material properties of Douglas fir/epoxy laminated wood composite material: With the generation of baseline data at two environmental conditions p 75 A87-28612

[NASA-TM-100151] p 186 A87-26399

Design of test specimens and procedures for generating material properties of Douglas fir/epoxy laminated wood composite material: With the generation of baseline data at two environmental conditions p 75 A87-28612

[NASA-TM-100151] p 186 A87-26399

Design of test specimens and procedures for generating material properties of Douglas fir/epoxy laminated wood composite material: With the generation of baseline data at two environmental conditions p 75 A87-28612

[NASA-TM-100151] p 186 A87-26399

Design of test specimens and procedures for generating material properties of Douglas fir/epoxy laminated wood composite material: With the generation of baseline data at two environmental conditions p 75 A87-28612

[NASA-TM-100151] p 186 A87-26399

Design of test specimens and procedures for generating material properties of Douglas fir/epoxy laminated wood composite material: With the generation of baseline data at two environmental conditions p 75 A87-28612

[NASA-TM-100151] p 186 A87-26399

Design of test specimens and procedures for generating material properties of Douglas fir/epoxy laminated wood composite material: With the generation of baseline data at two environmental conditions p 75 A87-28612

[NASA-TM-100151] p 186 A87-26399

Design of test specimens and procedures for generating material properties of Douglas fir/epoxy laminated wood composite material: With the generation of baseline data at two environmental conditions p 75 A87-28612

[NASA-TM-100151] p 186 A87-26399

Design of test specimens and procedures for generating material properties of Douglas fir/epoxy laminated wood composite material: With the generation of baseline data at two environmental conditions p 75 A87-28612

[NASA-TM-100151] p 186 A87-26399

Design of test specimens and procedures for generating material properties of Douglas fir/epoxy laminated wood composite material: With the generation of baseline data at two environmental conditions p 75 A87-28612

[NASA-TM-100151] p 186 A87-26399

Design of test specimens and procedures for generating material properties of Douglas fir/epoxy laminated wood composite material: With the generation of baseline data at two environmental conditions p 75 A87-28612

[NASA-TM-100151] p 186 A87-26399

Design of test specimens and procedures for generating material properties of Douglas fir/epoxy laminated wood composite material: With the generation of baseline data at two environmental conditions p 75 A87-28612

[NASA-TM-100151] p 186 A87-26399

Design of test specimens and procedures for generating material properties of Douglas fir/epoxy laminated wood composite material: With the generation of baseline data at two environmental conditions p 75 A87-28612

[NASA-TM-100151] p 186 A87-26399

Mechanical properties of SiC fiber-reinforced reaction-bonded Si3N4 composites p 73 A87-50094

A heater made from graphite composite material for potential deicing application p 17 N87-12559

[NASA-TM-88888] p 17 N87-12559

Ultrasonic determination of the elastic constants of the stiffness matrix for unidirectional fiberglass epoxy composites p 171 N87-13781

[NASA-CR-4034] p 171 N87-13781

Parameterized materials and dynamic response characterizations in unidirectional composites p 172 N87-13782

[NASA-CR-4032] p 172 N87-13782

Advanced composite combustor structural concepts program p 74 N87-20387

[NASA-CR-174733] p 74 N87-20387

Styrene-terminated polysulfone oligomers as matrix material for graphite reinforced composites: An initial study p 74 N87-21043

[NASA-TM-89846] p 74 N87-21043

Fiber reinforced superalloys p 75 N87-22811

[NASA-TM-89865] p 75 N87-22811

Effects of fiber motion on the acoustic behavior of an anisotropic, flexible fibrous material p 212 N87-25826

[NASA-TM-89884] p 212 N87-25826

Method of preparing fiber reinforced ceramic material [NASA-CASE-LEW-14392-1] p 106 N87-28656

[NASA-TM-89884] p 212 N87-25826

Method of preparing fiber reinforced ceramic material [NASA-CASE-LEW-14392-1] p 106 N87-28656

[NASA-TM-89884] p 212 N87-25826

Method of preparing fiber reinforced ceramic material [NASA-CASE-LEW-14392-1] p 106 N87-28656

[NASA-TM-89884] p 212 N87-25826

Method of preparing fiber reinforced ceramic material [NASA-CASE-LEW-14392-1] p 106 N87-28656

[NASA-TM-89884] p 212 N87-25826

Method of preparing fiber reinforced ceramic material [NASA-CASE-LEW-14392-1] p 106 N87-28656

[NASA-TM-89884] p 212 N87-25826

Method of preparing fiber reinforced ceramic material [NASA-CASE-LEW-14392-1] p 106 N87-28656

[NASA-TM-89884] p 212 N87-25826

Method of preparing fiber reinforced ceramic material [NASA-CASE-LEW-14392-1] p 106 N87-28656

[NASA-TM-89884] p 212 N87-25826

Method of preparing fiber reinforced ceramic material [NASA-CASE-LEW-14392-1] p 106 N87-28656

[NASA-TM-89884] p 212 N87-25826

Method of preparing fiber reinforced ceramic material [NASA-CASE-LEW-14392-1] p 106 N87-28656

[NASA-TM-89884] p 212 N87-25826

Method of preparing fiber reinforced ceramic material [NASA-CASE-LEW-14392-1] p 106 N87-28656

[NASA-TM-89884] p 212 N87-25826

Method of preparing fiber reinforced ceramic material [NASA-CASE-LEW-14392-1] p 106 N87-28656

[NASA-TM-89884] p 212 N87-25826

Method of preparing fiber reinforced ceramic material [NASA-CASE-LEW-14392-1] p 106 N87-28656

[NASA-TM-89884] p 212 N87-25826

Method of preparing fiber reinforced ceramic material [NASA-CASE-LEW-14392-1] p 106 N87-28656

[NASA-TM-89884] p 212 N87-25826

Method of preparing fiber reinforced ceramic material [NASA-CASE-LEW-14392-1] p 106 N87-28656

[NASA-TM-89884] p 212 N87-25826

Method of preparing fiber reinforced ceramic material [NASA-CASE-LEW-14392-1] p 106 N87-28656

[NASA-TM-89884] p 212 N87-25826

Method of preparing fiber reinforced ceramic material [NASA-CASE-LEW-14392-1] p 106 N87-28656

[NASA-TM-89884] p 212 N87-25826

Method of preparing fiber reinforced ceramic material [NASA-CASE-LEW-14392-1] p 106 N87-28656

[NASA-TM-89884] p 212 N87-25826

30 GHz monolithic balanced mixers using an ion-implanted FET-compatible 3-inch GaAs wafer process technology p 121 A87-34525

Optically controlled GaAs dual-gate MESFET and permeable base transistors p 123 N87-10232

[NASA-TM-88823] p 123 N87-10232

The 20 GHz GaAs monolithic power amplifier module development p 124 N87-11104

[NASA-CR-174742] p 124 N87-11104

The 20 GHz power GaAs FET development p 124 N87-16972

[NASA-CR-179546] p 124 N87-16972

Microwave performance of an optically controlled AlGaAs/GaAs high electron mobility transistor and GaAs MESFET p 125 N87-17993

[NASA-TM-88980] p 125 N87-17993

Apparatus for mounting a field emission cathode [NASA-CASE-LEW-14108-1] p 129 N87-28832

[NASA-TM-88980] p 125 N87-17993

Apparatus for mounting a field emission cathode [NASA-CASE-LEW-14108-1] p 129 N87-28832

[NASA-TM-88980] p 125 N87-17993

Apparatus for mounting a field emission cathode [NASA-CASE-LEW-14108-1] p 129 N87-28832

[NASA-TM-88980] p 125 N87-17993

Apparatus for mounting a field emission cathode [NASA-CASE-LEW-14108-1] p 129 N87-28832

[NASA-TM-88980] p 125 N87-17993

Apparatus for mounting a field emission cathode [NASA-CASE-LEW-14108-1] p 129 N87-28832

[NASA-TM-88980] p 125 N87-17993

Apparatus for mounting a field emission cathode [NASA-CASE-LEW-14108-1] p 129 N87-28832

[NASA-TM-88980] p 125 N87-17993

Apparatus for mounting a field emission cathode [NASA-CASE-LEW-14108-1] p 129 N87-28832

[NASA-TM-88980] p 125 N87-17993

Apparatus for mounting a field emission cathode [NASA-CASE-LEW-14108-1] p 129 N87-28832

[NASA-TM-88980] p 125 N87-17993

Apparatus for mounting a field emission cathode [NASA-CASE-LEW-14108-1] p 129 N87-28832

[NASA-TM-88980] p 125 N87-17993

Apparatus for mounting a field emission cathode [NASA-CASE-LEW-14108-1] p 129 N87-28832

[NASA-TM-88980] p 125 N87-17993

Apparatus for mounting a field emission cathode [NASA-CASE-LEW-14108-1] p 129 N87-28832

[NASA-TM-88980] p 125 N87-17993

Apparatus for mounting a field emission cathode [NASA-CASE-LEW-14108-1] p 129 N87-28832

[NASA-TM-88980] p 125 N87-17993

Apparatus for mounting a field emission cathode [NASA-CASE-LEW-14108-1] p 129 N87-28832

[NASA-TM-88980] p 125 N87-17993

Apparatus for mounting a field emission cathode [NASA-CASE-LEW-14108-1] p 129 N87-28832

[NASA-TM-88980] p 125 N87-17993

Apparatus for mounting a field emission cathode [NASA-CASE-LEW-14108-1] p 129 N87-28832

[NASA-TM-88980] p 125 N87-17993

Apparatus for mounting a field emission cathode [NASA-CASE-LEW-14108-1] p 129 N87-28832

[NASA-TM-88980] p 125 N87-17993

Apparatus for mounting a field emission cathode [NASA-CASE-LEW-14108-1] p 129 N87-28832

[NASA-TM-88980] p 125 N87-17993

Apparatus for mounting a field emission cathode [NASA-CASE-LEW-14108-1] p 129 N87-28832

[NASA-TM-88980] p 125 N87-17993

Apparatus for mounting a field emission cathode [NASA-CASE-LEW-14108-1] p 129 N87-28832

[NASA-TM-88980] p 125 N87-17993

Apparatus for mounting a field emission cathode [NASA-CASE-LEW-14108-1] p 129 N87-28832

[NASA-TM-88980] p 125 N87-17993

- Assessment of simplified composite micromechanics using three-dimensional finite-element analysis p 72 A87-19121
- Use of a corrugated surface to enhance radiation tolerance in a GaAs solar cell p 189 A87-19842
- An adaptive finite element strategy for complex flow problems [AIAA PAPER 87-0557] p 133 A87-22706
- Design concepts/parameters assessment and sensitivity analyses of select composite structural components p 175 A87-25407
- On the numerical performance of three-dimensional thick shell elements using a hybrid/mixed formulation p 175 A87-25924
- A probabilistic Hu-Washizu variational principle [AIAA PAPER 87-0764] p 176 A87-33579
- A versatile and low order hybrid stress element for general shell geometry [AIAA PAPER 87-0840] p 176 A87-33624
- A hybrid nonlinear programming method for design optimization p 201 A87-35718
- Optimal placement of critical speeds in rotor-bearing systems p 162 A87-38464
- Adaptive finite element methods for compressible flow problems p 4 A87-38496
- Recent advances in error estimation and adaptive improvement of finite element calculations p 204 A87-41239
- A quadrilateral shell element using a mixed formulation p 179 A87-53796
- On optimal design for the blade-root/hub interface in jet engines p 24 A87-11769
- A constitutive law for finite element contact problems with unclassical friction [NASA-TM-88838] p 180 A87-12924
- Composite interlaminar fracture toughness: Three-dimensional finite element modeling for mixed mode 1, 2 and 3 fracture [NASA-TM-88872] p 73 A87-13491
- Finite element modeling of electromagnetic propagation in composite structures [NASA-TM-88916] p 207 A87-14956
- Surface flaw reliability analysis of ceramic components with the SCARE finite element postprocessor program [NASA-TM-88901] p 181 A87-17087
- Structural properties of impact ices accreted on aircraft structures [NASA-CR-179580] p 182 A87-18121
- Finite element analysis of electromagnetic propagation in an absorbing wave guide [NASA-TM-88866] p 207 A87-18391
- Color postprocessing for 3-dimensional finite element mesh quality evaluation and evolving graphical workstation [NASA-CR-180215] p 202 A87-18997
- Elevated temperature crack growth [NASA-CR-179601] p 184 A87-22267
- Nonlinear heat transfer and structural analyses of SSME turbine blades p 184 A87-22779
- The NESSUS finite element code p 184 A87-22785
- Probabilistic finite elements p 185 A87-22790
- Finite element implementation of Robinson's unified viscoplastic model and its application to some uniaxial and multiaxial problems [NASA-TM-89891] p 185 A87-23010
- A simplified computer solution for the flexibility matrix of contacting teeth for spiral bevel gears [NASA-CR-179620] p 168 A87-23977
- Hub flexibility effects on propeller vibration [NASA-TM-89900] p 186 A87-24722
- A finite element model for wave propagation in an inhomogeneous material including experimental validation [NASA-TM-100149] p 207 A87-25821
- Finite element analysis of flexible, rotating blades [NASA-TM-89906] p 186 A87-26385
- Variational approach to probabilistic finite elements [NASA-CR-181343] p 206 A87-29212
- FINITE VOLUME METHOD**
- A diagonal implicit multigrid algorithm for the Euler equations [AIAA PAPER 87-0354] p 2 A87-22578
- Multigrid solution of inviscid transonic flow through rotating blade passages [AIAA PAPER 87-0608] p 3 A87-24992
- Composite grid and finite-volume LU implicit scheme for turbine flow analysis [AIAA PAPER 87-1129] p 5 A87-42078
- Composite grid and finite-volume LU implicit scheme for turbine flow analysis [NASA-TM-89828] p 12 A87-20235
- Thermodynamic evaluation of transonic compressor rotors using the finite volume approach [NASA-CR-180587] p 150 A87-23925

- FINIS**
- Turbulent heat transfer in corrugated-wall channels with and without fins p 134 A87-27709
- FIRE FIGHTING**
- Science and technology issues in spacecraft fire safety [AIAA PAPER 87-0467] p 39 A87-31107
- Science and technology issues in spacecraft fire safety [NASA-TM-88933] p 40 A87-16012
- FIRE PREVENTION**
- Science and technology issues in spacecraft fire safety [AIAA PAPER 87-0467] p 39 A87-31107
- Science and technology issues in spacecraft fire safety [NASA-TM-88933] p 40 A87-16012
- Fire safety concerns in space operations [NASA-TM-89848] p 40 A87-20342
- FLAME PROPAGATION**
- The flame structure and vorticity generated by a chemically reacting transverse jet p 76 A87-14116
- Gravitational effects on the structure and propagation of premixed flames [IAF PAPER 86-279] p 76 A87-15983
- Comparisons between thermodynamic and one-dimensional combustion models of spark-ignition engines p 161 A87-29275
- Flame radiation p 78 A87-11204
- Vortex-scalar element calculations of a diffusion flame stabilized on a plane mixing layer [NASA-TM-100133] p 2 A87-28501
- Bonding Lexan and sapphire to form high-pressure, flame-resistant window [NASA-TM-100188] p 159 A87-28880
- Spark ignition of monodisperse fuel sprays [NASA-CR-181404] p 80 A87-29635
- FLAMMABILITY**
- Bonding Lexan and sapphire to form high-pressure, flame-resistant window [NASA-TM-100188] p 159 A87-28880
- FLAT PLATES**
- Heat transfer in the stagnation region of the junction of a circular cylinder perpendicular to a flat plate p 131 A87-13019
- Endwall heat transfer in the junction region of a circular cylinder normal to a flat plate at 30 and 60 degrees from stagnation point of the cylinder [AIAA PAPER 87-0077] p 132 A87-22398
- Transition boiling heat transfer and the film transition regime p 143 A87-53589
- Flowfield measurements in a separated and reattached flat plate turbulent boundary layer [NASA-CR-4052] p 148 A87-21257
- An investigation of the flow characteristics in the blade endwall corner region [NASA-CR-4076] p 14 A87-29412
- FLEXIBILITY**
- A simplified computer solution for the flexibility matrix of contacting teeth for spiral bevel gears [NASA-CR-179620] p 168 A87-23977
- Hub flexibility effects on propeller vibration [NASA-TM-89900] p 186 A87-24722
- Effects of fiber motion on the acoustic behavior of an anisotropic, flexible fibrous material [NASA-TM-89884] p 212 A87-25826
- FLEXIBLE BODIES**
- A NASTHAN primer for the analysis of rotating flexible blades [NASA-TM-89861] p 184 A87-21375
- Finite element analysis of flexible, rotating blades [NASA-TM-89906] p 186 A87-26385
- FLEXIBLE SPACECRAFT**
- The 20th Aerospace Mechanics Symposium [NASA-CP-2423-REV] p 181 A87-16321
- FLIGHT CHARACTERISTICS**
- Polymer, metal, and ceramic matrix composites for advanced aircraft engine applications p 71 A87-15187
- Modeling of environmentally induced transients within satellites [AIAA PAPER 85-0387] p 42 A87-41611
- An evaluation of metallized propellants based on vehicle performance [AIAA PAPER 87-1773] p 53 A87-47003
- An evaluation of metallized propellants based on vehicle performance [NASA-TM-100104] p 64 A87-22806
- FLIGHT CONDITIONS**
- In-flight measurement of ice growth on an airfoil using an array of ultrasonic transducers [AIAA PAPER 87-0178] p 15 A87-22464
- Comparison of wet and dry growth in artificial and flight icing conditions p 16 A87-45635

FLIGHT SIMULATION

- Simulated flight acoustic investigation of treated ejector effectiveness on advanced mechanical suppressors for high velocity jet noise reduction [NASA-CR-4019] p 211 A87-17481
- Free-jet investigation of mechanically suppressed, high radius ratio coannular plug model nozzles [NASA-CR-3596] p 212 A87-29315
- FLIGHT TESTS**
- The voltage threshold for arcing for solar cells in Leo - Flight and ground test results [AIAA PAPER 86-0362] p 50 A87-40275
- Liquid droplet radiator development status --- waste heat rejection devices for future space vehicles [AIAA PAPER 87-1537] p 42 A87-43059
- Response of a small-turboshaft-engine compression system to inlet temperature distortion [NASA-TM-83765] p 23 A87-10100
- Flight test report of the NASA icing research airplane: Performance, stability, and control after flight through natural icing conditions [NASA-CR-179515] p 34 A87-11797
- Liquid droplet radiator development status [NASA-TM-89852] p 43 A87-20353
- FLIP-FLOPS**
- Design, implementation and investigation of an image guide-based optical flip-flop array [NASA-CR-181382] p 213 A87-30180
- FLOW CHARACTERISTICS**
- A numerical simulation of the inviscid flow through a counterrotating propeller [ASME PAPER 86-GT-138] p 3 A87-25395
- Icing of flow conditioners in a closed-loop wind tunnel [NASA-TM-89824] p 13 A87-23591
- An investigation of the flow characteristics in the blade endwall corner region [NASA-CR-4076] p 14 A87-29412
- FLOW COEFFICIENTS**
- Analysis of experimental shaft seal data for high-performance turbomachines - As for Space Shuttle main engines p 162 A87-45846
- FLOW DISTORTION**
- Perfect gas effects in compressible rapid distortion theory p 136 A87-31176
- A method for assessing effects of circumferential flow distortion on compressor stability p 7 A87-48722
- Viscous analyses for flow through subsonic and supersonic intakes p 30 A87-24469
- Calculations of inlet distortion induced compressor flowfield instability p 30 A87-24470
- Summary of investigations of engine response to distorted inlet conditions p 30 A87-24477
- FLOW DISTRIBUTION**
- Visualization of flows in a motored rotary combustion engine using holographic interferometry [AIAA PAPER 86-1557] p 19 A87-21514
- Laser velocimetry in turbulent flow fields - Particle response [AIAA PAPER 87-0118] p 132 A87-22426
- Multi-spark visualization of typical combustor flowfields p 134 A87-25281
- Modelling of jet- and swirl-stabilized reacting flows in axisymmetric combustors p 138 A87-38956
- Euler analysis of transonic propeller flows p 4 A87-39813
- Feasibility of mapping velocity flowfields in an SSME powerhead using laser anemometry techniques [AIAA PAPER 87-1306] p 154 A87-42374
- Spanwise structures in transitional flow around circular cylinders [AIAA PAPER 87-1383] p 140 A87-44940
- An experimental study on the effects of tip clearance on flow field and losses in an axial flow compressor rotor p 6 A87-46207
- Euler analysis of the three-dimensional flow field of a high-speed propeller - Boundary condition effects [ASME PAPER 87-GT-253] p 6 A87-48719
- Numerical simulation of the flow field and fuel sprays in an IC engine [SAE PAPER 870599] p 143 A87-48751
- Fuel-air mixing and combustion in a two-dimensional Wankel engine [SAE PAPER 870408] p 163 A87-48783
- Method for the determination of the three dimensional aerodynamic field of a rotor-stator combination in compressible flow [AIAA PAPER 87-1742] p 7 A87-50187
- CONDIF - A modified central-difference scheme for convective flows p 205 A87-53675
- Large perturbation flow field analysis and simulation for supersonic inlets [NASA-CR-174676] p 8 A87-10835
- Combustion overview p 78 A87-11181
- Host turbine heat transfer overview p 144 A87-11184

- Aerothermal modeling program, phase 2 p 24 N87-11200
- Calculation of two- and three-dimensional transonic cascade flow field using the Navier-Stokes equations p 144 N87-11220
- Assessment of a 3-D boundary layer code to predict heat transfer and flow losses in a turbine p 145 N87-11224
- An experimental study of the aerodynamics of a NACA 0012 airfoil with a simulated glaze ice accretion [NASA-CR-179897] p 8 N87-11701
- Measurements of the unsteady flow field within the stator row of a transonic axial-flow fan. 1: Measurement and analysis technique [NASA-TM-88945] p 10 N87-16789
- Measurements of the unsteady flow field within the stator row of a transonic axial-flow fan. Part 2: Results and discussion [NASA-TM-88946] p 10 N87-16790
- Euler analysis of the three dimensional flow field of a high-speed propeller: Boundary condition effects [NASA-TM-88955] p 10 N87-16798
- Transition mixing study [NASA-CR-175062] p 27 N87-16830
- Generation of a composite grid for turbine flows and consideration of a numerical scheme [NASA-TM-88890] p 11 N87-17662
- Design of 9.271-pressure-ratio 5-stage core compressor and overall performance for first 3 stages [NASA-TP-2597] p 27 N87-17699
- Experiments and modeling of dilution jet flow fields p 148 N87-20276
- Detailed flow surveys of turning vanes designed for a 0.1-scale model of NASA Lewis Research Center's proposed altitude wind tunnel [NASA-TP-2680] p 36 N87-20295
- Laser fringe anemometry for aero engine components p 110 N87-21176
- Flowfield measurements in a separated and reattached flat plate turbulent boundary layer [NASA-CR-4052] p 148 N87-21257
- Unsteady stator/rotor interaction p 149 N87-22767
- Simulation of multistage turbine flows p 149 N87-22768
- Method for the determination of the three-dimensional aerodynamic field of a rotor-stator combination to compressible flow [NASA-TM-100118] p 30 N87-23625
- Calculations of inlet distortion induced compressor flowfield instability p 30 N87-24470
- Turbulence modeling and surface heat transfer in a stagnation flow region [NASA-TM-100132] p 151 N87-26302
- Performance and aerodynamic braking of a horizontal-axis wind turbine from small-scale wind tunnel tests [NASA-CR-180812] p 198 N87-27327
- Three dimensional boundary layers in internal flows [NASA-CR-181336] p 152 N87-28860
- Control of shear flows by artificial excitation [NASA-TM-100201] p 15 N87-29420
- FLOW EQUATIONS**
- DOE/NASA automotive Stirling engine project - Overview 86 p 220 A87-18034
- Comparison of Hirs' equation with Moody's equation for determining rotordynamic coefficients of annular pressure seals [ASME PAPER 86-TRIB-19] p 161 A87-19529
- Multiply scaled constrained nonlinear equation solvers -- for nonlinear heat conduction problems p 137 A87-31406
- Comparison of generalized Reynolds and Navier Stokes equations for flow of a power law fluid p 142 A87-45852
- Third-moment closure of turbulence for predictions of separating and reattaching shear flows: A study of Reynolds-stress closure model [NASA-CR-177055] p 145 N87-11961
- A comparison of experimental and theoretical results for labyrinth gas seals [NASA-CR-180194] p 166 N87-18096
- FLOW GEOMETRY**
- Coherent structures and turbulence p 133 A87-22859
- Turbulence modeling for complex shear flows p 133 A87-23653
- Numerical prediction of cold turbulent flow in combustor configurations with different centerbody flame holders [ASME PAPER 86-WA/HT-50] p 140 A87-43715
- An LDA investigation of three-dimensional normal shock-boundary layer interactions in a corner [AIAA PAPER 87-1369] p 6 A87-44938
- Spanwise structures in transitional flow around circular cylinders [AIAA PAPER 87-1383] p 140 A87-44940

FLOW MEASUREMENT

- Two opposed lateral jets injected into swirling crossflow [AIAA PAPER 87-0307] p 132 A87-22549
- Two component laser velocimeter measurements of turbulence parameters downstream of an axisymmetric sudden expansion p 139 A87-40703
- A parametric study of the beam refraction problems across laser anemometer windows p 154 A87-40725
- Laser anemometry measurements of natural circulation flow in a scale model PWR reactor system -- Pressurized Water Reactor p 154 A87-40750
- Composite grid and finite-volume LU implicit scheme for turbine flow analysis [AIAA PAPER 87-1129] p 5 A87-42078
- Heat transfer and fluid mechanics measurements in transitional boundary layers on convex-curved surfaces [ASME PAPER 85-MT-60] p 143 A87-48726
- A critical analysis of transverse vorticity measurements in a large plane shear layer p 143 A87-52049
- User's manual for a TEACH computer program for the analysis of turbulent, swirling reacting flow in a research combustor [NASA-CR-179547] p 78 N87-11858
- Viscous analyses for flow through subsonic and supersonic intakes [NASA-TM-88831] p 9 N87-15173
- Four spot laser anemometer and optical access techniques for turbine applications [NASA-TM-88972] p 156 N87-18057
- Composite grid and finite-volume LU implicit scheme for turbine flow analysis [NASA-TM-89828] p 12 N87-20235
- Laser fringe anemometry for aero engine components p 110 N87-21176
- Combined fringe and Fabry-Perot laser anemometer for 3 component velocity measurements in turbine stator cascade facility p 110 N87-21183
- Beam-modulation methods in quantitative and flow-visualization holographic interferometry p 111 N87-21204
- Flowfield measurements in a separated and reattached flat plate turbulent boundary layer [NASA-CR-4052] p 148 N87-21257
- FLOW STABILITY**
- The generation of capillary instabilities on a liquid jet p 130 A87-12060
- Coherent motion in excited free shear flows [AIAA PAPER 85-0539] p 135 A87-30281
- On the spatial instability of piecewise linear free shear layers p 137 A87-31680
- The evolution of instabilities in the axisymmetric jet. I - The linear growth of disturbances near the nozzle. II - The flow resulting from the interaction between two waves p 138 A87-37256
- Shear flow instability generated by non-homogeneous external forcing p 142 A87-48047
- A method for assessing effects of circumferential flow distortion on compressor stability p 7 A87-48722
- Calculations of inlet distortion induced compressor flowfield instability p 30 N87-24470
- Controlled excitation of a cold turbulent swirling free jet [NASA-TM-100173] p 152 N87-27977
- FLOW THEORY**
- Perfect gas effects in compressible rapid distortion theory p 136 A87-31176
- FLOW VELOCITY**
- Agreement between experimental and theoretical effects of nitrogen gas flowrate on liquid jet atomization [AIAA PAPER 87-2138] p 141 A87-45427
- Radiative cooling of a layer with nonuniform velocity - A separable solution p 141 A87-45637
- Laser anemometers of hot-section applications p 155 N87-11187
- Experimental evaluation of wall Mach number distributions of the octagonal test section proposed for NASA Lewis Research Center's altitude wind tunnel [NASA-TP-2666] p 35 N87-17717
- Jet model for slot film cooling with effect of free-stream and coolant turbulence [NASA-TP-2655] p 146 N87-18034
- Agreement between experimental and theoretical effects of nitrogen gas flowrate on liquid jet atomization [NASA-TM-89821] p 156 N87-19684
- Combined fringe and Fabry-Perot laser anemometer for 3 component velocity measurements in turbine stator cascade facility p 110 N87-21183
- Development of gas-to-gas lift pad dynamic seals, volumes 1 and 2 [AIAA-CR-179486] p 168 N87-22245
- Turbulence characteristics of an axisymmetric reacting flow [NASA-CR-180697] p 152 N87-27973

FLOW VISUALIZATION

- Visualization of flows in a motored rotary combustion engine using holographic interferometry [AIAA PAPER 86-1557] p 19 A87-21514
- Multi-spark visualization of typical combustor flowfields p 134 A87-25281
- Flow visualization study of the effect of injection hole geometry on an inclined jet in crossflow p 155 A87-45842
- Simultaneous measurements of two-dimensional velocity and pressure fields in compressible flows through image-intensified detection of laser-induced fluorescence p 143 A87-52320
- Development of a turbomachinery design optimization procedure using a multiple-parameter nonlinear perturbation method [NASA-CR-3831] p 1 N87-10003
- Evaluation of diffuse-illumination holographic cinematography in a flutter cascade [NASA-TP-2593] p 156 N87-13731
- Beam-modulation methods in quantitative and flow-visualization holographic interferometry p 111 N87-21204
- Synchronization trigger control system for flow visualization [NASA-TM-89902] p 128 N87-23902
- FLOWMETERS**
- Three-dimensional trajectory analyses of two drop sizing instruments - PMS OAP and PMS FSSP -- Optical Array Probe and Forward Scattering Spectrometer Probe [AIAA PAPER 87-0180] p 132 A87-22466
- FLUID DYNAMICS**
- Coherent structures and turbulence p 133 A87-22859
- NASA-Chinese Aeronautical Establishment (CAE) Symposium [NASA-CP-2433] p 27 N87-20267
- FLUID FLOW**
- Numerical simulation of the flowfield in a motored two-dimensional Wankel engine p 138 A87-39812
- A model for fluid flow during saturated boiling on a horizontal cylinder p 139 A87-41173
- Liquid sheet radiator [AIAA PAPER 87-1525] p 140 A87-43048
- Comparison of generalized Reynolds and Navier Stokes equations for flow of a power law fluid p 142 A87-45852
- Refrigerated dynamic seal to 6.9 MPa (1000 psi) p 164 A87-50777
- Progress of Stirling cycle analysis and loss mechanism characterization [NASA-TM-88891] p 220 N87-13359
- Noise generated by flow through large butterfly valves [NASA-TM-88911] p 210 N87-16586
- Liquid sheet radiator [NASA-TM-89841] p 147 N87-18786
- FLUID INJECTION**
- Two opposed lateral jets injected into swirling crossflow [AIAA PAPER 87-0307] p 132 A87-22549
- FLUID JETS**
- Agreement between experimental and theoretical effects of nitrogen gas flowrate on liquid jet atomization [AIAA PAPER 87-2138] p 141 A87-45427
- Agreement between experimental and theoretical effects of nitrogen gas flowrate on liquid jet atomization [NASA-TM-89821] p 156 N87-19684
- FLUID MANAGEMENT**
- On-orbit cryogenic storage and resupply p 41 A87-18344
- Thermodynamic analysis and subscale modeling of space-based orbit transfer vehicle cryogenic propellant resupply [AIAA PAPER 87-1764] p 142 A87-48572
- Microgravity Fluid Management Symposium [NASA-CP-2465] p 108 N87-21141
- Cryogenic Fluid Management Flight Experiment (CFMFE) p 109 N87-21150
- Thermodynamic analysis and subscale modeling of space-based orbit transfer vehicle cryogenic propellant resupply [NASA-TM-89921] p 150 N87-22949
- Space station experiment definition: Long-term cryogenic fluid storage [NASA-CR-4072] p 151 N87-24641
- FLUIDS**
- Viscometer for low frequency, low shear rate measurements p 153 A87-13878
- FLUORESCENCE**
- Simultaneous measurements of two-dimensional velocity and pressure fields in compressible flows through image-intensified detection of laser-induced fluorescence p 143 A87-52320

FLUORIDES

- Effects of silver and group II fluoride solid lubricant additions to plasma-sprayed chromium carbide coatings for foil gas bearings to 650 C p 95 A87-22336
- Fluoride salts and container materials for thermal energy storage applications in the temperature range 973 to 1400 K
- [NASA-TM-89913] p 195 N87-24026
- Carbide-fluoride-silver self-lubricating composite
- [NASA-CASE-LEW-14196-2] p 169 N87-25585

FLUORINATION

- Effects of sequential treatment with fluorine and bromine on graphite fibers
- [NASA-TM-100106] p 104 N87-24574
- Synthesis, physical and chemical properties, and potential applications of graphite fluoride fibers
- [NASA-TM-100156] p 105 N87-26232
- Comparison of the tribological properties of fluorinated cokes and graphites
- [NASA-TM-100170] p 106 N87-29679

FLUOROHYDROCARBONS

- Substituted 1,1,1-triaryl-2,2,2-trifluoroethanes and processes for their synthesis --- synthetic routes to monomers for polyimides
- [NASA-CASE-LEW-14345-1] p 70 N87-14432
- New condensation polyimides containing 1,1,1-triaryl-2,2,2-trifluoroethane structures
- [NASA-CASE-LEW-14346-1] p 70 N87-14433

FLUOROPOLYMERS

- Substituted 1,1,1-triaryl-2,2,2-trifluoroethanes and processes for their synthesis --- synthetic routes to monomers for polyimides
- [NASA-CASE-LEW-14345-1] p 70 N87-14432
- New condensation polyimides containing 1,1,1-triaryl-2,2,2-trifluoroethane structures
- [NASA-CASE-LEW-14346-1] p 70 N87-14433

FLUTTER

- Analytical flutter investigation of a composite propfan model
- [AIAA PAPER 87-0738] p 178 A87-40497
- Optimization of cascade blade mistuning under flutter and forced response constraints p 24 N87-11732
- Analytical flutter investigation of a composite propfan model
- [NASA-TM-88944] p 182 N87-18115
- Unstalled flutter stability predictions and comparisons to test data for a composite prop-fan model
- [NASA-CR-179512] p 28 N87-21955
- Bladed disk vibration
- [NASA-CR-181203] p 31 N87-26908

FLUTTER ANALYSIS

- A technique for the prediction of airfoil flutter characteristics in separated flow
- [AIAA PAPER 87-0910] p 177 A87-33719
- Analytical and experimental investigation of mistuning in propfan flutter
- [AIAA PAPER 87-0739] p 178 A87-40496
- Concentrated mass effects on the flutter of a composite advanced turboprop model
- [NASA-TM-88854] p 180 N87-12017
- Analytical and experimental investigation of mistuning in propfan flutter
- [NASA-TM-88959] p 182 N87-18116
- A computational procedure for automated flutter analysis
- [NASA-TM-100171] p 187 N87-28058

FOIL BEARINGS

- Effects of silver and group II fluoride solid lubricant additions to plasma-sprayed chromium carbide coatings for foil gas bearings to 650 C p 95 A87-22336

FOLDING STRUCTURES

- Folding tilt rotor demonstrator feasibility study
- p 17 A87-19247

FORCED CONVECTION

- Prediction and rational correlation of thermophoretically reduced particle mass transfer to hot surfaces across laminar or turbulent forced-convection gas boundary layers
- p 133 A87-23449

FORCED VIBRATION

- Analysis of the vibratory excitation arising from spiral bevel gears
- [NASA-CR-4081] p 169 N87-25579

FORTRAN

- On the symbolic manipulation and code generation for elasto-plastic material matrices
- p 201 A87-18499

FRACTALS

- Stochastic and fractal analysis of fracture trajectories
- p 179 A87-51167

FRACTOGRAPHY

- Correlation of processing and sintering variables with the strength and radiography of silicon nitride
- p 94 A87-12938
- Slow crack growth in sintered silicon nitride
- p 98 A87-48989

FRACTURE MECHANICS

- SCARE - A postprocessor program to MSC/NASTRAN for reliability analysis of structural ceramic components [ASME PAPER 86-GT-34] p 174 A87-17988
- Compliance matrices for cracked bodies
- p 175 A87-25775
- Fault structures in rapidly quenched Ni-Mo binary alloys
- p 83 A87-32035
- Stochastic and fractal analysis of fracture trajectories
- p 179 A87-51167
- Fatigue and fracture: Overview
- p 179 N87-11183
- Analysis of mixed-mode crack propagation using the boundary integral method
- [NASA-CR-179518] p 180 N87-12915
- Unification of color postprocessing techniques for 3-dimensional computational mechanics
- [NASA-CR-180214] p 202 N87-18998
- Strain energy release rates of composite interlaminar end-notch and mixed-mode fracture: A sublaminate/ply level analysis and a computer code
- [NASA-TM-89827] p 74 N87-20389
- Structural Integrity and Durability of Reusable Space Propulsion Systems
- [NASA-CP-2471] p 62 N87-22766
- Fracture mechanics concepts in reliability analysis of monolithic ceramics
- [NASA-TM-100174] p 187 N87-27269
- Ductility and fracture in B2 FeAl alloys
- [NASA-CR-180810] p 93 N87-27771

FRACTURE STRENGTH

- Mechanism of strength degradation for hot corrosion of alpha-SiC
- p 95 A87-21470
- Fracture toughness of Si₃N₄ measured with short bar chevron-notched specimens
- p 96 A87-30621
- Composite interlaminar fracture toughness: Three-dimensional finite element modeling for mixed mode 1, 2 and 3 fracture
- [NASA-TM-88872] p 73 N87-13491
- Hot corrosion attack and strength degradation of SiC and Si(sub)3N(sub)4
- [NASA-TM-89820] p 102 N87-20425
- Macrocrack interaction with transverse array of microcracks
- [NASA-CR-180806] p 186 N87-25607

FRACTURING

- Deformation and fracture of single-crystal and sintered polycrystalline silicon carbide produced by cavitation
- [NASA-TM-88981] p 102 N87-20422

FREE CONVECTION

- Modeling free convective gravitational effects in chemical vapor deposition
- [AIAA PAPER 87-0313] p 133 A87-22552

FREE FLOW

- Coherent motion in excited free shear flows
- [AIAA PAPER 85-0539] p 135 A87-30281
- On the spatial instability of piecewise linear free shear layers
- p 137 A87-31680
- The generation of Tollmien-Schlichting waves by long wavelength free stream disturbances
- p 139 A87-41655

FREE JETS

- On self-preserving, variable-density, turbulent free jets
- p 130 A87-10920
- Particle-laden swirling free jets - Measurements and predictions
- [AIAA PAPER 87-0303] p 139 A87-42648
- Free jet feasibility study of a thermal acoustic shield concept for AST/VCE application: Dual stream nozzles
- [NASA-CR-3867] p 210 N87-10752
- Particle-laden swirling free jets: Measurements and predictions
- [NASA-TM-88904] p 26 N87-16826
- Controlled excitation of a cold turbulent swirling free jet
- [NASA-TM-100173] p 152 N87-27977

FREE RADICALS

- Iptycenes - Extended triptycenes
- p 69 A87-53654

FREE VIBRATION

- Three-dimensional vibrations of twisted cantilevered parallelepipeds
- p 173 A87-11106
- Free vibration analysis by BEM using particular integrals
- p 174 A87-13882

FREE-PISTON ENGINES

- A 1987 overview of free-piston Stirling technology for space power application
- [NASA-TM-89832] p 221 N87-21756

FREEZING

- Refrigerated dynamic seal to 6.9 MPa (1000 psi)
- p 164 A87-50777
- The mathematical modeling of rapid solidification processing
- [NASA-CR-179551] p 88 N87-13514
- User evaluation of photovoltaic-powered vaccine refrigerator/freezer systems
- [NASA-TM-88830] p 193 N87-18230

FREQUENCY ASSIGNMENT

- Intersatellite Link (ISL) application to commercial communications satellites. Volume 2: Technical final report
- [NASA-CR-179598-VOL-2] p 116 N87-19553
- Engineering calculations for communications satellite systems planning
- [NASA-CR-181112] p 117 N87-24605
- Optimization of orbital assignment and specification of service areas in satellite communications
- [NASA-CR-181273] p 118 N87-27882

FREQUENCY DIVISION MULTIPLE ACCESS

- Advanced space communications architecture study. Volume 1: Executive summary
- [NASA-CR-179591] p 115 N87-18696
- Satellite analog FDMA/FM to digital TDMA conversion
- [NASA-CR-179605] p 125 N87-20467
- On-board processing satellite network architecture and control study
- [NASA-CR-180817] p 44 N87-27711

FREQUENCY MODULATION

- Fiber-optic interferometer using frequency-modulated laser diodes
- p 153 A87-19186
- A study of the effect of group delay distortion on an SMSK satellite communications channel
- [NASA-TM-89835] p 116 N87-20450
- Beam-modulation methods in quantitative and flow-visualization holographic interferometry
- p 111 N87-21204
- Low-cost FM oscillator for capacitance type of blade tip clearance measurement system
- [NASA-TP-2746] p 31 N87-24481
- Detection of radio-frequency modulated optical signals by two and three terminal microwave devices
- [NASA-TM-100196] p 130 N87-29750

FREQUENCY RESPONSE

- Acceleration display system for aircraft zero-gravity research
- [NASA-TM-87358] p 156 N87-18801

FREQUENCY SHIFT KEYING

- A study of the effect of group delay distortion on an SMSK satellite communications channel
- [NASA-TM-89835] p 116 N87-20450

FRESNEL LENSES

- Development of a Fresnel lens concentrator for space application
- p 196 N87-26427

FRICTION

- Tribology of selected ceramics at temperatures to 900 C
- p 94 A87-12954
- Microstructure and surface chemistry of amorphous alloys important to their friction and wear behavior
- p 81 A87-15186
- Effects of silver and group II fluoride solid lubricant additions to plasma-sprayed chromium carbide coatings for foil gas bearings to 650 C
- p 95 A87-22336
- Effect of gimbal friction modelling technique on control stability and performance for Centaur upper stage
- [AIAA PAPER 87-2455] p 38 A87-50501
- A constitutive law for finite element contact problems with unclassical friction
- [NASA-TM-88838] p 180 N87-12924
- Effects of atmosphere on the tribological properties of a chromium carbide based coating for use to 760 deg C
- [NASA-TM-88894] p 101 N87-16140
- Effect of Gimbal friction modeling technique on control stability and performance for Centaur upper-stage
- [NASA-TM-89894] p 39 N87-22755
- SSME blade damper technology
- p 63 N87-22798
- Tribology theory versus experiment
- [NASA-TM-100108] p 71 N87-29599

FRICTION FACTOR

- Comparison of Hirs' equation with Moody's equation for determining rotordynamic coefficients of annular pressure seals
- [ASME PAPER 86-TRIB-19] p 161 A87-19529

FRICTION MEASUREMENT

- Oil film thickness measurement and analysis for an angular contact ball bearing operating in parched elastohydrodynamic lubrication
- [NASA-CR-179506] p 70 N87-16879

FRICTION REDUCTION

- SSME blade damper technology
- p 63 N87-22798
- Bladed disk vibration
- [NASA-CR-181203] p 31 N87-26908

FROST

- Icing of flow conditioners in a closed-loop wind tunnel
- [NASA-TM-89824] p 13 N87-23591

FUEL CELL POWER PLANTS

- Develop and test fuel cell powered on site integrated total energy systems. Phase 3: Full-scale power plant development
- [NASA-CR-175118] p 191 N87-11344
- Develop and test fuel cell powered on site integrated total energy systems: Phase 3: Full-scale power plant development
- [NASA-CR-175075] p 191 N87-11347

- Status of commercial fuel cell powerplant system development
[NASA-TM-89896] p 148 N87-22171
- FUEL CELLS**
- Performance study of a fuel cell Pt-on-C anode in presence of CO and CO₂ and calculation of adsorption parameters for CO poisoning p 188 A87-12338
- Materials characterization of phosphoric acid fuel cell system p 76 A87-23241
- Advanced technology for extended endurance alkaline fuel cells p 190 A87-33787
- Modeling for CO poisoning of a fuel cell anode p 191 A87-52288
- Develop and test fuel cell powered on site integrated total energy systems: Phase 3: Full-scale power plant development
[NASA-CR-175075] p 191 N87-11347
- Stress-life interrelationships associated with alkaline fuel cells
[NASA-TM-89881] p 194 N87-22307
- FUEL COMBUSTION**
- Fuel-air mixing and combustion in a two-dimensional Wankel engine
[SAE PAPER 870408] p 163 A87-48783
- Component testing of a ground based gas turbine steam cooled rich-burn primary zone combustor for emissions control of nitrogenous fuels
[NASA-TM-88873] p 191 N87-11345
- Thermodynamics and combustion modeling p 219 N87-20274
- Theoretical kinetic computations in complex reacting systems p 219 N87-20277
- The chemical shock tube as a tool for studying high-temperature chemical kinetics p 157 N87-20279
- Multispecies CARS measurements in turbulent combustion p 79 N87-23808
- Aviation fuel property effects on altitude relight
[NASA-CR-179582] p 107 N87-24578
- Turbulence characteristics of an axisymmetric reacting flow
[NASA-CR-180697] p 152 N87-27973
- FUEL CONSUMPTION**
- Automotive Stirling engine development program
[NASA-CR-174972] p 221 N87-20137
- FUEL CONTROL**
- Polymer, metal, and ceramic matrix composites for advanced aircraft engine applications p 71 A87-15187
- Self-regulating heater application to Shuttle/Centaur hydrazine fuel line thermal control
[AIAA PAPER 87-1570] p 43 A87-43081
- FUEL INJECTION**
- The effects of engine speed and injection characteristics on the flow field and fuel/air mixing in motored two-stroke diesel engines
[AIAA PAPER 87-0227] p 161 A87-22501
- Numerical simulation of the flowfield in a motored two-dimensional Wankel engine p 138 A87-39812
- Fuel-air mixing and combustion in a two-dimensional Wankel engine
[SAE PAPER 870408] p 163 A87-48783
- Estimation of instantaneous heat transfer coefficients for a direct-injection stratified-charge rotary engine
[SAE PAPER 870444] p 163 A87-48787
- FUEL PUMPS**
- The noncavitating performance and life of a small vane-type positive displacement pump in liquid hydrogen
[AIAA PAPER 86-1438] p 46 A87-17994
- Three-step labyrinth seal for high-performance turbomachines
[NASA-TP-1848] p 150 N87-23921
- Straight cylindrical seal for high-performance turbomachines
[NASA-TP-1850] p 150 N87-23936
- Three-step cylindrical seal for high-performance turbomachines
[NASA-TP-1849] p 151 N87-24639
- FUEL SPRAYS**
- Liquid fuel spray processes in high-pressure gas flow p 131 A87-13843
- The effects of engine speed and injection characteristics on the flow field and fuel/air mixing in motored two-stroke diesel engines
[AIAA PAPER 87-0227] p 161 A87-22501
- Effects of droplet interactions on droplet transport at intermediate Reynolds numbers
[AIAA PAPER 87-0137] p 134 A87-24926
- Prediction of the structure of fuel sprays in cylindrical combustion chambers p 20 A87-31277
- Two-phase measurements of a spray in the wake of a bluff body p 142 A87-46199
- Numerical simulation of the flow field and fuel sprays in an IC engine
[SAE PAPER 870599] p 143 A87-48751
- Two-phase flow p 147 N87-20272

- FUEL SYSTEMS**
- Simulation of multistage turbine flows p 149 N87-22768
- Antimisting kerosene JT3 engine fuel system integration study
[NASA-CR-4033] p 106 N87-24577
- FUEL TANKS**
- Temperature fields due to jet induced mixing in a typical OTV tank
[AIAA PAPER 87-2017] p 55 A87-52247
- FUEL TESTS**
- Degradation mechanisms of sulfur and nitrogen containing compounds during thermal stability testing of model fuels
[AIAA PAPER 87-2039] p 106 A87-45372
- FUEL-AIR RATIO**
- Numerical simulation of the flowfield in a motored two-dimensional Wankel engine p 138 A87-39812
- FUELS**
- Tribological properties of coal slurries
[NASA-TM-89930] p 104 N87-24565
- Spark ignition of monodisperse fuel sprays
[NASA-CR-181404] p 80 N87-29635
- FULL SCALE TESTS**
- Measurement of Centaur/Orbiter multiple reaction forces in a full-scale test rig p 38 A87-29448
- FUNCTIONS (MATHEMATICS)**
- Multigrid-sinc methods p 205 A87-52865
- FURNACES**
- Gravitational macrosegregation in binary Pb-Sn alloy ingots
[NASA-TM-89885] p 109 N87-24579
- FUSELAGES**
- Analysis and test evaluation of the dynamic response and stability of three advanced turboprop models
[NASA-CR-174814] p 32 N87-28555
- G**
- GADOLINIUM**
- Feasibility analysis of reciprocating magnetic heat pumps
[NASA-CR-180262] p 147 N87-19647
- GALACTIC EVOLUTION**
- Quasars as indicators of galactic ages p 223 A87-26927
- GALACTIC NUCLEI**
- Quasars as indicators of galactic ages p 223 A87-26927
- GALERKIN METHOD**
- Microstrip dispersion including anisotropic substrates p 123 A87-47621
- GALLIUM ARSENIDES**
- Indium phosphide solar cells - Status and prospects for use in space p 188 A87-18071
- High-efficiency GaAs solar concentrator cells for space and terrestrial applications p 188 A87-18073
- Advances in gallium arsenide monolithic microwave integrated-circuit technology for space communications systems p 120 A87-19091
- A 25.5 percent AMO gallium arsenide grating solar cell p 189 A87-19840
- Use of a corrugated surface to enhance radiation tolerance in a GaAs solar cell p 189 A87-19842
- Performance of GaAs and silicon concentrator cells under 1 MeV electron irradiation p 189 A87-19871
- A proposed GaAs-based superlattice solar cell structure with high efficiency and high radiation tolerance p 189 A87-19915
- Formation of a pn junction on an anisotropically etched GaAs surface using metalorganic chemical vapor deposition p 216 A87-21237
- Thermal and structural stability of cosputtered amorphous Ta(x)Cu(1-x) alloy thin films on GaAs p 216 A87-27198
- Nonlinear absorption in AlGaAs/GaAs multiple quantum well structures grown by metalorganic chemical vapor deposition p 217 A87-39687
- Optically controlled GaAs dual-gate MESFET and permeable base transistors
[NASA-TM-88823] p 123 N87-10232
- The 20 GHz GaAs monolithic power amplifier module development
[NASA-CR-174742] p 124 N87-11104
- Investigation of a GaAlAs Mach-Zehnder electro-optic modulator
[NASA-CR-179573] p 114 N87-16953
- The 20 GHz power GaAs FET development
[NASA-CR-179546] p 124 N87-16972
- The 60 GHz IMPATT diode development
[NASA-CR-179536] p 218 N87-17515
- Microwave performance of an optically controlled AlGaAs/GaAs high electron mobility transistor and GaAs MESFET
[NASA-TM-88980] p 125 N87-17993

- Propagation characteristics of some novel coplanar waveguide transmission lines on GaAs at MM-wave frequencies
[NASA-TM-89839] p 126 N87-20469
- AlGaAs growth by OMCVD using an excimer laser
[NASA-TM-88937] p 218 N87-23304
- Microwave characterization and modeling of GaAs/AlGaAs heterojunction bipolar transistors
[NASA-TM-100150] p 117 N87-26265
- Design considerations for a GaAs nipi doping superlattice solar cell p 196 N87-26422
- A V-grooved AlGaAs/GaAs passivated PN junction
[NASA-TM-100138] p 218 N87-27541
- A comparative study of the influence of buoyancy driven fluid flow on GaAs crystal growth p 219 N87-28741
- GAS ANALYSIS**
- In-situ analysis of hydrazine decomposition products
[AIAA PAPER 87-2122] p 54 A87-50198
- In-situ analysis of hydrazine decomposition products
[NASA-TM-89916] p 65 N87-23693
- GAS ATOMIZATION**
- Dendritic microstructure in argon atomized superalloy powders p 83 A87-24119
- GAS BEARINGS**
- Composition optimization of chromium carbide based solid lubricant coatings for foil gas bearings at temperatures to 650 C
[NASA-CR-179649] p 105 N87-26233
- GAS DENSITY**
- Resistojet plume and induced environment analysis
[NASA-TM-88957] p 66 N87-24536
- GAS DISCHARGES**
- Microwave electrothermal thruster performance in helium gas p 49 A87-31281
- GAS DYNAMICS**
- Particle cloud kinetics in microgravity
[AIAA PAPER 87-0577] p 107 A87-22716
- The near field behavior of turbulent gas jets in a long confinement p 135 A87-28976
- Preliminary design of turbopumps and related machinery
[NASA-RP-1170] p 11 N87-17665
- GAS FLOW**
- Gas particle radiator p 141 A87-45646
- GAS GENERATORS**
- A parametric study of a gas-generator air turbo ramjet (ATR)
[AIAA PAPER 86-1681] p 20 A87-41156
- In-situ analysis of hydrazine decomposition products
[AIAA PAPER 87-2122] p 54 A87-50198
- In-situ analysis of hydrazine decomposition products
[NASA-TM-89916] p 65 N87-23693
- GAS JETS**
- The near field behavior of turbulent gas jets in a long confinement p 135 A87-28976
- GAS MIXTURES**
- Ignition delay times of cyclopentene oxygen argon mixtures p 76 A87-12602
- A two-dimensional numerical study of the flow inside the combustion chamber of a motored rotary engine
[SAE PAPER 860615] p 161 A87-28624
- GAS PATH ANALYSIS**
- Ceramic high pressure gas path seal
[NASA-CR-180813] p 31 N87-26914
- GAS TEMPERATURE**
- Further development of the dynamic gas temperature measurement system. Volume 1: Technical efforts
[NASA-CR-179513-VOL-1] p 157 N87-19686
- GAS TURBINE ENGINES**
- An overview of the small engine component technology (SECT) studies --- commuter, rotorcraft, cruise missile and auxiliary power applications in year 2000
[AIAA PAPER 86-1542] p 19 A87-17993
- Fabrication and quality assurance processes for superhybrid composite fan blades p 72 A87-19123
- Soot loading in a generic gas turbine combustor
[AIAA PAPER 87-0297] p 19 A87-22544
- A computerized test system for thermal-mechanical fatigue crack growth p 153 A87-23899
- Comparison of calculated and experimental cascade performance for controlled-diffusion compressor stator blading
[ASME PAPER 86-GT-35] p 19 A87-25394
- Thin-film temperature sensors for gas turbine engines Problems and prospects p 153 A87-26109
- Prediction of the structure of fuel sprays in cylindrical combustion chambers p 20 A87-31277
- Optimization and analysis of gas turbine engine blades
[AIAA PAPER 87-0827] p 201 A87-33614
- Effects of multiple rows and noncircular orifices on dilution jet mixing p 138 A87-39805
- Advanced technology payoffs for future small propulsion systems p 21 A87-47081
- A technology development summary for the AGT101 advanced gas turbine program
[SAE PAPER 870466] p 163 A87-48790

- The Advanced Turbine Technology Applications Program (ATTAP)
 [SAE PAPER 870467] p 163 A87-48791
 Thermal-mechanical fatigue crack growth in B-1900-HF p 86 A87-49570
 Liner cooling research at NASA Lewis Research Center for gas turbine combustion chambers
 [AIAA PAPER 87-1828] p 22 A87-50189
 Hot section viewing system
 [NASA-CR-174773] p 155 N87-11144
 Evaluation results of the 700 deg C Chinese strain gages p 155 N87-11189
 Coating life prediction p 99 N87-11194
 Aerothermal modeling program, phase 2 p 24 N87-11200
 STAEBL: Structural tailoring of engine blades, phase 2 p 24 N87-11731
 Advanced Gas Turbine (AGT) Technology Project
 [NASA-CR-179484] p 164 N87-11995
 Scaled centrifugal compressor program
 [NASA-CR-174912] p 26 N87-14349
 Jet engine simulation with water ingestion through compressor
 [NASA-CR-179549] p 1 N87-15932
 Transition mixing study
 [NASA-CR-175062] p 27 N87-16830
 Combustion noise from gas turbine aircraft engines measurement of far-field levels
 [NASA-TM-88971] p 211 N87-17480
 Experimental evaluation of a translating nozzle sidewall radial turbine
 [NASA-TM-88963] p 27 N87-17701
 Creep fatigue life prediction for engine hot section materials (isotropic)
 [NASA-CR-174844] p 182 N87-18117
 Combustion research in the Internal Fluid Mechanics Division p 79 N87-20268
 Advanced composite combustor structural concepts program
 [NASA-CR-174733] p 74 N87-20387
 Nonisothermal elasto-visco-plastic response of shell-type structures p 185 N87-22796
 Fiber reinforced superalloys
 [NASA-TM-89865] p 75 N87-22811
 Life prediction and constitutive models for engine hot section anisotropic materials
 [NASA-CR-179594] p 29 N87-23622
 Liner cooling research at NASA Lewis Research Center
 [NASA-TM-100107] p 29 N87-23624
 Summary of investigations of engine response to distorted inlet conditions p 30 N87-24477
 Advanced Gas Turbine (AGT) Technology Development Project
 [NASA-CR-180818] p 222 N87-30225
- GAS TURBINES**
 Tribology of selected ceramics at temperatures to 900 C p 94 A87-12954
 Turbine airfoil deposition models p 24 N87-11191
 Mechanical behavior of thermal barrier coatings for gas turbine blades p 24 N87-11196
 Creep fatigue life prediction for engine hot section materials (isotropic): Two year update p 171 N87-11213
 Turbine airfoil gas side heat transfer p 144 N87-11219
 Assessment of a 3-D boundary layer code to predict heat transfer and flow losses in a turbine p 145 N87-11224
 Component testing of a ground based gas turbine steam cooled rich-burn primary zone combustor for emissions control of nitrogenous fuels
 [NASA-TM-88873] p 191 N87-11345
 Detonation wave compression in gas turbines
 [NASA-CR-179557] p 25 N87-13443
 Creep fatigue life prediction for engine hot section materials (ISOTROPIC)
 [NASA-CR-179550] p 181 N87-15491
 Measurement of heat transfer and pressure drop in rectangular channels with turbulence promoters
 [NASA-CR-4015] p 146 N87-17003
 Numerical calculations of turbulent reacting flow in a gas-turbine combustor
 [NASA-TM-89842] p 1 N87-20171
 Laser anemometry techniques for turbine applications
 [NASA-TM-88953] p 158 N87-22959
 Computation of full-coverage film-cooled airfoil temperatures by two methods and comparison with high heat flux data
 [NASA-TM-88931] p 150 N87-23934
 Compound cycle engine for helicopter application
 [NASA-CR-175110] p 31 N87-25323
- GASEOUS FUELS**
 Fuel-air mixing and combustion in a two-dimensional Wankel engine
 [SAE PAPER 870408] p 163 A87-48783

GASES

- Agreement between experimental and theoretical effects of nitrogen gas flowrate on liquid jet atomization
 [AIAA PAPER 87-2138] p 141 A87-45427
 Agreement between experimental and theoretical effects of nitrogen gas flowrate on liquid jet atomization
 [NASA-TM-89821] p 156 N87-19684

GATES (CIRCUITS)

- Optically controlled GaAs dual-gate MESFET and permeable base transistors
 [NASA-TM-88823] p 123 N87-10232
 The 20 GHz power GaAs FET development
 [NASA-CR-179546] p 124 N87-16972

GAUGE INVARIANCE

- Noncommutative-geometry model for closed bosonic strings p 207 A87-37542

GAUSS EQUATION

- On self-preserving, variable-density, turbulent free jets p 130 A87-10920

GEAR TEETH

- New generation methods for spur, helical, and spiral-bevel gears p 164 A87-53420
 New generation methods for spur, helical, and spiral-bevel gears
 [NASA-TM-88862] p 165 N87-15466
 Expansion of epicyclic gear dynamic analysis program
 [NASA-CR-179563] p 166 N87-19723
 Flexibility effects on tooth contact location in spiral bevel gear transmissions
 [NASA-CR-4055] p 166 N87-20552
 Gear tooth stress measurements on the UH-60A helicopter transmission
 [NASA-TP-2698] p 167 N87-22235
 Computer aided design and analysis of gear tooth geometry
 [NASA-CR-179611] p 168 N87-23969
 A simplified computer solution for the flexibility matrix of contacting teeth for spiral bevel gears
 [NASA-CR-179620] p 168 N87-23977
 Automated inspection and precision grinding of spiral bevel gears
 [NASA-CR-4083] p 169 N87-25578
 Analysis of the vibratory excitation arising from spiral bevel gears
 [NASA-CR-4081] p 169 N87-25579
 Generation of spiral bevel gears with conjugate tooth surfaces and tooth contact analysis
 [NASA-CR-4088] p 169 N87-26356
 An investigation of the dynamic response of spur gear teeth with moving loads
 [NASA-CR-179643] p 170 N87-29840
 Helical gears with circular arc teeth: Generation, geometry, precision and adjustment to errors, computer aided simulation of conditions of meshing and bearing contact
 [NASA-CR-4089] p 170 N87-29846

GEARS

- New generation methods for spur, helical, and spiral-bevel gears p 164 A87-53420
 Gear mesh compliance modeling p 164 A87-53422
 New generation methods for spur, helical, and spiral-bevel gears
 [NASA-TM-88862] p 165 N87-15466
 Common problems and pitfalls in gear design
 [NASA-TM-88858] p 165 N87-17033
 Gear mesh compliance modeling
 [NASA-TM-88843] p 166 N87-18092
 Predicted effect of dynamic load on pitting fatigue life for low-contact-ratio spur gears
 [NASA-TP-2610] p 166 N87-18095
 Cryogenic gear technology for an orbital transfer vehicle engine and tester design
 [NASA-CR-175102] p 110 N87-19539
 A simplified computer solution for the flexibility matrix of contacting teeth for spiral bevel gears
 [NASA-CR-179620] p 168 N87-23977
 A computer solution for the dynamic load, lubricant film thickness and surface temperatures in spiral bevel gears
 [NASA-CR-4077] p 169 N87-26358
 The design and analysis of single flank transmission error tester for loaded gears
 [NASA-CR-179621] p 169 N87-27197
 Advanced Prop-fan Engine Technology (APET) single- and counter-rotation gearbox/pitch change mechanism
 [NASA-CR-168114-VOL-1] p 32 N87-28552
 Advanced Propfan Engine Technology (APET) and single-rotation gearbox/pitch change mechanism
 [NASA-CR-168113] p 32 N87-28553
 Advanced Prop-fan Engine Technology (APET) single- and counter-rotation gearbox/pitch change mechanism
 [NASA-CR-168114-VOL-2] p 33 N87-28556
 Profile modification to minimize spur gear dynamic loading
 [NASA-TM-89901] p 170 N87-28918

- Helical gears with circular arc teeth: Generation, geometry, precision and adjustment to errors, computer aided simulation of conditions of meshing and bearing contact
 [NASA-CR-4089] p 170 N87-29846

GELS

- Sol-Gel synthesis of MgO-SiO₂ glass compositions having stable liquid-liquid immiscibility
 [NASA-TM-89905] p 103 N87-23750

GENERAL AVIATION AIRCRAFT

- Application of propan propulsion to general aviation
 [AIAA PAPER 86-2698] p 18 A87-17934
 Advanced technology payoffs for future small propulsion systems p 21 A87-47081
 Advanced liquid-cooled, turbocharged and intercooled stratified charge rotary engines for aircraft
 [SAE PAPER 871039] p 22 A87-48766

GEOMETRICAL THEORY OF DIFFRACTION

- Radar cross section of an open-ended circular waveguide Calculation of second-order diffraction terms p 112 A87-31626
 RCS of a coated circular waveguide terminated by a perfect conductor p 112 A87-42536

GEOMETRY

- Generation of spiral bevel gears with conjugate tooth surfaces and tooth contact analysis
 [NASA-CR-4088] p 169 N87-26356
 3-D inelastic analysis methods for hot section components. Volume 2: Advanced special functions models
 [NASA-CR-179517] p 186 N87-27267

GEOSYNCHRONOUS ORBITS

- Low power arcjet life issues
 [AIAA PAPER 87-1059] p 50 A87-39635
 An advanced geostationary communications platform p 112 A87-43165
 The use of satellites in non-geostationary orbits for unloading geostationary communication satellite traffic peaks. Volume 1: Executive summary
 [NASA-CR-179597-VOL-1] p 117 N87-21212
 The use of satellites in non-geostationary orbits for unloading geostationary communication satellite traffic peaks. Volume 2: Technical report
 [NASA-CR-179597-VOL-2] p 117 N87-21213
 Regenerative fuel cell study for satellites in GEO orbit
 [NASA-CR-179609] p 198 N87-27324

GIMBALS

- Effect of gimbal friction modelling technique on control stability and performance for Centaur upper stage
 [AIAA PAPER 87-2455] p 38 A87-50501
 Effect of Gimbal friction modeling technique on control stability and performance for Centaur upper-stage
 [NASA-TM-89894] p 39 N87-22755

GLASS

- Structure-to-property relationships in addition cured polymers. II - Resin Tg and composite initial mechanical properties of norbornenyl cured polyimide resins p 96 A87-38638
 Annealing of electron damage in mid-IR transmitting fluoride glass p 99 A87-53652
 Sol-Gel synthesis of MgO-SiO₂ glass compositions having stable liquid-liquid immiscibility
 [NASA-TM-89905] p 103 N87-23750

GLASS FIBER REINFORCED PLASTICS

- Acousto-ultrasonic input-output characterization of unidirectional fiber composite plate by SH waves
 [NASA-CR-4087] p 173 N87-26361

GLASS FIBERS

- Modes of vibration on square fiberglass epoxy composite thick plate
 [NASA-CR-4018] p 171 N87-13779
 Ultrasonic determination of the elastic constants of the stiffness matrix for unidirectional fiberglass epoxy composites
 [NASA-CR-4034] p 171 N87-13781

GLAZES

- The effect of laser glazing on life of ZrO₂ TBCs in cyclic burner rig tests
 [NASA-TM-88821] p 89 N87-14487

GLOW DISCHARGES

- Ion plated gold films: Properties, tribological behavior and performance
 [NASA-TM-88977] p 110 N87-17937

GOLD COATINGS

- Ion plated gold films: Properties, tribological behavior and performance
 [NASA-TM-88977] p 110 N87-17937

GRADIENTS

- Profile modification to minimize spur gear dynamic loading
 [NASA-TM-89901] p 170 N87-28918

GRAIN BOUNDARIES

- Grain boundary oxidation and fatigue crack growth at elevated temperatures p 81 A87-19368
 Processing-structure characterization of rheocast IN-100 superalloy p 82 A87-24116

- Defects in nickel-base superalloys p 86 A87-49790
- Grain boundary oxidation and fatigue crack growth at elevated temperatures [NASA-CR-179529] p 88 N87-11873
- High temperature monotonic and cyclic deformation in a directionally solidified nickel-base superalloy [NASA-CR-175101] p 90 N87-15303
- SSME single crystal turbine blade dynamics [NASA-CR-179644] p 186 N87-26384
- GRAIN SIZE**
- Ultrasonic verification of microstructural changes due to heat treatment p 208 A87-10772
- Processing-structure characterization of rheocast IN-100 superalloy p 82 A87-24116
- Effect of composition and grain size on slow plastic flow properties of NiAl between 1200 and 1400 K p 84 A87-36251
- GRAPHITE**
- Anticorrelation of Shubnikov-deHaas amplitudes and negative magnetoresistance magnitudes in intercalated pitch based graphite fibers p 217 A87-28295
- Thermal expansion behavior of graphite/glass and graphite/magnesium p 72 A87-38615
- Structure-to-property relationships in addition cured polymers. II - Resin Tg and composite initial mechanical properties of norbornenyl cured polyimide resins p 96 A87-38638
- Effects of milling brominated P-100 graphite fibers p 97 A87-41078
- On the effect of the $Fe(2+)/Fe(3+)$ redox couple on oxidation of carbon in hot H_3PO_4 p 78 A87-42677
- Microstructure-derived macroscopic residual resistance of brominated graphite fibers p 97 A87-48324
- Simultaneous electrical resistivity and mass uptake measurements in bromine intercalated fibers [NASA-TM-88900] p 70 N87-11841
- Thermal conductivity of pristine and brominated P-100 fibers [NASA-TM-88863] p 99 N87-11893
- Solid lubrication design methodology, phase 2 [NASA-CR-175114] p 221 N87-18470
- Styrene-terminated polysulfone oligomers as matrix material for graphite reinforced composites: An initial study [NASA-TM-89846] p 74 N87-21043
- Stability of bromine, iodine monochloride, copper (II) chloride, and nickel (II) chloride intercalated pitch-based graphite fibers [NASA-TM-89904] p 103 N87-24563
- Comparison of the tribological properties of fluorinated cokes and graphites [NASA-TM-100170] p 106 N87-29679
- GRAPHITE-EPOXY COMPOSITES**
- Assessment of simplified composite micromechanics using three-dimensional finite-element analysis p 72 A87-19121
- A heater made from graphite composite material for potential deicing application [AIAA PAPER 87-0025] p 17 A87-24905
- Mechanical and electrical properties of graphite fiber-epoxy composites made from pristine and bromine intercalated fibers p 73 A87-49799
- A heater made from graphite composite material for potential deicing application [NASA-TM-88888] p 17 N87-12559
- Design of an advanced wood composite rotor and development of wood composite blade technology [NASA-CR-174713] p 73 N87-17861
- Dynamic response and stability of a composite prop-fan model [NASA-CR-179528] p 28 N87-21956
- Dynamic response of two composite prop-fan models on a nacelle/wing/fuselage half model [NASA-CR-179589] p 18 N87-23615
- GRAPHITE-POLYIMIDE COMPOSITES**
- Specimen geometry effects on graphite/PMR-15 composites during thermo-oxidative aging p 71 A87-13145
- Counterface effects on the tribological properties of polyimide composites p 95 A87-27625
- Corrosion of graphite composites in phosphoric acid fuel cells p 72 A87-42684
- Styrene-terminated polysulfone oligomers as matrix material for graphite reinforced composites - An initial study p 98 A87-49370
- GRAPHITIZATION**
- Effects of graphitization on the environmental stability of brominated pitch-based fibers [NASA-TM-88899] p 100 N87-12679
- Effects of sequential treatment with fluorine and bromine on graphite fibers [NASA-TM-100106] p 104 N87-24574
- Synthesis, physical and chemical properties, and potential applications of graphite fluoride fibers [NASA-TM-100156] p 105 N87-26232

- GRAVITATIONAL EFFECTS**
- Gravitational effects on the structure and propagation of premixed flames [IAF PAPER 86-279] p 76 A87-15983
- Modeling free convective gravitational effects in chemical vapor deposition [AIAA PAPER 87-0313] p 133 A87-22552
- Gravitational macrosegregation in binary Pb-Sn alloy ingots [NASA-TM-89885] p 109 N87-24579
- A comparative study of the influence of buoyancy driven fluid flow on GaAs crystal growth p 219 N87-28741
- GREEN'S FUNCTIONS**
- Elastic interaction of a crack with a microcrack array. I - Formulation of the problem and general form of the solution. II - Elastic solution for two crack configurations (piecewise constant and linear approximations) p 178 A87-36926
- GRINDING (COMMINUTION)**
- Particle-size reduction of Si_3N_4 powder with Si_3N_4 milling hardware p 94 A87-12936
- GRINDING (MATERIAL REMOVAL)**
- Effects of surface removal on rolling-element fatigue [NASA-TM-88871] p 166 N87-18820
- GRIT**
- Effect of abrasive grit size on wear of manganese-zinc ferrite under three-body abrasion [NASA-TM-89879] p 104 N87-24566
- GROOVES**
- A V-grooved AlGaAs/GaAs passivated PN junction [NASA-TM-100138] p 218 N87-27541
- GROUND STATIONS**
- A photovoltaic power system and a low-power satellite earth station for Indonesia p 189 A87-19859
- GROUND TESTS**
- Modeling of environmentally induced transients within satellites [AIAA PAPER 85-0387] p 42 A87-41611
- Outdoor test stand performance of a convertible engine with variable inlet guide vanes for advanced rotorcraft propulsion [NASA-TM-88939] p 26 N87-16825
- Research opportunities in microgravity science and applications during shuttle hiatus [NASA-TM-88964] p 108 N87-16917
- Applications and requirements for real-time simulators in ground-test facilities [NASA-TP-2672] p 204 N87-23202
- Ground-based plasma contractor characterization [NASA-TM-100194] p 215 N87-28423
- GROWTH**
- Spatially growing disturbances in a two-stream, coplanar jet [NASA-TM-88949] p 10 N87-16799
- GUIDANCE SENSORS**
- Design, implementation and investigation of an image guide-based optical flip-flop array [NASA-CR-181382] p 213 N87-30180
- GUIDE VANES**
- Detailed flow surveys of turning vanes designed for a 0.1-scale model of NASA Lewis Research Center's proposed altitude wind tunnel [NASA-TP-2680] p 36 N87-20295
- Effect of variable inlet guide vanes on the operating characteristics of a tilt nacelle inlet/powerd fan model [NASA-TM-88983] p 14 N87-27628
- GUSTS**
- Influence of airfoil mean loading on convected gust interaction noise p 208 A87-13587
- H**
- HALL EFFECT**
- Compensation in epitaxial cubic SiC films p 216 A87-15071
- HARDNESS**
- Hardness of CaF_2 and BaF_2 solid lubricants at 25 to 670 deg C [NASA-TM-88979] p 102 N87-18670
- HARMONIC OSCILLATION**
- The impact damped harmonic oscillator in free decay [NASA-TM-89897] p 168 N87-23978
- HARMONICS**
- Cruise noise of counterrotation propeller at angle of attack in wind tunnel [NASA-TM-88869] p 210 N87-13252
- HAZARDS**
- Combustion of velcro in low gravity [NASA-TM-88970] p 102 N87-19518
- HEAT AFFECTED ZONE**
- The effect of electron beam welding on the creep rupture properties of a Nb-Zr-C alloy [NASA-TM-88892] p 88 N87-13513

- HEAT EXCHANGERS**
- Oxidizer heat exchangers for rocket engine operation in idle modes [AIAA PAPER 87-2117] p 52 A87-45418
- Low heat transfer oxidizer heat exchanger design and analysis [NASA-CR-179488] p 58 N87-15272
- Heat exchanger for electrothermal devices [NASA-CASE-LEW-14037-1] p 59 N87-16875
- High heat transfer oxidizer heat exchanger design and analysis --- RL10-2B engine [NASA-CR-179596] p 63 N87-22803
- HEAT FLUX**
- Experimental evaluation of heat transfer on a 1030:1 area ratio rocket nozzle [AIAA PAPER 87-2070] p 55 A87-52249
- Flame radiation p 78 N87-11204
- Conventionally cast and forged copper alloy for high-heat-flux thrust chambers [NASA-TP-2694] p 90 N87-16902
- Heat flux calibration facility capable of SSME conditions p 36 N87-22774
- Computation of full-coverage film-cooled airfoil temperatures by two methods and comparison with high heat flux data [NASA-TM-88931] p 150 N87-23934
- Experimental evaluation of heat transfer on a 1030:1 area ratio rocket nozzle [NASA-TP-2726] p 67 N87-25424
- HEAT PIPES**
- Heat pipe cooled rocket engines [AIAA PAPER 86-1567] p 48 A87-21516
- HEAT PUMPS**
- Feasibility analysis of reciprocating magnetic heat pumps [NASA-CR-180262] p 147 N87-19647
- HEAT RADIATORS**
- Solar dynamic space power system heat rejection p 47 A87-18175
- Liquid sheet radiator [AIAA PAPER 87-1525] p 140 A87-43048
- Measurement of heat transfer and pressure drop in rectangular channels with turbulence promoters [NASA-CR-4015] p 146 N87-17003
- Liquid sheet radiator [NASA-TM-89841] p 147 N87-18786
- High temperature radiator materials for applications in the low Earth orbital environment [NASA-TM-100190] p 93 N87-29662
- HEAT RESISTANT ALLOYS**
- Mechanical property anisotropy in superalloy EI-929 directionally solidified by an exothermic technique p 81 A87-11389
- Fiber-reinforced superalloy composites provide an added performance edge p 71 A87-12647
- The effects of tantalum on the microstructure of two polycrystalline nickel-base superalloys - B-1900 + Hf and MAR-M247 p 82 A87-24110
- Processing-structure characterization of rheocast IN-100 superalloy p 82 A87-24116
- Dendritic microstructure in argon atomized superalloy powders p 83 A87-24119
- Analysis of the solidified structure of rheocast and VADER processed nickel-base superalloy p 83 A87-28734
- Yielding and deformation behavior of the single crystal superalloy PWA 1480 p 84 A87-32040
- The sensitivity of mechanical properties of TFRS composites to variations in reaction zone size and properties --- Tungsten Fiber Reinforced Superalloys [AIAA PAPER 87-0757] p 72 A87-33577
- Heat's on to develop high-temperature materials p 85 A87-39897
- Understanding single-crystal superalloys p 85 A87-40928
- Application of single crystal superalloys for earth-to-orbit propulsion systems [AIAA PAPER 87-1976] p 85 A87-45336
- The characteristics of gamma-prime dislocation pairs in a nickel-base superalloy p 85 A87-46932
- The stability of lamellar gamma-gamma-prime structures --- nickel-base superalloy p 86 A87-48323
- Effect of 15 MPa hydrogen on creep-rupture properties of iron-base superalloys p 86 A87-49558
- Defects in nickel-base superalloys p 86 A87-49790
- Thermal stability of the nickel-base superalloy B-1900 + Hf with tantalum variations p 87 A87-51289
- The mathematical modeling of rapid solidification processing [NASA-CR-179551] p 88 N87-13514
- The cyclic stress-strain behavior of PWA 1480 at 650 deg C [NASA-TM-87311] p 89 N87-14483
- A study of the microstructure of a rapidly solidified nickel-base superalloy modified with boron [NASA-CR-179553] p 89 N87-14486

- The effect of Cr, Co, Al, Mo and Ta on a series of cast Ni-base superalloys on the stability of an aluminate coating during cyclic oxidation in Mach 0.3 burner rig
[NASA-TM-88840] p 89 N87-14488
- Elevated temperature tension, compression and creep-rupture behavior of (001)-oriented single crystal superalloy PWA 1480
[NASA-TM-88950] p 90 N87-17882
- A constitutive model for the inelastic multiaxial cyclic response of a nickel base superalloy Rene 80
[NASA-CR-3998] p 182 N87-18852
- Advanced composite combustor structural concepts program
[NASA-CR-174733] p 74 N87-20387
- Bithermal low-cycle fatigue behavior of a NiCoCrAlY-coated single crystal superalloy
[NASA-TM-89831] p 91 N87-20408
- Superalloy resources: Supply and availability
[NASA-TM-89866] p 91 N87-21077
- Application of single crystal superalloys for Earth-to-orbit propulsion systems
[NASA-TM-89877] p 91 N87-22034
- Progress on thin-film sensors for space propulsion technology
p 158 N87-22772
- Fatigue damage interaction behavior of PWA 1480
p 92 N87-22777
- Fiber reinforced superalloys
[NASA-TM-89865] p 75 N87-22811
- Life prediction and constitutive models for engine hot section anisotropic materials
[NASA-CR-179594] p 29 N87-23622
- A study of reduced chromium content in a nickel-base superalloy via element substitution and rapid solidification processing
[NASA-CR-179631] p 92 N87-25456
- Observations of directional gamma prime coarsening during engine operation
[NASA-TM-100105] p 92 N87-25459
- Toward improved durability in advanced combustors and turbines: Progress in the prediction of thermomechanical loads
[NASA-TM-88932] p 32 N87-28551
- Creep-rupture behavior of a developmental cast-iron-base alloy for use up to 800 deg C
[NASA-TM-100167] p 93 N87-28641
- Heat treatment for superalloy
[NASA-CASE-LEW-14262-1] p 93 N87-28647
- HEAT SHIELDING**
- Free jet feasibility study of a thermal acoustic shield concept for AST/VCE application: Dual stream nozzles
[NASA-CR-3867] p 210 N87-10752
- HEAT STORAGE**
- Selection of high temperature thermal energy storage materials for advanced solar dynamic space power systems
[NASA-TM-89886] p 149 N87-22174
- Impact of thermal energy storage properties on solar dynamic space power conversion system mass
[NASA-TM-89909] p 63 N87-22802
- Fluoride salts and container materials for thermal energy storage applications in the temperature range 973 to 1400 K
[NASA-TM-89913] p 195 N87-24026
- HEAT TRANSFER**
- Endwall heat transfer in the junction region of a circular cylinder normal to a flat plate at 30 and 60 degrees from stagnation point of the cylinder
[AIAA PAPER 87-0077] p 132 A87-22398
- Unsteady heat transfer and direct comparison to steady-state measurements in a rotor-wake experiment
p 136 A87-30720
- Two-phase flows and heat transfer within systems with ambient pressure above the thermodynamic critical pressure
p 136 A87-30728
- Efficient numerical simulation of an electrothermal de-icer pad
[AIAA PAPER 87-0024] p 137 A87-32190
- Opportunities and challenges in heat transfer - From the perspective of the government laboratory
p 109 A87-48313
- Heat transfer and fluid mechanics measurements in transitional boundary layers on convex-curved surfaces
[ASME PAPER 85-MT-60] p 143 A87-48726
- Experimental evaluation of heat transfer on a 1030:1 area ratio rocket nozzle
[AIAA PAPER 87-2070] p 55 A87-52249
- Host turbine heat transfer overview
p 144 N87-11184
- Turbine airfoil gas side heat transfer
p 144 N87-11219
- Assessment of a 3-D boundary layer code to predict heat transfer and flow losses in a turbine
p 145 N87-11224
- Progress of Stirling cycle analysis and loss mechanism characterization
[NASA-TM-88891] p 220 N87-13359

- Enhanced heat transfer combustor technology, subtasks 1 and 2, last C.1
[NASA-CR-179541] p 56 N87-13486
- Turbine vane external heat transfer. Volume 2. Numerical solutions of the Navier-Stokes equations for two- and three-dimensional turbine cascades with heat transfer
[NASA-CR-174828] p 145 N87-13661
- Low heat transfer oxidizer heat exchanger design and analysis
[NASA-CR-179488] p 58 N87-15272
- A general method for unsteady stagnation region heat transfer and results for model turbine flows
[NASA-TM-88903] p 146 N87-17002
- Measurement of heat transfer and pressure drop in rectangular channels with turbulence promoters
[NASA-CR-4015] p 146 N87-17003
- Performance and efficiency evaluation and heat release study of an outboard Marine Corporation Rotary Combustion Engine
[NASA-TM-88833] p 28 N87-20282
- Use of a liquid-crystal, heater-element composite for quantitative, high-resolution heat transfer coefficients on a turbine airfoil, including turbulence and surface roughness effects
[NASA-TM-87355] p 158 N87-22181
- Regenerative fuel cell study for satellites in GEO orbit
[NASA-TM-89914] p 194 N87-22310
- Progress in the prediction of unsteady heat transfer on turbine blades
p 149 N87-22769
- Nonlinear heat transfer and structural analyses of SSME turbine blades
p 184 N87-22779
- High heat transfer oxidizer heat exchanger design and analysis -- RL10-2B engine
[NASA-CR-179596] p 63 N87-22803
- Experimental evaluation of heat transfer on a 1030:1 area ratio rocket nozzle
[NASA-TP-2726] p 67 N87-25424
- Turbulence modeling and surface heat transfer in a stagnation flow region
[NASA-TM-100132] p 151 N87-26302
- Application of turbulence modeling to predict surface heat transfer in stagnation flow region of circular cylinder
[NASA-TP-2758] p 151 N87-27161
- Toward improved durability in advanced combustors and turbines: Progress in the prediction of thermomechanical loads
[NASA-TM-88932] p 32 N87-28551
- HEAT TRANSFER COEFFICIENTS**
- Heat transfer in the stagnation region of the junction of a circular cylinder perpendicular to a flat plate
p 131 A87-13019
- Effect of a rotor wake on the local heat transfer on the forward half of a circular cylinder
p 136 A87-30721
- Local heat transfer augmentation in channels with two opposite ribbed surfaces
p 136 A87-30732
- Volume-energy parameters for heat transfer to supercritical fluids
p 137 A87-32326
- Rotational effects on impingement cooling
p 141 A87-45838
- Estimation of instantaneous heat transfer coefficients for a direct-injection stratified-charge rotary engine
[SAE PAPER 870444] p 163 A87-48787
- Use of a liquid-crystal, heater-element composite for quantitative, high-resolution heat transfer coefficients on a turbine airfoil, including turbulence and surface roughness effects
[NASA-TM-87355] p 158 N87-22181
- Computation of full-coverage film-cooled airfoil temperatures by two methods and comparison with high heat flux data
[NASA-TM-88931] p 150 N87-23934
- HEAT TREATMENT**
- Ultrasonic verification of microstructural changes due to heat treatment
p 208 A87-10772
- Specimen geometry effects on graphite/PMR-15 composites during thermo-oxidative aging
p 71 A87-13145
- The characteristics of gamma-prime dislocation pairs in a nickel-base superalloy
p 85 A87-46932
- Effect of heat treatment on the fracture behaviour of directionally solidified (gamma/gamma-prime)-alpha alloy
p 86 A87-47932
- Heat treatment for superalloy
[NASA-CASE-LEW-14262-1] p 93 N87-28647
- Method of preparing fiber reinforced ceramic material
[NASA-CASE-LEW-14392-1] p 106 N87-28656
- HEATERS**
- A heater made from graphite composite material for potential deicing application
[AIAA PAPER 87-0025] p 17 A87-24905
- A heater made from graphite composite material for potential deicing application
[NASA-TM-88888] p 17 N87-12559

HELICAL FLOW

- Numerical simulation of transonic propeller flow using a three-dimensional small disturbance code employing novel helical coordinates
[AIAA PAPER 87-1162] p 5 A87-42107
- Numerical simulation of transonic propeller flow using a 3-dimensional small disturbance code employing novel helical coordinates
[NASA-TM-89826] p 12 N87-19350
- HELICOPTER CONTROL**
- A rotorcraft flight/propulsion control integration study
[NASA-CR-179574] p 18 N87-24457
- HELICOPTER ENGINES**
- Compound cycle engine program
p 23 A87-53428
- Compound cycle engine program
[NASA-TM-88879] p 25 N87-11790
- Compound cycle engine for helicopter application
[NASA-CR-175110] p 31 N87-25323
- Ceramic high pressure gas path seal
[NASA-CR-180813] p 31 N87-26914
- HELICOPTER PERFORMANCE**
- The 3600 hp split-torque helicopter transmission
[NASA-CR-174932] p 25 N87-11788
- HELICOPTERS**
- New generation methods for spur, helical, and spiral-bevel gears
p 164 A87-53420
- Compound cycle engine program
p 23 A87-53428
- Testing of UH-60A helicopter transmission in NASA Lewis 2240-kW (3000-hp) facility
[NASA-TP-2626] p 164 N87-10391
- The 3600 hp split-torque helicopter transmission
[NASA-CR-174932] p 25 N87-11788
- Compound cycle engine program
[NASA-TM-88879] p 25 N87-11790
- New generation methods for spur, helical, and spiral-bevel gears
[NASA-TM-88862] p 165 N87-15466
- Vibration characteristics of OH-58A helicopter main rotor transmission
[NASA-TP-2705] p 167 N87-20555
- Helicopter transmission testing at NASA Lewis Research Center
[NASA-TM-89912] p 168 N87-22978
- HELIUM**
- Microwave electrothermal thruster performance in helium gas
p 49 A87-31281
- Preliminary study of niobium alloy contamination by transport through helium
[NASA-TM-88952] p 90 N87-17884
- HEPTANES**
- Velocity profiles in laminar diffusion flames
[NASA-TP-2596] p 147 N87-18035
- HETEROJUNCTION DEVICES**
- Microwave characterization and modeling of GaAs/AlGaAs heterojunction bipolar transistors
[NASA-TM-100150] p 117 N87-26265
- HETEROJUNCTIONS**
- Variable angle of incidence spectroscopic ellipsometry Application to GaAs-Al(x)Ga(1-x)As multiple heterostructures
p 216 A87-20519
- HEURISTIC METHODS**
- Mathematical programming formulations for satellite synthesis
[NASA-CR-181151] p 44 N87-25419
- HIGH ASPECT RATIO**
- A detailed description of the uncertainty analysis for High Area Ratio Rocket Nozzle tests at the NASA Lewis Research Center
[NASA-TM-100203] p 68 N87-28602
- HIGH ELECTRON MOBILITY TRANSISTORS**
- Microwave performance of an optically controlled AlGaAs/GaAs high electron mobility transistor and GaAs MESFET
[NASA-TM-88980] p 125 N87-17993
- HIGH ENERGY PROPELLANTS**
- An evaluation of metallized propellants based on vehicle performance
[AIAA PAPER 87-1773] p 53 A87-47003
- An evaluation of metallized propellants based on vehicle performance
[NASA-TM-100104] p 64 N87-22806
- HIGH FREQUENCIES**
- Space Station 20-kHz power management and distribution system
p 49 A87-36913
- 20 kHz Space Station power system
p 51 A87-40378
- Control considerations for high frequency, resonant, power processing equipment used in large systems
[NASA-TM-89926] p 64 N87-23690
- HIGH GAIN**
- Absolute gain measurement by the image method under mismatched condition
[NASA-TM-88924] p 124 N87-16968
- HIGH PRESSURE**
- Liquid fuel spray processes in high-pressure gas flow
p 131 A87-13843

- Ceramic high pressure gas path seal
[NASA-CR-180813] p 31 N87-26914
- Bonding Lexan and sapphire to form high-pressure, flame-resistant window
[NASA-TM-100188] p 159 N87-26880
- HIGH RESOLUTION**
A high resolution shock capturing scheme for high Mach number internal flow
[NASA-CR-179523] p 10 N87-16804
- HIGH REYNOLDS NUMBER**
An unconditionally-stable central differencing scheme for high Reynolds number flows
[AIAA PAPER 87-0060] p 133 A87-24912
- Coherent motion in excited free shear flows
[AIAA PAPER 85-0539] p 135 A87-30281
- HIGH SPEED**
High-speed propeller noise predictions - Effects of boundary conditions used in blade loading calculations
[AIAA PAPER 87-0525] p 208 A87-24978
- Measured noise of a scale model high speed propeller at simulated takeoff/approach conditions
[AIAA PAPER 87-0526] p 208 A87-31109
- High speed wind tunnel tests of the PTA aircraft --- Propan Test Assessment Program
[SAE PAPER 861744] p 4 A87-32619
- Euler analysis of the three-dimensional flow field of a high-speed propeller - Boundary condition effects
[ASME PAPER 87-GT-253] p 6 A87-48719
- High-speed propeller noise predictions: Effects of boundary conditions used in blade loading calculations
[NASA-TM-88913] p 210 N87-14957
- Measured noise of a scale model high speed propeller at simulated takeoff/approach conditions
[NASA-TM-88920] p 211 N87-16588
- Euler analysis of the three dimensional flow field of a high-speed propeller: Boundary condition effects
[NASA-TM-88955] p 10 N87-16798
- HIGH STRENGTH ALLOYS**
Thermal-mechanical fatigue crack growth in B-1900 + Hf
p 86 A87-49570
- HIGH TEMPERATURE**
Effects of silver and group II fluoride solid lubricant additions to plasma-sprayed chromium carbide coatings for foil gas bearings to 650 C
p 95 A87-22336
- Concentration of carbon dioxide by a high-temperature electrochemical membrane cell
p 77 A87-27400
- Elevated temperature strengthening of a melt spun austenitic steel by TiB₂
p 87 A87-51639
- Results of an interlaboratory fatigue test program conducted on alloy 800H at room and elevated temperatures
p 87 A87-54370
- High-temperature constitutive modeling
p 179 N87-11210
- On 3-D inelastic analysis methods for hot section components (base program)
[NASA-CR-175060] p 180 N87-12923
- A viscoplastic constitutive theory for metal matrix composites at high temperature
[NASA-CR-179530] p 180 N87-13790
- Estimation of high temperature low cycle fatigue on the basis of inelastic strain and strainrate
[NASA-TM-88841] p 89 N87-14489
- Conventionally cast and forged copper alloy for high-heat-flux thrust chambers
[NASA-TP-2694] p 90 N87-16902
- Elevated temperature tension, compression and creep-rupture behavior of (001)-oriented single crystal superalloy PWA 1480
[NASA-TM-88950] p 90 N87-17882
- Oxide-dispersion-strengthened turbine blades, volume 1
[NASA-CR-179537-VOL-1] p 90 N87-17883
- Addition of polymers from 1,4,5,8-tetrahydro-1,4,5,8-diepoxyanthracene and Bis-dienes: Processable resins for high temperature application
[NASA-TM-89838] p 103 N87-20426
- Selection of high temperature thermal energy storage materials for advanced solar dynamic space power systems
[NASA-TM-89886] p 149 N87-22174
- High temperature static strain gage alloy development program
[NASA-CR-174833] p 157 N87-22179
- Elevated temperature crack growth
[NASA-CR-179601] p 184 N87-22267
- On 3-D inelastic analysis methods for hot section components. Volume 1: Special finite element models
[NASA-CR-179494] p 185 N87-22996
- Advanced high temperature static strain sensor development
[NASA-CR-179520] p 158 N87-25552
- Optical strain measurement system development
[NASA-CR-179646] p 159 N87-26326
- Exposure time considerations in high temperature low cycle fatigue
[NASA-TM-88934] p 187 N87-28944
- High temperature radiator materials for applications in the low Earth orbital environment
[NASA-TM-100190] p 93 N87-29662
- Advanced Gas Turbine (AGT) Technology Development Project
[NASA-CR-180818] p 222 N87-30225
- HIGH TEMPERATURE ENVIRONMENTS**
Stress rupture and creep behavior of a low pressure plasma-sprayed NiCoCrAlY coating alloy in air and vacuum
p 85 A87-43396
- High-temperature effect of hydrogen on sintered alpha-silicon carbide
[NASA-TM-88819] p 100 N87-14518
- HIGH TEMPERATURE GASES**
The chemical shock tube as a tool for studying high-temperature chemical kinetics
p 157 N87-20279
- HIGH TEMPERATURE LUBRICANTS**
Experimental evaluation of chromium-carbide-based solid lubricant coatings for use to 760 C
[NASA-CR-180808] p 105 N87-27053
- HIGH TEMPERATURE TESTS**
Effects of temperature and hold times on low cycle fatigue of Astroloy
p 85 A87-38541
- Analysis of experimental shaft seal data for high-performance turbomachines - As for Space Shuttle main engines
p 162 A87-45846
- Slow crack growth in sintered silicon nitride
p 98 A87-48989
- The cyclic stress-strain behavior of PWA 1480 at 650 deg C
[NASA-TM-87311] p 89 N87-14483
- Optical strain measuring techniques for high temperature tensile testing
[NASA-CR-179637] p 159 N87-26327
- A high temperature fatigue and structures testing facility
[NASA-TM-100151] p 186 N87-26399
- HIGH VACUUM**
Vacuum chamber pressure effects on thrust measurements of low Reynolds number nozzles
p 45 A87-14976
- HIGH VOLTAGES**
Development of the VOLT-A Shuttle experiment --- Volt Operating Limit Tests
p 41 A87-19907
- Coaxial tube tether/transmission line for manned nuclear space power
[NASA-CASE-LEW-14338-1] p 55 N87-10174
- Coaxial tube array space transmission line characterization
[NASA-TM-89864] p 62 N87-22003
- A study of Schwarz converters for nuclear powered spacecraft
[NASA-TM-89911] p 128 N87-23903
- HODOGRAPHS**
Lewis inverse design code (LINDES): Users manual
[NASA-TP-2676] p 12 N87-20238
- HOLDERS**
Apparatus for mounting a field emission cathode
[NASA-CASE-LEW-14108-1] p 129 N87-28832
- HOLE GEOMETRY (MECHANICS)**
Flow visualization study of the effect of injection hole geometry on an inclined jet in crossflow
p 155 A87-45842
- HOLLOW CATHODES**
Three dimensional simulation of the operation of a hollow cathode electron emitter on the Shuttle orbiter
p 119 A87-14084
- Hollow cathodes as electron emitting plasma contactors
Theory and computer modeling
[AIAA PAPER 87-0569] p 214 A87-22712
- Plasma contactors for electrodynamic tethers
p 214 A87-31211
- Hollow cathode-based plasma contactor experiments for electrodynamic tether
[AIAA PAPER 87-0572] p 214 A87-32192
- Investigation of beam-plasma interactions
[NASA-CR-180579] p 215 N87-22508
- HOLOGRAPHIC INTERFEROMETRY**
Visualization of flows in a motored rotary combustion engine using holographic interferometry
[AIAA PAPER 86-1557] p 19 A87-21514
- Evaluation of diffuse-illumination holographic cinematography in a flutter cascade
[NASA-TP-2593] p 156 N87-13731
- Beam-modulation methods in quantitative and flow-visualization holographic interferometry
p 111 N87-21204
- HOLOGRAPHY**
Evaluation of diffuse-illumination holographic cinematography in a flutter cascade
[NASA-TP-2593] p 156 N87-13731
- HOMOJUNCTIONS**
Recent developments in indium phosphide space solar cell research
[NASA-TM-100139] p 68 N87-26141
- Near-optimum design of the InP homojunction solar cell
[NASA-TP-2692] p 197 N87-26443
- HONEYCOMB STRUCTURES**
Experimental evaluation of honeycomb/screen configurations and short contraction section for NASA Lewis Research Center's altitude wind tunnel
[NASA-TP-2692] p 36 N87-23662
- HORIZONTAL ORIENTATION**
Development and testing of vortex generators for small horizontal axis wind turbines
[NASA-CR-179514] p 193 N87-18922
- HORSEPOWER**
Contingency power for small turboshaft engines using water injection into turbine cooling air
[AIAA PAPER 87-1906] p 21 A87-45289
- Contingency power for small turboshaft engines using water injection into turbine cooling air
[NASA-TM-89817] p 28 N87-20280
- HOT CORROSION**
Corrosion of metals and alloys in sulfate melts at 750 C
p 81 A87-17997
- Reactions occurring during the sulfation of sodium chloride deposited on alumina substrates
p 76 A87-20223
- Mechanism of strength degradation for hot corrosion of alpha-SiC
p 95 A87-21470
- The formation of volatile corrosion products during the mixed oxidation-chlorination of cobalt at 650 C
p 82 A87-23848
- Experimental verification of corrosive vapor deposition rate theory in high velocity burner rigs
p 143 A87-49551
- Surface protection
p 88 N87-11182
- Experimental verification of vapor deposition model in Mach 0.3 burner rigs
p 88 N87-11192
- Effects of surface chemistry on hot corrosion life
p 88 N87-11193
- Coating life prediction
p 99 N87-11194
- Hot corrosion attack and strength degradation of SiC and Si(sub)3N(sub)4
[NASA-TM-89820] p 102 N87-20425
- HOT ISOSTATIC PRESSING**
Effects of temperature and hold times on low cycle fatigue of Astroloy
p 85 A87-38541
- Fabrication of cooled radial turbine rotor
[NASA-CR-179503] p 25 N87-11789
- HOT PRESSING**
Fracture toughness of Si₃N₄ measured with short bar chevron-notched specimens
p 96 A87-30621
- HOT SURFACES**
Prediction and rational correlation of thermophoretically reduced particle mass transfer to hot surfaces across laminar or turbulent forced-convection gas boundary layers
p 133 A87-23449
- Advances in 3-D Inelastic Analysis Methods for hot section components
[AIAA PAPER 87-0719] p 177 A87-33645
- Hot section viewing system
[NASA-CR-174773] p 155 N87-11144
- Creep fatigue life prediction for engine hot section materials (isotropic)
[NASA-CR-174844] p 182 N87-18117
- On 3-D inelastic analysis methods for hot section components. Volume 1: Special finite element models
[NASA-CR-179494] p 185 N87-22996
- HOT-WIRE ANEMOMETERS**
A critical analysis of transverse vorticity measurements in a large plane shear layer
p 143 A87-52049
- HOUSINGS**
Refrigerated dynamic seal to 6.9 MPa (1000 psi)
p 164 A87-50777
- The T55-L-712 turbine engine compressor housing refurbishment project
[NASA-CR-179624] p 92 N87-23729
- HUBS**
The hub wall boundary layer development and losses in an axial flow compressor rotor passage
p 139 A87-41665
- On optimal design for the blade-root/hub interface in jet engines
p 24 N87-11769
- Hub flexibility effects on propfan vibration
[NASA-TM-89900] p 186 N87-24722
- HYBRID PROPELLANT ROCKET ENGINES**
Analysis of quasi-hybrid solid rocket booster concepts for advanced earth-to-orbit vehicles
[AIAA PAPER 87-2082] p 55 A87-52250
- Analysis of quasi-hybrid solid rocket booster concepts for advanced earth-to-orbit vehicles
[NASA-TP-2751] p 67 N87-25425
- HYDRAULIC EQUIPMENT**
The 20th Aerospace Mechanics Symposium
[NASA-CP-2423-REV] p 181 N87-16321

HYDRAZINE ENGINES

- Performance characterization of a low power hydrazine arcjet
[AIAA PAPER 87-1057] p 50 A87-39634
Self-regulating heater application to Shuttle/Centaur hydrazine fuel line thermal control
[AIAA PAPER 87-1570] p 43 A87-43081
Propulsion recommendations for space station free flying platforms p 67 N87-26129

HYDRAZINES

- In-situ analysis of hydrazine decomposition products
[AIAA PAPER 87-2122] p 54 A87-50198
A design study of hydrazine and biowaste resistojets
[NASA-CR-179510] p 57 N87-14425
Arcjet starting reliability: A multistart test on hydrogen/nitrogen mixtures
[NASA-TM-89867] p 61 N87-21998
In-situ analysis of hydrazine decomposition products
[NASA-TM-89916] p 65 N87-23693

HYDROBROMIDES

- Theoretical performance of hydrogen-bromine rechargeable SPE fuel cell p 199 N87-29945

HYDROCARBON COMBUSTION

- Empirical modeling of soot formation in shock-tube pyrolysis of aromatic hydrocarbons p 76 A87-12599
Ignition delay times of cyclopentene oxygen argon mixtures p 76 A87-12602
Long-term deposit formation in aviation turbine fuel at elevated temperature p 106 A87-14986

HYDROCARBON FUELS

- Volume-energy parameters for heat transfer to supercritical fluids p 137 A87-32326
Systematic development of reduced reaction mechanisms for dynamic modeling p 77 A87-33987
The chemical shock tube as a tool for studying high-temperature chemical kinetics p 157 N87-20279
Thermal stability of distillate hydrocarbon fuels
[NASA-CR-181412] p 107 N87-29706

HYDROCARBONS

- Triptycene - A D(3h) C(62) hydrocarbon with three U-shaped cavities p 69 A87-53656

HYDRODYNAMICS

- Overview of the 1986 free-piston Stirling SP-100 activities at the NASA Lewis Research Center p 160 A87-18033
Thermohydrodynamic analysis for laminar lubricating films
[NASA-TM-88845] p 144 N87-11124
Preliminary design of turbopumps and related machinery
[NASA-RP-1170] p 11 N87-17665

HYDROGEN

- Low power dc arcjet operation with hydrogen/nitrogen/ammonia mixtures
[AIAA PAPER 87-1948] p 53 A87-48575
Effect of 15 MPa hydrogen on creep-rupture properties of iron-base superalloys p 86 A87-49558
Hydrogen-air ignition torch
[NASA-TM-88882] p 38 N87-13470
Effect of water on hydrogen permeability
[NASA-TM-88898] p 221 N87-16664
Low power DC arcjet operation with hydrogen/nitrogen/ammonia mixtures
[NASA-TM-89876] p 64 N87-22804
Hydrogen oxidation mechanism with applications to (1) the chaperon efficiency of carbon dioxide and (2) vitiated air testing
[NASA-TM-100186] p 80 N87-28628

HYDROGEN CHLORIDES

- Reaction of iron with hydrogen chloride-oxygen mixtures at 550 C p 83 A87-32001

HYDROGEN EMBRITTLEMENT

- High-temperature effect of hydrogen on sintered alpha-silicon carbide
[NASA-TM-88819] p 100 N87-14518

HYDROGEN FUELS

- Arcjet starting reliability - A multistart test on hydrogen/nitrogen mixtures
[AIAA PAPER 87-1061] p 51 A87-41128

HYDROGEN OXYGEN ENGINES

- The noncavitating performance and life of a small vane-type positive displacement pump in liquid hydrogen
[AIAA PAPER 86-1438] p 46 A87-17994
Space station propulsion system technology
[NASA-TM-100108] p 66 N87-25422
Proven, long-life hydrogen/oxygen thrust chambers for space station propulsion p 68 N87-26133

HYDROGEN OXYGEN FUEL CELLS

- NASA Lewis evaluation of Regenerative Fuel Cell (RFC) systems p 123 N87-11073
Long range inhabited surface transportation system power source for the exploration of Mars (manned Mars mission) p 37 N87-17752
Regenerative fuel cell study for satellites in GEO orbit
[NASA-TM-89914] p 194 N87-22310

HYDROGENATION

- Rapid thermal annealing of Amorphous Hydrogenated Carbon (a-C:H) films
[NASA-TM-89859] p 218 N87-20821

HYDROSTATICS

- A fully coupled variable properties thermohydraulic model for a cryogenic hydrostatic journal bearing
[ASME PAPER 86-TRIB-55] p 161 A87-19536

HYPERSONIC FLOW

- Two- and three-dimensional viscous computations of a hypersonic inlet flow
[AIAA PAPER 87-0283] p 4 A87-31106
High angle of attack hypersonic aerodynamics
[AIAA PAPER 87-2548] p 7 A87-49101
Two- and three-dimensional viscous computations of a hypersonic inlet flow
[NASA-TM-88923] p 146 N87-15441
A high resolution shock capturing scheme for high Mach number internal flow
[NASA-CR-179523] p 10 N87-16804
Internal computational fluid mechanics on supercomputers for aerospace propulsion systems p 151 N87-26002

HYPERSONIC SPEED

- Reactivation study for NASA Lewis Research Center's Hypersonic Tunnel Facility
[AIAA PAPER 87-1886] p 34 A87-50190
Reactivation study for NASA Lewis Research Center's hypersonic tunnel facility
[NASA-TM-89918] p 36 N87-23664

HYPERSONIC VEHICLES

- Preliminary aerothermodynamic design method for hypersonic vehicles
[AIAA PAPER 87-2545] p 7 A87-49100

ICE

- An experimental study of the aerodynamics of a NACA 0012 airfoil with a simulated glaze ice accretion
[NASA-CR-179897] p 8 N87-11701

ICE FORMATION

- In-flight photogrammetric measurement of wing ice accretions
[AIAA PAPER 86-0483] p 15 A87-17995
Particle trajectory computer program for icing analysis of axisymmetric bodies - A progress report
[AIAA PAPER 87-0027] p 15 A87-22366
Navier Stokes solution of the flowfield over ice accretion shapes
[AIAA PAPER 87-0099] p 2 A87-22414
Numerical analysis of a NACA0012 airfoil with leading edge ice accretions
[AIAA PAPER 87-0101] p 2 A87-22415
In-flight measurement of ice growth on an airfoil using an array of ultrasonic transducers
[AIAA PAPER 87-0178] p 15 A87-22464
Experimental, water droplet impingement data on two-dimensional airfoils, axisymmetric inlet and Boeing 737-300 engine inlet
[AIAA PAPER 87-0097] p 17 A87-24918
Comparison of wet and dry growth in artificial and flight icing conditions p 16 A87-45635
Evaluation of icing drag coefficient correlations applied to ice propeller performance prediction
[SAE PAPER 871033] p 16 A87-48761
Flight test report of the NASA icing research airplane: Performance, stability, and control after flight through natural icing conditions p 34 N87-11797
Structural properties of impact ices accreted on aircraft structures
[NASA-CR-179580] p 182 N87-18121
Two-phase flow p 147 N87-20272
Icing of flow conditioners in a closed-loop wind tunnel
[NASA-TM-89824] p 13 N87-23591
New methods and materials for molding and casting ice formations
[NASA-TM-100126] p 16 N87-29470

IDEAL GAS

- Perfect gas effects in compressible rapid distortion theory p 136 A87-31176

IGNITION

- Low power arcjet thruster pulse ignition
[AIAA PAPER 87-1951] p 54 A87-50194
Aircraft accident report: NASA 712, Convair 990, N712NA, March Air Force Base, California, July 17, 1985, executive summary
[NASA-TM-87356-VOL-1] p 16 N87-21878
Low power arcjet thruster pulse ignition
[NASA-TM-100123] p 64 N87-23691
Aviation fuel property effects on altitude reflight
[NASA-CR-179582] p 107 N87-24578

IGNITION LIMITS

- Ignition delay times of cyclopentene oxygen argon mixtures p 76 A87-12602

IMAGE ANALYSIS

- Design, implementation and investigation of an image guide-based optical flip-flop array
[NASA-CR-181382] p 213 N87-30180

IMAGE MOTION COMPENSATION

- An adaptive algorithm for motion compensated color image coding p 113 A87-45466

IMAGE PROCESSING

- Towards effective interactive three-dimensional colour postprocessing p 201 A87-11895
A high quality image compression scheme for real-time applications p 111 A87-30801
An adaptive algorithm for motion compensated color image coding p 113 A87-45466
Computer control of a scanning electron microscope for digital image processing of thermal-wave images
[NASA-TM-100157] p 128 N87-26278

IMAGE RECONSTRUCTION

- Image data compression with vector quantization in the transform domain p 111 A87-30775

IMAGERY

- Absolute gain measurement by the image method under mismatched condition p 201 A87-11895
[NASA-TM-88924] p 124 N87-16968

IMAGING TECHNIQUES

- Effects of non-spherical drops on a phase Doppler spray analyzer p 152 A87-11048

IMPACT

- The impact damped harmonic oscillator in free decay
[NASA-TM-89897] p 168 N87-23978

IMPACT DAMAGE

- The survivability of large space-borne reflectors under atomic oxygen and micrometeoroid impact
[AIAA PAPER 87-0341] p 49 A87-31300
The survivability of large space-borne reflectors under atomic oxygen and micrometeoroid impact
[NASA-TM-88914] p 57 N87-14423

IMPACT LOADS

- Dynamic delamination buckling in composite laminates under impact loading: Computational simulation
[NASA-TM-100192] p 75 N87-28611

IMPEDANCE

- The radiation impedance of an electrodynamic tether with end connectors p 42 A87-42585

IMPINGEMENT

- Experimental, water droplet impingement data on two-dimensional airfoils, axisymmetric inlet and Boeing 737-300 engine inlet
[AIAA PAPER 87-0097] p 17 A87-24918
Rotational effects on impingement cooling p 141 A87-45838

IMPREGNATING

- Effect of impregnation method on cycle life of the nickel electrode p 188 A87-18105

IN-FLIGHT MONITORING

- In-flight measurement of ice growth on an airfoil using an array of ultrasonic transducers
[AIAA PAPER 87-0178] p 15 A87-22464

INCIDENCE

- Variable angle of incidence spectroscopic ellipsometry Application to GaAs-Al(x)Ga(1-x)As multiple heterostructures p 216 A87-20519
The measurement of boundary layers on a compressor blade in cascade at high positive incidence angle. 1: Experimental techniques and results
[NASA-CR-179491] p 25 N87-13441

- The measurement of boundary layers on a compressor blade in cascade at high positive incidence angle. 2: Data report
[NASA-CR-179492] p 25 N87-13442

INCOMPRESSIBLE FLOW

- Comparison of Hirs' equation with Moody's equation for determining rotordynamic coefficients of annular pressure seals
[ASME PAPER 86-TRIB-19] p 161 A87-19529
Time-marching solution of incompressible Navier-Stokes equations for internal flow p 138 A87-39450
A finite difference scheme for three-dimensional steady laminar incompressible flow
[NASA-TM-89851] p 148 N87-20504

INDIUM

- Performance of AlGaAs, GaAs and InGaAs cells after 1 MeV electron irradiation p 197 N87-26438

INDIUM ARSENIDES

- Microwave performance of a quarter-micrometer gate low-noise pseudomorphic InGaAs/AlGaAs modulation-doped field effect transistor p 121 A87-23745
Characterization of InGaAs/AlGaAs pseudomorphic modulation-doped field-effect transistors p 121 A87-23922

INDIUM PHOSPHIDES

Indium phosphide solar cells - Status and prospects for use in space p 188 A87-18071
 Potential for use of InP solar cells in the space radiation environment p 120 A87-19996
 Shallow n(+) diffusion into InP by an open-tube diffusion technique p 217 A87-30023
 Indium phosphide shallow homojunction solar cells made by metalorganic chemical vapor deposition p 123 A87-50047

Recent developments in indium phosphide space solar cell research [NASA-TM-100139] p 68 A87-26141
 Status of indium phosphide solar cell development at Spire p 197 A87-26440
 Comparative performance of diffused junction indium phosphide solar cells p 197 A87-26441
 Solar cells in bulk InP using an open tube diffusion process p 198 A87-26444
 Radiation damage in proton irradiated indium phosphide solar cells p 199 A87-29018

INDUCTION

Enhanced current flow through a plasma cloud by induction of plasma turbulence --- electrolytic diodes for generating power for spacecraft in low earth orbit [AIAA PAPER 87-0573] p 214 A87-22714

INELASTIC SCATTERING

The temperature dependence of inelastic light scattering from small particles for use in combustion diagnostic instrumentation [NASA-CR-180399] p 80 A87-28634

INELASTIC STRESS

On 3-D inelastic analysis methods for hot section components (base program) [NASA-CR-175060] p 180 A87-12923
 Estimation of high temperature low cycle fatigue on the basis of inelastic strain and strainrate [NASA-TM-88841] p 89 A87-14489
 On 3-D inelastic analysis methods for hot section components. Volume 1: Special finite element models [NASA-CR-179494] p 185 A87-22996
 3-D inelastic analysis methods for hot section components. Volume 2: Advanced special functions models [NASA-CR-179517] p 186 A87-27267

INERTIA

Centrifugal inertia effects in two-phase face seal films p 162 A87-37687
 An investigation of the dynamic response of spur gear teeth with moving loads [NASA-CR-179643] p 170 A87-29840

INFRARED IMAGERY

Computer control of a scanning electron microscope for digital image processing of thermal-wave images [NASA-TM-100157] p 128 A87-26278

INFRARED SPECTRA

Gas particle radiator [NASA-CASE-LEW-14297-1] p 156 A87-15452

INFRARED SPECTROMETERS

Investigation of PTFE transfer films by infrared emission spectroscopy and phase-locked ellipsometry [NASA-TM-89844] p 102 A87-20421

INGESTION (ENGINES)

Jet engine simulation with water ingestion through compressor [NASA-CR-179549] p 1 A87-15932
 Hot gas ingestion: From model results to full scale engine testing p 30 A87-24419

INHOMOGENEITY

A finite element model for wave propagation in an inhomogeneous material including experimental validation [NASA-TM-100149] p 207 A87-25821

INLET AIRFRAME CONFIGURATIONS

Mass and momentum turbulent transport experiments p 144 A87-11201

INLET FLOW

Stall transients of axial compression systems with inlet distortion p 3 A87-24010
 Starvation effects on the hydrodynamic lubrication of rigid nonconformal contacts in combined rolling and normal motion p 135 A87-27839
 Two- and three-dimensional viscous computations of a hypersonic inlet flow [AIAA PAPER 87-0283] p 4 A87-31106
 Lower-upper implicit scheme for high-speed inlet analysis p 6 A87-46781
 A method for assessing effects of circumferential flow distortion on compressor stability p 7 A87-48722
 Viscous analyses for flow through subsonic and supersonic intakes [NASA-TM-88831] p 9 A87-15173
 Two- and three-dimensional viscous computations of a hypersonic inlet flow [NASA-TM-88923] p 146 A87-15441

Viscous analyses for flow through subsonic and supersonic intakes p 30 A87-24469
 Calculations of inlet distortion induced compressor flowfield instability p 30 A87-24470
 Summary of investigations of engine response to distorted inlet conditions p 30 A87-24477

INLET NOZZLES

PTA test bed aircraft engine inlet model test report, revised [NASA-CR-174845] p 23 A87-10866
 Effect of variable inlet guide vanes on the operating characteristics of a tilt nacelle inlet/powered fan model [NASA-TM-88983] p 14 A87-27628

INLET PRESSURE

Two-phase flows and heat transfer within systems with ambient pressure above the thermodynamic critical pressure p 136 A87-30728
 Flame radiation p 168 A87-11204

INLET TEMPERATURE

Response of a small-turboshaft-engine compression system to inlet temperature distortion [NASA-TM-83765] p 23 A87-10100
 Summary of investigations of engine response to distorted inlet conditions p 30 A87-24477

INSPECTION

Automated inspection and precision grinding of spiral bevel gears [NASA-CR-4083] p 169 A87-25578

INSTRUMENT COMPENSATION

Fiber-optic photoelastic pressure sensor with fiber-loss compensation p 154 A87-34566

INSULATION

Structureborne noise control in advanced turboprop aircraft [AIAA PAPER 87-0530] p 209 A87-31110
 Structureborne noise control in advanced turboprop aircraft [NASA-TM-88947] p 211 A87-16587

INSULATORS

Ellipsometric and optical study of amorphous hydrogenated carbon films p 216 A87-23967

INTAKE SYSTEMS

Viscous analyses for flow through subsonic and supersonic intakes [NASA-TM-88831] p 9 A87-15173

INTEGRAL EQUATIONS

Extrapolation methods for divergent oscillatory infinite integrals that are defined in the sense of summability p 204 A87-35575
 Noncommutative-geometry model for closed bosonic strings p 207 A87-37542

INTEGRATED CIRCUITS

Advances in gallium arsenide monolithic microwave integrated-circuit technology for space communications systems p 120 A87-19091
 Analysis of optically controlled microwave/millimeter-wave device structures p 121 A87-23680
 A 30-GHz monolithic receiver p 121 A87-23953
 30 GHz monolithic balanced mixers using an ion-implanted FET-compatible 3-inch GaAs wafer process technology p 121 A87-34525
 20-GHz phased-array-fed antennas utilizing distributed MMIC modules p 112 A87-34527
 The 20 GHz GaAs monolithic power amplifier module development [NASA-CR-174742] p 124 A87-11104
 A design concept for an MMIC microstrip phased array [NASA-TM-88834] p 114 A87-14569
 Swept frequency technique for dispersion measurement of microstrip lines [NASA-TM-88836] p 124 A87-14597
 System architecture of MMIC-based large aperture arrays for space application [NASA-TM-89840] p 125 A87-20468
 Ion beam sputter etching [NASA-CASE-LEW-13899-1] p 110 A87-21160
 RF characterization of monolithic microwave and mm-wave ICs [NASA-TM-88948] p 117 A87-22065
 Swept frequency technique for dispersion measurement of microstrip lines [AD-P005420] p 118 A87-27848
 Monolithic Microwave Integrated Circuit (MMIC) technology for space communications applications [NASA-TM-100187] p 118 A87-27883
 APS-Workshop on Characterization of MMIC (Monolithic Microwave Integrated Circuit) Devices for Array Antenna [AD-P005398] p 118 A87-28763
 A design concept for an MMIC (Monolithic Microwave Integrated Circuit) microstrip phased array [AD-P005404] p 119 A87-28769

INTEGRATED ENERGY SYSTEMS

Status of commercial fuel cell powerplant system development [NASA-TM-89896] p 148 A87-22171

INTERACTIONAL AERODYNAMICS

Perfect gas effects in compressible rapid distortion theory p 136 A87-31176
 Investigation of two-dimensional shock-wave/boundary-layer interactions p 4 A87-39528
 An LDA investigation of three-dimensional normal shock-boundary layer interactions in a corner [AIAA PAPER 87-1369] p 6 A87-44938
 Nonlinear binary-mode interactions in a developing mixing layer p 142 A87-47158
 Internal computational fluid mechanics on supercomputers for aerospace propulsion systems p 151 A87-26002

INTERCALATION

Properties and potential applications of brominated P-100 carbon fibers p 95 A87-23702
 Simultaneous electrical resistivity and mass uptake measurements in bromine intercalated fibers [NASA-TM-88900] p 70 A87-11841
 Stability of bromine, iodine monochloride, copper (II) chloride, and nickel (II) chloride intercalated pitch-based graphite fibers [NASA-TM-89904] p 103 A87-24563

INTERFACES

On optimal design for the blade-root/hub interface in jet engines p 24 A87-11769
 Space station resistojet system requirements and interface definition study [NASA-CR-179581] p 60 A87-17848
 Identification of structural interface characteristics using component mode synthesis [NASA-TM-88960] p 185 A87-24006
 SINDA-NASTRAN interfacing program theoretical description and user's manual [NASA-TM-100158] p 187 A87-27268

INTERFACIAL TENSION

Tribology theory versus experiment [NASA-TM-100198] p 71 A87-29599

INTERFERENCE IMMUNITY

SMI adaptive antenna arrays for weak interfering signals --- Sample Matrix Inversion p 111 A87-20818

INTERFEROMETERS

Large aperture interferometer with phase-conjugate self-reference beam p 153 A87-17320
 Linear capacitive displacement sensor with frequency readout p 154 A87-42546

INTERGRANULAR CORROSION

Grain boundary oxidation and fatigue crack growth at elevated temperatures p 81 A87-19368

INTERMETALLICS

Effect of composition and grain size on slow plastic flow properties of NiAl between 1200 and 1400 K p 84 A87-36251

Nickel base coating alloy [NASA-CASE-LEW-13834-1] p 89 A87-14482
 Ductility and fracture in B2 FeAl alloys [NASA-CR-180810] p 93 A87-27771

INTERNAL COMBUSTION ENGINES

Comparisons between thermodynamic and one-dimensional combustion models of spark-ignition engines p 161 A87-29275
 Advanced Gas Turbine (AGT) Technology Project [NASA-CR-179484] p 164 A87-11995
 Thermodynamics and combustion modeling p 219 A87-20274
 Synchronization trigger control system for flow visualization [NASA-TM-89902] p 128 A87-23902

INTERNATIONAL COOPERATION

Optimization of orbital assignment and specification of service areas in satellite communications [NASA-CR-181273] p 118 A87-27882

INTERSTITIALS

Preliminary study of niobium alloy contamination by transport through helium [NASA-TM-88952] p 90 A87-17884

INVERSIONS

Lewis inverse design code (LINDS): Users manual [NASA-TP-2676] p 12 A87-20238
 SMI adaptive antenna arrays for weak interfering signals [NASA-CR-181330] p 119 A87-28813

INVERTED CONVERTERS (DC TO AC)

Description of a 20 kilohertz power distribution system p 120 A87-18115
 20 kHz Space Station power system p 51 A87-40378

INVESTIGATION

An analytical and experimental investigation of resistojet plumes [NASA-TM-88852] p 58 A87-14428

INVISCID FLOW

- Comparison of calculated and experimental cascade performance for controlled-diffusion compressor stator blading
[ASME PAPER 86-GT-35] p 19 A87-25394
- A numerical simulation of the inviscid flow through a counterrotating propeller
[ASME PAPER 86-GT-138] p 3 A87-25395
- Euler analysis of transonic propeller flows
p 4 A87-39813
- The utilization of parallel processing in solving the inviscid form of the average-passage equation system for multistage turbomachinery
[AIAA PAPER 87-1108] p 5 A87-42057
- Lower-upper implicit scheme for high-speed inlet analysis
p 6 A87-46781
- Large perturbation flow field analysis and simulation for supersonic inlets
[NASA-CR-174676] p 8 N87-10835
- ION BEAMS**
- Adhesion, friction and deformation of ion-beam-deposited boron nitride films
p 98 A87-49325
- Characterization of ion beam modified ceramic wear surfaces using Auger electron spectroscopy
p 98 A87-51304
- Adhesion, friction, and deformation of ion-beam-deposited boron nitride films
[NASA-TM-88902] p 100 N87-15305
- Heat exchanger for electrothermal devices
[NASA-CASE-LEW-14037-1] p 59 N87-16875
- Mechanical strength and tribological behavior of ion-beam deposited boron nitride films on non-metallic substrates
[NASA-TM-89818] p 101 N87-18668
- Ion beam sputter etching
[NASA-CASE-LEW-13899-1] p 110 N87-21160
- Enhanced thermal emittance of space radiators by ion-discharge chamber texturing
[NASA-TM-100137] p 207 N87-25823
- ION CURRENTS**
- Theory of plasma contactors used in the ionosphere
p 122 A87-41610
- A flooded-starved design for nickel-cadmium cells
p 123 N87-11086
- ION ENGINES**
- Performance characteristics of ring-cusp thrusters with xenon propellant
[AIAA PAPER 86-1392] p 46 A87-17992
- The NASA Electric Propulsion Program
[AIAA PAPER 87-1098] p 53 A87-45795
- Status of xenon ion propulsion technology
[AIAA PAPER 87-1003] p 53 A87-48677
- Nuclear powered Mars cargo transport mission utilizing advanced ion propulsion
[AIAA PAPER 87-1903] p 53 A87-50191
- Electric propulsion options for the SP-100 reference mission
[NASA-TM-88918] p 57 N87-14422
- The NASA Electric Propulsion Program
[NASA-TM-89856] p 61 N87-21037
- Precision tunable resonant microwave cavity
[NASA-CASE-LEW-13935-1] p 126 N87-21234
- Nuclear powered Mars cargo transport mission utilizing advanced ion propulsion
[NASA-TM-100109] p 65 N87-23692
- ION EXCHANGE MEMBRANE ELECTROLYTES**
- Electrochemical performance and transport properties of a Nafion membrane in a hydrogen-bromine cell environment
[NASA-TM-89862] p 79 N87-23718
- ION IMPLANTATION**
- Stoichiometric disturbances in compound semiconductors due to ion implantation
p 215 A87-12292
- 30 GHz monolithic balanced mixers using an ion-implanted FET-compatible 3-inch GaAs wafer process technology
p 121 A87-34525
- Friction and wear behaviour of ion beam modified ceramics
p 97 A87-47958
- ION INJECTION**
- The dynamic behavior of plasmas observed near geosynchronous orbit
p 200 A87-31322
- ION PLATING**
- Ion plated gold films: Properties, tribological behavior and performance
[NASA-TM-88977] p 110 N87-17937
- ION PROPULSION**
- Performance characteristics of ring-cusp thrusters with xenon propellant
[AIAA PAPER 86-1392] p 46 A87-17992
- Status of xenon ion propulsion technology
[AIAA PAPER 87-1003] p 53 A87-48677
- Nuclear powered Mars cargo transport mission utilizing advanced ion propulsion
[AIAA PAPER 87-1903] p 53 A87-50191

- Nuclear powered Mars cargo transport mission utilizing advanced ion propulsion
[NASA-TM-100109] p 65 N87-23692
- ION SCATTERING**
- Ram ion scattering caused by Space Shuttle v x B induced differential charging
p 200 A87-51713
- IRON**
- Reaction of iron with hydrogen chloride-oxygen mixtures at 550 C
p 83 A87-32001
- The effect of Tricresyl-Phosphate (TCP) as an additive on wear of iron (Fe)
[NASA-TM-100103] p 93 N87-27030
- IRON ALLOYS**
- Creep-rupture behavior of a developmental cast-iron-base alloy for use up to 800 deg C
[NASA-TM-100167] p 93 N87-28641
- IRRADIATION**
- Results of 1 MeV proton irradiation of front and back surfaces of silicon solar cells
p 197 N87-26435
- Radiation effects on power transistor performance
[NASA-CR-181188] p 129 N87-27099
- ISOTHERMAL FLOW**
- Centrifugal inertia effects in two-phase face seal films
p 162 A87-37687
- ISOTHERMAL PROCESSES**
- Calculation of thermomechanical fatigue life based on isothermal behavior
[NASA-TM-88864] p 183 N87-20565
- ISOTROPIC MEDIA**
- Creep fatigue life prediction for engine hot section materials (isotropic)
[NASA-CR-174844] p 182 N87-18117
- ITERATION**
- A multigrid LU-SSOR scheme for approximate Newton iteration applied to the Euler equations
[NASA-CR-179524] p 10 N87-16803
- ITERATIVE SOLUTION**
- Solution of elliptic PDEs by fast Poisson solvers using a local relaxation factor
p 204 A87-21968
- Microstrip dispersion including anisotropic substrates
p 123 A87-47621

J

J INTEGRAL

- J-integral estimates for cracks in infinite bodies
p 177 A87-35334

JET AIRCRAFT NOISE

- On broadband shock associated noise of supersonic jets
p 208 A87-11768
- Free jet feasibility study of a thermal acoustic shield concept for AST/VCE application: Dual stream nozzles
[NASA-CR-3867] p 210 N87-10752
- Free-jet acoustic investigation of high-radius-ratio conannular plug nozzles
[NASA-CR-3818] p 210 N87-10753

JET ENGINE FUELS

- Flame radiation
p 78 N87-11204

JET ENGINES

- On optimal design for the blade-root/hub interface in jet engines
p 24 N87-11769
- Jet engine simulation with water ingestion through compressor
[NASA-CR-179549] p 1 N87-15932
- Jet model for slot film cooling with effect of free-stream and coolant turbulence
[NASA-TP-2655] p 146 N87-18034
- Theoretical kinetic computations in complex reacting systems
p 219 N87-20277
- Antimisting kerosene JT3 engine fuel system integration study
[NASA-CR-4033] p 106 N87-24577
- Bladed disk vibration
[NASA-CR-181203] p 31 N87-26908

JET EXHAUST

- Advanced optical smoke meters for jet engine exhaust measurement
[NASA-CR-179459] p 155 N87-12829

JET FLOW

- The generation of capillary instabilities on a liquid jet
p 130 A87-12060
- Liquid fuel spray processes in high-pressure gas flow
p 131 A87-13843
- The flame structure and vorticity generated by a chemically reacting transverse jet
p 76 A87-14116
- Two opposed lateral jets injected into swirling crossflow
[AIAA PAPER 87-0307] p 132 A87-22549
- Spatially growing disturbances in a high velocity ratio two-stream, coplanar jet
[AIAA PAPER 87-0056] p 3 A87-24996
- Modelling of jet- and swirl-stabilized reacting flows in axisymmetric combustors
p 138 A87-38956
- Effects of multiple rows and noncircular orifices on dilution jet mixing
p 138 A87-39805

- Two-dimensional nozzle plume characteristics
[AIAA PAPER 87-2111] p 6 A87-45413
- Secondary stream and excitation effects on two-dimensional nozzle plume characteristics
[AIAA PAPER 87-2112] p 6 A87-45414
- Flow visualization study of the effect of injection hole geometry on an inclined jet in crossflow
p 155 A87-45842
- Computation of multi-dimensional viscous supersonic jet flow
[NASA-CR-4020] p 8 N87-13405
- Computation of multi-dimensional viscous supersonic flow
[NASA-CR-4021] p 9 N87-13406
- Spatially growing disturbances in a high velocity ratio two-stream, coplanar jet
[NASA-TM-88922] p 9 N87-14283
- Spatially growing disturbances in a two-stream, coplanar jet
[NASA-TM-88949] p 10 N87-16799
- A comparison of experimental and theoretical results for labyrinth gas seals
[NASA-CR-180194] p 166 N87-18096
- Secondary stream and excitation effects on two-dimensional nozzle plume characteristics
[NASA-TM-89813] p 12 N87-18539
- Two-dimensional nozzle plume characteristics
[NASA-TM-89812] p 12 N87-18540
- Experiments and modeling of dilution jet flow fields
p 148 N87-20276

JET MIXING FLOW

- On self-preserving, variable-density, turbulent free jets
p 130 A87-10920
- Numerical simulation of excited jet mixing layers
[AIAA PAPER 87-0016] p 131 A87-22361
- The near field behavior of turbulent gas jets in a long confinement
p 135 A87-28976
- Effects of multiple rows and noncircular orifices on dilution jet mixing
p 138 A87-39805
- Temperature fields due to jet induced mixing in a typical OTV tank
[AIAA PAPER 87-2017] p 55 A87-52247

JOINTS (JUNCTIONS)

- Heat transfer in the stagnation region of the junction of a circular cylinder perpendicular to a flat plate
p 131 A87-13019

- The 20th Aerospace Mechanics Symposium
[NASA-CP-2423-REV] p 181 N87-16321
- Identification of structural interface characteristics using component mode synthesis
[NASA-TM-88960] p 185 N87-24006

JOURNAL BEARINGS

- Thermal shaft effects on load-carrying capacity of a fully coupled, variable-properties cryogenic journal bearing
[ASLE PREPRINT 86-TC-6B-1] p 160 A87-19502
- Finite difference solution for a generalized Reynolds equation with homogeneous two-phase flow
p 141 A87-45851
- Effect of vibration amplitude on vapor cavitation in journal bearings
[NASA-TM-88826] p 145 N87-11962
- Effect of shaft frequency on cavitation in a journal bearing for noncentered circular whirl
[NASA-TM-88925] p 148 N87-22122
- Stability of a rigid rotor supported on flexible oil journal bearings
[NASA-TM-89899] p 151 N87-24646

JUDGMENTS

- NASA Lewis Research Center Futuring Workshop
[NASA-CR-179577] p 206 N87-27475

K

KEROSENE

- Antimisting kerosene JT3 engine fuel system integration study
[NASA-CR-4033] p 106 N87-24577

KINEMATICS

- Nonisothermal, elasto-visco-plastic response of shell-type structures
p 185 N87-22796
- Helical gears with circular arc teeth: Generation, geometry, precision and adjustment to errors, computer aided simulation of conditions of meshing and bearing contact
[NASA-CR-4089] p 170 N87-29846

KINETIC EQUATIONS

- An analysis for crack layer stability
p 176 A87-28982

KINETICS

- Theoretical kinetic computations in complex reacting systems
p 219 N87-20277
- Nonisothermal elasto-visco-plastic response of shell-type structures
p 185 N87-22796

Decoupled direct method for sensitivity analysis in combustion kinetics
[NASA-CR-179636] p 79 N87-24549

L

LABORATORIES

2000-hour cyclic endurance test of a laboratory model multipropellant resistojet
[AIAA PAPER 87-0993] p 52 A87-45725

Opportunities and challenges in heat transfer - From the perspective of the government laboratory p 109 A87-48313

Up close - Materials division of NASA-Lewis Research Center p 69 A87-51176

Research opportunities in microgravity science and applications during shuttle hiatus
[NASA-TM-88964] p 108 N87-16917

A 2000-hour cyclic endurance test of a laboratory model multipropellant resistojet
[NASA-TM-89854] p 167 N87-22237

LABYRINTH SEALS

A comparison of experimental and theoretical results for labyrinth gas seals
[NASA-CR-180194] p 166 N87-18096

Experimental rotordynamic coefficient results for teeth-on-rotor and teeth-on-stator labyrinth gas seals p 167 N87-22212

Development of gas-to-gas lift pad dynamic seals, volumes 1 and 2
[NASA-CR-179486] p 168 N87-22245

Three-step labyrinth seal for high-performance turbomachines
[NASA-TP-1848] p 150 N87-23921

LAMELLA (METALLURGY)

The stability of lamellar gamma-gamma-prime structures - nickel-base superalloy p 86 A87-48323

LAMINAR BOUNDARY LAYER

Prediction and rational correlation of thermophoretically reduced particle mass transfer to hot surfaces across laminar or turbulent forced-convection gas boundary layers p 133 A87-23449

The generation of Tollmien-Schlichting waves by long wavelength free stream disturbances p 139 A87-41655

Generation of Tollmien-Schlichting waves on interactive marginally separated flows p 144 A87-54365

LAMINAR FLOW

A general method for unsteady stagnation region heat transfer and results for model turbine flows
[NASA-TM-88903] p 146 N87-17002

Velocity profiles in laminar diffusion flames
[NASA-TP-2596] p 147 N87-18035

A finite difference scheme for three-dimensional steady laminar incompressible flow
[NASA-TM-89851] p 148 N87-20504

Progress in the prediction of unsteady heat transfer on turbine blades p 149 N87-22769

LAMINATES

Design concepts/parameters assessment and sensitivity analyses of select composite structural components p 175 A87-25407

A higher order theory of laminated composite cylindrical shells p 177 A87-35656

The role of near-surface plastic deformation in the wear of lamellar solids p 162 A87-48500

Composite interlaminar fracture toughness: Three-dimensional finite element modeling for mixed mode 1, 2 and 3 fracture p 73 N87-13491

Design of an advanced wood composite rotor and development of wood composite blade technology
[NASA-CR-174713] p 73 N87-17861

Design of test specimens and procedures for generating material properties of Douglas fir/epoxy laminated wood composite material: With the generation of baseline data at two environmental conditions p 75 N87-28612

[NASA-CR-174910] p 75 N87-28612

Application of adaptive antenna techniques to future commercial satellite communications. Executive summary
[NASA-CR-179566-SUMM] p 115 N87-16955

[NASA-CR-179566-SUMM] p 115 N87-16955

[NASA-CR-179566-SUMM] p 115 N87-16955

[NASA-CR-179566-SUMM] p 115 N87-16955

[NASA-CR-179566-SUMM] p 115 N87-16955

[NASA-CR-179566-SUMM] p 115 N87-16955

[NASA-CR-179566-SUMM] p 115 N87-16955

[NASA-CR-179566-SUMM] p 115 N87-16955

[NASA-CR-179566-SUMM] p 115 N87-16955

[NASA-CR-179566-SUMM] p 115 N87-16955

[NASA-CR-179566-SUMM] p 115 N87-16955

[NASA-CR-179566-SUMM] p 115 N87-16955

[NASA-CR-179566-SUMM] p 115 N87-16955

[NASA-CR-179566-SUMM] p 115 N87-16955

LARGE SPACE STRUCTURES

Radiation from large space structures in low earth orbit with induced ac currents p 42 A87-22738

The survivability of large space-borne reflectors under atomic oxygen and micrometeoroid impact
[AIAA PAPER 87-0612] p 49 A87-31300

The survivability of large space-borne reflectors under atomic oxygen and micrometeoroid impact
[NASA-TM-88914] p 57 N87-14423

System architecture of MMIC-based large aperture arrays for space application
[NASA-TM-89840] p 125 N87-20468

Control considerations for high frequency, resonant, power processing equipment used in large systems
[NASA-TM-89926] p 64 N87-23690

Nuclear reactor power for a space-based radar. SP-100 project
[NASA-TM-89295] p 213 N87-25838

LASER ANEMOMETERS

A parametric study of the beam refraction problems across laser anemometer windows p 154 A87-40725

Laser anemometry measurements of natural circulation flow in a scale model PWR reactor system - Pressurized Water Reactor p 154 A87-40750

Feasibility of mapping velocity flowfields in an SSME powerhead using laser anemometry techniques
[AIAA PAPER 87-1306] p 154 A87-42374

An LDA investigation of three-dimensional normal shock-boundary layer interactions in a corner
[AIAA PAPER 87-1369] p 6 A87-44938

Laser anemometers of hot-section applications p 155 N87-11187

Four spot laser anemometer and optical access techniques for turbine applications
[NASA-TM-88972] p 156 N87-18057

A computer controlled signal preprocessor for laser fringe anemometer applications
[NASA-TM-88982] p 157 N87-20516

Laser fringe anemometry for aero engine components p 110 N87-21176

Combined fringe and Fabry-Perot laser anemometer for 3 component velocity measurements in turbine stator cascade facility p 110 N87-21183

Laser anemometry techniques for turbine applications
[NASA-TM-88953] p 158 N87-22959

LASER APPLICATIONS

Effects of non-spherical drops on a phase Doppler spray analyzer p 152 A87-11048

Processing of laser formed SiC powder
[NASA-CR-179857] p 99 N87-11009

Advanced optical smoke meters for jet engine exhaust measurement
[NASA-CR-179459] p 155 N87-12829

The effect of laser glazing on life of ZrO₂ TBCs in cyclic burner rig tests p 89 N87-14487

Optical strain measurement system development, phase 1
[NASA-CR-179619] p 158 N87-22960

Processing of laser formed SiC powder
[NASA-CR-179638] p 104 N87-24573

LASER CUTTING

Fatigue life of laser cut metals
[NASA-CR-179501] p 164 N87-11158

LASER DOPPLER VELOCIMETERS

Laser velocimetry in turbulent flow fields - Particle response
[AIAA PAPER 87-0118] p 132 A87-22426

Measurement of a counter rotation propeller flowfield using a Laser Doppler Velocimeter
[AIAA PAPER 87-0008] p 3 A87-24901

Two component laser velocimeter measurements of turbulence parameters downstream of an axisymmetric sudden expansion p 139 A87-40703

An experimental study on the effects of tip clearance on flow field and losses in an axial flow compressor rotor p 6 A87-46207

Enhanced heat transfer combustor technology, subtasks 1 and 2, test C.1
[NASA-CR-179541] p 56 N87-13486

LASER INTERFEROMETRY

Performance comparison of two interferometric droplet sizing techniques p 153 A87-11049

Fiber-optic interferometer using frequency-modulated laser diodes p 153 A87-19186

LASER MICROSCOPY

Quantitative void characterization in structural ceramics by use of scanning laser acoustic microscopy p 171 A87-51974

LASER OUTPUTS

Evaluation of diffuse-illumination holographic cinematography in a flutter cascade
[NASA-TP-2593] p 156 N87-13731

Optical strain measurement system development
[NASA-CR-179646] p 159 N87-26326

LEADING EDGES

Numerical analysis of a NACA0012 airfoil with leading edge ice accretions
[AIAA PAPER 87-0101] p 2 A87-22415

Effect of a rotor wake on the local heat transfer on the forward half of a circular cylinder p 136 A87-30721

An experimental study of the aerodynamics of a NACA 0012 airfoil with a simulated glaze ice accretion
[NASA-CR-179897] p 8 N87-11701

LEAKAGE

Analysis of experimental shaft seal data for high-performance turbomachines - As for Space Shuttle main engines p 162 A87-45846

Refrigerated dynamic seal to 6.9 MPa (1000 psi) p 164 A87-50777

Development of gas-to-gas lift pad dynamic seals, volumes 1 and 2
[NASA-CR-179486] p 168 N87-22245

Three-step cylindrical seal for high-performance turbomachines
[NASA-TP-1849] p 151 N87-24639

LEVITATION MELTING

The alloy undercooling experiment on the Columbia STS 61-C Space Shuttle mission
[AIAA PAPER 87-0506] p 108 A87-45724

The alloy undercooling experiment on the Columbia STA 61-C space shuttle mission
[NASA-TM-88909] p 91 N87-18643

LEXAN (TRADEMARK)

Bonding Lexan and sapphire to form high-pressure, flame-resistant window
[NASA-TM-100188] p 159 N87-28880

LIFE (DURABILITY)

Effect of impregnation method on cycle life of the nickel electrode p 188 A87-18105

Re-examination of cumulative fatigue damage analysis - An engineering perspective p 174 A87-22128

Effect of hard particle impacts on the atomic oxygen survivability of reflector surfaces with transparent protective overcoats
[AIAA PAPER 87-0104] p 69 A87-22417

Design, construction and long life endurance testing of cathode assemblies for use in microwave high-power transmitting tubes p 123 N87-10237

A flooded-starved design for nickel-cadmium cells
[NASA-CR-175116] p 123 N87-11086

Turbine Engine Hot Section Technology, 1984
[NASA-CP-2339] p 179 N87-11180

Combustion overview p 78 N87-11181

Surface protection p 88 N87-11182

Fatigue and fracture: Overview p 179 N87-11183

Turbine airfoil deposition models p 24 N87-11191

Experimental verification of vapor deposition model in Mach 0.3 burner rigs p 88 N87-11192

Effects of surface chemistry on hot corrosion life p 88 N87-11193

Coating life prediction p 99 N87-11194

Introduction to life modeling of thermal barrier coatings p 99 N87-11195

Mechanical behavior of thermal barrier coatings for gas turbine blades p 24 N87-11196

High temperature stress-strain analysis p 179 N87-11209

High-temperature constitutive modeling p 179 N87-11210

Creep fatigue life prediction for engine hot section materials (isotropic): Two year update p 171 N87-11213

Turbine airfoil gas side heat transfer p 144 N87-11219

Effect of hard particle impacts on the atomic oxygen survivability of reflector surfaces with transparent protective overcoats
[NASA-TM-88874] p 56 N87-11838

Thermal barrier coating life prediction model development
[NASA-CR-179508] p 99 N87-11892

Selection of rolling-element bearing steels for long-life application
[NASA-TM-88881] p 164 N87-11993

The effect of electron beam welding on the creep rupture properties of a Nb-Zr-C alloy
[NASA-TM-88892] p 88 N87-13513

Thermal barrier coating life prediction model
[NASA-CR-179504] p 100 N87-13539

Thermal barrier coating life prediction model
[NASA-CR-175010] p 100 N87-13540

Effect of design variables, temperature gradients and speed of life and reliability of a rotating disk
[NASA-TM-88883] p 165 N87-13755

The effect of laser glazing on life of ZrO₂ TBCs in cyclic burner rig tests
[NASA-TM-88821] p 89 N87-14487

- Creep fatigue life prediction for engine hot section materials (ISOTROPIC) [NASA-CR-179550] p 181 N87-15491
- Ion plated gold films: Properties, tribological behavior and performance [NASA-TM-88977] p 110 N87-17937
- Predicted effect of dynamic load on pitting fatigue life for low-contact-ratio spur gears [NASA-TP-2610] p 166 N87-18095
- Effect of an oxygen plasma on uncoated thin aluminum reflecting films [NASA-TM-88982] p 61 N87-21999
- Environmental degradation of 316 stainless steel in high temperature low cycle fatigue [NASA-TM-89931] p 185 N87-24007
- Toward improved durability in advanced combustors and turbines: Progress in the prediction of thermomechanical loads [NASA-TM-88932] p 32 N87-28551
- Exposure time considerations in high temperature low cycle fatigue [NASA-TM-88934] p 187 N87-28944
- LIFE CYCLE COSTS**
- Cycle life of nickel-hydrogen cells. II - Accelerated cycle life test p 46 A87-18104
- LIFT**
- A comparative study of some dynamic stall models [NASA-TM-88917] p 183 N87-18883
- LIGHT BEAMS**
- A parametric study of the beam refraction problems across laser anemometer windows p 154 A87-40725
- LIGHT EMISSION**
- Loss-compensation technique for fiber-optic sensors and its application to displacement measurements p 154 A87-32152
- Loss-compensation of intensity-modulating fiber-optic sensors [NASA-TM-88825] p 124 N87-13637
- Detection of radio-frequency modulated optical signals by two and three terminal microwave devices [NASA-TM-100196] p 130 N87-29750
- LIGHT SCATTERING**
- Effects of non-spherical drops on a phase Doppler spray analyzer p 152 A87-11048
- The temperature dependence of inelastic light scattering from small particles for use in combustion diagnostic instrumentation [NASA-CR-180399] p 80 N87-28634
- LIGHTING EQUIPMENT**
- Design, development and deployment of public service photovoltaic power/load systems for the Gabonese Republic [NASA-CR-179603] p 195 N87-23030
- LIGHTNING**
- Mechanical and electrical properties of graphite fiber-epoxy composites made from pristine and bromine intercalated fibers p 73 A87-49799
- LIMITS (MATHEMATICS)**
- A generalized procedure for constructing an upwind based TVD scheme [NASA-TM-88926] p 205 N87-24132
- LINEAR OPERATORS**
- Solution methods for one-dimensional viscoelastic problems [AIAA PAPER 87-0804] p 176 A87-33604
- LINEAR PROGRAMMING**
- On orbital allotments for geostationary satellites [NASA-CR-181017] p 37 N87-22700
- LINEARIZATION**
- A linearized Euler analysis of unsteady flows in turbomachinery [NASA-CR-180987] p 149 N87-22948
- LININGS**
- Liner cooling research at NASA Lewis Research Center --- for gas turbine combustion chambers [AIAA PAPER 87-1828] p 22 A87-50189
- Demonstration of laser speckle system on burner liner cyclic rig [NASA-CR-179509] p 155 N87-10377
- Turbine Engine Hot Section Technology, 1984 [NASA-CP-2339] p 179 N87-11180
- Combustion overview p 78 N87-11181
- High temperature stress-strain analysis p 179 N87-11209
- Transition mixing study [NASA-CR-175062] p 27 N87-16830
- Conventionally cast and forged copper alloy for high-heat-flux thrust chambers [NASA-TP-2694] p 90 N87-16902
- Advanced composite combustor structural concepts program [NASA-CR-174733] p 74 N87-20387
- Liner cooling research at NASA Lewis Research Center [NASA-TM-100107] p 29 N87-23624
- LIQUID CHROMATOGRAPHY**
- Quantitative analysis of PMR-15 polyimide resin by HPLC p 69 A87-48314
- LIQUID COOLING**
- Test program to provide confidence in liquid oxygen cooling of hydrocarbon fueled rocket thrust chambers p 67 N87-26114
- LIQUID CRYSTALS**
- Use of a liquid-crystal, heater-element composite for quantitative, high-resolution heat transfer coefficients on a turbine airfoil, including turbulence and surface roughness effects [NASA-TM-87355] p 158 N87-22181
- LIQUID FLOW**
- The generation of capillary instabilities on a liquid jet p 130 A87-12060
- Numerical modeling of on-orbit propellant motion resulting from an impulsive acceleration [AIAA PAPER 87-1766] p 40 A87-48573
- Numerical modeling of on-orbit propellant motion resulting from an impulsive acceleration [NASA-TM-89873] p 41 N87-22757
- LIQUID HYDROGEN**
- The noncavitating performance and life of a small vane-type positive displacement pump in liquid hydrogen [AIAA PAPER 86-1438] p 46 A87-17994
- LIQUID METALS**
- Undercooling and crystallization behaviour of antimony droplets p 83 A87-28732
- LIQUID OXYGEN**
- Thermal shaft effects on load-carrying capacity of a fully coupled, variable-properties cryogenic journal bearing [ASLE PREPRINT 86-TC-6B-1] p 160 A87-19502
- Liquid oxygen cooling of high pressure LOX/hydrocarbon rocket thrust chambers [NASA-TM-88805] p 57 N87-14426
- Test program to provide confidence in liquid oxygen cooling of hydrocarbon fueled rocket thrust chambers p 67 N87-26114
- LIQUID PHASES**
- Cellular and dendritic growth in a binary melt - A marginal stability approach p 107 A87-10871
- LIQUID PROPELLANT ROCKET ENGINES**
- Preliminary design of turbopumps and related machinery [NASA-RP-1170] p 11 N87-17665
- Test program to provide confidence in liquid oxygen cooling of hydrocarbon fueled rocket thrust chambers p 67 N87-26114
- LIQUID ROCKET PROPELLANTS**
- Volume-energy parameters for heat transfer to supercritical fluids p 137 A87-32326
- An evaluation of metallized propellants based on vehicle performance [AIAA PAPER 87-1773] p 53 A87-47003
- A design study of hydrazine and biowaste resistojets [NASA-CR-179510] p 57 N87-14425
- Potential propellant storage and feed systems for space station resistojet propulsion options [NASA-CR-179457] p 59 N87-16065
- Investigation of a repetitive pulsed electrothermal thruster [NASA-CR-179464] p 59 N87-16878
- An evaluation of metallized propellants based on vehicle performance [NASA-TM-100104] p 64 N87-22806
- LIQUID-LIQUID INTERFACES**
- Equilibrium fluid interfaces in the absence of gravity p 136 A87-36790
- LIQUID-SOLID INTERFACES**
- Cellular-dendritic transition in directionally solidified binary alloys p 84 A87-32046
- LIQUID-VAPOR INTERFACES**
- Low-gravity experiments in critical phenomena p 107 A87-23159
- Equilibrium fluid interfaces in the absence of gravity p 138 A87-38790
- LOADS (FORCES)**
- Simplified composite micromechanics for predicting microstresses p 72 A87-20090
- Fracture toughness of Si3N4 measured with short bar chevron-notched specimens p 96 A87-30621
- Composite load spectra for select space propulsion structural components [NASA-CR-179496] p 55 N87-10176
- Analysis of mixed-mode crack propagation using the boundary integral method [NASA-CR-179518] p 180 N87-12915
- Structural properties of impact ices accreted on aircraft structures [NASA-CR-179580] p 182 N87-18121
- Fatigue damage interaction behavior of PWA 1480 p 92 N87-22777
- Composite load spectra for select space propulsion structural components p 63 N87-22793
- SINDA-NASTRAN interfacing program theoretical description and user's manual [NASA-TM-100158] p 187 N87-27268
- LOGIC CIRCUITS**
- Advances in gallium arsenide monolithic microwave integrated-circuit technology for space communications systems p 120 A87-19091
- LONG DURATION SPACE FLIGHT**
- PEGASUS: A multi-megawatt nuclear electric propulsion system p 59 N87-17787
- Power system technologies for the manned Mars mission p 60 N87-17789
- LONG TERM EFFECTS**
- Long-term deposit formation in aviation turbine fuel at elevated temperature p 106 A87-14986
- LONGITUDE**
- A satellite system synthesis model for orbital arc allotment optimization [NASA-CR-181150] p 37 N87-25341
- LONGITUDINAL WAVES**
- One-dimensional wave propagation in rods of variable cross section: A WKBJ solution [NASA-CR-4086] p 172 N87-24707
- LOSSES**
- Development of the VOLT-A Shuttle experiment --- Volt Operating Limit Tests p 41 A87-19907
- LOSSY MEDIA**
- RCS of a coated circular waveguide terminated by a perfect conductor p 112 A87-42536
- LOW FREQUENCIES**
- Viscometer for low frequency, low shear rate measurements p 153 A87-13878
- LOW GRAVITY MANUFACTURING**
- Particle cloud kinetics in microgravity [AIAA PAPER 87-0577] p 107 A87-22716
- The alloy undercooling experiment on the Columbia STS 61-C Space Shuttle mission [AIAA PAPER 87-0506] p 108 A87-45724
- Equipment concept design and development plans for microgravity science and applications research on space station: Combustion tunnel, laser diagnostic system, advanced modular furnace, integrated electronics laboratory [NASA-CR-179535] p 108 N87-15320
- The alloy undercooling experiment on the Columbia STA 61-C space shuttle mission [NASA-TM-88909] p 91 N87-18643
- Gravitational macrosegregation in binary Pb-Sn alloy ingots [NASA-TM-89885] p 109 N87-24579
- LOW NOISE**
- Microwave performance of a quarter-micrometer gate low-noise pseudomorphic InGaAs/AlGaAs modulation-doped field effect transistor p 121 A87-23745
- LOW PASS FILTERS**
- Measurement techniques for millimeter wave substrate mounted MMW antennas p 123 A87-45899
- LOW REYNOLDS NUMBER**
- Experimental study of low Reynolds number nozzles [AIAA PAPER 87-0992] p 51 A87-41102
- Experimental study of low Reynolds number nozzles [NASA-TM-89858] p 61 N87-20383
- Low Reynolds number nozzle flow study [NASA-TM-100130] p 67 N87-25426
- LOW SPEED**
- Size and shape of solid fuel diffusion flames in very slow speed flows [AIAA PAPER 87-2030] p 78 A87-52248
- LOW TEMPERATURE**
- Low heat transfer oxidizer heat exchanger design and analysis [NASA-CR-179488] p 58 N87-15272
- LOW THRUST**
- Small centrifugal pumps for low-thrust rockets p 50 A87-39808
- High heat transfer oxidizer heat exchanger design and analysis --- RL10-2B engine [NASA-CR-179596] p 63 N87-22803
- LOW THRUST PROPUSSION**
- High- and low-thrust propulsion systems for the Space Station [AIAA PAPER 87-0398] p 48 A87-24997
- LUBRICANTS**
- Effects of silver and group II fluoride solid lubricant additions to plasma-sprayed chromium carbide coatings for foil gas bearings to 650 C p 95 A87-22336
- A preliminary study of ester oxidation on an aluminum surface using chemiluminescence p 96 A87-37688
- How to evaluate solid lubricant films using a Pin-on-disk tribometer p 97 A87-42618
- Thermohydrodynamic analysis for laminar lubricating films [NASA-TM-88845] p 144 N87-11124

- Oil film thickness measurement and analysis for an angular contact ball bearing operating in parched elastohydrodynamic lubrication
[NASA-CR-179506] p 70 N87-16879
- The effect of Tricresyl-Phosphate (TCP) as an additive on wear of Iron (Fe)
[NASA-TM-100103] p 93 N87-27030
- LUBRICATION**
- A new chromium carbide-based tribological coating for use to 900 C with particular reference to the Stirling engine p 95 A87-26112
- Starvation effects on the hydrodynamic lubrication of rigid nonconformal contacts in combined rolling and normal motion p 135 A87-27839
- Lubricant effects on bearing life
[NASA-TM-88875] p 165 N87-15467
- Tribological properties of coal slurries
[NASA-TM-89930] p 104 N87-24565
- Stability of a rigid rotor supported on flexible oil journal bearings
[NASA-TM-89899] p 151 N87-24646
- A computer solution for the dynamic load, lubricant film thickness and surface temperatures in spiral bevel gears
[NASA-CR-4077] p 169 N87-26358

M

MACH NUMBER

- The supersonic through-flow turbofan for high Mach propulsion
[AIAA PAPER 87-2050] p 22 A87-50196
- A high resolution shock capturing scheme for high Mach number internal flow
[NASA-CR-179523] p 10 N87-16804
- Experimental evaluation of wall Mach number distributions of the octagonal test section proposed for NASA Lewis Research Center's altitude wind tunnel
[NASA-TP-2666] p 35 N87-17717
- The supersonic through-flow turbofan for high Mach propulsion
[NASA-TM-100114] p 30 N87-23626

MACH-ZEHNDER INTERFEROMETERS

- Investigation of a GaAlAs Mach-Zehnder electro-optic modulator
[NASA-CR-179573] p 114 N87-16953

MAGNESIUM OXIDES

- Plastic deformation of a magnesium oxide 001-plane surface produced by cavitation
[ASLE PREPRINT 86-TC-3D-1] p 94 A87-19504
- Sol-Gel synthesis of MgO-SiO₂ glass compositions having stable liquid-liquid immiscibility
[NASA-TM-89905] p 103 N87-23750

MAGNETIC FILMS

- RCS of a coated circular waveguide terminated by a perfect conductor p 112 A87-42536

MAGNETIC PROPERTIES

- Feasibility analysis of reciprocating magnetic heat pumps
[NASA-CR-180262] p 147 N87-19647

MAGNETIC STORMS

- Modeling of environmentally induced transients within satellites
[AIAA PAPER 85-0387] p 42 A87-41611

MAGNETORESISTIVITY

- Anticorrelation of Shubnikov-deHaas amplitudes and negative magnetoresistance magnitudes in intercalated pitch based graphite fibers p 217 A87-28295

MAGNETOSPHERIC ELECTRON DENSITY

- The dynamic behavior of plasmas observed near geosynchronous orbit p 200 A87-31322

MAGNETOSPHERIC ION DENSITY

- The dynamic behavior of plasmas observed near geosynchronous orbit p 200 A87-31322

MAN-COMPUTER INTERFACE

- A hybrid nonlinear programming method for design optimization p 201 A87-35718

MANGANESE

- Effect of abrasive grit size on wear of manganese-zinc ferrite under three-body abrasion
[NASA-TM-89879] p 104 N87-24566

MANIPULATORS

- The 20th Aerospace Mechanics Symposium
[NASA-CP-2423-REV] p 181 N87-16321

MANNED MARS MISSIONS

- Long range inhabited surface transportation system power source for the exploration of Mars (manned Mars mission) p 37 N87-17752
- Power system technologies for the manned Mars mission p 60 N87-17789

MANNED SPACE FLIGHT

- PEGASUS: A multi-megawatt nuclear electric propulsion system p 59 N87-17787
- Power system technologies for the manned Mars mission p 60 N87-17789

MANNED SPACECRAFT

- The potential impact of new power system technology on the design of a manned Space Station p 47 A87-18342
- Manned spacecraft electrical power systems p 49 A87-37291

MARS (PLANET)

- Nuclear powered Mars cargo transport mission utilizing advanced ion propulsion
[AIAA PAPER 87-1903] p 53 A87-50191
- PEGASUS: A multi-megawatt nuclear electric propulsion system p 59 N87-17787
- Power system technologies for the manned Mars mission p 60 N87-17789
- Nuclear powered Mars cargo transport mission utilizing advanced ion propulsion
[NASA-TM-100109] p 65 N87-23692

MARS SURFACE

- Long range inhabited surface transportation system power source for the exploration of Mars (manned Mars mission) p 37 N87-17752

MASKS

- Ion beam sputter etching
[NASA-CASE-LEW-13899-1] p 110 N87-21160

MASS

- Impact of thermal energy storage properties on solar dynamic space power conversion system mass
[NASA-TM-89909] p 63 N87-22802

MASS DISTRIBUTION

- Concentrated mass effects on the flutter of a composite advanced turboprop model
[NASA-TM-88854] p 180 N87-12017

MASS SPECTROSCOPY

- Oxygen-18 tracer study of the passive thermal oxidation of silicon p 78 A87-51187

MASS TRANSFER

- Prediction and rational correlation of thermophoretically reduced particle mass transfer to hot surfaces across laminar or turbulent forced-convection gas boundary layers p 133 A87-23449
- Mass and momentum turbulent transport experiments p 144 N87-11201
- Simultaneous electrical resistivity and mass uptake measurements in bromine intercalated fibers
[NASA-TM-88900] p 70 N87-11841

MATERIALS

- Materials characterization of phosphoric acid fuel cell system p 76 A87-23241

MATERIALS HANDLING

- An evaluation of candidate oxidation resistant materials for space applications in LEO
[NASA-TM-100122] p 105 N87-25480

MATERIALS SCIENCE

- Materials research and applications at NASA Lewis Research Center p 69 A87-38472
- Up close - Materials division of NASA-Lewis Research Center p 69 A87-51176

MATHEMATICAL MODELS

- Specimen geometry effects on graphite/PMR-15 composites during thermo-oxidative aging p 71 A87-13145

- A numerical simulation of the inviscid flow through a counterrotating propeller
[ASME PAPER 86-GT-138] p 3 A87-25395

- Analytical and experimental investigation of mistuning in propfan flutter
[AIAA PAPER 87-0739] p 178 A87-40496

- Analytical flutter investigation of a composite propfan model
[AIAA PAPER 87-0738] p 178 A87-40497

- Numerical modeling of on-orbit propellant motion resulting from an impulsive acceleration
[AIAA PAPER 87-1766] p 40 A87-48573

- Dendritic solidification in a binary alloy melt - Comparison of theory and experiment p 217 A87-48733

- The finite-difference time-domain (FD-TD) method for electromagnetic scattering and interaction problems p 113 A87-51403

- Gear mesh compliance modeling p 164 A87-53422
- The study of microstrip antenna arrays and related problems
[NASA-CR-179714] p 113 N87-10225

- Turbine Engine Hot Section Technology, 1984
[NASA-CP-2339] p 179 N87-11180

- Combustion overview p 78 N87-11181
- Fatigue and fracture: Overview p 179 N87-11183

- Aerothermal modeling program, phase 2 p 24 N87-11200

- High-temperature constitutive modeling p 179 N87-11210
- On 3-D inelastic analysis methods for hot section components (base program)
[NASA-CR-175060] p 180 N87-12923

- The mathematical modeling of rapid solidification processing
[NASA-CR-179551] p 88 N87-13514

- Alternative mathematical programming formulations for FSS synthesis

- [NASA-CR-180030] p 202 N87-14872
- LEO high voltage solar array arcing response model
[NASA-CR-180073] p 124 N87-16971

- Gear mesh compliance modeling

- [NASA-TM-88843] p 166 N87-18092
- Analytical flutter investigation of a composite propfan model
[NASA-TM-88944] p 182 N87-18115

- Analytical and experimental investigation of mistuning in propfan flutter
[NASA-TM-88959] p 182 N87-18116

- A constitutive model for the inelastic multiaxial cyclic response of a nickel base superalloy Rene 80
[NASA-CR-3998] p 182 N87-18852

- A comparative study of some dynamic stall models
[NASA-TM-88917] p 183 N87-18883

- Expansion of epicyclic gear dynamic analysis program
[NASA-CR-179563] p 166 N87-19723

- Analysis of shell-type structures subjected to time-dependent mechanical and thermal loading
[NASA-CR-180349] p 183 N87-19756

- Numerical calculations of turbulent reacting flow in a gas-turbine combustor
[NASA-TM-89842] p 1 N87-20171

- On the modelling of non-reactive and reactive turbulent combustor flows
[NASA-CR-4041] p 28 N87-20996

- Numerical modeling of on-orbit propellant motion resulting from an impulsive acceleration
[NASA-TM-89873] p 41 N87-22757

- Simulation of multistage turbine flows p 149 N87-22768
- Self-consistent inclusion of space-charge in the traveling wave tube
[NASA-TM-89928] p 128 N87-24630

- Mathematical programming formulations for satellite synthesis
[NASA-CR-181151] p 44 N87-25419

- Turbulence modeling and surface heat transfer in a stagnation flow region
[NASA-TM-100132] p 151 N87-26302

- Secondary electron generation, emission and transport: Effects on spacecraft charging and NASCAP models p 44 N87-26950

- 3-D inelastic analysis methods for hot section components. Volume 2: Advanced special functions models
[NASA-CR-179517] p 186 N87-27267

- Studies of unsteady viscous flows using a two-equation model of turbulence
[NASA-CR-181293] p 152 N87-27949

- Turbulence characteristics of an axisymmetric reacting flow
[NASA-CR-180697] p 152 N87-27973

- Spark ignition of monodisperse fuel sprays
[NASA-CR-181404] p 80 N87-29635

- The dynamic aspects of thermo-elasto-viscoplastic snap-through and creep buckling phenomena
[NASA-CR-181411] p 187 N87-29897

- Space Electrochemical Research and Technology (SERT)
[NASA-CP-2484] p 199 N87-29914

- Theoretical performance of hydrogen-bromine rechargeable SPE fuel cell p 199 N87-29945

- Modelling of multijunction cascade photovoltaics for space applications
[NASA-CR-181417] p 200 N87-29958

MATHEMATICAL PROGRAMMING

- Alternative mathematical programming formulations for FSS synthesis
[NASA-CR-180030] p 202 N87-14872

- On orbital allotments for geostationary satellites
[NASA-CR-181017] p 37 N87-22700

MATRICES (MATHEMATICS)

- Compliance matrices for cracked bodies p 175 A87-25775

- SMI adaptive antenna arrays for weak interfering signals
[NASA-CR-181330] p 119 N87-28813

MATRIX MATERIALS

- On the symbolic manipulation and code generation for elastoplastic material matrices p 201 A87-18499

- Styrene-terminated polysulfone oligomers as matrix material for graphite reinforced composites - An initial study p 98 A87-49370

- Mechanical properties of SiC fiber-reinforced reaction-bonded Si₃N₄ composites p 73 A87-50094

MEASURING INSTRUMENTS

- How to evaluate solid lubricant films using a Pin-on-disk tribometer p 97 A87-42618
- Advanced optical smoke meters for jet engine exhaust measurement
[NASA-CR-179459] p 155 N87-12829

- High temperature static strain gage alloy development program
[NASA-CR-174833] p 157 N87-22179
Measurement uncertainty for the Uniform Engine Testing Program conducted at NASA Lewis Research Center
[NASA-TM-88943] p 33 N87-28557

MECHANICAL DEVICES

- Apparatus for mounting a field emission cathode
[NASA-CASE-LEW-14108-1] p 129 N87-28832

MECHANICAL DRIVES

- New generation methods for spur, helical, and spiral-bevel gears p 164 A87-53420
New generation methods for spur, helical, and spiral-bevel gears
[NASA-TM-88862] p 165 N87-15466
Evaluation of a high-torque backlash-free roller actuator p 165 N87-16336
Generation of spiral bevel gears with conjugate tooth surfaces and tooth contact analysis
[NASA-CR-4088] p 169 N87-26356

MECHANICAL PROPERTIES

- Mechanical property anisotropy in superalloy EI-929 directionally solidified by an exothermic technique p 81 A87-11389
Correlation of processing and sintering variables with the strength and radiography of silicon nitride p 94 A87-12938
Sintering, microstructural, radiographic, and strength characterization of a high-purity Si₃N₄-based composition p 94 A87-12939
The sensitivity of mechanical properties of TFRS composites to variations in reaction zone size and properties — Tungsten Fiber Reinforced Superalloys [AIAA PAPER 87-0757] p 72 A87-33577
Composite space antenna structures - Properties and environmental effects p 72 A87-38610
Mechanical and electrical properties of graphite fiber-epoxy composites made from pristine and bromine intercalated fibers p 73 A87-49799
Mechanical properties of SiC fiber-reinforced reaction-bonded Si₃N₄ composites p 73 A87-50094
Surface protection p 88 N87-11182
PMR polyimide compositions for improved performance at 371 deg C p 73 N87-16071
Composite space antenna structures: Properties and environmental effects p 73 N87-16880
Structural properties of impact ices accreted on aircraft structures p 182 N87-18121
Ceramic matrix and resin matrix composites: A comparison p 74 N87-18615
Mechanical strength and tribological behavior of ion-beam deposited boron nitride films on non-metallic substrates p 101 N87-18668
A constitutive model for the inelastic multiaxial cyclic response of a nickel base superalloy Rene 80 [NASA-CR-3998] p 182 N87-18852
Boron nitride: Composition, optical properties and mechanical behavior [NASA-TM-89849] p 218 N87-25017

- MELT SPINNING**
Chill block melt spinning of nickel-molybdenum alloys p 86 A87-47902
Microstructures in rapidly solidified Ni-Mo alloys p 87 A87-51636
Elevated temperature strengthening of a melt spun austenitic steel by TiB₂ p 87 A87-51639
Cellular microstructure of chill block melt spun Ni-Mo alloys p 87 A87-54300
Primary arm spacing in chill block melt spun Ni-Mo alloys [NASA-TM-88887] p 88 N87-11875
The mathematical modeling of rapid solidification processing [NASA-CR-179551] p 88 N87-13514

- MELTING**
Combustion of velcro in low gravity [NASA-TM-88970] p 102 N87-19518

- MELTING POINTS**
Undercooling and crystallization behaviour of antimony droplets p 83 A87-28732

- MELTS (CRYSTAL GROWTH)**
Cellular and dendritic growth in a binary melt - A marginal stability approach p 107 A87-10871

- MERCURY ION ENGINES**
Plasma properties in electron-bombardment ion thrusters [AIAA PAPER 87-1076] p 51 A87-41135

- MESH**
An optimized top contact design for solar cell concentrators p 189 A87-19882

- Fatigue failure of regenerator screens in a high frequency Stirling engine [NASA-TM-88974] p 183 N87-18882

METAL COATINGS

- Degradation mechanisms in thermal-barrier coatings p 94 A87-12953
Low cycle fatigue behaviour of a plasma-sprayed coating material p 82 A87-24040
Adherent Al₂O₃ scales formed on undoped NiCrAl alloys p 84 A87-32045
Nickel base coating alloy [NASA-CASE-LEW-13834-1] p 89 N87-14482

- Effects of atmosphere on the tribological properties of a chromium carbide based coating for use to 760 deg C [NASA-TM-88894] p 101 N87-16140

METAL CRYSTALS

- A critical examination of the dendrite growth models
Comparison of theory with experimental data p 83 A87-25048

METAL FATIGUE

- Grain boundary oxidation and fatigue crack growth at elevated temperatures p 81 A87-19368
Low cycle fatigue behaviour of a plasma-sprayed coating material p 82 A87-24040
Effects of temperature and hold times on low cycle fatigue of Astroloy p 85 A87-38541
Grain boundary oxidation and fatigue crack growth at elevated temperatures [NASA-CR-179529] p 88 N87-11873
Fatigue damage interaction behavior of PWA 1480 p 92 N87-22777

- Probabilistic structural analysis to evaluate the structural durability of SSME critical components p 62 N87-22783

- Materials for Advanced Turbine Engines (MATE). Project 4: Erosion resistant compressor airfoil coating [NASA-CR-179622] p 92 N87-27029

METAL FILMS

- The sensitivity of mechanical properties of TFRS composites to variations in reaction zone size and properties — Tungsten Fiber Reinforced Superalloys [AIAA PAPER 87-0757] p 72 A87-33577
METAL FILMS
Thin-film temperature sensors for gas turbine engines Problems and prospects p 153 A87-26109
A review of recent advances in solid film lubrication p 161 A87-35332
Interactions of amorphous Ta(x)Cu(1-x) (x = 0.93 and 0.80) alloy films with Au overlayers and GaAs substrates p 217 A87-44562

METAL FLUORIDES

- Annealing of electron damage in mid-IR transmitting fluoride glass p 99 A87-53652

METAL FOILS

- A heater made from graphite composite material for potential deicing application [AIAA PAPER 87-0025] p 17 A87-24905
A heater made from graphite composite material for potential deicing application [NASA-TM-88888] p 17 N87-12559
Compositional optimization of chromium carbide based solid lubricant coatings for foil gas bearings at temperatures to 650 C [NASA-CR-179649] p 105 N87-26233

METAL GRINDING

- Automated inspection and precision grinding of spiral bevel gears [NASA-CR-4083] p 169 N87-25578

METAL MATRIX COMPOSITES

- Fiber-reinforced superalloy composites provide an added performance edge p 71 A87-12647
Polymer, metal, and ceramic matrix composites for advanced aircraft engine applications p 71 A87-15187

- Thermal expansion behavior of graphite/glass and graphite/magnesium p 72 A87-38615
A viscoplastic constitutive theory for metal matrix composites at high temperature [NASA-CR-179530] p 180 N87-13790

- Advanced composite combustor structural concepts program [NASA-CR-174733] p 74 N87-20387

- Analysis of an advanced technology subsonic turbofan incorporating revolutionary materials [NASA-TM-89868] p 29 N87-22680

- Probabilistic structural analysis to evaluate the structural durability of SSME critical components p 62 N87-22783

- METAL OXIDE SEMICONDUCTORS**
Behavior of inversion layers in 3C silicon carbide p 215 A87-11242

- METAL OXIDES**
Oxidation protection coatings for polymers [NASA-CASE-LEW-14072-3] p 103 N87-23736

METAL POWDER

- Dendritic microstructure in argon atomized superalloy powders p 83 A87-24119

METAL PROPELLANTS

- An evaluation of metallized propellants based on vehicle performance [AIAA PAPER 87-1773] p 53 A87-47003
An evaluation of metallized propellants based on vehicle performance [NASA-TM-100104] p 64 N87-22806

METAL SHELLS

- Nonisothermal elasto-visco-plastic response of shell-type structures p 185 N87-22796

METAL SURFACES

- Analysis of thermomechanical oxidation fields in thermal barrier coatings p 174 A87-14316
A preliminary study of ester oxidation on an aluminum surface using chemiluminescence p 96 A87-37688
A constitutive law for finite element contact problems with unclassical friction [NASA-TM-88838] p 180 N87-12924
Ester oxidation on an aluminum surface using chemiluminescence [NASA-TP-2611] p 101 N87-18666

METALLIC GLASSES

- Microstructure and surface chemistry of amorphous alloys important to their friction and wear behavior p 81 A87-15186

METALLOGRAPHY

- Further observations of SCC in alpha-beta brass Considerations regarding the appearance of crack arrest markings during SCC p 82 A87-23843
Dendritic microstructure in argon atomized superalloy powders p 83 A87-24119

METALS

- An evaluation of metallized propellants based on vehicle performance [AIAA PAPER 87-1773] p 53 A87-47003
Fatigue life of laser cut metals [NASA-CR-179501] p 164 N87-11158
Calculation of thermomechanical fatigue life based on isothermal behavior [NASA-TM-88864] p 183 N87-20565
An evaluation of metallized propellants based on vehicle performance [NASA-TM-100104] p 64 N87-22806

METEOROID PROTECTION

- Coaxial tube tether/transmission line for manned nuclear space power [NASA-CASE-LEW-14338-1] p 55 N87-10174

METHANE

- Temperature dependence (4K to 300K) of the electrical resistivity of methane grown carbon fibers p 97 A87-47375

METHYL COMPOUNDS

- The 2,5-diacetyl-1,4-dimethylbenzenes: Examples of bisphotonol equivalents [NASA-TM-89836] p 71 N87-22005

METHYL POLYSILOXANE

- Silsesquioxanes as precursors to ceramic composites [NASA-TM-89893] p 75 N87-25432

MICROCRACKS

- Elastic interaction of a crack with a microcrack array. I - Formulation of the problem and general form of the solution. II - Elastic solution for two crack configurations (piecewise constant and linear approximations) p 178 A87-36926

- Simplified composite micromechanics for predicting microstresses p 179 A87-49275

- Stochastic and fractal analysis of fracture trajectories p 179 A87-51167

- Macrocrack interaction with transverse array of microcracks [NASA-CR-180806] p 186 N87-25607

- MICROFIBERS**
Simplified composite micromechanics for predicting microstresses p 72 A87-20090

- MICROMECHANICS**
Assessment of simplified composite micromechanics using three-dimensional finite-element analysis p 72 A87-19121

- Simplified composite micromechanics for predicting microstresses p 72 A87-20090

- The sensitivity of mechanical properties of TFRS composites to variations in reaction zone size and properties — Tungsten Fiber Reinforced Superalloys [AIAA PAPER 87-0757] p 72 A87-33577

- Simplified composite micromechanics for predicting microstresses p 179 A87-49275

- MICROSTRIP ANTENNAS**
New simple feed network for an array module of four microstrip elements p 122 A87-41638

- The study of microstrip antenna arrays and related problems [NASA-CR-179714] p 113 N87-10225

- A design concept for an MMIC microstrip phased array
[NASA-TM-88834] p 114 N87-14569
- Microstrip antenna array with parasitic elements
[NASA-TM-89919] p 117 N87-22089
- An experimental investigation of parasitic microstrip arrays
[NASA-TM-100168] p 129 N87-27120
- A design concept for an MMIC (Monolithic Microwave Integrated Circuit) microstrip phased array
[AD-P005404] p 119 N87-28769
- MICROSTRIP TRANSMISSION LINES**
- Microstrip dispersion including anisotropic substrates
p 123 A87-47621
- Swept frequency technique for dispersion measurement of microstrip lines
[NASA-TM-88836] p 124 N87-14597
- A new model for broadband waveguide to microstrip transition design
[NASA-TM-88905] p 115 N87-16958
- Swept frequency technique for dispersion measurement of microstrip lines
[AD-P005420] p 118 N87-27848
- MICROSTRUCTURE**
- Ultrasonic verification of microstructural changes due to heat treatment
p 208 A87-10772
- Sintering, microstructural, radiographic, and strength characterization of a high-purity Si₃N₄-based composition
p 94 A87-12939
- Microstructure and surface chemistry of amorphous alloys important to their friction and wear behavior
p 81 A87-15186
- The effects of tantalum on the microstructure of two polycrystalline nickel-base superalloys - B-1900 + Hf and MAR-M247
p 82 A87-24110
- Antiphase boundaries in epitaxially grown beta-SiC
p 217 A87-30025
- Structure and tensile strength of LaS(1,4)
p 96 A87-38065
- The alloy undercooling experiment on the Columbia STS 61-C Space Shuttle mission
[AIAA PAPER 87-0506] p 108 A87-45724
- Microstructure-derived macroscopic residual resistance of brominated graphite fibers
p 97 A87-48324
- Thermal stability of the nickel-base superalloy B-1900 + Hf with tantalum variations
p 87 A87-51289
- Cellular microstructure of chill block melt spun Ni-Mo alloys
p 87 A87-54300
- A study of the microstructure of a rapidly solidified nickel-base superalloy modified with boron
[NASA-CR-179553] p 89 N87-14486
- The alloy undercooling experiment on the Columbia STA 61-C space shuttle mission
[NASA-TM-88909] p 91 N87-18643
- Ion beam sputter etching
[NASA-CASE-LEW-13899-1] p 110 N87-21160
- Processing of laser formed SiC powder
[NASA-CR-179638] p 104 N87-24573
- Boron nitride: Composition, optical properties and mechanical behavior
[NASA-TM-89849] p 218 N87-25017
- A study of reduced chromium content in a nickel-base superalloy via element substitution and rapid solidification processing
[NASA-CR-179631] p 92 N87-25456
- Observations of directional gamma prime coarsening during engine operation
[NASA-TM-100105] p 92 N87-25459
- Ductility and fracture in B2 FeAl alloys
[NASA-CR-180810] p 93 N87-27771
- MICROWAVE AMPLIFIERS**
- Calculation of secondary electron trajectories in multistage depressed collectors for microwave amplifiers
[NASA-TP-2664] p 125 N87-17991
- MICROWAVE ANTENNAS**
- 20-GHz phased-array-fed antennas utilizing distributed MMIC modules
p 112 A87-34527
- Measurement techniques for millimeter wave substrate mounted MMW antennas
p 121 A87-40926
- Measurement techniques for millimeter wave substrate mounted MMW antennas
p 123 A87-45899
- MICROWAVE CIRCUITS**
- Advances in gallium arsenide monolithic microwave integrated-circuit technology for space communications systems
p 120 A87-19091
- Microwave performance of a quarter-micrometer gate low-noise pseudomorphic InGaAs/AlGaAs modulation-doped field effect transistor
p 121 A87-23745
p 121 A87-23953
- 20-GHz phased-array-fed antennas utilizing distributed MMIC modules
p 112 A87-34527
- A design concept for an MMIC microstrip phased array
[NASA-TM-88834] p 114 N87-14569
- Swept frequency technique for dispersion measurement of microstrip lines
[NASA-TM-88836] p 124 N87-14597
- RF characterization of monolithic microwave and mm-wave ICs
[NASA-TM-88948] p 117 N87-22065
- Optically controlled microwave devices and circuits: Emerging applications in space communications systems
[NASA-TM-89869] p 127 N87-23900
- Monolithic Microwave Integrated Circuit (MMIC) technology for space communications applications
[NASA-TM-100187] p 118 N87-27883
- APS-Workshop on Characterization of MMIC (Monolithic Microwave Integrated Circuit) Devices for Array Antenna
[AD-P005398] p 118 N87-28763
- A design concept for an MMIC (Monolithic Microwave Integrated Circuit) microstrip phased array
[AD-P005404] p 119 N87-28769
- MICROWAVE EQUIPMENT**
- Analysis of optically controlled microwave/millimeter-wave device structures
p 121 A87-23680
- Optically controlled GaAs dual-gate MESFET and permeable base transistors
[NASA-TM-88823] p 123 N87-10232
- Optically controlled microwave devices and circuits: Emerging applications in space communications systems
[NASA-TM-89869] p 127 N87-23900
- Microwave characterization and modeling of GaAs/AlGaAs heterojunction bipolar transistors
[NASA-TM-100150] p 117 N87-26265
- APS-Workshop on Characterization of MMIC (Monolithic Microwave Integrated Circuit) Devices for Array Antenna
[AD-P005398] p 118 N87-28763
- Detection of radio-frequency modulated optical signals by two and three terminal microwave devices
[NASA-TM-100196] p 130 N87-29750
- MICROWAVE SENSORS**
- Loss-compensation technique for fiber-optic sensors and its application to displacement measurements
p 154 A87-32152
- Loss-compensation of intensity-modulating fiber-optic sensors
[NASA-TM-88825] p 124 N87-13637
- MICROWAVE TRANSMISSION**
- A new model for broadband waveguide to microstrip transition design
[NASA-TM-88905] p 115 N87-16958
- Propagation characteristics of some novel coplanar waveguide transmission lines on GaAs at MM-wave frequencies
[NASA-TM-89839] p 126 N87-20469
- Microstrip antenna array with parasitic elements
[NASA-TM-89919] p 117 N87-22089
- Automated measurement of the bit-error rate as a function of signal-to-noise ratio for microwave communications systems
[NASA-TM-89898] p 127 N87-22102
- Optimizing the antenna system of a microwave space power station: Implications for the selection of operating power, frequency and antenna size
[NASA-TM-100184] p 206 N87-30132
- MICROWAVE TUBES**
- Improvements in MDC and TWT overall efficiency through the application of carbon electrode surfaces --- Multistage Depressed Collectors
p 120 A87-20667
- MICROWAVES**
- Microwave electrothermal thruster performance in helium gas
p 49 A87-31281
- A review of research and development on the microwave-plasma electrothermal rocket
[AIAA PAPER 87-1011] p 49 A87-38008
- Microwave performance of an optically controlled AlGaAs/GaAs high electron mobility transistor and GaAs MESFET
[NASA-TM-88980] p 125 N87-17993
- Precision tunable resonant microwave cavity
[NASA-CASE-LEW-13935-1] p 126 N87-21234
- MILLIMETER WAVES**
- Analysis of optically controlled microwave/millimeter-wave device structures
p 121 A87-23680
- Measurement techniques for millimeter wave substrate mounted MMW antennas
p 121 A87-40926
- Measurement techniques for millimeter wave substrate mounted MMW antennas
p 123 A87-45899
- System architecture of MMIC-based large aperture arrays for space application
[NASA-TM-89840] p 125 N87-20468
- Propagation characteristics of some novel coplanar waveguide transmission lines on GaAs at MM-wave frequencies
[NASA-TM-89839] p 126 N87-20469
- RF characterization of monolithic microwave and mm-wave ICs
[NASA-TM-88948] p 117 N87-22065
- MILLING**
- Effects of milling brominated P-100 graphite fibers
p 97 A87-41078
- MILLING (MACHINING)**
- Particle-size reduction of Si₃N₄ powder with Si₃N₄ milling hardware
p 94 A87-12936
- MINIATURE ELECTRONIC EQUIPMENT**
- Ultra small electron beam amplifiers
p 122 A87-42681
- MINIATURIZATION**
- Measurement techniques for millimeter wave substrate mounted MMW antennas
p 123 A87-45899
- MINORITY CARRIERS**
- Use of a corrugated surface to enhance radiation tolerance in a GaAs solar cell
p 189 A87-19842
- The use of multiple EBIC curves and low voltage electron microscopy in the measurement of small diffusion lengths
p 197 N87-26434
- MIRRORS**
- Effect of hard particle impacts on the atomic oxygen survivability of reflector surfaces with transparent protective overcoats
[AIAA PAPER 87-0104] p 69 A87-22417
- The survivability of large space-borne reflectors under atomic oxygen and micrometeoroid impact
[AIAA PAPER 87-0341] p 49 A87-31300
- Effect of hard particle impacts on the atomic oxygen survivability of reflector surfaces with transparent protective overcoats
[NASA-TM-88874] p 56 N87-11838
- The survivability of large space-borne reflectors under atomic oxygen and micrometeoroid impact
[NASA-TM-88914] p 57 N87-14423
- MISALIGNMENT**
- New generation methods for spur, helical, and spiral-bevel gears
p 164 A87-53420
- New generation methods for spur, helical, and spiral-bevel gears
[NASA-TM-88862] p 165 N87-15466
- MISMATCH (ELECTRICAL)**
- Absolute gain measurement by the image method under mismatched condition
[NASA-TM-88924] p 124 N87-16968
- MISSILES**
- Preliminary aerothermodynamic design method for hypersonic vehicles
[AIAA PAPER 87-2545] p 7 A87-49100
- MISSION PLANNING**
- Advanced solar dynamic space power systems perspectives, requirements and technology needs
[NASA-TM-88884] p 56 N87-12606
- Centaur D1-A systems in a nutshell
[NASA-TM-88880] p 38 N87-15996
- High power/large area PV systems
p 198 N87-26452
- MIXING**
- Transition mixing study
[NASA-CR-175062] p 27 N87-16830
- Experiments and modeling of dilution jet flow fields
p 148 N87-20276
- Direct numerical simulations of a temporally evolving mixing layer subject to forcing
[NASA-TM-88896] p 150 N87-23933
- On the coalescence-dispersion modeling of turbulent molecular mixing
[NASA-TM-89910] p 2 N87-25292
- Enhanced mixing of an axisymmetric jet by aerodynamic excitation
[NASA-CR-175059] p 15 N87-29418
- MIXING CIRCUITS**
- 30 GHz monolithic balanced mixers using an ion-implanted FET-compatible 3-inch GaAs wafer process technology
p 121 A87-34525
- MIXING LENGTH FLOW THEORY**
- Short efficient ejector systems
[AIAA PAPER 87-1837] p 20 A87-45239
- Nonlinear binary-mode interactions in a developing mixing layer
p 142 A87-47158
- MODELS**
- 2000-hour cyclic endurance test of a laboratory model multipropellant resistojel
[AIAA PAPER 87-0993] p 52 A87-45725
- Preliminary performance characterizations of an engineering model multipropellant resistojel for space station application
[AIAA PAPER 87-2120] p 54 A87-50197
- Progress of Stirling cycle analysis and loss mechanism characterization
[NASA-TM-88891] p 220 N87-13359
- Thermal barrier coating life prediction model
[NASA-CR-175010] p 100 N87-13540
- Finite element modeling of electromagnetic propagation in composite structures
[NASA-TM-88916] p 207 N87-14956

- Communications satellite systems operations with the space station, volume 2
[NASA-CR-179527] p 206 N87-17473
- Noise reduction for model counterrotation propeller at cruise by reducing aft-propeller diameter
[NASA-TM-88936] p 211 N87-19057
- A 2000-hour cyclic endurance test of a laboratory model multipropellant resistorjet
[NASA-TM-89854] p 167 N87-22237
- Revised NASA axially symmetric ring model for coupled-cavity traveling-wave tubes
[NASA-TP-2675] p 127 N87-22923
- Preliminary performance characterizations of an engineering model multipropellant resistorjet for space station application
[NASA-TM-100113] p 111 N87-23821
- On the coalescence-dispersion modeling of turbulent molecular mixing
[NASA-TM-89910] p 2 N87-25292
- A finite element model for wave propagation in an inhomogeneous material including experimental validation
[NASA-TM-100149] p 207 N87-25821
- Microwave characterization and modeling of GaAs/AlGaAs heterojunction bipolar transistors
[NASA-TM-100150] p 117 N87-26265
- Application of turbulence modeling to predict surface heat transfer in stagnation flow region of circular cylinder
[NASA-TP-2758] p 151 N87-27161
- The effect of front-to-rear propeller spacing on the interaction noise of a model counterrotation propeller at cruise conditions
[NASA-TM-100121] p 212 N87-28396
- MODULATION**
Fiber-optic temperature sensor using a spectrum-modulating semiconductor etalon
[NASA-TM-100153] p 31 N87-25329
- MODULES**
Conceptual design and integration of a Space Station resistorjet propulsion assembly
[AIAA PAPER 87-1860] p 52 A87-45256
- Conceptual design and integration of a space station resistorjet propulsion assembly
[NASA-TM-89847] p 60 N87-20378
- MODULUS OF ELASTICITY**
Understanding single-crystal superalloys
p 85 A87-40928
- Gear mesh compliance modeling
p 164 A87-53422
- Ultrasonic determination of the elastic constants of the stiffness matrix for unidirectional fiberglass epoxy composites
[NASA-CR-4034] p 171 N87-13781
- Gear mesh compliance modeling
[NASA-TM-88843] p 166 N87-18092
- MOLDS**
New methods and materials for molding and casting ice formations
[NASA-TM-100126] p 16 N87-29470
- MOLECULAR BEAM EPITAXY**
Variable angle of incidence spectroscopic ellipsometry Application to GaAs-Al(x)Ga(1-x)As multiple heterostructures
p 216 A87-20519
- Characterization of InGaAs/AlGaAs pseudomorphic modulation-doped field-effect transistors
p 121 A87-23922
- MOLECULAR FLOW**
On the coalescence-dispersion modeling of turbulent molecular mixing
[NASA-TM-89910] p 2 N87-25292
- MOLECULAR STRUCTURE**
Iptycenes - Extended triptycenes
p 69 A87-53654
- MOLTEN SALTS**
Corrosion of metals and alloys in sulfate melts at 750 C
p 81 A87-17997
- Mechanism of strength degradation for hot corrosion of alpha-SiC
p 95 A87-21470
- Corrosion pitting of SiC by molten salts
p 76 A87-27165
- Fluoride salts and container materials for thermal energy storage applications in the temperature range 973 to 1400 K
[NASA-TM-89913] p 195 N87-24026
- MOLYBDENUM**
Primary arm spacing in chill block melt spun Ni-Mo alloys
[NASA-TM-88887] p 88 N87-11875
- MOLYBDENUM ALLOYS**
Fault structures in rapidly quenched Ni-Mo binary alloys
p 83 A87-32035
- Chill block melt spinning of nickel-molybdenum alloys
p 86 A87-47902
- Effect of heat treatment on the fracture behaviour of directionally solidified (gamma/gamma-prime)-alpha alloy
p 86 A87-47932
- Microstructures in rapidly solidified Ni-Mo alloys
p 87 A87-51636

- Cellular microstructure of chill block melt spun Ni-Mo alloys
p 87 A87-54300
- MOM (SEMICONDUCTORS)**
Technology for satellite power conversion
[NASA-CR-181057] p 66 N87-25420
- MOMENTUM TRANSFER**
Mass and momentum turbulent transport experiments
p 144 N87-11201
- MONITORS**
A simple method for monitoring surface temperatures in plasma treatments
p 160 A87-17269
- MONOMERS**
Structure-to-property relationships in addition cured polymers. II - Resin Tg and composite initial mechanical properties of norbornenyl cured polyimide resins
p 96 A87-38638
- Substituted 1,1,1-triaryl-2,2,2-trifluoroethanes and processes for their synthesis --- synthetic routes to monomers for polyimides
[NASA-CASE-LEW-14345-1] p 70 N87-14432
- New condensation polyimides containing 1,1,1-triaryl-2,2,2-trifluoroethane structures
[NASA-CASE-LEW-14346-1] p 70 N87-14433
- Thermo-oxidatively stable condensation polyimides containing 1,1,1-triaryl-2,2,2-trifluoroethane dianhydride and diamine monomers
[NASA-TM-89875] p 103 N87-22048
- MONTE CARLO METHOD**
Variational approach to probabilistic finite elements
[NASA-CR-181343] p 206 N87-29212
- MORPHOLOGY**
Adherent Al₂O₃ scales formed on undoped NiCrAl alloys
p 84 A87-32045
- Morphology of zirconia particles exposed to D.C. arc plasma jet
[NASA-TM-88927] p 90 N87-16113
- MULTIBEAM ANTENNAS**
Advances in gallium arsenide monolithic microwave integrated-circuit technology for space communications systems
p 120 A87-19091
- An assessment of the status and trends in satellite communications 1986-2000: An information document prepared for the Communications Subcommittee of the Space Applications Advisory Committee
[NASA-TM-88867] p 114 N87-13600
- MULTICHANNEL COMMUNICATION**
Onboard multichannel demultiplexer/demodulator
[NASA-CR-180821] p 119 N87-28819
- MULTIPATH TRANSMISSION**
Ray propagation path analysis of acousto-ultrasonic signals in composites
[NASA-TM-100148] p 173 N87-25589
- MULTIPROCESSING (COMPUTERS)**
A comparison of five benchmarks
[NASA-TM-88956] p 202 N87-17441

N

N-TYPE SEMICONDUCTORS

- Shallow n(+) diffusion into InP by an open-tube diffusion technique
p 217 A87-30023
- Observation of deep levels in cubic silicon carbide
p 122 A87-41089
- High-efficiency GaAs concentrator space cells
p 196 N87-26417

NASA PROGRAMS

- Space power - Emerging opportunities
[IAF PAPER 86-152] p 45 A87-15900
- Solar dynamic space power system heat rejection
p 47 A87-18175
- Up close - Materials division of NASA-Lewis Research Center
p 69 A87-51176
- The NASA strain gage laboratory
p 35 A87-52494
- NASA SPACE PROGRAMS**
Electrical power system design for the U.S. Space Station
p 46 A87-18068
- NASA Growth Space Station missions and candidate nuclear/solar power systems
p 48 A87-21807
- Materials research and applications at NASA Lewis Research Center
p 69 A87-38472
- A 20 GHz, high efficiency dual mode TWT for the ACTS program --- Advanced Communications Technology Satellite
p 122 A87-45511
- ACTS experiments program --- Advanced Communications Technology Satellite
p 113 A87-45513
- Research opportunities in microgravity science and applications during shuttle hiatus
[NASA-TM-88964] p 108 N87-16917
- Superalloy resources: Supply and availability
[NASA-TM-88966] p 91 N87-21077

NASTRAN

- A NASTRAN primer for the analysis of rotating flexible blades
[NASA-TM-89861] p 184 N87-21375

- Hub flexibility effects on propfan vibration
[NASA-TM-89900] p 186 N87-24722
- Finite element analysis of flexible, rotating blades
[NASA-TM-89906] p 186 N87-26385
- SINDA-NASTRAN interfacing program theoretical description and user's manual
[NASA-TM-100158] p 187 N87-27268
- NAVIER-STOKES EQUATION**
Navier Stokes solution of the flowfield over ice accretion shapes
[AIAA PAPER 87-0099] p 2 A87-22414
- An LU-SSOR scheme for the Euler and Navier-Stokes equations
[AIAA PAPER 87-0600] p 137 A87-34724
- Comparison of three explicit multigrid methods for the Euler and Navier-Stokes equations
[AIAA PAPER 87-0602] p 137 A87-34725
- Diffusion flame extinction in slow convection flow under microgravity environment
p 77 A87-38787
- Time-marching solution of incompressible Navier-Stokes equations for internal flow
p 138 A87-39450
- Turbulent solutions of the Navier-Stokes equations
p 139 A87-40932
- Comparison of generalized Reynolds and Navier Stokes equations for flow of a power law fluid
p 142 A87-45852
- Numerical simulations of unsteady, viscous, transonic flow over isolated and cascaded airfoils using a deforming grid
[AIAA PAPER 87-1316] p 7 A87-49649
- Calculation of two- and three-dimensional transonic cascade flow field using the Navier-Stokes equations
p 144 N87-11220
- Turbine vane external heat transfer. Volume 2. Numerical solutions of the Navier-Stokes equations for two- and three-dimensional turbine cascades with heat transfer
[NASA-CR-174828] p 145 N87-13661
- Comparison of three explicit multigrid methods for the Euler and Navier-Stokes equations
[NASA-TM-88878] p 1 N87-16784
- An LU-SSOR scheme for the Euler and Navier-Stokes equations
[NASA-CR-179556] p 11 N87-16806
- A Navier-Stokes solver using the LU-SSOR TVD algorithm
[NASA-CR-179608] p 13 N87-20243
- A finite difference scheme for three-dimensional steady laminar incompressible flow
[NASA-TM-89851] p 148 N87-20504
- Application of advanced computational codes in the design of an experiment for a supersonic throughflow fan rotor
[NASA-TM-88915] p 13 N87-22630
- Numerical simulations of unsteady, viscous, transonic flow over isolated and cascaded airfoils using a deforming grid
[NASA-TM-89890] p 13 N87-24435
- Viscous analyses for flow through subsonic and supersonic intakes
p 30 N87-24469
- Internal computational fluid mechanics on supercomputers for aerospace propulsion systems
p 151 N87-26002
- Three dimensional boundary layers in internal flows
[NASA-CR-181336] p 152 N87-28860
- NEAR FIELDS**
Computational aeroacoustics of propeller noise in the near and far field
[AIAA PAPER 87-0254] p 19 A87-24944
- The near field behavior of turbulent gas jets in a long confinement
p 135 A87-28976
- Detection of reflector surface error from near-field data: Effect of edge diffracted field
[NASA-TM-89920] p 117 N87-22874
- NETWORK SYNTHESIS**
A 30-GHz monolithic receiver
p 121 A87-23953
- A satellite system synthesis model for orbital arc allotment optimization
[NASA-CR-181150] p 37 N87-25341
- Mathematical programming formulations for satellite synthesis
[NASA-CR-181151] p 44 N87-25419
- NEUMANN PROBLEM**
On the validity of the modified equation approach to the stability analysis of finite-difference methods
[AIAA PAPER 87-1120] p 204 A87-42069
- NEUTRAL ATOMS**
Neutral atomic oxygen beam produced by ion charge exchange for Low Earth Orbital (LEO) simulation
p 79 N87-26188
- NEWTON METHODS**
A multigrid LU-SSOR scheme for approximate Newton iteration applied to the Euler equations
[NASA-CR-179524] p 10 N87-16803

NEWTON THEORY

- A multigrid LU-SSOR scheme for approximate Newton iteration applied to the Euler equations
[NASA-CR-179524] p 10 N87-16803

NICKEL

- Ultrasonic verification of microstructural changes due to heat treatment p 208 A87-10772
Corrosion of metals and alloys in sulfate melts at 750 C p 81 A87-17997
A point defect model for nickel electrode structures p 87 A87-52282
Primary arm spacing in chill block melt spun Ni-Mo alloys [NASA-TM-88887] p 88 N87-11875
Stability of bromine, iodine monochloride, copper (II) chloride, and nickel (II) chloride intercalated pitch-based graphite fibers [NASA-TM-89904] p 103 N87-24563

NICKEL ALLOYS

- Mechanical property anisotropy in superalloy El-929 directionally solidified by an exothermic technique p 81 A87-11389
Low cycle fatigue behaviour of a plasma-sprayed coating material p 82 A87-24040
The effects of tantalum on the microstructure of two polycrystalline nickel-base superalloys - B-1900 + Hf and MAR-M247 p 82 A87-24110
Processing-structure characterization of rheocast IN-100 superalloy p 82 A87-24116
Analysis of the solidified structure of rheocast and VADER processed nickel-base superalloy p 83 A87-28734
Fault structures in rapidly quenched Ni-Mo binary alloys p 83 A87-32035
Yielding and deformation behavior of the single crystal superalloy PWA 1480 p 84 A87-32040
Adherent Al₂O₃ scales formed on undoped NiCrAl alloys p 84 A87-32045
Analysis of NiAlTa precipitates in beta-NiAl + 2 at. pct Ta alloy p 84 A87-34888
Effect of composition and grain size on slow plastic flow properties of NiAl between 1200 and 1400 K p 84 A87-36251
Understanding single-crystal superalloys p 85 A87-40928
Dendritic growth of undercooled nickel-tin, I, II p 85 A87-41012
Stress rupture and creep behavior of a low pressure plasma-sprayed NiCoCrAlY coating alloy in air and vacuum p 85 A87-43396
Application of single crystal superalloys for earth-to-orbit propulsion systems [AIAA PAPER 87-1976] p 85 A87-45336
The characteristics of gamma-prime dislocation pairs in a nickel-base superalloy p 85 A87-46932
Chill block melt spinning of nickel-molybdenum alloys p 86 A87-47902
Effect of heat treatment on the fracture behaviour of directionally solidified (gamma/gamma-prime)-alpha alloy p 86 A87-47932
The stability of lamellar gamma-gamma-prime structures --- nickel-base superalloy p 86 A87-48323
Thermal-mechanical fatigue crack growth in B-1900 + Hf p 86 A87-49570
Defects in nickel-base superalloys p 86 A87-49790
Thermal stability of the nickel-base superalloy B-1900 + Hf with tantalum variations p 87 A87-51289
Microstructures in rapidly solidified Ni-Mo alloys p 87 A87-51636
Cellular microstructure of chill block melt spun Ni-Mo alloys p 87 A87-54300
Ultrasonic determination of recrystallization [NASA-TM-88855] p 171 N87-10399
Nickel base coating alloy [NASA-CASE-LEW-13834-1] p 89 N87-14482
The cyclic stress-strain behavior of PWA 1480 at 650 deg C [NASA-TM-87311] p 89 N87-14483
A study of the microstructure of a rapidly solidified nickel-base superalloy modified with boron [NASA-CR-179553] p 89 N87-14486
The effect of Cr, Co, Al, Mo and Ta on a series of cast Ni-base superalloys on the stability of an aluminide coating during cyclic oxidation in Mach 0.3 burner rig [NASA-TM-88840] p 89 N87-14488
High temperature monotonic and cyclic deformation in a directionally solidified nickel-base superalloy [NASA-CR-175101] p 90 N87-15303
Bithermal low-cycle fatigue behavior of a NiCoCrAlY-coated single crystal superalloy [NASA-TM-89831] p 91 N87-20408
Application of single crystal superalloys for Earth-to-orbit propulsion systems [NASA-TM-89877] p 91 N87-22034
Progress on thin-film sensors for space propulsion technology p 158 N87-22772

Fatigue damage interaction behavior of PWA 1480

- p 92 N87-22777
A study of reduced chromium content in a nickel-base superalloy via element substitution and rapid solidification processing [NASA-CR-179631] p 92 N87-25456
Observations of directional gamma prime coarsening during engine operation [NASA-TM-100105] p 92 N87-25459
Heat treatment for superalloy [NASA-CASE-LEW-14262-1] p 93 N87-28647
- NICKEL CADMIUM BATTERIES**
A flooded-starved design for nickel-cadmium cells p 123 N87-11086
A prediction model of the depth-of-discharge effect on the cycle life of a storage cell [NASA-TM-89915] p 194 N87-22311
- NICKEL COATINGS**
High temperature tensile and creep behaviour of low pressure plasma-sprayed Ni-Co-Cr-Al-Y coating alloy p 82 A87-23429
- NICKEL HYDROGEN BATTERIES**
Parametric and cycle tests of a 40-AH bipolar nickel-hydrogen battery p 46 A87-18093
Nickel-hydrogen separator development p 188 A87-18103
Cycle life of nickel-hydrogen cells. II - Accelerated cycle life test p 46 A87-18104
Effect of impregnation method on cycle life of the nickel electrode p 188 A87-18105
Initial performance of advanced designs for IPV nickel-hydrogen cells [NASA-TM-87282] p 192 N87-16445
Effect of storage and LEO cycling on manufacturing technology IPV nickel-hydrogen cells [NASA-TM-88883] p 194 N87-22308
Component variations and their effects on bipolar nickel-hydrogen cell performance [NASA-TM-89907] p 195 N87-23029
Test results of a 60 volt bipolar nickel-hydrogen battery [NASA-TM-89927] p 195 N87-24029
Effect of component compression on the initial performance of an IPV nickel-hydrogen cell [NASA-TM-100102] p 195 N87-24838
KOH concentration effect on cycle life of nickel-hydrogen cells p 199 N87-29920
- NIObIUM ALLOYS**
Preliminary study of niobium alloy contamination by transport through helium [NASA-TM-88952] p 90 N87-17884
Creep behavior of niobium alloy PWC-11 [NASA-TM-89834] p 91 N87-20405
Long-time creep behavior of Nb-12Zr alloy containing carbon [NASA-TM-100142] p 92 N87-26217
- NITRIDING**
Analysis of plasma-nitrided steels [NASA-TM-89815] p 91 N87-21078
- NITROGEN**
Arcjet starting reliability - A multistart test on hydrogen/nitrogen mixtures [AIAA PAPER 87-1061] p 51 A87-41128
Low power dc arcjet operation with hydrogen/nitrogen/ammonia mixtures [AIAA PAPER 87-1948] p 53 A87-48575
Low power DC arcjet operation with hydrogen/nitrogen/ammonia mixtures [NASA-TM-89876] p 64 N87-22804
Multispecies CARS measurements in turbulent combustion p 79 N87-23808
- NITROGEN COMPOUNDS**
Degradation mechanisms of sulfur and nitrogen containing compounds during thermal stability testing of model fuels [AIAA PAPER 87-2039] p 106 A87-45372
Component testing of a ground based gas turbine steam cooled rich-burn primary zone combustor for emissions control of nitrobenzene fuels [NASA-TM-88873] p 191 N87-11345
- NOISE**
Structureborne noise control in advanced turboprop aircraft [AIAA PAPER 87-0530] p 209 A87-31110
Structureborne noise control in advanced turboprop aircraft [NASA-TM-88947] p 211 N87-16587
- NOISE GENERATORS**
Noise generated by flow through large butterfly valves [NASA-TM-88911] p 210 N87-16586
- NOISE MEASUREMENT**
Measured noise of a scale model high speed propeller at simulated takeoff/approach conditions [AIAA PAPER 87-0526] p 208 A87-31109

- Measured noise of a scale model high speed propeller at simulated takeoff/approach conditions [NASA-TM-88920] p 211 N87-16588
Identification and proposed control of helicopter transmission noise at the source [NASA-TM-89312] p 18 N87-16816
Turbofan aft duct suppressor study. Contractor's data report of mode probe signal data [NASA-CR-175067] p 34 N87-29538
- NOISE PREDICTION**
High-speed propeller noise predictions: Effects of boundary conditions used in blade loading calculations [NASA-TM-88913] p 210 N87-14957
- NOISE PREDICTION (AIRCRAFT)**
High-speed propeller noise predictions - Effects of boundary conditions used in blade loading calculations [AIAA PAPER 87-0525] p 208 A87-24978
Coupled aerodynamic and acoustical predictions for turboprops [NASA-TM-87094] p 13 N87-23598
Turbofan aft duct suppressor study. Contractor's data report of mode probe signal data [NASA-CR-175067] p 34 N87-29538
Turbofan aft duct suppressor study [NASA-CR-175067] p 34 N87-29539
- NOISE PROPAGATION**
Noise generated by flow through large butterfly valves [NASA-TM-88911] p 210 N87-16586
- NOISE REDUCTION**
Free jet feasibility study of a thermal acoustic shield concept for AST/VCE application: Dual stream nozzles [NASA-CR-3867] p 210 N87-10752
Free-jet acoustic investigation of high-radius-ratio coannular plug nozzles [NASA-CR-3818] p 210 N87-10753
Cruise noise of counterrotation propeller at angle of attack in wind tunnel [NASA-TM-88869] p 210 N87-13252
Identification and proposed control of helicopter transmission noise at the source [NASA-TM-89312] p 18 N87-16816
Simulated flight acoustic investigation of treated ejector effectiveness on advanced mechanical suppressors for high velocity jet noise reduction [NASA-CR-4019] p 211 N87-17481
Noise reduction for model counterrotation propeller at cruise by reducing aft-propeller diameter [NASA-TM-88936] p 211 N87-19057
Free-jet investigation of mechanically suppressed, high radius ratio coannular plug model nozzles [NASA-CR-3596] p 212 N87-29315
Aerodynamic performance investigation of advanced mechanical suppressor and ejector nozzle concepts for jet noise reduction [NASA-CR-174860] p 33 N87-29534
Turbofan aft duct suppressor study. Contractor's data report of mode probe signal data [NASA-CR-175067] p 34 N87-29538
Turbofan aft duct suppressor study [NASA-CR-175067] p 34 N87-29539
- NOISE SPECTRA**
Combustion noise from gas turbine aircraft engines measurement of far-field levels [NASA-TM-88971] p 211 N87-17480
The effect of front-to-rear propeller spacing on the interaction noise of a model counterrotation propeller at cruise conditions [NASA-TM-100121] p 212 N87-28396
- NONDESTRUCTIVE TESTS**
Ultrasonic verification of microstructural changes due to heat treatment p 208 A87-10772
Nondestructive evaluation of adhesive bond strength using the stress wave factor technique p 170 A87-32200
Feasibility of mapping velocity flowfields in an SSME powerhead using laser anemometry techniques [AIAA PAPER 87-1306] p 154 A87-42374
Quantitative void characterization in structural ceramics by use of scanning laser acoustic microscopy p 171 A87-51974
Ultrasonic determination of recrystallization [NASA-TM-88855] p 171 N87-10399
Ultrasonic determination of the elastic constants of the stiffness matrix for unidirectional fiberglass epoxy composites [NASA-CR-4034] p 171 N87-13781
Nondestructive evaluation of structural ceramics [NASA-TM-88978] p 172 N87-18109
The acousto-ultrasonic approach [NASA-TM-89843] p 172 N87-20562
Laser anemometry techniques for turbine applications [NASA-TM-88953] p 158 N87-22959
Low-cost FM oscillator for capacitance type of blade tip clearance measurement system [NASA-TP-2746] p 31 N87-24481

- One-dimensional wave propagation in rods of variable cross section: A WKB solution
[NASA-CR-4086] p 172 N87-24707
- Ray propagation path analysis of acousto-ultrasonic signals in composites
[NASA-TM-100148] p 173 N87-25589
- Acousto-ultrasonic input-output characterization of unidirectional fiber composite plate by SH waves
[NASA-CR-4087] p 173 N87-26361
- Ultrasonic NDE of structural ceramics for power and propulsion systems
[NASA-TM-100147] p 173 N87-26362
- Fracture mechanics concepts in reliability analysis of monolithic ceramics
[NASA-TM-100174] p 187 N87-27269

NONISOTHERMAL PROCESSES

- Thermodynamically consistent constitutive equations for nonisothermal large-strain, elastoplastic, creep behavior
p 175 A87-27945

NONLINEAR EQUATIONS

- Multiphase scaled constrained nonlinear equation solvers --- for nonlinear heat conduction problems
p 137 A87-31406
- Separation of variables solution for non-linear radiative cooling
p 142 A87-48450

NONLINEAR PROGRAMMING

- A hybrid nonlinear programming method for design optimization
p 201 A87-35718

NONLINEAR SYSTEMS

- Influence of third-degree geometric nonlinearities on the vibration and stability of pretwisted, precone, rotating blades
p 21 A87-46228
- The effect of nonlinearities on the dynamic response of a large shuttle payload
[NASA-TM-88941] p 181 N87-18112
- A constitutive model for the inelastic multiaxial cyclic response of a nickel base superalloy Rene 80
[NASA-CR-3998] p 182 N87-18852
- NONLINEARITY**
- Bounding solutions of geometrically nonlinear viscoelastic problems
p 174 A87-20892
- Nonlinear vibration and stability of rotating, pretwisted, precone blades including Coriolis effects
p 178 A87-39896
- Influence of third-degree geometric nonlinearities on the vibration and stability of pretwisted, precone, rotating blades
p 21 A87-46228
- A generalized procedure for constructing an upwind based TVD scheme
[NASA-TM-88926] p 205 N87-24132

NOTCH SENSITIVITY

- Fracture toughness of Si3N4 measured with short bar chevron-notched specimens
p 96 A87-30621

NOTCH TESTS

- KI-solutions for single edge notch specimens under fixed end displacements
p 174 A87-15798
- Fracture toughness of Si3N4 measured with short bar chevron-notched specimens
p 96 A87-30621
- NOZZLE DESIGN**
- Free-jet investigation of mechanically suppressed, high radius ratio conical plug model nozzles
[NASA-CR-3596] p 212 N87-29315
- Automotive Stirling Engine Development Program
[NASA-CR-174873] p 222 N87-30223
- NOZZLE EFFICIENCY**
- Comparison of theoretical and experimental thrust performance of a 1030:1 area ratio rocket nozzle at a chamber pressure of 2413 kN/sq m (350 psia)
[AIAA PAPER 87-2069] p 52 A87-45390
- NOZZLE FLOW**
- The generation of capillary instabilities on a liquid jet
p 130 A87-12060
- Duct flows with swirl
[AIAA PAPER 87-0247] p 132 A87-22509
- The evolution of instabilities in the axisymmetric jet. I - The linear growth of disturbances near the nozzle. II - The flow resulting from the interaction between two waves
p 138 A87-37256
- Sound radiation from single and annular stream nozzles, with modal decomposition of in-duct acoustic power
p 209 A87-37629
- Secondary stream and excitation effects on two-dimensional nozzle plume characteristics
[AIAA PAPER 87-2112] p 6 A87-45414
- Experimental evaluation of heat transfer on a 1030:1 area ratio rocket nozzle
[AIAA PAPER 87-2070] p 55 A87-52249
- Effect of nozzle geometry on the resistojet exhaust plume
[AIAA PAPER 87-2121] p 55 A87-52252
- Secondary stream and excitation effects on two-dimensional nozzle plume characteristics
[NASA-TM-89813] p 12 N87-18539
- Experimental evaluation of heat transfer on a 1030:1 area ratio rocket nozzle
[NASA-TP-2726] p 67 N87-25424

- Low Reynolds number nozzle flow study
[NASA-TM-100130] p 67 N87-25426

NOZZLE GEOMETRY

- Experimental study of low Reynolds number nozzles
[AIAA PAPER 87-0992] p 51 A87-41102
- Secondary stream and excitation effects on two-dimensional nozzle plume characteristics
[AIAA PAPER 87-2112] p 6 A87-45414
- Effect of nozzle geometry on the resistojet exhaust plume
[AIAA PAPER 87-2121] p 55 A87-52252
- Experimental evaluation of a translating nozzle sidewall radial turbine
[NASA-TM-88963] p 27 N87-17701
- Secondary stream and excitation effects on two-dimensional nozzle plume characteristics
[NASA-TM-89813] p 12 N87-18539
- Experimental thrust performance of a high-area-ratio rocket nozzle
[NASA-TP-2720] p 60 N87-20381
- Experimental study of low Reynolds number nozzles
[NASA-TM-89858] p 61 N87-20383
- Experimental thrust performance of a high area-ratio rocket nozzle
p 65 N87-23809
- Aviation fuel property effects on altitude relight
[NASA-CR-179582] p 107 N87-24578
- A detailed description of the uncertainty analysis for High Area Ratio Rocket Nozzle tests at the NASA Lewis Research Center
[NASA-TM-100203] p 68 N87-28602

NOZZLE THRUST COEFFICIENTS

- Secondary stream and excitation effects on two-dimensional nozzle plume characteristics
[AIAA PAPER 87-2112] p 6 A87-45414
- Secondary stream and excitation effects on two-dimensional nozzle plume characteristics
[NASA-TM-89813] p 12 N87-18539

NOZZLES

- Simulated flight acoustic investigation of treated ejector effectiveness on advanced mechanical suppressors for high velocity jet noise reduction
[NASA-CR-4019] p 211 N87-17481

NUCLEAR ELECTRIC POWER GENERATION

- The potential impact of new power system technology on the design of a manned Space Station
p 47 A87-18342

NUCLEAR ELECTRIC PROPULSION

- Nuclear powered Mars cargo transport mission utilizing advanced ion propulsion
[AIAA PAPER 87-1903] p 53 A87-50191
- Nuclear powered Mars cargo transport mission utilizing advanced ion propulsion
[NASA-TM-100109] p 65 N87-23692

NUCLEAR POWER REACTORS

- PEGASUS: A multi-megawatt nuclear electric propulsion system
p 59 N87-17787
- Coaxial tube array space transmission line characterization
[NASA-TM-89864] p 62 N87-22003
- Nuclear reactor power for a space-based radar. SP-100 project
[NASA-TM-89295] p 213 N87-25838
- An assessment and validation study of nuclear reactors for low power space applications
[NASA-CR-180672] p 213 N87-27495

NUCLEAR REACTORS

- A study of Schwarz converters for nuclear powered spacecraft
[NASA-TM-89911] p 128 N87-23903

NUCLEATE BOILING

- A model for fluid flow during saturated boiling on a horizontal cylinder
p 139 A87-41173

NUMERICAL ANALYSIS

- Notes and comments on computational elastoplasticity - Some new models and their numerical implementation
p 173 A87-10893
- Solution of elliptic PDEs by fast Poisson solvers using a local relaxation factor
p 204 A87-21968
- Analysis of viscous transonic flow over airfoil sections
[AIAA PAPER 87-0420] p 4 A87-34723
- An LU-SSOR scheme for the Euler and Navier-Stokes equations
[AIAA PAPER 87-0600] p 137 A87-34724
- Elastic interaction of a crack with a microcrack array. I - Formulation of the problem and general form of the solution. II - Elastic solution for two crack configurations (piecewise constant and linear approximations)
p 178 A87-36926
- Numerical simulation of transonic propeller flow using a three-dimensional small disturbance code employing novel helical coordinates
[AIAA PAPER 87-1162] p 5 A87-42107
- Interactive graphics and analysis accuracy
p 202 A87-45900
- Multigrid-sinc methods
p 205 A87-52865

- An LU-SSOR scheme for the Euler and Navier-Stokes equations
[NASA-CR-179556] p 11 N87-16806
- Analysis of viscous transonic flow over airfoil sections
[NASA-TM-88912] p 146 N87-17001
- Generation of a composite grid for turbine flows and consideration of a numerical scheme
[NASA-TM-88890] p 11 N87-17662
- Jet model for slot film cooling with effect of free-stream and coolant turbulence
[NASA-TP-2655] p 146 N87-18034
- Numerical simulation of transonic propeller flow using a 3-dimensional small disturbance code employing novel helical coordinates
[NASA-TM-88826] p 12 N87-19350
- A Navier-Stokes solver using the LU-SSOR TVD algorithm
[NASA-CR-179608] p 13 N87-20243
- On the modelling of non-reactive and reactive turbulent combustor flows
[NASA-CR-4041] p 28 N87-20996
- Direct numerical simulations of a temporally evolving mixing layer subject to forcing
[NASA-TM-88896] p 150 N87-23933
- Low Reynolds number nozzle flow study
[NASA-TM-100130] p 67 N87-25426
- Reduction of the radar cross section of arbitrarily shaped cavity structures
[NASA-CR-180307] p 118 N87-27085

NUMERICAL CONTROL

- A rotorcraft flight/propulsion control integration study
[NASA-CR-179574] p 18 N87-24457

NUMERICAL FLOW VISUALIZATION

- Numerical simulation of excited jet mixing layers
[AIAA PAPER 87-0016] p 131 A87-22361
- Three-dimensional unsteady Euler solutions for propfans and counter-rotating propfans in transonic flow
[AIAA PAPER 87-1197] p 5 A87-42314
- Numerical simulation of the flow field and fuel sprays in an IC engine
[SAE PAPER 870599] p 143 A87-48751

NUMERICAL STABILITY

- An unconditionally-stable central differencing scheme for high Reynolds number flows
[AIAA PAPER 87-0060] p 133 A87-24912
- CONDIF - A modified central-difference scheme with unconditional stability and very low numerical diffusion
p 136 A87-30685
- On the validity of the modified equation approach to the stability analysis of finite-difference methods
[AIAA PAPER 87-1120] p 204 A87-42069

O

O RING SEALS

- Analysis of experimental shaft seal data for high-performance turbomachines - As for Space Shuttle main engines
p 162 A87-45846

OBLIQUE SHOCK WAVES

- Investigation of two-dimensional shock-wave/boundary-layer interactions
p 4 A87-39528

OCTANES

- Velocity profiles in laminar diffusion flames
[NASA-TP-2596] p 147 N87-18035

OH-58 HELICOPTER

- Identification and proposed control of helicopter transmission noise at the source
[NASA-TM-89312] p 18 N87-16816

ONBOARD DATA PROCESSING

- ACTS baseband processing --- Advanced Communications Technology Satellite
p 201 A87-45512

- On-board processing satellite network architecture and control study
[NASA-CR-180816] p 44 N87-27710

- On-board processing satellite network architecture and control study
[NASA-CR-180817] p 44 N87-27711

ONBOARD EQUIPMENT

- Onboard multichannel demultiplexer/demodulator
[NASA-CR-180821] p 119 N87-28819

ONE DIMENSIONAL FLOW

- Large perturbation flow field analysis and simulation for supersonic inlets
[NASA-CR-174676] p 8 N87-10835
- Thermodynamics and combustion modeling
p 219 N87-20274

OPEN CIRCUIT VOLTAGE

- A 25.5 percent AMO gallium arsenide grating solar cell
p 189 A87-19840

OPTICAL COMMUNICATION

Optical technologies for communication satellite applications; Proceedings of the Meeting, Los Angeles, CA, Jan. 21, 22, 1986
[SPIE-616] p 41 A87-26610
US long distance fiber optic networks: Technology, evolution and advanced concepts. Volume 1: Executive summary
[NASA-CR-179479] p 113 N87-11056

OPTICAL EQUIPMENT

Optically controlled GaAs dual-gate MESFET and permeable base transistors
[NASA-TM-88823] p 123 N87-10232
Microwave performance of an optically controlled AlGaAs/GaAs high electron mobility transistor and GaAs MESFET
[NASA-TM-88980] p 125 N87-17993
Referencing in fiber optic sensing systems
[NASA-TM-89822] p 126 N87-20475
Detection of radio-frequency modulated optical signals by two and three terminal microwave devices
[NASA-TM-100196] p 130 N87-29750
Design, implementation and investigation of an image guide-based optical flip-flop array
[NASA-CR-181382] p 213 N87-30180

OPTICAL HETERODYNING

Beam-modulation methods in quantitative and flow-visualization holographic interferometry
p 111 N87-21204

OPTICAL MEASUREMENT

Advanced optical smoke meters for jet engine exhaust measurement
[NASA-CR-179459] p 155 N87-12829

OPTICAL MEASURING INSTRUMENTS

A low-cost optical data acquisition system for vibration measurement
[NASA-TM-88907] p 181 N87-14730
Optical strain measuring techniques for high temperature tensile testing
[NASA-CR-179637] p 159 N87-26327

OPTICAL PROPERTIES

Boron nitride: Composition, optical properties and mechanical behavior
[NASA-TM-89849] p 218 N87-25017

OPTICAL RESONATORS

Linear capacitive displacement sensor with frequency readout
p 154 A87-42546

OPTICAL WAVEGUIDES

Investigation of a GaAlAs Mach-Zehnder electro-optic modulator
[NASA-CR-179573] p 114 N87-16953

OPTIMIZATION

Propeller design by optimization p 18 A87-14123
An optimized top contact design for solar cell concentrators p 189 A87-19882
Optimization and analysis of gas turbine engine blades
[AIAA PAPER 87-0827] p 201 A87-33614
Optimal placement of critical speeds in rotor-bearing systems p 162 A87-38464
Development of a turbomachinery design optimization procedure using a multiple-parameter nonlinear perturbation method
[NASA-CR-3831] p 1 N87-10003
STAEEL: Structural tailoring of engine blades, phase 2
p 24 N87-11731
Optimization of cascade blade mistuning under flutter and forced response constraints p 24 N87-11732
On optimal design for the blade-root/hub interface in jet engines p 24 N87-11769
Optimizing the antenna system of a microwave space power station: Implications for the selection of operating power, frequency and antenna size
[NASA-TM-100184] p 206 N87-30132

ORBIT SPECTRUM UTILIZATION

Intersatellite Link (ISL) application to commercial communications satellites. Volume 1: Executive summary
[NASA-CR-179598-VOL-1] p 116 N87-19552
Intersatellite Link (ISL) application to commercial communications satellites. Volume 2: Technical final report
[NASA-CR-179598-VOL-2] p 116 N87-19553
The use of satellites in non-geostationary orbits for unloading geostationary communication satellite traffic peaks. Volume 1: Executive summary
[NASA-CR-179597-VOL-1] p 117 N87-21212
The use of satellites in non-geostationary orbits for unloading geostationary communication satellite traffic peaks. Volume 2: Technical report
[NASA-CR-179597-VOL-2] p 117 N87-21213
On orbital allotments for geostationary satellites
[NASA-CR-181017] p 37 N87-22700
Optimization of orbital assignment and specification of service areas in satellite communications
[NASA-CR-181273] p 118 N87-27882

ORBIT TRANSFER VEHICLES

Status of advanced propulsion for space based orbital transfer vehicle
[IAF PAPER 86-183] p 48 A87-23239
Concepts for space maintenance of OTV engines
p 40 A87-41161
Concepts for space maintenance of OTV engines
p 37 A87-46000
Thermodynamic analysis and subscale modeling of space-based orbit transfer vehicle cryogenic propellant resupply
[AIAA PAPER 87-1764] p 142 A87-48572
Temperature fields due to jet induced mixing in a typical OTV tank
[AIAA PAPER 87-2017] p 55 A87-52247
Status of advanced propulsion for space based orbital transfer vehicle
[NASA-TM-88848] p 56 N87-10959
Cryogenic gear technology for an orbital transfer vehicle engine and tester design
[NASA-CR-175102] p 110 N87-19539
Thermodynamic analysis and subscale modeling of space-based orbit transfer vehicle cryogenic propellant resupply
[NASA-TM-89921] p 150 N87-22949
Concepts for space maintenance of OTV engines
p 67 N87-26097

ORBITAL MANEUVERING VEHICLES

Communications satellite systems operations with the space station. Volume 1: Executive summary
[NASA-CR-179526] p 206 N87-17472

ORBITAL MANEUVERS

Conceptual design and integration of a Space Station resistojet propulsion assembly
[AIAA PAPER 87-1860] p 52 A87-45256
Conceptual design and integration of a space station resistojet propulsion assembly
[NASA-TM-89847] p 60 N87-20378

ORBITAL MECHANICS

Alternative mathematical programming formulations for FSS synthesis
[NASA-CR-180030] p 202 N87-14872

ORBITAL SERVICING

On-orbit cryogenic storage and resupply
p 41 A87-18344
Concepts for space maintenance of OTV engines
p 37 A87-46000

ORBITS

A satellite system synthesis model for orbital arc allotment optimization
[NASA-CR-181150] p 37 N87-25341

ORDER-DISORDER TRANSFORMATIONS

Anticorrelation of Shubnikov-deHaas amplitudes and negative magnetoresistance magnitudes in intercalated pitch based graphite fibers
p 217 A87-28295

ORGANIC COMPOUNDS

Iptycenes - Extended triptycenes p 69 A87-53654
Simulation of fluid flows during growth of organic crystals in microgravity
[NASA-TM-88921] p 108 N87-16167

ORGANOMETALLIC COMPOUNDS

Formation of a pn junction on an anisotropically etched GaAs surface using metalorganic chemical vapor deposition
p 216 A87-21237
Indium phosphide shallow homojunction solar cells made by metalorganic chemical vapor deposition
p 123 A87-50047
Organometallic catalysts for primary phosphoric acid fuel cells
[NASA-CR-179490] p 193 N87-19804

ORGANOMETALLIC POLYMERS

Polymer precursors for ceramic matrix composites
[NASA-CR-179562] p 70 N87-14434

ORIFICE FLOW

Effects of multiple rows and noncircular orifices on dilution jet mixing
p 138 A87-39805
Experiments and modeling of dilution jet flow fields
p 148 N87-20276

ORR-SOMMERFELD EQUATIONS

On the spatial instability of piecewise linear free shear layers
p 137 A87-31680

ORTHOTROPISM

Thermal analysis of an orthotropic engineering body --- horizontal axis wind turbine rotor blade
p 173 A87-13496

OSCILLATING FLOW

Effect of flow oscillations on axial energy transport in a porous material
p 135 A87-27715
Influence of oscillation-induced diffusion on heat transfer in a uniformly heated channel
p 135 A87-27716
Shear flow instability generated by non-homogeneous external forcing
p 142 A87-48047

OSCILLATIONS

Numerical simulations of unsteady, viscous, transonic flow over isolated and cascaded airfoils using a deforming grid
[AIAA PAPER 87-1316] p 7 A87-49649
Numerical simulations of unsteady, viscous, transonic flow over isolated and cascaded airfoils using a deforming grid
[NASA-TM-89890] p 13 N87-24435

OSCILLATORS

Low-cost FM oscillator for capacitance type of blade tip clearance measurement system
[NASA-TP-2746] p 31 N87-24481

OXIDATION

Ignition delay times of cyclopentene oxygen argon mixtures
p 76 A87-12602
Degradation mechanisms in thermal-barrier coatings
p 94 A87-12953
Grain boundary oxidation and fatigue crack growth at elevated temperatures
p 81 A87-19368
A preliminary study of ester oxidation on an aluminum surface using chemiluminescence
p 96 A87-37688
On the effect of the Fe(2+)/Fe(3+) redox couple on oxidation of carbon in hot H3PO4
p 78 A87-42677
Oxygen-18 tracer study of the passive thermal oxidation of silicon
p 78 A87-51187
Grain boundary oxidation and fatigue crack growth at elevated temperatures
[NASA-CR-179529] p 88 N87-11873
Degradation mechanisms in thermal barrier coatings
[NASA-CR-89309] p 101 N87-17926
Ester oxidation on an aluminum surface using chemiluminescence
[NASA-TP-2611] p 101 N87-18666
Effect of an oxygen plasma on uncoated thin aluminum reflecting films
[NASA-TM-89882] p 61 N87-21999
The oxidation degradation of aromatic compounds
[NASA-CR-180588] p 79 N87-22020
Thermo-oxidatively stable condensation polyimides containing 1,1,1-triaryl-2,2,2-trifluoroethane dianhydride and diamine monomers
[NASA-TM-89875] p 103 N87-22048
Oxidation protection coatings for polymers
[NASA-CASE-LEW-14072-3] p 103 N87-23736
A study of reduced chromium content in a nickel-base superalloy via element substitution and rapid solidification processing
[NASA-CR-179631] p 92 N87-25456
The tribological behavior of polyphenyl ether and polyphenyl thioether aromatic lubricants
[NASA-TM-100166] p 105 N87-26231
Hydrogen oxidation mechanism with applications to (1) the chaperon efficiency of carbon dioxide and (2) vitiated air testing
[NASA-TM-100186] p 80 N87-28628

OXIDATION RESISTANCE

Specimen geometry effects on graphite/PMR-15 composites during thermo-oxidative aging
p 71 A87-13145
Analysis of thermomechanical oxidation fields in thermal barrier coatings
p 174 A87-14316
Protection of solar array blankets from attack by low earth orbital atomic oxygen
p 47 A87-19874
Oxidation-resistant reflective surfaces for solar dynamic power generation in near Earth orbit
[NASA-TM-88865] p 56 N87-10960
Nickel base coating alloy
[NASA-CASE-LEW-13834-1] p 89 N87-14482
The effect of Cr, Co, Al, Mo and Ta on a series of cast Ni-base superalloys on the stability of an aluminide coating during cyclic oxidation in Mach 0.3 burner rig
[NASA-TM-88840] p 89 N87-14488
PMR polyimide compositions for improved performance at 371 deg C
[NASA-TM-88942] p 73 N87-16071
Oxide-dispersion-strengthened turbine blades, volume 1
[NASA-CR-179537-VOL-1] p 90 N87-17883
An evaluation of candidate oxidation resistant materials for space applications in LEO
[NASA-TM-100122] p 105 N87-25480
An evaluation of candidate oxidation resistant materials
p 80 N87-26203

OXIDE FILMS

Oxidation protection coatings for polymers
[NASA-CASE-LEW-14072-3] p 103 N87-23736

OXIDES

High temperature solid oxide regenerative fuel cell for solar photovoltaic energy storage
[NASA-TM-89872] p 194 N87-23020

OXIDIZERS

Low heat transfer oxidizer heat exchanger design and analysis
[NASA-CR-179488] p 58 N87-15272

OXYGEN

- Reaction of iron with hydrogen chloride-oxygen mixtures at 550 C p 83 A87-32001
- Multispecies CARS measurements in turbulent combustion p 79 N87-23808
- Oxygen interaction with space-power materials [NASA-CR-181396] p 80 N87-29633
- OXYGEN ATOMS**
- Protection of solar array blankets from attack by low earth orbital atomic oxygen p 47 A87-19874
- Effect of an oxygen plasma on the physical and chemical properties of several fluids for the Liquid Droplet Radiator [AIAA PAPER 87-0080] p 42 A87-22401
- Neutral atomic oxygen beam produced by ion charge exchange for Low Earth Orbital (LEO) simulation p 79 N87-26188
- An evaluation of candidate oxidation resistant materials p 80 N87-26203
- OXYGEN 18**
- Oxygen-18 tracer study of the passive thermal oxidation of silicon p 78 A87-51187

P

P-N JUNCTIONS

- Cell performance and defect behavior in proton-irradiated lithium-counterdoped n(+)-p silicon solar cells p 216 A87-14222
- Formation of a pn junction on an anisotropically etched GaAs surface using metalorganic chemical vapor deposition p 216 A87-21237
- Comparative performance of diffused junction indium phosphide solar cells p 197 N87-26441
- Solar cells in bulk InP using an open tube diffusion process p 198 N87-26444
- A V-grooved AlGaAs/GaAs passivated PN junction [NASA-TM-100138] p 218 N87-27541
- Modelling of multijunction cascade photovoltaics for space applications [NASA-CR-181417] p 200 N87-29958

P-TYPE SEMICONDUCTORS

- High-efficiency GaAs concentrator space cells p 196 N87-26417

PACKET SWITCHING

- On-board processing satellite network architecture and control study [NASA-CR-180816] p 44 N87-27710
- On-board processing satellite network architecture and control study [NASA-CR-180817] p 44 N87-27711

PAINTS

- An evaluation of candidate oxidation resistant materials p 80 N87-26203

PALMGREN-MINER RULE

- Re-examination of cumulative fatigue damage analysis - An engineering perspective p 174 A87-22128

PANEL METHOD (FLUID DYNAMICS)

- A panel method for counter rotating propfans [AIAA PAPER 87-1890] p 21 A87-45279

PARABOLIC REFLECTORS

- Optimization of spherical facets for parabolic solar concentrators p 213 A87-18173
- Solar dynamic power systems for space station p 58 N87-16024

PARALLEL COMPUTERS

- Time-partitioning simulation models for calculation on parallel computers [NASA-TM-89850] p 203 N87-20766

PARALLEL PLATES

- Reduction of the radar cross section of arbitrarily shaped cavity structures [NASA-CR-180307] p 118 N87-27085

PARALLEL PROCESSING (COMPUTERS)

- The utilization of parallel processing in solving the inviscid form of the average-passage equation system for multistage turbomachinery [AIAA PAPER 87-1108] p 5 A87-42057
- Increasing processor utilization during parallel computation rundown p 202 A87-52541
- WEST-3 wind turbine simulator development. Volume 2: Verification [NASA-CR-174982] p 191 N87-10531
- WEST-3 wind turbine simulator development. Volume 1: Summary [NASA-CR-174981] p 192 N87-11348
- WEST-3 wind turbine simulator development [NASA-CR-174983] p 192 N87-12046
- A comparison of five benchmarks [NASA-TM-88956] p 202 N87-17441
- Automating the parallel processing of fluid and structural dynamics calculations [NASA-TM-89837] p 203 N87-19002

- Time-partitioning simulation models for calculation on parallel computers [NASA-TM-89850] p 203 N87-20766
- The hypercluster: A parallel processing test-bed architecture for computational mechanics applications [NASA-TM-89823] p 203 N87-20767

PARALLEL PROGRAMMING

- Mathematical model partitioning and packing for parallel computer calculation p 202 A87-52534

PARALLELEPIPEDS

- Three-dimensional vibrations of twisted cantilevered parallelepipeds p 173 A87-11106

PARAMETERIZATION

- Parameterized materials and dynamic response characterizations in unidirectional composites [NASA-CR-4032] p 172 N87-13782

PARTIAL DIFFERENTIAL EQUATIONS

- Solution of elliptic PDEs by fast Poisson solvers using a local relaxation factor p 204 A87-21968
- On the validity of the modified equation approach to the stability analysis of finite-difference methods [AIAA PAPER 87-1120] p 204 A87-42069
- Solution of elliptic partial differential equations by fast Poisson solvers using a local relaxation factor. 2: Two-step method [NASA-TP-2530] p 205 N87-14918
- An exponential finite difference technique for solving partial differential equations [NASA-TM-89874] p 205 N87-24930

PARTICLE BEAMS

- Effect of hard particle impacts on the atomic oxygen survivability of reflector surfaces with transparent protective overcoats [AIAA PAPER 87-0104] p 69 A87-22417
- Effect of hard particle impacts on the atomic oxygen survivability of reflector surfaces with transparent protective overcoats [NASA-TM-88874] p 56 N87-11838

PARTICLE DIFFUSION

- Shallow n(+) diffusion into InP by an open-tube diffusion technique p 217 A87-30023

PARTICLE INTERACTIONS

- Effects of droplet interactions on droplet transport at intermediate Reynolds numbers [AIAA PAPER 87-0137] p 134 A87-24926
- Effects of droplet interactions on droplet transport at intermediate Reynolds numbers [NASA-CR-179567] p 26 N87-14348

PARTICLE LADEN JETS

- Particle-laden swirling free jets - Measurements and predictions [AIAA PAPER 87-0303] p 139 A87-42648
- Particle-laden swirling free jets: Measurements and predictions [NASA-TM-88904] p 26 N87-16826

PARTICLE SIZE DISTRIBUTION

- Representation of the vaporization behavior of turbulent polydisperse sprays by 'equivalent' monodisperse sprays [AIAA PAPER 87-1954] p 141 A87-45325
- Gas particle radiator p 141 A87-45646
- Representation of the vaporization behavior of turbulent polydisperse sprays by equivalent monodisperse sprays [NASA-TM-88906] p 26 N87-16827

PARTICLE TRAJECTORIES

- Particle trajectory computer program for icing analysis of axisymmetric bodies - A progress report [AIAA PAPER 87-0027] p 15 A87-22366
- Calculation of secondary electron trajectories in multistage depressed collectors for microwave amplifiers [NASA-TP-2664] p 125 N87-17991

PARTICLES

- Morphology of zirconia particles exposed to D.C. arc plasma jet [NASA-TM-88927] p 90 N87-16113
- Four spot laser anemometer and optical access techniques for turbine applications [NASA-TM-88972] p 156 N87-18057
- The temperature dependence of inelastic light scattering from small particles for use in combustion diagnostic instrumentation [NASA-CR-180399] p 80 N87-28634

PARTITIONS (MATHEMATICS)

- Mathematical model partitioning and packing for parallel computer calculation p 202 A87-52534
- Time-partitioning simulation models for calculation on parallel computers [NASA-TM-89850] p 203 N87-20766

PASSIVITY

- A V-grooved AlGaAs/GaAs passivated PN junction [NASA-TM-100138] p 218 N87-27541

PECLET NUMBER

- Thermocapillary bubble migration for large Marangoni Numbers [NASA-CR-179628] p 109 N87-22865

PERFORATED PLATES

- Transonic interference reduction by limited ventilation wall panels [NASA-CR-175039] p 15 N87-29419

PERFORMANCE PREDICTION

- Comparisons between thermodynamic and one-dimensional combustion models of spark-ignition engines p 161 A87-29275
- High speed wind tunnel tests of the PTA aircraft - Propfan Test Assessment Program [SAE PAPER 861744] p 4 A87-32619
- Computer-based phosphoric acid fuel cell analytical tools Descriptions and usages p 190 A87-33788
- Performance studies on an axial flow compressor stage p 138 A87-37208
- Comparison of two procedures for predicting rocket engine nozzle performance [AIAA PAPER 87-2071] p 52 A87-45391
- Gas particle radiator p 141 A87-45646
- Evaluation of icing drag coefficient correlations applied to iced propeller performance prediction [SAE PAPER 871033] p 16 A87-48761
- Surface protection p 88 N87-11182
- High temperature stress-strain analysis p 179 N87-11209
- A comparative study of some dynamic stall models [NASA-TM-88917] p 183 N87-18883
- Performance and efficiency evaluation and heat release study of an outboard Marine Corporation Rotary Combustion Engine [NASA-TM-89833] p 28 N87-20282
- Comparison of two procedures for predicting rocket engine nozzle performance [NASA-TM-89814] p 60 N87-20379
- Calibration and comparison of the NASA Lewis free-piston Stirling engine model predictions with RE-1000 test data [NASA-TM-89853] p 222 N87-22561

PERFORMANCE TESTS

- The noncavitating performance and life of a small vane-type positive displacement pump in liquid hydrogen [AIAA PAPER 86-1438] p 46 A87-17994
- Parametric and cycle tests of a 40-AH bipolar nickel-hydrogen battery p 46 A87-18093
- Baseband processor development/test performance for 30/20 GHz SS-TDMA communication system p 111 A87-18310
- Overview of the new ASME Performance Test Code for wind turbines [ASME PAPER 86-JPGC-PTC-4] p 190 A87-25475
- The effect of nonlinearities on the dynamic response of a large Shuttle payload [AIAA PAPER 87-0857] p 40 A87-33697
- Performance studies on an axial flow compressor stage p 138 A87-37208
- An anemometer for highly turbulent or recirculating flows p 154 A87-37698
- Small centrifugal pumps for low-thrust rockets p 50 A87-39808
- Arcjet component conditions through a multistart test [AIAA PAPER 87-1060] p 51 A87-41127
- The effect of ambient pressure on the performance of a resistojel [AIAA PAPER 87-0991] p 52 A87-42181
- 2000-hour cyclic endurance test of a laboratory model multipropellant resistojel [AIAA PAPER 87-0993] p 52 A87-45725
- Preliminary performance characterizations of an engineering model multipropellant resistojel for space station application [AIAA PAPER 87-2120] p 54 A87-50197
- Evaluation results of the 700 deg C Chinese strain gages p 155 N87-11189
- Develop and test fuel cell powered on site integrated total energy systems. Phase 3: Full-scale power plant development [NASA-CR-175118] p 191 N87-11344
- Outdoor test stand performance of a convertible engine with variable inlet guide vanes for advanced rotorcraft propulsion [NASA-TM-88939] p 26 N87-16825
- A comparison of five benchmarks [NASA-TM-88956] p 202 N87-17441
- Design of 9.271-pressure-ratio 5-stage core compressor and overall performance for first 3 stages [NASA-TP-2597] p 27 N87-17699
- Experimental evaluation of a translating nozzle sidewall radial turbine [NASA-TM-88963] p 27 N87-17701
- Bit-error-rate testing of high-power 30-GHz traveling wave tubes for ground-terminal applications [NASA-TP-2635] p 115 N87-17971
- Solid lubrication design methodology, phase 2 [NASA-CR-175114] p 221 N87-18470

- Performance and efficiency evaluation and heat release study of an outboard Marine Corporation Rotary Combustion Engine
[NASA-TM-89833] p 28 N87-20282
- Arcjet component conditions through a multistart test
[NASA-TM-89857] p 61 N87-20382
- Arcjet starting reliability: A multistart test on hydrogen/nitrogen mixtures
[NASA-TM-89867] p 61 N87-21998
- Radiation and temperature effects in gallium arsenide, indium phosphide and silicon solar cells
[NASA-TM-89870] p 127 N87-22098
- A 2000-hour cyclic endurance test of a laboratory model multipropellant resistojel
[NASA-TM-89854] p 167 N87-22237
- Regenerative fuel cell study for satellites in GEO orbit
[NASA-TM-89914] p 194 N87-22310
- Helicopter transmission testing at NASA Lewis Research Center
[NASA-TM-89912] p 168 N87-22978
- Component variations and their effects on bipolar nickel-hydrogen cell performance
[NASA-TM-89907] p 195 N87-23029
- Preliminary performance characterizations of an engineering model multipropellant resistojel for space station application
[NASA-TM-100113] p 111 N87-23821
- Test results of a 60 volt bipolar nickel-hydrogen battery
[NASA-TM-89927] p 195 N87-24029
- Test program to provide confidence in liquid oxygen cooling of hydrocarbon fueled rocket thrust chambers
p 67 N87-26114
- Design and performance of controlled-diffusion stator compared with original double-circular-arc stator
[NASA-TM-100141] p 31 N87-26910
- The design and analysis of single flank transmission error tester for loaded gears
[NASA-CR-179621] p 169 N87-27197
- Measurement uncertainty for the Uniform Engine Testing Program conducted at NASA Lewis Research Center
[NASA-TM-88943] p 33 N87-28557
- Propan test assessment propan propulsion system static test report
[NASA-CR-179613] p 33 N87-29536
- Resonant AC power system proof-of-concept test program
[NASA-CR-175069-VOL-1] p 129 N87-29738
- Resonant AC power system proof-of-concept test program, volume 2, appendix 1
[NASA-CR-175069-VOL-2] p 130 N87-29739
- Performance and power regulation characteristics of two aileron-controlled rotors and a pitchable tip-controlled rotor on the Mod-O turbine
[NASA-TM-100136] p 200 N87-29956
- PERMEABILITY**
Effect of water on hydrogen permeability
[NASA-TM-88898] p 221 N87-16664
- PERTURBATION**
Spatially growing disturbances in a high velocity ratio two-stream, coplanar jet
[AIAA PAPER 87-0056] p 3 A87-24996
- Spatially growing disturbances in a high velocity ratio two-stream, coplanar jet
[NASA-TM-88922] p 9 N87-14283
- Spatially growing disturbances in a two-stream, coplanar jet
[NASA-TM-88949] p 10 N87-16799
- PERTURBATION THEORY**
Microstrip dispersion including anisotropic substrates
p 123 A87-47621
- Development of a turbomachinery design optimization procedure using a multiple-parameter nonlinear perturbation method
[NASA-CR-3831] p 1 N87-10003
- Probabilistic finite elements
p 185 N87-22790
- PHASE CONJUGATION**
Large aperture interferometer with phase-conjugate self-reference beam
p 153 A87-17320
- PHASE CONTROL**
A design concept for an MMIC microstrip phased array
[NASA-TM-88834] p 114 N87-14569
- PHASE DIAGRAMS**
Analysis of NiAlTa precipitates in beta-NiAl + 2 at. pct Ta alloy
p 84 A87-34888
- PHASE TRANSFORMATIONS**
Transition from a planar interface to cellular and dendritic structures during rapid solidification processing
p 81 A87-12029
- Cellular-dendritic transition in directionally solidified binary alloys
p 84 A87-32046
- PHASED ARRAYS**
20-GHz phased-array-fed antennas utilizing distributed MMIC modules
p 112 A87-34527
- A design concept for an MMIC microstrip phased array
[NASA-TM-88834] p 114 N87-14569
- Advanced space communications architecture study. Volume 2: Technical report
[NASA-CR-179592] p 115 N87-18695
- A design concept for an MMIC (Monolithic Microwave Integrated Circuit) microstrip phased array
[AD-P005404] p 119 N87-28769
- PHENYLS**
Silsequioxanes as precursors to ceramic composites
[NASA-TM-89893] p 75 N87-25432
- PHOSPHORIC ACID**
Materials characterization of phosphoric acid fuel cell system
p 76 A87-23241
- Develop and test fuel cell powered on site integrated total energy systems. Phase 3: Full-scale power plant development
[NASA-CR-175118] p 191 N87-11344
- PHOSPHORIC ACID FUEL CELLS**
Status of commercial phosphoric acid fuel cell power plant system development
p 190 A87-33777
- Computer-based phosphoric acid fuel cell analytical tools Descriptions and usages
p 190 A87-33788
- Catalyst and electrode research for phosphoric acid fuel cells
p 190 A87-33789
- On the effect of the Fe(2+)/Fe(3+) redox couple on oxidation of carbon in hot H₃PO₄
p 78 A87-42677
- Corrosion of graphite composites in phosphoric acid fuel cells
p 72 A87-42684
- Develop and test fuel cell powered on-site integrated total energy systems. Phase 3: Full-scale power plant development
[NASA-CR-175117] p 191 N87-11346
- Organometallic catalysts for primary phosphoric acid fuel cells
[NASA-CR-179490] p 193 N87-19804
- Status of commercial fuel cell powerplant system development
[NASA-TM-89896] p 148 N87-22171
- PHOTOABSORPTION**
Ellipsometric and optical study of amorphous hydrogenated carbon films
p 216 A87-23967
- PHOTOCHEMICAL REACTIONS**
The 2,5-diacyl-1,4-dimethylbenzenes: Examples of bisphenol equivalents
[NASA-TM-89836] p 71 N87-22005
- PHOTOELASTICITY**
Fiber-optic photoelastic pressure sensor with fiber-loss compensation
p 154 A87-34566
- PHOTOELECTRIC MATERIALS**
Solar concentrator materials development
p 213 A87-18171
- PHOTOGRAMMETRY**
In-flight photogrammetric measurement of wing ice accretions
[AIAA PAPER 86-0483] p 15 A87-17995
- Demonstration of laser speckle system on burner liner cyclic rig
[NASA-CR-179509] p 155 N87-10377
- PHOTOGRAPHIC PROCESSING**
Black-and-white photographic chemistry: A reference
[NASA-TM-87296] p 70 N87-10177
- PHOTOLYSIS**
AlGaAs growth by OMCVD using an excimer laser
[NASA-TM-88937] p 218 N87-23304
- PHOTOVOLTAIC CELLS**
Space power - Emerging opportunities
[IAF PAPER 86-152] p 45 A87-15900
- Proposal for superstructure based high efficiency photovoltaics
p 120 A87-19104
- Combination solar photovoltaic heat engine energy converter
p 190 A87-47088
- Electrical power system design for the US space station
[NASA-TM-88824] p 58 N87-15267
- User evaluation of photovoltaic-powered vaccine refrigerator/freezer systems
[NASA-TM-88830] p 193 N87-18230
- Performance characteristics of a combination solar photovoltaic heat engine energy converter
[NASA-TM-89908] p 195 N87-23028
- Combination photovoltaic-heat engine energy converter
[NASA-CASE-LEW-14252-1] p 196 N87-25630
- Recent developments in indium phosphide space solar cell research
[NASA-TM-100139] p 68 N87-26141
- Development of a Fresnel lens concentrator for space application
p 196 N87-26427
- The space station power system
p 198 N87-28960
- Status of space station power system
p 45 N87-29915
- Computer modelling of aluminum-gallium arsenide/gallium arsenide multilayer photovoltaics
[NASA-CR-181418] p 200 N87-29957
- Modelling of multijunction cascade photovoltaics for space applications
[NASA-CR-181417] p 200 N87-29958
- PHOTOVOLTAIC CONVERSION**
Electrical power system for the U.S. Space Station
[IAF PAPER 86-37] p 45 A87-16138
- A photovoltaic power system and a low-power satellite earth station for Indonesia
p 189 A87-19859
- Tunisia Renewable Energy Project systems description report
[NASA-TM-88789] p 192 N87-13856
- Space station WP-04 power system. Volume 1: Executive summary
[NASA-CR-179587-VOL-1] p 65 N87-23695
- Space station WP-04 power system. Volume 2: Study results
[NASA-CR-179587-VOL-2] p 65 N87-23696
- Issues in space photovoltaic research and technology
[NASA-TM-89922] p 128 N87-23901
- Space Photovoltaic Research and Technology 1986. High Efficiency, Space Environment, and Array Technology
[NASA-CP-2475] p 196 N87-26413
- Space station power system
p 68 N87-26447
- High power/large area PV systems
p 198 N87-26452
- Alternative power generation concepts for space
p 199 N87-28961
- PHOTOVOLTAIC EFFECT**
Design, development and deployment of public service photovoltaic power/load systems for the Gabonese Republic
[NASA-CR-179603] p 195 N87-23030
- Development of an advanced photovoltaic concentrator system for space applications
[NASA-TM-100101] p 66 N87-24531
- PIEZOELECTRICITY**
One-dimensional wave propagation in rods of variable cross section: A WKB solution
[NASA-CR-4086] p 172 N87-24707
- PIGGYBACK SYSTEMS**
Measurement of Centaur/Orbiter multiple reaction forces in a full-scale test rig
p 38 A87-29448
- PILOT PERFORMANCE**
Acceleration display system for aircraft zero-gravity research
[NASA-TM-87358] p 156 N87-18801
- PIPE FLOW**
CONDIF - A modified central-difference scheme for convective flows
p 205 A87-53675
- PIPES (TUBES)**
Propagation of sound waves in tubes of noncircular cross section
[NASA-TP-2601] p 9 N87-14284
- Three dimensional boundary layers in internal flows
[NASA-CR-181336] p 152 N87-28860
- PISTON ENGINES**
EHD analysis of and experiments on pumping Leningrader seals
[NASA-CR-179570] p 168 N87-22246
- PISTONS**
Overview of the 1986 free-piston Stirling SP-100 activities at the NASA Lewis Research Center
p 160 A87-18033
- Automotive Stirling Engine Development Program
[NASA-CR-174873] p 222 N87-30223
- PITCH (INCLINATION)**
Design and dynamic simulation of a fixed pitch 56 kW wind turbine drive train with a continuously variable transmission
[NASA-CR-179543] p 193 N87-17401
- Advanced Prop-fan Engine Technology (APET) single- and counter-rotation gearbox/pitch change mechanism
[NASA-CR-168114-VOL-2] p 33 N87-28556
- Performance and power regulation characteristics of two aileron-controlled rotors and a pitchable tip-controlled rotor on the Mod-O turbine
[NASA-TM-100136] p 200 N87-29956
- PITCH (MATERIAL)**
Anticorrelation of Shubnikov-deHaas amplitudes and negative magnetoresistance magnitudes in intercalated pitch based graphite fibers
p 217 A87-28295
- Effects of graphitization on the environmental stability of brominated pitch-based fibers
[NASA-TM-88899] p 100 N87-12679
- Stability of bromine, iodine monochloride, copper (II) chloride, and nickel (II) chloride intercalated pitch-based graphite fibers
[NASA-TM-89904] p 103 N87-24563
- PITCHING MOMENTS**
Advanced Propfan Engine Technology (APET) definition study, single and counter-rotation gearbox/pitch change mechanism design
[NASA-CR-168115] p 32 N87-28554

PITTING

PITTING

- Mechanism of strength degradation for hot corrosion of alpha-SiC p 95 A87-21470
Corrosion pitting of SiC by molten salts p 76 A87-27165
Predicted effect of dynamic load on pitting fatigue life for low-contact-ratio spur gears [NASA-TP-2610] p 166 N87-18095
Hot corrosion attack and strength degradation of SiC and Si(sub)3N(sub)4 [NASA-TM-89820] p 102 N87-20425

PLANE STRAIN

- Fracture toughness of Si3N4 measured with short bar chevron-notched specimens p 96 A87-30621

PLANE WAVES

- DOE/NASA automotive Stirling engine project - Overview 86 p 220 A87-18034
Rays versus modes - Pictorial display of energy flow in an open-ended waveguide p 112 A87-44075

PLASMA ACCELERATION

- Rail gun performance and plasma characteristics due to wall ablation p 214 A87-18735

PLASMA CLOUDS

- Enhanced current flow through a plasma cloud by induction of plasma turbulence --- electrodynamic tethers for generating power for spacecraft in low earth orbit [AIAA PAPER 87-0573] p 214 A87-22714
Theory of plasma contactors used in the ionosphere p 122 A87-41610
Enhanced current flow through a plasma cloud by induction of plasma turbulence p 214 A87-48241

PLASMA CONTROL

- Plasma contactors for electrodynamic tether [NASA-TM-88850] p 215 N87-18428
Ground-based plasma contractor characterization [NASA-TM-100194] p 215 N87-28423

PLASMA CURRENTS

- Enhanced current flow through a plasma cloud by induction of plasma turbulence --- electrodynamic tethers for generating power for spacecraft in low earth orbit [AIAA PAPER 87-0573] p 214 A87-22714

PLASMA DENSITY

- Rail gun performance and plasma characteristics due to wall ablation p 214 A87-18735
The voltage threshold for arcing for solar cells in Leo - Flight and ground test results [AIAA PAPER 86-0362] p 50 A87-40275
Theory of plasma contactors for electrodynamic tethered satellite systems p 122 A87-41609
Measurements of plasma density and turbulence near the shuttle orbiter [NASA-CR-180102] p 215 N87-16614

PLASMA DIAGNOSTICS

- Measurements of plasma parameters in the vicinity of the Space Shuttle p 200 A87-24672
A review of research and development on the microwave-plasma electrothermal rocket [AIAA PAPER 87-1011] p 49 A87-38008
Measurements of plasma density and turbulence near the shuttle orbiter [NASA-CR-180102] p 215 N87-16614

PLASMA DYNAMICS

- The dynamic behavior of plasmas observed near geosynchronous orbit p 200 A87-31322

PLASMA ENGINES

- A review of research and development on the microwave-plasma electrothermal rocket [AIAA PAPER 87-1011] p 49 A87-38008
A computer model for the recombination zone of a microwave-plasma electrothermal rocket [AIAA PAPER 87-1014] p 50 A87-38009
An analysis of electromagnetic coupling and eigenfrequencies for microwave electrothermal thruster discharges [AIAA PAPER 87-1012] p 51 A87-41111

PLASMA FREQUENCIES

- Plasma properties in electron-bombardment ion thrusters [AIAA PAPER 87-1076] p 51 A87-41135

PLASMA HEATING

- A simple method for monitoring surface temperatures in plasma treatments p 160 A87-17269

PLASMA INTERACTION EXPERIMENT

- Computer simulation of plasma electron collection by PIX-II --- solar array-space plasma interaction p 45 A87-17837
Environmentally-induced discharge transient coupling to spacecraft [NASA-CR-174922] p 43 N87-10946

PLASMA INTERACTIONS

- Effect of an oxygen plasma on the physical and chemical properties of several fluids for the Liquid Droplet Radiator [AIAA PAPER 87-0080] p 42 A87-22401
The dynamic behavior of plasmas observed near geosynchronous orbit p 200 A87-31322

Electron beam experiments at high altitudes

p 44 N87-26946

PLASMA JETS

- Morphology of zirconia particles exposed to D.C. arc plasma jet [NASA-TM-88927] p 90 N87-16113

PLASMA POTENTIALS

- Hollow cathodes as electron emitting plasma contactors Theory and computer modeling [AIAA PAPER 87-0569] p 214 A87-22712

PLASMA SHEATHS

- Theory of plasma contactors for electrodynamic tethered satellite systems p 122 A87-41609

PLASMA SPRAYING

- High temperature tensile and creep behaviour of low pressure plasma-sprayed Ni-Co-Cr-Al-Y coating alloy p 82 A87-23429

- Low cycle fatigue behaviour of a plasma-sprayed coating material p 82 A87-24040

- A new chromium carbide-based tribological coating for use to 900 C with particular reference to the Stirling engine p 95 A87-26112

- New ZrO2-Yb2O3 plasma-sprayed coatings for thermal barrier applications p 98 A87-53623

- Mechanical behavior of thermal barrier coatings for gas turbine blades p 24 N87-11196

- Thermal barrier coating life prediction model [NASA-CR-179504] p 100 N87-13539

- Morphology of zirconia particles exposed to D.C. arc plasma jet [NASA-TM-88927] p 90 N87-16113

- Effects of atmosphere on the tribological properties of a chromium carbide based coating for use to 760 deg C [NASA-TM-88894] p 101 N87-16140

- Materials for Advanced Turbine Engines (MATE). Project 4: Erosion resistant compressor airfoil coating [NASA-CR-179622] p 92 N87-27029

PLASMA TEMPERATURE

- Rail gun performance and plasma characteristics due to wall ablation p 214 A87-18735

PLASMA TURBULENCE

- Enhanced current flow through a plasma cloud by induction of plasma turbulence --- electrodynamic tethers for generating power for spacecraft in low earth orbit [AIAA PAPER 87-0573] p 214 A87-22714
Enhanced current flow through a plasma cloud by induction of plasma turbulence p 214 A87-48241

PLASMA WAVES

- Radiation from large space structures in low earth orbit with induced ac currents [AIAA PAPER 87-0612] p 42 A87-22738

PLASMAS (PHYSICS)

- Plasma assisted surface coating/modification processes: An emerging technology [NASA-TM-88885] p 110 N87-12708
Secondary electron generation, emission and transport: Effects on spacecraft charging and NASCAP models p 44 N87-26950

PLASTIC DEFORMATION

- Plastic deformation of a magnesium oxide 001-plane surface produced by cavitation [ASLE PREPRINT 86-TC-3D-1] p 94 A87-19504
Opening and closing of cracks at high cyclic strains p 84 A87-34661

- The role of near-surface plastic deformation in the wear of lamellar solids p 162 A87-48500

- Hardness of CaF2 and BaF2 solid lubricants at 25 to 670 deg C [NASA-TM-88979] p 102 N87-18670

- Optical strain measurement system development, phase 1 [NASA-CR-179619] p 158 N87-22960

PLASTIC FLOW

- Effect of composition and grain size on slow plastic flow properties of NiAl between 1200 and 1400 K p 84 A87-36251
Structure and tensile strength of LaS(1.4) p 96 A87-38065

- Stochastic and fractal analysis of fracture trajectories p 179 A87-51167

PLASTIC PROPERTIES

- Effect of composition and grain size on slow plastic flow properties of NiAl between 1200 and 1400 K p 84 A87-36251

- Thermomechanical behavior of plasma-sprayed ZrO2-Y2O3 coatings influenced by plasticity, creep and oxidation [NASA-TM-88940] p 147 N87-18784

PLATES (STRUCTURAL MEMBERS)

- Compliance matrices for cracked bodies p 175 A87-25775

PLENUM CHAMBERS

- Experimental evaluation of blockage ratio and plenum evacuation system flow effects on pressure distribution for bodies of revolution in 0.1 scale model test section of NASA Lewis Research Center's proposed altitude wind tunnel [NASA-TP-2702] p 36 N87-22694

PLUG NOZZLES

- Free-jet acoustic investigation of high-radius-ratio conannular plug nozzles [NASA-CR-3818] p 210 N87-10753

PLUMES

- An analytical and experimental investigation of resistojet plumes [AIAA PAPER 87-0399] p 48 A87-24998

- Two-dimensional nozzle plume characteristics [AIAA PAPER 87-2111] p 6 A87-45413

- Secondary stream and excitation effects on two-dimensional nozzle plume characteristics [AIAA PAPER 87-2112] p 6 A87-45414

- Langmuir probe surveys of an arcjet exhaust [AIAA PAPER 87-1950] p 54 A87-50193

- An analytical and experimental investigation of resistojet plumes [NASA-TM-88852] p 58 N87-14428

- Secondary stream and excitation effects on two-dimensional nozzle plume characteristics [NASA-TM-89813] p 12 N87-18539

- Two-dimensional nozzle plume characteristics [NASA-TM-89812] p 12 N87-18540

- Langmuir probe surveys of an arcjet exhaust [NASA-TM-89924] p 64 N87-22807

PLY ORIENTATION

- Design concepts/parameters assessment and sensitivity analyses of select composite structural components p 175 A87-25407
Simplified composite micromechanics for predicting microstresses p 179 A87-49275

POINT DEFECTS

- A point defect model for nickel electrode structures p 87 A87-52282

POINTING CONTROL SYSTEMS

- Solar dynamic power systems for space station p 58 N87-16024

POISSON RATIO

- Elastic interaction of a crack with a microcrack array. I - Formulation of the problem and general form of the solution. II - Elastic solution for two crack configurations (piecewise constant and linear approximations) p 178 A87-36926

POLARIZATION (WAVES)

- A new formulation of electromagnetic wave scattering using an on-surface radiation boundary condition approach p 112 A87-32829

POLARIZATION CHARACTERISTICS

- Performance study of a fuel cell Pt-on-C anode in presence of CO and CO2, and calculation of adsorption parameters for CO poisoning p 188 A87-12338
Radar cross section of an open-ended circular waveguide Calculation of second-order diffraction terms p 112 A87-31626

POLYCRYSTALS

- Ultrasonic verification of microstructural changes due to heat treatment p 208 A87-10772

- The effects of tantalum on the microstructure of two polycrystalline nickel-base superalloys - B-1900 + Hf and MAR-M247 p 82 A87-24110

- Deformation and fracture of single-crystal and sintered polycrystalline silicon carbide produced by cavitation [NASA-TM-88981] p 102 N87-20422

POLYIMIDE RESINS

- Structure-to-property relationships in addition cured polymers. II - Resin Tg and composite initial mechanical properties of norbornenyl cured polyimide resins p 96 A87-38638

- Quantitative analysis of PMR-15 polyimide resin by HPLC p 69 A87-48314

- PMR polyimide compositions for improved performance at 371 deg C [NASA-TM-88942] p 73 N87-16071

POLYIMIDES

- A mechanistic study of polyimide formation from diester-diacids p 70 A87-53671

- Substituted 1,1,1-triaryl-2,2,2-trifluoroethanes and processes for their synthesis --- synthetic routes to monomers for polyimides [NASA-CASE-LEW-14345-1] p 70 N87-14432

- New condensation polyimides containing 1,1,1-triaryl-2,2,2-trifluoroethane structures [NASA-CASE-LEW-14346-1] p 70 N87-14433

- Thermo-oxidatively stable condensation polyimides containing 1,1,1-triaryl-2,2,2-trifluoroethane dianhydride and diamine monomers [NASA-TM-89875] p 103 N87-22048

- Oxidation protection coatings for polymers [NASA-CASE-LEW-14072-3] p 103 N87-23736

POLYMER CHEMISTRY

- Substituted 1,1,1-triaryl-2,2,2-trifluoroethanes and processes for their synthesis --- synthetic routes to monomers for polyimides
[NASA-CASE-LEW-14345-1] p 70 N87-14432
- New condensation polyimides containing 1,1,1-triaryl-2,2,2-trifluoroethane structures
[NASA-CASE-LEW-14346-1] p 70 N87-14433

POLYMER MATRIX COMPOSITES

- Counterface effects on the tribological properties of polyimide composites p 95 A87-27625
- PMR polyimide compositions for improved performance at 371 deg C
[NASA-TM-88942] p 73 N87-16071
- Addition polymers from 1,4,5,8-tetrahydro-1,4,5,8-diepoxyanthracene and Bis-dienes: Processable resins for high temperature application
[NASA-TM-89838] p 103 N87-20426
- Styrene-terminated polysulfone oligomers as matrix material for graphite reinforced composites: An initial study
[NASA-TM-89846] p 74 N87-21043

POLYMERIC FILMS

- Tribological properties of polymer films and solid bodies in a vacuum environment
[NASA-TM-88966] p 101 N87-17906

POLYMERIZATION

- Structure-to-property relationships in addition cured polymers. II - Resin Tg and composite initial mechanical properties of norbornenyl cured polyimide resins
p 96 A87-38638
- A mechanistic study of polyimide formation from diester-diads
p 70 A87-53671
- New condensation polyimides containing 1,1,1-triaryl-2,2,2-trifluoroethane structures
[NASA-CASE-LEW-14346-1] p 70 N87-14433
- Polymer precursors for ceramic matrix composites
[NASA-CR-179562] p 70 N87-14434
- Styrene-terminated polysulfone oligomers as matrix material for graphite reinforced composites: An initial study
[NASA-TM-89846] p 74 N87-21043

POLYMERS

- Oxidation protection coatings for polymers
[NASA-CASE-LEW-14072-3] p 103 N87-23736

POLYPHENYL ETHER

- The tribological behavior of polyphenyl ether and polyphenyl thioether aromatic lubricants
[NASA-TM-100166] p 105 N87-26231

POLYSTYRENE

- An analysis for crack layer stability
p 176 A87-28982

POLYTETRAFLUOROETHYLENE

- Investigation of PTFE transfer films by infrared emission spectroscopy and phase-locked ellipsometry
[NASA-TM-89844] p 102 N87-20421

POROSITY

- Defects in nickel-base superalloys p 86 A87-49790
- Fatigue damage interaction behavior of PWA 1480
p 92 N87-22777

POROUS MATERIALS

- Effect of flow oscillations on axial energy transport in a porous material p 135 A87-27715

POTASSIUM HYDROXIDES

- KOH concentration effect on cycle life of nickel-hydrogen cells p 199 N87-29920

POWDER (PARTICLES)

- Particle-size reduction of Si₃N₄ powder with Si₃N₄ milling hardware p 94 A87-12936
- Colloidal characterization of ultrafine silicon carbide and silicon nitride powders p 95 A87-19625
- Processing of laser formed SiC powder
[NASA-CR-179857] p 99 N87-11009
- Processing of laser formed SiC powder
[NASA-CR-179638] p 104 N87-24573
- Stability and rheology of dispersions of silicon nitride and silicon carbide
[NASA-CR-179634] p 104 N87-25476

POWDER METALLURGY

- Analysis of the solidified structure of rheocast and VADER processed nickel-base superalloy
p 83 A87-28734

POWER

- Resonant AC power system proof-of-concept test program
[NASA-CR-175069-VOL-1] p 129 N87-29738

POWER AMPLIFIERS

- Ultra small electron beam amplifiers p 122 A87-42681
- The 20 GHz GaAs monolithic power amplifier module development
[NASA-CR-174742] p 124 N87-11104

POWER CONDITIONING

- Description of a 20 kilohertz power distribution system p 120 A87-18115

SP-100 Advanced Technology Program

- [NASA-TM-89888] p 194 N87-23027
- Control considerations for high frequency, resonant, power processing equipment used in large systems
[NASA-TM-89926] p 64 N87-23690
- A study of Schwarz converters for nuclear powered spacecraft
[NASA-TM-89911] p 128 N87-23903

POWER CONVERTERS

- Reliability and mass analysis of dynamic power conversion systems with parallel or standby redundancy p 190 A87-21823
- Space Station 20-kHz power management and distribution system p 49 A87-36913

POWER EFFICIENCY

- Evaluation of Stirling engine appendix gap losses p 160 A87-18037
- Proposal for superstructure based high efficiency photovoltaics p 120 A87-19104
- Improvements in MDC and TWT overall efficiency through the application of carbon electrode surfaces --- Multistage Depressed Collectors p 120 A87-20667

POWER FACTOR CONTROLLERS

- Resistojet control and power for high frequency ac buses
[AIAA PAPER 87-0994] p 122 A87-41103
- Resistojet control and power for high frequency ac buses
[NASA-TM-89860] p 126 N87-20477

POWER LINES

- Coaxial tube tether/transmission line for manned nuclear space power
[NASA-CASE-LEW-14338-1] p 55 N87-10174

POWER TRANSMISSION

- Optimizing the antenna system of a microwave space power station: Implications for the selection of operating power, frequency and antenna size
[NASA-TM-100184] p 206 N87-30132

PRECIPITATES

- Analysis of NiAlTa precipitates in beta-NiAl + 2 at. pct Ta alloy p 84 A87-34888

PRECIPITATION HARDENING

- Analysis of NiAlTa precipitates in beta-NiAl + 2 at. pct Ta alloy p 84 A87-34888
- Oxide-dispersion-strengthened turbine blades, volume 1
[NASA-CR-179537-VOL-1] p 90 N87-17883

PRECISION

- Analysis of the vibratory excitation arising from spiral bevel gears
[NASA-CR-4081] p 169 N87-25579

PREDICTION ANALYSIS TECHNIQUES

- Dynamic data acquisition, reduction, and analysis for the identification of high-speed compressor component post-stability characteristics
[AIAA PAPER 87-2089] p 162 A87-45398
- Turbine Engine Hot Section Technology, 1984
[NASA-CP-2339] p 179 N87-11180

Host turbine heat transfer overview

- p 144 N87-11184
- Turbine airfoil deposition models p 24 N87-11191
- Experimental verification of vapor deposition model in Mach 0.3 burner rigs p 88 N87-11192
- Effects of surface chemistry on hot corrosion life p 88 N87-11193

- Coating life prediction p 99 N87-11194
- Introduction to life modeling of thermal barrier coatings p 99 N87-11195
- Mechanical behavior of thermal barrier coatings for gas turbine blades p 24 N87-11196

- Aerothermal modeling program, phase 2 p 24 N87-11200
- High temperature stress-strain analysis p 179 N87-11209

- High-temperature constitutive modeling p 179 N87-11210
- Creep fatigue life prediction for engine hot section materials (isotropic): Two year update p 171 N87-11213

- Turbine airfoil gas side heat transfer p 144 N87-11219
- Calculation of two- and three-dimensional transonic cascade flow field using the Navier-Stokes equations p 144 N87-11220

- Gas flow environmental and heat transfer nonrotating 3D program p 145 N87-11223
- Assessment of a 3-D boundary layer code to predict heat transfer and flow losses in a turbine p 145 N87-11224

- Thermal barrier coating life prediction model
[NASA-CR-175010] p 100 N87-13540
- Turbine vane external heat transfer. Volume 2. Numerical solutions of the Navier-Stokes equations for two- and three-dimensional turbine cascades with heat transfer
[NASA-CR-174828] p 145 N87-13661

Creep fatigue life prediction for engine hot section materials (ISOTROPIC)

- [NASA-CR-179550] p 181 N87-15491
- Development of a rotor wake/vortex model. Volume 2: User's manual for computer program
[NASA-CR-174850-VOL-2] p 13 N87-20239

- Unstalled flutter stability predictions and comparisons to test data for a composite prop-fan model
[NASA-CR-179512] p 28 N87-21955

- Life prediction and constitutive models for engine hot section anisotropic materials
[NASA-CR-179594] p 29 N87-23622

- Self-consistent inclusion of space-charge in the traveling wave tube
[NASA-TM-89928] p 128 N87-24630

- Free-jet investigation of mechanically suppressed, high radius ratio conannular plug model nozzles
[NASA-CR-3596] p 212 N87-29315

PREDICTIONS

- Particle-laden swirling free jets - Measurements and predictions
[AIAA PAPER 87-0303] p 139 A87-42648

- Thermal barrier coating life prediction model development
[NASA-CR-179508] p 99 N87-11892

- Advanced solar dynamic space power systems perspectives, requirements and technology needs
[NASA-TM-88884] p 56 N87-12606

- Thermal barrier coating life prediction model
[NASA-CR-179504] p 100 N87-13539

- Particle-laden swirling free jets: Measurements and predictions
[NASA-TM-88904] p 26 N87-16826

- Calculation of thermomechanical fatigue life based on isothermal behavior
[NASA-TM-88864] p 183 N87-20565

- A prediction model of the depth-of-discharge effect on the cycle life of a storage cell
[NASA-TM-89915] p 194 N87-22311

- Progress in the prediction of unsteady heat transfer on turbine blades p 149 N87-22769
- Environmental degradation of 316 stainless steel in high temperature low cycle fatigue
[NASA-TM-89931] p 185 N87-24007

- Comparison of theoretical and experimental thrust performance of a 1030:1 area ratio rocket nozzle at a chamber pressure of 2413 kN/m² (350 psia)
[NASA-TP-2725] p 66 N87-25423

- Turbulence characteristics of an axisymmetric reacting flow
[NASA-CR-180697] p 152 N87-27973

PREFORMS

- Method of preparing fiber reinforced ceramic material
[NASA-CASE-LEW-14392-1] p 106 N87-28656

PREMIXED FLAMES

- Gravitational effects on the structure and propagation of premixed flames
[IAF PAPER 86-279] p 76 A87-15983

PREPROCESSING

- A computer controlled signal preprocessor for laser fringe anemometer applications
[NASA-TM-88982] p 157 N87-20516

PRESSING (FORMING)

- Improved consolidation of silicon carbide p 94 A87-12940

PRESSURE

- Airflow calibration and exhaust pressure/temperature survey of an F404, S/N 215-109, turbofan engine
[NASA-TM-100159] p 33 N87-29537

PRESSURE DISTRIBUTION

- A universal equation of state for solids p 219 A87-14665
- Acoustic power measurement for single and annular stream duct-nozzle systems utilizing a modal decomposition scheme p 209 A87-37628

- Simultaneous measurements of two-dimensional velocity and pressure fields in compressible flows through image-intensified detection of laser-induced fluorescence p 143 A87-52320

- A comparison of experimental and theoretical results for labyrinth gas seals
[NASA-CR-180194] p 166 N87-18096

- Experimental evaluation of honeycomb/screen configurations and short contraction section for NASA Lewis Research Center's altitude wind tunnel
[NASA-TP-2692] p 36 N87-23662

PRESSURE EFFECTS

- The effect of ambient pressure on the performance of a resistojet
[AIAA PAPER 87-0991] p 52 A87-42181

PRESSURE GRADIENTS

- Refrigerated dynamic seal to 6.9 MPa (1000 psi) p 164 A87-50777

PRESSURE MEASUREMENT

Acoustic power measurement for single and annular stream duct-nozzle systems utilizing a modal decomposition scheme p 209 A87-37628
Surface pressure measurements on the blade of an operating Mod-2 wind turbine with and without vortex generators [NASA-TM-89903] p 198 N87-26455

PRESSURE OSCILLATIONS

Summary of investigations of engine response to distorted inlet conditions p 30 N87-24477

PRESSURE SENSORS

Fiber-optic photoelastic pressure sensor with fiber-loss compensation p 154 A87-34566
Spectrum-modulating fiber-optic sensors for aircraft control systems [NASA-TM-89968] p 27 N87-17700

PRESSURE VESSELS

Initial performance of advanced designs for IPV nickel-hydrogen cells [NASA-TM-87282] p 192 N87-16445

PRESSURIZED WATER REACTORS

Laser anemometry measurements of natural circulation flow in a scale model PWR reactor system — Pressurized Water Reactor p 154 A87-40750

PRESTRESSING

Nonlinear vibration and stability of rotating, pretwisted, precone blades including Coriolis effects p 178 A87-39896

PRETREATMENT

Colloidal characterization of ultrafine silicon carbide and silicon nitride powders p 95 A87-19625

PROBABILITY THEORY

SCARE - A postprocessor program to MSC/NASTRAN for reliability analysis of structural ceramic components [ASME PAPER 86-GT-34] p 174 A87-17988
A probabilistic Hu-Washizu variational principle [AIAA PAPER 87-0764] p 176 A87-33579
Probabilistic structural analysis to quantify uncertainties associated with turbopump blades [AIAA PAPER 87-0766] p 176 A87-33581
Composite load spectra for select space propulsion structural components [NASA-CR-179496] p 55 N87-10176
Probabilistic structural analysis methods for space propulsion system components [NASA-TM-88861] p 181 N87-13794
Probabilistic structural analysis to evaluate the structural durability of SSME critical components p 62 N87-22783
Probabilistic Structural Analysis Methods (PSAM) for select space propulsion system structural components p 62 N87-22784
The NESSUS finite element code p 184 N87-22785
Probabilistic finite elements p 185 N87-22790
Composite load spectra for select space propulsion structural components p 63 N87-22793
Variational approach to probabilistic finite elements [NASA-CR-181343] p 206 N87-29212

PROBES

Precision tunable resonant microwave cavity [NASA-CASE-LEW-13935-1] p 126 N87-21234

PROBLEM SOLVING

An efficient method for solving the steady Euler equations [NASA-TM-87329] p 205 N87-11543
Solution of elliptic partial differential equations by fast Poisson solvers using a local relaxation factor. 2: Two-step method [NASA-TP-2530] p 205 N87-14918
Common problems and pitfalls in gear design [NASA-TM-88858] p 165 N87-17033
A Navier-Stokes solver using the LU-SSOR TVD algorithm [NASA-CR-179608] p 13 N87-20243
An exponential finite difference technique for solving partial differential equations [NASA-TM-89874] p 205 N87-24930
Thermo-elasto-viscoplastic analysis of problems in extension and shear [NASA-CR-181410] p 187 N87-29896

PROCESS CONTROL (INDUSTRY)

Particle cloud kinetics in microgravity [AIAA PAPER 87-0577] p 107 A87-22716
NDE reliability and process control for structural ceramics [ASME PAPER 87-GT-8] p 171 A87-48702
NDE reliability and process control for structural ceramics [NASA-TM-88870] p 171 N87-12910

PROJECT MANAGEMENT

Space experiment development process p 109 N87-21156

PROJECT PLANNING

Strategic plan, 1985 [NASA-TM-89263] p 219 N87-12384

Space station experiment definition: Long-term cryogenic fluid storage [NASA-CR-4072] p 151 N87-24641
Spacecraft 2000: The challenge of the future p 68 N87-26448

PROP-FAN TECHNOLOGY

Application of propfan propulsion to general aviation [AIAA PAPER 86-2698] p 18 A87-17934
High-speed propeller noise predictions - Effects of boundary conditions used in blade loading calculations [AIAA PAPER 87-0525] p 208 A87-24978
A model propulsion simulator for evaluating counter rotating blade characteristics [SAE PAPER 861715] p 20 A87-32607
High speed wind tunnel tests of the PTA aircraft — Propfan Test Assessment Program [SAE PAPER 861744] p 4 A87-32619
Structural tailoring of advanced turboprops [AIAA PAPER 87-0753] p 177 A87-33648
Analytical and experimental investigation of mistuning in propfan flutter [AIAA PAPER 87-0739] p 178 A87-40496
Analytical flutter investigation of a composite propfan model [AIAA PAPER 87-0738] p 178 A87-40497
Three-dimensional unsteady Euler solutions for propfans and counter-rotating propfans in transonic flow [AIAA PAPER 87-1197] p 5 A87-42314
A panel method for counter rotating propfans [AIAA PAPER 87-1890] p 21 A87-45279
Wind tunnel tests on a one-foot diameter SR-7L propfan model [AIAA PAPER 87-1892] p 6 A87-45281
Results of acoustic tests of a Prop-Fan model [AIAA PAPER 87-1894] p 209 A87-45282
Static tests of the propulsion system — Propfan Test Assessment program [AIAA PAPER 87-1728] p 23 A87-52245
Wind tunnel performance results of an aeroelastically scaled 2/9 model of the PTA flight test prop-fan [AIAA PAPER 87-1893] p 8 A87-52251
PTA test bed aircraft engine inlet model test report, revised [NASA-CR-174845] p 23 N87-10866
Analytical flutter investigation of a composite propfan model [NASA-TM-88944] p 182 N87-18115
Analytical and experimental investigation of mistuning in propfan flutter [NASA-TM-88959] p 182 N87-18116
Unstalled flutter stability predictions and comparisons to test data for a composite prop-fan model [NASA-CR-179512] p 28 N87-21955
Structural and aeroelastic analysis of the SR-7L propfan [NASA-TM-86877] p 184 N87-22273
Wind tunnel performance results of an aeroelastically scaled 2/9 model of the PTA flight test prop-fan [NASA-TM-89917] p 14 N87-25294
A computational procedure for automated flutter analysis [NASA-TM-100171] p 187 N87-28058
Advanced Prop-fan Engine Technology (APET) single- and counter-rotation gearbox/pitch change mechanism [NASA-CR-168114-VOL-1] p 32 N87-28552
Advanced Propfan Engine Technology (APET) definition study, single and counter-rotation gearbox/pitch change mechanism design [NASA-CR-168115] p 32 N87-28554
Advanced Prop-fan Engine Technology (APET) single- and counter-rotation gearbox/pitch change mechanism [NASA-CR-168114-VOL-2] p 33 N87-28556
Propfan test assessment testbed aircraft flutter model test report [NASA-CR-179458] p 14 N87-29413
Propfan test assessment propfan propulsion system static test report [NASA-CR-179613] p 33 N87-29536

PROPAGATION MODES

Elastic analysis of a mode II fatigue crack test specimen p 174 A87-17799

PROPELLANT PROPERTIES

A variable geometry combustor for broadened properties fuels [AIAA PAPER 87-1832] p 23 A87-52246

PROPELLANT TANKS

Development and test of the Shuttle/Centaur cryogenic tankage thermal protection system [AIAA PAPER 87-1557] p 43 A87-43073

PROPELLANT TESTS

Volume-energy parameters for heat transfer to supercritical fluids p 137 A87-32326

PROPELLANT TRANSFER

Thermodynamic analysis and subscale modeling of space-based orbit transfer vehicle cryogenic propellant resupply [AIAA PAPER 87-1764] p 142 A87-48572
Thermodynamic analysis and subscale modeling of space-based orbit transfer vehicle cryogenic propellant resupply [NASA-TM-89921] p 150 N87-22949

PROPELLANTS

Liquid oxygen cooling of high pressure LOX/hydrocarbon rocket thrust chambers [NASA-TM-88805] p 57 N87-14426
Water-propellant resistojets for man-tended platforms [NASA-TM-100110] p 68 N87-26135

PROPELLER BLADES

Structural tailoring of advanced turboprops [AIAA PAPER 87-0753] p 177 A87-33648
Influence of third-degree geometric nonlinearities on the vibration and stability of pretwisted, precone, rotating blades p 21 A87-46228
Wind tunnel performance results of an aeroelastically scaled 2/9 model of the PTA flight test prop-fan [AIAA PAPER 87-1893] p 8 A87-52251
Effect of angular inflow on the vibratory response of a counter-rotating propeller [NASA-CR-174819] p 8 N87-10840
Dynamic response and stability of a composite prop-fan model [NASA-CR-179528] p 28 N87-21956
Wind tunnel performance results of an aeroelastically scaled 2/9 model of the PTA flight test prop-fan [NASA-TM-89917] p 14 N87-25294
Propfan test assessment propfan propulsion system static test report [NASA-CR-179613] p 33 N87-29536

PROPELLER EFFICIENCY

Evaluation of icing drag coefficient correlations applied to iced propeller performance prediction [SAE PAPER 871033] p 16 A87-48761

PROPELLER FANS

Computational aeroacoustics of propeller noise in the near and far field [AIAA PAPER 87-0254] p 19 A87-24944
Wind tunnel performance results of an aeroelastically scaled 2/9 model of the PTA flight test prop-fan [AIAA PAPER 87-1893] p 8 A87-52251
Dynamic response and stability of a composite prop-fan model [NASA-CR-179528] p 28 N87-21956
Dynamic response of two composite prop-fan models on a nacelle/wing/fuselage half model [NASA-CR-179589] p 18 N87-23615
Wind tunnel performance results of an aeroelastically scaled 2/9 model of the PTA flight test prop-fan [NASA-TM-89917] p 14 N87-25294
Cruise noise of the 2/9th scale model of the Large-scale Advanced Propfan (LAP) propeller, SR-7A [NASA-TM-100175] p 212 N87-28398

PROPELLERS

Propeller design by optimization p 18 A87-14123
Measurement of a counter rotation propeller flowfield using a Laser Doppler Velocimeter [AIAA PAPER 87-0008] p 3 A87-24901
Experimental and theoretical study of propeller spinner/shank interference [AIAA PAPER 87-0145] p 3 A87-24929
High-speed propeller noise predictions - Effects of boundary conditions used in blade loading calculations [AIAA PAPER 87-0525] p 208 A87-24978
Off-design analysis of counter-rotating propeller configurations p 20 A87-27989
Measured noise of a scale model high speed propeller at simulated takeoff/approach conditions [AIAA PAPER 87-0526] p 208 A87-31109
Structureborne noise control in advanced turboprop aircraft [AIAA PAPER 87-0530] p 209 A87-31110
Euler analysis of transonic propeller flows p 4 A87-39813
Numerical simulation of transonic propeller flow using a three-dimensional small disturbance code employing novel helical coordinates [AIAA PAPER 87-1162] p 5 A87-42107
Euler analysis of the three-dimensional flow field of a high-speed propeller - Boundary condition effects [ASME PAPER 87-GT-253] p 6 A87-48719
High-speed propeller noise predictions: Effects of boundary conditions used in blade loading calculations [NASA-TM-88913] p 210 N87-14957
Structureborne noise control in advanced turboprop aircraft [NASA-TM-88947] p 211 N87-16587
Measured noise of a scale model high speed propeller at simulated takeoff/approach conditions [NASA-TM-88920] p 211 N87-16588

Euler analysis of the three dimensional flow field of a high-speed propeller: Boundary condition effects
[NASA-TM-88955] p 10 N87-16798

Noise reduction for model counterrotation propeller at cruise by reducing aft-propeller diameter
[NASA-TM-88936] p 211 N87-19057

Numerical simulation of transonic propeller flow using a 3-dimensional small disturbance code employing novel helical coordinates
[NASA-TM-89826] p 12 N87-19350

Coupled aerodynamic and acoustical predictions for turboprops
[NASA-TM-87094] p 13 N87-23598

The effect of front-to-rear propeller spacing on the interaction noise of a model counterrotation propeller at cruise conditions
[NASA-TM-100121] p 212 N87-28396

PROPULSION SYSTEM CONFIGURATIONS

Engine studies for future subsonic cruise missiles
[AIAA PAPER 86-1547] p 19 A87-21513

Propulsion recommendations for Space Station free flying platforms
p 49 A87-31134

Advanced technology payoffs for future small propulsion systems
p 21 A87-47081

A variable geometry combustor for broadened properties fuels
[AIAA PAPER 87-1832] p 23 A87-52246

Potential propellant storage and feed systems for space station resistojet propulsion options
[NASA-CR-179457] p 59 N87-16065

Space station propulsion system technology
[NASA-TM-100108] p 66 N87-25422

Internal computational fluid mechanics on supercomputers for aerospace propulsion systems
p 151 N87-26002

Propulsion recommendations for space station free flying platforms
p 67 N87-26129

Advanced Propan Engine Technology (APET) and single-rotation gearbox/pitch change mechanism
[NASA-CR-168113] p 32 N87-28553

PROPULSION SYSTEM PERFORMANCE

Propeller design by optimization
p 18 A87-14123

Performance characteristics of ring-cusp thrusters with xenon propellant
[AIAA PAPER 86-1392] p 46 A87-17992

Status of advanced propulsion for space based orbital transfer vehicle
[IAF PAPER 86-183] p 48 A87-23239

Microwave electrothermal thruster performance in helium gas
p 49 A87-31281

A model propulsion simulator for evaluating counter rotating blade characteristics
[SAE PAPER 861715] p 20 A87-32607

Performance characterization of a low power hydrazine arcjet
[AIAA PAPER 87-1057] p 50 A87-39634

Comparison of theoretical and experimental thrust performance of a 1030:1 area ratio rocket nozzle at a chamber pressure of 2413 kN/sq m (350 psia)
[AIAA PAPER 87-2069] p 52 A87-45390

Oxidizer heat exchangers for rocket engine operation in idle modes
[AIAA PAPER 87-2117] p 52 A87-45418

Status of xenon ion propulsion technology
[AIAA PAPER 87-1003] p 53 A87-48677

Static tests of the propulsion system --- Propan Test Assessment program
[AIAA PAPER 87-1728] p 23 A87-52245

Status of advanced propulsion for space based orbital transfer vehicle
[NASA-TM-88848] p 56 N87-10959

Summary of investigations of engine response to distorted inlet conditions
p 30 N87-24477

Propulsion recommendations for space station free flying platforms
p 67 N87-26129

Advanced Prop-fan Engine Technology (APET) single- and counter-rotation gearbox/pitch change mechanism
[NASA-CR-168114-VOL-1] p 32 N87-28552

PROPYL COMPOUNDS

Silsesquioxanes as precursors to ceramic composites
[NASA-TM-89893] p 75 N87-25432

PROTECTIVE COATINGS

Solar concentrator materials development
p 213 A87-18171

Protection of solar array blankets from attack by low earth orbital atomic oxygen
p 47 A87-19874

Carbon and carbon-coated electrodes for multistage depressed collectors for electron-beam devices - A technology review
p 120 A87-20666

Effect of hard particle impacts on the atomic oxygen survivability of reflector surfaces with transparent protective overcoats
[AIAA PAPER 87-0104] p 69 A87-22417

The survivability of large space-borne reflectors under atomic oxygen and micrometeoroid impact
[AIAA PAPER 87-0341] p 49 A87-31300

Stress rupture and creep behavior of a low pressure plasma-sprayed NiCoCrAlY coating alloy in air and vacuum
p 85 A87-43396

Oxidation-resistant reflective surfaces for solar dynamic power generation in near Earth orbit
[NASA-TM-88865] p 56 N87-10960

Surface protection
p 88 N87-11182

Turbine airfoil deposition models
p 24 N87-11191

Coating life prediction
p 99 N87-11194

Effect of hard particle impacts on the atomic oxygen survivability of reflector surfaces with transparent protective overcoats
p 56 N87-11838

Thermal barrier coating life prediction model development
[NASA-CR-179508] p 99 N87-11892

Plasma assisted surface coating/modification processes: An emerging technology
[NASA-TM-88885] p 110 N87-12708

Thermal barrier coating life prediction model
[NASA-CR-179504] p 100 N87-13539

Thermal barrier coating life prediction model
[NASA-CR-175010] p 100 N87-13540

The survivability of large space-borne reflectors under atomic oxygen and micrometeoroid impact
[NASA-TM-88914] p 57 N87-14423

Nickel base coating alloy
[NASA-CASE-LEW-13834-1] p 89 N87-14482

Effect of water on hydrogen permeability
[NASA-TM-88898] p 221 N87-16664

Oxide-dispersion-strengthened turbine blades, volume 1
[NASA-CR-179537-VOL-1] p 90 N87-17883

Degradation mechanisms in thermal barrier coatings
[NASA-TM-89309] p 101 N87-17926

Thermomechanical behavior of plasma-sprayed ZrO₂-Y₂O₃ coatings influenced by plasticity, creep and oxidation
[NASA-TM-88940] p 147 N87-18784

Bithermal low-cycle fatigue behavior of a NiCoCrAlY-coated single crystal superalloy
[NASA-TM-89831] p 91 N87-20408

Oxidation protection coatings for polymers
[NASA-CASE-LEW-14072-3] p 103 N87-23736

An evaluation of candidate oxidation resistant materials
p 80 N87-26203

Composition optimization of chromium carbide based solid lubricant coatings for foil gas bearings at temperatures to 650 C
[NASA-CR-179649] p 105 N87-26233

PROTON DAMAGE

Radiation damage in proton irradiated indium phosphide solar cells
p 199 N87-29018

PROTON IRRADIATION

Cell performance and defect behavior in proton-irradiated lithium-counterdoped n(+)-p silicon solar cells
p 216 A87-14222

Potential for use of InP solar cells in the space radiation environment
p 120 A87-19996

PROTOTYPES

Hot section viewing system
[NASA-CR-174773] p 155 N87-11144

PROVING

A finite element model for wave propagation in an inhomogeneous material including experimental validation
[NASA-TM-100149] p 207 N87-25821

Resonant AC power system proof-of-concept test program
[NASA-CR-175069-VOL-1] p 129 N87-29738

Resonant AC power system proof-of-concept test program, volume 2, appendix 1
[NASA-CR-175069-VOL-2] p 130 N87-29739

PULSE COMMUNICATION

Image data compression with vector quantization in the transform domain
p 111 A87-30775

PULSED JET ENGINES

Experiments on a repetitively pulsed electrothermal thruster
[AIAA PAPER 87-1043] p 50 A87-38017

Low power arcjet thruster pulse ignition
[AIAA PAPER 87-1951] p 54 A87-50194

Investigation of a repetitively pulsed electrothermal thruster
[NASA-CR-179464] p 59 N87-16878

Low power arcjet thruster pulse ignition
[NASA-TM-100123] p 64 N87-23691

PUMP SEALS

EHD analysis of and experiments on pumping Leningrader seals
[NASA-CR-179570] p 168 N87-22246

Three-step cylindrical seal for high-performance turbomachines
[NASA-TP-1849] p 151 N87-24639

PUMPS

Design, development and deployment of public service photovoltaic power/load systems for the Gabonese Republic
[NASA-CR-179603] p 195 N87-23030

PURITY

Processing of laser formed SiC powder
[NASA-CR-179857] p 99 N87-11009

PYROLYSIS

Shock-tube pyrolysis of acetylene - Sensitivity analysis of the reaction mechanism for soot formation
p 75 A87-12598

Empirical modeling of soot formation in shock-tube pyrolysis of aromatic hydrocarbons
p 76 A87-12599

PYROLYTIC GRAPHITE

Design, fabrication and performance of small, graphite electrode, multistage depressed collectors with 200-W, CW, 8- to 18-GHz traveling-wave tubes
[NASA-TP-2693] p 126 N87-20474

Q

QUALITY CONTROL

Fabrication and quality assurance processes for superhybrid composite fan blades
p 72 A87-19123

EMC and power quality standards for 20-kHz power distribution
[NASA-TM-89925] p 62 N87-22004

QUANTITATIVE ANALYSIS

Quantitative analysis of PMR-15 polyimide resin by HPLC
p 69 A87-48314

QUANTUM EFFICIENCY

Oxygen interaction with space-power materials
[NASA-CR-181396] p 80 N87-29633

QUANTUM WELLS

Nonlinear absorption in AlGaAs/GaAs multiple quantum well structures grown by metalorganic chemical vapor deposition
p 217 A87-39687

QUASARS

Quasars as indicators of galactic ages
p 223 A87-26927

R

RADAR ANTENNAS

Nuclear reactor power for a space-based radar. SP-100 project
[NASA-TM-89295] p 213 N87-25838

RADAR CROSS SECTIONS

Radar cross section of an open-ended circular waveguide Calculation of second-order diffraction terms
p 112 A87-31626

RCS of a coated circular waveguide terminated by a perfect conductor
p 112 A87-42536

Rays versus modes - Pictorial display of energy flow in an open-ended waveguide
p 112 A87-44075

Reduction of the radar cross section of arbitrarily shaped cavity structures
[NASA-CR-180307] p 118 N87-27085

RADIANT COOLING

Transient radiative cooling of a droplet-filled layer
p 135 A87-27712

Radiative cooling of a layer with nonuniform velocity - A separable solution
p 141 A87-45637

Separation of variables solution for non-linear radiative cooling
p 142 A87-48450

RADIANT FLUX DENSITY

Technology for satellite power conversion
[NASA-CR-181057] p 66 N87-25420

RADIATION ABSORPTION

Modeling the effects of wind tunnel wall absorption on the acoustic radiation characteristics of propellers
[AIAA PAPER 86-1876] p 208 A87-17991

RADIATION DAMAGE

Indium phosphide solar cells - Status and prospects for use in space
p 188 A87-18071

Annealing of electron damage in mid-IR transmitting fluoride glass
p 99 A87-53652

The use of multiple EBIC curves and low voltage electron microscopy in the measurement of small diffusion lengths
p 197 N87-26434

Results of 1 MeV proton irradiation of front and back surfaces of silicon solar cells
p 197 N87-26435

Performance of AlGaAs, GaAs and InGaAs cells after 1 MeV electron irradiation
p 197 N87-26438

Comparative performance of diffused junction indium phosphide solar cells
p 197 N87-26441

Radiation effects on power transistor performance
[NASA-CR-181188] p 129 N87-27099

Modelling of multijunction cascade photovoltaics for space applications
[NASA-CR-181417] p 200 N87-29958

RADIATION EFFECTS

- Potential for use of InP solar cells in the space radiation environment p 120 A87-19996
- Radiation and temperature effects in gallium arsenide, indium phosphide and silicon solar cells [NASA-TM-89870] p 127 N87-22098
- Recent developments in indium phosphide space solar cell research [NASA-TM-100139] p 68 N87-26141
- Radiation effects on power transistor performance [NASA-CR-181188] p 129 N87-27099
- Modelling of multijunction cascade photovoltaics for space applications [NASA-CR-181417] p 200 N87-29958

RADIATION TOLERANCE

- Use of a corrugated surface to enhance radiation tolerance in a GaAs solar cell p 189 A87-19842
- Performance of GaAs and silicon concentrator cells under 1 MeV electron irradiation p 189 A87-19871
- A proposed GaAs-based superlattice solar cell structure with high efficiency and high radiation tolerance p 189 A87-19915
- Status of indium phosphide solar cell development at Spire p 197 N87-26440
- Comparative performance of diffused junction indium phosphide solar cells p 197 N87-26441
- Near-optimum design of the InP homojunction solar cell p 197 N87-26443
- Computer modelling of aluminum-gallium arsenide/gallium arsenide multilayer photovoltaics [NASA-CR-181418] p 200 N87-29957

RADIATIVE HEAT TRANSFER

- Transient radiative cooling of a droplet-filled layer p 135 A87-27712
- Separation of variables solution for non-linear radiative cooling p 142 A87-48450
- Combustion overview p 78 N87-11181
- Modeling turbulent, reacting flow p 147 N87-20270

RADIO FREQUENCIES

- Precision tunable resonant microwave cavity [NASA-CASE-LEW-13935-1] p 126 N87-21234
- RF characterization of monolithic microwave and mm-wave ICs [NASA-TM-88948] p 117 N87-22065
- Detection of radio-frequency modulated optical signals by two and three terminal microwave devices [NASA-TM-100196] p 130 N87-29750

RADIO FREQUENCY HEATING

- A review of research and development on the microwave-plasma electrothermal rocket [AIAA PAPER 87-1011] p 49 A87-38008
- A computer model for the recombination zone of a microwave-plasma electrothermal rocket [AIAA PAPER 87-1014] p 50 A87-38009

RADIO FREQUENCY INTERFERENCE

- Electromagnetic emission experiences using electric propulsion systems - A survey [AIAA PAPER 87-2028] p 54 A87-50195
- Electromagnetic emission experiences using electric propulsion systems: A survey [NASA-TM-100120] p 64 N87-22805

RADIO RECEIVERS

- A 30-GHz monolithic receiver p 121 A87-23953

RADIOGRAPHY

- Correlation of processing and sintering variables with the strength and radiography of silicon nitride p 94 A87-12938
- Sintering, microstructural, radiographic, and strength characterization of a high-purity Si₃N₄-based composition p 94 A87-12939
- Probability of detection of internal voids in structural ceramics using microfocus radiography p 170 A87-14300
- NDE reliability and process control for structural ceramics [ASME PAPER 87-GT-8] p 171 A87-48702
- NDE reliability and process control for structural ceramics [NASA-TM-88870] p 171 N87-12910

RADIOMETERS

- Liquid fuel spray processes in high-pressure gas flow p 131 A87-13843

RAILGUN ACCELERATORS

- Rail gun performance and plasma characteristics due to wall ablation p 214 A87-18735

RAMAN SPECTRA

- A point defect model for nickel electrode structures p 87 A87-52282

RAMAN SPECTROSCOPY

- Multispecies CARS measurements in turbulent combustion p 79 N87-23808

RAMP FUNCTIONS

- Ramp-integration technique for capacitance-type blade-tip clearance measurement p 155 A87-45128

RANDOM NOISE

- Sound radiation from single and annular stream nozzles, with modal decomposition of in-duct acoustic power p 209 A87-37629

RANKINE CYCLE

- ANL/RBC: A computer code for the analysis of Rankine bottoming cycles, including system cost evaluation and off-design performance [NASA-CR-179462] p 220 N87-10777
- Compound cycle engine for helicopter application [NASA-CR-175110] p 31 N87-25323
- Technical and economic study of Stirling and Rankine cycle bottoming systems for heavy truck diesel engines [NASA-CR-180833] p 222 N87-28470

RANKING

- High power/large area PV systems p 198 N87-26452

RAPID QUENCHING (METALLURGY)

- Transition from a planar interface to cellular and dendritic structures during rapid solidification processing p 81 A87-12029
- Fault structures in rapidly quenched Ni-Mo binary alloys p 83 A87-32035
- Chill block melt spinning of nickel-molybdenum alloys p 86 A87-47902
- Cellular microstructure of chill block melt spun Ni-Mo alloys p 87 A87-54300
- Primary arm spacing in chill block melt spun Ni-Mo alloys [NASA-TM-88887] p 88 N87-11875
- The mathematical modeling of rapid solidification processing [NASA-CR-179551] p 88 N87-13514
- A study of reduced chromium content in a nickel-base superalloy via element substitution and rapid solidification processing [NASA-CR-179631] p 92 N87-25456

RAY TRACING

- A parametric study of the beam refraction problems across laser anemometer windows p 154 A87-40725
- Reduction of the radar cross section of arbitrarily shaped cavity structures [NASA-CR-180307] p 118 N87-27085

REACTION BONDING

- Fracture of flash oxidized, yttria-doped sintered reaction-bonded silicon nitride p 97 A87-47923
- Fiber reinforced ceramic material [NASA-CASE-LEW-14392-2] p 106 N87-27810

REACTION KINETICS

- Reactions occurring during the sulfation of sodium chloride deposited on alumina substrates p 76 A87-20223
- Reaction of iron with hydrogen chloride-oxygen mixtures at 550 C p 83 A87-32001
- Systematic development of reduced reaction mechanisms for dynamic modeling p 77 A87-33987
- Diffusion flame extinction in slow convection flow under microgravity environment p 77 A87-38787
- Fast algorithm for calculating chemical kinetics in turbulent reacting flow p 77 A87-38958
- A mechanistic study of polyimide formation from diester-diacids p 70 A87-53671
- Numerical calculations of turbulent reacting flow in a gas-turbine combustor [NASA-TM-89842] p 1 N87-20171
- The chemical shock tube as a tool for studying high-temperature chemical kinetics p 157 N87-20279
- The oxidation degradation of aromatic compounds [NASA-CR-180588] p 79 N87-22020

REACTION PRODUCTS

- Shock-tube pyrolysis of acetylene - Sensitivity analysis of the reaction mechanism for soot formation p 75 A87-12598
- Empirical modeling of soot formation in shock-tube pyrolysis of aromatic hydrocarbons p 76 A87-12599
- The formation of volatile corrosion products during the mixed oxidation-chlorination of cobalt at 650 C p 82 A87-23648

REACTOR DESIGN

- Reliability and mass analysis of dynamic power conversion systems with parallel or standby redundancy p 190 A87-21823

REAL TIME OPERATION

- A real-time simulation evaluation of an advanced detection, isolation and accommodation algorithm for sensor failures in turbine engines p 18 A87-13318
- A high quality image compression scheme for real-time applications p 111 A87-30801
- Applications and requirements for real-time simulators in ground-test facilities [NASA-TP-2672] p 204 N87-23202

REATTACHED FLOW

- Third-moment closure of turbulence for predictions of separating and reattaching shear flows: A study of Reynolds-stress closure model [NASA-CR-177055] p 145 N87-11961

RECHARGING

- Oxygen electrodes for rechargeable alkaline fuel cells p 199 N87-29940
- Theoretical performance of hydrogen-bromine rechargeable SPE fuel cell p 199 N87-29945

RECIPROCATION

- EHD analysis of and experiments on pumping Leningrader seals [NASA-CR-179570] p 168 N87-22246

RECIRCULATIVE FLUID FLOW

- Evaluation of new techniques for the calculation of internal recirculating flows [AIAA PAPER 87-0059] p 131 A87-22387
- Development and evaluation of improved numerical schemes for recirculating flows [AIAA PAPER 87-0061] p 134 A87-24913
- An anemometer for highly turbulent or recirculating flows p 154 A87-37698
- Numerical prediction of cold turbulent flow in combustor configurations with different centerbody flame holders [ASME PAPER 86-WA/HT-50] p 140 A87-43715

RECLAMATION

- The T55-L-712 turbine engine compressor housing refurbishment project [NASA-CR-179624] p 92 N87-23729

RECOMBINATION REACTIONS

- A computer model for the recombination zone of a microwave-plasma electrothermal rocket [AIAA PAPER 87-1014] p 50 A87-38009
- Diffusion length measurements in bulk and epitaxially grown 3-5 semiconductors using charge collection microscopy [NASA-TM-100128] p 129 N87-27121

RECRYSTALLIZATION

- Ultrasonic determination of recrystallization [NASA-TM-88855] p 171 N87-10399

RECTANGULAR PANELS

- Design concepts/parameters assessment and sensitivity analyses of select composite structural components p 175 A87-25407

RECTENNAS

- Technology for satellite power conversion [NASA-CR-180162] p 193 N87-18229
- Rectenna Technology Program: Ultra light 2.45 GHz rectenna 20 GHz rectenna [NASA-CR-179558] p 116 N87-19556
- Technology for satellite power conversion [NASA-CR-181057] p 66 N87-25420

RECURSIVE FUNCTIONS

- Self-consistent inclusion of space-charge in the traveling wave tube [NASA-TM-89928] p 128 N87-24630

REDOX CELLS

- On the effect of the Fe(2+)/Fe(3+) redox couple on oxidation of carbon in hot H₃PO₄ p 78 A87-42677

REDUCED GRAVITY

- Effects of transient propellant dynamics on deployment of large liquid stages in zero-gravity with application to Shuttle/Centaur [IAF PAPER 86-119] p 39 A87-15880
- Diffusion flame extinction in slow convection flow under microgravity environment p 77 A87-38787
- Equilibrium fluid interfaces in the absence of gravity p 138 A87-38790

- Liquid droplet radiator development status - waste heat rejection devices for future space vehicles [AIAA PAPER 87-1537] p 42 A87-43059

- Experiments on thermoacoustic convection heat transfer in gravity and zero-gravity environments [AIAA PAPER 87-1551] p 107 A87-43141

- Size and shape of solid fuel diffusion flames in very slow speed flows [AIAA PAPER 87-2030] p 78 A87-52248

- Gas particle radiator [NASA-CASE-LEW-14297-1] p 156 N87-15452
- Simulation of fluid flows during growth of organic crystals in microgravity [NASA-TM-88921] p 108 N87-16167

- Research opportunities in microgravity science and applications during shuttle hiatus [NASA-TM-88964] p 108 N87-16917

- Combustion of velcro in low gravity [NASA-TM-88970] p 102 N87-19518

- Liquid droplet radiator development status [NASA-TM-88952] p 43 N87-20353

- A comparative study of the influence of buoyancy driven fluid flow on GaAs crystal growth p 219 N87-28741

REDUNDANCY

- Reliability and mass analysis of dynamic power conversion systems with parallel or standby redundancy p 190 A87-21823

REDUNDANCY ENCODING

- Advanced detection, isolation and accommodation of sensor failures: Real-time evaluation [NASA-TP-2740] p 34 N87-25331

REFLECTOR ANTENNAS

- Detection of reflector surface error from near-field data:
Effect of edge diffracted field
[NASA-TM-88920] p 117 N87-22874

REFLECTORS

- Composite space antenna structures - Properties and environmental effects p 72 A87-38610
Oxidation-resistant reflective surfaces for solar dynamic power generation in near Earth orbit
[NASA-TM-88865] p 56 N87-10960
Composite space antenna structures: Properties and environmental effects
[NASA-TM-88859] p 73 N87-16880
Results of 1 MeV proton irradiation of front and back surfaces of silicon solar cells p 197 N87-26435

REFRACTION

- A parametric study of the beam refraction problems across laser anemometer windows p 154 A87-40725

REFRACTIVITY

- Ellipsometric and optical study of amorphous hydrogenated carbon films p 216 A87-23967

REFRACTORY COATINGS

- High temperature tensile and creep behaviour of low pressure plasma-sprayed Ni-Co-Cr-Al-Y coating alloy p 82 A87-23429
Low cycle fatigue behaviour of a plasma-sprayed coating material p 82 A87-24040

REFRACTORY MATERIALS

- Ethynylated aromatics as high temperature matrix resins p 96 A87-34850
Heat's on to develop high-temperature materials p 85 A87-39897

REFRACTORY METAL ALLOYS

- High temperature tensile and creep behaviour of low pressure plasma-sprayed Ni-Co-Cr-Al-Y coating alloy p 82 A87-23429
Thermal stability of the nickel-base superalloy B-1900 + Hf with tantalum variations p 87 A87-51289
Preliminary study of niobium alloy contamination by transport through helium
[NASA-TM-88952] p 90 N87-17884

REFRIGERATING

- Refrigerated dynamic seal to 6.9 MPa (1000 psi) p 164 A87-50777
User evaluation of photovoltaic-powered vaccine refrigerator/freezer systems
[NASA-TM-88830] p 193 N87-18230

REFUELING

- On-orbit cryogenic storage and resupply p 41 A87-18344

REGENERATIVE FUEL CELLS

- Alkaline water electrolysis technology for Space Station regenerative fuel cell energy storage p 46 A87-18107
NASA Lewis evaluation of Regenerative Fuel Cell (RFC) systems p 123 N87-11073
Regenerative fuel cell study for satellites in GEO orbit
[NASA-TM-89914] p 194 N87-22310
High temperature solid oxide regenerative fuel cell for solar photovoltaic energy storage
[NASA-TM-89872] p 194 N87-23020
Electrochemical performance and transport properties of a Nafion membrane in a hydrogen-bromine cell environment
[NASA-TM-89862] p 79 N87-23718
Regenerative fuel cell study for satellites in GEO orbit
[NASA-CR-179609] p 198 N87-27324
Space Electrochemical Research and Technology (SERT)
[NASA-CP-2484] p 199 N87-29914
Oxygen electrodes for rechargeable alkaline fuel cells p 199 N87-29940
Theoretical performance of hydrogen-bromine rechargeable SPE fuel cell p 199 N87-29945

REGENERATORS

- An overview of the small engine component technology (SECT) studies — commuter, rotorcraft, cruise missile and auxiliary power applications in year 2000
[AIAA PAPER 86-1542] p 19 A87-17993
Fatigue failure of regenerator screens in a high frequency Stirling engine
[NASA-TM-88974] p 183 N87-18882

REGULATIONS

- Aerodynamic performance investigation of advanced mechanical suppressor and ejector nozzle concepts for jet noise reduction
[NASA-CR-174860] p 33 N87-29534

REINFORCED PLATES

- Acousto-ultrasonic input-output characterization of unidirectional fiber composite plate by SH waves
[NASA-CR-4087] p 173 N87-26361

REINFORCING FIBERS

- Ceramic matrix and resin matrix composites: A comparison
[NASA-TM-89830] p 74 N87-18615

RELIABILITY

- NDE reliability and process control for structural ceramics
[ASME PAPER 87-GT-8] p 171 A87-48702
NDE reliability and process control for structural ceramics
[NASA-TM-88870] p 171 N87-12910
Effect of design variables, temperature gradients and speed of life and reliability of a rotating disk
[NASA-TM-88883] p 165 N87-13755
Surface flaw reliability analysis of ceramic components with the SCARE finite element postprocessor program
[NASA-TM-88901] p 181 N87-17087

RELIABILITY ANALYSIS

- Reliability and mass analysis of dynamic power conversion systems with parallel or standby redundancy p 190 A87-21823

- Fatigue criterion to system design, life, and reliability p 175 A87-27986

- Arcjet component conditions through a multistart test
[AIAA PAPER 87-1060] p 51 A87-41127

- Arcjet starting reliability - A multistart test on hydrogen/nitrogen mixtures
[AIAA PAPER 87-1061] p 51 A87-41128

- Arcjet component conditions through a multistart test
[NASA-TM-89857] p 61 N87-20382

- Arcjet starting reliability: A multistart test on hydrogen/nitrogen mixtures
[NASA-TM-89867] p 61 N87-21998

REMOTE SENSORS

- Advanced detection, isolation and accommodation of sensor failures: Real-time evaluation
[NASA-TP-2740] p 34 N87-25331

REQUIREMENTS

- Advanced solar dynamic space power systems perspectives, requirements and technology needs
[NASA-TM-88884] p 56 N87-12606
Power system technologies for the manned Mars mission p 60 N87-17789
High power/large area PV systems p 198 N87-26452

RESEARCH AIRCRAFT

- Flight test report of the NASA icing research airplane: Performance, stability, and control after flight through natural icing conditions
[NASA-CR-179515] p 34 N87-11797

RESEARCH AND DEVELOPMENT

- Space Station Power System issues p 47 A87-19877
A review of research and development on the microwave-plasma electrothermal rocket
[AIAA PAPER 87-1011] p 49 A87-38008
Materials research and applications at NASA Lewis Research Center p 69 A87-38472
Opportunities and challenges in heat transfer - From the perspective of the government laboratory p 109 A87-48313
The Advanced Turbine Technology Applications Program (ATTAP)
[SAE PAPER 870467] p 163 A87-48791
Research and technology
[NASA-TM-88868] p 223 N87-17656
Automotive Stirling Engine Development Program
[NASA-CR-174873] p 222 N87-30223

RESEARCH FACILITIES

- Reactivation study for NASA Lewis Research Center's Hypersonic Tunnel Facility
[AIAA PAPER 87-1886] p 34 A87-50190
Up close - Materials division of NASA-Lewis Research Center p 69 A87-51176
User's manual for a TEACH computer program for the analysis of turbulent, swirling reacting flow in a research combustor
[NASA-CR-179547] p 78 N87-11858
Overview of the 1986 free-piston Stirling activities at NASA Lewis Research Center
[NASA-TM-88895] p 221 N87-16663
Research opportunities in microgravity science and applications during shuttle hiatus
[NASA-TM-88964] p 108 N87-16917
Heat flux calibration facility capable of SSME conditions p 36 N87-22774
Helicopter transmission testing at NASA Lewis Research Center
[NASA-TM-89912] p 168 N87-22978
Reactivation study for NASA Lewis Research Center's hypersonic tunnel facility
[NASA-TM-89918] p 36 N87-23664
A detailed description of the uncertainty analysis for High Area Ratio Rocket Nozzle tests at the NASA Lewis Research Center
[NASA-TM-100203] p 68 N87-28602

RESEARCH MANAGEMENT

- Equipment concept design and development plans for microgravity science and applications research on space station: Combustion tunnel, laser diagnostic system, advanced modular furnace, integrated electronics laboratory
[NASA-CR-179535] p 108 N87-15320
Overview of the 1986 free-piston Stirling activities at NASA Lewis Research Center
[NASA-TM-88895] p 221 N87-16663
Research opportunities in microgravity science and applications during shuttle hiatus
[NASA-TM-88964] p 108 N87-16917
Space experiment development process p 109 N87-21156
Issues in space photovoltaic research and technology
[NASA-TM-89922] p 128 N87-23901

RESIN MATRIX COMPOSITES

- Polymer, metal, and ceramic matrix composites for advanced aircraft engine applications p 71 A87-15187

- Ethynylated aromatics as high temperature matrix resins p 96 A87-34850

- Ceramic matrix and resin matrix composites: A comparison
[NASA-TM-89830] p 74 N87-18615

- Ray propagation path analysis of acousto-ultrasonic signals in composites
[NASA-TM-100148] p 173 N87-25589

RESISTOJET ENGINES

- An analytical and experimental investigation of resistojets plumes
[AIAA PAPER 87-0399] p 48 A87-24998
Resistojet control and power for high frequency ac buses
[AIAA PAPER 87-0994] p 122 A87-41103
The effect of ambient pressure on the performance of a resistojets
[AIAA PAPER 87-0991] p 52 A87-42181
Conceptual design and integration of a Space Station resistojets propulsion assembly
[AIAA PAPER 87-1860] p 52 A87-45256
2000-hour cyclic endurance test of a laboratory model multipropellant resistojets
[AIAA PAPER 87-0993] p 52 A87-45725
Preliminary performance characterizations of an engineering model multipropellant resistojets for space station application
[AIAA PAPER 87-2120] p 54 A87-50197
Effect of nozzle geometry on the resistojets exhaust plume
[AIAA PAPER 87-2121] p 55 A87-52252
Electric propulsion options for the SP-100 reference mission
[NASA-TM-88918] p 57 N87-14422
A design study of hydrazine and biowaste resistojets
[NASA-CR-179510] p 57 N87-14425
An analytical and experimental investigation of resistojets plumes
[NASA-TM-88852] p 58 N87-14428
Potential propellant storage and feed systems for space station resistojets propulsion options
[NASA-CR-179457] p 59 N87-16065
Space station resistojets system requirements and interface definition study
[NASA-CR-179581] p 60 N87-17848
Conceptual design and integration of a space station resistojets propulsion assembly
[NASA-TM-88847] p 60 N87-20378
Resistojet control and power for high frequency ac buses
[NASA-TM-89860] p 126 N87-20477
A 2000-hour cyclic endurance test of a laboratory model multipropellant resistojets
[NASA-TM-89854] p 167 N87-22237
Preliminary performance characterizations of an engineering model multipropellant resistojets for space station application
[NASA-TM-100113] p 111 N87-23821
Resistojet plume and induced environment analysis
[NASA-TM-88957] p 66 N87-24536
Space station propulsion system technology
[NASA-TM-100108] p 66 N87-25422
Water-propellant resistojets for man-tended platforms
[NASA-TM-100110] p 68 N87-26135

RESONANCE

- Precision tunable resonant microwave cavity
[NASA-CASE-LEW-13935-1] p 126 N87-21234
Control considerations for high frequency, resonant, power processing equipment used in large systems
[NASA-TM-89926] p 64 N87-23690
Resonant AC power system proof-of-concept test program
[NASA-CR-175069-VOL-1] p 129 N87-29738

- Resonant AC power system proof-of-concept test program, volume 2, appendix 1
[NASA-CR-175069-VOL-2] p 130 N87-29739
- RESONANT VIBRATION**
Bladed disk vibration
[NASA-CR-181203] p 31 N87-26908
- RESTARTABLE ROCKET ENGINES**
Arcjet starting reliability: A multistart test on hydrogen/nitrogen mixtures
[NASA-TM-89867] p 61 N87-21998
- REYNOLDS EQUATION**
Finite difference solution for a generalized Reynolds equation with homogeneous two-phase flow
p 141 A87-45851
Comparison of generalized Reynolds and Navier Stokes equations for flow of a power law fluid
p 142 A87-45852
- REYNOLDS NUMBER**
Comparison of Hirs' equation with Moody's equation for determining rotordynamic coefficients of annular pressure seals
[ASME PAPER 86-TRIB-19] p 161 A87-19529
Effects of droplet interactions on droplet transport at intermediate Reynolds numbers
[AIAA PAPER 87-0137] p 134 A87-24926
Comparison of calculated and experimental cascade performance for controlled-diffusion compressor stator blading
[ASME PAPER 86-GT-35] p 19 A87-25394
Performance of two 10-lb/sec centrifugal compressors with different blade and shroud thicknesses operating over a range of Reynolds numbers
[AIAA PAPER 87-1745] p 22 A87-50188
Effects of droplet interactions on droplet transport at intermediate Reynolds numbers
[NASA-CR-179567] p 26 N87-14348
Performance of two 10-lb/sec centrifugal compressors with different blade and shroud thicknesses operating over a range of Reynolds numbers
[NASA-TM-100115] p 29 N87-23623
- REYNOLDS STRESS**
Comparison of pressure-strain correlation models for the flow behind a disk
p 131 A87-20897
Computation of rotating turbulent flow with an algebraic Reynolds stress model
p 140 A87-43384
Third-moment closure of turbulence for predictions of separating and reattaching shear flows: A study of Reynolds-stress closure model
[NASA-CR-177055] p 145 N87-11961
Turbulence characteristics of an axisymmetric reacting flow
[NASA-CR-180697] p 152 N87-27973
- RHEOCASTING**
Processing-structure characterization of rheocast IN-100 superalloy
p 82 A87-24116
Analysis of the solidified structure of rheocast and VADER processed nickel-base superalloy
p 83 A87-28734
- RHEOLOGY**
Stability and rheology of dispersions of silicon nitride and silicon carbide
[NASA-CR-179634] p 104 N87-25476
- RIBBONS**
Combustion of velcro in low gravity
[NASA-TM-88970] p 102 N87-19518
- RIGID ROTORS**
Stability of a rigid rotor supported on flexible oil journal bearings
[NASA-TM-89899] p 151 N87-24646
- RIGID STRUCTURES**
Starvation effects on the hydrodynamic lubrication of rigid nonconformal contacts in combined rolling and normal motion
p 135 A87-27839
- RINGS**
Revised NASA axially symmetric ring model for coupled-cavity traveling-wave tubes
[NASA-TP-2675] p 127 N87-22923
- RL-10 ENGINES**
High heat transfer oxidizer heat exchanger design and analysis --- RL10-2B engine
[NASA-CR-179596] p 63 N87-22803
- ROCKET ENGINE DESIGN**
Engine studies for future subsonic cruise missiles
[AIAA PAPER 86-1547] p 19 A87-21513
Heat pipe cooled rocket engines
[AIAA PAPER 86-1567] p 48 A87-21516
Feasibility of mapping velocity flowfields in an SSME powerhead using laser anemometry techniques
[AIAA PAPER 87-1306] p 154 A87-42374
Oxidizer heat exchangers for rocket engine operation in idle modes
[AIAA PAPER 87-2117] p 52 A87-45418
Concepts for space maintenance of OTV engines
p 37 A87-46000

- Preliminary design of turbopumps and related machinery
[NASA-RP-1170] p 11 N87-17665
- ROCKET ENGINES**
Small centrifugal pumps for low-thrust rockets
p 50 A87-39808
Application of single crystal superalloys for earth-to-orbit propulsion systems
[AIAA PAPER 87-1976] p 85 A87-45336
Comparison of two procedures for predicting rocket engine nozzle performance
[AIAA PAPER 87-2071] p 52 A87-45391
Liquid oxygen cooling of high pressure LOX/hydrocarbon rocket thrust chambers
[NASA-TM-88805] p 57 N87-14426
Breadboard RL10-11B low thrust operating mode
[NASA-CR-174914] p 58 N87-15269
Space station auxiliary thrust chamber technology
[NASA-CR-179552] p 59 N87-16874
Cryogenic gear technology for an orbital transfer vehicle engine and tester design
[NASA-CR-175102] p 110 N87-19539
Comparison of two procedures for predicting rocket engine nozzle performance
[NASA-TM-89814] p 60 N87-20379
Pretest uncertainty analysis for chemical rocket engine tests
[NASA-TM-89819] p 157 N87-20515
Application of single crystal superalloys for Earth-to-orbit propulsion systems
[NASA-TM-89877] p 91 N87-22034
Concepts for space maintenance of OTV engines
p 67 N87-26097
- ROCKET EXHAUST**
Resistojet plume and induced environment analysis
[NASA-TM-88957] p 66 N87-24536
- ROCKET NOZZLES**
Comparison of theoretical and experimental thrust performance of a 1030:1 area ratio rocket nozzle at a chamber pressure of 2413 kN/sq m (350 psia)
[AIAA PAPER 87-2069] p 52 A87-45390
Comparison of two procedures for predicting rocket engine nozzle performance
[AIAA PAPER 87-2071] p 52 A87-45391
Experimental evaluation of heat transfer on a 1030:1 area ratio rocket nozzle
[AIAA PAPER 87-2070] p 55 A87-52249
Theoretical kinetic computations in complex reacting systems
p 219 N87-20277
Comparison of two procedures for predicting rocket engine nozzle performance
[NASA-TM-89814] p 60 N87-20379
Experimental thrust performance of a high-area-ratio rocket nozzle
[NASA-TP-2720] p 60 N87-20381
Experimental thrust performance of a high area-ratio rocket nozzle
p 65 N87-23809
Comparison of theoretical and experimental thrust performance of a 1030:1 area ratio rocket nozzle at a chamber pressure of 2413 kN/m² (350 psia)
[NASA-TP-2725] p 66 N87-25423
Experimental evaluation of heat transfer on a 1030:1 area ratio rocket nozzle
[NASA-TP-2726] p 67 N87-25424
A detailed description of the uncertainty analysis for High Area Ratio Rocket Nozzle tests at the NASA Lewis Research Center
[NASA-1M-100203] p 66 N87-26602
- ROCKET OXIDIZERS**
Oxidizer heat exchangers for rocket engine operation in idle modes
[AIAA PAPER 87-2117] p 52 A87-45418
- ROCKET PROPELLANTS**
2000-hour cyclic endurance test of a laboratory model multipropellant resistojel
[AIAA PAPER 87-0993] p 52 A87-45725
Preliminary performance characterizations of an engineering model multipropellant resistojel for space station application
[AIAA PAPER 87-2120] p 54 A87-50197
A 2000-hour cyclic endurance test of a laboratory model multipropellant resistojel
[NASA-TM-89854] p 167 N87-22237
Preliminary performance characterizations of an engineering model multipropellant resistojel for space station application
[NASA-TM-100113] p 111 N87-23821
- ROCKET THRUST**
An analytical and experimental investigation of resistojel plumes
[AIAA PAPER 87-0399] p 48 A87-24998
An analytical and experimental investigation of resistojel plumes
[NASA-TM-88852] p 58 N87-14428

- Experimental thrust performance of a high-area-ratio rocket nozzle
[NASA-TP-2720] p 60 N87-20381
Experimental thrust performance of a high area-ratio rocket nozzle
p 65 N87-23809
Comparison of theoretical and experimental thrust performance of a 1030:1 area ratio rocket nozzle at a chamber pressure of 2413 kN/m² (350 psia)
[NASA-TP-2725] p 66 N87-25423
- RODS**
One-dimensional wave propagation in rods of variable cross section: A WKBJ solution
[NASA-CR-4086] p 172 N87-24707
- ROLLER BEARINGS**
Effect of interference fits on roller bearing fatigue life
p 162 A87-37686
Selection of rolling-element bearing steels for long-life application
[NASA-TM-88881] p 164 N87-11993
Analysis of mixed-mode crack propagation using the boundary integral method
[NASA-CR-179518] p 180 N87-12915
Lubricant effects on bearing life
[NASA-TM-88875] p 165 N87-15467
Effects of surface removal on rolling-element fatigue
[NASA-TM-88871] p 166 N87-18820
- ROLLERS**
Evaluation of a high-torque backlash-free roller actuator
p 165 N87-16336
- ROLLING CONTACT LOADS**
Lubricant effects on bearing life
[NASA-TM-88875] p 165 N87-15467
Effects of surface removal on rolling-element fatigue
[NASA-TM-88871] p 166 N87-18820
- ROLLING MOMENTS**
Starvation effects on the hydrodynamic lubrication of rigid nonconformal contacts in combined rolling and normal motion
p 135 A87-27839
- ROTARY ENGINES**
Visualization of flows in a motored rotary combustion engine using holographic interferometry
[AIAA PAPER 86-1557] p 19 A87-21514
A two-dimensional numerical study of the flow inside the combustion chamber of a motored rotary engine
[SAE PAPER 860615] p 161 A87-28624
Numerical simulation of the flowfield in a motored two-dimensional Wankel engine
p 138 A87-39812
Advanced liquid-cooled, turbocharged and intercooled stratified charge rotary engines for aircraft
[SAE PAPER 871039] p 22 A87-48766
Estimation of instantaneous heat transfer coefficients for a direct-injection stratified-charge rotary engine
[SAE PAPER 870444] p 163 A87-48787
Performance and efficiency evaluation and heat release study of an outboard Marine Corporation Rotary Combustion Engine
[NASA-TM-89833] p 28 N87-20282
- ROTARY STABILITY**
Influence of third-degree geometric nonlinearities on the vibration and stability of pretwisted, precone, rotating blades
p 21 A87-46228
- ROTARY WING AIRCRAFT**
Contingency power for small turboshaft engines using water injection into turbine cooling air
[AIAA PAPER 87-1906] p 21 A87-45289
Compound cycle engine program
p 23 A87-53428
Compound cycle engine program
[NASA-TM-88879] p 25 N87-11790
Outdoor test stand performance of a convertible engine with variable inlet guide vanes for advanced rotorcraft propulsion
[NASA-TM-88939] p 26 N87-16825
Contingency power for small turboshaft engines using water injection into turbine cooling air
[NASA-TM-89817] p 28 N87-20280
Experimental and analytical evaluation of dynamic load and vibration of a 2240-kW (300-hp) rotorcraft transmission
[NASA-TM-88975] p 167 N87-20556
- ROTARY WINGS**
Response of a small-turboshaft-engine compression system to inlet temperature distortion
[NASA-TM-83765] p 23 N87-10100
- ROTATING BODIES**
CONDIF - A modified central-difference scheme for convective flows
p 205 A87-53675
Finite element analysis of flexible, rotating blades
[NASA-TM-89906] p 186 N87-26385
- ROTATING DISKS**
Optimal placement of critical speeds in rotor-bearing systems
p 162 A87-38464
Effect of design variables, temperature gradients and speed of life and reliability of a rotating disk
[NASA-TM-88883] p 165 N87-13755

ROTATING FLUIDS

- Computation of rotating turbulent flow with an algebraic Reynolds stress model p 140 A87-43384
 Rotational effects on impingement cooling p 141 A87-45838

ROTATING SHAFTS

- Optimal placement of critical speeds in rotor-bearing systems p 162 A87-38464
 Analysis of experimental shaft seal data for high-performance turbomachines - As for Space Shuttle main engines p 162 A87-45846
 Finite difference solution for a generalized Reynolds equation with homogeneous two-phase flow p 141 A87-45851
 Development of gas-to-gas lift pad dynamic seals, volumes 1 and 2 [NASA-CR-179486] p 168 A87-22245

ROTATING STALLS

- Stall transients of axial compression systems with inlet distortion p 3 A87-24010
 Aerodynamic instability performance of an advanced high-pressure-ratio compression component [AIAA PAPER 86-1619] p 5 A87-41157

ROTATION

- Nonlinear vibration and stability of rotating, pretwisted, precone blades including Coriolis effects p 178 A87-39896

ROTOR AERODYNAMICS

- Rotor wake characteristics of a transonic axial-flow fan p 2 A87-20886
 High-speed propeller noise predictions - Effects of boundary conditions used in blade loading calculations [AIAA PAPER 87-0525] p 208 A87-24978
 Results of acoustic tests of a Prop-Fan model [AIAA PAPER 87-1894] p 209 A87-45282
 Aeroelastic control of stability and forced response of supersonic rotors by aerodynamic detuning p 21 A87-46249
 Vibration characteristics of OH-58A helicopter main rotor transmission [NASA-TP-2705] p 167 A87-20555
 Shock structure measured in a transonic fan using laser anemometry p 28 A87-21929
 Rotordynamic Instability Problems in High-Performance Turbomachinery, 1986 [NASA-CP-2443] p 167 A87-22199
 Experimental rotordynamic coefficient results for teeth-on-rotor and teeth-on-stator labyrinth gas seals p 167 A87-22212
 Unsteady stator/rotor interaction p 149 A87-22767

ROTOR BLADES

- Multigrid solution of inviscid transonic flow through rotating blade passages [AIAA PAPER 87-0608] p 3 A87-24992

ROTOR BLADES (TURBOMACHINERY)

- Stall transients of axial compression systems with inlet distortion p 3 A87-24010
 The effect of circumferential aerodynamic detuning on coupled bending-torsion unstalled supersonic flutter [ASME PAPER 86-GT-100] p 20 A87-25396
 Analytical and experimental investigation of mistuning in propfan flutter [AIAA PAPER 87-0739] p 178 A87-40496
 Turbine Engine Hot Section Technology, 1984 [NASA-CP-2339] p 179 A87-11180
 Turbine airfoil deposition models p 24 A87-11191
 Design of 9.271-pressure-ratio 5-stage core compressor and overall performance for first 3 stages [NASA-TP-2597] p 27 A87-17699
 Analytical and experimental investigation of mistuning in propfan flutter [NASA-TM-88959] p 182 A87-18116
 Development of a rotor wake/vortex model. Volume 2: User's manual for computer program [NASA-CR-174850-VOL-2] p 13 A87-20239
 Shock structure measured in a transonic fan using laser anemometry p 28 A87-21929
 Unstalled flutter stability predictions and comparisons to test data for a composite prop-fan model [NASA-CR-179512] p 28 A87-21955
 Application of advanced computational codes in the design of an experiment for a supersonic throughflow fan rotor [NASA-TM-88915] p 13 A87-22630
 Unsteady stator/rotor interaction p 149 A87-22767
 Dynamic response of two composite prop-fan models on a nacelle/wing/fuselage half model [NASA-CR-179589] p 18 A87-23615
 Low-cost FM oscillator for capacitance type of blade tip clearance measurement system [NASA-TP-2746] p 31 A87-24481
 High temperature static strain gage development contract, tasks 1 and 2 [NASA-CR-180811] p 159 A87-28869

- An investigation of the flow characteristics in the blade endwall corner region [NASA-CR-4076] p 14 A87-29412

ROTORCRAFT AIRCRAFT

- Advanced technology payoffs for future small propulsion systems p 21 A87-47081

ROTORS

- Modeling of multi-rotor torsional vibrations in rotating machinery using substructuring p 175 A87-28543
 Unsteady heat transfer and direct comparison to steady-state measurements in a rotor-wake experiment p 136 A87-30720
 Method for the determination of the three dimensional aerodynamic field of a rotor-stator combination in compressible flow [AIAA PAPER 87-1742] p 7 A87-50187
 Optimization of cascade blade mistuning under flutter and forced response constraints p 24 A87-11732
 Fabrication of cooled radial turbine rotor [NASA-CR-179503] p 25 A87-11789
 Design of an advanced wood composite rotor and development of wood composite blade technology [NASA-CR-174713] p 73 A87-17861
 Structural and aeroelastic analysis of the SR-7L propan [NASA-TM-86877] p 184 A87-22273
 Method for the determination of the three-dimensional aerodynamic field of a rotor-stator combination to compressible flow [NASA-TM-100118] p 30 A87-23625
 Wind tunnel evaluation of a truncated NACA 64-621 airfoil for wind turbine applications [NASA-CR-180803] p 196 A87-25621
 Performance and aerodynamic braking of a horizontal-axis wind turbine from small-scale wind tunnel tests [NASA-CR-180812] p 198 A87-27327
 Performance and power regulation characteristics of two airfoil-controlled rotors and a pitchable tip-controlled rotor on the Mod-O turbine [NASA-TM-100136] p 200 A87-29956
- RUN TIME (COMPUTERS)**
 Increasing processor utilization during parallel computation rundown p 202 A87-52541

S**SAFETY**

- 20 kHz Space Station power system p 51 A87-40378

SAFETY MANAGEMENT

- Science and technology issues in spacecraft fire safety [AIAA PAPER 87-0467] p 39 A87-31107
 Science and technology issues in spacecraft fire safety [NASA-TM-88933] p 40 A87-16012
 Fire safety concerns in space operations [NASA-TM-89848] p 40 A87-20342

SALT SPRAY TESTS

- Experimental verification of corrosive vapor deposition rate theory in high velocity burner rigs p 143 A87-49551

SAMPLING

- SMI adaptive antenna arrays for weak interfering signals [NASA-CR-181330] p 119 A87-28813

SAPPHIRE

- Bonding Lexan and sapphire to form high-pressure, flame-resistant window [NASA-TM-100188] p 159 A87-28880

SATELLITE ANTENNAS

- 20-GHz phased-array-fed antennas utilizing distributed MMIC modules p 112 A87-34527

SATELLITE COMMUNICATION

- Baseband processor development/test performance for 30/20 GHz SS-TDMA communication system p 111 A87-18310
 A photovoltaic power system and a low-power satellite earth station for Indonesia p 189 A87-19859
 SMI adaptive antenna arrays for weak interfering signals --- Sample Matrix Inversion p 111 A87-20818
 Optical technologies for communication satellite applications; Proceedings of the Meeting, Los Angeles, CA, Jan. 21, 22, 1986 [SPIE-616] p 41 A87-26610
 An advanced geostationary communications platform p 112 A87-43165
 Application of adaptive antenna techniques to future commercial satellite communication [NASA-CR-179566] p 115 A87-16954
 Application of adaptive antenna techniques to future commercial satellite communications. Executive summary [NASA-CR-179566-SUMM] p 115 A87-16955

- Advanced space communications architecture study. Volume 2: Technical report [NASA-CR-179592] p 115 A87-18695

- Performance of a Ka-band satellite system under variable transmitted signal power conditions [NASA-TM-88984] p 116 A87-18700

- Intersatellite Link (ISL) application to commercial communications satellites. Volume 2: Technical final report [NASA-CR-179598-VOL-2] p 116 A87-19553

- Unique bit-error-rate measurement system for satellite communication systems [NASA-TP-2699] p 116 A87-20448

- A study of the effect of group delay distortion on an SMSK satellite communications channel [NASA-TM-89835] p 116 A87-20450

- Microstrip antenna array with parasitic elements [NASA-TM-89919] p 117 A87-22089

- Onboard multichannel demultiplexer/demodulator [NASA-CR-180821] p 119 A87-28819

SATELLITE DESIGN

- Satellite analog FDMA/FM to digital TDMA conversion [NASA-CR-179605] p 125 A87-20467

SATELLITE NETWORKS

- Intersatellite Link (ISL) application to commercial communications satellites. Volume 1: Executive summary [NASA-CR-179598-VOL-1] p 116 A87-19552
 Intersatellite Link (ISL) application to commercial communications satellites. Volume 2: Technical final report [NASA-CR-179598-VOL-2] p 116 A87-19553
 Engineering calculations for communications satellite systems planning [NASA-CR-181112] p 117 A87-24605

SATELLITE ORBITS

- Engineering calculations for communications satellite systems planning [NASA-CR-180106] p 114 A87-16198
 Optimization of orbital assignment and specification of service areas in satellite communications [NASA-CR-181273] p 118 A87-27882

SATELLITE ORIENTATION

- Alternative mathematical programming formulations for FSS synthesis [NASA-CR-180030] p 202 A87-14872

SATELLITE POWER TRANSMISSION (TO EARTH)

- Technology for satellite power conversion [NASA-CR-180162] p 193 A87-18229
 Rectenna Technology Program: Ultra light 2.45 GHz rectenna 20 GHz rectenna [NASA-CR-179558] p 116 A87-19556

SATELLITE SOLAR POWER STATIONS

- Space Station Power System issues p 47 A87-19877

SATELLITE SURFACES

- Modeling of environmentally induced transients within satellites [AIAA PAPER 85-0387] p 42 A87-41611

SATELLITE TRANSMISSION

- Engineering calculations for communications satellite systems planning [NASA-CR-180106] p 114 A87-16198

SATELLITE-BORNE RADAR

- Nuclear reactor power for a space-based radar. SP-100 project [NASA-TM-89295] p 213 A87-25838

SCALARS

- Vortex-scalar element calculations of a diffusion flame stabilized on a plane mixing layer [NASA-TM-100133] p 2 A87-28501

SCALE (CORROSION)

- Analysis of thermomechanical oxidation fields in thermal barrier coatings p 174 A87-14316
 Adherent Al₂O₃ scales formed on undoped NiCrAl alloys p 84 A87-32045

SCALE EFFECT

- Scaled centrifugal compressor program [NASA-CR-174912] p 26 A87-14349
 Hot gas ingestion: From model results to full scale engine testing p 30 A87-24419

SCALE MODELS

- Cruise noise of the 2/9th scale model of the Large-scale Advanced Propfan (LAP) propeller, SR-7A [NASA-TM-100175] p 212 A87-28398

SCANNING

- Application of scanning acoustic microscopy to advanced structural ceramics [NASA-TM-89929] p 172 A87-23987
 Computer control of a scanning electron microscope for digital image processing of thermal-wave images [NASA-TM-100157] p 128 A87-26278

SCATHA SATELLITE

- Investigation of beam-plasma interactions [NASA-CR-180579] p 215 A87-22508

SCHOTTKY DIODES

- 30 GHz monolithic balanced mixers using an ion-implanted FET-compatible 3-inch GaAs wafer process technology p 121 A87-34525
Technology for satellite power conversion [NASA-CR-181057] p 66 N87-25420

SCREENS

- Experimental evaluation of honeycomb/screen configurations and short contraction section for NASA Lewis Research Center's altitude wind tunnel [NASA-TP-2692] p 36 N87-23662

SEALS (STOPPERS)

- Comparison of Hirs' equation with Moody's equation for determining rotordynamic coefficients of annular pressure seals [ASME PAPER 86-TRIB-19] p 161 A87-19529
Centrifugal inertia effects in two-phase face seal films p 162 A87-37687
Refrigerated dynamic seal to 6.9 MPa (1000 psi) p 164 A87-50777
Evaluation of seals for high-performance cryogenic turbomachines [NASA-TM-88919] p 146 N87-15442
Thermomechanical behavior of plasma-sprayed ZrO₂-Y₂O₃ coatings influenced by plasticity, creep and oxidation [NASA-TM-88940] p 147 N87-18784
EHD analysis of and experiments on pumping Leningrader seals [NASA-CR-179570] p 168 N87-22246
SSME blade damper technology p 63 N87-22798
Straight cylindrical seal for high-performance turbomachines [NASA-TP-1850] p 150 N87-23936
Experiments on dynamic stiffness and damping of tapered bore seals [NASA-TM-89895] p 169 N87-23984
Ceramic high pressure gas path seal [NASA-CR-180813] p 31 N87-26914

SECONDARY INJECTION

- Secondary stream and excitation effects on two-dimensional nozzle plume characteristics [AIAA PAPER 87-2112] p 6 A87-45414
Secondary stream and excitation effects on two-dimensional nozzle plume characteristics [NASA-TM-89813] p 12 N87-18539

SELECTION

- Selection of rolling-element bearing steels for long-life application [NASA-TM-88881] p 164 N87-11993

SELF LUBRICATION

- Carbide-fluoride-silver self-lubricating composite [NASA-CASE-LEW-14196-2] p 169 N87-25585
Experimental evaluation of chromium-carbide-based solid lubricant coatings for use to 760 C [NASA-CR-180808] p 105 N87-27053

SELF SEALING

- Refrigerated dynamic seal to 6.9 MPa (1000 psi) p 164 A87-50777

SEMICONDUCTING FILMS

- Growth and characterization of cubic SiC single-crystal films on Si p 217 A87-44875

SEMICONDUCTOR DEVICES

- Analysis of optically controlled microwave/millimeter-wave device structures p 121 A87-23680
Ellipsometric and optical study of amorphous hydrogenated carbon films p 216 A87-23967
Thermal and structural stability of cosputtered amorphous Ta(x)Cu(1-x) alloy thin films on GaAs p 216 A87-27198
Space station power semiconductor package [NASA-CR-180829] p 129 N87-28825

SEMICONDUCTORS (MATERIALS)

- Stoichiometric disturbances in compound semiconductors due to ion implantation p 215 A87-12292
Fiber-optic temperature sensor using a spectrum-modulating semiconductor etalon [NASA-TM-100153] p 31 N87-25329
Synthesis, physical and chemical properties, and potential applications of graphite fluoride fibers [NASA-TM-100156] p 105 N87-26232
The use of multiple EBIC curves and low voltage electron microscopy in the measurement of small diffusion lengths p 197 N87-26434

SENSITIVITY

- Sensitivity analysis and approximation methods for general eigenvalue problems [NASA-CR-179538] p 180 N87-12021
Decoupled direct method for sensitivity analysis in combustion kinetics [NASA-CR-179636] p 79 N87-24549

SENSORS

- Referencing in fiber optic sensing systems [NASA-TM-89822] p 126 N87-20475

SEPARATED FLOW

- Vacuum chamber pressure effects on thrust measurements of low Reynolds number nozzles p 45 A87-14976
Comparison of pressure-strain correlation models for the flow behind a disk p 131 A87-20897
Prediction of the structure of fuel sprays in cylindrical combustion chambers p 20 A87-31277
A technique for the prediction of airfoil flutter characteristics in separated flow [AIAA PAPER 87-0910] p 177 A87-33719
Third-moment closure of turbulence for predictions of separating and reattaching shear flows: A study of Reynolds-stress closure model [NASA-CR-177055] p 145 N87-11961
A comparative study of some dynamic stall models [NASA-TM-88917] p 183 N87-18883
Flowfield measurements in a separated and reattached flat plate turbulent boundary layer [NASA-CR-4052] p 148 N87-21257

SEPARATORS

- Nickel-hydrogen separator development p 188 A87-18103
Electrochemical performance and transport properties of a Nafion membrane in a hydrogen-bromine cell environment [NASA-TM-89862] p 79 N87-23718

SERVICE LIFE

- The noncavitating performance and life of a small vane-type positive displacement pump in liquid hydrogen [AIAA PAPER 86-1438] p 46 A87-17994
Fatigue criterion to system design, life, and reliability p 175 A87-27986
Lubricant effects on bearing life [NASA-TM-88875] p 165 N87-15467
Creep fatigue life prediction for engine hot section materials (isotropic) [NASA-CR-174844] p 182 N87-18117
Stress-life interrelationships associated with alkaline fuel cells [NASA-TM-89881] p 194 N87-22307
A prediction model of the depth-of-discharge effect on the cycle life of a storage cell [NASA-TM-89915] p 194 N87-22311
Life prediction and constitutive models for engine hot section anisotropic materials [NASA-CR-179594] p 29 N87-23622
KOH concentration effect on cycle life of nickel-hydrogen cells p 199 N87-29920

SHAFTS (MACHINE ELEMENTS)

- Factors that affect the fatigue strength of power transmission shafting and their impact on design p 160 A87-14656
Effect of shaft frequency on cavitation in a journal bearing for noncentered circular whirl [NASA-TM-88925] p 148 N87-22122
Generation of spiral bevel gears with conjugate tooth surfaces and tooth contact analysis [NASA-CR-4088] p 169 N87-26356

SHAPES

- New methods and materials for molding and casting ice formations [NASA-TM-100126] p 16 N87-29470

SHEAR FLOW

- Turbulence modeling for complex shear flows p 133 A87-23653
Shear flow instability generated by non-homogeneous external forcing p 142 A87-48047
A critical analysis of transverse vorticity measurements in a large plane shear layer p 143 A87-52049
Third-moment closure of turbulence for predictions of separating and reattaching shear flows: A study of Reynolds-stress closure model [NASA-CR-177055] p 145 N87-11961
Aeroacoustics of subsonic turbulent shear flows [NASA-TM-100165] p 212 N87-26615
Control of shear flows by artificial excitation [NASA-TM-100201] p 15 N87-29420

SHEAR LAYERS

- Viscometer for low frequency, low shear rate measurements p 153 A87-13878
Numerical simulation of excited jet mixing layers [AIAA PAPER 87-0016] p 131 A87-22361
Coherent motion in excited free shear flows [AIAA PAPER 85-0539] p 135 A87-30281
On the spatial instability of piecewise linear free shear layers p 137 A87-31680
Nonlinear binary-mode interactions in a developing mixing layer p 142 A87-47158
Enhanced mixing of an axisymmetric jet by aerodynamic excitation [NASA-CR-175059] p 15 N87-29418

SHEAR PROPERTIES

- Thermo-elasto-viscoplastic analysis of problems in extension and shear [NASA-CR-181410] p 187 N87-29896

SHEAR STRAIN

- A simplified computer solution for the flexibility matrix of contacting teeth for spiral bevel gears [NASA-CR-179620] p 168 N87-23977

SHEAR STRENGTH

- Specimen geometry effects on graphite/PMR-15 composites during thermo-oxidative aging p 71 A87-13145

SHEAR STRESS

- Simplified composite micromechanics for predicting microstresses p 72 A87-20090
Effect of interference fits on roller bearing fatigue life p 162 A87-37686
An investigation of the flow characteristics in the blade endwall corner region [NASA-CR-4076] p 14 N87-29412

SHELL THEORY

- A versatile and low order hybrid stress element for general shell geometry [AIAA PAPER 87-0840] p 176 A87-33624
A higher order theory of laminated composite cylindrical shells p 177 A87-35656
A quadrilateral shell element using a mixed formulation p 179 A87-53796

SHELLS (STRUCTURAL FORMS)

- On the numerical performance of three-dimensional thick shell elements using a hybrid/mixed formulation p 175 A87-25924
Analysis of shell-type structures subjected to time-dependent mechanical and thermal loading [NASA-CR-180349] p 183 N87-19756
The dynamic aspects of thermo-elasto-viscoplastic snap-through and creep buckling phenomena [NASA-CR-181411] p 187 N87-29897

SHOCK TUBES

- Shock-tube pyrolysis of acetylene - Sensitivity analysis of the reaction mechanism for soot formation p 75 A87-12598
Empirical modeling of soot formation in shock-tube pyrolysis of aromatic hydrocarbons p 76 A87-12599
The chemical shock tube as a tool for studying high-temperature chemical kinetics p 157 N87-20279

SHOCK WAVE INTERACTION

- Investigation of two-dimensional shock-wave/boundary-layer interactions p 4 A87-39528
Shock structure measured in a transonic fan using laser anemometry p 28 N87-21929

SHOCK WAVES

- On broadband shock associated noise of supersonic jets p 208 A87-11768
A high resolution shock capturing scheme for high Mach number internal flow [NASA-CR-179523] p 10 N87-16804
A linearized Euler analysis of unsteady flows in turbomachinery [NASA-CR-180987] p 149 N87-22948

SHORT CIRCUIT CURRENTS

- Proposal for superstructure based high efficiency photovoltaics p 120 A87-19104

SHORT TAKEOFF AIRCRAFT

- Hot gas ingestion: From model results to full scale engine testing p 30 N87-24419
Effect of variable inlet guide vanes on the operating characteristics of a tilt nacelle inlet/powered fan model [NASA-TM-88983] p 14 N87-27628

SHOT PEENING

- Shot peening for Ti-6Al-4V alloy compressor blades [NASA-TF-2711] p 104 N87-20556

SHROUDS

- Ceramic high pressure gas path seal [NASA-CR-180813] p 31 N87-26914
Aerodynamic performance investigation of advanced mechanical suppressor and ejector nozzle concepts for jet noise reduction [NASA-CR-174860] p 33 N87-29534

SIGNAL DISTORTION

- A study of the effect of group delay distortion on an SMSK satellite communications channel [NASA-TM-89835] p 116 N87-20450

SIGNAL ENCODING

- An adaptive algorithm for motion compensated color image coding p 113 A87-45466

SIGNAL FADING

- Performance of a Ka-band satellite system under variable transmitted signal power conditions [NASA-TM-88984] p 116 N87-18700

SIGNAL PROCESSING

- Baseband processor development/test performance for 30/20 GHz SS-TDMA communication system p 111 A87-18310
ACTS baseband processing - Advanced Communications Technology Satellite p 201 A87-45512

- Performance of a Ka-band satellite system under variable transmitted signal power conditions
[NASA-TM-88984] p 116 N87-18700
- A computer controlled signal preprocessor for laser fringe anemometer applications
[NASA-TM-88982] p 157 N87-20516
- SMI adaptive antenna arrays for weak interfering signals
[NASA-CR-181330] p 119 N87-28813
- Adaptive arrays for weak interfering signals: An experimental system
[NASA-CR-181181] p 119 N87-28814
- Onboard multichannel demultiplexer/demodulator
[NASA-CR-180821] p 119 N87-28819
- Oxygen interaction with space-power materials
[NASA-CR-181396] p 80 N87-29633
- SIGNAL TO NOISE RATIOS**
- Automated measurement of the bit-error rate as a function of signal-to-noise ratio for microwave communications systems
[NASA-TM-89898] p 127 N87-22102
- SILANES**
- Sol-Gel synthesis of MgO-SiO₂ glass compositions having stable liquid-liquid immiscibility
[NASA-TM-89905] p 103 N87-23750
- SILICA GLASS**
- Sol-Gel synthesis of MgO-SiO₂ glass compositions having stable liquid-liquid immiscibility
[NASA-TM-89905] p 103 N87-23750
- SILICON**
- Indium phosphide solar cells - Status and prospects for use in space p 188 N87-18071
- Further advances in silicon solar cell technology for space application p 188 N87-18074
- Potential for use of InP solar cells in the space radiation environment p 120 N87-19996
- TEM investigation of beta-SiC grown epitaxially on Si substrate by CVD p 97 N87-40927
- SILICON CARBIDES**
- Behavior of inversion layers in 3C silicon carbide p 215 N87-11242
- Improved consolidation of silicon carbide p 94 N87-12940
- Compensation in epitaxial cubic SiC films p 216 N87-15071
- Colloidal characterization of ultrafine silicon carbide and silicon nitride powders p 95 N87-19625
- Mechanism of strength degradation for hot corrosion of alpha-SiC p 95 N87-21470
- Corrosion pitting of SiC by molten salts p 76 N87-27165
- Antiphase boundaries in epitaxially grown beta-SiC p 217 N87-30025
- TEM investigation of beta-SiC grown epitaxially on Si substrate by CVD p 97 N87-40927
- Observation of deep levels in cubic silicon carbide p 122 N87-41089
- Comment on 'Temperature dependence of electrical properties of non-doped and nitrogen-doped beta-SiC single crystals grown by chemical vapor deposition' p 217 N87-42846
- Growth and characterization of cubic SiC single-crystal films on Si p 217 N87-44875
- SILICON NITRIDES**
- Particle-size reduction of Si₃N₄ powder with Si₃N₄ milling hardware p 94 N87-12936
- Correlation of processing and sintering variables with the strength and radiography of silicon nitride p 94 N87-12938
- Sintering, microstructural, radiographic, and strength characterization of a high-purity Si₃N₄-based composition p 94 N87-12939
- Colloidal characterization of ultrafine silicon carbide and silicon nitride powders p 95 N87-19625
- Fracture toughness of Si₃N₄ measured with short bar chevron-notched specimens p 96 N87-30621
- Fracture of flash oxidized, yttria-doped sintered reaction-bonded silicon nitride p 97 N87-47923
- Slow crack growth in sintered silicon nitride p 98 N87-48989
- Mechanical properties of SiC fiber-reinforced reaction-bonded Si₃N₄ composites p 73 N87-50094
- Characterization of ion beam modified ceramic wear surfaces using Auger electron spectroscopy p 98 N87-51304
- Quantitative void characterization in structural ceramics by use of scanning laser acoustic microscopy p 171 N87-51974
- Hot corrosion attack and strength degradation of SiC and Si(sub)3N(sub)4 [NASA-TM-89820] p 102 N87-20425
- Stability and rheology of dispersions of silicon nitride and silicon carbide [NASA-CR-179634] p 104 N87-25476
- SILICON OXIDES**
- Oxygen-18 tracer study of the passive thermal oxidation of silicon p 78 N87-51187
- SILOXANES**
- Silsesquioxanes as precursors to ceramic composites [NASA-TM-89893] p 75 N87-25432
- SILVER**
- Effects of silver and group II fluoride solid lubricant additions to plasma-sprayed chromium carbide coatings for foil gas bearings to 650 C p 95 N87-22336
- Effect of hard particle impacts on the atomic oxygen survivability of reflector surfaces with transparent protective overcoats p 56 N87-11838
- Carbide-fluoride-silver self-lubricating composite [NASA-CASE-LEW-14196-2] p 169 N87-25585
- SIMILARITY THEOREM**
- On similarity solutions for turbulent and heated round jets p 130 N87-10922
- SIMULATION**
- Numerical simulation of transonic propeller flow using a three-dimensional small disturbance code employing novel helical coordinates p 5 N87-42107
- [AIAA PAPER 87-1162] p 5 N87-42107
- WEST-3 wind turbine simulator development. Volume 1: Summary p 192 N87-11348
- Numerical simulation of transonic propeller flow using a 3-dimensional small disturbance code employing novel helical coordinates p 12 N87-19350
- Direct numerical simulations of a temporally evolving mixing layer subject to forcing p 150 N87-23933
- [NASA-TM-88896] p 150 N87-23933
- Experimental evaluation of corner turning vanes [NASA-TM-100143] p 37 N87-28571
- Oxygen interaction with space-power materials [NASA-CR-181396] p 80 N87-29633
- SIMULATORS**
- A model propulsion simulator for evaluating counter rotating blade characteristics [SAE PAPER 861715] p 20 N87-32607
- Applications and requirements for real-time simulators in ground-test facilities [NASA-TP-2672] p 204 N87-23202
- SINGLE CRYSTALS**
- Behavior of inversion layers in 3C silicon carbide p 215 N87-11242
- Antiphase boundaries in epitaxially grown beta-SiC p 217 N87-30025
- Yielding and deformation behavior of the single crystal superalloy PWA 1480 p 84 N87-32040
- Understanding single-crystal superalloys p 85 N87-40928
- Application of single crystal superalloys for earth-to-orbit propulsion systems [AIAA PAPER 87-1976] p 85 N87-45336
- The characteristics of gamma-prime dislocation pairs in a nickel-base superalloy p 85 N87-46932
- Comment on 'Temperature dependence of electrical properties of non-doped and nitrogen-doped beta-SiC single crystals grown by chemical vapor deposition' p 217 N87-42846
- Growth and characterization of cubic SiC single-crystal films on Si p 217 N87-44875
- Mechanical properties of SiC fiber-reinforced reaction-bonded Si₃N₄ composites p 73 N87-50094
- Processing of laser formed SiC powder [NASA-CR-179857] p 99 N87-11009
- High-temperature effect of hydrogen on sintered alpha-silicon carbide [NASA-TM-88819] p 100 N87-14518
- Deformation and fracture of single-crystal and sintered polycrystalline silicon carbide produced by cavitation [NASA-TM-88981] p 102 N87-20422
- Hot corrosion attack and strength degradation of SiC and Si(sub)3N(sub)4 [NASA-TM-89820] p 102 N87-20425
- Friction and wear of sintered Alpha SiC sliding against IN-718 alloy at 25 to 800 C in atmospheric air at ambient pressure [NASA-TM-87353] p 103 N87-22860
- Processing of laser formed SiC powder [NASA-CR-179638] p 104 N87-24573
- Stability and rheology of dispersions of silicon nitride and silicon carbide [NASA-CR-179634] p 104 N87-25476
- Method of preparing fiber reinforced ceramic material [NASA-CASE-LEW-14392-1] p 106 N87-28656
- SILICON DIOXIDE**
- Shallow n(+) diffusion into InP by an open-tube diffusion technique p 217 N87-30023
- SILICON FILMS**
- Compensation in epitaxial cubic SiC films p 216 N87-15071
- The stability of lamellar gamma-gamma-prime structures -- nickel-base superalloy p 86 N87-48323
- The cyclic stress-strain behavior of PWA 1480 at 650 deg C [NASA-TM-87311] p 89 N87-14483
- Elevated temperature tension, compression and creep-rupture behavior of (001)-oriented single crystal superalloy PWA 1480 [NASA-TM-88950] p 90 N87-17882
- Hardness of CaF₂ and BaF₂ solid lubricants at 25 to 670 deg C [NASA-TM-88979] p 102 N87-18670
- Bithermal low-cycle fatigue behavior of a NiCoCrAlY-coated single crystal superalloy [NASA-TM-89831] p 91 N87-20408
- Deformation and fracture of single-crystal and sintered polycrystalline silicon carbide produced by cavitation [NASA-TM-88981] p 102 N87-20422
- Application of single crystal superalloys for Earth-to-orbit propulsion systems [NASA-TM-89877] p 91 N87-22034
- Life prediction and constitutive models for engine hot section anisotropic materials [NASA-CR-179594] p 29 N87-23622
- SSME single crystal turbine blade dynamics [NASA-CR-179644] p 186 N87-26384
- SINGLE-PHASE FLOW**
- Laser anemometry measurements of natural circulation flow in a scale model PWR reactor system -- Pressurized Water Reactor p 154 N87-40750
- SINTERING**
- Correlation of processing and sintering variables with the strength and radiography of silicon nitride p 94 N87-12938
- Sintering, microstructural, radiographic, and strength characterization of a high-purity Si₃N₄-based composition p 94 N87-12939
- Improved consolidation of silicon carbide p 94 N87-12940
- Probability of detection of internal voids in structural ceramics using microfocus radiography p 170 N87-14300
- Fracture of flash oxidized, yttria-doped sintered reaction-bonded silicon nitride p 97 N87-47923
- Slow crack growth in sintered silicon nitride p 98 N87-48989
- High-temperature effect of hydrogen on sintered alpha-silicon carbide [NASA-TM-88819] p 100 N87-14518
- Deformation and fracture of single-crystal and sintered polycrystalline silicon carbide produced by cavitation [NASA-TM-88981] p 102 N87-20422
- Friction and wear of sintered Alpha SiC sliding against IN-718 alloy at 25 to 800 C in atmospheric air at ambient pressure [NASA-TM-87353] p 103 N87-22860
- Processing of laser formed SiC powder [NASA-CR-179638] p 104 N87-24573
- SIZE DETERMINATION**
- Quantitative void characterization in structural ceramics by use of scanning laser acoustic microscopy p 171 N87-51974
- SLIDING FRICTION**
- Friction and wear behaviour of ion beam modified ceramics p 97 N87-47958
- The role of near-surface plastic deformation in the wear of lamellar solids p 162 N87-48500
- SLURRIES**
- Tribological properties of coal slurries [NASA-TM-89930] p 104 N87-24565
- SMALL PERTURBATION FLOW**
- A method for assessing effects of circumferential flow distortion on compressor stability p 7 N87-48722
- SMOKE**
- Advanced optical smoke meters for jet engine exhaust measurement [NASA-CR-179459] p 155 N87-12829
- SODIUM**
- Experimental verification of corrosive vapor deposition rate theory in high velocity burner rigs p 143 N87-49551
- SODIUM CHLORIDES**
- Reactions occurring during the sulfation of sodium chloride deposited on alumina substrates p 76 N87-20223
- SOFTWARE ENGINEERING**
- Color postprocessing for 3-dimensional finite element mesh quality evaluation and evolving graphical workstation [NASA-CR-180215] p 202 N87-18997
- SOFTWARE TOOLS**
- The hypercluster: A parallel processing test-bed architecture for computational mechanics applications [NASA-TM-89823] p 203 N87-20767

SOL-GEL PROCESSES

Sol-Gel synthesis of MgO-SiO₂ glass compositions having stable liquid-liquid immiscibility
[NASA-TM-89905] p 103 N87-23750

SOLAR ARRAYS

Computer simulation of plasma electron collection by PIX-II — solar array-space plasma interaction p 45 A87-17837
Indium phosphide solar cells - Status and prospects for use in space p 188 A87-18071
Space station experiment definition: Advanced power system test bed
[NASA-CR-179502] p 58 N87-15270
Solar dynamic power systems for space station p 58 N87-16024
LEO high voltage solar array arcing response model [NASA-CR-180073] p 124 N87-16971
Space station WP-04 power system. Volume 1: Executive summary p 65 N87-23695
[NASA-CR-179587-VOL-1] p 65 N87-23695
Space station WP-04 power system. Volume 2: Study results p 65 N87-23696
[NASA-CR-179587-VOL-2] p 65 N87-23696
High power/large area PV systems p 198 N87-26452

SOLAR BLANKETS

Protection of solar array blankets from attack by low earth orbital atomic oxygen p 47 A87-19874

SOLAR CELLS

Cell performance and defect behavior in proton-irradiated lithium-counterdoped n(+)-p silicon solar cells p 216 A87-14222
Indium phosphide solar cells - Status and prospects for use in space p 188 A87-18071
High-efficiency GaAs solar concentrator cells for space and terrestrial applications p 188 A87-18073
Further advances in silicon solar cell technology for space application p 188 A87-18074
The potential impact of new power system technology on the design of a manned Space Station p 47 A87-18342
A 25.5 percent AMO gallium arsenide grating solar cell p 189 A87-19840
Use of a corrugated surface to enhance radiation tolerance in a GaAs solar cell p 189 A87-19842
Performance of GaAs and silicon concentrator cells under 1 MeV electron irradiation p 189 A87-19871
An optimized top contact design for solar cell concentrators p 189 A87-19882
Development of the VOLT-A Shuttle experiment — Volt Operating Limit Tests p 41 A87-19907
A proposed GaAs-based superlattice solar cell structure with high efficiency and high radiation tolerance p 189 A87-19915
Potential for use of InP solar cells in the space radiation environment p 120 A87-19996
The voltage threshold for arcing for solar cells in Leo - Flight and ground test results
[AIAA PAPER 86-0362] p 50 A87-40275
Combination solar photovoltaic heat engine energy converter p 190 A87-47088
Indium phosphide shallow homojunction solar cells made by metalorganic chemical vapor deposition p 123 A87-50047
LEO high voltage solar array arcing response model [NASA-CR-180073] p 124 N87-16971
Effect of an oxygen plasma on uncoated thin aluminum reflecting films p 61 N87-21999
[NASA-TM-89882] p 61 N87-21999
Radiation and temperature effects in gallium arsenide, indium phosphide and silicon solar cells p 127 N87-22098
[NASA-TM-89870] p 127 N87-22098
High temperature solid oxide regenerative fuel cell for solar photovoltaic energy storage p 194 N87-23020
[NASA-TM-89872] p 194 N87-23020
Issues in space photovoltaic research and technology [NASA-TM-89922] p 128 N87-23901
Combination photovoltaic-heat engine energy converter
[NASA-CASE-LEW-14252-1] p 196 N87-25630
Space Photovoltaic Research and Technology 1986. High Efficiency, Space Environment, and Array Technology
[NASA-CP-2475] p 196 N87-26413
High-efficiency GaAs concentrator space cells p 196 N87-26417
Design considerations for a GaAs nipi doping superlattice solar cell p 196 N87-26422
The effect of internal stresses on solar cell efficiency p 196 N87-26430
The use of multiple EBIC curves and low voltage electron microscopy in the measurement of small diffusion lengths p 197 N87-26434
Results of 1 MeV proton irradiation of front and back surfaces of silicon solar cells p 197 N87-26435

Performance of AlGaAs, GaAs and InGaAs cells after 1 MeV electron irradiation p 197 N87-26438
Status of indium phosphide solar cell development at Spire p 197 N87-26440
Comparative performance of diffused junction indium phosphide solar cells p 197 N87-26441
Near-optimum design of the InP homojunction solar cell p 197 N87-26443
Solar cells in bulk InP using an open tube diffusion process p 198 N87-26444
Radiation damage in proton irradiated indium phosphide solar cells p 199 N87-29018

SOLAR COLLECTORS

Solar concentrator materials development p 213 A87-18171
Optimization of spherical facets for parabolic solar concentrators p 213 A87-18173
An optimized top contact design for solar cell concentrators p 189 A87-19882
Development of an advanced photovoltaic concentrator system for space applications p 66 N87-24531
[NASA-TM-100101] p 66 N87-24531

SOLAR DYNAMIC POWER SYSTEMS

Space power - Emerging opportunities
[IAF PAPER 86-152] p 45 A87-15900
Electrical power system for the U.S. Space Station
[IAF PAPER 86-37] p 45 A87-16138
Solar concentrator materials development p 213 A87-18171
Optimization of spherical facets for parabolic solar concentrators p 213 A87-18173
Solar dynamic space power system heat rejection p 47 A87-18175
Effect of hard particle impacts on the atomic oxygen survivability of reflector surfaces with transparent protective overcoats p 69 A87-22417
[AIAA PAPER 87-0104] p 69 A87-22417
Oxidation-resistant reflective surfaces for solar dynamic power generation in near Earth orbit p 56 N87-10960
[NASA-TM-88865] p 56 N87-10960
Effect of hard particle impacts on the atomic oxygen survivability of reflector surfaces with transparent protective overcoats p 56 N87-11838
[NASA-TM-88874] p 56 N87-11838
Advanced solar dynamic space power systems perspectives, requirements and technology needs p 56 N87-12606
[NASA-TM-88884] p 56 N87-12606
Conceptual definition of a technology development mission for advanced solar dynamic power systems [NASA-CR-179482] p 192 N87-14771
Advanced Stirling conversion systems for terrestrial applications p 220 N87-15031
[NASA-TM-88897] p 220 N87-15031
Electrical power system design for the US space station p 58 N87-15267
[NASA-TM-88824] p 58 N87-15267
Selection of high temperature thermal energy storage materials for advanced solar dynamic space power systems p 149 N87-22174
[NASA-TM-89886] p 149 N87-22174
Impact of thermal energy storage properties on solar dynamic space power conversion system mass p 63 N87-22802
[NASA-TM-89909] p 63 N87-22802
Speculations on future opportunities to evolve Brayton powerplants aboard the space station p 39 N87-23674
[NASA-TM-89863] p 39 N87-23674
Space station WP-04 power system. Volume 1: Executive summary p 65 N87-23695
[NASA-CR-179587-VOL-1] p 65 N87-23695
Space station WP-04 power system. Volume 2: Study results p 65 N87-23696
[NASA-CR-179587-VOL-2] p 65 N87-23696
Issues in space photovoltaic research and technology [NASA-TM-89922] p 128 N87-23901
Fluoride salts and container materials for thermal energy storage applications in the temperature range 973 to 1400 K p 195 N87-24026
[NASA-TM-89913] p 195 N87-24026
Combination photovoltaic-heat engine energy converter
[NASA-CASE-LEW-14252-1] p 196 N87-25630
Space station electrical power system p 68 N87-26144
[NASA-TM-100140] p 68 N87-26144
Space station power system p 68 N87-26447
Status of space station power system p 45 N87-29915

SOLAR ENERGY

NASA Growth Space Station missions and candidate nuclear/solar power systems p 48 A87-21807
Impact of thermal energy storage properties on solar dynamic space power conversion system mass p 63 N87-22802
[NASA-TM-89909] p 63 N87-22802

SOLAR ENERGY CONVERSION

Combination solar photovoltaic heat engine energy converter p 190 A87-47088

Brayton cycle solarized advanced gas turbine
[NASA-CR-179559] p 220 N87-15030
Advanced Stirling conversion systems for terrestrial applications p 220 N87-15031
[NASA-TM-88897] p 220 N87-15031
Solar dynamic power systems for space station p 58 N87-16024
Combination photovoltaic-heat engine energy converter
[NASA-CASE-LEW-14252-1] p 196 N87-25630
Comparison of Stirling engines for use with a 25-kW disk-electric conversion system p 222 N87-27564
[NASA-TM-100111] p 222 N87-27564
Alternative power generation concepts for space p 199 N87-28961

SOLAR GENERATORS

User evaluation of photovoltaic-powered vaccine refrigerator/freezer systems p 193 N87-18230
[NASA-TM-88830] p 193 N87-18230
Performance characteristics of a combination solar photovoltaic heat engine energy converter
[NASA-TM-89908] p 195 N87-23028
Design, development and deployment of public service photovoltaic power/load systems for the Gabonese Republic p 195 N87-23030
[NASA-CR-179603] p 195 N87-23030

SOLAR REFLECTORS

The survivability of large space-borne reflectors under atomic oxygen and micrometeoroid impact p 49 A87-31300
[AIAA PAPER 87-0341] p 49 A87-31300
The survivability of large space-borne reflectors under atomic oxygen and micrometeoroid impact p 57 N87-14423
[NASA-TM-88914] p 57 N87-14423
Solar dynamic power systems for space station p 58 N87-16024

SOLAR THERMAL ELECTRIC POWER PLANTS

Advanced solar thermal technologies for the 21st century p 47 A87-18179
A photovoltaic power system and a low-power satellite earth station for Indonesia p 189 A87-19859
Tunisia Renewable Energy Project systems description report p 192 N87-13856
[NASA-TM-88789] p 192 N87-13856

SOLID ELECTRODES

Carbon and carbon-coated electrodes for multistage depressed collectors for electron-beam devices - A technology review p 120 A87-20666
Improvements in MDC and TWT overall efficiency through the application of carbon electrode surfaces — Multistage Depressed Collectors p 120 A87-20667
Catalyst and electrode research for phosphoric acid fuel cells p 190 A87-33789
Low power arcjet life issues p 50 A87-39635
[AIAA PAPER 87-1059] p 50 A87-39635
A point defect model for nickel electrode structures p 87 A87-52282

SOLID LUBRICANTS

Tribology of selected ceramics at temperatures to 900 C p 94 A87-12954
Counterface effects on the tribological properties of polyimide composites p 95 A87-27625
A review of recent advances in solid film lubrication p 161 A87-35332
Tribological properties of polymer films and solid bodies in a vacuum environment p 101 N87-17906
[NASA-TM-88966] p 101 N87-17906
Solid lubrication design methodology, phase 2 p 221 N87-18470
[NASA-CR-175114] p 221 N87-18470
Hardness of CaF₂ and BaF₂ solid lubricants at 25 to 670 deg C p 102 N87-18670
[NASA-TM-88979] p 102 N87-18670
Investigation of PTFE transfer films by infrared emission spectroscopy and phase-locked ellipsometry p 102 N87-20421
[NASA-TM-89844] p 102 N87-20421
Composition optimization of chromium carbide based solid lubricant coatings for foil gas bearings at temperatures to 650 C p 105 N87-26233
[NASA-CR-179649] p 105 N87-26233
Experimental evaluation of chromium-carbide-based solid lubricant coatings for use to 760 C p 105 N87-27053
[NASA-CR-180808] p 105 N87-27053

SOLID MECHANICS

Variational approach to probabilistic finite elements [NASA-CR-181343] p 206 N87-29212

SOLID PHASES

Compressibility of solids p 219 A87-51962

SOLID PROPELLANT COMBUSTION

Forced cocurrent smoldering combustion p 77 A87-40572
Size and shape of solid fuel diffusion flames in very slow speed flows
[AIAA PAPER 87-2030] p 78 A87-52248

SOLID STATE DEVICES

The 20 GHz spacecraft IMPATT solid state transmitter [NASA-CR-179545] p 124 N87-17989

SOLID-SOLID INTERFACES

Antiphase boundaries in epitaxially grown beta-SiC
p 217 A87-30025

SOLIDIFICATION

Transition from a planar interface to cellular and dendritic structures during rapid solidification processing
p 81 A87-12029

Processing-structure characterization of rheocast IN-100 superalloy
p 82 A87-24116

Dendritic microstructure in argon atomized superalloy powders
p 83 A87-24119

Analysis of the solidified structure of rheocast and VADER processed nickel-base superalloy
p 83 A87-28734

The alloy undercooling experiment on the Columbia STS 61-C Space Shuttle mission
[AIAA PAPER 87-0506] p 108 A87-45724

Microstructures in rapidly solidified Ni-Mo alloys
p 87 A87-51636

Primary arm spacing in chill block melt spun Ni-Mo alloys
[NASA-TM-88887] p 88 A87-11875

A study of the microstructure of a rapidly solidified nickel-base superalloy modified with boron
[NASA-CR-179553] p 89 A87-14486

High temperature monotonic and cyclic deformation in a directionally solidified nickel-base superalloy
[NASA-CR-175101] p 90 A87-15303

The alloy undercooling experiment on the Columbia STA 61-C space shuttle mission
[NASA-TM-88909] p 91 A87-18643

Gravitational macrosegregation in binary Pb-Sn alloy ingots
[NASA-TM-89885] p 109 A87-24579

A study of reduced chromium content in a nickel-base superalloy via element substitution and rapid solidification processing
[NASA-CR-179631] p 92 A87-25456

SOLIDS

A universal equation of state for solids
p 219 A87-14665

SOLUBILITY

Sol-Gel synthesis of MgO-SiO₂ glass compositions having stable liquid-liquid immiscibility
[NASA-TM-89905] p 103 A87-23750

SOOT

Shock-tube pyrolysis of acetylene - Sensitivity analysis of the reaction mechanism for soot formation
p 75 A87-12598

Empirical modeling of soot formation in shock-tube pyrolysis of aromatic hydrocarbons
p 76 A87-12599

Soot loading in a generic gas turbine combustor
[AIAA PAPER 87-0297] p 19 A87-22544

SOUND PROPAGATION

Turbofan aft duct suppressor study. Contractor's data report of mode probe signal data
[NASA-CR-175067] p 34 A87-29538

Turbofan aft duct suppressor study
[NASA-CR-175067] p 34 A87-29539

SOUND TRANSMISSION

Identification and proposed control of helicopter transmission noise at the source
[NASA-TM-89312] p 18 A87-16816

SOUND WAVES

Modeling the effects of wind tunnel wall absorption on the acoustic radiation characteristics of propellers
[AIAA PAPER 86-1876] p 208 A87-17991

Sound radiation from single and annular stream nozzles, with modal decomposition of in-duct acoustic power
p 209 A87-37629

Propagation of sound waves in tubes of noncircular cross section
[NASA-TP-2601] p 9 A87-14284

SPACE BASED RADAR

Nuclear reactor power for a space-based radar. SP-100 project
[NASA-TM-89295] p 213 A87-25838

SPACE CHARGE

Self-consistent inclusion of space-charge in the traveling wave tube
[NASA-TM-89928] p 128 A87-24630

SPACE COMMERCIALIZATION

Dendritic microstructure in argon atomized superalloy powders
p 83 A87-24119

A critical examination of the dendrite growth models. Comparison of theory with experimental data
p 83 A87-25048

Undercooling and crystallization behaviour of antimony droplets
p 83 A87-28732

Fault structures in rapidly quenched Ni-Mo binary alloys
p 83 A87-32035

Cellular-dendritic transition in directionally solidified binary alloys
p 84 A87-32046

The NASA Electric Propulsion Program
[AIAA PAPER 87-1098] p 53 A87-45795

Equipment concept design and development plans for microgravity science and applications research on space station: Combustion tunnel, laser diagnostic system, advanced modular furnace, integrated electronics laboratory
[NASA-CR-179535] p 108 A87-15320

Communications satellite systems operations with the space station, volume 2
[NASA-CR-179527] p 206 A87-17473

The NASA Electric Propulsion Program
[NASA-TM-89856] p 61 A87-21037

SPACE COMMUNICATION

Advanced space communications architecture study. Volume 1: Executive summary
[NASA-CR-179591] p 115 A87-18696

Optically controlled microwave devices and circuits: Emerging applications in space communications systems
[NASA-TM-89869] p 127 A87-23900

Monolithic Microwave Integrated Circuit (MMIC) technology for space communications applications
[NASA-TM-100187] p 118 A87-27883

SPACE ENVIRONMENT SIMULATION

Neutral atomic oxygen beam produced by ion charge exchange for Low Earth Orbital (LEO) simulation
p 79 A87-26188

SPACE EXPLORATION

Status of advanced propulsion for space based orbital transfer vehicle
[IAF PAPER 86-183] p 48 A87-23239

The NASA Electric Propulsion Program
[AIAA PAPER 87-1098] p 53 A87-45795

Status of advanced propulsion for space based orbital transfer vehicle
[NASA-TM-88848] p 56 A87-10959

Centaur D1-A systems in a nutshell
[NASA-TM-88880] p 38 A87-15996

The NASA Electric Propulsion Program
[NASA-TM-89856] p 61 A87-21037

SPACE MAINTENANCE

Concepts for space maintenance of OTV engines
p 40 A87-41161

Concepts for space maintenance of OTV engines
p 67 A87-26097

SPACE PLASMAS

Computer simulation of plasma electron collection by PIX-II - solar array-space plasma interaction
p 45 A87-17837

Development of the VOLT-A Shuttle experiment - Volt Operating Limit Tests
p 41 A87-19907

Enhanced current flow through a plasma cloud by induction of plasma turbulence - electrodynamic tethers for generating power for spacecraft in low earth orbit
[AIAA PAPER 87-0573] p 214 A87-22714

Plasma contactors for electrodynamic tethers
p 214 A87-31211

Hollow cathode-based plasma contactor experiments for electrodynamic tether
[AIAA PAPER 87-0572] p 214 A87-32192

Theory of plasma contactors for electrodynamic tethered satellite systems
p 122 A87-41609

LEO high voltage solar array arcing response model
[NASA-CR-180073] p 124 A87-16971

Electron beam experiments at high altitudes
p 44 A87-26946

SPACE PLATFORMS

Propulsion recommendations for Space Station free flying platforms
p 49 A87-31134

An advanced geostationary communications platform
p 112 A87-43165

Electrical power system design for the US space station
[NASA-TM-88824] p 58 A87-15267

Propulsion recommendations for space station free flying platforms
p 67 A87-26129

SPACE POWER REACTORS

Overview of the 1986 free-piston Stirling SP-100 activities at the NASA Lewis Research Center
p 160 A87-18033

A feasibility assessment of nuclear reactor power system concepts for the NASA Growth Space Station
p 47 A87-18154

Solar dynamic space power system heat rejection
p 47 A87-18175

NASA Growth Space Station missions and candidate nuclear/solar power systems
p 48 A87-21807

Reliability and mass analysis of dynamic power conversion systems with parallel or standby redundancy
p 190 A87-21823

Coaxial tube tether/transmission line for manned nuclear space power
[NASA-CASE-LEW-14338-1] p 55 A87-10174

Coaxial tube array space transmission line characterization
[NASA-TM-89864] p 62 A87-22003

SP-100 Advanced Technology Program
[NASA-TM-89888] p 194 A87-23027

Speculations on future opportunities to evolve Brayton powerplants aboard the space station
[NASA-TM-89863] p 39 A87-23674

An assessment and validation study of nuclear reactors for low power space applications
[NASA-CR-180672] p 213 A87-27495

SPACE POWER UNIT REACTORS

Alternative power generation concepts for space
p 199 A87-28961

SPACE PROCESSING

Particle cloud kinetics in microgravity
[AIAA PAPER 87-0577] p 107 A87-22716

Experiments on thermocoustic convection heat transfer in gravity and zero-gravity environments
[AIAA PAPER 87-1651] p 107 A87-43141

Up close - Materials division of NASA-Lewis Research Center
p 69 A87-51176

Equipment concept design and development plans for microgravity science and applications research on space station: Combustion tunnel, laser diagnostic system, advanced modular furnace, integrated electronics laboratory
[NASA-CR-179535] p 108 A87-15320

Simulation of fluid flows during growth of organic crystals in microgravity
[NASA-TM-88921] p 108 A87-16167

SPACE SHUTTLE BOOSTERS

Analysis of quasi-hybrid solid rocket booster concepts for advanced earth-to-orbit vehicles
[AIAA PAPER 87-2082] p 55 A87-52250

Analysis of quasi-hybrid solid rocket booster concepts for advanced earth-to-orbit vehicles
[NASA-TP-2751] p 67 A87-25425

SPACE SHUTTLE MAIN ENGINE

Feasibility of mapping velocity flowfields in an SSME powerhead using laser anemometry techniques
[AIAA PAPER 87-1306] p 154 A87-42374

Application of single crystal superalloys for earth-to-orbit propulsion systems
[AIAA PAPER 87-1976] p 85 A87-45336

Composite load spectra for select space propulsion structural components
[NASA-CR-179496] p 55 A87-10176

Probabilistic structural analysis methods for space propulsion system components
[NASA-TM-88861] p 181 A87-13794

Conventionally cast and forged copper alloy for high-heat-flux thrust chambers
[NASA-TP-2694] p 90 A87-16902

Application of single crystal superalloys for Earth-to-orbit propulsion systems
[NASA-TM-88877] p 91 A87-22034

Structural Integrity and Durability of Reusable Space Propulsion Systems
[NASA-CP-2471] p 62 A87-22766

Unsteady stator/rotor interaction
p 149 A87-22767

Simulation of multistage turbine flows
p 149 A87-22768

Progress on thin-film sensors for space propulsion technology
p 158 A87-22772

Heat flux calibration facility capable of SSME conditions
p 36 A87-22774

Nonlinear heat transfer and structural analyses of SSME turbine blades
p 184 A87-22779

Probabilistic structural analysis to evaluate the structural durability of SSME critical components
p 62 A87-22783

Probabilistic Structural Analysis Methods (PSAM) for select space propulsion system structural components
p 62 A87-22784

Composite load spectra for select space propulsion structural components
p 63 A87-22793

Structural tailoring using the SSME/STAEBL code
p 63 A87-22795

SSME blade damper technology
p 63 A87-22798

Three-step labyrinth seal for high-performance turbomachines
[NASA-TP-1848] p 150 A87-23921

Straight cylindrical seal for high-performance turbomachines
[NASA-TP-1850] p 150 A87-23936

Three-step cylindrical seal for high-performance turbomachines
[NASA-TP-1849] p 151 A87-24639

SSME single crystal turbine blade dynamics
[NASA-CR-179644] p 186 A87-26384

SPACE SHUTTLE ORBITERS

Three dimensional simulation of the operation of a hollow cathode electron emitter on the Shuttle orbiter
p 119 A87-14084

Measurements of plasma parameters in the vicinity of the Space Shuttle
p 200 A87-24672

Measurement of Centaur/Orbiter multiple reaction forces in a full-scale test rig
p 38 A87-29448

Manned spacecraft electrical power systems
p 49 A87-37291

- Preliminary aerothermodynamic design method for hypersonic vehicles p 7 A87-49100
- Measurements of plasma density and turbulence near the shuttle orbiter [NASA-CR-180102] p 215 N87-16614
- SPACE SHUTTLE PAYLOADS**
- On-orbit cryogenic storage and resupply p 41 A87-18344
- The effect of nonlinearities on the dynamic response of a large Shuttle payload [AIAA PAPER 87-0857] p 40 A87-33697
- Liquid droplet radiator development status --- waste heat rejection devices for future space vehicles [AIAA PAPER 87-1537] p 42 A87-43059
- The alloy undercooling experiment on the Columbia STS 61-C Space Shuttle mission [AIAA PAPER 87-0506] p 108 A87-45724
- The effect of nonlinearities on the dynamic response of a large shuttle payload [NASA-TM-88941] p 181 N87-18112
- The alloy undercooling experiment on the Columbia STA 61-C space shuttle mission [NASA-TM-88909] p 91 N87-18643
- Liquid droplet radiator development status [NASA-TM-89852] p 43 N87-20353
- Design, development and test of shuttle/Centaur G-prime cryogenic tankage thermal protection systems [NASA-TM-89825] p 43 N87-23685
- Gravitational macrosegregation in binary Pb-Sn alloy ingots [NASA-TM-89885] p 109 N87-24579
- SPACE SHUTTLES**
- Effects of transient propellant dynamics on deployment of large liquid stages in zero-gravity with application to Shuttle/Centaur [IAF PAPER 86-119] p 39 A87-15880
- Ram ion scattering caused by Space Shuttle v x B induced differential charging p 200 A87-51713
- Space experiment development process p 109 N87-21156
- SPACE SIMULATORS**
- Neutral atomic oxygen beam produced by ion charge exchange for Low Earth Orbital (LEO) simulation p 79 N87-26188
- SPACE STATION POWER SUPPLIES**
- Power is the keystone --- for space station p 45 A87-16929
- Alkaline water electrolysis technology for Space Station regenerative fuel cell energy storage p 46 A87-18107
- A feasibility assessment of nuclear reactor power system concepts for the NASA Growth Space Station p 47 A87-18154
- Space Station Power System issues p 47 A87-19877
- NASA Growth Space Station missions and candidate nuclear/solar power systems p 48 A87-21807
- Automating the U.S. Space Station's electrical power system p 48 A87-23646
- Advanced technology for extended endurance alkaline fuel cells p 190 A87-33787
- 20 kHz Space Station power system p 51 A87-40378
- Coaxial tube tether/transmission line for manned nuclear space power [NASA-CASE-LEW-14338-1] p 55 N87-10174
- Space station electric power system requirements and design [NASA-TM-89889] p 62 N87-22001
- Speculations on future opportunities to evolve Brayton powerplants aboard the space station [NASA-TM-89863] p 39 N87-23674
- Space station WP-04 power system. Volume 1: Executive summary [NASA-CR-179587-VOL-1] p 65 N87-23695
- Space station WP-04 power system. Volume 2: Study results [NASA-CR-179587-VOL-2] p 65 N87-23696
- Status of space station power system p 45 N87-29915
- SPACE STATION PROPULSION**
- High- and low-thrust propulsion systems for the Space Station [AIAA PAPER 87-0398] p 48 A87-24997
- Propulsion recommendations for Space Station free flying platforms p 49 A87-31134
- Conceptual design and integration of a Space Station resistojet propulsion assembly [AIAA PAPER 87-1860] p 52 A87-45256
- Effect of nozzle geometry on the resistojet exhaust plume [AIAA PAPER 87-2121] p 55 A87-52252
- Conceptual design and integration of a space station resistojet propulsion assembly [NASA-TM-89847] p 60 N87-20378

- Proven, long-life hydrogen/oxygen thrust chambers for space station propulsion p 68 N87-26133
- Space station propulsion-ECLSS interaction study [NASA-CR-175093] p 69 N87-29594
- SPACE STATIONS**
- Electrical power system for the U.S. Space Station [IAF PAPER 86-37] p 45 A87-16138
- Electrical power system design for the U.S. Space Station p 46 A87-18068
- Solar dynamic space power system heat rejection p 47 A87-18175
- An analytical and experimental investigation of resistojet plumes [AIAA PAPER 87-0399] p 48 A87-24998
- Science and technology issues in spacecraft fire safety [AIAA PAPER 87-0467] p 39 A87-31107
- Space Station 20-kHz power management and distribution system p 49 A87-36913
- 20 kHz Space Station power system p 51 A87-40378
- Resistojet control and power for high frequency ac buses [AIAA PAPER 87-0994] p 122 A87-41103
- Liquid droplet radiator development status --- waste heat rejection devices for future space vehicles [AIAA PAPER 87-1537] p 42 A87-43059
- Preliminary performance characterizations of an engineering model multipropellant resistojet for space station application [AIAA PAPER 87-2120] p 54 A87-50197
- Strategic plan, 1985 [NASA-TM-89263] p 219 N87-12384
- High- and low-thrust propulsion systems for the space station [NASA-TM-88877] p 57 N87-14427
- An analytical and experimental investigation of resistojet plumes [NASA-TM-88852] p 58 N87-14428
- Conceptual definition of a technology development mission for advanced solar dynamic power systems [NASA-CR-179482] p 192 N87-14771
- Electrical power system design for the US space station [NASA-TM-88824] p 58 N87-15267
- Space station experiment definition: Advanced power system test bed [NASA-CR-179502] p 58 N87-15270
- Equipment concept design and development plans for microgravity science and applications research on space station: Combustion tunnel, laser diagnostic system, advanced modular furnace, integrated electronics laboratory [NASA-CR-179535] p 108 N87-15320
- Science and technology issues in spacecraft fire safety [NASA-TM-88933] p 40 N87-16012
- Solar dynamic power systems for space station p 58 N87-16024
- Potential propellant storage and feed systems for space station resistojet propulsion options [NASA-CR-179457] p 59 N87-16065
- The 20th Aerospace Mechanics Symposium [NASA-CP-2423-REV] p 181 N87-16321
- Space station auxiliary thrust chamber technology [NASA-CR-179552] p 59 N87-16874
- Communications satellite systems operations with the space station. Volume 1: Executive summary [NASA-CR-179526] p 206 N87-17472
- Communications satellite systems operations with the space station, volume 2 [NASA-CR-179527] p 206 N87-17473
- Research and technology [NASA-TM-88868] p 223 N87-17656
- Space station resistojet system requirements and interface definition study [NASA-CR-179581] p 60 N87-17848
- Fire safety concerns in space operations [NASA-TM-89848] p 40 N87-20342
- Liquid droplet radiator development status [NASA-TM-89852] p 43 N87-20353
- Resistojet control and power for high frequency ac buses [NASA-TM-89860] p 126 N87-20477
- Space station electric power system requirements and design [NASA-TM-89889] p 62 N87-22001
- Coaxial tube array space transmission line characterization [NASA-TM-89864] p 62 N87-22003
- EMC and power quality standards for 20-kHz power distribution [NASA-CR-89925] p 62 N87-22004
- Performance characteristics of a combination solar photovoltaic heat engine energy converter [NASA-TM-89908] p 195 N87-23028

- Control considerations for high frequency, resonant, power processing equipment used in large systems [NASA-TM-89926] p 64 N87-23690
- Space station WP-04 power system. Volume 1: Executive summary [NASA-CR-179587-VOL-1] p 65 N87-23695
- Space station WP-04 power system. Volume 2: Study results [NASA-CR-179587-VOL-2] p 65 N87-23696
- Preliminary performance characterizations of an engineering model multipropellant resistojet for space station application [NASA-TM-100113] p 111 N87-23821
- Space station experiment definition: Long-term cryogenic fluid storage [NASA-CR-4072] p 151 N87-24641
- Space station propulsion system technology [NASA-TM-100108] p 66 N87-25422
- Proven, long-life hydrogen/oxygen thrust chambers for space station propulsion p 68 N87-26133
- Water-propellant resistojets for man-tended platforms [NASA-TM-100110] p 68 N87-26135
- Space station electrical power system [NASA-TM-100140] p 68 N87-26144
- Space station power system p 68 N87-26447
- Space station power semiconductor package [NASA-CR-180829] p 129 N87-28825
- The space station power system p 198 N87-28960
- SPACE TRANSPORTATION SYSTEM**
- Development and test of the Shuttle/Centaur cryogenic tankage thermal protection system [AIAA PAPER 87-1557] p 43 A87-43073
- SPACEBORNE EXPERIMENTS**
- Low-gravity experiments in critical phenomena p 107 A87-23159
- ACTS experiments program --- Advanced Communications Technology Satellite p 113 A87-45513
- Ram ion scattering caused by Space Shuttle v x B induced differential charging p 200 A87-51713
- Space station experiment definition: Long-term cryogenic fluid storage [NASA-CR-4072] p 151 N87-24641
- SPACECRAFT**
- Centaur D1-A systems in a nutshell [NASA-TM-88880] p 38 N87-15996
- SPACECRAFT ANTENNAS**
- Composite space antenna structures - Properties and environmental effects p 72 A87-38610
- Thermal expansion behavior of graphite/glass and graphite/magnesium p 72 A87-38615
- An assessment of the status and trends in satellite communications 1986-2000: An information document prepared for the Communications Subcommittee of the Space Applications Advisory Committee [NASA-TM-88867] p 114 N87-13600
- Composite space antenna structures: Properties and environmental effects [NASA-TM-88859] p 73 N87-16880
- Application of adaptive antenna techniques to future commercial satellite communication [NASA-CR-179566] p 115 N87-16954
- Advanced space communications architecture study. Volume 2: Technical report [NASA-CR-179592] p 115 N87-18695
- System architecture of MMIC-based large aperture arrays for space application [NASA-TM-89840] p 125 N87-20468
- SPACECRAFT CABIN ATMOSPHERES**
- Concentration of carbon dioxide by a high-temperature electrochemical membrane cell p 77 A87-27400
- SPACECRAFT CHARGING**
- Three dimensional simulation of the operation of a hollow cathode electron emitter on the Shuttle orbiter p 119 A87-14084
- Hollow cathodes as electron emitting plasma contactors Theory and computer modeling [AIAA PAPER 87-0569] p 214 A87-22712
- Radiation from large space structures in low earth orbit with induced ac currents [AIAA PAPER 87-0612] p 42 A87-22738
- Plasma contactors for electrodynamic tethers p 214 A87-31211
- Modeling of environmentally induced transients within satellites [AIAA PAPER 85-0387] p 42 A87-41611
- Ram ion scattering caused by Space Shuttle v x B induced differential charging p 200 A87-51713
- Environmentally-induced discharge transient coupling to spacecraft [NASA-CR-174922] p 43 N87-10946
- Secondary electron generation, emission and transport: Effects on spacecraft charging and NASCAP models p 44 N87-26950

SPACECRAFT COMMUNICATION

An assessment of the status and trends in satellite communications 1986-2000: An information document prepared for the Communications Subcommittee of the Space Applications Advisory Committee
[NASA-TM-88867] p 114 N87-13600

The 20 GHz spacecraft IMPATT solid state transmitter
[NASA-CR-179545] p 124 N87-17989

SPACECRAFT COMPONENTS

The effect of electron beam welding on the creep rupture properties of a Nb-Zr-C alloy
[NASA-TM-88892] p 88 N87-13513

Identification of structural interface characteristics using component mode synthesis
[NASA-TM-88960] p 185 N87-24006

A high temperature fatigue and structures testing facility
[NASA-TM-100151] p 186 N87-26399

Spacecraft 2000: The challenge of the future
p 68 N87-26448

SPACECRAFT CONFIGURATIONS

NASA Growth Space Station missions and candidate nuclear/solar power systems p 48 A87-21807

The space station power system p 198 N87-28960

Status of space station power system p 45 N87-29915

SPACECRAFT CONSTRUCTION MATERIALS

Oxidation protection coatings for polymers
[NASA-CASE-LEW-14072-3] p 103 N87-23736

An evaluation of candidate oxidation resistant materials p 80 N87-26203

SPACECRAFT CONTAMINATION

Resistojet plume and induced environment analysis
[NASA-TM-88957] p 66 N87-24536

SPACECRAFT DESIGN

Spacecraft 2000 - The challenge of the future
p 37 A87-18064

The potential impact of new power system technology on the design of a manned Space Station
p 47 A87-18342

Spacecraft 2000: The challenge of the future
p 68 N87-26448

Status of space station power system p 45 N87-29915

SPACECRAFT DOCKING

Effects of transient propellant dynamics on deployment of large liquid stages in zero-gravity with application to Shuttle/Centaur
[IAF PAPER 86-119] p 39 A87-15880

SPACECRAFT ENVIRONMENTS

Resistojet plume and induced environment analysis
[NASA-TM-88957] p 66 N87-24536

Space station propulsion-ECLSS interaction study
[NASA-CR-175093] p 69 N87-29594

SPACECRAFT INSTRUMENTS

The 20th Aerospace Mechanics Symposium
[NASA-CP-2423-REV] p 181 N87-16321

SPACECRAFT LAUNCHING

Communications satellite systems operations with the space station. Volume 1: Executive summary
[NASA-CR-179526] p 206 N87-17472

SPACECRAFT LUBRICATION

Tribological properties of polymer films and solid bodies in a vacuum environment
[NASA-TM-88966] p 101 N87-17906

SPACECRAFT MAINTENANCE

Concepts for space maintenance of OTV engines
p 37 A87-46000

SPACECRAFT MOTION

Numerical modeling of on-orbit propellant motion resulting from an impulsive acceleration
[AIAA PAPER 87-1766] p 40 A87-48573

Numerical modeling of on-orbit propellant motion resulting from an impulsive acceleration
[NASA-TM-89873] p 41 N87-22757

SPACECRAFT POWER SUPPLIES

Space power development impact on technology requirements
[IAF PAPER 86-143] p 41 A87-15894

Space power - Emerging opportunities
[IAF PAPER 86-152] p 45 A87-15900

Electrical power system for the U.S. Space Station
[IAF PAPER 86-37] p 45 A87-16138

Spacecraft 2000 - The challenge of the future
p 37 A87-18064

Electrical power system design for the U.S. Space Station
p 46 A87-18068

Further advances in silicon solar cell technology for space application
p 188 A87-18074

Parametric and cycle tests of a 40-AH bipolar nickel-hydrogen battery
p 46 A87-18093

Cycle life of nickel-hydrogen cells. II - Accelerated cycle life test
p 46 A87-18104

Optimization of spherical facets for parabolic solar concentrators
p 213 A87-18173

Advanced solar thermal technologies for the 21st century p 47 A87-18179

Enhanced current flow through a plasma cloud by induction of plasma turbulence — electrodynamic tethers for generating power for spacecraft in low earth orbit
[AIAA PAPER 87-0573] p 214 A87-22714

Plasma contactors for electrodynamic tethers
p 214 A87-31211

Manned spacecraft electrical power systems
p 49 A87-37291

Resistojet control and power for high frequency ac buses
[AIAA PAPER 87-0994] p 122 A87-41103

The radiation impedance of an electrodynamic tether with end connectors
p 42 A87-42585

Liquid droplet radiator development status — waste heat rejection devices for future space vehicles
[AIAA PAPER 87-1537] p 42 A87-43059

Combination solar photovoltaic heat engine energy converter
p 190 A87-47088

Enhanced current flow through a plasma cloud by induction of plasma turbulence
p 214 A87-48241

Coaxial tube tether/transmission line for manned nuclear space power
[NASA-CASE-LEW-14338-1] p 55 N87-10174

Advanced solar dynamic space power systems perspectives, requirements and technology needs
[NASA-TM-88884] p 56 N87-12606

Conceptual definition of a technology development mission for advanced solar dynamic power systems
[NASA-CR-179482] p 192 N87-14771

Advanced Stirling conversion systems for terrestrial applications
[NASA-TM-88897] p 220 N87-15031

Electrical power system design for the US space station
[NASA-TM-88824] p 58 N87-15267

Solar dynamic power systems for space station
p 58 N87-16024

Initial performance of advanced designs for IPV nickel-hydrogen cells
[NASA-TM-87282] p 192 N87-16445

Overview of the 1986 free-piston Stirling activities at NASA Lewis Research Center
[NASA-TM-88895] p 221 N87-16663

PEGASUS: A multi-megawatt nuclear electric propulsion system
p 59 N87-17787

Power system technologies for the manned Mars mission
p 60 N87-17789

Liquid droplet radiator development status
[NASA-TM-89852] p 43 N87-20353

Resistojet control and power for high frequency ac buses
[NASA-TM-89860] p 126 N87-20477

A 1987 overview of free-piston Stirling technology for space power application
[NASA-TM-89832] p 221 N87-21756

Coaxial tube array space transmission line characterization
[NASA-TM-89864] p 62 N87-22003

EMC and power quality standards for 20-kHz power distribution
[NASA-TM-89925] p 62 N87-22004

Selection of high temperature thermal energy storage materials for advanced solar dynamic space power systems
[NASA-TM-89886] p 149 N87-22174

A prediction model of the depth-of-discharge effect on the cycle life of a storage cell
[NASA-TM-89915] p 194 N87-22311

High temperature solid oxide regenerative fuel cell for solar photovoltaic energy storage
[NASA-TM-89872] p 194 N87-23020

Control considerations for high frequency, resonant, power processing equipment used in large systems
[NASA-TM-89926] p 64 N87-23690

Issues in space photovoltaic research and technology
[NASA-TM-89922] p 128 N87-23901

A study of Schwarz converters for nuclear powered spacecraft
[NASA-TM-89911] p 128 N87-23903

Fluoride salts and container materials for thermal energy storage applications in the temperature range 973 to 1400 K
[NASA-TM-89913] p 195 N87-24026

Test results of a 60 volt bipolar nickel-hydrogen battery
[NASA-TM-89927] p 195 N87-24029

Development of an advanced photovoltaic concentrator system for space applications
[NASA-TM-100101] p 66 N87-24531

Arcjet power supply and start circuit
[NASA-CASE-LEW-14374-1] p 36 N87-25335

Nuclear reactor power for a space-based radar. SP-100 project
[NASA-TM-89295] p 213 N87-25838

Recent developments in indium phosphide space solar cell research
[NASA-TM-100139] p 68 N87-26141

Space station electrical power system
[NASA-TM-100140] p 68 N87-26144

Space Photovoltaic Research and Technology 1986. High Efficiency, Space Environment, and Array Technology
[NASA-CP-2475] p 196 N87-26413

Development of a Fresnel lens concentrator for space application
p 196 N87-26427

Space station power system
p 68 N87-26447

An assessment and validation study of nuclear reactors for low power space applications
[NASA-CR-180672] p 213 N87-27495

Space station power semiconductor package
[NASA-CR-180829] p 129 N87-28825

The space station power system
p 198 N87-28960

Alternative power generation concepts for space
p 199 N87-28961

Radiation damage in proton irradiated indium phosphide solar cells
p 199 N87-29018

High temperature radiator materials for applications in the low Earth orbital environment
[NASA-TM-100190] p 93 N87-29662

KOH concentration effect on cycle life of nickel-hydrogen cells
p 199 N87-29920

Theoretical performance of hydrogen-bromine rechargeable SPE fuel cell
p 199 N87-29945

SPACECRAFT PROPULSION

Performance characteristics of ring-cusp thrusters with xenon propellant
[AIAA PAPER 86-1392] p 46 A87-17992

High- and low-thrust propulsion systems for the Space Station
[AIAA PAPER 87-0398] p 48 A87-24997

Plasma contactors for electrodynamic tethers
p 214 A87-31211

Arcjet starting reliability - A multistart test on hydrogen/nitrogen mixtures
[AIAA PAPER 87-1061] p 51 A87-41128

Plasma properties in electron-bombardment ion thrusters
[AIAA PAPER 87-1076] p 51 A87-41135

Concepts for space maintenance of OTV engines
p 40 A87-41161

Composite load spectra for select space propulsion structural components
[NASA-CR-179496] p 55 N87-10176

High- and low-thrust propulsion systems for the space station
[NASA-TM-88877] p 57 N87-14427

Space station auxiliary thrust chamber technology
[NASA-CR-179552] p 59 N87-16874

Space station resistojet system requirements and interface definition study
[NASA-CR-179581] p 60 N87-17848

Structural Integrity and Durability of Reusable Space Propulsion Systems
[NASA-CP-2471] p 62 N87-22766

Progress on thin-film sensors for space propulsion technology
p 158 N87-22772

Probabilistic Structural Analysis Methods (PSAM) for select space propulsion system structural components
p 62 N87-22784

Composite load spectra for select space propulsion structural components
p 63 N87-22793

Propulsion recommendations for space station free flying platforms
p 67 N87-26129

Water-propellant resistojets for man-tended platforms
[NASA-TM-100110] p 68 N87-26135

SPACECRAFT RADIATORS

Effect of an oxygen plasma on the physical and chemical properties of several fluids for the Liquid Droplet Radiator
[AIAA PAPER 87-0080] p 42 A87-22401

Transient radiative cooling of a droplet-filled layer
p 135 A87-27712

Liquid sheet radiator
[AIAA PAPER 87-1525] p 140 A87-43048

Liquid droplet radiator development status — waste heat rejection devices for future space vehicles
[AIAA PAPER 87-1537] p 42 A87-43059

The design and performance of a multi-stream droplet generator for the liquid droplet radiator
[AIAA PAPER 87-1538] p 140 A87-44842

Gas particle radiator
p 141 A87-45646

Gas particle radiator
[NASA-CASE-LEW-14297-1] p 156 N87-15452

Liquid sheet radiator
[NASA-TM-89841] p 147 N87-18786

Liquid droplet radiator development status
[NASA-TM-89852] p 43 N87-20353

Enhanced thermal emittance of space radiators by ion-discharge chamber texturing
[NASA-TM-100137] p 207 N87-25823

- High temperature radiator materials for applications in the low Earth orbital environment
[NASA-TM-100190] p 93 N87-29662
- SPACECRAFT STRUCTURES**
Polymer, metal, and ceramic matrix composites for advanced aircraft engine applications
p 71 A87-15187
Spacecraft 2000: The challenge of the future
p 68 N87-26448
- SPACING**
The effect of front-to-rear propeller spacing on the interaction noise of a model counterrotation propeller at cruise conditions
[NASA-TM-100121] p 212 N87-28396
- SPARK GAPS**
Multi-spark visualization of typical combustor flowfields
p 134 A87-25281
Spark ignition of monodisperse fuel sprays
[NASA-CR-181404] p 80 N87-29635
- SPARK IGNITION**
Comparisons between thermodynamic and one-dimensional combustion models of spark-ignition engines
p 161 A87-29275
Spark ignition of monodisperse fuel sprays
[NASA-CR-181404] p 80 N87-29635
- SPATIAL DISTRIBUTION**
Spatially growing disturbances in a high velocity ratio two-stream, coplanar jet
[AIAA PAPER 87-0056] p 3 A87-24996
On the spatial instability of piecewise linear free shear layers
p 137 A87-31680
Spatially growing disturbances in a high velocity ratio two-stream, coplanar jet
[NASA-TM-88922] p 9 N87-14283
Spatially growing disturbances in a two-stream, coplanar jet
[NASA-TM-88949] p 10 N87-16799
- SPECIFIC IMPULSE**
Comparison of theoretical and experimental thrust performance of a 1030:1 area ratio rocket nozzle at a chamber pressure of 2413 kN/sq m (350 psia)
[AIAA PAPER 87-2069] p 52 A87-45390
The NASA/USAF arcjet research and technology program
[AIAA PAPER 87-1946] p 54 A87-50192
The NASA/USAF arcjet research and technology program
[NASA-TM-100112] p 66 N87-24525
- SPECIMEN GEOMETRY**
Specimen geometry effects on graphite/PMR-15 composites during thermo-oxidative aging
p 71 A87-13145
Results of an interlaboratory fatigue test program conducted on alloy 800H at room and elevated temperatures
p 87 A87-54370
- SPECKLE PATTERNS**
Demonstration of laser speckle system on burner liner cyclic rig
[NASA-CR-179509] p 155 N87-10377
Optical strain measurement system development, phase 1
[NASA-CR-179619] p 158 N87-22960
Optical strain measurement system development
[NASA-CR-179646] p 159 N87-26326
- SPECTROPHOTOVOLTAICS**
Proposal for superstructure based high efficiency photovoltaics
p 120 A87-19104
- SPECTROSCOPY**
Observation of deep levels in cubic silicon carbide
p 122 A87-41089
- SPECTRUM ANALYSIS**
Fiber-optic temperature sensor using a spectrum-modulating semiconductor etalon
[NASA-TM-100153] p 31 N87-25329
- SPEED CONTROL**
The effects of engine speed and injection characteristics on the flow field and fuel/air mixing in motored two-stroke diesel engines
[AIAA PAPER 87-0227] p 161 A87-22501
- SPINNERS**
Experimental and theoretical study of propeller spinner/shank interference
[AIAA PAPER 87-0145] p 3 A87-24929
- SPLINE FUNCTIONS**
Efficient numerical simulation of an electrothermal de-icer pad
[AIAA PAPER 87-0024] p 137 A87-32190
- SPRAY CHARACTERISTICS**
Effects of non-spherical drops on a phase Doppler spray analyzer
p 152 A87-11048
Performance comparison of two interferometric droplet sizing techniques
p 153 A87-11049
Two-phase flow measurements of a spray in a turbulent flow
[AIAA PAPER 87-0062] p 132 A87-22388

- Representation of the vaporization behavior of turbulent polydisperse sprays by 'equivalent' monodisperse sprays
[AIAA PAPER 87-1954] p 141 A87-45325
Two-phase measurements of a spray in the wake of a bluff body
p 142 A87-46199
Representation of the vaporization behavior of turbulent polydisperse sprays by equivalent monodisperse sprays
[NASA-TM-88906] p 26 N87-16827
Spark ignition of monodisperse fuel sprays
[NASA-CR-181404] p 80 N87-29635
- SPRAY NOZZLES**
Representation of the vaporization behavior of turbulent polydisperse sprays by 'equivalent' monodisperse sprays
[AIAA PAPER 87-1954] p 141 A87-45325
Representation of the vaporization behavior of turbulent polydisperse sprays by equivalent monodisperse sprays
[NASA-TM-88906] p 26 N87-16827
Two-phase flow
p 147 N87-20272
- SPRAYED COATINGS**
Low cycle fatigue behaviour of a plasma-sprayed coating material
p 82 A87-24040
Stress rupture and creep behavior of a low pressure plasma-sprayed NiCoCrAlY coating alloy in air and vacuum
p 85 A87-43396
New ZrO₂-Yb₂O₃ plasma-sprayed coatings for thermal barrier applications
p 98 A87-53623
- SPUTTERING**
Plasma assisted surface coating/modification processes: An emerging technology
[NASA-TM-88885] p 110 N87-12708
The 20th Aerospace Mechanics Symposium
[NASA-CP-2423-REV] p 181 N87-16321
Ion beam sputter etching
[NASA-CASE-LEW-13899-1] p 110 N87-21160
- SQUEEZE FILMS**
Starvation effects on the hydrodynamic lubrication of rigid nonconformal contacts in combined rolling and normal motion
p 135 A87-27839
- STABILITY**
Spatially growing disturbances in a high velocity ratio two-stream, coplanar jet
[AIAA PAPER 87-0056] p 3 A87-24996
Nonlinear vibration and stability of rotating, pretwisted, precone blades including Coriolis effects
p 178 A87-39896
Spatially growing disturbances in a high velocity ratio two-stream, coplanar jet
[NASA-TM-88922] p 9 N87-14283
Rotordynamic Instability Problems in High-Performance Turbomachinery, 1986
[NASA-CP-2443] p 167 N87-22199
Stability of bromine, iodine monochloride, copper (II) chloride, and nickel (II) chloride intercalated pitch-based graphite fibers
[NASA-TM-89904] p 103 N87-24563
Stability of a rigid rotor supported on flexible oil journal bearings
[NASA-TM-89899] p 151 N87-24646
Analysis and test evaluation of the dynamic response and stability of three advanced turboprop models
[NASA-CR-174814] p 32 N87-28555
- STACKS**
Develop and test fuel cell powered on-site integrated total energy systems. Phase 3: Full-scale power plant development
[NASA-CR-175117] p 191 N87-11346
Develop and test fuel cell powered on site integrated total energy systems: Phase 3: Full-scale power plant development
[NASA-CH-175075] p 191 N87-11347
Component variations and their effects on bipolar nickel-hydrogen cell performance
[NASA-TM-89907] p 195 N87-23029
- STAGNATION FLOW**
Turbulence modeling and surface heat transfer in a stagnation flow region
[NASA-TM-100132] p 151 N87-26302
Application of turbulence modeling to predict surface heat transfer in stagnation flow region of circular cylinder
[NASA-TP-2758] p 151 N87-27161
- STAGNATION POINT**
Heat transfer in the stagnation region of the junction of a circular cylinder perpendicular to a flat plate
p 131 A87-13019
Endwall heat transfer in the junction region of a circular cylinder normal to a flat plate at 30 and 60 degrees from stagnation point of the cylinder
[AIAA PAPER 87-0077] p 132 A87-22398
A general method for unsteady stagnation region heat transfer and results for model turbine flows
[NASA-TM-88903] p 146 N87-17002
Progress in the prediction of unsteady heat transfer on turbine blades
p 149 N87-22769
Turbulence modeling and surface heat transfer in a stagnation flow region
[NASA-TM-100132] p 151 N87-26302

STAINLESS STEELS

- Environmental degradation of 316 stainless steel in high temperature low cycle fatigue
[NASA-TM-89931] p 185 N87-24007
- STARTING**
Arcjet starting reliability - A multistart test on hydrogen/nitrogen mixtures
[AIAA PAPER 87-1061] p 51 A87-41128
Arcjet starting reliability: A multistart test on hydrogen/nitrogen mixtures
[NASA-TM-89867] p 61 N87-21998
Arcjet power supply and start circuit
[NASA-CASE-LEW-14374-1] p 36 N87-25335
- STATIC CHARACTERISTICS**
Advanced high temperature static strain sensor development
[NASA-CR-179520] p 158 N87-25552
- STATIC TESTS**
Static tests of the propulsion system --- Propan Test Assessment program
[AIAA PAPER 87-1728] p 23 A87-52245
High temperature static strain gage alloy development program
[NASA-CR-174833] p 157 N87-22179
Three-step labyrinth seal for high-performance turbomachines
[NASA-TP-1848] p 150 N87-23921
- STATIONKEEPING**
Low power arcjet life issues
[AIAA PAPER 87-1059] p 50 A87-39635
- STATISTICAL ANALYSIS**
Probability of detection of internal voids in structural ceramics using microfocus radiography
p 170 A87-14300
NDE reliability and process control for structural ceramics
[ASME PAPER 87-GT-8] p 171 A87-48702
NDE reliability and process control for structural ceramics
[NASA-TM-88870] p 171 N87-12910
- STATOR BLADES**
Unsteady flows in a single-stage transonic axial-flow fan stator row
[NASA-TM-88929] p 11 N87-16805
Unsteady stator/rotor interaction
p 149 N87-22767
- STATORS**
Comparison of calculated and experimental cascade performance for controlled-diffusion compressor stator blading
[ASME PAPER 86-GT-35] p 19 A87-25394
Method for the determination of the three dimensional aerodynamic field of a rotor-stator combination in compressible flow
[AIAA PAPER 87-1742] p 7 A87-50187
Turbine airfoil deposition models
p 24 N87-11191
Measurements of the unsteady flow field within the stator row of a transonic axial-flow fan. 1: Measurement and analysis technique
[NASA-TM-88945] p 10 N87-16789
Measurements of the unsteady flow field within the stator row of a transonic axial-flow fan. Part 2: Results and discussion
[NASA-TM-88946] p 10 N87-16790
Development of a rotor wake/vortex model. Volume 2: User's manual for computer program
[NASA-CR-174850-VOL-2] p 13 N87-20239
Method for the determination of the three-dimensional aerodynamic field of a rotor-stator combination to compressible flow
[NASA-TM-100118] p 30 N87-23625
Design and performance of controlled-diffusion stator compared with original double-circular-arc stator
[NASA-TM-100141] p 31 N87-26910
- STEADY STATE**
An efficient method for solving the steady Euler equations
[NASA-TM-87329] p 205 N87-11543
A finite difference scheme for three-dimensional steady laminar incompressible flow
[NASA-TM-89851] p 148 N87-20504
- STEAM**
Component testing of a ground based gas turbine steam cooled rich-burn primary zone combustor for emissions control of nitrogenous fuels
[NASA-TM-88873] p 191 N87-11345
- STEELS**
Selection of rolling-element bearing steels for long-life application
[NASA-TM-88881] p 164 N87-11993
Analysis of plasma-nitrided steels
[NASA-TM-89815] p 91 N87-21078
- STIFFNESS**
Experiments on dynamic stiffness and damping of tapered bore seals
[NASA-TM-89895] p 169 N87-23984

A computer solution for the dynamic load, lubricant film thickness and surface temperatures in spiral bevel gears [NASA-CR-4077] p 169 N87-26358

STIFFNESS MATRIX
An efficient quadrilateral element for plate bending analysis p 178 A87-45994
Ultrasonic determination of the elastic constants of the stiffness matrix for unidirectional fiberglass epoxy composites [NASA-CR-4034] p 171 N87-13781

STIRLING CYCLE
Tribology of selected ceramics at temperatures to 900 C p 94 A87-12954
Space power - Emerging opportunities [IAF PAPER 86-152] p 45 A87-15900
Overview of the 1986 free-piston Stirling SP-100 activities at the NASA Lewis Research Center p 160 A87-18033
A new chromium carbide-based tribological coating for use to 900 C with particular reference to the Stirling engine p 95 A87-26112
Mod II engine performance [SAE PAPER 870101] p 163 A87-48780
Overview of the 1986 free-piston Stirling activities at NASA Lewis Research Center [NASA-TM-88895] p 221 N87-16663
EHD analysis of and experiments on pumping Leningrad seals [NASA-CR-179570] p 168 N87-22246
Technical and economic study of Stirling and Rankine cycle bottoming systems for heavy truck diesel engines [NASA-CR-180833] p 222 N87-28470

STIRLING ENGINES
DOE/NASA automotive Stirling engine project - Overview 86 p 220 A87-18034
Testing of a variable-stroke Stirling engine p 160 A87-18036
Evaluation of Stirling engine appendix gap losses p 160 A87-18037
A new chromium carbide-based tribological coating for use to 900 C with particular reference to the Stirling engine p 95 A87-26112
Automotive Stirling engine system component review [SAE PAPER 870102] p 163 A87-48781
Ceramic automotive Stirling engine program [NASA-CR-175042] p 192 N87-12047
Progress of Stirling cycle analysis and loss mechanism characterization [NASA-TM-88891] p 220 N87-13359
Advanced Stirling conversion systems for terrestrial applications [NASA-TM-88897] p 220 N87-15031
Overview of the 1986 free-piston Stirling activities at NASA Lewis Research Center [NASA-TM-88895] p 221 N87-16663
Effect of water on hydrogen permeability [NASA-TM-88898] p 221 N87-16664
Fatigue failure of regenerator screens in a high frequency Stirling engine [NASA-TM-88974] p 183 N87-18882
Automotive Stirling engine development program [NASA-CR-174972] p 221 N87-20137
A 1987 overview of free-piston Stirling technology for space power application [NASA-TM-89832] p 221 N87-21756
Calibration and comparison of the NASA Lewis free-piston Stirling engine model predictions with RE-1000 test data [NASA-TM-89853] p 222 N87-22561
Automotive Stirling engine development program: A success [NASA-TM-89892] p 222 N87-22562
Comparison of Stirling engines for use with a 25-kW disk-electric conversion system [NASA-TM-100111] p 222 N87-27564
Creep-rupture behavior of a developmental cast-iron-base alloy for use up to 800 deg C [NASA-TM-100167] p 93 N87-28641
Automotive Stirling Engine Development Program [NASA-CR-174873] p 222 N87-30223

STOCHASTIC PROCESSES
A probabilistic Hu-Washizu variational principle [AIAA PAPER 87-0764] p 176 A87-33579
Stochastic and fractal analysis of fracture trajectories p 179 A87-51167

STOCKPILING
Superalloy resources: Supply and availability [NASA-TM-89866] p 91 N87-21077

STOICHIOMETRY
Stoichiometric disturbances in compound semiconductors due to ion implantation p 215 A87-12292
A point defect model for nickel electrode structures p 87 A87-52282

STORAGE BATTERIES
A prediction model of the depth-of-discharge effect on the cycle life of a storage cell p 194 N87-22311
Test results of a 60 volt bipolar nickel-hydrogen battery [NASA-TM-89927] p 195 N87-24029

STRAIN ENERGY RELEASE RATE
Strain energy release rates of composite interlaminar end-notch and mixed-mode fracture: A sublimate/ply level analysis and a computer code [NASA-TM-89827] p 74 N87-20389

STRAIN GAGES
The NASA strain gage laboratory p 35 A87-52494
Evaluation results of the 700 deg C Chinese strain gages p 155 N87-11189
High temperature static strain gage alloy development program [NASA-CR-174833] p 157 N87-22179
Optical strain measurement system development, phase 1 [NASA-CR-179619] p 158 N87-22960
Advanced high temperature static strain sensor development [NASA-CR-179520] p 158 N87-25552
Optical strain measuring techniques for high temperature tensile testing [NASA-CR-179637] p 159 N87-26327
High temperature static strain gage development contract, tasks 1 and 2 [NASA-CR-180811] p 159 N87-28869
Thin film strain gage development program [NASA-CR-174707] p 159 N87-28883

STRAIN MEASUREMENT
Demonstration of laser speckle system on burner liner cyclic rig [NASA-CR-179509] p 155 N87-10377
A mechanism for precise linear and angular adjustment utilizing flexures p 165 N87-16342
Advanced high temperature static strain sensor development [NASA-CR-179520] p 158 N87-25552
Optical strain measurement system development [NASA-CR-179646] p 159 N87-26326

STRAIN RATE
Estimation of high temperature low cycle fatigue on the basis of inelastic strain and strainrate [NASA-TM-88841] p 89 N87-14489

STRATEGIC MATERIALS
Superalloy resources: Supply and availability [NASA-TM-89866] p 91 N87-21077

STRATEGY
Strategic plan, 1985 [NASA-TM-89263] p 219 N87-12384

STRESS ANALYSIS
Elastic analysis of a mode II fatigue crack test specimen p 174 A87-17799
Assessment of simplified composite micromechanics using three-dimensional finite-element analysis p 72 A87-19121
On the numerical performance of three-dimensional thick shell elements using a hybrid/mixed formulation p 175 A87-25924
J-integral estimates for cracks in infinite bodies p 177 A87-35334
Effect of interference fits on roller bearing fatigue life p 162 A87-37686
Simplified composite micromechanics for predicting microstresses p 179 A87-49275
Creep fatigue life prediction for engine hot section materials (ISOTROPIC) [NASA-CR-179550] p 181 N87-15491
A constitutive model for the inelastic multiaxial cyclic response of a nickel base superalloy Rene 80 [NASA-CR-3998] p 182 N87-18852
On 3-D inelastic analysis methods for hot section components. Volume 1: Special finite element models [NASA-CR-179494] p 185 N87-22996
3-D inelastic analysis methods for hot section components. Volume 2: Advanced special functions models [NASA-CR-179517] p 186 N87-27267
Variational approach to probabilistic finite elements [NASA-CR-181343] p 206 N87-29212
Propfan test assessment propfan propulsion system static test report [NASA-CR-179613] p 33 N87-29536

STRESS CORROSION CRACKING
Further observations of SCC in alpha-beta brass Considerations regarding the appearance of crack arrest markings during SCC p 82 A87-23843

STRESS DISTRIBUTION
The effects of crack surface friction and roughness on crack tip stress fields [NASA-TM-88976] p 183 N87-18881

STRESS INTENSITY FACTORS
KI-solutions for single edge notch specimens under fixed end displacements p 174 A87-15798
Analysis of mixed-mode crack propagation using the boundary integral method [NASA-CR-179518] p 180 N87-12915

STRESS MEASUREMENT
Gear tooth stress measurements on the UH-60A helicopter transmission [NASA-TP-2698] p 167 N87-22235

STRESS WAVES
Nondestructive evaluation of adhesive bond strength using the stress wave factor technique p 170 A87-32200
Acousto-ultrasonic input-output characterization of unidirectional fiber composite plate by SH waves [NASA-CR-4087] p 173 N87-26361

STRESS-STRAIN RELATIONSHIPS
Comparison of pressure-strain correlation models for the flow behind a disk p 131 A87-20897
J-integral estimates for cracks in infinite bodies p 177 A87-35334
Fatigue and fracture: Overview p 179 N87-11183
The cyclic stress-strain behavior of PWA 1480 at 650 deg C [NASA-TM-87311] p 89 N87-14483
High temperature monotonic and cyclic deformation in a directionally solidified nickel-base superalloy [NASA-CR-175101] p 90 N87-15303
Nonlinear heat transfer and structural analyses of SSME turbine blades p 184 N87-22779
Observations of directional gamma prime coarsening during engine operation [NASA-TM-100105] p 92 N87-25459

STRESSES
Expansion of epicyclic gear dynamic analysis program [NASA-CR-179563] p 166 N87-19723
Strain energy release rates of composite interlaminar end-notch and mixed-mode fracture: A sublimate/ply level analysis and a computer code [NASA-TM-89827] p 74 N87-20389
Stress-life interrelationships associated with alkaline fuel cells [NASA-TM-89881] p 194 N87-22307

STRAIN THEORY
Noncommutative-geometry model for closed bosonic strings p 207 A87-37542

STRUCTURAL ANALYSIS
Notes and comments on computational elastoplasticity - Some new models and their numerical implementation p 173 A87-10893
On the symbolic manipulation and code generation for elasto-plastic material matrices p 201 A87-18499
Conforming versus non-conforming boundary elements in three-dimensional elastostatics p 175 A87-22775
Design concepts/parameters assessment and sensitivity analyses of select composite structural components p 175 A87-25407
Solution methods for one-dimensional viscoelastic problems [AIAA PAPER 87-0804] p 176 A87-33604
A versatile and low order hybrid stress element for general shell geometry [AIAA PAPER 87-0840] p 176 A87-33624
Advances in 3-D Inelastic Analysis Methods for hot section components [AIAA PAPER 87-0719] p 177 A87-33645
Crack layer theory p 178 A87-40056
High temperature stress-strain analysis p 179 N87-11209
High-temperature constitutive modeling p 179 N87-11210
Creep fatigue life prediction for engine hot section materials (isotropic): Two year update p 171 N87-11213
STAEBL: Structural tailoring of engine blades, phase 2 p 24 N87-11731
Probabilistic structural analysis methods for space propulsion system components [NASA-TM-88861] p 181 N87-13794
Computational composite mechanics for aerospace propulsion structures [NASA-TM-88965] p 74 N87-18614
Unification of color postprocessing techniques for 3-dimensional computational mechanics [NASA-CR-180214] p 202 N87-18998
Analysis of shell-type structures subjected to time-dependent mechanical and thermal loading [NASA-CR-180349] p 183 N87-19756
Analysis of plasma-nitrided steels [NASA-TM-89815] p 91 N87-21078
Unstalled flutter stability predictions and comparisons to test data for a composite prop-fan model [NASA-CR-179512] p 28 N87-21955
Nonlinear heat transfer and structural analyses of SSME turbine blades p 184 N87-22779

- Probabilistic structural analysis to evaluate the structural durability of SSME critical components p 62 N87-22783
- Probabilistic Structural Analysis Methods (PSAM) for select space propulsion system structural components p 62 N87-22784
- The NESSUS finite element code p 184 N87-22785
- Finite element implementation of Robinson's unified viscoplastic model and its application to some uniaxial and multiaxial problems p 185 N87-23010
- Application of scanning acoustic microscopy to advanced structural ceramics [NASA-TM-89929] p 172 N87-23987
- Finite element analysis of flexible, rotating blades [NASA-TM-89906] p 186 N87-26385
- A high temperature fatigue and structures testing facility [NASA-TM-100151] p 186 N87-26399
- Propan test assessment testbed aircraft flutter model test report [NASA-CR-179458] p 14 N87-29413
- STRUCTURAL DESIGN**
- Probabilistic structural analysis to quantify uncertainties associated with turbopump blades [AIAA PAPER 87-0766] p 176 A87-33581
- Optimal placement of critical speeds in rotor-bearing systems p 162 A87-38464
- The voltage threshold for arcing for solar cells in Leo - Flight and ground test results [AIAA PAPER 86-0362] p 50 A87-40275
- A flooded-starved design for nickel-cadmium cells p 123 N87-11086
- Progress of Stirling cycle analysis and loss mechanism characterization [NASA-TM-88891] p 220 N87-13359
- Space station electric power system requirements and design [NASA-TM-89889] p 62 N87-22001
- Regenerative fuel cell study for satellites in GEO orbit [NASA-TM-89914] p 194 N87-22310
- Interactive color display of 3-D engineering analysis results [NASA-CR-180589] p 203 N87-22422
- Probabilistic Structural Analysis Methods (PSAM) for select space propulsion system structural components p 62 N87-22784
- Aerodynamic performance investigation of advanced mechanical suppressor and ejector nozzle concepts for jet noise reduction [NASA-CR-174860] p 33 N87-29534
- STRUCTURAL DESIGN CRITERIA**
- NASA Lewis evaluation of Regenerative Fuel Cell (RFC) systems p 123 N87-11073
- The 3600 hp split-torque helicopter transmission [NASA-CR-174932] p 25 N87-11788
- Space station experiment definition: Advanced power system test bed [NASA-CR-179502] p 58 N87-15270
- Feasibility analysis of reciprocating magnetic heat pumps [NASA-CR-180262] p 147 N87-19647
- Computer modelling of aluminum-gallium arsenide/gallium arsenide multilayer photovoltaics [NASA-CR-181418] p 200 N87-29957
- STRUCTURAL ENGINEERING**
- A probabilistic Hu-Washizu variational principle [AIAA PAPER 87-0764] p 176 A87-33579
- STRUCTURAL MEMBERS**
- Identification of structural interface characteristics using component mode synthesis [NASA-TM-88960] p 185 N87-24006
- STRUCTURAL RELIABILITY**
- Structural Integrity and Durability of Reusable Space Propulsion Systems [NASA-CP-2471] p 62 N87-22766
- Probabilistic Structural Analysis Methods (PSAM) for select space propulsion system structural components p 62 N87-22784
- The NESSUS finite element code p 184 N87-22785
- STRUCTURAL VIBRATION**
- Free vibration analysis by BEM using particular integrals p 174 A87-13882
- Structureborne noise control in advanced turboprop aircraft [AIAA PAPER 87-0530] p 209 A87-31110
- Influence of third-degree geometric nonlinearities on the vibration and stability of pretwisted, precone, rotating blades p 21 A87-46228
- Structureborne noise control in advanced turboprop aircraft [NASA-TM-88947] p 211 N87-16587
- STRUTS**
- Solar dynamic power systems for space station p 58 N87-16024
- STYRENES**
- Styrene-terminated polysulfone oligomers as matrix material for graphite reinforced composites: An initial study [NASA-TM-89846] p 74 N87-21043
- SUBCRITICAL FLOW**
- Two-phase flows and heat transfer within systems with ambient pressure above the thermodynamic critical pressure p 136 A87-30728
- SUBSONIC FLOW**
- Viscous analyses for flow through subsonic and supersonic intakes [NASA-TM-88831] p 9 N87-15173
- Viscous analyses for flow through subsonic and supersonic intakes p 30 N87-24469
- Aerodynamics of subsonic turbulent shear flows [NASA-TM-100165] p 212 N87-26615
- SUBSONIC SPEED**
- Engine studies for future subsonic cruise missiles [AIAA PAPER 86-1547] p 19 A87-21513
- SUBSTRATES**
- Reactions occurring during the sulfation of sodium chloride deposited on alumina substrates p 76 A87-20223
- TEM investigation of beta-SiC grown epitaxially on Si substrate by CVD p 97 A87-40927
- Adhesion, friction, and deformation of ion-beam-deposited boron nitride films [NASA-TM-88902] p 100 N87-15305
- SUBSTRUCTURES**
- Modeling of multi-rotor torsional vibrations in rotating machinery using substructuring p 175 A87-28543
- SULFATES**
- Corrosion of metals and alloys in sulfate melts at 750 C p 81 A87-17997
- SULFATION**
- Reactions occurring during the sulfation of sodium chloride deposited on alumina substrates p 76 A87-20223
- SULFIDES**
- Structure and tensile strength of LaS₂(1.4) p 96 A87-38065
- SULFONES**
- Styrene-terminated polysulfone oligomers as matrix material for graphite reinforced composites: An initial study [NASA-TM-89846] p 74 N87-21043
- SULFUR**
- Solar cells in bulk InP using an open tube diffusion process p 198 N87-26444
- SULFUR COMPOUNDS**
- Degradation mechanisms of sulfur and nitrogen containing compounds during thermal stability testing of model fuels [AIAA PAPER 87-2039] p 106 A87-45372
- SUPERCOOLING**
- Dendritic growth of undercooled nickel-tin, I, II p 85 A87-41012
- SUPERCritical FLUIDS**
- Volume-energy parameters for heat transfer to supercritical fluids p 137 A87-32326
- SUPERCritical PRESSURES**
- Two-phase flows and heat transfer within systems with ambient pressure above the thermodynamic critical pressure p 136 A87-30728
- SUPERHYBRID MATERIALS**
- Fabrication and quality assurance processes for superhybrid composite fan blades p 72 A87-19123
- SUPERLATTICES**
- A proposed GaAs-based superlattice solar cell structure with high efficiency and high radiation tolerance p 189 A87-19915
- Design considerations for a GaAs nipi doping superlattice solar cell p 196 N87-26422
- Computer modelling of aluminum-gallium arsenide/gallium arsenide multilayer photovoltaics [NASA-CR-181418] p 200 N87-29957
- SUPERSONIC AIRCRAFT**
- The supersonic through-flow turbofan for high Mach propulsion [AIAA PAPER 87-2050] p 22 A87-50196
- The supersonic through-flow turbofan for high Mach propulsion [NASA-TM-100114] p 30 N87-23626
- SUPERSONIC CRUISE AIRCRAFT RESEARCH**
- The supersonic through-flow turbofan for high Mach propulsion [AIAA PAPER 87-2050] p 22 A87-50196
- The supersonic through-flow turbofan for high Mach propulsion [NASA-TM-100114] p 30 N87-23626
- SUPERSONIC FLOW**
- An adaptive finite element strategy for complex flow problems [AIAA PAPER 87-0557] p 133 A87-22706
- Aeroelastic control of stability and forced response of supersonic rotors by aerodynamic detuning p 21 A87-46249
- Supersonic through-flow fan design [AIAA PAPER 87-1746] p 22 A87-48571
- Computation of multi-dimensional viscous supersonic flow [NASA-CR-4021] p 9 N87-13406
- Viscous analyses for flow through subsonic and supersonic intakes [NASA-TM-88831] p 9 N87-15173
- Application of advanced computational codes in the design of an experiment for a supersonic throughflow fan rotor [NASA-TM-88915] p 13 N87-22630
- Supersonic through-flow fan design [NASA-TM-88908] p 29 N87-22681
- SUPERSONIC FLUTTER**
- The effect of circumferential aerodynamic detuning on coupled bending-torsion unstalled supersonic flutter [ASME PAPER 86-GT-100] p 20 A87-25396
- SUPERSONIC INLETS**
- Large perturbation flow field analysis and simulation for supersonic inlets [NASA-CR-174676] p 8 N87-10835
- Computation of multi-dimensional viscous supersonic jet flow [NASA-CR-4020] p 8 N87-13405
- Viscous analyses for flow through subsonic and supersonic intakes [NASA-TM-88831] p 9 N87-15173
- Viscous analyses for flow through subsonic and supersonic intakes p 30 N87-24469
- SUPERSONIC JET FLOW**
- On broadband shock associated noise of supersonic jets p 208 A87-11768
- SUPERSONIC NOZZLES**
- Supersonic through-flow fan design [AIAA PAPER 87-1746] p 22 A87-48571
- Supersonic through-flow fan design [NASA-TM-88908] p 29 N87-22681
- SUPERSONIC TRANSPORTS**
- Simulated flight acoustic investigation of treated ejector effectiveness on advanced mechanical suppressors for high velocity jet noise reduction [NASA-CR-4019] p 211 N87-17481
- SUPERSONIC TURBINES**
- The supersonic through-flow turbofan for high Mach propulsion [AIAA PAPER 87-2050] p 22 A87-50196
- Measurements of the unsteady flow field within the stator row of a transonic axial-flow fan. Part 2: Results and discussion [NASA-TM-88946] p 10 N87-16790
- The supersonic through-flow turbofan for high Mach propulsion [NASA-TM-100114] p 30 N87-23626
- SUPERSONIC WIND TUNNELS**
- Investigation of two-dimensional shock-wave/boundary-layer interactions p 4 A87-39528
- SUPPRESSORS**
- Free jet feasibility study of a thermal acoustic shield concept for AST/VCE application: Dual stream nozzles [NASA-CR-3867] p 210 N87-10752
- SURFACE CRACKS**
- Compliance matrices for cracked bodies p 175 A87-25775
- SURFACE FINISHING**
- Formation of a pn junction on an anisotropically etched GaAs surface using metalorganic chemical vapor deposition p 216 A87-21237
- Plasma assisted surface coating/modification processes: An emerging technology [NASA-TM-88885] p 110 N87-12708
- SURFACE GEOMETRY**
- A note on the generation of Tollmien-Schlichting waves by sudden surface-curvature change p 144 A87-54366
- SURFACE LAYERS**
- Comparison of calculated and experimental cascade performance for controlled-diffusion compressor stator blading [ASME PAPER 86-GT-35] p 19 A87-25394
- SURFACE NOISE INTERACTIONS**
- Enhanced mixing of an axisymmetric jet by aerodynamic excitation [NASA-CR-175059] p 15 N87-29418
- SURFACE PROPERTIES**
- Plastic deformation of a magnesium oxide 001-plane surface produced by cavitation [ASLE PREPRINT 86-TC-3D-1] p 94 A87-19504
- Colloidal characterization of ultrafine silicon carbide and silicon nitride powders p 95 A87-19625
- Transition boiling heat transfer and the film transition regime p 143 A87-53589

A constitutive law for finite element contact problems with unclassical friction
[NASA-TM-88838] p 180 N87-12924

Surface flaw reliability analysis of ceramic components with the SCARE finite element postprocessor program
[NASA-TM-88901] p 181 N87-17087

Ion beam sputter etching
[NASA-CASE-LEW-13899-1] p 110 N87-21160

Detection of reflector surface error from near-field data: Effect of edge diffracted field
[NASA-TM-89920] p 117 N87-22874

Application of turbulence modeling to predict surface heat transfer in stagnation flow region of circular cylinder
[NASA-TP-2758] p 151 N87-27161

SURFACE REACTIONS
Effects of surface chemistry on hot corrosion life
p 88 N87-11193

Stability and rheology of dispersions of silicon nitride and silicon carbide
[NASA-CR-179634] p 104 N87-25476

Diffusion length measurements in bulk and epitaxially grown 3-5 semiconductors using charge collection microscopy
[NASA-TM-100128] p 129 N87-27121

SURFACE ROUGHNESS
The effects of crack surface friction and roughness on crack tip stress fields
[NASA-TM-88976] p 183 N87-18881

Use of a liquid-crystal, heater-element composite for quantitative, high-resolution heat transfer coefficients on a turbine airfoil, including turbulence and surface roughness effects
[NASA-TM-87355] p 158 N87-22181

SURFACE STABILITY
The role of near-surface plastic deformation in the wear of lamellar solids
p 162 A87-48500

Characterization of ion beam modified ceramic wear surfaces using Auger electron spectroscopy
p 98 A87-51304

SURFACE TEMPERATURE
A simple method for monitoring surface temperatures in plasma treatments
p 160 A87-17269

A computer solution for the dynamic load, lubricant film thickness and surface temperatures in spiral bevel gears
[NASA-CR-4077] p 169 N87-26358

SURFACE VEHICLES
Long range inhabited surface transportation system power source for the exploration of Mars (manned Mars mission)
p 37 N87-17752

SURGES
Environmentally-induced discharge transient coupling to spacecraft
[NASA-CR-174922] p 43 N87-10946

Summary of investigations of engine response to distorted inlet conditions
p 30 N87-24477

SURVIVAL
The survivability of large space-borne reflectors under atomic oxygen and micrometeoroid impact
[AIAA PAPER 87-0341] p 49 A87-31300

The survivability of large space-borne reflectors under atomic oxygen and micrometeoroid impact
[NASA-TM-88914] p 57 N87-14423

SWEEP FREQUENCY
Swept frequency technique for dispersion measurement of microstrip lines
[NASA-TM-88836] p 124 N87-14597

Swept frequency technique for dispersion measurement of microstrip lines
[AD-P005420] p 118 N87-27848

SWIRLING
Duct flows with swirl
[AIAA PAPER 87-0247] p 132 A87-22509

Two opposed lateral jets injected into swirling crossflow
[AIAA PAPER 87-0307] p 132 A87-22549

Modelling of jet- and swirl-stabilized reacting flows in axisymmetric combustors
p 138 A87-38956

Particle-laden swirling free jets - Measurements and predictions
[AIAA PAPER 87-0303] p 139 A87-42648

User's manual for a TEACH computer program for the analysis of turbulent, swirling reacting flow in a research combustor
[NASA-CR-179547] p 78 N87-11858

Particle-laden swirling free jets: Measurements and predictions
[NASA-TM-88904] p 26 N87-16826

Controlled excitation of a cold turbulent swirling free jet
[NASA-TM-100173] p 152 N87-27977

SWITCHES
Radiation effects on power transistor performance
[NASA-CR-181188] p 129 N87-27099

SWITCHING CIRCUITS
Space station power semiconductor package
[NASA-CR-180829] p 129 N87-28825

SYMBOLIC PROGRAMMING
On the symbolic manipulation and code generation for elastoplastic material matrices
p 201 A87-18499

SYNCHRONISM
Synchronization trigger control system for flow visualization
[NASA-TM-89902] p 128 N87-23902

SYNCHRONOUS SATELLITES
Performance characterization of a low power hydrazine arcjet
[AIAA PAPER 87-1057] p 50 A87-39634

An assessment of the status and trends in satellite communications 1986-2000: An information document prepared for the Communications Subcommittee of the Space Applications Advisory Committee
[NASA-TM-88867] p 114 N87-13600

Alternative mathematical programming formulations for FSS synthesis
[NASA-CR-180030] p 202 N87-14872

The use of satellites in non-geostationary orbits for unloading geostationary communication satellite traffic peaks. Volume 1: Executive summary
[NASA-CR-179597-VOL-1] p 117 N87-21212

The use of satellites in non-geostationary orbits for unloading geostationary communication satellite traffic peaks. Volume 2: Technical report
[NASA-CR-179597-VOL-2] p 117 N87-21213

On orbital allotments for geostationary satellites
[NASA-CR-181017] p 37 N87-22700

SYNTHESIS (CHEMISTRY)
Triptycene - A D(3h) C(62) hydrocarbon with three U-shaped cavities
p 69 A87-53656

Substituted 1,1,1-triaryl-2,2,2-trifluoroethanes and processes for their synthesis --- synthetic routes to monomers for polyimides
[NASA-CASE-LEW-14345-1] p 70 N87-14432

New condensation polyimides containing 1,1,1-triaryl-2,2,2-trifluoroethane structures
[NASA-CASE-LEW-14346-1] p 70 N87-14433

Polymer precursors for ceramic matrix composites
[NASA-CR-179562] p 70 N87-14434

Thermo-oxidatively stable condensation polyimides containing 1,1,1-triaryl-2,2,2-trifluoroethane dianhydride and diamine monomers
[NASA-TM-89875] p 103 N87-22048

Processing of laser formed SiC powder
[NASA-CR-179638] p 104 N87-24573

SYSTEMS ANALYSIS
Advanced solar dynamic space power systems perspectives, requirements and technology needs
[NASA-TM-88884] p 56 N87-12606

Viscous analyses for flow through subsonic and supersonic intakes
[NASA-TM-88831] p 9 N87-15173

Advanced space communications architecture study. Volume 2: Technical report
[NASA-CR-179592] p 115 N87-18695

Unique bit-error-rate measurement system for satellite communication systems
[NASA-TP-2699] p 116 N87-20448

Aerodynamic performance investigation of advanced mechanical suppressor and ejector nozzle concepts for jet noise reduction
[NASA-CR-174860] p 33 N87-29534

SYSTEMS ENGINEERING
Fatigue criterion to system design, life, and reliability
p 175 A87-27986

Advanced space communications architecture study. Volume 1: Executive summary
[NASA-CR-179591] p 115 N87-18696

System architecture of MMIC-based large aperture arrays for space application
[NASA-TM-89840] p 125 N87-20468

Probabilistic Structural Analysis Methods (PSAM) for select space propulsion system structural components
p 62 N87-22784

Design, development and deployment of public service photovoltaic power/load systems for the Gabonese Republic
[NASA-CR-179603] p 195 N87-23030

SYSTEMS INTEGRATION
A rotorcraft flight/propulsion control integration study
[NASA-CR-179574] p 18 N87-24457

SYSTOLIC ARRAYS
A high quality image compression scheme for real-time applications
p 111 A87-30801

T

TAKEOFF
Analysis of Convair 990 rejected-takeoff accident with emphasis on decision making, training and procedures
[NASA-TM-100189] p 16 N87-29471

TAKEOFF RUNS
Aircraft accident report: NASA 712, Convair 990, N712NA, March Air Force Base, California, July 17, 1985, executive summary
[NASA-TM-87356-VOL-1] p 16 N87-21878

Aircraft accident report: NASA 712, Convair 990, N712NA, March Air Force Base, California, July 17, 1985, facts and analysis
[NASA-TM-87356-VOL-2] p 16 N87-21879

TANTALUM
The effects of tantalum on the microstructure of two polycrystalline nickel-base superalloys - B-1900 + Hf and MAR-M247
p 82 A87-24110

TANTALUM ALLOYS
Thermal and structural stability of cosputtered amorphous Ta(x)Cu(1-x) alloy thin films on GaAs
p 216 A87-27198

Analysis of NiAlTa precipitates in beta-NiAl + 2 at. pct Ta alloy
p 84 A87-34888

Interactions of amorphous Ta(x)Cu(1-x) (x = 0.93 and 0.80) alloy films with Au overlayers and GaAs substrates
p 217 A87-44562

TAPERING
Experiments on dynamic stiffness and damping of tapered bore seals
[NASA-TM-89895] p 169 N87-23984

TECHNOLOGICAL FORECASTING
US long distance fiber optic networks: Technology, evolution and advanced concepts. Volume 3: Advanced networks and economics
[NASA-CR-179481] p 114 N87-11915

Speculations on future opportunities to evolve Brayton powerplants aboard the space station
[NASA-TM-89863] p 39 N87-23674

NASA Lewis Research Center Futuring Workshop
[NASA-CR-179577] p 206 N87-27475

TECHNOLOGY ASSESSMENT
An overview of the small engine component technology (SECT) studies --- commuter, rotorcraft, cruise missile and auxiliary power applications in year 2000
[AIAA PAPER 86-1542] p 19 A87-17993

Further advances in silicon solar cell technology for space application
p 188 A87-18074

Status of commercial phosphoric acid fuel cell power plant system development
p 190 A87-33777

ACTS experiments program --- Advanced Communications Technology Satellite
p 113 A87-45513

US long distance fiber optic networks: Technology, evolution and advanced concepts. Volume 3: Advanced networks and economics
[NASA-CR-179481] p 114 N87-11915

Advanced solar dynamic space power systems perspectives, requirements and technology needs
[NASA-TM-88884] p 56 N87-12606

Conceptual definition of a technology development mission for advanced solar dynamic power systems
[NASA-CR-179482] p 192 N87-14771

Cryogenic gear technology for an orbital transfer vehicle engine and tester design
[NASA-CR-175102] p 110 N87-19539

Intersatellite Link (ISL) application to commercial communications satellites. Volume 1: Executive summary
[NASA-CR-179598-VOL-1] p 116 N87-19552

Intersatellite Link (ISL) application to commercial communications satellites. Volume 2: Technical final report
[NASA-CR-179598-VOL-2] p 116 N87-19553

Cryogenic Fluid Management Flight Experiment (CFMFE)
p 109 N87-21150

Automotive Stirling engine development program: A success
[NASA-TM-89892] p 222 N87-22562

NASA Lewis Research Center Futuring Workshop
[NASA-CR-179577] p 206 N87-27475

Alternative power generation concepts for space
p 199 N87-28961

TECHNOLOGY UTILIZATION
Space power development impact on technology requirements
[IAF PAPER 86-143] p 41 A87-15894

Materials research and applications at NASA Lewis Research Center
p 69 A87-38472

The Advanced Turbine Technology Applications Program (ATTAP)
[SAE PAPER 870467] p 163 A87-48791

US long distance fiber optic networks: Technology, evolution and advanced concepts. Volume 1: Executive summary
[NASA-CR-179479] p 113 N87-11056

Advanced Propfan Engine Technology (APET) definition study, single and counter-rotation gearbox/pitch change mechanism design
[NASA-CR-168115] p 32 N87-28554

TELECOMMUNICATION

US long distance fiber optic networks: Technology, evolution and advanced concepts. Volume 2: Fiber optic technology and long distance networks
[NASA-CR-179480] p 113 N87-11057

Automated measurement of the bit-error rate as a function of signal-to-noise ratio for microwave communications systems
[NASA-TM-89898] p 127 N87-22102

TEMPERATURE CONTROL

Self-regulating heater application to Shuttle/Centaur hydrazine fuel line thermal control
[AIAA PAPER 87-1570] p 43 A87-43081

TEMPERATURE DEPENDENCE

Low cycle fatigue behaviour of a plasma-sprayed coating material p 82 A87-24040
Comment on 'Temperature dependence of electrical properties of non-doped and nitrogen-doped beta-SiC single crystals grown by chemical vapor deposition' p 217 A87-42846

Temperature dependence (4K to 300K) of the electrical resistivity of methane grown carbon fibers p 97 A87-47375

The temperature dependence of inelastic light scattering from small particles for use in combustion diagnostic instrumentation
[NASA-CR-180399] p 80 N87-28634

TEMPERATURE DISTRIBUTION

Thermal analysis of an orthotropic engineering body --- horizontal axis wind turbine rotor blade p 173 A87-13496

Efficient numerical simulation of an electrothermal de-icer pad
[AIAA PAPER 87-0024] p 137 A87-32190

Temperature fields due to jet induced mixing in a typical QTV tank
[AIAA PAPER 87-2017] p 55 A87-52247

Thermocapillary bubble migration for large Marangoni Numbers
[NASA-CR-179628] p 109 N87-22865

Vortex-scalar element calculations of a diffusion flame stabilized on a plane mixing layer
[NASA-TM-100133] p 2 N87-28501

TEMPERATURE EFFECTS

Reaction of iron with hydrogen chloride-oxygen mixtures at 550 C p 83 A87-32001

Effects of temperature and hold times on low cycle fatigue of Astroloy p 85 A87-38541

Nonlinear absorption in AlGaAs/GaAs multiple quantum well structures grown by metalorganic chemical vapor deposition p 217 A87-39687

Thermohydrodynamic analysis for laminar lubricating films
[NASA-TM-88845] p 144 N87-11124

High temperature monotonic and cyclic deformation in a directionally solidified nickel-base superalloy
[NASA-CR-175101] p 90 N87-15303

Radiation and temperature effects in gallium arsenide, indium phosphide and silicon solar cells
[NASA-TM-89870] p 127 N87-22098

Experimental evaluation of chromium-carbide-based solid lubricant coatings for use to 760 C
[NASA-CR-180808] p 105 N87-27053

High temperature static strain gage development contract, tasks 1 and 2
[NASA-CR-180811] p 159 N87-28869

Thermocapillary bubble migration for large Marangoni Numbers
[NASA-CR-179628] p 109 N87-22865

Thermocapillary bubble migration for large Marangoni Numbers
[NASA-CR-179628] p 109 N87-22865

TEMPERATURE GRADIENTS

Cellular and dendritic growth in a binary melt - A marginal stability approach p 107 A87-10871

Effect of design variables, temperature gradients and speed of life and reliability of a rotating disk
[NASA-TM-88883] p 165 N87-13755

Elevated temperature crack growth
[NASA-CR-179601] p 184 N87-22267

Thermocapillary bubble migration for large Marangoni Numbers
[NASA-CR-179628] p 109 N87-22865

TEMPERATURE MEASUREMENT

A simple method for monitoring surface temperatures in plasma treatments p 160 A87-17269

Thin-film temperature sensors for gas turbine engines Problems and prospects p 153 A87-26109

Further development of the dynamic gas temperature measurement system. Volume 1: Technical efforts
[NASA-CR-179513-VOL-1] p 157 N87-19686

Progress on thin-film sensors for space propulsion technology p 158 N87-22772

Heat flux calibration facility capable of SSME conditions p 36 N87-22774

Airflow calibration and exhaust pressure/temperature survey of an F404, S/N 215-109, turbofan engine
[NASA-TM-100159] p 33 N87-29537

TEMPERATURE MEASURING INSTRUMENTS

Further development of the dynamic gas temperature measurement system. Volume 1: Technical efforts
[NASA-CR-179513-VOL-1] p 157 N87-19686

TEMPERATURE PROFILES

Velocity profiles in laminar diffusion flames
[NASA-TP-2596] p 147 N87-18035

TEMPERATURE SENSORS

Thin-film temperature sensors for gas turbine engines Problems and prospects p 153 A87-26109

Spectrum-modulating fiber-optic sensors for aircraft control systems
[NASA-TM-88968] p 27 N87-17700

Fiber-optic temperature sensor using a spectrum-modulating semiconductor etalon
[NASA-TM-100153] p 31 N87-25329

TEMPORAL DISTRIBUTION

Two opposed lateral jets injected into swirling crossflow
[AIAA PAPER 87-0307] p 132 A87-22549

TENSILE PROPERTIES

High temperature tensile and creep behaviour of low pressure plasma-sprayed Ni-Co-Cr-Al-Y coating alloy
[NASA-TM-100194] p 82 A87-23429

TENSILE STRENGTH

Structure and tensile strength of LaS(1,4) p 96 A87-38065

Heat treatment for superalloy
[NASA-CASE-LEW-14262-1] p 93 N87-28647

TENSILE STRESS

The stability of lamellar gamma-gamma-prime structures --- nickel-base superalloy p 86 A87-48323

Elevated temperature tension, compression and creep-rupture behavior of (001)-oriented single crystal superalloy PWA 1480
[NASA-TM-88950] p 90 N87-17882

The effect of internal stresses on solar cell efficiency p 196 N87-26430

TENSILE TESTS

Yielding and deformation behavior of the single crystal superalloy PWA 1480 p 84 A87-32040

Ethynylated aromatics as high temperature matrix resins p 96 A87-34850

Elevated temperature strengthening of a melt spun austenitic steel by TiB2 p 87 A87-51639

Optical strain measuring techniques for high temperature tensile testing
[NASA-CR-179637] p 159 N87-26327

TEST EQUIPMENT

The hypercluster: A parallel processing test-bed architecture for computational mechanics applications
[NASA-TM-89823] p 203 N87-20767

TEST FACILITIES

Full-scale thrust reverser testing in an altitude facility
[AIAA PAPER 87-1788] p 34 A87-45203

Reactivation study for NASA Lewis Research Center's Hypersonic Tunnel Facility
[AIAA PAPER 87-1886] p 34 A87-50190

The NASA strain gage laboratory p 35 A87-52494

Conceptual definition of a technology development mission for advanced solar dynamic power systems
[NASA-CR-179482] p 192 N87-14771

A distributed data acquisition system for aeronautics test facilities
[NASA-TM-88961] p 35 N87-16851

Research opportunities in microgravity science and applications during shuttle hiatus
[NASA-TM-88964] p 108 N87-16917

Full-scale thrust reverser testing in an altitude facility
[NASA-TM-88967] p 35 N87-18575

Applications and requirements for real-time simulators in ground-test facilities
[NASA-TP-2672] p 204 N87-23202

Reactivation study for NASA Lewis Research Center's hypersonic tunnel facility
[NASA-TM-88918] p 36 N87-23664

A high temperature fatigue and structures testing facility
[NASA-TM-100151] p 186 N87-26399

Ground-based plasma contractor characterization
[NASA-TM-100194] p 215 N87-28423

TEST FIRING

Breadboard RL10-11B low thrust operating mode
[NASA-TM-174914] p 58 N87-15269

TEST STANDS

Measurement of Centaur/Orbiter multiple reaction forces in a full-scale test rig p 38 A87-29448

Outdoor test stand performance of a convertible engine with variable inlet guide vanes for advanced rotorcraft propulsion
[NASA-TM-88939] p 26 N87-16825

The design and analysis of single flank transmission error tester for loaded gears
[NASA-CR-179621] p 169 N87-27197

TETHERED BALLOONS

Theory of plasma contactors used in the ionosphere p 122 A87-41610

TETHERED SATELLITES

Hollow cathode-based plasma contactor experiments for electrodynamic tether
[AIAA PAPER 87-0572] p 214 A87-32192

Theory of plasma contactors for electrodynamic tethered satellite systems p 122 A87-41609

Theory of plasma contactors used in the ionosphere p 122 A87-41610

Enhanced current flow through a plasma cloud by induction of plasma turbulence p 214 A87-48241

Electrodynamic tether p 44 N87-26449

TETHERING

Enhanced current flow through a plasma cloud by induction of plasma turbulence --- electrodynamic tethers for generating power for spacecraft in low earth orbit
[AIAA PAPER 87-0573] p 214 A87-22714

Coaxial tube array space transmission line characterization
[NASA-TM-89864] p 62 N87-22003

Investigation of beam-plasma interactions
[NASA-CR-180579] p 215 N87-22508

Electrodynamic tether p 44 N87-26449

Ground-based plasma contractor characterization
[NASA-TM-100194] p 215 N87-28423

TETHERLINES

Three dimensional simulation of the operation of a hollow cathode electron emitter on the Shuttle orbiter p 119 A87-14084

Hollow cathode-based plasma contactor experiments for electrodynamic tether
[AIAA PAPER 87-0572] p 214 A87-32192

The radiation impedance of an electrodynamic tether with end connectors p 42 A87-42585

Coaxial tube tether/transmission line for manned nuclear space power
[NASA-CASE-LEW-14338-1] p 55 N87-10174

TEXTURES

Enhanced thermal emittance of space radiators by ion-discharge chamber texturing
[NASA-TM-100137] p 207 N87-25823

THERMAL ABSORPTION

Separation of variables solution for non-linear radiative cooling p 142 A87-48450

THERMAL ANALYSIS

Thermal analysis of an orthotropic engineering body --- horizontal axis wind turbine rotor blade p 173 A87-13496

Thermal analysis of an orthotropic engineering body --- horizontal axis wind turbine rotor blade p 173 A87-13496

Thermal analysis of an orthotropic engineering body --- horizontal axis wind turbine rotor blade p 173 A87-13496

Thermal analysis of an orthotropic engineering body --- horizontal axis wind turbine rotor blade p 173 A87-13496

Thermal analysis of an orthotropic engineering body --- horizontal axis wind turbine rotor blade p 173 A87-13496

Thermal analysis of an orthotropic engineering body --- horizontal axis wind turbine rotor blade p 173 A87-13496

Thermal analysis of an orthotropic engineering body --- horizontal axis wind turbine rotor blade p 173 A87-13496

Thermal analysis of an orthotropic engineering body --- horizontal axis wind turbine rotor blade p 173 A87-13496

Thermal analysis of an orthotropic engineering body --- horizontal axis wind turbine rotor blade p 173 A87-13496

Thermal analysis of an orthotropic engineering body --- horizontal axis wind turbine rotor blade p 173 A87-13496

Thermal analysis of an orthotropic engineering body --- horizontal axis wind turbine rotor blade p 173 A87-13496

Thermal analysis of an orthotropic engineering body --- horizontal axis wind turbine rotor blade p 173 A87-13496

Thermal analysis of an orthotropic engineering body --- horizontal axis wind turbine rotor blade p 173 A87-13496

Thermal analysis of an orthotropic engineering body --- horizontal axis wind turbine rotor blade p 173 A87-13496

Thermal analysis of an orthotropic engineering body --- horizontal axis wind turbine rotor blade p 173 A87-13496

Thermal analysis of an orthotropic engineering body --- horizontal axis wind turbine rotor blade p 173 A87-13496

Thermal analysis of an orthotropic engineering body --- horizontal axis wind turbine rotor blade p 173 A87-13496

Thermal analysis of an orthotropic engineering body --- horizontal axis wind turbine rotor blade p 173 A87-13496

Thermal analysis of an orthotropic engineering body --- horizontal axis wind turbine rotor blade p 173 A87-13496

Thermal analysis of an orthotropic engineering body --- horizontal axis wind turbine rotor blade p 173 A87-13496

Thermal analysis of an orthotropic engineering body --- horizontal axis wind turbine rotor blade p 173 A87-13496

Thermal analysis of an orthotropic engineering body --- horizontal axis wind turbine rotor blade p 173 A87-13496

Thermal analysis of an orthotropic engineering body --- horizontal axis wind turbine rotor blade p 173 A87-13496

Thermal analysis of an orthotropic engineering body --- horizontal axis wind turbine rotor blade p 173 A87-13496

Thermal analysis of an orthotropic engineering body --- horizontal axis wind turbine rotor blade p 173 A87-13496

Thermal analysis of an orthotropic engineering body --- horizontal axis wind turbine rotor blade p 173 A87-13496

Thermal analysis of an orthotropic engineering body --- horizontal axis wind turbine rotor blade p 173 A87-13496

THERMAL EMISSION

Enhanced thermal emittance of space radiators by ion-discharge chamber texturing
[NASA-TM-100137] p 207 N87-25823

THERMAL ENERGY

Selection of high temperature thermal energy storage materials for advanced solar dynamic space power systems
[NASA-TM-89886] p 149 N87-22174

THERMAL EXPANSION

Mechanisms by which heat release affects the flow field in a chemically reacting, turbulent mixing layer
[AIAA PAPER 87-0131] p 134 A87-24925
Composite space antenna structures - Properties and environmental effects p 72 A87-38610
Thermal expansion behavior of graphite/glass and graphite/magnesium p 72 A87-38615
Composite space antenna structures: Properties and environmental effects
[NASA-TM-88859] p 73 N87-16880

THERMAL FATIGUE

A computerized test system for thermal-mechanical fatigue crack growth p 153 A87-23899

THERMAL INSULATION

Thermal barrier coating life prediction model development
[NASA-CR-179508] p 99 N87-11892
Thermal barrier coating life prediction model
[NASA-CR-179504] p 100 N87-13539
Thermal barrier coating life prediction model
[NASA-CR-175010] p 100 N87-13540
The effect of laser glazing on life of ZrO₂ TBCs in cyclic burner rig tests
[NASA-TM-88821] p 89 N87-14487

THERMAL PROTECTION

Development and test of the Shuttle/Centaur cryogenic tankage thermal protection system
[AIAA PAPER 87-1557] p 43 A87-43073
Degradation mechanisms in thermal barrier coatings
[NASA-TM-89309] p 101 N87-17926
Design, development and test of shuttle/Centaur G-prime cryogenic tankage thermal protection systems
[NASA-TM-89825] p 43 N87-23685

THERMAL RADIATION

Computer control of a scanning electron microscope for digital image processing of thermal-wave images
[NASA-TM-100157] p 128 N87-26278

THERMAL RESISTANCE

Degradation mechanisms in thermal-barrier coatings p 94 A87-12953
Bonding Lexan and sapphire to form high-pressure, flame-resistant window
[NASA-TM-100188] p 159 N87-28880

THERMAL SIMULATION

Multiply scaled constrained nonlinear equation solvers -- for nonlinear heat conduction problems p 137 A87-31406

THERMAL STABILITY

Specimen geometry effects on graphite/PMR-15 composites during thermo-oxidative aging p 71 A87-13145

Thermal and structural stability of cosputtered amorphous Ta(x)Cu(1-x) alloy thin films on GaAs p 216 A87-27198

Degradation mechanisms of sulfur and nitrogen containing compounds during thermal stability testing of model fuels
[AIAA PAPER 87-2039] p 106 A87-45372

Thermal stability of the nickel-base superalloy B-1900 + Hf with tantalum variations p 87 A87-51289

PMR polyimide compositions for improved performance at 371 deg C
[NASA-TM-88942] p 73 N87-16071

Thermo-oxidatively stable condensation polyimides containing 1,1,1-triary-2,2,2-trifluoroethane dianhydride and diamine monomers
[NASA-TM-89875] p 103 N87-22048

The tribological behavior of polyphenyl ether and polyphenyl thioether aromatic lubricants
[NASA-TM-100166] p 105 N87-26231

Thermal stability of distillate hydrocarbon fuels
[NASA-CR-181412] p 107 N87-29706

THERMAL STRESSES

SINDA-NASTRAN interfacing program theoretical description and user's manual
[NASA-TM-100158] p 187 N87-27268

Toward improved durability in advanced combustors and turbines: Progress in the prediction of thermomechanical loads
[NASA-TM-88932] p 32 N87-28551

THERMOCHEMISTRY

Plasma assisted surface coating/modification processes: An emerging technology
[NASA-TM-88885] p 110 N87-12708

THERMOCOUPLES

Thin-film temperature sensors for gas turbine engines Problems and prospects p 153 A87-26109
Further development of the dynamic gas temperature measurement system. Volume 1: Technical efforts
[NASA-CR-179513-VOL-1] p 157 N87-19686
Progress on thin-film sensors for space propulsion technology p 158 N87-22772

THERMODYNAMIC CYCLES

Combination solar photovoltaic heat engine energy converter p 190 A87-47088
ANL/RBC: A computer code for the analysis of Rankine bottoming cycles, including system cost evaluation and off-design performance p 220 N87-10777
Compound cycle engine for helicopter application
[NASA-CR-175110] p 31 N87-25323

THERMODYNAMIC EFFICIENCY

Combination solar photovoltaic heat engine energy converter p 190 A87-47088

THERMODYNAMIC PROPERTIES

A universal equation of state for solids p 219 A87-14665
Progress of Stirling cycle analysis and loss mechanism characterization
[NASA-TM-88891] p 220 N87-13359
Feasibility analysis of reciprocating magnetic heat pumps
[NASA-CR-180262] p 147 N87-19647
Thermodynamics and combustion modeling p 219 N87-20274

THERMODYNAMICS

Thermodynamically consistent constitutive equations for nonisothermal large-strain, elastoplastic, creep behavior p 175 A87-27945
Comparisons between thermodynamic and one-dimensional combustion models of spark-ignition engines p 161 A87-29275
Crack layer theory p 178 A87-40056
NASA-Chinese Aeronautical Establishment (CAE) Symposium
[NASA-CP-2433] p 27 N87-20267
Thermodynamics and combustion modeling p 219 N87-20274

Theoretical kinetic computations in complex reacting systems p 219 N87-20277

Calculation of thermomechanical fatigue life based on isothermal behavior
[NASA-TM-88864] p 183 N87-20565

Thermocapillary bubble migration for large Marangoni Numbers
[NASA-CR-179628] p 109 N87-22865

Thermodynamic evaluation of transonic compressor rotors using the finite volume approach
[NASA-CR-180587] p 150 N87-23925

THERMOELASTICITY

Thermo-elasto-viscoplastic analysis of problems in extension and shear
[NASA-CR-181410] p 187 N87-29896

THERMOELECTRIC GENERATORS

Speculations on future opportunities to evolve Brayton powerplants aboard the space station
[NASA-TM-89863] p 39 N87-23674

THERMOHYDRAULICS

A fully coupled variable properties thermohydraulic model for a cryogenic hydrostatic journal bearing
[ASME PAPER 86-TRIB-55] p 161 A87-19536

THERMO-MECHANICAL TREATMENT

Thermal-mechanical fatigue crack growth in B-1900 + Hf p 86 A87-49570

THERMOMETERS

Fiber-optic thermometer using temperature dependent absorption, broadband detection, and time domain referencing p 153 A87-25948

THERMOPHORESIS

Prediction and rational correlation of thermophoretically reduced particle mass transfer to hot surfaces across laminar or turbulent forced-convection gas boundary layers p 133 A87-23449

THERMOPLASTIC RESINS

Corrosion of graphite composites in phosphoric acid fuel cells p 72 A87-42684

THERMOSETTING RESINS

Styrene-terminated polysulfone oligomers as matrix material for graphite reinforced composites: An initial study
[NASA-TM-89846] p 74 N87-21043

THERMOVISCOELASTICITY

Non-isothermal elastoviscoplastic snap-through and creep buckling of shallow arches
[AIAA PAPER 87-0806] p 176 A87-33605

THICK PLATES

Three-dimensional vibrations of twisted cantilevered parallelepipeds p 173 A87-11106
An efficient quadrilateral element for plate bending analysis p 178 A87-45994

THREE DIMENSIONAL COMPOSITES

Modes of vibration on square fiberglass epoxy composite thick plate
[NASA-CR-4018] p 171 N87-13779

THICK WALLS

On the numerical performance of three-dimensional thick shell elements using a hybrid/mixed formulation p 175 A87-25924

THICKNESS

Performance of two 10-lb/sec centrifugal compressors with different blade and shroud thicknesses operating over a range of Reynolds numbers
[AIAA PAPER 87-1745] p 22 A87-50188

Performance of two 10-lb/sec centrifugal compressors with different blade and shroud thicknesses operating over a range of Reynolds numbers
[NASA-TM-100115] p 29 N87-23623

THIN FILMS

A simple method for monitoring surface temperatures in plasma treatments p 160 A87-17269
Thin-film temperature sensors for gas turbine engines Problems and prospects p 153 A87-26109
Thermal and structural stability of cosputtered amorphous Ta(x)Cu(1-x) alloy thin films on GaAs p 216 A87-27198

A review of recent advances in solid film lubrication p 161 A87-35332

How to evaluate solid lubricant films using a Pin-on-disk tribometer p 87 A87-42618

Comparison of generalized Reynolds and Navier Stokes equations for flow of a power law fluid p 142 A87-45852

Adhesion, friction and deformation of ion-beam-deposited boron nitride films p 98 A87-49325

Thermohydrodynamic analysis for laminar lubricating films
[NASA-TM-88845] p 144 N87-11124

Adhesion, friction, and deformation of ion-beam-deposited boron nitride films
[NASA-TM-88902] p 100 N87-15305

Ion plated gold films: Properties, tribological behavior and performance
[NASA-TM-88977] p 110 N87-17937

Mechanical strength and tribological behavior of ion-beam deposited boron nitride films on non-metallic substrates
[NASA-TM-89818] p 101 N87-18668

Investigation of PTFE transfer films by infrared emission spectroscopy and phase-locked ellipsometry
[NASA-TM-89844] p 102 N87-20421

Rapid thermal annealing of Amorphous Hydrogenated Carbon (a-C:H) films
[NASA-TM-88859] p 218 N87-20821

Traveling-wave-tube efficiency improvement by a low-cost technique for deposition of carbon on multistage depressed collector
[NASA-TP-2719] p 126 N87-21239

Effect of an oxygen plasma on uncoated thin aluminum reflecting films
[NASA-TM-88882] p 61 N87-21999

Progress on thin-film sensors for space propulsion technology p 158 N87-22772

AlGaAs growth by OMCVD using an excimer laser
[NASA-TM-88937] p 218 N87-23304

A computer solution for the dynamic load, lubricant film thickness and surface temperatures in spiral bevel gears
[NASA-CR-4077] p 169 N87-26358

Thin film strain gage development program
[NASA-CR-174707] p 159 N87-28883

THIN PLATES

An efficient quadrilateral element for plate bending analysis p 178 A87-45994

THIN WALLED SHELLS

Nonisothermal elasto-visco-plastic response of shell-type structures p 185 N87-22796

THREE DIMENSIONAL BODIES

On the numerical performance of three-dimensional thick shell elements using a hybrid/mixed formulation p 175 A87-25924

Composite interlaminar fracture toughness: Three-dimensional finite element modeling for mixed mode 1, 2 and 3 fracture
[NASA-TM-88872] p 73 N87-13491

THREE DIMENSIONAL BOUNDARY LAYER

An experimental investigation of compressible three-dimensional boundary layer flow in annular diffusers
[AIAA PAPER 87-0366] p 3 A87-24954

Assessment of a 3-D boundary layer code to predict heat transfer and flow losses in a turbine p 145 N87-11224

THREE DIMENSIONAL COMPOSITES

Assessment of simplified composite micromechanics using three-dimensional finite-element analysis p 72 A87-19121

THREE DIMENSIONAL FLOW

- An L-U implicit multigrid algorithm for the three-dimensional Euler equations
[AIAA PAPER 87-0453] p 133 A87-22645
- Two- and three-dimensional viscous computations of a hypersonic inlet flow
[AIAA PAPER 87-0283] p 4 A87-31106
- Euler analysis of transonic propeller flows
p 4 A87-39813
- Numerical simulation of transonic propeller flow using a three-dimensional small disturbance code employing novel helical coordinates
[AIAA PAPER 87-1162] p 5 A87-42107
- Three-dimensional unsteady Euler solutions for propfans and counter-rotating propfans in transonic flow
[AIAA PAPER 87-1197] p 5 A87-42314
- An LDA investigation of three-dimensional normal shock-boundary layer interactions in a corner
[AIAA PAPER 87-1369] p 6 A87-44938
- Euler analysis of the three-dimensional flow field of a high-speed propeller - Boundary condition effects
[ASME PAPER 87-GT-253] p 6 A87-48719
- Method for the determination of the three dimensional aerodynamic field of a rotor-stator combination in compressible flow
[AIAA PAPER 87-1742] p 7 A87-50187
- Gas flow environmental and heat transfer nonrotating 3D program
p 145 A87-11223
- Calculation of water drop trajectories to and about arbitrary three-dimensional lifting and nonlifting bodies in potential airflow
[NASA-CR-3935] p 8 A87-11694
- On 3-D inelastic analysis methods for hot section components (base program)
[NASA-CR-175060] p 180 A87-12923
- Computation of multi-dimensional viscous supersonic jet flow
[NASA-CR-4020] p 8 A87-13405
- Computation of multi-dimensional viscous supersonic flow
[NASA-CR-4021] p 9 A87-13406
- Evaluation of diffuse-illumination holographic cinematography in a flutter cascade
[NASA-TP-2593] p 156 A87-13731
- Two- and three-dimensional viscous computations of a hypersonic inlet flow
[NASA-TM-88923] p 146 A87-15441
- Euler analysis of the three dimensional flow field of a high-speed propeller: Boundary condition effects
[NASA-TM-88955] p 10 A87-16798
- Numerical simulation of transonic propeller flow using a 3-dimensional small disturbance code employing novel helical coordinates
[NASA-TM-89826] p 12 A87-19350
- Experiments and modeling of dilution jet flow fields
p 148 A87-20276
- A finite difference scheme for three-dimensional steady laminar incompressible flow
[NASA-TM-89851] p 148 A87-20504
- Application of advanced computational codes in the design of an experiment for a supersonic throughflow fan rotor
[NASA-TM-88915] p 13 A87-22630
- Method for the determination of the three-dimensional aerodynamic field of a rotor-stator combination to compressible flow
[NASA-TM-100118] p 30 A87-23625
- Three dimensional boundary layers in internal flows
[NASA-CR-181336] p 152 A87-28860
- THREE DIMENSIONAL MOTION**
- Three-dimensional vibrations of twisted cantilevered parallelepipeds
p 173 A87-11106
- Three-dimensional trajectory analyses of two drop sizing instruments - PMS OAP and PMS FSSP - Optical Array Probe and Forward Scattering Spectrometer Probe
[AIAA PAPER 87-0180] p 132 A87-22466
- THRUST**
- Low power arcjet thruster pulse ignition
[AIAA PAPER 87-1951] p 54 A87-50194
- Low power arcjet thruster pulse ignition
[NASA-TM-100123] p 64 A87-23691
- THRUST AUGMENTATION**
- A design study of hydrazine and biowaste resistojets
[NASA-CR-179510] p 57 A87-14425
- THRUST CHAMBERS**
- Heat pipe cooled rocket engines
[AIAA PAPER 86-1567] p 48 A87-21516
- Comparison of theoretical and experimental thrust performance of a 1030:1 area ratio rocket nozzle at a chamber pressure of 2413 kN/sq m (350 psia)
[AIAA PAPER 87-2069] p 52 A87-45390
- Test program to provide confidence in liquid oxygen cooling of hydrocarbon fueled rocket thrust chambers
p 67 A87-26114
- Proven, long-life hydrogen/oxygen thrust chambers for space station propulsion
p 68 A87-26133

THRUST MEASUREMENT

- Vacuum chamber pressure effects on thrust measurements of low Reynolds number nozzles
p 45 A87-14976
- An analysis of electromagnetic coupling and eigenfrequencies for microwave electrothermal thruster discharges
[AIAA PAPER 87-1012] p 51 A87-41111
- THRUST REVERSAL**
- Full-scale thrust reverser testing in an altitude facility
[AIAA PAPER 87-1788] p 34 A87-45203
- Full-scale thrust reverser testing in an altitude facility
[NASA-TM-88967] p 35 A87-18575
- THRUST VECTOR CONTROL**
- High- and low-thrust propulsion systems for the Space Station
[AIAA PAPER 87-0398] p 48 A87-24997
- An analytical and experimental investigation of resistojet plumes
[AIAA PAPER 87-0399] p 48 A87-24998
- Conceptual design and integration of a Space Station resistojet propulsion assembly
[AIAA PAPER 87-1860] p 52 A87-45256
- High- and low-thrust propulsion systems for the space station
[NASA-TM-88877] p 57 A87-14427
- An analytical and experimental investigation of resistojet plumes
[NASA-TM-88852] p 58 A87-14428
- Conceptual design and integration of a space station resistojet propulsion assembly
[NASA-TM-89847] p 60 A87-20378
- THRUST-WEIGHT RATIO**
- Polymer, metal, and ceramic matrix composites for advanced aircraft engine applications
p 71 A87-15187
- THRUSTORS**
- Microwave electrothermal thruster performance in helium gas
p 49 A87-31261
- TILT ROTOR AIRCRAFT**
- Folding tilt rotor demonstrator feasibility study
p 17 A87-19247
- TIME**
- Time-partitioning simulation models for calculation on parallel computers
[NASA-TM-89850] p 203 A87-20766
- TIME DEPENDENCE**
- Exposure time considerations in high temperature low cycle fatigue
[NASA-TM-88934] p 187 A87-28944
- TIME DIVISION MULTIPLE ACCESS**
- Baseband processor development/test performance for 30/20 GHz SS-TDMA communication system
p 111 A87-18310
- ACTS baseband processing - Advanced Communications Technology Satellite
p 201 A87-45512
- Satellite analog FDMA/FM to digital TDMA conversion
[NASA-CR-179605] p 125 A87-20467
- On-board processing satellite network architecture and control study
[NASA-CR-180816] p 44 A87-27710
- On-board processing satellite network architecture and control study
[NASA-CR-180817] p 44 A87-27711
- TIME DIVISION MULTIPLEXING**
- On-board processing satellite network architecture and control study
[NASA-CR-180816] p 44 A87-27710
- On-board processing satellite network architecture and control study
[NASA-CR-180817] p 44 A87-27711
- TIME LAG**
- Ignition delay times of cyclopentene oxygen argon mixtures
p 76 A87-12602
- TIME MARCHING**
- Time-marching solution of incompressible Navier-Stokes equations for internal flow
p 138 A87-39450
- Thermodynamic evaluation of transonic compressor rotors using the finite volume approach
[NASA-CR-180587] p 150 A87-23925
- TIME SERIES ANALYSIS**
- Engineering calculations for communications satellite systems planning
[NASA-CR-180106] p 114 A87-16198
- TIME TEMPERATURE PARAMETER**
- Non-isothermal elastoviscoplastic snap-through and creep buckling of shallow arches
[AIAA PAPER 87-0806] p 176 A87-33605
- TIP SPEED**
- An experimental study on the effects of tip clearance on flow field and losses in an axial flow compressor rotor
p 6 A87-46207
- Cruise noise of the 2/9th scale model of the Large-scale Advanced Propfan (LAP) propeller, SR-7A
[NASA-TM-100175] p 212 A87-28398

TIRES

- Aircraft accident report: NASA 712, Convair 990, N712NA, March Air Force Base, California, July 17, 1985, executive summary
[NASA-TM-87356-VOL-1] p 16 A87-21878
- Aircraft accident report: NASA 712, Convair 990, N712NA, March Air Force Base, California, July 17, 1985, facts and analysis
[NASA-TM-87356-VOL-2] p 16 A87-21879
- TITANIUM ALLOYS**
- Elevated temperature strengthening of a melt spun austenitic steel by TiB₂
p 87 A87-51639
- Shot peening for Ti-6Al-4V alloy compressor blades
[NASA-TP-2711] p 184 A87-20566
- TITANIUM CARBIDES**
- Characterization of ion beam modified ceramic wear surfaces using Auger electron spectroscopy
p 98 A87-51304
- TOLLMIEIN-SCHLICHTING WAVES**
- Nonlinear critical layers eliminate the upper branch of spatially growing Tollmien-Schlichting waves
p 131 A87-12251
- The generation of Tollmien-Schlichting waves by long wavelength free stream disturbances
p 139 A87-41655
- Generation of Tollmien-Schlichting waves on interactive marginally separated flows
p 144 A87-54365
- A note on the generation of Tollmien-Schlichting waves by sudden surface-curvature change
p 144 A87-54366
- TOLUENE**
- The oxidation degradation of aromatic compounds
[NASA-CR-180588] p 79 A87-22020
- TORCHES**
- Hydrogen-air ignition torch
[NASA-TM-88882] p 38 A87-13470
- TORQUE**
- Evaluation of a high-torque backlash-free roller actuator
p 165 A87-16336
- TORQUE CONVERTERS**
- The 3600 hp split-torque helicopter transmission
[NASA-CR-174932] p 25 A87-11788
- TORSION**
- The effect of circumferential aerodynamic detuning on coupled bending-torsion unstalled supersonic flutter
[ASME PAPER 86-GT-100] p 20 A87-25396
- Influence of third-degree geometric nonlinearities on the vibration and stability of pretwisted, precone, rotating blades
p 21 A87-46228
- TORSIONAL STRESS**
- Aeroelastic control of stability and forced response of supersonic rotors by aerodynamic detuning
p 21 A87-46249
- TORSIONAL VIBRATION**
- Modeling of multi-rotor torsional vibrations in rotating machinery using substructuring
p 175 A87-28543
- Nonlinear vibration and stability of rotating, pretwisted, precone blades including Coriolis effects
p 178 A87-39896
- TRACE ELEMENTS**
- Oxygen-18 tracer study of the passive thermal oxidation of silicon
p 78 A87-51187
- TRAJECTORY ANALYSIS**
- Three-dimensional trajectory analyses of two drop sizing instruments - PMS OAP and PMS FSSP - Optical Array Probe and Forward Scattering Spectrometer Probe
[AIAA PAPER 87-0180] p 132 A87-22466
- Flow visualization study of the effect of injection hole geometry on an inclined jet in crossflow
p 155 A87-45842
- Calculation of water drop trajectories to and about arbitrary three-dimensional lifting and nonlifting bodies in potential airflow
[NASA-CR-3935] p 8 A87-11694
- TRANSATMOSPHERIC VEHICLES**
- High angle of attack hypersonic aerodynamics
[AIAA PAPER 87-2548] p 7 A87-49101
- TRANSDUCANCE**
- Characterization of InGaAs/AlGaAs pseudomorphic modulation-doped field-effect transistors
p 121 A87-23922
- TRANSFER ORBITS**
- Effects of transient propellant dynamics on deployment of large liquid stages in zero-gravity with application to Shuttle/Centaur
[IAF PAPER 86-119] p 39 A87-15880
- Status of advanced propulsion for space based orbital transfer vehicle
[IAF PAPER 86-183] p 48 A87-23239
- Status of advanced propulsion for space based orbital transfer vehicle
[NASA-TM-88848] p 56 A87-10959
- TRANSFERRING**
- Investigation of PTFE transfer films by infrared emission spectroscopy and phase-locked ellipsometry
[NASA-TM-89844] p 102 A87-20421

TRANSFORMATIONS (MATHEMATICS)

- Bounding solutions of geometrically nonlinear viscoelastic problems p 174 A87-20892
 Extrapolation methods for divergent oscillatory infinite integrals that are defined in the sense of summability p 204 A87-35575

TRANSIENT HEATING

- Efficient numerical simulation of an electrothermal de-icer pad [AIAA PAPER 87-0024] p 137 A87-32190

TRANSIENT RESPONSE

- Transient radiative cooling of a droplet-filled layer p 135 A87-27712
 Modeling of environmentally induced transients within satellites [AIAA PAPER 85-0387] p 42 A87-41611
 Separation of variables solution for non-linear radiative cooling p 142 A87-48450

TRANSISTORS

- Radiation effects on power transistor performance [NASA-CR-181188] p 129 A87-27099

TRANSITION FLOW

- Spanwise structures in transitional flow around circular cylinders [AIAA PAPER 87-1383] p 140 A87-44940
 Transition boiling heat transfer and the film transition regime p 143 A87-53589
 Transition mixing study [NASA-CR-175062] p 27 A87-16830

TRANSMISSION

- A study of Schwarz converters for nuclear powered spacecraft [NASA-TM-89911] p 128 A87-23903
 Profile modification to minimize spur gear dynamic loading [NASA-TM-89901] p 170 A87-28918

TRANSMISSION EFFICIENCY

- Image data compression with vector quantization in the transform domain p 111 A87-30775
 US long distance fiber optic networks: Technology, evolution and advanced concepts. Volume 1: Executive summary [NASA-CR-179479] p 113 A87-11056
 Bit-error-rate testing of high-power 30-GHz traveling wave tubes for ground-terminal applications [NASA-TP-2635] p 115 A87-17971
 Rectenna Technology Program: Ultra light 2.45 GHz rectenna 20 GHz rectenna [NASA-CR-179558] p 116 A87-19556

TRANSMISSION LINES

- Propagation characteristics of some novel coplanar waveguide transmission lines on GaAs at MM-wave frequencies [NASA-TM-89839] p 126 A87-20469
 Coaxial tube array space transmission line characterization [NASA-TM-89864] p 62 A87-22003

TRANSMISSION LOSS

- Helical gears with circular arc teeth: Generation, geometry, precision and adjustment to errors, computer aided simulation of conditions of meshing and bearing contact [NASA-CR-4089] p 170 A87-29846

TRANSMISSIONS (MACHINE ELEMENTS)

- Testing of UH-60A helicopter transmission in NASA Lewis 2240-kW (3000-hp) facility [NASA-TP-2626] p 164 A87-10391
 The 3600 hp split-torque helicopter transmission [NASA-CR-174932] p 25 A87-11788
 Common problems and pitfalls in gear design [NASA-TM-88858] p 165 A87-17033
 Design and dynamic simulation of a fixed pitch 56 kW wind turbine drive train with a continuously variable transmission [NASA-CR-179543] p 193 A87-17401
 Flexibility effects on tooth contact location in spiral bevel gear transmissions [NASA-CR-4055] p 166 A87-20552
 Vibration characteristics of OH-58A helicopter main rotor transmission [NASA-TP-2705] p 167 A87-20555
 Experimental and analytical evaluation of dynamic load and vibration of a 2240-kW (300-hp) rotorcraft transmission [NASA-TM-88975] p 167 A87-20556
 Gear tooth stress measurements on the UH-60A helicopter transmission [NASA-TP-2698] p 167 A87-22235
 Helicopter transmission testing at NASA Lewis Research Center [NASA-TM-89912] p 168 A87-22978
 The design and analysis of single flank transmission error tester for loaded gears [NASA-CR-179621] p 169 A87-27197

TRANSMISSIVITY

- Spectrum-modulating fiber-optic sensors for aircraft control systems [NASA-TM-88968] p 27 A87-17700

TRANSMITTERS

- The 20 GHz power GaAs FET development [NASA-CR-179546] p 124 A87-16972
 The 20 GHz spacecraft IMPATT solid state transmitter [NASA-CR-179545] p 124 A87-17989

TRANSONIC COMPRESSORS

- Measurements of the unsteady flow field within the stator row of a transonic axial-flow fan. 1: Measurement and analysis technique [NASA-TM-88945] p 10 A87-16789

TRANSONIC FLOW

- Rotor wake characteristics of a transonic axial-flow fan p 2 A87-20886
 An L-U implicit multigrid algorithm for the three-dimensional Euler equations [AIAA PAPER 87-0453] p 133 A87-22645
 Multigrid solution of inviscid transonic flow through rotating blade passages [AIAA PAPER 87-0608] p 3 A87-24992
 Analysis of viscous transonic flow over airfoil sections [AIAA PAPER 87-0420] p 4 A87-34723
 An LU-SSOR scheme for the Euler and Navier-Stokes equations [AIAA PAPER 87-0600] p 137 A87-34724
 Three-dimensional unsteady Euler solutions for propfans and counter-rotating propfans in transonic flow [AIAA PAPER 87-1197] p 5 A87-42314
 Calculation of two- and three-dimensional transonic cascade flow field using the Navier-Stokes equations p 144 A87-11220
 Unsteady flows in a single-stage transonic axial-flow fan stator row [NASA-TM-88929] p 11 A87-16805
 An LU-SSOR scheme for the Euler and Navier-Stokes equations [NASA-CR-179556] p 11 A87-16806
 Analysis of viscous transonic flow over airfoil sections [NASA-TM-88912] p 146 A87-17001
 Beam-modulation methods in quantitative and flow-visualization holographic interferometry p 111 A87-21204
 Shock structure measured in a transonic fan using laser anemometry p 28 A87-21929

TRANSONIC WIND TUNNELS

- Transonic interference reduction by limited ventilation wall panels [NASA-CR-175039] p 15 A87-29419

TRANSPORT PROPERTIES

- CONDIF - A modified central-difference scheme with unconditional stability and very low numerical diffusion p 136 A87-30685
 Effects of droplet interactions on droplet transport at intermediate Reynolds numbers [NASA-CR-179567] p 26 A87-14348
 Preliminary study of niobium alloy contamination by transport through helium [NASA-TM-88952] p 90 A87-17884
 Electrochemical performance and transport properties of a Nafion membrane in a hydrogen-bromine cell environment [NASA-TM-89862] p 79 A87-23718
 Secondary electron generation, emission and transport: Effects on spacecraft charging and NASCAP models p 44 A87-26950

TRAVELING WAVE TUBES

- Carbon and carbon-coated electrodes for multistage depressed collectors for electron-beam devices - A technology review p 120 A87-20666
 Improvements in MDC and TWT overall efficiency through the application of carbon electrode surfaces --- Multistage Depressed Collectors p 120 A87-20667
 TWT efficiency improvement by a low-cost technique for deposition of carbon on MDC electrodes p 121 A87-30199
 A 20 GHz, high efficiency dual mode TWT for the ACTS program --- Advanced Communications Technology Satellite p 122 A87-45511
 Bit-error-rate testing of high-power 30-GHz traveling wave tubes for ground-terminal applications [NASA-TP-2635] p 115 A87-17971
 Performance of textured carbon on copper electrode multistage depressed collectors with medium-power traveling wave tubes [NASA-TP-2665] p 125 A87-17990
 Calculation of secondary electron trajectories in multistage depressed collectors for microwave amplifiers [NASA-TP-2664] p 125 A87-17991
 Design, fabrication and performance of small, graphite electrode, multistage depressed collectors with 200-W, CW, 8- to 18-GHz traveling-wave tubes [NASA-TP-2693] p 126 A87-20474

- Traveling-wave-tube efficiency improvement by a low-cost technique for deposition of carbon on multistage depressed collector [NASA-TP-2719] p 126 A87-21239
 Revised NASA axially symmetric ring model for coupled-cavity traveling-wave tubes [NASA-TP-2675] p 127 A87-22923
 Self-consistent inclusion of space-charge in the traveling wave tube [NASA-TM-89928] p 128 A87-24630
 Analytical and experimental performance of a dual-mode traveling wave tube and multistage depressed collector [NASA-TP-2752] p 128 A87-25532

TRENDS

- An assessment of the status and trends in satellite communications 1986-2000: An information document prepared for the Communications Subcommittee of the Space Applications Advisory Committee [NASA-TM-88867] p 114 A87-13600

TRIBOLOGY

- Tribology of selected ceramics at temperatures to 900 C p 94 A87-12954
 Microstructure and surface chemistry of amorphous alloys important to their friction and wear behavior p 81 A87-15186
 Counterface effects on the tribological properties of polyimide composites p 95 A87-27625
 A review of recent advances in solid film lubrication p 161 A87-35332
 How to evaluate solid lubricant films using a Pin-on-disk tribometer p 97 A87-42618
 Effects of atmosphere on the tribological properties of a chromium carbide based coating for use to 760 deg C [NASA-TM-88894] p 101 A87-16140
 The 20th Aerospace Mechanics Symposium [NASA-CP-2423-REV] p 181 A87-16321
 Tribological properties of polymer films and solid bodies in a vacuum environment [NASA-TM-88966] p 101 A87-17906
 Ion plated gold films: Properties, tribological behavior and performance [NASA-TM-88977] p 110 A87-17937
 Mechanical strength and tribological behavior of ion-beam deposited boron nitride films on non-metallic substrates [NASA-TM-89818] p 101 A87-18668
 Effect of shaft frequency on cavitation in a journal bearing for noncentered circular whirl [NASA-TM-88925] p 148 A87-22122
 Tribological properties of coal slurries [NASA-TM-89930] p 104 A87-24565
 Effect of abrasive grit size on wear of manganese-zinc ferrite under three-body abrasion [NASA-TM-89879] p 104 A87-24566
 Stability of a rigid rotor supported on flexible oil journal bearings [NASA-TM-89899] p 151 A87-24646
 The tribological behavior of polyphenyl ether and polyphenyl thioether aromatic lubricants [NASA-TM-100166] p 105 A87-26231
 The effect of Tricresyl-Phosphate (TCP) as an additive on wear of Iron (Fe) [NASA-TM-100103] p 93 A87-27030
 Tribology theory versus experiment [NASA-TM-100198] p 71 A87-29599
 Comparison of the tribological properties of fluorinated cokes and graphites [NASA-TM-100170] p 106 A87-29679
- TRIGGER CIRCUITS**
 Synchronization trigger control system for flow visualization [NASA-TM-89902] p 128 A87-23902
- TRUCKS**
 Technical and economic study of Stirling and Rankine cycle bottoming systems for heavy truck diesel engines [NASA-CR-180833] p 222 A87-28470
- TRUSSES**
 A hybrid nonlinear programming method for design optimization p 201 A87-35718
- TUNGSTEN**
 The sensitivity of mechanical properties of TFRS composites to variations in reaction zone size and properties --- Tungsten Fiber Reinforced Superalloys [AIAA PAPER 87-0757] p 72 A87-33577
 Fiber reinforced superalloys [NASA-TM-89865] p 75 A87-22811
- TUNING**
 The effect of circumferential aerodynamic detuning on coupled bending-torsion unstalled supersonic flutter [ASME PAPER 86-GT-100] p 20 A87-25396
 Analytical and experimental investigation of mistuning in propfan flutter [AIAA PAPER 87-0739] p 178 A87-40496
 Optimization of cascade blade mistuning under flutter and forced response constraints p 24 A87-11732

- Analytical and experimental investigation of mistuning in propfan flutter
[NASA-TM-88959] p 182 N87-18116
- Precision tunable resonant microwave cavity
[NASA-CASE-LEW-13935-1] p 126 N87-21234
- ### TUNISIA
- Tunisia Renewable Energy Project systems description report
[NASA-TM-88789] p 192 N87-13856
- ### TURBINE BLADES
- Thermal analysis of an orthotropic engineering body — horizontal axis wind turbine rotor blade p 173 A87-13496
- Local heat transfer augmentation in channels with two opposite ribbed surfaces p 136 A87-30732
- Probabilistic structural analysis to quantify uncertainties associated with turbopump blades
[AIAA PAPER 87-0766] p 176 A87-33581
- Optimization and analysis of gas turbine engine blades
[AIAA PAPER 87-0827] p 201 A87-33614
- Advances in 3-D Inelastic Analysis Methods for hot section components
[AIAA PAPER 87-0719] p 177 A87-33645
- Understanding single-crystal superalloys p 85 A87-40928
- Application of single crystal superalloys for earth-to-orbit propulsion systems
[AIAA PAPER 87-1746] p 85 A87-45336
- Rotational effects on impingement cooling p 141 A87-45838
- Supersonic through-flow fan design
[AIAA PAPER 87-1746] p 22 A87-48571
- WEST-3 wind turbine simulator development. Volume 2: Verification
[NASA-CR-174982] p 191 N87-10531
- Mechanical behavior of thermal barrier coatings for gas turbine blades p 24 N87-11196
- STAEBL: Structural tailoring of engine blades, phase 2 p 24 N87-11731
- Optimization of cascade blade mistuning under flutter and forced response constraints p 24 N87-11732
- On optimal design for the blade-root/hub interface in jet engines p 24 N87-11769
- Fabrication of cooled radial turbine rotor
[NASA-CR-179503] p 25 N87-11789
- Generation of a composite grid for turbine flows and consideration of a numerical scheme
[NASA-TM-88890] p 11 N87-17662
- Design of an advanced wood composite rotor and development of wood composite blade technology
[NASA-CR-174713] p 73 N87-17861
- Oxide-dispersion-strengthened turbine blades, volume 1
[NASA-CR-179537-VOL-1] p 90 N87-17883
- Lewis inverse design code (LIDES): Users manual
[NASA-TP-2676] p 12 N87-20238
- Application of single crystal superalloys for Earth-to-orbit propulsion systems
[NASA-TM-89877] p 91 N87-22034
- Structural and aeroelastic analysis of the SR-7L propfan
[NASA-TM-86877] p 184 N87-22273
- Supersonic through-flow fan design
[NASA-TM-88908] p 29 N87-22681
- Progress in the prediction of unsteady heat transfer on turbine blades p 149 N87-22769
- Progress on thin-film sensors for space propulsion technology p 158 N87-22772
- Nonlinear heat transfer and structural analyses of SSME turbine blades p 184 N87-22779
- Probabilistic structural analysis to evaluate the structural durability of SSME critical components p 62 N87-22783
- Probabilistic Structural Analysis Methods (PSAM) for select space propulsion system structural components p 62 N87-22784
- Structural tailoring using the SSME/STAEBL code p 63 N87-22795
- SSME blade damper technology p 63 N87-22798
- A linearized Euler analysis of unsteady flows in turbomachinery
[NASA-CR-180987] p 149 N87-22948
- SSME single crystal turbine blade dynamics
[NASA-CR-179644] p 186 N87-26384
- Finite element analysis of flexible, rotating blades
[NASA-TM-89906] p 186 N87-26385
- Surface pressure measurements on the blade of an operating Mod-2 wind turbine with and without vortex generators
[NASA-TM-89903] p 198 N87-26455
- Bladed disk vibration
[NASA-CR-181203] p 31 N87-26908
- Design of test specimens and procedures for generating material properties of Douglas fir/epoxy laminated wood composite material: With the generation of baseline data at two environmental conditions
[NASA-CR-174910] p 75 N87-28612
- ### TURBINE ENGINES
- A real-time simulation evaluation of an advanced detection, isolation and accommodation algorithm for sensor failures in turbine engines p 18 A87-13318
- Long-term deposit formation in aviation turbine fuel at elevated temperature p 106 A87-14986
- The utilization of parallel processing in solving the inviscid form of the average-passage equation system for multistage turbomachinery
[AIAA PAPER 87-1108] p 5 A87-42057
- Full-scale thrust reverser testing in an altitude facility
[AIAA PAPER 87-1788] p 34 A87-45203
- Mathematical model partitioning and packing for parallel computer calculation p 202 A87-52534
- Compound cycle engine program p 23 A87-53428
- Turbine Engine Hot Section Technology, 1984
[NASA-CP-2339] p 179 N87-11180
- Combustion overview p 78 N87-11181
- Fatigue and fracture: Overview p 179 N87-11183
- Host turbine heat transfer overview p 144 N87-11184
- Laser anemometers of hot-section applications p 155 N87-11187
- Effects of surface chemistry on hot corrosion life p 88 N87-11193
- Introduction to life modeling of thermal barrier coatings p 99 N87-11195
- Compound cycle engine program
[NASA-TM-88879] p 25 N87-11790
- Turbine vane external heat transfer. Volume 2. Numerical solutions of the Navier-Stokes equations for two- and three-dimensional turbine cascades with heat transfer
[NASA-CR-174828] p 145 N87-13661
- Four spot laser anemometer and optical access techniques for turbine applications
[NASA-TM-88972] p 156 N87-18057
- Full-scale thrust reverser testing in an altitude facility
[NASA-TM-88967] p 35 N87-18575
- The T55-L-712 turbine engine compressor housing refurbishment project
[NASA-CR-179624] p 92 N87-23729
- Advanced detection, isolation and accommodation of sensor failures: Real-time evaluation
[NASA-TP-2740] p 34 N87-25331
- Ceramic high pressure gas path seal
[NASA-CR-180813] p 31 N87-26914
- Materials for Advanced Turbine Engines (MATE). Project 4: Erosion resistant compressor airfoil coating
[NASA-CR-179622] p 92 N87-27029
- Toward improved durability in advanced combustors and turbines: Progress in the prediction of thermomechanical loads
[NASA-TM-88932] p 32 N87-28551
- ### TURBINE PUMPS
- Probabilistic structural analysis to quantify uncertainties associated with turbopump blades
[AIAA PAPER 87-0766] p 176 A87-33581
- Application of single crystal superalloys for earth-to-orbit propulsion systems
[AIAA PAPER 87-1976] p 85 A87-45336
- Application of single crystal superalloys for Earth-to-orbit propulsion systems
[NASA-TM-89877] p 91 N87-22034
- Heat flux calibration facility capable of SSME conditions p 36 N87-22774
- Nonlinear heat transfer and structural analyses of SSME turbine blades p 184 N87-22779
- Probabilistic structural analysis to evaluate the structural durability of SSME critical components p 62 N87-22783
- SSME blade damper technology p 63 N87-22798
- Straight cylindrical seal for high-performance turbomachines
[NASA-TP-1850] p 150 N87-23936
- Three-step cylindrical seal for high-performance turbomachines
[NASA-TP-1849] p 151 N87-24639
- SSME single crystal turbine blade dynamics
[NASA-CR-179644] p 186 N87-26384
- Bladed disk vibration
[NASA-CR-181203] p 31 N87-26908
- ### TURBINES
- Calculation of two- and three-dimensional transonic cascade flow field using the Navier-Stokes equations p 144 N87-11220
- A general method for unsteady stagnation region heat transfer and results for model turbine flows
[NASA-TM-88903] p 146 N87-17002
- Combined fringe and Fabry-Perot laser anemometer for 3 component velocity measurements in turbine stator cascade facility p 110 N87-21183
- Simulation of multistage turbine flows p 149 N87-22768
- ### TURBOCOMPRESSORS
- Stall transients of axial compression systems with inlet distortion p 3 A87-24010
- Performance studies on an axial flow compressor stage p 138 A87-37208
- The hub wall boundary layer development and losses in an axial flow compressor rotor passage p 139 A87-41665
- An experimental study on the effects of tip clearance on flow field and losses in an axial flow compressor rotor p 6 A87-46207
- Supersonic through-flow fan design
[AIAA PAPER 87-1746] p 22 A87-48571
- A method for assessing effects of circumferential flow distortion on compressor stability p 7 A87-48722
- Advanced liquid-cooled, turbocharged and intercooled stratified charge rotary engines for aircraft
[SAE PAPER 871039] p 22 A87-48766
- Method for the determination of the three dimensional aerodynamic field of a rotor-stator combination in compressible flow
[AIAA PAPER 87-1742] p 7 A87-50187
- Compound cycle engine program p 23 A87-53428
- Compound cycle engine program
[NASA-TM-88879] p 25 N87-11790
- Unsteady flows in a single-stage transonic axial-flow fan stator row
[NASA-TM-88929] p 11 N87-16805
- Rotordynamic Instability Problems in High-Performance Turbomachinery, 1986
[NASA-CP-2443] p 167 N87-22199
- Supersonic through-flow fan design
[NASA-TM-88908] p 29 N87-22681
- Method for the determination of the three-dimensional aerodynamic field of a rotor-stator combination to compressible flow
[NASA-TM-100118] p 30 N87-23625
- Calculations of inlet distortion induced compressor flowfield instability p 30 N87-24470
- ### TURBOFAN ENGINES
- A real-time simulation evaluation of an advanced detection, isolation and accommodation algorithm for sensor failures in turbine engines p 18 A87-13318
- An overview of the small engine component technology (SECT) studies — commuter, rotorcraft, cruise missile and auxiliary power applications in year 2000
[AIAA PAPER 86-1542] p 19 A87-17993
- Engine studies for future subsonic cruise missiles
[AIAA PAPER 86-1547] p 19 A87-21513
- Aircraft turbofan noise p 209 A87-31144
- NASA/GE advanced low emissions combustor program
[AIAA PAPER 87-2035] p 21 A87-45369
- Supersonic through-flow fan design
[AIAA PAPER 87-1746] p 22 A87-48571
- The supersonic through-flow turbofan for high Mach propulsion
[AIAA PAPER 87-2050] p 22 A87-50196
- Full-scale engine demonstration of an advanced sensor failure detection isolation, and accommodation algorithm — Preliminary results
[AIAA PAPER 87-2259] p 22 A87-50422
- Scaled centrifugal compressor program
[NASA-CR-174912] p 26 N87-14349
- Measurements of the unsteady flow field within the stator row of a transonic axial-flow fan. Part 2: Results and discussion
[NASA-TM-88940] p 10 N87-16790
- Unsteady flows in a single-stage transonic axial-flow fan stator row
[NASA-TM-88929] p 11 N87-16805
- Full-scale engine demonstration of an advanced sensor failure detection, isolation and accommodation algorithm: Preliminary results
[NASA-TM-88980] p 127 N87-22097
- Analysis of an advanced technology subsonic turbofan incorporating revolutionary materials
[NASA-TM-89868] p 29 N87-22680
- Supersonic through-flow fan design
[NASA-TM-88908] p 29 N87-22681
- The supersonic through-flow turbofan for high Mach propulsion
[NASA-TM-100114] p 30 N87-23626
- Aviation fuel property effects on altitude relight
[NASA-CR-179582] p 107 N87-24578
- Effect of variable inlet guide vanes on the operating characteristics of a tilt nacelle inlet/powered fan model
[NASA-TM-88983] p 14 N87-27628
- Advanced Propfan Engine Technology (APET) and single-rotation gearbox/pitch change mechanism
[NASA-CR-168113] p 32 N87-28553
- Airflow calibration and exhaust pressure/temperature survey of an F404, S/N 215-109, turbofan engine
[NASA-TM-100159] p 33 N87-29537

- Turbofan aft duct suppressor study. Contractor's data report of mode probe signal data
[NASA-CR-175067] p 34 N87-29538
- Turbofan aft duct suppressor study
[NASA-CR-175067] p 34 N87-29539
- TURBOFANS**
- Modeling the effects of wind tunnel wall absorption on the acoustic radiation characteristics of propellers
[AIAA PAPER 86-1876] p 208 A87-17991
- Supersonic through-flow fan design
[AIAA PAPER 87-1746] p 22 A87-48571
- Measurements of the unsteady flow field within the stator row of a transonic axial-flow fan. 1: Measurement and analysis technique
[NASA-TM-88945] p 10 N87-16789
- Supersonic through-flow fan design
[NASA-TM-88908] p 29 N87-22681
- TURBOJET ENGINES**
- Measurement uncertainty for the Uniform Engine Testing Program conducted at NASA Lewis Research Center
[NASA-TM-88943] p 33 N87-28557
- Thin film strain gage development program
[NASA-CR-174707] p 159 N87-28883
- TURBOMACHINE BLADES**
- Development of a turbomachinery design optimization procedure using a multiple-parameter nonlinear perturbation method
[NASA-CR-3831] p 1 N87-10003
- TURBOMACHINERY**
- The utilization of parallel processing in solving the inviscid form of the average-passage equation system for multistage turbomachinery
[AIAA PAPER 87-1108] p 5 A87-42057
- Composite grid and finite-volume LU implicit scheme for turbine flow analysis
[AIAA PAPER 87-1129] p 5 A87-42078
- Analysis of experimental shaft seal data for high-performance turbomachines - As for Space Shuttle main engines
p 162 A87-45846
- Evaluation of seals for high-performance cryogenic turbomachines
[NASA-TM-88919] p 146 N87-15442
- A method for calculating turbulent boundary layers and losses in the flow channels of turbomachines
[NASA-TM-88928] p 9 N87-15944
- Generation of a composite grid for turbine flows and consideration of a numerical scheme
p 11 N87-17662
- Composite grid and finite-volume LU implicit scheme for turbine flow analysis
[NASA-TM-88928] p 12 N87-20235
- Laser fringe anemometry for aero engine components
p 110 N87-21176
- Rotordynamic Instability Problems in High-Performance Turbomachinery, 1986
[NASA-CP-2443] p 167 N87-22199
- Unsteady stator/rotor interaction
p 149 N87-22767
- A linearized Euler analysis of unsteady flows in turbomachinery
[NASA-CR-180987] p 149 N87-22948
- Three-step labyrinth seal for high-performance turbomachines
[NASA-TP-1848] p 150 N87-23921
- Straight cylindrical seal for high-performance turbomachines
[NASA-TP-1850] p 150 N87-23936
- Design and performance of controlled-diffusion stator compared with original double-circular-arc stator
[NASA-TM-100141] p 31 N87-26910
- TURBOPROP AIRCRAFT**
- Structureborne noise control in advanced turboprop aircraft
[AIAA PAPER 87-0530] p 209 A87-31110
- Euler analysis of transonic propeller flows
p 4 A87-39813
- Concentrated mass effects on the flutter of a composite advanced turboprop model
[NASA-TM-88854] p 180 N87-12017
- Structureborne noise control in advanced turboprop aircraft
[NASA-TM-88947] p 211 N87-16587
- Coupled aerodynamic and acoustical predictions for turboprops
[NASA-TM-87094] p 13 N87-23598
- Analysis and test evaluation of the dynamic response and stability of three advanced turboprop models
[NASA-CR-174814] p 32 N87-28555
- TURBOPROP ENGINES**
- An overview of the small engine component technology (SECT) studies --- commuter, rotorcraft, cruise missile and auxiliary power applications in year 2000
[AIAA PAPER 86-1542] p 19 A87-17993
- A numerical simulation of the inviscid flow through a counterrotating propeller
[ASME PAPER 86-GT-138] p 3 A87-25395
- Structural tailoring of advanced turboprops
[AIAA PAPER 87-0753] p 177 A87-33648
- Wind tunnel performance results of an aeroelastically scaled 2/9 model of the PTA flight test prop-fan
[AIAA PAPER 87-1893] p 8 A87-52251
- Strategic plan, 1985
[NASA-TM-89263] p 219 N87-12384
- Dynamic response of two composite prop-fan models on a nacelle/wing/fuselage half model
[NASA-CR-179589] p 18 N87-23615
- Wind tunnel performance results of an aeroelastically scaled 2/9 model of the PTA flight test prop-fan
[NASA-TM-89917] p 14 N87-25294
- Advanced Propfan Engine Technology (APET) and single-rotation gearbox/pitch change mechanism
[NASA-CR-168113] p 32 N87-28553
- Advanced Propfan Engine Technology (APET) definition study, single and counter-rotation gearbox/pitch change mechanism design
[NASA-CR-168115] p 32 N87-28554
- TURBORAMJET ENGINES**
- A parametric study of a gas-generator airturbo ramjet (ATR)
[AIAA PAPER 86-1681] p 20 A87-41156
- TURBOSHAFTS**
- Contingency power for small turboshaft engines using water injection into turbine cooling air
[AIAA PAPER 87-1906] p 21 A87-45289
- Contingency power for small turboshaft engines using water injection into turbine cooling air
[NASA-TM-89817] p 28 N87-20280
- TURBULENCE**
- User's manual for a TEACH computer program for the analysis of turbulent, swirling reacting flow in a research combustor
[NASA-CR-179547] p 78 N87-11858
- Measurement of heat transfer and pressure drop in rectangular channels with turbulence promoters
[NASA-CR-4015] p 146 N87-17003
- Flowfield measurements in a separated and reattached flat plate turbulent boundary layer
[NASA-CR-4052] p 148 N87-21257
- Direct numerical simulations of a temporally evolving mixing layer subject to forcing
[NASA-TM-88896] p 150 N87-23933
- Application of turbulence modeling to predict surface heat transfer in stagnation flow region of circular cylinder
[NASA-TP-2758] p 151 N87-27161
- TURBULENCE EFFECTS**
- Jet model for slot film cooling with effect of free-stream and coolant turbulence
[NASA-TP-2655] p 146 N87-18034
- Experimental evaluation of honeycomb/screen configurations and short contraction section for NASA Lewis Research Center's altitude wind tunnel
[NASA-TP-2692] p 36 N87-23662
- Initial turbulence effect on jet evolution with and without tonal excitation
[NASA-TM-100178] p 14 N87-27629
- TURBULENCE BOUNDARY LAYER**
- Prediction and rational correlation of thermophoretically reduced particle mass transfer to hot surfaces across laminar or turbulent forced-convection gas boundary layers
p 133 A87-23449
- Investigation of two-dimensional shock-wave/boundary-layer interactions
p 4 A87-39528
- An experimental study of the development of longitudinal vortex pairs embedded in a turbulent boundary layer
[AIAA PAPER 87-1309] p 139 A87-42376
- A critical analysis of transverse vorticity measurements in a large plane shear layer
p 143 A87-52049
- A method for calculating turbulent boundary layers and losses in the flow channels of turbomachines
[NASA-TM-88928] p 9 N87-15944
- Turbulence modeling and surface heat transfer in a stagnation flow region
[NASA-TM-100132] p 151 N87-26302
- TURBULENCE DIFFUSION**
- On self-preserving, variable-density, turbulent free jets
p 130 A87-10920
- Comparisons between thermodynamic and one-dimensional combustion models of spark-ignition engines
p 161 A87-29275
- TURBULENCE FLOW**
- Two-phase flow measurements of a spray in a turbulent flow
[AIAA PAPER 87-0062] p 132 A87-22388
- Laser velocimetry in turbulent flow fields - Particle response
[AIAA PAPER 87-0118] p 132 A87-22426
- Coherent structures and turbulence
p 133 A87-22859
- Turbulence modeling for complex shear flows
p 133 A87-23653
- Coherent motion in excited free shear flows
[AIAA PAPER 85-0539] p 135 A87-30281
- An anemometer for highly turbulent or recirculating flows
p 154 A87-37698
- Fast algorithm for calculating chemical kinetics in turbulent reacting flow
p 77 A87-38958
- Two component laser velocimeter measurements of turbulence parameters downstream of an axisymmetric sudden expansion
p 139 A87-40703
- Turbulent solutions of the Navier-Stokes equations
p 139 A87-40932
- Computation of rotating turbulent flow with an algebraic Reynolds stress model
p 140 A87-43384
- Numerical prediction of cold turbulent flow in combustor configurations with different centerbody flame holders
[ASME PAPER 86-WA/HT-50] p 140 A87-37115
- On direct numerical simulations of turbulent reacting flows
[AIAA PAPER 87-1324] p 140 A87-44930
- Mass and momentum turbulent transport experiments
p 144 N87-11201
- Third-moment closure of turbulence for predictions of separating and reattaching shear flows: A study of Reynolds-stress closure model
[NASA-CR-177055] p 145 N87-11961
- A method for calculating turbulent boundary layers and losses in the flow channels of turbomachines
[NASA-TM-88928] p 9 N87-15944
- Four spot laser anemometer and optical access techniques for turbine applications
[NASA-TM-88972] p 156 N87-18057
- Modeling turbulent, reacting flow
p 147 N87-20270
- On the modelling of non-reactive and reactive turbulent combustor flows
[NASA-CR-4041] p 28 N87-20996
- Progress in the prediction of unsteady heat transfer on turbine blades
p 149 N87-22769
- Experimental evaluation of honeycomb/screen configurations and short contraction section for NASA Lewis Research Center's altitude wind tunnel
[NASA-TP-2692] p 36 N87-23662
- Multispecies CARS measurements in turbulent combustion
p 79 N87-23808
- Thermodynamic evaluation of transonic compressor rotors using the finite volume approach
[NASA-CR-180587] p 150 N87-23925
- On the coalescence-dispersion modeling of turbulent molecular mixing
[NASA-TM-89910] p 2 N87-25292
- Turbulence modeling and surface heat transfer in a stagnation flow region
[NASA-TM-100132] p 151 N87-26302
- Aeroacoustics of subsonic turbulent shear flows
[NASA-TM-100165] p 212 N87-26615
- Studies of unsteady viscous flows using a two-equation model of turbulence
[NASA-CR-181293] p 152 N87-27949
- Turbulence characteristics of an axisymmetric reacting flow
[NASA-CR-180697] p 152 N87-27973
- Vortex-scalar element calculations of a diffusion flame stabilized on a plane mixing layer
[NASA-TM-100133] p 2 N87-28501
- TURBULENCE HEAT TRANSFER**
- On similarity solutions for turbulent and heated round jets
p 130 A87-10922
- Turbulent heat transfer in corrugated wall channels with and without fins
p 134 A87-27709
- TURBULENCE JETS**
- On self-preserving, variable-density, turbulent free jets
p 130 A87-10920
- On similarity solutions for turbulent and heated round jets
p 130 A87-10922
- Multi-spark visualization of typical combustor flowfields
p 134 A87-25281
- The near field behavior of turbulent gas jets in a long confinement
p 135 A87-28976
- The evolution of instabilities in the axisymmetric jet. I - The linear growth of disturbances near the nozzle. II - The flow resulting from the interaction between two waves
p 138 A87-37256
- Mass and momentum turbulent transport experiments
p 144 N87-11201
- Initial turbulence effect on jet evolution with and without tonal excitation
[NASA-TM-100178] p 14 N87-27629
- Controlled excitation of a cold turbulent swirling free jet
[NASA-TM-100173] p 152 N87-27977
- TURBULENCE MIXING**
- On similarity solutions for turbulent and heated round jets
p 130 A87-10922
- Mechanisms by which heat release affects the flow field in a chemically reacting, turbulent mixing layer
[AIAA PAPER 87-0131] p 134 A87-24925

Fuel-air mixing and combustion in a two-dimensional Wankel engine
[SAE PAPER 870408] p 163 A87-48783

TURBULENT WAKES

Comparison of pressure-strain correlation models for the flow behind a disk p 131 A87-20897
Two-phase measurements of a spray in the wake of a bluff body p 142 A87-46199

TWISTING

Three-dimensional vibrations of twisted cantilevered parallelepipeds p 173 A87-11106

TWO DIMENSIONAL BODIES

Secondary stream and excitation effects on two-dimensional nozzle plume characteristics
[AIAA PAPER 87-2112] p 6 A87-45414
Secondary stream and excitation effects on two-dimensional nozzle plume characteristics
[NASA-TM-89813] p 12 A87-18539

TWO DIMENSIONAL FLOW

Finite analytic numerical solution of two-dimensional channel flow over a backward-facing step p 131 A87-13506

A two-dimensional numerical study of the flow inside the combustion chamber of a motored rotary engine
[SAE PAPER 860615] p 161 A87-28624

Two- and three-dimensional viscous computations of a hypersonic inlet flow
[AIAA PAPER 87-0283] p 4 A87-31106
Adaptive finite element methods for compressible flow problems p 4 A87-38496
Time-marching solution of incompressible Navier-Stokes equations for internal flow p 138 A87-39450
Investigation of two-dimensional shock-wave/boundary-layer interactions p 4 A87-39528

Heat transfer and fluid mechanics measurements in transitional boundary layers on convex-curved surfaces
[ASME PAPER 85-MT-60] p 143 A87-48726
Simultaneous measurements of two-dimensional velocity and pressure fields in compressible flows through image-intensified detection of laser-induced fluorescence p 143 A87-52320

Computation of multi-dimensional viscous supersonic jet flow
[NASA-CR-4020] p 8 A87-13405

Computation of multi-dimensional viscous supersonic flow
[NASA-CR-4021] p 9 A87-13406

Two- and three-dimensional viscous computations of a hypersonic inlet flow
[NASA-TM-88923] p 146 A87-15441

TWO DIMENSIONAL JETS

Two-dimensional nozzle plume characteristics
[AIAA PAPER 87-2111] p 6 A87-45413
Two-dimensional nozzle plume characteristics
[NASA-TM-89812] p 12 A87-18540

TWO PHASE FLOW

Two-phase flow measurements of a spray in a turbulent flow
[AIAA PAPER 87-0062] p 132 A87-22388
Navier Stokes solution of the flowfield over ice accretion shapes
[AIAA PAPER 87-0099] p 2 A87-22414
Laser velocimetry in turbulent flow fields - Particle response
[AIAA PAPER 87-0118] p 132 A87-22426

Two-phase flows and heat transfer within systems with ambient pressure above the thermodynamic critical pressure p 136 A87-30728
Gas particle radiator p 141 A87-45646

Finite difference solution for a generalized Reynolds equation with homogeneous two-phase flow p 141 A87-45851

Two-phase measurements of a spray in the wake of a bluff body p 142 A87-46199

Two-phase flow p 147 A87-20272

U**UH-60A HELICOPTER**

Gear tooth stress measurements on the UH-60A helicopter transmission
[NASA-TP-2698] p 167 A87-22235

A rotorcraft flight/propulsion control integration study
[NASA-CR-179574] p 18 A87-24457

ULTRASONIC FLAW DETECTION

Quantitative void characterization in structural ceramics by use of scanning laser acoustic microscopy p 171 A87-51974

Ultrasonic determination of recrystallization
[NASA-TM-88855] p 171 A87-10399

ULTRASONIC RADIATION

Ultrasonic verification of microstructural changes due to heat treatment p 208 A87-10772

Ultrasonic determination of recrystallization
[NASA-TM-88855] p 171 A87-10399

ULTRASONIC TESTS

Nondestructive evaluation of adhesive bond strength using the stress wave factor technique p 170 A87-32200

Modes of vibration on square fiberglass epoxy composite thick plate
[NASA-CR-4018] p 171 A87-13779

Ultrasonic determination of the elastic constants of the stiffness matrix for unidirectional fiberglass epoxy composites
[NASA-CR-4034] p 171 A87-13781

Nondestructive evaluation of structural ceramics
[NASA-TM-88978] p 172 A87-18109

Ultrasonic NDE of structural ceramics for power and propulsion systems
[NASA-TM-100147] p 173 A87-26362

ULTRASONIC WAVE TRANSDUCERS

In-flight measurement of ice growth on an airfoil using an array of ultrasonic transducers
[AIAA PAPER 87-0178] p 15 A87-22464

ULTRASONICS

Ultrasonic verification of microstructural changes due to heat treatment p 208 A87-10772

The acousto-ultrasonic approach
[NASA-TM-89843] p 172 A87-20562

Ray propagation path analysis of acousto-ultrasonic signals in composites
[NASA-TM-100148] p 173 A87-25589

Acousto-ultrasonic input-output characterization of unidirectional fiber composite plate by SH waves
[NASA-CR-4087] p 173 A87-26361

UNIVERSE

The large-scale peculiar velocity field in flat models of the universe p 223 A87-40651

UNSTEADY FLOW

Numerical simulation of excited jet mixing layers
[AIAA PAPER 87-0016] p 131 A87-22361
Aircraft turbofan noise p 209 A87-31144

Numerical simulation of the flowfield in a motored two-dimensional Wankel engine p 138 A87-39812

Three-dimensional unsteady Euler solutions for propfans and counter-rotating propfans in transonic flow
[AIAA PAPER 87-1197] p 5 A87-42314

Aeroelastic control of stability and forced response of supersonic rotors by aerodynamic detuning p 21 A87-46249

Measurements of the unsteady flow field within the stator row of a transonic axial-flow fan. 1: Measurement and analysis technique
[NASA-TM-88945] p 10 A87-16789

Measurements of the unsteady flow field within the stator row of a transonic axial-flow fan. Part 2: Results and discussion
[NASA-TM-88946] p 10 A87-16790

Unsteady flows in a single-stage transonic axial-flow fan stator row
[NASA-TM-88929] p 11 A87-16805

A general method for unsteady stagnation region heat transfer and results for model turbine flows
[NASA-TM-88903] p 146 A87-17002

Unsteady stator/rotor interaction p 149 A87-22767

A linearized Euler analysis of unsteady flows in turbomachinery
[NASA-CR-180987] p 149 A87-22948

Calculations of inlet distortion induced compressor flowfield instability p 30 A87-24470

Studies of unsteady viscous flows using a two-equation model of turbulence
[NASA-CR-181293] p 152 A87-27949

UPLINKING

Engineering calculations for communications satellite systems planning
[NASA-CR-181112] p 117 A87-24605

USER MANUALS (COMPUTER PROGRAMS)

ANL/RBC: A computer code for the analysis of Rankine bottoming cycles, including system cost evaluation and off-design performance
[NASA-CR-179462] p 220 A87-10777

User's manual for a TEACH computer program for the analysis of turbulent, swirling reacting flow in a research combustor
[NASA-CR-179547] p 78 A87-11858

Expansion of epicyclic gear dynamic analysis program
[NASA-CR-179563] p 166 A87-19723

Lewis inverse design code (LINDES): Users manual
[NASA-TP-2676] p 12 A87-20238

Development of a rotor wake/vortex model. Volume 2: User's manual for computer program
[NASA-CR-174850-VOL-2] p 13 A87-20239

A NASTRAN primer for the analysis of rotating flexible blades
[NASA-TM-89861] p 184 A87-21375

SINDA-NASTRAN interfacing program theoretical description and user's manual
[NASA-TM-100158] p 187 A87-27268

USER REQUIREMENTS

Space station experiment definition: Advanced power system test bed
[NASA-CR-179502] p 58 A87-15270

User evaluation of photovoltaic-powered vaccine refrigerator/freezer systems
[NASA-TM-88830] p 193 A87-18230

Advanced space communications architecture study. Volume 2: Technical report
[NASA-CR-179592] p 115 A87-18695

V**VACCINES**

User evaluation of photovoltaic-powered vaccine refrigerator/freezer systems
[NASA-TM-88830] p 193 A87-18230

VACUUM MELTING

Analysis of the solidified structure of rheocast and VADER processed nickel-base superalloy p 83 A87-28734

VANADIUM

Shot peening for Ti-6Al-4V alloy compressor blades
[NASA-TP-2711] p 184 A87-20566

VANES

Advances in 3-D Inelastic Analysis Methods for hot section components
[AIAA PAPER 87-0719] p 177 A87-33645

Experimental evaluation of two turning vane designs for fan drive corner of 0.1-scale model of NASA Lewis Research Center's proposed altitude wind tunnel
[NASA-TP-2646] p 35 A87-18576

Use of a liquid-crystal, heater-element composite for quantitative, high-resolution heat transfer coefficients on a turbine airfoil, including turbulence and surface roughness effects
[NASA-TM-87355] p 158 A87-22181

Experimental evaluation of corner turning vanes
[NASA-TM-100143] p 37 A87-28571

High temperature static strain gage development contract, tasks 1 and 2
[NASA-CR-180811] p 159 A87-28869

VAPOR DEPOSITION

Formation of a pn junction on an anisotropically etched GaAs surface using metalorganic chemical vapor deposition p 216 A87-21237

Modeling free convective gravitational effects in chemical vapor deposition
[AIAA PAPER 87-0313] p 133 A87-22552

Shallow n(+) diffusion into InP by an open-tube diffusion technique p 217 A87-30023

Nonlinear absorption in AlGaAs/GaAs multiple quantum well structures grown by metalorganic chemical vapor deposition p 217 A87-39687

TEM investigation of beta-SiC grown epitaxially on Si substrate by CVD p 97 A87-40927

Comment on 'Temperature dependence of electrical properties of non-doped and nitrogen-doped beta-SiC single crystals grown by chemical vapor deposition' p 217 A87-42846

Experimental verification of corrosive vapor deposition rate theory in high velocity burner rigs p 143 A87-49551

Indium phosphide shallow homojunction solar cells made by metalorganic chemical vapor deposition p 123 A87-50047

Experimental verification of vapor deposition model in Mach 0.3 burner rigs p 88 A87-11192

The 60 GHz IMPATT diode development
[NASA-CR-179536] p 218 A87-17515

AlGaAs growth by OMCVD using an excimer laser
[NASA-TM-88937] p 218 A87-23304

High-efficiency GaAs concentrator space cells p 196 A87-26417

Status of indium phosphide solar cell development at Spire p 197 A87-26440

VAPOR PHASE EPITAXY

Antiphase boundaries in epitaxially grown beta-SiC p 217 A87-30025

VAPOR PHASES

Two-phase measurements of a spray in the wake of a bluff body p 142 A87-46199

VAPORIZING

Agreement between experimental and theoretical effects of nitrogen gas flowrate on liquid jet atomization
[AIAA PAPER 87-2138] p 141 A87-45427

Agreement between experimental and theoretical effects of nitrogen gas flowrate on liquid jet atomization
[NASA-TM-89821] p 156 A87-19684

VARIABILITY

- Component variations and their effects on bipolar nickel-hydrogen cell performance
[NASA-TM-89907] p 195 N87-23029
- Effect of variable inlet guide vanes on the operating characteristics of a tilt nacelle inlet/powered fan model
[NASA-TM-88983] p 14 N87-27628

VARIABLE GEOMETRY STRUCTURES

- A versatile and low order hybrid stress element for general shell geometry
[AIAA PAPER 87-0840] p 176 A87-33624
- A variable geometry combustor for broadened properties fuels
[AIAA PAPER 87-1832] p 23 A87-52246

VARIABLE STREAM CONTROL ENGINES

- Outdoor test stand performance of a convertible engine with variable inlet guide vanes for advanced rotorcraft propulsion
[NASA-TM-88939] p 26 N87-16825

VARIABLE THRUST

- High heat transfer oxidizer heat exchanger design and analysis — RL10-2B engine
[NASA-CR-179596] p 63 N87-22803

VARIATIONAL PRINCIPLES

- On the numerical performance of three-dimensional thick shell elements using a hybrid/mixed formulation
p 175 A87-25924
- A probabilistic Hu-Washizu variational principle
[AIAA PAPER 87-0764] p 176 A87-33579
- An efficient quadrilateral element for plate bending analysis
p 178 A87-45994

VECTORS (MATHEMATICS)

- Extrapolation methods for vector sequences
p 203 A87-53631

VELOCITY

- Experimental verification of corrosive vapor deposition rate theory in high velocity burner rigs
p 143 A87-49551
- An investigation of the dynamic response of spur gear teeth with moving loads
[NASA-CR-179643] p 170 N87-29840

VELOCITY DISTRIBUTION

- The large-scale peculiar velocity field in flat models of the universe
p 223 A87-40651
- Radiative cooling of a layer with nonuniform velocity - A separable solution
p 141 A87-45637

VELOCITY MEASUREMENT

- Measurement of a counter rotation propeller flowfield using a Laser Doppler Velocimeter
[AIAA PAPER 87-0008] p 3 A87-24901
- Simultaneous measurements of two-dimensional velocity and pressure fields in compressible flows through image-intensified detection of laser-induced fluorescence
p 143 A87-52320
- Velocity profiles in laminar diffusion flames
[NASA-TP-2596] p 147 N87-18035
- Combined fringe and Fabry-Perot laser anemometer for 3 component velocity measurements in turbine stator cascade facility
p 110 N87-21183
- Thermocapillary bubble migration for large Marangoni Numbers
[NASA-CR-179628] p 109 N87-22865

VERSATILITY

- 20 kHz Space Station power system
p 51 A87-40378

VERTICAL LANDING

- Hot gas ingestion: From model results to full scale engine testing
p 30 N87-24419

VERTICAL TAKEOFF AIRCRAFT

- Effect of variable inlet guide vanes on the operating characteristics of a tilt nacelle inlet/powered fan model
[NASA-TM-88983] p 14 N87-27628

VERY LARGE SCALE INTEGRATION

- A high quality image compression scheme for real-time applications
p 111 A87-30801

VIBRATION

- Hub flexibility effects on propfan vibration
[NASA-TM-89900] p 186 N87-24722
- Propfan test assessment testbed aircraft flutter model test report
[NASA-CR-179458] p 14 N87-29413

VIBRATION DAMPING

- Experiments on dynamic stiffness and damping of tapered bore seals
[NASA-TM-89895] p 169 N87-23984

VIBRATION EFFECTS

- Analysis of the vibratory excitation arising from spiral bevel gears
[NASA-CR-4081] p 169 N87-25579

VIBRATION ISOLATORS

- SSME blade damper technology
p 63 N87-22798

VIBRATION MEASUREMENT

- Testing of UH-60A helicopter transmission in NASA Lewis 2240-kW (3000-hp) facility
[NASA-TP-2626] p 164 N87-10391

- A low-cost optical data acquisition system for vibration measurement
[NASA-TM-88907] p 181 N87-14730
- Vibration characteristics of OH-58A helicopter main rotor transmission
[NASA-TP-2705] p 167 N87-20555
- Experimental and analytical evaluation of dynamic load and vibration of a 2240-kW (300-hp) rotorcraft transmission
[NASA-TM-88975] p 167 N87-20556

VIBRATION MODE

- Modeling of multi-rotor torsional vibrations in rotating machinery using substructuring
p 175 A87-28543
- Modes of vibration on square fiberglass epoxy composite thick plate
[NASA-CR-4018] p 171 N87-13779

VIBRATIONAL STRESS

- Effect of vibration amplitude on vapor cavitation in journal bearings
[NASA-TM-88826] p 145 N87-11962

VIBRATORY LOADS

- Effect of angular inflow on the vibratory response of a counter-rotating propeller
[NASA-CR-174819] p 8 N87-10840

VIEWING

- Hot section viewing system
[NASA-CR-174773] p 155 N87-11144

VISCOELASTICITY

- Bounding solutions of geometrically nonlinear viscoelastic problems
p 174 A87-20892
- Solution methods for one-dimensional viscoelastic problems
[AIAA PAPER 87-0804] p 176 A87-33604

VISCOMETERS

- Viscometer for low frequency, low shear rate measurements
p 153 A87-13878

VISCOPLASTICITY

- Thermodynamically consistent constitutive equations for nonisothermal large-strain, elastoplastic, creep behavior
p 175 A87-27945
- Non-isothermal elastoviscoplastic snap-through and creep buckling of shallow arches
[AIAA PAPER 87-0806] p 176 A87-33605
- A viscoplastic constitutive theory for metal matrix composites at high temperature
[NASA-CR-179530] p 180 N87-13790
- Analysis of shell-type structures subjected to time-dependent mechanical and thermal loading
[NASA-CR-180349] p 183 N87-19756
- Nonisothermal elasto-visco-plastic response of shell-type structures
p 185 N87-22796
- Finite element implementation of Robinson's unified viscoplastic model and its application to some uniaxial and multiaxial problems
[NASA-TM-89891] p 185 N87-23010
- Thermo-elasto-viscoplastic analysis of problems in extension and shear
[NASA-CR-181410] p 187 N87-29896

VISCOUS FLOW

- Two- and three-dimensional viscous computations of a hypersonic inlet flow
[AIAA PAPER 87-0283] p 4 A87-31106
- Analysis of viscous transonic flow over airfoil sections
[AIAA PAPER 87-0420] p 4 A87-34723
- Gas flow environmental and heat transfer nonrotating 3D program
p 145 N87-11223
- Computation of multi-dimensional viscous supersonic jet flow
[NASA-CR-4020] p 8 N87-13405
- Computation of multi-dimensional viscous supersonic flow
[NASA-CR-4021] p 9 N87-13406
- Viscous analyses for flow through subsonic and supersonic intakes
[NASA-TM-88831] p 9 N87-15173
- Two- and three-dimensional viscous computations of a hypersonic inlet flow
[NASA-TM-88923] p 146 N87-15441
- Analysis of viscous transonic flow over airfoil sections
[NASA-TM-88912] p 146 N87-17001
- Thermodynamic evaluation of transonic compressor rotors using the finite volume approach
[NASA-CR-180587] p 150 N87-23925
- Viscous analyses for flow through subsonic and supersonic intakes
p 30 N87-24469
- Studies of unsteady viscous flows using a two-equation model of turbulence
[NASA-CR-181293] p 152 N87-27949

VOIDS

- Probability of detection of internal voids in structural ceramics using microfocus radiography
p 170 A87-14300
- Quantitative void characterization in structural ceramics by use of scanning laser acoustic microscopy
p 171 A87-51974

VOLATILITY

- The formation of volatile corrosion products during the mixed oxidation-chlorination of cobalt at 650 C
p 82 A87-23848

VOLT-AMPERE CHARACTERISTICS

- Proposal for superstructure based high efficiency photovoltaics
p 120 A87-19104
- Microwave performance of a quarter-micrometer gate low-noise pseudomorphic InGaAs/AlGaAs modulation-doped field effect transistor
p 121 A87-23745
- Characterization of InGaAs/AlGaAs pseudomorphic modulation-doped field-effect transistors
p 121 A87-23922

- Low power dc arcjet operation with hydrogen/nitrogen/ammonia mixtures
[AIAA PAPER 87-1948] p 53 A87-48575
- Modeling for CO poisoning of a fuel cell anode
p 191 A87-52288

- Low power DC arcjet operation with hydrogen/nitrogen/ammonia mixtures
[NASA-TM-89876] p 64 N87-22804

VORTEX GENERATORS

- Development and testing of vortex generators for small horizontal axis wind turbines
[NASA-CR-179514] p 193 N87-18922
- Surface pressure measurements on the blade of an operating Mod-2 wind turbine with and without vortex generators
[NASA-TM-89903] p 198 N87-26455

VORTEX SHEDDING

- Rotor wake characteristics of a transonic axial-flow fan
p 2 A87-20886
- A comparative study of some dynamic stall models
[NASA-TM-88917] p 183 N87-18883

VORTICES

- Endwall heat transfer in the junction region of a circular cylinder normal to a flat plate at 30 and 60 degrees from stagnation point of the cylinder
[AIAA PAPER 87-0077] p 132 A87-22398
- Effect of a rotor wake on the local heat transfer on the forward half of a circular cylinder
p 136 A87-30721

- An experimental study of the development of longitudinal vortex pairs embedded in a turbulent boundary layer
[AIAA PAPER 87-1309] p 139 A87-42376
- Development of a rotor wake/vortex model. Volume 2: User's manual for computer program
[NASA-CR-174850-VOL-2] p 13 N87-20239
- Vortex-scalar element calculations of a diffusion flame stabilized on a plane mixing layer
[NASA-TM-100133] p 2 N87-28501
- Enhanced mixing of an axisymmetric jet by aerodynamic excitation
[NASA-CR-175059] p 15 N87-29418

VORTICITY

- The flame structure and vorticity generated by a chemically reacting transverse jet
p 76 A87-14116
- Perfect gas effects in compressible rapid distortion theory
p 136 A87-31176
- A critical analysis of transverse vorticity measurements in a large plane shear layer
p 143 A87-52049

W**WAFERS**

- The 60 GHz IMPATT diode development
[NASA-CR-179536] p 218 N87-17515
- Solar cells in bulk InP using an open tube diffusion process
p 198 N87-26444

WAKES

- Rotor wake characteristics of a transonic axial-flow fan
p 2 A87-20886
- Unsteady heat transfer and direct comparison to steady-state measurements in a rotor-wake experiment
p 136 A87-30720
- Measurements of plasma density and turbulence near the shuttle orbiter
[NASA-CR-180102] p 215 N87-16614

WALL FLOW

- The hub wall boundary layer development and losses in an axial flow compressor rotor passage
p 139 A87-41665
- Transonic interference reduction by limited ventilation wall panels
[NASA-CR-175039] p 15 N87-29419

WALL JETS

- Jet model for slot film cooling with effect of free-stream and coolant turbulence
[NASA-TP-2655] p 146 N87-18034

WALL TEMPERATURE

- Experimental evaluation of heat transfer on a 1030:1 area ratio rocket nozzle
[AIAA PAPER 87-2070] p 55 A87-52249

- Enhanced heat transfer combustor technology, subtasks 1 and 2, test C.1
[NASA-CR-179541] p 56 N87-13486
- Experimental evaluation of heat transfer on a 1030:1 area ratio rocket nozzle
[NASA-TP-2726] p 67 N87-25424
- WANKEL ENGINES**
- Numerical simulation of the flowfield in a motored two-dimensional Wankel engine p 138 A87-39812
- Fuel-air mixing and combustion in a two-dimensional Wankel engine
[SAE PAPER 870408] p 163 A87-48783
- WASTE ENERGY UTILIZATION**
- A design study of hydrazine and biowaste resistojets
[NASA-CR-179510] p 57 N87-14425
- Technical and economic study of Stirling and Rankine cycle bottoming systems for heavy truck diesel engines
[NASA-CR-180833] p 222 N87-28470
- WASTE HEAT**
- Transient radiative cooling of a droplet-filled layer
p 135 A87-27712
- WATER**
- Jet engine simulation with water ingestion through compressor
[NASA-CR-179549] p 1 N87-15932
- Water-propellant resistojets for man-tended platforms
[NASA-TM-100110] p 68 N87-26135
- WATER INJECTION**
- Contingency power for small turboshaft engines using water injection into turbine cooling air
[AIAA PAPER 87-1906] p 21 A87-45289
- Investigation of a repetitive pulsed electrothermal thruster
[NASA-CR-179464] p 59 N87-16878
- Contingency power for small turboshaft engines using water injection into turbine cooling air
[NASA-TM-89817] p 28 N87-20280
- WATER RESOURCES**
- Design, development and deployment of public service photovoltaic power/load systems for the Gabonese Republic
[NASA-CR-179603] p 195 N87-23030
- WAVE ATTENUATION**
- Ultrasonic verification of microstructural changes due to heat treatment p 208 A87-10772
- Ultrasonic determination of recrystallization
[NASA-TM-88855] p 171 N87-10399
- WAVE DISPERSION**
- Swept frequency technique for dispersion measurement of microstrip lines
[AD-P005420] p 118 N87-27848
- WAVE GENERATION**
- A note on the generation of Tollmien-Schlichting waves by sudden surface-curvature change p 144 A87-54366
- WAVE INTERACTION**
- Rays versus modes - Pictorial display of energy flow in an open-ended waveguide p 112 A87-44075
- WAVE PROPAGATION**
- DOE/NASA automotive Stirling engine project - Overview 86 p 220 A87-18034
- Forced cocurrent smoldering combustion p 77 A87-40572
- Generation of Tollmien-Schlichting waves on interactive marginally separated flows p 144 A87-54365
- Propagation of sound waves in tubes of noncircular cross section
[NASA-TP-2601] p 9 N87-14284
- Finite element modeling of electromagnetic propagation in composite structures
[NASA-TM-88916] p 207 N87-14956
- Finite element analysis of electromagnetic propagation in an absorbing wave guide
[NASA-TM-88866] p 207 N87-18391
- Propagation characteristics of some novel coplanar waveguide transmission lines on GaAs at MM-wave frequencies
[NASA-TM-89839] p 126 N87-20469
- One-dimensional wave propagation in rods of variable cross section: A WKBJ solution
[NASA-CR-4086] p 172 N87-24707
- A finite element model for wave propagation in an inhomogeneous material including experimental validation
[NASA-TM-100149] p 207 N87-25821
- Computer control of a scanning electron microscope for digital image processing of thermal-wave images
[NASA-TM-100157] p 128 N87-26278
- WAVE SCATTERING**
- The finite-difference time-domain (FD-TD) method for electromagnetic scattering and interaction problems p 113 A87-51403
- WAVEGUIDES**
- Rays versus modes - Pictorial display of energy flow in an open-ended waveguide p 112 A87-44075

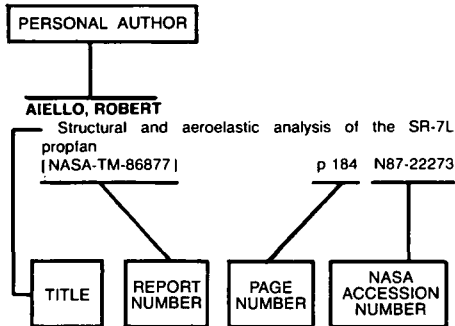
- A new model for broadband waveguide to microstrip transition design
[NASA-TM-88905] p 115 N87-16958
- Finite element analysis of electromagnetic propagation in an absorbing wave guide
[NASA-TM-88866] p 207 N87-18391
- Propagation characteristics of some novel coplanar waveguide transmission lines on GaAs at MM-wave frequencies
[NASA-TM-89839] p 126 N87-20469
- Reduction of the radar cross section of arbitrarily shaped cavity structures
[NASA-CR-180307] p 118 N87-27085
- WEAR**
- Tribology of selected ceramics at temperatures to 900 C p 94 A87-12954
- Microstructure and surface chemistry of amorphous alloys important to their friction and wear behavior p 81 A87-15186
- Effects of silver and group II fluoride solid lubricant additions to plasma-sprayed chromium carbide coatings for foil gas bearings to 650 C p 95 A87-22336
- Counterface effects on the tribological properties of polyimide composites p 95 A87-27625
- Composition optimization of self-lubricating chromium-carbide-based composite coatings for use to 760 C p 96 A87-27838
- How to evaluate solid lubricant films using a Pin-on-disk tribometer p 97 A87-42618
- Effects of atmosphere on the tribological properties of a chromium carbide based coating for use to 760 deg C
[NASA-TM-88894] p 101 N87-16140
- Tribological properties of polymer films and solid bodies in a vacuum environment p 101 N87-17906
- Friction and wear of sintered Alpha SiC sliding against IN-718 alloy at 25 to 800 C in atmospheric air at ambient pressure
[NASA-TM-87353] p 103 N87-22860
- Effect of abrasive grit size on wear of manganese-zinc ferrite under three-body abrasion p 104 N87-24566
- Tribology theory versus experiment
[NASA-TM-100198] p 71 N87-29599
- WEAR RESISTANCE**
- The role of near-surface plastic deformation in the wear of lamellar solids p 162 A87-48500
- Materials for Advanced Turbine Engines (MATE). Project 4: Erosion resistant compressor airfoil coating
[NASA-CR-179622] p 92 N87-27029
- The effect of Tricresyl-Phosphate (TCP) as an additive on wear of Iron (Fe)
[NASA-TM-100103] p 93 N87-27030
- Experimental evaluation of chromium-carbide-based solid lubricant coatings for use to 760 C
[NASA-CR-180808] p 105 N87-27053
- WEAR TESTS**
- Friction and wear behaviour of ion beam modified ceramics p 97 A87-47958
- Characterization of ion beam modified ceramic wear surfaces using Auger electron spectroscopy p 98 A87-51304
- WEIBULL DENSITY FUNCTIONS**
- Fracture mechanics concepts in reliability analysis of monolithic ceramics
[NASA-TM-100174] p 187 N87-27269
- WEIGHT ANALYSIS**
- Long range inhabited surface transportation system power source for the exploration of Mars (manned Mars mission) p 37 N87-17752
- WEIGHTLESSNESS**
- Equilibrium fluid interfaces in the absence of gravity p 138 A87-38790
- Microgravity Fluid Management Symposium
[NASA-CP-2465] p 108 N87-21141
- WELD STRENGTH**
- Nondestructive evaluation of adhesive bond strength using the stress wave factor technique p 170 A87-32200
- WENTZEL-KRAMER-BRILLOUIN METHOD**
- One-dimensional wave propagation in rods of variable cross section: A WKBJ solution
[NASA-CR-4086] p 172 N87-24707
- WIENER HOPF EQUATIONS**
- Radar cross section of an open-ended circular waveguide Calculation of second-order diffraction terms p 112 A87-31626
- Microstrip dispersion including anisotropic substrates p 123 A87-47621
- WIND TUNNEL APPARATUS**
- Measurement of Centaur/Orbiter multiple reaction forces in a full-scale test rig p 38 A87-29448
- Experimental evaluation of wall Mach number distributions of the octagonal test section proposed for NASA Lewis Research Center's altitude wind tunnel
[NASA-TP-2666] p 35 N87-17717

- Experimental evaluation of two turning vane designs for fan drive corner of 0.1-scale model of NASA Lewis Research Center's proposed altitude wind tunnel
[NASA-TP-2646] p 35 N87-18576
- Detailed flow surveys of turning vanes designed for a 0.1-scale model of NASA Lewis Research Center's proposed altitude wind tunnel
[NASA-TP-2680] p 36 N87-20295
- WIND TUNNEL CALIBRATION**
- Experimental evaluation of honeycomb/screen configurations and short contraction section for NASA Lewis Research Center's altitude wind tunnel
[NASA-TP-2692] p 36 N87-23662
- WIND TUNNEL DRIVES**
- Experimental evaluation of two turning vane designs for fan drive corner of 0.1-scale model of NASA Lewis Research Center's proposed altitude wind tunnel
[NASA-TP-2646] p 35 N87-18576
- Detailed flow surveys of turning vanes designed for a 0.1-scale model of NASA Lewis Research Center's proposed altitude wind tunnel
[NASA-TP-2680] p 36 N87-20295
- WIND TUNNEL MODELS**
- Measured noise of a scale model high speed propeller at simulated takeoff/approach conditions
[AIAA PAPER 87-0526] p 208 A87-31109
- Noise generated by flow through large butterfly valves
[NASA-TM-88911] p 210 N87-16586
- Measured noise of a scale model high speed propeller at simulated takeoff/approach conditions
[NASA-TM-88920] p 211 N87-16588
- Experimental evaluation of blockage ratio and plenum evacuation system flow effects on pressure distribution for bodies of revolution in 0.1 scale model test section of NASA Lewis Research Center's proposed altitude wind tunnel
[NASA-TP-2702] p 36 N87-22694
- WIND TUNNEL TESTS**
- Experimental and theoretical study of propeller spinner/shank interference
[AIAA PAPER 87-0145] p 3 A87-24929
- An experimental investigation of compressible three-dimensional boundary layer flow in annular diffusers
[AIAA PAPER 87-0366] p 3 A87-24954
- High speed wind tunnel tests of the PTA aircraft --- Proplan Test Assessment Program
[SAE PAPER 861744] p 4 A87-32619
- Effects of multiple rows and noncircular orifices on dilution jet mixing p 138 A87-39805
- Short efficient ejector systems
[AIAA PAPER 87-1837] p 20 A87-45239
- Wind tunnel tests on a one-foot diameter SR-7L proplan model
[AIAA PAPER 87-1892] p 6 A87-45281
- Shear flow instability generated by non-homogeneous external forcing p 142 A87-48047
- The acoustic experimental investigation of counterrotating propeller configurations
[SAE PAPER 871031] p 210 A87-48760
- Wind tunnel performance results of an aerodynamically scaled 2/9 model of the PTA flight test prop-fan
[AIAA PAPER 87-1893] p 8 A87-52251
- An experimental study of the aerodynamics of a NACA 0012 airfoil with a simulated glaze ice accretion
[NASA-CR-179897] p 8 N87-11701
- Cruise noise of counterrotation propeller at angle of attack in wind tunnel
[NASA-TM-88869] p 210 N87-13252
- Noise generated by flow through large butterfly valves
[NASA-TM-88911] p 210 N87-16586
- Experimental evaluation of blockage ratio and plenum evacuation system flow effects on pressure distribution for bodies of revolution in 0.1 scale model test section of NASA Lewis Research Center's proposed altitude wind tunnel
[NASA-TP-2702] p 36 N87-22694
- Icing of flow conditioners in a closed-loop wind tunnel
[NASA-TM-89824] p 13 N87-23591
- Wind tunnel performance results of an aerodynamically scaled 2/9 model of the PTA flight test prop-fan
[NASA-TM-89917] p 14 N87-25294
- Wind tunnel evaluation of a truncated NACA 64-621 airfoil for wind turbine applications
[NASA-CR-180803] p 196 N87-25621
- Performance and aerodynamic braking of a horizontal-axis wind turbine from small-scale wind tunnel tests
[NASA-CR-180812] p 198 N87-27327
- Cruise noise of the 2/9th scale model of the Large-scale Advanced Proplan (LAP) propeller, SR-7A
[NASA-TM-100175] p 212 N87-28398
- Analysis and test evaluation of the dynamic response and stability of three advanced turboprop models
[NASA-CR-174814] p 32 N87-28555

- Aerodynamic performance investigation of advanced mechanical suppressor and ejector nozzle concepts for jet noise reduction
[NASA-CR-174860] p 33 N87-29534
- WIND TUNNEL WALLS**
Modeling the effects of wind tunnel wall absorption on the acoustic radiation characteristics of propellers
[AIAA PAPER 86-1876] p 208 A87-17991
Experimental evaluation of wall Mach number distributions of the octagonal test section proposed for NASA Lewis Research Center's altitude wind tunnel
[NASA-TP-2666] p 35 N87-17717
- WIND TUNNELS**
Reactivation study for NASA Lewis Research Center's Hypersonic Tunnel Facility
[AIAA PAPER 87-1886] p 34 A87-50190
Strategic plan, 1985
[NASA-TM-89263] p 219 A87-12384
Reactivation study for NASA Lewis Research Center's hypersonic tunnel facility
[NASA-TM-89918] p 36 N87-23664
Experimental evaluation of corner turning vanes
[NASA-TM-100143] p 37 N87-28571
- WIND TURBINES**
Thermal analysis of an orthotropic engineering body --- horizontal axis wind turbine rotor blade
p 173 A87-13496
Overview of the new ASME Performance Test Code for wind turbines
[ASME PAPER 86-JPGC-PTC-4] p 190 A87-25475
WEST-3 wind turbine simulator development. Volume 2: Verification
[NASA-CR-174982] p 191 N87-10531
WEST-3 wind turbine simulator development. Volume 1: Summary
[NASA-CR-174981] p 192 N87-11348
WEST-3 wind turbine simulator development
[NASA-CR-174983] p 192 N87-12046
Utility interconnection issues for wind power generation
[NASA-CR-175056] p 193 N87-17400
Design and dynamic simulation of a fixed pitch 56 kW wind turbine drive train with a continuously variable transmission
[NASA-CR-179543] p 193 N87-17401
Design of an advanced wood composite rotor and development of wood composite blade technology
[NASA-CR-174713] p 73 N87-17861
Development and testing of vortex generators for small horizontal axis wind turbines
[NASA-CR-179514] p 193 N87-18922
Wind tunnel evaluation of a truncated NACA 64-621 airfoil for wind turbine applications
[NASA-CR-180803] p 196 N87-25621
Surface pressure measurements on the blade of an operating Mod-2 wind turbine with and without vortex generators
[NASA-TM-89903] p 198 N87-26455
Performance and aerodynamic braking of a horizontal-axis wind turbine from small-scale wind tunnel tests
[NASA-CR-180812] p 198 N87-27327
Design of test specimens and procedures for generating material properties of Douglas fir/epoxy laminated wood composite material: With the generation of baseline data at two environmental conditions
[NASA-CR-174910] p 75 N87-28612
Performance and power regulation characteristics of two airfoil-controlled rotors and a pitchable tip-controlled rotor on the Mod-O turbine
[NASA-TM-100136] p 200 N87-29956
- WINDOWS**
Bonding Lexan and sapphire to form high-pressure, flame-resistant window
[NASA-TM-100188] p 159 N87-28880
- WINDOWS (APERTURES)**
A parametric study of the beam refraction problems across laser anemometer windows
p 154 A87-40725
- WINDPOWER UTILIZATION**
Utility interconnection issues for wind power generation
[NASA-CR-175056] p 193 N87-17400
Wind tunnel evaluation of a truncated NACA 64-621 airfoil for wind turbine applications
[NASA-CR-180803] p 196 N87-25621
- WINDPOWERED GENERATORS**
Utility interconnection issues for wind power generation
[NASA-CR-175056] p 193 N87-17400
Design and dynamic simulation of a fixed pitch 56 kW wind turbine drive train with a continuously variable transmission
[NASA-CR-179543] p 193 N87-17401
- WING NACELLE CONFIGURATIONS**
Dynamic response of two composite prop-fan models on a nacelle/wing/fuselage half model
[NASA-CR-179589] p 18 N87-23615
- WING TANKS**
Aircraft accident report: NASA 712, Convair 990, N712NA, March Air Force Base, California, July 17, 1985, executive summary
[NASA-TM-87356-VOL-1] p 16 N87-21878
- WINGS**
In-flight photogrammetric measurement of wing ice accretions
[AIAA PAPER 86-0483] p 15 A87-17995
- WIRE CLOTH**
Fatigue failure of regenerator screens in a high frequency Stirling engine
[NASA-TM-88974] p 183 N87-18882
- WOOD**
Thermal analysis of an orthotropic engineering body --- horizontal axis wind turbine rotor blade
p 173 A87-13496
Design of an advanced wood composite rotor and development of wood composite blade technology
[NASA-CR-174713] p 73 N87-17861
Design of test specimens and procedures for generating material properties of Douglas fir/epoxy laminated wood composite material: With the generation of baseline data at two environmental conditions
[NASA-CR-174910] p 75 N87-28612
- WORKING FLUIDS**
Effect of an oxygen plasma on the physical and chemical properties of several fluids for the Liquid Droplet Radiator
[AIAA PAPER 87-0080] p 42 A87-22401
Preliminary study of niobium alloy contamination by transport through helium
[NASA-TM-88952] p 90 N87-17884
- WORKLOADS (PSYCHOPHYSIOLOGY)**
Identification and proposed control of helicopter transmission noise at the source
[NASA-TM-89312] p 18 N87-16816
- WORKSTATIONS**
Color postprocessing for 3-dimensional finite element mesh quality evaluation and evolving graphical workstation
[NASA-CR-180215] p 202 N87-18997
Interactive color display of 3-D engineering analysis results
[NASA-CR-180589] p 203 N87-22422
- X**
- X RAY ANALYSIS**
Correlation of processing and sintering variables with the strength and radiography of silicon nitride
p 94 A87-12938
Sintering, microstructural, radiographic, and strength characterization of a high-purity Si₃N₄-based composition
p 94 A87-12939
- X RAY INSPECTION**
NDE reliability and process control for structural ceramics
[ASME PAPER 87-GT-8] p 171 A87-48702
NDE reliability and process control for structural ceramics
[NASA-TM-88870] p 171 N87-12910
- XENON**
Performance characteristics of ring-cusp thrusters with xenon propellant
[AIAA PAPER 86-1392] p 46 A87-17992
Status of xenon ion propulsion technology
[AIAA PAPER 87-1003] p 53 A87-48677
- Y**
- YIELD STRENGTH**
Yielding and deformation behavior of the single crystal superalloy PWA 1480
p 84 A87-32040
- YTTERBIUM COMPOUNDS**
New ZrO₂-Yb₂O₃ plasma-sprayed coatings for thermal barrier applications
p 98 A87-53623
- YTTRIUM OXIDES**
Fracture of flash oxidized, yttria-doped sintered reaction-bonded silicon nitride
p 97 A87-47923
- Z**
- ZINC**
Effect of abrasive grit size on wear of manganese-zinc ferrite under three-body abrasion
[NASA-TM-89879] p 104 N87-24566
- ZIRCONIUM**
Nickel base coating alloy
[NASA-CASE-LEW-13834-1] p 89 N87-14482
- Morphology of zirconia particles exposed to D.C. arc plasma jet
[NASA-TM-88927] p 90 N87-16113
Long-time creep behavior of Nb-1Zr alloy containing carbon
[NASA-TM-100142] p 92 N87-26217
- ZIRCONIUM OXIDES**
New ZrO₂-Yb₂O₃ plasma-sprayed coatings for thermal barrier applications
p 98 A87-53623
The effect of laser glazing on life of ZrO₂ TBCs in cyclic burner rig tests
[NASA-TM-88821] p 89 N87-14487

PERSONAL AUTHOR INDEX

Typical Personal Author Index Listing



Listings in this index are arranged alphabetically by personal author. The title of the document provides the user with a brief description of the subject matter. The report number helps to indicate the type of document listed (e.g., NASA report, translation, NASA contractor report). The page and accession numbers are located beneath and to the right of the title. Under any one author's name the accession numbers are arranged in sequence.

A

- AADLAND, RANDALL S.**
Ground-based plasma contractor characterization
[NASA-TM-100194] p 215 N87-28423
- ABDELWAHAB, A. A.**
Image data compression with vector quantization in the transform domain p 111 A87-30775
- ABDELWAHAB, MAHMOOD**
Full-scale engine demonstration of an advanced sensor failure detection isolation, and accommodation algorithm - Preliminary results
[AIAA PAPER 87-2259] p 22 A87-50422
- Full-scale engine demonstration of an advanced sensor failure detection, isolation and accommodation algorithm: Preliminary results
[NASA-TM-89880] p 127 N87-22097
- Summary of investigations of engine response to distorted inlet conditions p 30 N87-24477
- Measurement uncertainty for the Uniform Engine Testing Program conducted at NASA Lewis Research Center [NASA-TM-88943] p 33 N87-28557
- ABDUL-AZIZ, A.**
Nonlinear heat transfer and structural analyses of SSME turbine blades p 184 N87-22779
- ABEL, J. F.**
Towards effective interactive three-dimensional colour postprocessing p 201 A87-11895
- Interactive graphics and analysis accuracy p 202 A87-45900
- ABEL, JOHN F.**
Interactive color display of 3-D engineering analysis results
[NASA-CR-180589] p 203 N87-22422
- ABEL, PHILLIP**
Up close - Materials division of NASA-Lewis Research Center p 69 A87-51176
- ABEL, PHILLIP B.**
Nondestructive evaluation of structural ceramics [NASA-TM-88978] p 172 N87-18109
- ACOSTA, R.**
A design concept for an MMIC microstrip phased array [NASA-TM-88834] p 114 N87-14569

- ACOSTA, ROBERTO**
An experimental investigation of parasitic microstrip arrays [NASA-TM-100168] p 129 N87-27120
- A design concept for an MMIC (Monolithic Microwave Integrated Circuit) microstrip phased array [AD-P005404] p 119 N87-28769
- ACOSTA, ROBERTO J.**
Microstrip antenna array with parasitic elements [NASA-TM-89919] p 117 N87-22089
- Detection of reflector surface error from near-field data: Effect of edge diffracted field [NASA-TM-89920] p 117 N87-22874
- ACOSTA, WALDO A.**
Liner cooling research at NASA Lewis Research Center [AIAA PAPER 87-1828] p 22 A87-50189
- Liner cooling research at NASA Lewis Research Center [NASA-TM-100107] p 29 N87-23624
- ADAMCZYK, J. J.**
A numerical simulation of the inviscid flow through a counterrotating propeller [ASME PAPER 86-GT-138] p 3 A87-25395
- Measurements of the unsteady flow field within the stator row of a transonic axial-flow fan. 1: Measurement and analysis technique [NASA-TM-88945] p 10 N87-16789
- Measurements of the unsteady flow field within the stator row of a transonic axial-flow fan. Part 2: Results and discussion [NASA-TM-88946] p 10 N87-16790
- ADAMCZYK, JOHN J.**
The utilization of parallel processing in solving the inviscid form of the average-passage equation system for multistage turbomachinery [AIAA PAPER 87-1108] p 5 A87-42057
- Simulation of multistage turbine flows p 149 N87-22768
- ADAMOVSKY, GRIGORY**
Fiber-optic thermometer using temperature dependent absorption, broadband detection, and time domain referencing p 153 A87-25948
- Referencing in fiber optic sensing systems [NASA-TM-89822] p 126 N87-20475
- Amplitude spectrum modulation technique for analog data processing in fiber optic sensing system with temporal separation of channels [NASA-TM-100152] p 159 N87-25562
- ADAMS, J. C., JR.**
Large perturbation flow field analysis and simulation for supersonic inlets [NASA-CR-174676] p 8 N87-10835
- ADDY, H. E.**
Estimation of instantaneous heat transfer coefficients for a direct-injection stratified-charge rotary engine [SAE PAPER 870444] p 163 A87-48787
- Performance and efficiency evaluation and heat release study of an outboard Marine Corporation Rotary Combustion Engine [NASA-TM-89833] p 28 N87-20282
- AGGARWAL, B. B.**
Solid lubrication design methodology, phase 2 [NASA-CR-175114] p 221 N87-18470
- AGGARWAL, S. K.**
Representation of the vaporization behavior of turbulent polydisperse sprays by 'equivalent' monodisperse sprays [AIAA PAPER 87-1954] p 141 A87-45325
- Representation of the vaporization behavior of turbulent polydisperse sprays by equivalent monodisperse sprays [NASA-TM-88906] p 26 N87-16827
- AHMAD, S.**
Free vibration analysis by BEM using particular integrals p 174 A87-13882
- AHMED, SAAD A.**
The near field behavior of turbulent gas jets in a long confinement p 135 A87-28976
- AIELLO, ROBERT**
Structural and aeroelastic analysis of the SR-7L propfan [NASA-TM-86877] p 184 N87-22273

- AIELLO, ROBERT A.**
A NASTRAN primer for the analysis of rotating flexible blades [NASA-TM-89861] p 184 N87-21375
- Dynamic delamination buckling in composite laminates under impact loading: Computational simulation [NASA-TM-100192] p 75 N87-28611
- AIGRET, G. G.**
Fabrication of cooled radial turbine rotor [NASA-CR-179503] p 25 N87-11789
- AKSUN, M. I.**
Microwave performance of a quarter-micrometer gate low-noise pseudomorphic InGaAs/AlGaAs modulation-doped field effect transistor p 121 A87-23745
- ALEXANDER, D. R.**
Effects of non-spherical drops on a phase Doppler spray analyzer p 152 A87-11048
- ALGER, DONALD L.**
Overview of the 1986 free-piston Stirling activities at NASA Lewis Research Center [NASA-TM-88895] p 221 N87-16663
- Fatigue failure of regenerator screens in a high frequency Stirling engine [NASA-TM-88974] p 183 N87-18882
- A 1987 overview of free-piston Stirling technology for space power application [NASA-TM-89832] p 221 N87-21756
- ALI, S. K.**
A critical analysis of transverse vorticity measurements in a large plane shear layer p 143 A87-52049
- ALJABRI, A. S.**
High speed wind tunnel tests of the PTA aircraft [SAE PAPER 861744] p 4 A87-32619
- ALJABRI, ABDULLAH S.**
Wind tunnel tests on a one-foot diameter SR-7L propfan model [AIAA PAPER 87-1892] p 6 A87-45281
- ALLEN, D. J.**
Testing of a variable-stroke Stirling engine p 160 A87-18036
- ALSTON, W. B.**
Substituted 1,1,1-triaryl-2,2,2-trifluoroethanes and processes for their synthesis [NASA-CASE-LEW-14345-1] p 70 N87-14432
- New condensation polyimides containing 1,1,1-triaryl-2,2,2-trifluoroethane structures [NASA-CASE-LEW-14346-1] p 70 N87-14433
- ALSTON, WILLIAM B.**
Structure-to-property relationships in addition cured polymers. II - Resin Tg and composite initial mechanical properties of norbornenyl cured polyimide resins p 96 A87-38638
- A mechanistic study of polyimide formation from diester-diacids p 70 A87-53671
- Thermo-oxidatively stable condensation polyimides containing 1,1,1-triaryl-2,2,2-trifluoroethane dianhydride and diamine monomers [NASA-TM-89875] p 103 N87-22048
- ALTEROVITZ, S. A.**
Compensation in epitaxial cubic SiC films p 216 A87-15071
- Ellipsometric and optical study of amorphous hydrogenated carbon films p 216 A87-23967
- Comment on 'Temperature dependence of electrical properties of non-doped and nitrogen-doped beta-SiC single crystals grown by chemical vapor deposition' p 217 A87-42846
- Adhesion, friction and deformation of ion-beam-deposited boron nitride films p 98 A87-49325
- ALTEROVITZ, SAMUEL A.**
Variable angle of incidence spectroscopic ellipsometry Application to GaAs-Al(x)Ga(1-x)As multiple heterostructures p 216 A87-20519
- Adhesion, friction, and deformation of ion-beam-deposited boron nitride films [NASA-TM-88902] p 100 N87-15305
- Mechanical strength and tribological behavior of ion-beam deposited boron nitride films on non-metallic substrates [NASA-TM-89818] p 101 N87-18668

B

- Rapid thermal annealing of Amorphous Hydrogenated Carbon (a-C:H) films
[NASA-TM-89859] p 218 N87-20821
- Boron nitride: Composition, optical properties and mechanical behavior
[NASA-TM-89849] p 218 N87-25017
- ALTIDIS, P. C.**
Flexibility effects on tooth contact location in spiral bevel gear transmissions
[NASA-CR-4055] p 166 N87-20552
- AMANO, R. S.**
Comparison of pressure-strain correlation models for the flow behind a disk p 131 A87-20897
Turbulent heat transfer in corrugated-wall channels with and without fins p 134 A87-27709
Third-moment closure of turbulence for predictions of separating and reattaching shear flows: A study of Reynolds-stress closure model
[NASA-CR-177055] p 145 N87-11961
- AMICK, ROBERT**
Long range inhabited surface transportation system power source for the exploration of Mars (manned Mars mission) p 37 N87-17752
- ANAND, M. S.**
An unconditionally-stable central differencing scheme for high Reynolds number flows
[AIAA PAPER 87-0060] p 133 A87-24912
- ANAND, YOGI**
The 60 GHz IMPATT diode development
[NASA-CR-179536] p 218 N87-17515
- ANDERSEN, BERNHARD H.**
Internal computational fluid mechanics on supercomputers for aerospace propulsion systems p 151 N87-26002
- ANDERSON, O. L.**
Assessment of a 3-D boundary layer code to predict heat transfer and flow losses in a turbine p 145 N87-11224
- ANDERSON, R. D.**
Advanced Propan Engine Technology (APET) definition study, single and counter-rotation gearbox/pitch change mechanism design
[NASA-CR-168115] p 32 N87-28554
- ANDERSON, W. L.**
Thin film strain gage development program
[NASA-CR-174707] p 159 N87-28883
- ANDERSON, WILLIAM**
Evaluation of a high-torque backlash-free roller actuator p 165 N87-16336
- ANNEN, K. D.**
Modeling free convective gravitational effects in chemical vapor deposition
[AIAA PAPER 87-0313] p 133 A87-22552
- ANSPAUGH, B. E.**
Results of 1 MeV proton irradiation of front and back surfaces of silicon solar cells p 197 N87-26435
- ANTCLIFF, RICHARD R.**
Multispecies CARS measurements in turbulent combustion p 79 N87-23808
- ANTHAN, D. J.**
Fiber-optic photoelastic pressure sensor with fiber-loss compensation p 154 A87-34566
Loss-compensation of intensity-modulating fiber-optic sensors
[NASA-TM-88825] p 124 N87-13637
- ANTHAN, DONALD J.**
Fiber-optic temperature sensor using a spectrum-modulating semiconductor etalon
[NASA-TM-100153] p 31 N87-25329
- ANTOINE, A. C.**
Catalyst and electrode research for phosphoric acid fuel cells p 190 A87-33789
- ANTOLOVICH, STEPHEN D.**
Yielding and deformation behavior of the single crystal superalloy PWA 1480 p 84 A87-32040
- APELIAN, D.**
Analysis of the solidified structure of rheocast and VADER processed nickel-base superalloy p 83 A87-28734
- APELIAN, DIRAN**
Processing-structure characterization of rheocast IN-100 superalloy p 82 A87-24116
- ARD, K. E.**
Thermal expansion behavior of graphite/glass and graphite/magnesium p 72 A87-38615
- ARMSTRONG, ELIZABETH S.**
Test program to provide confidence in liquid oxygen cooling of hydrocarbon fueled rocket thrust chambers p 67 N87-26114
- ARON, PAUL R.**
AlGaAs growth by OMCVD using an excimer laser
[NASA-TM-88937] p 218 N87-23304
- ARP, V. D.**
Volume-energy parameters for heat transfer to supercritical fluids p 137 A87-32326

- ARPASI, DALE J.**
Mathematical model partitioning and packing for parallel computer calculation p 202 A87-52534
Automating the parallel processing of fluid and structural dynamics calculations
[NASA-TM-89837] p 203 N87-19002
Applications and requirements for real-time simulators in ground-test facilities
[NASA-TP-2672] p 204 N87-23202
- ARRISON, ANNE**
A V-grooved AlGaAs/GaAs passivated PN junction
[NASA-TM-100138] p 218 N87-27541
- ARSENAUX, P. J.**
Analysis and test evaluation of the dynamic response and stability of three advanced turboprop models
[NASA-CR-174814] p 32 N87-28555
- ARTH, C. H.**
An assessment of the status and trends in satellite communications 1986-2000: An information document prepared for the Communications Subcommittee of the Space Applications Advisory Committee
[NASA-TM-88867] p 114 N87-13600
- ARYA, V. K.**
Finite element implementation of Robinson's unified viscoplastic model and its application to some uniaxial and multiaxial problems
[NASA-TM-89891] p 185 N87-23010
- ASMUSSEN, J.**
Microwave electrothermal thruster performance in helium gas p 49 A87-31281
An analysis of electromagnetic coupling and eigenfrequencies for microwave electrothermal thruster discharges
[AIAA PAPER 87-1012] p 51 A87-41111
- ASMUSSEN, JES**
A review of research and development on the microwave-plasma electrothermal rocket
[AIAA PAPER 87-1011] p 49 A87-38008
- ATLURI, S. N.**
Notes and comments on computational elastoplasticity - Some new models and their numerical implementation p 173 A87-10893
- ATTWOOD, S.**
Baseband processor development/test performance for 30/20 GHz SS-TDMA communication system p 111 A87-18310
- AUGUST, R.**
Effect of design variables, temperature gradients and speed of life and reliability of a rotating disk
[NASA-TM-88883] p 165 N87-13755
- AUSTIN, P. J., JR.**
Computation of full-coverage film-cooled airfoil temperatures by two methods and comparison with high heat flux data
[NASA-TM-88931] p 150 N87-23934
- AVILA, R. E.**
Behavior of inversion layers in 3C silicon carbide p 215 A87-11242
Stoichiometric disturbances in compound semiconductors due to ion implantation p 215 A87-12292
- AWKER, R. W.**
Application of propan propulsion to general aviation
[AIAA PAPER 86-2698] p 18 A87-17934
- AYDELOTT, J. C.**
Temperature fields due to jet induced mixing in a typical OTV tank
[AIAA PAPER 87-2017] p 55 A87-52247
- AYDELOTT, JOHN C.**
Thermodynamic analysis and subscale modeling of space-based orbit transfer vehicle cryogenic propellant resupply p 142 A87-48572
Numerical modeling of on-orbit propellant motion resulting from an impulsive acceleration
[AIAA PAPER 87-1766] p 40 A87-48573
Numerical modeling of on-orbit propellant motion resulting from an impulsive acceleration
[NASA-TM-89873] p 41 N87-22757
Thermodynamic analysis and subscale modeling of space-based orbit transfer vehicle cryogenic propellant resupply
[NASA-TM-89921] p 150 N87-22949
- AYERS, S. R.**
Solar concentrator materials development p 213 A87-18171
- AYLESWORTH, K. D.**
Thermal and structural stability of cosputtered amorphous Ta(x)Cu(1-x) alloy thin films on GaAs p 216 A87-27198
- AYYAGARI, MURTHY**
The 60 GHz IMPATT diode development
[NASA-CR-179536] p 218 N87-17515

BAAKLINI, G. Y.

- Correlation of processing and sintering variables with the strength and radiography of silicon nitride p 94 A87-12938
- Probability of detection of internal voids in structural ceramics using microfocus radiography p 170 A87-14300
- NDE reliability and process control for structural ceramics
[ASME PAPER 87-GT-8] p 171 A87-48702
Quantitative void characterization in structural ceramics by use of scanning laser acoustic microscopy p 171 A87-51974
- NDE reliability and process control for structural ceramics
[NASA-TM-88870] p 171 N87-12910
- BAAKLINI, GEORGE Y.**
Nondestructive evaluation of structural ceramics
[NASA-TM-88978] p 172 N87-18109
Ultrasonic NDE of structural ceramics for power and propulsion systems
[NASA-TM-100147] p 173 N87-26362
- BACHALO, W. D.**
Two-phase flow measurements of a spray in a turbulent flow
[AIAA PAPER 87-0062] p 132 A87-22388
Laser velocimetry in turbulent flow fields - Particle response
[AIAA PAPER 87-0118] p 132 A87-22426
Two-phase measurements of a spray in the wake of a bluff body p 142 A87-46199
- BADDOUR, MAURICE F.**
Absolute gain measurement by the image method under mismatched condition
[NASA-TM-88924] p 124 N87-16968
- BADER, CLAYTON H.**
Potential propellant storage and feed systems for space station resistojet propulsion options
[NASA-CR-179457] p 59 N87-16065
- BAGHERLEE, A.**
Turbulent heat transfer in corrugated-wall channels with and without fins p 134 A87-27709
- BAILEY, B. C.**
Towards effective interactive three-dimensional colour postprocessing p 201 A87-11895
- BAILEY, BRUCE CHARLES**
Unification of color postprocessing techniques for 3-dimensional computational mechanics
[NASA-CR-180214] p 202 N87-18998
- BAILEY, R. S.**
High temperature static strain gage alloy development program
[NASA-CR-174833] p 157 N87-22179
Advanced high temperature static strain sensor development
[NASA-CR-179520] p 158 N87-25552
High temperature static strain gage development contract, tasks 1 and 2
[NASA-CR-180811] p 159 N87-28869
- BAILEY, S. G.**
Formation of a pn junction on an anisotropically etched GaAs surface using metalorganic chemical vapor deposition p 216 A87-21237
- BAILEY, SHEILA G.**
A V-grooved AlGaAs/GaAs passivated PN junction
[NASA-TM-100138] p 218 N87-27541
- BAILY, R. D.**
Enhanced heat transfer combustor technology, subtasks 1 and 2, task C.1
[NASA-CR-179541] p 56 N87-13486
- BAK, M. J.**
On 3-D inelastic analysis methods for hot section components (base program)
[NASA-CR-175060] p 180 N87-12923
- BALAN, C.**
A model propulsion simulator for evaluating counter rotating blade characteristics
[SAE PAPER 861715] p 20 A87-32607
- BALASUBRAMANIAM, R.**
Simulation of fluid flows during growth of organic crystals in microgravity
[NASA-TM-88921] p 108 N87-16167
Thermocapillary bubble migration for large Marangoni Numbers
[NASA-CR-179628] p 109 N87-22865
- BALDWIN, RICHARD S.**
Electrochemical performance and transport properties of a Nafion membrane in a hydrogen-bromine cell environment
[NASA-TM-89862] p 79 N87-23718
- BALLARINI, R.**
Compliance matrices for cracked bodies p 175 A87-25775

- BALLARINI, ROBERTO**
The effects of crack surface friction and roughness on crack tip stress fields
[NASA-TM-88976] p 183 N87-18881
- BALODIS, VILNIS**
Space station power semiconductor package
[NASA-CR-180829] p 129 N87-28825
- BALSA, T. F.**
On the spatial instability of piecewise linear free shear layers
p 137 A87-31680
- BANERJEE, P. K.**
Free vibration analysis by BEM using particular integrals
p 174 A87-13882
Conforming versus non-conforming boundary elements in three-dimensional elastostatics p 175 A87-22775
On 3-D inelastic analysis methods for hot section components (base program)
[NASA-CR-175060] p 180 N87-12923
3-D inelastic analysis methods for hot section components. Volume 2: Advanced special functions models
[NASA-CR-179517] p 186 N87-27267
- BANHOLZER, W. F.**
Oxidation-resistant reflective surfaces for solar dynamic power generation in near Earth orbit
[NASA-TM-88865] p 56 N87-10960
- BANKS, B. A.**
Properties and potential applications of brominated P-100 carbon fibers
p 95 A87-23702
- BANKS, BRUCE**
An evaluation of candidate oxidation resistant materials for space applications in LEO
[NASA-TM-100122] p 105 N87-25480
Neutral atomic oxygen beam produced by ion charge exchange for Low Earth Orbital (LEO) simulation
p 79 N87-26188
An evaluation of candidate oxidation resistant materials
p 80 N87-26203
- BANKS, BRUCE A.**
Protection of solar array blankets from attack by low earth orbital atomic oxygen
p 47 A87-19874
Ion beam sputter etching
[NASA-CASE-LEW-13899-1] p 110 N87-21160
Oxidation protection coatings for polymers
[NASA-CASE-LEW-14072-3] p 103 N87-23736
High temperature radiator materials for applications in the low Earth orbital environment
[NASA-TM-100190] p 93 N87-29662
- BANSAL, NAROTTAM P.**
Annealing of electron damage in mid-IR transmitting fluoride glass
p 99 A87-53652
Sol-Gel synthesis of MgO-SiO₂ glass compositions having stable liquid-liquid immiscibility
[NASA-TM-88905] p 103 N87-23750
- BANSAL, P. N.**
Analysis and test evaluation of the dynamic response and stability of three advanced turboprop models
[NASA-CR-174814] p 32 N87-28555
- BANYAI, MARK**
Long range inhabited surface transportation system power source for the exploration of Mars (manned Mars mission)
p 37 N87-17752
- BARAONA, COSMO**
High power/large area PV systems
p 198 N87-26452
- BARAONA, COSMO R.**
Space station power system
p 68 N87-26447
The space station power system
p 198 N87-28960
Status of space station power system
p 45 N87-29915
- BARBAY, G.**
Environmentally-induced discharge transient coupling to spacecraft
[NASA-CR-174922] p 43 N87-10946
- BARBAY, GORDON J.**
Modeling of environmentally induced transients within satellites
[AIAA PAPER 85-0387] p 42 A87-41611
- BARKER, L.**
A design study of hydrazine and biowaste resistojets
[NASA-CR-179510] p 57 N87-14425
- BARNETT, ALLEN M.**
An optimized top contact design for solar cell concentrators
p 189 A87-19882
- BARRANGER, JOHN P.**
Ramp-integration technique for capacitance-type blade-tip clearance measurement
p 155 A87-45128
Low-cost FM oscillator for capacitance type of blade tip clearance measurement system
[NASA-TP-2746] p 31 N87-24481
- BARRETT, C. A.**
Nickel base coating alloy
[NASA-CASE-LEW-13834-1] p 89 N87-14482
- The effect of Cr, Co, Al, Mo and Ta on a series of cast Ni-base superalloys on the stability of an aluminide coating during cyclic oxidation in Mach 0.3 burner rig
[NASA-TM-88840] p 89 N87-14488
- BARTEL, H. W.**
Static tests of the propulsion system
[AIAA PAPER 87-1728] p 23 A87-52245
- BARTEL, JOHN**
Advanced liquid-cooled, turbocharged and intercooled stratified charge rotary engines for aircraft
[SAE PAPER 871039] p 22 A87-48766
- BARTOLOTTA, PAUL A.**
A high temperature fatigue and structures testing facility
[NASA-TM-100151] p 186 N87-26399
- BARTON, J. M.**
Euler analysis of transonic propeller flows
p 4 A87-39813
- BASHIR-HASHEMI, ABDOLLAH**
Iptycenes - Extended triptycenes
p 69 A87-53654
Triptycene - A D(3h) C(62) hydrocarbon with three U-shaped cavities
p 69 A87-53656
- BASSETT, DUANE E.**
The design and analysis of single flank transmission error tester for loaded gears
[NASA-CR-179621] p 169 N87-27197
- BASU, P.**
Centrifugal inertia effects in two-phase face seal films
p 162 A87-37687
- BATRA, R.**
Design, construction and long life endurance testing of cathode assemblies for use in microwave high-power transmitting tubes
[NASA-CR-175116] p 123 N87-10237
- BATHAUER, BYRON E.**
Aircraft accident report: NASA 712, Convair 990, N712NA, March Air Force Base, California, July 17, 1985, executive summary
[NASA-TM-87356-VOL-1] p 16 N87-21878
Aircraft accident report: NASA 712, Convair 990, N712NA, March Air Force Base, California, July 17, 1985, facts and analysis
[NASA-TM-87356-VOL-2] p 16 N87-21879
Analysis of Convair 990 rejected-takeoff accident with emphasis on decision making, training and procedures
[NASA-TM-100189] p 16 N87-29471
- BAUHAHN, P.**
30 GHz monolithic balanced mixers using an ion-implanted FET-compatible 3-inch GaAs wafer process technology
p 121 A87-34525
- BAUMEISTER, K. J.**
Modeling the effects of wind tunnel wall absorption on the acoustic radiation characteristics of propellers
[AIAA PAPER 86-1876] p 208 A87-17991
Finite element modeling of electromagnetic propagation in composite structures
[NASA-TM-88916] p 207 N87-14956
- BAUMEISTER, KENNETH J.**
Finite element analysis of electromagnetic propagation in an absorbing wave guide
[NASA-TM-88866] p 207 N87-18391
A finite element model for wave propagation in an inhomogeneous material including experimental validation
[NASA-TM-100149] p 207 N87-25821
- BEATTIE, J. R.**
Plasma properties in electron-bombardment ion thrusters
[AIAA PAPER 87-1076] p 51 A87-41135
Status of xenon ion propulsion technology
[AIAA PAPER 87-1003] p 53 A87-48677
- BEATTY, RICHARD**
Nuclear reactor power for a space-based radar. SP-100 project
[NASA-TM-89295] p 213 N87-25838
- BEDIAKO, E. D.**
Aerodynamic performance investigation of advanced mechanical suppressor and ejector nozzle concepts for jet noise reduction
[NASA-CR-174860] p 33 N87-29534
- BEELER, R. M.**
Centrifugal inertia effects in two-phase face seal films
p 162 A87-37687
- BEHEIM, G.**
Fiber-optic interferometer using frequency-modulated laser diodes
p 153 A87-19186
Fiber-optic photoelastic pressure sensor with fiber-loss compensation
p 154 A87-34566
Loss-compensation of intensity-modulating fiber-optic sensors
[NASA-TM-88825] p 124 N87-13637
- BEHEIM, GLENN**
Loss-compensation technique for fiber-optic sensors and its application to displacement measurements
p 154 A87-32152
- Spectrum-modulating fiber-optic sensors for aircraft control systems
[NASA-TM-88968] p 27 N87-17700
Fiber-optic temperature sensor using a spectrum-modulating semiconductor etalon
[NASA-TM-100153] p 31 N87-25329
- BELK, D. M.**
Three-dimensional unsteady Euler solutions for propfans and counter-rotating propfans in transonic flow
[AIAA PAPER 87-1197] p 5 A87-42314
- BELLOWS, A. H.**
A comparative study of the influence of buoyancy driven fluid flow on GaAs crystal growth
p 219 N87-28741
- BELYTSCHKO, T.**
A probabilistic Hu-Washizu variational principle
[AIAA PAPER 87-0764] p 176 A87-33579
Variational approach to probabilistic finite elements
[NASA-CR-181343] p 206 N87-29212
- BELYTSCHKO, TED**
Probabilistic finite elements
p 185 N87-22790
- BENSON, THOMAS J.**
Two- and three-dimensional viscous computations of a hypersonic inlet flow
[AIAA PAPER 87-0283] p 4 A87-31106
Two- and three-dimensional viscous computations of a hypersonic inlet flow
[NASA-TM-88923] p 146 N87-15441
Internal computational fluid mechanics on supercomputers for aerospace propulsion systems
p 151 N87-26002
- BENTS, D. J.**
Coaxial tube tether/transmission line for manned nuclear space power
[NASA-CASE-LEW-14338-1] p 55 N87-10174
- BENTS, DAVE**
Power system technologies for the manned Mars mission
p 60 N87-17789
- BENTS, DAVID J.**
Coaxial tube array space transmission line characterization
[NASA-TM-89864] p 62 N87-22003
High temperature solid oxide regenerative fuel cell for solar photovoltaic energy storage
[NASA-TM-89872] p 194 N87-23020
- BERCAW, R. W.**
Spacecraft 2000 - The challenge of the future
p 37 A87-18064
- BERCAW, ROBERT W.**
Spacecraft 2000: The challenge of the future
p 68 N87-26448
- BEREMAND, D. G.**
DOE/NASA automotive Stirling engine project - Overview 86
p 220 A87-18034
- BERG, R. F.**
Viscometer for low frequency, low shear rate measurements
p 153 A87-13878
- BERGER, BRETT**
Contingency power for small turboshaft engines using water injection into turbine cooling air
[AIAA PAPER 87-1906] p 21 A87-45289
Contingency power for small turboshaft engines using water injection into turbine cooling air
[NASA-TM-89817] p 28 N87-20280
- BERGGREN, R.**
Evaluation of Stirling engine appendix gap losses
p 160 A87-18037
- BERKMAN, D. K.**
Heat pipe cooled rocket engines
[AIAA PAPER 86-1567] p 48 A87-21516
- BERKOPEC, F.**
Power system technologies for the manned Mars mission
p 60 N87-17789
- BERKOPEC, FRANK**
PEGASUS: A multi-megawatt nuclear electric propulsion system
p 59 N87-17787
- BERKOVITS, A.**
Estimation of high temperature low cycle fatigue on the basis of inelastic strain and strain rate
[NASA-TM-88841] p 89 N87-14489
- BERLAD, A. L.**
Particle cloud kinetics in microgravity
[AIAA PAPER 87-0577] p 107 A87-22716
- BERMAN, ALBERT**
Space station power semiconductor package
[NASA-CR-180829] p 129 N87-28825
- BERNATOWICZ, D. T.**
Electrical power system design for the U.S. Space Station
p 46 A87-18068
- BERNATOWICZ, DANIEL T.**
Electrical power system design for the US space station
[NASA-TM-88824] p 58 N87-15267
- BERNDT, C. C.**
Mechanical behavior of thermal barrier coatings for gas turbine blades
p 24 N87-11196

BESSENDORF, MICHAEL H.

Stochastic and fractal analysis of fracture trajectories
[NASA-CR-179545] p 179 N87-51167

BEST, T.

The 20 GHz spacecraft IMPATT solid state transmitter
[NASA-CR-179545] p 124 N87-17989

BESTERFIELD, G.

Variational approach to probabilistic finite elements
[NASA-CR-181343] p 206 N87-29212

BESTERFIELD, G. H.

A probabilistic Hu-Washizu variational principle
[AIAA PAPER 87-0764] p 176 A87-33579

BHANDARI, PRADEEP

Nuclear reactor power for a space-based radar. SP-100 project
[NASA-TM-89295] p 213 N87-25838

BHASIN, K. B.

Advances in gallium arsenide monolithic microwave integrated-circuit technology for space communications systems
p 120 A87-19091

Optically controlled GaAs dual-gate MESFET and permeable base transistors
[NASA-TM-88823] p 123 N87-10232

System architecture of MMIC-based large aperture arrays for space application
[NASA-TM-89840] p 125 N87-20468

RF characterization of monolithic microwave and mm-wave ICs
[NASA-TM-88948] p 117 N87-22065

Detection of radio-frequency modulated optical signals by two and three terminal microwave devices
[NASA-TM-100196] p 130 N87-29750

BHASIN, KUL

Optical technologies for communication satellite applications; Proceedings of the Meeting, Los Angeles, CA, Jan. 21, 22, 1986
[SPIE-616] p 41 A87-26610

BHASIN, KUL B.

Analysis of optically controlled microwave/millimeter-wave device structures
p 121 A87-23680

Optically controlled microwave devices and circuits: Emerging applications in space communications systems
[NASA-TM-89869] p 127 N87-23900

Monolithic Microwave Integrated Circuit (MMIC) technology for space communications applications
[NASA-TM-100187] p 118 N87-27883

BHASIN, KUL B.

Microwave performance of an optically controlled AlGaAs/GaAs high electron mobility transistor and GaAs MESFET
[NASA-TM-88980] p 125 N87-17993

BHASIN, PUNEET

Mathematical programming formulations for satellite synthesis
[NASA-CR-181151] p 44 N87-25419

BHATT, RAMAKRISHNA T.

Mechanical properties of SiC fiber-reinforced reaction-bonded Si₃N₄ composites
p 73 A87-50094

Method of preparing fiber reinforced ceramic material
[NASA-CASE-LEW-14392-1] p 106 N87-28656

BHATTACHARYYA, S.

Effect of 15 MPa hydrogen on creep-rupture properties of iron-base superalloys
p 86 A87-49558

BHUTIANI, P. K.

Free-jet acoustic investigation of high-radius-ratio conannular plug nozzles
[NASA-CR-3818] p 210 N87-10753

BIESIADNY, T. J.

Response of a small-turboshaft-engine compression system to inlet temperature distortion
[NASA-TM-83765] p 23 N87-10100

BIESIADNY, THOMAS J.

Contingency power for small turboshaft engines using water injection into turbine cooling air
[AIAA PAPER 87-1906] p 21 A87-45289

Contingency power for small turboshaft engines using water injection into turbine cooling air
[NASA-TM-89817] p 28 N87-20280

Hot gas ingestion: From model results to full scale engine testing
p 30 N87-24419

Summary of investigations of engine response to distorted inlet conditions
p 30 N87-24477

Measurement uncertainty for the Uniform Engine Testing Program conducted at NASA Lewis Research Center
[NASA-TM-88943] p 33 N87-28557

BIFANO, WILLIAM J.

Development of the VOLT-A Shuttle experiment
p 41 A87-19907

BIRKS, N.

Reactions occurring during the sulfation of sodium chloride deposited on alumina substrates
p 76 A87-20223

BITTKER, DAVID A.

Theoretical kinetic computations in complex reacting systems
p 219 N87-20277

Hydrogen oxidation mechanism with applications to (1) the chaperon efficiency of carbon dioxide and (2) vitiated air testing
[NASA-TM-100186] p 80 N87-28628

BLACK, RICHARD E.

Research opportunities in microgravity science and applications during shuttle hiatus
[NASA-TM-88964] p 108 N87-16917

BLANCHARD, W. K.

Further observations of SCC in alpha-beta brass
Considerations regarding the appearance of crack arrest markings during SCC
p 82 A87-23843

BLECH, RICHARD A.

Time-partitioning simulation models for calculation on parallel computers
[NASA-TM-89850] p 203 N87-20766

The hypercluster: A parallel processing test-bed architecture for computational mechanics applications
[NASA-TM-89823] p 203 N87-20767

Applications and requirements for real-time simulators in ground-test facilities
[NASA-TP-2672] p 204 N87-23202

BLINN, ROGER F.

Short efficient ejector systems
[AIAA PAPER 87-1837] p 20 A87-45239

BLOOMFIELD, H. S.

A feasibility assessment of nuclear reactor power system concepts for the NASA Growth Space Station
p 47 A87-18154

BLOOMFIELD, HARVEY

Nuclear reactor power for a space-based radar. SP-100 project
[NASA-TM-89295] p 213 N87-25838

BLOOMFIELD, HARVEY S.

Reliability and mass analysis of dynamic power conversion systems with parallel or standby redundancy
p 190 A87-21823

BLUMENTHAL, PHILIP Z.

A distributed data acquisition system for aeronautics test facilities
[NASA-TM-88961] p 35 N87-16851

BOBER, L. J.

Euler analysis of transonic propeller flows
p 4 A87-39813

BOBER, LAWRENCE J.

Method for the determination of the three dimensional aerodynamic field of a rotor-stator combination in compressible flow
[AIAA PAPER 87-1742] p 7 A87-50187

Method for the determination of the three-dimensional aerodynamic field of a rotor-stator combination to compressible flow
[NASA-TM-100118] p 30 N87-23625

BOBULA, G. A.

Compound cycle engine program
p 23 A87-53428

Compound cycle engine program
[NASA-TM-88879] p 25 N87-11790

BODONYI, R. J.

Three dimensional boundary layers in internal flows
[NASA-CR-181336] p 152 N87-28860

BOLDMAN, DONALD R.

Experimental evaluation of two turning vane designs for fan drive corner of 0.1-scale model of NASA Lewis Research Center's proposed altitude wind tunnel
[NASA-TP-2646] p 35 N87-18576

Detailed flow surveys of turning vanes designed for a 0.1-scale model of NASA Lewis Research Center's proposed altitude wind tunnel
[NASA-TP-2680] p 36 N87-20295

Experimental evaluation of corner turning vanes
[NASA-TM-100143] p 37 N87-28571

BOND, T. H.

Estimation of instantaneous heat transfer coefficients for a direct-injection stratified-charge rotary engine
[SAE PAPER 870444] p 163 A87-48787

Performance and efficiency evaluation and heat release study of an outboard Marine Corporation Rotary Combustion Engine
[NASA-TM-89833] p 28 N87-20282

BOROUGH, MARK

NASA Lewis Research Center Futuring Workshop
[NASA-CR-179577] p 206 N87-27475

BORREGO, J. M.

Comparative performance of diffused junction indium phosphide solar cells
p 197 N87-26441

Solar cells in bulk InP using an open tube diffusion process
p 198 N87-26444

BOTHRA, S.

Solar cells in bulk InP using an open tube diffusion process
p 198 N87-26444

BOTSIS, J.

An analysis for crack layer stability
p 176 A87-28982

BOWEN, H. K.

Processing of laser formed SiC powder
[NASA-CR-179857] p 99 N87-11009

Processing of laser formed SiC powder
[NASA-CR-179638] p 104 N87-24573

BOWLES, J. V.

Folding tilt rotor demonstrator feasibility study
p 17 A87-19247

BOWLES, K. J.

Specimen geometry effects on graphite/PMR-15 composites during thermo-oxidative aging
p 71 A87-13145

BOWLES, KENNETH J.

Styrene-terminated polysulfone oligomers as matrix material for graphite reinforced composites - An initial study
p 98 A87-49370

Styrene-terminated polysulfone oligomers as matrix material for graphite reinforced composites: An initial study
[NASA-TM-89846] p 74 N87-21043

BOYD, GARY L.

A technology development summary for the AGT101 advanced gas turbine program
[SAE PAPER 870466] p 163 A87-48790

BOYD, LINDA SMITH

Expansion of epicyclic gear dynamic analysis program
[NASA-CR-179563] p 166 N87-19723

BOZEK, JOHN M.

Development of the VOLT-A Shuttle experiment
p 41 A87-19907

BRABBS, T.

Ignition delay times of cyclopentene oxygen argon mixtures
p 76 A87-12602

BRABBS, THEODORE A.

The chemical shock tube as a tool for studying high-temperature chemical kinetics
p 157 N87-20279

Hydrogen oxidation mechanism with applications to (1) the chaperon efficiency of carbon dioxide and (2) vitiated air testing
[NASA-TM-100186] p 80 N87-28628

BRADY, JOYCE

An evaluation of candidate oxidation resistant materials for space applications in LEO
[NASA-TM-100122] p 105 N87-25480

High temperature radiator materials for applications in the low Earth orbital environment
[NASA-TM-100190] p 93 N87-29662

BRAGG, M. B.

An experimental study of the aerodynamics of a NACA 0012 airfoil with a simulated glaze ice accretion
[NASA-CR-179897] p 8 N87-11701

BRAITHWAITE, WILLIS M.

Summary of investigations of engine response to distorted inlet conditions
p 30 N87-24477

BRANDHORST, H. W.

Space power - Emerging opportunities
[IAF PAPER 86-152] p 45 A87-15900

BRANDHORST, H. W., JR.

Spacecraft 2000 - The challenge of the future
p 37 A87-18064

BRANDHORST, HENRY W., JR.

Spacecraft 2000: The challenge of the future
p 68 N87-26448

Alternative power generation concepts for space
p 199 N87-28961

BRANDT, BRUCE

Anticorrelation of Shubnikov-deHaas amplitudes and negative magnetoresistance magnitudes in intercalated pitch based graphite fibers
p 217 A87-28295

BRAUN, M. J.

Thermal shaft effects on load-carrying capacity of a fully coupled, variable-properties cryogenic journal bearing
[ASLE PREPRINT 86-TC-6B-1] p 160 A87-19502

A fully coupled variable properties thermohydraulic model for a cryogenic hydrostatic journal bearing
[ASME PAPER 86-TRIB-55] p 161 A87-19536

Two-phase flows and heat transfer within systems with ambient pressure above the thermodynamic critical pressure
p 136 A87-30728

Analysis of experimental shaft seal data for high-performance turbomachines - As for Space Shuttle main engines
p 162 A87-45846

Finite difference solution for a generalized Reynolds equation with homogeneous two-phase flow
p 141 A87-45851

Comparison of generalized Reynolds and Navier Stokes equations for flow of a power law fluid
p 142 A87-45852

Refrigerated dynamic seal to 6.9 MPa (1000 psi)
p 164 A87-50777

Evaluation of seals for high-performance cryogenic turbomachines
[NASA-TM-88919] p 146 N87-15442

BRAUSCH, J. F.

Free jet feasibility study of a thermal acoustic shield concept for AST/VCE application: Dual stream nozzles
[NASA-CR-3867] p 210 N87-10752

- Simulated flight acoustic investigation of treated ejector effectiveness on advanced mechanical suppressors for high velocity jet noise reduction
[NASA-CR-4019] p 211 N87-17481
- Free-jet investigation of mechanically suppressed, high radius ratio conical plug model nozzles
[NASA-CR-3596] p 212 N87-29315
- BRDAR, MARKO**
Neutral atomic oxygen beam produced by ion charge exchange for Low Earth Orbital (LEO) simulation
p 79 N87-26188
- BREER, M. D.**
Experimental, water droplet impingement data on two-dimensional airfoils, axisymmetric inlet and Boeing 737-300 engine inlet
[AIAA PAPER 87-0097] p 17 A87-24918
- BRENNAN, SCOTT M.**
Space station propulsion-ECLSS interaction study
[NASA-CR-175093] p 69 N87-29594
- BREWE, D. E.**
Starvation effects on the hydrodynamic lubrication of rigid nonconformal contacts in combined rolling and normal motion
p 135 A87-27839
- Thermohydrodynamic analysis for laminar lubricating films
[NASA-TM-88845] p 144 N87-11124
- Effect of vibration amplitude on vapor cavitation in journal bearings
[NASA-TM-88826] p 145 N87-11962
- BREWE, DAVID E.**
Effect of shaft frequency on cavitation in a journal bearing for noncentered circular whirl
[NASA-TM-88925] p 148 N87-22122
- Stability of a rigid rotor supported on flexible oil journal bearings
[NASA-TM-88999] p 151 N87-24646
- BREYLEY, L. R.**
An analytical and experimental investigation of resistojet plumes
[NASA-TM-88852] p 58 N87-14428
- BREYLEY, LORANELL**
Effect of nozzle geometry on the resistojet exhaust plume
[AIAA PAPER 87-2121] p 55 A87-52252
- BREYLEY, LORANELL R.**
An analytical and experimental investigation of resistojet plumes
[AIAA PAPER 87-0399] p 48 A87-24998
- BREZINSKY, KENNETH**
The oxidation degradation of aromatic compounds
[NASA-CR-180588] p 79 N87-22020
- BRINDLEY, P. K.**
Further observations of SCC in alpha-beta brass
Considerations regarding the appearance of crack arrest markings during SCC p 82 A87-23843
- BRINDLEY, PAMELA K.**
The sensitivity of mechanical properties of TFRS composites to variations in reaction zone size and properties
[AIAA PAPER 87-0757] p 72 A87-33577
- BRINKER, D. J.**
Indium phosphide solar cells - Status and prospects for use in space p 188 A87-18071
- BRINKER, DAVID**
A proposed GaAs-based superlattice solar cell structure with high efficiency and high radiation tolerance
p 189 A87-19915
- Design considerations for a GaAs nipi doping superlattice solar cell
p 196 N87-26422
- BRINKER, DAVID J.**
Recent developments in indium phosphide space solar cell research
[NASA-TM-100139] p 68 N87-26141
- BROOKS, B. M.**
Dynamic response and stability of a composite prop-fan model
[NASA-CR-179528] p 28 N87-21956
- Analysis and test evaluation of the dynamic response and stability of three advanced turboprop models
[NASA-CR-174814] p 32 N87-28555
- BROOKS, BENNETT M.**
Dynamic response of two composite prop-fan models on a nacelle/wing/fuselage half model
[NASA-CR-179589] p 18 N87-23615
- BROWN, G. V.**
Nonlinear vibration and stability of rotating, pretwisted, precone blades including Coriolis effects
p 178 A87-39896
- A low-cost optical data acquisition system for vibration measurement
[NASA-TM-88907] p 181 N87-14730
- The impact damped harmonic oscillator in free decay
[NASA-TM-89897] p 168 N87-23978
- BROWN, K. W.**
Structural tailoring of advanced turboprops
[AIAA PAPER 87-0753] p 177 A87-33648
- STAEBL: Structural tailoring of engine blades, phase 2
p 24 N87-11731
- BROWN, L.**
Baseband processor development/test performance for 30/20 GHz SS-TDMA communication system
p 111 A87-18310
- BROWN, P. C.**
Results of acoustic tests of a Prop-Fan model
[AIAA PAPER 87-1894] p 209 A87-45282
- Effect of angular inflow on the vibratory response of a counter-rotating propeller
[NASA-CR-174819] p 8 N87-10840
- BROWN, W. F., JR.**
Elastic analysis of a mode II fatigue crack test specimen
p 174 A87-17799
- BROWN, WILLIAM C.**
Rectenna Technology Program: Ultra light 2.45 GHz rectenna 20 GHz rectenna
[NASA-CR-179558] p 116 N87-19556
- BRUTON, WILLIAM M.**
Advanced detection, isolation and accommodation of sensor failures: Real-time evaluation
[NASA-TP-2740] p 34 N87-25331
- BU-ABBUD, GEORGE H.**
Variable angle of incidence spectroscopic ellipsometry Application to GaAs-Al(x)Ga(1-x)As multiple heterostructures
p 216 A87-20519
- BUCKLEY, D. H.**
Microstructure and surface chemistry of amorphous alloys important to their friction and wear behavior
p 81 A87-15186
- Plastic deformation of a magnesium oxide 001-plane surface produced by cavitation
[ASLE PREPRINT 86-TC-3D-1] p 94 A87-19504
- Adhesion, friction and deformation of ion-beam-deposited boron nitride films
p 98 A87-49325
- BUCKLEY, DONALD H.**
Adhesion, friction, and deformation of ion-beam-deposited boron nitride films
[NASA-TM-88902] p 100 N87-15305
- Mechanical strength and tribological behavior of ion-beam deposited boron nitride films on non-metallic substrates
[NASA-TM-88918] p 101 N87-18668
- Deformation and fracture of single-crystal and sintered polycrystalline silicon carbide produced by cavitation
[NASA-TM-88981] p 102 N87-20422
- BUDHANI, R. C.**
Thin-film temperature sensors for gas turbine engines
Problems and prospects p 153 A87-26109
- BUGGELN, R. C.**
Computation of multi-dimensional viscous supersonic jet flow
[NASA-CR-4020] p 8 N87-13405
- Computation of multi-dimensional viscous supersonic flow
[NASA-CR-4021] p 9 N87-13406
- BULZAN, D. L.**
Particle-laden swirling free jets - Measurements and predictions
[AIAA PAPER 87-0303] p 139 A87-42648
- Particle-laden swirling free jets: Measurements and predictions
[NASA-TM-88904] p 26 N87-16826
- BUNSHAH, R. F.**
Thin-film temperature sensors for gas turbine engines
Problems and prospects p 153 A87-26109
- BUNTING, BRUCE G.**
Investigation of PTFE transfer films by infrared emission spectroscopy and phase-locked ellipsometry
[NASA-TM-89844] p 102 N87-20421
- BURCAT, A.**
Ignition delay times of cyclopentene oxygen argon mixtures
p 76 A87-12602
- BURCHAM, R. E.**
Analysis of experimental shaft seal data for high-performance turbomachines - As for Space Shuttle main engines
p 162 A87-45846
- BURGESS, R. M.**
Small centrifugal pumps for low-thrust rockets
p 50 A87-39808
- BURLEY, RICHARD R.**
Experimental evaluation of wall Mach number distributions of the octagonal test section proposed for NASA Lewis Research Center's altitude wind tunnel
[NASA-TP-2666] p 35 N87-17717
- Experimental evaluation of blockage ratio and plenum evacuation system flow effects on pressure distribution for bodies of revolution in 0.1 scale model test section of NASA Lewis Research Center's proposed altitude wind tunnel
[NASA-TP-2702] p 36 N87-22694
- Experimental evaluation of honeycomb/screen configurations and short contraction section for NASA Lewis Research Center's altitude wind tunnel
[NASA-TP-2692] p 36 N87-23662
- BURNS, MAUREEN E.**
Airflow calibration and exhaust pressure/temperature survey of an F404, S/N 215-109, turbofan engine
[NASA-TM-100159] p 33 N87-29537
- BURTON, R. L.**
Experiments on a repetitively pulsed electrothermal thruster
[AIAA PAPER 87-1043] p 50 A87-38017
- Investigation of a repetitively pulsed electrothermal thruster
[NASA-CR-179464] p 59 N87-16878
- BUYUKDURA, O. M.**
Engineering calculations for communications satellite systems planning
[NASA-CR-180106] p 114 N87-16198
- BUYUKDURA, O. MERIH**
Optimization of orbital assignment and specification of service areas in satellite communications
[NASA-CR-181273] p 118 N87-27882
- BUZZARD, R. J.**
Elastic analysis of a mode II fatigue crack test specimen
p 174 A87-17799
- BYERS, DAVID C.**
The NASA Electric Propulsion Program
[AIAA PAPER 87-1098] p 53 A87-45795
- The NASA Electric Propulsion Program
[NASA-TM-89856] p 61 N87-21037

C

- CALANDRA, M.**
Cryogenic gear technology for an orbital transfer vehicle engine and tester design
[NASA-CR-175102] p 110 N87-19539
- CALCO, FRANK S.**
Precision tunable resonant microwave cavity
[NASA-CASE-LEW-13935-1] p 126 N87-21234
- CALDWELL, R. J.**
Gear mesh compliance modeling p 164 A87-53422
- Gear mesh compliance modeling
[NASA-TM-88843] p 166 N87-18092
- CAMPANELLA, S. JOSEPH**
On-board processing satellite network architecture and control study
[NASA-CR-180816] p 44 N87-27710
- On-board processing satellite network architecture and control study
[NASA-CR-180817] p 44 N87-27711
- Onboard multichannel demultiplexer/demodulator
[NASA-CR-180821] p 119 N87-28819
- CAMPBELL, D. P.**
Measurement techniques for millimeter wave substrate mounted MMW antennas
p 121 A87-40926
- Measurement techniques for millimeter wave substrate mounted MMW antennas
p 123 A87-45899
- Technology for satellite power conversion
[NASA-CR-180162] p 193 N87-18229
- Technology for satellite power conversion
[NASA-CR-181057] p 66 N87-25420
- CAO, H. V.**
Performance and aerodynamic braking of a horizontal-axis wind turbine from small-scale wind tunnel tests
[NASA-CR-180812] p 198 N87-27327
- CAREK, GERALD A.**
Shot peening for Ti-6Al-4V alloy compressor blades
[NASA-TP-2711] p 184 N87-20566
- CARGILL, G.**
Scaled centrifugal compressor program
[NASA-CR-174912] p 26 N87-14349
- CARLSON, A. W.**
Solar dynamic space power system heat rejection
p 47 A87-18175
- CARLSON, R. L.**
Analysis of shell-type structures subjected to time-dependent mechanical and thermal loading
[NASA-CR-180349] p 183 N87-19756
- Nonisothermal elasto-visco-plastic response of shell-type structures
p 185 N87-22796
- CARLSON, ROBERT L.**
Thermodynamically consistent constitutive equations for nonisothermal large-strain, elastoplastic, creep behavior
p 175 A87-27945
- CARNEY, KELLY S.**
The effect of nonlinearities on the dynamic response of a large Shuttle payload
[AIAA PAPER 87-0857] p 40 A87-33697
- The effect of nonlinearities on the dynamic response of a large shuttle payload
[NASA-TM-88941] p 181 N87-18112

CARPENTER, M. H.

- The effects of engine speed and injection characteristics on the flow field and fuel/air mixing in motored two-stroke diesel engines
[AIAA PAPER 87-0227] p 161 A87-22501
- Numerical simulation of the flow field and fuel sprays in an IC engine
[SAE PAPER 870599] p 143 A87-48751

CARUSO, J. J.

- Assessment of simplified composite micromechanics using three-dimensional finite-element analysis
p 72 A87-19121

CASSIDY, J. F.

- Space power development impact on technology requirements
[IAF PAPER 86-143] p 41 A87-15894

CASTOR, J. G.

- Compound cycle engine program p 23 A87-53428
- Compound cycle engine program
[NASA-TM-88879] p 25 A87-11790

CASTOR, JERE G.

- Compound cycle engine for helicopter application
[NASA-CR-175110] p 31 A87-25323

CATALDO, R. L.

- Parametric and cycle tests of a 40-AH bipolar nickel-hydrogen battery p 46 A87-18093

CATALDO, ROBERT L.

- Component variations and their effects on bipolar nickel-hydrogen cell performance
[NASA-TM-89907] p 195 A87-23029

CATALDO, RUSSELL L.

- Test results of a 60 volt bipolar nickel-hydrogen battery
[NASA-TM-89927] p 195 A87-24029

CAUGHEY, D. A.

- An L-U implicit multigrid algorithm for the three-dimensional Euler equations
[AIAA PAPER 87-0453] p 133 A87-22645

CAUGHEY, DAVID A.

- A diagonal implicit multigrid algorithm for the Euler equations
[AIAA PAPER 87-0354] p 2 A87-22578

- Multigrid solution of inviscid transonic flow through rotating blade passages
[AIAA PAPER 87-0608] p 3 A87-24992

CAULFIELD, THOMAS

- Fiber reinforced superalloys
[NASA-TM-89865] p 75 A87-22811

CAVALIERE, A.

- Quasars as indicators of galactic ages p 223 A87-26927

CAWLEY, J. D.

- Oxygen-18 tracer study of the passive thermal oxidation of silicon p 78 A87-51187

CEBECI, T.

- Progress in the prediction of unsteady heat transfer on turbine blades p 149 A87-22769

CEBECI, TUNCER

- A general method for unsteady stagnation region heat transfer and results for model turbine flows
[NASA-TM-88903] p 146 A87-17002

CELESTINA, M. L.

- A numerical simulation of the inviscid flow through a counterrotating propeller
[ASME PAPER 86-GT-138] p 3 A87-25395

CELESTINA, MARK L.

- The utilization of parallel processing in solving the inviscid form of the average-passage equation system for multistage turbomachinery
[AIAA PAPER 87-1108] p 5 A87-42057

CERNANSKY, N. P.

- Degradation mechanisms of sulfur and nitrogen containing compounds during thermal stability testing of model fuels
[AIAA PAPER 87-2039] p 106 A87-45372

CERNANSKY, NICHOLAS P.

- Spark ignition of monodisperse fuel sprays
[NASA-CR-181404] p 80 A87-29635
- Thermal stability of distillate hydrocarbon fuels
[NASA-CR-181412] p 107 A87-29706

CHALMERS, H.

- On-board processing satellite network architecture and control study
[NASA-CR-180816] p 44 A87-27710

CHALMERS, HARVEY

- On-board processing satellite network architecture and control study
[NASA-CR-180817] p 44 A87-27711

CHAMIS, C. C.

- Assessment of simplified composite micromechanics using three-dimensional finite-element analysis
p 72 A87-19121

- Fabrication and quality assurance processes for superhybrid composite fan blades p 72 A87-19123

- Design concepts/parameters assessment and sensitivity analyses of select composite structural components p 175 A87-25407

- Structural tailoring of advanced turboprops
[AIAA PAPER 87-0753] p 177 A87-33648

- Composite interlaminar fracture toughness: Three-dimensional finite element modeling for mixed mode 1, 2 and 3 fracture
[NASA-TM-88872] p 73 A87-13491

- Probabilistic structural analysis methods for space propulsion system components
[NASA-TM-88861] p 181 A87-13794

- Strain energy release rates of composite interlaminar end-notch and mixed-mode fracture: A sublaminate/ply level analysis and a computer code
[NASA-TM-89827] p 74 A87-20389

CHAMIS, CHRISTOS C.

- Simplified composite micromechanics for predicting microstresses p 72 A87-20090

- Probabilistic structural analysis to quantify uncertainties associated with turbopump blades
[AIAA PAPER 87-0766] p 176 A87-33581

- Advances in 3-D Inelastic Analysis Methods for hot section components
[AIAA PAPER 87-0719] p 177 A87-33645

- Simplified composite micromechanics for predicting microstresses p 179 A87-49275

- Computational composite mechanics for aerospace propulsion structures
[NASA-TM-88965] p 74 A87-18614

- Probabilistic structural analysis to evaluate the structural durability of SSME critical components p 62 A87-22783

- Dynamic delamination buckling in composite laminates under impact loading: Computational simulation
[NASA-TM-100192] p 75 A87-28611

CHANG, CHING-DER

- A 30-GHz monolithic receiver p 121 A87-23953

CHANG, G. C.

- Mechanical behavior of thermal barrier coatings for gas turbine blades p 24 A87-11196

CHANG, HAO

- Temperature dependence (4K to 300K) of the electrical resistivity of methane grown carbon fibers p 97 A87-47375

CHANG, J.

- Slow crack growth in sintered silicon nitride p 98 A87-48989

CHANG, S. C.

- Solution of elliptic partial differential equations by fast Poisson solvers using a local relaxation factor. 2: Two-step method
[NASA-TP-2530] p 205 A87-14918

CHANG, S. H.

- Computer aided design and analysis of gear tooth geometry
[NASA-CR-179611] p 168 A87-23969

CHANG, SIN-CHUNG

- Solution of elliptic PDEs by fast Poisson solvers using a local relaxation factor p 204 A87-21968

- On the validity of the modified equation approach to the stability analysis of finite-difference methods
[AIAA PAPER 87-1120] p 204 A87-42069

CHANG, T. Y.

- On the symbolic manipulation and code generation for elastoplastic material matrices p 201 A87-18499

- On the numerical performance of three-dimensional thick shell elements using a hybrid/mixed formulation p 175 A87-25924

- An efficient quadrilateral element for plate bending analysis p 178 A87-45994

- A quadrilateral shell element using a mixed formulation p 179 A87-53796

CHAO, C.

- 30 GHz monolithic balanced mixers using an ion-implanted FET-compatible 3-inch GaAs wafer process technology p 121 A87-34525

CHAO, H. C.

- A computer solution for the dynamic load, lubricant film thickness and surface temperatures in spiral bevel gears
[NASA-CR-4077] p 169 A87-26358

CHAO, P. C.

- Microwave performance of a quarter-micrometer gate low-noise pseudomorphic InGaAs/AlGaAs modulation-doped field effect transistor p 121 A87-23745

CHEN, C.-J.

- Finite analytic numerical solution of two-dimensional channel flow over a backward-facing step p 131 A87-13506

CHEN, CHIUN-HSUN

- Diffusion flame extinction in slow convection flow under microgravity environment p 77 A87-38787

- Size and shape of solid fuel diffusion flames in very slow speed flows
[AIAA PAPER 87-2030] p 78 A87-52248

CHEN, S. H.

- A panel method for counter rotating propfans
[AIAA PAPER 87-1890] p 21 A87-45279

CHEN, W. J.

- Optimal placement of critical speeds in rotor-bearing systems p 162 A87-38464

CHENG, H. S.

- A simplified computer solution for the flexibility matrix of contacting teeth for spiral bevel gears
[NASA-CR-179620] p 168 A87-23977

- A computer solution for the dynamic load, lubricant film thickness and surface temperatures in spiral bevel gears
[NASA-CR-4077] p 169 A87-26358

CHENG, J.-J. A.

- Analysis of the solidified structure of rheocast and VADER processed nickel-base superalloy p 83 A87-28734

CHENG, JUNG-JEN ALLEN

- Processing-structure characterization of rheocast IN-100 superalloy p 82 A87-24116

CHERRETTE, ALAN R.

- Detection of reflector surface error from near-field data: Effect of edge diffracted field
[NASA-TM-89920] p 117 A87-22874

CHIAPPETTA, L. M.

- User's manual for a TEACH computer program for the analysis of turbulent, swirling reacting flow in a research combustor
[NASA-CR-179547] p 78 A87-11858

CHILDS, DARA W.

- Experimental rotordynamic coefficient results for teeth-on-rotor and teeth-on-stator labyrinth gas seals p 167 A87-22212

CHILDS, MORRIS E.

- An experimental investigation of compressible three-dimensional boundary layer flow in annular diffusers
[AIAA PAPER 87-0366] p 3 A87-24954

CHIMA, RODRICK V.

- Comparison of three explicit multigrid methods for the Euler and Navier-Stokes equations
[AIAA PAPER 87-0602] p 137 A87-34725

- Comparison of three explicit multigrid methods for the Euler and Navier-Stokes equations
[NASA-TM-88878] p 1 A87-16784

- Time-partitioning simulation models for calculation on parallel computers
[NASA-TM-89850] p 203 A87-20766

- Application of advanced computational codes in the design of an experiment for a supersonic throughflow fan rotor
[NASA-TM-88915] p 13 A87-22630

- Unsteady stator/rotor interaction p 149 A87-22767

CHOE, S. J.

- Effects of temperature and hold times on low cycle fatigue of Astroloy p 85 A87-38541

CHOI, H. C.

- Macrocrack interaction with transverse array of microcracks
[NASA-CR-180806] p 186 A87-25607

CHOI, K. Y.

- Endwall heat transfer in the junction region of a circular cylinder normal to a flat plate at 30 and 60 degrees from stagnation point of the cylinder
[AIAA PAPER 87-0077] p 132 A87-22398

CHOO, Y.

- Generation of a composite grid for turbine flows and consideration of a numerical scheme
[NASA-TM-88890] p 11 A87-17662

CHOO, YUNG K.

- Composite grid and finite-volume LU implicit scheme for turbine flow analysis
[AIAA PAPER 87-1129] p 5 A87-42078

- Composite grid and finite-volume LU implicit scheme for turbine flow analysis
[NASA-TM-89828] p 12 A87-20235

CHOREY, C. M.

- Antiphase boundaries in epitaxially grown beta-SiC p 217 A87-30025

- TEM investigation of beta-SiC grown epitaxially on Si substrate by CVD p 97 A87-40927

CHOU, R.

- Reduction of the radar cross section of arbitrarily shaped cavity structures
[NASA-CR-180307] p 118 A87-27085

CHOU, RI-CHEE

- Rays versus modes - Pictorial display of energy flow in an open-ended waveguide p 112 A87-44075

CHOW, EDWIN

- Nuclear reactor power for a space-based radar. SP-100 project
[NASA-TM-89295] p 213 A87-25838

- CHOY, FRED K.**
Experimental and analytical evaluation of dynamic load and vibration of a 2240-kW (300-hp) rotorcraft transmission
[NASA-TM-88975] p 167 N87-20556
- CHRISS, R. M.**
An LDA investigation of three-dimensional normal shock-boundary layer interactions in a corner
[AIAA PAPER 87-1369] p 6 A87-44938
- CHRISTNER, L. G.**
Performance study of a fuel cell Pt-on-C anode in presence of CO and CO₂, and calculation of adsorption parameters for CO poisoning p 188 A87-12338
On the effect of the Fe(2+)/Fe(3+) redox couple on oxidation of carbon in hot H₃PO₄ p 78 A87-42677
Corrosion of graphite composites in phosphoric acid fuel cells p 152 A87-42684
Modeling for CO poisoning of a fuel cell anode p 191 A87-52288
- CHU, M. L.**
Structural properties of impact ices accreted on aircraft structures
[NASA-CR-179580] p 182 N87-18121
- CHUANG, ISAAC**
A detailed description of the uncertainty analysis for High Area Ratio Rocket Nozzle tests at the NASA Lewis Research Center
[NASA-TM-100203] p 68 N87-28602
- CHUBB, DONALD L.**
Liquid sheet radiator
[AIAA PAPER 87-1525] p 140 A87-43048
Gas particle radiator p 141 A87-45646
Combination solar photovoltaic heat engine energy converter p 190 A87-47088
Gas particle radiator
[NASA-CASE-LEW-14297-1] p 156 N87-15452
Liquid sheet radiator
[NASA-TM-89841] p 147 N87-18786
Performance characteristics of a combination solar photovoltaic heat engine energy converter
[NASA-TM-89908] p 195 N87-23028
Combination photovoltaic-heat engine energy converter
[NASA-CASE-LEW-14252-1] p 196 N87-25630
- CHUDNOVSKY, A.**
An analysis for crack layer stability p 176 A87-28982
Elastic interaction of a crack with a microcrack array. I - Formulation of the problem and general form of the solution. II - Elastic solution for two crack configurations (piecewise constant and linear approximations) p 178 A87-36926
Crack layer theory p 178 A87-40056
- CHUE, R.**
Calculations of inlet distortion induced compressor flowfield instability p 30 N87-24470
- CHUN, K. S.**
Estimation of instantaneous heat transfer coefficients for a direct-injection stratified-charge rotary engine
[SAE PAPER 870444] p 163 A87-48787
Performance and efficiency evaluation and heat release study of an outboard Marine Corporation Rotary Combustion Engine
[NASA-TM-89833] p 28 N87-20282
Synchronization trigger control system for flow visualization
[NASA-TM-89902] p 128 N87-23902
- CHUNG, B. T. F.**
Thermomechanical behavior of plasma-sprayed ZrO₂-Y₂O₃ coatings influenced by plasticity, creep and oxidation
[NASA-TM-88940] p 147 N87-18784
- CIANCONE, MICHAEL L.**
Flow visualization study of the effect of injection hole geometry on an inclined jet in crossflow p 155 A87-45842
- CIARDULLO, SAMUEL W.**
Evaluation of capillary reinforced composites for anti-icing
[AIAA PAPER 87-0023] p 17 A87-24904
- CIVINSKAS, KESTUTIS C.**
Composite grid and finite-volume LU implicit scheme for turbine flow analysis
[AIAA PAPER 87-1129] p 5 A87-42078
Composite grid and finite-volume LU implicit scheme for turbine flow analysis
[NASA-TM-89828] p 12 N87-20235
- CLAING, R. G.**
Thin film strain gage development program
[NASA-CR-174707] p 159 N87-28883
- CLARK, B. J.**
High-speed propeller noise predictions - Effects of boundary conditions used in blade loading calculations
[AIAA PAPER 87-0525] p 208 A87-24978
- Euler analysis of the three-dimensional flow field of a high-speed propeller - Boundary condition effects
[ASME PAPER 87-GT-253] p 6 A87-48719
High-speed propeller noise predictions: Effects of boundary conditions used in blade loading calculations
[NASA-TM-88913] p 210 N87-14957
Euler analysis of the three dimensional flow field of a high-speed propeller: Boundary condition effects
[NASA-TM-88955] p 10 N87-16798
- CLARK, BRUCE J.**
Coupled aerodynamic and acoustical predictions for turboprops
[NASA-TM-87094] p 13 N87-23598
- CLARK, DAVID A.**
Contingency power for small turboshaft engines using water injection into turbine cooling air
[AIAA PAPER 87-1906] p 21 A87-45289
Contingency power for small turboshaft engines using water injection into turbine cooling air
[NASA-TM-89817] p 28 N87-20280
- CLARK, RALPH**
A proposed GaAs-based superlattice solar cell structure with high efficiency and high radiation tolerance p 189 A87-19915
Design considerations for a GaAs nipi doping superlattice solar cell p 196 N87-26422
- CLARY, D. W.**
Shock-tube pyrolysis of acetylene - Sensitivity analysis of the reaction mechanism for soot formation p 75 A87-12598
Empirical modeling of soot formation in shock-tube pyrolysis of aromatic hydrocarbons p 76 A87-12599
- CLAUS, RUSSELL W.**
Modeling turbulent, reacting flow p 147 N87-20270
Direct numerical simulations of a temporally evolving mixing layer subject to forcing
[NASA-TM-88896] p 150 N87-23933
- CLOPP, WILLIAM**
An advanced geostationary communications platform p 112 A87-43165
- CLOUD, STANLEY D.**
The temperature dependence of inelastic light scattering from small particles for use in combustion diagnostic instrumentation
[NASA-CR-180399] p 80 N87-28634
- COCHRAN, THOMAS H.**
Space station electrical power system
[NASA-TM-100140] p 68 N87-26144
- COE, H. H.**
Testing of UH-60A helicopter transmission in NASA Lewis 2240-kW (3000-hp) facility
[NASA-TP-2626] p 164 N87-10391
- COE, HAROLD H.**
Effect of interference fits on roller bearing fatigue life p 162 A87-37686
- COHEN, J.**
The evolution of instabilities in the axisymmetric jet. I - The linear growth of disturbances near the nozzle. II - The flow resulting from the interaction between two waves p 138 A87-37256
- COHEN, LAWRENCE M.**
Simultaneous measurements of two-dimensional velocity and pressure fields in compressible flows through image-intensified detection of laser-induced fluorescence p 143 A87-52320
- COHEN, R. S.**
Degradation mechanisms of sulfur and nitrogen containing compounds during thermal stability testing of model fuels
[AIAA PAPER 87-2039] p 106 A87-45372
- COLE, GARY L.**
Automating the parallel processing of fluid and structural dynamics calculations
[NASA-TM-89837] p 203 N87-19002
- COLEMAN, E. B.**
Effects of multiple rows and noncircular orifices on dilution jet mixing p 138 A87-39805
- COLES-HAMILTON, CAROLYN**
Selection of high temperature thermal energy storage materials for advanced solar dynamic space power systems
[NASA-TM-89886] p 149 N87-22174
- COLES-HAMILTON, CAROLYN E.**
Impact of thermal energy storage properties on solar dynamic space power conversion system mass
[NASA-TM-89909] p 63 N87-22802
- COLES, C. E.**
Advanced solar dynamic space power systems perspectives, requirements and technology needs
[NASA-TM-88884] p 56 N87-12606
- COLES, CAROLYN E.**
Effect of an oxygen plasma on the physical and chemical properties of several fluids for the Liquid Droplet Radiator
[AIAA PAPER 87-0080] p 42 A87-22401
- COLLIN, ROBERT E.**
Microstrip dispersion including anisotropic substrates p 123 A87-47621
- CONCUS, P.**
Equilibrium fluid interfaces in the absence of gravity p 138 A87-38790
- CONNOLLY, D. J.**
Advances in gallium arsenide monolithic microwave integrated-circuit technology for space communications systems p 120 A87-19091
- CONNOLLY, DENIS J.**
Monolithic Microwave Integrated Circuit (MMIC) technology for space communications applications
[NASA-TM-100187] p 118 N87-27883
- CONTOLATIS, A.**
30 GHz monolithic balanced mixers using an ion-implanted FET-compatible 3-inch GaAs wafer process technology p 121 A87-34525
- COOK, T. S.**
Thermal barrier coating life prediction model
[NASA-CR-179504] p 100 N87-13539
- COOMES, EDMUND P.**
PEGASUS: A multi-megawatt nuclear electric propulsion system p 59 N87-17787
- COOPER, A. R.**
Oxygen-18 tracer study of the passive thermal oxidation of silicon p 78 A87-51187
- COOPER, L. P.**
Status of advanced propulsion for space based orbital transfer vehicle
[NASA-TM-88848] p 56 N87-10959
- COOPER, LARRY P.**
Status of advanced propulsion for space based orbital transfer vehicle
[IAF PAPER 86-183] p 48 A87-23239
- CORBAN, ROBERT R.**
Experimental evaluation of wall Mach number distributions of the octagonal test section proposed for NASA Lewis Research Center's altitude wind tunnel
[NASA-TP-2666] p 35 N87-17717
- CORNELL, C. C.**
Experimental and theoretical study of propeller spinner/shank interference
[AIAA PAPER 87-0145] p 3 A87-24929
- CORNILSEN, BAHNE C.**
A point defect model for nickel electrode structures p 87 A87-52282
- CORRIGAN, ROBERT D.**
Performance and power regulation characteristics of two airion-controlled rotors and a pitchable tip-controlled rotor on the Mod-O turbine
[NASA-TM-100136] p 200 N87-29956
- COWLEY, S. J.**
Generation of Tollmien-Schlichting waves on interactive marginally separated flows p 144 A87-54365
- COY, J. J.**
New generation methods for spur, helical, and spiral-bevel gears p 164 A87-53420
New generation methods for spur, helical, and spiral-bevel gears
[NASA-TM-88862] p 165 N87-15466
- COY, JOHN J.**
Identification and proposed control of helicopter transmission noise at the source
[NASA-TM-89312] p 18 N87-16816
Vibration characteristics of OH-58A helicopter main rotor transmission
[NASA-TP-2705] p 167 N87-20555
Helicopter transmission testing at NASA Lewis Research Center
[NASA-TM-89912] p 168 N87-22978
- CRADDOCK, JAMES N.**
The sensitivity of mechanical properties of TFRS composites to variations in reaction zone size and properties
[AIAA PAPER 87-0757] p 72 A87-33577
- CRAIG, G.**
A model propulsion simulator for evaluating counter rotating blade characteristics
[SAE PAPER 861715] p 20 A87-32607
- CRAIG, JAMES E.**
Visualization of flows in a motored rotary combustion engine using holographic interferometry
[AIAA PAPER 86-1557] p 19 A87-21514
- CRANDELL, M.**
The 20 GHz power GaAs FET development
[NASA-CR-179546] p 124 N87-16972
- CRAWFORD, R. A.**
Gas flow environmental and heat transfer nonrotating 3D program p 145 N87-11223
- CRAWLEY, EDWARD F.**
A linearized Euler analysis of unsteady flows in turbomachinery
[NASA-CR-180987] p 149 N87-22948

CRIMP, MARTIN A.

Ductility and fracture in B2 FeAl alloys
[NASA-CR-180810] p 93 N87-27771

CRONIN, M.

Automotive Stirling engine development program
[NASA-CR-174972] p 221 N87-20137
Automotive Stirling Engine Development Program
[NASA-CR-174873] p 222 N87-30223

CRUSE, T. A.

Probabilistic Structural Analysis Methods (PSAM) for select space propulsion system structural components p 62 N87-22784

CURRAN, F. M.

Performance characterization of a low power hydrazine arcjet
[AIAA PAPER 87-1057] p 50 A87-39634
Low power arcjet life issues
[AIAA PAPER 87-1059] p 50 A87-39635

CURRAN, FRANCIS M.

Low power dc arcjet operation with hydrogen/nitrogen/ammonia mixtures
[AIAA PAPER 87-1948] p 53 A87-48575
In-situ analysis of hydrazine decomposition products
[AIAA PAPER 87-2122] p 54 A87-50198
Low power DC arcjet operation with hydrogen/nitrogen/ammonia mixtures
[NASA-TM-89876] p 64 N87-22804
In-situ analysis of hydrazine decomposition products
[NASA-TM-89916] p 65 N87-23693

CURRAN, FRANK M.

Arcjet component conditions through a multistart test
[AIAA PAPER 87-1060] p 51 A87-41127
Arcjet starting reliability - A multistart test on hydrogen/nitrogen mixtures
[AIAA PAPER 87-1061] p 51 A87-41128
Arcjet component conditions through a multistart test
[NASA-TM-89857] p 61 N87-20382
Arcjet starting reliability: A multistart test on hydrogen/nitrogen mixtures
[NASA-TM-89867] p 61 N87-21998

CURREN, ARTHUR N.

Carbon and carbon-coated electrodes for multistage depressed collectors for electron-beam devices - A technology review p 120 A87-20666
Performance of textured carbon on copper electrode multistage depressed collectors with medium-power traveling wave tubes
[NASA-TP-2665] p 125 N87-17990

CURTIS, H. B.

Performance of GaAs and silicon concentrator cells under 1 MeV electron irradiation p 189 A87-19871

CURTIS, HENRY B.

Performance of AlGaAs, GaAs and InGaAs cells after 1 MeV electron irradiation p 197 N87-26438

CUTA, JUDITH M.

PEGASUS: A multi-megawatt nuclear electric propulsion system p 59 N87-17787

D**DAHELE, J. S.**

An experimental investigation of parasitic microstrip arrays
[NASA-TM-100168] p 129 N87-27120

DAHL, MILO D.

A finite element model for wave propagation in an inhomogeneous material including experimental validation
[NASA-TM-100149] p 207 N87-25821
Effects of fiber motion on the acoustic behavior of an anisotropic, flexible fibrous material
[NASA-TM-89884] p 212 N87-25826

DALTON, C.

A model for fluid flow during saturated boiling on a horizontal cylinder p 139 A87-41173

DAMORE, LISA

Silsesquioxanes as precursors to ceramic composites
[NASA-TM-89893] p 75 N87-25432

DANGELO, N.

Measurements of plasma parameters in the vicinity of the Space Shuttle p 200 A87-24672
Measurements of plasma density and turbulence near the shuttle orbiter
[NASA-CR-180102] p 215 N87-16614

DANIS, ALLEN M.

Spark ignition of monodisperse fuel sprays
[NASA-CR-181404] p 80 N87-29635

DAPKUS, P. D.

Nonlinear absorption in AlGaAs/GaAs multiple quantum well structures grown by metalorganic chemical vapor deposition p 217 A87-39687

DARLING, CLIFF

The T55-L-712 turbine engine compressor housing refurbishment project
[NASA-CR-179624] p 92 N87-23729

DAT, ROVINDRA

The 60 GHz IMPATT diode development
[NASA-CR-179536] p 218 N87-17515

DAUGHERTY, ELAINE S.

Automated measurement of the bit-error rate as a function of signal-to-noise ratio for microwave communications systems
[NASA-TM-89898] p 127 N87-22102

DAVIDIAN, KENNETH J.

Comparison of two procedures for predicting rocket engine nozzle performance
[AIAA PAPER 87-2071] p 52 A87-45391

Comparison of two procedures for predicting rocket engine nozzle performance
[NASA-TM-89814] p 60 N87-20379

Pretest uncertainty analysis for chemical rocket engine tests
[NASA-TM-89819] p 157 N87-20515

A detailed description of the uncertainty analysis for High Area Ratio Rocket Nozzle tests at the NASA Lewis Research Center
[NASA-TM-100203] p 68 N87-28602

DAVIS, V. A.

Three dimensional simulation of the operation of a hollow cathode electron emitter on the Shuttle orbiter
[NASA-TM-100203] p 119 A87-14084

Hollow cathodes as electron emitting plasma contactors
Theory and computer modeling
[AIAA PAPER 87-0569] p 214 A87-22712

Ram ion scattering caused by Space Shuttle v x B induced differential charging p 200 A87-51713

DAWSON, JEFF M.

The utilization of parallel processing in solving the inviscid form of the average-passage equation system for multistage turbomachinery
[AIAA PAPER 87-1108] p 5 A87-42057

DAYTON, J. A., JR.

Ultra small electron beam amplifiers p 122 A87-42681

DE JONGHE, L. C.

Degradation mechanisms in thermal-barrier coatings p 94 A87-12953

DE WITT, K. J.

Efficient numerical simulation of an electrothermal de-icer pad
[AIAA PAPER 87-0024] p 137 A87-32190
The effect of ambient pressure on the performance of a resistojet
[AIAA PAPER 87-0991] p 52 A87-42181

DEADMORE, D.

Tribology of selected ceramics at temperatures to 900 C p 94 A87-12954

DEADMORE, DANIEL L.

Hardness of CaF₂ and BaF₂ solid lubricants at 25 to 670 deg C
[NASA-TM-88979] p 102 N87-18670

Friction and wear of sintered Alpha SiC sliding against IN-718 alloy at 25 to 800 C in atmospheric air at ambient pressure
[NASA-TM-87353] p 103 N87-22860

DECHOW, CURTIS

Design of an advanced wood composite rotor and development of wood composite blade technology
[NASA-CR-174713] p 73 N87-17861

DECKER, A. J.

Evaluation of diffuse-illumination holographic cinematography in a flutter cascade
[NASA-TP-2593] p 156 N87-13731

DECKER, ARTHUR J.

Beam-modulation methods in quantitative and flow-visualization holographic interferometry p 111 N87-21204

DEFELICE, DAVID M.

Thermodynamic analysis and subscale modeling of space-based orbit transfer vehicle cryogenic propellant resupply
[AIAA PAPER 87-1764] p 142 A87-48572

Cryogenic Fluid Management Flight Experiment (CFMFE) p 109 N87-21150

Thermodynamic analysis and subscale modeling of space-based orbit transfer vehicle cryogenic propellant resupply
[NASA-TM-89921] p 150 N87-22949

DEININGER, WILLIAM

Nuclear reactor power for a space-based radar. SP-100 project
[NASA-TM-89295] p 213 N87-25838

DEISSLER, R. G.

Turbulent solutions of the Navier-Stokes equations p 139 A87-40932

DEJONGHE, L. C.

Degradation mechanisms in thermal barrier coatings
[NASA-TM-89309] p 101 N87-17926

DELAAT, J. C.

A real-time simulation evaluation of an advanced detection, isolation and accommodation algorithm for sensor failures in turbine engines p 18 A87-13318

DELAAT, JOHN C.

Full-scale engine demonstration of an advanced sensor failure detection isolation, and accommodation algorithm - Preliminary results p 22 A87-50422

Full-scale engine demonstration of an advanced sensor failure detection, isolation and accommodation algorithm: Preliminary results
[NASA-TM-89880] p 127 N87-22097

Advanced detection, isolation and accommodation of sensor failures: Real-time evaluation
[NASA-TP-2740] p 34 N87-25331

DELANEY, B. R.

A model propulsion simulator for evaluating counter rotating blade characteristics
[SAE PAPER 861715] p 20 A87-32607

DELLACORTE, CHRIS

Composition optimization of self-lubricating chromium-carbide-based composite coatings for use to 760 C p 86 A87-27838

Effects of atmosphere on the tribological properties of a chromium carbide based coating for use to 760 deg C
[NASA-TM-88894] p 101 N87-16140

DELLACORTE, CHRISTOPHER

Composition optimization of chromium carbide based solid lubricant coatings for foil gas bearings at temperatures to 650 C
[NASA-CR-179649] p 105 N87-26233

Experimental evaluation of chromium-carbide-based solid lubricant coatings for use to 760 C
[NASA-CR-180808] p 105 N87-27053

DELOMBARD, RICHARD

A photovoltaic power system and a low-power satellite earth station for Indonesia p 189 A87-19859

DEMASI, J. T.

Thermal barrier coating life prediction model development
[NASA-CR-179508] p 99 N87-11892

DEPAUW, JAMES F.

Space experiment development process p 109 N87-21156

DESALVO, GREGORY C.

An optimized top contact design for solar cell concentrators p 189 A87-19882

DEUTSCH, S.

The measurement of boundary layers on a compressor blade in cascade at high positive incidence angle. 1: Experimental techniques and results
[NASA-CR-179491] p 25 N87-13441

The measurement of boundary layers on a compressor blade in cascade at high positive incidence angle. 2: Data report
[NASA-CR-179492] p 25 N87-13442

DEVANCE, DARRELL

Space station power semiconductor package
[NASA-CR-180829] p 129 N87-28825

DEVER, TERESE

An evaluation of candidate oxidation resistant materials p 80 N87-26203

DEVER, TERESE

An evaluation of candidate oxidation resistant materials for space applications in LEO
[NASA-TM-100122] p 105 N87-25480

DEVLOO, PH.

An adaptive finite element strategy for complex flow problems
[AIAA PAPER 87-0557] p 133 A87-22706

Adaptive finite element methods for compressible flow problems p 4 A87-38496

Recent advances in error estimation and adaptive improvement of finite element calculations p 204 A87-41239

DEWITT, K. J.

Numerical prediction of cold turbulent flow in combustor configurations with different centerbody flame holders
[ASME PAPER 86-WA/HT-50] p 140 A87-43715

DHAR, H. P.

Performance study of a fuel cell Pt-on-C anode in presence of CO and CO₂, and calculation of adsorption parameters for CO poisoning p 188 A87-12338

On the effect of the Fe(2+)/Fe(3+) redox couple on oxidation of carbon in hot H₃PO₄ p 78 A87-42677

Corrosion of graphite composites in phosphoric acid fuel cells p 72 A87-42684

Modeling for CO poisoning of a fuel cell anode p 191 A87-52288

DIAMOND, W. A.

Analysis of experimental shaft seal data for high-performance turbomachines - As for Space Shuttle main engines p 162 A87-45846

DIAS, J. B.

The NESSUS finite element code p 184 N87-22785

- DICARLO, J. A.**
Polymer, metal, and ceramic matrix composites for advanced aircraft engine applications p 71 A87-15187
- DIECK, RONALD H.**
A detailed description of the uncertainty analysis for High Area Ratio Rocket Nozzle tests at the NASA Lewis Research Center [NASA-TM-100203] p 68 N87-28602
- DIFILIPPO, FRANK**
An evaluation of candidate oxidation resistant materials for space applications in LEO [NASA-TM-100122] p 105 N87-25480
An evaluation of candidate oxidation resistant materials p 80 N87-26203
- DILLEHAY, M. E.**
A heater made from graphite composite material for potential deicing application [NASA-TM-88888] p 17 N87-12559
- DILLEHAY, MICHAEL E.**
A heater made from graphite composite material for potential deicing application [AIAA PAPER 87-0025] p 17 A87-24905
Effects of milling brominated P-100 graphite fibers p 97 A87-41078
- DITTMAR, J. H.**
Cruise noise of counterrotation propeller at angle of attack in wind tunnel [NASA-TM-88869] p 210 N87-13252
- DITTMAR, JAMES H.**
Noise reduction for model counterrotation propeller at cruise by reducing aft-propeller diameter [NASA-TM-88936] p 211 N87-19057
The effect of front-to-rear propeller spacing on the interaction noise of a model counterrotation propeller at cruise conditions [NASA-TM-100121] p 212 N87-28396
Cruise noise of the 2/9th scale model of the Large-scale Advanced Propfan (LAP) propeller, SR-7A [NASA-TM-100175] p 212 N87-28398
- DIXON, J.**
Communications satellite systems operations with the space station. Volume 1: Executive summary [NASA-CR-179526] p 206 N87-17472
Communications satellite systems operations with the space station, volume 2 [NASA-CR-179527] p 206 N87-17473
- DODDS, W. J.**
A variable geometry combustor for broadened properties fuels [AIAA PAPER 87-1832] p 23 A87-52246
- DOHERTY, ROGER D.**
Processing-structure characterization of rheocast IN-100 superalloy p 82 A87-24116
- DOLCE, JAMES L.**
Automating the U.S. Space Station's electrical power system p 48 A87-23646
- DOLGOPOLSKY, A.**
Elastic interaction of a crack with a microcrack array. I - Formulation of the problem and general form of the solution. II - Elastic solution for two crack configurations (piecewise constant and linear approximations) p 178 A87-36926
- DOMBRO, LOUIS**
A 20 GHz, high efficiency dual mode TWT for the ACTS program p 122 A87-45511
- DOONG, W.**
The use of satellites in non-geostationary orbits for unloading geostationary communication satellite traffic peaks. Volume 1: Executive summary [NASA-CR-179597-VOL-1] p 117 N87-21212
The use of satellites in non-geostationary orbits for unloading geostationary communication satellite traffic peaks. Volume 2: Technical report [NASA-CR-179597-VOL-2] p 117 N87-21213
- DOREMUS, ROBERT H.**
Annealing of electron damage in mid-IR transmitting fluoride glass p 99 A87-53652
- DOS REIS, HENRIQUE L. M.**
Nondestructive evaluation of adhesive bond strength using the stress wave factor technique p 170 A87-32200
- DOSANJH, SUDIP S.**
Forced cocurrent smoldering combustion p 77 A87-40572
- DOWLING, N. E.**
Opening and closing of cracks at high cyclic strains p 84 A87-34661
J-integral estimates for cracks in infinite bodies p 177 A87-35334
- DOWNEY, ALAN N.**
A new model for broadband waveguide to microstrip transition design [NASA-TM-88905] p 115 N87-16958
- DRAKE, M. C.**
Simulation of fluid flows during growth of organic crystals in microgravity [NASA-TM-88921] p 108 N87-16167
- DRAPER, SUSAN L.**
Observations of directional gamma prime coarsening during engine operation [NASA-TM-100105] p 92 N87-25459
- DRESHFIELD, R. L.**
Application of single crystal superalloys for earth-to-orbit propulsion systems [AIAA PAPER 87-1976] p 85 A87-45336
Application of single crystal superalloys for Earth-to-orbit propulsion systems [NASA-TM-89877] p 91 N87-22034
- DRESHFIELD, ROBERT L.**
Understanding single-crystal superalloys p 85 A87-40928
Defects in nickel-base superalloys p 86 A87-49790
Observations of directional gamma prime coarsening during engine operation [NASA-TM-100105] p 92 N87-25459
- DRIGGERS, T.**
Satellite analog FDMA/FM to digital TDMA conversion [NASA-CR-179605] p 125 N87-20467
- DUFFY, S. F.**
A viscoplastic constitutive theory for metal matrix composites at high temperature [NASA-CR-179530] p 180 N87-13790
- DUNCAN, G.**
Cryogenic gear technology for an orbital transfer vehicle engine and tester design [NASA-CR-175102] p 110 N87-19539
- DUQUETTE, D. J.**
Effects of temperature and hold times on low cycle fatigue of Astroloy p 85 A87-38541
- DURBIN, E. J.**
An anemometer for highly turbulent or recirculating flows p 154 A87-37698
- DURBIN, P. A.**
Nonlinear critical layers eliminate the upper branch of spatially growing Tollmien-Schlichting waves p 131 A87-12251
An anemometer for highly turbulent or recirculating flows p 154 A87-37698
Shear flow instability generated by non-homogeneous external forcing p 142 A87-48047
Asymptotic analysis of corona discharge from thin electrodes [NASA-TP-2645] p 215 N87-14998
- DUSTIN, M. O.**
Advanced solar dynamic space power systems perspectives, requirements and technology needs [NASA-TM-88884] p 56 N87-12606
- DVORAK, S. D.**
Dynamic data acquisition, reduction, and analysis for the identification of high-speed compressor component post-stability characteristics [AIAA PAPER 87-2089] p 162 A87-45398

E

- EATON, JOHN K.**
An experimental study of the development of longitudinal vortex pairs embedded in a turbulent boundary layer [AIAA PAPER 87-1309] p 139 A87-42376
- EBERHARDT, R. N.**
On-orbit cryogenic storage and resupply p 41 A87-18344
- EBIHARA, BEN T.**
Improvements in MDC and TWT overall efficiency through the application of carbon electrode surfaces p 120 A87-20667
TWT efficiency improvement by a low-cost technique for deposition of carbon on MDC electrodes p 121 A87-30199
Design, fabrication and performance of small, graphite electrode, multistage depressed collectors with 200-W, CW, 8- to 18-GHz traveling-wave tubes [NASA-TP-2693] p 126 N87-20474
Traveling-wave-tube efficiency improvement by a low-cost technique for deposition of carbon on multistage depressed collector [NASA-TP-2719] p 126 N87-21239
Apparatus for mounting a field emission cathode [NASA-CASE-LEW-14108-1] p 129 N87-28832
- ECK, T. G.**
Oxygen interaction with space-power materials [NASA-CR-181396] p 80 N87-29633
- ECKERLE, W. A.**
Soot loading in a generic gas turbine combustor [AIAA PAPER 87-0297] p 19 A87-22544
- EDUCATO, JAMES LOUIS**
Modelling of multijunction cascade photovoltaics for space applications [NASA-CR-181417] p 200 N87-29958
- EDWARD, BRYAN**
APS-Workshop on Characterization of MMIC (Monolithic Microwave Integrated Circuit) Devices for Array Antenna [AD-P005398] p 118 N87-28763
- EGGER, R. A.**
Solar concentrator materials development p 213 A87-18171
Oxidation-resistant reflective surfaces for solar dynamic power generation in near Earth orbit [NASA-TM-88865] p 56 N87-10960
- EISENBERG, J. D.**
Folding tilt rotor demonstrator feasibility study p 17 A87-19247
- EKSTEDT, E. E.**
NASA/GE advanced low emissions combustor program [AIAA PAPER 87-2035] p 21 A87-45369
- ELANGOVAN, E.**
Experimental, water droplet impingement data on two-dimensional airfoils, axisymmetric inlet and Boeing 737-300 engine inlet [AIAA PAPER 87-0097] p 17 A87-24918
- ELFE, T. B.**
Optimization of spherical facets for parabolic solar concentrators p 213 A87-18173
- ELLEMAN, DANIEL D.**
Research opportunities in microgravity science and applications during shuttle hiatus [NASA-TM-88964] p 108 N87-16917
- ELLIS, J. R.**
Results of an interlaboratory fatigue test program conducted on alloy 800H at room and elevated temperatures p 87 A87-54370
High-temperature constitutive modeling p 179 N87-11210
A viscoplastic constitutive theory for metal matrix composites at high temperature [NASA-CR-179530] p 180 N87-13790
A mechanism for precise linear and angular adjustment utilizing flexures p 165 N87-16342
- ELMORE, D. L.**
Further development of the dynamic gas temperature measurement system. Volume 1: Technical efforts [NASA-CR-179513-VOL-1] p 157 N87-19686
- ELROD, H. G.**
Thermohydrodynamic analysis for laminar lubricating films [NASA-TM-88845] p 144 N87-11124
- ENDRES, N. M.**
Composite space antenna structures - Properties and environmental effects p 72 A87-38610
- ENDRES, NED M.**
Composite space antenna structures: Properties and environmental effects [NASA-TM-88859] p 73 N87-16880
- ENGLAND, J. E.**
Development and test of the Shuttle/Centaur cryogenic tankage thermal protection system [AIAA PAPER 87-1557] p 43 A87-43073
- ENGLAND, JAMES E.**
Design, development and test of shuttle/Centaur G-prime cryogenic tankage thermal protection systems [NASA-TM-89825] p 43 N87-23685
- ENGLISH, ROBERT E.**
Speculations on future opportunities to evolve Brayton powerplants aboard the space station [NASA-TM-89863] p 39 N87-23674
- ENSIGN, C. ROBERT**
Toward improved durability in advanced combustors and turbines: Progress in the prediction of thermomechanical loads [NASA-TM-88932] p 32 N87-28551
- ENSWORTH, CLINTON B. F., III**
Performance and power regulation characteristics of two aileron-controlled rotors and a pitchable tip-controlled rotor on the Mod-O turbine [NASA-TM-100136] p 200 N87-29956
- EPSTEIN, A. H.**
Rotor wake characteristics of a transonic axial-flow fan p 2 A87-20886
Rotational effects on impingement cooling p 141 A87-45838
- ERICKSON, C. M.**
Concepts for space maintenance of OTV engines p 40 A87-41161
Concepts for space maintenance of OTV engines p 37 A87-46000
Concepts for space maintenance of OTV engines p 67 N87-26097
- ERIKSON, R. J.**
Optimization of spherical facets for parabolic solar concentrators p 213 A87-18173

ERNST, MICHAEL A.

- A NASTRAN primer for the analysis of rotating flexible blades
[NASA-TM-89861] p 184 N87-21375
Hub flexibility effects on propfan vibration
[NASA-TM-89900] p 186 N87-24722
- ERST, W.**
Automotive Stirling engine development program
[NASA-CR-174972] p 221 N87-20137
Automotive Stirling Engine Development Program
[NASA-CR-174873] p 222 N87-30223
- ERSON, L.**
Application of adaptive antenna techniques to future commercial satellite communication
[NASA-CR-179566] p 115 N87-16954
Application of adaptive antenna techniques to future commercial satellite communications. Executive summary
[NASA-CR-179566-SUMM] p 115 N87-16955
- EUSEPI, M. W.**
EHD analysis of and experiments on pumping Leningrader seals
[NASA-CR-179570] p 168 N87-22246
- EVERSMAN, W.**
Modeling the effects of wind tunnel wall absorption on the acoustic radiation characteristics of propellers
[AIAA PAPER 86-1876] p 208 A87-17991
- EVERSON, KENT**
A photovoltaic power system and a low-power satellite earth station for Indonesia p 189 A87-19859
- EWELL, RICHARD**
Nuclear reactor power for a space-based radar. SP-100 project
[NASA-TM-89295] p 213 N87-25838

F

FAETH, G. M.

- Particle-laden swirling free jets - Measurements and predictions
[AIAA PAPER 87-0303] p 139 A87-42648
Particle-laden swirling free jets: Measurements and predictions
[NASA-TM-88904] p 26 N87-16826
- FARELL, C.**
Spanwise structures in transitional flow around circular cylinders
[AIAA PAPER 87-1383] p 140 A87-44940
- FARNHAM, T.**
The design and performance of a multi-stream droplet generator for the liquid droplet radiator
[AIAA PAPER 87-1538] p 140 A87-44842
- FAROKHI, S.**
Controlled excitation of a cold turbulent swirling free jet
[NASA-TM-100173] p 152 N87-27977
- FAROOQUE, M.**
Corrosion of graphite composites in phosphoric acid fuel cells p 72 A87-42684
- FARRELL, R.**
Automotive Stirling engine development program
[NASA-CR-174972] p 221 N87-20137
Automotive Stirling Engine Development Program
[NASA-CR-174873] p 222 N87-30223
- FAYMON, K. A.**
Spacecraft 2000 - The challenge of the future p 37 A87-18064
- FAYMON, KARL A.**
Automating the U.S. Space Station's electrical power system p 48 A87-23646
Spacecraft 2000: The challenge of the future p 68 N87-26448
- FEAR, J. S.**
NASA/GE advanced low emissions combustor program
[AIAA PAPER 87-2035] p 21 A87-45369
A variable geometry combustor for broadened properties fuels
[AIAA PAPER 87-1832] p 23 A87-52246
- FEKADE, KONJIT**
Observation of deep levels in cubic silicon carbide p 122 A87-41089
- FEKE, DONALD L.**
Colloidal characterization of ultrafine silicon carbide and silicon nitride powders p 95 A87-19625
Stability and rheology of dispersions of silicon nitride and silicon carbide
[NASA-CR-179634] p 104 N87-25476
- FERGUSON, DALE C.**
Development of the VOLT-A Shuttle experiment p 41 A87-19907
The voltage threshold for arcing for solar cells in Leo - Flight and ground test results
[AIAA PAPER 86-0362] p 50 A87-40275

FERGUSON, T. V.

- Feasibility of mapping velocity flowfields in an SSME powerhead using laser anemometry techniques
[AIAA PAPER 87-1306] p 154 A87-42374
- FERNANDEZ-PELLO, A. CARLOS**
Forced cocurrent smoldering combustion p 77 A87-40572
- FERRANTE, J.**
A universal equation of state for solids p 219 A87-14665
Compressibility of solids p 219 A87-51962
Analysis of plasma-nitrided steels
[NASA-TM-89815] p 91 N87-21078
- FERRANTE, JOHN**
The effect of Tricresyl-Phosphate (TCP) as an additive on wear of Iron (Fe)
[NASA-TM-100103] p 93 N87-27030
Tribology theory versus experiment
[NASA-TM-100198] p 71 N87-29599
- FESTER, D. A.**
On-orbit cryogenic storage and resupply p 41 A87-18344
- FILPUS, JOHN W.**
A review of research and development on the microwave-plasma electrothermal rocket
[AIAA PAPER 87-1011] p 49 A87-38008
A computer model for the recombination zone of a microwave-plasma electrothermal rocket
[AIAA PAPER 87-1014] p 50 A87-38009
- FIORINTINO, A.**
Antimitting kerosene JT3 engine fuel system integration study
[NASA-CR-4033] p 106 N87-24577
- FISKE, G. H.**
Turbobfan aft duct suppressor study. Contractor's data report of mode probe signal data
[NASA-CR-175067] p 34 N87-29538
Turbobfan aft duct suppressor study
[NASA-CR-175067] p 34 N87-29539
- FISKE, M. R.**
Equipment concept design and development plans for microgravity science and applications research on space station: Combustion tunnel, laser diagnostic system, advanced modular furnace, integrated electronics laboratory
[NASA-CR-179535] p 108 N87-15320
- FITZGERALD, T. J.**
Space power development impact on technology requirements
[IAF PAPER 86-143] p 41 A87-15894
- FLEETER, S.**
The effect of circumferential aerodynamic detuning on coupled bending-torsion unstalled supersonic flutter
[ASME PAPER 86-GT-100] p 20 A87-25396
- FLEETER, SANFORD**
Aeroelastic control of stability and forced response of supersonic rotors by aerodynamic detuning p 21 A87-46249
- FLEISCHER, D.**
Experiments on a repetitively pulsed electrothermal thruster
[AIAA PAPER 87-1043] p 50 A87-38017
Investigation of a repetitive pulsed electrothermal thruster
[NASA-CR-179464] p 59 N87-16878
- FLEMING, DAVID P.**
Experiments on dynamic stiffness and damping of tapered bore seals
[NASA-TM-89895] p 169 N87-23984
- FLEMINGS, M. C.**
Dendritic growth of undercooled nickel-tin. I, II p 85 A87-41012
- FLEMINGS, MERTON C.**
The alloy undercooling experiment on the Columbia STS 61-C Space Shuttle mission
[AIAA PAPER 87-0506] p 108 A87-45724
The alloy undercooling experiment on the Columbia STA 61-C space shuttle mission
[NASA-TM-88909] p 91 N87-18643
- FLOOD, DENNIS J.**
Issues in space photovoltaic research and technology
[NASA-TM-89922] p 128 N87-23901
- FORCE, DALE A.**
Calculation of secondary electron trajectories in multistage depressed collectors for microwave amplifiers
[NASA-TP-2664] p 125 N87-17991
Analytical and experimental performance of a dual-mode traveling wave tube and multistage depressed collector
[NASA-TP-2752] p 128 N87-25532
- FORD, C. W.**
High-efficiency GaAs solar concentrator cells for space and terrestrial applications p 188 A87-18073
High-efficiency GaAs concentrator space cells p 196 N87-26417

FORD, WILLIAM F.

- Extrapolation methods for vector sequences p 203 A87-53631
- FORDYCE, J. S.**
The potential impact of new power system technology on the design of a manned Space Station p 47 A87-18342
- FORESTIERI, A. F.**
Space Station Power System issues p 47 A87-19877
- FORMAN, RALPH**
Apparatus for mounting a field emission cathode
[NASA-CASE-LEW-14108-1] p 129 N87-28832
- FORSYTH, D. W.**
Computational aeroacoustics of propeller noise in the near and far field
[AIAA PAPER 87-0254] p 19 A87-24944
- FOSS, J. F.**
A critical analysis of transverse vorticity measurements in a large plane shear layer p 143 A87-52049
- FOUTCH, DAVID W.**
Size and shape of solid fuel diffusion flames in very slow speed flows
[AIAA PAPER 87-2030] p 78 A87-52248
- FOWLIS, WILLIAM K.**
Simulation of fluid flows during growth of organic crystals in microgravity
[NASA-TM-88921] p 108 N87-16167
- FOX, DENNIS S.**
Hot corrosion attack and strength degradation of SiC and Si(sub)3N(sub)4
[NASA-TM-89820] p 102 N87-20425
- FRANCISCUS, LEO C.**
The supersonic through-flow turbobfan for high Mach propulsion
[AIAA PAPER 87-2050] p 22 A87-50196
The supersonic through-flow turbobfan for high Mach propulsion
[NASA-TM-100114] p 30 N87-23626
- FRASCA, ALBERT J.**
Radiation effects on power transistor performance
[NASA-CR-181188] p 129 N87-27099
- FRASCH, L. L.**
An analysis of electromagnetic coupling and eigenfrequencies for microwave electrothermal thruster discharges
[AIAA PAPER 87-1012] p 51 A87-41111
- FRASCH, LYDELL L.**
A review of research and development on the microwave-plasma electrothermal rocket
[AIAA PAPER 87-1011] p 49 A87-38008
- FREEDMAN, M. R.**
Particle-size reduction of Si3N4 powder with Si3N4 milling hardware p 94 A87-12936
Improved consolidation of silicon carbide p 94 A87-12940
- FREEMAN, JON C.**
Self-consistent inclusion of space-charge in the traveling wave tube
[NASA-TM-89928] p 128 N87-24630
- FRELING, M.**
Materials for Advanced Turbine Engines (MATE). Project 4: Erosion resistant compressor airfoil coating
[NASA-CR-179622] p 92 N87-27029
- FRENKLACH, M.**
Shock-tube pyrolysis of acetylene - Sensitivity analysis of the reaction mechanism for soot formation p 75 A87-12598
Empirical modeling of soot formation in shock tube pyrolysis of aromatic hydrocarbons p 76 A87-12599
Systematic development of reduced reaction mechanisms for dynamic modeling p 77 A87-33987
- FREUND, G. A., JR.**
Experimental, water droplet impingement data on two-dimensional airfoils, axisymmetric inlet and Boeing 737-300 engine inlet
[AIAA PAPER 87-0097] p 17 A87-24918
- FRIEDMAN, ROBERT**
Science and technology issues in spacecraft fire safety
[AIAA PAPER 87-0467] p 39 A87-31107
Science and technology issues in spacecraft fire safety
[NASA-TM-88933] p 40 N87-16012
Fire safety concerns in space operations
[NASA-TM-89848] p 40 N87-20342
- FRIEDRICH, L. A.**
Materials for Advanced Turbine Engines (MATE). Project 4: Erosion resistant compressor airfoil coating
[NASA-CR-179622] p 92 N87-27029
- FRINT, HAROLD**
Automated inspection and precision grinding of spiral bevel gears
[NASA-CR-4083] p 169 N87-25578

FRITSCH, KLAUS

- Linear capacitive displacement sensor with frequency readout p 154 A87-42546
- Spectrum-modulating fiber-optic sensors for aircraft control systems [NASA-TM-88968] p 27 N87-17700
- Fiber-optic temperature sensor using a spectrum-modulating semiconductor etalon [NASA-TM-100153] p 31 N87-25329

FRITTS, S. D.

- Theoretical performance of hydrogen-bromine rechargeable SPE fuel cell p 199 N87-29945

FRONEK, DENNIS L.

- A distributed data acquisition system for aeronautics test facilities [NASA-TM-88961] p 35 N87-16851

FRYXELL, R. E.

- Effects of surface chemistry on hot corrosion life p 88 N87-11193

FU, K.-C.

- Thermal analysis of an orthotropic engineering body p 173 N87-13496

FUJIKAWA, GENE

- Bit-error-rate testing of high-power 30-GHz traveling wave tubes for ground-terminal applications [NASA-TP-2635] p 115 N87-17971
- Performance of a Ka-band satellite system under variable transmitted signal power conditions [NASA-TM-88984] p 116 N87-18700

FUJITA, TOSHIO

- Nuclear reactor power for a space-based radar. SP-100 project [NASA-TM-89295] p 213 N87-25838

FUNG, C. D.

- Behavior of inversion layers in 3C silicon carbide p 215 A87-11242
- Stoichiometric disturbances in compound semiconductors due to ion implantation p 215 A87-12292

FURST, R. B.

- Small centrifugal pumps for low-thrust rockets p 50 A87-39808

FUSARO, ROBERT L.

- Counterface effects on the tribological properties of polyimide composites p 95 A87-27625
- How to evaluate solid lubricant films using a Pin-on-disk tribometer p 97 A87-42618
- Tribological properties of polymer films and solid bodies in a vacuum environment p 101 N87-17906
- Tribological properties of coal slurries [NASA-TM-89930] p 104 N87-24565
- Comparison of the tribological properties of fluorinated cokes and graphites [NASA-TM-100170] p 106 N87-29679

G

GABB, T. P.

- Low cycle fatigue behaviour of a plasma-sprayed coating material p 82 A87-24040
- The characteristics of gamma-prime dislocation pairs in a nickel-base superalloy p 85 A87-46932
- The cyclic stress-strain behavior of PWA 1480 at 650 deg C [NASA-TM-87311] p 89 N87-14483
- Bithermal low-cycle fatigue behavior of a NiCoCrAlY-coated single crystal superalloy [NASA-TM-89831] p 91 N87-20408

GAHN, RANDALL F.

- Component variations and their effects on bipolar nickel-hydrogen cell performance [NASA-TM-89907] p 195 N87-23029
- Test results of a 60 volt bipolar nickel-hydrogen battery [NASA-TM-89927] p 195 N87-24029
- Effect of component compression on the initial performance of an IPV nickel-hydrogen cell [NASA-TM-100102] p 195 N87-24838

GAIER, J. R.

- Properties and potential applications of brominated P-100 carbon fibers p 95 A87-23702
- Microstructure-derived macroscopic residual resistance of brominated graphite fibers p 97 A87-48324
- Effects of graphitization on the environmental stability of brominated pitch-based fibers [NASA-TM-88899] p 100 N87-12679

GAIER, JAMES R.

- Effects of milling brominated P-100 graphite fibers p 97 A87-41078
- Stability of bromine, iodine monochloride, copper (II) chloride, and nickel (II) chloride intercalated pitch-based graphite fibers [NASA-TM-89904] p 103 N87-24563

GALECKI, DIANE L.

- Nuclear powered Mars cargo transport mission utilizing advanced ion propulsion [AIAA PAPER 87-1903] p 53 A87-50191
- Nuclear powered Mars cargo transport mission utilizing advanced ion propulsion [NASA-TM-100109] p 65 N87-23692

GALLAGHER, J. J.

- Measurement techniques for millimeter wave substrate mounted MMW antennas p 121 A87-40926
- Measurement techniques for millimeter wave substrate mounted MMW antennas p 123 A87-45899
- Technology for satellite power conversion [NASA-CR-180162] p 193 N87-18229
- Technology for satellite power conversion [NASA-CR-181057] p 66 N87-25420

GALLER, DONALD E.

- Breadboard RL10-11B low thrust operating mode [NASA-CR-174914] p 58 N87-15269

GALLO, C.

- Design and dynamic simulation of a fixed pitch 56 kW wind turbine drive train with a continuously variable transmission [NASA-CR-179543] p 193 N87-17401

GARCIA, DANA

- Styrene-terminated polysulfone oligomers as matrix material for graphite reinforced composites - An initial study p 98 A87-49370
- Styrene-terminated polysulfone oligomers as matrix material for graphite reinforced composites: An initial study [NASA-TM-89846] p 74 N87-21043

GARDINER, W. C., JR.

- Shock-tube pyrolysis of acetylene - Sensitivity analysis of the reaction mechanism for soot formation p 75 A87-12598

GARDNER, LLOYD B.

- The alloy undercooling experiment on the Columbia STS 61-C Space Shuttle mission [AIAA PAPER 87-0506] p 108 A87-45724
- The alloy undercooling experiment on the Columbia STA 61-C space shuttle mission [NASA-TM-88909] p 91 N87-18643

GAYDA, J.

- Low cycle fatigue behaviour of a plasma-sprayed coating material p 82 A87-24040
- Bithermal low-cycle fatigue behavior of a NiCoCrAlY-coated single crystal superalloy [NASA-TM-89831] p 91 N87-20408

GAZZANIGA, J. A.

- Off-design analysis of counter-rotating propeller configurations p 20 A87-27989

GAZZANIGA, JOHN A.

- The acoustic experimental investigation of counterrotating propeller configurations [SAE PAPER 871031] p 210 A87-48760

GEDEON, S. R.

- An assessment and validation study of nuclear reactors for low power space applications [NASA-CR-180672] p 213 N87-27495

GEDWILL, M. A.

- Coating life prediction p 99 N87-11194

GEDYMIN, JON S.

- Characterization of InGaAs/AlGaAs pseudomorphic modulation-doped field-effect transistors p 121 A87-23922

GEIER, JAMES V.

- Near-optimum design of the InP homojunction solar cell p 197 N87-26443

GELDER, THOMAS F.

- Detailed flow surveys of turning vanes designed for a 0.1-scale model of NASA Lewis Research Center's proposed altitude wind tunnel [NASA-TP-2680] p 36 N87-20295

- Design and performance of controlled-diffusion stator compared with original double-circular-arc stator [NASA-TM-100141] p 31 N87-26910

- Experimental evaluation of corner turning vanes [NASA-TM-100143] p 37 N87-28571

GELLER, B. D.

- 20-GHz phased-array-fed antennas utilizing distributed MMIC modules p 112 A87-34527

GEMEINER, RUSSEL P.

- Component variations and their effects on bipolar nickel-hydrogen cell performance [NASA-TM-89907] p 195 N87-23029
- Test results of a 60 volt bipolar nickel-hydrogen battery [NASA-TM-89927] p 195 N87-24029

GENERAZIO, E. R.

- Ultrasonic verification of microstructural changes due to heat treatment p 208 A87-10772
- Quantitative void characterization in structural ceramics by use of scanning laser acoustic microscopy p 171 A87-51974

- Ultrasonic determination of recrystallization [NASA-TM-88855] p 171 N87-10399

GENERAZIO, EDWARD R.

- Ultrasonic NDE of structural ceramics for power and propulsion systems [NASA-TM-100147] p 173 N87-26362

GENG, STEVEN M.

- Calibration and comparison of the NASA Lewis free-piston Stirling engine model predictions with RE-1000 test data [NASA-TM-89853] p 222 N87-22561

GEORGEKUTTY, T.

- Equipment concept design and development plans for microgravity science and applications research on space station: Combustion tunnel, laser diagnostic system, advanced modular furnace, integrated electronics laboratory [NASA-CR-179535] p 108 N87-15320

GERTZ, J. B.

- Rotor wake characteristics of a transonic axial-flow fan p 2 A87-20886

GHANDHI, S. K.

- Comparative performance of diffused junction indium phosphide solar cells p 197 N87-26441
- Solar cells in bulk InP using an open tube diffusion process p 198 N87-26444

GHANDHI, SORAB K.

- Shallow n(+) diffusion into InP by an open-tube diffusion technique p 217 A87-30023

GHONIEM, AHMED F.

- Vortex-scalar element calculations of a diffusion flame stabilized on a plane mixing layer [NASA-TM-100133] p 2 N87-28501

GHOSE, HIREN M.

- The effect of Tricresyl-Phosphate (TCP) as an additive on wear of Iron (Fe) [NASA-TM-100103] p 93 N87-27030

GHOSH, M. K.

- Starvation effects on the hydrodynamic lubrication of rigid nonconformal contacts in combined rolling and normal motion p 135 A87-27839

GHOSH, L. J.

- Analysis of mixed-mode crack propagation using the boundary integral method [NASA-CR-179518] p 180 N87-12915

GIARRATANO, P. J.

- Volume-energy parameters for heat transfer to supercritical fluids p 137 A87-32326

GIELDA, T. P.

- Navier Stokes solution of the flowfield over ice accretion shapes [AIAA PAPER 87-0099] p 2 A87-22414

GIESLER, F. J.

- Navier Stokes solution of the flowfield over ice accretion shapes [AIAA PAPER 87-0099] p 2 A87-22414

GILBERT, PERCY

- Computer control of a scanning electron microscope for digital image processing of thermal-wave images [NASA-TM-100157] p 128 N87-26278

GILCHRIST, GEORGE

- The T55-L-712 turbine engine compressor housing refurbishment project [NASA-CR-179624] p 92 N87-23729

GILJE, R. I.

- Space power development impact on technology requirements [IAF PAPER 86-143] p 41 A87-15894

GILLE, J. P.

- On-orbit cryogenic storage and resupply p 41 A87-18344

GINER, JOSE

- Oxygen electrodes for rechargeable alkaline fuel cells p 199 N87-29940

GINTY, C. A.

- Composite space antenna structures - Properties and environmental effects p 72 A87-38610

GINTY, CAROL A.

- Composite space antenna structures: Properties and environmental effects [NASA-TM-88859] p 73 N87-16880

GIOULEKAS, A.

- Enhanced current flow through a plasma cloud by induction of plasma turbulence [AIAA PAPER 87-0573] p 214 A87-22714

GIOVANNETTI, A. J.

- Long-term deposit formation in aviation turbine fuel at elevated temperature p 106 A87-14986

GIVI, PEYMAN

- On the coalescence-dispersion modeling of turbulent molecular mixing [NASA-TM-89910] p 2 N87-25292
- Vortex-scalar element calculations of a diffusion flame stabilized on a plane mixing layer [NASA-TM-100133] p 2 N87-28501

GLADDEN, H. J.

Computation of full-coverage film-cooled airfoil temperatures by two methods and comparison with high heat flux data
[NASA-TM-88931] p 150 N87-23934

GLASGOW, T. K.

Microstructures in rapidly solidified Ni-Mo alloys
p 87 A87-51636
Elevated temperature strengthening of a melt spun austenitic steel by TiB₂ p 87 A87-51639
Cellular microstructure of chill block melt spun Ni-Mo alloys p 87 A87-54300
Primary arm spacing in chill block melt spun Ni-Mo alloys
[NASA-TM-88887] p 88 N87-11875

GLASGOW, THOMAS K.

Chill block melt spinning of nickel-molybdenum alloys
p 86 A87-47902
Research opportunities in microgravity science and applications during shuttle hiatus
[NASA-TM-88964] p 108 N87-16917

GLASSMAN, IRVIN

The oxidation degradation of aromatic compounds
[NASA-CR-180588] p 79 N87-22020

GLIEBE, P. R.

Development of a rotor wake/vortex model. Volume 2: User's manual for computer program
[NASA-CR-174850-VOL-2] p 13 N87-20239

GODLEWSKI, M. P.

A 25.5 percent AMO gallium arsenide grating solar cell
p 189 A87-19840

GOEKOGLU, S. A.

Experimental verification of vapor deposition model in Mach 0.3 burner rigs
p 88 N87-11192

GOEL, P.

Third-moment closure of turbulence for predictions of separating and reattaching shear flows: A study of Reynolds-stress closure model
[NASA-CR-177055] p 145 N87-11961

GOKOGLU, SULEYMAN A.

Prediction and rational correlation of thermophoretically reduced particle mass transfer to hot surfaces across laminar or turbulent forced-convection gas boundary layers
p 133 A87-23449
Experimental verification of corrosive vapor deposition rate theory in high velocity burner rigs
p 143 A87-49551

GOLDMAN, LOUIS J.

Combined fringe and Fabry-Perot laser anemometer for 3 component velocity measurements in turbine stator cascade facility
p 110 N87-21183

GOLDSTEIN, M. E.

The generation of capillary instabilities on a liquid jet
p 130 A87-12060
Nonlinear critical layers eliminate the upper branch of spatially growing Tollmien-Schlichting waves
p 131 A87-12251
The generation of Tollmien-Schlichting waves by long wavelength free stream disturbances
p 139 A87-41655
Generation of Tollmien-Schlichting waves on interactive marginally separated flows
p 144 A87-54365
A note on the generation of Tollmien-Schlichting waves by sudden surface-curvature change
p 144 A87-54366

GOLDSTEIN, MARVIN E.

Aeroacoustics of subsonic turbulent shear flows
[NASA-TM-100165] p 212 N87-26615

GOLDSTEIN, S. A.

Experiments on a repetitively pulsed electrothermal thruster
[AIAA PAPER 87-1043] p 50 A87-38017
Investigation of a repetitive pulsed electrothermal thruster
[NASA-CR-179464] p 59 N87-16878

GONSALVEZ, D. J. A.

Alternative mathematical programming formulations for FSS synthesis
[NASA-CR-180030] p 202 N87-14872

GONSALVEZ, DAVID J. A.

On orbital allotments for geostationary satellites
[NASA-CR-181017] p 37 N87-22700

GONZALEZ-SANABRIA, O. D.

NASA Lewis evaluation of Regenerative Fuel Cell (RFC) systems
p 123 N87-11073

GONZALEZ-SANABRIA, O. D.

Nickel-hydrogen separator development
p 188 A87-18103

GONZALEZ-SANABRIA, OLGA

Regenerative fuel cell study for satellites in GEO orbit
[NASA-TM-89914] p 194 N87-22310
Test results of a 60 volt bipolar nickel-hydrogen battery
[NASA-TM-89927] p 195 N87-24029

GONZALEZ-SANABRIA, OLGA D.

Component variations and their effects on bipolar nickel-hydrogen cell performance
[NASA-TM-89907] p 195 N87-23029

GORADIA, C.

Cell performance and defect behavior in proton-irradiated lithium-counterdoped n(+)-p silicon solar cells
p 216 A87-14222

GORADIA, CHANDRA

A proposed GaAs-based superlattice solar cell structure with high efficiency and high radiation tolerance
p 189 A87-19915

Design considerations for a GaAs nipi doping superlattice solar cell
p 196 N87-26422
Near-optimum design of the InP homojunction solar cell
p 197 N87-26443

GORDAN, ANDREW L.

Centaur D1-A systems in a nutshell
[NASA-TM-88880] p 38 N87-15996

GORDON, J. D.

Space power development impact on technology requirements
[IAF PAPER 86-143] p 41 A87-15894

GORECKI, JOY

Silsesquioxanes as precursors to ceramic composites
[NASA-TM-89893] p 75 N87-25432

GOUKER, M. A.

Measurement techniques for millimeter wave substrate mounted MMW antennas
p 121 A87-40926
Measurement techniques for millimeter wave substrate mounted MMW antennas
p 123 A87-45899
Technology for satellite power conversion
[NASA-CR-180162] p 193 N87-18229
Technology for satellite power conversion
[NASA-CR-181057] p 66 N87-25420

GOULD, RICHARD D.

Two component laser velocimeter measurements of turbulence parameters downstream of an axisymmetric sudden expansion
p 139 A87-40703
Turbulence characteristics of an axisymmetric reacting flow
[NASA-CR-180697] p 152 N87-27973

GOVILA, R. K.

Fracture of flash oxidized, yttria-doped sintered reaction-bonded silicon nitride
p 97 A87-47923

GRABER, E. J.

Static tests of the propulsion system
[AIAA PAPER 87-1728] p 23 A87-52245

GRADY, JOSEPH E.

Dynamic delamination buckling in composite laminates under impact loading: Computational simulation
[NASA-TM-100192] p 75 N87-28611

GRAF, W.

On the numerical performance of three-dimensional thick shell elements using a hybrid/mixed formulation
p 175 A87-25924
A quadrilateral shell element using a mixed formulation
p 179 A87-53796

GRAHAM, RONALD E.

Effect of gimbal friction modelling technique on control stability and performance for Centaur upper stage
[AIAA PAPER 87-2455] p 38 A87-50501
Effect of Gimbal friction modeling technique on control stability and performance for Centaur upper-stage
[NASA-TM-89894] p 39 N87-22755

GRANT, H. P.

Advanced high temperature static strain sensor development
[NASA-CR-179520] p 158 N87-25552

High temperature static strain gage development contract, tasks 1 and 2
[NASA-CR-180811] p 159 N87-28869

Thin film strain gage development program
[NASA-CR-174707] p 159 N87-28883

GRATZ, R. F.

Substituted 1,1,1-triaryl-2,2,2-trifluoroethanes and processes for their synthesis
[NASA-CASE-LEW-14345-1] p 70 N87-14432
New condensation polyimides containing 1,1,1-triaryl-2,2,2-trifluoroethane structures
[NASA-CASE-LEW-14346-1] p 70 N87-14433

GRATZ, ROY F.

Thermo-oxidatively stable condensation polyimides containing 1,1,1-triaryl-2,2,2-trifluoroethane dianhydride and diamine monomers
[NASA-TM-89875] p 103 N87-22048

GRAVES, J. A.

Undercooling and crystallization behaviour of antimony droplets
p 83 A87-28732

GRAY, HUGH R.

Heat's on to develop high-temperature materials
p 85 A87-39897

GREBER, ISAAC

Investigation of two-dimensional shock-wave/boundary-layer interactions
p 4 A87-39528

GREEN, JAMES M.

An evaluation of metallized propellants based on vehicle performance
[AIAA PAPER 87-1773] p 53 A87-47003

An evaluation of metallized propellants based on vehicle performance
[NASA-TM-100104] p 64 N87-22806

GREENBERG, DONALD P.

Interactive color display of 3-D engineering analysis results
[NASA-CR-180589] p 203 N87-22422

GREGOREK, G. M.

Wind tunnel evaluation of a truncated NACA 64-621 airfoil for wind turbine applications
[NASA-CR-180803] p 196 N87-25621

GREITZER, E. M.

A method for assessing effects of circumferential flow distortion on compressor stability
p 7 A87-48722
Calculations of inlet distortion induced compressor flowfield instability
p 30 N87-24470

GRIFFIN, J. H.

Bladed disk vibration
[NASA-CR-181203] p 31 N87-26908

GRIFFIN, J. M.

An analysis of electromagnetic coupling and eigenfrequencies for microwave electrothermal thruster discharges
[AIAA PAPER 87-1012] p 51 A87-41111

GRIFFIN, JERRY H.

SSE blade damper technology
p 63 N87-22798

GRIFFIN, STAN A.

Measurement of Centaur/Orbiter multiple reaction forces in a full-scale test rig
p 38 A87-29448

GRIFFITH, P. C.

Design, implementation and investigation of an image guide-based optical flip-flop array
[NASA-CR-181382] p 213 N87-30180

GRISNIK, S. P.

Vacuum chamber pressure effects on thrust measurements of low Reynolds number nozzles
p 45 A87-14976

GRISNIK, STANLEY P.

Experimental study of low Reynolds number nozzles
[AIAA PAPER 87-0992] p 51 A87-41102
Experimental study of low Reynolds number nozzles
[NASA-TM-89858] p 61 N87-20383

GROBSTEIN, T. L.

The effect of electron beam welding on the creep rupture properties of a Nb-Zr-C alloy
[NASA-TM-88892] p 88 N87-13513
Creep behavior of niobium alloy PWC-11
[NASA-TM-89834] p 91 N87-20405

GROENEWEG, J. F.

High-speed propeller noise predictions - Effects of boundary conditions used in blade loading calculations
[AIAA PAPER 87-0525] p 208 A87-24978
Aircraft turbofan noise
p 209 A87-31144
Euler analysis of the three-dimensional flow field of a high-speed propeller - Boundary condition effects
[ASME PAPER 87-GT-253] p 6 A87-48719
High-speed propeller noise predictions: Effects of boundary conditions used in blade loading calculations
[NASA-TM-88913] p 210 N87-14957
Euler analysis of the three dimensional flow field of a high-speed propeller: Boundary condition effects
[NASA-TM-88955] p 10 N87-16798

GROESBECK, DONALD E.

Effects of fiber motion on the acoustic behavior of an anisotropic, flexible fibrous material
[NASA-TM-89884] p 212 N87-25826

GROSS, B.

Elastic analysis of a mode II fatigue crack test specimen
p 174 A87-17799

GROSSMAN, MERLIN

Nuclear reactor power for a space-based radar. SP-100 project
[NASA-TM-89295] p 213 N87-25838

GRUBER, ROBERT P.

Resistojet control and power for high frequency ac buses
[AIAA PAPER 87-0994] p 122 A87-41103
Low power arcjet thruster pulse ignition
[AIAA PAPER 87-1951] p 54 A87-50194
Resistojet control and power for high frequency ac buses
[NASA-TM-89860] p 126 N87-20477
Low power arcjet thruster pulse ignition
[NASA-TM-100123] p 64 N87-23691
Arcjet power supply and start circuit
[NASA-CASE-LEW-14374-1] p 36 N87-25335

GRUDKOWSKI, T. W.

Advanced high temperature static strain sensor development
[NASA-CR-179520] p 158 N87-25552

- GULBRANDSEN, N. C.**
Small centrifugal pumps for low-thrust rockets
p 50 A87-39808
- GULINO, D. A.**
Solar concentrator materials development
p 213 A87-18171
Oxidation-resistant reflective surfaces for solar dynamic power generation in near Earth orbit
[NASA-TM-88865] p 56 N87-10960
Effect of hard particle impacts on the atomic oxygen survivability of reflector surfaces with transparent protective overcoats
[NASA-TM-88874] p 56 N87-11838
The survivability of large space-borne reflectors under atomic oxygen and micrometeoroid impact
[NASA-TM-88914] p 57 N87-14423
- GULINO, DANIEL A.**
Effect of an oxygen plasma on the physical and chemical properties of several fluids for the Liquid Droplet Radiator
[AIAA PAPER 87-0080] p 42 A87-22401
Effect of hard particle impacts on the atomic oxygen survivability of reflector surfaces with transparent protective overcoats
[AIAA PAPER 87-0104] p 69 A87-22417
The survivability of large space-borne reflectors under atomic oxygen and micrometeoroid impact
[AIAA PAPER 87-0341] p 49 A87-31300
Effect of an oxygen plasma on uncoated thin aluminum reflecting films
[NASA-TM-89882] p 61 N87-21999
- GUPTA, B. K.**
Effects of surface chemistry on hot corrosion life
p 88 N87-11193
- GUPTA, I. J.**
SMI adaptive antenna arrays for weak interfering signals
[NASA-CR-181330] p 119 N87-28813
- GUPTA, INDER J.**
SMI adaptive antenna arrays for weak interfering signals
p 111 A87-20818
- GUSTAFSON, E.**
Solar dynamic space power system heat rejection
p 47 A87-18175
- GUTIERREZ-MIRAVETE, E.**
The mathematical modeling of rapid solidification processing
[NASA-CR-179551] p 88 N87-13514
- GYATT, G. W.**
Development and testing of vortex generators for small horizontal axis wind turbines
[NASA-CR-179514] p 193 N87-18922
- GYEKENYESI, J. P.**
SCARE - A postprocessor program to MSC/NASTRAN for reliability analysis of structural ceramic components
[ASME PAPER 86-GT-34] p 174 A87-17988
- GYEKENYESI, JOHN P.**
Surface flaw reliability analysis of ceramic components with the SCARE finite element postprocessor program
[NASA-TM-88901] p 181 N87-17087
Fracture mechanics concepts in reliability analysis of monolithic ceramics
[NASA-TM-100174] p 187 N87-27269
- GYEKENYESI, JOHN Z.**
Optical strain measuring techniques for high temperature tensile testing
[NASA-CR-179637] p 159 N87-26327
- H**
- HAAG, T. W.**
Performance characterization of a low power hydrazine arcjet
[AIAA PAPER 87-1057] p 50 A87-39634
- HAAG, THOMAS W.**
Arcjet component conditions through a multistart test
[AIAA PAPER 87-1060] p 51 A87-41127
Arcjet starting reliability - A multistart test on hydrogen/nitrogen mixtures
[AIAA PAPER 87-1061] p 51 A87-41128
Preliminary performance characterizations of an engineering model multipropellant resistojel for space station application
[AIAA PAPER 87-2120] p 54 A87-50197
Arcjet component conditions through a multistart test
[NASA-TM-89857] p 61 N87-20382
Arcjet starting reliability: A multistart test on hydrogen/nitrogen mixtures
[NASA-TM-89867] p 61 N87-21998
Preliminary performance characterizations of an engineering model multipropellant resistojel for space station application
[NASA-TM-100113] p 111 N87-23821
- HAAS, JEFFREY E.**
Reactivation study for NASA Lewis Research Center's Hypersonic Tunnel Facility
[AIAA PAPER 87-1886] p 34 A87-50190
Reactivation study for NASA Lewis Research Center's hypersonic tunnel facility
[NASA-TM-89918] p 36 N87-23664
- HADINGER, PETER J.**
Advanced space communications architecture study. Volume 2: Technical report
[NASA-CR-179592] p 115 N87-18695
Advanced space communications architecture study. Volume 1: Executive summary
[NASA-CR-179591] p 115 N87-18696
- HADY, WILLIAM F.**
Advanced liquid-cooled, turbocharged and intercooled stratified charge rotary engines for aircraft
[SAE PAPER 871039] p 22 A87-48766
- HAFTKA, R. T.**
Optimization of cascade blade mistuning under flutter and forced response constraints
p 24 N87-11732
Sensitivity analysis and approximation methods for general eigenvalue problems
[NASA-CR-179538] p 180 N87-12021
- HAFTKA, RAPHAEL T.**
Approximations to eigenvalues of modified general matrices
[AIAA PAPER 87-0947] p 177 A87-33756
- HAGEDORN, N. H.**
NASA Lewis evaluation of Regenerative Fuel Cell (RFC) systems
p 123 N87-11073
- HAGGERTY, J. S.**
Processing of laser formed SiC powder
[NASA-CR-179857] p 99 N87-11009
Processing of laser formed SiC powder
[NASA-CR-179638] p 104 N87-24573
- HAIJAR, J. F.**
Towards effective interactive three-dimensional colour postprocessing
p 201 A87-11895
- HALFORD, G. R.**
Re-examination of cumulative fatigue damage analysis - An engineering perspective
p 174 A87-22128
Fatigue and fracture: Overview
p 179 N87-11183
Bilthermal low-cycle fatigue behavior of a NiCoCrAlY-coated single crystal superalloy
[NASA-TM-89831] p 91 N87-20408
Exposure time considerations in high temperature low cycle fatigue
[NASA-TM-88934] p 187 N87-28944
- HALFORD, GARY R.**
Calculation of thermomechanical fatigue life based on isothermal behavior
[NASA-TM-88864] p 183 N87-20565
Environmental degradation of 316 stainless steel in high temperature low cycle fatigue
[NASA-TM-89931] p 185 N87-24007
- HALL, KENNETH C.**
A linearized Euler analysis of unsteady flows in turbomachinery
[NASA-CR-180987] p 149 N87-22948
- HALLINAN, G. J.**
Electrical power system for the U.S. Space Station
[IAF PAPER 86-37] p 45 A87-16138
Space station WP-04 power system. Volume 1: Executive summary
[NASA-CR-179587-VOL-1] p 65 N87-23695
Space station WP-04 power system. Volume 2: Study results
[NASA-CR-179587-VOL-2] p 65 N87-23696
- HALLORAN, J. W.**
Oxygen-18 tracer study of the passive thermal oxidation of silicon
p 78 A87-51187
- HALLUM, G. W.**
High-temperature effect of hydrogen on sintered alpha-silicon carbide
[NASA-TM-88819] p 100 N87-14518
- HAMAKER, H. C.**
High-efficiency GaAs solar concentrator cells for space and terrestrial applications
p 188 A87-18073
High-efficiency GaAs concentrator space cells
p 196 N87-26417
- HAMBOURGER, PAUL D.**
Effects of milling brominated P-100 graphite fibers
p 97 A87-41078
- HAMINS, A.**
Gravitational effects on the structure and propagation of premixed flames
[IAF PAPER 86-279] p 76 A87-15983
- HAMMER, A. N.**
Fabrication of cooled radial turbine rotor
[NASA-CR-179503] p 25 N87-11789
- HAMROCK, B. J.**
Starvation effects on the hydrodynamic lubrication of rigid nonconformal contacts in combined rolling and normal motion
p 135 A87-27839
- HAN, J. C.**
Local heat transfer augmentation in channels with two opposite ribbed surfaces
p 136 A87-30732
Measurement of heat transfer and pressure drop in rectangular channels with turbulence promoters
[NASA-CR-4015] p 146 N87-17003
- HANCOCK, J. P.**
PTA test bed aircraft engine inlet model test report, revised
[NASA-CR-174845] p 23 N87-10886
- HANDSCHUH, R. F.**
New generation methods for spur, helical, and spiral-bevel gears
p 164 A87-53420
New generation methods for spur, helical, and spiral-bevel gears
[NASA-TM-88862] p 165 N87-15466
- HANDSCHUH, ROBERT F.**
Identification and proposed control of helicopter transmission noise at the source
[NASA-TM-89312] p 18 N87-16816
An exponential finite difference technique for solving partial differential equations
[NASA-TM-89874] p 205 N87-24930
- HANKEY, W. L.**
Numerical simulation of excited jet mixing layers
[AIAA PAPER 87-0016] p 131 A87-22361
Navier Stokes solution of the flowfield over ice accretion shapes
[AIAA PAPER 87-0099] p 2 A87-22414
- HANNAH, MICHAEL**
Aircraft accident report: NASA 712, Convair 990, N712NA, March Air Force Base, California, July 17, 1985, executive summary
[NASA-TM-87356-VOL-1] p 16 N87-21878
Aircraft accident report: NASA 712, Convair 990, N712NA, March Air Force Base, California, July 17, 1985, facts and analysis
[NASA-TM-87356-VOL-2] p 16 N87-21879
- HANSEN, I. G.**
Description of a 20 kilohertz power distribution system
p 120 A87-18115
- HANSEN, IRVING G.**
Space Station 20-kHz power management and distribution system
p 49 A87-36913
20 kHz Space Station power system
p 51 A87-40378
EMC and power quality standards for 20-kHz power distribution
[NASA-TM-89925] p 62 N87-22004
- HANSMAN, R. JOHN, JR.**
In-flight measurement of ice growth on an airfoil using an array of ultrasonic transducers
[AIAA PAPER 87-0178] p 15 A87-22464
Comparison of wet and dry growth in artificial and flight icing conditions
p 16 A87-45635
- HANSON, RONALD K.**
Simultaneous measurements of two-dimensional velocity and pressure fields in compressible flows through image-intensified detection of laser-induced fluorescence
p 143 A87-52320
- HARDY, T. L.**
Low power arcjet life issues
[AIAA PAPER 87-1059] p 50 A87-39635
Electric propulsion options for the SP-100 reference mission
[NASA-TM-88918] p 57 N87-14422
- HARDY, TERRY L.**
Low power dc arcjet operation with hydrogen/nitrogen/ammonia mixtures
[AIAA PAPER 87-1948] p 53 A87-48575
Low power DC arcjet operation with hydrogen/nitrogen/ammonia mixtures
[NASA-TM-89876] p 64 N87-22804
- HARF, FREDRIC H.**
The alloy undercooling experiment on the Columbia STS 61-C Space Shuttle mission
[AIAA PAPER 87-0506] p 108 A87-45724
The alloy undercooling experiment on the Columbia STA 61-C space shuttle mission
[NASA-TM-88909] p 91 N87-18643
Heat treatment for superalloy
[NASA-CASE-LEW-14262-1] p 93 N87-28647
- HARIZ, A.**
Nonlinear absorption in AlGaAs/GaAs multiple quantum well structures grown by metalorganic chemical vapor deposition
p 217 A87-39687
- HARLOFF, G. J.**
Preliminary aerothermodynamic design method for hypersonic vehicles
[AIAA PAPER 87-2545] p 7 A87-49100
- HARLOFF, GARY J.**
High angle of attack hypersonic aerodynamics
[AIAA PAPER 87-2548] p 7 A87-49101
- HARMON, B. S.**
Thermal stability of the nickel-base superalloy B-1900 + Hf with tantalum variations
p 87 A87-51289

HARRINGTON, DOUGLAS E.

Experimental evaluation of wall Mach number distributions of the octagonal test section proposed for NASA Lewis Research Center's altitude wind tunnel [NASA-TP-2666] p 35 N87-17717

Experimental evaluation of blockage ratio and plenum evacuation system flow effects on pressure distribution for bodies of revolution in 0.1 scale model test section of NASA Lewis Research Center's proposed altitude wind tunnel [NASA-TP-2702] p 36 N87-22694

Experimental evaluation of honeycomb/screen configurations and short contraction section for NASA Lewis Research Center's altitude wind tunnel [NASA-TP-2692] p 36 N87-23662

HARRIS, G. L.

Observation of deep levels in cubic silicon carbide p 122 A87-41089

HARRISON, G. L.

Measurement of a counter rotation propeller flowfield using a Laser Doppler Velocimeter [AIAA PAPER 87-0008] p 3 A87-24901

HART, HAROLD

Iptycenes - Extended triptycenes p 69 A87-53654
Triptycene - A D(3h) C(62) hydrocarbon with three U-shaped cavities p 69 A87-53656

HART, R. E., JR.

Potential for use of InP solar cells in the space radiation environment p 120 A87-19996

Radiation and temperature effects in gallium arsenide, indium phosphide and silicon solar cells [NASA-TM-89870] p 127 N87-22098

Comparative performance of diffused junction indium phosphide solar cells p 197 N87-26441

Radiation damage in proton irradiated indium phosphide solar cells p 199 N87-29018

HART, RUSSELL E., JR.

Performance of AlGaAs, GaAs and InGaAs cells after 1 MeV electron irradiation p 197 N87-26438

HARTLEY, J. G.

Feasibility analysis of reciprocating magnetic heat pumps [NASA-CR-180262] p 147 N87-19647

HARTMAN, L. A.

The role of near-surface plastic deformation in the wear of lamellar solids p 162 A87-48500

HARVEY, P. R.

Structural tailoring of advanced turboprops [AIAA PAPER 87-0753] p 177 A87-33648

HASTINGS, D. E.

Enhanced current flow through a plasma cloud by induction of plasma turbulence [AIAA PAPER 87-0573] p 214 A87-22714

Radiation from large space structures in low earth orbit with induced ac currents [AIAA PAPER 87-0612] p 42 A87-22738

Theory of plasma contactors used in the ionosphere p 122 A87-41610

Enhanced current flow through a plasma cloud by induction of plasma turbulence p 214 A87-48241

HASTINGS, DANIEL E.

The radiation impedance of an electrodynamic tether with end connectors p 42 A87-42585

HATHAWAY, M. D.

Rotor wake characteristics of a transonic axial-flow fan p 2 A87-20886

Measurements of the unsteady flow field within the stator row of a transonic axial-flow fan. 1: Measurement and analysis technique [NASA-TM-88945] p 10 N87-16789

Measurements of the unsteady flow field within the stator row of a transonic axial-flow fan. Part 2: Results and discussion [NASA-TM-88946] p 10 N87-16790

HATHAWAY, MICHAEL D.

Unsteady flows in a single-stage transonic axial-flow fan stator row [NASA-TM-88929] p 11 N87-16805

Design and performance of controlled-diffusion stator compared with original double-circular-arc stator [NASA-TM-100141] p 31 N87-26910

HATTORI, S.

Plastic deformation of a magnesium oxide 001-plane surface produced by cavitation [ASLE PREPRINT 86-TC-3D-1] p 94 A87-19504

HATTORI, SHUJI

Deformation and fracture of single-crystal and sintered polycrystalline silicon carbide produced by cavitation [NASA-TM-88981] p 102 N87-20422

HAUCK, K. E.

The role of near-surface plastic deformation in the wear of lamellar solids p 162 A87-48500

HAUGLAND, E. J.

Compensation in epitaxial cubic SiC films p 216 A87-15071

Comment on 'Temperature dependence of electrical properties of non-doped and nitrogen-doped beta-SiC single crystals grown by chemical vapor deposition' p 217 A87-42846

HAVEN, V. E.

Indium phosphide shallow homojunction solar cells made by metalorganic chemical vapor deposition p 123 A87-50047

HAW, R. C.

A critical analysis of transverse vorticity measurements in a large plane shear layer p 143 A87-52049

HAWKES, THADDEUS A.

An advanced geostationary communications platform p 112 A87-43165

HAWLEY, MARTIN C.

A review of research and development on the microwave-plasma electrothermal rocket [AIAA PAPER 87-1011] p 49 A87-38008

A computer model for the recombination zone of a microwave-plasma electrothermal rocket [AIAA PAPER 87-1014] p 50 A87-38009

HAY, STUART S.

Preliminary performance characterizations of an engineering model multipropellant resistojel for space station application [AIAA PAPER 87-2120] p 54 A87-50197

Preliminary performance characterizations of an engineering model multipropellant resistojel for space station application [NASA-TM-100113] p 111 N87-23821

HAYKIN, T.

Jet engine simulation with water ingestion through compressor [NASA-CR-179549] p 1 N87-15932

HAZARIKA, BIRINCHI K.

An investigation of the flow characteristics in the blade endwall corner region [NASA-CR-4076] p 14 N87-29412

HEBSUR, M. G.

High temperature tensile and creep behaviour of low pressure plasma-sprayed Ni-Co-Cr-Al-Y coating alloy p 82 A87-23429

Stress rupture and creep behavior of a low pressure plasma-sprayed NiCoCrAlY coating alloy in air and vacuum p 85 A87-43396

HEBSUR, MOHAN G.

Elevated temperature tension, compression and creep-rupture behavior of (001)-oriented single crystal superalloy PWA 1480 [NASA-TM-88950] p 90 N87-17882

HECKEL, R. W.

The effects of tantalum on the microstructure of two polycrystalline nickel-base superalloys - B-1900 + Hf and MAR-M247 p 82 A87-24110

HECKERT, BRUCE J.

Space station resistojel system requirements and interface definition study [NASA-CR-179581] p 60 N87-17848

HEITMAN, P. W.

Slow crack growth in sintered silicon nitride p 98 A87-48989

HEITOR, M.

Gravitational effects on the structure and propagation of premixed flames [IAF PAPER 86-279] p 76 A87-15983

HELDT, L. A.

Further observations of SCC in alpha-beta brass. Considerations regarding the appearance of crack arrest markings during SCC p 82 A87-23843

HELLER, J. A.

A feasibility assessment of nuclear reactor power system concepts for the NASA Growth Space Station p 47 A87-18154

HELLER, JACK

Nuclear reactor power for a space-based radar. SP-100 project [NASA-TM-89295] p 213 N87-25838

HELLER, JACK A.

NASA Growth Space Station missions and candidate nuclear/solar power systems p 48 A87-21807

HEMANN, JOHN H.

Optical strain measuring techniques for high temperature tensile testing [NASA-CR-179637] p 159 N87-26327

HEMCKER, K. J.

Microstructures in rapidly solidified Ni-Mo alloys p 87 A87-51636

HEMCKER, KEVIN J.

Chill block melt spinning of nickel-molybdenum alloys p 86 A87-47902

HEMMINGER, J. A.

The noncavitating performance and life of a small vane-type positive displacement pump in liquid hydrogen [AIAA PAPER 86-1438] p 46 A87-17994

HENDERSON, T.

Microwave performance of a quarter-micrometer gate low-noise pseudomorphic InGaAs/AlGaAs modulation-doped field effect transistor p 121 A87-23745

HENDRICKS, R. C.

Thermal shaft effects on load-carrying capacity of a fully coupled, variable-properties cryogenic journal bearing [ASLE PREPRINT 86-TC-6B-1] p 160 A87-19502

A fully coupled variable properties thermohydraulic model for a cryogenic hydrostatic journal bearing [ASME PAPER 86-TRIB-55] p 161 A87-19536

Two-phase flows and heat transfer within systems with ambient pressure above the thermodynamic critical pressure p 136 A87-30728

Volume-energy parameters for heat transfer to supercritical fluids p 137 A87-32326

Analysis of experimental shaft seal data for high-performance turbomachines - As for Space Shuttle main engines p 162 A87-45846

Finite difference solution for a generalized Reynolds equation with homogeneous two-phase flow p 141 A87-45851

Comparison of generalized Reynolds and Navier Stokes equations for flow of a power law fluid p 142 A87-45852

Evaluation of seals for high-performance cryogenic turbomachines [NASA-TM-88919] p 146 N87-15442

HENDRICKS, ROBERT C.

Refrigerated dynamic seal to 6.9 MPa (1000 psi) p 164 A87-50777

Thermomechanical behavior of plasma-sprayed ZrO₂-Y₂O₃ coatings influenced by plasticity, creep and oxidation [NASA-TM-88940] p 147 N87-18784

Three-step labyrinth seal for high-performance turbomachines [NASA-TP-1848] p 150 N87-23921

Straight cylindrical seal for high-performance turbomachines [NASA-TP-1850] p 150 N87-23936

Three-step cylindrical seal for high-performance turbomachines [NASA-TP-1849] p 151 N87-24639

HERBELL, T. P.

Particle-size reduction of Si₃N₄ powder with Si₃N₄ milling hardware p 94 A87-12936

High-temperature effect of hydrogen on sintered alpha-silicon carbide [NASA-TM-88819] p 100 N87-14518

HERCZFELD, P. R.

System architecture of MMIC-based large aperture arrays for space application [NASA-TM-88940] p 125 N87-20468

HERRERA, J. I.

Utility interconnection issues for wind power generation [NASA-CR-175056] p 193 N87-17400

HICKS, YOLANDA R.

Visualization of flows in a motored rotary combustion engine using holographic interferometry [AIAA PAPER 86-1557] p 19 A87-21514

HIGUCHI, H.

Spanwise structures in transitional flow around circular cylinders [AIAA PAPER 87-1383] p 140 A87-44940

HILLER, BERNHARD

Simultaneous measurements of two-dimensional velocity and pressure fields in compressible flows through image-intensified detection of laser-induced fluorescence p 143 A87-52320

HILLERY, R. V.

Thermal barrier coating life prediction model [NASA-CR-179504] p 100 N87-13539

Thermal barrier coating life prediction model [NASA-CR-175010] p 100 N87-13540

HINCKEL, J. N.

Heat transfer in the stagnation region of the junction of a circular cylinder perpendicular to a flat plate p 131 A87-13019

HINDES, CHIP

Automotive Stirling engine system component review [SAE PAPER 870102] p 163 A87-48781

HINES, B. D.

Concepts for space maintenance of OTV engines p 40 A87-41161

Concepts for space maintenance of OTV engines p 37 A87-46000

Concepts for space maintenance of OTV engines p 67 N87-26097

HINGST, W. R.

An LDA investigation of three-dimensional normal shock-boundary layer interactions in a corner [AIAA PAPER 87-1369] p 6 A87-44938

- HINGST, WARREN R.**
Investigation of two-dimensional shock-wave/boundary-layer interactions p 4 A87-39528
- HINTZ, M. B.**
Further observations of SCC in alpha-beta brass
Considerations regarding the appearance of crack arrest markings during SCC p 82 A87-23843
- HIPPENSTEELE, STEVEN A.**
Use of a liquid-crystal, heater-element composite for quantitative, high-resolution heat transfer coefficients on a turbine airfoil, including turbulence and surface roughness effects [NASA-TM-87355] p 158 N87-22181
- HIRSCHBEIN, M. S.**
STAEBL: Structural tailoring of engine blades, phase 2 p 24 N87-11731
- HIRSCHBEIN, MURRAY**
Structural and aeroelastic analysis of the SR-7L propan [NASA-TM-86877] p 184 N87-22273
- HO, H.**
Composite load spectra for select space propulsion structural components [NASA-CR-179496] p 55 N87-10176
- HO, K.-S.**
Finite analytic numerical solution of two-dimensional channel flow over a backward-facing step p 131 A87-13506
- HOAG, DAVID**
The 60 GHz IMPATT diode development [NASA-CR-179536] p 218 N87-17515
- HOBBART, H. F.**
Evaluation results of the 700 deg C Chinese strain gages p 155 N87-11189
- HOBBART, HOWARD F.**
The NASA strain gage laboratory p 35 A87-52494
- HOBERECHT, M. A.**
Alkaline water electrolysis technology for Space Station regenerative fuel cell energy storage p 46 A87-18107
- HOCHSTEIN, J. I.**
Temperature fields due to jet induced mixing in a typical OTV tank [AIAA PAPER 87-2017] p 55 A87-52247
- HOCHSTEIN, JOHN I.**
Numerical modeling of on-orbit propellant motion resulting from an impulsive acceleration [AIAA PAPER 87-1766] p 40 A87-48573
Numerical modeling of on-orbit propellant motion resulting from an impulsive acceleration [NASA-TM-89873] p 41 N87-22757
- HOERST, D. J.**
Simulated flight acoustic investigation of treated ejector effectiveness on advanced mechanical suppressors for high velocity jet noise reduction [NASA-CR-4019] p 211 N87-17481
- HOFFMAN, D. J.**
An analytical and experimental investigation of resistojet plumes [NASA-TM-88852] p 58 N87-14428
- HOFFMAN, DAVID J.**
An analytical and experimental investigation of resistojet plumes [AIAA PAPER 87-0399] p 48 A87-24998
Effect of nozzle geometry on the resistojet exhaust plume [AIAA PAPER 87-2121] p 55 A87-52252
Resistojet plume and induced environment analysis [NASA-TM-88957] p 66 N87-24536
- HOFFMAN, J. A.**
WEST-3 wind turbine simulator development [NASA-CR-174983] p 192 N87-12046
- HOFFMAN, R. W.**
Oxygen interaction with space-power materials [NASA-CR-181396] p 80 N87-29633
- HOFFMAN, R., JR.**
Analysis of plasma-nitrided steels [NASA-TM-89815] p 91 N87-21078
- HOGAN, ROBERT J.**
Aircraft accident report: NASA 712, Convair 990, N712NA, March Air Force Base, California, July 17, 1985, executive summary [NASA-TM-87356-VOL-1] p 16 N87-21878
Aircraft accident report: NASA 712, Convair 990, N712NA, March Air Force Base, California, July 17, 1985, facts and analysis [NASA-TM-87356-VOL-2] p 16 N87-21879
- HOLDEMAN, J. D.**
Effects of multiple rows and noncircular orifices on dilution jet mixing p 138 A87-39805
- HOLDEMAN, JAMES D.**
Experiments and modeling of dilution jet flow fields p 148 N87-20276
- HOLLANSWORTH, J. E.**
An assessment of the status and trends in satellite communications 1986-2000: An information document prepared for the Communications Subcommittee of the Space Applications Advisory Committee [NASA-TM-88867] p 114 N87-13600
- HOLMAN, R.**
Noncommutative-geometry model for closed bosonic strings p 207 A87-37542
- HONEY, F.**
Analysis of plasma-nitrided steels [NASA-TM-89815] p 91 N87-21078
- HONEY, FRANK C.**
The effect of Tricresyl-Phosphate (TCP) as an additive on wear of Iron (Fe) [NASA-TM-100103] p 93 N87-27030
- HOPKINS, D. A.**
Optimization and analysis of gas turbine engine blades [AIAA PAPER 87-0827] p 201 A87-33614
- HOPKINS, DALE A.**
The sensitivity of mechanical properties of TFRS composites to variations in reaction zone size and properties [AIAA PAPER 87-0757] p 72 A87-33577
- HORSTEIN, MICHAEL**
Advanced space communications architecture study. Volume 2: Technical report [NASA-CR-179592] p 115 N87-18695
Advanced space communications architecture study. Volume 1: Executive summary [NASA-CR-179591] p 115 N87-18696
- HOSNY, W. M.**
Aerodynamic instability performance of an advanced high-pressure-ratio compression component [AIAA PAPER 86-1619] p 5 A87-41157
Dynamic data acquisition, reduction, and analysis for the identification of high-speed compressor component post-stability characteristics [AIAA PAPER 87-2089] p 162 A87-45398
- HOTES, DEBORAH**
An evaluation of candidate oxidation resistant materials for space applications in LEO [NASA-TM-100122] p 105 N87-25480
An evaluation of candidate oxidation resistant materials p 80 N87-26203
High temperature radiator materials for applications in the low Earth orbital environment [NASA-TM-100190] p 93 N87-29662
- HOUSER, DONALD R.**
The design and analysis of single flank transmission error tester for loaded gears [NASA-CR-179621] p 169 N87-27197
- HOUSER, M. J.**
Two-phase flow measurements of a spray in a turbulent flow [AIAA PAPER 87-0062] p 132 A87-22388
Laser velocimetry in turbulent flow fields - Particle response [AIAA PAPER 87-0118] p 132 A87-22426
Two-phase measurements of a spray in the wake of a bluff body p 142 A87-46199
- HOWARTH, R.**
Automotive Stirling engine development program [NASA-CR-174972] p 221 N87-20137
Automotive Stirling Engine Development Program [NASA-CR-174873] p 222 N87-30223
- HOWE, M.**
Recent advances in error estimation and adaptive improvement of finite element calculations p 204 A87-41239
- HOWES, W. L.**
Large aperture interferometer with phase-conjugate self-reference beam p 153 A87-17320
- HOYNIK, D.**
The effect of circumferential aerodynamic detuning on coupled bending-torsion unstalled supersonic flutter [ASME PAPER 86-GT-100] p 20 A87-25396
- HOYNIK, DANIEL**
Aeroelastic control of stability and forced response of supersonic rotors by aerodynamic detuning p 21 A87-46249
- HSU, C. Y.**
A simplified computer solution for the flexibility matrix of contacting teeth for spiral bevel gears [NASA-CR-179620] p 168 N87-23977
- HUANG, S. C.**
Evaluation of Stirling engine appendix gap losses p 160 A87-18037
- HUANG, SHYAN-CHERNG**
Mod II engine performance [SAE PAPER 870101] p 163 A87-48780
- HUCKELBRIDGE, A. A.**
Identification of structural interface characteristics using component mode synthesis [NASA-TM-88960] p 185 N87-24006
- HUFF, DENNIS L.**
Analysis of viscous transonic flow over airfoil sections [AIAA PAPER 87-0420] p 4 A87-34723
Numerical simulations of unsteady, viscous, transonic flow over isolated and cascaded airfoils using a deforming grid [AIAA PAPER 87-1316] p 7 A87-49649
Analysis of viscous transonic flow over airfoil sections [NASA-TM-88912] p 146 N87-17001
Numerical simulations of unsteady, viscous, transonic flow over isolated and cascaded airfoils using a deforming grid [NASA-TM-88890] p 13 N87-24435
- HUFF, RONALD G.**
Noise generated by flow through large butterfly valves [NASA-TM-88911] p 210 N87-16586
Identification and proposed control of helicopter transmission noise at the source [NASA-TM-89312] p 18 N87-16816
- HUGHES, W. F.**
Centrifugal inertia effects in two-phase face seal films p 162 A87-37687
- HULL, DAVID R.**
Fatigue failure of regenerator screens in a high frequency Stirling engine [NASA-TM-88974] p 183 N87-18882
Observations of directional gamma prime coarsening during engine operation [NASA-TM-100105] p 92 N87-25459
- HULLIGAN, DAVID**
Effect of water on hydrogen permeability [NASA-TM-88898] p 221 N87-16664
- HULSE, C. O.**
High temperature static strain gage alloy development program [NASA-CR-174833] p 157 N87-22179
Advanced high temperature static strain sensor development [NASA-CR-179520] p 158 N87-25552
High temperature static strain gage development contract, tasks 1 and 2 [NASA-CR-180811] p 159 N87-28869
- HULTGREN, LENNART S.**
A note on the generation of Tollmien-Schlichting waves by sudden surface-curvature change p 144 A87-54366
- HUMENIK, F. M.**
A model propulsion simulator for evaluating counter rotating blade characteristics [SAE PAPER 861715] p 20 A87-32607
- HUMES, R. L.**
In-flight photogrammetric measurement of wing ice accretions [AIAA PAPER 86-0483] p 15 A87-17995
- HUMES, ROBERT L.**
In-flight measurement of ice growth on an airfoil using an array of ultrasonic transducers [AIAA PAPER 87-0178] p 15 A87-22464
- HUNG, C. C.**
Properties and potential applications of brominated P-100 carbon fibers p 95 A87-23702
Thermal conductivity of pristine and brominated P-100 fibers [NASA-TM-88863] p 99 N87-11893
A heater made from graphite composite material for potential deicing application [NASA-TM-88868] p 17 N87-12559
- HUNG, CHING-CHEH**
A heater made from graphite composite material for potential deicing application [AIAA PAPER 87-0025] p 17 A87-24905
Effects of sequential treatment with fluorine and bromine on graphite fibers [NASA-TM-100106] p 104 N87-24574
Synthesis, physical and chemical properties, and potential applications of graphite fluoride fibers [NASA-TM-100156] p 105 N87-26232
- HUNTER, SCOTT D.**
Oil film thickness measurement and analysis for an angular contact ball bearing operating in parched elastohydrodynamic lubrication [NASA-CR-179506] p 70 N87-16879
- HURON, ERIC S.**
High temperature monotonic and cyclic deformation in a directionally solidified nickel-base superalloy [NASA-CR-175101] p 90 N87-15303
- HURWITZ, F. I.**
Ethylnated aromatics as high temperature matrix resins p 96 A87-34850
- HURWITZ, FRANCES I.**
Ceramic matrix and resin matrix composites: A comparison [NASA-TM-89830] p 74 N87-18615
Silsesquioxanes as precursors to ceramic composites [NASA-TM-89893] p 75 N87-25432

- HUSS, JANICE E.**
A comparison of five benchmarks
[NASA-TM-88956] p 202 N87-17441
- HUSSAIN, A. K. M. FAZLE**
Coherent structures and turbulence
p 133 A87-22859
- HUSTON, EDWARD S.**
The NASA/USAF arcjet research and technology program
[AIAA PAPER 87-1946] p 54 A87-50192
The NASA/USAF arcjet research and technology program
[NASA-TM-100112] p 66 N87-24525
- HUSTON, R. L.**
Computer aided design and analysis of gear tooth geometry
[NASA-CR-179611] p 168 N87-23969
- HUYNH, HUNG T.**
A finite difference scheme for three-dimensional steady laminar incompressible flow
[NASA-TM-89851] p 148 N87-20504
- HWANG, B. C.**
On similarity solutions for turbulent and heated round jets
p 130 A87-10922
- HWANG, DANNY P.**
A finite difference scheme for three-dimensional steady laminar incompressible flow
[NASA-TM-89851] p 148 N87-20504
- HYATT, LIZBETH H.**
Silsesquioxanes as precursors to ceramic composites
[NASA-TM-89893] p 75 N87-25432
- MYNES, T. P.**
A method for assessing effects of circumferential flow distortion on compressor stability
p 7 A87-48722
Calculations of inlet distortion induced compressor flowfield instability
p 30 N87-24470
- IBRAHIM, M. Y.**
Measurement of heat transfer and pressure drop in rectangular channels with turbulence promoters
[NASA-CR-4015] p 146 N87-17003
- INGEBO, R. D.**
Liquid fuel spray processes in high-pressure gas flow
p 131 A87-13843
- INGEBO, ROBERT D.**
Agreement between experimental and theoretical effects of nitrogen gas flowrate on liquid jet atomization
[AIAA PAPER 87-2138] p 141 A87-45427
Agreement between experimental and theoretical effects of nitrogen gas flowrate on liquid jet atomization
[NASA-TM-89821] p 156 N87-19684
- INGRAFFEA, ANTHONY R.**
Interactive color display of 3-D engineering analysis results
[NASA-CR-180589] p 203 N87-22422
- IRVINE, THOMAS B.**
Solar dynamic power systems for space station
p 58 N87-16024
- IYER, N. S.**
Opening and closing of cracks at high cyclic strains
p 84 A87-34661

J

- JACKSON, T. A.**
Performance comparison of two interferometric droplet sizing techniques
p 153 A87-11049
- JACOB, K. I.**
Three-dimensional vibrations of twisted cantilevered parallelepipeds
p 173 A87-11106
- JACOBSON, B. O.**
Effect of vibration amplitude on vapor cavitation in journal bearings
[NASA-TM-88826] p 145 N87-11962
- JACOBSON, N. S.**
The formation of volatile corrosion products during the mixed oxidation-chlorination of cobalt at 650 C
p 82 A87-23848
Corrosion pitting of SiC by molten salts
p 76 A87-27165
Reaction of iron with hydrogen chloride-oxygen mixtures at 550 C
p 83 A87-32001
- JACOBSON, NATHAN S.**
Mechanism of strength degradation for hot corrosion of alpha-SiC
p 95 A87-21470
Hot corrosion attack and strength degradation of SiC and Si(sub)3N(sub)4
[NASA-TM-89820] p 102 N87-20425
- JACOBSON, T. P.**
Tribology of selected ceramics at temperatures to 900 C
p 94 A87-12954

- JAFFE, LEONARD**
Nuclear reactor power for a space-based radar. SP-100 project
[NASA-TM-89295] p 213 N87-25838
- JAMEIKIS, S. M.**
Advanced high temperature static strain sensor development
[NASA-CR-179520] p 158 N87-25552
- JAMESON, ANTHONY**
An LU-SSOR scheme for the Euler and Navier-Stokes equations
[AIAA PAPER 87-0600] p 137 A87-34724
Lower-upper implicit scheme for high-speed inlet analysis
p 6 A87-46781
- JAMESON, ANTONY**
A multigrid LU-SSOR scheme for approximate Newton iteration applied to the Euler equations
[NASA-CR-179524] p 10 N87-16803
A high resolution shock capturing scheme for high Mach number internal flow
[NASA-CR-179523] p 10 N87-16804
An LU-SSOR scheme for the Euler and Navier-Stokes equations
[NASA-CR-179556] p 11 N87-16806
- JANARDAN, B. A.**
Free jet feasibility study of a thermal acoustic shield concept for AST/VCE application: Dual stream nozzles
[NASA-CR-3867] p 210 N87-10752
Free-jet acoustic investigation of high-radius-ratio conannular plug nozzles
[NASA-CR-3818] p 210 N87-10753
Free-jet investigation of mechanically suppressed, high radius ratio conannular plug model nozzles
[NASA-CR-3596] p 212 N87-29315
- JANOWSKI, G. M.**
The effects of tantalum on the microstructure of two polycrystalline nickel-base superalloys - B-1900 + Hf and MAR-M247
p 82 A87-24110
Thermal stability of the nickel-base superalloy B-1900 + Hf with tantalum variations
p 87 A87-51289
- JANUS, J. M.**
Three-dimensional unsteady Euler solutions for propfans and counter-rotating propfans in transonic flow
[AIAA PAPER 87-1197] p 5 A87-42314
- JARRETT, OLIN, JR.**
Multispecies CARS measurements in turbulent combustion
p 79 N87-23808
- JAWORSKE, D. A.**
Properties and potential applications of brominated P-100 carbon fibers
p 95 A87-23702
Simultaneous electrical resistivity and mass uptake measurements in bromine intercalated fibers
[NASA-TM-88900] p 70 N87-11841
- JAWORSKE, DONALD A.**
Mechanical and electrical properties of graphite fiber-epoxy composites made from pristine and bromine intercalated fibers
p 73 A87-49799
- JAYARAMAN, N.**
Fault structures in rapidly quenched Ni-Mo binary alloys
p 83 A87-32035
Microstructures in rapidly solidified Ni-Mo alloys
p 87 A87-51636
- JENG, D.-R.**
Thermal analysis of an orthotropic engineering body
p 173 A87-13496
- JENNESS, C. M. J.**
Propan test assessment testbed aircraft flutter model test report
[NASA-CR-173458] p 14 N87-29413
- JETLEY, R. L.**
Space station experiment definition: Long-term cryogenic fluid storage
[NASA-CR-4072] p 151 N87-24641
- JI, HYUN-CHUL**
Temperature fields due to jet induced mixing in a typical OTV tank
[AIAA PAPER 87-2017] p 55 A87-52247
- JOHNS, ALBERT L.**
Hot gas ingestion: From model results to full scale engine testing
p 30 N87-24419
- JOHNSON, B. V.**
Mass and momentum turbulent transport experiments
p 144 N87-11201
- JOHNSON, PAUL E.**
Design of test specimens and procedures for generating material properties of Douglas fir/epoxy laminated wood composite material: With the generation of baseline data at two environmental conditions
[NASA-CR-174910] p 75 N87-28612
- JOHNSTON, JAMES C.**
A mechanistic study of polyimide formation from diester-diols
p 70 A87-53671
- JONES, BARBARA I.**
Alternative power generation concepts for space
p 199 N87-28961

- JONES, MICHAEL R.**
Modeling of environmentally induced transients within satellites
[AIAA PAPER 85-0387] p 42 A87-41611
- JONES, R. E.**
High- and low-thrust propulsion systems for the space station
[NASA-TM-88877] p 57 N87-14427
- JONES, ROBERT E.**
High- and low-thrust propulsion systems for the Space Station
[AIAA PAPER 87-0398] p 48 A87-24997
Space station propulsion system technology
[NASA-TM-100108] p 66 N87-25422
Water-propellant resistojets for man-tended platforms
[NASA-TM-100110] p 68 N87-26135
Computer control of a scanning electron microscope for digital image processing of thermal-wave images
[NASA-TM-100157] p 128 N87-26278
- JONES, WILLIAM H.**
Increasing processor utilization during parallel computation rundown
p 202 A87-52541
Combined aerodynamic and structural dynamic problem emulating routines (CASPER): Theory and implementation
[NASA-TP-2418] p 11 N87-17669
- JONES, WILLIAM R., JR.**
A preliminary study of ester oxidation on an aluminum surface using chemiluminescence
p 96 A87-37688
Ester oxidation on an aluminum surface using chemiluminescence
[NASA-TP-2611] p 101 N87-18666
Investigation of PTFE transfer films by infrared emission spectroscopy and phase-locked ellipsometry
[NASA-TM-89844] p 102 N87-20421
The tribological behavior of polyphenyl ether and polyphenyl thioether aromatic lubricants
[NASA-TM-100166] p 105 N87-26231
- JONGEWARD, G. A.**
Computer simulation of plasma electron collection by PIX-II
p 45 A87-17837
- JORDAN, J. L.**
Flight test report of the NASA icing research airplane: Performance, stability, and control after flight through natural icing conditions
[NASA-CR-179515] p 34 N87-11797
- JORGENSEN, PHILIP C. E.**
Unsteady stator/rotor interaction
p 149 N87-22767
- JOSHI, M. C.**
Turbofan aft duct suppressor study. Contractor's data report of mode probe signal data
[NASA-CR-175067] p 34 N87-29538
Turbofan aft duct suppressor study
[NASA-CR-175067] p 34 N87-29539
- JOSHI, N. D.**
Particle cloud kinetics in microgravity
[AIAA PAPER 87-0577] p 107 A87-22716
- JOU, W.-H.**
Propeller design by optimization
p 18 A87-14123
On direct numerical simulations of turbulent reacting flows
[AIAA PAPER 87-1324] p 140 A87-44930
- JUHASZ, A. J.**
Advanced solar dynamic space power systems perspectives, requirements and technology needs
[NASA-TM-88884] p 56 N87-12606
- JUHASZ, ALBERT**
Selection of high temperature thermal energy storage materials for advanced solar dynamic space power systems
[NASA-TM-89886] p 149 N87-22174
- JUHASZ, ALBERT J.**
Reliability and mass analysis of dynamic power conversion systems with parallel or standby redundancy
p 190 A87-21823
Impact of thermal energy storage properties on solar dynamic space power conversion system mass
[NASA-TM-89909] p 63 N87-22802
Alternative power generation concepts for space
p 199 N87-28961

K

- KACHANOV, M.**
Elastic interaction of a crack with a microcrack array. I - Formulation of the problem and general form of the solution. II - Elastic solution for two crack configurations (piecewise constant and linear approximations)
p 178 A87-36926
- KACHARE, R.**
Results of 1 MeV proton irradiation of front and back surfaces of silicon solar cells
p 197 N87-26435
- KACZYNSKI, K. J.**
Experimental thrust performance of a high area-ratio rocket nozzle
p 65 N87-23809

KACZYNSKI, KENNETH J.

Comparison of theoretical and experimental thrust performance of a 1030:1 area ratio rocket nozzle at a chamber pressure of 2413 kN/sq m (350 psia)
[AIAA PAPER 87-2069] p 52 A87-45390

Experimental evaluation of heat transfer on a 1030:1 area ratio rocket nozzle
[AIAA PAPER 87-2070] p 55 A87-52249

Experimental thrust performance of a high-area-ratio rocket nozzle
[NASA-TP-2720] p 60 N87-20381

Comparison of theoretical and experimental thrust performance of a 1030:1 area ratio rocket nozzle at a chamber pressure of 2413 kN/m² (350 psia)
[NASA-TP-2725] p 66 N87-25423

Experimental evaluation of heat transfer on a 1030:1 area ratio rocket nozzle
[NASA-TP-2726] p 67 N87-25424

KADAMBI, J. R.

Laser anemometry measurements of natural circulation flow in a scale model PWR reactor system
p 154 A87-40750

KAERCHER, ARTHUR

Particle trajectory computer program for icing analysis of axisymmetric bodies - A progress report
[AIAA PAPER 87-0027] p 15 A87-22366

KAFALES, J. A.

A comparative study of the influence of buoyancy driven fluid flow on GaAs crystal growth
p 219 N87-28741

KAILASANATH, K.

Systematic development of reduced reaction mechanisms for dynamic modeling
p 77 A87-33987

KALLURI, S.

Exposure time considerations in high temperature low cycle fatigue
[NASA-TM-88934] p 187 N87-28944

KALLURI, SREERAMESH

Environmental degradation of 316 stainless steel in high temperature low cycle fatigue
[NASA-TM-88931] p 185 N87-24007

KAM, M.

System architecture of MMIC-based large aperture arrays for space application
[NASA-TM-89840] p 125 N87-20468

KAMINAR, N. R.

High-efficiency GaAs solar concentrator cells for space and terrestrial applications
p 188 A87-18073

KANG, DAVID S.

A versatile and low order hybrid stress element for general shell geometry
[AIAA PAPER 87-0840] p 176 A87-33624

KANG, M. P.

Concentration of carbon dioxide by a high-temperature electrochemical membrane cell
p 77 A87-27400

KANIC, P. G.

Oxidizer heat exchangers for rocket engine operation in idle modes
[AIAA PAPER 87-2117] p 52 A87-45418

Low heat transfer oxidizer heat exchanger design and analysis
[NASA-CR-179488] p 58 N87-15272

KANIC, PAUL G.

High heat transfer oxidizer heat exchanger design and analysis
[NASA-CR-179596] p 63 N87-22803

KARAGOZIAN, A. R.

The flame structure and vorticity generated by a chemically reacting transverse jet
p 76 A87-14116

KARCHMER, ALLAN M.

Identification and proposed control of helicopter transmission noise at the source
[NASA-TM-89312] p 18 N87-16816

KARJALA, PHILIP J.

A point defect model for nickel electrode structures
p 87 A87-52282

KARKI, K. C.

Development and evaluation of improved numerical schemes for recirculating flows
[AIAA PAPER 87-0061] p 134 A87-24913

KASUBA, R.

Design and dynamic simulation of a fixed pitch 56 kW wind turbine drive train with a continuously variable transmission
[NASA-CR-179543] p 193 N87-17401

KASZETA, WILLIAM J.

Design, development and deployment of public service photovoltaic power/load systems for the Gabonese Republic
[NASA-CR-179603] p 195 N87-23030

KATZ, I.

Three dimensional simulation of the operation of a hollow cathode electron emitter on the Shuttle orbiter
p 119 A87-14084

Computer simulation of plasma electron collection by PIX-II
p 45 A87-17837

Hollow cathodes as electron emitting plasma contactors
Theory and computer modeling

[AIAA PAPER 87-0569] p 214 A87-22712

Theory of plasma contactors for electrodynamic tethered satellite systems
p 122 A87-41609

Ram ion scattering caused by Space Shuttle v x B induced differential charging
p 200 A87-51713

KATZ, IRA

Secondary electron generation, emission and transport: Effects on spacecraft charging and NASCAP models
p 44 N87-26950

KAUFMAN, A.

Develop and test fuel cell powered on site integrated total energy systems. Phase 3: Full-scale power plant development
[NASA-CR-175118] p 191 N87-11344

Develop and test fuel cell powered on-site integrated total energy systems. Phase 3: Full-scale power plant development
[NASA-CR-175117] p 191 N87-11346

Develop and test fuel cell powered on site integrated total energy systems: Phase 3: Full-scale power plant development
[NASA-CR-175075] p 191 N87-11347

Nonlinear heat transfer and structural analyses of SSME turbine blades
p 184 N87-22779

Finite element implementation of Robinson's unified viscoplastic model and its application to some uniaxial and multiaxial problems
[NASA-TM-88891] p 185 N87-23010

KAUTZ, HAROLD E.

Ray propagation path analysis of acousto-ultrasonic signals in composites
[NASA-TM-100148] p 173 N87-25589

KAWASE, M.

Nonlinear absorption in AlGaAs/GaAs multiple quantum well structures grown by metalorganic chemical vapor deposition
p 217 A87-39687

KAZA, K. R. V.

A technique for the prediction of airfoil flutter characteristics in separated flow
[AIAA PAPER 87-0910] p 177 A87-33719

Nonlinear vibration and stability of rotating, pretwisted, precone blades including Coriolis effects
p 178 A87-39896

Analytical flutter investigation of a composite propfan model
[AIAA PAPER 87-0738] p 178 A87-40497

Influence of third-degree geometric nonlinearities on the vibration and stability of pretwisted, precone, rotating blades
p 21 A87-46228

Concentrated mass effects on the flutter of a composite advanced turboprop model
[NASA-TM-88854] p 180 N87-12017

Analytical flutter investigation of a composite propfan model
[NASA-TM-88944] p 182 N87-18115

A comparative study of some dynamic stall models
[NASA-TM-88917] p 183 N87-18883

KAZA, KRISHNA RAO V.

Analytical and experimental investigation of mistuning in propfan flutter
[AIAA PAPER 87-0739] p 178 A87-40496

Analytical and experimental investigation of mistuning in propfan flutter
[NASA-TM-88959] p 182 N87-18116

A computational procedure for automated flutter analysis
[NASA-TM-100171] p 187 N87-28058

KAZAROFF, JOHN M.

Conventionally cast and forged copper alloy for high-heat-flux thrust chambers
[NASA-TP-2694] p 90 N87-16902

KEAVNEY, C. J.

Indium phosphide shallow homojunction solar cells made by metalorganic chemical vapor deposition
p 123 A87-50047

Status of indium phosphide solar cell development at Spire
p 197 N87-26440

KEITH, T. G., JR.

Efficient numerical simulation of an electrothermal de-icer pad
[AIAA PAPER 87-0024] p 137 A87-32190

The effect of ambient pressure on the performance of a resistojet
[AIAA PAPER 87-0991] p 52 A87-42181

Numerical prediction of cold turbulent flow in combustor configurations with different centerbody flame holders
[ASME PAPER 86-WA-HT-50] p 140 A87-43715

An LDA investigation of three-dimensional normal shock-boundary layer interactions in a corner.
[AIAA PAPER 87-1369] p 6 A87-44938

KENNEDY, F. E.

The role of near-surface plastic deformation in the wear of lamellar solids
p 162 A87-48500

KERCZEWSKI, ROBERT J.

Performance of a Ka-band satellite system under variable transmitted signal power conditions
[NASA-TM-88984] p 116 N87-18700

A study of the effect of group delay distortion on an SMSK satellite communications channel
[NASA-TM-89835] p 116 N87-20450

Automated measurement of the bit-error rate as a function of signal-to-noise ratio for microwave communications systems
[NASA-TM-89898] p 127 N87-22102

KERREBROCK, J. L.

Rotational effects on impingement cooling
p 141 A87-45838

KERSCHEN, E. J.

Influence of airfoil mean loading on convected gust interaction noise
p 208 A87-13587

Perfect gas effects in compressible rapid distortion theory
p 136 A87-31176

KERWIN, PAUL T.

The Advanced Turbine Technology Applications Program (ATTAP)
[SAE PAPER 870467] p 163 A87-48791

KESSLER, JOEL R.

A 30-GHz monolithic receiver
p 121 A87-23953

KETTERSON, ANDREW A.

Characterization of InGaAs/AlGaAs pseudomorphic modulation-doped field-effect transistors
p 121 A87-23922

KHANDELWAL, P. K.

Slow crack growth in sintered silicon nitride
p 98 A87-48989

KHANDELWAL, SURESH

Method for the determination of the three dimensional aerodynamic field of a rotor-stator combination in compressible flow
[AIAA PAPER 87-1742] p 7 A87-50187

Method for the determination of the three-dimensional aerodynamic field of a rotor-stator combination to compressible flow
[NASA-TM-100118] p 30 N87-23625

KHEYRANDISH, K.

A model for fluid flow during saturated boiling on a horizontal cylinder
p 139 A87-41173

KHONSARI, M. M.

Effect of shaft frequency on cavitation in a journal bearing for noncentered circular whirl
[NASA-TM-88925] p 148 N87-22122

KHONSARI, MICHAEL M.

Stability of a rigid rotor supported on flexible oil journal bearings
[NASA-TM-89899] p 151 N87-24646

KIDWELL, JAMES R.

A technology development summary for the AGT101 advanced gas turbine program
[SAE PAPER 870466] p 163 A87-48790

KIEL, ROBERT

Structural and aeroelastic analysis of the SR-7L propfan
[NASA-TM-86877] p 184 N87-22273

KIEL, ROBERT E.

SSME blade damper technology
p 63 N87-22798

KIKUCHI, N.

On optimal design for the blade-root/hub interface in jet engines
p 24 N87-11769

KIM, H. J.

Spanwise structures in transitional flow around circular cylinders
[AIAA PAPER 87-1383] p 140 A87-44940

KIM, K. S.

Thermal barrier coating life prediction model
[NASA-CR-179504] p 100 N87-13539

Elevated temperature crack growth
[NASA-CR-179601] p 184 N87-22267

KIM, WALTER S.

Progress on thin-film sensors for space propulsion technology
p 158 N87-22772

KIM, Y. N.

Computation of multi-dimensional viscous supersonic jet flow
[NASA-CR-4020] p 8 N87-13405

Computation of multi-dimensional viscous supersonic flow
[NASA-CR-4021] p 9 N87-13406

KING, DAVID Q.

PEGASUS: A multi-megawatt nuclear electric propulsion system
p 59 N87-17787

KING, R. B.

Catalyst and electrode research for phosphoric acid fuel cells
p 190 A87-33789

KIRBY, MARK S.

In-flight measurement of ice growth on an airfoil using an array of ultrasonic transducers
[AIAA PAPER 87-0178] p 15 A87-22464

Comparison of wet and dry growth in artificial and flight icing conditions
p 16 A87-45635

KIRCHGESSNER, THOMAS A.

Airflow calibration and exhaust pressure/temperature survey of an F404, S/N 215-109, turbofan engine
[NASA-TM-100159] p 33 N87-29537

KISER, J. D.

Particle-size reduction of Si₃N₄ powder with Si₃N₄ milling hardware p 94 A87-12936
Sintering, microstructural, radiographic, and strength characterization of a high-purity Si₃N₄-based composition p 94 A87-12939

KLANN, G. A.

Response of a small-turboshaft-engine compression system to inlet temperature distortion
[NASA-TM-83765] p 23 N87-10100

KLANN, GARY A.

Contingency power for small turboshaft engines using water injection into turbine cooling air
[AIAA PAPER 87-1906] p 21 A87-45289
Contingency power for small turboshaft engines using water injection into turbine cooling air
[NASA-TM-89817] p 28 N87-20280

KLEIN, A. C.

An assessment and validation study of nuclear reactors for low power space applications
[NASA-CR-180672] p 213 N87-27495

KLEM, JOHN

Characterization of InGaAs/AlGaAs pseudomorphic modulation-doped field-effect transistors
p 121 A87-23922

KLIMA, STANLEY J.

Nondestructive evaluation of structural ceramics
[NASA-TM-88978] p 172 N87-18109
Application of scanning acoustic microscopy to advanced structural ceramics
[NASA-TM-89929] p 172 N87-23987

KLIMEK, R.

Particle cloud kinetics in microgravity
[AIAA PAPER 87-0577] p 107 A87-22716

KMIEC, T. D.

Oxidizer heat exchangers for rocket engine operation in idle modes
[AIAA PAPER 87-2117] p 52 A87-45418
Low heat transfer oxidizer heat exchanger design and analysis
[NASA-CR-179488] p 58 N87-15272

KMIEC, THOMAS D.

Breadboard RL10-11B low thrust operating mode
[NASA-CR-174914] p 58 N87-15269
High heat transfer oxidizer heat exchanger design and analysis
[NASA-CR-179596] p 63 N87-22803

KNEILE, K. R.

Large perturbation flow field analysis and simulation for supersonic inlets
[NASA-CR-174676] p 8 N87-10835

KNIP, GERALD, JR.

Analysis of an advanced technology subsonic turbofan incorporating revolutionary materials
[NASA-TM-89868] p 29 N87-22680

KNOLL, R. H.

Development and test of the Shuttle/Centaur cryogenic tankage thermal protection system
[AIAA PAPER 87-1557] p 43 A87-43073

KNOLL, RICHARD H.

Design, development and test of shuttle/Centaur G-prime cryogenic tankage thermal protection systems
[NASA-TM-89825] p 43 N87-23685

KNOTT, P. R.

Free-jet acoustic investigation of high-radius-ratio conannular plug nozzles
[NASA-CR-3818] p 210 N87-10753
Free-jet investigation of mechanically suppressed, high radius ratio conannular plug model nozzles
[NASA-CR-3596] p 212 N87-29315

KNOWLES, S. C.

Performance characterization of a low power hydrazine arcjet
[AIAA PAPER 87-1057] p 50 A87-39634
Low power arcjet life issues
[AIAA PAPER 87-1059] p 50 A87-39635

KNOWLES, STEVEN C.

Electromagnetic emission experiences using electric propulsion systems - A survey
[AIAA PAPER 87-2028] p 54 A87-50195
Electromagnetic emission experiences using electric propulsion systems: A survey
[NASA-TM-100120] p 64 N87-22805

KONNHORST, PAUL

Engineering calculations for communications satellite systems planning
[NASA-CR-181112] p 117 N87-24605

KOHOUT, L. L.

Advanced solar thermal technologies for the 21st century p 47 A87-18179
NASA Lewis evaluation of Regenerative Fuel Cell (RFC) systems p 123 N87-11073

KOHOUT, LISA

Long range inhabited surface transportation system power source for the exploration of Mars (manned Mars mission) p 37 N87-17752

KOLAVENNU, V.

Satellite analog FDMA/FM to digital TDMA conversion
[NASA-CR-179605] p 125 N87-20467

KOO, J. J.

Rotational effects on impingement cooling
p 141 A87-45838

KOPANSKI, J. J.

Behavior of inversion layers in 3C silicon carbide
p 215 A87-11242

KORKAN, K. D.

Computational aeroacoustics of propeller noise in the near and far field
[AIAA PAPER 87-0254] p 19 A87-24944
Off-design analysis of counter-rotating propeller configurations p 20 A87-27989
Evaluation of icing drag coefficient correlations applied to iced propeller performance prediction
[SAE PAPER 871033] p 16 A87-48761

KOSALY, GEORGE

On the coalescence-dispersion modeling of turbulent molecular mixing
[NASA-TM-89910] p 2 N87-25292

KOSMAHL, H. G.

Ultra small electron beam amplifiers
p 122 A87-42681

KOSMAHL, HENRY G.

Analytical and experimental performance of a dual-mode traveling wave tube and multistage depressed collector
[NASA-TP-2752] p 128 N87-25532

KOSSOWSKY, R.

Friction and wear behaviour of ion beam modified ceramics p 97 A87-47958

KOST, A.

Nonlinear absorption in AlGaAs/GaAs multiple quantum well structures grown by metalorganic chemical vapor deposition p 217 A87-39687

KRAFT, R. E.

Turbofan aft duct suppressor study. Contractor's data report of mode probe signal data
[NASA-CR-175067] p 34 N87-29538
Turbofan aft duct suppressor study
[NASA-CR-175067] p 34 N87-29539

KRAINER, A.

Progress in the prediction of unsteady heat transfer on turbine blades p 149 N87-22769

KRAINER, ANDREAS

A general method for unsteady stagnation region heat transfer and results for model turbine flows
[NASA-TM-88903] p 146 N87-17002

KRAMARCHUK, IHOR

Automated measurement of the bit-error rate as a function of signal-to-noise ratio for microwave communications systems
[NASA-TM-89898] p 127 N87-22102

Computer control of a scanning electron microscope for digital image processing of thermal-wave images
[NASA-TM-100157] p 128 N87-26278

KRAMER, SAUNDERS B.

The Advanced Turbine Technology Applications Program (ATTAP)
[SAE PAPER 870467] p 163 A87-48791

KRAUTZ, HAROLD E.

Nondestructive evaluation of adhesive bond strength using the stress wave factor technique p 170 A87-32200

KREINER, DANIEL M.

A technology development summary for the AGT101 advanced gas turbine program
[SAE PAPER 870466] p 163 A87-48790

KREJSA, EUGENE A.

Identification and proposed control of helicopter transmission noise at the source
[NASA-TM-89312] p 18 N87-16816

Combustion noise from gas turbine aircraft engines measurement of far-field levels
[NASA-TM-88971] p 211 N87-17480

KRETCH, BRIAN E.

Microstrip dispersion including anisotropic substrates p 123 A87-47621

KRIEGSMANN, GREGORY A.

A new formulation of electromagnetic wave scattering using an on-surface radiation boundary condition approach p 112 A87-32829

KRISHNA MURTHY, A. V.

A higher order theory of laminated composite cylindrical shells p 177 A87-35656

KRISHNA, LALA

Multiply scaled constrained nonlinear equation solvers p 137 A87-31406

KROSKIEWICZ, STEVEN M.

Full-scale engine demonstration of an advanced sensor failure detection isolation, and accommodation algorithm
- Preliminary results
[AIAA PAPER 87-2259] p 22 A87-50422
Full-scale engine demonstration of an advanced sensor failure detection, isolation and accommodation algorithm: Preliminary results
[NASA-TM-89880] p 127 N87-22097

KUBO, I.

Technical and economic study of Stirling and Rankine cycle bottoming systems for heavy truck diesel engines
[NASA-CR-180833] p 222 N87-28470

KUCZMARSKI, MARIA A.

Growth and characterization of cubic SiC single-crystal films on Si p 217 A87-44875

KUKULKA, J. R.

Further advances in silicon solar cell technology for space application p 188 A87-18074

KUMAKAWA, A.

Volume-energy parameters for heat transfer to supercritical fluids p 137 A87-32326

KUMAR, K.

Polymer precursors for ceramic matrix composites
[NASA-CR-179562] p 70 N87-14434

KUMAR, MAHENDRA

Dendritic microstructure in argon atomized superalloy powders p 83 A87-24119

KUNATH, R. R.

System architecture of MMIC-based large aperture arrays for space application
[NASA-TM-89840] p 125 N87-20468

KUNIK, WILLIAM G.

Two- and three-dimensional viscous computations of a hypersonic inlet flow
[AIAA PAPER 87-0283] p 4 A87-31106

Two- and three-dimensional viscous computations of a hypersonic inlet flow
[NASA-TM-88923] p 146 N87-15441

Application of advanced computational codes in the design of an experiment for a supersonic throughflow fan rotor
[NASA-TM-88915] p 13 N87-22630

KURTH, R. E.

Composite load spectra for select space propulsion structural components
[NASA-CR-179496] p 55 N87-10176

KURTH, W. S.

Measurements of plasma parameters in the vicinity of the Space Shuttle p 200 A87-24672

KUSH, A. K.

Performance study of a fuel cell Pt-on-C anode in presence of CO and CO₂, and calculation of adsorption parameters for CO poisoning p 188 A87-12338
On the effect of the Fe(2+)/Fe(3+) redox couple on oxidation of carbon in hot H₃PO₄ p 78 A87-42677
Corrosion of graphite composites in phosphoric acid fuel cells p 72 A87-42684
Modeling for CO poisoning of a fuel cell anode p 191 A87-52288

KUSSMAUL, MICHAEL

An evaluation of candidate oxidation resistant materials p 80 N87-26203
High temperature radiator materials for applications in the low Earth orbital environment
[NASA-TM-100190] p 93 N87-29662

KUSSMAUL, MICHAEL T.

Enhanced thermal emittance of space radiators by ion-discharge chamber texturing
[NASA-TM-100137] p 207 N87-25823

KWATRA, S. C.

Image data compression with vector quantization in the transform domain p 111 A87-30775

KWATRA, SUBHASH C.

An adaptive algorithm for motion compensated color image coding p 113 A87-45466

L

LABED, RICHARD

An evaluation of candidate oxidation resistant materials p 80 N87-26203

LABUS, THOMAS L.

Space station electrical power system
[NASA-TM-100140] p 68 N87-26144

LACY, D. E.

Advanced solar dynamic space power systems perspectives, requirements and technology needs
[NASA-TM-88884] p 56 N87-12606

LACY, DOVIE E.

Selection of high temperature thermal energy storage materials for advanced solar dynamic space power systems
[NASA-TM-89886] p 149 N87-22174

- Impact of thermal energy storage properties on solar dynamic space power conversion system mass
[NASA-TM-89909] p 63 N87-22802
- LAFLEN, J. H.**
Elevated temperature crack growth
[NASA-CR-179601] p 184 N87-22267
- LAGRAFF, J. E.**
Unsteady heat transfer and direct comparison to steady-state measurements in a rotor-wake experiment
p 136 A87-30720
- LAKSHMINARAYANA, B.**
Turbulence modeling for complex shear flows
p 133 A87-23653
The hub wall boundary layer development and losses in an axial flow compressor rotor passage
p 139 A87-41665
Computation of rotating turbulent flow with an algebraic Reynolds stress model
p 140 A87-43384
An experimental study on the effects of tip clearance on flow field and losses in an axial flow compressor rotor
p 6 A87-46207
- LANKFORD, J.**
Friction and wear behaviour of ion beam modified ceramics
p 97 A87-47958
Characterization of ion beam modified ceramic wear surfaces using Auger electron spectroscopy
p 98 A87-51304
- LANT, CHRISTIAN T.**
Optical strain measurement system development, phase 1
[NASA-CR-179619] p 158 N87-22960
Optical strain measurement system development
[NASA-CR-179646] p 159 N87-26326
- LAPRADE, N.**
System architecture of MMIC-based large aperture arrays for space application
[NASA-TM-89840] p 125 N87-20468
- LAPRADE, NICK**
APS-Workshop on Characterization of MMIC (Monolithic Microwave Integrated Circuit) Devices for Array Antenna
[AD-P005398] p 118 N87-28763
- LARK, R. F.**
Fabrication and quality assurance processes for superhybrid composite fan blades
p 72 A87-19123
- LARSON, A. V.**
Feasibility analysis of reciprocating magnetic heat pumps
[NASA-CR-180262] p 147 N87-19647
- LAUER, JAMES L.**
Investigation of PTFE transfer films by infrared emission spectroscopy and phase-locked ellipsometry
[NASA-TM-89844] p 102 N87-20421
- LAUVER, RICHARD W.**
Quantitative analysis of PMR-15 polyimide resin by HPLC
p 69 A87-48314
- LAW, S. P.**
Wind tunnel evaluation of a truncated NACA 64-621 airfoil for wind turbine applications
[NASA-CR-180803] p 196 N87-25621
- LAWLER, J. S.**
Utility interconnection issues for wind power generation
[NASA-CR-175056] p 193 N87-17400
- LAWRENCE, C.**
Nonlinear vibration and stability of rotating, pretwisted, precone blades including Coriolis effects
p 178 A87-39896
Identification of structural interface characteristics using component mode synthesis
[NASA-TM-89960] p 185 N87-24006
- LAWRENCE, CHARLES**
A NASTRAN primer for the analysis of rotating flexible blades
[NASA-TM-89861] p 184 N87-21375
Structural and aeroelastic analysis of the SR-71 propan
[NASA-TM-86877] p 184 N87-22273
Hub flexibility effects on propan vibration
[NASA-TM-89900] p 186 N87-24722
- LAXMANAN, V.**
Cellular and dendritic growth in a binary melt - A marginal stability approach
p 107 A87-10871
Transition from a planar interface to cellular and dendritic structures during rapid solidification processing
p 81 A87-12029
A critical examination of the dendrite growth models
Comparison of theory with experimental data
p 83 A87-25048
Cellular-dendritic transition in directionally solidified binary alloys
p 84 A87-32046
Dendritic solidification in a binary alloy melt - Comparison of theory and experiment
p 217 A87-48733
Gravitational macrosegregation in binary Pb-Sn alloy ingots
[NASA-TM-89885] p 109 N87-24579
- LE, M.**
Alkaline water electrolysis technology for Space Station regenerative fuel cell energy storage
p 46 A87-18107
- LEBED, RICHARD**
High temperature radiator materials for applications in the low Earth orbital environment
[NASA-TM-100190] p 93 N87-29662
- LEBURTON, J. P.**
Proposal for superstructure based high efficiency photovoltaics
p 120 A87-19104
- LEE, B. S.**
20-GHz phased-array-fed antennas utilizing distributed MMIC modules
p 112 A87-34527
- LEE, C. M.**
Estimation of instantaneous heat transfer coefficients for a direct-injection stratified-charge rotary engine
[SAE PAPER 870444] p 163 A87-48787
Performance and efficiency evaluation and heat release study of an outboard Marine Corporation Rotary Combustion Engine
[NASA-TM-89833] p 28 N87-20282
- LEE, C. S.**
Radar cross section of an open-ended circular waveguide Calculation of second-order diffraction terms
p 112 A87-31626
- LEE, CHOON S.**
RCS of a coated circular waveguide terminated by a perfect conductor
p 112 A87-42536
- LEE, DAVID Y.**
Visualization of flows in a motored rotary combustion engine using holographic interferometry
[AIAA PAPER 86-1557] p 19 A87-21514
- LEE, E. A.**
Application of adaptive antenna techniques to future commercial satellite communication
[NASA-CR-179566] p 115 N87-16954
Application of adaptive antenna techniques to future commercial satellite communications. Executive summary
[NASA-CR-179566-SUMM] p 115 N87-16955
- LEE, H. C.**
Nonlinear absorption in AlGaAs/GaAs multiple quantum well structures grown by metalorganic chemical vapor deposition
p 217 A87-39687
- LEE, HONG-TAO**
Generation of spiral bevel gears with conjugate tooth surfaces and tooth contact analysis
[NASA-CR-4088] p 169 N87-26356
- LEE, JOHN D.**
Transonic interference reduction by limited ventilation wall panels
[NASA-CR-175039] p 15 N87-29419
- LEE, K. F.**
An experimental investigation of parasitic microstrip arrays
[NASA-TM-100168] p 129 N87-27120
- LEE, KAI F.**
Microstrip antenna array with parasitic elements
[NASA-TM-89919] p 117 N87-22089
- LEE, R. Q.**
A design concept for an MMIC microstrip phased array
[NASA-TM-88834] p 114 N87-14569
Swept frequency technique for dispersion measurement of microstrip lines
[NASA-TM-88836] p 124 N87-14597
- LEE, R. Q. H.**
New simple feed network for an array module of four microstrip elements
p 122 A87-41638
- LEE, RICHARD Q.**
Absolute gain measurement by the image method under mismatched condition
[NASA-TM-88924] p 124 N87-16968
Microstrip antenna array with parasitic elements
[NASA-TM-89919] p 117 N87-22089
An experimental investigation of parasitic microstrip arrays
[NASA-TM-100168] p 129 N87-27120
Swept frequency technique for dispersion measurement of microstrip lines
[AD-P005420] p 118 N87-27848
A design concept for an MMIC (Monolithic Microwave Integrated Circuit) microstrip phased array
[AD-P005404] p 119 N87-28769
- LEE, S. S.**
Modes of vibration on square fiberglass epoxy composite thick plate
[NASA-CR-4018] p 171 N87-13779
- LEE, S. W.**
Radar cross section of an open-ended circular waveguide Calculation of second-order diffraction terms
p 112 A87-31626
Reduction of the radar cross section of arbitrarily shaped cavity structures
[NASA-CR-180307] p 118 N87-27085
- LEE, SHONG W.**
Detection of reflector surface error from near-field data: Effect of edge diffracted field
[NASA-TM-89920] p 117 N87-22874
- LEE, SHUNG-WU**
RCS of a coated circular waveguide terminated by a perfect conductor
p 112 A87-42536
Rays versus modes - Pictorial display of energy flow in an open-ended waveguide
p 112 A87-44075
- LEE, Y. Y.**
The formation of volatile corrosion products during the mixed oxidation-chlorination of cobalt at 650 C
p 82 A87-23848
- LEIB, S. J.**
The generation of capillary instabilities on a liquid jet
p 130 A87-12060
Generation of Tollmien-Schlichting waves on interactive marginally separated flows
p 144 A87-54365
- LEISSA, A.**
Three-dimensional vibrations of twisted cantilevered parallelpiped
p 173 A87-11106
- LEISSLER, GEORGE W.**
The T55-L-712 turbine engine compressor housing refurbishment project
[NASA-CR-179624] p 92 N87-23729
- LEKAN, J.**
An assessment of the status and trends in satellite communications 1986-2000: An information document prepared for the Communications Subcommittee of the Space Applications Advisory Committee
[NASA-TM-88867] p 114 N87-13600
- LEKAN, JACK**
An advanced geostationary communications platform
p 112 A87-43165
- LEMKEY, F. D.**
High temperature static strain gage alloy development program
[NASA-CR-174833] p 157 N87-22179
- LEON, R. P.**
Formation of a pn junction on an anisotropically etched GaAs surface using metalorganic chemical vapor deposition
p 216 A87-21237
The use of multiple EBIC curves and low voltage electron microscopy in the measurement of small diffusion lengths
p 197 N87-26434
Diffusion length measurements in bulk and epitaxially grown 3-5 semiconductors using charge collection microscopy
[NASA-TM-100128] p 129 N87-27121
- LEON, ROSA P.**
Use of a corrugated surface to enhance radiation tolerance in a GaAs solar cell
p 189 A87-19842
A V-grooved AlGaAs/GaAs passivated PN junction
[NASA-TM-100138] p 218 N87-27541
- LEOWENTHAL, S. H.**
Factors that affect the fatigue strength of power transmission shafting and their impact on design
p 160 A87-14656
- LEVINE, S. R.**
Surface protection
p 88 N87-11182
- LEVINE, STANLEY R.**
Heat's on to develop high-temperature materials
p 85 A87-39897
- LEVIS, C. A.**
Alternative mathematical programming formulations for FSS synthesis
[NASA-CR-180030] p 202 N87-14872
Engineering calculations for communications satellite systems planning
[NASA-CR-180106] p 114 N87-16198
- LEVIS, CURT A.**
Optimization of orbital assignment and specification of service areas in satellite communications
[NASA-CR-181273] p 118 N87-27882
- LEVY, ALEXANDER**
Regenerative fuel cell study for satellites in GEO orbit
[NASA-TM-89914] p 194 N87-22310
Regenerative fuel cell study for satellites in GEO orbit
[NASA-CR-179609] p 198 N87-27324
- LEVY, RALPH**
Duct flows with swirl
[AIAA PAPER 87-0247] p 132 A87-22509
- LEWICKI, D. G.**
Gear mesh compliance modeling
p 164 A87-53422
Gear mesh compliance modeling
[NASA-TM-88843] p 166 N87-18092
- LEWICKI, DAVID G.**
Identification and proposed control of helicopter transmission noise at the source
[NASA-TM-89312] p 18 N87-16816
Predicted effect of dynamic load on pitting fatigue life for low-contact-ratio spur gears
[NASA-TP-2610] p 166 N87-18095
Vibration characteristics of OH-58A helicopter main rotor transmission
[NASA-TP-2705] p 167 N87-20555

- Helicopter transmission testing at NASA Lewis Research Center
[NASA-TM-89912] p 168 N87-22978
- LEZBERG, ERWIN A.**
Hydrogen oxidation mechanism with applications to (1) the chaperon efficiency of carbon dioxide and (2) vitiated air testing
[NASA-TM-100186] p 80 N87-28628
- LIAO, PETER**
Acousto-ultrasonic input-output characterization of unidirectional fiber composite plate by SH waves
[NASA-CR-4087] p 173 N87-26361
- LIBBY, P. A.**
Gravitational effects on the structure and propagation of premixed flames
[IAF PAPER 86-279] p 76 A87-15983
- LIEBERT, CURT H.**
Heat flux calibration facility capable of SSME conditions
p 36 N87-22774
- LIENHARD, J. H.**
A model for fluid flow during saturated boiling on a horizontal cylinder
p 139 A87-41173
Transition boiling heat transfer and the film transition regime
p 143 A87-53589
- LILLEY, D. G.**
Two opposed lateral jets injected into swirling crossflow
[AIAA PAPER 87-0307] p 132 A87-22549
Multi-spark visualization of typical combustor flowfields
p 134 A87-25281
- LILLINGTON, D. R.**
Further advances in silicon solar cell technology for space application
p 188 A87-18074
- LIM, H. S.**
Cycle life of nickel-hydrogen cells. II - Accelerated cycle life test
p 46 A87-18104
- LIM, HONG S.**
A prediction model of the depth-of-discharge effect on the cycle life of a storage cell
[NASA-TM-89915] p 194 N87-22311
KOH concentration effect on cycle life of nickel-hydrogen cells
p 199 N87-29920
- LIN, CHIN-SHUN**
Numerical calculations of turbulent reacting flow in a gas-turbine combustor
[NASA-TM-89842] p 1 N87-20171
- LIN, CHOW-MING**
An adaptive algorithm for motion compensated color image coding
p 113 A87-45466
- LIN, HSIANG HSI**
Profile modification to minimize spur gear dynamic loading
[NASA-TM-89901] p 170 N87-28918
- LIN, L. S.**
Creep fatigue life prediction for engine hot section materials (ISOTROPIC)
[NASA-CR-179550] p 181 N87-15491
- LIN, LI-SEN JIM**
Creep fatigue life prediction for engine hot section materials (isotropic)
[NASA-CR-174844] p 182 N87-18117
- LINASK, I.**
Life prediction and constitutive models for engine hot section anisotropic materials
[NASA-CR-179594] p 29 N87-23622
- LINDER, C.**
Scaled centrifugal compressor program
[NASA-CR-174912] p 26 N87-14349
- LING, H.**
Reduction of the radar cross section of arbitrarily shaped cavity structures
[NASA-CR-180307] p 118 N87-27085
- LING, HAO**
Rays versus modes - Pictorial display of energy flow in an open-ended waveguide
p 112 A87-44075
- LIOTTA, G. C.**
Ceramic high pressure gas path seal
[NASA-CR-180813] p 31 N87-26914
- LIOW, M. S.**
An efficient method for solving the steady Euler equations
[NASA-TM-87329] p 205 N87-11543
- LIOW, MENG-SING**
A generalized procedure for constructing an upwind-based TVD scheme
[AIAA PAPER 87-0355] p 4 A87-32191
A generalized procedure for constructing an upwind based TVD scheme
[NASA-TM-88926] p 205 N87-24132
- LITT, M. H.**
Polymer precursors for ceramic matrix composites
[NASA-CR-179562] p 70 N87-14434
- LITTLE, B. H., JR.**
High speed wind tunnel tests of the PTA aircraft
[SAE PAPER 861744] p 4 A87-32619
- LITTLE, J. K.**
Response of a small-turboshaft-engine compression system to inlet temperature distortion
[NASA-TM-83765] p 23 N87-10100
- LITVIN, F. L.**
New generation methods for spur, helical, and spiral-bevel gears
p 164 A87-53420
New generation methods for spur, helical, and spiral-bevel gears
[NASA-TM-88862] p 165 N87-15466
- LITVIN, FAYDOR L.**
Generation of spiral bevel gears with conjugate tooth surfaces and tooth contact analysis
[NASA-CR-4088] p 169 N87-26356
Helical gears with circular arc teeth: Generation, geometry, precision and adjustment to errors, computer aided simulation of conditions of meshing and bearing contact
[NASA-CR-4089] p 170 N87-29846
- LIU, CAROL S.**
A 30-GHz monolithic receiver
p 121 A87-23953
- LIU, D. C.**
Ellipsometric and optical study of amorphous hydrogenated carbon films
p 216 A87-23967
Adhesion, friction and deformation of ion-beam-deposited boron nitride films
p 98 A87-49325
- LIU, DAVID C.**
Adhesion, friction, and deformation of ion-beam-deposited boron nitride films
[NASA-TM-88902] p 100 N87-15305
- LIU, H. W.**
Grain boundary oxidation and fatigue crack growth at elevated temperatures
p 81 A87-19368
Grain boundary oxidation and fatigue crack growth at elevated temperatures
[NASA-CR-179529] p 88 N87-11873
- LIU, J. T. C.**
Nonlinear binary-mode interactions in a developing mixing layer
p 142 A87-47158
- LIU, LOUIS C. T.**
A 30-GHz monolithic receiver
p 121 A87-23953
- LIU, T. M.**
On self-preserving, variable-density, turbulent free jets
p 130 A87-10920
- LIU, W. K.**
A probabilistic Hu-Washizu variational principle
[AIAA PAPER 87-0764] p 176 A87-33579
Variational approach to probabilistic finite elements
[NASA-CR-181343] p 206 N87-29212
- LO, Y. T.**
New simple feed network for an array module of four microstrip elements
p 122 A87-41638
The study of microstrip antenna arrays and related problems
[NASA-CR-179714] p 113 N87-10225
- LOEFFLER, IRVIN J.**
Structureborne noise control in advanced turboprop aircraft
[AIAA PAPER 87-0530] p 209 A87-31110
Structureborne noise control in advanced turboprop aircraft
[NASA-TM-88947] p 211 N87-16587
- LOHMANN, R. P.**
Advanced composite combustor structural concepts program
[NASA-CR-174733] p 74 N87-20387
- LONG, JIN**
A 20 GHz, high efficiency dual mode TWT for the ACTS program
p 122 A87-45511
- LONG, MARTIN**
Synthesis, physical and chemical properties, and potential applications of graphite fluoride fibers
[NASA-TM-100156] p 105 N87-26232
- LOTTIG, ROY A.**
Full-scale thrust reverser testing in an altitude facility
[AIAA PAPER 87-1788] p 34 A87-45203
Full-scale thrust reverser testing in an altitude facility
[NASA-TM-88967] p 35 N87-18575
- LOUVIERE, ALLEN J.**
Water-propellant resistojets for man-tended platforms
[NASA-TM-100110] p 68 N87-26135
- LOWELL, C. E.**
Nickel base coating alloy
[NASA-CASE-LEW-13834-1] p 89 N87-14482
- LOYSELLE, PATRICIA L.**
A point defect model for nickel electrode structures
p 87 A87-52282
- LU, C.**
Computer-based phosphoric acid fuel cell analytical tools Descriptions and usages
p 190 A87-33788
- LU, C. Y.**
Estimation of instantaneous heat transfer coefficients for a direct-injection stratified-charge rotary engine
[SAE PAPER 870444] p 163 A87-48787
- LUDLOW, GERRY**
Space station power semiconductor package
[NASA-CR-180829] p 129 N87-28825
- LUO, JIHEI**
Iptycenes - Extended triptycenes
p 69 A87-53654
- LYONS, VALERIE J.**
Velocity profiles in laminar diffusion flames
[NASA-TP-2596] p 147 N87-18035

M

- MACIAG, CAROLYN**
Effects of sequential treatment with fluorine and bromine on graphite fibers
[NASA-TM-100106] p 104 N87-24574
- MACKAY, R. A.**
The stability of lamellar gamma-gamma-prime structures
p 86 A87-48323
- MACMILLAN, H. F.**
High-efficiency GaAs concentrator space cells
p 196 N87-26417
- MACNEIL, P. N.**
Development and test of the Shuttle/Centaur cryogenic tankage thermal protection system
[AIAA PAPER 87-1557] p 43 A87-43073
- MACNEIL, PETER N.**
Design, development and test of shuttle/Centaur G-prime cryogenic tankage thermal protection systems
[NASA-TM-89825] p 43 N87-23685
- MAJUGI, R. K.**
Free jet feasibility study of a thermal acoustic shield concept for AST/VCE application: Dual stream nozzles
[NASA-CR-3867] p 210 N87-10752
Free-jet acoustic investigation of high-radius-ratio conannular plug nozzles
[NASA-CR-3818] p 210 N87-10753
Development of a rotor wake/vortex model. Volume 2: User's manual for computer program
[NASA-CR-174850-VOL-2] p 13 N87-20239
Free-jet investigation of mechanically suppressed, high radius ratio conannular plug model nozzles
[NASA-CR-3596] p 212 N87-29315
- MAJUMDAR, BANKIM C.**
Stability of a rigid rotor supported on flexible oil journal bearings
[NASA-TM-89899] p 151 N87-24646
- MALIK, S. N.**
Elevated temperature crack growth
[NASA-CR-179601] p 184 N87-22267
- MALTEZOS, DIMITRIOS G.**
Particle trajectory computer program for icing analysis of axisymmetric bodies - A progress report
[AIAA PAPER 87-0027] p 15 A87-22366
- MANDELL, M. J.**
Three dimensional simulation of the operation of a hollow cathode electron emitter on the Shuttle orbiter
p 119 A87-14084
Computer simulation of plasma electron collection by PIX-II
p 45 A87-17837
Hollow cathodes as electron emitting plasma contactors Theory and computer modeling
[AIAA PAPER 87-0569] p 214 A87-22712
- MANDELL, MYRON**
Secondary electron generation, emission and transport: Effects on spacecraft charging and NASCAP models
p 44 N87-26950
- MANDERSCHIED, JANE M.**
Fracture mechanics concepts in reliability analysis of monolithic ceramics
[NASA-TM-100174] p 187 N87-27269
- MANI, A.**
Variational approach to probabilistic finite elements
[NASA-CR-181343] p 206 N87-29212
- MANNING, ROBERT M.**
Optimizing the antenna system of a microwave space power station: Implications for the selection of operating power, frequency and antenna size
[NASA-TM-100184] p 206 N87-30132
- MANOLIS, G. D.**
Conforming versus non-conforming boundary elements in three-dimensional elastostatics
p 175 A87-22775
- MANORY, R. R.**
A simple method for monitoring surface temperatures in plasma treatments
p 160 A87-17269
- MANSON, S. S.**
Re-examination of cumulative fatigue damage analysis - An engineering perspective
p 174 A87-22128
Exposure time considerations in high temperature low cycle fatigue
[NASA-TM-88934] p 187 N87-28944
- MANSON, S. STANFORD**
Environmental degradation of 316 stainless steel in high temperature low cycle fatigue
[NASA-TM-89931] p 185 N87-24007

- MANZELLA, D. H.**
The effect of ambient pressure on the performance of a resistor
[AIAA PAPER 87-0991] p 52 A87-42181
- MANZO, MICHELLE A.**
Component variations and their effects on bipolar nickel-hydrogen cell performance
[NASA-TM-89907] p 195 N87-23029
Test results of a 60 volt bipolar nickel-hydrogen battery
[NASA-TM-89927] p 195 N87-24029
- MARCHAND, N.**
KI-solutions for single edge notch specimens under fixed end displacements p 174 A87-15798
A computerized test system for thermal-mechanical fatigue crack growth p 153 A87-23899
Thermal-mechanical fatigue crack growth in B-1900 + HF p 86 A87-49570
- MARGLE, JANICE M.**
Velocity profiles in laminar diffusion flames
[NASA-TP-2596] p 147 N87-18035
- MARINO, D.**
Design, construction and long life endurance testing of cathode assemblies for use in microwave high-power transmitting tubes
[NASA-CR-175116] p 123 N87-10237
- MARINOS, CHARALAMPUS**
Heat exchanger for electrothermal devices
[NASA-CASE-LEW-14037-1] p 59 N87-16875
- MARK, WILLIAM D.**
Analysis of the vibratory excitation arising from spiral bevel gears
[NASA-CR-4081] p 169 N87-25579
- MARLOW, FRANK J.**
Aircraft accident report: NASA 712, Convair 990, N712NA, March Air Force Base, California, July 17, 1985, executive summary
[NASA-TM-87356-VOL-1] p 16 N87-21878
Aircraft accident report: NASA 712, Convair 990, N712NA, March Air Force Base, California, July 17, 1985, facts and analysis
[NASA-TM-87356-VOL-2] p 16 N87-21879
- MARQUES, E. R. C.**
Modes of vibration on square fiberglass epoxy composite thick plate
[NASA-CR-4018] p 171 N87-13779
Ultrasonic determination of the elastic constants of the stiffness matrix for unidirectional fiberglass epoxy composites
[NASA-CR-4034] p 171 N87-13781
Parameterized materials and dynamic response characterizations in unidirectional composites
[NASA-CR-4032] p 172 N87-13782
- MARTIN, M. R.**
Fatigue life of laser cut metals
[NASA-TM-879501] p 164 N87-11158
- MARTIN, R. A.**
Advanced technology for extended endurance alkaline fuel cells p 190 A87-33787
- MARTIN, R. E.**
Effects of transient propellant dynamics on deployment of large liquid stages in zero-gravity with application to Shuttle/Centaur
[IAF PAPER 86-119] p 39 A87-15880
- MARTIN, RONALD E.**
Stress-life interrelationships associated with alkaline fuel cells
[NASA-TM-89881] p 194 N87-22307
- MARTINDALE, W. R.**
Large perturbation flow field analysis and simulation for supersonic inlets
[NASA-CR-174676] p 8 N87-10835
- MARTINEZ, A.**
Concepts for space maintenance of OTV engines p 40 A87-41161
Concepts for space maintenance of OTV engines p 37 A87-46000
Concepts for space maintenance of OTV engines p 67 N87-26097
- MARTZ, J. E.**
Tunisia Renewable Energy Project systems description report
[NASA-TM-88789] p 192 N87-13856
- MARU, H. C.**
Performance study of a fuel cell Pt-on-C anode in presence of CO and CO₂, and calculation of adsorption parameters for CO poisoning p 188 A87-12338
- MASSELINK, WILLIAM T.**
Characterization of InGaAs/AlGaAs pseudomorphic modulation-doped field-effect transistors p 121 A87-23922
- MASTERS, P. A.**
Liquid oxygen cooling of high pressure LOX/hydrocarbon rocket thrust chambers
[NASA-TM-88805] p 57 N87-14426
- MATERNA, DAVID M.**
Investigation of a GaAlAs Mach-Zehnder electro-optic modulator
[NASA-CR-179573] p 114 N87-16953
- MATOSSIAN, J. N.**
Plasma properties in electron-bombardment ion thrusters
[AIAA PAPER 87-1076] p 51 A87-41135
Status of xenon ion propulsion technology
[AIAA PAPER 87-1003] p 53 A87-48677
- MATTHEWS, E. W.**
Application of adaptive antenna techniques to future commercial satellite communication
[NASA-CR-179566] p 115 N87-16954
Application of adaptive antenna techniques to future commercial satellite communications. Executive summary
[NASA-CR-179566-SUMM] p 115 N87-16955
- MATULA, R. A.**
Empirical modeling of soot formation in shock-tube pyrolysis of aromatic hydrocarbons p 76 A87-12599
- MATUS, G.**
Growth and characterization of cubic SiC single-crystal films on Si p 217 A87-44875
- MATUS, L. G.**
Compensation in epitaxial cubic SiC films p 216 A87-15071
Comment on "Temperature dependence of electrical properties of non-doped and nitrogen-doped beta-SiC single crystals grown by chemical vapor deposition" p 217 A87-42846
- MAYS, J. C.**
Oxide-dispersion-strengthened turbine blades, volume 1
[NASA-CR-179537-VOL-1] p 90 N87-17883
- MAZARIS, G. A.**
Formation of a pn junction on an anisotropically etched GaAs surface using metalorganic chemical vapor deposition p 216 A87-21237
- MCCARDLE, JACK G.**
Outdoor test stand performance of a convertible engine with variable inlet guide vanes for advanced rotorcraft propulsion
[NASA-TM-88939] p 26 N87-16825
- MCCARTHY, G. T.**
Aircraft accident report: NASA 712, Convair 990, N712NA, March Air Force Base, California, July 17, 1985, executive summary
[NASA-TM-87356-VOL-1] p 16 N87-21878
Aircraft accident report: NASA 712, Convair 990, N712NA, March Air Force Base, California, July 17, 1985, facts and analysis
[NASA-TM-87356-VOL-2] p 16 N87-21879
- MCDANIELS, D. L.**
Polymer, metal, and ceramic matrix composites for advanced aircraft engine applications p 71 A87-15187
- MCDANIELS, D. L.**
Fiber-reinforced superalloy composites provide an added performance edge p 71 A87-12647
- MCDONALD, GLEN E.**
Thermomechanical behavior of plasma-sprayed ZrO₂-Y₂O₃ coatings influenced by plasticity, creep and oxidation
[NASA-TM-88940] p 147 N87-18784
- MCDONALD, H.**
Calculation of two- and three-dimensional transonic cascade flow field using the Navier-Stokes equations p 144 N87-11220
Computation of multi-dimensional viscous supersonic jet flow
[NASA-CR-4020] p 8 N87-13405
Computation of multi-dimensional viscous supersonic flow
[NASA-CR-4021] p 9 N87-13406
Turbine vane external heat transfer. Volume 2. Numerical solutions of the Navier-Stokes equations for two- and three-dimensional turbine cascades with heat transfer
[NASA-CR-174828] p 145 N87-13661
- MCGAW, MICHAEL A.**
Fatigue damage interaction behavior of PWA 1480 p 92 N87-22777
A high temperature fatigue and structures testing facility
[NASA-TM-100151] p 186 N87-26399
- MCGEE, OLIVER G.**
A NASTRAN primer for the analysis of rotating flexible blades
[NASA-TM-89861] p 184 N87-21375
Finite element analysis of flexible, rotating blades
[NASA-TM-89906] p 186 N87-26385
- MCILWAIN, C. E.**
The dynamic behavior of plasmas observed near geosynchronous orbit p 200 A87-31322
- MCKINZIE, D. J.**
An anemometer for highly turbulent or recirculating flows p 154 A87-37698
- MCKNIGHT, R. C.**
In-flight photogrammetric measurement of wing ice accretions
[AIAA PAPER 86-0483] p 15 A87-17995
- MCKNIGHT, ROBERT C.**
In-flight measurement of ice growth on an airfoil using an array of ultrasonic transducers
[AIAA PAPER 87-0178] p 15 A87-22464
- MCLALLIN, K. L.**
Solar dynamic space power system heat rejection p 47 A87-18175
- MCLENNAN, G. A.**
ANL/RBC: A computer code for the analysis of Rankine bottoming cycles, including system cost evaluation and off-design performance
[NASA-CR-179462] p 220 N87-10777
- MCMURRY, C. B.**
Two opposed lateral jets injected into swirling crossflow
[AIAA PAPER 87-0307] p 132 A87-22549
- MCMURTY, P. A.**
Mechanisms by which heat release affects the flow field in a chemically reacting, turbulent mixing layer
[AIAA PAPER 87-0131] p 134 A87-24925
- MCNALLAN, M. J.**
The formation of volatile corrosion products during the mixed oxidation-chlorination of cobalt at 650 C p 82 A87-23848
- MEACHER, J.**
Automotive Stirling engine development program
[NASA-CR-174972] p 221 N87-20137
Automotive Stirling Engine Development Program
[NASA-CR-174873] p 222 N87-30223
- MEADOR, MARY ANN**
Iptycenes - Extended triptycenes p 69 A87-53654
- MEADOR, MARY ANN B.**
A mechanistic study of polyimide formation from diester-diacids p 70 A87-53671
Addition polymers from 1,4,5,8-tetrahydro-1,4,5,8-diepoxyanthracene and Bis-dienes: Processable resins for high temperature application
[NASA-TM-89838] p 103 N87-20426
- MEADOR, MICHAEL A.**
A preliminary study of ester oxidation on an aluminum surface using chemiluminescence p 96 A87-37688
Ester oxidation on an aluminum surface using chemiluminescence
[NASA-TP-2611] p 101 N87-18666
The 2,5-diacyl-1,4-dimethylbenzenes: Examples of bisphenol equivalents
[NASA-TM-89836] p 71 N87-22005
- MEHALIC, CHARLES M.**
Full-scale thrust reverser testing in an altitude facility
[AIAA PAPER 87-1788] p 34 A87-45203
Full-scale thrust reverser testing in an altitude facility
[NASA-TM-88967] p 35 N87-18575
- MEHMED, O.**
Analytical flutter investigation of a composite propfan model
[AIAA PAPER 87-0738] p 178 A87-40497
Analytical flutter investigation of a composite propfan model
[NASA-TM-89944] p 182 N87-18115
- MEHMED, ORAL**
Analytical and experimental investigation of mistuning in propfan flutter
[AIAA PAPER 87-0739] p 178 A87-40496
Analytical and experimental investigation of mistuning in propfan flutter
[NASA-TM-88959] p 182 N87-18116
- MENDELSON, A.**
Analysis of mixed-mode crack propagation using the boundary integral method
[NASA-CR-179518] p 180 N87-12915
- MENG, PHILLIP R.**
Space station propulsion system technology
[NASA-TM-100108] p 66 N87-25422
- MERRILL, W. C.**
A real-time simulation evaluation of an advanced detection, isolation and accommodation algorithm for sensor failures in turbine engines p 18 A87-13318
- MERRILL, WALTER C.**
Full-scale engine demonstration of an advanced sensor failure detection, isolation, and accommodation algorithm - Preliminary results
[AIAA PAPER 87-2259] p 22 A87-50422
Full-scale engine demonstration of an advanced sensor failure detection, isolation and accommodation algorithm: Preliminary results
[NASA-TM-89880] p 127 N87-22097

- Advanced detection, isolation and accommodation of sensor failures: Real-time evaluation
[NASA-TP-2740] p 34 N87-25331
- METCALFE, R. W.**
Mechanisms by which heat release affects the flow field in a chemically reacting, turbulent mixing layer
[AIAA PAPER 87-0131] p 134 A87-24925
- METZ, ROGER N.**
LEO high voltage solar array arcing response model
[NASA-CR-180073] p 124 N87-16971
- METZGER, F.B.**
Results of acoustic tests of a Prop-Fan model
[AIAA PAPER 87-1894] p 209 A87-45282
- MEYER, T. G.**
Life prediction and constitutive models for engine hot section anisotropic materials
[NASA-CR-179594] p 29 N87-23622
- MEYERS, A.**
Specimen geometry effects on graphite/PMR-15 composites during thermo-oxidative aging
p 71 A87-13145
- MEYERS, G. D.**
Effects of multiple rows and noncircular orifices on dilution jet mixing
p 138 A87-39805
- MICHAL, G. M.**
Analysis of NiAl₂ precipitates in beta-NiAl + 2 at. pct Ta alloy
p 84 A87-34888
Elevated temperature strengthening of a melt spun austenitic steel by TiB₂
p 87 A87-51639
- MIESKOWSKI, D. M.**
Sintering, microstructural, radiographic, and strength characterization of a high-purity Si₃N₄-based composition
p 94 A87-12939
- MIGRA, R. P.**
Advanced solar dynamic space power systems perspectives, requirements and technology needs
[NASA-TM-88884] p 56 N87-12606
Conceptual definition of a technology development mission for advanced solar dynamic power systems
[NASA-CR-179482] p 192 N87-14771
- MILDICE, J. W.**
Control considerations for high frequency, resonant, power processing equipment used in large systems
[NASA-TM-89926] p 64 N87-23690
- MILES, J. H.**
Spatially growing disturbances in a high velocity ratio two-stream, coplanar jet
[NASA-TM-88922] p 9 N87-14283
- MILES, JEFFREY H.**
Spatially growing disturbances in a high velocity ratio two-stream, coplanar jet
[AIAA PAPER 87-0056] p 3 A87-24996
Spatially growing disturbances in a two-stream, coplanar jet
[NASA-TM-88949] p 10 N87-16799
- MILLAN, P. P., JR.**
Oxide-dispersion-strengthened turbine blades, volume 1
[NASA-CR-179537-VOL-1] p 90 N87-17883
- MILLARD, M. L.**
Improved consolidation of silicon carbide
p 94 A87-12940
- MILLER, DEAN R.**
Performance and power regulation characteristics of two aireron-controlled rotors and a pitchable tip-controlled rotor on the Mod-O turbine
[NASA-TM-100136] p 200 N87-29956
- MILLER, E. F.**
An assessment of the status and trends in satellite communications 1986-2000: An information document prepared for the Communications Subcommittee of the Space Applications Advisory Committee
[NASA-TM-88867] p 114 N87-13600
- MILLER, J.**
Thermal conductivity of pristine and brominated P-100 fibers
[NASA-TM-88863] p 99 N87-11893
- MILLER, R. A.**
Degradation mechanisms in thermal-barrier coatings
p 94 A87-12953
Introduction to life modeling of thermal barrier coatings
p 99 N87-11195
Degradation mechanisms in thermal barrier coatings
[NASA-TM-89309] p 101 N87-17926
- MILLER, THOMAS L.**
Evaluation of icing drag coefficient correlations applied to iced propeller performance prediction
[SAE PAPER 871033] p 16 A87-48761
- MILLIGAN, WALTER W.**
Yielding and deformation behavior of the single crystal superalloy PWA 1480
p 84 A87-32040
- MILLIS, MARC G.**
Acceleration display system for aircraft zero-gravity research
[NASA-TM-87358] p 156 N87-18801
- MILNER, EDWARD J.**
Mathematical model partitioning and packing for parallel computer calculation
p 202 A87-52534
Time-partitioning simulation models for calculation on parallel computers
[NASA-TM-89850] p 203 N87-20766
- MINER, R. V.**
High temperature tensile and creep behaviour of low pressure plasma-sprayed Ni-Co-Cr-Al-Y coating alloy
p 82 A87-23429
Low cycle fatigue behaviour of a plasma-sprayed coating material
p 82 A87-24040
Stress rupture and creep behavior of a low pressure plasma-sprayed NiCoCrAlY coating alloy in air and vacuum
p 85 A87-43396
The characteristics of gamma-prime dislocation pairs in a nickel-base superalloy
p 85 A87-46932
Bithermal low-cycle fatigue behavior of a NiCoCrAlY-coated single crystal superalloy
[NASA-TM-89831] p 91 N87-20408
- MINER, ROBERT V.**
Elevated temperature tension, compression and creep-rupture behavior of (001)-oriented single crystal superalloy PWA 1480
[NASA-TM-88950] p 90 N87-17882
- MIRTIKH, MICHAEL**
An evaluation of candidate oxidation resistant materials
p 80 N87-26203
- MIRTIKH, MICHAEL J.**
Protection of solar array blankets from attack by low earth orbital atomic oxygen
p 47 A87-19874
Heat exchanger for electrothermal devices
[NASA-CASE-LEW-14037-1] p 59 N87-16875
Oxidation protection coatings for polymers
[NASA-CASE-LEW-14072-3] p 103 N87-23736
Enhanced thermal emittance of space radiators by ion-discharge chamber texturing
[NASA-TM-100137] p 207 N87-25823
High temperature radiator materials for applications in the low Earth orbital environment
[NASA-TM-100190] p 93 N87-29662
- MISEGADES, KENT P.**
The utilization of parallel processing in solving the inviscid form of the average-passage equation system for multistage turbomachinery
[AIAA PAPER 87-1108] p 5 A87-42057
- MISRA, A. K.**
Corrosion of metals and alloys in sulfate melts at 750 C
p 81 A87-17997
- MISRA, AJAY K.**
Fluoride salts and container materials for thermal energy storage applications in the temperature range 973 to 1400 K
[NASA-TM-89913] p 195 N87-24026
- MITCHELL, A. M.**
Testing of UH-60A helicopter transmission in NASA Lewis 2240-kW (3000-hp) facility
[NASA-TP-2626] p 164 N87-10391
- MITCHELL, STEPHEN C.**
Evaluation of capillary reinforced composites for anti-icing
[AIAA PAPER 87-0023] p 17 A87-24904
- MITCHELL, T. E.**
TEM investigation of beta-SiC grown epitaxially on Si substrate by CVD
p 97 A87-40927
- MITTRA, RAJ**
APS-Workshop on Characterization of MMIC (Monolithic Microwave Integrated Circuit) Devices for Array Antenna
[AD-P005398] p 118 N87-28763
- MIYOSHI, K.**
Tribology of selected ceramics at temperatures to 900 C
p 94 A87-12954
Microstructure and surface chemistry of amorphous alloys important to their friction and wear behavior
p 81 A87-15186
Plastic deformation of a magnesium oxide 001-plane surface produced by cavitation
[ASLE PREPRINT 86-TC-3D-1] p 94 A87-19504
Adhesion, friction and deformation of ion-beam-deposited boron nitride films
p 98 A87-49325
- MIYOSHI, KAZUHISA**
Adhesion, friction, and deformation of ion-beam-deposited boron nitride films
[NASA-TM-88902] p 100 N87-15305
Mechanical strength and tribological behavior of ion-beam deposited boron nitride films on non-metallic substrates
[NASA-TM-89818] p 101 N87-18668
Deformation and fracture of single-crystal and sintered polycrystalline silicon carbide produced by cavitation
[NASA-TM-88981] p 102 N87-20422
Effect of abrasive grit size on wear of manganese-zinc ferrite under three-body abrasion
[NASA-TM-89879] p 104 N87-24566
- Boron nitride: Composition, optical properties and mechanical behavior
[NASA-TM-89849] p 218 N87-25017
- MJOLSNES, R. C.**
Some plane curvature approximations
p 204 A87-49821
- MJOLSNES, RAYMOND C.**
Numerical modeling of on-orbit propellant motion resulting from an impulsive acceleration
[AIAA PAPER 87-1766] p 40 A87-48573
Numerical modeling of on-orbit propellant motion resulting from an impulsive acceleration
[NASA-TM-89873] p 41 N87-22757
- MOAT, RICHARD L.**
ACTS baseband processing
p 201 A87-45512
- MOET, A.**
An analysis for crack layer stability
p 176 A87-28982
- MOLDOVER, M. R.**
Viscometer for low frequency, low shear rate measurements
p 153 A87-13878
- MOLDOVER, MICHAEL R.**
Low-gravity experiments in critical phenomena
p 107 A87-23159
- MOLE, PHILIP J.**
Measurement of Centaur/Orbiter multiple reaction forces in a full-scale test rig
p 38 A87-29448
- MONGIA, H. C.**
Development and evaluation of improved numerical schemes for recirculating flows
[AIAA PAPER 87-0061] p 134 A87-24913
- MONGIA, HUKAM C.**
An unconditionally-stable central differencing scheme for high Reynolds number flows
[AIAA PAPER 87-0060] p 133 A87-24912
- MOORE, F. K.**
Stall transients of axial compression systems with inlet distortion
p 3 A87-24010
- MOORE, JOAN G.**
Thermodynamic evaluation of transonic compressor rotors using the finite volume approach
[NASA-CR-180587] p 150 N87-23925
- MOORE, JOHN**
Thermodynamic evaluation of transonic compressor rotors using the finite volume approach
[NASA-CR-180587] p 150 N87-23925
- MOORE, ROYCE D.**
Supersonic through-flow fan design
[AIAA PAPER 87-1746] p 22 A87-48571
Performance of two 10-lb/sec centrifugal compressors with different blade and shroud thicknesses operating over a range of Reynolds numbers
[AIAA PAPER 87-1745] p 22 A87-50188
Experimental evaluation of two turning vane designs for fan drive corner of 0.1-scale model of NASA Lewis Research Center's proposed altitude wind tunnel
[NASA-TP-2646] p 35 N87-18576
Detailed flow surveys of turning vanes designed for a 0.1-scale model of NASA Lewis Research Center's proposed altitude wind tunnel
[NASA-TP-2680] p 36 N87-20295
Supersonic through-flow fan design
[NASA-TM-88908] p 29 N87-22681
Performance of two 10-lb/sec centrifugal compressors with different blade and shroud thicknesses operating over a range of Reynolds numbers
[NASA-TM-100115] p 29 N87-23623
Experimental evaluation of corner turning vanes
[NASA-TM-100143] p 37 N87-28571
- MOORE, T. J.**
Elevated temperature strengthening of a melt spun austenitic steel by TiB₂
p 87 A87-51639
The effect of electron beam welding on the creep rupture properties of a Nb-Zr-C alloy
[NASA-TM-88892] p 88 N87-13513
Creep behavior of niobium alloy PWC-11
[NASA-TM-89834] p 91 N87-20405
- MOORE, THOMAS J.**
Preliminary study of niobium alloy contamination by transport through helium
[NASA-TM-88952] p 90 N87-17884
Fatigue failure of regenerator screens in a high frequency Stirling engine
[NASA-TM-88974] p 183 N87-18882
- MORALES, WILFREDO**
A preliminary study of ester oxidation on an aluminum surface using chemiluminescence
p 96 A87-37688
Ester oxidation on an aluminum surface using chemiluminescence
[NASA-TP-2611] p 101 N87-18666
- MOREHOUSE, K. A.**
Unsteady heat transfer and direct comparison to steady-state measurements in a rotor-wake experiment
p 136 A87-30720

- MOREHOUSE, KIM A.**
Effect of a rotor wake on the local heat transfer on the forward half of a circular cylinder p 136 A87-30721
- MOREL, D. E.**
Solar concentrator materials development p 213 A87-18171
- MORENO, V.**
Creep fatigue life prediction for engine hot section materials (isotropic): Two year update p 171 N87-11213
- MORENO, VITO**
Creep fatigue life prediction for engine hot section materials (isotropic) [NASA-CR-174844] p 182 N87-18117
- MOREY, D. C.**
An assessment and validation study of nuclear reactors for low power space applications [NASA-CR-180672] p 213 N87-27495
- MOREY, W. W.**
Hot section viewing system [NASA-CR-174773] p 155 N87-11144
Advanced high temperature static strain sensor development [NASA-CR-179520] p 158 N87-25552
- MORIN, BRUCE L.**
Short efficient ejector systems [AIAA PAPER 87-1837] p 20 A87-45239
- MORKOC, HADIS**
Microwave performance of a quarter-micrometer gate low-noise pseudomorphic InGaAs/AlGaAs modulation-doped field effect transistor p 121 A87-23745
- MORREN, W. EARL**
2000-hour cyclic endurance test of a laboratory model multipropellant resistojet [AIAA PAPER 87-0993] p 52 A87-45725
Preliminary performance characterizations of an engineering model multipropellant resistojet for space station application [AIAA PAPER 87-2120] p 54 A87-50197
A 2000-hour cyclic endurance test of a laboratory model multipropellant resistojet [NASA-TM-89854] p 167 N87-22237
Preliminary performance characterizations of an engineering model multipropellant resistojet for space station application [NASA-TM-100113] p 111 N87-23821
Water-propellant resistojets for man-tended platforms [NASA-TM-100110] p 68 N87-26135
- MOSS, LARRY A.**
Analytical and experimental investigation of mistuning in propfan flutter [AIAA PAPER 87-0739] p 178 A87-40496
Analytical and experimental investigation of mistuning in propfan flutter [NASA-TM-88959] p 182 N87-18116
SSME single crystal turbine blade dynamics [NASA-CR-179644] p 186 N87-26384
- MOTSINGER, R. E.**
Simulated flight acoustic investigation of treated ejector effectiveness on advanced mechanical suppressors for high velocity jet noise reduction [NASA-CR-4019] p 211 N87-17481
Turbofan aft duct suppressor study. Contractor's data report of mode probe signal data [NASA-CR-175067] p 34 N87-29538
Turbofan aft duct suppressor study [NASA-CR-175067] p 34 N87-29539
- MOUNT-CAMPBELL, C. A.**
Alternative mathematical programming formulations for FSS synthesis [NASA-CR-180030] p 202 N87-14872
Engineering calculations for communications satellite systems planning [NASA-CR-180106] p 114 N87-16198
- MOUNT-CAMPBELL, CLARK A.**
On orbital allotments for geostationary satellites [NASA-CR-181017] p 37 N87-22700
- MOUNT, ROBERT E.**
Advanced liquid-cooled, turbocharged and intercooled stratified charge rotary engines for aircraft [SAE PAPER 871039] p 22 A87-48766
- MUENNEMANN, FRANK**
A 20 GHz, high efficiency dual mode TWT for the ACTS program p 122 A87-45511
- MULAC, R. A.**
A numerical simulation of the inviscid flow through a counterrotating propeller [ASME PAPER 86-GT-138] p 3 A87-25395
Three-dimensional unsteady Euler solutions for propfans and counter-rotating propfans in transonic flow [AIAA PAPER 87-1197] p 5 A87-42314
- MULAC, RICHARD A.**
The utilization of parallel processing in solving the inviscid form of the average-passage equation system for multistage turbomachinery [AIAA PAPER 87-1108] p 5 A87-42057
Simulation of multistage turbine flows p 149 N87-22768
- MULARZ, E. J.**
Aerothermal modeling program, phase 2 p 24 N87-11200
- MULARZ, EDWARD J.**
Combustion research in the Internal Fluid Mechanics Division p 79 N87-20268
- MULLEN, R. L.**
Two-phase flows and heat transfer within systems with ambient pressure above the thermodynamic critical pressure p 136 A87-30728
Analysis of experimental shaft seal data for high-performance turbomachines - As for Space Shuttle main engines p 162 A87-45846
Finite difference solution for a generalized Reynolds equation with homogeneous two-phase flow p 141 A87-45851
Comparison of generalized Reynolds and Navier Stokes equations for flow of a power law fluid p 142 A87-45852
Refrigerated dynamic seal to 6.9 MPa (1000 psi) p 164 A87-50777
- MUNTZ, E. P.**
The design and performance of a multi-stream droplet generator for the liquid droplet radiator [AIAA PAPER 87-1538] p 140 A87-44842
- MURPHY, G.**
Measurements of plasma parameters in the vicinity of the Space Shuttle p 200 A87-24672
Measurements of plasma density and turbulence near the shuttle orbiter [NASA-CR-180102] p 215 N87-16614
- MURTHY, D. V.**
Analytical flutter investigation of a composite propfan model [AIAA PAPER 87-0738] p 178 A87-40497
Optimization of cascade blade mistuning under flutter and forced response constraints p 24 N87-11732
Sensitivity analysis and approximation methods for general eigenvalue problems [NASA-CR-179538] p 180 N87-12021
Analytical flutter investigation of a composite propfan model [NASA-TM-88944] p 182 N87-18115
- MURTHY, DURBHA V.**
Approximations to eigenvalues of modified general matrices [AIAA PAPER 87-0947] p 177 A87-33756
A computational procedure for automated flutter analysis [NASA-TM-100171] p 187 N87-28058
- MURTHY, K. N. S.**
The hub wall boundary layer development and losses in an axial flow compressor rotor passage p 139 A87-41665
An experimental study on the effects of tip clearance on flow field and losses in an axial flow compressor rotor p 6 A87-46207
- MURTHY, P. L. N.**
Composite interlaminar fracture toughness: Three-dimensional finite element modeling for mixed mode 1, 2 and 3 fracture [NASA-TM-88872] p 73 N87-13491
- MURTHY, S. N. B.**
Jet engine simulation with water ingestion through compressor [NASA-CR-179549] p 1 N87-15932
- MYERS, IRA**
Power system technologies for the manned Mars mission p 60 N87-17789
- MYERS, M. R.**
Influence of airfoil mean loading on convected gust interaction noise p 208 A87-13587
Perfect gas effects in compressible rapid distortion theory p 136 A87-31176
- NAFIS, SURAIYA**
Temperature dependence (4K to 300K) of the electrical resistivity of methane grown carbon fibers p 97 A87-47375
- NAGAMATSU, H. T.**
Heat transfer in the stagnation region of the junction of a circular cylinder perpendicular to a flat plate p 131 A87-13019
- Endwall heat transfer in the junction region of a circular cylinder normal to a flat plate at 30 and 60 degrees from stagnation point of the cylinder [AIAA PAPER 87-0077] p 132 A87-22398
- NAGIEGAAL, J. C.**
The NESSUS finite element code p 184 N87-22785
- NAGPAL, VINOD K.**
Probabilistic structural analysis to quantify uncertainties associated with turbopump blades [AIAA PAPER 87-0766] p 176 A87-33581
- NAHRA, HENRY K.**
Protection of solar array blankets from attack by low earth orbital atomic oxygen p 47 A87-19874
- NAINIGER, JOSEPH J.**
NASA Growth Space Station missions and candidate nuclear/solar power systems p 48 A87-21807
- NAKANISHI, S.**
Microwave electrothermal thruster performance in helium gas p 49 A87-31281
- NAKANISHI, SHIGEO**
Precision tunable resonant microwave cavity [NASA-CASE-LEW-13935-1] p 126 N87-21234
- NAKAZAWA, S.**
On 3-D inelastic analysis methods for hot section components (base program) [NASA-CR-175060] p 180 N87-12923
The NESSUS finite element code p 184 N87-22785
On 3-D inelastic analysis methods for hot section components. Volume 1: Special finite element models [NASA-CR-179494] p 185 N87-22996
- NALL, MARSHA**
Structural and aeroelastic analysis of the SR-7L propfan [NASA-TM-86877] p 184 N87-22273
- NALL, MARSHA M.**
Solar dynamic power systems for space station p 58 N87-16024
- NALLASAMY, M.**
High-speed propeller noise predictions - Effects of boundary conditions used in blade loading calculations [AIAA PAPER 87-0525] p 208 A87-24978
Euler analysis of the three-dimensional flow field of a high-speed propeller - Boundary condition effects [ASME PAPER 87-GT-253] p 6 A87-48719
High-speed propeller noise predictions: Effects of boundary conditions used in blade loading calculations [NASA-TM-88913] p 210 N87-14957
Euler analysis of the three dimensional flow field of a high-speed propeller: Boundary condition effects [NASA-TM-88955] p 10 N87-16798
- NAMER, IZAK**
Spark ignition of monodisperse fuel sprays [NASA-CR-181404] p 80 N87-29635
- NARAYANAN, G. V.**
Analytical flutter investigation of a composite propfan model [AIAA PAPER 87-0738] p 178 A87-40497
Analytical flutter investigation of a composite propfan model [NASA-TM-88944] p 182 N87-18115
- NATARAJAN, V.**
Anticorrelation of Shubnikov-deHaas amplitudes and negative magnetoresistance magnitudes in intercalated pitch based graphite fibers p 217 A87-28295
- NATHAL, M. V.**
Analysis of NiAlTa precipitates in beta-NiAl + 2 at. pct Ta alloy p 84 A87-34888
The stability of lamellar gamma-gamma-prime structures p 86 A87-48323
- NEFF, R. E.**
Space station experiment definition: Advanced power system test bed [NASA-CR-179502] p 58 N87-15270
- NELSON, C. C.**
Comparison of Hirs' equation with Moody's equation for determining rotordynamic coefficients of annular pressure seals [ASME PAPER 86-TRIB-19] p 161 A87-19529
- NELSON, H. D.**
Optimal placement of critical speeds in rotor-bearing systems p 162 A87-38464
- NELSON, R. S.**
Creep fatigue life prediction for engine hot section materials (ISOTROPIC) [NASA-CR-179550] p 181 N87-15491
- NEMETH, NOEL N.**
Surface flaw reliability analysis of ceramic components with the SCARE finite element postprocessor program [NASA-TM-88901] p 181 N87-17087
- NESBITT, J. A.**
Coating life prediction p 99 N87-11194
- NEWELL, J. F.**
Composite load spectra for select space propulsion structural components [NASA-CR-179496] p 55 N87-10176

N

- Composite load spectra for select space propulsion structural components p 63 N87-22793
- NEWTON, JAMES E.**
Icing of flow conditioners in a closed-loop wind tunnel [NASA-TM-89824] p 13 N87-23591
- NG, WING-FAI**
Two- and three-dimensional viscous computations of a hypersonic inlet flow [AIAA PAPER 87-0283] p 4 A87-31106
Two- and three-dimensional viscous computations of a hypersonic inlet flow [NASA-TM-88923] p 146 N87-15441
- NGAN, Y. C.**
The 20 GHz spacecraft IMPATT solid state transmitter [NASA-CR-179545] p 124 N87-17989
- NGUYEN, D. T.**
Comparison of Hirs' equation with Moody's equation for determining rotordynamic coefficients of annular pressure seals [ASME PAPER 86-TRIB-19] p 161 A87-19529
- NGUYEN, H. L.**
The effects of engine speed and injection characteristics on the flow field and fuel/air mixing in motored two-stroke diesel engines [AIAA PAPER 87-0227] p 161 A87-22501
Numerical simulation of the flowfield in a motored two-dimensional Wankel engine p 138 A87-39812
Numerical simulation of the flow field and fuel sprays in an IC engine [SAE PAPER 870599] p 143 A87-48751
Performance and efficiency evaluation and heat release study of an outboard Marine Corporation Rotary Combustion Engine [NASA-TM-89833] p 28 N87-20282
- NGUYEN, T.**
Satellite analog FDMA/FM to digital TDMA conversion [NASA-CR-179605] p 125 N87-20467
The use of satellites in non-geostationary orbits for unloading geostationary communication satellite traffic peaks. Volume 1: Executive summary [NASA-CR-179597-VOL-1] p 117 N87-21212
The use of satellites in non-geostationary orbits for unloading geostationary communication satellite traffic peaks. Volume 2: Technical report [NASA-CR-179597-VOL-2] p 117 N87-21213
- NICHOLSON, STEPHEN**
Thermodynamic evaluation of transonic compressor rotors using the finite volume approach [NASA-CR-180587] p 150 N87-23925
- NIEDWIECKI, R. W.**
An overview of the small engine component technology (SECT) studies [AIAA PAPER 86-1542] p 19 A87-17993
- NISS, T. G.**
Turbulent heat transfer in corrugated-wall channels with and without fins p 134 A87-27709
- NIGHTINGALE, N.**
Automotive Stirling Engine Development Program [NASA-CR-174873] p 222 N87-30223
- NIINO, M.**
Volume-energy parameters for heat transfer to supercritical fluids p 137 A87-32326
- NIKITOPOULOS, D. E.**
Nonlinear binary-mode interactions in a developing mixing layer p 142 A87-47158
- NIKJOOY, M.**
Modelling of jet- and swirl-stabilized reacting flows in axisymmetric combustors p 138 A87-38956
- NIKJOOY, MOHAMMAD**
On the modelling of non-reactive and reactive turbulent combustor flows [NASA-CR-4041] p 28 N87-20996
- NISSLEY, D. M.**
Life prediction and constitutive models for engine hot section anisotropic materials [NASA-CR-179594] p 29 N87-23622
- NISSLEY, DAVID**
Creep fatigue life prediction for engine hot section materials (isotropic) [NASA-CR-174844] p 182 N87-18117
- NORED, D. L.**
Electrical power system for the U.S. Space Station [IAF PAPER 86-37] p 45 A87-16138
Electrical power system design for the U.S. Space Station p 46 A87-18068
- NORED, DONALD L.**
Manned spacecraft electrical power systems p 49 A87-37291
Electrical power system design for the US space station [NASA-TM-88824] p 58 N87-15267
- NORMENT, H. G.**
Three-dimensional trajectory analyses of two drop sizing instruments - PMS OAP and PMS FSSP [AIAA PAPER 87-0180] p 132 A87-22466

- Calculation of water drop trajectories to and about arbitrary three-dimensional lifting and nonlifting bodies in potential airflow [NASA-CR-3935] p 8 N87-11694
- NORRIS, P. P.**
Life prediction and constitutive models for engine hot section anisotropic materials [NASA-CR-179594] p 29 N87-23622
- NORTH, C. M.**
The impact damped harmonic oscillator in free decay [NASA-TM-89897] p 168 N87-23978
- NYLAND, TED W.**
Surface pressure measurements on the blade of an operating Mod-2 wind turbine with and without vortex generators [NASA-TM-89903] p 198 N87-26455

O

- OBERTHART, M. L.**
New simple feed network for an array module of four microstrip elements p 122 A87-41638
- OBERLE, L. G.**
Laser anemometers of hot-section applications p 155 N87-11187
- OBERLE, LAWRENCE G.**
A computer controlled signal preprocessor for laser fringe anemometer applications [NASA-TM-88982] p 157 N87-20516
Laser anemometry techniques for turbine applications [NASA-TM-88953] p 158 N87-22959
- OBRIEN, J. E.**
Unsteady heat transfer and direct comparison to steady-state measurements in a rotor-wake experiment p 136 A87-30720
- OCHI, SIMEON C. U.**
One-dimensional wave propagation in rods of variable cross section: A WKBJ solution [NASA-CR-4086] p 172 N87-24707
- ODEN, J. T.**
An adaptive finite element strategy for complex flow problems [AIAA PAPER 87-0557] p 133 A87-22706
Adaptive finite element methods for compressible flow problems p 4 A87-38496
Recent advances in error estimation and adaptive improvement of finite element calculations p 204 A87-41239
- OH, J. E.**
Thermal and structural stability of cosputtered amorphous Ta(x)Cu(1-x) alloy thin films on GaAs p 216 A87-27198
- OH, JAE E.**
Interactions of amorphous Ta(x)Cu(1-x) (x = 0.93 and 0.80) alloy films with Au overlayers and GaAs substrates p 217 A87-44562
- OKADA, T.**
Plastic deformation of a magnesium oxide 001-plane surface produced by cavitation [ASLE PREPRINT 86-TC-3D-1] p 94 A87-19504
- OKADA, TSUNENORI**
Deformation and fracture of single-crystal and sintered polycrystalline silicon carbide produced by cavitation [NASA-TM-88981] p 102 N87-20422
- OKISHI, T. H.**
Measurements of the unsteady flow field within the stator row of a transonic axial-flow fan. 1: Measurement and analysis technique [NASA-TM-88945] p 10 N87-16789
Measurements of the unsteady flow field within the stator row of a transonic axial-flow fan. Part 2: Results and discussion [NASA-TM-88946] p 10 N87-16790
- OLBERT, S.**
Radiation from large space structures in low earth orbit with induced ac currents [AIAA PAPER 87-0612] p 42 A87-22738
- OLEN, CARL**
Neutral atomic oxygen beam produced by ion charge exchange for Low Earth Orbital (LEO) simulation p 79 N87-26188
- OLSEN, R. C.**
Electron beam experiments at high altitudes p 44 N87-26946
- OLSEN, RICHARD C.**
Investigation of beam-plasma interactions [NASA-CR-180579] p 215 N87-22508
- OLSON, B.**
Develop and test fuel cell powered on site integrated total energy systems. Phase 3: Full-scale power plant development [NASA-CR-175118] p 191 N87-11344

- Develop and test fuel cell powered on-site integrated total energy systems. Phase 3: Full-scale power plant development [NASA-CR-175117] p 191 N87-11346
Develop and test fuel cell powered on site integrated total energy systems: Phase 3: Full-scale power plant development [NASA-CR-175075] p 191 N87-11347
- OLSON, D. A.**
Degradation mechanisms in thermal-barrier coatings p 94 A87-12953
Degradation mechanisms in thermal barrier coatings [NASA-TM-89309] p 101 N87-17926
- OLSON, SANDRA L.**
Combustion of velcro in low gravity [NASA-TM-88970] p 102 N87-19518
- OM, DEEPAK**
An experimental investigation of compressible three-dimensional boundary layer flow in annular diffusers [AIAA PAPER 87-0366] p 3 A87-24954
- ONEILL, MARK J.**
Development of an advanced photovoltaic concentrator system for space applications [NASA-TM-100101] p 66 N87-24531
Development of a Fresnel lens concentrator for space application p 196 N87-26427
- ONG, L. H.**
Two opposed lateral jets injected into swirling crossflow [AIAA PAPER 87-0307] p 132 A87-22549
- ORAN, E. S.**
Systematic development of reduced reaction mechanisms for dynamic modeling p 77 A87-33987
- ORME, MELISSA**
The design and performance of a multi-stream droplet generator for the liquid droplet radiator [AIAA PAPER 87-1538] p 140 A87-44842
- OROURKE, D. M.**
Propfan test assessment propfan propulsion system static test report [NASA-CR-179613] p 33 N87-29536
- OSHIDA, Y.**
Grain boundary oxidation and fatigue crack growth at elevated temperatures p 81 A87-19368
Grain boundary oxidation and fatigue crack growth at elevated temperatures [NASA-CR-179529] p 88 N87-11873
- OSONITSCH, CHARLES**
Particle trajectory computer program for icing analysis of axisymmetric bodies - A progress report [AIAA PAPER 87-0027] p 15 A87-22366
- OSWALD, F. B.**
Testing of UH-60A helicopter transmission in NASA Lewis 2240-kW (3000-hp) facility [NASA-TP-2626] p 164 N87-10391
- OSWALD, FRED B.**
Experimental and analytical evaluation of dynamic load and vibration of a 2240-kW (300-hp) rotorcraft transmission [NASA-TM-88975] p 167 N87-20556
Gear tooth stress measurements on the UH-60A helicopter transmission p 167 N87-22235
Profile modification to minimize spur gear dynamic loading [NASA-TM-89901] p 170 N87-28918
- OWEN, ALBERT K.**
A parametric study of the beam refraction problems across laser anemometer windows p 154 A87-40725

P

- PADOVAN, J.**
Analysis of thermomechanical oxidation fields in thermal barrier coatings p 174 A87-14316
Thermomechanical behavior of plasma-sprayed ZrO₂-Y₂O₃ coatings influenced by plasticity, creep and oxidation [NASA-TM-88940] p 147 N87-18784
- PADOVAN, JOE**
Multiply scaled constrained nonlinear equation solvers p 137 A87-31406
- PADOVAN, P.**
Analysis of thermomechanical oxidation fields in thermal barrier coatings p 174 A87-14316
- PAGE, R. J.**
A design study of hydrazine and biowaste resistojets [NASA-CR-179510] p 57 N87-14425
- PAGEL, L. L.**
Hot gas ingestion: From model results to full scale engine testing p 30 N87-24419
- PAGNI, PATRICK J.**
Forced cocurrent smoldering combustion p 77 A87-40572

- PALCO, R. L.**
In-flight photogrammetric measurement of wing ice accretions
[AIAA PAPER 86-0483] p 15 A87-17995
- PALLINI, R. A.**
Solid lubrication design methodology, phase 2
[NASA-CR-175114] p 221 N87-18470
- PAMPREEN, RON**
Engine studies for future subsonic cruise missiles
[AIAA PAPER 86-1547] p 19 A87-21513
- PANTHAKI, M. J.**
Interactive graphics and analysis accuracy
p 202 A87-45900
- PANTHAKI, MALCOLM J.**
Color postprocessing for 3-dimensional finite element mesh quality evaluation and evolving graphical workstation
[NASA-CR-180215] p 202 N87-18997
- PAPADAKIS, M.**
Experimental, water droplet impingement data on two-dimensional airfoils, axisymmetric inlet and Boeing 737-300 engine inlet
[AIAA PAPER 87-0097] p 17 A87-24918
- PARANG, MASOOD**
Experiments on thermoacoustic convection heat transfer in gravity and zero-gravity environments
[AIAA PAPER 87-1651] p 107 A87-43141
- PARAT, K. K.**
Comparative performance of diffused junction indium phosphide solar cells
p 197 N87-26441
Solar cells in bulk InP using an open tube diffusion process
p 198 N87-26444
- PARAT, KRISHNA K.**
Shallow $n(+)$ diffusion into InP by an open-tube diffusion technique
p 217 A87-30023
- PARK, J. S.**
Local heat transfer augmentation in channels with two opposite ribbed surfaces
p 136 A87-30732
Measurement of heat transfer and pressure drop in rectangular channels with turbulence promoters
[NASA-CR-4015] p 146 N87-17003
- PARKS, D. E.**
Three dimensional simulation of the operation of a hollow cathode electron emitter on the Shuttle orbiter
p 119 A87-14084
Hollow cathodes as electron emitting plasma contactors
Theory and computer modeling
[AIAA PAPER 87-0569] p 214 A87-22712
Theory of plasma contactors for electrodynamic tethered satellite systems
p 122 A87-41609
- PARKS, D. M.**
KI-solutions for single edge notch specimens under fixed end displacements
p 174 A87-15798
- PARR, R. A.**
Application of single crystal superalloys for earth-to-orbit propulsion systems
[AIAA PAPER 87-1976] p 85 A87-45336
Application of single crystal superalloys for Earth-to-orbit propulsion systems
[NASA-TM-89877] p 91 N87-22034
- PARSONS, ROGER L.**
Effect of an oxygen plasma on uncoated thin aluminum reflecting films
[NASA-TM-89882] p 61 N87-21999
- PASSERELLO, C. E.**
An investigation of the dynamic response of spur gear teeth with moving loads
[NASA-CR-179643] p 170 N87-29840
- PATANKAR, S. V.**
Development and evaluation of improved numerical schemes for recirculating flows
[AIAA PAPER 87-0061] p 134 A87-24913
- PATEL, D. N.**
Modeling for CO poisoning of a fuel cell anode
p 191 A87-52288
- PATHARE, V.**
Analysis of NiAlTa precipitates in beta-NiAl + 2 at. pct Ta alloy
p 84 A87-34888
- PATRICK, WILLIAM P.**
Flowfield measurements in a separated and reattached flat plate turbulent boundary layer
[NASA-CR-4052] p 148 N87-21257
- PATTERSON, M. J.**
Performance characteristics of ring-cusp thrusters with xenon propellant
[AIAA PAPER 86-1392] p 46 A87-17992
Electric propulsion options for the SP-100 reference mission
[NASA-TM-88918] p 57 N87-14422
- PATTERSON, MICHAEL**
Electrodynamic tether
p 44 N87-26449
- PATTERSON, MICHAEL J.**
Plasma contactors for electrodynamic tethers
p 214 A87-31211
- Hollow cathode-based plasma contactor experiments for electrodynamic tether
[AIAA PAPER 87-0572] p 214 A87-32192
Nuclear powered Mars cargo transport mission utilizing advanced ion propulsion
[AIAA PAPER 87-1903] p 53 A87-50191
Power system technologies for the manned Mars mission
p 60 N87-17789
Plasma contactors for electrodynamic tether
[NASA-TM-88850] p 215 N87-18428
Nuclear powered Mars cargo transport mission utilizing advanced ion propulsion
p 65 N87-23692
Ground-based plasma contractor characterization
[NASA-TM-100194] p 215 N87-28423
- PATTERSON, MIKE J.**
PEGASUS: A multi-megawatt nuclear electric propulsion system
p 59 N87-17787
- PAULEY, WAYNE R.**
An experimental study of the development of longitudinal vortex pairs embedded in a turbulent boundary layer
[AIAA PAPER 87-1309] p 139 A87-42376
- PAVLI, A. J.**
Experimental thrust performance of a high area-ratio rocket nozzle
p 65 N87-23809
- PAVLI, ALBERT J.**
Comparison of theoretical and experimental thrust performance of a 1030:1 area ratio rocket nozzle at a chamber pressure of 2413 kN/sq m (350 psia)
[AIAA PAPER 87-2069] p 52 A87-45390
Experimental evaluation of heat transfer on a 1030:1 area ratio rocket nozzle
[AIAA PAPER 87-2070] p 55 A87-52249
Experimental thrust performance of a high-area-ratio rocket nozzle
[NASA-TP-2720] p 60 N87-20381
Comparison of theoretical and experimental thrust performance of a 1030:1 area ratio rocket nozzle at a chamber pressure of 2413 kN/m² (350 psia)
[NASA-TP-2725] p 66 N87-25423
Experimental evaluation of heat transfer on a 1030:1 area ratio rocket nozzle
[NASA-TP-2726] p 67 N87-25424
- PECK, R. E.**
Modelling of jet- and swirl-stabilized reacting flows in axisymmetric combustors
p 138 A87-38956
- PECKHAM, R. J.**
Low heat transfer oxidizer heat exchanger design and analysis
[NASA-CR-179488] p 58 N87-15272
- PECKHAM, RICHARD J.**
High heat transfer oxidizer heat exchanger design and analysis
[NASA-CR-179596] p 63 N87-22803
- PEET, SHELLEY**
TWT efficiency improvement by a low-cost technique for deposition of carbon on MDC electrodes
p 121 A87-30199
Traveling-wave-tube efficiency improvement by a low-cost technique for deposition of carbon on multistage depressed collector
[NASA-TP-2719] p 126 N87-21239
- PELACCIO, D. G.**
Feasibility of mapping velocity flowfields in an SSME powerhead using laser anemometry techniques
[AIAA PAPER 87-1306] p 154 A87-42374
- PELLOUX, R. M.**
KI-solutions for single edge notch specimens under fixed end displacements
p 174 A87-15798
A computerized test system for thermal-mechanical fatigue crack growth
p 153 A87-23899
Thermal-mechanical fatigue crack growth in B-1900 + Hf
p 86 A87-49570
- PENG, C. K.**
Microwave performance of a quarter-micrometer gate low-noise pseudomorphic InGaAs/AlGaAs modulation-doped field effect transistor
p 121 A87-23745
- PENG, CHIN-KUN**
Characterization of InGaAs/AlGaAs pseudomorphic modulation-doped field-effect transistors
p 121 A87-23922
- PENKO, P. F.**
Vacuum chamber pressure effects on thrust measurements of low Reynolds number nozzles
p 45 A87-14976
The effect of ambient pressure on the performance of a resistojet
[AIAA PAPER 87-0991] p 52 A87-42181
- PENKO, PAUL F.**
Heat exchanger for electrothermal devices
[NASA-CASE-LEW-14037-1] p 59 N87-16875
- PENNLIN, JAMES A.**
A comparison of five benchmarks
[NASA-TM-88956] p 202 N87-17441
- PEREPEZKO, J. H.**
Undercooling and crystallization behaviour of antimony droplets
p 83 A87-28732
- PEREZ-DAVIS, M. E.**
Advanced solar thermal technologies for the 21st century
p 47 A87-18179
- PETERSEN, ROBERT A.**
Coherent motion in excited free shear flows
[AIAA PAPER 85-0539] p 135 A87-30281
- PETRASEK, D. W.**
Fiber-reinforced superalloy composites provide an added performance edge
p 71 A87-12647
- PETRASEK, DONALD W.**
The sensitivity of mechanical properties of TFRS composites to variations in reaction zone size and properties
[AIAA PAPER 87-0757] p 72 A87-33577
Fiber reinforced superalloys
[NASA-TM-89865] p 75 N87-22811
- PETRIE, S. L.**
Preliminary aerothermodynamic design method for hypersonic vehicles
[AIAA PAPER 87-2545] p 7 A87-49100
- PHARES, W. J.**
Large perturbation flow field analysis and simulation for supersonic inlets
[NASA-CR-174676] p 8 N87-10835
- PHUCHAROEN, W.**
Mechanical behavior of thermal barrier coatings for gas turbine blades
p 24 N87-11196
- PIAN, THEODORE H. H.**
A versatile and low order hybrid stress element for general shell geometry
[AIAA PAPER 87-0840] p 176 A87-33624
- PICCONE, T. J.**
Dendritic growth of undercooled nickel-tin. I, II
p 85 A87-41012
- PICCONE, THOMAS J.**
The alloy undercooling experiment on the Columbia STS 61-C Space Shuttle mission
[AIAA PAPER 87-0506] p 108 A87-45724
The alloy undercooling experiment on the Columbia STA 61-C space shuttle mission
[NASA-TM-88909] p 91 N87-18643
- PICKETT, J.**
Measurements of plasma parameters in the vicinity of the Space Shuttle
p 200 A87-24672
Measurements of plasma density and turbulence near the shuttle orbiter
[NASA-CR-180102] p 215 N87-16614
- PIKE, JAMES A.**
Expansion of epicyclic gear dynamic analysis program
[NASA-CR-179563] p 166 N87-19723
- PILSNER, B. H.**
Thermal barrier coating life prediction model
[NASA-CR-179504] p 100 N87-13539
Thermal barrier coating life prediction model
[NASA-CR-175010] p 100 N87-13540
- PILTCH, NANCY D.**
Fiber-optic thermometer using temperature dependent absorption, broadband detection, and time domain referencing
p 153 A87-25948
- PINTZ, A.**
Design and dynamic simulation of a fixed pitch 56 kW wind turbine drive train with a continuously variable transmission
[NASA-CR-179543] p 193 N87-17401
- PIROUZ, P.**
Antiphase boundaries in epitaxially grown beta-SiC
p 217 A87-30025
TEM investigation of beta-SiC grown epitaxially on Si substrate by CVD
p 97 A87-40927
- PISZCZOR, MICHAEL F.**
Development of a Fresnel lens concentrator for space application
p 196 N87-26427
- PISZCZOR, MICHAEL F., JR.**
Use of a corrugated surface to enhance radiation tolerance in a GaAs solar cell
p 189 A87-19842
Development of an advanced photovoltaic concentrator system for space applications
[NASA-TM-100101] p 66 N87-24531
- PITZ, R. W.**
Advanced optical smoke meters for jet engine exhaust measurement
[NASA-CR-179459] p 155 N87-12829
- PLATZ, S. J.**
Flight test report of the NASA icing research airplane: Performance, stability, and control after flight through natural icing conditions
[NASA-CR-179515] p 34 N87-11797
- PLATZER, M. F.**
Progress in the prediction of unsteady heat transfer on turbine blades
p 149 N87-22769

PLATZER, MAX F.

A general method for unsteady stagnation region heat transfer and results for model turbine flows
[NASA-TM-88903] p 146 N87-17002

PLESHA, M. E.

A constitutive law for finite element contact problems with unclassified friction
[NASA-TM-88838] p 180 N87-12924

PLESHA, MICHAEL E.

The effects of crack surface friction and roughness on crack tip stress fields
[NASA-TM-88976] p 183 N87-18881

PLETKA, B. J.

The effects of tantalum on the microstructure of two polycrystalline nickel-base superalloys - B-1900 + Hf and MAR-M247 p 82 A87-24110
Thermal stability of the nickel-base superalloy B-1900 + Hf with tantalum variations p 87 A87-51289

PODBOY, GARY G.

Wind tunnel performance results of an aeroelastically scaled 2/9 model of the PTA flight test prop-fan [AIAA PAPER 87-1893] p 8 A87-52251
Wind tunnel performance results of an aeroelastically scaled 2/9 model of the PTA flight test prop-fan [NASA-TM-89917] p 14 N87-25294

POLEY, W. A.

An assessment of the status and trends in satellite communications 1986-2000: An information document prepared for the Communications Subcommittee of the Space Applications Advisory Committee
[NASA-TM-88867] p 114 N87-13600

POLLARD, H. E.

Space station experiment definition: Advanced power system test bed
[NASA-CR-179502] p 58 N87-15270

PONCHAK, G. E.

RF characterization of monolithic microwave and mm-wave ICs
[NASA-TM-88948] p 117 N87-22065

PONCHAK, GEORGE E.

A new model for broadband waveguide to microstrip transition design
[NASA-TM-88905] p 115 N87-16958

PONTANO, B.

On-board processing satellite network architecture and control study
[NASA-CR-180816] p 44 N87-27710

PONTANO, BENJAMIN A.

On-board processing satellite network architecture and control study
[NASA-CR-180817] p 44 N87-27711

PONTONIDES, H. C.

Effect of variable inlet guide vanes on the operating characteristics of a tilt nacelle inlet/powered fan model
[NASA-TM-88983] p 14 N87-27628

POPE, A. N.

Development of gas-to-gas lift pad dynamic seals, volumes 1 and 2
[NASA-CR-179486] p 168 N87-22245

PORRO, A. R.

An LDA investigation of three-dimensional normal shock-boundary layer interactions in a corner
[AIAA PAPER 87-1369] p 6 A87-44938

POSTA, S. J.

A low-cost optical data acquisition system for vibration measurement
[NASA-TM-88907] p 181 N87-14730

POTAPCZUK, MARK G.

Numerical analysis of a NACA0012 airfoil with leading edge ice accretions
[AIAA PAPER 87-0101] p 2 A87-22415

POUCH, J. J.

Ellipsometric and optical study of amorphous hydrogenated carbon films p 216 A87-23967
Thermal and structural stability of cosputtered amorphous Ta(x)Cu(1-x) alloy thin films on GaAs p 216 A87-27198
Adhesion, friction and deformation of ion-beam-deposited boron nitride films p 98 A87-49325

POUCH, JOHN J.

Interactions of amorphous Ta(x)Cu(1-x) (x = 0.93 and 0.80) alloy films with Au overlayers and GaAs substrates p 217 A87-44562

Adhesion, friction, and deformation of ion-beam-deposited boron nitride films [NASA-TM-88902] p 100 N87-15305
Mechanical strength and tribological behavior of ion-beam deposited boron nitride films on non-metallic substrates [NASA-TM-89818] p 101 N87-18668
Rapid thermal annealing of Amorphous Hydrogenated Carbon (a-C:H) films [NASA-TM-89859] p 218 N87-20821

AlGaAs growth by OMCVD using an excimer laser [NASA-TM-88937] p 218 N87-23304

Boron nitride: Composition, optical properties and mechanical behavior [NASA-TM-89849] p 218 N87-25017

Computer control of a scanning electron microscope for digital image processing of thermal-wave images [NASA-TM-100157] p 128 N87-26278

POVINELLI, LOUIS A.

Viscous analyses for flow through subsonic and supersonic intakes [NASA-TM-88831] p 9 N87-15173
Viscous analyses for flow through subsonic and supersonic intakes p 30 N87-24469

POWELL, J. A.

Antiphase boundaries in epitaxially grown beta-SiC p 217 A87-30025
TEM investigation of beta-SiC grown epitaxially on Si substrate by CVD p 97 A87-40927

POWELL, J. ANTHONY

Growth and characterization of cubic SiC single-crystal films on Si p 217 A87-44875

POWERS, WILLIAM O.

A study of reduced chromium content in a nickel-base superalloy via element substitution and rapid solidification processing [NASA-CR-179631] p 92 N87-25456

PRADHAN, D. C.

Mechanical property anisotropy in superalloy EI-929 directionally solidified by an exothermic technique p 81 A87-11389

PRAKASH, S.

Thin-film temperature sensors for gas turbine engines Problems and prospects p 153 A87-26109

PRATT, D. T.

Fast algorithm for calculating chemical kinetics in turbulent reacting flow p 77 A87-38958

PREISER, U. Z.

Rotational effects on impingement cooling p 141 A87-45838

PREKWS, A.

Comparison of generalized Reynolds and Navier Stokes equations for flow of a power law fluid p 142 A87-45852

PRESLER, A.

Power system technologies for the manned Mars mission p 60 N87-17789

PRESLER, A. F.

Computer-based phosphoric acid fuel cell analytical tools Descriptions and usages p 190 A87-33788

PRESZ, WALTER M., JR.

Short efficient ejector systems [AIAA PAPER 87-1837] p 20 A87-45239

PRICE, H. G.

Liquid oxygen cooling of high pressure LOX/hydrocarbon rocket thrust chambers [NASA-TM-88805] p 57 N87-14426

PRICE, HAROLD G.

Proven, long-life hydrogen/oxygen thrust chambers for space station propulsion p 68 N87-26133

PRICE, J.

An adaptive finite element strategy for complex flow problems [AIAA PAPER 87-0557] p 133 A87-22706

PRICE, K.

Communications satellite systems operations with the space station. Volume 1: Executive summary [NASA-CR-179526] p 206 N87-17472

Communications satellite systems operations with the space station, volume 2 [NASA-CR-179527] p 206 N87-17473

The use of satellites in non-geostationary orbits for unloading geostationary communication satellite traffic peaks. Volume 1: Executive summary [NASA-CR-179597-VOL-1] p 117 N87-21212

The use of satellites in non-geostationary orbits for unloading geostationary communication satellite traffic peaks. Volume 2: Technical report [NASA-CR-179597-VOL-2] p 117 N87-21213

PROBST, H. B.

Materials research and applications at NASA Lewis Research Center p 69 A87-38472
Structural ceramics in heat engines - The NASA viewpoint p 98 A87-53352

PRZYBYSEWSKI, J. S.

High temperature static strain gage development contract, tasks 1 and 2 [NASA-CR-180811] p 159 N87-28869

Thin film strain gage development program [NASA-CR-174707] p 159 N87-28883

PSICHOGIOS, T. P.

Fabrication of cooled radial turbine rotor [NASA-CR-179503] p 25 N87-11789

PUDICK, S.

Develop and test fuel cell powered on site integrated total energy systems. Phase 3: Full-scale power plant development [NASA-CR-175118] p 191 N87-11344

Develop and test fuel cell powered on-site integrated total energy systems. Phase 3: Full-scale power plant development [NASA-CR-175117] p 191 N87-11346

Develop and test fuel cell powered on site integrated total energy systems: Phase 3: Full-scale power plant development [NASA-CR-175075] p 191 N87-11347

PUGH, D. W.

Development of gas-to-gas lift pad dynamic seals, volumes 1 and 2 [NASA-CR-179486] p 168 N87-22245

PURVIS, CAROLYN

Secondary electron generation, emission and transport: Effects on spacecraft charging and NASCAP models p 44 N87-26950

Q

QAQISH, WALID

Optical strain measurement system development, phase 1 [NASA-CR-179619] p 158 N87-22960
Optical strain measurement system development [NASA-CR-179646] p 159 N87-26326

QIAN, X. W.

Microstructure-derived macroscopic residual resistance of brominated graphite fibers p 97 A87-48324

QUEALY, A.

Three-dimensional trajectory analyses of two drop sizing instruments - PMS OAP and PMS FSSP [AIAA PAPER 87-0180] p 132 A87-22466

R

RADCLIFFE, M. D.

Simulation of fluid flows during growth of organic crystals in microgravity [NASA-TM-88921] p 108 N87-16167

RADHAKRISHNAN, K.

Fast algorithm for calculating chemical kinetics in turbulent reacting flow p 77 A87-38958

RADHAKRISHNAN, KRISHNAN

Decoupled direct method for sensitivity analysis in combustion kinetics [NASA-CR-179636] p 79 N87-24549

RAGEN, M. A.

Solid lubrication design methodology, phase 2 [NASA-CR-175114] p 221 N87-18470

RAITHBY, G. D.

Evaluation of new techniques for the calculation of internal recirculating flows [AIAA PAPER 87-0059] p 131 A87-22387

RAJ, RISHI S.

An investigation of the flow characteristics in the blade endwall corner region [NASA-CR-4076] p 14 N87-29412

RAJAN, M.

Optimal placement of critical speeds in rotor-bearing systems p 162 A87-38464

RAJAN, S. D.

A hybrid nonlinear programming method for design optimization p 201 A87-35718
Optimal placement of critical speeds in rotor-bearing systems p 162 A87-38464

RAMACHANDRA, SRIDHAR M.

Method for the determination of the three dimensional aerodynamic field of a rotor-stator combination in compressible flow [AIAA PAPER 87-1742] p 7 A87-50187

Method for the determination of the three-dimensional aerodynamic field of a rotor-stator combination to compressible flow [NASA-TM-100118] p 30 N87-23625

RAMAKRISHNAN, R.

Acoustic power measurement for single and annular stream duct-nozzle systems utilizing a modal decomposition scheme p 209 A87-37628

RAMAMOORTHY, P. A.

A high quality image compression scheme for real-time applications p 111 A87-30801

RAMAN, G.

Initial turbulence effect on jet evolution with and without tonal excitation [NASA-TM-100178] p 14 N87-27629

RAMAN, GANESH

Enhanced mixing of an axisymmetric jet by aerodynamic excitation [NASA-CR-175059] p 15 N87-29418

RAMASWAMY, V. G.

A constitutive model for the inelastic multiaxial cyclic response of a nickel base superalloy Rene 80 [NASA-CR-3998] p 182 N87-18852

- RAMILISON, J. M.**
Transition boiling heat transfer and the film transition regime p 143 A87-53589
- RAMINS, PETER**
Improvements in MDC and TWT overall efficiency through the application of carbon electrode surfaces p 120 A87-20667
TWT efficiency improvement by a low-cost technique for deposition of carbon on MDC electrodes p 121 A87-30199
Performance of textured carbon on copper electrode multistage depressed collectors with medium-power traveling wave tubes [NASA-TP-2665] p 125 A87-17990
Design, fabrication and performance of small, graphite electrode, multistage depressed collectors with 200-W, CW, 8- to 18-GHz traveling-wave tubes [NASA-TP-2693] p 126 A87-20474
Traveling-wave-tube efficiency improvement by a low-cost technique for deposition of carbon on multistage depressed collector p 126 A87-21239
Analytical and experimental performance of a dual-mode traveling wave tube and multistage depressed collector [NASA-TP-2752] p 128 A87-25532
- RAMOS, J. I.**
The effects of engine speed and injection characteristics on the flow field and fuel/air mixing in motored two-stroke diesel engines [AIAA PAPER 87-0227] p 161 A87-22501
Comparisons between thermodynamic and one-dimensional combustion models of spark-ignition engines p 161 A87-29275
Numerical simulation of the flow field and fuel sprays in an IC engine [SAE PAPER 870599] p 143 A87-48751
Fuel-air mixing and combustion in a two-dimensional Wankel engine [SAE PAPER 870408] p 163 A87-48783
- RAMSEY, J. K.**
Concentrated mass effects on the flutter of a composite advanced turboprop model [NASA-TM-88854] p 180 A87-12017
- RAPP, DOUGLAS C.**
Analysis of quasi-hybrid solid rocket booster concepts for advanced earth-to-orbit vehicles [AIAA PAPER 87-2082] p 55 A87-52250
Analysis of quasi-hybrid solid rocket booster concepts for advanced earth-to-orbit vehicles [NASA-TP-2751] p 67 A87-25425
- RASHID, J. M.**
Materials for Advanced Turbine Engines (MATE). Project 4: Erosion resistant compressor airfoil coating [NASA-CR-179622] p 92 A87-27029
- RATAJCZAK, A. F.**
Tunisia Renewable Energy Project systems description report [NASA-TM-88789] p 192 A87-13856
- RATAJCZAK, ANTHONY F.**
User evaluation of photovoltaic-powered vaccine refrigerator/freezer systems [NASA-TM-88830] p 193 A87-18230
- RAWLIN, V. K.**
Electric propulsion options for the SP-100 reference mission [NASA-TM-88918] p 57 A87-14422
- RAY, P. K.**
Rail gun performance and plasma characteristics due to wall ablation p 214 A87-18735
- RAYMONDO, P.**
Advanced high temperature static strain sensor development [NASA-CR-179520] p 158 A87-25552
- REDD, L. R.**
Propulsion recommendations for Space Station free flying platforms p 49 A87-31134
Propulsion recommendations for space station free flying platforms p 67 A87-26129
- REDDOCH, T. W.**
Utility interconnection issues for wind power generation [NASA-CR-175056] p 193 A87-17400
- REDDY, K. T.**
Degradation mechanisms of sulfur and nitrogen containing compounds during thermal stability testing of model fuels [AIAA PAPER 87-2039] p 106 A87-45372
- REDDY, KISHENKUMAR TADISINA**
Thermal stability of distillate hydrocarbon fuels [NASA-CR-181412] p 107 A87-29706
- REDDY, T. S. R.**
A higher order theory of laminated composite cylindrical shells p 177 A87-35656
A comparative study of some dynamic stall models [NASA-TM-88917] p 183 A87-18883
- REEHORST, ANDREW L.**
New methods and materials for molding and casting ice formations [NASA-TM-100126] p 16 A87-29470
- REILLY, C. H.**
Alternative mathematical programming formulations for FSS synthesis [NASA-CR-180030] p 202 A87-14872
Engineering calculations for communications satellite systems planning [NASA-CR-180106] p 114 A87-16198
- REILLY, CHARLES H.**
On orbital allotments for geostationary satellites [NASA-CR-181017] p 37 A87-22700
Engineering calculations for communications satellite systems planning [NASA-CR-181112] p 117 A87-24605
A satellite system synthesis model for orbital arc allotment optimization [NASA-CR-181150] p 37 A87-25341
Mathematical programming formulations for satellite synthesis [NASA-CR-181151] p 44 A87-25419
- RENO, C.**
Generation of a composite grid for turbine flows and consideration of a numerical scheme [NASA-TM-88890] p 11 A87-17662
- REPAS, G. A.**
Hydrogen-air ignition torch [NASA-CR-88882] p 38 A87-13470
- REPAS, GEORGE A.**
Conventionally cast and forged copper alloy for high-heat-flux thrust chambers [NASA-TP-2694] p 90 A87-16902
- REYNARD, WILLIAM D.**
Aircraft accident report: NASA 712, Convair 990, N712NA, March Air Force Base, California, July 17, 1985, executive summary [NASA-TM-87356-VOL-1] p 16 A87-21878
Aircraft accident report: NASA 712, Convair 990, N712NA, March Air Force Base, California, July 17, 1985, facts and analysis [NASA-TM-87356-VOL-2] p 16 A87-21879
- REYNOLDS, C. N.**
Advanced Prop-fan Engine Technology (APET) single- and counter-rotation gearbox/pitch change mechanism [NASA-CR-168114-VOL-1] p 32 A87-28552
Advanced Prop-fan Engine Technology (APET) single- and counter-rotation gearbox/pitch change mechanism [NASA-CR-168114-VOL-2] p 33 A87-28556
- REYNOLDS, R.**
Transition mixing study [NASA-CR-175062] p 27 A87-16830
- RICE, E. J.**
Aircraft turbofan noise p 209 A87-31144
Initial turbulence effect on jet evolution with and without tonal excitation [NASA-TM-100178] p 14 A87-27629
Controlled excitation of a cold turbulent swirling free jet [NASA-TM-100173] p 152 A87-27977
Control of shear flows by artificial excitation [NASA-TM-100201] p 15 A87-29420
- RICE, EDWARD J.**
Effects of fiber motion on the acoustic behavior of an anisotropic, flexible fibrous material [NASA-TM-89884] p 212 A87-25826
- RICHARDS, W. B.**
Propagation of sound waves in tubes of noncircular cross section [NASA-TP-2601] p 9 A87-14284
- RICHARDSON, WILLIAM R.**
Bonding Lexan and sapphire to form high-pressure, flame-resistant window [NASA-TM-100188] p 159 A87-28880
- RICHEY, A.**
Automotive Stirling engine development program [NASA-CR-174972] p 221 A87-20137
Automotive Stirling Engine Development Program [NASA-CR-174873] p 222 A87-30223
- RICHEY, ALBERT E.**
Mod II engine performance [SAE PAPER 870101] p 163 A87-48780
- RICHTER, G. PAUL**
Proven, long-life hydrogen/oxygen thrust chambers for space station propulsion p 68 A87-26133
New methods and materials for molding and casting ice formations [NASA-TM-100126] p 16 A87-29470
- RIECKE, G.**
Automotive Stirling engine development program [NASA-CR-174972] p 221 A87-20137
Automotive Stirling Engine Development Program [NASA-CR-174873] p 222 A87-30223
- RIFF, R.**
Non-isothermal elastoviscoplastic snap-through and creep buckling of shallow arches [AIAA PAPER 87-0806] p 176 A87-33605
Analysis of shell-type structures subjected to time-dependent mechanical and thermal loading [NASA-CR-180349] p 183 A87-19756
Nonisothermal elasto-visco-plastic response of shell-type structures p 185 A87-22796
Thermo-elasto-viscoplastic analysis of problems in extension and shear [NASA-CR-181410] p 187 A87-29896
The dynamic aspects of thermo-elasto-viscoplastic snap-through and creep buckling phenomena [NASA-CR-181411] p 187 A87-29897
- RIFF, RICHARD**
Thermodynamically consistent constitutive equations for nonisothermal large-strain, elastoplastic, creep behavior p 175 A87-27945
- RILEY, J. J.**
Mechanisms by which heat release affects the flow field in a chemically reacting, turbulent mixing layer [AIAA PAPER 87-0131] p 134 A87-24925
- RILEY, JAMES J.**
On direct numerical simulations of turbulent reacting flows [AIAA PAPER 87-1324] p 140 A87-44930
- RIZK, M. H.**
Propeller design by optimization p 18 A87-14123
- ROBACK, R.**
Mass and momentum turbulent transport experiments p 144 A87-11201
- ROBERTS, GARY D.**
Quantitative analysis of PMR-15 polyimide resin by HPLC p 69 A87-48314
Simulation of fluid flows during growth of organic crystals in microgravity [NASA-TM-88921] p 108 A87-16167
- ROBERTSON, THOMAS F.**
Hydrogen oxidation mechanism with applications to (1) the chaperon efficiency of carbon dioxide and (2) vitiated air testing [NASA-TM-100186] p 80 A87-28628
- ROBINSON, D. N.**
High-temperature constitutive modeling p 179 A87-11210
A viscoplastic constitutive theory for metal matrix composites at high temperature [NASA-CR-179530] p 180 A87-13790
- ROBINSON, W. W.**
Further development of the dynamic gas temperature measurement system. Volume 1: Technical efforts [NASA-CR-179513-VOL-1] p 157 A87-19686
- ROBSON, R. R.**
Status of xenon ion propulsion technology [AIAA PAPER 87-1003] p 53 A87-48677
- ROCHE, J. C.**
Computer simulation of plasma electron collection by PIX-II p 45 A87-17837
- ROCHE, JAMES C.**
Secondary electron generation, emission and transport: Effects on spacecraft charging and NASCAP models p 44 A87-26950
- RODGERS, C.**
Fabrication of cooled radial turbine rotor [NASA-CR-179503] p 25 A87-11789
- ROELKE, R. J.**
Efficient numerical simulation of an electrothermal de-icer pad [AIAA PAPER 87-0024] p 137 A87-32190
- ROELKE, RICHARD J.**
Experimental evaluation of a translating nozzle sidewall radial turbine [NASA-TM-88963] p 27 A87-17701
- ROGERS, R. CLAYTON**
Multispecies CARS measurements in turbulent combustion p 79 A87-23808
- ROGO, CASIMIR**
Experimental evaluation of a translating nozzle sidewall radial turbine [NASA-TM-88963] p 27 A87-17701
- ROHDE, J. E.**
Host turbine heat transfer overview p 144 A87-11184
- ROHN, DOUGLAS A.**
Evaluation of a high-torque backlash-free roller actuator p 165 A87-16336
- ROMANOVSKY, R. R.**
RF characterization of monolithic microwave and mm-wave ICs [NASA-TM-88948] p 117 A87-22065
- ROMANOVSKY, ROBERT R.**
Microwave characterization and modeling of GaAs/AlGaAs heterojunction bipolar transistors [NASA-TM-100150] p 117 A87-26265

- Monolithic Microwave Integrated Circuit (MMIC) technology for space communications applications [NASA-TM-100187] p 118 N87-27883
- ROSE, GAYLE E.**
Wind tunnel performance results of an aeroelastically scaled 2/9 model of the PTA flight test prop-fan [AIAA PAPER 87-1893] p 8 A87-52251
Wind tunnel performance results of an aeroelastically scaled 2/9 model of the PTA flight test prop-fan [NASA-TM-89917] p 14 N87-25294
- ROSE, J. H.**
A universal equation of state for solids p 219 A87-14665
Compressibility of solids p 219 A87-51962
- ROSE, L. J.**
Propulsion recommendations for Space Station free flying platforms p 49 A87-31134
Propulsion recommendations for space station free flying platforms p 67 N87-26129
- ROSENTHAL, BRUCE N.**
Research opportunities in microgravity science and applications during shuttle hiatus [NASA-TM-88964] p 108 N87-16917
- ROSFJORD, T. J.**
Soot loading in a generic gas turbine combustor [AIAA PAPER 87-0297] p 19 A87-22544
- ROSNER, D. E.**
Turbine airfoil deposition models p 24 N87-11191
- ROSNER, DANIEL E.**
Prediction and rational correlation of thermophoretically reduced particle mass transfer to hot surfaces across laminar or turbulent forced-convection gas boundary layers p 133 A87-23449
- ROSS, H.**
Particle cloud kinetics in microgravity [AIAA PAPER 87-0577] p 107 A87-22716
- ROST, MARTIN C.**
Variable angle of incidence spectroscopic ellipsometry Application to GaAs-Al(x)Ga(1-x)As multiple heterostructures p 216 A87-20519
- ROTH, D. J.**
Probability of detection of internal voids in structural ceramics using microfocus radiography p 170 A87-14300
Quantitative void characterization in structural ceramics by use of scanning laser acoustic microscopy p 171 A87-51974
- ROTH, DON J.**
Ultrasonic NDE of structural ceramics for power and propulsion systems [NASA-TM-100147] p 173 N87-26362
- RUBINSTEIN, A. A.**
Macrocrack interaction with transverse array of microcracks [NASA-CR-180806] p 186 N87-25607
- RUBINSTEIN, ROBERT**
Probabilistic structural analysis to quantify uncertainties associated with turbopump blades [AIAA PAPER 87-0766] p 176 A87-33581
Structural tailoring using the SSME/STAEBL code p 63 N87-22795
- RUDOFF, R.**
Laser velocimetry in turbulent flow fields - Particle response [AIAA PAPER 87-0118] p 132 A87-22426
- RUDOFF, R. C.**
Two-phase flow measurements of a spray in a turbulent flow [AIAA PAPER 87-0062] p 132 A87-22388
Two-phase measurements of a spray in the wake of a bluff body p 142 A87-46199
- RUNCHAL, AKSHAI K.**
An unconditionally-stable central differencing scheme for high Reynolds number flows [AIAA PAPER 87-0060] p 133 A87-24912
CONDIF - A modified central-difference scheme with unconditional stability and very low numerical diffusion p 136 A87-30685
CONDIF - A modified central-difference scheme for convective flows p 205 A87-53675
- RUSSELL, LOUIS M.**
Use of a liquid-crystal, heater-element composite for quantitative, high-resolution heat transfer coefficients on a turbine airfoil, including turbulence and surface roughness effects [NASA-TM-87355] p 158 N87-22181
- RUTLEDGE, SHARON**
An evaluation of candidate oxidation resistant materials for space applications in LEO [NASA-TM-100122] p 105 N87-25480
Neutral atomic oxygen beam produced by ion charge exchange for Low Earth Orbital (LEO) simulation p 79 N87-26188
An evaluation of candidate oxidation resistant materials p 80 N87-26203

- RUTLEDGE, SHARON K.**
Protection of solar array blankets from attack by low earth orbital atomic oxygen p 47 A87-19874
Ion beam sputter etching [NASA-CASE-LEW-13899-1] p 110 N87-21160
High temperature radiator materials for applications in the low Earth orbital environment [NASA-TM-100190] p 93 N87-29662
- RUTLEDGE, D. G. C.**
A rotorcraft flight/propulsion control integration study [NASA-CR-179574] p 18 N87-24457

S

- SABOURIN, D.**
Baseband processor development/test performance for 30/20 GHz SS-TDMA communication system p 111 A87-18310
- SACKSTEDER, KURT R.**
Science and technology issues in spacecraft fire safety [AIAA PAPER 87-0467] p 39 A87-31107
Science and technology issues in spacecraft fire safety [NASA-TM-88933] p 40 N87-16012
- SALAH-EDDINE, ADEL**
Experiments on thermoacoustic convection heat transfer in gravity and zero-gravity environments [AIAA PAPER 87-1651] p 107 A87-43141
- SALEEB, A. F.**
On the symbolic manipulation and code generation for elastoplastic material matrices p 201 A87-18499
On the numerical performance of three-dimensional thick shell elements using a hybrid/mixed formulation p 175 A87-25924
An efficient quadrilateral element for plate bending analysis p 178 A87-45994
A quadrilateral shell element using a mixed formulation p 179 A87-53796
- SALEM, JONATHAN A.**
Fracture toughness of Si3N4 measured with short bar chevron-notched specimens p 96 A87-30621
- SALIK, J.**
Analysis of plasma-nitrided steels [NASA-TM-88815] p 91 N87-21078
- SALIKUDDIN, M.**
Acoustic power measurement for single and annular stream duct-nozzle systems utilizing a modal decomposition scheme p 209 A87-37628
Sound radiation from single and annular stream nozzles, with modal decomposition of in-duct acoustic power p 209 A87-37629
- SALTSMAN, JAMES F.**
Calculation of thermomechanical fatigue life based on isothermal behavior [NASA-TM-88864] p 183 N87-20565
- SALTZ, LARRY E.**
Experimental study of low Reynolds number nozzles [AIAA PAPER 87-0992] p 51 A87-41102
Experimental study of low Reynolds number nozzles [NASA-TM-88858] p 61 N87-20383
- SAMUELSEN, G. S.**
Performance comparison of two interferometric droplet sizing techniques p 153 A87-11049
- SANDERS, W. A.**
Correlation of processing and sintering variables with the strength and radiography of silicon nitride p 94 A87-12938
Sintering, microstructural, radiographic, and strength characterization of a high-purity Si3N4-based composition p 94 A87-12939
- SANGER, N. L.**
Comparison of calculated and experimental cascade performance for controlled-diffusion compressor stator blading [ASME PAPER 86-GT-35] p 19 A87-25394
- SANKAR, L. N.**
A technique for the prediction of airfoil flutter characteristics in separated flow [AIAA PAPER 87-0910] p 177 A87-33719
Analysis of viscous transonic flow over airfoil sections [AIAA PAPER 87-0420] p 4 A87-34723
Analysis of viscous transonic flow over airfoil sections [NASA-TM-88912] p 146 N87-17001
Studies of unsteady viscous flows using a two-equation model of turbulence [NASA-CR-181293] p 152 N87-27949
- SANTORO, GILBERT J.**
Experimental verification of corrosive vapor deposition rate theory in high velocity burner rigs p 143 A87-49551
- SANZ, JOSE M.**
Lewis inverse design code (LINDES): Users manual [NASA-TP-2676] p 12 N87-20238

- SARGISSON, D. F.**
Advanced Propan Engine Technology (APET) and single-rotation gearbox/pitch change mechanism [NASA-CR-168113] p 32 N87-28553
- SARMA, GARIMELLA R.**
Ramp-integration technique for capacitance-type blade-tip clearance measurement p 155 A87-45128
- SARMIENTO, CHARLES J.**
Low power arcjet thruster pulse ignition [AIAA PAPER 87-1951] p 54 A87-50194
Low power arcjet thruster pulse ignition [NASA-TM-100123] p 64 N87-23691
- SATTAR, M. A.**
Advanced composite combustor structural concepts program [NASA-CR-174733] p 74 N87-20387
- SAVAGE, M.**
Gear mesh compliance modeling p 164 A87-53422
Gear mesh compliance modeling [NASA-TM-88843] p 166 N87-18092
Flexibility effects on tooth contact location in spiral bevel gear transmissions [NASA-CR-4055] p 166 N87-20552
- SAVINELL, ROBERT F.**
Theoretical performance of hydrogen-bromine rechargeable SPE fuel cell p 199 N87-29945
- SAVINO, J. M.**
Advanced solar dynamic space power systems perspectives, requirements and technology needs [NASA-TM-88884] p 56 N87-12606
- SAYEGH, SOHEIL**
Onboard multichannel demultiplexer/demodulator [NASA-CR-180821] p 119 N87-28819
- SCARLOTTI, R. D.**
Space station experiment definition: Long-term cryogenic fluid storage [NASA-CR-4072] p 151 N87-24641
- SCARPELLI, AUGUST R.**
Precision tunable resonant microwave cavity [NASA-CASE-LEW-13935-1] p 126 N87-21234
- SCAVUZZO, R. J.**
Structural properties of impact ices accreted on aircraft structures [NASA-CR-179580] p 182 N87-18121
- SCHAFER, STEVE**
Comparison of three explicit multigrid methods for the Euler and Navier-Stokes equations [AIAA PAPER 87-0602] p 137 A87-34725
Multigrid-sinc methods p 205 A87-52865
Comparison of three explicit multigrid methods for the Euler and Navier-Stokes equations [NASA-TM-88878] p 1 N87-16784
- SCHARRER, JOSEPH K.**
Experimental rotordynamic coefficient results for teeth-on-rotor and teeth-on-stator labyrinth gas seals p 167 N87-22212
- SCHARRER, JOSEPH KIRK**
A comparison of experimental and theoretical results for labyrinth gas seals [NASA-CR-180194] p 166 N87-18096
- SCHAUB, S. A.**
Effects of non-spherical drops on a phase Doppler spray analyzer p 152 A87-11048
- SCHIEER, D. D.**
Small centrifugal pumps for low-thrust rockets p 50 A87-39808
Status of advanced propulsion for space based orbital transfer vehicle [NASA-TM-88848] p 56 N87-10959
- SCHIEER, DEAN D.**
Status of advanced propulsion for space based orbital transfer vehicle [IAF PAPER 86-183] p 48 A87-23239
- SCHERTLER, RONALD J.**
ACTS experiments program p 113 A87-45513
- SCHETTINO, JOHN C.**
The Advanced Turbine Technology Applications Program (ATTAP) [SAE PAPER 87-0467] p 163 A87-48791
- SCHUEERMANN, COULSON M.**
Preliminary study of niobium alloy contamination by transport through helium [NASA-TM-88952] p 90 N87-17884
Fatigue failure of regenerator screens in a high frequency Stirling engine [NASA-TM-88974] p 183 N87-18882
Creep-rupture behavior of a developmental cast-iron-base alloy for use up to 800 deg C [NASA-TM-100167] p 93 N87-28641
- SCHINSTOCK, W. C.**
Flight test report of the NASA icing research airplane: Performance, stability, and control after flight through natural icing conditions [NASA-CR-179515] p 34 N87-11797

- SCHMIDT, JAMES F.**
Supersonic through-flow fan design
[AIAA PAPER 87-1746] p 22 A87-48571
Application of advanced computational codes in the design of an experiment for a supersonic throughflow fan rotor
[NASA-TM-88915] p 13 N87-22630
Supersonic through-flow fan design
[NASA-TM-88908] p 29 N87-22681
Design and performance of controlled-diffusion stator compared with original double-circular-arc stator
[NASA-TM-100141] p 31 N87-26910
- SCHNEIDER, S. J.**
Laser anemometry measurements of natural circulation flow in a scale model PWR reactor system
p 154 A87-40750
- SCHNEIDER, STEVEN J.**
Space station propulsion system technology
[NASA-TM-100108] p 66 N87-25422
- SCHOCK, H. J.**
A two-dimensional numerical study of the flow inside the combustion chamber of a motored rotary engine
[SAE PAPER 860615] p 161 A87-28624
Numerical simulation of the flowfield in a motored two-dimensional Wankel engine p 138 A87-39812
Numerical simulation of the flow field and fuel sprays in an IC engine
[SAE PAPER 870599] p 143 A87-48751
Fuel-air mixing and combustion in a two-dimensional Wankel engine
[SAE PAPER 870408] p 163 A87-48783
- SCHOCK, HAROLD J.**
Visualization of flows in a motored rotary combustion engine using holographic interferometry
[AIAA PAPER 86-1557] p 19 A87-21514
- SCHOENDORF, J. F.**
Creep fatigue life prediction for engine hot section materials (ISOTROPIC)
[NASA-CR-179550] p 181 N87-15491
- SCHREINER, K. E.**
Control considerations for high frequency, resonant, power processing equipment used in large systems
[NASA-TM-89926] p 64 N87-23690
- SCHRUBENS, DALE L.**
Tribological properties of coal slurries
[NASA-TM-89930] p 104 N87-24565
- SCHUBERT, F. H.**
Alkaline water electrolysis technology for Space Station regenerative fuel cell energy storage p 46 A87-18107
- SCHULTZ, D. F.**
Combustion overview p 78 N87-11181
Component testing of a ground based gas turbine steam cooled rich-burn primary zone combustor for emissions control of nitrogenous fuels
[NASA-TM-88873] p 191 N87-11345
- SCHUMANN, LAWRENCE F.**
A method for calculating turbulent boundary layers and losses in the flow channels of turbomachines
[NASA-TM-88928] p 9 N87-15944
- SCHWARTZ, H. J.**
The potential impact of new power system technology on the design of a manned Space Station p 47 A87-18342
- SCHWARZE, GENE E.**
A study of Schwarz converters for nuclear powered spacecraft
[NASA-TM-89911] p 128 N87-23903
- SCOTT, J. N.**
Numerical simulation of excited jet mixing layers
[AIAA PAPER 87-0016] p 131 A87-22361
Navier Stokes solution of the flowfield over ice accretion shapes
[AIAA PAPER 87-0099] p 2 A87-22414
- SCOTT, JAMES R.**
Coupled aerodynamic and acoustical predictions for turboprops
[NASA-TM-87094] p 13 N87-23598
- SCUDDER, L. R.**
Tunisia Renewable Energy Project systems description report
[NASA-TM-88789] p 192 N87-13856
- SEASHOLTZ, R. G.**
Laser anemometers of hot-section applications
p 155 N87-11187
- SEASHOLTZ, RICHARD G.**
Combined fringe and Fabry-Perot laser anemometer for 3 component velocity measurements in turbine stator cascade facility p 110 N87-21183
- SEEMAN, M. P.**
Effects of non-spherical drops on a phase Doppler spray analyzer p 152 A87-11048
- SEGALL, B.**
Compensation in epitaxial cubic SiC films p 216 A87-15071
- Comment on 'Temperature dependence of electrical properties of non-doped and nitrogen-doped beta-SiC single crystals grown by chemical vapor deposition' p 217 A87-42846
- SEHANOBISH, K.**
An analysis for crack layer stability p 176 A87-28982
- SEIDEL, ROBERT C.**
Solar dynamic power systems for space station p 58 N87-16024
- SELLMYER, D. J.**
Thermal and structural stability of cosputtered amorphous Ta(x)Cu(1-x) alloy thin films on GaAs p 216 A87-27198
- SELLMYER, DAVID J.**
Temperature dependence (4K to 300K) of the electrical resistivity of methane grown carbon fibers p 97 A87-47375
- SEN, SIDDHARTHA**
Noncommutative-geometry model for closed bosonic strings p 207 A87-37542
- SENNEFF, J. M.**
Space station auxiliary thrust chamber technology
[NASA-CR-179552] p 59 N87-16874
- SERAFINI, J. S.**
An analytical and experimental investigation of resistojet plumes
[NASA-TM-88852] p 58 N87-14428
- SERAFINI, JOHN S.**
An analytical and experimental investigation of resistojet plumes
[AIAA PAPER 87-0399] p 48 A87-24998
Effect of nozzle geometry on the resistojet exhaust plume
[AIAA PAPER 87-2121] p 55 A87-52252
- SERAFINI, T. T.**
Polymer, metal, and ceramic matrix composites for advanced aircraft engine applications p 71 A87-15187
- SETTER, ROBERT N.**
A distributed data acquisition system for aeronautics test facilities
[NASA-TM-88961] p 35 N87-16851
- SHAFFER, NANETTE**
Stability of bromine, iodine monochloride, copper (II) chloride, and nickel (II) chloride intercalated pitch-based graphite fibers
[NASA-TM-89904] p 103 N87-24563
- SHALKHAUSER, K. A.**
RF characterization of monolithic microwave and mm-wave ICs
[NASA-TM-88948] p 117 N87-22065
- SHALKHAUSER, KURT A.**
Bit-error-rate testing of high-power 30-GHz traveling wave tubes for ground-terminal applications
[NASA-TP-2635] p 115 N87-17971
- SHALTENS, R. K.**
DOE/NASA automotive Stirling engine project - Overview 86 p 220 A87-18034
Advanced Stirling conversion systems for terrestrial applications
[NASA-TM-88897] p 220 N87-15031
- SHALTENS, RICHARD K.**
Comparison of Stirling engines for use with a 25-kW disk-electric conversion system
[NASA-TM-100111] p 222 N87-27564
- SHAMROTH, S. J.**
Calculation of two- and three-dimensional transonic cascade flow field using the Navier-Stokes equations p 144 N87-11220
Turbine vane external heat transfer. Volume 2. Numerical solutions of the Navier-Stokes equations for two- and three-dimensional turbine cascades with heat transfer
[NASA-CR-174828] p 145 N87-13661
- SHANNON, JOHN L. JR.**
Fracture toughness of Si3N4 measured with short bar chevron-notched specimens p 96 A87-30621
- SHARMA, K. K.**
Mechanical property anisotropy in superalloy EI-929 directionally solidified by an exothermic technique p 81 A87-11389
- SHARMA, L. K.**
Feasibility of mapping velocity flowfields in an SSME powerhead using laser anemometry techniques
[AIAA PAPER 87-1306] p 154 A87-42374
- SHARP, G. RICHARD**
Thermal expansion behavior of graphite/glass and graphite/magnesium p 72 A87-38615
- SHAW, R. J.**
Three-dimensional trajectory analyses of two drop sizing instruments - PMS OAP and PMS FSSP
[AIAA PAPER 87-0180] p 132 A87-22466
Evaluation of icing drag coefficient correlations applied to iced propeller performance prediction
[SAE PAPER 871033] p 16 A87-48761
- SHAW, ROBERT J.**
Particle trajectory computer program for icing analysis of axisymmetric bodies - A progress report
[AIAA PAPER 87-0027] p 15 A87-22366
- SHEIBLEY, D. W.**
Advanced technology for extended endurance alkaline fuel cells p 190 A87-33787
- SHEIBLEY, DEAN W.**
Status of space station power system p 45 N87-29915
- SHELTON, S. V.**
Feasibility analysis of reciprocating magnetic heat pumps
[NASA-CR-180262] p 147 N87-19647
- SHIH, T. I.-P.**
Numerical simulation of the flowfield in a motored two-dimensional Wankel engine p 138 A87-39812
Fuel-air mixing and combustion in a two-dimensional Wankel engine
[SAE PAPER 870408] p 163 A87-48783
- SHIH, T. I.-P.**
A two-dimensional numerical study of the flow inside the combustion chamber of a motored rotary engine
[SAE PAPER 860615] p 161 A87-28624
- SHINDE, S. L.**
Degradation mechanisms in thermal-barrier coatings p 94 A87-12953
Degradation mechanisms in thermal barrier coatings
[NASA-TM-89309] p 101 N87-17926
- SHIOHARA, Y.**
Dendritic growth of undercooled nickel-tin. I, II p 85 A87-41012
- SHIOHARA, YUH**
The alloy undercooling experiment on the Columbia STS 61-C Space Shuttle mission
[AIAA PAPER 87-0506] p 108 A87-45724
The alloy undercooling experiment on the Columbia STA 61-C space shuttle mission
[NASA-TM-88909] p 91 N87-18643
- SHREEVE, R. P.**
Comparison of calculated and experimental cascade performance for controlled-diffusion compressor stator blading
[ASME PAPER 86-GT-35] p 19 A87-25394
- SHUEN, J. S.**
Representation of the vaporization behavior of turbulent polydisperse sprays by 'equivalent' monodisperse sprays
[AIAA PAPER 87-1954] p 141 A87-45325
Effects of droplet interactions on droplet transport at intermediate Reynolds numbers p 26 N87-14348
Representation of the vaporization behavior of turbulent polydisperse sprays by equivalent monodisperse sprays
[NASA-TM-88906] p 26 N87-16827
- SHUEN, J.-S.**
Particle-laden swirling free jets - Measurements and predictions
[AIAA PAPER 87-0303] p 139 A87-42648
Particle-laden swirling free jets: Measurements and predictions
[NASA-TM-88904] p 26 N87-16826
- SHUEN, JIAN-SHUN**
Effects of droplet interactions on droplet transport at intermediate Reynolds numbers
[AIAA PAPER 87-0137] p 134 A87-24926
Prediction of the structure of fuel sprays in cylindrical combustion chambers p 20 A87-31277
- SHUEY, L. W.**
An investigation of the dynamic response of spur gear teeth with moving loads
[NASA-CR-179643] p 170 N87-29840
- SHYNE, RICKY J.**
Experimental evaluation of two turning vane designs for fan drive corner of 0.1-scale model of NASA Lewis Research Center's proposed altitude wind tunnel
[NASA-TP-2646] p 35 N87-18576
Detailed flow surveys of turning vanes designed for a 0.1-scale model of NASA Lewis Research Center's proposed altitude wind tunnel
[NASA-TP-2680] p 36 N87-20295
Experimental evaluation of corner turning vanes
[NASA-TM-100143] p 37 N87-28571
- SIDDIQI, S.**
20-GHz phased-array-fed antennas utilizing distributed MMIC modules p 112 A87-34527
- SIDI, AVRAM**
Extrapolation methods for divergent oscillatory infinite integrals that are defined in the sense of summability p 204 A87-35575
Extrapolation methods for vector sequences p 203 A87-53631
- SIEGEL, R.**
Transient radiative cooling of a droplet-filled layer p 135 A87-27712
Effect of flow oscillations on axial energy transport in a porous material p 135 A87-27715

- Influence of oscillation-induced diffusion on heat transfer in a uniformly heated channel p 135 A87-27716
- SIEGEL, ROBERT**
Radiative cooling of a layer with nonuniform velocity - A separable solution p 141 A87-45637
Separation of variables solution for non-linear radiative cooling p 142 A87-48450
- SIGNORELLI, ROBERT A.**
Fiber reinforced superalloys [NASA-TM-89865] p 75 N87-22811
- SILVER, DEAN**
Measurement uncertainty for the Uniform Engine Testing Program conducted at NASA Lewis Research Center [NASA-TM-88943] p 33 N87-28557
- SIMETKOSKY, M.**
Automotive Stirling engine development program [NASA-CR-174972] p 221 N87-20137
Automotive Stirling Engine Development Program [NASA-CR-174873] p 222 N87-30223
- SIMTSES, G. J.**
Non-isothermal elastoviscoplastic snap-through and creep buckling of shallow arches [AIAA PAPER 87-0806] p 176 A87-33605
Analysis of shell-type structures subjected to time-dependent mechanical and thermal loading [NASA-CR-180349] p 183 N87-19756
Nonisothermal elasto-visco-plastic response of shell-type structures p 185 N87-22796
Thermo-elasto-viscoplastic analysis of problems in extension and shear [NASA-CR-181410] p 187 N87-29896
The dynamic aspects of thermo-elasto-viscoplastic snap-through and creep buckling phenomena [NASA-CR-181411] p 187 N87-29897
- SIMTSES, GEORGE J.**
Bounding solutions of geometrically nonlinear viscoelastic problems p 174 A87-20892
Thermodynamically consistent constitutive equations for nonisothermal large-strain, elastoplastic, creep behavior p 175 A87-27945
Solution methods for one-dimensional viscoelastic problems [AIAA PAPER 87-0804] p 176 A87-33604
- SIMON, FREDERICK F.**
Flow visualization study of the effect of injection hole geometry on an inclined jet in crossflow p 155 A87-45842
Jet model for slot film cooling with effect of free-stream and coolant turbulence [NASA-TP-2655] p 146 N87-18034
- SIMON, M. A.**
Low power arcjet life issues [AIAA PAPER 87-1059] p 50 A87-39635
- SIMON, T. W.**
Heat transfer and fluid mechanics measurements in transitional boundary layers on convex-curved surfaces [ASME PAPER 85-MT-60] p 143 A87-48726
- SIMON, WILLIAM E.**
Manned spacecraft electrical power systems p 49 A87-37291
- SIMONEAU, R. J.**
Unsteady heat transfer and direct comparison to steady-state measurements in a rotor-wake experiment p 136 A87-30720
Progress in the prediction of unsteady heat transfer on turbine blades p 149 N87-22769
- SIMONEAU, ROBERT J.**
Effect of a rotor wake on the local heat transfer on the forward half of a circular cylinder p 136 A87-30721
Opportunities and challenges in heat transfer - From the perspective of the government laboratory p 109 A87-48313
A general method for unsteady stagnation region heat transfer and results for model turbine flows [NASA-TM-88903] p 146 N87-17002
- SIMONS, R. N.**
Optically controlled GaAs dual-gate MESFET and permeable base transistors [NASA-TM-88823] p 123 N87-10232
Detection of radio-frequency modulated optical signals by two and three terminal microwave devices [NASA-TM-100196] p 130 N87-29750
- SIMONS, RAINEE N.**
Analysis of optically controlled microwave/millimeter-wave device structures p 121 A87-23680
Microwave performance of an optically controlled AlGaAs/GaAs high electron mobility transistor and GaAs MESFET [NASA-TM-88980] p 125 N87-17993
Propagation characteristics of some novel coplanar waveguide transmission lines on GaAs at MM-wave frequencies [NASA-TM-89839] p 126 N87-20469
- Optically controlled microwave devices and circuits: Emerging applications in space communications systems [NASA-TM-89869] p 127 N87-23900
Microwave characterization and modeling of GaAs/AlGaAs heterojunction bipolar transistors [NASA-TM-100150] p 117 N87-26265
- SIMONYI, P. SUSAN**
Shock structure measured in a transonic fan using laser anemometry p 28 N87-21929
- SITARAM, N.**
Performance studies on an axial flow compressor stage p 138 A87-37208
- SKEBE, STANLEY A.**
Investigation of two-dimensional shock-wave/boundary-layer interactions p 4 A87-39528
- SKOCH, GARY J.**
Performance of two 10-lb/sec centrifugal compressors with different blade and shroud thicknesses operating over a range of Reynolds numbers [AIAA PAPER 87-1745] p 22 A87-50188
Performance of two 10-lb/sec centrifugal compressors with different blade and shroud thicknesses operating over a range of Reynolds numbers [NASA-TM-100115] p 29 N87-23623
- SLABE, M. E.**
Effects of graphitization on the environmental stability of brominated pitch-based fibers [NASA-TM-88899] p 100 N87-12679
- SLABE, MELISSA**
Effects of sequential treatment with fluorine and bromine on graphite fibers [NASA-TM-100106] p 104 N87-24574
- SLABE, MELISSA E.**
Stability of bromine, iodine monochloride, copper (II) chloride, and nickel (II) chloride intercalated pitch-based graphite fibers [NASA-TM-89904] p 103 N87-24563
- SLABY, J. G.**
Overview of the 1986 free-piston Stirling SP-100 activities at the NASA Lewis Research Center p 160 A87-18033
- SLABY, JACK G.**
A 1987 overview of free-piston Stirling technology for space power application [NASA-TM-89832] p 221 N87-21756
- SLINEY, H. E.**
Tribology of selected ceramics at temperatures to 900 C p 94 A87-12954
- SLINEY, HAROLD E.**
Effects of silver and group II fluoride solid lubricant additions to plasma-sprayed chromium carbide coatings for foil gas bearings to 650 C p 95 A87-22336
A new chromium carbide-based tribological coating for use to 900 C with particular reference to the Stirling engine p 95 A87-26112
Composition optimization of self-lubricating chromium-carbide-based composite coatings for use to 760 C p 96 A87-27838
Heat's on to develop high-temperature materials p 85 A87-39897
Effects of atmosphere on the tribological properties of a chromium carbide based coating for use to 760 deg C [NASA-TM-88894] p 101 N87-16140
Mechanical strength and tribological behavior of ion-beam deposited boron nitride films on non-metallic substrates [NASA-TM-89818] p 101 N87-18668
Hardness of CaF₂ and BaF₂ solid lubricants at 25 to 670 deg C [NASA-TM-88979] p 102 N87-18670
Friction and wear of sintered Alpha SiC sliding against IN-718 alloy at 25 to 800 C in atmospheric air at ambient pressure [NASA-TM-87353] p 103 N87-22860
Carbide-fluoride-silver self-lubricating composite [NASA-CASE-LEW-14196-2] p 169 N87-25585
- SLOAT, DAVID**
The 60 GHz IMPATT diode development [NASA-CR-179536] p 218 N87-17515
- SMALLEY, ROBERT R.**
A distributed data acquisition system for aeronautics test facilities [NASA-TM-88961] p 35 N87-16851
- SMETANA, J.**
A design concept for an MMIC microstrip phased array [NASA-TM-88834] p 114 N87-14569
- SMETANA, JERRY**
APS-Workshop on Characterization of MMIC (Monolithic Microwave Integrated Circuit) Devices for Array Antenna [AD-P005398] p 118 N87-28763
A design concept for an MMIC (Monolithic Microwave Integrated Circuit) microstrip phased array [AD-P005404] p 119 N87-28769
- SMIALEK, J. L.**
Corrosion pitting of SiC by molten salts p 76 A87-27165
- SMIALEK, JAMES L.**
Mechanism of strength degradation for hot corrosion of alpha-SiC p 95 A87-21470
Adherent Al₂O₃ scales formed on undoped NiCrAl alloys p 84 A87-32045
Hot corrosion attack and strength degradation of SiC and Si(sub)3N(sub)4 [NASA-TM-89820] p 102 N87-20425
- SMITH, A. F.**
Dynamic response and stability of a composite prop-fan model [NASA-CR-179528] p 28 N87-21956
Analysis and test evaluation of the dynamic response and stability of three advanced turboprop models [NASA-CR-174814] p 32 N87-28555
- SMITH, ARTHUR F.**
Dynamic response of two composite prop-fan models on a nacelle/wing/fuselage half model [NASA-CR-179589] p 18 N87-23615
- SMITH, DAVID A.**
Extrapolation methods for vector sequences p 203 A87-53631
- SMITH, G.**
Automotive Stirling engine development program [NASA-CR-174972] p 221 N87-20137
Automotive Stirling Engine Development Program [NASA-CR-174873] p 222 N87-30223
- SMITH, J. R.**
A universal equation of state for solids p 219 A87-14665
Compressibility of solids p 219 A87-51962
- SMITH, M. M.**
Feasibility analysis of reciprocating magnetic heat pumps [NASA-CR-180262] p 147 N87-19647
- SMITH, R. J.**
Turbulent heat transfer in corrugated-wall channels with and without fins p 134 A87-27709
- SMITH, T. A.**
Experimental thrust performance of a high area-ratio rocket nozzle p 65 N87-23809
- SMITH, T. E.**
Effect of design variables, temperature gradients and speed of life and reliability of a rotating disk [NASA-TM-88883] p 165 N87-13755
- SMITH, TAMARA A.**
Experimental study of low Reynolds number nozzles [AIAA PAPER 87-0992] p 51 A87-41102
Comparison of theoretical and experimental thrust performance of a 1030:1 area ratio rocket nozzle at a chamber pressure of 2413 kN/sq m (350 psia) [AIAA PAPER 87-2069] p 52 A87-45390
Experimental evaluation of heat transfer on a 1030:1 area ratio rocket nozzle [AIAA PAPER 87-2070] p 55 A87-52249
Experimental thrust performance of a high-area-ratio rocket nozzle [NASA-TP-2720] p 60 N87-20381
Experimental study of low Reynolds number nozzles [NASA-TM-89858] p 61 N87-20383
Comparison of theoretical and experimental thrust performance of a 1030:1 area ratio rocket nozzle at a chamber pressure of 2413 kN/m² (350 psia) [NASA-TP-2725] p 66 N87-25423
Experimental evaluation of heat transfer on a 1030:1 area ratio rocket nozzle [NASA-TP-2726] p 67 N87-25424
- SMITH, TODD E.**
SSME single crystal turbine blade dynamics [NASA-CR-179644] p 186 N87-26384
- SMITH, W. W.**
Performance characterization of a low power hydrazine arcjet [AIAA PAPER 87-1057] p 50 A87-39634
- SMITH, WAYNE A.**
Multigrid solution of inviscid transonic flow through rotating blade passages [AIAA PAPER 87-0608] p 3 A87-24992
- SMITHRICK, J. J.**
Effect of impregnation method on cycle life of the nickel electrode p 188 A87-18105
- SMITHRICK, JOHN J.**
Initial performance of advanced designs for IPV nickel-hydrogen cells [NASA-TM-87282] p 192 N87-16445
Effect of storage and LEO cycling on manufacturing technology IPV nickel-hydrogen cells [NASA-TM-89883] p 194 N87-22308
- SMOAK, RICHARD H.**
Structure and tensile strength of LaS(1.4) p 96 A87-38065

SNYDER, AARON

- Numerical simulation of transonic propeller flow using a three-dimensional small disturbance code employing novel helical coordinates
[AIAA PAPER 87-1162] p 5 A87-42107
- Numerical simulation of transonic propeller flow using a 3-dimensional small disturbance code employing novel helical coordinates
[NASA-TM-89826] p 12 N87-19350

SNYDER, C.

- Ignition delay times of cyclopentene oxygen argon mixtures p 76 A87-12602

SNYDER, CHRISTOPHER A.

- A parametric study of a gas-generator air turbo ramjet (ATR)
[AIAA PAPER 86-1681] p 20 A87-41156

SNYDER, PAUL G.

- Variable angle of incidence spectroscopic ellipsometry Application to GaAs-Al(x)Ga(1-x)As multiple heterostructures p 216 A87-20519

SO, R. M. C.

- On self-preserving, variable-density, turbulent free jets p 130 A87-10920
- On similarity solutions for turbulent and heated round jets p 130 A87-10922
- Modelling of jet- and swirl-stabilized reacting flows in axisymmetric combustors p 138 A87-38956

SO, RONALD M. C.

- The near field behavior of turbulent gas jets in a long confinement p 135 A87-28976
- On the modelling of non-reactive and reactive turbulent combustor flows
[NASA-CR-4041] p 28 N87-20996

SOARES, FOLA R.

- Modeling of multi-rotor torsional vibrations in rotating machinery using substructuring p 175 A87-28543

SOEDER, RONALD H.

- Summary of investigations of engine response to distorted inlet conditions p 30 N87-24477

SOH, W. Y.

- Time-marching solution of incompressible Navier-Stokes equations for internal flow p 138 A87-39450

SOKOLOV, V.

- 30 GHz monolithic balanced mixers using an ion-implanted FET-compatible 3-inch GaAs wafer process technology p 121 A87-34525

SOKOLOWSKI, DANIEL E.

- Toward improved durability in advanced combustors and turbines: Progress in the prediction of thermomechanical loads
[NASA-TM-88932] p 32 N87-28551

SOLIN, S. A.

- Microstructure-derived macroscopic residual resistance of brominated graphite fibers p 97 A87-48324

SOLLARS, TERESA A.

- Shuttle/Centaur G-prime composite adapters damage tolerance/repair test program
[AIAA PAPER 87-0792] p 38 A87-33592

SORBELLO, R. M.

- 20-GHz phased-array-fed antennas utilizing distributed MMIC modules p 112 A87-34527

SOTOS, RAYMOND G.

- Combustion of velcro in low gravity
[NASA-TM-88970] p 102 N87-19518

SOVEY, J. S.

- Vacuum chamber pressure effects on thrust measurements of low Reynolds number nozzles p 45 A87-14976

SOVEY, JAMES S.

- 2000-hour cyclic endurance test of a laboratory model multipropellant resistojel
[AIAA PAPER 87-0993] p 52 A87-45725
- Electromagnetic emission experiences using electric propulsion systems - A survey
[AIAA PAPER 87-2028] p 54 A87-50195
- Preliminary performance characterizations of an engineering model multipropellant resistojel for space station application
[AIAA PAPER 87-2120] p 54 A87-50197
- Heat exchanger for electrothermal devices
[NASA-CASE-LEW-14037-1] p 59 N87-16875
- A 2000-hour cyclic endurance test of a laboratory model multipropellant resistojel
[NASA-TM-89854] p 167 N87-22237
- Electromagnetic emission experiences using electric propulsion systems: A survey
[NASA-TM-100120] p 64 N87-22805
- Oxidation protection coatings for polymers
[NASA-CASE-LEW-14072-3] p 103 N87-23736
- Preliminary performance characterizations of an engineering model multipropellant resistojel for space station application
[NASA-TM-100113] p 111 N87-23821
- Space station propulsion system technology
[NASA-TM-100108] p 66 N87-25422

- Water-propellant resistojets for man-tended platforms
[NASA-TM-100110] p 68 N87-26135

SOVIE, RONALD J.

- SP-100 Advanced Technology Program
[NASA-TM-89888] p 194 N87-23027

SPALVINS, T.

- A review of recent advances in solid film lubrication processes: An emerging technology
[NASA-TM-88885] p 110 N87-12708

SPALVINS, TALIVALDIS

- Ion plated gold films: Properties, tribological behavior and performance
[NASA-TM-88977] p 110 N87-17937

SPECK, J. S.

- A study of the microstructure of a rapidly solidified nickel-base superalloy modified with boron
[NASA-CR-179553] p 89 N87-14486

SPENCER, M. G.

- Observation of deep levels in cubic silicon carbide p 122 A87-41089

SPERA, DAVID A.

- Overview of the new ASME Performance Test Code for wind turbines
[ASME PAPER 86-JPGC-PTC-4] p 190 A87-25475

SPITZER, M. B.

- Indium phosphide shallow homojunction solar cells made by metalorganic chemical vapor deposition p 123 A87-50047
- Status of indium phosphide solar cell development at Spire p 197 N87-26440

SPRADLEY, L. W.

- An adaptive finite element strategy for complex flow problems
[AIAA PAPER 87-0557] p 133 A87-22706

SPRING, J.

- Design and dynamic simulation of a fixed pitch 56 kW wind turbine drive train with a continuously variable transmission
[NASA-CR-179543] p 193 N87-17401

SRIDHAR, S.

- WEST-3 wind turbine simulator development. Volume 2: Verification
[NASA-CR-174982] p 191 N87-10531
- WEST-3 wind turbine simulator development. Volume 1: Summary
[NASA-CR-174981] p 192 N87-11348
- WEST-3 wind turbine simulator development
[NASA-CR-174983] p 192 N87-12046

SRINIVASAN, R.

- Effects of multiple rows and noncircular orifices on dilution jet mixing p 138 A87-39805

SRIRAMAMURTHY, A. M.

- Effect of heat treatment on the fracture behaviour of directionally solidified (gamma/gamma-prime)-alpha alloy p 86 A87-47932

STAHARA, S. S.

- Development of a turbomachinery design optimization procedure using a multiple-parameter nonlinear perturbation method
[NASA-CR-3831] p 1 N87-10003

STAHL, M.

- A heater made from graphite composite material for potential deicing application
[NASA-TM-88888] p 17 N87-12559

STAHL, MARK

- A heater made from graphite composite material for potential deicing application
[AIAA PAPER 87-0025] p 17 A87-24905
- Effects of sequential treatment with fluorine and bromine on graphite fibers
[NASA-TM-100106] p 104 N87-24574
- Synthesis, physical and chemical properties, and potential applications of graphite fluoride fibers
[NASA-TM-100156] p 105 N87-26232

STANG, DAVID B.

- Noise reduction for model counterrotation propeller at cruise by reducing aft-propeller diameter
[NASA-TM-88936] p 211 N87-19057
- Cruise noise of the 2/9th scale model of the Large-scale Advanced Propfan (LAP) propeller, SR-7A
[NASA-TM-100175] p 212 N87-28398

STATLER, R. L.

- Radiation and temperature effects in gallium arsenide, indium phosphide and silicon solar cells
[NASA-TM-89870] p 127 N87-22098

STEARN, CARL A.

- Heat's on to develop high-temperature materials p 85 A87-39897

STECURA, STEPHAN

- New ZrO₂-Yb₂O₃ plasma-sprayed coatings for thermal barrier applications p 98 A87-53623

STEDMAN, JAMES K.

- Stress-life interrelationships associated with alkaline fuel cells
[NASA-TM-89881] p 194 N87-22307
- Regenerative fuel cell study for satellites in GEO orbit
[NASA-CR-179609] p 198 N87-27324

STEENKEN, W. G.

- Aerodynamic instability performance of an advanced high-pressure-ratio compression component
[AIAA PAPER 86-1619] p 5 A87-41157
- Dynamic data acquisition, reduction, and analysis for the identification of high-speed compressor component post-stability characteristics
[AIAA PAPER 87-2089] p 162 A87-45398

STEFKO, GEORGE L.

- Wind tunnel performance results of an aeroelastically scaled 2/9 model of the PTA flight test prop-fan
[AIAA PAPER 87-1893] p 8 A87-52251
- Wind tunnel performance results of an aeroelastically scaled 2/9 model of the PTA flight test prop-fan
[NASA-TM-89917] p 14 N87-25294

STEGEMAN, J. D.

- Numerical simulation of the flowfield in a motored two-dimensional Wankel engine p 138 A87-39812
- Numerical simulation of the flow field and fuel sprays in an IC engine
[SAE PAPER 870599] p 143 A87-48751

STEIN, S. E.

- Shock-tube pyrolysis of acetylene - Sensitivity analysis of the reaction mechanism for soot formation p 75 A87-12598

STEINETZ, B. M.

- A constitutive law for finite element contact problems with unclassified friction
[NASA-TM-88838] p 180 N87-12924

STEINETZ, BRUCE M.

- Evaluation of a high-torque backlash-free roller actuator p 165 N87-16336

STEINKE, RONALD J.

- Supersonic through-flow fan design
[AIAA PAPER 87-1746] p 22 A87-48571
- Design of 9.271-pressure-ratio 5-stage core compressor and overall performance for first 3 stages
[NASA-TP-2597] p 27 N87-17699

- Application of advanced computational codes in the design of an experiment for a supersonic throughflow fan rotor
[NASA-TM-88915] p 13 N87-22630

- Supersonic through-flow fan design
[NASA-TM-88908] p 29 N87-22681

STENGER, FRANK

- Multigrid-sinc methods p 205 A87-52865

STEPHENS, J. R.

- Fiber-reinforced superalloy composites provide an added performance edge p 71 A87-12647

STEPHENS, JOSEPH R.

- Heat's on to develop high-temperature materials p 85 A87-39897
- Superalloy resources: Supply and availability
[NASA-TM-89866] p 91 N87-21077

STETSON, K. A.

- Demonstration of laser speckle system on burner liner cyclic rig
[NASA-CR-179509] p 155 N87-10377
- Advanced high temperature static strain sensor development
[NASA-CR-179520] p 158 N87-25552

STEVENS, G. H.

- An assessment of the status and trends in satellite communications 1986-2000: An information document prepared for the Communications Subcommittee of the Space Applications Advisory Committee
[NASA-TM-88867] p 114 N87-13600

STEVENS, N. J.

- Environmentally-induced discharge transient coupling to spacecraft
[NASA-CR-174922] p 43 N87-10946

STEVENS, N. JOHN

- Modeling of environmentally induced transients within satellites
[AIAA PAPER 85-0387] p 42 A87-41611

STEVENSON, S. M.

- An assessment of the status and trends in satellite communications 1986-2000: An information document prepared for the Communications Subcommittee of the Space Applications Advisory Committee
[NASA-TM-88867] p 114 N87-13600

STEVENSON, WARREN H.

- Two component laser velocimeter measurements of turbulence parameters downstream of an axisymmetric sudden expansion p 139 A87-40703
- Turbulence characteristics of an axisymmetric reacting flow
[NASA-CR-180697] p 152 N87-27973

T

- STEWART, W. A.**
Laser anemometry measurements of natural circulation flow in a scale model PWR reactor system
p 154 A87-40750
- STIDHAM, CURT**
Neutral atomic oxygen beam produced by ion charge exchange for Low Earth Orbital (LEO) simulation
p 79 N87-26188
- STINESPRING, C. D.**
Modeling free convective gravitational effects in chemical vapor deposition
[AIAA PAPER 87-0313] p 133 A87-22552
- STOKLOS, JANIS H.**
Aircraft accident report: NASA 712, Convair 990, N712NA, March Air Force Base, California, July 17, 1985, executive summary
[NASA-TM-87356-VOL-1] p 16 N87-21878
Aircraft accident report: NASA 712, Convair 990, N712NA, March Air Force Base, California, July 17, 1985, facts and analysis
[NASA-TM-87356-VOL-2] p 16 N87-21879
- STOLOFF, N. S.**
Effects of temperature and hold times on low cycle fatigue of Astroloy
p 85 A87-38541
- STONE, JAMES R.**
The NASA/USAF arcjet research and technology program
[AIAA PAPER 87-1946] p 54 A87-50192
The NASA/USAF arcjet research and technology program
[NASA-TM-100112] p 66 N87-24525
- STONER, W. A.**
A design study of hydrazine and biowaste resistojets
[NASA-CR-179510] p 57 N87-14425
- STOTTS, ROBERT**
Automotive Stirling engine system component review
[SAE PAPER 870102] p 163 A87-48781
- STOVER, JOHN**
NASA Lewis Research Center Futuring Workshop
[NASA-CR-179577] p 206 N87-27475
- STRAZISAR, A. J.**
Rotor wake characteristics of a transonic axial-flow fan
p 2 A87-20886
An LDA investigation of three-dimensional normal shock-boundary layer interactions in a corner
[AIAA PAPER 87-1369] p 6 A87-44938
Measurements of the unsteady flow field within the stator row of a transonic axial-flow fan. 1: Measurement and analysis technique
[NASA-TM-88945] p 10 N87-16789
Measurements of the unsteady flow field within the stator row of a transonic axial-flow fan. Part 2: Results and discussion
[NASA-TM-88946] p 10 N87-16790
- STRAZISAR, ANTHONY J.**
Laser fringe anemometry for aero engine components
p 110 N87-21176
Shock structure measured in a transonic fan using laser anemometry
p 28 N87-21929
- STROEBEL, THOMAS**
Design of an advanced wood composite rotor and development of wood composite blade technology
[NASA-CR-174713] p 73 N87-17861
- STROUBOULIS, T.**
An adaptive finite element strategy for complex flow problems
[AIAA PAPER 87-0557] p 133 A87-22706
Adaptive finite element methods for compressible flow problems
p 4 A87-38496
Recent advances in error estimation and adaptive improvement of finite element calculations
p 204 A87-41239
- STUART, THOMAS A.**
A study of Schwarz converters for nuclear powered spacecraft
[NASA-TM-89911] p 128 N87-23903
- STUBSTAD, JOHN M.**
Bounding solutions of geometrically nonlinear viscoelastic problems
p 174 A87-20892
Solution methods for one-dimensional viscoelastic problems
[AIAA PAPER 87-0804] p 176 A87-33604
- STUDER, A.**
Gravitational macrosegregation in binary Pb-Sn alloy ingots
[NASA-TM-89885] p 109 N87-24579
- STUPICA, J. W.**
Cell performance and defect behavior in proton-irradiated lithium-counterdoped n(+)-p silicon solar cells
p 216 A87-14222
- STURGIS, J. D.**
Optimization of spherical facets for parabolic solar concentrators
p 213 A87-18173

- SUBRAHMANYAM, K. B.**
Nonlinear vibration and stability of rotating, pretwisted, precone blades including Coriolis effects
p 178 A87-39896
Influence of third-degree geometric nonlinearities on the vibration and stability of pretwisted, precone, rotating blades
p 21 A87-46228
- SUDER, K. L.**
Measurements of the unsteady flow field within the stator row of a transonic axial-flow fan. 1: Measurement and analysis technique
[NASA-TM-88945] p 10 N87-16789
Measurements of the unsteady flow field within the stator row of a transonic axial-flow fan. Part 2: Results and discussion
[NASA-TM-88946] p 10 N87-16790
- SUDER, KENNETH L.**
Design and performance of controlled-diffusion stator compared with original double-circular-arc stator
[NASA-TM-100141] p 31 N87-26910
- SULLIVAN, J. P.**
Measurement of a counter rotation propeller flowfield using a Laser Doppler Velocimeter
[AIAA PAPER 87-0008] p 3 A87-24901
- SULLIVAN, R. L.**
Utility interconnection issues for wind power generation
[NASA-CR-175056] p 193 N87-17400
- SULLIVAN, TIMOTHY L.**
The effect of nonlinearities on the dynamic response of a large Shuttle payload
[AIAA PAPER 87-0857] p 40 A87-33697
The effect of nonlinearities on the dynamic response of a large shuttle payload
[NASA-TM-88941] p 181 N87-18112
- SUNDBERG, GALE R.**
Space Station 20-kHz power management and distribution system
p 49 A87-36913
- SURPRENANT, V. A.**
The role of near-surface plastic deformation in the wear of lamellar solids
p 162 A87-48500
- SUTTER, JAMES K.**
Simulation of fluid flows during growth of organic crystals in microgravity
[NASA-TM-88921] p 108 N87-16167
- SWAFFORD, T. W.**
Three-dimensional unsteady Euler solutions for propfans and counter-rotating propfans in transonic flow
[AIAA PAPER 87-1197] p 5 A87-42314
- SWANSON, G. A.**
Life prediction and constitutive models for engine hot section anisotropic materials
[NASA-CR-179594] p 29 N87-23622
- SWARTZ, BLAIR**
Some plane curvature approximations
p 204 A87-49821
- SWARTZ, C. K.**
Cell performance and defect behavior in proton-irradiated lithium-counterdoped n(+)-p silicon solar cells
p 216 A87-14222
Performance of GaAs and silicon concentrator cells under 1 MeV electron irradiation
p 189 A87-19871
Potential for use of InP solar cells in the space radiation environment
p 120 A87-19996
Radiation and temperature effects in gallium arsenide, indium phosphide and silicon solar cells
[NASA-TM-89870] p 127 N87-22098
Comparative performance of diffused junction indium phosphide solar cells
p 197 N87-26441
Radiation damage in proton irradiated indium phosphide solar cells
p 199 N87-29018
- SWETTE, LARRY**
Oxygen electrodes for rechargeable alkaline fuel cells
p 199 N87-29940
- SWITZER, COLLEEN A.**
Coaxial tube array space transmission line characterization
[NASA-TM-89864] p 62 N87-22003
- SYED, A. A.**
Turbofan aft duct suppressor study. Contractor's data report of mode probe signal data
[NASA-CR-175067] p 34 N87-29538
Turbofan aft duct suppressor study
[NASA-CR-175067] p 34 N87-29539
- SZALAY, A.**
Quasars as indicators of galactic ages
p 223 A87-26927
- SZETELA, E. J.**
Long-term deposit formation in aviation turbine fuel at elevated temperature
p 106 A87-14986

- T'EN, JAMES S.**
Size and shape of solid fuel diffusion flames in very slow speed flows
[AIAA PAPER 87-2030] p 78 A87-52248
- TABATA, W. K.**
Automotive Stirling engine development program: A success
[NASA-TM-89892] p 222 N87-22562
- TACINA, R. R.**
Conceptual design and integration of a Space Station resistojet propulsion assembly
[AIAA PAPER 87-1860] p 52 A87-45256
- TACINA, ROBERT R.**
Two-phase flow
p 147 N87-20272
Conceptual design and integration of a space station resistojet propulsion assembly
[NASA-TM-89847] p 60 N87-20378
Space station propulsion system technology
[NASA-TM-100108] p 66 N87-25422
- TAFLOVE, A.**
The finite-difference time-domain (FD-TD) method for electromagnetic scattering and interaction problems
p 113 A87-51403
- TAFLOVE, ALLEN**
A new formulation of electromagnetic wave scattering using an on-surface radiation boundary condition approach
p 112 A87-32829
- TAGHAVI, R.**
Controlled excitation of a cold turbulent swirling free jet
[NASA-TM-100173] p 152 N87-27977
- TAM, C. K. W.**
On broadband shock associated noise of supersonic jets
p 208 A87-11768
- TAM, L. T.**
Evaluation of seals for high-performance cryogenic turbomachines
[NASA-TM-88919] p 146 N87-15442
- TAN, C. S.**
Calculations of inlet distortion induced compressor flowfield instability
p 30 N87-24470
- TAN, H. Q.**
On the symbolic manipulation and code generation for elasto-plastic material matrices
p 201 A87-18499
- TAYLOR, ARTHUR**
Two- and three-dimensional viscous computations of a hypersonic inlet flow
[AIAA PAPER 87-0283] p 4 A87-31106
Two- and three-dimensional viscous computations of a hypersonic inlet flow
[NASA-TM-88923] p 146 N87-15441
- TAYLOR, J. E.**
On optimal design for the blade-root/hub interface in jet engines
p 24 N87-11769
- TAYLOR, J. H.**
Dynamic data acquisition, reduction, and analysis for the identification of high-speed compressor component post-stability characteristics
[AIAA PAPER 87-2089] p 162 A87-45398
- TENNYSON, R. C.**
Solar concentrator materials development
p 213 A87-18171
- TEREN, FRED**
Space station electric power system requirements and design
[NASA-TM-89889] p 62 N87-22001
- TEW, R. C., JR.**
Progress of Stirling cycle analysis and loss mechanism characterization
[NASA-TM-88891] p 220 N87-13359
- TEWARI, S. N.**
Mechanical property anisotropy in superalloy El-929 directionally solidified by an exothermic technique
p 81 A87-11389
Dendritic microstructure in argon atomized superalloy powders
p 83 A87-24119
A critical examination of the dendrite growth models. Comparison of theory with experimental data
p 83 A87-25048
Fault structures in rapidly quenched Ni-Mo binary alloys
p 83 A87-32035
Cellular-dendritic transition in directionally solidified binary alloys
p 84 A87-32046
Effect of heat treatment on the fracture behaviour of directionally solidified (gamma/gamma-prime)-alpha alloy
p 86 A87-47932
Microstructures in rapidly solidified Ni-Mo alloys
p 87 A87-51636
Cellular microstructure of chill block melt spun Ni-Mo alloys
p 87 A87-54300
Primary arm spacing in chill block melt spun Ni-Mo alloys
[NASA-TM-88887] p 88 N87-11875

- THALLER, L. H.**
A flooded-starved design for nickel-cadmium cells
p 123 N87-11086
- THALLER, LAWRENCE H.**
Stress-life interrelationships associated with alkaline fuel cells
[NASA-TM-89881] p 194 N87-22307
A prediction model of the depth-of-discharge effect on the cycle life of a storage cell
[NASA-TM-89915] p 194 N87-22311
- THIEME, L. G.**
Testing of a variable-stroke Stirling engine
p 160 A87-18036
- THOMAS, CHARLES**
NASA Lewis Research Center Futuring Workshop
[NASA-CR-179577] p 206 N87-27475
- THOMAS, R. L.**
Power is the keystone
p 45 A87-16929
- THOMPSON, H. DOYLE**
Two component laser velocimeter measurements of turbulence parameters downstream of an axisymmetric sudden expansion
p 139 A87-40703
Turbulence characteristics of an axisymmetric reacting flow
[NASA-CR-180697] p 152 N87-27973
- THOMPSON, R. L.**
High temperature stress-strain analysis
p 179 N87-11209
- TIDMAN, D. A.**
Experiments on a repetitively pulsed electrothermal thruster
[AIAA PAPER 87-1043] p 50 A87-38017
Investigation of a repetitive pulsed electrothermal thruster
[NASA-CR-179464] p 59 N87-16878
- TIEN, JOHN K.**
Fiber reinforced superalloys
[NASA-TM-89865] p 75 N87-22811
- TITRAN, R. H.**
Effect of 15 MPa hydrogen on creep-rupture properties of iron-base superalloys
p 86 A87-49558
The effect of electron beam welding on the creep rupture properties of a Nb-Zr-C alloy
[NASA-TM-88892] p 88 N87-13513
Creep behavior of niobium alloy PWC-11
[NASA-TM-89834] p 91 N87-20405
Long-time creep behavior of Nb-1Zr alloy containing carbon
[NASA-TM-100142] p 92 N87-26217
- TITRAN, ROBERT H.**
Creep-rupture behavior of a developmental cast-iron-base alloy for use up to 800 deg C
[NASA-TM-100167] p 93 N87-28641
- TOMAZIC, WILLIAM A.**
Effect of water on hydrogen permeability
[NASA-TM-88898] p 221 N87-16664
- TOMPKINS, STEPHEN S.**
Thermal expansion behavior of graphite/glass and graphite/magnesium
p 72 A87-38615
- TORRES, FELIX J.**
Use of a liquid-crystal, heater-element composite for quantitative, high-resolution heat transfer coefficients on a turbine airfoil, including turbulence and surface roughness effects
[NASA-TM-87355] p 158 N87-22181
- TORREY, MARTIN D.**
Numerical modeling of on-orbit propellant motion resulting from an impulsive acceleration
[AIAA PAPER 87-1766] p 40 A87-48573
Numerical modeling of on-orbit propellant motion resulting from an impulsive acceleration
[NASA-TM-89873] p 41 N87-22757
- TOTH, J.**
Heat pipe cooled rocket engines
[AIAA PAPER 86-1567] p 48 A87-21516
- TOWNE, CHARLES E.**
Viscous analyses for flow through subsonic and supersonic intakes
[NASA-TM-88831] p 9 N87-15173
Viscous analyses for flow through subsonic and supersonic intakes
p 30 N87-24469
- TOWNSEND, DENNIS P.**
Common problems and pitfalls in gear design
[NASA-TM-88858] p 165 N87-17033
Experimental and analytical evaluation of dynamic load and vibration of a 2240-kW (300-hp) rotorcraft transmission
[NASA-TM-88975] p 167 N87-20556
Profile modification to minimize spur gear dynamic loading
[NASA-TM-89901] p 170 N87-28918
- TRAN, T.**
A high quality image compression scheme for real-time applications
p 111 A87-30801
- TRIBBLE, A.**
Measurements of plasma density and turbulence near the shuttle orbiter
[NASA-CR-180102] p 215 N87-16614
- TSAI, TOMMY M.**
Duct flows with swirl
[AIAA PAPER 87-0247] p 132 A87-22509
- TSAY, C.-B. P.**
New generation methods for spur, helical, and spiral-bevel gears
p 164 A87-53420
New generation methods for spur, helical, and spiral-bevel gears
[NASA-TM-88862] p 165 N87-15466
- TSAY, CHUNG-BIAU**
Helical gears with circular arc teeth: Generation, geometry, precision and adjustment to errors, computer aided simulation of conditions of meshing and bearing contact
[NASA-CR-4089] p 170 N87-29846
- TSUNG, W.-J.**
New generation methods for spur, helical, and spiral-bevel gears
p 164 A87-53420
New generation methods for spur, helical, and spiral-bevel gears
[NASA-TM-88862] p 165 N87-15466
- TSUNG, WEI-JIUNG**
Generation of spiral bevel gears with conjugate tooth surfaces and tooth contact analysis
[NASA-CR-4088] p 169 N87-26356
- TURAN, A.**
Evaluation of new techniques for the calculation of internal recirculating flows
[AIAA PAPER 87-0059] p 131 A87-22387
- TURK, M. A.**
Advanced technology payoffs for future small propulsion systems
p 21 A87-47081
- TURKEL, ELI**
Comparison of three explicit multigrid methods for the Euler and Navier-Stokes equations
[AIAA PAPER 87-0602] p 137 A87-34725
Comparison of three explicit multigrid methods for the Euler and Navier-Stokes equations
[NASA-TM-88878] p 1 N87-16784
- TURNBERG, J. E.**
Static tests of the propulsion system
[AIAA PAPER 87-1728] p 23 A87-52245
Effect of angular inflow on the vibratory response of a counter-rotating propeller
[NASA-CR-174819] p 8 N87-10840
Unstalled flutter stability predictions and comparisons to test data for a composite prop-fan model
[NASA-CR-179512] p 28 N87-21955
Analysis and test evaluation of the dynamic response and stability of three advanced turbo-prop models
[NASA-CR-174814] p 32 N87-28555
- TURNER, A.**
The use of satellites in non-geostationary orbits for unloading geostationary communication satellite traffic peaks. Volume 1: Executive summary
[NASA-CR-179597-VOL-1] p 117 N87-21212
The use of satellites in non-geostationary orbits for unloading geostationary communication satellite traffic peaks. Volume 2: Technical report
[NASA-CR-179597-VOL-2] p 117 N87-21213
- TURNER, E. R.**
Turbine airfoil gas side heat transfer
p 144 N87-11219
- TURNER, MICHAEL S.**
The large-scale peculiar velocity field in flat models of the universe
p 223 A87-40651
- U**
- UHRAN, M. L.**
Equipment concept design and development plans for microgravity science and applications research on space station: Combustion tunnel, laser diagnostic system, advanced modular furnace, integrated electronics laboratory
[NASA-CR-179535] p 108 N87-15320
- ULBRICHT, T. E.**
The noncavitating performance and life of a small vane-type positive displacement pump in liquid hydrogen
[AIAA PAPER 86-1438] p 46 A87-17994
- UMASHANKAR, K. R.**
The finite-difference time-domain (FD-TD) method for electromagnetic scattering and interaction problems
p 113 A87-51403
- UMASHANKAR, KORADAR R.**
A new formulation of electromagnetic wave scattering using an on-surface radiation boundary condition approach
p 112 A87-32829
- UMSTATTER, HOLLY L.**
Visualization of flows in a motored rotary combustion engine using holographic interferometry
[AIAA PAPER 86-1557] p 19 A87-21514
- UNKRICH, DAVID B.**
Self-regulating heater application to Shuttle/Centaur hydrazine fuel line thermal control
[AIAA PAPER 87-1570] p 43 A87-43081
- V**
- VAGNETTI, F.**
Quasars as indicators of galactic ages
p 223 A87-26927
- VALISETTY, R. R.**
Strain energy release rates of composite interlaminar end-notch and mixed-mode fracture: A sublimate/ply level analysis and a computer code
[NASA-TM-89827] p 74 N87-20389
- VAN DIEP, G. PHAM**
The design and performance of a multi-stream droplet generator for the liquid droplet radiator
[AIAA PAPER 87-1538] p 140 A87-44842
- VAN DOORMAAL, J. P.**
Evaluation of new techniques for the calculation of internal recirculating flows
[AIAA PAPER 87-0059] p 131 A87-22387
- VANCO, M. R.**
An overview of the small engine component technology (SECT) studies
[AIAA PAPER 86-1542] p 19 A87-17993
- VANDEBRINK, D. J.**
Optimization and analysis of gas turbine engine blades
[AIAA PAPER 87-0827] p 201 A87-33614
- VANDINE, LESLIE**
Regenerative fuel cell study for satellites in GEO orbit
[NASA-TM-89914] p 194 N87-22310
- VANDINE, LESLIE L.**
Regenerative fuel cell study for satellites in GEO orbit
[NASA-CR-179609] p 198 N87-27324
- VANNUCCI, RAYMOND D.**
Heat's on to develop high-temperature materials
p 85 A87-39897
Styrene-terminated polysulfone oligomers as matrix material for graphite reinforced composites - An initial study
p 98 A87-49370
Mechanical and electrical properties of graphite fiber-epoxy composites made from pristine and bromine intercalated fibers
p 73 A87-49799
PMR polyimide compositions for improved performance at 371 deg C
[NASA-TM-88942] p 73 N87-16071
Styrene-terminated polysulfone oligomers as matrix material for graphite reinforced composites: An initial study
[NASA-TM-89846] p 74 N87-21043
- VANOVERBECK, THOMAS**
Multispecies CARS measurements in turbulent combustion
p 79 N87-23808
- VANSTONE, R. H.**
Elevated temperature crack growth
[NASA-CR-179601] p 184 N87-22267
- VARNER, M. O.**
Large perturbation flow field analysis and simulation for supersonic inlets
[NASA-CR-174676] p 8 N87-10835
- VARY, ALEX**
The acousto-ultrasonic approach
[NASA-TM-89843] p 172 N87-20562
Application of scanning acoustic microscopy to advanced structural ceramics
[NASA-TM-89929] p 172 N87-23987
Ultrasonic NDE of structural ceramics for power and propulsion systems
[NASA-TM-100147] p 173 N87-26362
- VEDULA, K.**
Analysis of NiAlTa precipitates in beta-NiAl + 2 at. pct Ta alloy
p 84 A87-34888
- VENKATARAMANI, K.**
Aviation fuel property effects on altitude reflight
[NASA-CR-179582] p 107 N87-24578
- VENKATESH, SRINIVASAN**
Materials characterization of phosphoric acid fuel cell system
p 76 A87-23241
- VERNON, S. M.**
Indium phosphide shallow homojunction solar cells made by metalorganic chemical vapor deposition
p 123 A87-50047
Status of indium phosphide solar cell development at Spire
p 197 N87-26440
- VERZWYVELT, S. A.**
Cycle life of nickel-hydrogen cells. II - Accelerated cycle life test
p 46 A87-18104
KOH concentration effect on cycle life of nickel-hydrogen cells
p 199 N87-29920

VINET, P.

- A universal equation of state for solids
p 219 A87-14665
- Compressibility of solids
p 219 A87-51962
- VIRSHUP, G. F.**
High-efficiency GaAs solar concentrator cells for space and terrestrial applications
p 188 A87-18073
- High-efficiency GaAs concentrator space cells
p 196 N87-26417

VISWANATHAN, R.

- Modeling of environmentally induced transients within satellites
[AIAA PAPER 85-0387]
p 42 A87-41611
- Environmentally-induced discharge transient coupling to spacecraft
[NASA-CR-174922]
p 43 N87-10946

VITTORIO, NICOLA

- The large-scale peculiar velocity field in flat models of the universe
p 223 A87-40651

VLCEK, B. L.

- Evaluation of seals for high-performance cryogenic turbomachines
[NASA-TM-88919]
p 146 N87-15442

VOGT, P. G.

- Free-jet acoustic investigation of high-radius-ratio conical plug nozzles
[NASA-CR-3818]
p 210 N87-10753

VON GLAHN, UWE H.

- Two-dimensional nozzle plume characteristics
[AIAA PAPER 87-2111]
p 6 A87-45413
- Secondary stream and excitation effects on two-dimensional nozzle plume characteristics
[AIAA PAPER 87-2112]
p 6 A87-45414

VONGLAHN, UWE H.

- Secondary stream and excitation effects on two-dimensional nozzle plume characteristics
[NASA-TM-89813]
p 12 N87-18539
- Two-dimensional nozzle plume characteristics
[NASA-TM-89812]
p 12 N87-18540

W

WAGENKNECHT, C. D.

- Aerodynamic performance investigation of advanced mechanical suppressor and ejector nozzle concepts for jet noise reduction
[NASA-CR-174860]
p 33 N87-29534

WAGNER, LEE

- Space station power semiconductor package
[NASA-CR-180829]
p 129 N87-28825

WAGNER, M.

- Proposal for superstructure based high efficiency photovoltaics
p 120 A87-19104

WAGNER, MICHAEL BRODERICK

- Computer modelling of aluminum-gallium arsenide/gallium arsenide multilayer photovoltaics
[NASA-CR-181418]
p 200 N87-29957

WAGNER, R. C.

- Effects of silver and group II fluoride solid lubricant additions to plasma-sprayed chromium carbide coatings for foil gas bearings to 650 C
p 95 A87-22336

WALKER, E. D.

- Black-and-white photographic chemistry: A reference
[NASA-TM-87296]
p 70 N87-10177

WALKER, ERNIE D.

- Bonding Lexan and sapphire to form high-pressure, flame-resistant window
[NASA-TM-100188]
p 159 N87-28880

WALKER, K. P.

- Life prediction and constitutive models for engine hot section anisotropic materials
[NASA-CR-179594]
p 29 N87-23622

WALLACE, J. F.

- Gravitational macrosegregation in binary Pb-Sn alloy ingots
[NASA-TM-89885]
p 109 N87-24579

WALOWIT, J. A.

- EHD analysis of and experiments on pumping Leningrader seals
[NASA-CR-179570]
p 168 N87-22246

WALSH, FRASER

- Organometallic catalysts for primary phosphoric acid fuel cells
[NASA-CR-179490]
p 193 N87-19804

WALTON, ERIC K.

- Engineering calculations for communications satellite systems planning
[NASA-CR-181112]
p 117 N87-24605

WANG, C. L.

- Develop and test fuel cell powered on site integrated total energy systems. Phase 3: Full-scale power plant development
[NASA-CR-175118]
p 191 N87-11344

- Develop and test fuel cell powered on-site integrated total energy systems. Phase 3: Full-scale power plant development
[NASA-CR-175117]
p 191 N87-11346
- Develop and test fuel cell powered on site integrated total energy systems: Phase 3: Full-scale power plant development
[NASA-CR-175075]
p 191 N87-11347

WANG, CHI R.

- Turbulence modeling and surface heat transfer in a stagnation flow region
[NASA-TM-100132]
p 151 N87-26302

- Application of turbulence modeling to predict surface heat transfer in stagnation flow region of circular cylinder
[NASA-TP-2758]
p 151 N87-27161

WANG, COU-WAY

- Optimization of orbital assignment and specification of service areas in satellite communications
[NASA-CR-181273]
p 118 N87-27882

WANG, J.

- The radiation impedance of an electrodynamic tether with end connectors
p 42 A87-42585

WANG, L.

- Gravitational macrosegregation in binary Pb-Sn alloy ingots
[NASA-TM-89885]
p 109 N87-24579

WANG, P. S.

- On the symbolic manipulation and code generation for elastoplastic material matrices
p 201 A87-18499

WANG, SHING-KUO

- A 30-GHz monolithic receiver
p 121 A87-23953

WANG, T.

- Heat transfer and fluid mechanics measurements in transitional boundary layers on convex-curved surfaces
[ASME PAPER 85-MT-60]
p 143 A87-48726

WAPPES, LORAN J.

- Resonant AC power system proof-of-concept test program
[NASA-CR-175069-VOL-1]
p 129 N87-29738

WARD, DONALD L.

- Triptycene - A D(3h) C(62) hydrocarbon with three U-shaped cavities
p 69 A87-53656

WARD, JAMES

- Adaptive arrays for weak interfering signals: An experimental system
[NASA-CR-181181]
p 119 N87-28814

WARFIELD, MATTHEW J.

- Computation of rotating turbulent flow with an algebraic Reynolds stress model
p 140 A87-43384

WARNER, J. D.

- Ellipsometric and optical study of amorphous hydrogenated carbon films
p 216 A87-23967

WARNER, JOSEPH D.

- Rapid thermal annealing of Amorphous Hydrogenated Carbon (a-C:H) films
[NASA-TM-89859]
p 218 N87-20821

- AlGaAs growth by OMCVD using an excimer laser
[NASA-TM-88937]
p 218 N87-23304

- Boron nitride: Composition, optical properties and mechanical behavior
[NASA-TM-89849]
p 218 N87-25017

WARSHAY, M.

- Status of commercial phosphoric acid fuel cell power plant system development
p 190 A87-33777

WARSHAY, MARVIN

- Status of commercial fuel cell powerplant system development
[NASA-TM-89896]
p 148 N87-22171

WASEL, ROBERT A.

- The NASA Electric Propulsion Program
[AIAA PAPER 87-1098]
p 53 A87-45795

- The NASA Electric Propulsion Program
[NASA-TM-89856]
p 61 N87-21037

WATKINS, W. B.

- Further development of the dynamic gas temperature measurement system. Volume 1: Technical efforts
[NASA-CR-179513-VOL-1]
p 157 N87-19686

WAWRZYNEK, P. A.

- Interactive graphics and analysis accuracy
p 202 A87-45900

WEAR, J. D.

- Flame radiation
p 78 N87-11204

WEAR, W. O.

- Equipment concept design and development plans for microgravity science and applications research on space station: Combustion tunnel, laser diagnostic system, advanced modular furnace, integrated electronics laboratory
[NASA-CR-179535]
p 108 N87-15320

WEBB, BRENT J.

- PEGASUS: A multi-megawatt nuclear electric propulsion system
p 59 N87-17787

WEDEVEN, L. D.

- Solid lubrication design methodology, phase 2
[NASA-CR-175114]
p 221 N87-18470

WEI, W.

- Friction and wear behaviour of ion beam modified ceramics
p 97 A87-47958
- Characterization of ion beam modified ceramic wear surfaces using Auger electron spectroscopy
p 98 A87-51304

WEIKLE, D. H.

- Laser anemometers of hot-section applications
p 155 N87-11187

WEINBERG, B. C.

- Calculation of two- and three-dimensional transonic cascade flow field using the Navier-Stokes equations
p 144 N87-11220

- Turbine vane external heat transfer. Volume 2. Numerical solutions of the Navier-Stokes equations for two- and three-dimensional turbine cascades with heat transfer
[NASA-CR-174828]
p 145 N87-13661

WEINBERG, I.

- Cell performance and defect behavior in proton-irradiated lithium-counterdoped n(+)-p silicon solar cells
p 216 A87-14222

- Indium phosphide solar cells - Status and prospects for use in space
p 188 A87-18071

- Potential for use of InP solar cells in the space radiation environment
p 120 A87-19996

- Radiation and temperature effects in gallium arsenide, indium phosphide and silicon solar cells
[NASA-TM-89870]
p 127 N87-22098

- Comparative performance of diffused junction indium phosphide solar cells
p 197 N87-26441

- Radiation damage in proton irradiated indium phosphide solar cells
p 199 N87-29018

WEINBERG, IRVING

- Recent developments in indium phosphide space solar cell research
[NASA-TM-100139]
p 68 N87-26141

- Near-optimum design of the InP homojunction solar cell
p 197 N87-26443

WEIZER, V. G.

- A 25.5 percent AM0 gallium arsenide grating solar cell
p 189 A87-19840

- Results of 1 MeV proton irradiation of front and back surfaces of silicon solar cells
p 197 N87-26435

WEIZER, VICTOR G.

- The effect of internal stresses on solar cell efficiency
p 196 N87-26430

WELSCH, G.

- The characteristics of gamma-prime dislocation pairs in a nickel-base superalloy
p 85 A87-46932

WELSCH, G. E.

- The cyclic stress-strain behavior of PWA 1480 at 650 deg C
[NASA-TM-87311]
p 89 N87-14483

WENTZ, W. H., JR.

- Performance and aerodynamic braking of a horizontal-axis wind turbine from small-scale wind tunnel tests
[NASA-CR-180812]
p 198 N87-27327

WERNET, MARK P.

- Four spot laser anemometer and optical access techniques for turbine applications
[NASA-TM-88972]
p 156 N87-18057

- Laser anemometry techniques for turbine applications
[NASA-TM-88953]
p 158 N87-22959

WERTH, J.

- Develop and test fuel cell powered on site integrated total energy systems. Phase 3: Full-scale power plant development
[NASA-CR-175118]
p 191 N87-11344

- Develop and test fuel cell powered on-site integrated total energy systems. Phase 3: Full-scale power plant development
[NASA-CR-175117]
p 191 N87-11346

- Develop and test fuel cell powered on site integrated total energy systems: Phase 3: Full-scale power plant development
[NASA-CR-175075]
p 191 N87-11347

WERTHEN, J. G.

- High-efficiency GaAs solar concentrator cells for space and terrestrial applications
p 188 A87-18073

- High-efficiency GaAs concentrator space cells
p 196 N87-26417

WEST, H.

- A model propulsion simulator for evaluating counter rotating blade characteristics
[SAE PAPER 861715]
p 20 A87-32607

WESTFALL, L. J.

- Fiber-reinforced superalloy composites provide an added performance edge
p 71 A87-12647

WEYANDT, C.

- Communications satellite systems operations with the space station. Volume 1: Executive summary
[NASA-CR-179526]
p 206 N87-17472

- Communications satellite systems operations with the space station, volume 2
[NASA-CR-179527]
p 206 N87-17473

- The use of satellites in non-geostationary orbits for unloading geostationary communication satellite traffic peaks. Volume 1: Executive summary
[NASA-CR-179597-VOL-1] p 117 N87-21212
- The use of satellites in non-geostationary orbits for unloading geostationary communication satellite traffic peaks. Volume 2: Technical report
[NASA-CR-179597-VOL-2] p 117 N87-21213
- WHALEN, M. V.**
Vacuum chamber pressure effects on thrust measurements of low Reynolds number nozzles
p 45 A87-14976
- WHALEN, MARGARET V.**
In-situ analysis of hydrazine decomposition products
[AIAA PAPER 87-2122] p 54 A87-50198
In-situ analysis of hydrazine decomposition products
[NASA-TM-89916] p 65 N87-23693
Low Reynolds number nozzle flow study
[NASA-TM-100130] p 67 N87-25426
- WHEELER, DONALD R.**
Preliminary study of niobium alloy contamination by transport through helium
[NASA-TM-88952] p 90 N87-17884
- WHEELER, R. L., III**
Thermal shaft effects on load-carrying capacity of a fully coupled, variable-properties cryogenic journal bearing
[ASLE PREPRINT 86-TC-6B-1] p 160 A87-19502
A fully coupled variable properties thermohydraulic model for a cryogenic hydrostatic journal bearing
[ASME PAPER 86-TRIB-55] p 161 A87-19536
Finite difference solution for a generalized Reynolds equation with homogeneous two-phase flow
p 141 A87-45851
- WHELAN, J. A.**
Develop and test fuel cell powered on site integrated total energy systems. Phase 3: Full-scale power plant development
[NASA-CR-175118] p 191 N87-11344
Develop and test fuel cell powered on-site integrated total energy systems. Phase 3: Full-scale power plant development
[NASA-CR-175117] p 191 N87-11346
Develop and test fuel cell powered on site integrated total energy systems. Phase 3: Full-scale power plant development
[NASA-CR-175075] p 191 N87-11347
- WHIPPLE, E. C.**
The dynamic behavior of plasmas observed near geosynchronous orbit
p 200 A87-31322
- WHITE, ALAN**
The design and performance of a multi-stream droplet generator for the liquid droplet radiator
[AIAA PAPER 87-1538] p 140 A87-44842
- WHITE, C.**
Transition mixing study
[NASA-CR-175062] p 27 N87-16830
- WHITE, C. D.**
Effects of multiple rows and noncircular orifices on dilution jet mixing
p 138 A87-39805
- WHITE, G.**
The 3600 hp split-torque helicopter transmission
[NASA-CR-174932] p 25 N87-11788
- WHITE, J. E.**
Optimization of spherical facets for parabolic solar concentrators
p 213 A87-18173
- WHITE, K. ALAN, III**
Liquid droplet radiator development status
[AIAA PAPER 87-1537] p 42 A87-43059
Liquid sheet radiator
[NASA-TM-89841] p 147 N87-18786
Liquid droplet radiator development status
[NASA-TM-89852] p 43 N87-20353
- WHITE, K. ALLAN, III**
Liquid sheet radiator
[AIAA PAPER 87-1525] p 140 A87-43048
- WHITEHAIR, S.**
Microwave electrothermal thruster performance in helium gas
p 49 A87-31281
- WHITEHAIR, STANLEY**
A review of research and development on the microwave-plasma electrothermal rocket
[AIAA PAPER 87-1011] p 49 A87-38008
- WHITELY, STAN**
The 60 GHz IMPATT diode development
[NASA-CR-179536] p 218 N87-17515
- WHITFIELD, D. L.**
Three-dimensional unsteady Euler solutions for propfans and counter-rotating propfans in transonic flow
[AIAA PAPER 87-1197] p 5 A87-42314
- WHITMAN, PAMELA K.**
Colloidal characterization of ultrafine silicon carbide and silicon nitride powders
p 95 A87-19625
- WHITTENBERGER, J. DANIEL**
Effect of composition and grain size on slow plastic flow properties of NiAl between 1200 and 1400 K
p 84 A87-36251
- Structure and tensile strength of LaS(1.4)
p 96 A87-38065
- Fluoride salts and container materials for thermal energy storage applications in the temperature range 973 to 1400 K
[NASA-TM-89913] p 195 N87-24026
- WHYTE, WAYNE A.**
An adaptive algorithm for motion compensated color image coding
p 113 A87-45466
- WILBUR, PAUL J.**
Plasma contactors for electrodynamic tethers
p 214 A87-31211
Plasma contactors for electrodynamic tether
[NASA-TM-88850] p 215 N87-18428
- WILES, K. J.**
Effects of non-spherical drops on a phase Doppler spray analyzer
p 152 A87-11048
- WILL, HERBERT A.**
The NASA strain gage laboratory
p 35 A87-52494
- WILLIAMS, J. H., JR.**
Modes of vibration on square fiberglass epoxy composite thick plate
[NASA-CR-4018] p 171 N87-13779
Ultrasonic determination of the elastic constants of the stiffness matrix for unidirectional fiberglass epoxy composites
[NASA-CR-4034] p 171 N87-13781
Parameterized materials and dynamic response characterizations in unidirectional composites
[NASA-CR-4032] p 172 N87-13782
- WILLIAMS, JAMES H., JR.**
One-dimensional wave propagation in rods of variable cross section: A WKB solution
[NASA-CR-4086] p 172 N87-24707
Acousto-ultrasonic input-output characterization of unidirectional fiber composite plate by SH waves
[NASA-CR-4087] p 173 N87-26361
- WILLIAMS, M. H.**
A panel method for counter rotating propfans
[AIAA PAPER 87-1890] p 21 A87-45279
- WILLIAMS, MARC**
Analytical and experimental investigation of mistuning in propfan flutter
[AIAA PAPER 87-0739] p 178 A87-40496
Analytical and experimental investigation of mistuning in propfan flutter
[NASA-TM-88959] p 182 N87-18116
- WILLIAMS, W. D.**
Formation of a pn junction on an anisotropically etched GaAs surface using metalorganic chemical vapor deposition
p 216 A87-21237
- WILLIAMS, WALLACE D.**
Computer control of a scanning electron microscope for digital image processing of thermal-wave images
[NASA-TM-100157] p 128 N87-26278
- WILSON, JEFFREY D.**
Revised NASA axially symmetric ring model for coupled-cavity traveling-wave tubes
[NASA-TP-2675] p 127 N87-22923
- WILSON, R. B.**
On 3-D inelastic analysis methods for hot section components (base program)
[NASA-CR-175060] p 180 N87-12923
3-D inelastic analysis methods for hot section components. Volume 2: Advanced special functions models
[NASA-CR-179517] p 186 N87-27267
- WILT, DAVID M.**
AlGaAs growth by OMCVD using an excimer laser
[NASA-TM-88937] p 218 N87-23304
- WINDMILLER, MARY JO**
Unique bit-error-rate measurement system for satellite communication systems
[NASA-TP-2699] p 116 N87-20448
- WINEGAR, STEVEN R.**
SINDA-NASTRAN interfacing program theoretical description and user's manual
[NASA-TM-100158] p 187 N87-27268
- WING, KAM LIU**
Probabilistic finite elements
p 185 N87-22790
- WINNICK, J.**
Concentration of carbon dioxide by a high-temperature electrochemical membrane cell
p 77 A87-27400
- WINSOR, E. A.**
Gravitational macrosegregation in binary Pb-Sn alloy ingots
[NASA-TM-89885] p 109 N87-24579
- WINSOR, EDWARD A.**
The alloy undercooling experiment on the Columbia STS 61-C Space Shuttle mission
[AIAA PAPER 87-0506] p 108 A87-45724
The alloy undercooling experiment on the Columbia STS 61-C space shuttle mission
[NASA-TM-88909] p 91 N87-18643
- WINSOR, N. K.**
Investigation of a repetitive pulsed electrothermal thruster
[NASA-CR-179464] p 59 N87-16878
- WINTUCKY, W. T.**
An overview of the small engine component technology (SECT) studies
[AIAA PAPER 86-1542] p 19 A87-17993
Compound cycle engine program
p 23 A87-53428
Compound cycle engine program
[NASA-TM-88879] p 25 N87-11790
- WISE, JOSEPH**
High power/large area PV systems
p 198 N87-26452
- WISLICENUS, GEORGE F.**
Preliminary design of turbopumps and related machinery
[NASA-RP-1170] p 11 N87-17665
- WISOR, G. D.**
Gear mesh compliance modeling
p 164 A87-53422
Gear mesh compliance modeling
[NASA-TM-88843] p 166 N87-18092
- WITHERS, C. C.**
Static tests of the propulsion system
[AIAA PAPER 87-1728] p 23 A87-52245
- WOJTCZUK, S.**
Detection of radio-frequency modulated optical signals by two and three terminal microwave devices
[NASA-TM-100196] p 130 N87-29750
- WOLFF, F.**
Control considerations for high frequency, resonant, power processing equipment used in large systems
[NASA-TM-89926] p 64 N87-23690
- WOLFF, FREDRICK J.**
20 kHz Space Station power system
p 51 A87-40378
- WOOD, JERRY R.**
Supersonic through-flow fan design
[AIAA PAPER 87-1746] p 22 A87-48571
Shock structure measured in a transonic fan using laser anemometry
p 28 N87-21929
Application of advanced computational codes in the design of an experiment for a supersonic throughflow fan rotor
[NASA-TM-88915] p 13 N87-22630
Supersonic through-flow fan design
[NASA-TM-88908] p 29 N87-22681
- WOODWARD, RICHARD P.**
Measured noise of a scale model high speed propeller at simulated takeoff/approach conditions
[AIAA PAPER 87-0526] p 208 A87-31109
Measured noise of a scale model high speed propeller at simulated takeoff/approach conditions
[NASA-TM-88920] p 211 N87-16588
- WOOLAM, J. A.**
Thermal and structural stability of cosputtered amorphous Ta(x)Cu(1-x) alloy thin films on GaAs
p 216 A87-27198
- WOOLLAM, JOHN A.**
Variable angle of incidence spectroscopic ellipsometry Application to GaAs-Al(x)Ga(1-x)As multiple heterostructures
p 216 A87-20519
Anticorrelation of Shubnikov-deHaas amplitudes and negative magnetoresistance magnitudes in intercalated pitch based graphite fibers
p 217 A87-28295
Interactions of amorphous Ta(x)Cu(1-x) (x = 0.93 and 0.80) alloy films with Au overlayers and GaAs substrates
p 217 A87-44562
Temperature dependence (4K to 300K) of the electrical resistivity of methane grown carbon fibers
p 97 A87-47375
- WOOLLETT, R. R.**
Effect of variable inlet guide vanes on the operating characteristics of a tilt nacelle inlet/powered fan model
[NASA-TM-88983] p 14 N87-27628
- WORTMAN, A.**
Detonation wave compression in gas turbines
[NASA-CR-179557] p 25 N87-13443
- WRIGHT, W. B.**
Efficient numerical simulation of an electrothermal de-icer pad
[AIAA PAPER 87-0024] p 137 A87-32190
- WU, C. S.**
Reactions occurring during the sulfation of sodium chloride deposited on alumina substrates
p 76 A87-20223
- WU, JIUNN-CHI**
A technique for the prediction of airfoil flutter characteristics in separated flow
[AIAA PAPER 87-0910] p 177 A87-33719
Analysis of viscous transonic flow over airfoil sections
[AIAA PAPER 87-0420] p 4 A87-34723
Analysis of viscous transonic flow over airfoil sections
[NASA-TM-88912] p 146 N87-17001

- Studies of unsteady viscous flows using a two-equation model of turbulence
[NASA-CR-181293] p 152 N87-27949
- WU, Y.**
Dendritic growth of undercooled nickel-tin. I, II
p 85 A87-41012
- WU, YANZHONG**
The alloy undercooling experiment on the Columbia STS 61-C Space Shuttle mission
[AIAA PAPER 87-0506] p 108 A87-45724
The alloy undercooling experiment on the Columbia STA 61-C space shuttle mission
[NASA-TM-88909] p 91 N87-18643
- WYGNANSKI, I.**
The evolution of instabilities in the axisymmetric jet. I - The linear growth of disturbances near the nozzle. II - The flow resulting from the interaction between two waves
p 138 A87-37256
- WYGNANSKI, ISRAEL J.**
Coherent motion in excited free shear flows
[AIAA PAPER 85-0539] p 135 A87-30281

X

- XIARU, Y.**
Analysis of thermomechanical oxidation fields in thermal barrier coatings
p 174 A87-14316

Y

- YAGER, THOMAS J.**
Aircraft accident report: NASA 712, Convair 990, N712NA, March Air Force Base, California, July 17, 1985, executive summary
[NASA-TM-87356-VOL-1] p 16 N87-21878
Aircraft accident report: NASA 712, Convair 990, N712NA, March Air Force Base, California, July 17, 1985, facts and analysis
[NASA-TM-87356-VOL-2] p 16 N87-21879
- YAMAGUCHI, MASAFUMI**
Radiation damage in proton irradiated indium phosphide solar cells
p 199 N87-29018
- YAMAMOTO, O.**
Euler analysis of transonic propeller flows
p 4 A87-39813
- YANG, R. J.**
Calculation of two- and three-dimensional transonic cascade flow field using the Navier-Stokes equations
p 144 N87-11220
Turbine vane external heat transfer. Volume 2. Numerical solutions of the Navier-Stokes equations for two- and three-dimensional turbine cascades with heat transfer
[NASA-TP-174828] p 145 N87-13661
- YANG, S. L.**
A two-dimensional numerical study of the flow inside the combustion chamber of a motored rotary engine
[SAE PAPER 860615] p 161 A87-28624
- YEH, F. C.**
Computation of full-coverage film-cooled airfoil temperatures by two methods and comparison with high heat flux data
[NASA-TM-88931] p 150 N87-23934
- YEH, FREDERICK C.**
Turbulence modeling and surface heat transfer in a stagnation flow region
[NASA-TM-100132] p 151 N87-26302
Application of turbulence modeling to predict surface heat transfer in stagnation flow region of circular cylinder
[NASA-TP-2758] p 151 N87-27161
- YOKOTA, JEFFREY W.**
An L-U implicit multigrid algorithm for the three-dimensional Euler equations
[AIAA PAPER 87-0453] p 133 A87-22645
- YOON, S.**
Generation of a composite grid for turbine flows and consideration of a numerical scheme
[NASA-TM-88890] p 11 N87-17662
- YOON, SEOKKWAN**
An LU-SSOR scheme for the Euler and Navier-Stokes equations
[AIAA PAPER 87-0600] p 137 A87-34724
Composite grid and finite-volume LU implicit scheme for turbine flow analysis
[AIAA PAPER 87-1129] p 5 A87-42078
Lower-upper implicit scheme for high-speed inlet analysis
p 6 A87-46781
A multigrid LU-SSOR scheme for approximate Newton iteration applied to the Euler equations
[NASA-CR-179524] p 10 N87-16803
A high resolution shock capturing scheme for high Mach number internal flow
[NASA-CR-179523] p 10 N87-16804

- An LU-SSOR scheme for the Euler and Navier-Stokes equations
[NASA-CR-179556] p 11 N87-16806
Composite grid and finite-volume LU implicit scheme for turbine flow analysis
[NASA-TM-89828] p 12 N87-20235
A Navier-Stokes solver using the LU-SSOR TVD algorithm
[NASA-CR-179608] p 13 N87-20243
- YOUNG, S. LEE**
Intersatellite Link (ISL) application to commercial communications satellites. Volume 1: Executive summary
[NASA-CR-179598-VOL-1] p 116 N87-19552
Intersatellite Link (ISL) application to commercial communications satellites. Volume 2: Technical final report
[NASA-CR-179598-VOL-2] p 116 N87-19553
- YOUNGBLOOD, W. W.**
Equipment concept design and development plans for microgravity science and applications research on space station: Combustion tunnel, laser diagnostic system, advanced modular furnace, integrated electronics laboratory
[NASA-CR-179535] p 108 N87-15320
- YU, M. H.**
The near field behavior of turbulent gas jets in a long confinement
p 135 A87-28976
- YUNG, C. N.**
Numerical prediction of cold turbulent flow in combustor configurations with different centerbody flame holders
[ASME PAPER 86-WA-HT-50] p 140 A87-43715

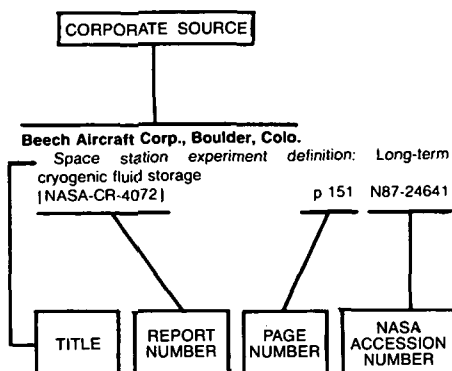
Z

- ZAGHLOUL, A. I.**
20-GHz phased-array-fed antennas utilizing distributed MMIC modules
p 112 A87-34527
- ZAGHLOUL, AMIR**
APS-Workshop on Characterization of MMIC (Monolithic Microwave Integrated Circuit) Devices for Array Antenna
[AD-P005398] p 118 N87-28763
- ZAMAN, K. B. M. Q.**
Initial turbulence effect on jet evolution with and without tonal excitation
[NASA-TM-100178] p 14 N87-27629
Control of shear flows by artificial excitation
[NASA-TM-100201] p 15 N87-29420
- ZANA, L. M.**
An analytical and experimental investigation of resistojet plumes
[NASA-TM-88852] p 58 N87-14428
- ZANA, LYNETTE M.**
Effect of nozzle geometry on the resistojet exhaust plume
[AIAA PAPER 87-2121] p 55 A87-52252
- ZANA, LYNETTE M.**
An analytical and experimental investigation of resistojet plumes
[AIAA PAPER 87-0399] p 48 A87-24998
Langmuir probe surveys of an arcjet exhaust
[AIAA PAPER 87-1950] p 54 A87-50193
Electromagnetic emission experiences using electric propulsion systems - A survey
[AIAA PAPER 87-2028] p 54 A87-50195
Electromagnetic emission experiences using electric propulsion systems: A survey
[NASA-TM-100120] p 64 N87-22805
Langmuir probe surveys of an arcjet exhaust
[NASA-TM-89924] p 64 N87-22807
- ZAPLATYNSKY, I.**
The effect of laser glazing on life of ZrO₂ TBCs in cyclic burner rig tests
[NASA-TM-88821] p 89 N87-14487
The effect of Cr, Co, Al, Mo and Ta on a series of cast Ni-base superalloys on the stability of an aluminide coating during cyclic oxidation in Mach 0.3 burner rig
[NASA-TM-88840] p 89 N87-14488
- ZAPLATYNSKY, ISIDOR**
Morphology of zirconia particles exposed to D.C. arc plasma jet
[NASA-TM-88927] p 90 N87-16113
- ZARETSKY, E. V.**
Selection of rolling-element bearing steels for long-life application
[NASA-TM-88881] p 164 N87-11993
Effect of design variables, temperature gradients and speed of life and reliability of a rotating disk
[NASA-TM-88883] p 165 N87-13755
- ZARETSKY, ERWIN V.**
Effect of interference fits on roller bearing fatigue life
p 162 A87-37686
Lubricant effects on bearing life
[NASA-TM-88875] p 165 N87-15467

- Effects of surface removal on rolling-element fatigue
[NASA-TM-88871] p 166 N87-18820
- ZARETSKY, ERWIN Y.**
Fatigue criterion to system design, life, and reliability
p 175 A87-27986
- ZAVESKY, RALPH J.**
Heat exchanger for electrothermal devices
[NASA-CASE-LEW-14037-1] p 59 N87-16875
- ZEINER, P. K.**
Advanced technology payoffs for future small propulsion systems
p 21 A87-47081
- ZELEZNIK, FRANK J.**
Thermodynamics and combustion modeling
p 219 N87-20274
- ZERKLE, RONALD D.**
Evaluation of capillary reinforced composites for anti-icing
[AIAA PAPER 87-0023] p 17 A87-24904
- ZHANG, J.**
An experimental study on the effects of tip clearance on flow field and losses in an axial flow compressor rotor
p 6 A87-46207
- ZHOU, PEIZHEN**
Observation of deep levels in cubic silicon carbide
p 122 A87-41089
- ZIERKE, W. C.**
The measurement of boundary layers on a compressor blade in cascade at high positive incidence angle. 1: Experimental techniques and results
[NASA-CR-179491] p 25 N87-13441
The measurement of boundary layers on a compressor blade in cascade at high positive incidence angle. 2: Data report
[NASA-CR-179492] p 25 N87-13442
- ZINOLABEDINI, REZA**
Mechanical and electrical properties of graphite fiber-epoxy composites made from pristine and bromine intercalated fibers
p 73 A87-49799
- ZURAWSKI, ROBERT L.**
An evaluation of metallized propellants based on vehicle performance
[AIAA PAPER 87-1773] p 53 A87-47003
Analysis of quasi-hybrid solid rocket booster concepts for advanced earth-to-orbit vehicles
[AIAA PAPER 87-2082] p 55 A87-52250
An evaluation of metallized propellants based on vehicle performance
[NASA-TM-100104] p 64 N87-22806
Analysis of quasi-hybrid solid rocket booster concepts for advanced earth-to-orbit vehicles
[NASA-TP-2751] p 67 N87-25425
- ZUTECK, MICHAEL**
Design of an advanced wood composite rotor and development of wood composite blade technology
[NASA-CR-174713] p 73 N87-17861

CORPORATE SOURCE INDEX

Typical Corporate Source Index Listing



Listings in this index are arranged alphabetically by corporate source. The title of the document is used to provide a brief description of the subject matter. The page number and the accession number are included in each entry to assist the user in locating the abstract in the abstract section. If applicable, a report number is also included as an aid in identifying the document.

A

- Advanced Scientific Computing Ltd., Waterloo (Ontario).**
Evaluation of new techniques for the calculation of internal recirculating flows
[AIAA PAPER 87-0059] p 131 A87-22387
- Aerodyne Products Corp., Billerica, Mass.**
Modelling free convective gravitational effects in chemical vapor deposition
[AIAA PAPER 87-0313] p 133 A87-22552
- Aerodyne Research, Inc., Billerica, Mass.**
Modelling free convective gravitational effects in chemical vapor deposition
[AIAA PAPER 87-0313] p 133 A87-22552
- Aerojet Strategic Propulsion Co., Sacramento, Calif.**
Fast algorithm for calculating chemical kinetics in turbulent reacting flow
p 77 A87-38958
- Aerojet TechSystems Co., Sacramento, Calif.**
Heat pipe cooled rocket engines
[AIAA PAPER 86-1567] p 48 A87-21516
- Aerometrics, Inc., Mountain View, Calif.**
Two-phase flow measurements of a spray in a turbulent flow
[AIAA PAPER 87-0062] p 132 A87-22388
Laser velocimetry in turbulent flow fields - Particle response
[AIAA PAPER 87-0118] p 132 A87-22426
Two-phase measurements of a spray in the wake of a bluff body
p 142 A87-46199
- AeroVironment, Inc., Monrovia, Calif.**
Development and testing of vortex generators for small horizontal axis wind turbines
[NASA-CR-179514] p 193 N87-18922
- Agency for International Development, Washington, D.C.**
Tunisia Renewable Energy Project systems description report
[NASA-TM-88789] p 192 N87-13856

Air Force Armament Lab., Eglin AFB, Fla.

Three-dimensional unsteady Euler solutions for propfans and counter-rotating propfans in transonic flow
[AIAA PAPER 87-1197] p 5 A87-42314

Air Force Rocket Propulsion Lab., Edwards AFB, Calif.

The NASA/USAF arcjet research and technology program
[AIAA PAPER 87-1946] p 54 A87-50192

Akron Univ., Ohio.

Analysis of thermomechanical oxidation fields in thermal barrier coatings
p 174 A87-14316
On the symbolic manipulation and code generation for elasto-plastic material matrices
p 201 A87-18499

Thermal shaft effects on load-carrying capacity of a fully coupled, variable-properties cryogenic journal bearing
[ASLE PREPRINT 86-TC-68-1] p 160 A87-19502

A fully coupled variable properties thermohydraulic model for a cryogenic hydrostatic journal bearing
[ASME PAPER 86-TRIB-55] p 161 A87-19536

Numerical analysis of a NACA0012 airfoil with leading edge ice accretions
[AIAA PAPER 87-0101] p 2 A87-22415

An analytical and experimental investigation of resistojet plumes
[AIAA PAPER 87-0399] p 48 A87-24998

On the numerical performance of three-dimensional thick shell elements using a hybrid/mixed formulation
p 175 A87-25924

Two-phase flows and heat transfer within systems with ambient pressure above the thermodynamic critical pressure
p 136 A87-30728

Multiply scaled constrained nonlinear equation solvers
p 137 A87-31406

Analysis of experimental shaft seal data for high-performance turbomachines - As for Space Shuttle main engines
p 162 A87-45846

Finite difference solution for a generalized Reynolds equation with homogeneous two-phase flow
p 141 A87-45851

Comparison of generalized Reynolds and Navier Stokes equations for flow of a power law fluid
p 142 A87-45852

An efficient quadrilateral element for plate bending analysis
p 178 A87-45994

Refrigerated dynamic seal to 6.9 MPa (1000 psi)
p 164 A87-50777

Effect of nozzle geometry on the resistojet exhaust plume
[AIAA PAPER 87-2121] p 55 A87-52252

Gear mesh compliance modeling
p 164 A87-53422

A quadrilateral shell element using a mixed formulation
p 179 A87-53796

Results of an interlaboratory fatigue test program conducted on alloy 800H at room and elevated temperatures
p 87 A87-54370

High-temperature constitutive modeling
p 179 A87-11210

A viscoplastic constitutive theory for metal matrix composites at high temperature
[NASA-CR-179530] p 180 A87-13790

A mechanism for precise linear and angular adjustment utilizing flexures
p 165 A87-16342

Structural properties of impact ices accreted on aircraft structures
[NASA-CR-179580] p 182 A87-18121

Flexibility effects on tooth contact location in spiral bevel gear transmissions
[NASA-CR-4055] p 166 A87-20552

Alabama Univ., Huntsville.
Investigation of beam-plasma interactions
[NASA-CR-180579] p 215 A87-22508

Electron beam experiments at high altitudes
p 44 A87-26946

Ames Lab., Iowa.
Compressibility of solids
p 219 A87-51962

Analex Corp., Cleveland, Ohio.
Microwave electrothermal thruster performance in helium gas
p 49 A87-31281

Ultra small electron beam amplifiers
p 122 A87-42681

Analex Corp., Dayton, Ohio.

Experimental verification of vapor deposition model in Mach 0.3 burner rigs
p 88 N87-11192

Analytic and Computational Research, Inc., Los Angeles, Calif.

An unconditionally-stable central differencing scheme for high Reynolds number flows.
[AIAA PAPER 87-0060] p 133 A87-24912

CONDIF - A modified central-difference scheme with unconditional stability and very low numerical diffusion
p 136 A87-30685

CONDIF - A modified central-difference scheme for convective flows
p 205 A87-53675

Argonne National Lab., Ill.

ANL/RBC: A computer code for the analysis of Rankine bottoming cycles, including system cost evaluation and off-design performance
[NASA-CR-179462] p 220 N87-10777

Arizona State Univ., Tempe.

On self-preserving, variable-density, turbulent free jets
p 130 A87-10920

On similarity solutions for turbulent and heated round jets
p 130 A87-10922

The near field behavior of turbulent gas jets in a long confinement
p 135 A87-28976

A hybrid nonlinear programming method for design optimization
p 201 A87-35718

Optimal placement of critical speeds in rotor-bearing systems
p 162 A87-38464

Modelling of jet- and swirl-stabilized reacting flows in axisymmetric combustors
p 138 A87-38956

On the modelling of non-reactive and reactive turbulent combustor flows
[NASA-CR-4041] p 28 A87-20996

Arizona Univ., Tucson.

Influence of airfoil mean loading on convected gust interaction noise
p 208 A87-13587

Coherent motion in excited free shear flows
[AIAA PAPER 85-0539] p 135 A87-30281

Perfect gas effects in compressible rapid distortion theory
p 136 A87-31176

On the spatial instability of piecewise linear free shear layers
p 137 A87-31680

The evolution of instabilities in the axisymmetric jet. I - The linear growth of disturbances near the nozzle. II - The flow resulting from the interaction between two waves
p 138 A87-37256

Army Aviation Research and Development Command, Cleveland, Ohio.

New generation methods for spur, helical, and spiral-bevel gears
p 164 A87-53420

Gear mesh compliance modeling
p 164 A87-53422

Compound cycle engine program
p 23 A87-53428

Vibration characteristics of OH-58A helicopter main rotor transmission
[NASA-TP-2705] p 167 A87-20555

The T55-L-712 turbine engine compressor housing refurbishment project
[NASA-CR-179624] p 92 A87-23729

Army Propulsion Lab., Cleveland, Ohio.

Rotor wake characteristics of a transonic axial-flow fan
p 2 A87-20886

Structure-to-property relationships in addition cured polymers. II - Resin Tg and composite initial mechanical properties of norbornenyl cured polyimide resins
p 96 A87-38638

Composite grid and finite-volume LU implicit scheme for turbine flow analysis
[AIAA PAPER 87-1129] p 5 A87-42078

Contingency power for small turboshaft engines using water injection into turbine cooling air
[AIAA PAPER 87-1906] p 21 A87-45289

Performance of two 10-lb/sec centrifugal compressors with different blade and shroud thicknesses operating over a range of Reynolds numbers
[AIAA PAPER 87-1745] p 22 A87-50188

Liner cooling research at NASA Lewis Research Center
[AIAA PAPER 87-1828] p 22 A87-50189

Atmospheric Science Associates, Bedford, Mass.

- Three-dimensional trajectory analyses of two drop sizing instruments - PMS OAP and PMS FSSP
[AIAA PAPER 87-0180] p 132 A87-22466
- Calculation of water drop trajectories to and about arbitrary three-dimensional lifting and nonlifting bodies in potential airflow
[NASA-CR-3935] p 8 N87-11694
- Avco-Everett Research Lab., Mass.**
Evaluation of new techniques for the calculation of internal recirculating flows
[AIAA PAPER 87-0059] p 131 A87-22387

B

- Beech Aircraft Corp., Boulder, Colo.**
Space station experiment definition: Long-term cryogenic fluid storage
[NASA-CR-4072] p 151 N87-24641
- Beech Aircraft Corp., Wichita, Kans.**
Application of propfan propulsion to general aviation
[AIAA PAPER 86-2698] p 18 A87-17934
- Boeing Aerospace Co., Kent, Wash.**
Space station propulsion-ECLSS interaction study
[NASA-CR-175093] p 69 N87-29594
- Boeing Co., Seattle, Wash.**
A model propulsion simulator for evaluating counter rotating blade characteristics
[SAE PAPER 861715] p 20 A87-32607
- Boeing Commercial Airplane Co., Seattle, Wash.**
An experimental investigation of compressible three-dimensional boundary layer flow in annular diffusers
[AIAA PAPER 87-0366] p 3 A87-24954
- Boeing Military Airplane Development, Wichita, Kans.**
Experimental, water droplet impingement data on two-dimensional airfoils, axisymmetric inlet and Boeing 737-300 engine inlet
[AIAA PAPER 87-0097] p 17 A87-24918
- Bolt, Beranek, and Newman, Inc., Cambridge, Mass.**
Analysis of the vibratory excitation arising from spiral bevel gears
[NASA-CR-4081] p 169 N87-25579
- Brown Univ., Providence, R. I.**
Nonlinear binary-mode interactions in a developing mixing layer
p 142 A87-47158

C

- California Univ., Berkeley.**
Equilibrium fluid interfaces in the absence of gravity
p 138 A87-38790
- Forced cocurrent smoldering combustion
p 77 A87-40572
- The large-scale peculiar velocity field in flat models of the universe
p 223 A87-40651
- California Univ., Berkeley. Lawrence Berkeley Lab.**
Degradation mechanisms in thermal-barrier coatings
p 94 A87-12953
- California Univ., Irvine.**
Performance comparison of two interferometric droplet sizing techniques
p 153 A87-11049
- California Univ., La Jolla.**
Gravitational effects on the structure and propagation of premixed flames
[IAF PAPER 86-279] p 76 A87-15983
- Particle cloud kinetics in microgravity
[AIAA PAPER 87-0577] p 107 A87-22716
- The dynamic behavior of plasmas observed near geosynchronous orbit
p 200 A87-31322
- California Univ., Los Angeles.**
The flame structure and vorticity generated by a chemically reacting transverse jet
p 76 A87-14116
- Thin-film temperature sensors for gas turbine engines
Problems and prospects
p 153 A87-26109
- Calspan Field Services, Inc., Arnold AFS, Tenn.**
In-flight photogrammetric measurement of wing ice accretions
[AIAA PAPER 86-0483] p 15 A87-17995
- In-flight measurement of ice growth on an airfoil using an array of ultrasonic transducers
[AIAA PAPER 87-0178] p 15 A87-22464
- Cambridge Univ. (England).**
A method for assessing effects of circumferential flow distortion on compressor stability
p 7 A87-48722
- Calculations of inlet distortion induced compressor flowfield instability
p 30 N87-24470
- Carnegie-Mellon Univ., Pittsburgh, Pa.**
The effects of engine speed and injection characteristics on the flow field and fuel/air mixing in motored two-stroke diesel engines
[AIAA PAPER 87-0227] p 161 A87-22501

- Comparisons between thermodynamic and one-dimensional combustion models of spark-ignition engines
p 161 A87-29275
- Centrifugal inertia effects in two-phase face seal films
p 162 A87-37687
- Numerical simulation of the flow field and fuel sprays in an IC engine
[SAE PAPER 870599] p 143 A87-48751
- Fuel-air mixing and combustion in a two-dimensional Wankel engine
[SAE PAPER 870408] p 163 A87-48783
- Bladed disk vibration
[NASA-CR-181203] p 31 N87-26908
- Case Western Reserve Univ., Cleveland, Ohio.**
Cellular and dendritic growth in a binary melt - A marginal stability approach
p 107 A87-10871
- Behavior of inversion layers in 3C silicon carbide
p 215 A87-11242
- Transition from a planar interface to cellular and dendritic structures during rapid solidification processing
p 81 A87-12029
- Stoichiometric disturbances in compound semiconductors due to ion implantation
p 215 A87-12292
- Compensation in epitaxial cubic SiC films
p 216 A87-15071
- Colloidal characterization of ultrafine silicon carbide and silicon nitride powders
p 95 A87-19625
- Re-examination of cumulative fatigue damage analysis - An engineering perspective
p 174 A87-22128
- Effects of silver and group II fluoride solid lubricant additions to plasma-sprayed chromium carbide coatings for foil gas bearings to 650 C
p 95 A87-22336
- Compliance matrices for cracked bodies
p 175 A87-25775
- An analysis for crack layer stability
p 176 A87-28982
- Antiphase boundaries in epitaxially grown beta-SiC
p 217 A87-30025
- TWT efficiency improvement by a low-cost technique for deposition of carbon on MDC electrodes
p 121 A87-30199
- Two-phase flows and heat transfer within systems with ambient pressure above the thermodynamic critical pressure
p 136 A87-30728
- Cellular-dendritic transition in directionally solidified binary alloys
p 84 A87-32046
- Analysis of NiAlTa precipitates in beta-NiAl + 2 at. pct Ta alloy
p 84 A87-34888
- Investigation of two-dimensional shock-wave/boundary-layer interactions
p 4 A87-39528
- Crack layer theory
p 178 A87-40056
- Laser anemometry measurements of natural circulation flow in a scale model PWR reactor system
p 154 A87-40750
- TEM investigation of beta-SiC grown epitaxially on Si substrate by CVD
p 97 A87-40927
- Comment on 'Temperature dependence of electrical properties of non-doped and nitrogen-doped beta-SiC single crystals grown by chemical vapor deposition'
p 217 A87-42846
- Analysis of experimental shaft seal data for high-performance turbomachines - As for Space Shuttle main engines
p 162 A87-45846
- Finite difference solution for a generalized Reynolds equation with homogeneous two-phase flow
p 141 A87-45851
- Comparison of generalized Reynolds and Navier Stokes equations for flow of a power law fluid
p 142 A87-45852
- The characteristics of gamma-prime dislocation pairs in a nickel-base superalloy
p 85 A87-46932
- Microstrip dispersion including anisotropic substrates
p 123 A87-47621
- Experimental verification of corrosive vapor deposition rate theory in high velocity burner rigs
p 143 A87-49551
- Method for the determination of the three dimensional aerodynamic field of a rotor-stator combination in compressible flow
[AIAA PAPER 87-1742] p 7 A87-50187
- Refrigerated dynamic seal to 6.9 MPa (1000 psi)
p 164 A87-50777
- Oxygen-18 tracer study of the passive thermal oxidation of silicon
p 78 A87-51187
- Elevated temperature strengthening of a melt spun austenitic steel by TiB₂
p 87 A87-51639
- Size and shape of solid fuel diffusion flames in very slow speed flows
[AIAA PAPER 87-2030] p 78 A87-52248
- Analysis of mixed-mode crack propagation using the boundary integral method
[NASA-CR-179518] p 180 N87-12915
- Polymer precursors for ceramic matrix composites
[NASA-CR-179562] p 70 N87-14434

- Oil film thickness measurement and analysis for an angular contact ball bearing operating in parched elastohydrodynamic lubrication
[NASA-CR-179506] p 70 N87-16879
- Investigation of a GaAlAs Mach-Zehnder electro-optic modulator
[NASA-CR-179573] p 114 N87-16953
- Thermocapillary bubble migration for large Marangoni Numbers
[NASA-CR-179628] p 109 N87-22865
- Environmental degradation of 316 stainless steel in high temperature low cycle fatigue
[NASA-TM-89931] p 185 N87-24007
- Stability and rheology of dispersions of silicon nitride and silicon carbide
[NASA-CR-179634] p 104 N87-25476
- Composition optimization of chromium carbide based solid lubricant coatings for foil gas bearings at temperatures to 650 C
[NASA-CR-179649] p 105 N87-26233
- Experimental evaluation of chromium-carbide-based solid lubricant coatings for use to 760 C
[NASA-CR-180808] p 105 N87-27053
- Ductility and fracture in B2 FeAl alloys
[NASA-CR-180810] p 93 N87-27771
- Oxygen interaction with space-power materials
[NASA-CR-181396] p 80 N87-29633
- Theoretical performance of hydrogen-bromine rechargeable SPE fuel cell
p 199 N87-29945
- Ceramic Process Systems, Lexington, Mass.**
Oxygen-18 tracer study of the passive thermal oxidation of silicon
p 78 A87-51187
- CHAM of North America, Inc., Huntsville, Ala.**
Comparison of generalized Reynolds and Navier Stokes equations for flow of a power law fluid
p 142 A87-45852
- Chicago Univ., Ill.**
The large-scale peculiar velocity field in flat models of the universe
p 223 A87-40651
- Helical gears with circular arc teeth: Generation, geometry, precision and adjustment to errors, computer aided simulation of conditions of meshing and bearing contact
[NASA-CR-4089] p 170 N87-29846
- Cincinnati Univ., Ohio.**
A high quality image compression scheme for real-time applications
p 111 A87-30801
- Fault structures in rapidly quenched Ni-Mo binary alloys
p 83 A87-32035
- Microstructures in rapidly solidified Ni-Mo alloys
p 87 A87-51636
- A constitutive model for the inelastic multiaxial cyclic response of a nickel base superalloy Rene 80
[NASA-CR-3998] p 182 N87-18852
- Computer aided design and analysis of gear tooth geometry
[NASA-CR-179611] p 168 N87-23969
- City Coll. of the City Univ. of New York.**
An investigation of the flow characteristics in the blade endwall corner region
[NASA-CR-4076] p 14 N87-29412
- Clarkson Univ., Potsdam, N.Y.**
Soot loading in a generic gas turbine combustor
[AIAA PAPER 87-0297] p 19 A87-22544
- Clemson Univ., S.C.**
Heat transfer and fluid mechanics measurements in transitional boundary layers on convex-curved surfaces
[ASME PAPER 85-MT-60] p 143 A87-48726
- Cleveland State Univ., Ohio.**
Correlation of processing and sintering variables with the strength and radiography of silicon nitride
p 94 A87-12938
- Cell performance and defect behavior in proton-irradiated lithium-counterdoped n(+)-p silicon solar cells
p 216 A87-14222
- Probability of detection of internal voids in structural ceramics using microfocus radiography
p 170 A87-14300
- Solar concentrator materials development
p 213 A87-18171
- A proposed GaAs-based superlattice solar cell structure with high efficiency and high radiation tolerance
p 189 A87-19915
- A heater made from graphite composite material for potential deicing application
[AIAA PAPER 87-0025] p 17 A87-24905
- Cellular-dendritic transition in directionally solidified binary alloys
p 84 A87-32046
- Fiber-optic photoelastic pressure sensor with fiber-loss compensation
p 154 A87-34566
- Effects of milling brominated P-100 graphite fibers
p 97 A87-41078
- Estimation of instantaneous heat transfer coefficients for a direct-injection stratified-charge rotary engine
[SAE PAPER 870444] p 163 A87-48787

- Mechanical and electrical properties of graphite fiber-epoxy composites made from pristine and bromine intercalated fibers p 73 A87-49799
- Quantitative void characterization in structural ceramics by use of scanning laser acoustic microscopy p 171 A87-51974
- Cellular microstructure of chill block melt spun Ni-Mo alloys p 87 A87-54300
- Mechanical behavior of thermal barrier coatings for gas turbine blades p 24 A87-11196
- Design and dynamic simulation of a fixed pitch 56 kW wind turbine drive train with a continuously variable transmission [NASA-CR-179543] p 193 A87-17401
- Effects of sequential treatment with fluorine and bromine on graphite fibers [NASA-TM-100106] p 104 A87-24574
- Optical strain measuring techniques for high temperature tensile testing [NASA-CR-179637] p 159 A87-26327
- Enhanced mixing of an axisymmetric jet by aerodynamic excitation [NASA-CR-175059] p 15 A87-29418
- Colby Coll., Waterville, Maine.**
- LEO high voltage solar array arcing response model [NASA-CR-180073] p 124 A87-16971
- College of Western New England, Springfield, Mass.**
- Short efficient ejector systems [AIAA PAPER 87-1837] p 20 A87-45239
- Colorado State Univ., Fort Collins.**
- Plasma contactors for electrodynamic tethers p 214 A87-31211
- Plasma contactors for electrodynamic tether [NASA-TM-88850] p 215 A87-18428
- Communications Satellite Corp., Clarksburg, Md.**
- 20-GHz phased-array-fed antennas utilizing distributed MMIC modules p 112 A87-34527
- On-board processing satellite network architecture and control study [NASA-CR-180816] p 44 A87-27710
- On-board processing satellite network architecture and control study [NASA-CR-180817] p 44 A87-27711
- Onboard multichannel demultiplexer/demodulator [NASA-CR-180821] p 119 A87-28819
- Communications Satellite Corp., Washington, D.C.**
- Intersatellite Link (ISL) application to commercial communications satellites. Volume 1: Executive summary [NASA-CR-179598-VOL-1] p 116 A87-19552
- Intersatellite Link (ISL) application to commercial communications satellites. Volume 2: Technical final report [NASA-CR-179598-VOL-2] p 116 A87-19553
- Cooper Union for the Advancement of Science and Art, New York.**
- Stochastic and fractal analysis of fracture trajectories p 179 A87-51167
- Cornell Univ., Ithaca, N.Y.**
- Towards effective interactive three-dimensional colour postprocessing p 201 A87-11895
- A diagonal implicit multigrid algorithm for the Euler equations [AIAA PAPER 87-0354] p 2 A87-22578
- An L-U implicit multigrid algorithm for the three-dimensional Euler equations [AIAA PAPER 87-0453] p 133 A87-22645
- Stall transients of axial compression systems with inlet distortion p 3 A87-24010
- Multigrid solution of inviscid transonic flow through rotating blade passages [AIAA PAPER 87-0608] p 3 A87-24992
- Interactive graphics and analysis accuracy p 202 A87-45900
- Color postprocessing for 3-dimensional finite element mesh quality evaluation and evolving graphical workstation [NASA-CR-180215] p 202 A87-18997
- Unification of color postprocessing techniques for 3-dimensional computational mechanics [NASA-CR-180214] p 202 A87-18998
- Interactive color display of 3-D engineering analysis results [NASA-CR-180589] p 203 A87-22422
- Cray Research, Inc., Mendota Heights, Minn.**
- The utilization of parallel processing in solving the inviscid form of the average-passage equation system for multistage turbomachinery [AIAA PAPER 87-1108] p 5 A87-42057
- Cummins Engine Co., Inc., Columbus, Ind.**
- Technical and economic study of Stirling and Rankine cycle bottoming systems for heavy truck diesel engines [NASA-CR-180833] p 222 A87-28470

D

- Dartmouth Coll., Hanover, N.H.**
- The role of near-surface plastic deformation in the wear of lamellar solids p 162 A87-48500
- Dawn Engineering, Plano, Tex.**
- A photovoltaic power system and a low-power satellite earth station for Indonesia p 189 A87-19859
- Dayton Univ., Ohio.**
- Numerical simulation of excited jet mixing layers [AIAA PAPER 87-0016] p 131 A87-22361
- Navier Stokes solution of the flowfield over ice accretion shapes [AIAA PAPER 87-0099] p 2 A87-22414
- Design of test specimens and procedures for generating material properties of Douglas fir/epoxy laminated wood composite material: With the generation of baseline data at two environmental conditions [NASA-CR-174910] p 75 A87-28612
- Defence Metallurgical Research Lab., Hyderabad (India).**
- Mechanical property anisotropy in superalloy EI-929 directionally solidified by an exothermic technique p 81 A87-11389
- Dendritic microstructure in argon atomized superalloy powders p 83 A87-24119
- Effect of heat treatment on the fracture behaviour of directionally solidified (gamma/gamma-prime)-alpha alloy p 86 A87-47932
- Defence Research and Development Lab., Hyderabad (India).**
- Mechanical property anisotropy in superalloy EI-929 directionally solidified by an exothermic technique p 81 A87-11389
- Delaware Univ., Newark.**
- An optimized top contact design for solar cell concentrators p 189 A87-19882
- Elastic interaction of a crack with a microcrack array. I - Formulation of the problem and general form of the solution. II - Elastic solution for two crack configurations (piecewise constant and linear approximations) p 178 A87-36926
- Department of Energy, Washington, D.C.**
- The Advanced Turbine Technology Applications Program (ATTAP) [SAE PAPER 87-0467] p 163 A87-48791
- Solid lubrication design methodology, phase 2 [NASA-CR-175114] p 221 A87-18470
- Drexel Univ., Philadelphia, Pa.**
- Processing-structure characterization of rheocast IN-100 superalloy p 82 A87-24116
- Analysis of the solidified structure of rheocast and VADER processed nickel-base superalloy p 83 A87-28734
- Degradation mechanisms of sulfur and nitrogen containing compounds during thermal stability testing of model fuels [AIAA PAPER 87-2039] p 106 A87-45372
- Spark ignition of monodisperse fuel sprays [NASA-CR-181404] p 80 A87-29635
- Thermal stability of distillate hydrocarbon fuels [NASA-CR-181412] p 107 A87-29706
- Duke Univ., Durham, N.C.**
- Extrapolation methods for vector sequences p 203 A87-53631

E

- ECO Energy Conversion, Somerville, Mass.**
- Organometallic catalysts for primary phosphoric acid fuel cells [NASA-CR-179490] p 193 A87-19804
- Ecole Polytechnique Federale de Lausanne (Switzerland).**
- Thermal-mechanical fatigue crack growth in B-1900+Hf p 86 A87-49570
- Electrotek Concepts, Inc., Knoxville, Tenn.**
- Utility interconnection issues for wind power generation [NASA-CR-175056] p 193 A87-17400
- Embry-Riddle Aeronautical Univ., Prescott, Ariz.**
- Measurement of a counter rotation propeller flowfield using a Laser Doppler Velocimeter [AIAA PAPER 87-0008] p 3 A87-24901
- Energy Research Corp., Danbury, Conn.**
- Performance study of a fuel cell Pt-on-C anode in presence of CO and CO₂ and calculation of adsorption parameters for CO poisoning p 188 A87-12338
- On the effect of the Fe(2+)/Fe(3+) redox couple on oxidation of carbon in hot H₃PO₄ p 78 A87-42677
- Corrosion of graphite composites in phosphoric acid fuel cells p 72 A87-42684
- Modeling for CO poisoning of a fuel cell anode p 191 A87-52288

Garrett Turbine Engine Co., Phoenix, Ariz.

- Engelhard Corp., Edison, N.J.**
- Develop and test fuel cell powered on site integrated total energy systems. Phase 3: Full-scale power plant development [NASA-CR-175118] p 191 A87-11344
- Develop and test fuel cell powered on-site integrated total energy systems. Phase 3: Full-scale power plant development [NASA-CR-175117] p 191 A87-11346
- Develop and test fuel cell powered on site integrated total energy systems: Phase 3: Full-scale power plant development [NASA-CR-175075] p 191 A87-11347
- Eotvoes Lorand Univ., Budapest (Hungary).**
- Quasars as indicators of galactic ages p 223 A87-26927
- Ethyl Corp., Baton Rouge, La.**
- Shock-tube pyrolysis of acetylene - Sensitivity analysis of the reaction mechanism for soot formation p 75 A87-12598

F

- Fermi National Accelerator Lab., Batavia, Ill.**
- Quasars as indicators of galactic ages p 223 A87-26927
- Florida State Univ., Tallahassee.**
- On broadband shock associated noise of supersonic jets p 208 A87-11768
- Florida Univ., Gainesville.**
- A two-dimensional numerical study of the flow inside the combustion chamber of a motored rotary engine [SAE PAPER 860615] p 161 A87-28624
- Numerical simulation of the flowfield in a motored two-dimensional Wankel engine p 138 A87-39812
- Fuel-air mixing and combustion in a two-dimensional Wankel engine [SAE PAPER 870408] p 163 A87-48783
- Flow Research, Inc., Kent, Wash.**
- Propeller design by optimization p 18 A87-14123
- Mechanisms by which heat release affects the flow field in a chemically reacting, turbulent mixing layer [AIAA PAPER 87-0131] p 134 A87-24925
- On direct numerical simulations of turbulent reacting flows [AIAA PAPER 87-1324] p 140 A87-44930
- Ford Aerospace and Communications Corp., Palo Alto, Calif.**
- Space station experiment definition: Advanced power system test bed [NASA-CR-179502] p 58 A87-15270
- Application of adaptive antenna techniques to future commercial satellite communication [NASA-CR-179566] p 115 A87-16954
- Application of adaptive antenna techniques to future commercial satellite communications. Executive summary [NASA-CR-179566-SUMM] p 115 A87-16955
- Communications satellite systems operations with the space station. Volume 1: Executive summary [NASA-CR-179526] p 206 A87-17472
- Communications satellite systems operations with the space station, volume 2 [NASA-CR-179527] p 206 A87-17473
- Satellite analog FDMA/FM to digital TDMA conversion [NASA-CR-179605] p 125 A87-20467
- The use of satellites in non-geostationary orbits for unloading geostationary communication satellite traffic peaks. Volume 1: Executive summary [NASA-CR-179597-VOL-1] p 117 A87-21212
- The use of satellites in non-geostationary orbits for unloading geostationary communication satellite traffic peaks. Volume 2: Technical report [NASA-CR-179597-VOL-2] p 117 A87-21213
- Ford Motor Co., Dearborn, Mich.**
- Fracture of flash oxidized, yttria-doped sintered reaction-bonded silicon nitride p 97 A87-47923
- Fukui Univ. (Japan).**
- Plastic deformation of a magnesium oxide 001-plane surface produced by cavitation [ASLE PREPRINT 86-TC-3D-1] p 94 A87-19504

G

- Garrett Corp., Phoenix, Ariz.**
- Compound cycle engine program p 23 A87-53428
- Garrett Turbine Engine Co., Phoenix, Ariz.**
- Finite analytic numerical solution of two-dimensional channel flow over a backward-facing step p 131 A87-13506
- Effects of multiple rows and noncircular orifices on dilution jet mixing p 138 A87-39805
- Advanced technology payoffs for future small propulsion systems p 21 A87-47081

- A technology development summary for the AGT101 advanced gas turbine program [SAE PAPER 870466] p 163 A87-48790
- Scaled centrifugal compressor program [NASA-CR-174912] p 26 N87-14349
- Brayton cycle solarized advanced gas turbine [NASA-CR-179559] p 220 N87-15030
- Transition mixing study [NASA-CR-175062] p 27 N87-16830
- Oxide-dispersion-strengthened turbine blades, volume 1 [NASA-CR-179537-VOL-1] p 90 N87-17883
- Compound cycle engine for helicopter application [NASA-CR-175110] p 31 N87-25323
- Advanced Gas Turbine (AGT) Technology Development Project [NASA-CR-180818] p 222 N87-30225
- General Dynamics/Convair, San Diego, Calif.**
- Measurement of Centaur/Orbiter multiple reaction forces in a full-scale test rig p 38 A87-29448
- General Dynamics Corp., San Diego, Calif.**
- Effects of transient propellant dynamics on deployment of large liquid stages in zero-gravity with application to Shuttle/Centaur [IAF PAPER 86-119] p 39 A87-15880
- Shuttle/Centaur G-prime composite adapters damage tolerance/repair test program [AIAA PAPER 87-0792] p 38 A87-33592
- Development and test of the Shuttle/Centaur cryogenic tankage thermal protection system [AIAA PAPER 87-1557] p 43 A87-43073
- Self-regulating heater application to Shuttle/Centaur hydrazine fuel line thermal control [AIAA PAPER 87-1570] p 43 A87-43081
- Control considerations for high frequency, resonant, power processing equipment used in large systems [NASA-TM-89926] p 64 N87-23690
- Resonant AC power system proof-of-concept test program [NASA-CR-175069-VOL-1] p 129 N87-29738
- Resonant AC power system proof-of-concept test program, volume 2, appendix 1 [NASA-CR-175069-VOL-2] p 130 N87-29739
- General Electric Co., Cincinnati, Ohio.**
- Evaluation of capillary reinforced composites for anti-icing [AIAA PAPER 87-0023] p 17 A87-24904
- Aerodynamic instability performance of an advanced high-pressure-ratio compression component [AIAA PAPER 86-1619] p 5 A87-41157
- Dynamic data acquisition, reduction, and analysis for the identification of high-speed compressor component post-stability characteristics [AIAA PAPER 87-2089] p 162 A87-45398
- Free jet feasibility study of a thermal acoustic shield concept for AST/VCE application: Dual stream nozzles [NASA-CR-3867] p 210 N87-10752
- Free-jet acoustic investigation of high-radius-ratio conical plug nozzles [NASA-CR-3818] p 210 N87-10753
- Thermal barrier coating life prediction model [NASA-CR-179504] p 100 N87-13539
- Thermal barrier coating life prediction model [NASA-CR-175010] p 100 N87-13540
- Simulated flight acoustic investigation of treated ejector effectiveness on advanced mechanical suppressors for high velocity jet noise reduction [NASA-CR-4019] p 211 N87-17481
- Development of a rotor wake/vortex model. Volume 2: User's manual for computer program [NASA-CR-174850-VOL-2] p 13 N87-20239
- Development of gas-to-gas lift pad dynamic seals, volumes 1 and 2 [NASA-CR-179486] p 168 N87-22245
- Elevated temperature crack growth [NASA-CR-179601] p 184 N87-22267
- Aviation fuel property effects on altitude relight [NASA-CR-179582] p 107 N87-24578
- Advanced Propan Engine Technology (APET) and single-rotation gearbox/pitch change mechanism [NASA-CR-168113] p 32 N87-28553
- Free-jet investigation of mechanically suppressed, high radius ratio conical plug model nozzles [NASA-CR-3596] p 212 N87-29315
- Aerodynamic performance investigation of advanced mechanical suppressor and ejector nozzle concepts for jet noise reduction [NASA-CR-174860] p 33 N87-29534
- Turbofan aft duct suppressor study. Contractor's data report of mode probe signal data [NASA-CR-175067] p 34 N87-29538
- Turbofan aft duct suppressor study [NASA-CR-175067] p 34 N87-29539
- General Electric Co., Evendale, Ohio.**
- Improved consolidation of silicon carbide p 94 A87-12940
- NASA/GE advanced low emissions combustor program [AIAA PAPER 87-2035] p 21 A87-45369
- A variable geometry combustor for broadened properties fuels [AIAA PAPER 87-1832] p 23 A87-52246
- General Electric Co., Fairfield, Conn.**
- A model propulsion simulator for evaluating counter rotating blade characteristics [SAE PAPER 861715] p 20 A87-32607
- Effects of surface chemistry on hot corrosion life p 88 N87-11193
- General Electric Co., Lynn, Mass.**
- Ceramic high pressure gas path seal [NASA-CR-180813] p 31 N87-26914
- General Electric Co., Schenectady, N.Y.**
- Dynamic data acquisition, reduction, and analysis for the identification of high-speed compressor component post-stability characteristics [AIAA PAPER 87-2089] p 162 A87-45398
- Advanced optical smoke meters for jet engine exhaust measurement [NASA-CR-179459] p 155 N87-12829
- General Electric Co., Syracuse, N.Y.**
- Microwave performance of a quarter-micrometer gate low-noise pseudomorphic InGaAs/AlGaAs modulation-doped field effect transistor p 121 A87-23745
- General Motors Corp., Detroit, Mich.**
- Turbine airfoil gas side heat transfer p 144 N87-11219
- General Motors Corp., Indianapolis, Ind.**
- An unconditionally-stable central differencing scheme for high Reynolds number flows [AIAA PAPER 87-0060] p 133 A87-24912
- Development and evaluation of improved numerical schemes for recirculating flows [AIAA PAPER 87-0061] p 134 A87-24913
- Slow crack growth in sintered silicon nitride p 98 A87-48989
- Advanced Gas Turbine (AGT) Technology Project [NASA-CR-179484] p 164 N87-11995
- Turbine vane external heat transfer. Volume 2. Numerical solutions of the Navier-Stokes equations for two- and three-dimensional turbine cascades with heat transfer [NASA-CR-174828] p 145 N87-13661
- Advanced Propan Engine Technology (APET) definition study, single and counter-rotation gearbox/pitch change mechanism design [NASA-CR-168115] p 32 N87-28554
- General Motors Research Labs., Warren, Mich.**
- A universal equation of state for solids p 219 A87-14665
- Compressibility of solids p 219 A87-51962
- Georgia Inst. of Tech., Atlanta.**
- Notes and comments on computational elastoplasticity - Some new models and their numerical implementation p 173 A87-10893
- Optimization of spherical facets for parabolic solar concentrators p 213 A87-18173
- Bounding solutions of geometrically nonlinear viscoelastic problems p 174 A87-20892
- Concentration of carbon dioxide by a high-temperature electrochemical membrane cell p 77 A87-27400
- Thermodynamically consistent constitutive equations for nonisothermal large-strain, elastoplastic, creep behavior p 175 A87-27945
- Yielding and deformation behavior of the single crystal superalloy PWA 1480 p 84 A87-32040
- Solution methods for one-dimensional viscoelastic problems [AIAA PAPER 87-0804] p 176 A87-33604
- Non-isothermal elastoviscoplastic snap-through and creep buckling of shallow arches [AIAA PAPER 87-0806] p 176 A87-33605
- A technique for the prediction of airfoil flutter characteristics in separated flow [AIAA PAPER 87-0910] p 177 A87-33719
- Analysis of viscous transonic flow over airfoil sections [AIAA PAPER 87-0420] p 4 A87-34723
- Measurement techniques for millimeter wave substrate mounted MMW antennas p 121 A87-40926
- Measurement techniques for millimeter wave substrate mounted MMW antennas p 123 A87-45899
- High temperature monotonic and cyclic deformation in a directionally solidified nickel-base superalloy [NASA-CR-175101] p 90 N87-15303
- Feasibility analysis of reciprocating magnetic heat pumps [NASA-CR-180262] p 147 N87-19647
- Analysis of shell-type structures subjected to time-dependent mechanical and thermal loading [NASA-CR-180349] p 183 N87-19756
- Nonisothermal elasto-visco-plastic response of shell-type structures p 185 N87-22796
- Technology for satellite power conversion [NASA-CR-181057] p 66 N87-25420
- Studies of unsteady viscous flows using a two-equation model of turbulence [NASA-CR-181293] p 152 N87-27949
- Thermo-elasto-viscoplastic analysis of problems in extension and shear [NASA-CR-181410] p 187 N87-29896
- The dynamic aspects of thermo-elasto-viscoplastic snap-through and creep buckling phenomena [NASA-CR-181411] p 187 N87-29897
- Georgia Tech Research Inst., Atlanta.**
- Technology for satellite power conversion [NASA-CR-180162] p 193 N87-18229
- Giner, Inc., Waltham, Mass.**
- Oxygen electrodes for rechargeable alkaline fuel cells p 199 N87-29940
- Goodrich (B. F.) Co., Brecksville, Ohio.**
- Styrene-terminated polysulfone oligomers as matrix material for graphite reinforced composites - An initial study p 98 A87-49370
- Gougeon Bros., Inc., Bay City, Mich.**
- Design of an advanced wood composite rotor and development of wood composite blade technology [NASA-CR-174713] p 73 N87-17861
- Grumman Aerospace Corp., Bethpage, N.Y.**
- Solar dynamic space power system heat rejection p 47 A87-18175
- Particle trajectory computer program for icing analysis of axisymmetric bodies - A progress report [AIAA PAPER 87-0027] p 15 A87-22366
- Grumman Data Systems Corp., Bethpage, N.Y.**
- Particle trajectory computer program for icing analysis of axisymmetric bodies - A progress report [AIAA PAPER 87-0027] p 15 A87-22366
- GT-Devices, Alexandria, Va.**
- Experiments on a repetitively pulsed electrothermal thruster [AIAA PAPER 87-1043] p 50 A87-38017
- Investigation of a repetitively pulsed electrothermal thruster [NASA-CR-179464] p 59 N87-16878
- GTE Labs., Inc., Waltham, Mass.**
- A comparative study of the influence of buoyancy driven fluid flow on GaAs crystal growth p 219 N87-28741

H

- Hamilton Standard, Windsor Locks, Conn.**
- Results of acoustic tests of a Prop-Fan model [AIAA PAPER 87-1894] p 209 A87-45282
- Effect of angular inflow on the vibratory response of a counter-rotating propeller [NASA-CR-174819] p 8 N87-10840
- Expansion of epicyclic gear dynamic analysis program [NASA-CR-179563] p 166 N87-19723
- Unstalled flutter stability predictions and comparisons to test data for a composite prop-fan model [NASA-CR-179512] p 28 N87-21955
- Dynamic response and stability of a composite prop-fan model [NASA-CR-179528] p 28 N87-21956
- Dynamic response of two composite prop-fan models on a nacelle/wing/fuselage half model [NASA-CR-179589] p 18 N87-23615
- Hamilton Standard Div., United Aircraft Corp., Windsor Locks, Conn.**
- Static tests of the propulsion system [AIAA PAPER 87-1728] p 23 A87-52245
- Harris Corp., Melbourne, Fla.**
- Optimization of spherical facets for parabolic solar concentrators p 213 A87-18173
- Thermal expansion behavior of graphite/glass and graphite/magnesium p 72 A87-38615
- Harris Government Aerospace Systems Div., Melbourne, Fla.**
- Solar concentrator materials development p 213 A87-18171
- Honeywell, Inc., Bloomington, Minn.**
- 30 GHz monolithic balanced mixers using an ion-implanted FET-compatible 3-inch GaAs wafer process technology p 121 A87-34525
- Houston Univ., Tex.**
- Coherent structures and turbulence p 133 A87-22859
- A model for fluid flow during saturated boiling on a horizontal cylinder p 139 A87-41173
- Transition boiling heat transfer and the film transition regime p 143 A87-53589
- Howard Univ., Washington, D. C.**
- Observation of deep levels in cubic silicon carbide p 122 A87-41089
- Howmet Turbine Components Corp., White Hall, Mich.**
- Thermal stability of the nickel-base superalloy B-1900 + Hf with tantalum variations p 87 A87-51289

- Hughes Aircraft Co., El Segundo, Calif.**
RCS of a coated circular waveguide terminated by a perfect conductor p 112 A87-42536
- Hughes Aircraft Co., Los Angeles, Calif.**
Modeling of environmentally induced transients within satellites
[AIAA PAPER 85-0387] p 42 A87-41611
Environmentally-induced discharge transient coupling to spacecraft
[NASA-CR-174922] p 43 N87-10946
- Hughes Aircraft Co., Torrance, Calif.**
A 30-GHz monolithic receiver p 121 A87-23953
- Hughes Research Labs., Malibu, Calif.**
Cycle life of nickel-hydrogen cells. II - Accelerated cycle life test p 46 A87-18104
Plasma properties in electron-bombardment ion thrusters
[AIAA PAPER 87-1076] p 51 A87-41135
Status of xenon ion propulsion technology
[AIAA PAPER 87-1003] p 53 A87-48677
KOH concentration effect on cycle life of nickel-hydrogen cells p 199 N87-29920

- IBM Federal Systems Div., Gaithersburg, Md.**
Microstrip dispersion including anisotropic substrates p 123 A87-47621

- IGI Consulting, Inc., Boston, Mass.**
US long distance fiber optic networks: Technology, evolution and advanced concepts. Volume 1: Executive summary
[NASA-CR-179479] p 113 N87-11056
US long distance fiber optic networks: Technology, evolution and advanced concepts. Volume 2: Fiber optic technology and long distance networks
[NASA-CR-179480] p 113 N87-11057
US long distance fiber optic networks: Technology, evolution and advanced concepts. Volume 3: Advanced networks and economics
[NASA-CR-179481] p 114 N87-11915

- Illinois Univ., Chicago.**
The formation of volatile corrosion products during the mixed oxidation-chlorination of cobalt at 650 C p 82 A87-23848
A new formulation of electromagnetic wave scattering using an on-surface radiation boundary condition approach p 112 A87-32829
Elastic interaction of a crack with a microcrack array. I - Formulation of the problem and general form of the solution. II - Elastic solution for two crack configurations (piecewise constant and linear approximations) p 178 A87-36926
The finite-difference time-domain (FD-TD) method for electromagnetic scattering and interaction problems p 113 A87-51403
New generation methods for spur, helical, and spiral-bevel gears p 164 A87-53420
Generation of spiral bevel gears with conjugate tooth surfaces and tooth contact analysis
[NASA-CR-4088] p 169 N87-26356

- Illinois Univ., Urbana.**
Proposal for superstructure based high efficiency photovoltaics p 120 A87-19104
Microwave performance of a quarter-micrometer gate low-noise pseudomorphic InGaAs/AlGaAs modulation-doped field effect transistor p 121 A87-23745
Characterization of InGaAs/AlGaAs pseudomorphic modulation-doped field-effect transistors p 121 A87-23922
Radar cross section of an open-ended circular waveguide Calculation of second-order diffraction terms p 112 A87-31626
Nondestructive evaluation of adhesive bond strength using the stress wave factor technique p 170 A87-32200
New simple feed network for an array module of four microstrip elements p 122 A87-41638
RCS of a coated circular waveguide terminated by a perfect conductor p 112 A87-42536
Rays versus modes - Pictorial display of energy flow in an open-ended waveguide p 112 A87-44075

- Illinois Univ., Urbana-Champaign.**
The study of microstrip antenna arrays and related problems
[NASA-CR-179714] p 113 N87-10225
A study of reduced chromium content in a nickel-base superalloy via element substitution and rapid solidification processing
[NASA-CR-179631] p 92 N87-25456
Reduction of the radar cross section of arbitrarily shaped cavity structures
[NASA-CR-180307] p 118 N87-27085

- Computer modelling of aluminum-gallium arsenide/gallium arsenide multilayer photovoltaics
[NASA-CR-181418] p 200 N87-29957
Modelling of multijunction cascade photovoltaics for space applications
[NASA-CR-181417] p 200 N87-29958
- Imperial Coll. of Science and Technology, London (England).**
Generation of Tollmien-Schlichting waves on interactive marginally separated flows p 144 A87-54365
- Indian Inst. of Science, Bangalore.**
A higher order theory of laminated composite cylindrical shells p 177 A87-35656
- Indian Inst. of Tech., Madras.**
Performance studies on an axial flow compressor stage p 138 A87-37208
- Indiana Univ., Indianapolis.**
Three dimensional boundary layers in internal flows
[NASA-CR-181336] p 152 N87-28860
- Instituto de Estudos Avancados, Sao Jose dos Campos (Brazil).**
Heat transfer in the stagnation region of the junction of a circular cylinder perpendicular to a flat plate p 131 A87-13019
- International Fuel Cells Corp., South Windsor, Conn.**
Advanced technology for extended endurance alkaline fuel cells p 190 A87-33787
Regenerative fuel cell study for satellites in GEO orbit
[NASA-CR-179609] p 198 N87-27324
- International Telecommunications Satellite Organization, El Segundo, Calif.**
20-GHz phased-array-fed antennas utilizing distributed MMIC modules p 112 A87-34527
- Iowa State Univ. of Science and Technology, Ames.**
A universal equation of state for solids p 219 A87-14665

- Iowa Univ., Iowa City.**
Finite analytic numerical solution of two-dimensional channel flow over a backward-facing step p 131 A87-13506
Measurements of plasma parameters in the vicinity of the Space Shuttle p 200 A87-24672
Measurements of plasma density and turbulence near the shuttle orbiter
[NASA-CR-180102] p 215 N87-16614
- ISTAR, Inc., Santa Monica, Calif.**
Detonation wave compression in gas turbines
[NASA-CR-179557] p 25 N87-13443

J

- Jet Propulsion Lab., California Inst. of Tech., Pasadena.**
Structure and tensile strength of LaS(1,4) p 96 A87-38065
Nuclear reactor power for a space-based radar. SP-100 project
[NASA-TM-89295] p 213 N87-25838
- John Carroll Univ., Cleveland, Ohio.**
Linear capacitive displacement sensor with frequency readout p 154 A87-42546
- John Deere Technologies International, Inc., Wood-Ridge, N.J.**
Advanced liquid-cooled, turbocharged and intercooled stratified charge rotary engines for aircraft
[SAE PAPER 871039] p 22 A87-48766

K

- Kent State Univ., Ohio.**
On the symbolic manipulation and code generation for elastoplastic material matrices p 201 A87-18499
- Kohlman Systems Research, Inc., Lawrence, Kans.**
Flight test report of the NASA icing research airplane: Performance, stability, and control after flight through natural icing conditions
[NASA-CR-179515] p 34 N87-11797

L

- Life Systems, Inc., Cleveland, Ohio.**
Alkaline water electrolysis technology for Space Station regenerative fuel cell energy storage p 46 A87-18107
- Lockheed-Georgia Co., Marietta.**
High speed wind tunnel tests of the PTA aircraft
[SAE PAPER 861744] p 4 A87-32619
Acoustic power measurement for single and annular stream duct-nozzle systems utilizing a modal decomposition scheme p 209 A87-37628
Sound radiation from single and annular stream nozzles, with modal decomposition of in-duct acoustic power p 209 A87-37629

- Wind tunnel tests on a one-foot diameter SR-7L propan model
[AIAA PAPER 87-1892] p 6 A87-45281
Static tests of the propulsion system
[AIAA PAPER 87-1728] p 23 A87-52245
PTA test bed aircraft engine inlet model test report, revised
[NASA-CR-174845] p 23 N87-10866
Propan test assessment testbed aircraft flutter model test report
[NASA-CR-179458] p 14 N87-29413
Propan test assessment propan propulsion system static test report
[NASA-CR-179613] p 33 N87-29536
- Lockheed Missiles and Space Co., Huntsville, Ala.**
An adaptive finite element strategy for complex flow problems
[AIAA PAPER 87-0557] p 133 A87-22706
- Los Alamos National Lab., N. Mex.**
Numerical modeling of on-orbit propellant motion resulting from an impulsive acceleration
[AIAA PAPER 87-1766] p 40 A87-48573
Some plane curvature approximations p 204 A87-49821
Nuclear reactor power for a space-based radar. SP-100 project
[NASA-TM-89295] p 213 N87-25838
- Louisiana State Univ., Baton Rouge.**
Shock-tube pyrolysis of acetylene - Sensitivity analysis of the reaction mechanism for soot formation p 75 A87-12598
Empirical modeling of soot formation in shock-tube pyrolysis of aromatic hydrocarbons p 76 A87-12599

M

- M/A-COM, Inc., Burlington, Mass.**
The 60 GHz IMPATT diode development
[NASA-CR-179536] p 218 N87-17515
- MARC Analysis Research Corp., Palo Alto, Calif.**
The NESSUS finite element code p 184 N87-22785
- Martin Marietta Aerospace, Denver, Colo.**
On-orbit cryogenic storage and resupply p 41 A87-18344
Propulsion recommendations for space station free flying platforms p 67 N87-26129
- Martin Marietta Corp., Denver, Colo.**
Propulsion recommendations for Space Station free flying platforms p 49 A87-31134
- Massachusetts Inst. of Tech., Cambridge.**
KI-solutions for single edge notch specimens under fixed end displacements p 174 A87-15798
Rotor wake characteristics of a transonic axial-flow fan p 2 A87-20886
In-flight measurement of ice growth on an airfoil using an array of ultrasonic transducers
[AIAA PAPER 87-0178] p 15 A87-22464
Enhanced current flow through a plasma cloud by induction of plasma turbulence
[AIAA PAPER 87-0573] p 214 A87-22714
Radiation from large space structures in low earth orbit with induced arc currents
[AIAA PAPER 87-0612] p 42 A87-22738
A computerized test system for thermal-mechanical fatigue crack growth p 153 A87-23899
Anticorrelation of Shubnikov-deHaas amplitudes and negative magnetoresistance magnitudes in intercalated pitch based graphite fibers p 217 A87-28295
A versatile and low order hybrid stress element for general shell geometry
[AIAA PAPER 87-0840] p 176 A87-33624
Dendritic growth of undercooled nickel-tin. I, II p 85 A87-41012
Theory of plasma contactors used in the ionosphere p 122 A87-41610
The radiation impedance of an electrodynamic tether with end connectors p 42 A87-42585
Comparison of wet and dry growth in artificial and flight icing conditions p 16 A87-45635
The alloy undercooling experiment on the Columbia STS 61-C Space Shuttle mission
[AIAA PAPER 87-0506] p 108 A87-45724
Rotational effects on impingement cooling p 141 A87-45838
Enhanced current flow through a plasma cloud by induction of plasma turbulence p 214 A87-48241
Thermal-mechanical fatigue crack growth in B-1900+Hf p 86 A87-49570
Processing of laser formed SiC powder
[NASA-CR-179857] p 99 N87-11009
The mathematical modeling of rapid solidification processing
[NASA-CR-179551] p 88 N87-13514

- Modes of vibration on square fiberglass epoxy composite thick plate
[NASA-CR-4018] p 171 N87-13779
- Ultrasonic determination of the elastic constants of the stiffness matrix for unidirectional fiberglass epoxy composites
[NASA-CR-4034] p 171 N87-13781
- Parameterized materials and dynamic response characterizations in unidirectional composites
[NASA-CR-4032] p 172 N87-13782
- A study of the microstructure of a rapidly solidified nickel-base superalloy modified with boron
[NASA-CR-179553] p 89 N87-14486
- A linearized Euler analysis of unsteady flows in turbomachinery
[NASA-CR-180987] p 149 N87-22948
- Processing of laser formed SiC powder
[NASA-CR-179638] p 104 N87-24573
- One-dimensional wave propagation in rods of variable cross section: A WKBJ solution
[NASA-CR-4086] p 172 N87-24707
- Acousto-ultrasonic input-output characterization of unidirectional fiber composite plate by SH waves
[NASA-CR-4087] p 173 N87-26361
- Maxwell Labs., Inc., San Diego, Calif.**
Ram ion scattering caused by Space Shuttle v x B induced differential charging p 200 N87-51713
- Mechanical Technology, Inc., Latham, N. Y.**
Evaluation of Stirling engine appendix gap losses
Mod II engine performance p 160 N87-18037
- [SAE PAPER 870101] p 163 N87-48780
- Automotive Stirling engine system component review
[SAE PAPER 870102] p 163 N87-48781
- Fatigue life of laser cut metals
[NASA-CR-179501] p 164 N87-11158
- Ceramic automotive Stirling engine program
[NASA-CR-175042] p 192 N87-12047
- Automotive Stirling engine development program
[NASA-CR-174972] p 221 N87-20137
- EHD analysis of and experiments on pumping Leningrader seals
[NASA-CR-179570] p 168 N87-22246
- Automotive Stirling Engine Development Program
[NASA-CR-174873] p 222 N87-30223
- Medical Coll. of Ohio, Toledo.**
Specimen geometry effects on graphite/PMR-15 composites under thermo-oxidative aging p 71 N87-13145
- Metallurgical and Engineering Consultants Ltd., Ranchi (India).**
Effect of 15 MPa hydrogen on creep-rupture properties of iron-base superalloys p 86 N87-49558
- Michigan State Univ., East Lansing.**
Microwave electrothermal thruster performance in helium gas p 49 N87-31281
- A review of research and development on the microwave-plasma electrothermal rocket
[AIAA PAPER 87-1011] p 49 N87-38008
- A computer model for the recombination zone of a microwave-plasma electrothermal rocket
[AIAA PAPER 87-1014] p 50 N87-38009
- An analysis of electromagnetic coupling and eigenfrequencies for microwave electrothermal thruster discharges
[AIAA PAPER 87-1012] p 51 N87-41111
- Microstructure-derived macroscopic residual resistance of brominated graphite fibers p 97 N87-48324
- A critical analysis of transverse vorticity measurements in a large plane shear layer p 143 N87-52049
- Iptycenes - Extended triptycenes p 69 N87-53654
- Triptycene - A D(3h) C(62) hydrocarbon with three U-shaped cavities p 69 N87-53656
- Michigan Technological Univ., Houghton.**
Further observations of SCC in alpha-beta brass
Considerations regarding the appearance of crack arrest markings during SCC p 82 N87-23843
- The effects of tantalum on the microstructure of two polycrystalline nickel-base superalloys - B-1900 + Hf and MAR-M247 p 82 N87-24110
- Thermal stability of the nickel-base superalloy B-1900 + Hf with tantalum variations p 87 N87-51289
- A point defect model for nickel electrode structures p 87 N87-52282
- An investigation of the dynamic response of spur gear teeth with moving loads
[NASA-CR-179643] p 170 N87-29840
- Michigan Univ., Ann Arbor.**
Particle-laden swirling free jets - Measurements and predictions
[AIAA PAPER 87-0303] p 139 N87-42648
- On optimal design for the blade-root/hub interface in jet engines p 24 N87-11769
- Microsemi Corp., Torrance, Calif.**
Space station power semiconductor package
[NASA-CR-180829] p 129 N87-28825

- Minnesota Univ., Minneapolis.**
Development and evaluation of improved numerical schemes for recirculating flows
[AIAA PAPER 87-0061] p 134 N87-24913
- Spanwise structures in transitional flow around circular cylinders
[AIAA PAPER 87-1383] p 140 N87-44940
- Heat transfer and fluid mechanics measurements in transitional boundary layers on convex-curved surfaces
[ASME PAPER 85-MT-60] p 143 N87-48726
- Mississippi State Univ., Mississippi State.**
Three-dimensional unsteady Euler solutions for propfans and counter-rotating propfans in transonic flow
[AIAA PAPER 87-1197] p 5 N87-42314
- Missouri Univ., Rolla.**
Modeling the effects of wind tunnel wall absorption on the acoustic radiation characteristics of propellers
[AIAA PAPER 86-1876] p 208 N87-17991
- Motorola, Inc., Phoenix, Ariz.**
ACTS baseband processing p 201 N87-45512
- Motorola, Inc., Scottsdale, Ariz.**
Baseband processor development/test performance for 30/20 GHz SS-TDMA communication system p 111 N87-18310

N

- National Aeronautics and Space Administration, Washington, D.C.**
The NASA Electric Propulsion Program
[AIAA PAPER 87-1098] p 53 N87-45795
- National Aeronautics and Space Administration, Ames Research Center, Moffett Field, Calif.**
Folding tilt rotor demonstrator feasibility study p 17 N87-19247
- National Aeronautics and Space Administration, Lyndon B. Johnson Space Center, Houston, Tex.**
Manned spacecraft electrical power systems p 49 N87-37291
- National Aeronautics and Space Administration, Langley Research Center, Hampton, Va.**
The effects of engine speed and injection characteristics on the flow field and fuel/air mixing in motored two-stroke diesel engines
[AIAA PAPER 87-0227] p 161 N87-22501
- Thermal expansion behavior of graphite/glass and graphite/magnesium p 72 N87-38615
- Numerical simulation of the flow field and fuel sprays in an IC engine
[SAE PAPER 870599] p 143 N87-48751
- Multiphase CARS measurements in turbulent combustion p 79 N87-23808
- National Aeronautics and Space Administration, Marshall Space Flight Center, Huntsville, Ala.**
Application of single crystal superalloys for earth-to-orbit propulsion systems
[AIAA PAPER 87-1976] p 85 N87-45336
- The alloy undercooling experiment on the Columbia STS 61-C Space Shuttle mission
[AIAA PAPER 87-0506] p 108 N87-45724
- National Aerospace Lab., Kakuda (Japan).**
Volume-energy parameters for heat transfer to supercritical fluids p 137 N87-32326
- National Bureau of Standards, Boulder, Colo.**
Volume-energy parameters for heat transfer to supercritical fluids p 137 N87-32326
- National Bureau of Standards, Gaithersburg, Md.**
Viscometer for low frequency, low shear rate measurements p 153 N87-13878
- Low-gravity experiments in critical phenomena p 107 N87-23159
- National Bureau of Standards, Washington, D.C.**
Shock-tube pyrolysis of acetylene - Sensitivity analysis of the reaction mechanism for soot formation p 75 N87-12598
- National Chiao Tung Univ., Hsinchu (Taiwan).**
New generation methods for spur, helical, and spiral-bevel gears p 164 N87-53420
- Naval Postgraduate School, Monterey, Calif.**
Comparison of calculated and experimental cascade performance for controlled-diffusion compressor stator blading
[ASME PAPER 86-GT-35] p 19 N87-25394
- Naval Research Lab., Washington, D.C.**
Systematic development of reduced reaction mechanisms for dynamic modeling p 77 N87-33987
- Naval Ship Research and Development Center, Annapolis, Md.**
On similarity solutions for turbulent and heated round jets p 130 N87-10922
- Nebraska Univ., Lincoln.**
Effects of non-spherical drops on a phase Doppler spray analyzer p 152 N87-11048
- Variable angle of incidence spectroscopic ellipsometry Application to GaAs-Al(x)Ga(1-x)As multiple heterostructures p 216 N87-20519
- Thermal and structural stability of cosputtered amorphous Ta(x)Cu(1-x) alloy thin films on GaAs p 216 N87-27198
- Anticorrelation of Shubnikov-deHaas amplitudes and negative magnetoresistance magnitudes in intercalated pitch based graphite fibers p 217 N87-28295
- Interactions of amorphous Ta(x)Cu(1-x) (x = 0.93 and 0.80) alloy films with Au overlayers and GaAs substrates p 217 N87-44562
- Temperature dependence (4K to 300K) of the electrical resistivity of methane grown carbon fibers p 97 N87-47375

Nevada Univ., Las Vegas.

- The temperature dependence of inelastic light scattering from small particles for use in combustion diagnostic instrumentation
[NASA-CR-180399] p 80 N87-28634

Nielsen Engineering and Research, Inc., Mountain View, Calif.

- Development of a turbomachinery design optimization procedure using a multiple-parameter nonlinear perturbation method
[NASA-CR-3831] p 1 N87-10003

Northwestern Univ., Evanston, Ill.

- A new formulation of electromagnetic wave scattering using an on-surface radiation boundary condition approach p 112 N87-32829
- A probabilistic Hu-Washizu variational principle
[AIAA PAPER 87-0764] p 176 N87-33579
- The finite-difference time-domain (FD-TD) method for electromagnetic scattering and interaction problems p 113 N87-51403
- Probabilistic finite elements p 185 N87-22790
- A simplified computer solution for the flexibility matrix of contacting teeth for spiral bevel gears
[NASA-CR-179620] p 168 N87-23977
- A computer solution for the dynamic load, lubricant film thickness and surface temperatures in spiral bevel gears
[NASA-CR-4077] p 169 N87-26358
- Variational approach to probabilistic finite elements
[NASA-CR-181343] p 206 N87-29212

O

Ohio State Univ., Columbus.

- Three-dimensional vibrations of twisted cantilevered parallelepipeds p 173 N87-11106
- SML adaptive antenna arrays for weak interfering signals p 111 N87-20818
- Starvation effects on the hydrodynamic lubrication of rigid nonconformal contacts in combined rolling and normal motion p 135 N87-27839
- Oxygen-18 tracer study of the passive thermal oxidation of silicon p 78 N87-51187
- An experimental study of the aerodynamics of a NACA 0012 airfoil with a simulated glaze ice accretion
[NASA-CR-179897] p 8 N87-11701
- Alternative mathematical programming formulations for FSS synthesis
[NASA-CR-180030] p 202 N87-14872
- Engineering calculations for communications satellite systems planning
[NASA-CR-180106] p 114 N87-16198
- On orbital allotments for geostationary satellites
[NASA-CR-181017] p 37 N87-22700
- Engineering calculations for communications satellite systems planning
[NASA-CR-181112] p 117 N87-24605
- A satellite system synthesis model for orbital arc allotment optimization
[NASA-CR-181150] p 37 N87-25341
- Mathematical programming formulations for satellite synthesis
[NASA-CR-181151] p 44 N87-25419
- Wind tunnel evaluation of a truncated NACA 64-621 airfoil for wind turbine applications
[NASA-CR-180803] p 196 N87-25621
- The design and analysis of single flank transmission error tester for loaded gears
[NASA-CR-179621] p 169 N87-27197
- Optimization of orbital assignment and specification of service areas in satellite communications
[NASA-CR-181273] p 118 N87-27882
- SML adaptive antenna arrays for weak interfering signals
[NASA-CR-181330] p 119 N87-28813
- Adaptive arrays for weak interfering signals: An experimental system
[NASA-CR-181181] p 119 N87-28814
- Transonic interference reduction by limited ventilation wall panels
[NASA-CR-175039] p 15 N87-29419

- Design, implementation and investigation of an image guide-based optical flip-flop array
[NASA-CR-181382] p 213 N87-30180
- Oklahoma State Univ., Stillwater.**
Two opposed lateral jets injected into swirling crossflow
[AIAA PAPER 87-0307] p 132 A87-22549
Multi-spark visualization of typical combustor flowfields
p 134 A87-25281

- Oregon State Univ., Corvallis.**
An assessment and validation study of nuclear reactors for low power space applications
[NASA-CR-180672] p 213 N87-27495

P

- Page (R. J.) Co., Santa Ana, Calif.**
A design study of hydrazine and biowaste resistojets
[NASA-CR-179510] p 57 N87-14425
- Paragon Pacific, Inc., El Segundo, Calif.**
WEST-3 wind turbine simulator development. Volume 1: Summary
[NASA-CR-174981] p 192 N87-11348
- Paragon Pacific, Inc., Torrance, Calif.**
WEST-3 wind turbine simulator development. Volume 2: Verification
[NASA-CR-174982] p 191 N87-10531
WEST-3 wind turbine simulator development
[NASA-CR-174983] p 192 N87-12046
- Pennsylvania State Univ., State College.**
Friction and wear behaviour of ion beam modified ceramics
p 97 A87-47958
The measurement of boundary layers on a compressor blade in cascade at high positive incidence angle. 1: Experimental techniques and results
[NASA-CR-179491] p 25 N87-13441
The measurement of boundary layers on a compressor blade in cascade at high positive incidence angle. 2: Data report
[NASA-CR-179492] p 25 N87-13442

- Pennsylvania State Univ., University Park.**
Shock-tube pyrolysis of acetylene - Sensitivity analysis of the reaction mechanism for soot formation
p 75 A87-12598
Turbulence modeling for complex shear flows
p 133 A87-23653
Systematic development of reduced reaction mechanisms for dynamic modeling
p 77 A87-33987
The hub wall boundary layer development and losses in an axial flow compressor rotor passage
p 139 A87-41665
Computation of rotating turbulent flow with an algebraic Reynolds stress model
p 140 A87-43384
An experimental study on the effects of tip clearance on flow field and losses in an axial flow compressor rotor
p 6 A87-46207

- Pittsburgh Univ., Pa.**
Reactions occurring during the sulfation of sodium chloride deposited on alumina substrates
p 76 A87-20223
- Pratt and Whitney Aircraft, East Hartford, Conn.**
Creep fatigue life prediction for engine hot section materials (isotropic): Two year update
p 171 N87-11213
Thermal barrier coating life prediction model development
[NASA-CR-179508] p 99 N87-11892
On 3-D inelastic analysis methods for hot section components (base program)
[NASA-CR-175060] p 180 N87-12923
Creep fatigue life prediction for engine hot section materials (ISOTROPIC)
[NASA-CR-179550] p 181 N87-15491
Creep fatigue life prediction for engine hot section materials (isotropic)
[NASA-CR-174844] p 182 N87-18117
Advanced composite combustor structural concepts program
[NASA-CR-174733] p 74 N87-20387
On 3-D inelastic analysis methods for hot section components. Volume 1: Special finite element models
[NASA-CR-179494] p 185 N87-22996
Antimisting kerosene JT3 engine fuel system integration study
[NASA-CR-4033] p 106 N87-24577
Materials for Advanced Turbine Engines (MATE). Project 4: Erosion resistant compressor airfoil coating
[NASA-CR-179622] p 92 N87-27029
3-D inelastic analysis methods for hot section components. Volume 2: Advanced special functions models
[NASA-CR-179517] p 186 N87-27267

- Pratt and Whitney Aircraft, West Palm Beach, Fla.**
Breadboard RL10-11B low thrust operating mode
[NASA-CR-174914] p 58 N87-15269

- Low heat transfer oxidizer heat exchanger design and analysis
[NASA-CR-179488] p 58 N87-15272
Cryogenic gear technology for an orbital transfer vehicle engine and tester design
[NASA-CR-175102] p 110 N87-19539
Further development of the dynamic gas temperature measurement system. Volume 1: Technical efforts
[NASA-CR-179513-VOL-1] p 157 N87-19686
High heat transfer oxidizer heat exchanger design and analysis
[NASA-CR-179596] p 63 N87-22803
- Pratt and Whitney Aircraft Group, East Hartford, Conn.**
Structural tailoring of advanced turboprops
[AIAA PAPER 87-0753] p 177 A87-33648
Life prediction and constitutive models for engine hot section anisotropic materials
[NASA-CR-179594] p 29 N87-23622
Thin film strain gage development program
[NASA-CR-174707] p 159 N87-28883
- Pratt and Whitney Aircraft Group, West Palm Beach, Fla.**
Oxidizer heat exchangers for rocket engine operation in idle modes
[AIAA PAPER 87-2117] p 52 A87-45418
- Princeton Univ., N. J.**
An LU-SSOR scheme for the Euler and Navier-Stokes equations
[AIAA PAPER 87-0600] p 137 A87-34724
An anemometer for highly turbulent or recirculating flows
p 154 A87-37698
Lower-upper implicit scheme for high-speed inlet analysis
p 6 A87-46781
The oxidation degradation of aromatic compounds
[NASA-CR-180588] p 79 N87-22020

- Purdue Univ., West Lafayette, Ind.**
Measurement of a counter rotation propeller flowfield using a Laser Doppler Velocimeter
[AIAA PAPER 87-0008] p 3 A87-24901
The effect of circumferential aerodynamic detuning on coupled bending-torsion unstalled supersonic flutter
[ASME PAPER 86-GT-100] p 20 A87-25396
Analytical and experimental investigation of mistuning in propfan flutter
[AIAA PAPER 87-0739] p 178 A87-40496
Two component laser velocimeter measurements of turbulence parameters downstream of an axisymmetric sudden expansion
p 139 A87-40703
A panel method for counter rotating propfans
[AIAA PAPER 87-1890] p 21 A87-45279
Aeroelastic control of stability and forced response of supersonic rotors by aerodynamic detuning
p 21 A87-46249
Preliminary performance characterizations of an engineering model multipropellant resistojets for space station application
[AIAA PAPER 87-2120] p 54 A87-50197
Jet engine simulation with water ingestion through compressor
[NASA-CR-179549] p 1 N87-15932
Turbulence characteristics of an axisymmetric reacting flow
[NASA-CR-180697] p 152 N87-27973

R

- Raytheon Co., Waltham, Mass.**
Rectenna Technology Program: Ultra light 2.45 GHz rectenna 20 GHz rectenna
[NASA-CR-179558] p 116 N87-19556
- Rensselaer Polytechnic Inst., Troy, N.Y.**
Heat transfer in the stagnation region of the junction of a circular cylinder perpendicular to a flat plate
p 131 A87-13019
Endwall heat transfer in the junction region of a circular cylinder normal to a flat plate at 30 and 60 degrees from stagnation point of the cylinder
[AIAA PAPER 87-0077] p 132 A87-22398
Shallow $n(+)$ diffusion into InP by an open-tube diffusion technique
p 217 A87-30023
Effects of temperature and hold times on low cycle fatigue of Astroloy
p 85 A87-38541
Annealing of electron damage in mid-IR transmitting fluoride glass
p 99 A87-53652
Solar cells in bulk InP using an open tube diffusion process
p 198 N87-26444
- Rocket Research Corp., Redmond, Wash.**
Performance characterization of a low power hydrazine arcjet
[AIAA PAPER 87-1057] p 50 A87-39634
Low power arcjet life issues
[AIAA PAPER 87-1059] p 50 A87-39635
Experimental study of low Reynolds number nozzles
[AIAA PAPER 87-0992] p 51 A87-41102
Electromagnetic emission experiences using electric

- propulsion systems - A survey
[AIAA PAPER 87-2028] p 54 A87-50195
- Rockwell International Corp., Canoga Park, Calif.**
Electrical power system for the U.S. Space Station
[IAF PAPER 86-37] p 45 A87-16138
Small centrifugal pumps for low-thrust rockets
p 50 A87-39808
Concepts for space maintenance of OTV engines
p 40 A87-41161
Feasibility of mapping velocity flowfields in an SSME powerhead using laser anemometry techniques
[AIAA PAPER 87-1306] p 154 A87-42374
Analysis of experimental shaft seal data for high-performance turbomachines - As for Space Shuttle main engines
p 162 A87-45846

- Concepts for space maintenance of OTV engines
p 37 A87-46000
Composite load spectra for select space propulsion structural components
[NASA-CR-179496] p 55 N87-10176
Enhanced heat transfer combustor technology, subtasks 1 and 2, task C.1
[NASA-CR-179541] p 56 N87-13486
Space station resistojets system requirements and interface definition study
[NASA-CR-179581] p 60 N87-17848
Composite load spectra for select space propulsion structural components
p 63 N87-22793
Space station WP-04 power system. Volume 1: Executive summary
[NASA-CR-179587-VOL-1] p 65 N87-23695
Space station WP-04 power system. Volume 2: Study results
[NASA-CR-179587-VOL-2] p 65 N87-23696
Concepts for space maintenance of OTV engines
p 67 N87-26097

- Rockwell International Corp., Downey, Calif.**
Modeling of multi-rotor torsional vibrations in rotating machinery using substructuring
p 175 A87-28543
- Rohr Industries, Inc., Chula Vista, Calif.**
On self-preserving, variable-density, turbulent free jets
p 130 A87-10920

- Rome Univ. (Italy).**
Quasars as indicators of galactic ages
p 223 A87-26927
- Rose-Hulman Inst. of Tech., Terre Haute, Ind.**
The impact damped harmonic oscillator in free decay
[NASA-TM-89897] p 168 N87-23978

S

- Scientific Research Associates, Inc., Glastonbury, Conn.**
Duct flows with swirl
[AIAA PAPER 87-0247] p 132 A87-22509
Calculation of two- and three-dimensional transonic cascade flow field using the Navier-Stokes equations
p 144 N87-11220
Computation of multi-dimensional viscous supersonic jet flow
[NASA-CR-4020] p 8 N87-13405
Computation of multi-dimensional viscous supersonic flow
[NASA-CR-4021] p 9 N87-13406
- Sikorsky Aircraft, Stratford, Conn.**
A rotorcraft flight/propulsion control integration study
[NASA-CR-179574] p 18 N87-24457
Automated inspection and precision grinding of spiral bevel gears
[NASA-CR-4083] p 169 N87-25578
- SKF Industries, Inc., King of Prussia, Pa.**
Solid lubrication design methodology, phase 2
[NASA-CR-175114] p 221 N87-18470
- Solar Turbines International, San Diego, Calif.**
Fabrication of cooled radial turbine rotor
[NASA-CR-179503] p 25 N87-11789
- Solavolt International, Phoenix, Ariz.**
Design, development and deployment of public service photovoltaic power/load systems for the Gabonese Republic
[NASA-CR-179603] p 195 N87-23030
- Southwest Research Inst., San Antonio, Tex.**
Friction and wear behaviour of ion beam modified ceramics
p 97 A87-47958
Characterization of ion beam modified ceramic wear surfaces using Auger electron spectroscopy
p 98 A87-51304
Probabilistic Structural Analysis Methods (PSAM) for select space propulsion system structural components
p 62 N87-22784

Spectrolab, Inc., Sylmar, Calif.

Further advances in silicon solar cell technology for space application p 188 A87-18074

Spectron Development Labs., Inc., Costa Mesa, Calif.

Visualization of flows in a motored rotary combustion engine using holographic interferometry [AIAA PAPER 86-1557] p 19 A87-21514

Spire Corp., Bedford, Mass.

Indium phosphide hollow homojunction solar cells made by metalorganic chemical vapor deposition p 123 A87-50047

Status of indium phosphide solar cell development at Spire p 197 N87-26440

Stanford Univ., Calif.

An experimental study of the development of longitudinal vortex pairs embedded in a turbulent boundary layer [AIAA PAPER 87-1309] p 139 A87-42376

Simultaneous measurements of two-dimensional velocity and pressure fields in compressible flows through image-intensified detection of laser-induced fluorescence p 143 A87-52320

State Univ. of New York, Buffalo.

Free vibration analysis by BEM using particular integrals p 174 A87-13882

Conforming versus non-conforming boundary elements in three-dimensional elastostatics p 175 A87-22775

State Univ. of New York, Farmingdale.

Particle trajectory computer program for icing analysis of axisymmetric bodies - A progress report [AIAA PAPER 87-0027] p 15 A87-22366

Sverdrup Technology, Inc., Arnold Air Force Station, Tenn.

Three-dimensional unsteady Euler solutions for propfans and counter-rotating propfans in transonic flow [AIAA PAPER 87-1197] p 5 A87-42314

The acoustic experimental investigation of counterrotating propeller configurations [SAE PAPER 87-1031] p 210 A87-48760

Large perturbation flow field analysis and simulation for supersonic inlets [NASA-CR-174676] p 8 N87-10835

Optical strain measurement system development [NASA-CR-179646] p 159 N87-26326

Sverdrup Technology, Inc., Middleburg Heights, Ohio.

Evaluation of icing drag coefficient correlations applied to iced propeller performance prediction [SAE PAPER 87-1033] p 16 A87-48761

High angle of attack hypersonic aerodynamics [AIAA PAPER 87-2548] p 7 A87-49101

Sverdrup Technology, Inc., Cleveland, Ohio.

Testing of a variable-stroke Stirling engine p 160 A87-18036

Three-dimensional trajectory analyses of two drop sizing instruments - PMS OAP and PMS FSSP [AIAA PAPER 87-0180] p 132 A87-22466

Effects of droplet interactions on droplet transport at intermediate Reynolds numbers [AIAA PAPER 87-0137] p 134 A87-24926

High-speed propeller noise predictions - Effects of boundary conditions used in blade loading calculations [AIAA PAPER 87-0525] p 208 A87-24978

A numerical simulation of the inviscid flow through a counterrotating propeller [ASME PAPER 86-GT-138] p 3 A87-25395

Prediction of the structure of fuel sprays in cylindrical combustion chambers p 20 A87-31277

Probabilistic structural analysis to quantify uncertainties associated with turbopump blades [AIAA PAPER 87-0766] p 176 A87-33581

An LU-SSOR scheme for the Euler and Navier-Stokes equations [AIAA PAPER 87-0600] p 137 A87-34724

Composite space antenna structures - Properties and environmental effects p 72 A87-38610

Time-marching solution of incompressible Navier-Stokes equations for internal flow p 138 A87-39450

Euler analysis of transonic propeller flows p 4 A87-39813

Analytical and experimental investigation of mistuning in propfan flutter [AIAA PAPER 87-0739] p 178 A87-40496

Analytical flutter investigation of a composite propfan model [AIAA PAPER 87-0738] p 178 A87-40497

The utilization of parallel processing in solving the inviscid form of the average-passage equation system for multistage turbomachinery [AIAA PAPER 87-1108] p 5 A87-42057

Composite grid and finite-volume LU implicit scheme for turbine flow analysis [AIAA PAPER 87-1129] p 5 A87-42078

Three-dimensional unsteady Euler solutions for propfans and counter-rotating propfans in transonic flow [AIAA PAPER 87-1197] p 5 A87-42314

Particle-laden swirling free jets - Measurements and predictions [AIAA PAPER 87-0303] p 139 A87-42648

Representation of the vaporization behavior of turbulent polydisperse sprays by 'equivalent' monodisperse sprays [AIAA PAPER 87-1954] p 141 A87-45325

Lower-upper implicit scheme for high-speed inlet analysis p 6 A87-46781

An evaluation of metallized propellants based on vehicle performance [AIAA PAPER 87-1773] p 53 A87-47003

Euler analysis of the three-dimensional flow field of a high-speed propeller - Boundary condition effects [ASME PAPER 87-GT-253] p 6 A87-48719

Preliminary aerothermodynamic design method for hypersonic vehicles [AIAA PAPER 87-2545] p 7 A87-49100

Method for the determination of the three dimensional aerodynamic field of a rotor-stator combination in compressible flow [AIAA PAPER 87-1742] p 7 A87-50187

Nuclear powered Mars cargo transport mission utilizing advanced ion propulsion [AIAA PAPER 87-1903] p 53 A87-50191

Analysis of quasi-hybrid solid rocket booster concepts for advanced earth-to-orbit vehicles [AIAA PAPER 87-2082] p 55 A87-52250

Wind tunnel performance results of an aeroelastically scaled 2/9 model of the PTA flight test prop-fan [AIAA PAPER 87-1893] p 8 A87-52251

Effects of droplet interactions on droplet transport at intermediate Reynolds numbers [NASA-CR-179567] p 26 N87-14348

Conceptual definition of a technology development mission for advanced solar dynamic power systems [NASA-CR-179482] p 192 N87-14771

Potential propellant storage and feed systems for space station resistojet propulsion options [NASA-CR-179457] p 59 N87-16065

A multigrid LU-SSOR scheme for approximate Newton iteration applied to the Euler equations [NASA-CR-179524] p 10 N87-16803

A high resolution shock capturing scheme for high Mach number internal flow [NASA-CR-179523] p 10 N87-16804

An LU-SSOR scheme for the Euler and Navier-Stokes equations [NASA-CR-179556] p 11 N87-16806

A Navier-Stokes solver using the LU-SSOR TVD algorithm [NASA-CR-179608] p 13 N87-20243

Optical strain measurement system development, phase 1 [NASA-CR-179619] p 158 N87-22960

The T55-L-712 turbine engine compressor housing refurbishment project [NASA-CR-179624] p 92 N87-23729

Environmental degradation of 316 stainless steel in high temperature low cycle fatigue [NASA-TM-89931] p 185 N87-24007

Decoupled direct method for sensitivity analysis in combustion kinetics [NASA-CR-179636] p 79 N87-24549

Wind tunnel performance results of an aeroelastically scaled 2/9 model of the PTA flight test prop-fan [NASA-TM-89917] p 14 N87-25294

SSME single crystal turbine blade dynamics [NASA-CR-179644] p 186 N87-26384

Syracuse Univ., N. Y.

Grain boundary oxidation and fatigue crack growth at elevated temperatures p 81 A87-19368

Unsteady heat transfer and direct comparison to steady-state measurements in a rotor-wake experiment p 136 A87-30720

Grain boundary oxidation and fatigue crack growth at elevated temperatures [NASA-CR-179529] p 88 N87-11873

Systems Science and Software, La Jolla, Calif.

Three dimensional simulation of the operation of a hollow cathode electron emitter on the Shuttle orbiter p 119 A87-14084

Computer simulation of plasma electron collection by PIX-II p 45 A87-17837

Hollow cathodes as electron emitting plasma contactors Theory and computer modeling [AIAA PAPER 87-0569] p 214 A87-22712

Theory of plasma contactors for electrodynamic tethered satellite systems p 122 A87-41609

T**Technion - Israel Inst. of Tech., Haifa.**

Ignition delay times of cyclopentene oxygen argon

mixtures p 76 A87-12602

Extrapolation methods for divergent oscillatory infinite integrals that are defined in the sense of summability p 204 A87-35575

Extrapolation methods for vector sequences p 203 A87-53631

Tel-Aviv Univ. (Israel).

Coherent motion in excited free shear flows [AIAA PAPER 85-0539] p 135 A87-30281

The evolution of instabilities in the axisymmetric jet. I - The linear growth of disturbances near the nozzle. II - The flow resulting from the interaction between two waves p 138 A87-37256

Temple Univ., Philadelphia, Pa.

Degradation mechanisms of sulfur and nitrogen containing compounds during thermal stability testing of model fuels [AIAA PAPER 87-2039] p 106 A87-45372

Tennessee Univ., Knoxville.

Experiments on thermoacoustic convection heat transfer in gravity and zero-gravity environments [AIAA PAPER 87-1651] p 107 A87-43141

Tennessee Univ. Space Inst., Tullahoma.

Gas flow environmental and heat transfer nonrotating 3D program p 145 N87-11223

Texas A&M Univ., College Station.

Comparison of Hirs' equation with Moody's equation for determining rotordynamic coefficients of annular pressure seals [ASME PAPER 86-TRIB-19] p 161 A87-19529

Experimental and theoretical study of propeller spinner/shank interference [AIAA PAPER 87-0145] p 3 A87-24929

Computational aeroacoustics of propeller noise in the near and far field [AIAA PAPER 87-0254] p 19 A87-24944

Off-design analysis of counter-rotating propeller configurations p 20 A87-27989

Local heat transfer augmentation in channels with two opposite ribbed surfaces p 136 A87-30732

Evaluation of icing drag coefficient correlations applied to iced propeller performance prediction [SAE PAPER 87-1033] p 16 A87-48761

Measurement of heat transfer and pressure drop in rectangular channels with turbulence promoters [NASA-CR-4015] p 146 N87-17003

A comparison of experimental and theoretical results for labyrinth gas seals [NASA-CR-180194] p 166 N87-18096

Experimental rotordynamic coefficient results for teeth-on-rotor and teeth-on-stator labyrinth gas seals p 167 N87-22212

Texas Instruments, Inc., Dallas.

The 20 GHz GaAs monolithic power amplifier module development [NASA-CR-174742] p 124 N87-11104

Texas Univ., Austin.

Shock-tube pyrolysis of acetylene - Sensitivity analysis of the reaction mechanism for soot formation p 75 A87-12598

An adaptive finite element strategy for complex flow problems [AIAA PAPER 87-0557] p 133 A87-22706

Adaptive finite element methods for compressible flow problems p 4 A87-38496

Recent advances in error estimation and adaptive improvement of finite element calculations p 204 A87-41239

Rays versus modes - Pictorial display of energy flow in an open-ended waveguide p 112 A87-44075

Textron Bell Aerospace Co., Buffalo, N. Y.

Space station auxiliary thrust chamber technology [NASA-CR-179552] p 59 N87-16874

The Futures Group, Glastonbury, Conn.

NASA Lewis Research Center Futuring Workshop [NASA-CR-179577] p 206 N87-27475

Thermacore, Inc., Lancaster, Pa.

Heat pipe cooled rocket engines [AIAA PAPER 86-1567] p 48 A87-21516

Toledo Univ., Ohio.

Thermal analysis of an orthotropic engineering body p 173 A87-13496

Image data compression with vector quantization in the transform domain p 111 A87-30775

Efficient numerical simulation of an electrothermal de-icer pad [AIAA PAPER 87-0024] p 137 A87-32190

Approximations to eigenvalues of modified general matrices [AIAA PAPER 87-0947] p 177 A87-33756

Analytical flutter investigation of a composite propfan model [AIAA PAPER 87-0738] p 178 A87-40497

The effect of ambient pressure on the performance of a resistojet

- [AIAA PAPER 87-0991] p 52 A87-42181
Numerical prediction of cold turbulent flow in combustor configurations with different centerbody flame holders
[ASME PAPER 86-WA/HT-50] p 140 A87-43715
An LDA investigation of three-dimensional normal shock-boundary layer interactions in a corner
[AIAA PAPER 87-1369] p 6 A87-44938
An adaptive algorithm for motion compensated color image coding p 113 A87-45466
Numerical simulation of the flow field and fuel sprays in an IC engine
[SAE PAPER 870599] p 143 A87-48751
Toronto Univ. (Ontario).
Solar concentrator materials development p 213 A87-18171
Transmission Research, Inc., Cleveland, Ohio.
The 3600 hp split-torque helicopter transmission
[NASA-CR-174932] p 25 N87-11788
Trinity Coll., Dublin (Ireland).
Noncommutative-geometry model for closed bosonic strings p 207 A87-37542
TRW Electronic Systems Group, Redondo Beach, Calif.
The 20 GHz power GaAs FET development
[NASA-CR-179546] p 124 N87-16972
The 20 GHz spacecraft IMPATT solid state transmitter
[NASA-CR-179545] p 124 N87-17989
Advanced space communications architecture study.
Volume 2: Technical report
[NASA-CR-179592] p 115 N87-18695
Advanced space communications architecture study.
Volume 1: Executive summary
[NASA-CR-179591] p 115 N87-18696
TRW, Inc., Redondo Beach, Calif.
Space power development impact on technology requirements
[IAF PAPER 86-143] p 41 A87-15894
A 30-GHz monolithic receiver p 121 A87-23953
Tufts Univ., Medford, Mass.
Elastic interaction of a crack with a microcrack array. I - Formulation of the problem and general form of the solution. II - Elastic solution for two crack configurations (piecewise constant and linear approximations) p 178 A87-36926
Tulane Univ., New Orleans, La.
Macrocrack interaction with transverse array of microcracks
[NASA-CR-180806] p 186 N87-25607
Tuskegee Inst., Ala.
Rail gun performance and plasma characteristics due to wall ablation p 214 A87-18735

U

- United Technologies Corp., East Hartford, Conn.**
Demonstration of laser speckle system on burner liner cyclic rig
[NASA-CR-179509] p 155 N87-10377
Hot section viewing system
[NASA-CR-174773] p 155 N87-11144
Advanced Prop-fan Engine Technology (APET) single- and counter-rotation gearbox/pitch change mechanism
[NASA-CR-168114-VOL-1] p 32 N87-28552
Advanced Prop-fan Engine Technology (APET) single- and counter-rotation gearbox/pitch change mechanism
[NASA-CR-168114-VOL-2] p 33 N87-28556
United Technologies Corp., Windsor Locks, Conn.
Analysis and test evaluation of the dynamic response and stability of three advanced turboprop models
[NASA-CR-174814] p 32 N87-28555
United Technologies Research Center, East Hartford, Conn.
Long-term deposit formation in aviation turbine fuel at elevated temperature p 106 A87-14986
Soot loading in a generic gas turbine combustor
[AIAA PAPER 87-0297] p 19 A87-22544
Investigation of two-dimensional shock-wave/boundary-layer interactions p 4 A87-39528
Short efficient ejector systems
[AIAA PAPER 87-1837] p 20 A87-45239
Mass and momentum turbulent transport experiments p 144 A87-11201
Assessment of a 3-D boundary layer code to predict heat transfer and flow losses in a turbine p 145 N87-11224
User's manual for a TEACH computer program for the analysis of turbulent, swirling reacting flow in a research combustor
[NASA-CR-179547] p 78 N87-11858
Flowfield measurements in a separated and reattached flat plate turbulent boundary layer
[NASA-CR-4052] p 148 N87-21257
High temperature static strain gage alloy development program

- [NASA-CR-174833] p 157 N87-22179
Advanced high temperature static strain sensor development
[NASA-CR-179520] p 158 N87-25552
High temperature static strain gage development contract, tasks 1 and 2
[NASA-CR-180811] p 159 N87-28869
University of Southern California, Los Angeles.
Nonlinear absorption in AlGaAs/GaAs multiple quantum well structures grown by metalorganic chemical vapor deposition p 217 A87-39687
The design and performance of a multi-stream droplet generator for the liquid droplet radiator
[AIAA PAPER 87-1538] p 140 A87-44842
University of Southern Illinois, Carbondale.
The sensitivity of mechanical properties of TFRS composites to variations in reaction zone size and properties
[AIAA PAPER 87-0757] p 72 A87-33577
University of Western Michigan, Kalamazoo.
Optimization and analysis of gas turbine engine blades
[AIAA PAPER 87-0827] p 201 A87-33614
Utah Univ., Salt Lake City.
Multigrid-sinc methods p 205 A87-52865

V

- Varian Associates, Palo Alto, Calif.**
High-efficiency GaAs solar concentrator cells for space and terrestrial applications p 188 A87-18073
High-efficiency GaAs concentrator space cells p 196 N87-26417
Virginia Polytechnic Inst. and State Univ., Blacksburg.
Two- and three-dimensional viscous computations of a hypersonic inlet flow
[AIAA PAPER 87-0283] p 4 A87-31106
Approximations to eigenvalues of modified general matrices
[AIAA PAPER 87-0947] p 177 A87-33756
Opening and closing of cracks at high cyclic strains p 84 A87-34661
J-integral estimates for cracks in infinite bodies p 177 A87-35334
Optimization of cascade blade mistuning under flutter and forced response constraints p 24 N87-11732
Sensitivity analysis and approximation methods for general eigenvalue problems
[NASA-CR-179538] p 180 N87-12021
Thermodynamic evaluation of transonic compressor rotors using the finite volume approach
[NASA-CR-180587] p 150 N87-23925

W

- Washington Univ., Seattle.**
Mechanisms by which heat release affects the flow field in a chemically reacting, turbulent mixing layer
[AIAA PAPER 87-0131] p 134 A87-24925
An experimental investigation of compressible three-dimensional boundary layer flow in annular diffusers
[AIAA PAPER 87-0366] p 3 A87-24954
On direct numerical simulations of turbulent reacting flows
[AIAA PAPER 87-1324] p 140 A87-44930
Washington Univ., St. Louis, Mo.
Numerical modeling of on-orbit propellant motion resulting from an impulsive acceleration
[AIAA PAPER 87-1766] p 40 A87-48573
Temperature fields due to jet induced mixing in a typical OTV tank
[AIAA PAPER 87-2017] p 55 A87-52247
Waterloo Univ. (Ontario).
Evaluation of new techniques for the calculation of internal recirculating flows
[AIAA PAPER 87-0059] p 131 A87-22387
Watkins-Johnson Co., Palo Alto, Calif.
A 20 GHz, high efficiency dual mode TWT for the ACTS program p 122 A87-45511
Design, construction and long life endurance testing of cathode assemblies for use in microwave high-power transmitting tubes
[NASA-CR-175116] p 123 N87-10237
Westinghouse Electric Corp., Pittsburgh, Pa.
Materials characterization of phosphoric acid fuel cell system p 76 A87-23241
Laser anemometry measurements of natural circulation flow in a scale model PWR reactor system p 154 A87-40750
Wichita State Univ., Kans.
Experimental, water droplet impingement data on two-dimensional airfoils, axisymmetric inlet and Boeing 737-300 engine inlet
[AIAA PAPER 87-0097] p 17 A87-24918

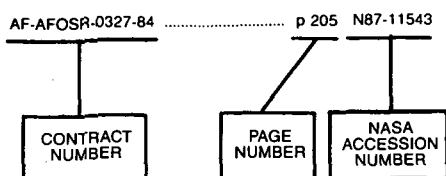
- Performance and aerodynamic braking of a horizontal-axis wind turbine from small-scale wind tunnel tests
[NASA-CR-180812] p 198 N87-27327
Williams International, Walled Lake, Mich.
Engine studies for future subsonic cruise missiles
[AIAA PAPER 86-1547] p 19 A87-21513
Wisconsin Univ., Madison.
Undercooling and crystallization behaviour of antimony droplets p 83 A87-28732
Wisconsin Univ., Milwaukee.
Comparison of pressure-strain correlation models for the flow behind a disk p 131 A87-20897
Turbulent heat transfer in corrugated-wall channels with and without fins p 134 A87-27709
Third-moment closure of turbulence for predictions of separating and reattaching shear flows: A study of Reynolds-stress closure model
[NASA-CR-177055] p 145 N87-11961
Wittenberg Univ., Springfield, Ohio.
Radiation effects on power transistor performance
[NASA-CR-181188] p 129 N87-27099
Wyle Labs., Inc., Huntsville, Ala.
Equipment concept design and development plans for microgravity science and applications research on space station: Combustion tunnel, laser diagnostic system, advanced modular furnace, integrated electronics laboratory
[NASA-CR-179535] p 108 N87-15320

Y

- Yale Univ., New Haven, Conn.**
Prediction and rational correlation of thermophoretically reduced particle mass transfer to hot surfaces across laminar or turbulent forced-convection gas boundary layers p 133 A87-23449
Turbine airfoil deposition models p 24 N87-11191

CONTRACT NUMBER INDEX

Typical Contract Number Index Listing



Listings in this index are arranged alphanumerically by contract number. Under each contract number the NASA accession numbers denoting documents that have been produced as a result of research done under that contract are arranged in ascending order. The NASA accession number denotes the number by which the citation is identified. Preceding the accession number is the page number on which the citation may be found.

AF-AFOSR-0327-84 p 205 N87-11543
 AF-AFOSR-0356-84 p 2 N87-28501
 AF-AFOSR-84-0034 p 133 A87-23449
 AF-AFOSR-84-0321 p 178 A87-36926
 AF-AFOSR-84-305 p 217 A87-39687
 AF-AFOSR-85-0297 p 217 A87-39687
 DA PROJ. 1L1-61102-AH-45 p 164 N87-11158
 p 166 N87-20552
 p 92 N87-23729
 p 31 N87-25323
 DA PROJ. 1L1-612209-AH-76 p 25 N87-11789
 DA PROJ. 1L1-62209-AH-76 p 25 N87-11790
 p 26 N87-14349
 p 146 N87-17003
 p 169 N87-25578
 DAAA15-85-K-0001 p 152 A87-11048
 DAAG29-84-K-0184 p 178 A87-36926
 DAAL03-86-K-0134 p 183 N87-18881
 DE-AC02-81ER-10941 p 82 A87-23843
 DE-AC03-76SF-00098 p 94 A87-12953
 p 138 A87-38790
 p 101 N87-17926
 DE-AI01-76ET-20320 p 191 N87-10531
 p 192 N87-11348
 p 192 N87-12046
 p 193 N87-17400
 p 193 N87-17401
 p 193 N87-18922
 p 198 N87-26455
 p 200 N87-29956
 DE-AI01-79ET-20320 p 73 N87-17861
 p 75 N87-28612
 DE-AI01-79ET-20485 p 193 N87-18230
 DE-AI01-85CE-50112 p 192 N87-12047
 p 221 N87-16664
 p 168 N87-22246
 p 222 N87-22562
 p 93 N87-28641
 p 222 N87-30223
 DE-AI01-85CE-50162 p 105 N87-27053
 DE-AI01-86CE-50162 p 220 N87-10777
 p 101 N87-16140
 p 222 N87-28470
 DE-AI03-86SF-16013 p 213 N87-25838
 DE-AI03-86SF-16310 p 88 N87-13513
 p 90 N87-17884
 p 91 N87-20405
 p 92 N87-26217
 DE-AI21-80ET-17088 p 193 N87-19804
 p 148 N87-22171
 DE-AT03-84ER-40161 p 223 A87-40651

DE-AT04-85AL-33408 p 220 N87-15031
 DE-FG03-86ER-13608 p 139 A87-42376
 DE-FG22-80PC-30247 p 76 A87-12599
 DEN3-167 p 97 A87-47923
 p 163 A87-48790
 p 222 N87-30225
 DEN3-168 p 98 A87-48989
 p 164 N87-11995
 DEN3-17 p 98 A87-48989
 DEN3-181 p 220 N87-15030
 DEN3-206 p 193 N87-19804
 DEN3-217 p 86 A87-49558
 p 191 N87-11344
 p 191 N87-11346
 p 191 N87-11347
 DEN3-247 p 191 N87-10531
 p 192 N87-11348
 p 192 N87-12046
 DEN3-260 p 73 N87-17861
 DEN3-286 p 75 N87-28612
 DEN3-290 p 188 A87-12338
 p 76 A87-23241
 p 78 A87-42677
 p 72 A87-42684
 p 191 A87-52288
 DEN3-303 p 86 A87-49558
 DEN3-311 p 192 N87-12047
 DEN3-323 p 221 N87-18470
 DEN3-32 p 160 A87-18037
 p 163 A87-48780
 p 163 A87-48781
 p 221 N87-20137
 p 222 N87-30223
 DEN3-343 p 168 N87-22246
 DEN3-347 p 195 N87-23030
 DEN3-352 p 97 A87-47958
 p 98 A87-51304
 DEN3-361 p 222 N87-28470
 DEN3-367 p 193 N87-18922
 DTFA03-81-A-00154 p 106 N87-24577
 DTFA03-83-A00328 p 1 N87-15932
 F04611-84-K-0026 p 140 A87-44842
 F04701-77-C-0062 p 200 A87-31322
 F08635-83-C-0052 p 153 A87-11049
 F49620-82-K-0033 p 167 N87-22212
 F49620-83-K-0004 p 143 A87-52320
 F49620-85-C-0067 p 140 A87-44930
 F49620-86-C-0078 p 132 A87-22426
 p 142 A87-46199
 INTELSAT-INTEL-375 p 53 A87-48677
 JPL-955870 p 99 A87-53652
 NAG1-224 p 177 A87-33756
 NAG1-379 p 142 A87-47158
 NAG2-31 p 31 N87-26908
 NAG2-373 p 2 A87-22578
 NAG3-102 p 4 A87-39528
 NAG3-109 p 15 N87-29419
 NAG3-122 p 14 N87-29412
 NAG3-146 p 138 A87-38790
 NAG3-14 p 82 A87-24116
 p 83 A87-28734
 NAG3-154 p 216 A87-20519
 p 216 A87-27198
 p 217 A87-44562
 NAG3-159 p 202 N87-14872
 p 114 N87-16198
 p 37 N87-22700
 p 117 N87-24605
 p 37 N87-25341
 p 44 N87-25419
 p 118 N87-27882
 NAG3-163 p 121 A87-23745
 NAG3-166 p 162 A87-37687
 NAG3-167 p 130 A87-10920
 p 130 A87-10922
 p 138 A87-38956
 p 28 N87-20996
 NAG3-181 p 166 N87-18096
 NAG3-182 p 208 A87-11768
 NAG3-183 p 106 A87-45372
 p 107 N87-29706
 NAG3-201 p 24 N87-11191
 NAG3-216 p 82 A87-24110

NAG3-21 p 87 A87-51289
 p 161 A87-22501
 p 161 A87-29275
 p 143 A87-48751
 NAG3-223 p 179 A87-51167
 NAG3-22 p 85 A87-38541
 NAG3-239 p 107 A87-43141
 NAG3-23 p 178 A87-36926
 NAG3-256 p 174 A87-14316
 NAG3-260 p 130 A87-10920
 p 130 A87-10922
 p 135 A87-28976
 p 138 A87-38956
 p 28 N87-20996
 NAG3-272 p 3 A87-24929
 NAG3-280 p 174 A87-15798
 p 153 A87-23899
 p 86 A87-49570
 NAG3-282 p 121 A87-40926
 p 123 A87-45899
 p 193 N87-18229
 p 66 N87-25420
 NAG3-285 p 143 A87-52320
 NAG3-286 p 143 A87-48726
 NAG3-28 p 8 N87-11701
 NAG3-292 p 131 A87-13019
 p 132 A87-22398
 p 77 A87-38958
 NAG3-294 p 201 A87-18499
 NAG3-298 p 160 A87-19502
 NAG3-304 p 49 A87-31281
 NAG3-305 p 51 A87-41111
 p 201 A87-18499
 NAG3-307 p 175 A87-25924
 p 178 A87-45994
 p 179 A87-53796
 NAG3-309 p 6 A87-44938
 NAG3-310 p 79 N87-22020
 NAG3-312 p 99 N87-11009
 p 104 N87-24573
 NAG3-3143 p 168 N87-23977
 NAG3-325 p 92 N87-25456
 NAG3-328 p 171 N87-13779
 p 171 N87-13781
 p 172 N87-13782
 p 172 N87-24702
 p 173 N87-26361
 NAG3-330 p 196 N87-25621
 NAG3-335 p 141 A87-45838
 NAG3-337 p 185 N87-24007
 p 187 N87-28944
 NAG3-33 p 176 A87-33624
 NAG3-344 p 170 N87-29840
 NAG3-346 p 173 A87-10893
 NAG3-347 p 177 A87-33756
 p 24 N87-11732
 p 180 N87-12021
 NAG3-348 p 81 A87-19368
 p 88 N87-11873
 NAG3-349 p 3 A87-24010
 NAG3-354 p 20 A87-27989
 p 210 A87-48760
 NAG3-355 p 140 A87-43715
 NAG3-357 p 208 A87-13587
 p 136 A87-31176
 NAG3-363 p 138 A87-39812
 p 163 A87-48783
 NAG3-365 p 88 N87-13514
 p 89 N87-14486
 p 153 A87-25948
 NAG3-366 p 80 N87-28634
 NAG3-368 p 173 A87-13496
 NAG3-373 p 3 A87-24954
 NAG3-376 p 87 A87-54370
 NAG3-379 p 179 N87-11210
 p 180 N87-13790
 p 165 N87-16342
 NAG3-382 p 80 N87-29635
 NAG3-388 p 24 N87-11769
 NAG3-389 p 215 A87-11242
 p 215 A87-12292
 NAG3-391 p 175 A87-28543
 NAG3-395 p 201 A87-11895

NAG3-396	p 202	A87-45900	NAG3-595	p 97	A87-48324	NAS3-23038	p 33	N87-29534
NAG3-408	p 202	N87-18997	NAG3-597	p 85	A87-41012	NAS3-23044	p 32	N87-28553
NAG3-416	p 202	N87-18998	NAG3-600	p 147	N87-19647	NAS3-23045	p 32	N87-28552
NAG3-418	p 203	N87-22422	NAG3-604	p 217	A87-30023		p 33	N87-28556
NAG3-422	p 180	N87-12915		p 198	N87-26444	NAS3-23046	p 32	N87-28554
NAG3-424	p 133	A87-22859	NAG3-610	p 20	A87-45239	NAS3-23156	p 155	N87-11144
NAG3-42	p 2	A87-22415	NAG3-613	p 121	A87-23922	NAS3-23164	p 50	A87-39808
	p 113	N87-10225	NAG3-61	p 4	A87-39528	NAS3-23169	p 157	N87-22179
	p 189	A87-19882	NAG3-620	p 215	N87-22508	NAS3-23174	p 31	N87-26914
	p 173	A87-11106		p 44	N87-26946	NAS3-23250	p 112	A87-34527
	p 111	A87-30775	NAG3-634	p 152	A87-11048	NAS3-23275	p 211	N87-17481
	p 113	A87-45466	NAG3-635	p 112	A87-32829	NAS3-23277	p 26	N87-14349
	p 122	A87-41089		p 113	A87-51403	NAS3-23278	p 145	N87-11223
NAG3-431	p 83	A87-28732	NAG3-637	p 55	A87-52252	NAS3-23284	p 74	N87-20387
NAG3-436	p 84	A87-34661	NAG3-645	p 2	A87-22578	NAS3-23288	p 171	N87-11213
NAG3-438	p 177	A87-35334		p 133	A87-22645		p 181	N87-15491
NAG3-443	p 77	A87-40572		p 3	A87-24992		p 182	N87-18117
NAG3-446	p 70	N87-14434	NAG3-654	p 76	A87-15983	NAS3-23293	p 88	N87-11192
NAG3-449	p 200	A87-24672	NAG3-655	p 170	N87-29846	NAS3-23339	p 218	N87-17515
	p 215	N87-16614	NAG3-665	p 2	A87-22414	NAS3-23346	p 123	N87-10237
NAG3-44	p 76	A87-20223	NAG3-6662	p 16	A87-45635	NAS3-23353	p 69	N87-29594
NAG3-451	p 153	A87-26109	NAG3-666	p 15	A87-22464	NAS3-23355	p 41	A87-18344
NAG3-460	p 135	A87-30281	NAG3-670	p 69	A87-53654	NAS3-23356	p 121	A87-34525
	p 138	A87-37256		p 69	A87-53656	NAS3-23357	p 121	A87-23953
NAG3-468	p 95	A87-19625	NAG3-671	p 143	A87-52049	NAS3-23531	p 140	A87-44930
	p 104	N87-25476	NAG3-673	p 142	A87-47158	NAS3-23542	p 76	A87-12599
NAG3-475	p 112	A87-31626	NAG3-67	p 31	N87-26908	NAS3-23634	p 48	A87-21516
	p 112	A87-42536	NAG3-681	p 214	A87-22714	NAS3-23681	p 13	N87-20239
	p 112	A87-44075		p 214	A87-48241	NAS3-23682	p 8	N87-10835
NAG3-477	p 118	N87-27085	NAG3-689	p 161	A87-22501	NAS3-23695	p 144	N87-11219
	p 75	A87-12598		p 143	A87-48751		p 144	N87-11220
	p 76	A87-12599		p 163	A87-48783		p 145	N87-13661
	p 77	A87-33987	NAG3-695	p 42	A87-22738	NAS3-23697	p 174	A87-13882
NAG3-479	p 182	N87-18121		p 42	A87-42585		p 180	N87-12923
NAG3-481	p 1	N87-15932	NAG3-696	p 80	N87-29633		p 185	N87-22996
NAG3-485	p 137	A87-31680	NAG3-730	p 177	A87-33719		p 186	N87-27267
NAG3-48	p 169	N87-26356	NAG3-749	p 159	N87-26327	NAS3-23703	p 169	N87-25579
NAG3-490	p 215	A87-11242	NAG3-751	p 186	N87-25607	NAS3-23716	p 145	N87-11224
	p 215	A87-12292	NAG3-752	p 213	N87-27495	NAS3-23722	p 159	N87-28869
NAG3-499	p 21	A87-45279	NAG3-767	p 5	A87-42314	NAS3-23773	p 40	A87-41161
NAG3-500	p 199	N87-29945	NAG3-768	p 152	N87-27949		p 37	A87-46000
NAG3-502	p 139	A87-40703	NAG3-76	p 214	A87-18735		p 56	N87-13486
	p 152	N87-27973	NAG3-793	p 129	N87-27099		p 67	N87-26097
NAG3-503	p 84	A87-32040	NAG3-95	p 217	A87-28295	NAS3-23775	p 51	A87-41135
	p 90	N87-15303		p 97	A87-47375	NAS3-23781	p 124	N87-11104
NAG3-507	p 120	A87-19104	NASA ORDER C-21030	p 206	N87-27475	NAS3-23790	p 122	A87-45511
	p 200	N87-29957	NASA ORDER C-67846-D	p 204	A87-49821		p 201	A87-45512
	p 200	N87-29958	NASA ORDER C-80000-E	p 75	A87-12598	NAS3-23858	p 110	N87-19539
NAG3-519	p 87	A87-52282	NASA ORDER C-80002-E	p 220	N87-10777	NAS3-23860	p 51	A87-41135
NAG3-522	p 139	A87-42376	NASA ORDER C-86129-D	p 153	A87-13878		p 53	A87-48677
NAG3-526	p 131	A87-22361		p 107	A87-23159	NAS3-23863	p 57	N87-14425
NAG3-528	p 152	N87-28860	NASA ORDER C-99066-G	p 183	N87-18881	NAS3-23869	p 42	A87-41611
NAG3-529	p 217	A87-39687		p 1	N87-20171		p 43	N87-10946
NAG3-533	p 143	A87-48751	NASA ORDER P-192815-D	p 97	A87-47923	NAS3-23876	p 188	A87-18073
NAG3-534	p 174	A87-20892	NAS1-17894	p 133	A87-22706		p 196	N87-26417
	p 175	A87-27945	NAS3-13475	p 11	N87-17665	NAS3-23881	p 119	A87-14084
	p 176	A87-33604	NAS3-181	p 161	A87-19529		p 45	A87-17837
	p 176	A87-33605		p 167	N87-22212		p 214	A87-22712
	p 183	N87-19756	NAS3-20043	p 168	N87-22245		p 122	A87-41609
	p 185	N87-22796	NAS3-20072	p 92	N87-27029	NAS3-23893	p 200	A87-51713
	p 187	N87-29896	NAS3-20073	p 90	N87-17883		p 49	A87-31134
	p 187	N87-29897	NAS3-20619	p 210	N87-10753		p 67	N87-26129
NAG3-535	p 176	A87-33579	NAS3-20797	p 209	A87-37628	NAS3-23926	p 88	N87-11193
	p 185	N87-22790		p 209	A87-37629	NAS3-23927	p 182	N87-18852
	p 206	N87-29212	NAS3-20836	p 1	N87-10003	NAS3-23931	p 25	N87-11788
NAG3-536	p 111	A87-20818	NAS3-21262	p 159	N87-28883	NAS3-23934	p 133	A87-22552
	p 119	N87-28813	NAS3-21608	p 212	N87-29315	NAS3-23939	p 29	N87-23622
	p 119	N87-28814	NAS3-22027	p 9	N87-13406	NAS3-23940	p 184	N87-22267
NAG3-537	p 139	A87-41173	NAS3-22126	p 158	N87-25552	NAS3-23942	p 164	N87-11158
	p 143	A87-53589	NAS3-22137	p 210	N87-10752	NAS3-23943	p 100	N87-13539
NAG3-541	p 169	N87-27197	NAS3-22146	p 8	N87-11694		p 100	N87-13540
NAG3-543	p 76	A87-14116	NAS3-22234	p 198	N87-27324	NAS3-23944	p 99	N87-11892
NAG3-546	p 131	A87-20897	NAS3-22238	p 46	A87-18104	NAS3-23967	p 175	A87-22775
	p 134	A87-27709		p 199	N87-29920	NAS3-24083	p 5	A87-41157
	p 145	N87-11961	NAS3-22393	p 32	N87-28555	NAS3-24084	p 155	N87-12829
NAG3-549	p 132	A87-22549	NAS3-22492	p 124	N87-17989	NAS3-24088	p 28	N87-21955
	p 134	A87-25281	NAS3-22502	p 111	A87-18310		p 28	N87-21956
NAG3-54	p 137	A87-31406	NAS3-22503	p 124	N87-16972		p 18	N87-23615
NAG3-553	p 185	N87-24007	NAS3-22513	p 25	N87-11789	NAS3-24091	p 106	A87-14986
	p 187	N87-28944	NAS3-22755	p 32	N87-28555	NAS3-24105	p 20	A87-31277
NAG3-55	p 164	A87-53422	NAS3-22759	p 8	N87-13405		p 77	A87-38958
	p 166	N87-18092	NAS3-22764	p 116	N87-19556		p 4	A87-39813
	p 166	N87-20552	NAS3-22766	p 34	N87-29538		p 7	A87-49100
NAG3-563	p 93	N87-27771		p 34	N87-29539		p 7	A87-49101
NAG3-566	p 17	A87-24918	NAS3-22770	p 148	N87-21257		p 26	N87-14348
NAG3-567	p 109	N87-22865	NAS3-22771	p 144	N87-11201		p 192	N87-14771
NAG3-571	p 154	A87-42546		p 78	N87-11858		p 59	N87-16065
NAG3-576	p 124	N87-16971	NAS3-22777	p 129	N87-29738		p 10	N87-16803
NAG3-578	p 55	A87-52247		p 130	N87-29739		p 10	N87-16804
NAG3-580	p 201	A87-35718	NAS3-22901	p 39	A87-15880		p 11	N87-16806
	p 162	A87-38464		p 38	A87-29448		p 193	N87-17400
NAG3-582	p 111	A87-30801		p 38	A87-33592		p 13	N87-20243
NAG3-585	p 176	A87-28982		p 43	A87-43073		p 158	N87-22960
	p 178	A87-40056		p 43	A87-43081		p 92	N87-23729
NAG3-590	p 133	A87-23449		p 43	N87-23685		p 79	N87-24549
NAG3-593	p 150	N87-23925	NAS3-22902	p 58	N87-15269		p 159	N87-26326

CONTRACT NUMBER INDEX

505-62-21

NAS3-24211	p 186	N87-26384	NAS5-21055	p 200	A87-31322	307-07-01	p 218	N87-23304
	p 5	A87-41157	NAS7-918	p 213	N87-25838	307-51-00	p 114	N87-16953
	p 162	A87-45398	NAS8-32807	p 200	A87-24672	324-01-00	p 25	N87-13443
NAS3-24215	p 107	N87-24578		p 215	N87-16614	480-43-02	p 206	N87-17472
NAS3-24217	p 106	N87-24577	NAS8-33982	p 200	A87-31322		p 206	N87-17473
NAS3-24222	p 209	A87-45282	NAS8-36647	p 4	A87-38496	480-52-02	p 192	N87-14771
	p 8	N87-10840		p 204	A87-41239	481-01-02	p 66	N87-25422
NAS3-24223	p 19	A87-22544	NATO-343/85	p 142	A87-47158	481-02-02	p 57	N87-14427
NAS3-24224	p 132	A87-22509	NAVAIR TASK AIR-310E	p 19	A87-25394		p 58	N87-14428
NAS3-24227	p 136	A87-30732	NCC3-19	p 97	A87-41078		p 59	N87-16065
	p 146	N87-17003	NCC3-25	p 216	A87-15071		p 60	N87-17848
NAS3-24228	p 157	N87-19686	NCC3-27	p 24	N87-11196		p 60	N87-20378
NAS3-24229	p 134	A87-24925	NCC3-29	p 123	A87-47621		p 66	N87-24536
	p 140	A87-44930	NCC3-30	p 95	A87-22336		p 68	N87-26135
NAS3-24238	p 58	N87-15269		p 70	N87-16879	481-50-32	p 56	N87-10960
	p 58	N87-15272		p 105	N87-26233		p 56	N87-11838
NAS3-24253	p 206	N87-17472		p 105	N87-27053		p 57	N87-14423
	p 206	N87-17473	NCC3-45	p 133	A87-23449		p 187	N87-27268
NAS3-24339	p 4	A87-32619	NCC3-46	p 175	A87-25775	481-51-02	p 68	N87-26144
	p 6	A87-45281		p 183	N87-18881	481-52-02	p 105	N87-25480
	p 23	A87-52245	NCC3-49	p 15	N87-29418	481-54-02	p 62	N87-22001
	p 23	N87-10866	NCC3-54	p 114	N87-16953		p 62	N87-22004
	p 14	N87-29413	NCC3-6	p 193	N87-17401		p 64	N87-23690
	p 33	N87-29536	NGL-05-005-007	p 200	A87-31322	485-40-02	p 65	N87-23695
NAS3-24340	p 27	N87-16830	NGL-22-009-640	p 15	A87-22464		p 65	N87-23696
NAS3-24343	p 18	N87-24457		p 16	A87-45635	485-49-02	p 58	N87-15267
NAS3-24346	p 31	N87-25323	NGT-36-027-805	p 78	A87-52248	505-05-12	p 104	N87-24573
NAS3-24349	p 18	A87-17934	NGT-36-027-807	p 217	A87-30025	505-31-04	p 26	N87-14348
NAS3-24350	p 153	A87-11049		p 97	A87-40927		p 205	N87-14918
	p 133	A87-24912	NGT-39-009-802	p 140	A87-43384		p 1	N87-16784
	p 134	A87-24913	NIH-GM-15997	p 69	A87-53654		p 26	N87-16827
	p 136	A87-30685	NSF ATM-83-08366	p 200	A87-31322	505-31-3B	p 210	N87-10753
	p 205	A87-53675	NSF ATM-83-51914	p 202	A87-45900	505-31-32	p 34	N87-29538
NAS3-24351	p 131	A87-22387	NSF CHE-83-19578	p 69	A87-53654		p 34	N87-29539
NAS3-24353	p 106	N87-24577		p 69	A87-53656	505-31-4K	p 146	N87-17003
NAS3-24356	p 154	A87-42374	NSF CHE-84-03823	p 69	A87-53656	505-31-52	p 159	N87-28883
NAS3-24382	p 55	N87-10176	NSF CPE-83-51849	p 199	N87-29945	505-32-6A	p 23	N87-10100
	p 63	N87-22793	NSF CPE-84-0481	p 2	N87-28501	505-33-62	p 88	N87-13514
NAS3-24386	p 17	A87-24904	NSF DMR-85-17223	p 97	A87-48324		p 89	N87-14486
NAS3-24389	p 62	N87-22784	NSF ECS-83-11345	p 112	A87-44075		p 101	N87-18666
	p 184	N87-22785	NSF ECS-85-15777	p 113	A87-51403		p 102	N87-20421
NAS3-24533	p 18	A87-14123	NSF INT-82-19963	p 200	A87-31322		p 105	N87-26231
NAS3-24543	p 19	A87-21513	NSF INT-84-19546	p 216	A87-27198	505-40-5A	p 11	N87-17669
NAS3-24544	p 21	A87-47081	NSF INT-85-14196	p 142	A87-47158	505-40-74	p 210	N87-10752
NAS3-24547	p 34	N87-11797	NSF MCS-83-00578	p 112	A87-32829		p 204	N87-23202
NAS3-24614	p 166	N87-19723	NSF MEA-80-06806	p 132	A87-22398	505-40-90	p 148	N87-20504
NAS3-24615	p 155	N87-10377	NSF MEA-82-10876	p 135	A87-30281		p 212	N87-29315
NAS3-24635	p 199	N87-29940		p 138	A87-37256	505-41-5A	p 43	N87-20353
NAS3-24636	p 50	A87-38017	NSF MEA-82-18708	p 139	A87-41173	505-42-32	p 25	N87-11788
	p 59	N87-16878		p 143	A87-53589	505-42-94	p 169	N87-25579
NAS3-24649	p 122	A87-41610	NSF MEA-83-05960	p 76	A87-14116	505-43-42	p 8	N87-10835
NAS3-24654	p 108	N87-15320	NSF MED-80-06806	p 131	A87-13019	505-45-54	p 8	N87-11694
NAS3-24656	p 59	N87-16874	NSF MSM-83-20307	p 142	A87-47158		p 15	N87-29419
NAS3-24658	p 60	N87-17848	NSG-3032	p 138	A87-37208	505-45-58	p 13	N87-23598
NAS3-24661	p 151	N87-24641		p 6	A87-46207	505-53-01	p 73	N87-16071
NAS3-24662	p 129	N87-28825	NSG-3079	p 149	N87-22948	505-62-OK	p 169	N87-25578
NAS3-24664	p 58	N87-15270	NSG-3135	p 3	A87-24901	505-62-OK	p 164	N87-11158
	p 219	N87-28741	NSG-3143	p 169	N87-26358	505-62-00	p 156	N87-13731
NAS3-24665	p 47	A87-18175	NSG-3150	p 200	A87-31322	505-62-01	p 155	N87-12829
NAS3-24666	p 213	A87-18173	NSG-3160	p 203	A87-53631		p 124	N87-13637
	p 65	N87-23695	NSG-3188	p 168	N87-23969		p 126	N87-20475
	p 65	N87-23696	NSG-3208	p 7	A87-48722		p 127	N87-22097
NAS3-24670	p 213	A87-18171		p 30	N87-24470		p 31	N87-24481
	p 213	A87-18173	NSG-3212	p 133	A87-23653		p 31	N87-25329
NAS3-24672	p 188	A87-18074		p 139	A87-41665		p 34	N87-25331
NAS3-24682	p 113	N87-11056	NSG-3253	p 162	A87-48500		p 158	N87-25552
	p 113	N87-11057	NSG-3264	p 25	N87-13441		p 159	N87-25562
	p 114	N87-11915		p 25	N87-13442	505-62-02	p 9	N87-14284
NAS3-24738	p 52	A87-45418	NSG-3266	p 133	A87-23653	505-62-11	p 28	N87-20282
	p 63	N87-22803		p 140	A87-43384		p 128	N87-23902
NAS3-24743	p 115	N87-18695	NSG-3277	p 198	N87-27327	505-62-21	p 205	N87-11543
	p 115	N87-18696	NSG-3291	p 78	A87-51187		p 8	N87-13405
NAS3-2483	p 162	A87-45398	NSG-3299	p 49	A87-38008		p 25	N87-13441
NAS3-24844	p 132	A87-22388		p 50	A87-38009		p 25	N87-13442
	p 132	A87-22426	NSG-3302	p 213	N87-30180		p 9	N87-14283
	p 142	A87-46199	NSG-3305	p 131	A87-13506		p 207	N87-14956
NAS3-24849	p 133	A87-22706	NSG-7623	p 200	A87-31322		p 9	N87-15173
	p 4	A87-38496	NSG-7645	p 85	A87-41012		p 146	N87-15441
	p 204	A87-41239	N00014-78-C-0636	p 173	A87-10893		p 9	N87-15944
NAS3-24854	p 25	N87-13443	N00014-80-C-0706	p 174	A87-15798		p 10	N87-16789
NAS3-24857	p 123	A87-50047	N00014-83-C-9151	p 153	A87-11049		p 10	N87-16790
	p 197	N87-26440	N00014-84-C-0359	p 140	A87-44930		p 10	N87-16799
NAS3-24871	p 196	N87-26427	N00014-84-K-0409	p 4	A87-38496		p 10	N87-16803
NAS3-24884	p 116	N87-19552		p 204	A87-41239		p 10	N87-16804
	p 116	N87-19553	N00014-85-K-0126	p 133	A87-22859		p 11	N87-16806
NAS3-24885	p 119	N87-28819	N00014-87-K-0174	p 140	A87-44930		p 26	N87-16826
NAS3-24886	p 44	N87-27710	N60530-85-C-0191	p 138	A87-38956		p 146	N87-18034
	p 44	N87-27711		p 28	N87-20996		p 147	N87-18035
NAS3-24890	p 125	N87-20467	N7405-ENG-26	p 165	N87-16342		p 207	N87-18391
NAS3-24891	p 117	N87-21212	PASA-NASA/DSB-5710-2-79	p 193	N87-18230		p 203	N87-19002
	p 117	N87-21213	PROJ. 3244	p 193	N87-18229		p 12	N87-19350
NAS3-24892	p 115	N87-16954	RF PROJ. 712620/762009	p 8	N87-11701		p 1	N87-20171
	p 115	N87-16955	USSJCSTC-020	p 161	A87-29275		p 12	N87-20235
NAS3-25068	p 140	A87-44842	W-7405-ENG-36	p 204	A87-49821		p 12	N87-20238
NAS3-25465	p 169	N87-25578	W-7405-ENG-82	p 219	A87-14665		p 13	N87-20243
NAS3-354	p 19	A87-24944		p 219	A87-51962		p 27	N87-20267

	p 203 N87-20766		p 205 N87-24930		p 64 N87-23691
	p 203 N87-20767		p 169 N87-26356		p 65 N87-23692
	p 28 N87-20996		p 169 N87-26358		p 65 N87-23693
	p 158 N87-22181		p 169 N87-27197		p 111 N87-23821
	p 13 N87-22630		p 170 N87-28918		p 66 N87-24525
	p 150 N87-23921		p 170 N87-29840		p 67 N87-25426
	p 150 N87-23933		p 170 N87-29846	506-43-11	p 171 N87-10399
	p 150 N87-23936	505-63-81	p 144 N87-11124		p 110 N87-12708
	p 205 N87-24132		p 145 N87-11962		p 171 N87-13779
	p 79 N87-24549		p 70 N87-16879		p 171 N87-13781
	p 151 N87-24639		p 75 N87-22811		p 172 N87-13782
	p 2 N87-25292	505-65-38	p 33 N87-28557		p 70 N87-14434
	p 207 N87-25821	505-68-01	p 91 N87-21077		p 100 N87-15305
	p 212 N87-25826	505-68-11	p 34 N87-11797		p 110 N87-17937
	p 151 N87-26302		p 17 N87-12559		p 74 N87-18615
	p 151 N87-27161		p 182 N87-18121		p 101 N87-18668
	p 14 N87-27629		p 13 N87-23591		p 102 N87-20422
	p 152 N87-27977		p 16 N87-29470		p 172 N87-20562
	p 2 N87-28501	505-68-51	p 26 N87-16825		p 91 N87-22034
	p 80 N87-28628	505-69-41	p 29 N87-22680		p 104 N87-24566
	p 15 N87-29418		p 107 N87-24578		p 172 N87-24707
	p 15 N87-29420	505-69-61	p 30 N87-23626		p 75 N87-25432
505-62-22	p 150 N87-23934	505-83-11	p 180 N87-12915		p 173 N87-25589
505-62-3A	p 210 N87-16586	505-90-01	p 215 N87-14998		p 159 N87-26327
	p 211 N87-17481		p 91 N87-21078		p 173 N87-26361
	p 35 N87-17717		p 212 N87-26615		p 173 N87-26362
	p 35 N87-18576		p 93 N87-27030	506-44-2A	p 125 N87-20468
	p 36 N87-22694		p 71 N87-29599	506-44-2C	p 218 N87-20821
	p 36 N87-23662	505-90-28	p 100 N87-12679		p 218 N87-25017
505-62-3B	p 35 N87-16851		p 103 N87-24563	506-44-21	p 123 N87-10232
	p 36 N87-23664	506-00-00	p 213 N87-25838		p 114 N87-16953
	p 33 N87-29537	506-40-31	p 59 N87-16878		p 115 N87-16958
505-62-38	p 35 N87-18575	506-41-11	p 127 N87-22098		p 124 N87-16968
505-62-51	p 164 N87-10391		p 195 N87-23028		p 218 N87-17515
	p 165 N87-15466		p 128 N87-23901		p 125 N87-17991
	p 165 N87-17033		p 66 N87-24531		p 125 N87-17993
	p 166 N87-18092		p 68 N87-26141		p 126 N87-20469
	p 166 N87-18095		p 196 N87-26413		p 126 N87-20474
	p 167 N87-20556		p 129 N87-27121		p 126 N87-21239
505-62-61	p 29 N87-22681		p 218 N87-27541		p 117 N87-22065
505-62-71	p 28 N87-20280	506-41-21	p 194 N87-22307		p 127 N87-22923
505-62-91	p 12 N87-18539		p 194 N87-22308		p 127 N87-23900
	p 12 N87-18540		p 194 N87-22310		p 128 N87-25532
	p 14 N87-27628		p 194 N87-22311		p 117 N87-26265
505-63-01	p 89 N87-14483		p 195 N87-23029		p 128 N87-26278
	p 89 N87-14487		p 79 N87-23718		p 129 N87-27120
	p 89 N87-14488		p 195 N87-24029		p 118 N87-27883
	p 90 N87-16113		p 195 N87-24838		p 130 N87-29750
	p 90 N87-17882		p 198 N87-27324	506-48-21	p 150 N87-22949
	p 90 N87-17883		p 199 N87-29914	506-49-22	p 69 N87-29594
	p 101 N87-17906	506-41-3A	p 195 N87-24026	506-49-38	p 40 N87-16012
	p 102 N87-18670	506-41-3B	p 91 N87-20405		p 40 N87-20342
	p 91 N87-20408	506-41-3D	p 222 N87-22561		p 108 N87-21141
	p 103 N87-20426	506-41-31	p 56 N87-12606	506-55-22	p 57 N87-14425
	p 74 N87-21043		p 221 N87-16663	506-55-52	p 192 N87-16445
	p 71 N87-22005		p 221 N87-21756	506-55-72	p 43 N87-10946
	p 103 N87-22048		p 61 N87-21999	506-58-22	p 114 N87-14569
	p 148 N87-22122		p 62 N87-22003		p 124 N87-14597
	p 103 N87-22860		p 149 N87-22174		p 117 N87-22089
	p 92 N87-23729		p 63 N87-22802		p 117 N87-22874
	p 104 N87-24565		p 194 N87-23020	506-62-21	p 9 N87-13406
	p 151 N87-24646		p 194 N87-23027		p 1 N87-15932
	p 92 N87-25456		p 128 N87-23903	506-63-11	p 166 N87-18820
	p 92 N87-25459		p 104 N87-24574	533-04-1A	p 155 N87-11144
	p 105 N87-26233		p 207 N87-25823		p 179 N87-11180
	p 92 N87-27029		p 105 N87-26232		p 157 N87-22179
	p 105 N87-27053		p 93 N87-29662		p 186 N87-27267
	p 93 N87-27771	506-41-38	p 88 N87-13513	533-04-11	p 155 N87-10377
	p 106 N87-29679	506-41-4R	p 99 N87-11893		p 88 N87-11873
505-63-11	p 164 N87-11993	506-41-41	p 70 N87-11841		p 99 N87-11892
	p 180 N87-12021	506-41-5A	p 147 N87-18786		p 156 N87-18057
	p 180 N87-12924	506-42-11	p 38 N87-13470		p 182 N87-18852
	p 73 N87-13491		p 64 N87-22806		p 157 N87-20516
	p 165 N87-13755		p 158 N87-22960		p 158 N87-22959
	p 89 N87-14489		p 67 N87-25425		p 185 N87-22996
	p 165 N87-15467		p 159 N87-26326		p 29 N87-23622
	p 182 N87-18115		p 68 N87-28602		p 186 N87-26399
	p 182 N87-18116	506-42-21	p 56 N87-10959		p 32 N87-28551
	p 74 N87-18614		p 56 N87-13486		p 159 N87-28869
	p 74 N87-20389		p 110 N87-19539	533-04-12	p 145 N87-13661
	p 183 N87-20565		p 60 N87-20379	533-05-01	p 172 N87-18109
	p 184 N87-21375		p 157 N87-20515		p 187 N87-27269
	p 168 N87-23978		p 41 N87-22757	533-05-11	p 171 N87-12910
	p 169 N87-23984		p 66 N87-25423		p 181 N87-17087
	p 185 N87-24006		p 67 N87-25424		p 102 N87-20425
	p 186 N87-24722	506-42-22	p 90 N87-16902		p 104 N87-25476
	p 187 N87-28058	506-42-31	p 57 N87-14422	533-13-00	p 55 N87-10176
	p 75 N87-28611		p 61 N87-20382		p 181 N87-13794
505-63-31	p 181 N87-14730		p 61 N87-20383	533-43-11	p 172 N87-23987
505-63-51	p 166 N87-19723		p 126 N87-20477	535-03-01	p 180 N87-12017
	p 166 N87-20552		p 61 N87-21037		p 210 N87-13252
	p 167 N87-20555		p 61 N87-21998		p 211 N87-16588
	p 167 N87-22235		p 167 N87-22237		p 10 N87-16798
	p 168 N87-22978		p 64 N87-22804		p 146 N87-17001
	p 168 N87-23969		p 64 N87-22805		p 211 N87-17480
	p 168 N87-23977		p 64 N87-22807		p 183 N87-18883

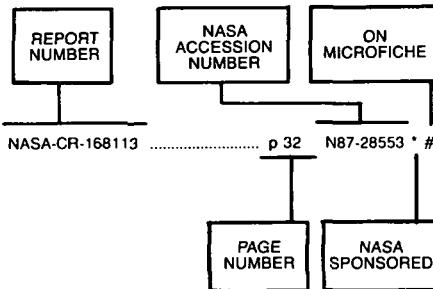
CONTRACT NUMBER INDEX

927-60-00

	p 211	N87-19057
	p 30	N87-23625
	p 13	N87-24435
	p 186	N87-26385
	p 212	N87-28396
	p 212	N87-28398
	p 33	N87-29536
535-03-12	p 23	N87-10866
	p 184	N87-22273
535-03	p 211	N87-16587
535-05-01	p 25	N87-11789
	p 11	N87-17665
	p 27	N87-17701
	p 148	N87-21257
	p 29	N87-23623
	p 29	N87-23624
	p 31	N87-26910
	p 37	N87-28571
535-05-12	p 26	N87-14349
545-03-01	p 14	N87-25294
553-03-04	p 186	N87-26384
553-12-00	p 146	N87-15442
553-13-00	p 57	N87-14426
	p 146	N87-17002
	p 147	N87-18784
	p 183	N87-18881
	p 167	N87-22199
	p 62	N87-22766
	p 185	N87-23010
	p 186	N87-25607
	p 187	N87-28944
553-13-80	p 185	N87-24007
650-20-26	p 44	N87-27711
	p 119	N87-28819
650-60-22	p 124	N87-17989
650-60-23	p 116	N87-18700
	p 116	N87-20448
	p 116	N87-20450
	p 127	N87-22102
650-60-26	p 114	N87-13600
	p 115	N87-16954
	p 115	N87-16955
	p 115	N87-18695
	p 115	N87-18696
	p 125	N87-20467
	p 117	N87-21212
	p 117	N87-21213
	p 44	N87-27710
650-66-22	p 124	N87-16972
674-22-05	p 156	N87-18801
	p 102	N87-19518
674-24-05	p 109	N87-22865
674-25-05	p 88	N87-11875
	p 108	N87-16167
	p 109	N87-24579
674-26-05	p 103	N87-23750
674-27-05	p 108	N87-16917
679-40-00	p 73	N87-16880
	p 128	N87-24630
694-03-03	p 91	N87-18643
	p 159	N87-28880
760-66-15	p 206	N87-27475
776-33-41	p 200	N87-29956
776-54-01	p 193	N87-18230
776-81-63	p 220	N87-15031
	p 222	N87-27564
778-17-01	p 148	N87-22171
778-34-12	p 101	N87-16140
778-35-13	p 220	N87-13359
	p 100	N87-14518
	p 221	N87-16664
	p 222	N87-22562
906-70-25	p 215	N87-18428
	p 215	N87-28423
917-60-00	p 38	N87-15996
917-60-01	p 43	N87-23685
927-60-00	p 181	N87-18112

REPORT/ACCESSION NUMBER INDEX

Typical Report Number Index Listing



Listings in this index are arranged alphanumerically by report number. The page number indicates the page on which the citation is located. The accession number denotes the number by which the citation is identified. An asterisk (*) indicates that the item is a NASA report. A pound sign (#) indicates that the item is available on microfiche.

A-3244 p 66 N87-25420 * #

AD-A170906 p 166 N87-18095 * #

AD-A171480 p 90 N87-15303 * #

AD-A173875 p 29 N87-23622 * #

AD-A175473 p 11 N87-17662 * #

AD-A178145 p 165 N87-15466 * #

AD-A178164 p 9 N87-15944 * #

AD-A180007 p 31 N87-25323 * #

AD-A180364 p 167 N87-20555 * #

AD-A183088 p 107 N87-24578 * #

AD-A183726 p 169 N87-25578 * #

AD-P005398 p 118 N87-28763 * #

AD-P005404 p 119 N87-28769 * #

AD-P005420 p 118 N87-27848 * #

AIAA PAPER 85-0387 p 42 A87-41611 * #

AIAA PAPER 85-0539 p 135 A87-30281 * #

AIAA PAPER 86-0362 p 50 A87-40275 * #

AIAA PAPER 86-0483 p 15 A87-17995 * #

AIAA PAPER 86-1392 p 46 A87-17992 * #

AIAA PAPER 86-1438 p 46 A87-17994 * #

AIAA PAPER 86-1542 p 19 A87-17993 * #

AIAA PAPER 86-1547 p 19 A87-21513 * #

AIAA PAPER 86-1557 p 19 A87-21514 * #

AIAA PAPER 86-1567 p 48 A87-21516 * #

AIAA PAPER 86-1619 p 5 A87-41157 * #

AIAA PAPER 86-1681 p 20 A87-41156 * #

AIAA PAPER 86-1876 p 208 A87-17991 * #

AIAA PAPER 86-2698 p 18 A87-17934 * #

AIAA PAPER 87-0008 p 3 A87-24901 * #

AIAA PAPER 87-0016 p 131 A87-22361 * #

AIAA PAPER 87-0023 p 17 A87-24904 * #

AIAA PAPER 87-0024 p 137 A87-32190 * #

AIAA PAPER 87-0025 p 17 A87-24905 * #

AIAA PAPER 87-0027 p 15 A87-22366 * #

AIAA PAPER 87-0056 p 3 A87-24996 * #

AIAA PAPER 87-0059 p 131 A87-22387 * #

AIAA PAPER 87-0060 p 133 A87-24912 * #

AIAA PAPER 87-0061 p 134 A87-24913 * #

AIAA PAPER 87-0062 p 132 A87-22388 * #

AIAA PAPER 87-0077 p 132 A87-22398 * #

AIAA PAPER 87-0080 p 42 A87-22401 * #

AIAA PAPER 87-0097 p 17 A87-24918 * #

AIAA PAPER 87-0099 p 2 A87-22414 * #

AIAA PAPER 87-0101 p 2 A87-22415 * #

AIAA PAPER 87-0104 p 69 A87-22417 * #

AIAA PAPER 87-0118 p 132 A87-22426 * #

AIAA PAPER 87-0131 p 134 A87-24925 * #

AIAA PAPER 87-0137 p 134 A87-24926 * #

AIAA PAPER 87-0145 p 3 A87-24929 * #

AIAA PAPER 87-0178 p 15 A87-22464 * #

AIAA PAPER 87-0180 p 132 A87-22466 * #

AIAA PAPER 87-0227 p 161 A87-22501 * #

AIAA PAPER 87-0247 p 132 A87-22509 * #

AIAA PAPER 87-0254 p 19 A87-24944 * #

AIAA PAPER 87-0283 p 4 A87-31106 * #

AIAA PAPER 87-0297 p 19 A87-22544 * #

AIAA PAPER 87-0303 p 139 A87-42648 * #

AIAA PAPER 87-0307 p 132 A87-22549 * #

AIAA PAPER 87-0313 p 133 A87-22552 * #

AIAA PAPER 87-0341 p 49 A87-31300 * #

AIAA PAPER 87-0354 p 2 A87-22578 * #

AIAA PAPER 87-0355 p 4 A87-32191 * #

AIAA PAPER 87-0366 p 3 A87-24954 * #

AIAA PAPER 87-0398 p 48 A87-24997 * #

AIAA PAPER 87-0399 p 48 A87-24998 * #

AIAA PAPER 87-0420 p 4 A87-34723 * #

AIAA PAPER 87-0453 p 133 A87-22645 * #

AIAA PAPER 87-0467 p 39 A87-31107 * #

AIAA PAPER 87-0506 p 108 A87-45724 * #

AIAA PAPER 87-0525 p 208 A87-24978 * #

AIAA PAPER 87-0526 p 208 A87-31109 * #

AIAA PAPER 87-0530 p 209 A87-31110 * #

AIAA PAPER 87-0557 p 133 A87-22706 * #

AIAA PAPER 87-0569 p 214 A87-22712 * #

AIAA PAPER 87-0572 p 214 A87-32192 * #

AIAA PAPER 87-0573 p 214 A87-22714 * #

AIAA PAPER 87-0577 p 107 A87-22716 * #

AIAA PAPER 87-0600 p 137 A87-34724 * #

AIAA PAPER 87-0602 p 137 A87-34725 * #

AIAA PAPER 87-0608 p 3 A87-24992 * #

AIAA PAPER 87-0612 p 42 A87-22738 * #

AIAA PAPER 87-0719 p 177 A87-33645 * #

AIAA PAPER 87-0738 p 178 A87-40497 * #

AIAA PAPER 87-0739 p 178 A87-40496 * #

AIAA PAPER 87-0753 p 177 A87-33648 * #

AIAA PAPER 87-0757 p 72 A87-33577 * #

AIAA PAPER 87-0764 p 176 A87-33579 * #

AIAA PAPER 87-0766 p 176 A87-33581 * #

AIAA PAPER 87-0792 p 38 A87-33592 * #

AIAA PAPER 87-0804 p 176 A87-33604 * #

AIAA PAPER 87-0806 p 176 A87-33605 * #

AIAA PAPER 87-0827 p 201 A87-33614 * #

AIAA PAPER 87-0840 p 176 A87-33624 * #

AIAA PAPER 87-0857 p 40 A87-33697 * #

AIAA PAPER 87-0910 p 177 A87-33719 * #

AIAA PAPER 87-0947 p 177 A87-33756 * #

AIAA PAPER 87-0991 p 52 A87-42181 * #

AIAA PAPER 87-0992 p 51 A87-41102 * #

AIAA PAPER 87-0993 p 52 A87-45725 * #

AIAA PAPER 87-0994 p 122 A87-41103 * #

AIAA PAPER 87-1003 p 53 A87-48677 * #

AIAA PAPER 87-1011 p 49 A87-38008 * #

AIAA PAPER 87-1012 p 51 A87-41111 * #

AIAA PAPER 87-1014 p 50 A87-38009 * #

AIAA PAPER 87-1043 p 50 A87-38017 * #

AIAA PAPER 87-1057 p 50 A87-39634 * #

AIAA PAPER 87-1059 p 50 A87-39635 * #

AIAA PAPER 87-1060 p 51 A87-41127 * #

AIAA PAPER 87-1061 p 51 A87-41128 * #

AIAA PAPER 87-1076 p 51 A87-41135 * #

AIAA PAPER 87-1098 p 53 A87-45795 * #

AIAA PAPER 87-1108 p 5 A87-42057 * #

AIAA PAPER 87-1120 p 204 A87-42069 * #

AIAA PAPER 87-1129 p 5 A87-42078 * #

AIAA PAPER 87-1162 p 5 A87-42107 * #

AIAA PAPER 87-1197 p 5 A87-42314 * #

AIAA PAPER 87-1306 p 154 A87-42374 * #

AIAA PAPER 87-1309 p 139 A87-42376 * #

AIAA PAPER 87-1316 p 7 A87-49649 * #

AIAA PAPER 87-1324 p 140 A87-44930 * #

AIAA PAPER 87-1369 p 6 A87-44938 * #

AIAA PAPER 87-1383 p 140 A87-44940 * #

AIAA PAPER 87-1525 p 140 A87-43048 * #

AIAA PAPER 87-1537 p 42 A87-43059 * #

AIAA PAPER 87-1538 p 140 A87-44842 * #

AIAA PAPER 87-1557 p 43 A87-43073 * #

AIAA PAPER 87-1570 p 43 A87-43081 * #

AIAA PAPER 87-1651 p 107 A87-43141 * #

AIAA PAPER 87-1728 p 23 A87-52245 * #

AIAA PAPER 87-1742 p 7 A87-50187 * #

AIAA PAPER 87-1745 p 22 A87-50188 * #

AIAA PAPER 87-1746 p 22 A87-48571 * #

AIAA PAPER 87-1764 p 142 A87-48572 * #

AIAA PAPER 87-1766 p 40 A87-48573 * #

AIAA PAPER 87-1773 p 53 A87-47003 * #

AIAA PAPER 87-1788 p 34 A87-45203 * #

AIAA PAPER 87-1828 p 22 A87-50189 * #

AIAA PAPER 87-1832 p 23 A87-52246 * #

AIAA PAPER 87-1837 p 20 A87-45239 * #

AIAA PAPER 87-1860 p 52 A87-45256 * #

AIAA PAPER 87-1886 p 34 A87-50190 * #

AIAA PAPER 87-1890 p 21 A87-45279 * #

AIAA PAPER 87-1892 p 6 A87-45281 * #

AIAA PAPER 87-1893 p 8 A87-52251 * #

AIAA PAPER 87-1894 p 209 A87-45282 * #

AIAA PAPER 87-1903 p 53 A87-50191 * #

AIAA PAPER 87-1906 p 21 A87-45289 * #

AIAA PAPER 87-1946 p 54 A87-50192 * #

AIAA PAPER 87-1948 p 53 A87-48575 * #

AIAA PAPER 87-1950 p 54 A87-50193 * #

AIAA PAPER 87-1951 p 54 A87-50194 * #

AIAA PAPER 87-1954 p 141 A87-45325 * #

AIAA PAPER 87-1976 p 85 A87-45336 * #

AIAA PAPER 87-2017 p 55 A87-52247 * #

AIAA PAPER 87-2028 p 54 A87-50195 * #

AIAA PAPER 87-2030 p 78 A87-52248 * #

AIAA PAPER 87-2035 p 21 A87-45369 * #

AIAA PAPER 87-2039 p 106 A87-45372 * #

AIAA PAPER 87-2050 p 22 A87-50196 * #

AIAA PAPER 87-2069 p 52 A87-45390 * #

AIAA PAPER 87-2070 p 55 A87-52249 * #

AIAA PAPER 87-2071 p 52 A87-45391 * #

AIAA PAPER 87-2082 p 55 A87-52250 * #

AIAA PAPER 87-2089 p 162 A87-45398 * #

AIAA PAPER 87-2111 p 6 A87-45413 * #

AIAA PAPER 87-2112 p 6 A87-45414 * #

AIAA PAPER 87-2117 p 52 A87-45418 * #

AIAA PAPER 87-2120 p 54 A87-50197 * #

AIAA PAPER 87-2121 p 55 A87-52252 * #

AIAA PAPER 87-2122 p 54 A87-50198 * #

AIAA PAPER 87-2138 p 141 A87-45427 * #

AIAA PAPER 87-2259 p 22 A87-50422 * #

AIAA PAPER 87-2455 p 38 A87-50501 * #

AIAA PAPER 87-2545 p 7 A87-49100 * #

AIAA PAPER 87-2548 p 7 A87-49101 * #

AIAA-86-0041 p 10 N87-16799 * #

AIAA-86-1079 p 205 N87-11543 * #

AIAA-87-0056 p 9 N87-14283 * #

AIAA-87-0137 p 26 N87-14348 * #

AIAA-87-0283 p 146 N87-15441 * #

AIAA-87-0303 p 26 N87-16826 * #

AIAA-87-0355 p 205 N87-24132 * #

AIAA-87-0420 p 146 N87-17001 * #

AIAA-87-0467 p 40 N87-16012 * #

AIAA-87-0525 p 210 N87-14957 * #

AIAA-87-0526 p 211 N87-16588 * #

AIAA-87-0530 p 111 N87-16587 * #

AIAA-87-0600 p 21 N87-16806 * #

AIAA-87-0738 p 182 N87-18115 * #

AIAA-87-0739 p 182 N87-18116 * #

AIAA-87-0992 p 61 N87-20383 * #

AIAA-87-0993 p 167 N87-22237 * #

AIAA-87-0994 p 126 N87-20477 * #

AIAA-87-1060 p 61 N87-20382 * #

AIAA-87-1061 p 61 N87-21998 * #

AIAA-87-1098 p 61 N87-21037 * #

AIAA-87-1316 p 13 N87-24435 * #

AIAA-87-1557 p 43 N87-23685 * #

AIAA-87-1742 p 30 N87-23625 * #

AIAA-87-1745 p 29 N87-23623 * #

AIAA-87-1746 p 29 N87-22681 * #

AIAA-87-1764 p 150 N87-22949 * #

AIAA-87-1766 p 41 N87-22757 * #

AIAA-87-1773 p 64 N87-22806 * #

AIAA-87-1788 p 35 N87-18575 * #

AIAA-87-1828 p 29 N87-23624 * #

AIAA-87-1886 p 36 N87-23664 * #

AIAA-87-1893 p 14 N87-25294 * #

AIAA-87-1903 p 65 N87-23692 * #

AIAA-87-1906 p 28 N87-20280 * #

AIAA-87-1946 p 66 N87-24525 * #

AIAA-87-1948 p 64 N87-22804 * #

AIAA-87-1950 p 64 N87-22807 * #

AIAA-87-1976 p 91 N87-22034 * #

AIAA-87-2028 p 64 N87-22805 * #

AIAA-87-2050 p 30 N87-23626 * #

AIAA-87-2069 p 66 N87-25423 * #

REPORT

AIAA-87-2070	p 67	N87-25424 * #	DOE/NASA-0241/20	p 191	N87-11346 * #	E-3145	p 35	N87-17717 * #
AIAA-87-2082	p 67	N87-25425 * #	DOE/NASA-0247/1-VOL-1	p 192	N87-11348 * #	E-3149	p 57	N87-14426 * #
AIAA-87-2111	p 12	N87-18540 * #	DOE/NASA-0247/2	p 191	N87-10531 * #	E-3151	p 215	N87-14998 * #
AIAA-87-2112	p 12	N87-18539 * #	DOE/NASA-0286-1	p 75	N87-28612 * #	E-3152	p 70	N87-16879 * #
AIAA-87-2120	p 111	N87-23821 * #	DOE/NASA-0311/1	p 192	N87-12047 * #	E-3164	p 146	N87-17003 * #
AIAA-87-2122	p 65	N87-23693 * #	DOE/NASA-0361-1	p 222	N87-28470 * #	E-3168	p 89	N87-14489 * #
AIAA-87-2138	p 156	N87-19684 * #	DOE/NASA-33408-2	p 222	N87-27564 * #	E-3175	p 35	N87-18576 * #
AIAA-87-2259	p 127	N87-22097 * #	DOE/NASA-33408/1	p 220	N87-15031 * #	E-3180	p 100	N87-14518 * #
AIAA-87-2722	p 15	N87-29420 * #	DOE/NASA-50112-68	p 221	N87-16664 * #	E-3181	p 180	N87-12924 * #
AIAA-87-2725	p 14	N87-27629 * #	DOE/NASA-50112/67	p 220	N87-13359 * #	E-3183-1	p 123	N87-10232 * #
AIAA-87-9003	p 62	N87-22001 * #	DOE/NASA/-13111/16	p 191	N87-11345 * #	E-3184	p 150	N87-23936 * #
AIAA-87-9034	p 66	N87-24531 * #	DOE/NASA/0006-3	p 193	N87-17401 * #	E-3185	p 151	N87-24639 * #
AIAA-87-9035	p 195	N87-23028 * #	DOE/NASA/0030-2	p 105	N87-27053 * #	E-3186	p 150	N87-23921 * #
AIAA-87-9053	p 68	N87-26141 * #	DOE/NASA/0032-25	p 222	N87-30223 * #	E-3189	p 204	N87-23202 * #
AIAA-87-9069	p 222	N87-27564 * #	DOE/NASA/0032-26	p 221	N87-20137 * #	E-3190	p 11	N87-16805 * #
AIAA-87-9080	p 194	N87-22311 * #	DOE/NASA/0032-80/7	p 222	N87-30223 * #	E-3195	p 171	N87-13779 * #
AIAA-87-9081	p 148	N87-22171 * #	DOE/NASA/0167-11	p 222	N87-30225 * #	E-3196	p 125	N87-17991 * #
AIAA-87-9198	p 194	N87-22307 * #	DOE/NASA/0168-10	p 164	N87-11995 * #	E-3198	p 124	N87-13637 * #
AIAA-87-9200	p 194	N87-22310 * #	DOE/NASA/0206-16	p 193	N87-19804 * #	E-3200	p 145	N87-11962 * #
AIAA-87-9203	p 194	N87-23020 * #	DOE/NASA/0247-3	p 192	N87-12046 * #	E-3206	p 193	N87-18230 * #
AIAA-87-9226	p 195	N87-24026 * #	DOE/NASA/0260-1	p 73	N87-17861 * #	E-3209	p 9	N87-15173 * #
AIAA-87-9232	p 194	N87-23027 * #	DOE/NASA/0323-2	p 221	N87-18470 * #	E-3210	p 8	N87-13405 * #
AIAA-87-9257	p 195	N87-24838 * #	DOE/NASA/0330-2	p 196	N87-25621 * #	E-3211	p 114	N87-14569 * #
AIAA-87-9260	p 195	N87-23029 * #	DOE/NASA/0343-1	p 168	N87-22246 * #	E-3213	p 124	N87-14597 * #
AIAA-87-9262	p 195	N87-24029 * #	DOE/NASA/0367-1	p 193	N87-18922 * #	E-3215	p 165	N87-15466 * #
AIAA-87-9314	p 128	N87-23903 * #	DOE/NASA/16310-1	p 88	N87-13513 * #	E-3216	p 127	N87-22923 * #
AIAA-87-9318	p 194	N87-22308 * #	DOE/NASA/16310-2	p 90	N87-17884 * #	E-3220	p 12	N87-20238 * #
AIAA-87-9353	p 64	N87-23690 * #	DOE/NASA/16310-3	p 91	N87-20405 * #	E-3221	p 165	N87-17033 * #
AIAA-87-9355	p 62	N87-22004 * #	DOE/NASA/16310-4	p 92	N87-26217 * #	E-3222	p 73	N87-16880 * #
AIAA-87-9442	p 63	N87-22802 * #	DOE/NASA/17088-5	p 148	N87-22171 * #	E-3225	p 181	N87-17087 * #
ALLISON-EDR-11984	p 145	N87-13661 * #	DOE/NASA/20320-72	p 198	N87-26455 * #	E-3229	p 166	N87-18092 * #
ANL/CT-86-3	p 220	N87-10777 * #	DOE/NASA/20320-73	p 200	N87-29956 * #	E-3230	p 166	N87-18820 * #
AR-1	p 55	N87-10176 * #	DOE/NASA/20485-80	p 193	N87-18230 * #	E-3231	p 33	N87-28557 * #
AR-1	p 100	N87-13540 * #	DOE/NASA/3277-4	p 198	N87-27327 * #	E-3233	p 144	N87-11124 * #
AR-2	p 99	N87-11892 * #	DOE/NASA/4105-3	p 198	N87-17400 * #	E-3236-1	p 60	N87-20381 * #
AR-2	p 100	N87-13539 * #	DOE/NASA/50112-69	p 193	N87-17400 * #	E-3238	p 56	N87-10959 * #
AR-2	p 182	N87-18117 * #	DOE/NASA/50112-70	p 222	N87-22562 * #	E-3242	p 215	N87-18428 * #
ASLE PREPRINT 86-TC-3D-1	p 94	A87-19504 *	DOE/NASA/50194-44	p 93	N87-28641 * #	E-3243	p 58	N87-14428 * #
ASLE PREPRINT 86-TC-6B-1	p 160	A87-19502 *	DOE/NASA/80002-1	p 101	N87-16140 * #	E-3247	p 180	N87-12017 * #
ASME PAPER 85-MT-60	p 143	A87-48726 * #	D483-10060-1	p 69	N87-29594 * #	E-3248	p 171	N87-10399 * #
ASME PAPER 86-GT-100	p 20	A87-25396 * #	E-2177	p 210	N87-10753 * #	E-3253	p 165	N87-15467 * #
ASME PAPER 86-GT-138	p 3	A87-25395 * #	E-2198	p 23	N87-10100 * #	E-3254	p 148	N87-21257 * #
ASME PAPER 86-GT-34	p 174	A87-17988 * #	E-2267	p 179	N87-11180 * #	E-3255	p 9	N87-14283 * #
ASME PAPER 86-GT-35	p 19	A87-25394 * #	E-2278	p 11	N87-17669 * #	E-3258	p 92	N87-26217 * #
ASME PAPER 86-JPGC-PTC-4	p 190	A87-25475 * #	E-2338	p 184	N87-22273 * #	E-3259	p 117	N87-22065 * #
ASME PAPER 86-TRIB-19	p 161	A87-19529 * #	E-2392	p 210	N87-10752 * #	E-3263	p 99	N87-11893 * #
ASME PAPER 86-TRIB-55	p 161	A87-19536 * #	E-2472	p 212	N87-29315 * #	E-3264	p 9	N87-15944 * #
ASME PAPER 86-WA/HT-50	p 140	A87-43715 * #	E-2528-1	p 205	N87-14918 * #	E-3267	p 36	N87-22694 * #
ASME PAPER 87-GT-253	p 6	A87-48719 * #	E-2589	p 27	N87-17699 * #	E-3268	p 56	N87-10960 * #
ASME PAPER 87-GT-8	p 171	A87-48702 * #	E-2647	p 101	N87-18666 * #	E-3270	p 114	N87-13600 * #
ASR-2	p 180	N87-12923 * #	E-2687	p 8	N87-11694 * #	E-3271	p 171	N87-13781 * #
ASR-2	p 29	N87-23622 * #	E-2688	p 13	N87-23598 * #	E-3272	p 172	N87-13782 * #
ASR-3	p 185	N87-22996 * #	E-2690	p 9	N87-14284 * #	E-3274	p 110	N87-12708 * #
AT86D002	p 221	N87-18470 * #	E-2879	p 147	N87-18035 * #	E-3275	p 210	N87-13252 * #
AV-FR-86/822	p 193	N87-18922 * #	E-2883	p 93	N87-27030 * #	E-3276	p 171	N87-12910 * #
AVSCOM-TR-86-C-21	p 166	N87-18095 * #	E-2904	p 181	N87-16321 * #	E-3278	p 73	N87-13491 * #
AVSCOM-TR-86-C-25	p 146	N87-17003 * #	E-2935	p 115	N87-16958 * #	E-3279	p 180	N87-13790 * #
AVSCOM-TR-86-C-42	p 167	N87-20555 * #	E-2937	p 156	N87-13731 * #	E-3280	p 191	N87-11345 * #
AVSCOM-TR-87-C-10	p 168	N87-22978 * #	E-2940	p 183	N87-20565 * #	E-3281	p 56	N87-11838 * #
AVSCOM-TR-87-C-11	p 169	N87-25578 * #	E-2941	p 164	N87-10391 * #	E-3285	p 57	N87-14427 * #
AVSCOM-TR-87-C-12	p 151	N87-24646 * #	E-2961	p 146	N87-18034 * #	E-3286	p 25	N87-11790 * #
AVSCOM-TR-87-C-13	p 168	N87-23969 * #	E-2989	p 166	N87-18095 * #	E-3287	p 38	N87-15996 * #
AVSCOM-TR-87-C-15	p 169	N87-27197 * #	E-2992	p 192	N87-16445 * #	E-3288	p 164	N87-11993 * #
AVSCOM-TR-87-C-16	p 168	N87-23977 * #	E-2996	p 115	N87-17971 * #	E-3290	p 38	N87-13470 * #
AVSCOM-TR-87-C-17	p 169	N87-26358 * #	E-3006	p 70	N87-10177 * #	E-3291	p 165	N87-13755 * #
AVSCOM-TR-87-C-19	p 205	N87-24930 * #	E-3007	p 89	N87-14488 * #	E-3292	p 56	N87-12606 * #
AVSCOM-TR-87-C-20	p 92	N87-23729 * #	E-3015	p 181	N87-13794 * #	E-3293	p 26	N87-14348 * #
AVSCOM-TR-87-C-21	p 29	N87-23623 * #	E-3021	p 158	N87-22181 * #	E-3294	p 36	N87-20295 * #
AVSCOM-TR-87-C-22	p 169	N87-26356 * #	E-3023	p 74	N87-18614 * #	E-3297	p 88	N87-11875 * #
AVSCOM-TR-87-C-23	p 170	N87-29840 * #	E-3026	p 89	N87-14487 * #	E-3298	p 17	N87-12559 * #
AVSCOM-TR-87-C-25	p 31	N87-26910 * #	E-3033	p 27	N87-20267 * #	E-3300	p 26	N87-16827 * #
AVSCOM-TR-87-C-7	p 103	N87-22048 * #	E-3038	p 89	N87-14483 * #	E-3301	p 11	N87-17662 * #
AVSCOM-TR-87-C-8	p 29	N87-23624 * #	E-3051	p 205	N87-11543 * #	E-3302	p 220	N87-13359 * #
BAC-ER-18056-8	p 151	N87-24641 * #	E-3069	p 182	N87-18852 * #	E-3304	p 90	N87-16902 * #
CONF-860152-7	p 101	N87-17926 * #	E-3073	p 58	N87-15267 * #	E-3305	p 91	N87-21077 * #
CR-R86091	p 28	N87-20996 * #	E-3074	p 90	N87-17682 * #	E-3306	p 91	N87-20405 * #
CTR-0723-87001	p 222	N87-28470 * #	E-3099	p 126	N87-20474 * #	E-3307	p 26	N87-16826 * #
DE86-015142	p 101	N87-17926 * #	E-3103	p 10	N87-16804 * #	E-3308	p 88	N87-13513 * #
DOE/NASA-0181	p 220	N87-15030 * #	E-3104	p 10	N87-16803 * #	E-3311	p 101	N87-16140 * #
DOE/NASA-0241-21	p 191	N87-11344 * #	E-3105	p 11	N87-16806 * #	E-3312	p 221	N87-16663 * #
DOE/NASA-0241/19	p 191	N87-11347 * #	E-3107	p 103	N87-22860 * #	E-3313	p 150	N87-23933 * #
			E-3110	p 16	N87-21878 * #	E-3314	p 220	N87-15031 * #
			E-3111	p 16	N87-21879 * #	E-3321	p 221	N87-16664 * #
			E-3117	p 156	N87-18801 * #	E-3322	p 116	N87-20448 * #
			E-3124	p 192	N87-13856 * #	E-3323	p 100	N87-12679 * #
			E-3126	p 1	N87-16784 * #	E-3324	p 70	N87-11841 * #
			E-3132	p 192	N87-14771 * #	E-3325	p 90	N87-16113 * #
			E-3133	p 207	N87-18391 * #	E-3326	p 100	N87-15305 * #
			E-3134	p 211	N87-17481 * #	E-3329	p 146	N87-17002 * #
			E-3136	p 167	N87-22199 * #	E-3330	p 181	N87-14730 * #
			E-3142	p 36	N87-23662 * #	E-3332	p 91	N87-18643 * #
			E-3143	p 125	N87-17990 * #	E-3333	p 125	N87-17993 * #
						E-3335	p 126	N87-20469 * #
						E-3336	p 210	N87-16586 * #
						E-3337	p 210	N87-14957 * #

REPORT NUMBER INDEX

GARRETT-31-6190

E-3338	p 57	N87-14423 * #	E-3485	p 221	N87-21756 * #	E-3629	p 64	N87-23690 * #
E-3339	p 13	N87-22630 * #	E-3488	p 28	N87-20282 * #	E-3631	p 195	N87-24029 * #
E-3340	p 146	N87-17001 * #	E-3491	p 116	N87-20450 * #	E-3632	p 172	N87-23987 * #
E-3341	p 207	N87-14956 * #	E-3492	p 29	N87-22681 * #	E-3633	p 128	N87-24630 * #
E-3342	p 183	N87-18883 * #	E-3493	p 71	N87-22005 * #	E-3634	p 104	N87-24565 * #
E-3343	p 57	N87-14422 * #	E-3494	p 203	N87-19002 * #	E-3635	p 79	N87-24549 * #
E-3346	p 93	N87-28641 * #	E-3495	p 103	N87-20426 * #	E-3636	p 185	N87-24007 * #
E-3348	p 146	N87-15442 * #	E-3497	p 147	N87-18786 * #	E-3637	p 66	N87-24531 * #
E-3349	p 40	N87-16012 * #	E-3499	p 13	N87-20243 * #	E-3639	p 64	N87-22806 * #
E-3352	p 211	N87-16588 * #	E-3500	p 14	N87-29412 * #	E-3641	p 65	N87-23692 * #
E-3354	p 108	N87-16167 * #	E-3501	p 1	N87-20171 * #	E-3642	p 92	N87-25459 * #
E-3356	p 146	N87-15441 * #	E-3504	p 172	N87-20562 * #	E-3644	p 104	N87-24574 * #
E-3357	p 167	N87-22235 * #	E-3505	p 102	N87-20421 * #	E-3645	p 64	N87-23691 * #
E-3359	p 124	N87-16968 * #	E-3506	p 199	N87-29914 * #	E-3647	p 29	N87-23624 * #
E-3360	p 166	N87-20552 * #	E-3510	p 43	N87-20353 * #	E-3648	p 66	N87-25422 * #
E-3361	p 148	N87-22122 * #	E-3511	p 40	N87-20342 * #	E-3649	p 68	N87-26135 * #
E-3362	p 211	N87-16587 * #	E-3512	p 62	N87-22766 * #	E-3650	p 173	N87-26361 * #
E-3364	p 205	N87-24132 * #	E-3513	p 148	N87-20504 * #	E-3651	p 172	N87-24707 * #
E-3366	p 59	N87-16065 * #	E-3514	p 218	N87-25017 * #	E-3655	p 222	N87-27564 * #
E-3367	p 102	N87-20422 * #	E-3515	p 109	N87-22865 * #	E-3656	p 66	N87-24525 * #
E-3368	p 167	N87-20555 * #	E-3517	p 203	N87-20766 * #	E-3657	p 111	N87-23821 * #
E-3369	p 158	N87-22959 * #	E-3519	p 218	N87-20821 * #	E-3659	p 30	N87-23626 * #
E-3372	p 150	N87-23934 * #	E-3520	p 222	N87-22561 * #	E-3660	p 29	N87-23623 * #
E-3374	p 32	N87-28551 * #	E-3521	p 167	N87-22237 * #	E-3662	p 30	N87-23625 * #
E-3375	p 187	N87-28944 * #	E-3523	p 66	N87-25423 * #	E-3667	p 212	N87-28396 * #
E-3378	p 211	N87-19057 * #	E-3524	p 61	N87-21037 * #	E-3669	p 105	N87-25480 * #
E-3379	p 218	N87-23304 * #	E-3525	p 61	N87-20382 * #	E-3670	p 169	N87-26356 * #
E-3380	p 167	N87-20556 * #	E-3526	p 61	N87-20383 * #	E-3671	p 186	N87-26384 * #
E-3384	p 26	N87-16825 * #	E-3527	p 126	N87-20477 * #	E-3672	p 80	N87-28628 * #
E-3385	p 147	N87-18784 * #	E-3528	p 184	N87-21375 * #	E-3673	p 16	N87-29470 * #
E-3386	p 108	N87-21141 * #	E-3529	p 79	N87-23718 * #	E-3674	p 186	N87-26385 * #
E-3387	p 181	N87-18112 * #	E-3530	p 39	N87-23674 * #	E-3677	p 129	N87-27121 * #
E-3390	p 73	N87-16071 * #	E-3531	p 62	N87-22003 * #	E-3678	p 159	N87-26326 * #
E-3392	p 182	N87-18115 * #	E-3532	p 13	N87-24435 * #	E-3679	p 67	N87-25426 * #
E-3393	p 10	N87-16789 * #	E-3533	p 75	N87-22811 * #	E-3681	p 105	N87-26233 * #
E-3394	p 10	N87-16790 * #	E-3538	p 61	N87-21998 * #	E-3682	p 151	N87-26302 * #
E-3398	p 10	N87-16799 * #	E-3540	p 169	N87-26358 * #	E-3683	p 2	N87-28501 * #
E-3399	p 10	N87-16798 * #	E-3541	p 170	N87-29846 * #	E-3686	p 200	N87-29956 * #
E-3401	p 90	N87-17884 * #	E-3542	p 29	N87-22680 * #	E-3687	p 207	N87-25823 * #
E-3407	p 211	N87-17480 * #	E-3543	p 127	N87-23900 * #	E-3688	p 218	N87-27541 * #
E-3408	p 151	N87-24646 * #	E-3544	p 205	N87-24930 * #	E-3690	p 68	N87-26141 * #
E-3410	p 66	N87-24536 * #	E-3546	p 127	N87-22098 * #	E-3692	p 68	N87-26144 * #
E-3411	p 202	N87-17441 * #	E-3547	p 41	N87-22757 * #	E-3694	p 31	N87-26910 * #
E-3412	p 182	N87-18116 * #	E-3549	p 194	N87-23020 * #	E-3695	p 37	N87-28571 * #
E-3415	p 185	N87-24006 * #	E-3550	p 158	N87-22960 * #	E-3698	p 130	N87-29750 * #
E-3416	p 126	N87-21239 * #	E-3551	p 103	N87-22048 * #	E-3699	p 105	N87-26232 * #
E-3417	p 35	N87-16851 * #	E-3552	p 169	N87-23984 * #	E-3702	p 14	N87-27629 * #
E-3418	p 151	N87-27161 * #	E-3553	p 64	N87-22804 * #	E-3705	p 173	N87-26362 * #
E-3419	p 27	N87-17701 * #	E-3554	p 67	N87-25425 * #	E-3706	p 173	N87-25589 * #
E-3420	p 108	N87-16917 * #	E-3556	p 91	N87-22034 * #	E-3712	p 186	N87-26399 * #
E-3424	p 105	N87-26231 * #	E-3558	p 67	N87-25424 * #	E-3713	p 105	N87-27053 * #
E-3425	p 110	N87-17937 * #	E-3559	p 104	N87-24566 * #	E-3714	p 159	N87-25562 * #
E-3429	p 101	N87-17906 * #	E-3561	p 127	N87-22097 * #	E-3715	p 31	N87-25329 * #
E-3430	p 184	N87-20566 * #	E-3562	p 194	N87-22307 * #	E-3719	p 128	N87-26278 * #
E-3431	p 103	N87-24563 * #	E-3563	p 195	N87-24026 * #	E-3720	p 187	N87-27268 * #
E-3435	p 35	N87-18575 * #	E-3564	p 61	N87-21999 * #	E-3730	p 212	N87-26615 * #
E-3436	p 27	N87-17700 * #	E-3566	p 194	N87-22308 * #	E-3731	p 129	N87-27120 * #
E-3438	p 102	N87-19518 * #	E-3568	p 212	N87-25826 * #	E-3735	p 106	N87-29679 * #
E-3439	p 101	N87-18668 * #	E-3569	p 149	N87-22174 * #	E-3736	p 187	N87-28058 * #
E-3440	p 156	N87-18057 * #	E-3570	p 109	N87-24579 * #	E-3741	p 152	N87-27977 * #
E-3442	p 91	N87-21078 * #	E-3571	p 92	N87-23729 * #	E-3743	p 187	N87-27269 * #
E-3443	p 183	N87-18882 * #	E-3576	p 194	N87-23027 * #	E-3746	p 212	N87-28398 * #
E-3445	p 183	N87-18881 * #	E-3577	p 62	N87-22001 * #	E-3761	p 206	N87-30132 * #
E-3446	p 172	N87-18109 * #	E-3579	p 222	N87-22562 * #	E-3763	p 118	N87-27883 * #
E-3447	p 33	N87-29537 * #	E-3580	p 169	N87-25579 * #	E-3769	p 159	N87-28880 * #
E-3448	p 102	N87-18670 * #	E-3581	p 75	N87-25432 * #	E-3771	p 16	N87-29471 * #
E-3449	p 128	N87-23902 * #	E-3582	p 39	N87-22755 * #	E-3772	p 93	N87-29662 * #
E-3450	p 196	N87-26413 * #	E-3583	p 185	N87-23010 * #	E-3779	p 75	N87-28611 * #
E-3451	p 28	N87-20996 * #	E-3585	p 127	N87-22102 * #	E-3784	p 215	N87-28423 * #
E-3452	p 157	N87-20516 * #	E-3586	p 148	N87-22171 * #	E-3791	p 71	N87-29599 * #
E-3453	p 14	N87-27628 * #	E-3587	p 168	N87-23978 * #	E-3794	p 15	N87-29420 * #
E-3454	p 116	N87-18700 * #	E-3588	p 128	N87-23903 * #	E-3799	p 68	N87-28602 * #
E-3455	p 31	N87-24481 * #	E-3590	p 195	N87-24838 * #	E-7389	p 11	N87-17665 * #
E-3456	p 12	N87-18540 * #	E-3591	p 195	N87-23028 * #			
E-3457	p 12	N87-18539 * #	E-3593	p 117	N87-26265 * #			
E-3458	p 60	N87-20379 * #	E-3595	p 198	N87-26455 * #	EDR-11283	p 32	N87-28554 * #
E-3462	p 28	N87-20280 * #	E-3596	p 186	N87-24722 * #	EDR-12344	p 164	N87-11995 * #
E-3463	p 151	N87-24641 * #	E-3597	p 170	N87-28918 * #			
E-3465	p 157	N87-20515 * #	E-3599	p 103	N87-23750 * #	ESL-TR-712257-5	p 213	N87-30180 * #
E-3466	p 102	N87-20425 * #	E-3600	p 195	N87-23029 * #			
E-3467	p 156	N87-19684 * #	E-3601	p 63	N87-22802 * #	FAA/CT-TN87/1	p 1	N87-15932 * #
E-3468	p 126	N87-20475 * #	E-3602	p 2	N87-25292 * #			
E-3469	p 203	N87-20767 * #	E-3603	p 168	N87-22978 * #	FCR-8347	p 198	N87-27324 * #
E-3470	p 128	N87-25532 * #	E-3604	p 169	N87-25578 * #			
E-3471	p 207	N87-25821 * #	E-3607	p 194	N87-22310 * #	FR-18683-2	p 58	N87-15269 * #
E-3472	p 74	N87-21043 * #	E-3608	p 194	N87-22311 * #	FR-19135-2	p 58	N87-15272 * #
E-3473	p 43	N87-23685 * #	E-3609	p 65	N87-23693 * #	FR-19289-2	p 63	N87-22803 * #
E-3474	p 13	N87-23591 * #	E-3610	p 14	N87-25294 * #			
E-3475	p 12	N87-19350 * #	E-3614	p 36	N87-23664 * #	FSR-DR-15-VOL-1	p 65	N87-23695 * #
E-3476	p 74	N87-20389 * #	E-3615	p 117	N87-22089 * #	FSR-DR-15-VOL-2	p 65	N87-23696 * #
E-3477	p 12	N87-20235 * #	E-3616	p 117	N87-22874 * #			
E-3479	p 34	N87-25331 * #	E-3617	p 150	N87-22949 * #	GARRETT-21-5278-1	p 90	N87-17883 * #
E-3481	p 74	N87-18615 * #	E-3618	p 64	N87-22805 * #	GARRETT-21-5464	p 26	N87-14349 * #
E-3482	p 125	N87-20468 * #	E-3620	p 128	N87-23901 * #	GARRETT-21-5723	p 27	N87-16830 * #
E-3483	p 60	N87-20378 * #	E-3623	p 64	N87-22807 * #	GARRETT-31-3725(11)	p 222	N87-30225 * #
E-3484	p 91	N87-20408 * #	E-3626	p 62	N87-22004 * #	GARRETT-31-6190	p 220	N87-15030 * #

GBI-ER-11	p 73	N87-17861 * #	NAS 1.15:100165	p 212	N87-26615 * #	NAS 1.15:88906	p 26	N87-16827 * #
GTDB6-5	p 59	N87-16878 * #	NAS 1.15:100166	p 105	N87-26231 * #	NAS 1.15:88907	p 181	N87-14730 * #
HSE-10853	p 166	N87-19723 * #	NAS 1.15:100168	p 129	N87-27120 * #	NAS 1.15:88908	p 29	N87-22681 * #
HSE-11056	p 28	N87-21955 * #	NAS 1.15:100170	p 106	N87-29679 * #	NAS 1.15:88909	p 91	N87-18643 * #
HSE-11057	p 28	N87-21956 * #	NAS 1.15:100171	p 187	N87-28058 * #	NAS 1.15:88911	p 210	N87-16586 * #
HSE-11058	p 18	N87-23615 * #	NAS 1.15:100173	p 152	N87-27977 * #	NAS 1.15:88912	p 146	N87-17001 * #
HSE-8945	p 32	N87-28555 * #	NAS 1.15:100174	p 187	N87-27269 * #	NAS 1.15:88913	p 210	N87-14957 * #
IAF PAPER 86-119	p 39	A87-15880 * #	NAS 1.15:100175	p 212	N87-28398 * #	NAS 1.15:88914	p 57	N87-14423 * #
IAF PAPER 86-143	p 41	A87-15894 * #	NAS 1.15:100178	p 14	N87-27629 * #	NAS 1.15:88915	p 13	N87-22630 * #
IAF PAPER 86-152	p 45	A87-15900 * #	NAS 1.15:100184	p 206	N87-30132 * #	NAS 1.15:88916	p 207	N87-14956 * #
IAF PAPER 86-183	p 48	A87-23239 * #	NAS 1.15:100186	p 80	N87-28628 * #	NAS 1.15:88917	p 183	N87-18883 * #
IAF PAPER 86-279	p 76	A87-15983 * #	NAS 1.15:100187	p 118	N87-27883 * #	NAS 1.15:88918	p 57	N87-14422 * #
IAF PAPER 86-37	p 45	A87-16138 * #	NAS 1.15:100188	p 159	N87-28880 * #	NAS 1.15:88919	p 146	N87-15442 * #
IAF-86-183	p 56	N87-10959 * #	NAS 1.15:100189	p 16	N87-29471 * #	NAS 1.15:88920	p 211	N87-16588 * #
IAF-87-234	p 68	N87-26144 * #	NAS 1.15:100190	p 93	N87-29662 * #	NAS 1.15:88921	p 108	N87-16167 * #
IAF-87-259	p 68	N87-26135 * #	NAS 1.15:100192	p 75	N87-28611 * #	NAS 1.15:88922	p 9	N87-14283 * #
IAF-87-491	p 118	N87-27883 * #	NAS 1.15:100194	p 215	N87-28423 * #	NAS 1.15:88923	p 146	N87-15441 * #
ICOMP-86-1	p 180	N87-12924 * #	NAS 1.15:100196	p 130	N87-29750 * #	NAS 1.15:88924	p 124	N87-16968 * #
ICOMP-86-3	p 1	N87-16784 * #	NAS 1.15:100198	p 71	N87-29599 * #	NAS 1.15:88925	p 148	N87-22122 * #
ICOMP-87-1	p 183	N87-18881 * #	NAS 1.15:100201	p 15	N87-29420 * #	NAS 1.15:88926	p 205	N87-24132 * #
ICOMP-87-2	p 1	N87-20171 * #	NAS 1.15:100203	p 68	N87-28602 * #	NAS 1.15:88927	p 90	N87-16113 * #
ICOMP-87-3	p 2	N87-25292 * #	NAS 1.15:87329	p 184	N87-22273 * #	NAS 1.15:88928	p 9	N87-15944 * #
ICOMP-87-4	p 2	N87-28501 * #	NAS 1.15:87355	p 13	N87-23598 * #	NAS 1.15:88929	p 11	N87-16805 * #
JM/87-4	p 150	N87-23925 * #	NAS 1.15:87356-VOL-1	p 192	N87-16445 * #	NAS 1.15:88931	p 150	N87-23934 * #
JPL-PUB-86-47	p 213	N87-25838 * #	NAS 1.15:87356-VOL-2	p 70	N87-10177 * #	NAS 1.15:88932	p 32	N87-28551 * #
KSR-86-01	p 34	N87-11797 * #	NAS 1.15:87358	p 89	N87-14483 * #	NAS 1.15:88933	p 40	N87-16012 * #
LBL-21043	p 101	N87-17926 * #	NAS 1.15:88789	p 205	N87-11543 * #	NAS 1.15:88934	p 187	N87-28944 * #
LG85ER0012-REV	p 23	N87-10866 * #	NAS 1.15:88819	p 103	N87-22860 * #	NAS 1.15:88936	p 211	N87-19057 * #
LG85ER0187	p 14	N87-29413 * #	NAS 1.15:88821	p 158	N87-22181 * #	NAS 1.15:88937	p 218	N87-23304 * #
LG86ER0173	p 33	N87-29536 * #	NAS 1.15:88823	p 16	N87-21878 * #	NAS 1.15:88939	p 26	N87-16825 * #
L86R1350	p 14	N87-29413 * #	NAS 1.15:88824	p 16	N87-21879 * #	NAS 1.15:88940	p 147	N87-18784 * #
L87R1488	p 33	N87-29536 * #	NAS 1.15:88825	p 156	N87-18801 * #	NAS 1.15:88941	p 181	N87-18112 * #
M/NAFA/TR-1	p 1	N87-15932 * #	NAS 1.15:88826	p 192	N87-13856 * #	NAS 1.15:88942	p 73	N87-16071 * #
MTI-85ASE445SA7	p 222	N87-30223 * #	NAS 1.15:88830	p 57	N87-14426 * #	NAS 1.15:88943	p 33	N87-28557 * #
MTI-85ASE476SA8	p 221	N87-20137 * #	NAS 1.15:88831	p 100	N87-14518 * #	NAS 1.15:88944	p 182	N87-18115 * #
MTI-85SESD24	p 192	N87-12047 * #	NAS 1.15:88832	p 89	N87-14487 * #	NAS 1.15:88945	p 10	N87-16789 * #
MTI-86TR33	p 168	N87-22246 * #	NAS 1.15:88833	p 123	N87-10232 * #	NAS 1.15:88946	p 10	N87-16790 * #
MTI-86TR40	p 164	N87-11158 * #	NAS 1.15:88834	p 58	N87-15267 * #	NAS 1.15:88947	p 211	N87-16587 * #
NAS 1.15:100101	p 66	N87-24531 * #	NAS 1.15:88836	p 124	N87-14597 * #	NAS 1.15:88948	p 117	N87-22065 * #
NAS 1.15:100102	p 195	N87-24838 * #	NAS 1.15:88838	p 180	N87-12924 * #	NAS 1.15:88949	p 10	N87-16799 * #
NAS 1.15:100103	p 93	N87-27030 * #	NAS 1.15:88840	p 89	N87-14488 * #	NAS 1.15:88950	p 90	N87-17882 * #
NAS 1.15:100104	p 64	N87-22806 * #	NAS 1.15:88841	p 89	N87-14489 * #	NAS 1.15:88951	p 90	N87-17884 * #
NAS 1.15:100105	p 92	N87-25459 * #	NAS 1.15:88843	p 166	N87-18092 * #	NAS 1.15:88952	p 158	N87-22959 * #
NAS 1.15:100106	p 104	N87-24574 * #	NAS 1.15:88844	p 144	N87-11124 * #	NAS 1.15:88953	p 10	N87-16798 * #
NAS 1.15:100107	p 29	N87-23624 * #	NAS 1.15:88845	p 56	N87-10959 * #	NAS 1.15:88956	p 202	N87-17441 * #
NAS 1.15:100108	p 66	N87-25422 * #	NAS 1.15:88846	p 215	N87-18428 * #	NAS 1.15:88957	p 66	N87-24536 * #
NAS 1.15:100109	p 65	N87-23692 * #	NAS 1.15:88847	p 58	N87-14428 * #	NAS 1.15:88959	p 182	N87-18116 * #
NAS 1.15:100110	p 68	N87-26135 * #	NAS 1.15:88848	p 180	N87-12017 * #	NAS 1.15:88960	p 185	N87-24006 * #
NAS 1.15:100111	p 222	N87-27564 * #	NAS 1.15:88849	p 171	N87-10399 * #	NAS 1.15:88961	p 35	N87-16851 * #
NAS 1.15:100112	p 66	N87-24525 * #	NAS 1.15:88850	p 165	N87-17033 * #	NAS 1.15:88962	p 27	N87-17701 * #
NAS 1.15:100113	p 111	N87-23821 * #	NAS 1.15:88851	p 73	N87-16880 * #	NAS 1.15:88963	p 108	N87-16917 * #
NAS 1.15:100114	p 30	N87-23626 * #	NAS 1.15:88852	p 181	N87-13794 * #	NAS 1.15:88964	p 74	N87-18614 * #
NAS 1.15:100115	p 29	N87-23623 * #	NAS 1.15:88853	p 165	N87-15466 * #	NAS 1.15:88965	p 101	N87-17906 * #
NAS 1.15:100118	p 30	N87-23625 * #	NAS 1.15:88854	p 99	N87-11893 * #	NAS 1.15:88966	p 35	N87-18575 * #
NAS 1.15:100120	p 64	N87-22805 * #	NAS 1.15:88855	p 183	N87-20565 * #	NAS 1.15:88967	p 27	N87-17700 * #
NAS 1.15:100121	p 212	N87-28396 * #	NAS 1.15:88856	p 56	N87-10960 * #	NAS 1.15:88968	p 102	N87-19518 * #
NAS 1.15:100122	p 105	N87-25480 * #	NAS 1.15:88857	p 207	N87-18391 * #	NAS 1.15:88969	p 211	N87-17480 * #
NAS 1.15:100123	p 64	N87-23691 * #	NAS 1.15:88858	p 114	N87-13600 * #	NAS 1.15:88970	p 156	N87-18057 * #
NAS 1.15:100126	p 16	N87-29470 * #	NAS 1.15:88859	p 223	N87-17656 * #	NAS 1.15:88971	p 183	N87-18882 * #
NAS 1.15:100128	p 129	N87-27121 * #	NAS 1.15:88860	p 210	N87-13252 * #	NAS 1.15:88972	p 167	N87-20556 * #
NAS 1.15:100130	p 67	N87-25426 * #	NAS 1.15:88861	p 171	N87-12910 * #	NAS 1.15:88973	p 183	N87-18881 * #
NAS 1.15:100132	p 151	N87-26302 * #	NAS 1.15:88862	p 166	N87-18820 * #	NAS 1.15:88974	p 110	N87-17937 * #
NAS 1.15:100133	p 2	N87-28501 * #	NAS 1.15:88863	p 73	N87-13491 * #	NAS 1.15:88975	p 172	N87-18109 * #
NAS 1.15:100136	p 200	N87-29956 * #	NAS 1.15:88864	p 191	N87-11345 * #	NAS 1.15:88976	p 102	N87-18670 * #
NAS 1.15:100137	p 207	N87-25823 * #	NAS 1.15:88865	p 56	N87-11838 * #	NAS 1.15:88977	p 125	N87-17993 * #
NAS 1.15:100138	p 218	N87-27541 * #	NAS 1.15:88866	p 165	N87-15467 * #	NAS 1.15:88978	p 102	N87-20422 * #
NAS 1.15:100139	p 68	N87-26141 * #	NAS 1.15:88867	p 57	N87-14427 * #	NAS 1.15:88979	p 157	N87-20516 * #
NAS 1.15:100140	p 68	N87-26144 * #	NAS 1.15:88868	p 1	N87-16784 * #	NAS 1.15:88980	p 14	N87-27628 * #
NAS 1.15:100141	p 31	N87-26910 * #	NAS 1.15:88869	p 38	N87-15996 * #	NAS 1.15:88981	p 116	N87-18700 * #
NAS 1.15:100142	p 92	N87-26217 * #	NAS 1.15:88870	p 164	N87-11993 * #	NAS 1.15:88982	p 219	N87-12384 * #
NAS 1.15:100143	p 37	N87-28571 * #	NAS 1.15:88871	p 38	N87-13470 * #	NAS 1.15:88983	p 213	N87-25838 * #
NAS 1.15:100147	p 173	N87-26362 * #	NAS 1.15:88872	p 165	N87-13755 * #	NAS 1.15:88984	p 101	N87-17926 * #
NAS 1.15:100148	p 173	N87-25589 * #	NAS 1.15:88873	p 56	N87-12606 * #	NAS 1.15:88985	p 18	N87-16816 * #
NAS 1.15:100149	p 207	N87-25821 * #	NAS 1.15:88874	p 110	N87-12708 * #	NAS 1.15:88986	p 12	N87-18540 * #
NAS 1.15:100150	p 117	N87-26265 * #	NAS 1.15:88875	p 88	N87-11875 * #	NAS 1.15:88987	p 12	N87-18539 * #
NAS 1.15:100151	p 186	N87-26399 * #	NAS 1.15:88876	p 17	N87-12559 * #	NAS 1.15:88988	p 60	N87-20379 * #
NAS 1.15:100152	p 159	N87-25562 * #	NAS 1.15:88877	p 11	N87-17662 * #	NAS 1.15:88989	p 91	N87-21078 * #
NAS 1.15:100153	p 31	N87-25329 * #	NAS 1.15:88878	p 220	N87-13359 * #	NAS 1.15:88990	p 28	N87-20280 * #
NAS 1.15:100156	p 105	N87-26232 * #	NAS 1.15:88879	p 88	N87-13513 * #	NAS 1.15:88991	p 101	N87-18668 * #
NAS 1.15:100157	p 128	N87-26278 * #	NAS 1.15:88880	p 101	N87-16140 * #	NAS 1.15:88992	p 157	N87-20515 * #
NAS 1.15:100158	p 187	N87-27268 * #	NAS 1.15:88881	p 221	N87-16663 * #	NAS 1.15:88993	p 102	N87-20425 * #
NAS 1.15:100159	p 33	N87-29537 * #	NAS 1.15:88882	p 150	N87-23933 * #	NAS 1.15:88994	p 156	N87-19684 * #
			NAS 1.15:88883	p 220	N87-15031 * #	NAS 1.15:88995	p 126	N87-20475 * #
			NAS 1.15:88884	p 221	N87-16664 * #	NAS 1.15:88996	p 203	N87-20767 * #
			NAS 1.15:88885	p 100	N87-12679 * #	NAS 1.15:88997	p 13	N87-23591 * #
			NAS 1.15:88886	p 70	N87-11841 * #	NAS 1.15:88998	p 43	N87-23685 * #
			NAS 1.15:88887	p 181	N87-17087 * #	NAS 1.15:88999	p 221	N87-21756 * #
			NAS 1.15:88888	p 100	N87-15305 * #	NAS 1.15:89000	p 28	N87-20282 * #
			NAS 1.15:88889	p 146	N87-17002 * #	NAS 1.15:89001	p 91	N87-20405 * #
			NAS 1.15:88890	p 26	N87-16826 * #	NAS 1.15:89002	p 116	N87-20450 * #
			NAS 1.15:88891	p 115	N87-16958 * #	NAS 1.15:89003	p 71	N87-22005 * #

REPORT NUMBER INDEX

NAS 1.26:181336

NAS 1.15:89837	p 23	N87-19002 * #	NAS 1.26:174713	p 73	N87-17861 * #	NAS 1.26:179556	p 11	N87-16806 * #
NAS 1.15:89838	p 103	N87-20426 * #	NAS 1.26:174733	p 74	N87-20387 * #	NAS 1.26:179557	p 25	N87-13443 * #
NAS 1.15:89839	p 126	N87-20469 * #	NAS 1.26:174742	p 124	N87-11104 * #	NAS 1.26:179558	p 116	N87-19556 * #
NAS 1.15:89840	p 125	N87-20468 * #	NAS 1.26:174773	p 155	N87-11144 * #	NAS 1.26:179559	p 220	N87-15030 * #
NAS 1.15:89841	p 147	N87-18786 * #	NAS 1.26:174814	p 32	N87-28555 * #	NAS 1.26:179562	p 70	N87-14434 * #
NAS 1.15:89842	p 1	N87-20171 * #	NAS 1.26:174819	p 8	N87-10840 * #	NAS 1.26:179563	p 166	N87-19723 * #
NAS 1.15:89843	p 172	N87-20562 * #	NAS 1.26:174828	p 145	N87-13661 * #	NAS 1.26:179566-SUMM	p 115	N87-16955 * #
NAS 1.15:89844	p 102	N87-20421 * #	NAS 1.26:174833	p 157	N87-22179 * #	NAS 1.26:179566	p 115	N87-16954 * #
NAS 1.15:89846	p 74	N87-21043 * #	NAS 1.26:174844	p 182	N87-18117 * #	NAS 1.26:179567	p 26	N87-14348 * #
NAS 1.15:89847	p 60	N87-20378 * #	NAS 1.26:174845	p 23	N87-10866 * #	NAS 1.26:179570	p 168	N87-22246 * #
NAS 1.15:89848	p 40	N87-20342 * #	NAS 1.26:174850-VOL-2	p 13	N87-20239 * #	NAS 1.26:179573	p 114	N87-16953 * #
NAS 1.15:89849	p 218	N87-25017 * #	NAS 1.26:174860	p 33	N87-29534 * #	NAS 1.26:179574	p 18	N87-24457 * #
NAS 1.15:89850	p 203	N87-20766 * #	NAS 1.26:174873	p 222	N87-30223 * #	NAS 1.26:179577	p 206	N87-27475 * #
NAS 1.15:89851	p 148	N87-20504 * #	NAS 1.26:174910	p 75	N87-28612 * #	NAS 1.26:179580	p 182	N87-18121 * #
NAS 1.15:89852	p 43	N87-20353 * #	NAS 1.26:174912	p 26	N87-14349 * #	NAS 1.26:179581	p 60	N87-17848 * #
NAS 1.15:89853	p 222	N87-22561 * #	NAS 1.26:174914	p 58	N87-15269 * #	NAS 1.26:179582	p 107	N87-24578 * #
NAS 1.15:89854	p 167	N87-22237 * #	NAS 1.26:174922	p 43	N87-10946 * #	NAS 1.26:179587-VOL-1	p 65	N87-23695 * #
NAS 1.15:89856	p 61	N87-21037 * #	NAS 1.26:174932	p 25	N87-11788 * #	NAS 1.26:179587-VOL-2	p 65	N87-23696 * #
NAS 1.15:89857	p 61	N87-20382 * #	NAS 1.26:174972	p 221	N87-20137 * #	NAS 1.26:179589	p 18	N87-23615 * #
NAS 1.15:89858	p 61	N87-20383 * #	NAS 1.26:174981	p 192	N87-11348 * #	NAS 1.26:179591	p 115	N87-18696 * #
NAS 1.15:89859	p 218	N87-20821 * #	NAS 1.26:174982	p 191	N87-10531 * #	NAS 1.26:179592	p 115	N87-18695 * #
NAS 1.15:89860	p 126	N87-20477 * #	NAS 1.26:174983	p 192	N87-12046 * #	NAS 1.26:179594	p 29	N87-23622 * #
NAS 1.15:89861	p 184	N87-21375 * #	NAS 1.26:175010	p 100	N87-13540 * #	NAS 1.26:179596	p 63	N87-22803 * #
NAS 1.15:89862	p 79	N87-23718 * #	NAS 1.26:175039	p 15	N87-29419 * #	NAS 1.26:179597-VOL-1	p 117	N87-21212 * #
NAS 1.15:89863	p 39	N87-23674 * #	NAS 1.26:175042	p 192	N87-12047 * #	NAS 1.26:179597-VOL-2	p 117	N87-21213 * #
NAS 1.15:89864	p 62	N87-22003 * #	NAS 1.26:175056	p 193	N87-17400 * #	NAS 1.26:179598-VOL-1	p 116	N87-19552 * #
NAS 1.15:89865	p 75	N87-22811 * #	NAS 1.26:175059	p 15	N87-29418 * #	NAS 1.26:179598-VOL-2	p 116	N87-19553 * #
NAS 1.15:89866	p 91	N87-21077 * #	NAS 1.26:175060	p 180	N87-12923 * #	NAS 1.26:179601	p 184	N87-22267 * #
NAS 1.15:89867	p 61	N87-21998 * #	NAS 1.26:175062	p 27	N87-16830 * #	NAS 1.26:179603	p 195	N87-23030 * #
NAS 1.15:89868	p 29	N87-22680 * #	NAS 1.26:175067	p 34	N87-29538 * #	NAS 1.26:179605	p 125	N87-20467 * #
NAS 1.15:89869	p 127	N87-23900 * #	NAS 1.26:175067	p 34	N87-29539 * #	NAS 1.26:179608	p 13	N87-20243 * #
NAS 1.15:89870	p 127	N87-22098 * #	NAS 1.26:175069-VOL-1	p 129	N87-29738 * #	NAS 1.26:179609	p 198	N87-27324 * #
NAS 1.15:89872	p 194	N87-23020 * #	NAS 1.26:175069-VOL-2	p 130	N87-29739 * #	NAS 1.26:179611	p 168	N87-23969 * #
NAS 1.15:89873	p 41	N87-22757 * #	NAS 1.26:175075	p 191	N87-11347 * #	NAS 1.26:179613	p 33	N87-29536 * #
NAS 1.15:89874	p 205	N87-24930 * #	NAS 1.26:175093	p 69	N87-29594 * #	NAS 1.26:179619	p 158	N87-22960 * #
NAS 1.15:89875	p 103	N87-22048 * #	NAS 1.26:175101	p 90	N87-15303 * #	NAS 1.26:179620	p 168	N87-23977 * #
NAS 1.15:89876	p 64	N87-22804 * #	NAS 1.26:175102	p 110	N87-19539 * #	NAS 1.26:179621	p 169	N87-27197 * #
NAS 1.15:89877	p 91	N87-22034 * #	NAS 1.26:175110	p 31	N87-25323 * #	NAS 1.26:179622	p 92	N87-27029 * #
NAS 1.15:89879	p 104	N87-24566 * #	NAS 1.26:175114	p 221	N87-18470 * #	NAS 1.26:179624	p 92	N87-23729 * #
NAS 1.15:89880	p 127	N87-22097 * #	NAS 1.26:175116	p 123	N87-10237 * #	NAS 1.26:179628	p 109	N87-22865 * #
NAS 1.15:89881	p 194	N87-22307 * #	NAS 1.26:175117	p 191	N87-11346 * #	NAS 1.26:179631	p 92	N87-25456 * #
NAS 1.15:89882	p 61	N87-21999 * #	NAS 1.26:175118	p 191	N87-11344 * #	NAS 1.26:179634	p 104	N87-25476 * #
NAS 1.15:89883	p 194	N87-22308 * #	NAS 1.26:177055	p 145	N87-11961 * #	NAS 1.26:179636	p 79	N87-24549 * #
NAS 1.15:89884	p 212	N87-25826 * #	NAS 1.26:179457	p 59	N87-16065 * #	NAS 1.26:179637	p 159	N87-26327 * #
NAS 1.15:89885	p 109	N87-24579 * #	NAS 1.26:179458	p 14	N87-29413 * #	NAS 1.26:179638	p 104	N87-24573 * #
NAS 1.15:89886	p 149	N87-22174 * #	NAS 1.26:179459	p 155	N87-12829 * #	NAS 1.26:179643	p 170	N87-29840 * #
NAS 1.15:89888	p 194	N87-23027 * #	NAS 1.26:179462	p 220	N87-10777 * #	NAS 1.26:179644	p 186	N87-26384 * #
NAS 1.15:89889	p 62	N87-22001 * #	NAS 1.26:179464	p 59	N87-16878 * #	NAS 1.26:179646	p 159	N87-26326 * #
NAS 1.15:89890	p 13	N87-24435 * #	NAS 1.26:179479	p 113	N87-11056 * #	NAS 1.26:179649	p 105	N87-26233 * #
NAS 1.15:89891	p 185	N87-23010 * #	NAS 1.26:179480	p 113	N87-11057 * #	NAS 1.26:179714	p 113	N87-10225 * #
NAS 1.15:89892	p 222	N87-22562 * #	NAS 1.26:179481	p 114	N87-11915 * #	NAS 1.26:179857	p 99	N87-11009 * #
NAS 1.15:89893	p 75	N87-25432 * #	NAS 1.26:179482	p 192	N87-14771 * #	NAS 1.26:179897	p 8	N87-11701 * #
NAS 1.15:89894	p 39	N87-22755 * #	NAS 1.26:179484	p 164	N87-11995 * #	NAS 1.26:180030	p 202	N87-14872 * #
NAS 1.15:89895	p 169	N87-23984 * #	NAS 1.26:179486	p 168	N87-22245 * #	NAS 1.26:180073	p 124	N87-16971 * #
NAS 1.15:89896	p 148	N87-22171 * #	NAS 1.26:179488	p 58	N87-15272 * #	NAS 1.26:180102	p 215	N87-16614 * #
NAS 1.15:89897	p 168	N87-23978 * #	NAS 1.26:179490	p 193	N87-19804 * #	NAS 1.26:180106	p 114	N87-16198 * #
NAS 1.15:89898	p 127	N87-22102 * #	NAS 1.26:179491	p 25	N87-13441 * #	NAS 1.26:180162	p 193	N87-18229 * #
NAS 1.15:89899	p 151	N87-24646 * #	NAS 1.26:179492	p 25	N87-13442 * #	NAS 1.26:180194	p 166	N87-18096 * #
NAS 1.15:89900	p 186	N87-24722 * #	NAS 1.26:179494	p 185	N87-22996 * #	NAS 1.26:180214	p 202	N87-18998 * #
NAS 1.15:89901	p 170	N87-28918 * #	NAS 1.26:179496	p 55	N87-10176 * #	NAS 1.26:180215	p 202	N87-18997 * #
NAS 1.15:89902	p 128	N87-23902 * #	NAS 1.26:179501	p 164	N87-11158 * #	NAS 1.26:180262	p 147	N87-19647 * #
NAS 1.15:89903	p 198	N87-26455 * #	NAS 1.26:179502	p 58	N87-15270 * #	NAS 1.26:180307	p 118	N87-27085 * #
NAS 1.15:89904	p 103	N87-24563 * #	NAS 1.26:179503	p 25	N87-11789 * #	NAS 1.26:180349	p 183	N87-19756 * #
NAS 1.15:89905	p 103	N87-23750 * #	NAS 1.26:179504	p 100	N87-13539 * #	NAS 1.26:180399	p 80	N87-28634 * #
NAS 1.15:89906	p 186	N87-26385 * #	NAS 1.26:179506	p 70	N87-16879 * #	NAS 1.26:180579	p 215	N87-22508 * #
NAS 1.15:89907	p 195	N87-23029 * #	NAS 1.26:179508	p 99	N87-11892 * #	NAS 1.26:180587	p 150	N87-23925 * #
NAS 1.15:89908	p 195	N87-23028 * #	NAS 1.26:179509	p 155	N87-10377 * #	NAS 1.26:180588	p 79	N87-22020 * #
NAS 1.15:89909	p 63	N87-22802 * #	NAS 1.26:179510	p 57	N87-14425 * #	NAS 1.26:180589	p 203	N87-22422 * #
NAS 1.15:89910	p 2	N87-25292 * #	NAS 1.26:179512	p 28	N87-21955 * #	NAS 1.26:180672	p 213	N87-27493 * #
NAS 1.15:89911	p 128	N87-23903 * #	NAS 1.26:179513-VOL-1	p 157	N87-19686 * #	NAS 1.26:180697	p 152	N87-27975 * #
NAS 1.15:89912	p 168	N87-22978 * #	NAS 1.26:179514	p 193	N87-18922 * #	NAS 1.26:180803	p 196	N87-25621 * #
NAS 1.15:89913	p 195	N87-24026 * #	NAS 1.26:179515	p 34	N87-11797 * #	NAS 1.26:180806	p 186	N87-25607 * #
NAS 1.15:89914	p 194	N87-22310 * #	NAS 1.26:179517	p 186	N87-27267 * #	NAS 1.26:180808	p 105	N87-27053 * #
NAS 1.15:89915	p 194	N87-22311 * #	NAS 1.26:179518	p 180	N87-12915 * #	NAS 1.26:180810	p 93	N87-27771 * #
NAS 1.15:89916	p 65	N87-23693 * #	NAS 1.26:179520	p 158	N87-25552 * #	NAS 1.26:180811	p 159	N87-28869 * #
NAS 1.15:89917	p 14	N87-25294 * #	NAS 1.26:179523	p 10	N87-16804 * #	NAS 1.26:180812	p 198	N87-27327 * #
NAS 1.15:89918	p 36	N87-23664 * #	NAS 1.26:179524	p 10	N87-16803 * #	NAS 1.26:180813	p 31	N87-26914 * #
NAS 1.15:89919	p 117	N87-22089 * #	NAS 1.26:179526	p 206	N87-17472 * #	NAS 1.26:180816	p 44	N87-27710 * #
NAS 1.15:89920	p 117	N87-22874 * #	NAS 1.26:179527	p 206	N87-17473 * #	NAS 1.26:180817	p 44	N87-27711 * #
NAS 1.15:89921	p 150	N87-22949 * #	NAS 1.26:179528	p 28	N87-21956 * #	NAS 1.26:180818	p 222	N87-30225 * #
NAS 1.15:89922	p 128	N87-23901 * #	NAS 1.26:179529	p 88	N87-11873 * #	NAS 1.26:180821	p 119	N87-28819 * #
NAS 1.15:89924	p 64	N87-22807 * #	NAS 1.26:179530	p 180	N87-13790 * #	NAS 1.26:180829	p 129	N87-28825 * #
NAS 1.15:89925	p 62	N87-22004 * #	NAS 1.26:179535	p 108	N87-15320 * #	NAS 1.26:180833	p 222	N87-28470 * #
NAS 1.15:89926	p 64	N87-23690 * #	NAS 1.26:179536	p 218	N87-17515 * #	NAS 1.26:180987	p 149	N87-22948 * #
NAS 1.15:89927	p 195	N87-24029 * #	NAS 1.26:179537-VOL-1	p 90	N87-17883 * #	NAS 1.26:181017	p 37	N87-22700 * #
NAS 1.15:89928	p 128	N87-24630 * #	NAS 1.26:179538	p 180	N87-12021 * #	NAS 1.26:181057	p 66	N87-25420 * #
NAS 1.15:89929	p 172	N87-23987 * #	NAS 1.26:179541	p 56	N87-13486 * #	NAS 1.26:181112	p 117	N87-24605 * #
NAS 1.15:89930	p 104	N87-24565 * #	NAS 1.26:179543	p 193	N87-17401 * #	NAS 1.26:181150	p 37	N87-25341 * #
NAS 1.15:89931	p 185	N87-24007 * #	NAS 1.26:179545	p 124	N87-17989 * #	NAS 1.26:181151	p 44	N87-25419 * #
NAS 1.26:100167	p 93	N87-28641 * #	NAS 1.26:179546	p 124	N87-16972 * #	NAS 1.26:181181	p 119	N87-28814 * #
NAS 1.26:168113	p 32	N87-28553 * #	NAS 1.26:179547	p 78	N87-11858 * #	NAS 1.26:181188	p 129	N87-27099 * #
NAS 1.26:168114-VOL-1	p 32	N87-28552 * #	NAS 1.26:179549	p 1	N87-15932 * #	NAS 1.26:181203	p 31	N87-26908 * #
NAS 1.26:168114-VOL-2	p 33	N87-28556 * #	NAS 1.26:179550	p 181	N87-15491 * #	NAS 1.26:181273	p 118	N87-27882 * #
NAS 1.26:168115	p 32	N87-28554 * #	NAS 1.26:179551	p 88	N87-13514 * #	NAS 1.26:181293	p 152	N87-27949 * #
NAS 1.26:174676	p							

NAS 1.26:181343	p 206	N87-29212	#	NASA-CASE-LEW-14072-3	p 103	N87-23736	*	NASA-CR-179512	p 28	N87-21955	*
NAS 1.26:181382	p 213	N87-30180	#	NASA-CASE-LEW-14108-1	p 129	N87-28832	*	NASA-CR-179513-VOL-1	p 157	N87-19686	*
NAS 1.26:181396	p 80	N87-29633	#	NASA-CASE-LEW-14196-2	p 169	N87-25585	#	NASA-CR-179514	p 193	N87-18922	*
NAS 1.26:181404	p 80	N87-29635	#	NASA-CASE-LEW-14252-1	p 196	N87-25630	#	NASA-CR-179515	p 34	N87-11797	*
NAS 1.26:181410	p 187	N87-29896	#	NASA-CASE-LEW-14262-1	p 93	N87-28647	*	NASA-CR-179517	p 186	N87-27267	*
NAS 1.26:181411	p 187	N87-29897	#	NASA-CASE-LEW-14297-1	p 156	N87-15452	#	NASA-CR-179518	p 180	N87-12915	*
NAS 1.26:181412	p 107	N87-29706	#	NASA-CASE-LEW-14338-1	p 55	N87-10174	*	NASA-CR-179520	p 158	N87-25552	*
NAS 1.26:181417	p 200	N87-29958	#	NASA-CASE-LEW-14345-1	p 70	N87-14432	#	NASA-CR-179523	p 10	N87-16804	*
NAS 1.26:181418	p 200	N87-29957	#	NASA-CASE-LEW-14346-1	p 70	N87-14433	*	NASA-CR-179524	p 10	N87-16803	*
NAS 1.26:3596	p 212	N87-29315	#	NASA-CASE-LEW-14374-1	p 36	N87-25335	#	NASA-CR-179526	p 206	N87-17472	*
NAS 1.26:3818	p 210	N87-10753	*	NASA-CASE-LEW-14392-1	p 106	N87-28656	*	NASA-CR-179527	p 206	N87-17473	*
NAS 1.26:3831	p 1	N87-10003	*	NASA-CASE-LEW-14392-2	p 106	N87-27810	#	NASA-CR-179528	p 28	N87-21956	*
NAS 1.26:3867	p 210	N87-10752	*	NASA-CP-2339	p 179	N87-11180	#	NASA-CR-179529	p 88	N87-11873	*
NAS 1.26:3935	p 8	N87-11694	*	NASA-CP-2423-REV	p 181	N87-16321	#	NASA-CR-179530	p 180	N87-13790	*
NAS 1.26:3998	p 182	N87-18852	#	NASA-CP-2433	p 27	N87-20267	#	NASA-CR-179535	p 108	N87-15320	*
NAS 1.26:4015	p 146	N87-17003	#	NASA-CP-2443	p 167	N87-22199	#	NASA-CR-179536	p 218	N87-17515	*
NAS 1.26:4018	p 171	N87-13779	#	NASA-CP-2465	p 108	N87-21141	#	NASA-CR-179537-VOL-1	p 90	N87-17883	*
NAS 1.26:4019	p 211	N87-17481	#	NASA-CP-2471	p 62	N87-22766	#	NASA-CR-179538	p 180	N87-12021	*
NAS 1.26:4020	p 8	N87-13405	#	NASA-CP-2475	p 196	N87-26413	#	NASA-CR-179541	p 56	N87-13486	*
NAS 1.26:4021	p 9	N87-13406	#	NASA-CP-2484	p 199	N87-29914	#	NASA-CR-179543	p 193	N87-17401	*
NAS 1.26:4032	p 172	N87-13782	#	NASA-CR-168113	p 32	N87-28553	#	NASA-CR-179545	p 124	N87-16972	*
NAS 1.26:4033	p 106	N87-24577	#	NASA-CR-168114-VOL-1	p 32	N87-28552	*	NASA-CR-179547	p 78	N87-11858	*
NAS 1.26:4034	p 171	N87-13781	#	NASA-CR-168114-VOL-2	p 33	N87-28556	#	NASA-CR-179549	p 1	N87-15932	*
NAS 1.26:4041	p 28	N87-20996	#	NASA-CR-168115	p 32	N87-28554	#	NASA-CR-179550	p 181	N87-15491	*
NAS 1.26:4052	p 148	N87-21257	#	NASA-CR-174676	p 8	N87-10835	#	NASA-CR-179551	p 88	N87-13514	*
NAS 1.26:4055	p 166	N87-20552	#	NASA-CR-174707	p 159	N87-28883	#	NASA-CR-179552	p 59	N87-16874	*
NAS 1.26:4072	p 151	N87-24641	#	NASA-CR-174713	p 73	N87-17861	*	NASA-CR-179553	p 89	N87-14486	*
NAS 1.26:4076	p 14	N87-29412	#	NASA-CR-174733	p 74	N87-20387	#	NASA-CR-179556	p 11	N87-16806	*
NAS 1.26:4077	p 169	N87-26358	#	NASA-CR-174742	p 124	N87-11104	#	NASA-CR-179557	p 25	N87-13443	*
NAS 1.26:4081	p 169	N87-25579	#	NASA-CR-174773	p 155	N87-11144	#	NASA-CR-179558	p 116	N87-19556	*
NAS 1.26:4083	p 169	N87-25578	#	NASA-CR-174814	p 32	N87-28555	#	NASA-CR-179559	p 220	N87-15030	*
NAS 1.26:4086	p 172	N87-24707	#	NASA-CR-174819	p 8	N87-10840	#	NASA-CR-179562	p 70	N87-14434	*
NAS 1.26:4087	p 173	N87-26361	#	NASA-CR-174828	p 145	N87-13661	#	NASA-CR-179563	p 166	N87-19723	*
NAS 1.26:4088	p 169	N87-26356	#	NASA-CR-174833	p 157	N87-22179	#	NASA-CR-179566-SUMM	p 115	N87-16955	*
NAS 1.26:4089	p 170	N87-29846	#	NASA-CR-174844	p 182	N87-18117	#	NASA-CR-179567	p 115	N87-16954	*
NAS 1.26:83765	p 23	N87-10100	#	NASA-CR-174845	p 23	N87-10866	#	NASA-CR-179570	p 26	N87-14348	*
NAS 1.26:88879	p 179	N87-11180	#	NASA-CR-174850-VOL-2	p 13	N87-20239	#	NASA-CR-179571	p 168	N87-22246	*
NAS 1.55:2339	p 181	N87-16321	#	NASA-CR-174860	p 33	N87-29534	*	NASA-CR-179573	p 114	N87-16953	*
NAS 1.55:2423-REV	p 179	N87-16321	#	NASA-CR-174873	p 222	N87-30223	#	NASA-CR-179574	p 18	N87-24457	*
NAS 1.55:2433	p 27	N87-20267	#	NASA-CR-174910	p 75	N87-28612	#	NASA-CR-179577	p 206	N87-27475	*
NAS 1.55:2443	p 167	N87-22199	#	NASA-CR-174912	p 26	N87-14349	#	NASA-CR-179580	p 182	N87-18121	*
NAS 1.55:2465	p 108	N87-21141	#	NASA-CR-174914	p 58	N87-15269	#	NASA-CR-179581	p 60	N87-17848	*
NAS 1.55:2471	p 62	N87-22766	#	NASA-CR-174922	p 43	N87-10946	#	NASA-CR-179582	p 107	N87-24578	*
NAS 1.55:2475	p 196	N87-26413	#	NASA-CR-174932	p 25	N87-11788	#	NASA-CR-179587-VOL-1	p 65	N87-23695	*
NAS 1.55:2484	p 199	N87-29914	#	NASA-CR-174972	p 221	N87-20137	#	NASA-CR-179587-VOL-2	p 65	N87-23696	*
NAS 1.60:1848	p 150	N87-23921	#	NASA-CR-174981	p 192	N87-11348	#	NASA-CR-179589	p 18	N87-23615	*
NAS 1.60:1849	p 151	N87-24639	#	NASA-CR-174982	p 191	N87-10531	#	NASA-CR-179591	p 115	N87-18696	*
NAS 1.60:1850	p 150	N87-23936	#	NASA-CR-174983	p 192	N87-12046	#	NASA-CR-179592	p 115	N87-18695	*
NAS 1.60:2418	p 11	N87-17669	#	NASA-CR-175010	p 100	N87-13540	#	NASA-CR-179594	p 29	N87-23622	*
NAS 1.60:2530	p 205	N87-14918	#	NASA-CR-175039	p 15	N87-29419	#	NASA-CR-179596	p 63	N87-22803	*
NAS 1.60:2593	p 156	N87-13731	#	NASA-CR-175042	p 192	N87-12047	#	NASA-CR-179597-VOL-1	p 117	N87-21212	*
NAS 1.60:2596	p 147	N87-18035	#	NASA-CR-175056	p 193	N87-17400	#	NASA-CR-179597-VOL-2	p 117	N87-21213	*
NAS 1.60:2597	p 27	N87-17699	#	NASA-CR-175059	p 15	N87-29418	#	NASA-CR-179598-VOL-1	p 116	N87-19552	*
NAS 1.60:2601	p 9	N87-14284	#	NASA-CR-175060	p 180	N87-12923	#	NASA-CR-179598-VOL-2	p 116	N87-19553	*
NAS 1.60:2610	p 166	N87-18095	#	NASA-CR-175062	p 27	N87-16830	#	NASA-CR-179601	p 184	N87-22267	*
NAS 1.60:2611	p 101	N87-18666	#	NASA-CR-175067	p 34	N87-29538	#	NASA-CR-179603	p 195	N87-23030	*
NAS 1.60:2626	p 164	N87-10391	#	NASA-CR-175067	p 34	N87-29539	#	NASA-CR-179605	p 125	N87-20467	*
NAS 1.60:2635	p 115	N87-17971	#	NASA-CR-175067	p 34	N87-29539	#	NASA-CR-179608	p 13	N87-20243	*
NAS 1.60:2645	p 215	N87-14998	#	NASA-CR-175069-VOL-1	p 129	N87-29738	#	NASA-CR-179609	p 198	N87-27324	*
NAS 1.60:2646	p 35	N87-18576	#	NASA-CR-175069-VOL-2	p 130	N87-29739	#	NASA-CR-179611	p 168	N87-23969	*
NAS 1.60:2655	p 146	N87-18034	#	NASA-CR-175075	p 191	N87-11347	#	NASA-CR-179613	p 33	N87-29536	*
NAS 1.60:2664	p 125	N87-17991	#	NASA-CR-175093	p 69	N87-29594	#	NASA-CR-179619	p 158	N87-22960	*
NAS 1.60:2665	p 125	N87-17990	#	NASA-CR-175101	p 90	N87-15303	#	NASA-CR-179620	p 168	N87-23977	*
NAS 1.60:2666	p 35	N87-17717	#	NASA-CR-175102	p 110	N87-19539	#	NASA-CR-179621	p 169	N87-27197	*
NAS 1.60:2672	p 204	N87-23202	#	NASA-CR-175110	p 31	N87-25323	#	NASA-CR-179622	p 92	N87-27029	*
NAS 1.60:2675	p 127	N87-22923	#	NASA-CR-175116	p 221	N87-18470	#	NASA-CR-179624	p 92	N87-23729	*
NAS 1.60:2676	p 12	N87-20238	#	NASA-CR-175116	p 123	N87-10237	#	NASA-CR-179628	p 109	N87-22865	*
NAS 1.60:2680	p 36	N87-20295	#	NASA-CR-175117	p 191	N87-11346	#	NASA-CR-179631	p 92	N87-25456	*
NAS 1.60:2682	p 35	N87-23662	#	NASA-CR-175118	p 191	N87-11344	#	NASA-CR-179633	p 104	N87-25476	*
NAS 1.60:2693	p 126	N87-20474	#	NASA-CR-175055	p 145	N87-11961	#	NASA-CR-179636	p 79	N87-24549	*
NAS 1.60:2694	p 90	N87-16902	#	NASA-CR-179457	p 59	N87-16065	#	NASA-CR-179637	p 159	N87-26327	*
NAS 1.60:2698	p 167	N87-22235	#	NASA-CR-179458	p 14	N87-29413	#	NASA-CR-179638	p 104	N87-24573	*
NAS 1.60:2699	p 116	N87-20448	#	NASA-CR-179459	p 155	N87-12829	#	NASA-CR-179643	p 170	N87-29840	*
NAS 1.60:2702	p 36	N87-22694	#	NASA-CR-179462	p 220	N87-10777	#	NASA-CR-179644	p 186	N87-26384	*
NAS 1.60:2705	p 167	N87-20555	#	NASA-CR-179464	p 59	N87-16878	#	NASA-CR-179646	p 159	N87-26326	*
NAS 1.60:2711	p 184	N87-20566	#	NASA-CR-179479	p 113	N87-11056	#	NASA-CR-179649	p 105	N87-26233	*
NAS 1.60:2719	p 126	N87-21239	#	NASA-CR-179480	p 113	N87-11057	#	NASA-CR-179714	p 113	N87-10225	*
NAS 1.60:2720	p 60	N87-20381	#	NASA-CR-179481	p 114	N87-11915	#	NASA-CR-179857	p 99	N87-11009	*
NAS 1.60:2725	p 66	N87-25423	#	NASA-CR-179482	p 192	N87-14771	#	NASA-CR-179897	p 8	N87-11701	*
NAS 1.60:2726	p 67	N87-25424	#	NASA-CR-179484	p 164	N87-11995	#	NASA-CR-180030	p 202	N87-14872	*
NAS 1.60:2740	p 34	N87-25331	#	NASA-CR-179486	p 168	N87-22245	#	NASA-CR-180073	p 124	N87-16971	*
NAS 1.60:2746	p 31	N87-24481	#	NASA-CR-179488	p 58	N87-15272	*	NASA-CR-180102	p 215	N87-16614	*
NAS 1.60:2751	p 67	N87-25425	#	NASA-CR-179490	p 193	N87-19804	#	NASA-CR-180106	p 114	N87-16198	*
NAS 1.60:2752	p 128	N87-25532	#	NASA-CR-179491	p 25	N87-13441	#	NASA-CR-180162	p 193	N87-18229	*
NAS 1.60:2758	p 151	N87-27161	#	NASA-CR-179492	p 25	N87-13442	#	NASA-CR-180194	p 166	N87-18096	*
NAS 1.61:1170	p 11	N87-17665	#	NASA-CR-179494	p 185	N87-22996	#	NASA-CR-180214	p 202	N87-18998	*
NAS 1.71:LEW-14297-1	p 156	N87-15452	#	NASA-CR-179496	p 55	N87-10176	#	NASA-CR-180215	p 202	N87-18997	*
NAS 1.71:LEW-14338-1	p 55	N87-10174	#	NASA-CR-179501	p 164	N87-11158	#	NASA-CR-180262	p 147	N87-19647	*
NAS 1.71:LEW-14345-1	p 70	N87-14432	#	NASA-CR-179502	p 58	N87-15270	#	NASA-CR-180307	p 118	N87-27085	*
NAS 1.71:LEW-14346-1	p 70	N87-14433	#	NASA-CR-179503	p 25	N87-11789	#	NASA-CR-180349	p 183	N87-19756	*
NAS 1.71:LEW-14392-2	p 106	N87-27810	#	NASA-CR-179504	p 100	N87-13539	#	NASA-CR-180399	p 80	N87-28634	*
NASA-CASE-LEW-13834-1	p 89	N87-14482	*	NASA-CR-179505	p 70	N87-16879	#	NASA-CR-180579	p 215	N87-22508	*
NASA-CASE-LEW-13899-1	p 110	N87-21160	*	NASA-CR-179508	p 99	N87-11892	#	NASA-CR-180587	p 150	N87-23925	

REPORT NUMBER INDEX

NASA-TM-89817

NASA-CR-180672	p 213	N87-27495 * #	NASA-TM-100141	p 31	N87-26910 * #	NASA-TM-88885	p 110	N87-12708 * #
NASA-CR-180697	p 152	N87-27973 * #	NASA-TM-100142	p 92	N87-26217 * #	NASA-TM-88887	p 88	N87-11875 * #
NASA-CR-180803	p 196	N87-25621 * #	NASA-TM-100143	p 37	N87-28571 * #	NASA-TM-88888	p 17	N87-12559 * #
NASA-CR-180806	p 186	N87-25607 * #	NASA-TM-100147	p 173	N87-26362 * #	NASA-TM-88890	p 11	N87-17662 * #
NASA-CR-180808	p 105	N87-27053 * #	NASA-TM-100148	p 173	N87-25589 * #	NASA-TM-88891	p 220	N87-13359 * #
NASA-CR-180810	p 93	N87-27771 * #	NASA-TM-100149	p 207	N87-25821 * #	NASA-TM-88892	p 88	N87-13513 * #
NASA-CR-180811	p 159	N87-28869 * #	NASA-TM-100150	p 117	N87-26265 * #	NASA-TM-88894	p 101	N87-16140 * #
NASA-CR-180812	p 198	N87-27327 * #	NASA-TM-100151	p 186	N87-26399 * #	NASA-TM-88895	p 221	N87-16663 * #
NASA-CR-180813	p 31	N87-26914 * #	NASA-TM-100152	p 159	N87-25562 * #	NASA-TM-88896	p 150	N87-23933 * #
NASA-CR-180816	p 44	N87-27710 * #	NASA-TM-100153	p 31	N87-25329 * #	NASA-TM-88897	p 220	N87-15031 * #
NASA-CR-180817	p 44	N87-27711 * #	NASA-TM-100156	p 105	N87-26232 * #	NASA-TM-88898	p 221	N87-16664 * #
NASA-CR-180818	p 222	N87-30225 * #	NASA-TM-100157	p 128	N87-26278 * #	NASA-TM-88899	p 100	N87-12679 * #
NASA-CR-180821	p 119	N87-28819 * #	NASA-TM-100158	p 187	N87-27268 * #	NASA-TM-88900	p 70	N87-11841 * #
NASA-CR-180829	p 129	N87-28825 * #	NASA-TM-100159	p 33	N87-29537 * #	NASA-TM-88901	p 181	N87-17087 * #
NASA-CR-180833	p 222	N87-28470 * #	NASA-TM-100165	p 212	N87-26615 * #	NASA-TM-88902	p 100	N87-15305 * #
NASA-CR-180987	p 149	N87-22948 * #	NASA-TM-100166	p 105	N87-26231 * #	NASA-TM-88903	p 146	N87-17002 * #
NASA-CR-181017	p 37	N87-22700 * #	NASA-TM-100167	p 93	N87-28641 * #	NASA-TM-88904	p 26	N87-16826 * #
NASA-CR-181057	p 66	N87-25420 * #	NASA-TM-100168	p 129	N87-27120 * #	NASA-TM-88905	p 115	N87-16958 * #
NASA-CR-181112	p 117	N87-24605 * #	NASA-TM-100170	p 106	N87-29679 * #	NASA-TM-88906	p 26	N87-16827 * #
NASA-CR-181150	p 37	N87-25341 * #	NASA-TM-100171	p 187	N87-28058 * #	NASA-TM-88907	p 181	N87-14730 * #
NASA-CR-181151	p 44	N87-25419 * #	NASA-TM-100173	p 152	N87-27977 * #	NASA-TM-88908	p 29	N87-22681 * #
NASA-CR-181181	p 119	N87-28814 * #	NASA-TM-100174	p 187	N87-27269 * #	NASA-TM-88909	p 91	N87-18643 * #
NASA-CR-181188	p 129	N87-27099 * #	NASA-TM-100175	p 212	N87-28398 * #	NASA-TM-88911	p 210	N87-16586 * #
NASA-CR-181203	p 31	N87-26908 * #	NASA-TM-100178	p 14	N87-27629 * #	NASA-TM-88912	p 146	N87-17001 * #
NASA-CR-181273	p 118	N87-27882 * #	NASA-TM-100184	p 206	N87-30132 * #	NASA-TM-88913	p 210	N87-14957 * #
NASA-CR-181293	p 152	N87-27949 * #	NASA-TM-100186	p 80	N87-28628 * #	NASA-TM-88914	p 57	N87-14423 * #
NASA-CR-181330	p 119	N87-28813 * #	NASA-TM-100187	p 118	N87-27883 * #	NASA-TM-88915	p 13	N87-22630 * #
NASA-CR-181336	p 152	N87-28860 * #	NASA-TM-100188	p 159	N87-28880 * #	NASA-TM-88916	p 207	N87-14956 * #
NASA-CR-181343	p 206	N87-29212 * #	NASA-TM-100189	p 16	N87-29471 * #	NASA-TM-88917	p 183	N87-18883 * #
NASA-CR-181382	p 213	N87-30180 * #	NASA-TM-100190	p 93	N87-29662 * #	NASA-TM-88918	p 57	N87-14422 * #
NASA-CR-181396	p 80	N87-29633 * #	NASA-TM-100192	p 75	N87-28611 * #	NASA-TM-88919	p 146	N87-15442 * #
NASA-CR-181404	p 80	N87-29635 * #	NASA-TM-100194	p 215	N87-28423 * #	NASA-TM-88920	p 211	N87-16588 * #
NASA-CR-181410	p 187	N87-29896 * #	NASA-TM-100196	p 130	N87-29750 * #	NASA-TM-88921	p 108	N87-16167 * #
NASA-CR-181411	p 187	N87-29897 * #	NASA-TM-100198	p 71	N87-29599 * #	NASA-TM-88922	p 9	N87-14283 * #
NASA-CR-181412	p 107	N87-29706 * #	NASA-TM-100201	p 15	N87-29420 * #	NASA-TM-88923	p 146	N87-15441 * #
NASA-CR-181417	p 200	N87-29958 * #	NASA-TM-100203	p 68	N87-28602 * #	NASA-TM-88924	p 124	N87-16968 * #
NASA-CR-181418	p 200	N87-29957 * #	NASA-TM-83765	p 23	N87-10100 * #	NASA-TM-88925	p 148	N87-22122 * #
NASA-CR-3596	p 212	N87-29315 * #	NASA-TM-86877	p 184	N87-22273 * #	NASA-TM-88926	p 205	N87-24132 * #
NASA-CR-3818	p 210	N87-10753 * #	NASA-TM-87094	p 13	N87-23598 * #	NASA-TM-88927	p 90	N87-16113 * #
NASA-CR-3831	p 1	N87-10003 * #	NASA-TM-87282	p 192	N87-16445 * #	NASA-TM-88928	p 9	N87-15944 * #
NASA-CR-3867	p 210	N87-10752 * #	NASA-TM-87296	p 70	N87-10177 * #	NASA-TM-88929	p 11	N87-16805 * #
NASA-CR-3935	p 8	N87-11694 * #	NASA-TM-87311	p 89	N87-14483 * #	NASA-TM-88931	p 150	N87-23934 * #
NASA-CR-3998	p 182	N87-18852 * #	NASA-TM-87329	p 205	N87-11543 * #	NASA-TM-88932	p 32	N87-28551 * #
NASA-CR-4015	p 146	N87-17003 * #	NASA-TM-87353	p 103	N87-22860 * #	NASA-TM-88933	p 40	N87-16012 * #
NASA-CR-4018	p 171	N87-13779 * #	NASA-TM-87355	p 158	N87-22181 * #	NASA-TM-88934	p 187	N87-28944 * #
NASA-CR-4019	p 211	N87-17481 * #	NASA-TM-87356-VOL-1	p 16	N87-21878 * #	NASA-TM-88936	p 211	N87-19057 * #
NASA-CR-4020	p 8	N87-13405 * #	NASA-TM-87356-VOL-2	p 16	N87-21879 * #	NASA-TM-88937	p 218	N87-23304 * #
NASA-CR-4021	p 9	N87-13406 * #	NASA-TM-87358	p 156	N87-18801 * #	NASA-TM-88939	p 26	N87-16825 * #
NASA-CR-4032	p 172	N87-13782 * #	NASA-TM-88789	p 192	N87-13856 * #	NASA-TM-88940	p 147	N87-18784 * #
NASA-CR-4033	p 106	N87-24577 * #	NASA-TM-88805	p 57	N87-14426 * #	NASA-TM-88941	p 181	N87-18112 * #
NASA-CR-4034	p 171	N87-13781 * #	NASA-TM-88819	p 100	N87-14518 * #	NASA-TM-88942	p 73	N87-16071 * #
NASA-CR-4041	p 28	N87-20996 * #	NASA-TM-88821	p 89	N87-14487 * #	NASA-TM-88943	p 33	N87-28557 * #
NASA-CR-4052	p 148	N87-21257 * #	NASA-TM-88823	p 123	N87-10232 * #	NASA-TM-88944	p 182	N87-18115 * #
NASA-CR-4055	p 166	N87-20552 * #	NASA-TM-88824	p 58	N87-15267 * #	NASA-TM-88945	p 10	N87-16789 * #
NASA-CR-4072	p 151	N87-24641 * #	NASA-TM-88825	p 124	N87-13637 * #	NASA-TM-88946	p 10	N87-16790 * #
NASA-CR-4076	p 14	N87-29412 * #	NASA-TM-88826	p 145	N87-11962 * #	NASA-TM-88947	p 211	N87-16587 * #
NASA-CR-4077	p 169	N87-26358 * #	NASA-TM-88830	p 193	N87-18230 * #	NASA-TM-88948	p 117	N87-22065 * #
NASA-CR-4081	p 169	N87-25579 * #	NASA-TM-88831	p 9	N87-15173 * #	NASA-TM-88949	p 10	N87-16799 * #
NASA-CR-4083	p 169	N87-25578 * #	NASA-TM-88834	p 114	N87-14569 * #	NASA-TM-88950	p 90	N87-17882 * #
NASA-CR-4086	p 172	N87-24707 * #	NASA-TM-88834	p 119	N87-28769 * #	NASA-TM-88952	p 90	N87-17884 * #
NASA-CR-4087	p 173	N87-26361 * #	NASA-TM-88836	p 124	N87-14597 * #	NASA-TM-88953	p 158	N87-22959 * #
NASA-CR-4088	p 169	N87-26356 * #	NASA-TM-88838	p 180	N87-12924 * #	NASA-TM-88955	p 10	N87-16798 * #
NASA-CR-4089	p 170	N87-29846 * #	NASA-TM-88840	p 89	N87-14488 * #	NASA-TM-88956	p 202	N87-17441 * #
			NASA-TM-88841	p 89	N87-14489 * #	NASA-TM-88957	p 66	N87-24536 * #
NASA-RP-1170	p 11	N87-17665 * #	NASA-TM-88843	p 166	N87-18092 * #	NASA-TM-88959	p 182	N87-18116 * #
			NASA-TM-88845	p 144	N87-11124 * #	NASA-TM-88960	p 185	N87-24006 * #
NASA-TM-100101	p 66	N87-24531 * #	NASA-TM-88848	p 56	N87-10959 * #	NASA-TM-88961	p 35	N87-16851 * #
NASA-TM-100102	p 195	N87-24838 * #	NASA-TM-88850	p 215	N87-18428 * #	NASA-TM-88963	p 27	N87-17701 * #
NASA-TM-100103	p 93	N87-27030 * #	NASA-TM-88852	p 58	N87-14428 * #	NASA-TM-88964	p 108	N87-16917 * #
NASA-TM-100104	p 64	N87-22808 * #	NASA-TM-88854	p 180	N87-12017 * #	NASA-TM-88965	p 74	N87-18814 * #
NASA-TM-100105	p 92	N87-25459 * #	NASA-TM-88855	p 171	N87-10399 * #	NASA-TM-88966	p 101	N87-17906 * #
NASA-TM-100106	p 104	N87-24574 * #	NASA-TM-88858	p 165	N87-17033 * #	NASA-TM-88967	p 35	N87-18575 * #
NASA-TM-100107	p 29	N87-23624 * #	NASA-TM-88859	p 73	N87-16880 * #	NASA-TM-88968	p 27	N87-17700 * #
NASA-TM-100108	p 66	N87-25422 * #	NASA-TM-88861	p 181	N87-13794 * #	NASA-TM-88970	p 102	N87-19518 * #
NASA-TM-100109	p 65	N87-23692 * #	NASA-TM-88862	p 165	N87-15466 * #	NASA-TM-88971	p 211	N87-17480 * #
NASA-TM-100110	p 68	N87-26135 * #	NASA-TM-88863	p 99	N87-11893 * #	NASA-TM-88972	p 156	N87-18057 * #
NASA-TM-100111	p 222	N87-27564 * #	NASA-TM-88864	p 183	N87-20565 * #	NASA-TM-88974	p 183	N87-18882 * #
NASA-TM-100112	p 66	N87-24525 * #	NASA-TM-88865	p 56	N87-10960 * #	NASA-TM-88975	p 167	N87-20556 * #
NASA-TM-100113	p 111	N87-23821 * #	NASA-TM-88866	p 207	N87-18391 * #	NASA-TM-88976	p 183	N87-18881 * #
NASA-TM-100114	p 30	N87-23626 * #	NASA-TM-88867	p 114	N87-13600 * #	NASA-TM-88977	p 110	N87-17937 * #
NASA-TM-100115	p 29	N87-23623 * #	NASA-TM-88868	p 223	N87-17656 * #	NASA-TM-88978	p 172	N87-18109 * #
NASA-TM-100118	p 30	N87-23625 * #	NASA-TM-88869	p 210	N87-13252 * #	NASA-TM-88979	p 102	N87-18670 * #
NASA-TM-100120	p 64	N87-22805 * #	NASA-TM-88870	p 171	N87-12910 * #	NASA-TM-88980	p 125	N87-17993 * #
NASA-TM-100121	p 212	N87-28396 * #	NASA-TM-88871	p 166	N87-18820 * #	NASA-TM-88981	p 102	N87-20422 * #
NASA-TM-100122	p 105	N87-25480 * #	NASA-TM-88872	p 73	N87-13491 * #	NASA-TM-88982	p 157	N87-20516 * #
NASA-TM-100123	p 64	N87-23691 * #	NASA-TM-88873	p 191	N87-11345 * #	NASA-TM-88983	p 14	N87-27628 * #
NASA-TM-100126	p 16	N87-29470 * #	NASA-TM-88874	p 56	N87-11838 * #	NASA-TM-88984	p 116	N87-18700 * #
NASA-TM-100128	p 129	N87-27121 * #	NASA-TM-88875	p 165	N87-15467 * #	NASA-TM-89263	p 219	N87-12384 * #
NASA-TM-100130	p 67	N87-25426 * #	NASA-TM-88877	p 57	N87-14427 * #	NASA-TM-89295	p 213	N87-25838 * #
NASA-TM-100132	p 151	N87-26302 * #	NASA-TM-88878	p 1	N87-16784 * #	NASA-TM-89309	p 101	N87-17926 * #
NASA-TM-100133	p 2	N87-28501 * #	NASA-TM-88879	p 25	N87-11790 * #	NASA-TM-89312	p 18	N87-16816 * #
NASA-TM-100136	p 200	N87-29956 * #	NASA-TM-88880	p 38	N87-15996 * #	NASA-TM-89812	p 12	N87-18540 * #
NASA-TM-100137	p 207	N87-25823 * #	NASA-TM-88881	p 164	N87-11993 * #	NASA-TM-89813	p 12	N87-18539 * #
NASA-TM-100138	p 218	N87-27541 * #	NASA-TM-88882	p 38	N87-13470 * #	NASA-TM-89814	p 60	N87-20379 * #
NASA-TM-100139	p 68	N87-26141 * #	NASA-TM-88883	p 165	N87-13755 * #	NASA-TM-89815	p 91	N87-21078 * #
NASA-TM-100140	p 68	N87-26144 * #	NASA-TM-88884	p 56	N87-12606 * #	NASA-TM-89817	p 28	N87-20280 * #

NASA-TM-89818	p 101	N87-18668 * #	NASA-TM-89920	p 117	N87-22874 * #	RI/RD86-199	p 56	N87-13486 * #
NASA-TM-89819	p 157	N87-20515 * #	NASA-TM-89921	p 150	N87-22949 * #	RI/RD87-109	p 60	N87-17848 * #
NASA-TM-89820	p 102	N87-20425 * #	NASA-TM-89922	p 128	N87-23901 * #			
NASA-TM-89821	p 156	N87-19684 * #	NASA-TM-89924	p 64	N87-22807 * #	R81AEG484	p 212	N87-29315 * #
NASA-TM-89822	p 126	N87-20475 * #	NASA-TM-89925	p 62	N87-22004 * #	R83-915540-27	p 78	N87-11858 * #
NASA-TM-89823	p 203	N87-20767 * #	NASA-TM-89926	p 64	N87-23690 * #	R83AEB122-3	p 33	N87-29534 * #
NASA-TM-89824	p 13	N87-23591 * #	NASA-TM-89927	p 195	N87-24029 * #	R83AEB566	p 34	N87-29539 * #
NASA-TM-89825	p 43	N87-23685 * #	NASA-TM-89928	p 128	N87-24630 * #	R83AEB574	p 210	N87-10753 * #
NASA-TM-89826	p 12	N87-19350 * #	NASA-TM-89929	p 172	N87-23987 * #	R83AEB592	p 32	N87-28553 * #
NASA-TM-89827	p 74	N87-20389 * #	NASA-TM-89930	p 104	N87-24565 * #	R84-925830-33	p 155	N87-11144 * #
NASA-TM-89828	p 12	N87-20235 * #	NASA-TM-89931	p 185	N87-24007 * #	R85-915952-13	p 157	N87-22179 * #
NASA-TM-89830	p 74	N87-18615 * #				R85AEB304	p 100	N87-13540 * #
NASA-TM-89831	p 91	N87-20408 * #	NASA-TP-1848	p 150	N87-23921 * #	R85AEB518	p 211	N87-17481 * #
NASA-TM-89832	p 221	N87-21756 * #	NASA-TP-1849	p 151	N87-24639 * #	R86-927298-10	p 155	N87-10377 * #
NASA-TM-89833	p 28	N87-20282 * #	NASA-TP-1850	p 150	N87-23936 * #	R86-995875-28	p 158	N87-25552 * #
NASA-TM-89834	p 91	N87-20405 * #	NASA-TP-2418	p 11	N87-17669 * #	R86AEB511	p 100	N87-13539 * #
NASA-TM-89835	p 116	N87-20450 * #	NASA-TP-2530	p 205	N87-14918 * #	R87-AEB432	p 168	N87-22245 * #
NASA-TM-89836	p 71	N87-22005 * #	NASA-TP-2593	p 156	N87-13731 * #	R87-916527-1	p 159	N87-28869 * #
NASA-TM-89837	p 203	N87-19002 * #	NASA-TP-2596	p 147	N87-18035 * #	R87AEB111	p 107	N87-24578 * #
NASA-TM-89838	p 103	N87-20426 * #	NASA-TP-2597	p 27	N87-17699 * #			
NASA-TM-89839	p 126	N87-20469 * #	NASA-TP-2601	p 9	N87-14284 * #	S/N-36778	p 124	N87-16972 * #
NASA-TM-89840	p 125	N87-20468 * #	NASA-TP-2610	p 166	N87-18095 * #	S/N-36779	p 124	N87-17989 * #
NASA-TM-89841	p 147	N87-18786 * #	NASA-TP-2611	p 101	N87-18666 * #	SAE PAPER 860615	p 161	A87-28624 *
NASA-TM-89842	p 1	N87-20171 * #	NASA-TP-2626	p 164	N87-10391 * #	SAE PAPER 861715	p 20	A87-32607 *
NASA-TM-89843	p 172	N87-20562 * #	NASA-TP-2635	p 115	N87-17971 * #	SAE PAPER 861744	p 4	A87-32619 *
NASA-TM-89844	p 102	N87-20421 * #	NASA-TP-2645	p 215	N87-14998 * #	SAE PAPER 870101	p 163	A87-48780 *
NASA-TM-89846	p 74	N87-21043 * #	NASA-TP-2646	p 35	N87-18576 * #	SAE PAPER 870102	p 163	A87-48781 *
NASA-TM-89847	p 60	N87-20378 * #	NASA-TP-2655	p 146	N87-18034 * #	SAE PAPER 870408	p 163	A87-48783 *
NASA-TM-89848	p 40	N87-20342 * #	NASA-TP-2664	p 125	N87-17991 * #	SAE PAPER 870444	p 163	A87-48787 *
NASA-TM-89849	p 218	N87-25017 * #	NASA-TP-2665	p 125	N87-17990 * #	SAE PAPER 870466	p 163	A87-48790 *
NASA-TM-89850	p 203	N87-20766 * #	NASA-TP-2666	p 35	N87-17717 * #	SAE PAPER 870467	p 163	A87-48791 *
NASA-TM-89851	p 148	N87-20504 * #	NASA-TP-2672	p 204	N87-23202 * #	SAE PAPER 870599	p 143	A87-48751 *
NASA-TM-89852	p 43	N87-20353 * #	NASA-TP-2675	p 127	N87-22923 * #	SAE PAPER 871031	p 210	A87-48760 *
NASA-TM-89853	p 222	N87-22561 * #	NASA-TP-2676	p 12	N87-20238 * #	SAE PAPER 871033	p 16	A87-48761 *
NASA-TM-89854	p 167	N87-22237 * #	NASA-TP-2680	p 36	N87-20295 * #	SAE PAPER 871039	p 22	A87-48766 *
NASA-TM-89856	p 61	N87-21037 * #	NASA-TP-2692	p 36	N87-23662 * #			
NASA-TM-89857	p 61	N87-20382 * #	NASA-TP-2693	p 126	N87-20474 * #	SAE-PAPER-870450	p 128	N87-23902 * #
NASA-TM-89858	p 61	N87-20383 * #	NASA-TP-2694	p 90	N87-16902 * #	SER-510220	p 169	N87-25578 * #
NASA-TM-89859	p 218	N87-20821 * #	NASA-TP-2698	p 167	N87-22235 * #	SER-760606	p 18	N87-24457 * #
NASA-TM-89860	p 126	N87-20477 * #	NASA-TP-2699	p 116	N87-20448 * #	SPIE-616	p 41	A87-26610 *
NASA-TM-89861	p 184	N87-21375 * #	NASA-TP-2702	p 36	N87-22694 * #	SR86-R-4938-39	p 25	N87-11789 * #
NASA-TM-89862	p 79	N87-23718 * #	NASA-TP-2705	p 167	N87-20555 * #	TF/86/9	p 145	N87-11961 * #
NASA-TM-89863	p 39	N87-23674 * #	NASA-TP-2711	p 184	N87-20566 * #	TR-716548-6	p 202	N87-14872 * #
NASA-TM-89864	p 62	N87-22003 * #	NASA-TP-2719	p 126	N87-21239 * #	TR-716688-1	p 114	N87-16198 * #
NASA-TM-89865	p 75	N87-22811 * #	NASA-TP-2720	p 60	N87-20381 * #	TR-716688-4	p 44	N87-25419 * #
NASA-TM-89866	p 91	N87-21077 * #	NASA-TP-2725	p 66	N87-25423 * #	TR-716688-5	p 37	N87-25341 * #
NASA-TM-89867	p 61	N87-21998 * #	NASA-TP-2726	p 67	N87-25424 * #	TRC-SEAL-3-87	p 166	N87-18096 * #
NASA-TM-89868	p 29	N87-22680 * #	NASA-TP-2740	p 34	N87-25331 * #	UDR-TR-85-45	p 75	N87-28612 * #
NASA-TM-89869	p 127	N87-23900 * #	NASA-TP-2746	p 31	N87-24481 * #	UILU-ENG-87-2560	p 118	N87-27085 * #
NASA-TM-89870	p 127	N87-22098 * #	NASA-TP-2751	p 67	N87-25425 * #	UILU-TR-87-6	p 118	N87-27085 * #
NASA-TM-89872	p 194	N87-23020 * #	NASA-TP-2752	p 128	N87-25532 * #	US-PATENT-APPL-SN-038560	p 106	N87-27810 * #
NASA-TM-89873	p 41	N87-22757 * #	NASA-TP-2758	p 151	N87-27161 * #	US-PATENT-APPL-SN-054983	p 169	N87-25585 * #
NASA-TM-89874	p 205	N87-24930 * #				US-PATENT-APPL-SN-060200	p 36	N87-25335 * #
NASA-TM-89875	p 103	N87-22048 * #	NEAR-TR-295	p 1	N87-10003 * #	US-PATENT-APPL-SN-071678	p 196	N87-25630 * #
NASA-TM-89876	p 64	N87-22804 * #	OS-TR-718688-2	p 37	N87-22700 * #	US-PATENT-APPL-SN-478131	p 89	N87-14482 * #
NASA-TM-89877	p 91	N87-22034 * #	OS-TR-718688-2	p 37	N87-22700 * #	US-PATENT-APPL-SN-636463	p 59	N87-16875 * #
NASA-TM-89879	p 104	N87-24566 * #	OSU-NE-8702	p 213	N87-27495 * #	US-PATENT-APPL-SN-700255	p 126	N87-21234 * #
NASA-TM-89880	p 127	N87-22097 * #	OSU-TR-716111-5	p 119	N87-28813 * #	US-PATENT-APPL-SN-732321	p 129	N87-28832 * #
NASA-TM-89881	p 194	N87-22307 * #	P/W/GPD-FR-19381-VOL-1	p 157	N87-19686 * #	US-PATENT-APPL-SN-775350	p 110	N87-21150 * #
NASA-TM-89882	p 61	N87-21999 * #	PCG-REPT-85-1	p 202	N87-18998 * #	US-PATENT-APPL-SN-832296	p 93	N87-28647 * #
NASA-TM-89883	p 194	N87-22308 * #	PCG-REPT-87-1	p 202	N87-18997 * #	US-PATENT-APPL-SN-834977	p 103	N87-23736 * #
NASA-TM-89884	p 212	N87-25826 * #	PPI-FID-300086-VOL-3	p 192	N87-12046 * #	US-PATENT-APPL-SN-886149	p 106	N87-28656 * #
NASA-TM-89885	p 109	N87-24579 * #	PPI-FID-300101-VOL-1	p 192	N87-11348 * #	US-PATENT-APPL-SN-897239	p 55	N87-10174 * #
NASA-TM-89886	p 149	N87-22174 * #	PPI-FID-300102-VOL-2	p 191	N87-10531 * #	US-PATENT-APPL-SN-917125	p 156	N87-15452 * #
NASA-TM-89888	p 194	N87-23027 * #	PT-6807	p 116	N87-19556 * #	US-PATENT-APPL-SN-924474	p 70	N87-14432 * #
NASA-TM-89889	p 62	N87-22001 * #	PW/GPD-FR-19177	p 110	N87-19539 * #	US-PATENT-APPL-SN-934470	p 70	N87-14433 * #
NASA-TM-89890	p 13	N87-24435 * #	PWA-5574-206	p 92	N87-27029 * #	US-PATENT-CLASS-148-162	p 93	N87-28647 * #
NASA-TM-89891	p 185	N87-23010 * #	PWA-5628-69	p 159	N87-28883 * #	US-PATENT-CLASS-148-410	p 93	N87-28647 * #
NASA-TM-89892	p 222	N87-22562 * #	PWA-5869-88-VOL-1	p 32	N87-28552 * #	US-PATENT-CLASS-148-429	p 89	N87-14482 * #
NASA-TM-89893	p 75	N87-25432 * #	PWA-5869-88-VOL-2	p 33	N87-28556 * #	US-PATENT-CLASS-156-345	p 110	N87-21160 * #
NASA-TM-89894	p 39	N87-22755 * #	PWA-5890-24	p 74	N87-20387 * #	US-PATENT-CLASS-156-643	p 110	N87-21160 * #
NASA-TM-89895	p 169	N87-23984 * #	PWA-5894-34	p 182	N87-18117 * #	US-PATENT-CLASS-156-646	p 110	N87-21160 * #
NASA-TM-89896	p 148	N87-22171 * #	PWA-5940-36	p 180	N87-12923 * #	US-PATENT-CLASS-156-659.1	p 110	N87-21160 * #
NASA-TM-89897	p 168	N87-23978 * #	PWA-5940-46-VOL-1	p 185	N87-22996 * #	US-PATENT-CLASS-156-661.1	p 110	N87-21160 * #
NASA-TM-89898	p 127	N87-22102 * #	PWA-5940-46-VOL-2	p 186	N87-27267 * #	US-PATENT-CLASS-156-904	p 110	N87-21160 * #
NASA-TM-89899	p 151	N87-24646 * #	PWA-5968-47	p 29	N87-23622 * #	US-PATENT-CLASS-204-298	p 110	N87-21160 * #
NASA-TM-89900	p 186	N87-24722 * #	QR-17	p 191	N87-11347 * #	US-PATENT-CLASS-219-275	p 59	N87-16875 * #
NASA-TM-89901	p 170	N87-28918 * #	QR-18	p 191	N87-11346 * #	US-PATENT-CLASS-250-423-R	p 126	N87-21234 * #
NASA-TM-89902	p 128	N87-23902 * #	QR-19	p 191	N87-11344 * #	US-PATENT-CLASS-264-332	p 106	N87-28656 * #
NASA-TM-89903	p 198	N87-26455 * #	REPT-6451	p 169	N87-25579 * #	US-PATENT-CLASS-264-60	p 106	N87-28656 * #
NASA-TM-89904	p 103	N87-24563 * #	REPT-716548-7	p 118	N87-27882 * #	US-PATENT-CLASS-313-237	p 129	N87-28832 * #
NASA-TM-89905	p 103	N87-23750 * #	REPT-716688-3	p 117	N87-24605 * #	US-PATENT-CLASS-313-278	p 129	N87-28832 * #
NASA-TM-89906	p 186	N87-26385 * #	REPT-764038/716109	p 169	N87-27197 * #	US-PATENT-CLASS-315-111.81	p 126	N87-21234 * #
NASA-TM-89907	p 195	N87-23029 * #	REPT-8911-950001	p 59	N87-16874 * #			
NASA-TM-89908	p 195	N87-23028 * #	RI/RD86-123	p 55	N87-10176 * #			
NASA-TM-89909	p 63	N87-22802 * #						
NASA-TM-89910	p 2	N87-25292 * #						
NASA-TM-89911	p 128	N87-23903 * #						
NASA-TM-89912	p 168	N87-22978 * #						
NASA-TM-89913	p 195	N87-24026 * #						
NASA-TM-89914	p 194	N87-22310 * #						
NASA-TM-89915	p 194	N87-22311 * #						
NASA-TM-89916	p 65	N87-23693 * #						
NASA-TM-89917	p 14	N87-25294 * #						
NASA-TM-89918	p 36	N87-23664 * #						
NASA-TM-89919	p 117	N87-22089 * #						

REPORT NUMBER INDEX

WDL-TR11068

US-PATENT-CLASS-420-460	p 89	N87-14482 *
US-PATENT-CLASS-428-367	p 106	N87-28656 *
US-PATENT-CLASS-428-421	p 103	N87-23736 *
US-PATENT-CLASS-428-422	p 103	N87-23736 *
US-PATENT-CLASS-428-447	p 103	N87-23736 *
US-PATENT-CLASS-428-473.5	p 103	N87-23736 *
US-PATENT-CLASS-428-702	p 103	N87-23736 *
US-PATENT-CLASS-60-203.1	p 59	N87-16875 *
US-PATENT-4,608,821	p 59	N87-16875 *
US-PATENT-4,610,736	p 89	N87-14482 *
US-PATENT-4,620,898	p 110	N87-21160 *
US-PATENT-4,642,523	p 126	N87-21234 *
US-PATENT-4,664,980	p 103	N87-23736 *
US-PATENT-4,676,846	p 93	N87-28647 *
US-PATENT-4,687,964	p 129	N87-28832 *
US-PATENT-4,689,188	p 106	N87-28656 *
USAAVCOM-TR-87-C-2	p 18	N87-16816 * #
USAAVSCOM-TR-84-C-13	p 23	N87-10100 * #
USAAVSCOM-TR-85-C-13	p 26	N87-14349 * #
USAAVSCOM-TR-86-C-15	p 31	N87-25323 * #
USAAVSCOM-TR-86-C-19	p 90	N87-15303 * #
USAAVSCOM-TR-86-C-26	p 145	N87-11962 * #
USAAVSCOM-TR-86-C-27	p 165	N87-15466 * #
USAAVSCOM-TR-86-C-28	p 166	N87-18092 * #
USAAVSCOM-TR-86-C-29	p 11	N87-16805 * #
USAAVSCOM-TR-86-C-30	p 10	N87-16789 * #
USAAVSCOM-TR-86-C-31	p 10	N87-16790 * #
USAAVSCOM-TR-86-C-32	p 28	N87-20280 * #
USAAVSCOM-TR-86-C-33	p 144	N87-11124 * #
USAAVSCOM-TR-86-C-34	p 164	N87-11158 * #
USAAVSCOM-TR-86-C-36	p 9	N87-15944 * #
USAAVSCOM-TR-86-C-37	p 25	N87-11790 * #
USAAVSCOM-TR-86-C-38	p 11	N87-17662 * #
USAAVSCOM-TR-86-C-41	p 148	N87-22122 * #
USAAVSCOM-TR-87-C-5	p 12	N87-20235 * #
WDL-TR-10941-SUMM	p 115	N87-16955 * #
WDL-TR-10941	p 115	N87-16954 * #
WDL-TR10939	p 58	N87-15270 * #
WDL-TR11068	p 125	N87-20467 * #



National Aeronautics and
Space Administration

Report Documentation Page

1. Report No. NASA TM-100910	2. Government Accession No.	3. Recipient's Catalog No.	
4. Title and Subtitle Bibliography of Lewis Research Center Technical Publications Announced in 1987		5. Report Date June 1988	6. Performing Organization Code
		8. Performing Organization Report No. E-4162	
7. Author(s)		10. Work Unit No. None	
		11. Contract or Grant No.	
9. Performing Organization Name and Address National Aeronautics and Space Administration Lewis Research Center Cleveland, Ohio 44135-3191		13. Type of Report and Period Covered Technical Memorandum	
		14. Sponsoring Agency Code	
12. Sponsoring Agency Name and Address National Aeronautics and Space Administration Washington, D.C. 20546-0001			
15. Supplementary Notes Compiled by Technical Information Services Division, Lewis Research Center.			
16. Abstract This compilation of abstracts describes and indexes the technical reporting that resulted from the scientific and engineering work performed and managed by the Lewis Research Center in 1987. All the publications were announced in the 1987 issues of STAR (Scientific and Technical Aerospace Reports) and/or IAA (International Aerospace Abstracts). Included are research reports, journal articles, conference presentations, patents and patent applications, and theses.			
17. Key Words (Suggested by Author(s)) Bibliographies Abstracts Documentation Indexes (Documentation)		18. Distribution Statement Unclassified - Unlimited Subject Category 82	
19. Security Classif. (of this report) Unclassified	20. Security Classif. (of this page) Unclassified	21. No of pages 365	22. Price* A16

National Aeronautics and
Space Administration

Lewis Research Center
Cleveland, Ohio 44135

Official Business
Penalty for Private Use \$300

FOURTH CLASS MAIL

ADDRESS CORRECTION REQUESTED



Postage and Fees Paid
National Aeronautics and
Space Administration
NASA 451

NASA
